THE HYDRAULIC CHARACTERISTICS OF CHANNELS WITH OVERBANK FLOOD PLAIN FLOW

A THESIS SUBMITTED TO THE UNIVERSITY OF GLASGOW FOR THE DEGREE OF DOCTOR OF PHILOSOPHY IN THE DEPARTMENT OF CIVIL ENGINEERING, UNIVERSITY OF GLASGOW

JAMES I. BAIRD BSc. HONS

OCTOBER 1984.

TO MY PARENTS

Acknowledgement

The author wishes to express his gratitude to the following people:-

To Prof Hugh B Sutherland for his support and encouragement in obtaining the necessary funding.

Dr D A Ervine, my supervisor for his continued effort

All the other staff of the Civil Engineering Department, in particular Dr G Herbertson.

Alan Gray, Department technician for his skills in constructing the physical model.

John Love, Chief Technician and all the other staff in the work shop.

To my parents for their help and understanding.

Finally to my wife Janice for her sustaining influence throughout.

Summary.

The work presented in this thesis is an extensive experimental study into the hydraulic behaviour of smooth rectangular compound channels when overbank flow occurs on the flood plain. The effect of a turbulent shear mechanism, which exists at the channel/flood plain boundary, is investigated for a range of sixteen different geometrical cross-sections with constant boundary roughness but varying water surface slopes and channel flow depths.

The early chapters in this thesis attempt to establish the nature and context of the problem and so provide an outline of the past research carried out in the field of channel/flood plain interaction. Chapter Three essentially describes the design and construction of the physical model for the expermental study. It is hoped that the proposed model study will give a clear understanding of the turbulent mechanism and it's relevance in determining rating curves for rivers, developing mathematical models and establishing design criteria for flood protection schemes.

The experimental work presented can essentially be divided into three main areas :

(a) The recording of local velocities throughout the channel section and so investigate the effect of the shear interaction on the distribution of velocities in the channel and flood plain.

(b) The recording of boundary shear stresses around the perimeter of the channel and flood plain to evaluate the effect

of the interaction mechanism on the distribution of the boundary shear stress.

(c) The determination of non-dimensional rating curves to compare the measured discharges with predicted discharges based on conventional discharge-stage equations.

The geometrical parameters which influence the channel/flood plain interaction will be indicated in later chapters. The analysis of the experimental results attempts to present a relationship between such parameters and the interaction mechanism. From consideration of force-momentum equations the out of balance forces which exist in the channel and flood plain can be directly related to an Apparent shear force which exists between the channel and the flood plain. An interesting relationship is established between the apparent shear force and the geometrical parameters given for each geometry tested. The mean velocities in the channel and flood plain during overbank flow are also calculated and the effect of the channel/flood plain interaction is related to the associated frictional resistance of the channel to flow.

It will be shown that the intensity of this turbulent shear mechanism is dependent on ΔV, the relative depth Yf/Yc, Bf/Bc, Bc/h and Bf/h where ΔV is the difference in mean velocities in the channel and flood plain, Yc and Yfare the channel and flood plain depths respectively, Bc and Bf are the channel and flood plain widths respectively and h is the bankfull depth in the channel.

CONTENTS

LIST OF SYMBOLS

A	Area term.
Ac	Cross sectional area of main channel
Af	Cross sectional area of flood plain
At	Cross sectional area of total channel
B	Width term
Bc	Main channel width
Bf	Flood plain width
Bt	Total channel width
b	subscript denotes bankfull
C	Function describing geometrical parameters
c	subscript denotes main channel
D	Depth of flow in channel
d	Depth of flow in flood plain
F	Function describing geometrical parameters
F1	" " " " " " " "
F2	" " " " " " " "
F3	" " " " " " " "
f	subscript denotes flood plain
fp	subscript denotes flood plain
g	Gravitational constant
h	Bankfull depth
k	kinetic energy term
ℓ	Mixing length term
n	Mannings coefficient of friction
n_c	Mannings n for the channel
n_f	Mannings n for the flood plain
P	Dynamic pressure head

p_o	Static pressure head
Pc	Wetted Perimeter (2*Yc+Bc)
Pc'	Wetted Perimeter (Yc+h+Bc)
Pf	Wetted Perimeter (2*Yf+Bf)
Pf'	Wetted Perimeter (Yf+Bf)
R	Hydraulic radius of section
Rc	Hydraulic radius of channel
Rc'	Hydraulic radius of channel during interaction
Rf	Hydraulic radius of flood plain section
Rf'	Hydraulic radius of flood plain during interaction
Re	Reynolds Number
S	Longitudinal slope of channel
Sa	Apparent shear force
T	Length term
t	subscript denotes total channel parameter
U	Velocity component
u	Mean velocity component
u'	Fluctuating velocity component
U*	Shear velocity
V	Velocity term
Vb	Bankfull velocity
V_c'	Mean velocity in channel
V_f'	Mean velocity in flood plain
V	Mean velocity in total cross section
$\bar{v}$	Mean velocity term
v'	Fluctuating velocity component
W	Width term

W	Directional velocity component
$\overline{W}$	Mean velocity component
w'	Flucuating velocity component
x	Distance from channel entrance
x^*	Term introduced in Patel's relationship
Y	Depth term
y*	Term introduced in Patel's relationship
z	Length term across the channel/flood plain
α	Energy correction coefficient
α_1	Term used to describe slope of relationships
β	Momentum correction coefficient
γ	Term to describe velocity gradient
ε	Eddy viscosity
μ	Viscosity term
ν	Kinematic viscosity
ρ	Density of water
τ	denotes shear stress
τ_a	Apparent shear stress
ψ	Linearisation term
'	Denotes a parameter during interaction

CHAPTER ONE

GENERAL BACKGROUND

Table of Contents

1.1 Background.

Water is perhaps the most fundamental and necessary resource available to mankind. It arrives on land in the form of precipitation and returns to the sea by means of river channels. For the most part, river channels adequately convey the water back to the sea but occasionally, under conditions of high rainfall and large flow rates, the river channel may overtop its banks and flow onto the flood plain with possible danger to life and property. This process of overspilling onto adjacent land area is known as river flooding and the nature, extent and frequency of such flooding is described briefly in Section 1.2.

The river flood plain itself has always been an attractive area for human settlement. Fertile land, a good water supply, transport and fishing have been major factors governing the steady encroachment of man onto the flood plain. When overbank flow does occur, danger to life and property is a distinct possibility and steps are frequently required to minimise such risks. This is termed FLOOD CONTROL and is discussed briefly in Section 1.3.

The hydraulic behaviour of overbank flow situations is complicated and various hydraulic mechanisms are introduced during overbank flow. Initially the point of inundation of the flood plain may be characterised by a lateral flow in a similar manner to a side weir. Furthermore, overbank flow is more likely to occur in regions of sinuous meanders where the flow patterns exhibit a higher order of complexity. This may

be characterised for instance, with overbank flow re-entering the river at a point further along the meander and certainly usually produces non-uniform flood plain widths, and strongly three dimensional flow patterns. On top of this, overbank flooding often occurs during rapidly changing unsteady flow conditions with the effective slope of the water surface profile producing a hysteresis effect on the stage-discharge relationship.

One particular mechanism which forms the subject of this thesis involves a turbulent interaction between the faster moving river channel flow and and the slower moving flood plain flow. The turbulent interaction causes an extra resistance to flow in the main river channel, rather like the head losses associated with a sudden expansion. The effect of the turbulent interaction mechanism between the channel and the flood plain, in particular, the effects of the interaction on velocity distributions throughout the channel and flood plain cross sections, the boundary shear stress distribution and stage-discharge relationships during overbank flow are investigated. A brief description of the turbulent interaction problem is given in Section 1.4.

1.2 Nature of River Floods.

It is perhaps appropriate at an early stage to attempt a definition for a river flood. Ven Te Chow (Ref 11) suggested that " a flood is a relatively high flow which overtaxes the natural channel provided for the runoff". Ward (Ref 68) suggested the definition " A flood is a body of water

which rises to overflow land which is not normally submerged." So essentially a river flood is a high volume of flow which can no longer be contained within the channel banks.

The primary function of any river is to convey water from its associated catchment area to the sea as part of the hydrological cycle. As time passes, the river will form an equilibrium with the surrounding topography, depending on the discharge which is normally transported through the river. Occasionally however, due to unusual hydrologic conditions, excess water will be passed down the river channel which can no longer contain the flood. Under these conditions, the river will overtop its banks and spill onto the adjacent land known as the flood plain. The flood plain tends to be low flat land which can extend anything from a few metres to tens of kilometres away from the river.

The causes of flooding vary, but by far the most common is excessive rainfall either for a very short time or over prolonged periods. Flash floods experienced in the summer months can cause problems due to their extreme intensity. A noteable example is the Lynmouth flood which occurred on 15th August 1953. Over 24 hours an average of 143 mm of rain fell over the catchment with some areas experiencing 228mm of rainfall. Thirty four people were killed and excessive damage was caused to property. River flooding is most frequent during the spring months with prolonged periods of rain combining with the snow melt in the higher reaches of the river.

A further cause of flooding is the combination of

high rainfall with the occurrence of high tides and storm surges in the lower reaches of large rivers. A noteable example of this type of flood must be the Thames estuary where the construction of a barrier has been necessary to prevent the possible flooding of the inner London area. Less frequent causes of flooding might include seismic activity or the possibility of dam failures.

The extent of overbank flooding onto river flood plains is governed not only by the factors outlined above, but by a range of topographical and other physical features which exist in the river valley. The permeability of the catchment geology will effect the amount of ground water flow. The degree of saturation before a storm can influence the response of a river to a storm. The slope of the river basin will effect the rate of runoff from the land. Such factors play a major role in influencing the flood as it passes down the river reach. The hydraulic characteristics of the river channel itself to some extent control the amount of flooding which will occur from a given storm. The roughness of the channel bed affords increased resistance to channel flow resulting in increased flooding. The extent of meandering which occurs in the river will effect the rate of flow down the channel. This factor is perhaps the most important as evidenced by the fact that most overbank flow problems occur in the lower reaches of the river course.

It can be seen therefore that a variety of factors influence the extent and frequency of flooding in a natural river.

1.3 Flood Control.

The problem of developing satisfactory methods of flood control has arisen because man has chosen to occupy the flood plain because of its attractive features. Therefore much effort has gone into developing methods of preventing rivers from inundating their occupied flood plains. The most effective flood control measures are best carried out in the light of extensive knowledge regarding the character and behaviour of a flood wave. The response of a particular river to a given storm must be established before any efficient form of flood control can be deployed. The frequency of flood waves of different sizes must also be determined, often requiring historical data. The need to classify storms and their frequency has led to the development of the concept of the "Return Period" of a flood. This is defined as the period of time between two events which equal or exceed a given flood level. Thus a flood with a return period of one hundred years can be expected to occur statistically once every one hundred years.

The design flood from which a potential flood plain zone is to be protected, is determined by the economic costs of protection. If a high degree of flood control is necessary, say in an urban area, then the design flood must have a greater return period. Usually a compromise or "optimum" is reached between the costs of flood damage and the capital costs incurred in constructing flood control works.

Very little can be done in the short term to prevent damage to properties from flooding, therefore attention

must be given by the engineer to the options available in the design of long term flood control systems. The three main methods of longer term flood control are as follows :

(a) <u>The construction of flood walls and/or levées to contain the flood flow within a reduced flood plain.</u>

Essentially a levée is an earth dyke constructed from material taken from a nearby borrow pit. Since most rivers meander within the flood plain, and the extent of meandering varies with time due to erosion and deposition, the levées or flood walls are usually constructed a suitable distance away from the river, outside the limits of river meandering. Also, the retaining wall or levée must satisfy similar safety criteria employed in the design of small dams. The main disadvantage of levées or flood walls is that although the flooding problems are alleviated at the flood control area, the problems of flooding downstream are increased. This is because the flood wave takes a shorter time to pass through the flood control zone and therefore increases the discharge passing down the river in the lower reaches. An example of the effect of the constrictions caused by flood retention was presented by Belt (Ref 5) when he reported that a 200 year flood on the Mississippi became a 30 year flood after the extensive use of flood walls. This increase in water levels was attributed to the man made levées and navigation works which have reduced the cross sectional flow area of the river.

(b) The increase of the storage capacity on the river and flood plains and the possible diversion of flow from the river. Perhaps the simplest example of this method of flood control is the construction of a regulating reservoir in the catchment river upstream of the flood protected zone. Normally the level of water in the reservoir upstream of the dam is maintained at a depth which would enable the reservoir to act as a storage basin during times of extremely high rainfall. Occasionally due to the flat topography of the catchment, it is not always possible to construct a regulating reservoir and on such occasions the construction of a smaller detention basin adjacent to the flood plain, upstream of the flood protected area is a feasible alternative. Such detention basins are constructed at such an elevation as to allow flow into the basin as extreme flooding occurs. An example of the design of a detention basin is given by Mosonyi (Ref 33). As the water level rises, the peak of the flood wave is diverted to the detention basin, and later on, as the flood diminishes, the excess volume is released back into the river. Sometimes the flood plain can be improved to act more efficiently as a storage basin and thus attenuating the flood peak by storage.

(c) Improvement of the carrying capacity of a channel and its flood plains. The discharge capacity of a river can be improved by the use of the following techniques.

(i) Reduction of the bed roughness of the river

channel or flood plain.

(ii) An enlargement of the river cross section by deepening or widening the channel.

(iii) Shortening the river by eliminating or by-passing severe meanders.

The difficulty in adopting river training techniques is that the modification to the river results in an imbalance in the river system regarding the sedimental bed load and storage capacity of the river. The balance is redressed naturally by the increased removal of sediment from the upper reach into or through the protected area. Any river protected in this way may need occasional or even continuous dredging of the bed.

Often a flood protected zone will have adopted a number of the methods described, depending on the suitability and cost of deployment of such methods.

1.4 Hydraulic Behaviour of Overbank Flow.

It has been indicated previously that before any system of flood control can be introduced into a particular flood risk zone, a detailed knowledge of the flow behaviour and a historical appreciation of the flood frequencies should be understood. Since overbank flow is caused by the passage of a large flood wave through the river section, the analysis of the hydraulic mechanisms involved is further complicated by the unsteady nature of the flow.

During inundation of the flood plain, it is

possible to consider the channel banks acting as a broad crested weir with the depth of flow over these banks giving an estimate of the overspill on to the flood plain which is behaving like a storage basin. Mathematical models often consider the problem in this way. It is debatable at this stage whether the flood plain acts merely as a storage basin or whether it also contributes to the overall discharge of the channel. If considered as a separate contributing channel, then the roughness coefficient for the flood plain should be selected to allow for the increased bed roughness afforded from the growth of vegetation and hedges and the compound discharge obtained by the addition of the total channel and flood plain discharges separately. The storage or floodway capacities of a river can be better understood by an appreciation of the topographical conditions which exist in the river reach. A further contributing factor to the amount of water transferred onto the flood plain is the convection of flow by the natural meandering of the river. As the flow in a river approaches a bend, the inertial forces which exist in the flow cause the flow to maintain its direction thus transferring flow onto the flood plain. Secondary currents can also encourage flow onto the flood plain in this way and to consider this type of flow in terms of mathematical modelling is very difficult since it involves two dimensional or even three dimensional modelling of the flow. Most models to date involve the introduction of an empirical term into the one dimensional Saint - Venant equations, which may include factors relating to the meander of the channel within the flood plain.

Another factor which influences the carrying capacity of a river during overbank flow is the subject of this thesis. During times of high flood, the flow in the channel is much greater than the flow in the flood plain. The difference in velocity between the faster moving water in the channel and the slower moving water in the flood plain leads to the development of a turbulent shear zone at the channel/flood plain junction. Prandtl showed that in turbulent flow, the turbulent shear stress at any point is proportional to the velocity gradient:

$$\tau = \rho k^2 \ell^2 \left(\frac{dV}{dy}\right)^2 \qquad (1.1)$$

Similarly, because of the existence of a velocity gradient (in plan) across the width of channel and flood plain, it follows that a turbulent shear stress will exist at the channel/flood plain boundary.

The work presented in this thesis establishes the existence of this turbulent interaction mechanism and investigates a range of parameters which effect it. This work investigates in particular the effect of a range of channel and flood plain widths, the bankfull depth, the longitudinal bed slope and a range of velocity conditions on the degree of interaction between channel and flood plain. It should be pointed out that the variation in channel and flood plain roughness was not investigated although this is an important aspect. Attempts are also made to produce semi-empirical relationships for this process to cover the range of parameters

tested.

It must be remembered that this work is a laboratory investigation and therefore the idealised conditions of a smooth straight channel with one flood plain have been chosen. The channel flow operated with steady uniform flow at all times. It is necessary, at this time, to point out that such idealised conditions will never exist in the field. The channel and flood plain boundaries are likely to vary in size and shape, the boundary roughness is sure to vary significantly. It will be unlikely that the river will achieve steady state flow due to the unsteady nature of the flood wave passing through the river, and the effect of possible meanders with a three dimensional flow configuration is also ignored.

Very little data is available to demonstrate the turbulent shear mechanism in the field, but until such information is available, it is hoped that the work presented in this thesis will improve our current understanding of the interaction which exists between a channel and its flood plain.

The ultimate aim of the work therefore, is to obtain a clearer understanding of the processes involved in overbank flow, and to apply the results to more accurate predictions of the stage-discharge relationship, the distribution of boundary shear stresses and the likely effects on sediment transport, and also to provide raw data and more accurate empirical constants for use in mathematical models based on the Saint-Venant Equations as well as the new breed of turbulence models being developed in Germany.

CHAPTER TWO

PREVIOUS INVESTIGATIONS

Table of Contents

2.1 Introduction.

An attempt has been made in this chapter to draw together various aspects of past research in hydraulic engineering concerning the behaviour of rivers and channels during overbank flow. Prior to the early Sixties, very little was known of the complex flow patterns which exist between a channel and its associated flood plains, but more recent developments have led to a clearer understanding of the hydraulic mechanisms involved, at least at the level of model studies.

There appear to be three major reasons why consideration should be given to the hydraulic behaviour of channels with flood plain flow.

(a) A knowledge of the nature of rating curves, or stage-discharge relationships, during overbank flow would lead to more accurate and reliable discharge predictions during flooding, and would also provide more accurate data for the design of flood embankments and levées.

(b) The boundary shear distribution around the perimeter of the channel and flood plain is altered considerably by channel/flood plain interaction as will be discovered later in this chapter. This nonuniformity of boundary shear stress is likely to have important implications with regard to the erosion and sedimentation processes of a river and its flood plain.

(c) An understanding of the complex flow behaviour between a

channel and its flood plain will enable the development of more accurate unsteady flow equations in mathematical models. Such models are used to predict the stage and discharge in relation to distance and time in river channels and a neglection of the channel/flood plain interaction mechanism may result in erroneous predictions.

The three main areas outlined above are considered separately in this literature review although it should be pointed out that many of the papers discussed overlap into two or three of these areas. A further short section is also included concerning the resistance to flow and friction factors for channel flow when no overbank flow is occurring, with all the discharge confined to the main channel.

2.2 Rating Curves and Velocity Profiles.

The first recorded investigation into the problem of channel/flood plain interaction was by the Russian engineer Georgi Vasilyevich Zheleznyakov (Ref 74). In an innovative study he carried out tests in a 5.2 metre wide flume. Parabolic shaped main channels, 0.45 m and 0.6 m wide, with flood plains on either side, were used to exhibit the interaction mechanism between the channel and flood plain. Discharges in the channel varied between 6.9 litres/sec and 51.4 litres/sec and bed slopes ranging from 1/1000 to 1/2000 were tested. The results of one of his experiments are indicated on Fig 2.1 demonstrating quite clearly the effect of appreciable turbulent mixing between the

flow in the deep main channel and the flow in the shallow flood plain, and the considerable reduction in main channel velocity during the interaction. Zheleznyakov observed the formation of turbulent eddies and large scale vorticies with vertical axes at the channel/flood plain junction, and also noted that the interaction mechanism or "Kinematic Effect" was characterised by a reduction in main channel velocities and an increase in flood plain velocities close to the main channel.

Zheleznyakov recognised that the energy structure of the flow was significantly altered and proposed the following energy balance equation:

$$\Delta E_c = \Delta E_f + \Delta E_e \qquad (2.1)$$

where ΔE_c represents the difference in kinetic energy between the isolated and interacting flows in the main channel, ΔE_f represents the kinetic energy added to the flood plain flow from the main channel and ΔE_e represents the amount of energy spent on the formation of eddies and vorticies in the mixing region. In other words, the amount of energy transferred to the flood plain is less than the energy leaving the main channel. The energy Equation is difficult to apply in this situation since the energy loss in the turbulent vorticies at the channel/flood plain junction is unknown, or at least difficult to quantify.

Zheleznyakov also presented field test results (Ref 75) as shown in Fig 2.2. Again he observed significant

reductions in channels velocities at low flood plain depths during overbank flow due to the interaction effect. A definite scaling relationship between the models and full scale rivers for the interaction effect was not presented.

In a subsequent paper (Ref 76), Zheleznyakov identified three stages of interacting flow:

$$\frac{dV_c}{dY_f} < 0 \quad \left\{ \text{Channel velocity is decreasing with increasing flood plain depths} \right.$$

$$\frac{dV_c}{dY_f} = 0 \quad \left\{ \text{Channel velocity is reduced to a minimum.} \right.$$

$$\frac{dV_c}{dY_f} > 0 \quad \left\{ \text{Channel velocity is increasing with increasing flood plain depths.} \right.$$

In other words, the effect of the interaction increases to a maximum at low flood plain depths and decreases with subsequent increases in flood plain depths. This appears to be in agreement with Myers work (Ref 34, Ref 35, Ref 36), which will be discussed later in the chapter, and argues essentially that the total shear force due to the interaction which apparently retards the main channel flow and assists the flood plain flow, is maximised at a particular flood plain depth. Zheleznyakov stated that the value of the relative depth, Yc/Yf (where Yc is the channel depth and Yf is the flood plain depth)

at which the reduction in channel velocity was a maximum, increased with Bc/Bf, where Bc is the channel width and Bf is the flood plain width. He also found that the discharge reduction in the main channel increased with increasing Bf/Bc as can be seen in Fig 2.3.

Thus Zheleznyakov found that the channel/flood plain interaction plays a significant role in the estimation of discharge, velocity and resistance to flow, especially at low flood plain depths. For a relative depth Yf/Yc =0.15 for instance, the channel discharge could be reduced by as much as 32% compared with the bankfull discharge. Also tests carried out in the field suggested that the discharge could be reduced by 15%-30% relative to the bankfull discharge. Zheleznyakov attempted to quantify the reduction in discharge due to the channel/flood plain interaction and suggested the following relationship:

$$Q = K_c Q_c + K_f Q_f \qquad (2.2)$$

where Qc and Qf are the discharges in the channel and flood plain respectively, under isolated or non-interacting conditions Kc and Kf are coefficients for the channel and flood plain respectively, where Kc was found to vary between 0.6 and 1.05 and Kf was found to vary between 1.0 and 1.2. Other experimenters (Ref 2) have found K_c to vary between 0.73 and 0.99, and K_f to vary between 1.01 and 1.3.

Zheleznyakov furthered his work with Novakova (Ref 77) by investigating the influence of the interaction effect on an erodible channel model. Three series of experiments were carried out, the first series in a flume 23 metres long and 3.88 metres wide, and the second and third series in a flume 14.3 metres long and 0.98 metres wide. In each series of tests the relative roughness of the channel was varied. In Series One tests, the channel was significantly rougher than the flood plain, while in Series Two tests, the channel and flood plain had boundaries of equal roughness. Finally, in Series Three tests, the flood plain boundary was rougher than the channel boundary. Results from series one tests indicated little interaction between the channel and flood plain and in some cases suggested an increase in the main channel velocity at low flood plain depths. This would suggest an energy and momentum transfer from the flood plain to the main channel. The results of series one and two tests are shown in Fig 2.4 indicating the importance of the relative roughnesses of the channel and flood plain. Generally, the flood plain will be rougher than the main channel in the field due to vegatation growth. The friction coefficients for the channel and flood plain allow the estimation of the mean velocities in the channel and flood plain under isolated conditions. As Zheleznyakov correctly observed, the difference in channel and flood plain mean velocities significantly influences the magnitude of the channel/flood plain interaction.

Zheleznyakov also observed a certain amount of

hysteresis in the stage-discharge curves produced from experiments. The interaction effect significantly reformed the channel cross section by transferring sand from the flood plain to the channel bed. The channel bed then rose, reducing the relative depth Yf/Yc until the overall channel stabilized. This is one possible explanation of the hysteresis effect, although it should be pointed out that Sellin (Ref 54, Ref 55) found the same effect on a channel with a rigid boundary. Therefore the effect is much more likely to be a function of the slope of the water surface profile as in river rating curves.

Work carried out by Agasieva and Barikyan (Ref 2) confirmed Zheleznyakov's results. Their tests were carried out in two separate channels, with main channel widths of 1.21 metres and 2.10 metres and a range of flood plain widths. Their results were found to be in general agreement with Zheleznyakov's experiments and the following equations were suggested for the modified Chezy coefficient for channel/flood plain interaction:

$$Cr = C\left(1 - \frac{1{\cdot}15}{1+Y_c/Y_f}\right) \quad \text{for } Y_c/Y_f \geqslant 1{\cdot}8 \qquad (2.3)$$

$$Cr = C\left(0{\cdot}45 + \frac{0{\cdot}45}{1+Y_c/Y_f}\right) \quad \text{for } Y_c/Y_f \leqslant 1{\cdot}8 \qquad (2.4)$$

where C is Chezy's coefficient calculated from Pavlovski's formula $C=\frac{R^y}{n}$ and Cr is the modified Chezy's coefficient applied to the overall channel/flood plain cross section. Details of the Pavlovski formula is given in a short section at

the end of this chapter.

In 1962, Spitsin (Ref 57) carried out research into the behaviour of a trapezoidal channel with a channel bed width of 1.66 metres during overbank flow. To compare the flow in the main channel under interacting and isolated conditions, he inserted a glass wall at the channel/flood plain junction. Again Spitsin's results were in broad agreement with the findings of previous investigations. Since he was able to calculate the energy existing in the channel and flood plain under isolated and interacting conditions, he proposed the following equations in an attempt to quantify the changes in energy in both the flood plain and channel after the restructuring of the flow:

$$\Delta E_c = -\frac{\alpha \rho A_c}{2}\left(\overline{V_c}^3 - \overline{V_c'}^3\right) \qquad (2.5)$$

$$\Delta E_f = \frac{\alpha \rho A_f}{2}\left(\overline{V_f}^3 - \overline{V_f}^3\right) \qquad (2.6)$$

where ΔEc and ΔEf are changes in energy in the channel and flood plain due to the interaction mechanism, Vc and Vf are the mean channel and flood plain velocities under non-interacting conditions V_c' and V_f' are the mean channel and flood plain velocities under interacting conditions and Ac and Af are the corresponding cross sectional areas of the channel and flood plain. α is the energy correction coefficient which allows for the non-uniform distribution of velocity throughout the cross section. Spitsin found that the amount of energy transmitted to

the flood plain from the channel was never greater than 25% of the total energy lost from the main channel, suggesting that at least 75% of the energy lost from the main channel was dissipated in the formation of eddies and vorticies in the turbulent shear layer at the channel/flood plain interface. At this stage it became apparent that the conservation of momentum across the channel/flood plain section might be a preferable analytical technique in view of the large unknown energy loss during interaction.

In 1960, Sellin (Ref 54, Ref 55) commenced similar work at the University of Bristol. His investigations were carried out in a 6.1 metres long, 0.457 metres wide flume with symmetrical flood plains constructed from fibre glass. The resulting bankfull depth was 0.0445 m. Initial tests indicated depressions on the water surface caused by large scale vortices transporting momentum from regions of high velocity to regions of slower flow on the flood plain. Sellin attempted to quantify the extent of these vorticies by using two similar photographic techniques. Initially he made use of the Schlieren optical system which involves photographing reflections of light off the water surface. The intensity of the illumination gives an indication of the slope of the water surface at that particular point. Thus the Schlieren principle can be used as a method of photographing the depressions on the water surface, generated by the vorticity mechanism.

A more conventional photographic method was also

adopted using fine aluminium powder sprinkled on the water surface. A 35 mm camera was mounted on an instrument carriage which could be driven along the flume in the direction of flow at any desired velocity. With a given exposure time the vorticies could clearly be identified. Sellin was therefore able to measure the pitch between the large scale vorticies and found statistically, that the average pitch was about twice the channel width. It cannot be presumed that the same pitch length will apply to other geometries since Sellin maintained the same channel width throughout his work.

Sellin proceeded to measure point velocities throughout the channel cross-section using a Pitot tube and recorded cross sectional traverses at four different stations along the length of the channel and finally averaged these results to give a mean velocity contour profile. This procedure was repeated for flow under isolated or non-interacting conditions and the results are shown in Fig 2.5. Each contour represents the local velocity divided by the mean channel velocity and it was noted by Sellin that during interacting conditions, the maximum velocity filament was depressed below the water surface and away from the interacting regions. Another effect of the interaction mechanism was the reduction of velocities in the main channel , especially near the channel/flood plain junction. This would be in general agreement with Zheleznyakov's findings.

Sellin recognised the need to establish a relationship between stage and discharge for channels during overbank flow.

Some of his results are shown on Fig 2.6 represented by curve 1 for the full cross-sectional area. As soon as the flood plain is inundated, a distinct change in the relationship between the stage and discharge occurs as shown by curve 1. It is interesting to note that curve 2, the stage/discharge relationship for the isolated channel, has a different slope from the relationship of stage and discharge below bankfull depth. Since walls of similar roughness were inserted at the channel banks to contain the flow, there should be no significant change in the slope of the stage/discharge curve. No satisfactory reason was given for this phenomenon but the possibility exists that Sellin may have been operating unintentionally with a 'draw down' water surface profile at depths greater than bankfull level. This is also reflected in the low values of Manning's "n" obtained at relatively small Reynolds numbers. If the stage/discharge relationship on curve 2 gives overestimated discharges for a given depth above bankfull level, then it follows that curve 4 also gives overestimated discharges for a given flood plain depth. This is evident since the full section discharge should, at high relative depths, exceed the discharge predicted by curve 4, the summation of the discharges of the channel and flood plain under isolated conditions. It is likely that the full cross-section begins to behave like a single channel at high relative depths, whereas the insertion of a wall between the channel and flood plain gives added resistance to flow at high flood plain depths. In Fig 2.6, at no point does

curve 1 ever seem likely to exceed curve 4 and if anything, both curves are diverging.

The introduction of permeable flood walls on the channel bank was found by Sellin to have interesting effects on the discharge capacity of the model at low flood plain depths. Sellin intended to restrict the formation of vorticies but at the same time allowing cross channel flow to occur. Two types of flood wall were adopted.

(a) 6 mm round dowels at pitches of 25 mm and 50 mm.

(b) Thin aluminium sheets with 6 mm vertical slots at 12 mm intervals.

Fig 2.7(a) shows the effect of each flood wall arrangement on the stage/discharge relationship indicating, for the dowel design, the greater the pitch the less drag exerted on the flow. At low flood plain depths the use of the Aluminium sheet as the flood wall resulted in a slightly increased carrying capacity of the channel. Sellin roughened the bed of the flood plain as it was thought that the interacting problem was heightened by a lower velocity on the flood plain and the flood wall strip used on the previous tests would be more beneficial for the roughened flood plain case. Fig 2.7(b) shows that this was indeed the case. At channel depths greater than 56 mm, the wall imposed a greater resistance to flow.

In summary, Sellin observed the formation of large scale vorticies and was successful in photographing them. He proceeded to show the effect of the channel/flood plain

interaction mechanism on the stage/discharge curve, identifying a reduction in discharge at depths just above bankfull depth. In an attempt to minimise turbulent eddies at the channel/flood plain junction, he introduced various flood walls resulting in rating curve relationships.

In 1967, Townsend (Ref 63, Ref 64) carried out an experimental investigation using a 9 - 10 metre long perspex flume of width 0.61 metres. An asymmetrical cross section with a channel flanked by only one flood plain was chosen in an attempt to eliminate any compensating effects a symmetrical channel might have on the behaviour of the flow during overbank flow. The main channel was 0.254 metres wide and the flood plain was 0.356 metres wide. His work involved the measurement of turbulence intensities in the longitudinal and transverse directions, and the results of his work are discussed in Section 2.3. However he did augment Sellins work by taking velocity traverses during isolated and interacting flow conditions. The results of two of his tests are shown on Fig 2.8 and illustrate a distinct lateral distortion of the maximum velocity filament away from the interaction region.

In his paper in 1967, Posey (Ref 42) highlighted the problems associated with the use of the hydraulic radius in estimating discharges in rivers with overbank flow. The hydraulic radius is defined as the cross-sectional area of a channel divided by its wetted perimeter. As a flood inundates the flood plain, there is a sudden increase in the wetted

perimeter with only a small increase in the total channel cross-sectional area. This implies that at just above bankfull level, the hydraulic radius, as commonly calculated, is suddenly reduced and if conventional relationships are used to estimate discharge (such as Chezy or Manning) then the predicted discharge will also be reduced, since the discharge is a function of the hydraulic radius. Since the actual discharge is not reduced, better methods of estimating the discharge in compound channels are required. Posey has outlined four possible methods which might be used in situations described above:-

(i) Consider the whole cross-sectional area of the compound channel and divide it by the total wetted perimeter. As previously mentioned, this method underestimates the discharge at low flood plain depths.

(ii) Divide the channel and flood plains by imaginary walls at the channel/flood plain junction and compute the discharge for each section including the vertical imaginary walls for the calculation of the hydraulic radius for each section. The disadvantage of this method is that no allowance is made for the turbulent shear interaction and momentum transfer which occurs across each division line. Neglection of this channel/flood plain interaction will lead to overestimation of discharges at low flood plain depths.

(iii) Method (iii) is similar to method two except that the imaginary walls are exduded in the calculations of the

hydraulic radius for each section.

(iv) Method (iv) is perhaps the most complicated approach and involves the introduction of imaginary walls inclined towards the centre of the channel from the channel bank. The hydraulic radius is then weighted by considering the area of the section it represents, against the total cross-sectional area.

Posey found that method (ii) was the most accurate method at low flood plain depths, whereas at greater depths, method (i) became more accurate. However, Posey neglected the interactive turbulent shear mechanism, and none of the four methods satisfactorily predicted the discharge at low flood plain depths.

In 1967, Toebes and Sooky (Ref 61, Ref 62) investigated the effects of overbank flow on meandering channels in a flume 73.15 metres long and 1.18 metres wide. Their experiments consisted of the measurement of velocity distributions, free surface elevations and streamline patterns. They suggested a method of analysing overbank flow conditions by dividing the channel into two sections by a horizontal line from one channel bank to the other. Considering the Darcy-Weisbach Equation for open channel flow:-

$$Q = A\left(\frac{8gRS}{f}\right)^{1/2} \qquad (2.7)$$

Toebes and Sooky proposed the following Equation for overbank flow:-

$$Q_{total} = A_1\left[\frac{8gA_1S}{(P_1-b+T)f_1}\right]^{1/2} + A_2\left[\frac{8gA_3S}{(P_3+T)f_3}\right]^{1/2} \qquad (2.8)$$

where A_2 is the area of the channel and flood plain above the horizontal division line, A_1 and A_3 are the cross-sectional areas of the channel section (of width b) below the horizontal line for straight and meandering channels respectively, S is the bed slope, P_1 and P_3 are the corresponding wetted perimeters and f_1 and f_3 are the friction factors. Recognising that there would be some fluid transfer between the channel and flood plain sections, the subsequent energy losses could be taken into account by introducing a solid boundary of equivalent length T into the above equation. Toebes and Sooky found T to be a function of the bed slope, bankfull depth, roughness and relative widths of the channel and flood plain. Their work on meandering channels with flood plains also suggested, that as the mean velocities decreased, the interaction losses increased and by varying the overbank depth the intensity of the interaction could be maximised. It should be remembered that the experiments carried out by Toebes and Sooky involved a meandering channel contained within a flood plain thus making comparison with other investigators somewhat difficult. Their results, however are in general agreement with previous investigations.

In 1973, Yen and Overton (Ref 72, Ref 73) recognised

the inadequacies of the methods proposed for discharge estimation in rivers with overbank flow. They proposed a method which involved the selection of division lines across which, the net momentum transfer was zero. These lines would therefore be excluded in the calculation of the hydraulic radius since by definition, no shear stress exists on division lines through which no momentum is transferred. From experimental data obtained from Udeozo's work (Ref 66), velocity contours were drawn and, by drawing a straight line from the corner of the channel/flood plain boundary, perpendicular to the isovels, division lines could be determined. The angle of inclination of these division lines θ, was seen to vary approximately uniformly for varying channel depths as shown on Fig 2.9. The relative widths of the channel and flood plain also influenced θ and the relationship between Y/b, B/b, and θ is shown on Fig 2.9. Yen and Overton reported that their method was more satisfactory for discharge assessment than any other proposed method and consists of estimating θ from Fig 2.9, from which division lines are drawn on the cross-section of the channel and the discharge is computed for the different sections and summed. Unfortunately the bankfull depth d, was not included as a parameter having an effect on the angle θ.

In 1977, James and Brown (Ref 27) carried out an extensive study into the nature of the turbulent shear interaction between a channel and its flood plain. Their experiments were carried out in a flume 26.82 metres long,

1.52 metres wide and 0.457 metres deep. Tests were carried out on asymmetric and symmetric cross sections of varying channel and flood plain widths. Since the main channel was trapezoidal in shape, there was a less rapid change in the depth of flow across the channel. However the investigators did note some interaction between the channel and flood plain and suggested an empirical adjustment to the Manning resistance Equation applied to the total cross section. Fig 2.10 shows the results of their work. They suggested that the flood plain/channel width ratio, Bf/Bc, and Yc/h (the channel depth divided by the bankfull depth) influenced the extent and degree of the interaction, with the existence of one or two flood plains being of little importance.

They introduced a factor $1/\phi = n/n_b$ where n is the equivalent Manning's n value at any depth above bankfull level and n_b is the Manning's n when the flow is at bankfull depth. From curve fitting techniques, Brown and James found that ϕ could be found from the relationship:-

$$1/\phi = \frac{n}{n_b} = a\alpha^{-b} \qquad (2.9)$$

where α represents the the aspect ratio $((Wf_1 + Wf_2)/Wch)$, the ratio of the total flood plain width to the channel width, and a and b can be determined from Fig 2.10. ϕ can then be applied to a modified Manning's equation:-

$$Q = \phi \frac{A_T R^{2/3} S^{1/2}}{n} \qquad (2.10)$$

where A_T is the total cross sectional area and R is the hydraulic radius based on the single channel method and S is the channel slope. One difficulty of the method above is that the results are based on tests carried out on a channel with inclined side walls which may have the effect of dispersing the interaction over a wider region, altering the hydraulic characteristics of the turbulent shear mechanism.

The energy principle which is frequently used in the analysis of open channel flows has been modified by Blalock and Sturm (Ref 7) for problems involving overbank flow. The specific energy for an open channel is given by:-

$$E = y + \frac{\alpha Q^2}{2gA^2} \qquad (2.11)$$

where y is the depth of flow in the channel, Q is the total discharge, A is the total cross sectional area of the channel, $\alpha = \frac{\sum V^3 dA}{\bar{V}^3 A}$ as given by Chow (Ref 10) is introduced to allow for the nonuniform distribution of flow throughout the channel cross-section, V is the velocity of an element of flow of area dA and $\bar{V}$ is the mean velocity of the total flow. Differentiation of Equation (2.11) assuming that α is independent of channel depth, leads to :-

$$\frac{dE}{dy} = 1 - \frac{\alpha Q^2}{g A^3} \frac{dA}{dy} \qquad (2.12)$$

where $\frac{dA}{dy} = T$, the top width of the water surface. One method of calculating the minimum specific energy of the flow is to assume that α is unity. Then the Froude number is given by :-

$$Fr = \left(\frac{Q^2 T}{g A^3} \right)^{1/2} \qquad (2.13)$$

For a compound channel, α should be included in the Froude number to account for the variation of local velocities across the whole channel and the Froude number can thus be given as:-

$$Fr = \left(\frac{\alpha Q^2 T}{g A^3} \right)^{1/2} \qquad (2.14)$$

Blalock and Sturm suggest that α varies with depth of flow and therefore differentiation of Equation (2.11) yields :-

$$\frac{dE}{dy} = 1 - \frac{\alpha Q^2}{g A^3} \frac{dA}{dy} + \frac{Q^2}{2g A^2} \frac{d\alpha}{dy} \qquad (2.15)$$

yielding a Froude number of:-

$$Fr = \left(\frac{\alpha Q^2 T}{g A^3} - \frac{Q^2}{2gA^2} \frac{d\alpha}{dy} \right) \qquad (2.16)$$

Blalock and Sturm carried out experiments in a tilting steel flume 24.38 metres long, 1.07 m wide and 0.46 metres deep. The single flood plain was 0.77 m wide and the channel width was

0.3 metres. The bankfull depth was set at 0.16 metres. These experiments were used to establish the accuracy of equations (2.13), (2.14), (2.15) and (2.16) in predicting the minimum specific energy. It was found that Equation (2.16) agreed best with experimental results and suggested that two critical depths (depths at which the minimum specific energy occurs) could exist; one below bankfull and one above. The concept of two critical depths is very relevant to open channel flow calculations since the principle of minimum specific energy is used to estimate flow depths over control sections such as weirs, sluice gates, etc.

Investigative work into the problem of channel/flood plain interaction has invariably taken the form of experimental model studies. Very few full scale test results are available due to the difficulties in obtaining stage/discharge data during overbank flow. However, Bhowmik and Demissie (Ref 6) in 1982 presented data from two rivers in the United States and Fig 2.11 shows the rating curves obtained from these two rivers. It can be seen that, for both rivers there is a significant reduction in the main channel velocity during overbank flow. These observations are in broad agreement with the findings from models in the laboratory, but little can be said about scale effects at this stage, except that the interaction plays an important role in both full scale rivers and models, and to neglect this phenomenon in discharge estimation is likely to lead to inaccurate stage-discharge relationships.

A recently updated British Standard, BS3680:Part 3C (Ref 9) contains a method proposed by Zheleznyakov for the estimation of discharge in rivers during overbank flow. It involves the use of a modified Chezy's coefficient in Chezy's equation:-

$$Q = C A\sqrt{RS} \qquad (2.17)$$

where
$$C = \frac{R^{1/y}}{n} \qquad (2.18)$$

and
$$y = \frac{1}{\log R}\left[\left(\frac{1}{2} - \frac{n\sqrt{g}}{0.26}(1-\log R)\right) + \sqrt{n\,\frac{1}{4}\left(\frac{1}{n} - \frac{\sqrt{g}}{0.13}(1-\log R)\right)^2 + \frac{\sqrt{g}}{0.13}\left(\frac{1}{n} + g\log R\right)}\right] \qquad (2.19)$$

Chezy's Equation is directly related to Manning's "n" when y = 1/6. R is the hydraulic mean radius. Equation (2.18) is Pavlovski's formula modified to allow for the kinematic or interaction effect. This method will be discussed in a later chapter and compared to experimental data.

In 1980, Crcry (Ref 12, Ref 13, Ref 14) carried cut extensive tests in a flume described in Sectien 2.3.2. Crcry's mcdel ccnsisted cf an asymmetric ccmpcund channel, i.e. a channel flanked by cnly cne flccd plain. By inserting a mcveable perspex wall, Crcry was able tc test 4 different main channel widths and use was made cf a laser dcppler anemcmetry system tc give instantanecus pcint velccities and turbulence levels

throughout the channel/flood plain cross-section. The point velocity measurements were integrated over the whole cross-sectional area giving a mean total channel discharge within 0.7% of the measured discharge, thus demonstrating the usefulness of the laser system. Crory plotted isovel contours of the cross-sections and found that the maximum velocity filament in the channel was depressed below the water surface and away from the centreline of the channel, towards the noninteracting side of the main channel. This was in agreement with Townsend (Ref 63, Ref 64). Crory observed at low flood plain depths, the maximum velocity filament occurred at the channel/flood plain junction. However, as the flood plain depth increases, ie around Yf/Yc = 0.14-0.27, the maximum velocity filament in the flood plain moves away from the channel/flood plain junction, further into the flood plain. This occurence can be seen on Fig 2.12 and is attributed to the shedding of vorticies in the highly turbulent mixing zone.

Crory also compared her results with Rajaratnam and Ahmadi (Ref 3, Ref 47, Ref 48) who proposed equations (2.24) and (2.26) for the velocity distribution in the main channel and flood plain respectively. Reasonable agreement was found with the main channel distribution, but the results for the flood plain however, disagreed with Rajaratnam and Ahmadi's theoretical model. Equation (2.26) does require that the flood plain be wide enough for the undisturbed flood plain velocity to be reached and therefore Crory assumed that her flood plain was too small.

It has been shown in this section that the interaction mechanism does play a major role in influencing the velocity distribution and discharge carrying capacity of a channel an flood plain during overbank flow and to neglect such a mechanism may result in serious errors in the predicted discharge for a given stage.

One aspect of the research of Wormleaton, Allen and Hadjipanos(Ref 70, Ref 22), whose work will be described in the following section, involved the investigation into the advantages and disadvantages of available methods of estimating discharge by subdividing the channel and flood plains into various sections. Fig 2.13 shows the relationships between the observed and calculated discharges with increasing flood plain depth, for different methods of subdivision, based on their results. Vertical, horizontal and diagonal division lines have been considered, with options on the inclusion or exclusion of the division lines in the calculation of the hydraulic radius for each subsection. The diagonal lines extend from one corner of the channel bank to the centreline of the main channel at the water surface. It can be seen that there is no obvious method which improves the accuracy of the discharge estimation, although Wormleaton et al, have shown that for rougher flood plains, methods which have diagonal or horizontal division lines, with the division lines included in the calculation, give a more accurate estimation of the discharge during overbank flow.

2.3 Shear Stress Measurements.

2.3.1 Introduction.

Recent developments in experimental methods have enabled investigators to analyse the behaviour of flow and understand more fully the turbulent shear patterns which exist in the channel during overbank flow. Two methods of analysis have developed in this field. First, the measurement of boundary shear around the channel flood plain perimeter has permitted investigators to develop the force-momentum Equation and establish "Apparent shear forces" on any plane within the flow. Turbulence measurements have been recorded by researchers using the hot wire anemometer technique, the Laser doppler anemometry system or a dye injection technique affording a estimation of the Reynolds shear stress.

2.3.2 Boundary shear Measurements.

In 1965, Cruff (Ref 15) made use of the Preston tube technique as well as the Karman - Prandtl logarithmic velocity-law to estimate the boundary shear stress resulting from uniform flow in a rectangular channel. A Preston tube was traversed around the boundary of a rectangular channel and an estimation of the boundary shear stress distribution obtained. From considerations of the longitudinal force equilibrium Equation , an apparent shear force, which is essentially an "out of balance" force, could be calculated to act on any vertical

plane in the flow.

Consider the element of fluid shown on Fig 2.14 with each face numbered 1 to 6. If the symmetry of the channel is considered, it can be said that there is no transfer of flow and therefore no transfer of momentum across the centre plane of the channel. It is therefore assumed that the apparent shear force acting on side 3 is zero. Considering the forces acting on the fluid element:-

$$\tau_a y + \tau_{o(1)} x = \rho g x y \sin\theta \qquad (2.20)$$

where $\tau_{o(1)}$ is the average shear stress acting on side 1, τ_a is the apparent shear stress acting on side 4. If θ is small enough ($<5^\circ$) then $\sin\theta$ can be taken as the slope of the channel bed. Uniform flow exists and the hydraulic forces acting on faces 5 and 6 can be eliminated because of their equality. The length of the element is taken as unity. Cruff used this method to calculate the amount of momentum transported from one region to another and therefore the apparent shear stress at any section. This approach was to be used by later investigations including the work presented in this thesis. Cruff was able to show the extent over which a wall would influence the flow in the channel. His results suggested that the walls influenced the flow a distance of 6 times the water depth from the wall.

Although Cruff did not measure boundary shear stresses in a channel with overbank flow, his work established a

method to enable investigators to calculate the apparent shear stress and hence momentum transfer between a channel and its flood plain. Wright and Carstens (Ref 71) used the Preston tube technique to measure boundary shear stresses in a closed conduit aerodynamic model 6 metres long. Three different cross-sectional shapes were tested as shown in Fig 2.15. Air was passed through the channel and the shear stress distribution was recorded by a small Preston tube, 0.69 mm OD. Velocity traverses were also recorded and typical cross sections with isovels are shown on Fig 2.14. Considering the equilibrium of forces acting on the main channel, an apparent shear stress at the channel/flood plain junction could be calculated and this was found to be of the same order of magnitude as the average shear stress in the main channel. Wright and Carstens suggested that the imaginary plane between the channel and flood plain be considered a solid boundary when calculating the mean shear stress in the channel, and the mean shear stress in the channel be regarded as a propulsive force acting on the flood plain. Wright and Carstens verified the mean shear stress around the whole periphery of the channel by comparing the total shear force acting on the boundary with the pressure gradient along the channel length. They found that τ_o , the average shear stress obtained from the Preston tube was 20% less than the shear stress obtained from the pressure gradient. It is not clear why such a large discrepancy existed in the force balance-shear equation. Furthermore, other investigators have suggested that the apparent shear stress at

the junction plane can be as much as 20 times the average shear stress in the main channel.

In 1972, Ghosh and Jena (Ref 20) investigated the distribution of boundary shear stress for rough and smooth walls in a compound channel. Their experiments were carried out in a 8.5 metre long flume with a main channel width of 0.203 metres flanked by two flood plains, each of width 76 mm. The bankfull depth of the channel was 0.102 metres and a bed slope of 0.00525 was maintained for all experiments. Ghosh and Jena obtained the boundary shear distribution along the wetted perimeter of the total channel for various depths of flow using the Preston tube technique combined with the Patel calibration. Fig 2.16 shows the results of two of their experiments on a compound channel with a smooth boundary and it can be seen that the shear stress distribution is distinctly non-uniform in nature. The maximum shear stress on the channel bed occurs approximately midway between the centre line and corner, and the maximum shear in the flood plain always occurs at the channel/flood plain junction. Ghosh and Jena made no direct reference to the interaction between a channel and its flood plain, but results obtained by them can be used to determine the extent of any interaction which was taking place during their tests. From the experimental results of the shear distribution it is possible by planimetry to calculate τ_c' ,the average shear stress in the channel during interaction. Applying the "out of balance" force relationship previously used by Wright and Carstens (Ref 71) it is possible

to calculate the apparent shear stress which acts at the channel/flood plain junction. This has been carried out and the findings of Ghosh and Jena's tests on smooth channels are presented in Chapter 6.

Ghosh and Jena found that by roughening the total periphery of the channel and flood plain the boundary shear in the channel could be redistributed with the maximum shear in the channel bed now occurring at the channel centreline. This redistribution of boundary shear was confirmed by Ghosh and Mehta (Ref 19) who investigated the effects of roughening various parts of the channel/flood plain periphery. Four cases of roughness were tested:-

(a) all smooth

(b) all rough

(c) flood plain rough

(d) channel and flood plain beds rough, walls smooth

For similar channel depths Ghosh and Mehta found a wide variation in the shear distribution around the total perimeter of the channel and concluded that this was due to the complex interaction and circulatory behaviour of the flow.

In 1975, further work was carried out by Myers and Elsawy (Ref 34, Ref 36) into the effects of the existence of a flood plain on the boundary shear distribution of a channel. Using the same flume as Townsend (Ref 63, Ref 64) and Crory (Ref 12, Ref 13, Ref 14), Myers used the Preston tube technique (Ref 43) and Patels calibration (Ref 40) to determine the

magnitude and distribution of boundary shear in a compound channel. To check the validity of Preston and Patels work, Myers equated the weight component of the flow to the average shear stress acting against the flow and found the maximum difference to be 8.14%. Fig 2.17 presents the shear distribution in the main channel for a selection of tests with both the shear distribution for non-interacting (or isolated) and interacting flow presented. It can be seen that the average shear in the main channel is reduced during channel/flood plain interaction. It was found that this average shear stress could be reduced by as much as 20% at very low flood plain depths. At greater flood plain depths the reduction in shear stress decreased.

The boundary shear stress distribution in the flood plain is shown in Fig 2.18 for a number of tests. Comparing the distributon of shear on the flood plain for isolated and interacting flows, it can be seen that the boundary shear is significantly increased during interaction. Myers and Elsawy found that the average flood plain shear could increase by as much as 200% with an increase of 270% in maximum flood plain shear at low flood plain depths. As the flood plain depth increased, the increase in shear due to channel/flood plain interaction was reduced.

The implications of these results are important in flood plain design and positioning of levées and flood walls, since a river will react by erosion and deposition to any non-uniformity of the shear stress distribution. The reaction to

increased boundary shear on the flood plain may result in increased erosion on the flood plain, especially in areas close to the main channel, with deposition occurring in lower velocity areas away from the main channel.

In 1977, Myers (Ref 35) presented a paper in the Journal of Hydraulic Research quantifying the "Apparent shear force" which is a measure of the momentum transfer between a channel and its flood plain during flow interaction. This is essentially an out of balance force resisting channel flow and assisting flood plain flow. Using the data from previous work (Ref 36, Ref 34) Myers proposed the following Equation :-

$$W\sin\theta = S_{frict} + S_a \qquad (2.21)$$

where $W\sin\theta$ is the weight component of flow in the main channel acting in the direction of flow, S_{frict} is the frictional drag force exerted by the bed and sides of the main channel and S_a is the Apparent shear force which acts against the main channel flow and is considered conceptually to act at the vertical junction between the channel and the flood plain. The apparent shear force can be given as :-

$$S_a = W\sin\theta - S_{frict} \qquad (2.22)$$

Now $W\sin\theta$ is equal to $\rho g A_c S$ where A_c is the main channel cross-sectional area and S is the bed slope of the channel.

Since $\rho g A_c S$ can be calculated and S_{frict} can be measured by integrating boundary shear around the channel perimeter, it is possible to calculate the apparent shear force. Fig 2.19 shows the calculated apparent shear force for the ten tests carried out by Myers. It is clear that the maximum apparent shear force occurs at a relative depth Yf/Yc , in the region of 0.3. This would explain the findings of other investigations (Ref 74, Ref 75, Ref 76, Ref 61) which revealed that the interaction effect was a maximum at a relative depth in the channel of around 0.3. The apparent shear force essentially represents the extra resistance to flow in the main channel and the extra assistance to flow in the flood plain. Myers found that the apparent shear force could represent as much as 25% of the channel flow weight component, i.e. :

$$\frac{\tau_a \ Y_f}{\rho g A_c S} = 0{\cdot}25 \qquad (2.23)$$

where the apparent shear force Sa is given by the "apparent shear stress" τ_a multiplied by the flood plain depth.

The apparent shear stress obtained from Myers results is shown on Fig 2.20 over a range of relative depths. It can be seen that the apparent shear stress is a maximum when the flood plain is just inundated, at very low flood plain depths.

Using the method described by Cruff (Ref 15), it is possible to calculate the apparent shear force on any vertical plane in the channel or flood plain and a plot of apparent shear

force against distance from the left wall in the channel is shown on Fig 2.21(a) for Myers results. At the channel/flood plain junction there exists a discontinuity in apparent shear force , the amount of discontinuity being given by the total drag force which is exerted on the main channel channel wall below the flood plain bank. It is also noted that there is a definite distance from the left hand wall, within the main channel, where the apparent shear force equals zero. At this vertical plane there is zero momentum transfer and it can be seen that at greater relative depths the plane of zero momentum transfer is displaced further from the interaction zone. It would be expected that the plane of zero apparent shear would occur on the centre line of a rectangular channel when not interacting with a flood plain. Myers proved this to be the case and compared his results in a nondimensional form with those of Cruff (Ref 15). The results are shown on Fig 2.21(b).

In 1979, a further piece of research was presented by Rajaratnam and Ahmadi (Ref 22, Ref 47). Tests were carried out in a channel 18.29 metres long, 1.22 metres wide and 0.9 metres deep. A main channel 0.2032 metres wide, flanked by two flood plains, each 0.508 metres wide was used to exhibit the interaction mechanism in a symmetrical compound channel. Velocity traverses and boundary shear stresses were recorded. Analysis of velocity profiles revealed that the lateral velocity profiles at different depths in the main channel exhibited similarity and could be described by the Equation :-

$$\frac{U - U'_m}{U_m - U'_m} = 1 - 0{\cdot}75\eta^2 \qquad (2.24)$$

The symbols are represented on Fig 2.22, and η is equal to z/b_m where b_m is a length scale for the main channel which is equal to z when :-

$$\frac{U - U'_m}{U_m - U'_m} = 0{\cdot}25 \qquad (2.25)$$

U is the velocity in the main channel a distance z from the centreline. The flood plain lateral velocity profiles could be described by the equation:-

$$\frac{U - U_\infty}{U'_m - U_\infty} = e^{-{\cdot}693\eta'^2} \qquad (2.26)$$

where $\eta' = \frac{z'}{b_f}$ and b_f is a length scale which is equal to z' when :-

$$\frac{U - U_\infty}{U'_\infty - U_\infty} = 0{\cdot}5 \qquad (2.27)$$

Rajaratnam and Ahmadi showed that length scales b_m and b_f which represent the lateral turbulent mixing could be represented by:-

$$\frac{b_m}{d} = 0{\cdot}92\,\frac{D}{d} - 1{\cdot}32 \qquad (2.28)$$

and $$\frac{b_f}{d} = 2{\cdot}02 \cdot \frac{D}{d} - 2{\cdot}71 \qquad (2.29)$$

Due to the overlapping of the interaction regions in the main channel for the symmetric case, Rajaratnam and Ahmadi (Ref 22, Ref 48) extended their work to an asymmetrical cross section with a main channel of width 0.708 metres and a flood plain width of 0.508 m. Again there were similarities in the lateral velocity profiles at various depths of flow and the channel profiles could be represented by equations (2.24) and (2.25). The velocity profiles on the flood plain could again be described by equations (2.26) and (2.27). A similar analysis was carried out on the boundary shear stress distribution on the flood plain and the shear stress τ_o at any point in the flood plain is described by:-

$$\frac{\tau_o - \tau_{o\infty}}{\tau'_{om} - \tau_{o\infty}} = e^{-0{\cdot}693\left(\frac{z'}{b_\tau}\right)^2} \qquad (2.30)$$

where b_τ is a shear stress length scale and is equal to z' when :-

$$\frac{\tau_o - \tau_{o\infty}}{\tau_{om} - \tau_{o\infty}} = 0{\cdot}5 \qquad (2.31)$$

A further length scale b_t was was introduced and was equal to the total width of the channel and flood plain over which the interaction would influence the velocity profiles. The relationships of b_m, b_f, b_τ and b_t are shown on Fig 2.23 and are

described by the equations:-

$$\frac{b_m}{d} = 3{\cdot}78\left(\frac{D}{d} - 1\right) \qquad (2.32)$$

$$\frac{b_f}{d} = 0{\cdot}64\left(\frac{D}{d} - 1\right) \qquad (2.33)$$

$$\frac{b_I}{d} = 0{\cdot}64\left(\frac{D}{d} - 1\right) \qquad (2.34)$$

and

$$\frac{b_t}{d} = 5{\cdot}95\left(\frac{D}{d} - 1\right) \qquad (2.35)$$

Rearranging Equation (2.35) can show that b_t, the total spreading width of the turbulent shear layer is approximately equal to 6h where h is the bankfull depth. This gives an indication of the width of channel and flood plain over which the interaction mechanism influences the flow. Equations (2.32) to (2.35) also demonstrate quite clearly that the turbulent mechanism is strongly related to the bankfull depth and the channel and flood plain depths.

Rajaratnam and Ahmadi considered the turbulent mean shear stress on any vertical plane in the flood plain which was a result of any channel/flood plain interaction. They integrated this mean shear stress over a distance of $2.5b_\tau$ into the flood plain and found that the following relationship could be derived:-

$$\frac{\overline{\tau_*}}{\tau_{o\infty}} = 0.15\left(\frac{D}{d} - 1\right)^2 \qquad (2.36)$$

where $\overline{\tau_*}$ is the turbulent mean shear stress which acts at the channel/flood plain junction. $\overline{\tau_*}$ has certain similarities with Myers' apparent shear stress, τ_a and the validity of this relationship will be discussed with respect to results presented in this thesis in a later chapter. $\overline{\tau_*}$ is a physical shear stress average whereas τ_a is purely conceptual.

In summary, Rajaratnam and Ahmadi found that the velocity profiles in the channel and flood plain could be described by equations developed by them. Shear stress profiles in the flood plain could also be described by a proposed equation and integration of this equation over the flood plain yielded a relationship between $\overline{\tau_*}$ and D/d. Rajaratnam and Ahmadi also showed that the mixing zone extended a distance of 6 times the bankfull depth across the channel and flood plain.

Extensive tests on channel/flood plain interaction were carried out by Hadjipanos, et al, (Ref 22, Ref 69, Ref 70) in a flume 9.65 metres long with a main channel width of 0.288 metres, flanked by two flood plains, each of width 0.46 metres and a bankfull depth of 0.12 metres as shown on Fig 2.24. Four different series of tests were carried out , the first series with smooth flood plains and the second, third and fourth series with different arrangements of hemispherical roughness elements on both flood plains. In all cases the main channel was hydraulically smooth. Hadjipanos realised that the

hydraulic characteristics of the flow in a channel with no channel/flood plain interaction had to be established before any satisfactory method of analysis could be developed for overbank flow. For this reason extensive testing of rectangular channels with the roughness arrangements described above was carried out. Hadjipanos discovered that Manning's Equation adequately described the relationship between discharge and stage and therefore made use of Manning's Equation to estimate the discharge for isolated flow conditions. After the roughness coefficients were established, 36 runs of overbank flow were carried out for various values of the relative depth and relative boundary roughness. Shear stress measurements and velocity traverses were recorded for each run throughout the channel/flood plain cross section. From the results, a relationship was developed for the estimation of τ_a , the apparent shear stress from various geometrical and flow parameters :-

$$\tau_a = 13{\cdot}84(\Delta V)^{0{\cdot}882}\left(\frac{Y_c}{h}\right)^{-3{\cdot}123}\left(\frac{B_c}{B_f}\right)^{0{\cdot}727} \qquad (2.37)$$

B_c and B_f are the channel and flood plain widths, ΔV is the difference in mean velocity between the channel and flood plain (the velocities based on the channel and flood plain being isolated from each other), Y_c is the depth of flow in the main channel and h is the bankfull depth. Their results together with other investigators are shown on Fig 2.24. The relationship appears to be a promising one and will be discussed in

relationship to the results presented in this thesis in a later chapter.

Crory and Elsawy (Ref 12, Ref 13, Ref 14) carried out experimental tests on the same perspex flume used by Townsend (Ref 63, Ref 64) and Myers (Ref 34, Ref 36, Ref 35). A perspex wall was inserted into the main channel, along its length to give four different channel widths of 0.254 m, 0.203 m, 0.153 m and 0.102 m. Boundary shear stress distributions around the total periphery were measured using a Preston tube of OD 1.82 mm. Their work also involved extensive turbulence intensity and point velocity measurements using a Laser doppler anemometry system, and will be described in Section 2.3.2 when turbulence experiments carried out will be reviewed. Using the information obtained from a total of 16 runs of varying channel widths and flow depths, Crory and Elsawy were able to calculate the apparent shear stress acting at the channel/flood plain junction. Fig 2.25 shows the relationship between the apparent shear stress τ_a, and ΔU and $\Delta U'$, where ΔU and $\Delta U'$ are the mean velocity differences between the channel and the flood plain calculated from isolated and interacting flows respectively. It can be seen that as Bf/Bc increases, the apparent shear stress increases. This will be shown to be in general agreement with the results presented in this thesis and a direct comparison will be presented in a later chapter. Crory's work suggested that the apparent shear stress could be up to 25 times greater than the average shear stress around the channel periphery, ρgRS. This

would appear to disagree with Wright and Carsten's suggestion that the apparent shear stress was of the same order of magnitude as the average shear stress in the channel.

Crory also developed equations based on geometrical parameters to predict the relationship between the shear stress under isolated and interacting conditions for both the channel and the flood plain:-

$$\Phi_c = \frac{\tau_c'}{\tau_c} = \frac{\tau_c'}{\rho g R_c S} = 1 - \frac{B_c h^2}{B_f A_c} \qquad (2.38)$$

and

$$\Phi_f = \frac{\tau_f'}{\tau_f} = \frac{\tau_f'}{\rho g R_f S} = 1 + \frac{B_c h^2}{B_f A_f} \qquad (2.39)$$

Equation (2.38) can be rewritten :

$$\frac{\tau_c'}{\tau_c} = 1 - \frac{B_c}{B_f} \cdot \frac{h^2}{B_c Y_c} \qquad (2.40)$$

which leads to

$$\frac{\tau_c'}{\tau_c} = 1 - \frac{h^2}{B_f Y_c} \qquad (2.41)$$

Equation (2.41) can be expressed in the form :

$$\frac{\tau_c'}{\tau_c} = 1 - \left(\frac{h}{B_f}\right)\left(\frac{h}{Y_c}\right) \qquad (2.41(a))$$

which does not appear satisfactory when the flood plain depth is small ($h/Yc \to 1$) combined with small flood plain widths, when $h/Bf \to 1$. Then τ_c' / τ_c tends towards zero which cannot be the case. Now from a consideration of the forces acting on the flow

in the channel :-

$$\tau_c' P_c' + \tau_a Y_f = \tau_c P_c \qquad (2.42)$$

where $\tau_c = \rho g R_c S$ (2.43)

and $P_c = B_c + 2Y_c$; $P_c = B_c + Y_c + h$ (2.44)

Pc and Pc' represents the solid wetted perimeter in the channel during isolated and interacting flow conditions, τ_a is the apparent shear stress acting at the channel/flood plain junction, τ_c' and τ_c are the average shear stresses in the channel during interaction or isolation of the flow respectively. Now for low flood plain depths $Pc' \approx Pc$ and Equation (2.42) gives:-

$$\tau_a Y_f \approx \tau_c P_c - \tau_c' P_c \qquad (2.45)$$

which gives $$\tau_a Y_f \approx \rho g A_c S - \tau_c' P_c \qquad (2.46)$$

dividing by $\rho g A_c S$ gives $$\frac{\tau_a Y_f}{\rho g A_c S} \doteq 1 - \frac{\tau_c'}{\tau_c} \qquad (2.47)$$

Combining Equation (2.41) and (2.47) gives

$$1 - \frac{\tau_a Y_f}{\rho g A_c S} \approx 1 - \frac{h^2}{B_f Y_c} \qquad (2.48)$$

which simplfies to $$\frac{\tau_a Y_f}{\rho g A_c S} \approx \frac{h^2}{B_f Y_c} \qquad (2.49)$$

rearranging gives $$\tau_a \approx \frac{h^2}{B_f Y_c} \frac{\rho g A_c S}{Y_f} \qquad (2.50)$$

or $$\frac{\tau a}{\rho g Y_f S} \approx \frac{B_c}{B_f} \cdot \left(\frac{h}{Y_f}\right)^2 \approx \frac{B_c}{B_f} \left(\frac{Y_c}{Y_f} - 1\right)^2 \qquad (2.51)$$

Equation (2.51) is now in a similar form as that proposed by Rajaratnam and Ahmadi in Equation (2.36), although $\overline{\tau_*}$ in Equation (2.36) is a physical shear stress whereas τ_a in Equation (2.51) is purely conceptual. The significance of this relationship to the results presented in this thesis will be discussed in Chapter 6.

In summary, the Preston tube has been used extensively in the determination of the boundary shear stress distribution in channels with overbank flow. A knowledge of the shear distribution has permitted investigators to establish the apparent shear force or out of balance force which exist between a channel and its flood plain. This method has therefore been used to obtain some of the results presented in this thesis and also to compare with the apparent shear stresses obtained in previous research work.

2.3.3 Turbulence Measurements.

As previously stated, a turbulent shear mechanism exists, acting at the channel/flood plain junction during overbank flow. This turbulent shear mechanism is recognised by the visible existence of vorticies and large scale eddies on the water surface. In 1967, Townsend (Ref 63, Ref 64) investigated the intensities of turbulence occurring during overbank flow in a flume described in Section 2.2. Townsend used two separate methods to measure the turbulence intensity of compound channel flow. First, he measured the lateral turbulence intensity, or rather the RMS value $\sqrt{\overline{(v')^2}}$, using a dye injection technique. v' is the fluctuating velocity component of the flow in the lateral direction. The angle of dispersion of the dye injected into the flow has been shown by Taylor(Ref 59) to be proportional to $\sqrt{\overline{(v')^2}}$. Townsend's results shown on Fig 2.26 indicate that at regions close to the channel/flood plain boundary, the intensity of lateral turbulence increases by 30% compared to the turbulence in the main channel centre. More recent measurements of the half spreading angle of a shear layer, have indicated values in the range 3°-11° giving a total spreading angle of 6°-22° which is in good agreement with Townsend's results.

Secondly, the longitudinal turbulence intensity RMS value $\sqrt{\overline{(u')^2}}$, where u' is the fluctuating velocity component in the longitudinal direction of flow, was measured using the hot wire anemometry system. Fig 2.27 shows the results of three tests carried out using this system, each test being carried out

at a different relative depth. The relative longitudinal turbulence near the channel/flood plain boundary was found to be approximately twice the intensity elsewhere in the main channel. It can also be observed that the intensity of the turbulence is significantly reduced as the depth in the flood plain increases. This is to be expected as the degree of turbulent shear mixing decreases with increasing relative depth as shown by previous investigators. It can be seen that the maximum longitudinal turbulence intensity occurs in the main channel, very close to the channel/flood plain junction.

Fig 2.28 presents Townsend's results of the relative lateral and longitudinal turbulence intensities with the local velocities included. Here it can be seen that the longitudinal turbulence levels are greater than those in the lateral direction, or $u' > v'$.

Townsend's work introduced a new aspect to the channel/flood plain interaction during overbank flow in that for the first time an appreciation of the magnitude and extent of the turbulence intensities were recorded, although it is not clear how these results may be used in practice, except in the k-ε turbulence model currently being developed by Rodi(Ref 52).

Crory(Ref 12, Ref 13, Ref 14) made use of the Laser doppler anemometry system to measure average velocities and turbulence intensities in the longitudinal direction of flow in a compound channel. This method involves passing two laser beams through the flow to a point of convergence and the generation of

interference fringes at the point of convergence. Receiving optics combined with a frequency tracker translate the fringes or doppler bursts into velocity and RMS turbulence readings. This system has four main advantages :-

(a) The measuring device does not interfere with the flow

(b) The system is not contaminated by the flow as in the hot wire or hot film anemometry systems.

(c) It is calibration free.

(d) It can measure the instantaneous velocity and therefore over a period of time establish the mean local velocity and the associated fluctuating velocity component.

Using the same channel as described in Section 2.3.1, Crory was able to obtain results which were in broad agreement with Townsend's. She observed that the turbulence intensities were minimised at maximum velocity filaments and also noted that the maximum turbulence intensity in the channel occurred just inside the main channel, near the channel/flood plain junction.

Crory also attempted to relate the apparent shear stress τ_a to the fluid shear or Reynolds stress τ_r at the channel/flood plain junction. The Reynolds shear stress τ_r , at any point in the flow is given by:-

$$\tau_r = \rho \overline{u' v'} \qquad (2.52)$$

where u' and v' are the fluctuating velocity components in the longitudinal and transverse directions respectively. If isotropic turbulence is assumed, ie u'= v', then Equation (2.52) becomes :-

$$\tau_r = \rho . u'^2 \qquad (2.53)$$

To find the fluid shear τ_r at the channel/flood plain junction, the value of u' at a depth, half of the flood plain depth was chosen. Crory then plotted τ_r against τ_a. The results are shown on Fig 2.29 and it can be seen that there is a large degree of scatter in the results. A comparison of the relative magnitudes can be noted with an approximate relationship being given as :-

$$\tau_a \approx 3\rho(u')^2 \approx 3\tau_r \qquad (2.54)$$

Townsend has shown on Fig 2.28 that the assumption of u'= v' is not strictly correct. However, since Crory was able to measure only the longitudinal velocity component, no comparison between u' and v' obtained from her results could be made. The validity of correlating the apparent shear stress τa, with the estimated Reynolds stress τ_r , is not in question, as high Reynolds stresses are found in regions of intense shear, and hence extensive momentum transfer between layers. τa on the other hand is a gross parameter to describe momentum transfer from one large body of fluid to another and hence in some ways τa is

linked to the local Reynolds stress at the channel/flood plain junction.

Both Crory and Townsend have demonstrated the significant increase in turbulence which exists at the channel/flood plain interface. They have shown that the turbulence intensity is related to the relative depth Yc/Yf which confirms the findings of previous investigators in their calculations of the apparent shear stress.

2.4 Mathematical Models.

2.4.1 Introduction.

The traditional approach to analysing the flow characteristics of a particular river reach is to construct a scale model of the river in question. The costs of such an investigation are becoming prohibitive for two main reasons. First, there are limitations imposed on the model from scaling laws and if a particularly long river reach is to be modelled, then a model of several hundred feet in length may require to be constructed. Secondly, as demands on a river as a natural resource increase, more accurate modelling is required.

With the development of the computer and the reduction in associated computing costs, it is inevitable that a great deal of recent effort has been spent on the development of mathematical models which give reasonable predictions of stage and discharge in a river with respect to distance along the river

and time.

The fundamental equations of flow are known but for the present are too complex to be solved directly by computer and therefore simplifications must be made. The Navier-Stokes equations for 3 dimensional incompressible flow are given as follows :-

$$\frac{\delta u}{\delta t} + \left(\frac{\delta u}{\delta x} + \frac{\delta u}{\delta y} + \frac{\delta u}{\delta z}\right) = \frac{1}{\rho} - \frac{\delta P}{\delta x} + \nabla^2 u \qquad (2.55(a))$$

$$\frac{\delta v}{\delta t} + \left(\frac{\delta v}{\delta x} + \frac{\delta v}{\delta y} + \frac{\delta v}{\delta z}\right) = \frac{1}{\rho} - \frac{\delta P}{\delta y} + \nabla^2 v \qquad (2.55(b))$$

$$\frac{\delta w}{\delta t} + \left(\frac{\delta w}{\delta x} + \frac{\delta w}{\delta y} + \frac{\delta w}{\delta z}\right) = \frac{1}{\rho} - \frac{\delta P}{\delta z} + \nabla^2 w \qquad (2.55(c))$$

If it is assumed that the vertical accelerations of flow are negligible compared with gravity then Equation (2.55(c)) can be neglected. By integrating equations (2.55(a)) and (2.55(b)) over the depth of flow these equations give the two dimensional flow equations. Further integration over the width of the channel and eliminating viscous terms gives the one dimensional equations :-

$$\frac{\delta Q}{\delta t} + \frac{\delta(\beta Q)}{\delta x} + gA\left(\frac{\delta h}{\delta x} + S_f\right) = 0 \qquad (2.56)$$

This equation is known as the one dimensional Equation of momentum.

From a consideration of continuity the equation for 3 dimensional flow is given as :-

$$\frac{\delta u}{\delta x} + \frac{\delta v}{\delta y} + \frac{\delta w}{\delta z} = 0 \qquad (2.57)$$

By similar integration given to the momentum equation, the continuity Equation can be reduced to :-

$$\frac{\delta A}{\delta t} + \frac{\delta Q}{\delta x} = q \qquad (2.58)$$

for one dimensional flow where Q is the discharge through a particular section of cross-sectional area A, q is the lateral inflow or outflow at the reach of length x. β is the momentum correcton factor, h is the depth of the channel and S_f is the energy slope.

Equations (2.58) and (2.56) can be solved by various numerical methods giving values of Q and h with respect to distance along the river reach and time.

2.4.2 Previous Investigations.

From evidence presented in this chapter, it is expected that during overbank flow, additional resistance to flow will be encountered due to the high turbulent shear which exists between a channel and its flood plains. Various modifications have been made to the equations of continuity and momentum to allow for overbank flow in straight and meandering channels and a brief description of some proposals are given.

Radojkovic (Ref 45) presented a method in 1976 where the momentum and continuity equations were modified to

accommodate the reduction in shear in the main channel due to channel/flood plain interaction. From the boundary shear distribution results obtained from Myers and Elsawy (Ref 34, Ref 36) and Ghosh and Jena (Ref 20), Radojkovic was able to analyse the energy transfer mechanism at the channel/flood plain junction. He proposed the following equations :-

$$\Phi_{mc} = \frac{E^f_{mc}}{E^w_{mc}} = \frac{\tau_{mc}}{\rho g R_{mc} S} \qquad (2.59)$$

and

$$\Phi_{fp} = \frac{E^f_{fp}}{E^w_{fp}} = \frac{\tau_{fp}}{\rho g R_{fp} S} \qquad (2.60)$$

for the channel and flood plain. The subscripts $_{fp}$ and $_{mc}$ represent parameters in the flood plain and channel respectively, E^f is the energy dissipated along the solid boundary walls due to friction, E^W is the energy due to the work of gravity and τ is the mean shear stress along the solid boundary during overbank flow. Radojkovic also proposed the energy ratios :-

$$\Psi_{mc} = \frac{E^t \quad E^d}{E^f_{mc}} \qquad (2.61)$$

$$E^t$$

and

$$\Psi_{fp} = \frac{}{E^f_{fp}} \qquad (2.62)$$

where E^t is the total energy transferred from the main channel to the flood plain, E^d is the energy dissipated through eddies generated along the junction between the main channel and flood

plain. The relationship between these parameters are given as :-

$$\Psi_{mc} = \frac{(1 - \Phi_{mc})}{\Phi_{mc}} \qquad (2.63)$$

and $$\Psi_{fp} = \frac{(\Phi_{fp} - 1)}{\Phi_{fp}} \qquad (2.64)$$

Radojkovic suggested that the dimensionless parameters Ψ_{mc} , Ψ_{fp} , Φ_{mc} and Φ_{fp} are functions of the geometrical properties of the channel. A general relationship is presented on Fig 2.30. Using the dimensionless parameters Radojkovic proposed a relationship between the discharges in the channel and flood plain during interaction :-

$$\frac{Q_{mc}}{Q_{fp}} = \frac{n_{fp}}{n_{mc}} \cdot \frac{A_{mc}}{A_{fp}} \cdot \frac{R_{mc}^{2/3}}{R_{fp}^{2/3}} \cdot \sqrt{\frac{\Phi_{mc}}{\Phi_{fp}}} \qquad (2.65)$$

where Q is the discharge, A is the cross sectional area and n is Manning's roughness coefficient. He also presented modifications to the equations of unsteady flow, (2.56) and (2.58). The Equation of momentum becomes :-

$$\frac{1}{g}\frac{\delta V_{mc}}{\delta t} + \frac{V_{mc}}{g}\frac{\delta V_{mc}}{\delta x} + \frac{\delta Z_{mc}}{\delta x} = -\frac{\tau_{mc}}{\rho g R_{mc}}\Phi_{mc} + \frac{(1-m)V_{mc}q}{g A_{mc}} \qquad (2.66(a))$$

for the main channel and

$$\frac{1}{g}\frac{\delta V_{fp}}{\delta t} + \frac{V_{fp}}{g}\frac{\delta V_{fp}}{\delta x} + \frac{\delta Z_{fp}}{\delta x} = -\frac{\tau_{fp}}{\rho g R_{fp}}\Phi_{fp} + m\frac{V_{fp}q}{g A_{fp}} \qquad (2.66(b))$$

for the flood plain. m is used to define the lateral flow conditions in the sense that m = 1 for lateral flow from the channel to the flood plain and m = 0 for vice-versa. The introduction of the terms $\frac{\tau_{mc}\Phi_{mc}}{\rho g R_{mc}}$ and $\frac{\tau_{fp}\Phi_{fp}}{\rho g R_{fp}}$ allow for the interaction mechanism. No evidence was presented by Radojkovic to show the advantages of the proposed modification to the unsteady flow equations, therefore the validity of his proposal cannot be confirmed.

In 1976, Tingsanchali and Ackermann (Ref 60) proposed a method which allowed for the nonuniform distribution of the momentum flux through the total width of the channel and flood plains. They proposed a momentum correction factor M in the form :-

$$M = \frac{\sum_{i=1}^{n} \rho Q_i V_i}{\rho Q V} \qquad (2.67)$$

where the number of sections is n and Q_i and V_i are the discharges and velocities in the ith sub-section, Q is the total discharge through the channel and V is the mean channel velocity. This Equation is used to modify the Equation of momentum, Equation (2.56) and M can be calculated by estimating the discharges and velocities for each section using Manning's equation. In this method no allowance is made for the turbulent interaction between the channel and flood plain.

A further method of analysis in meandering channels was proposed by Fread (Ref 17) and involved the

influence of river sinuosity on the relative amounts of flow carried by the channel and flood plain. Again no attempt was made to quantify the amount of energy lost due to channel/flood plain interaction.

A mathematical model called FLUCOMP (Ref 16) has been developed for unsteady open channel flow at the Hydraulic Research Station. When considering a channel/flood plain section, the program calculates the discharge for each subsection using Manning's equation. Price (Ref 44) correctly suggests that the turbulent shear which exists between the channel section and the flood plain section is dependent on the difference between the mean main channel velocity and the mean flood plain velocity. However, to minimise complications, he suggests that the shear layers be considered vertical and be regarded as rough surfaces.

2.4.3 Turbulence Models.

Flow in rivers is always turbulent meaning that the flow in any component of direction fluctuates about a mean value. By adopting a statistical approach the instantaneous velocities in the longitudinal, lateral and vertical directions are given by :-

$$u = \bar{u} + u' \qquad (2.68(a))$$

$$v = \bar{v} + v' \qquad (2.68(b))$$

and

$$w = \bar{w} + w' \qquad (2.68(c))$$

where $\bar{u}$, $\bar{v}$ and $\bar{w}$ are the mean velocity components, u',v' and w' are the fluctuations of velocity. If vertical components (w) are ignored, differentiation of the product gives :-

$$\frac{\delta}{\delta y}\left[(\bar{u}+u')(\bar{v}+v')\right] = \frac{\delta}{\delta y}(\bar{u}.\bar{v} \quad \overline{u'.v'}) \qquad (2.69)$$

Adopting this statistical approach and arguing from a physical basis, it is possible to show that the turbulent shear stress within a flow τ_r , is equal to $\rho u'v'$. This is termed the Reynolds stress and is a measure of the momentum transfer at any given point within the flow. Various proposals have been made to model the Reynolds stress, most of which are based on the eddy viscosity concept which assumes that the turbulent stresses are proportional to the mean velocity gradients. Rodi (Ref 52) gives the Reynolds stresses in the form :

$$-u'v' = \nu_t\left(\frac{\delta u}{\delta y} - \frac{\delta v}{\delta x}\right) - \frac{2}{3}k \qquad (2.70)$$

where k is the kinetic energy of the fluctuating motion given by :-

$$k = 1/2(u'^2 + v'^2 + w'^2) \qquad (2.71)$$

ν_t is the eddy viscosity of the flow which varies throughout the channel cross-section and difficulty is experienced in attempting to estimate the value of ν_t at any point in the flow.

Various models have been suggested for estimating ν_t which vary in complexity. Perhaps the simplest models are the mixing length models which suggest that :-

$$\nu_t = \ell_m^2 \left|\frac{\delta u}{\delta y}\right| \qquad (2.72)$$

where ℓ_m is a mixing length which is a measure of the movement of an element of fluid.

For more complex flow patterns such as overbank flow, more sophisticated models are necessary to estimate ν_t. The eddy viscosity relationship can be generalised as follows :-

$$\nu_t \propto \hat{V} L \qquad (2.73)$$

where $\hat{V}$ is a velocity scale and L is a length scale characterised by the large scale turbulent motion. A suitable velocity scale incorporated by most models is $\sqrt{k}$, where k is given by Equation (2.71). Thus Equation (2.73) becomes :-

$$\nu_t = C'_\mu \sqrt{k}\ L \qquad (2.74)$$

This is known as the Kolmogorov - Prandtl expression, where C_μ' is an empirical constant and k can be found by solving a transport Equation in terms of k.

The length scale L can also solved by manipulation of the Navier Stokes Equation by the dissipation rate ε , where

$$\varepsilon = C_d \cdot \frac{k^{3/2}}{L} \qquad (2.75)$$

and C_d is a further empircal constant. Rodi(Ref 52) produced a simplified relationship in the form :-

$$\nu_t = C_\mu \frac{k^2}{\varepsilon} \qquad (2.76)$$

k and ε can be found from partial differential equations, given by Rodi and a value of ν_t can be obtained. This enables Equation (2.70) to be solved, thus yielding a theoretical soluton to the Reynolds stresses.

The continuity and momentum equations can now be considered as three dimensional flow or depth averaged flow with the Reynolds stresses or turbulent stresses incorporated into the model. Velocity distributions and shear profiles can be calculated for a given channel geometry. Most models assume that the eddy viscosity is isotropic, ie is the same for all the Reynolds stresses at a particular point in the flow. Such an assumption has been made in a model presented by Rodi, Celik and

Keller (Ref 53) which compares Rajaratnam and Ahmadi's experimental data (Ref 48) with the velocity and bed shear profiles predicted by the turbulence model. Fig 2.31 shows that the velocity profiles compared well. However the theoretical model bed shear prediction is overestimated by around 25% in the main channel. The reason for this is not known at the present, although it may be due to the fact that Rajaratnam underestimated the main channel boundary shear during the interaction condition.

2.5 Rectangular Channel Flow.

Most investigators have used the Darcy-Wiesbach equation, Manning's Equation or Chezy's Equation in the estimation of discharge in rivers with overbank flow. It would seem logical that a precise knowledge of the suitability of such equations in rectangular channels be established before any attempt to apply them to the flow behaviour in compound channels is made. Hadjipanos (Ref 22) was aware of this need and carried out extensive tests on rectangular channels before investigating the nature of the flow in compound channels.

Many attempts have been made to develop satisfactory equations for open channel flow which apply over a wide range of Reynolds numbers, roughness, and channel geometries. These equations take the general form :

$$Q = f(\text{geometrical parameters \& roughness}) \qquad (2.77)$$

One of the earliest empirical equations to be developed was the Chezy formula, based on a squared relationship between the boundary shear stress and the mean velocity :-

$$Q = C.A.\sqrt{RS} \qquad (2.78)$$

where Q is the channel discharge, A is the cross sectional area, R is the hydraulic radius, defined as the cross sectional area of the channel divided by the wetted perimeter of the channel, S is the friction slope of the flow or in the case of uniform flow, S is the slope of the bed. Chezy's coefficient, C, has been given by various formulae :-

(i) Ganguillet and Kutter,

$$C = \frac{41{\cdot}65 - \frac{0{\cdot}00281}{S} - \frac{1{\cdot}811}{n}}{1 + \left(41{\cdot}65 + \frac{0{\cdot}00281}{S}\right)\frac{n}{\sqrt{R}}} \qquad (2.79)$$

n is Kutters n and is very similar to Manning's n.

(ii) Bazin

$$C = \frac{157{\cdot}6}{1 + \frac{m}{R}} \qquad (2.80)$$

where m varies between 0.109 and 3.17.

(iii) Pavlovskis formula,

$$C = \frac{R^y}{n} \qquad (2.81)$$

where $y = 2{\cdot}5\sqrt{n} - 0{\cdot}13 - 0{\cdot}75\sqrt{R}\,(\sqrt{n} - 0{\cdot}1)$ (2.82(a))

and n is Manning's n. Pavlovski also proposed a simpler Equation for estimating y,

$$y = 1.5\sqrt{n} \text{ for } R<1 \text{ metre} \qquad (2.82(b))$$

and

$$y = 1.3\sqrt{n} \text{ for } R>1 \text{ metre} \qquad (2.82(c))$$

Pavlovski's formula is still widely used by Russian engineers today.

(iv) In 1889, Manning (Ref 32) proposed,

$$C = \frac{R^{1/6}}{n} \qquad (2.83)$$

where n is Manning's n.

Using Manning's proposed Equation for Chezy's coefficient, Chezy's Equation becomes,

$$Q = \frac{A}{n} R^{2/3}\sqrt{S} \qquad (2.84)$$

This formula has become known as Manning's Equation and because of its simplicity it has become the most widely used of all the empirical equations. Values of n for can be found in most

hydraulic text books and are generally assumed constant for a particular channel bed roughness. Chow (Ref 10) presents a comphrehensive description of most rough surfaces and their associated Manning's n value.

Weisbach first introduced the dimensionless friction coefficient f in the Darcy relationship for pipe flow in the form :-

$$S = \frac{f \quad V^2}{4 \, R \quad 2g} \qquad (2.85)$$

where S is the friction slope, R is the hydraulic radius for the channel, V is the mean channel velocity and g is the acceleration due to gravity. Blasius, drawing on the boundary layer theory developed by Prandtl, proposed that the friction factor was a function of the Reynold's number alone for smooth turbulent flow. He proposed that, for Re<100,000 :-

$$f = \frac{0{\cdot}316}{Re^{1/4}} \qquad (2.86)$$

where Re is the Reynold's number and is equal to $4VR/\nu$ where V and R have the usual definitions and ν is the kinematic viscosity of the fluid.

In 1932, Prandtl proposed the well known friction factor Equation for smooth pipes :-

$$\frac{1}{\sqrt{f}} = 2{\cdot}0 \log(Re\sqrt{f}) - 0{\cdot}8 \qquad (2.87)$$

where $f=2gDS/V^2$ and D is the internal diameter of the pipe. This Equation has become known as the smooth pipe equation. Nikuradse later demonstrated that for rough walled pipes, with sufficiently high Reynold's numbers, the friction factor f becomes independent of the Reynold's number and dependent on the ratio of an equivalent roughness of the pipe and the wall diameter.

From the Prandtl mixing length theory, the following Equation was developed :-

$$\frac{U}{U_*} = 5{\cdot}75 \log \frac{y U_*}{\nu} + 5{\cdot}5 \qquad (2.88)$$

where U_* is the shear velocity and is defined as $\sqrt{\frac{\tau_o}{\rho}}$ where τ_o is the boundary shear stress at the wall and ρ is the density of the fluid. ν is the kinematic viscosity and U is the velocity at a point of distance y from the wall. Integration of Equation (2.88) over the pipe radius will yield the smooth pipe Equation (2.87).

Keulegan (Ref 31) using a similar method of analysis, proposed a similar Equation applied to smooth open channels in the form :-

$$\frac{1}{\sqrt{f}} = 2{\cdot}0 \log(Re\sqrt{f}) - 1{\cdot}08 \qquad (2.89)$$

The general form of this Equation can be written as :-

$$\frac{1}{\sqrt{f}} = A \log (Re\sqrt{f}) - B \qquad (2.90)$$

The choice of the values of A and B in open channels have varied according to the results of each investigator. Henderson (Ref 24) and Chow (Ref 10) have suggested that the smooth pipe Equation (2.87) is adequate for analysing open channel flow, i.e. A=2.0 and B=0.8.

The combination of smooth and rough equations brought the development of the Colebrook-White Equation :-

$$\frac{1}{\sqrt{f}} = -2{\cdot}0 \log \left[\frac{k_s}{14{\cdot}83R} + \frac{2{\cdot}52}{Re\sqrt{f}} \right] \qquad (2.91)$$

where k_s is the equivalent roughness of the pipe surface. If k_s=0.0 then Equation (2.91) reduces to Equation (2.87). Ackers (Ref 1) made use of the Colebrook-White Equation and presented the Equation in a series of charts to enable the speedy solution of Equation (2.91). Since the work presented in this thesis is confined to hydraulically smooth surfaces in open channels, no further consideration will be given to equations which include roughness parameters.

Reinus (Ref 51) found that for wide, smooth rectangular channels, A=2.0 and B=1.06.

Based on a total of 49 experimental tests, Tracy and Lester (Ref 65) found the values of A and B to be 2.03 and

1.3 respectively. Rao (Ref 50) found that A=2.12 and B=1.83. Thus it has become apparent that the smooth pipe Equation is not necessarily applicable to smooth rectangular channels, the latter giving friction factors generally 5-15% greater than friction factors obtained from Equation (2.87).

Kazimipour and Apelt (Ref 29) suggested the introduction of a shape factor ψ, in the form :-

$$\psi = \frac{F(\frac{B}{y_{av}})}{\sqrt{P/B}} = \frac{\psi_2}{\psi_1} \qquad (2.92)$$

where B is the channel width, y_{av} is the average depth of flow, P is the wetted perimeter and F, in this case designates a function which is shown on Fig 2.32(a). A modified friction factor is obtained from :

$$F^* = \frac{F}{\psi} \qquad (2.93)$$

where f is the friction factor obtained from the pipe flow equation, (2.87). Shih and Gregg's results (Ref 56) and Tracy and Lester's results (Ref 65) were analysed using this method and the results were encouraging. In 1982, Kazimipour and Apelt (Ref 30) presented their own results using the relationships in equations (2.92) and (2.93) and found the results were favourable as shown on Fig 2.32(b). The results indicate the possibility of altering open channel results to fit the smooth pipe equation. It can be seen that Kazimipour's method adjusts the data

satisfactorily to fit the smooth pipe flow equation.

A similar method was developed by Pillai (Ref 41) who suggested that the significant shape factor was the ratio (P/R), the wetted perimeter to hydraulic radius.

In 1982, Myers (Ref 37) carried out experiments in a rectangular channel with widths 0.755 m, 0.505 m and 0.202 m permitting the testing of a wide range of width to depth ratios. He found from his data that A=2.1 and B=1.56. Table 2.1 presents a comparison of the different values of A and B obtained from different investigations. Myers agreed that the width to depth ratio was an important factor in determining the friction factor but also recognised, as did Henderson (Ref 24), that other factors such as the free surface, secondary flows and the nonuniformity of the boundary shear stress distribution may influence the friction factor coefficient. Myers compared his results with Kazimipour and Apelt (Ref 29, Ref 30) and Pillai (Ref 41) and found that their methods improved the divergency of his own open channel results (compared to the smooth pipe flow Equation) from 8% to around 2%.

2.6 Summary.

In this literature review, the significance of the interaction mechanism which acts between a channel and its flood plain has been investigated. It has been shown that the discharge capacity and velocity distribution can be altered significantly during channel/flood plain interaction, with a

complete redistribution of shear stress occurring. In the light of such evidence it has been decided to carry out an experimental investigation in this field.

It has been shown that the relative depth of flow, Yc/Yf strongly influences the magnitude of this turbulent shear mechanism with the relative widths of the channel and flood plain also playing an important role. It has been shown that the bankfull depth can determine the width of the interaction across the channel and flood plain. In essence, where a severe velocity gradient exists, a turbulent shear layer will develop and the parameters which influence the velocity in the channel and flood plain, influence the intensity of the interaction. The relative roughness of the channel and flood plain again effect the interaction, however in this investigation it has been decided to avoid varying the boundary roughness coefficients in order to carry out an in depth study of the geometrical and flow parameters.

Perhaps, it may be possible to summarise some of the parameters which appear to influence the degree of channel/flood plain interaction. The parameters can be given in the general format :

$$\text{Degree of interaction} = fn\left(\frac{Y_f}{Y_c}, \Delta V, \frac{B_c}{B_f}, \frac{B_f}{h}, \frac{B_c}{h}, S, \frac{n_c}{n_f}\right) \qquad (2.94)$$

where Yf is the flood plain depth of flow

Yc is the main channel depth of flow

ΔV is the velocity difference (Vc -Vf)

Bf is the flood plain width

Bc is the channel width

h is the bankfull depth

S is the longitudinal slope

n_f is the flood plain roughness coefficient

and n_c is the channel roughness coefficient

In this study attention will be given to studying the influence of each geometrical parameter such as channel and flood plain widths, bankfull depth, channel slope and the channel and flood plain flow depths.

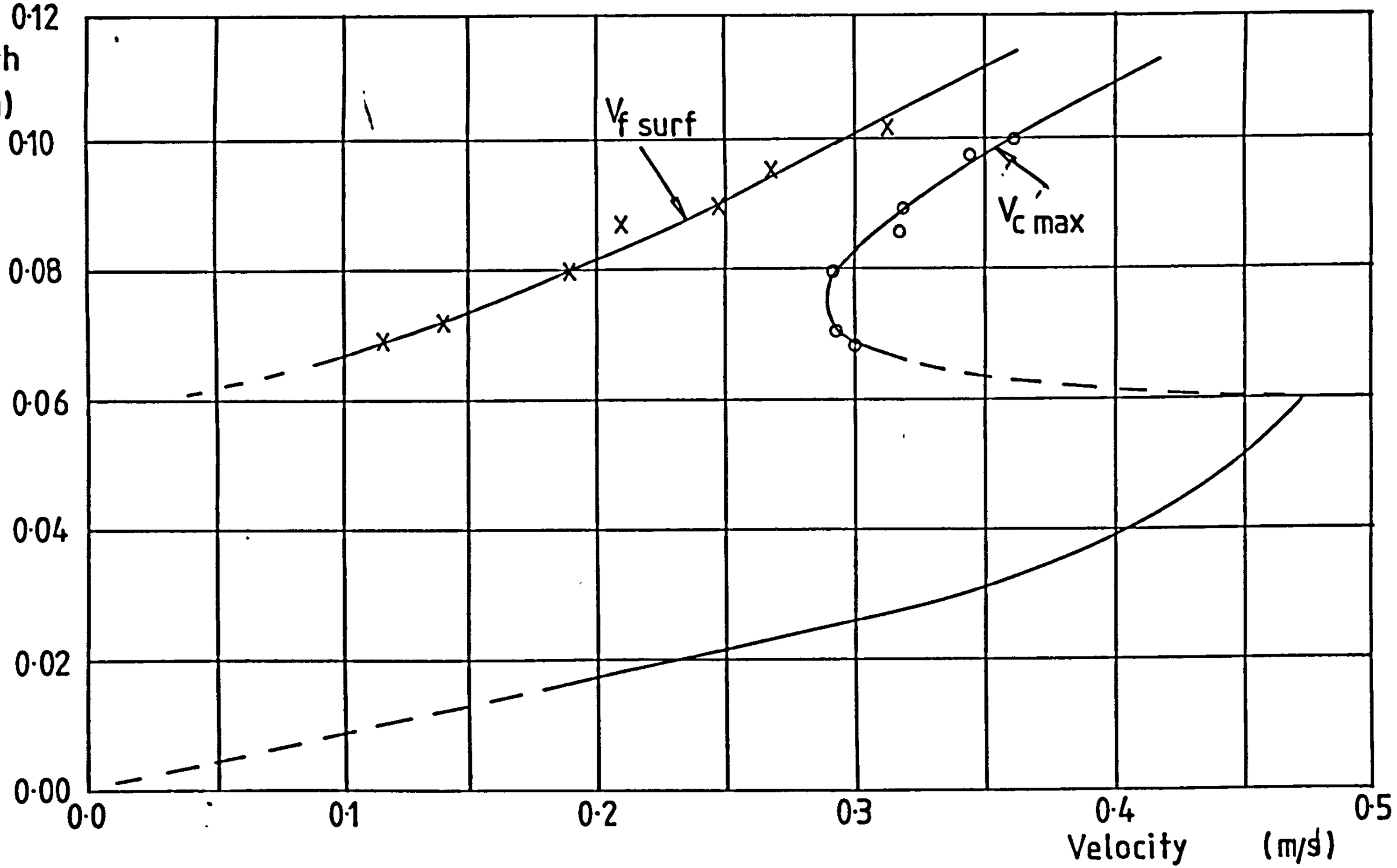

Fig 2·1 GRAPH OF MAXIMUM CHANNEL VELOCITY AND FLOOD PLAIN SURFACE VELOCITY

$B_c = 0{\cdot}6m$, $B_f = 2{\cdot}4m$, $h = 0{\cdot}06m$ (ZHELEZNYAKOV)

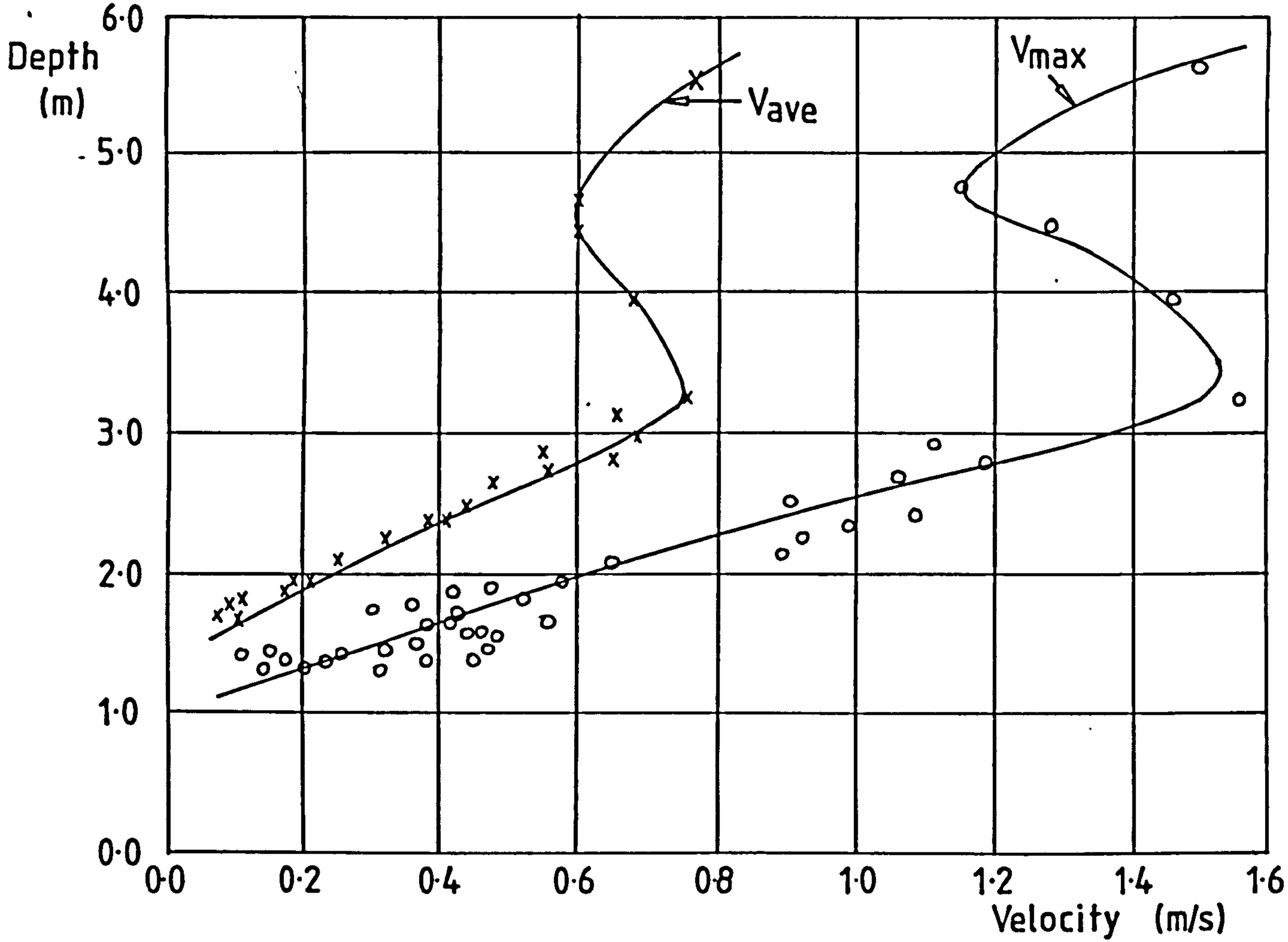

Fig 2·2 GRAPH OF THE AVERAGE AND MAXIMUM VELOCITIES IN A NATURAL RIVER DURING FLOODING (ZHELEZNYAKOV)

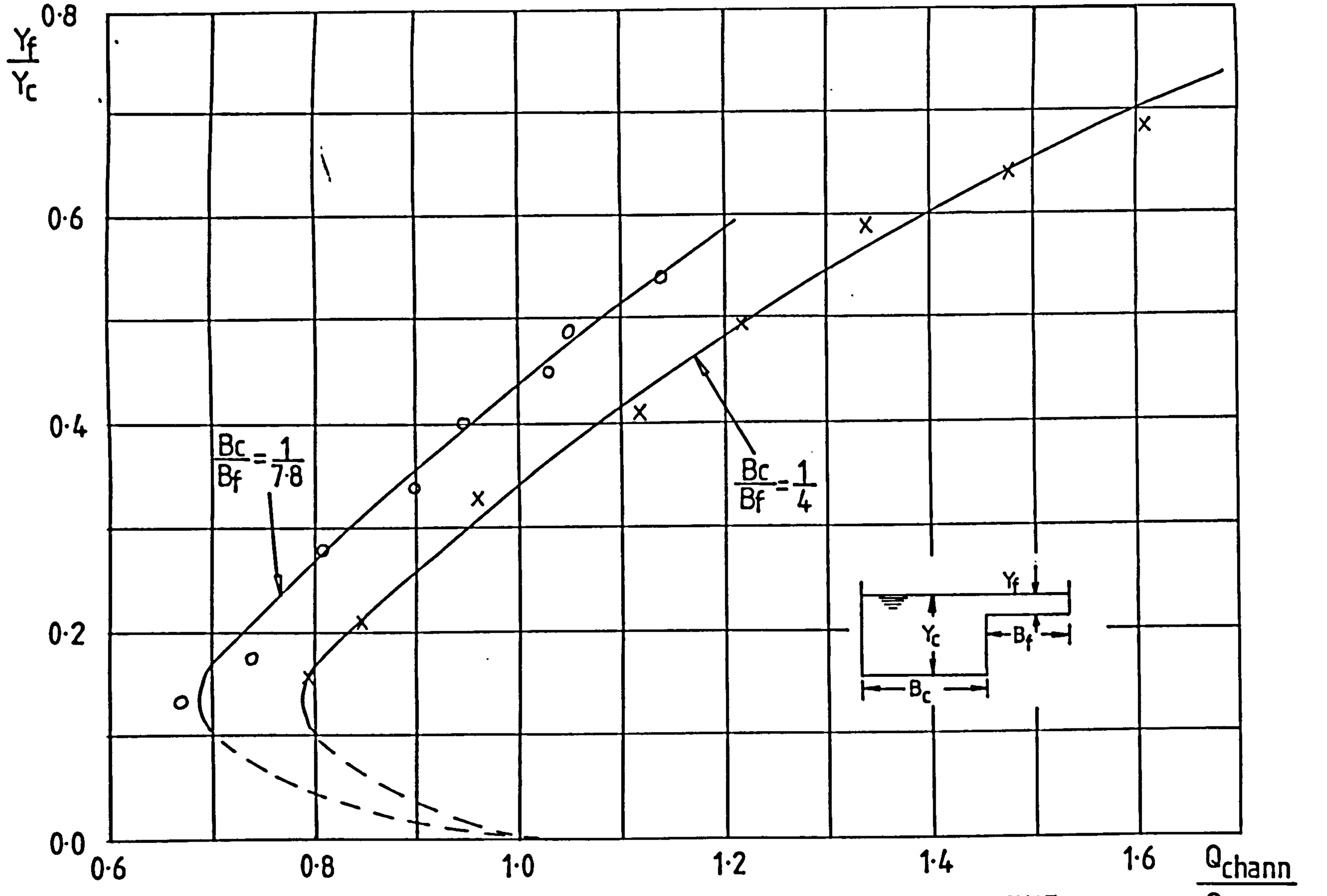

Fig 2·3 GRAPH SHOWING THE EFFECT OF B_c/B_f ON THE CARRYING CAPACITY OF A CHANNEL. (ZHELEZNYAKOV)

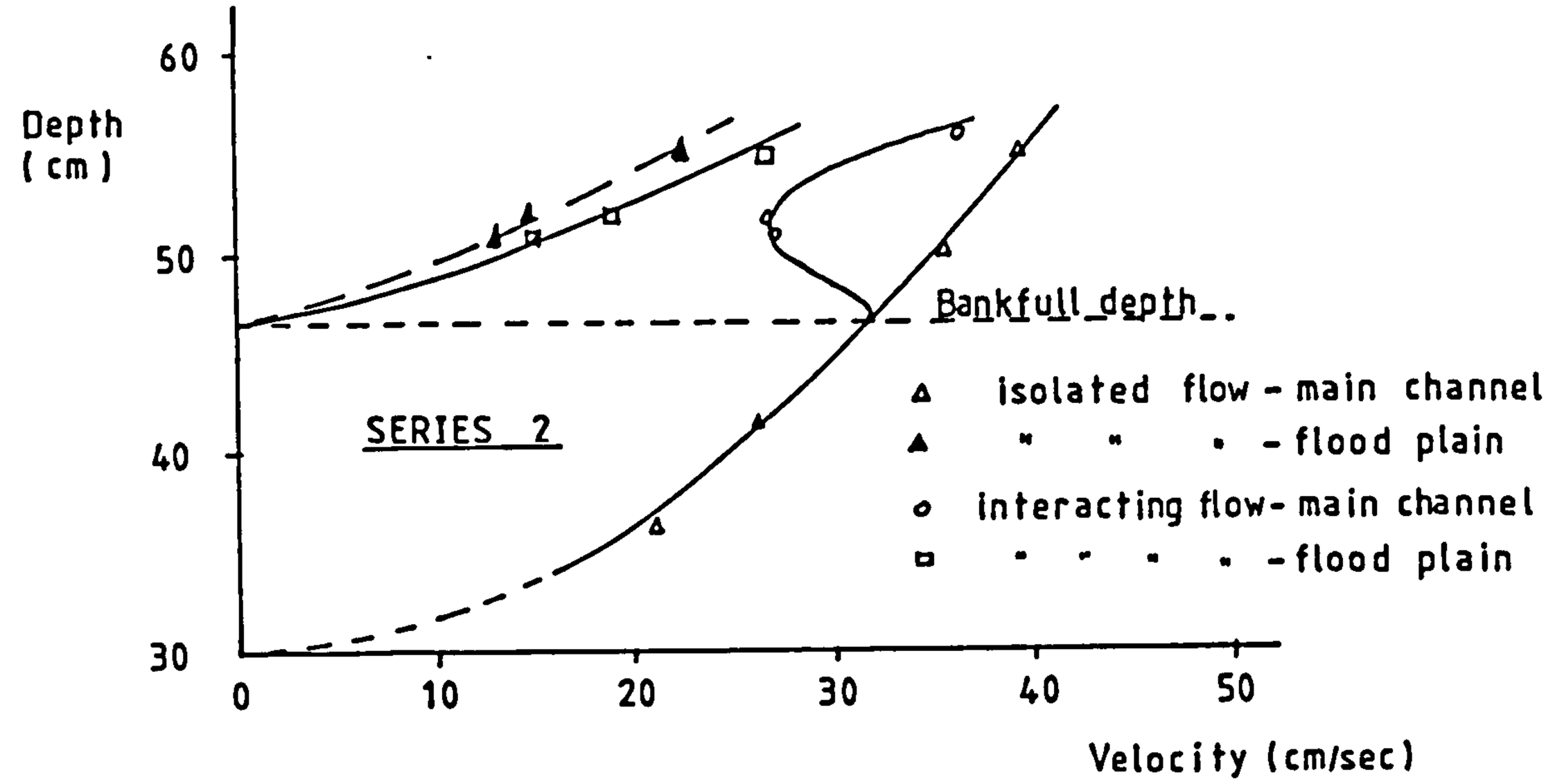

(a) Channel & flood plain with equal roughness coefficients.

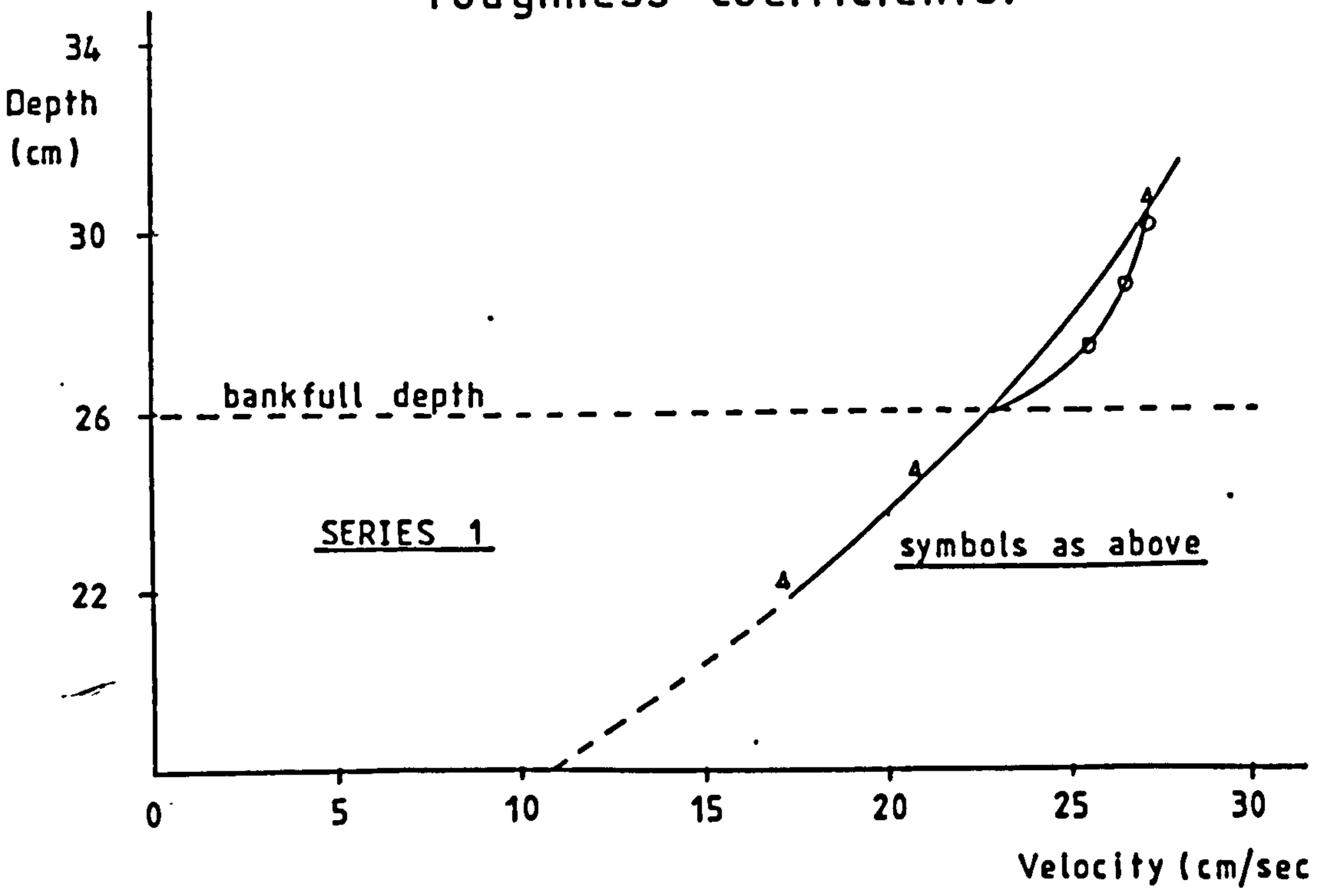

(b) Channel rougher than flood plain.

Fig 2·4 INFLUENCE OF RELATIVE ROUGHNESS ON THE STAGE-DISCHARGE CURVE (ZHELEZNYAKOV & NOVIKOVA)

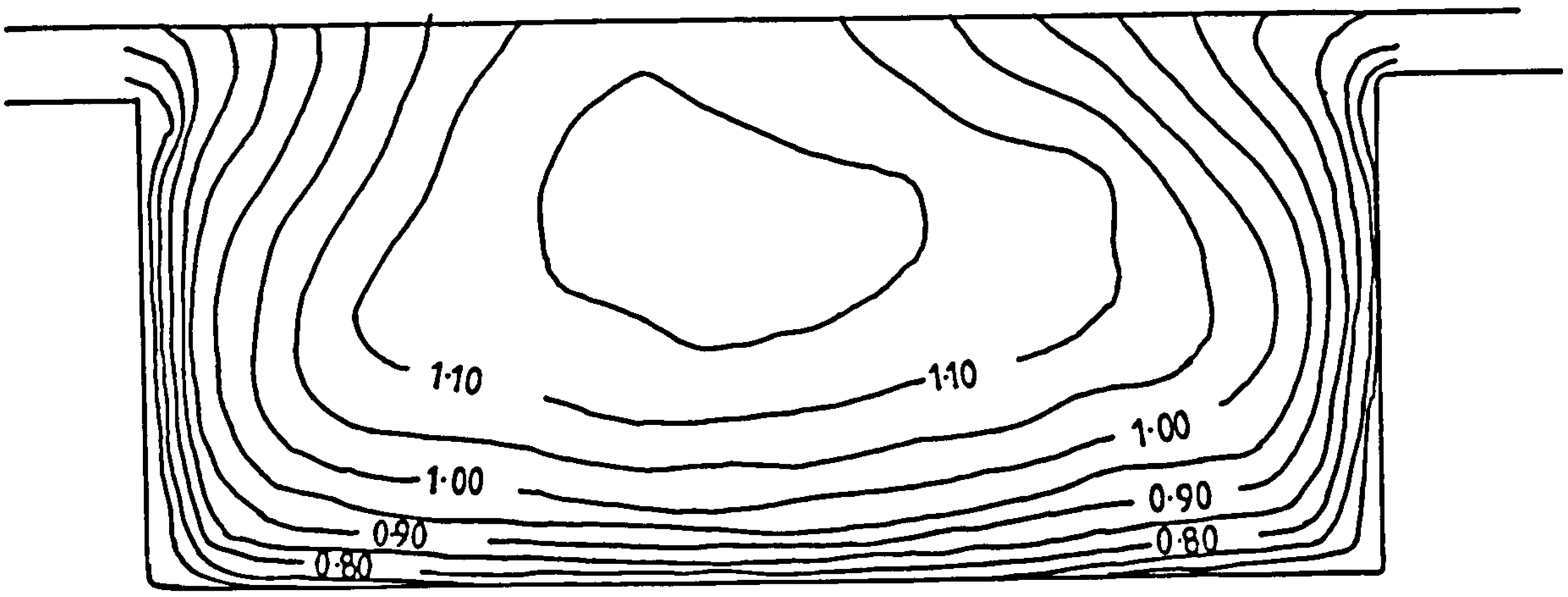

(a) FLOW IN MAIN CHANNEL DURING INTERACTION

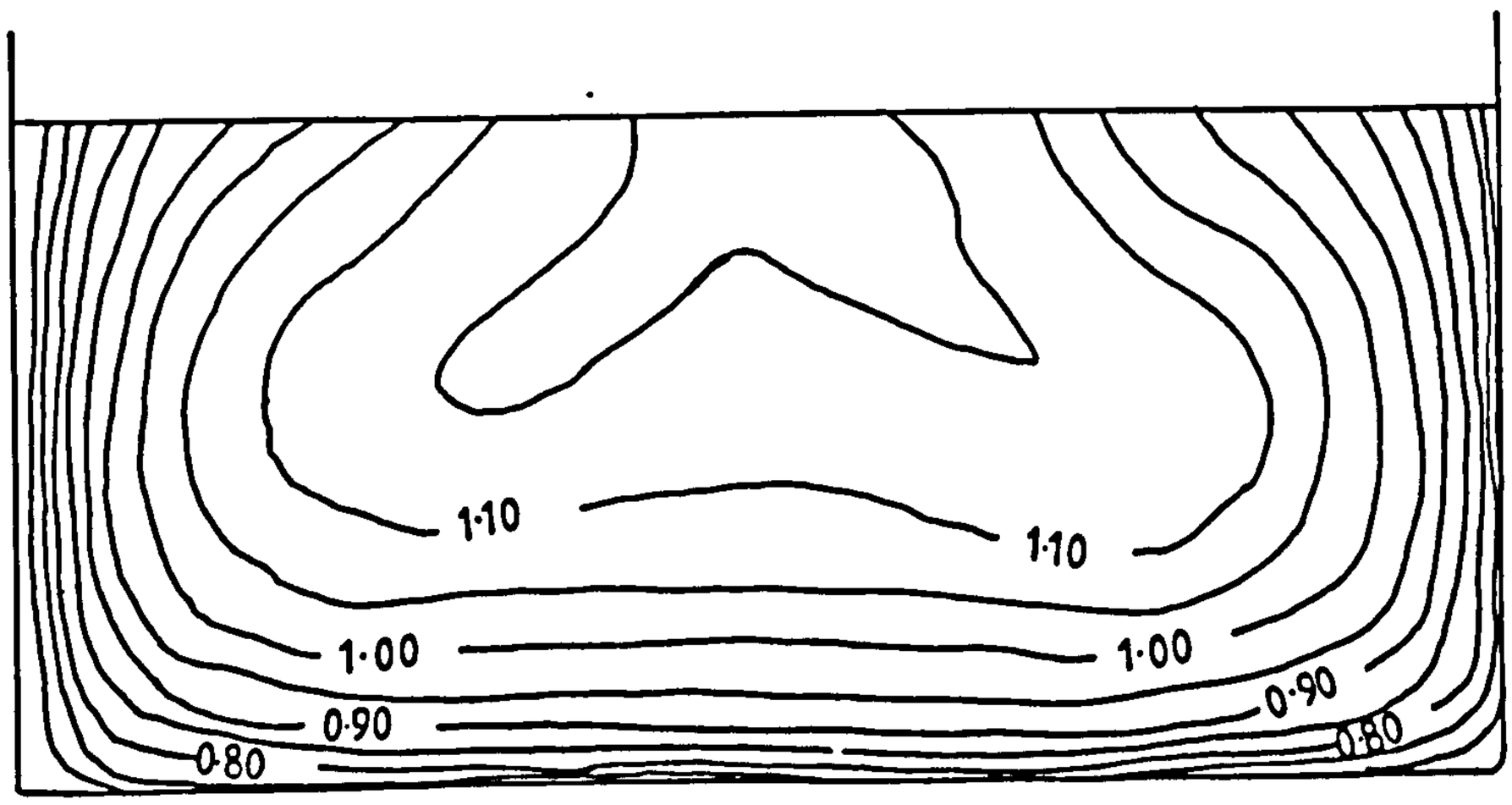

(b) FLOW CONFINED TO MAIN CHANNEL

Fig 2·5 GRAPHS SHOWING EQUAL VELOCITY-RATIO CONTOURS DURING INTERACTING AND ISOLATED CONDITIONS. (SELLIN)

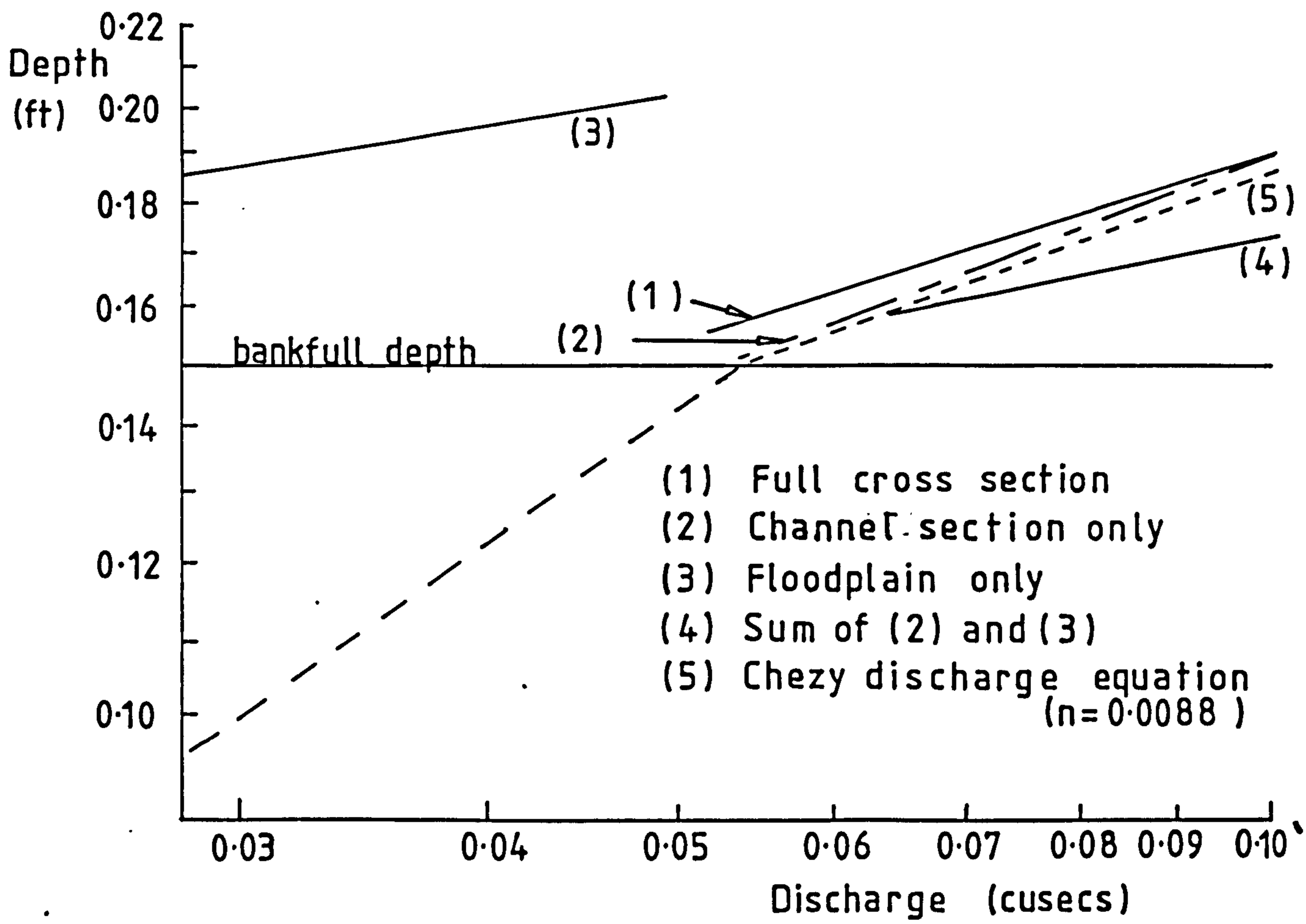

Fig 2·6 DISCHARGE OF FULL CROSS SECTION COMPARED WITH THAT OF THE CROSS SECTION ELEMENTS AND THE CHEZY EQUATION (SELLIN)

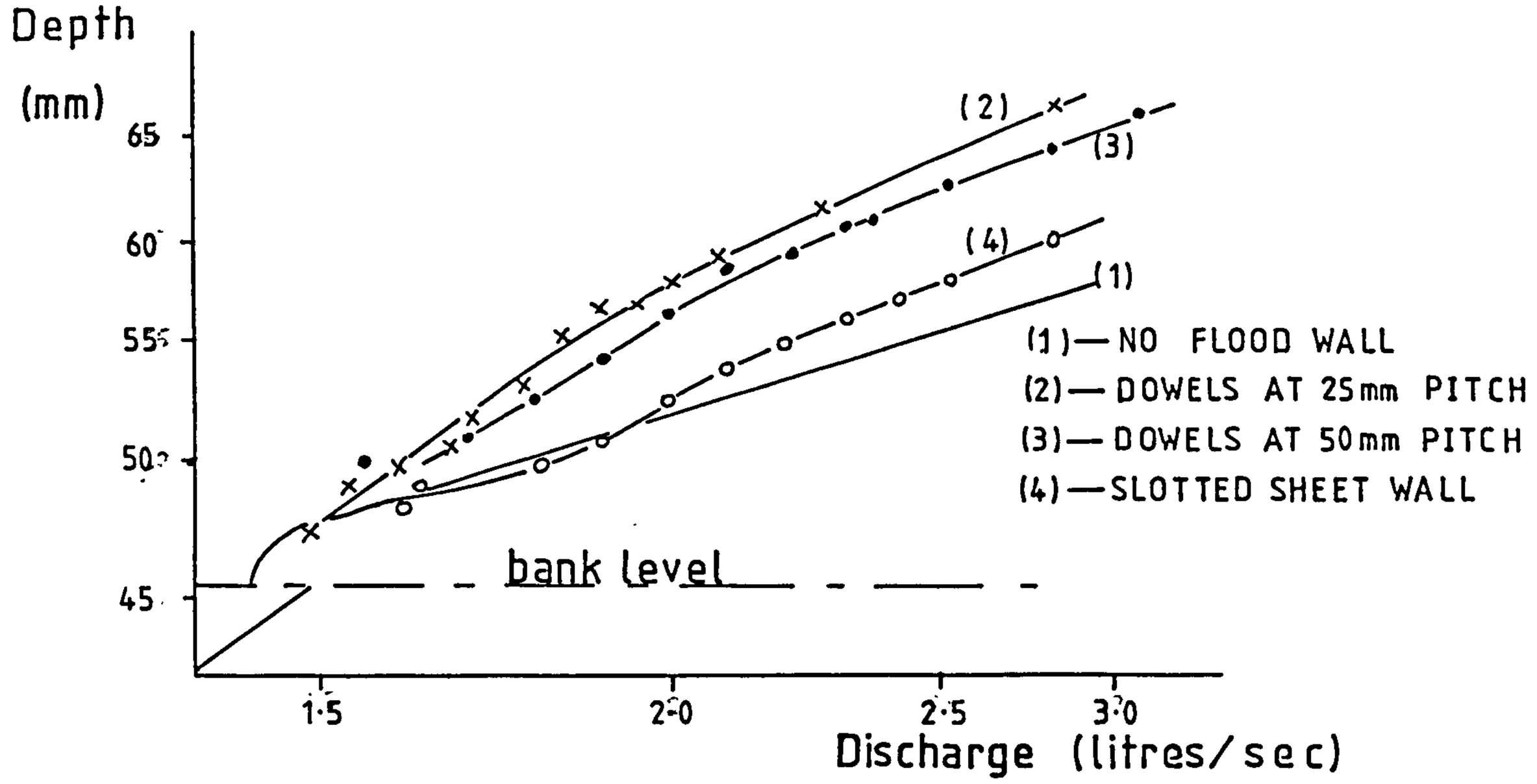

A. CHANNEL DISCHARGE MODIFIED BY USE OF VARIOUS PERMEABLE FLOOD WALLS (SMOOTH FLOOD PLAIN)

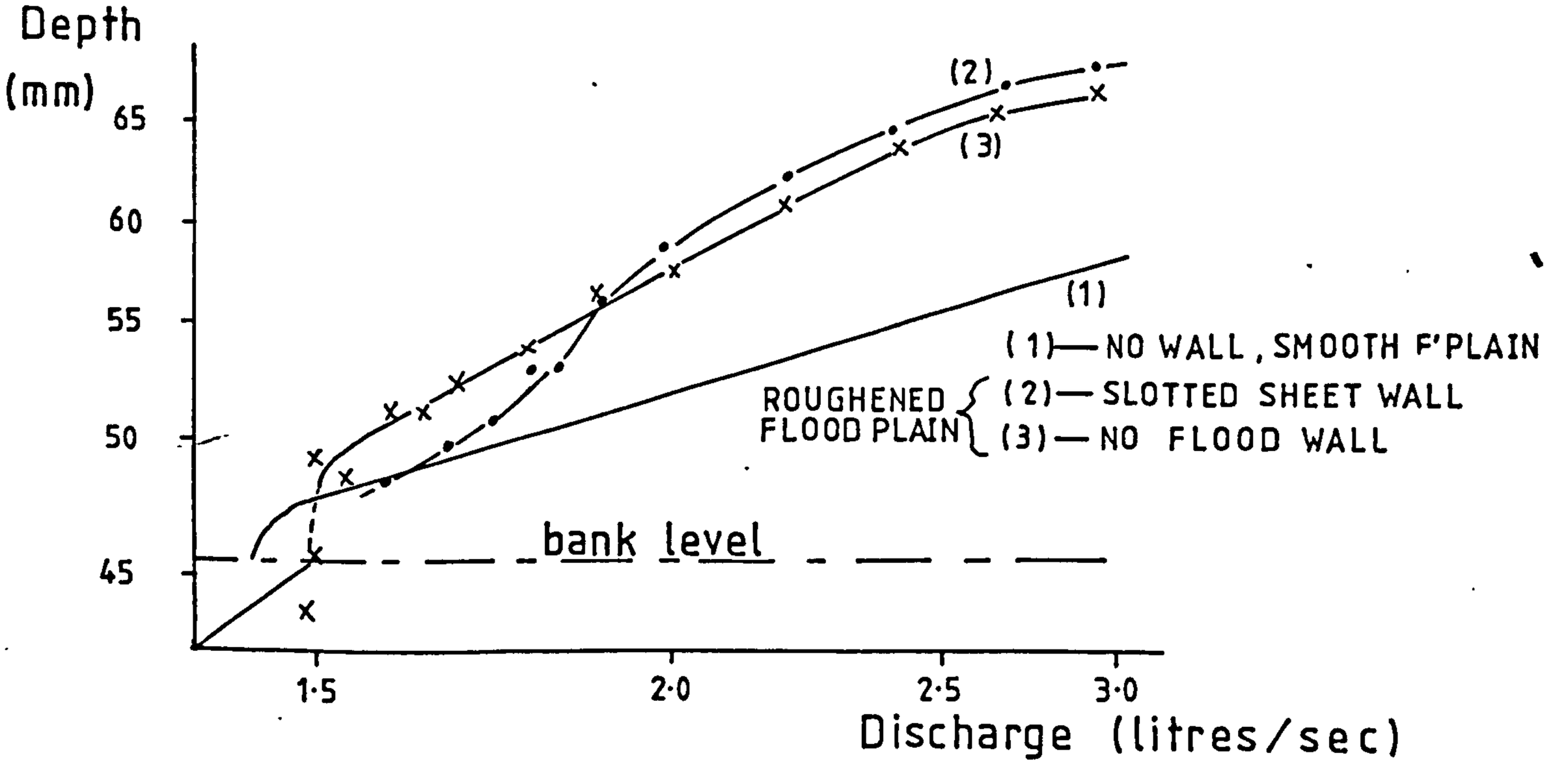

B. DISCHARGE OF CHANNEL WITH ROUGHENED FLOOD PLAIN

FIG 2·7 (SELLIN)

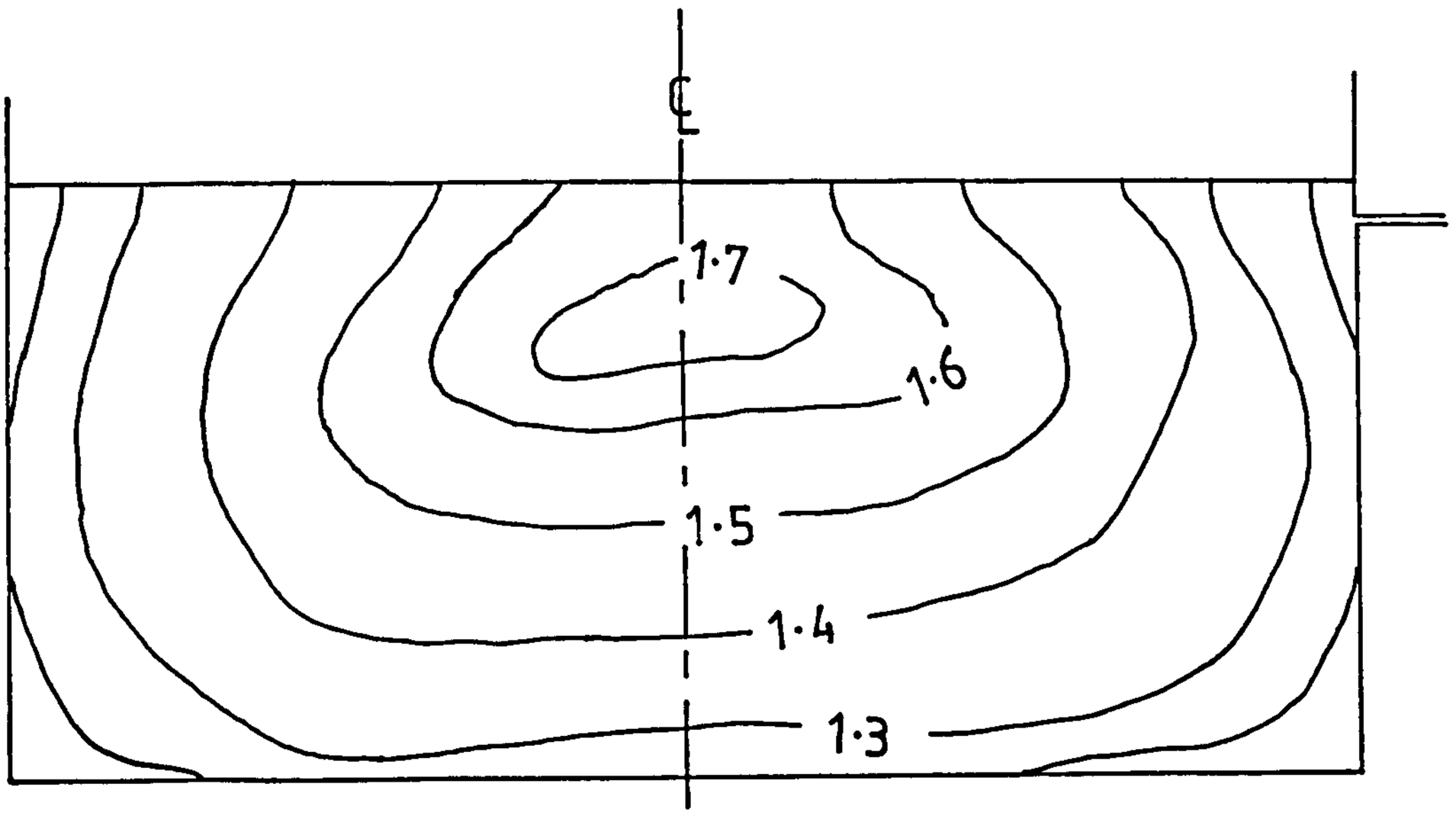

A. ISOLATED

all contours are in feet per sec.

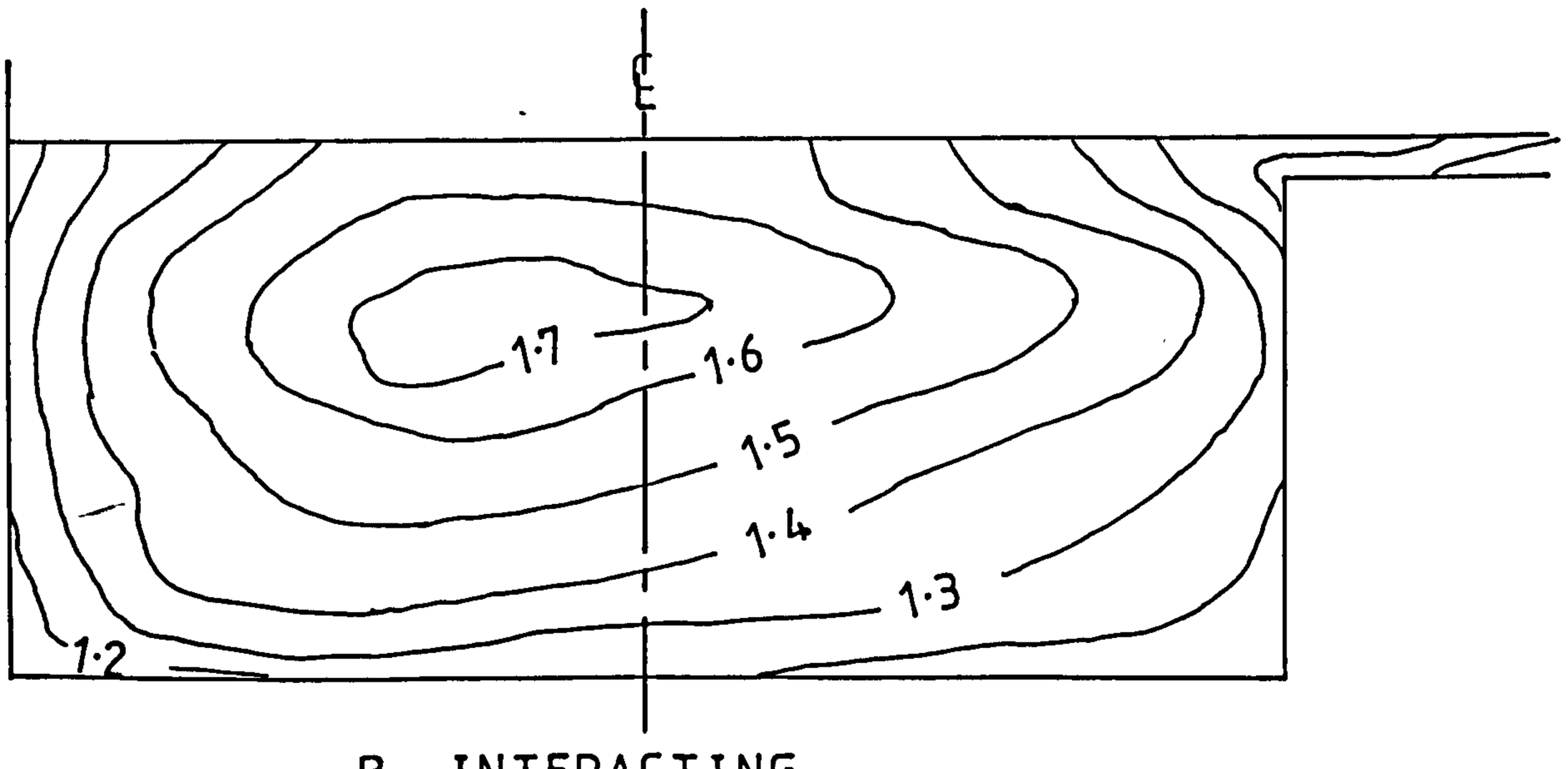

B. INTERACTING

Fig 2·8 COMPARISON OF VELOCITY TRAVERSES UNDER ISOLATED AND INTERACTING CONDITIONS. (Townsend)

Symbol	B/b
△	6·45
○	6·45
▲	3·22
●	3·22
×	3·22

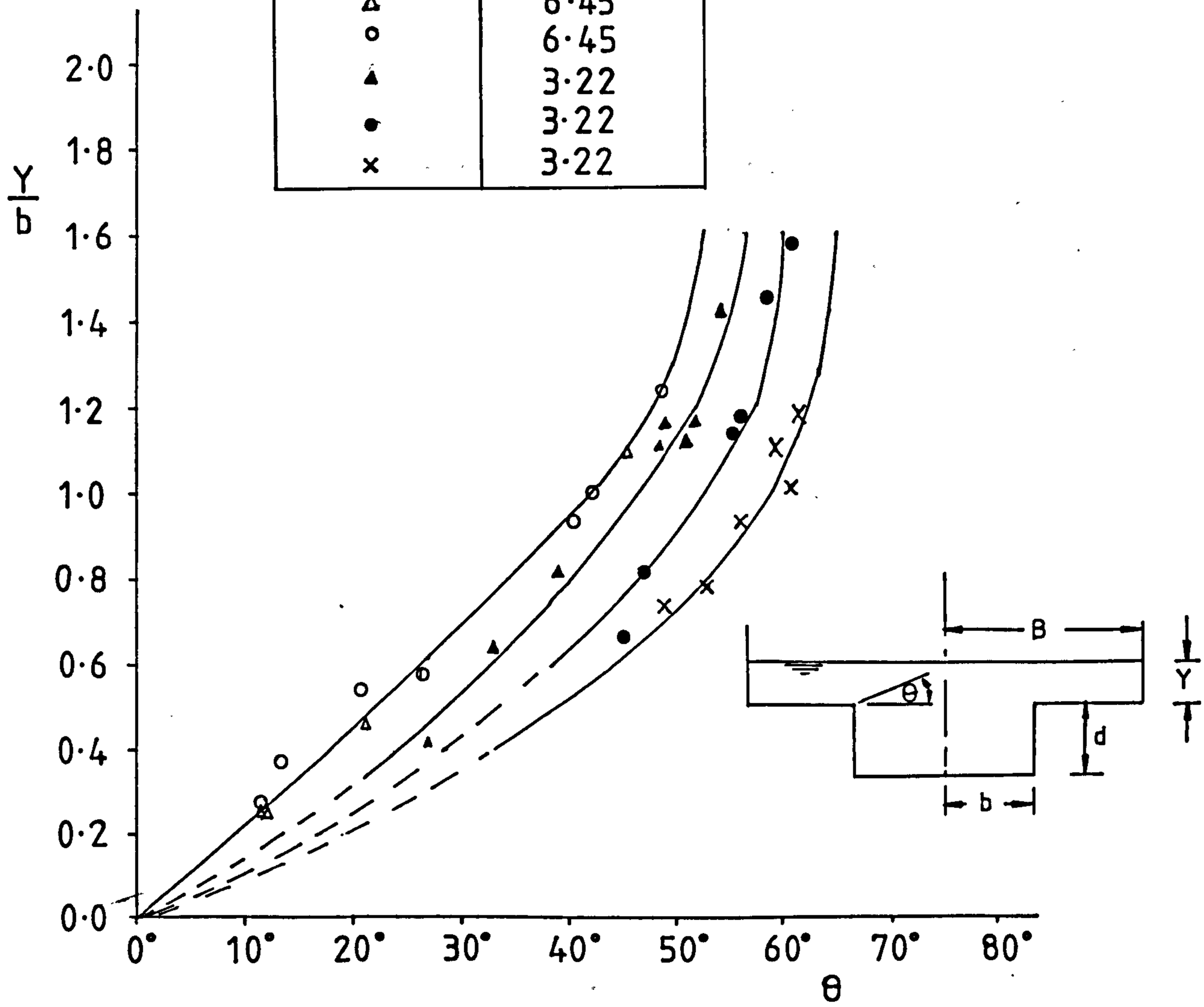

Fig 2·9 INCLINATION OF DIVISION LINES FOR TURBULENT FLOW (YEN & OVERTON)

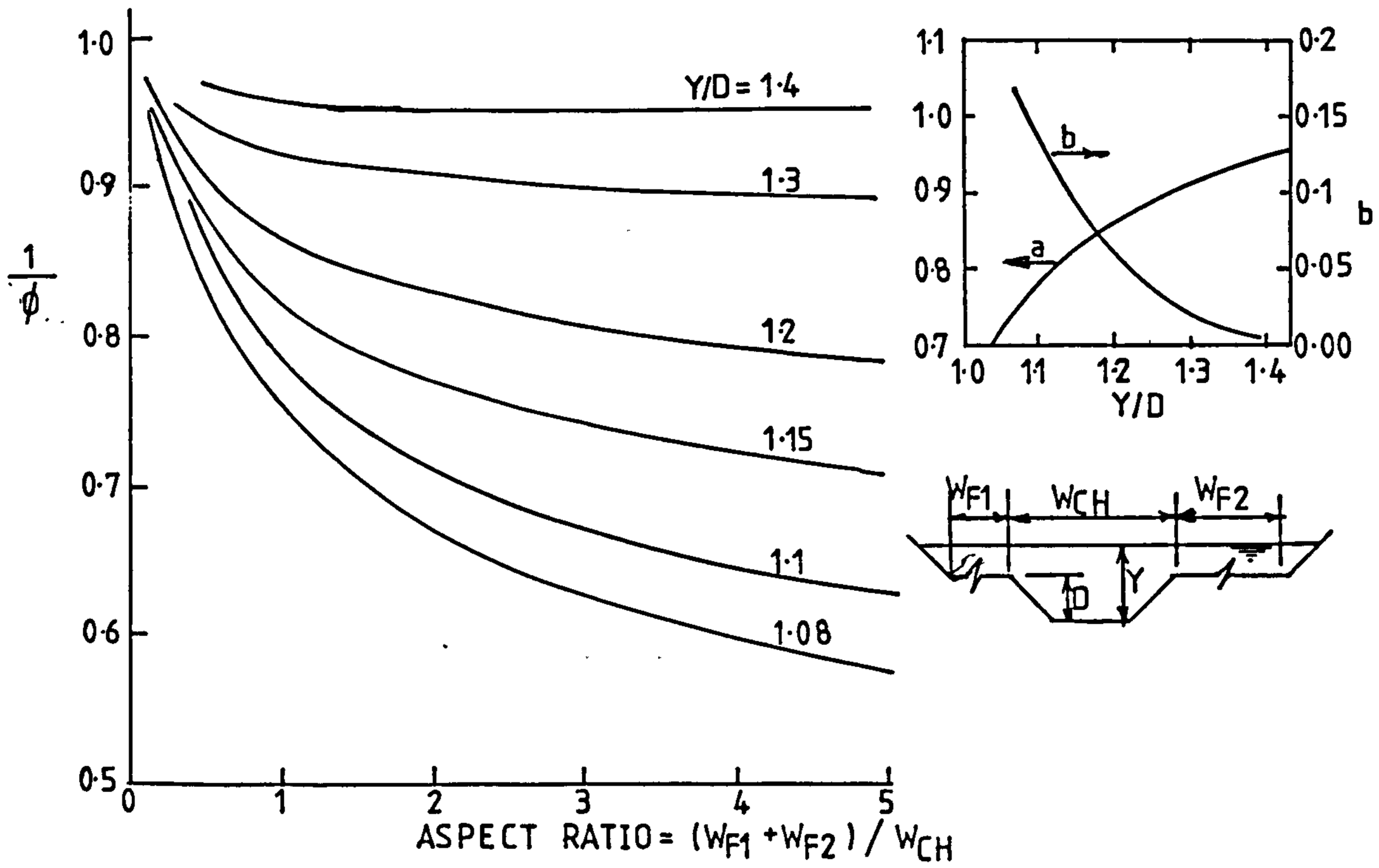

Fig 2·10 Correction factors for flood flow

(James & Brown)

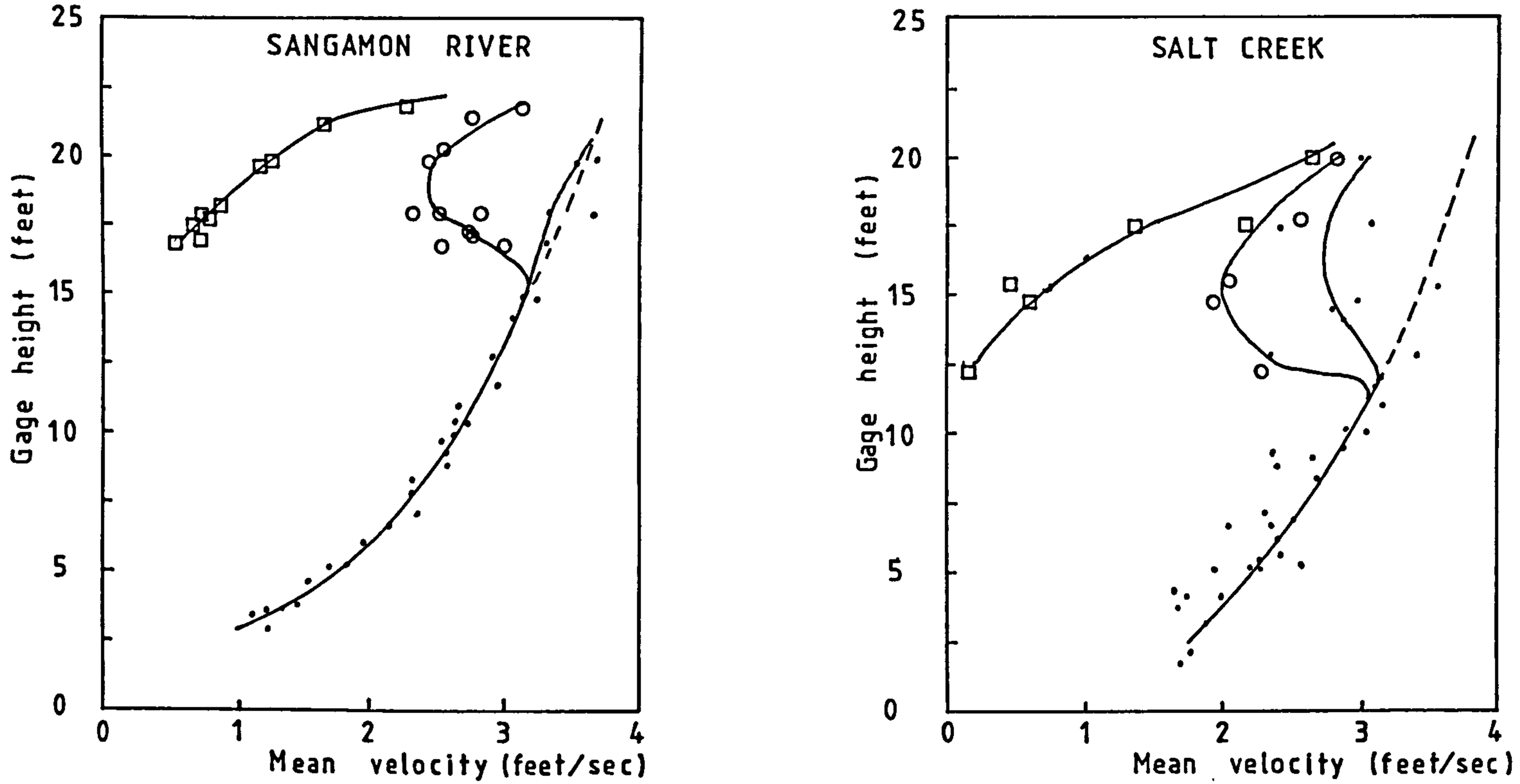

Fig 2·11 Variation of average velocity in main channel, flood plain and composite cross section with stage (Bhowmik & Demissie)

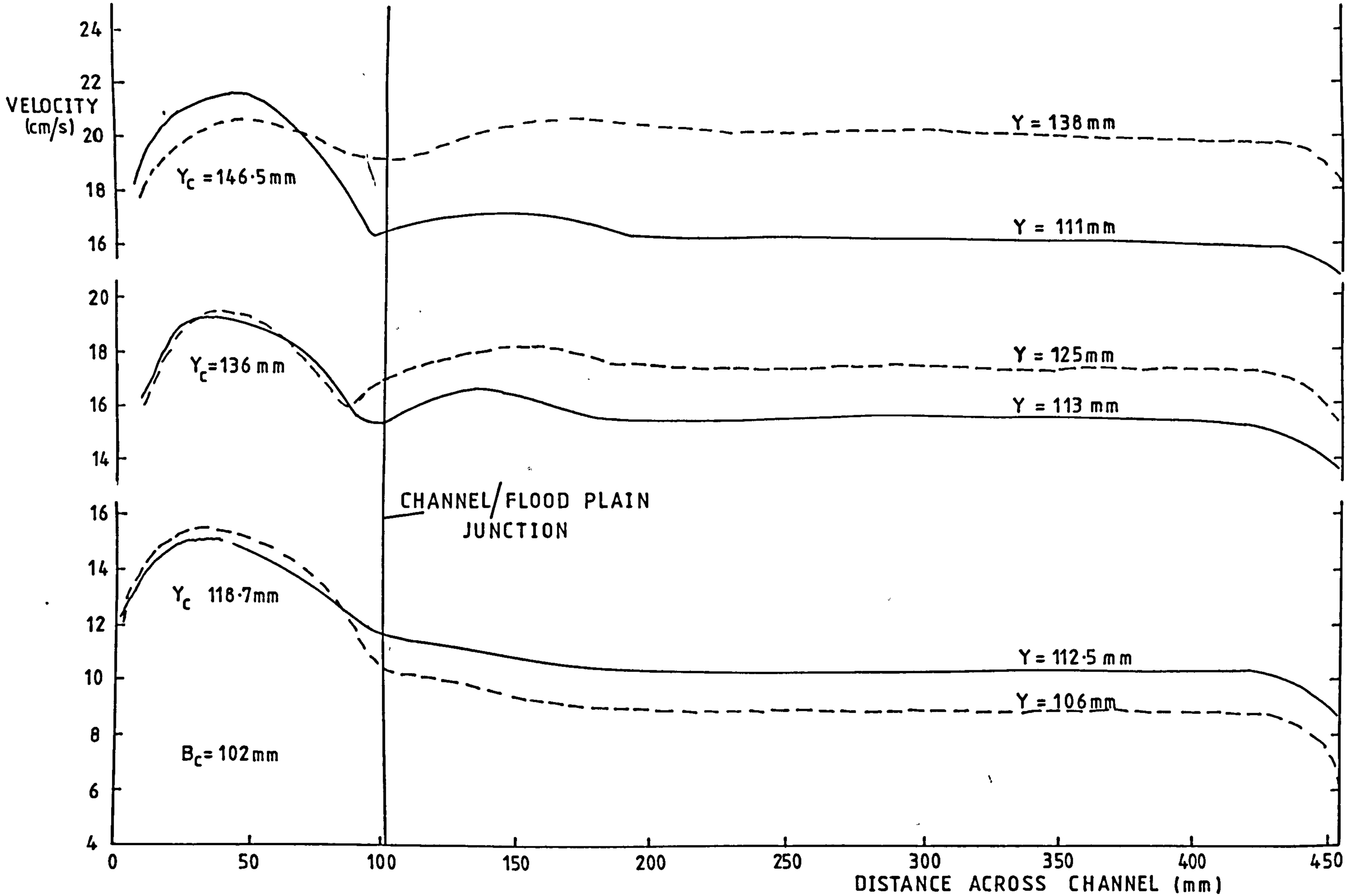

Fig 2·12 Velocity distributions at depths above flood plain bed (CRORY)

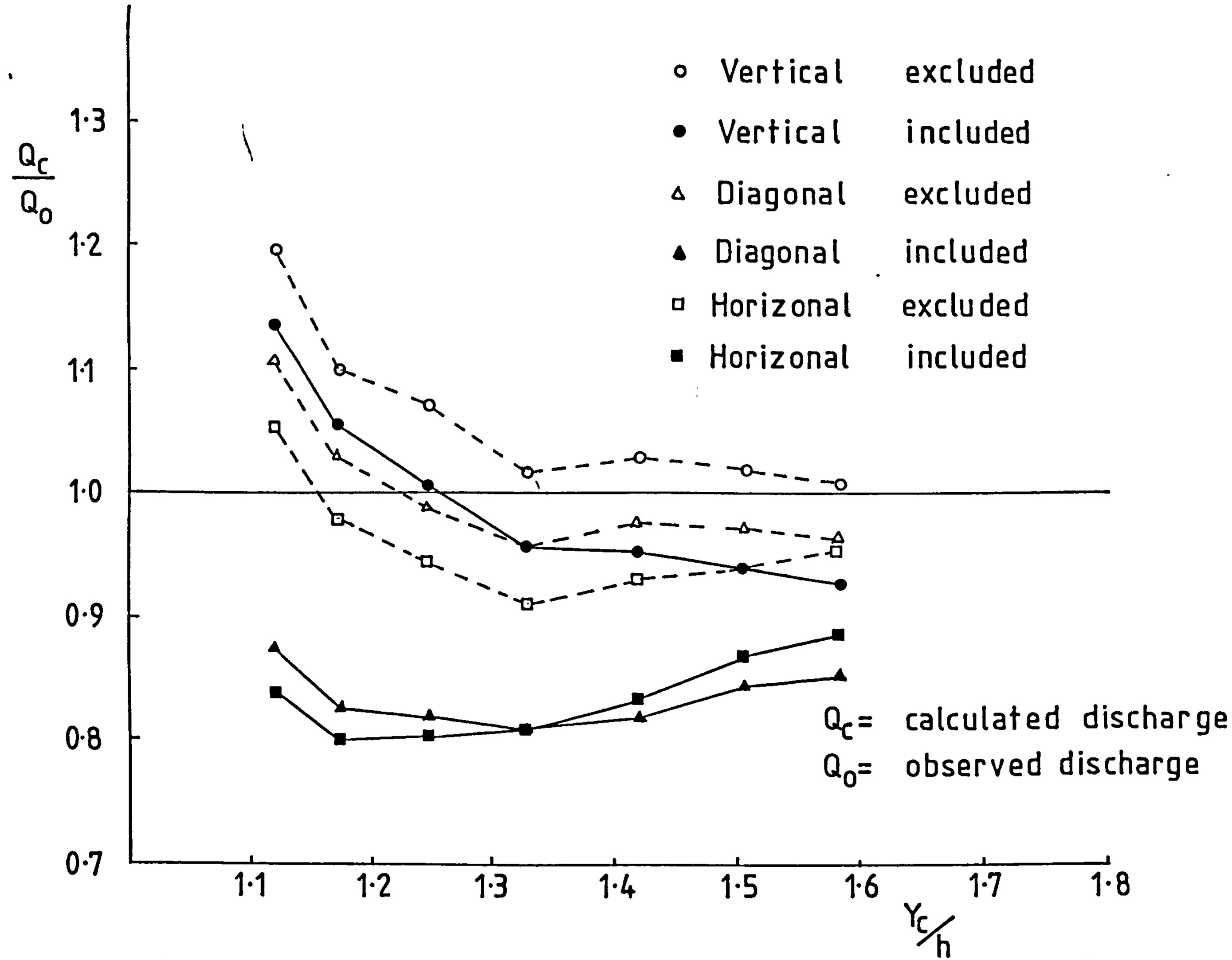

Fig 2·13 Effect of different division lines in the calculation of discharge (Wormleaton, Allen and Hadjipanos)

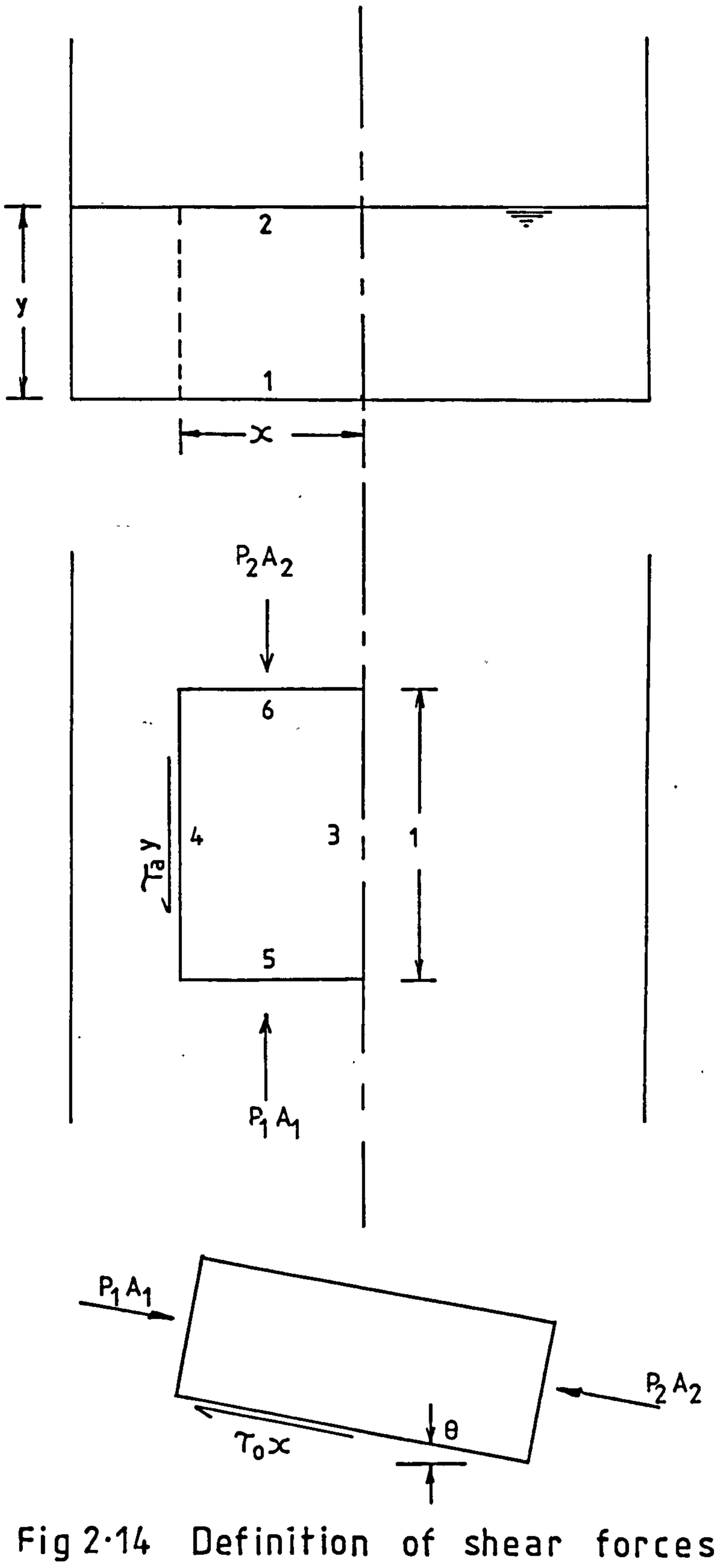

Fig 2·14 Definition of shear forces in the momentum equation (Cruff)

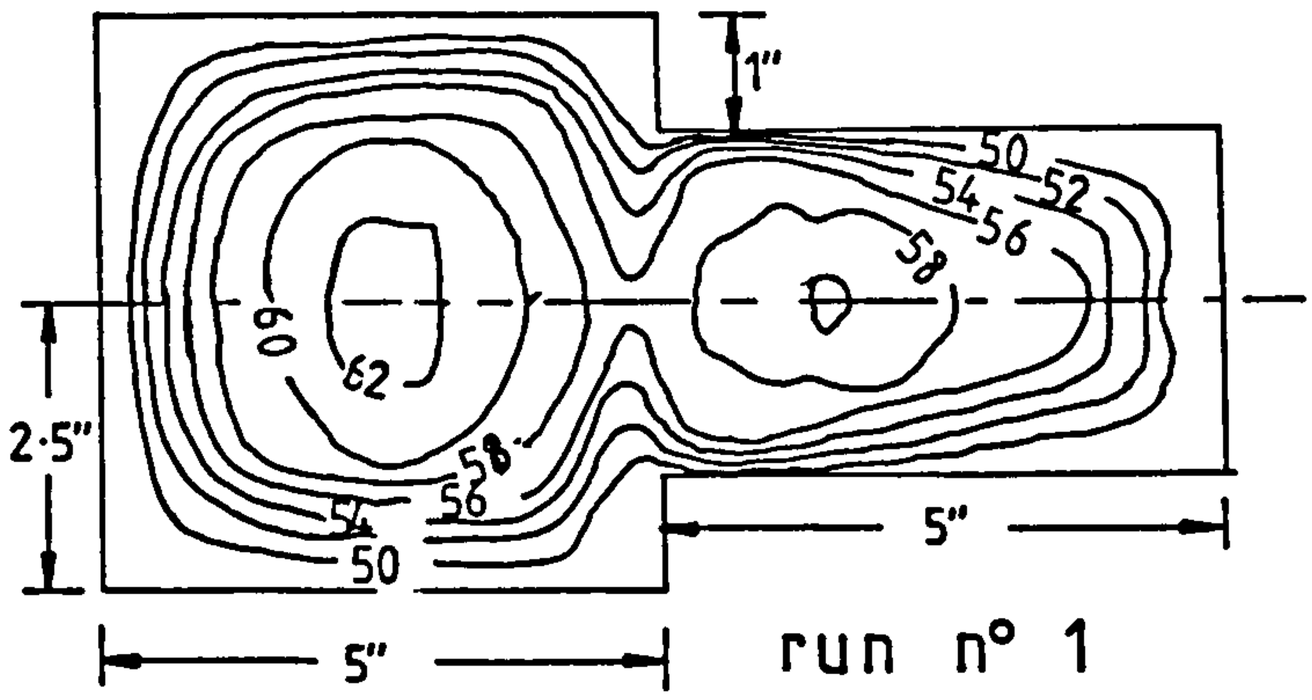

Fig2·15 CROSS SECTIONAL DIMENSIONS
AND ISOVELS (WRIGHT & CARSTENS)

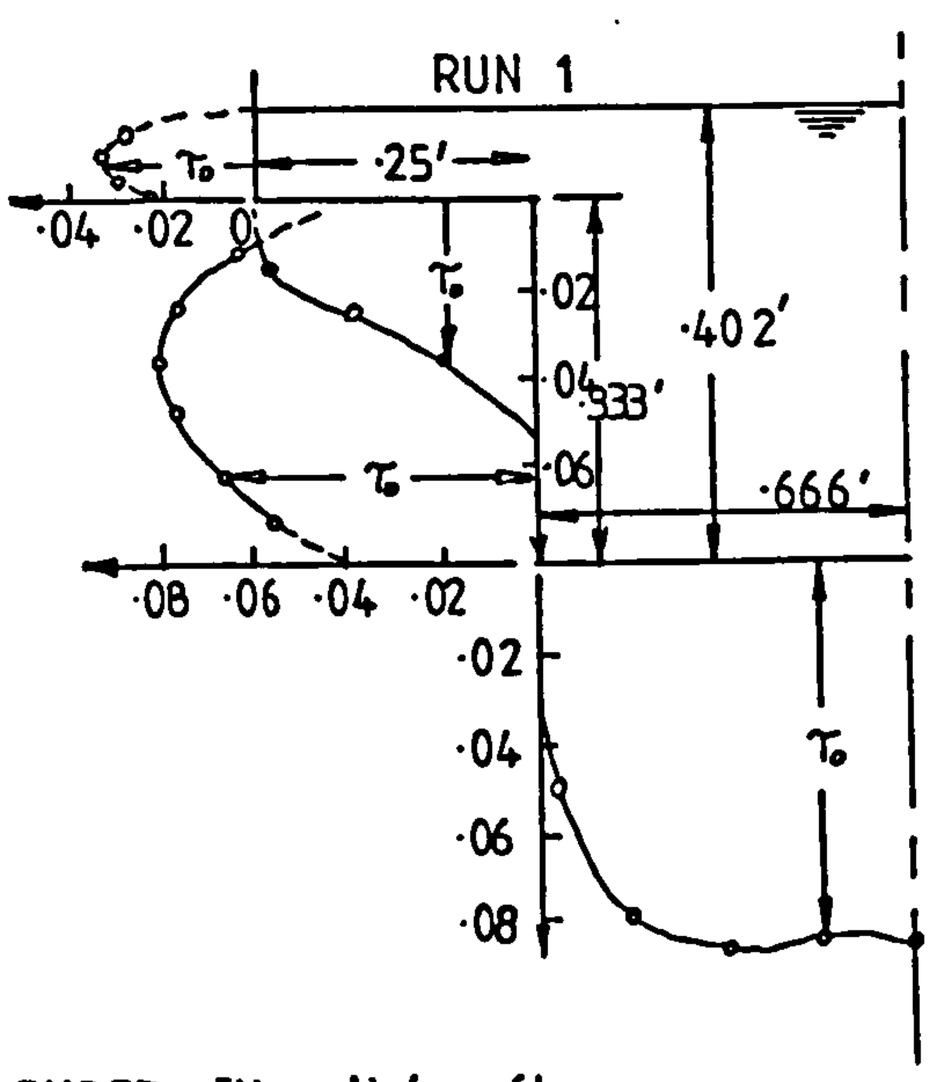

TAU IS MEASURED IN lb/sq. ft

DIMENSIONS ARE IN FEET

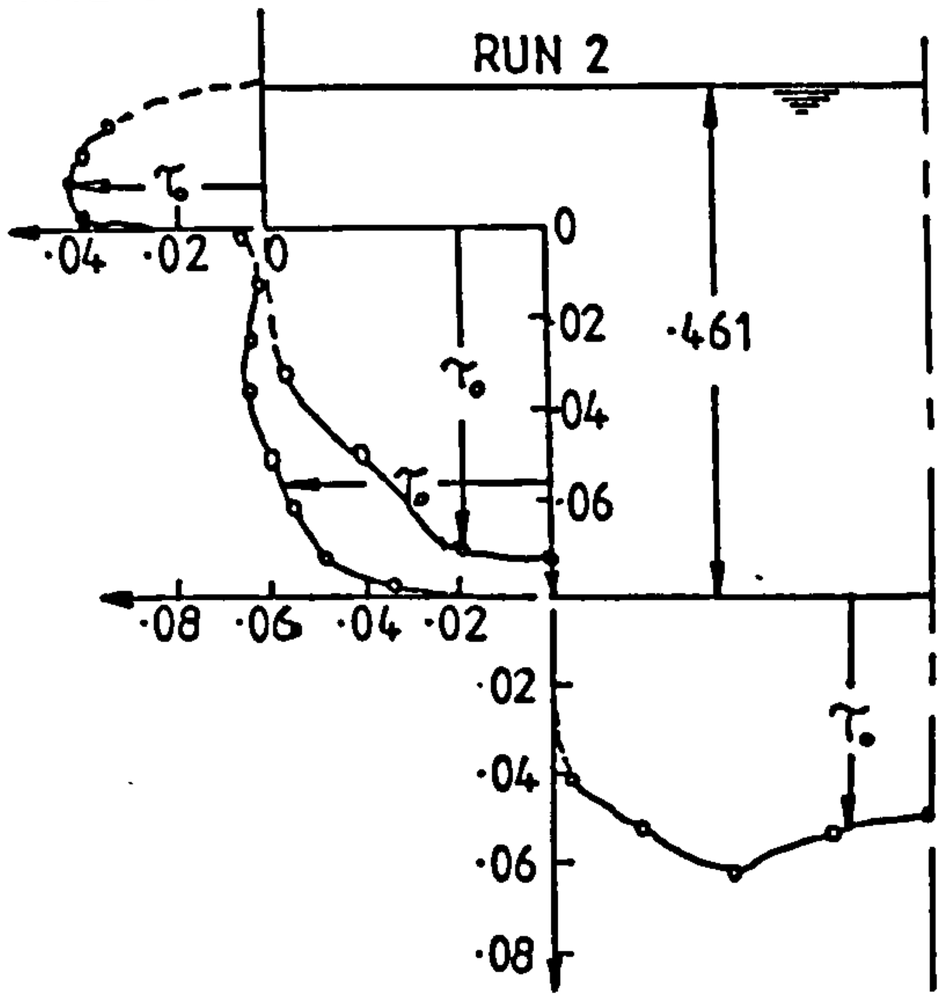

Fig 2·16 Boundary shear distribution in a compound channel (Ghosh & Jena)

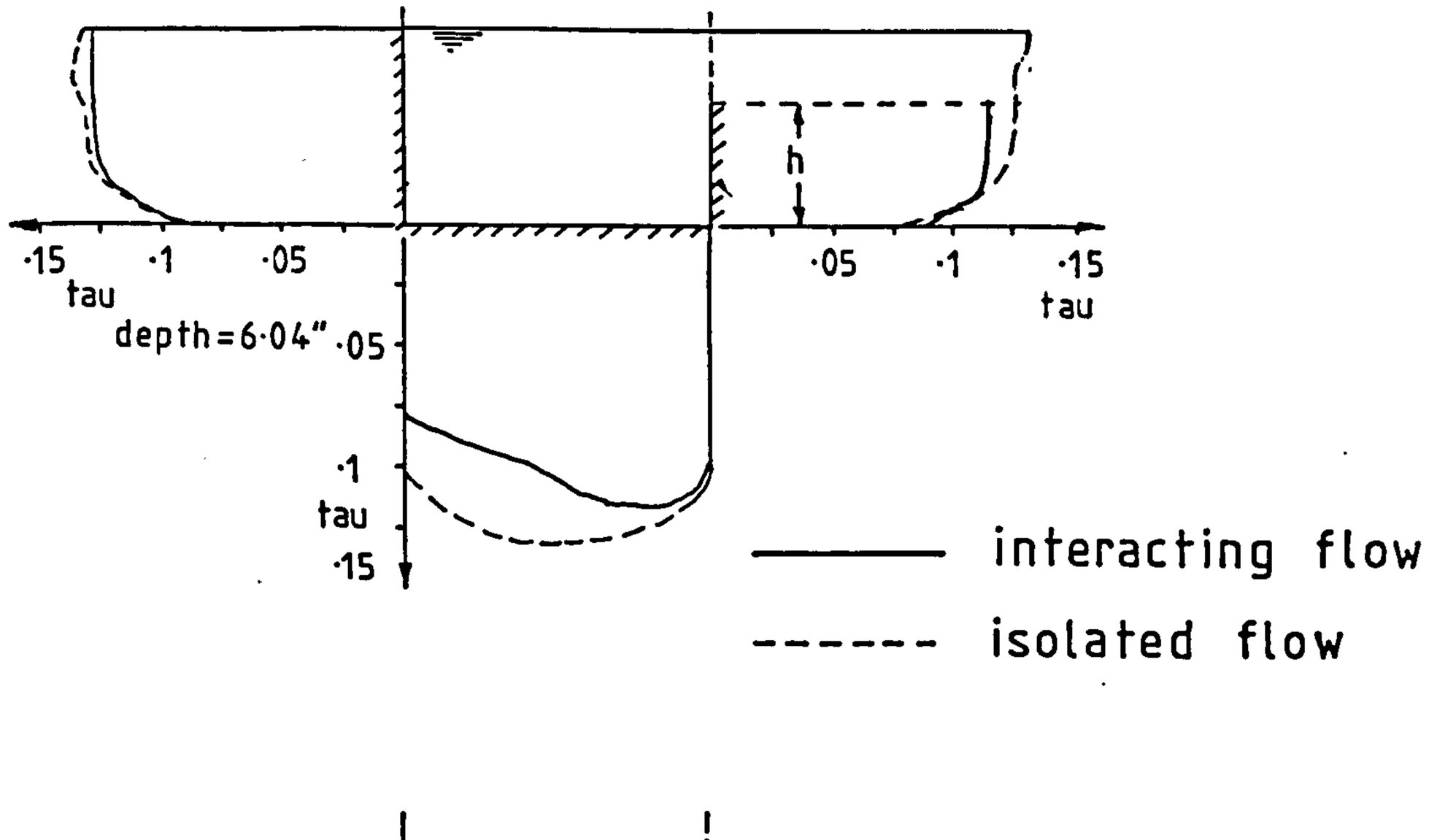

Fig 2·17 COMPARISON OF SHEAR DISTRIBUTIONS IN CHANNEL UNDER ISOLATED AND INTERACTING CONDITIONS (MYERS & ELSAWY)

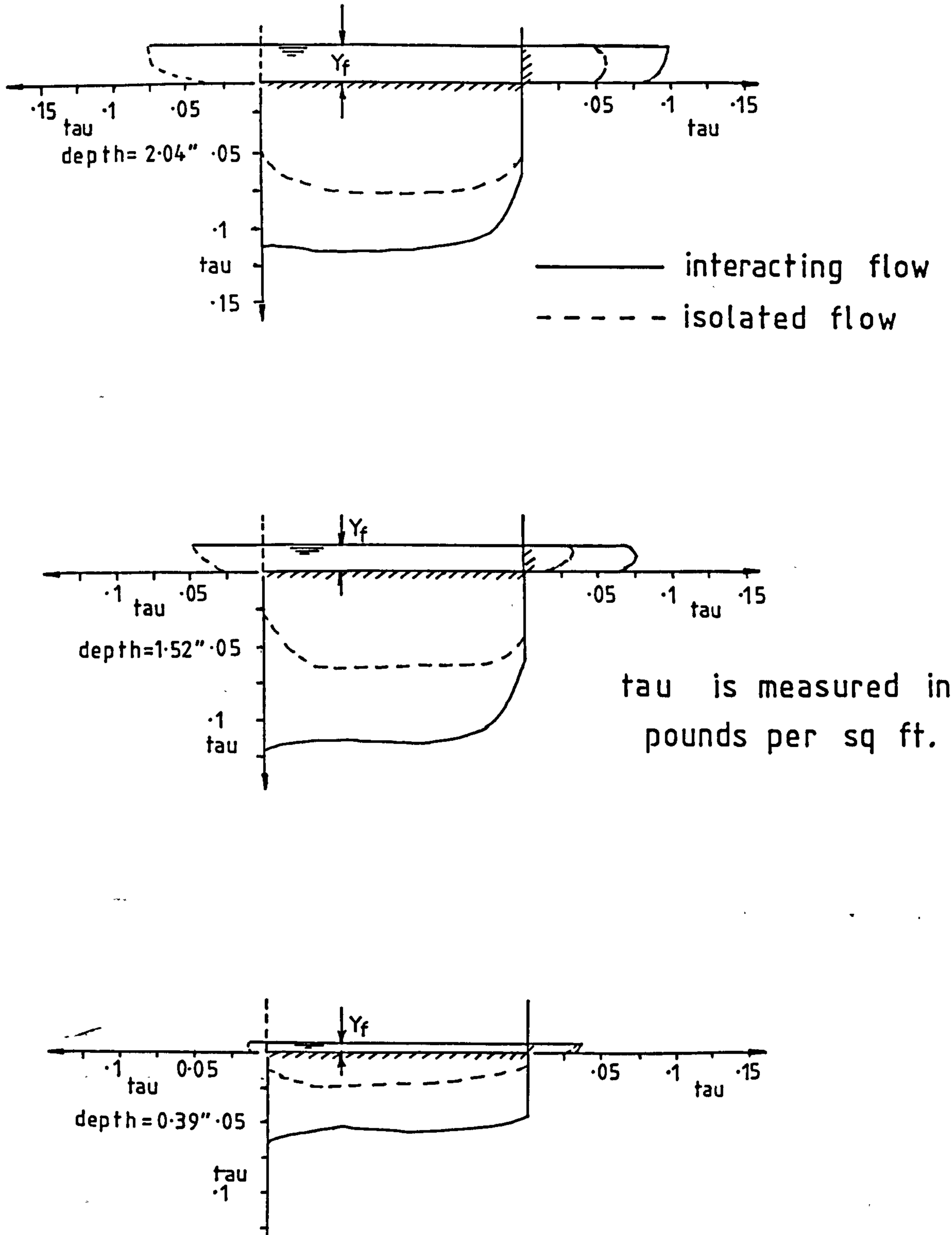

Fig 2·18 COMPARISON OF FLOOD PLAIN SHEAR DISTRIBUTIONS UNDER ISOLATED AND INTERACTING CONDITIONS (MYERS & ELSAWY)

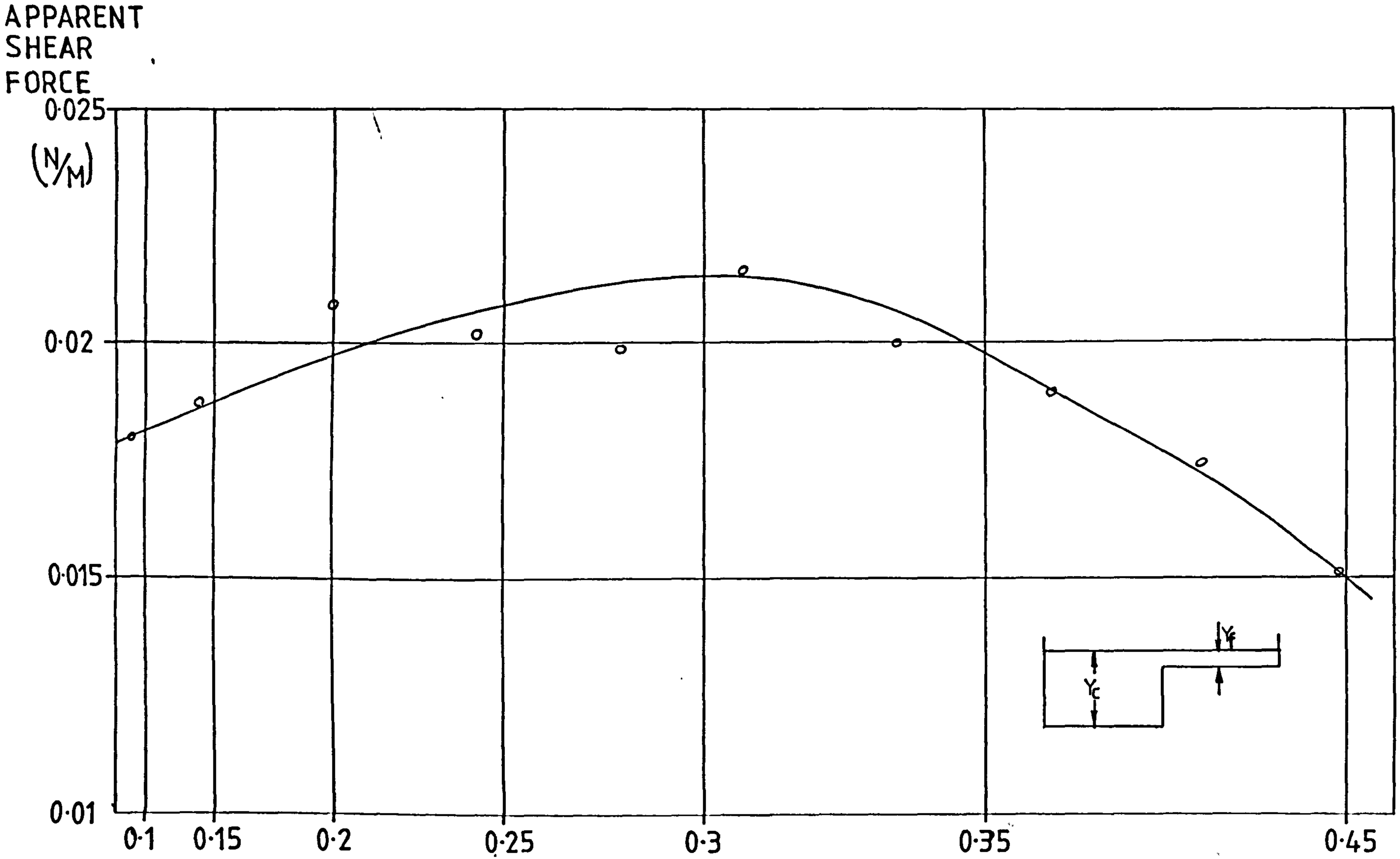

Fig 2·19 APPARENT SHEAR FORCE VERSES RELATIVE DEPTH (MYERS)

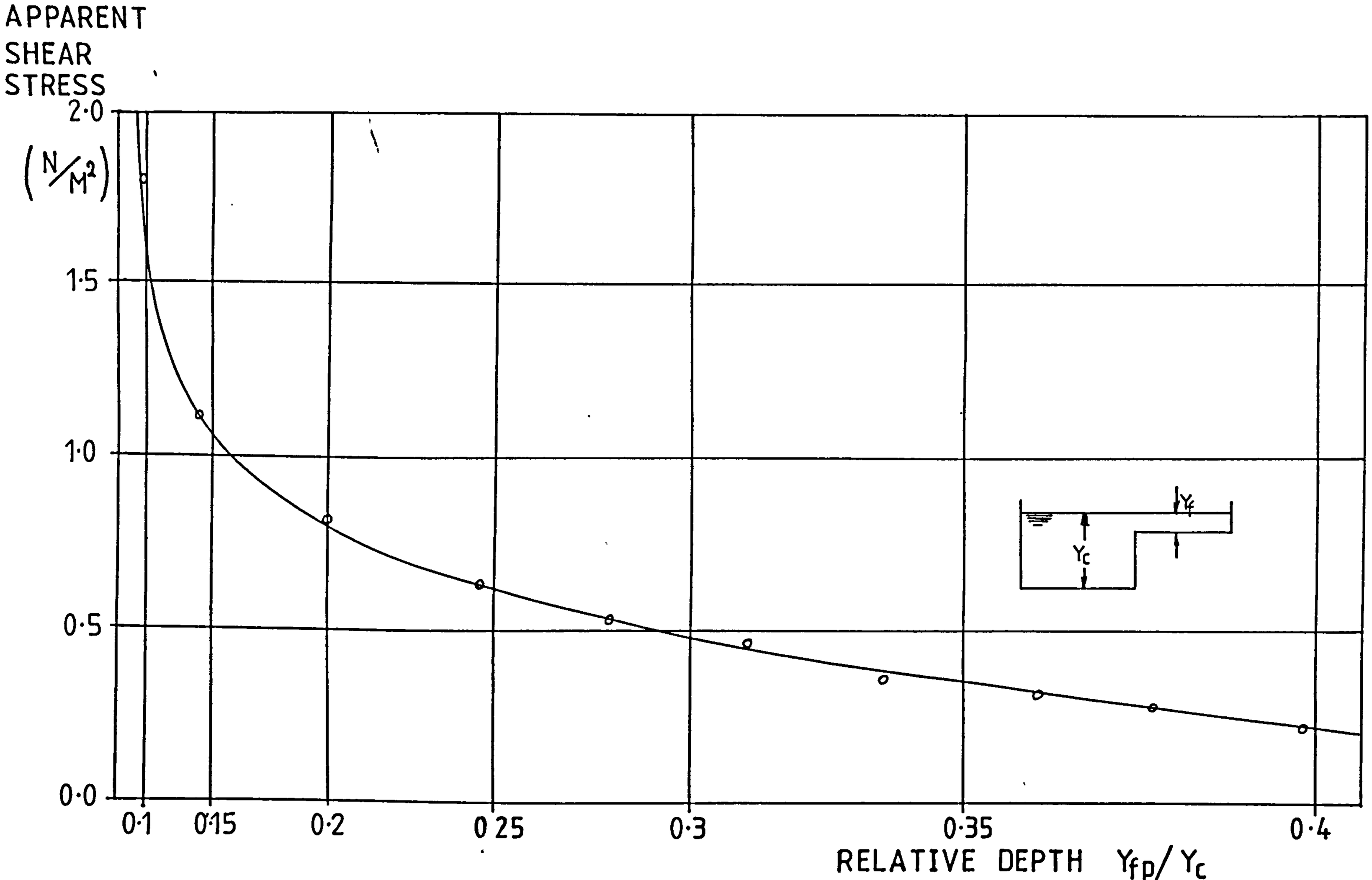

Fig 2·20 APPARENT SHEAR STRESS VERSES RELATIVE DEPTH (MYERS)

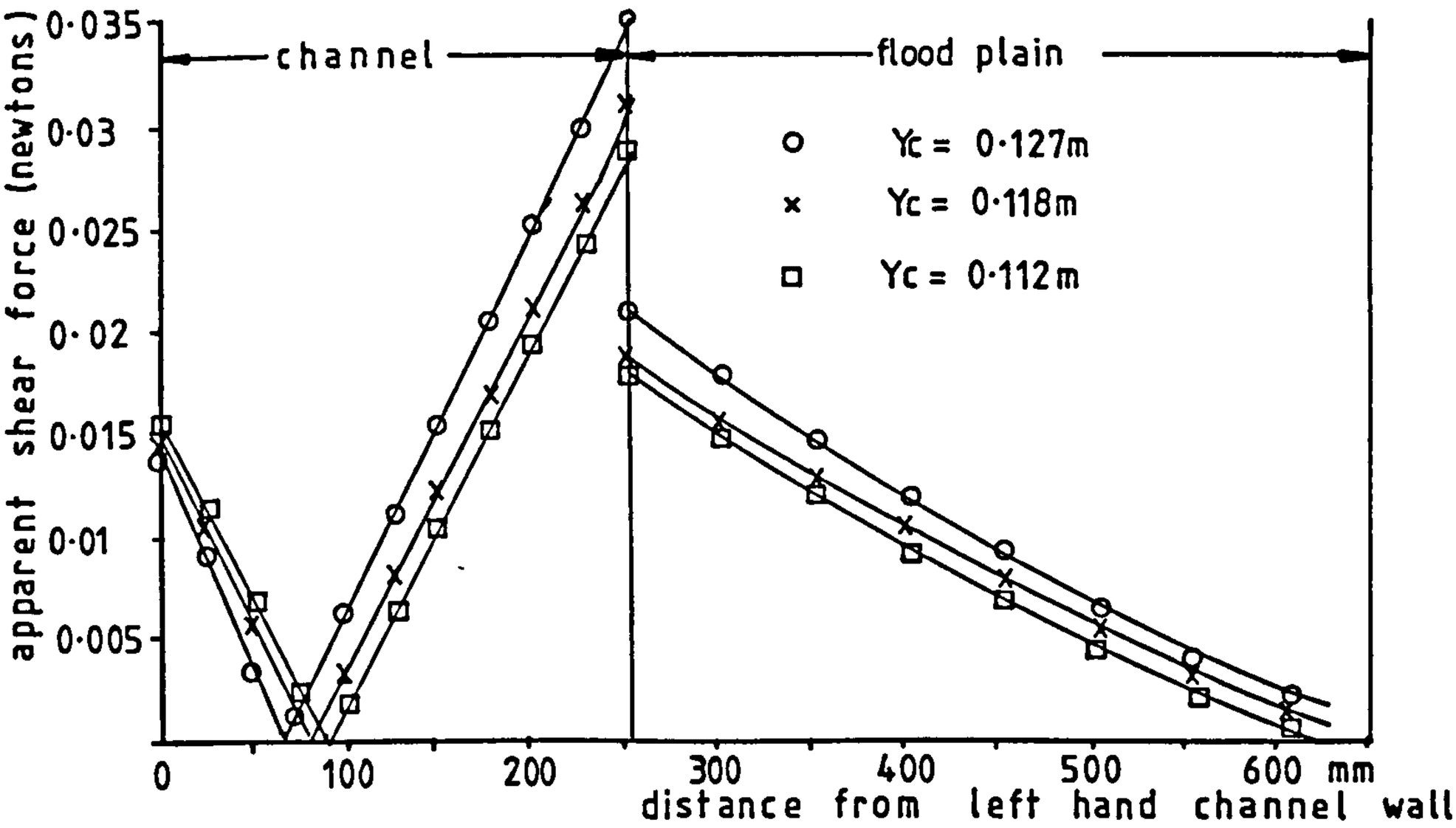

(a) Apparent shear force at interfaces throughout the full cross-section.

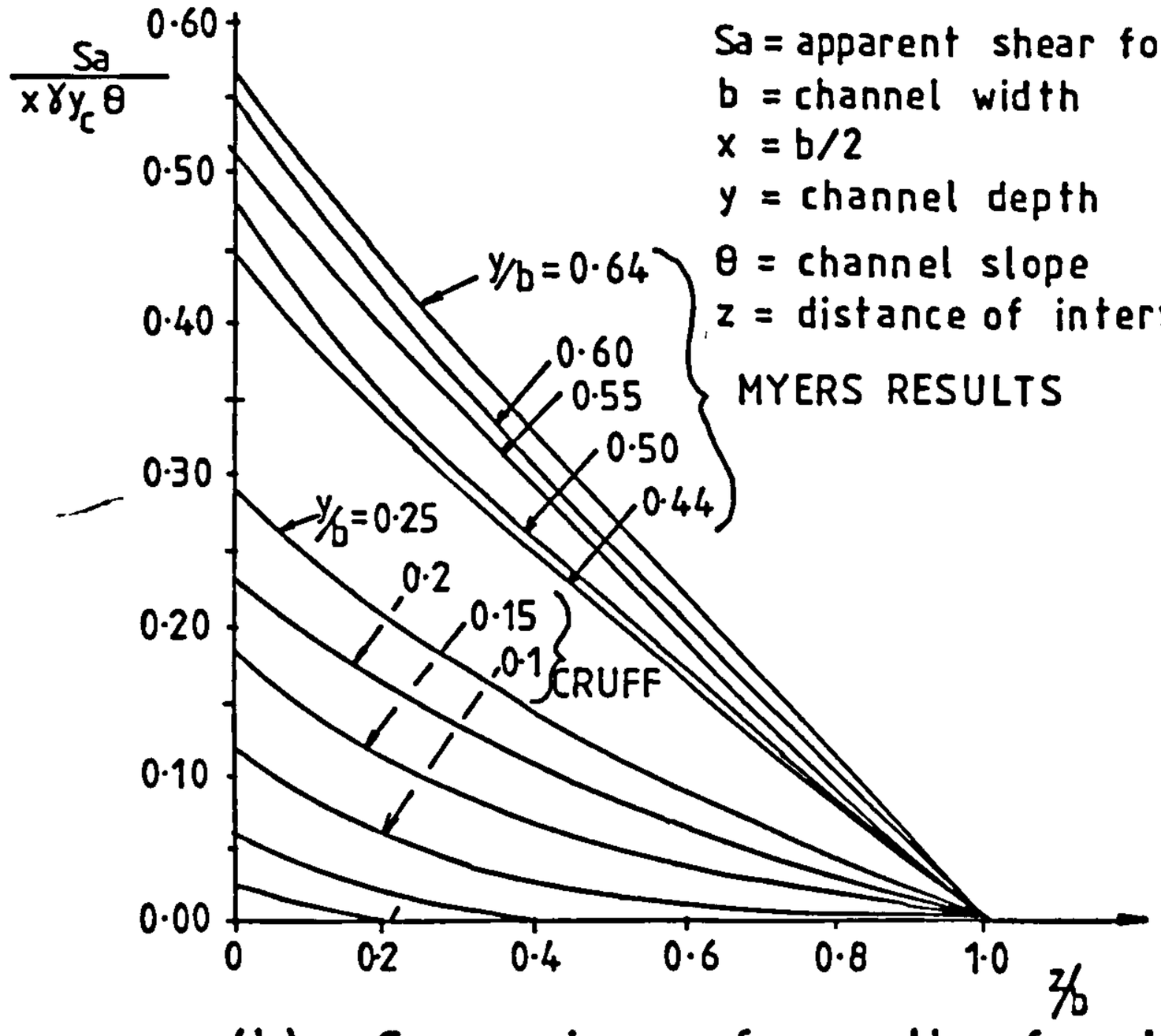

(b) Comparison of results for isolated case with Cruff's

Fig 2·21 (MYERS)

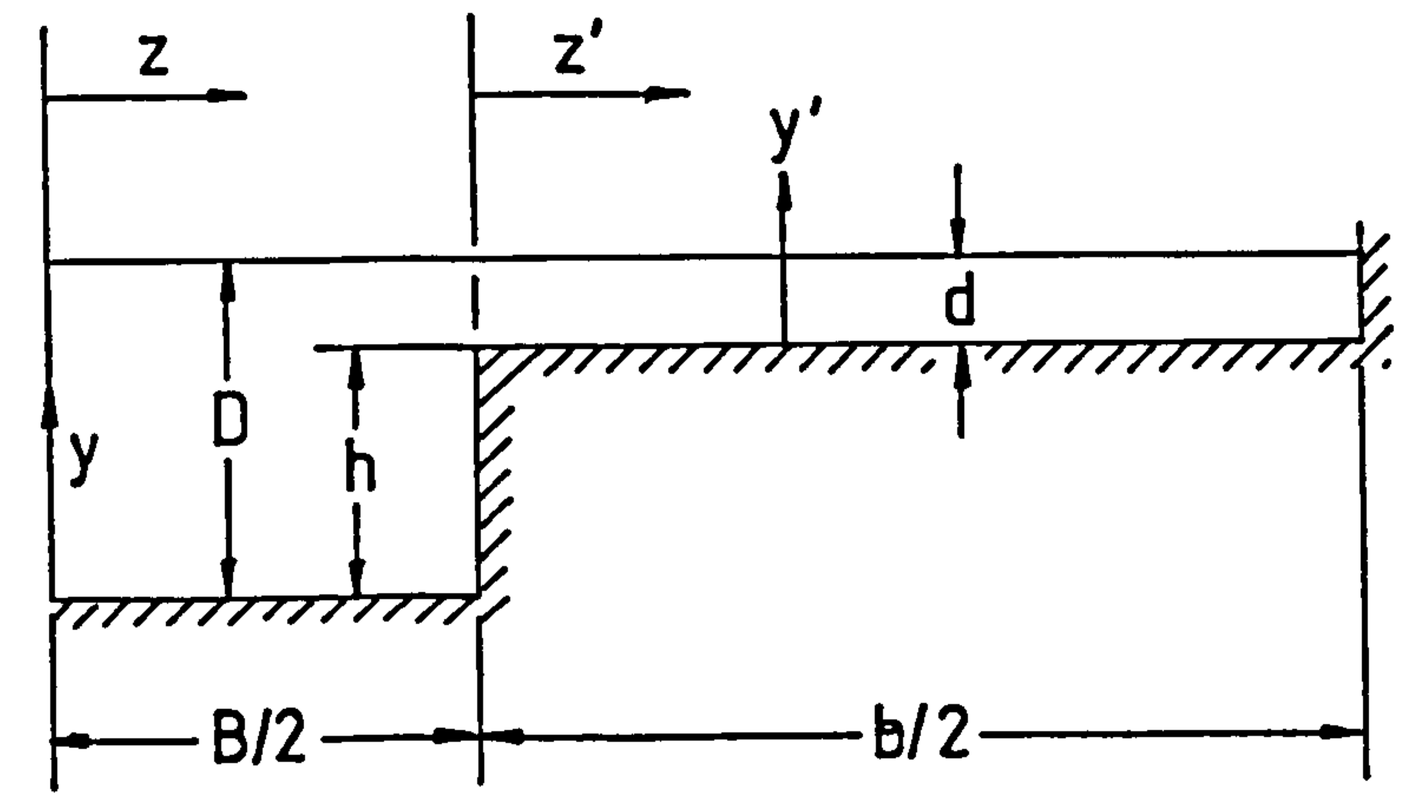

(a) (half) Sectional view

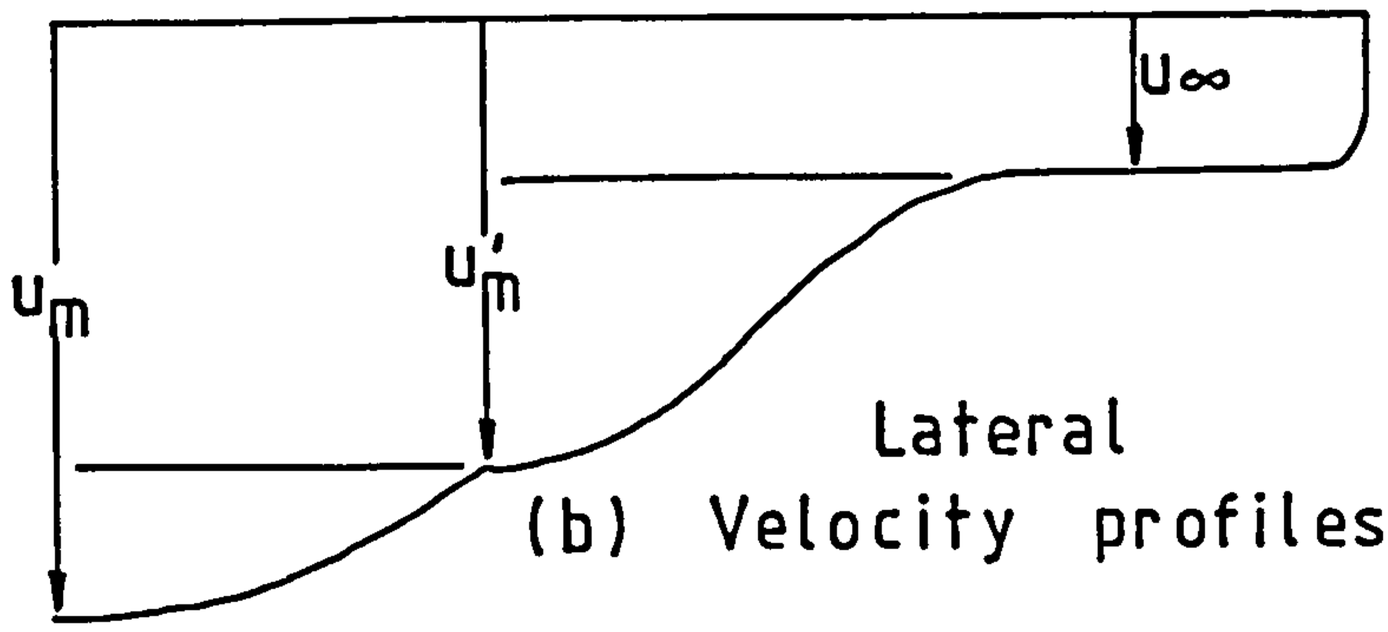

Lateral

(b) Velocity profiles

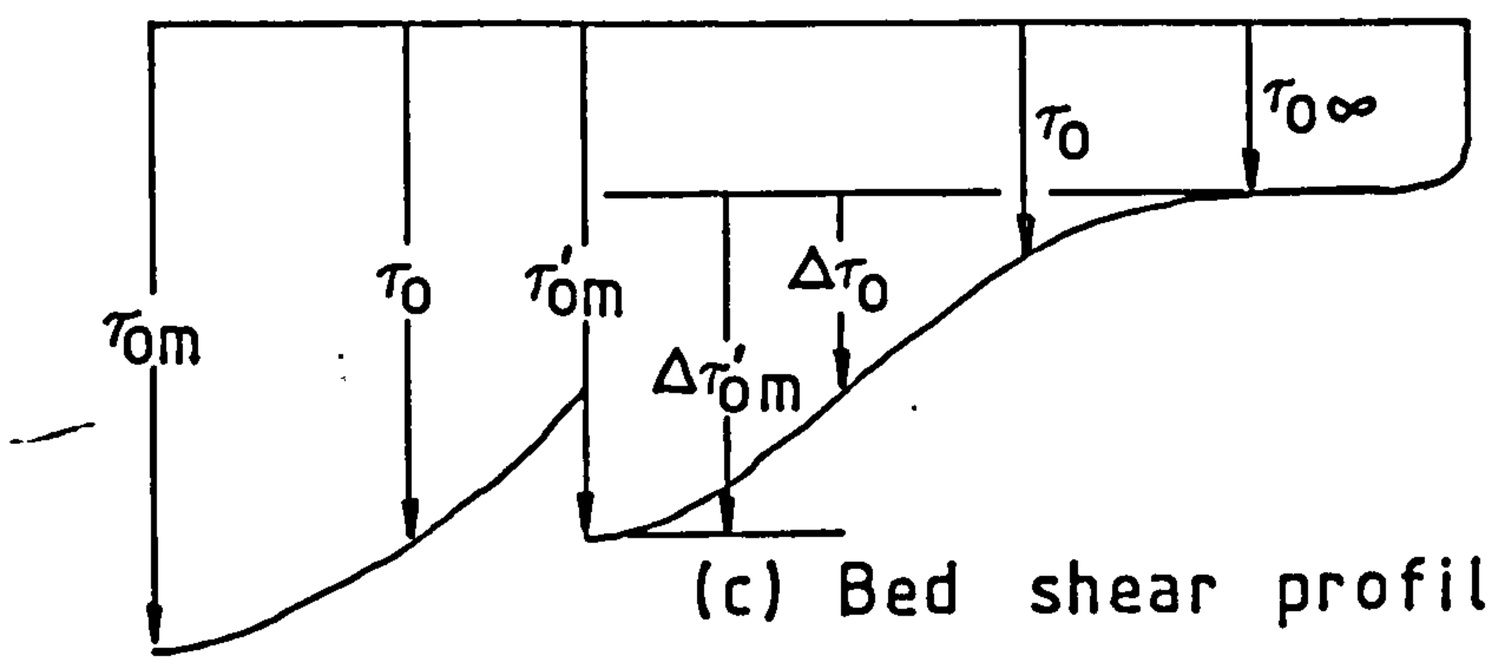

(c) Bed shear profiles

Fig 2·22 DEFINITION SKETCHES (RAJARATNAM & AHMADI)

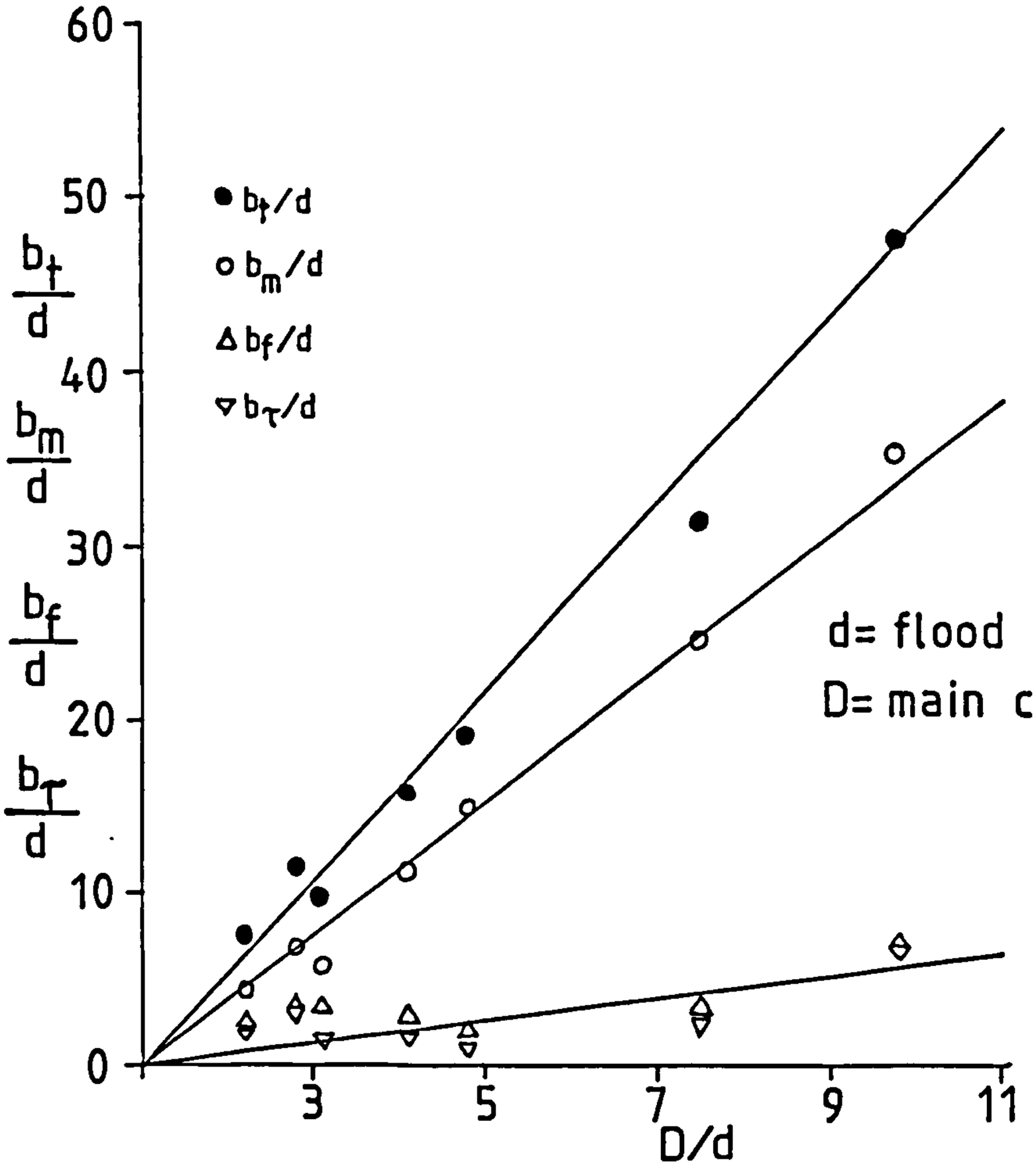

Fig2·23 STUDY OF LENGTH SCALES
(RAJARATNAM AND AHMADI)

$$\tau_{av} = 13{\cdot}84\left(\frac{h}{y_c}\right)^{3{\cdot}123} \cdot (\Delta V)^{0{\cdot}882} \cdot \left(\frac{B_c}{B_f}\right)^{0{\cdot}727}$$

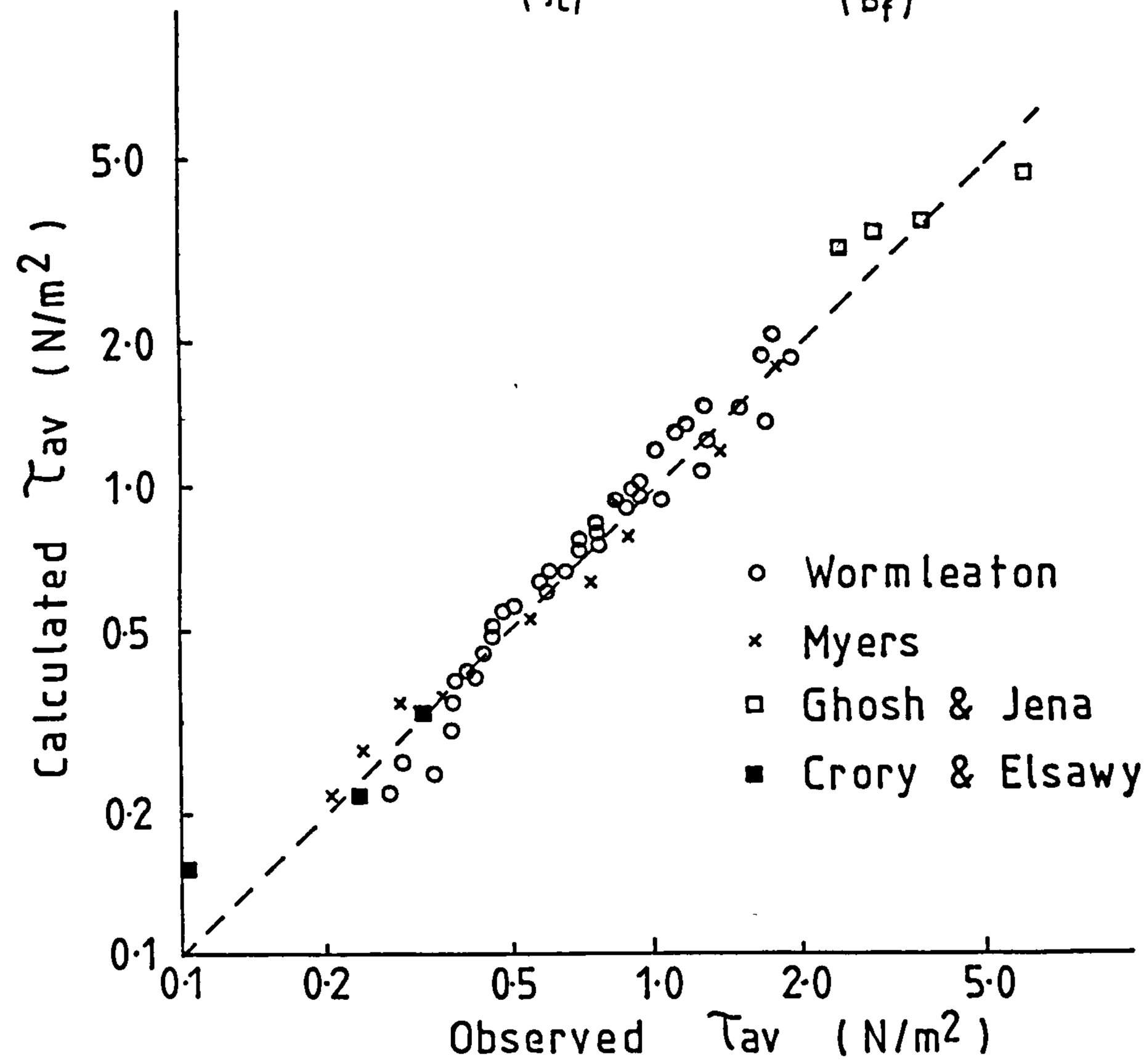

Fig 2·24 Proposed method of estimating τ_{av} (Wormleaton, Allen & Hadjipanos)

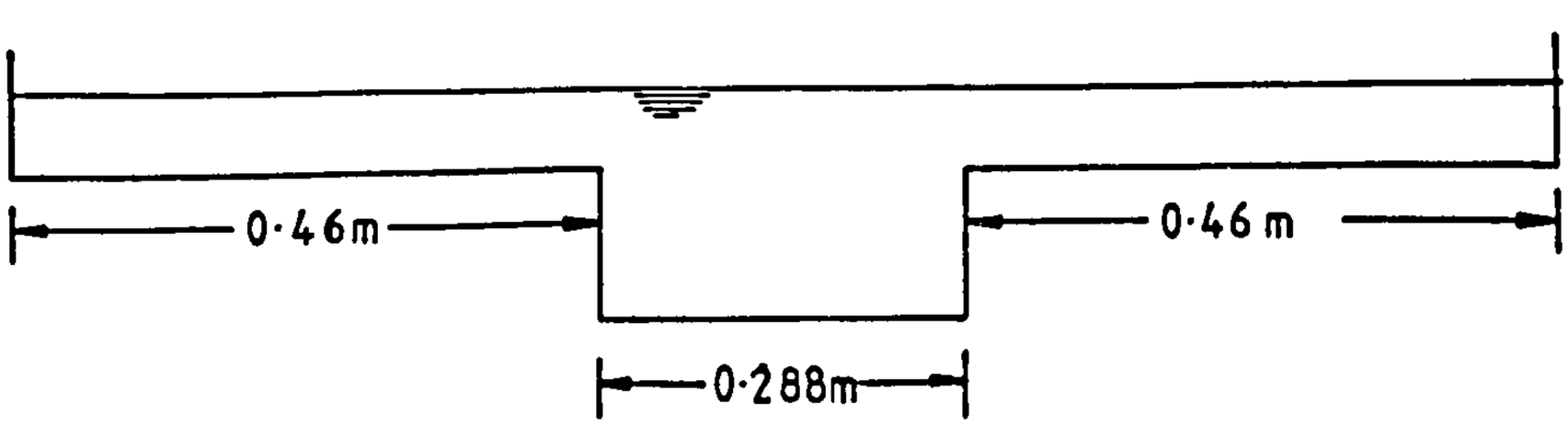

Symbol	B_f/B_c	Symbol
△	1·40	▲
X	1·75	✳
□	2·33	■
○	3·50	●

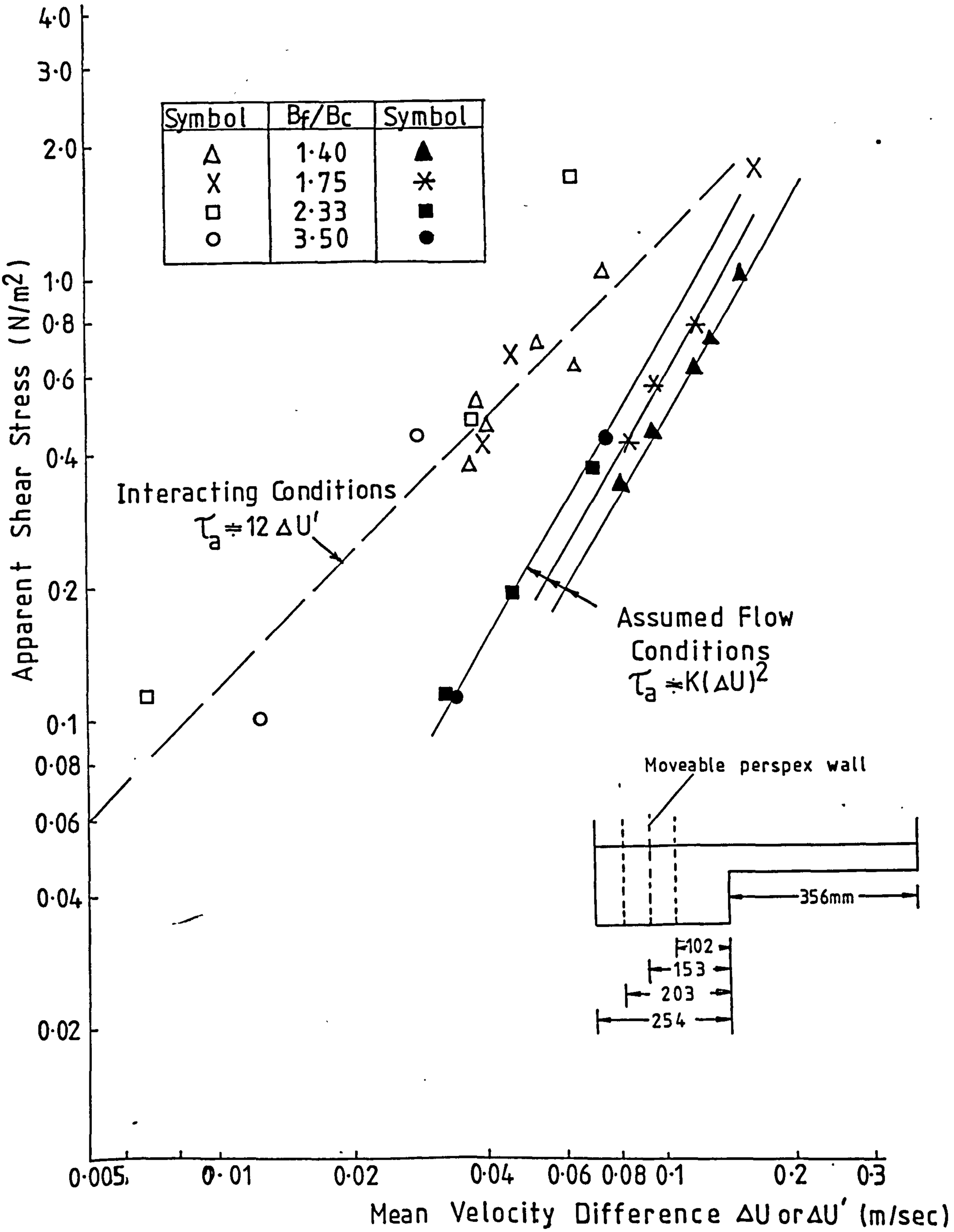

Fig 2·25 Relationship between apparent shear stress and mean velocity differences under isolated and assumed flow conditions (Crory)[106]

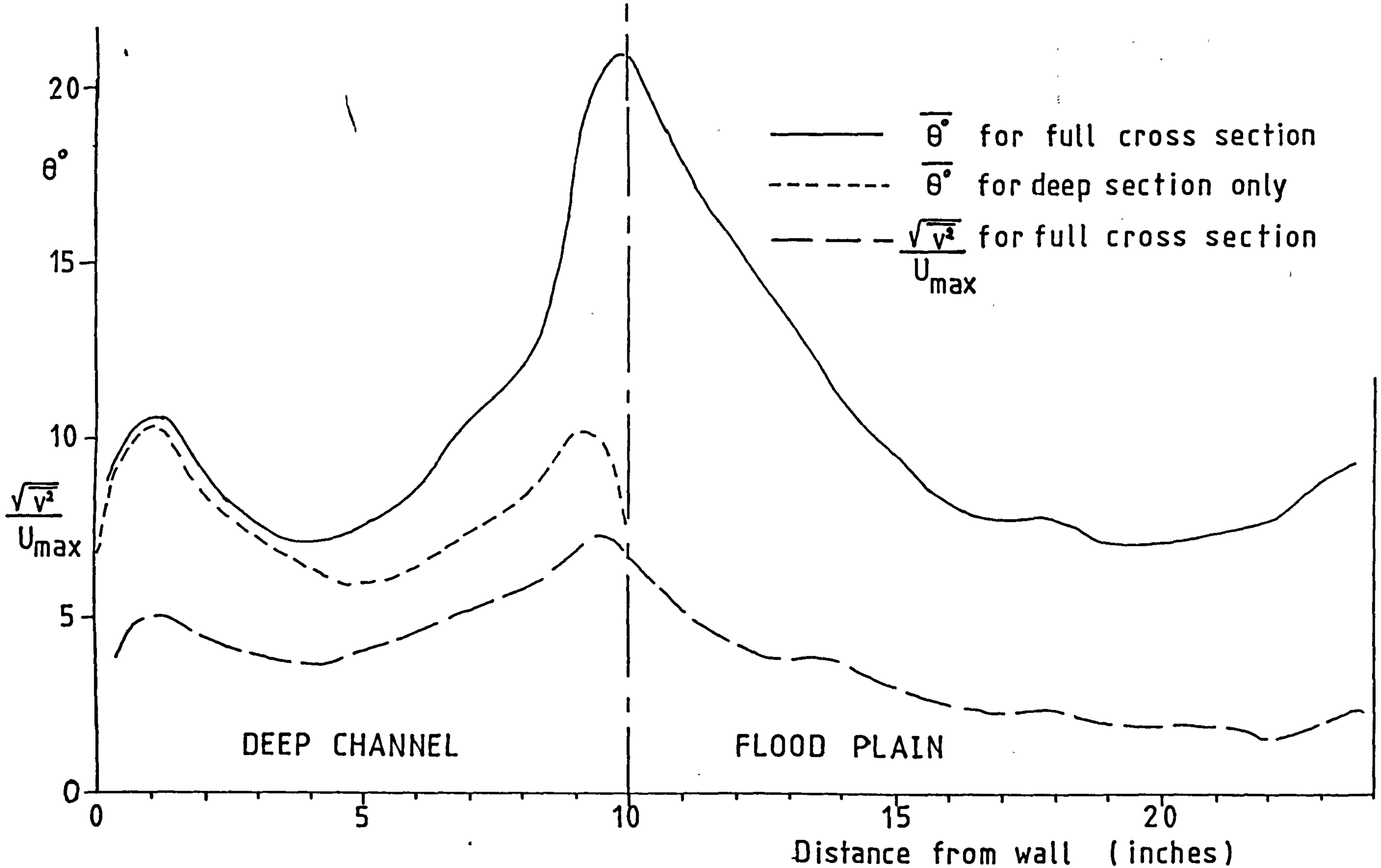

Fig2·26 A PLOT OF CONE ANGLE VALUES WITH CORRESPONDING VALUES OF $\sqrt{\overline{v^2}}/U_{max}$ (TOWNSEND)

SYMBOL	d (ins)	Re_f/Re_c
———	0·3	0·042
— — —	0·5	0·071
- - - - - -	1·0	0·181

d = depth of flow in flood plain

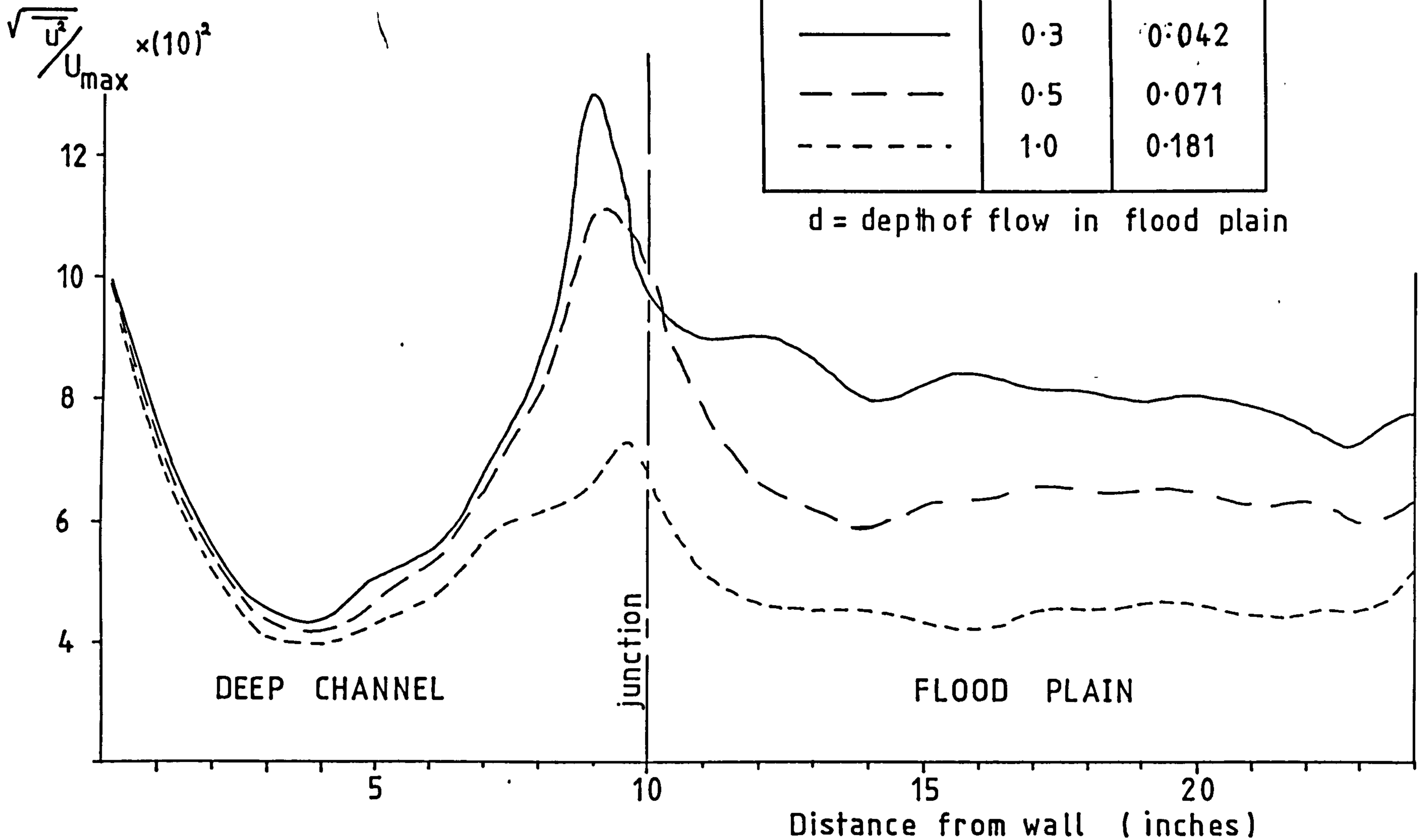

Fig 2·27 THE EFFECT OF AN INCREASE IN THE REYNOLDS No RATIO ON THE TURBULENCE INTENSITY IN THE DIRECTION OF FLOW (TOWNSEND)

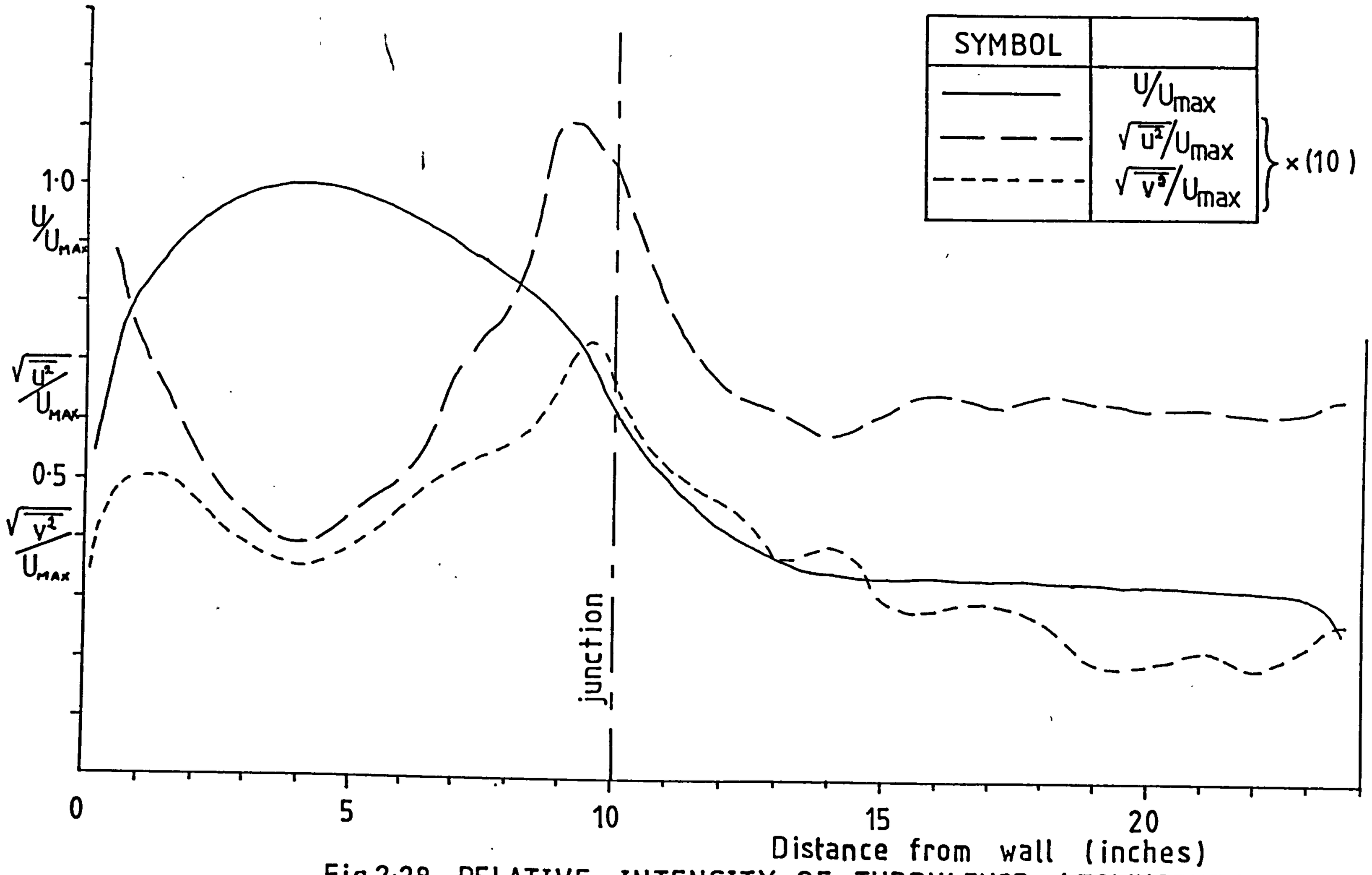

Fig 2·28 RELATIVE INTENSITY OF TURBULENCE (TOWNSEND)

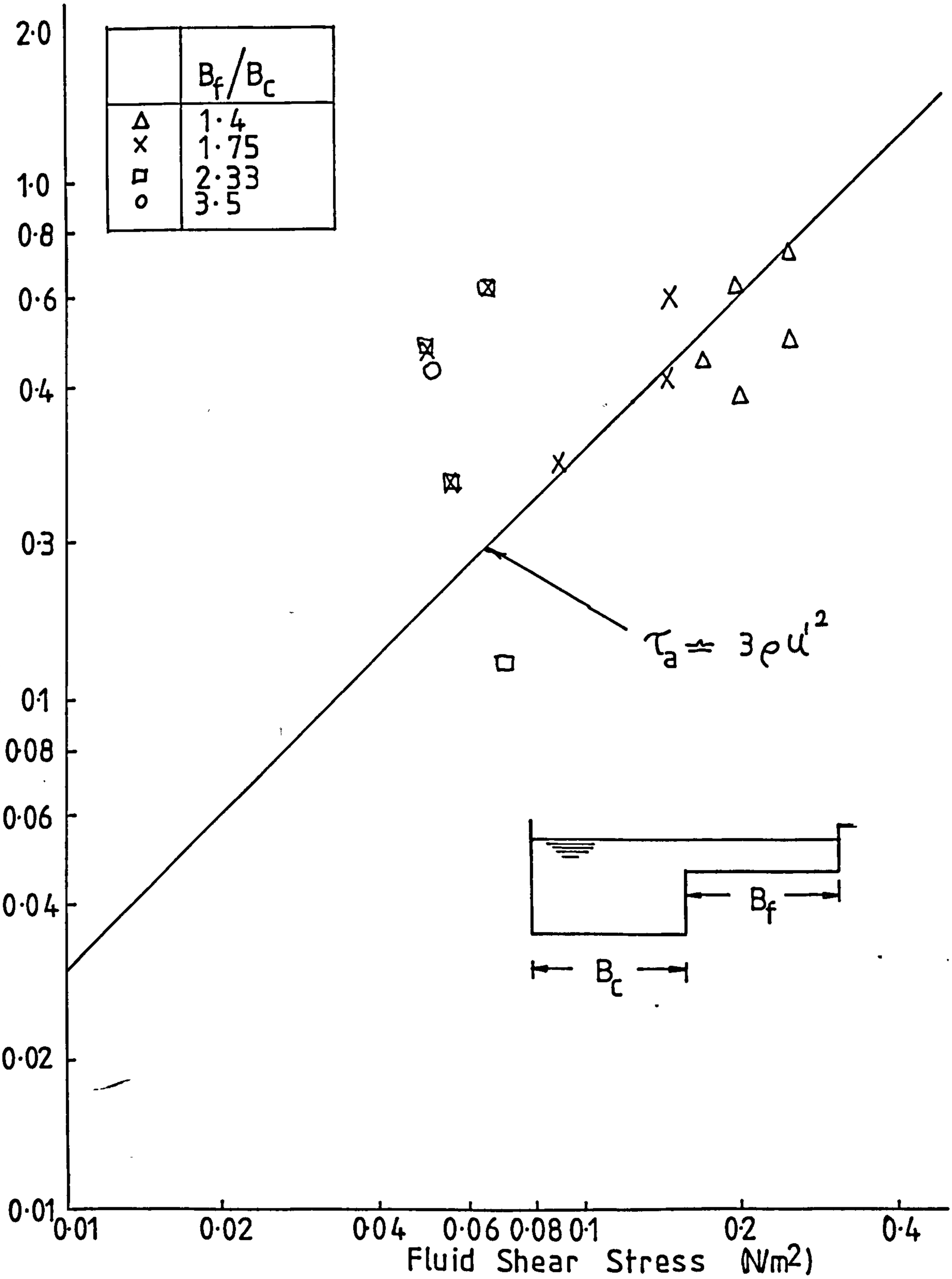

Fig 2·29 Relationship between apparent shear stress and fluid shear stress at interface (Crory)

▲,△ MAIN CHANNEL

●,○ FLOOD PLAIN

△,○ GHOSH & JENA

▲,● MYERS & ELSAWY

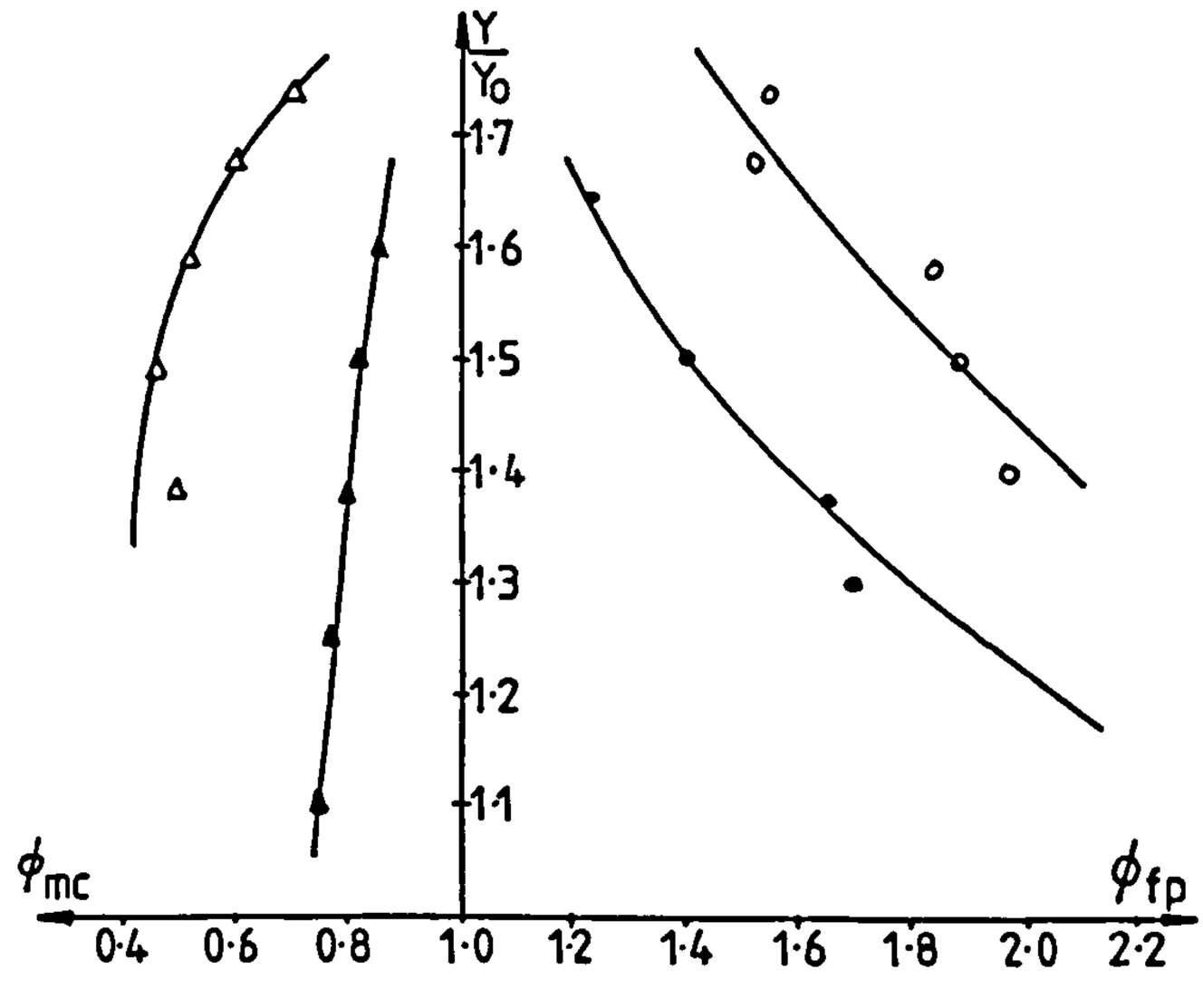

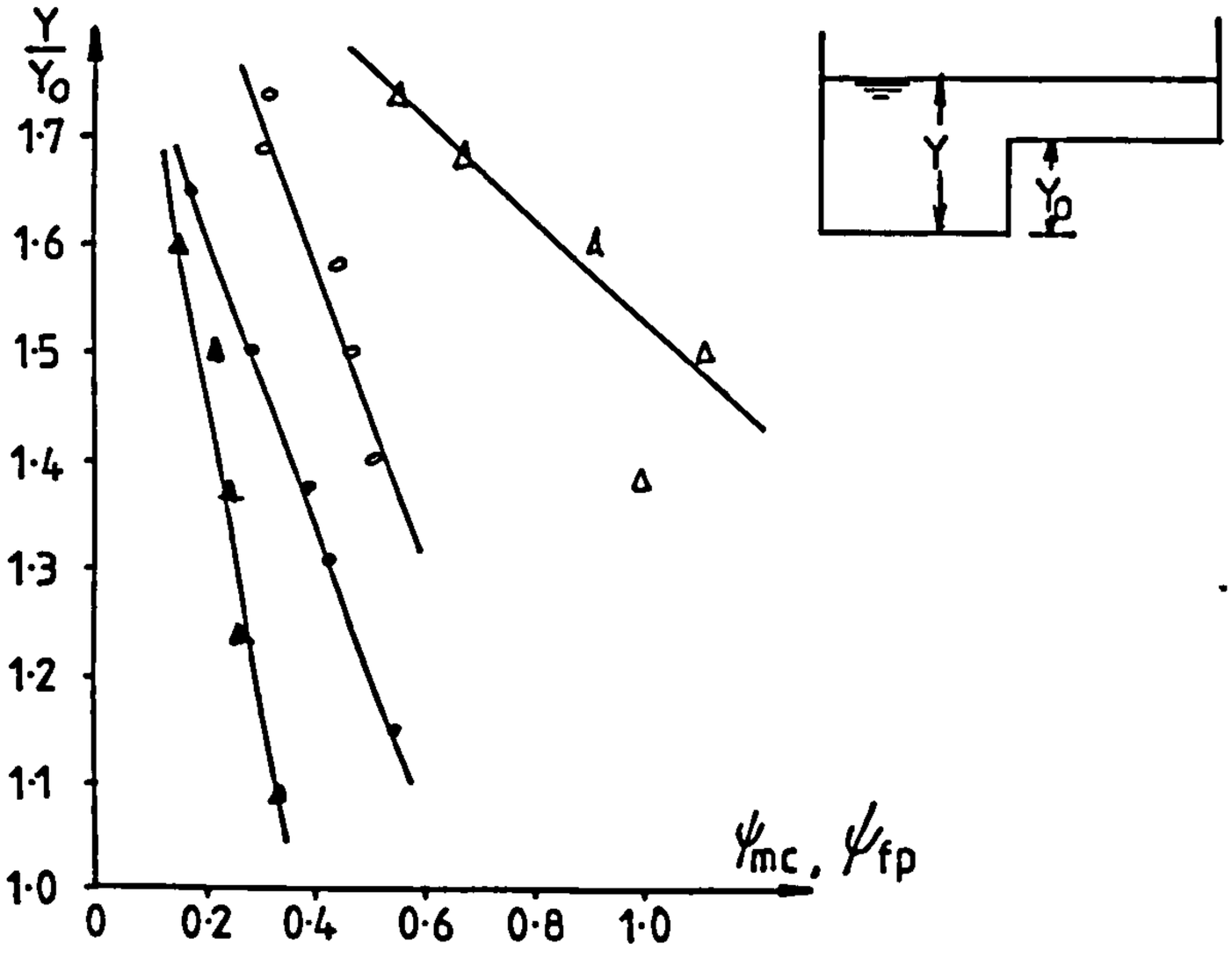

Fig 2·30 Compound channel parameters (Radojkovic)

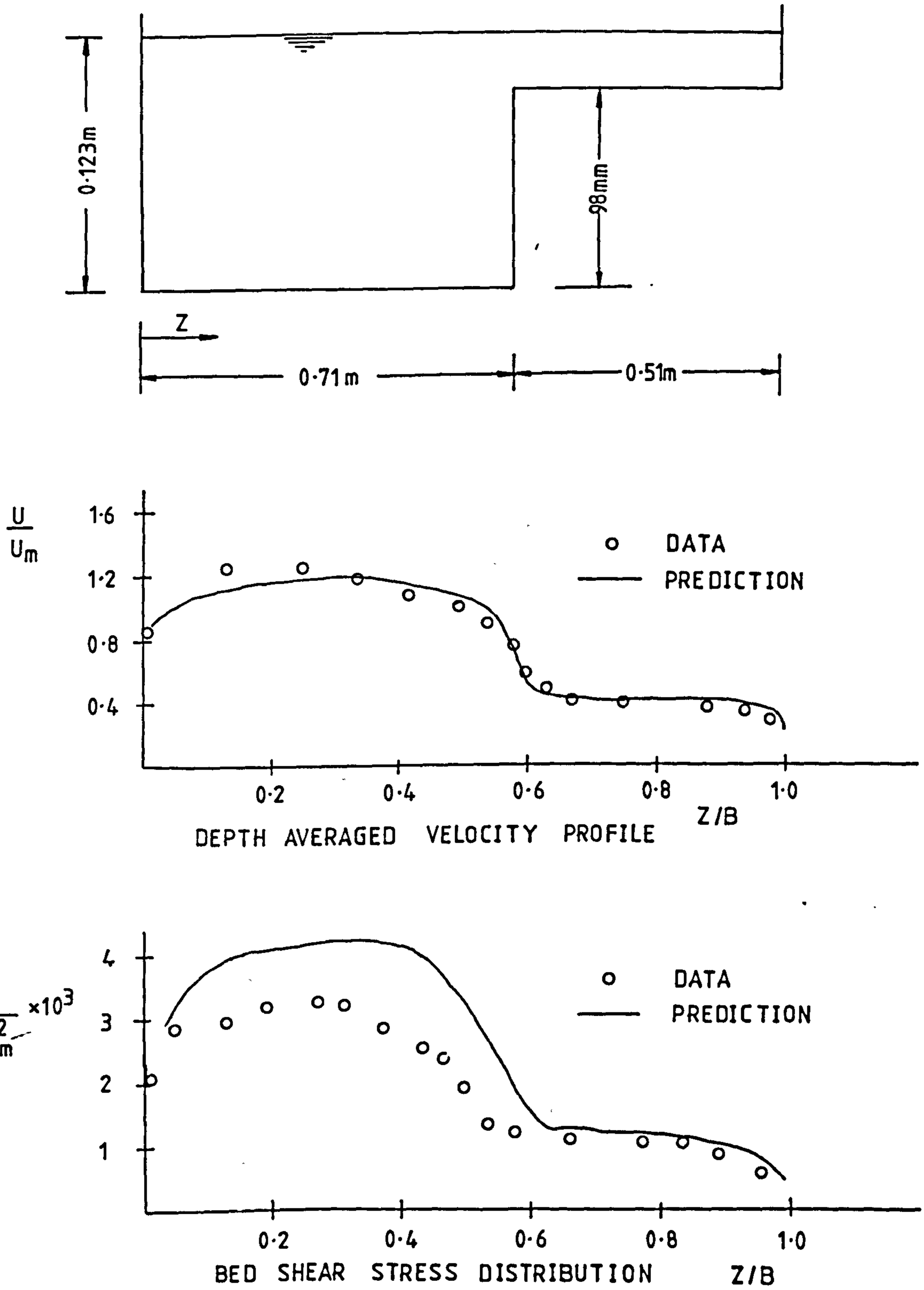

Fig 2·31 Comparison of experimental results and the k-ε turbulence model.

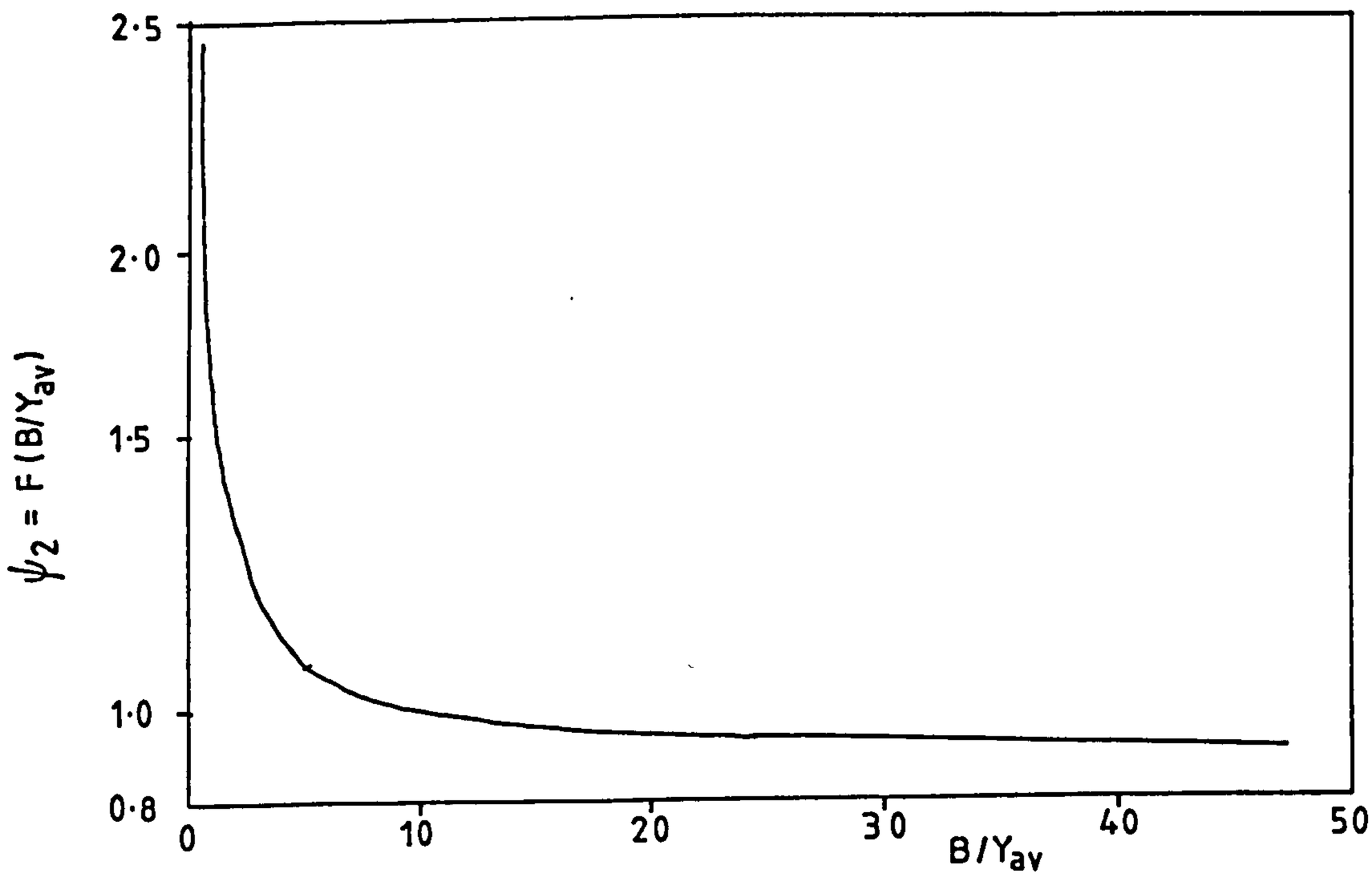

(a) shape parameter ψ_2 against B/Y_{av}

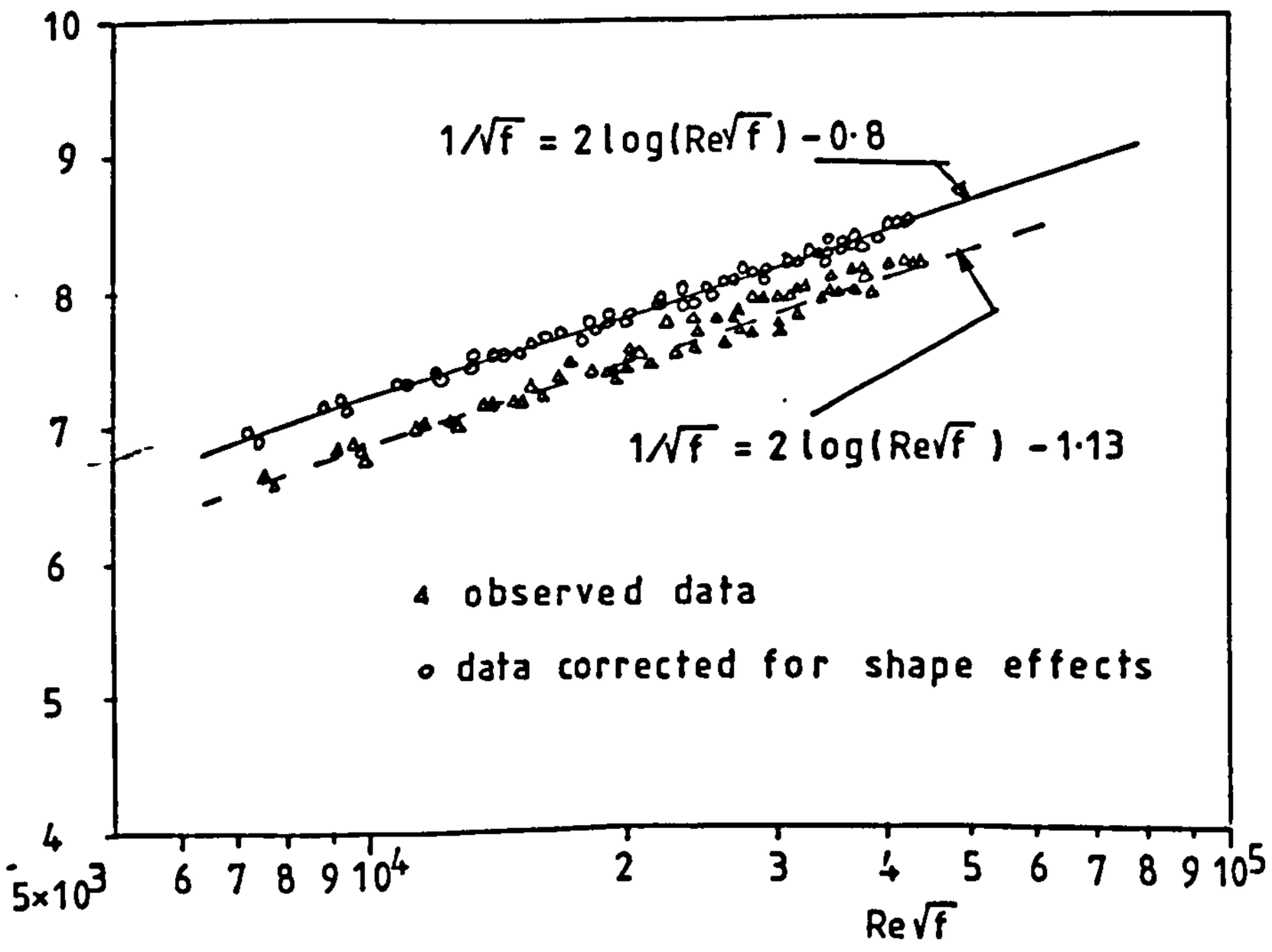

(b) Kazemipour's method applied to observed data.

Fig 2·32

$$\frac{1}{\sqrt{f}} = A \log(Re\sqrt{f}) - B$$

INVESTIGATION	Value of A	Value of B
Smooth pipe	2·0	0·08
Keulegan	2·03	1·08
Reinus	2·00	1·06
Tracy & Lester	2·03	1·30
Rao	2·12	1·83
Myers	2·10	1·56

Table 2·1 Comparison of constants in open channel flow equation. (Myers)

CHAPTER THREE

EXPERIMENTAL METHODS AND APPARATUS

Table of Contents

3.4.1 Introduction.

3.4.2 Orifice Plate Design and Construction.

3.4.3 Water Surface and Bed Slope Profile Determination.

3.4.4 Pressure Transducer and it's Calibration.

3.4.5 Pitot Tube Selection and Calibration.

3.4.6 Shear Stress Measurements.

3.5 Experimental Procedure.

3.1 Introduction.

An experimental investigation has been carried out on the effect of various channel geometry parameters on the interaction mechanism which exists between a channel and its associated flood plain during overbank flow. At an early stage of the project, the possibility of obtaining full scale measurements in a natural river was considered. However, this proposal was dismissed because of the infrequency of a suitable flood and also because of dangers likely to be experienced during flow gauging in high flood waters.

It was therefore decided, for the present, that a model study would be the only reasonable direction to pursue. In a model study, each geometrical parameter and flow condition could be controlled thus permitting an extensive study into the relationship between each flow and geometrical parameter and the channel/flood plain mechanism.

Having completed the literature review, it has become clear that certain parameters significantly effect the channel/flood plain interaction mechanism:-

$$\text{Degree of interaction} = fn\left[\frac{n_c}{n_f}, \frac{Y_c}{Y_f}, \frac{\Delta V}{V_c}, \frac{B_c}{B_f}, \frac{B_c}{h}, \frac{B_f}{h}, S\right] \quad (3.1)$$

In this present study n_c/n_f is held constant. However the other parameters are systematically varied. No facility existed in the Dept of Civil Engineering, University of Glasgow for such a model study, therefore a flume had to be designed and constructed. This chapter gives details of all design considerations and the constructional procedure. Also included is a description of the instrumentation used to obtain the necessary data with details of their calibration. Finally a description is given of the experimental procedure adopted for a typical experimental test run.

3.2 General Design Considerations of the Model.

It was decided at the design stage that the flume should be available for use by the Civil Engineering Department after the current research program was completed. The flume would therefore require features which may not be necessary for this present study into the overbank flow mechanism.

A recirculating system was chosen for construction because no facility existed in the laboratory for storing large volumes of water. Water flowing out of the channel flume would be held in a small sump tank and then pumped by pipe, to the channel inlet tank and back along the flume.

It was considered important to be able to compare any results obtained with previous findings by other

investigators. The depths of flow and Reynolds numbers in the flood plain had also to be such that fully developed turbulent flow would exist on the flood plain, or at least, laminar flow would not occur on the flood plain. It was therefore decided to design the flume to carry flows up to 250 mm deep. A minimum freeboard of 50 mm was allowed resulting in a design depth of flume of 300 mm.

Two considerations were applied in the selection of the flume width. First, data by Chow(Ref 10) suggests that the channel width may be taken as 3-5 times the water depth to enable the side wall effects of the channel to be fully developed. Secondly, since the purpose of any open channel model is to simulate flow behaviour in natural rivers, consideration should be given to regime theory and its implications for the ratio of channel width to depth of a river. Nixon (Ref 39) suggested that for a self-formed river, the channel cross-sectional shape would remain stable provided the following equations are satisfied:

$$W = 1{\cdot}65\ Q_b^{1/2} \qquad (3.2)$$

$$Y = 0{\cdot}545\ Q_b^{1/3} \qquad (3.3)$$

where W is the water surface width, Y is the water depth and Q_b is the bankfull discharge. All dimensions are in feet. Combining Equation (3.2) and Equation (3.3) and converting to SI units yields:

$$W = 2{\cdot}263\, Y^{3/2} \qquad (3.4)$$

This suggests a channel width of around 3-15 times wider than the water depth. The final channel width chosen for the model was 800 mm which would satisfy both considerations outlined above.

The length of the channel flume requires careful consideration especially when uniform flow conditions and fully developed turbulent flow conditions are required simultaneously. Regarding the first of these conditions, it should be noted that any channel flow will naturally attempt to form uniform flow (ie the water surface slope = the bed slope) and the distance required for the flow to reach its normal depth can be of the order of several kilometres. A channel operating under uniform flow conditions is required in this research work, but the channel flume length was limited by space available. In establishing uniform flow conditions, the common practice is to set the depth of flow in the channel at the normal depth by adjusting levels at a control section in the flume, such as a tail gate. The depth of flow over the end weir will be approximately the critical depth, and therefore for subcritical flow, the height of the tailgate above the channel bed should be set such that the tail gate height + the critical depth + the critical velocity head is equal to the normal depth + normal velocity head.

$$H_{tg} + \frac{3}{2} Y_{cr} \doteq Y_n + \frac{q^2}{2 g Y_n^2} \qquad (3.5)$$

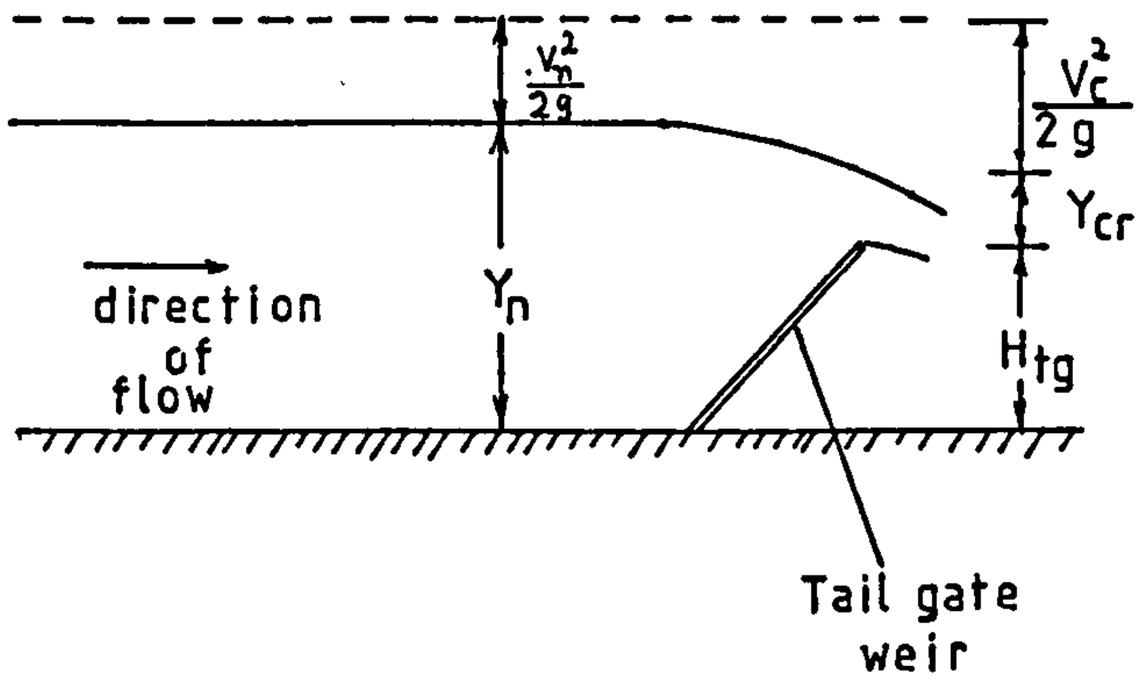

This was the approach adopted in this study for obtaining uniform flow. However, since the uniform flow was obtained artificially, the station at which readings were taken had to be a suitable distance away from the tail gate weir. This would prevent the weir from influencing the flow behaviour in the channel significantly

A second consideration regarding the channel length is the development of the boundary layer along the channel flume. As the flow enters the channel, the local velocities throughout the flow cross section are approximately equal. As the water travels down the flume, the channel bed and to some extent , the walls resist the flow, and the distance into the flow which is influenced by the channel boundary is known as the boundary layer. When the boundary layer reaches the water surface, the flow is considered to have a fully developed

turbulent structure. Fig 3.1, obtained from the United States Geological Survey (Ref 67), shows the relationship between the depth of flow in the channel d, the distance downstream from the channel entrance x, and the mean channel velocity V_o for fully developed turbulent conditions. The boundary layer growth can also be given by the equation:

$$\frac{d}{x} = \frac{0.38}{\left(\frac{V_o x}{\nu}\right)^{0.2}} \qquad (3.6)$$

where all dimensions are in feet. d is the channel depth, x is the distance downstream from the channel entrance, and ν is the kinematic viscosity of the water. If a channel depth of 0.5 ft is assumed with a velocity of 1.0 ft/sec then the required channel length is around 7.6 m.

The flume length was finally chosen by considering the length of the laboratory in which the model was to be situated. The total length of the laboratory was 10.5 m, and the final length of flume chosen was 8.5 m. This length is comparable to that of previous investigators including Sellin, Wormleaton, Myers etc, but is still a little too short to ensure a fully developed turbulent structure for the full range of tests carried out.

The channel slope was designed to tilt at slopes between the horizontal and 1/50, although the range of slopes actually tested varied from 1/800 to 1/3000. This range of slope

was thought to encompass a wide range of natural river slopes as shown by Jansen (Ref 28).

It was possible to obtain estimates of the range of discharges required for this research work using Manning's equation:

$$Q = \frac{1}{n} A R^{2/3} \sqrt{S} \qquad (3.7)$$

where Q is the discharge, A is the cross-sectional area, R is the hydraulic radius of the channel (A/P), S is the channel slope and n is Manning's n, estimated as 0.01 for glass reinforced plastic (the material from which the flume was constructed). The discharge range which was considered suitable was taken as 0-60 litres/sec and a pump with the appropriate pump characteristic was later installed.

From the literature review, it is apparent that several geometrical parameters may influence the interaction mechanism. These parameters may be summarised as:

Bc, the channel width

Bf, the flood plain width

Yc, the depth of flow in the channel

Yf, the depth of flow on the flood plain

h, the bankfull depth

and S, the longitudinal bed slope.

Each parameter could be varied by the introduction of rectangular flood plain sections of varying width and height. It is generally necessary to obtain at least three different values of each parameter for a satisfactory analysis of the results.

With this in mind, three main channel widths of 200 mm, 400 mm and 600 mm, three flood plain widths of 200 mm, 400 mm and 600 mm, and three bankfull depths of 50 mm, 100 mm and 150 mm were considered suitable. The cross-section of the channel and the values of h, Bc and Bf for each geometry tested are shown on Fig 3.2. It can be seen from Fig 3.2 that an asymmetrical channel shape was chosen for experimental consideration. This arrangement was chosen for two reasons. First, one flood plain would permit the development of only one turbulent interaction mechanism between the channel and flood plain thus obviating the possibility of two overlapping turbulent shear regions which may occur if flood plains on either side of the channel are used. Secondly, the amount of time, expense and width of channel necessary to construct two sets of similar flood plain sections would be too great. It was therefore considered appropriate to use only one flood plain.

The sump tank, from which the water was drawn into the pump was required to contain a large volume of water, and its design was dependent on two factors. First, the water level in the sump tank could not be allowed to fall below a level of 150 mm above the intake pipe to the pump. Any water depth below this design depth would encourage air intake to the pump by the formation of a large vortex immediately above the pipe entrance. Secondly, the volume of water which would occupy the inlet tank and the channel flume would require storage in the sump tank when the model was not in use. From these considerations, it was calculated that the storage capacity of the sump tank would need to be at least 3.2 m^3 . This volume was easily obtained by flanging together two large water tanks, each of size 186 cm x 122 cm x 100 cm, giving a total volume of 4.54 m^3.

With the design considerations outlined above, the model was designed and constructed and this work is described in the next section.

3.3 Design and Construction.

3.3.1 Flume Construction.

The final model is shown on Fig 3.3 with the experimental flume 8.5 m long, 0.8 m wide and 0.3 m in depth, as discussed in the previous section. It was decided to construct the flume from glass reinforced plastic in two identical

sections, each 4.25 m long, including 8 mm steel reinforcing bars encased into the underside of the flume at 1.0 m intervals to give the flume added rigidity. Extra strength was afforded to the channel by incorporating a flange along the top edge of the flume. A cross-section of the channel flume is shown on Fig 3.4. The stiffening arrangements are clearly shown.

A flange with steel sheet reinforcing was attached to one end of each flume section, and the two flanges were bolted together to give the complete full length of flume. Any discontinuity in the inside of the flume at the flange joint was eliminated by the use of a plastic cataloy filler material.

The glass reinforced plastic flume rested on a rigid framework structure composed of heavy duty bolted "handy angle" sections, and the framework in turn rested on a continuous bench structure. The rigid frame incorporated the facility to vary the longitudinal channel slope from 0 to 1/50 using a jacking system along the length of the flume. Fourteen screw jack arrangements were incorporated into the frame and the general arrangement of one of these jacking points is shown in Fig 3.5. A fixed pivot was incorporated at the entrance end of the frame, about which the channel would rotate and is shown on Fig 3.9.

3.3.2 Sump Tanks.

The capacity of the sump tanks was given in the previous section as 4.54 m^3 and two galvinised steel tanks, each of size 1.86 m x 1.22 m x 1.0 m, were flanged together in the arrangement shown on Fig 3.6. The tanks were positioned and a hole of 150 mm diameter was cut into one of the tanks. A small pipe section about 1 m long was fitted to this hole and connected to the pump at its other end and incorporated a 150 mm butterfly valve, enabling the sump tanks to be isolated from the pump during periods of necessary maintenance. The general arrangement of this pipe section is shown on Fig 3.7.

3.3.3 Pump.

Consideration was now given to the selection of the pump and its ability to discharge up to 60 litres/sec through the system. The total head loss through the system was estimated at 2.8 metres at a discharge of 40.0 litres/sec. Losses from pipe bends, sudden expansions, gate valve and orifice plate losses and general frictional losses were all considered. The static head required by the pump was taken as 0.5 metres. The pump finally chosen was a MYSON MSK 150-4210 centrifugal pump and its characteristics are shown on Fig 3.7 and Fig 3.8 respectively. There are two particular features of this pump which are worth considering. First, the pump must always operate under flooded conditions and this is why the sump tank was

carefully designed to give a minimum drawdown level 150 mm above the level of the 150 mm delivery pipe. Secondly, the pump operates at a constant r.p.m thus necessitating the introduction of a control valve in the pipe system downstream of the pump.

3.3.4 Gate valve and Inlet Tank.

A 150 mm gate valve was connected to the downstream side of the pump, permitting the operator to exercise considerable control over the discharge through the system. The gate valve is shown on Fig 3.7.

A pipe of length 3.5 m and internal diameter 150 mm was then attached to the gate valve and incorporated an orifice plate a distance of 2.25 m away downstream from the gate valve. The orifice plate was used to measure the total water discharge and details of it's design is given later in this chapter.

A galvinised steel inlet tank of size 1.22 m x 1.22 m x 1.22 m was positioned on top of concrete blocks at the flume entrance. A rectangular section was cut out of the tank to allow the flume section to rest inside the inlet tank. It was essential for the joint between the flume and inlet tank to be watertight, and also be suitably flexible to allow the variation of channel slopes to occur. It was therefore necessary to design a special sealing joint which would satisfy all necessary

requirements. A steel flange was "fibre-glassed" around the underside of the channel, at the edge of the inlet tank. A rubber sheet was then clamped onto this flange and the inlet tank. This gave a watertight, yet flexible joint which is illustrated on Fig 3.9.

A hole of 150 mm diameter was cut into the inlet tank to allow the pipe system from the pump to be fitted. Again a 150 mm butterfly valve was incorporated into this length to allow the isolation of the top inlet tank from the pipe system. A short length of flexible duct was used to complete the pipe system. The flexible pipe was necessary to accommodate the height difference between the two pipe sections to be joined by the flexible duct.

The model was now filled with water and checked for watertightness, and fortunately few modificatons were necessary to the system so the next phase of construction could be carried out.

3.3.5 Tailgate Weir.

As previously discussed, a tail gate was necessary to act as a control section for the channel flow. A brass plate, 800 mm x 200 mm x 5mm thick was hinged to the inside of the downstream end of the flume. Rubber seals prevented any significant leakage between the brass plate and the flume side

walls. A screwed rod arrangement, as illustrated on Fig 3.10, was attached to the brass plate and by this mechanism, the gate could be raised or lowered.

3.3.6 Flow Straighteners.

Flow straightener tubes were placed over the total channel cross- section, at the entrance to the flume. These tubes assisted the boundary layer growth by reducing the large scale transverse velocities formed in the inlet tank and had a significant effect on the surface roughness of the flow entering the flume. The honeycomb arrangement of the tubes is shown on Fig 3.11 and Fig 3.12. It was later decided to reduce the turbulent roughness and large scale eddies in the inlet tank by attaching a "T-piece" pipe section to the pipe entrance in the inlet tank. The "T-piece" helped to disperse the flow as it entered the inlet tank and can be seen on Fig 3.12.

3.3.7 Instrument Carriage.

It was necessary to design and construct an instrument carriage which would support any necessary measurement devices and also allow instruments to be positioned anywhere in the flow. This was achieved by constructing a carriage which could run longitudinally along steel rails which were attached to the top flanges of the flume. Special lock clamps were incorporated into the carriage which allowed the carriage to be

fixed at any position along the flume. Two further rails were constructed on top of this carriage, perpendicular to the direction of flow as shown on Fig 3.13. Along these rails a smaller carriage would run which would carry the instrumentation and could be winched across the flume by the rotation of a handle attached to the larger carriage. This permitted accurate positioning of the instrumentation across the width of the flow. The small instrument carriage was designed to carry a water level recorder in the form of a pointer gauge which was used to measure the bed slope, the water surface slope and the flow depth. The pointer gauge would be positioned either on the channel bed or just touching the water surface and a surveying level, positioned at the top end of the flume, would read a scale which was attached to the pointer gauge. This was found to be the most accurate method of confirming uniform flow. A Pitot static tube and a Preston tube could also be attached to the small instrument carriage, permitting the determination of point velocities and boundary shear stress measurements in the channel and flood plain. The height of these instruments above the channel bed could be determined by a scale and pointer attached to the instrument carriage. The general arrangement of the instrument carriage is shown on Fig 3.13.

The model flume was now complete and ready for modification to the requirements of the current study.

3.3.8 Flood Plain Design and Construction.

For ease of construction, it was decided to construct each wooden flood plain section in three identical lengths and following completion, lay them end to end along the length of the flume with the joints sealed with tape. Since the marine plywood used for the construction of the sections was available in sheets of size 2.44 m length x 1.22 m width, it was decided to construct each wooden section in lengths of 2.44 m, giving a total flood plain length of 7.32 m. As previously mentioned, it was decided to investigate three different flood plain widths, namely, 200 mm, 400 mm and 600 mm. The widths were obtained by constructing three separate sets of flood plains of widths 200 mm, 400 mm and 600 mm. The three different bankfull depths of 150 mm, 100 mm and 50 mm were obtained by first constructing each section of flood plain at a height of 150 mm and then, after tests were completed at that height, removing 50 mm off the vertical sides of the sections to give a new channel bankfull depth of 100 mm. This procedure was then repeated to give a bankfull depth of 50 mm. Various methods of construction were attempted and it was soon apparent that the use of marine plywood on the top and sides of the section was necessary to prevent warping of the wood. The final arrangement of the construction of a wooden section is shown on Fig 3.14. Pinewood was used on the underside of the flood plain to connect the top and sides of the wooden section together. Each section was treated with five coats of varnish on the inside and outside

of the sections to reduce water penetration. The buoyancy of each wooden section was calculated and a suitable volume of concrete was encased into the inside of each section. The concrete was fixed in position by steel reinforcing bars attached to the pinewood. Finally the concrete surface was given a thick coating of fibre glass resin. The wooden sections were now heavy enough to lie firmly on the base of the flume when submerged.

A total of nine flood plain sections were finally constructed and various combinations of these sections gave 18 possible cross sectional arrangements. These configurations are shown on Fig 3.15. Between 8 and 10 tests were carried out for each cross-sectional geometry. Unfortunately no tests were carried out using the geometry, channel width 600 mm, flood plain width 200 mm and bankfull depth 50 mm. This was due to the concrete in the inside of this set of flood plains exceeding the specified depth, thus not permitting a bankfull depth of 50 mm to be achieved. Only one test run was carried out with the geometry, channel width 600 mm, flood plain width 200 mm and bankfull depth 150 mm. At this geometry, difficulties were experienced in measuring the water surface profile at the high discharges necessary to achieve overbank flow.

Therefore, only 16 geometry configurations were extensively tested and each of these geometries are decribed by a letter of the alphabet as shown on Fig 3.15. A total of 136 test runs were achieved covering all 16 cross sectional geometries.

It was also necessary to construct different transition sections for each flood plain geometry. These transition sections were positioned at the entrance of the channel and allowed water to flow smoothly onto the flood plain. A master mould was built and various inserts allowed a variety of transitional sections to be cast from concrete. The concrete used contained little aggregate which gave the surface a smooth finish.

3.4 Instrumentation.

3.4.1 Introduction.

Each of the 136 test runs involved the accurate measurement and recording of the following parameters :-

(i) Water discharge rate. (ii) Depth of flow in channel and flood plain. (iii) Longitudinal bed slope and water surface slope. (iv) Point velocities throughout the channel and flood plain. (v) Boundary shear stresses around the channel and flood plain. The instrumentation used to record the above parameters will now be discussed and details of any necessary calibration will be described

3.4.2 Orifice Plate Design and Construction.

The most reasonable method of measuring the channel discharge efficiently and cheaply was to commission one of the devices outlined in BS1042:PART 1:1964. It was decided that the simplest device to fit was the orifice plate with pressure tappings a distance of D and D/2 upstream and downstream from the orifice plate, where D is the internal diameter of the pipe.

An orifice plate is essentially a circular disc with a hole of known diameter in the centre. The orifice plate is inserted into the pipeline acting as a contraction to the flow, and producing an energy or head loss as the flow passes through the throat of the orifice plate. This energy loss can be conveniently measured on a manometer by measuring the pressure difference between the two pressure tappings upstream and downstream of the orifice plate. According to BS1042:PART1:1964

$$Q = 0{\cdot}01252\ C\ Z\ \varepsilon\ E\ d^2\sqrt{\frac{h}{\rho_w}} \qquad (3.8)$$

where Q is the discharge through the orifice in m^3/hour, C is the basic correction coefficient, Z is a Reynolds number correction factor, ε is the expansibility factor which for incompressible flow can be taken as 1.0, E is a "velocity of approach" factor, h is the difference in pressure (in mm

water) between the upstream and downstream pressure tappings at the orifice plate, ρ_w is the density of water and d is the diameter of the orifice throat. The following values for each parameter are given below and were calculated from methods specified in BS1042:PART1:1964.

ρ_w = 998 kg/m^3

C = 0·6064

Z = 1·02

E = 1·206

d = 114 mm

ε = 1·0

The orifice plate details are shown on Fig 3.16 and Fig 3.17. The orifice plate throat diameter was taken as 114 mm as it was considered important to obtain a reasonable head difference h over a wide range of discharges. If the water manometer was used to measure discharges in excess of 40 litres/sec then the expected value of h would be around 2000 - 3000 mm. It was therefore decided to utilise two manometers, one containing water for the measurement of low discharges, and the other, containing mercury would be capable of measuring high discharges. Both manometers are clearly shown on Fig 3.18.

An important point of consideration in the design of the orifice plate is the required distances upstream and downstream from the orifice plate to another

device such as a pipe bend or a gate valve. The minimum distance required downstream from the plate is 7 pipe diameters which is equivalent to 1.02 m. This requirement was satisfied. However, the minimum distance required upstream is dependent on the gate valve opening. With the gate valve 3/4 closed the required distance to the gate valve from the orifice is 60 pipe diameters or 9.05 m. With the gate valve fully open the required distance is 27 pipe diameters or 4.05 m. Unfortunately this requirement could not be satisfied since the maximum available distance between the gate valve and the orifice was 2.25 m. It was decided to overlook this problem and take extra care in the calibration check on the orifice plate in its final position.

Calibration of the orifice plate was carried out by measuring the volume of water drawn from the 4.5 m sump tanks in a given time. This time was short enough to prevent any water from recirculating through the system and back into the sump tanks. The levels in the manometer were then read and the discharge was then estimated from Equation (3.8). The results of a number of such tests are shown on Fig 3.19 and it can be clearly seen that for a wide range of discharges the orifice plate prediction of the discharge compares very well with the measured discharge. On the basis of these results the orifice was considered a satisfactory flow measurement device in the system.

3.4.3 Water Surface and Bed Slope Profile Determination.

The water surface profile and bed slope were determined by using a surveying level shown on Fig 3.20, combined with a pointer gauge and graduated scale carried on the instrument carriage as shown on Fig 3.27. The surveying level permitted level accuracy of ± 0.1 mm to be measured. Fig 3.21 shows a typical water surface profile and channel bed profile. Considering the bed profile it can be seen that it is difficult to associate a particular bed slope with it's profile. Attempts were made to improve the profile by finely adjusting each jacking point. This was partly unsuccessful because of small undulations of the bed of the glass fibre channel. It was finally decided to consider the range of possible bed slopes and find an average slope. Throughout the tests the bed slope was changed by adjusting the jacking arrangement to give a range of average bed slopes.

The water surface slope was set by first considering the average bed slope and then adjusting the tail gate weir until the water surface profile was approximately similar to the bed slope. Again some difficulties were experienced in estimating the water surface slope, probably due to the formation of small waves

and general disturbances. However with experience, the water surface slope could be measured more accurately than the bed slope as can be seen on Fig 3.21. The range of possible water surface slopes is less than the range of bed slopes.

3.4.4 Pressure Transducer and it's Calibration.

It was decided to use a Pitot static tube and a Preston tube to measure the local velocities and shear stresses in the channel. A method of measuring the small pressure differences from the static and dynamic tubes was therefore necessary. One possible approach was to connect both tubes to an inclined manometer or micro-manometer. However the main disadvantage of this approach was that the time taken for the manometer to respond to the differential pressures could be as long as 20 minutes. This would mean a single run could take as long as 24 hours to complete.

Following a visit to Prof. Rajaratnam, University of Alberta, Canada, it was finally decided to use a low head pressure transducer which had the advantage of being able to respond rapidly to the pressure differences. The only known available pressure transducer which would give accurate pressure difference readings at very low pressure differences was the Validyne DP103 Diaphragm Magnetic Reluctance, Ultra-low head Pressure Transducer.

Considerable delivery delay was experienced with this device as it had to be imported from the United States.

A simplified schematic diagram is shown on Fig 3.22. A thin diaphragm of magnetically permeable material is supported by two symmetrical assemblies. Imbedded in each assembly is a small magnetic E-core. The diaphragm completes the magnetic circuit in each E-core. The application of pressure to either side of the transducer increases or decreases the gap between the diaphragm and the E-core in either assembly. The magnetic reluctance of each core varies with the gap, thus determining the induction ratio. This ratio is measured in an AC bridge circuit in which the output voltage is proportional to the pressure. A sine wave excitation is applied to both the inductance ratio arms of the transducer and the output was demodulated and amplified using a carrier demodulator specially constructed in the Electronic workshop in The Department of Civil Engineering at the University of Glasgow. An LCD circuit was used to display an output DC voltage which was proportional to the differential pressure obtained from the transducer. Both the pressure transducer and the carrier demodulator are shown on Fig 3.23. One advantage of the DP103 pressure transducer is that a wide range of differential pressures can be measured by simply selecting a diaphragm from the 16 different diaphragm thicknesses available. Diaphragm 16 was chosen to give the appropriate

diaphragm deflection for the anticipated pressure difference. This diaphragm would give a linear relationship between the output voltage and the differential pressure up to a pressure difference of 35 mm head of water. This pressure difference is equivalent to a velocity of 0.83 metres/sec in the channel flow. Velocities in excess of this were never anticipated. The zero and gain controls on the carrier demodulator were adjusted until a reading of 100 on the carrier demodulator was equivalent to a pressure difference of 10.0 mm of water across the pressure transducer. Thus a reading of 1 on the digital display is equivalent to a head of 0.1 mm, and for readings alternating between two values, the instrument is accurate down to 0.05 mm. The procedure for the initial setting and calibration of the pressure transducer was as follows:

1. The beaker arrangement shown on Fig 3.24 was set up. Both beakers were connected to the pressure transducer and the inclined manometer shown on Fig 3.25. Valve A, when open, allowed flow to take place between the beakers.

2. Valve A was opened and both beakers were half filled with water. The pipe system was bled to eliminate any air pockets in any part of the tubes. It was important to remove all traces of air on either side of the transducer diaphragm.

3. With valve A open, the water levels in both beakers were equal. The inclined manometer was inclined at 19.5° to the horizontal. Any difference in water level in the manometer was magnified by a factor of three. The zero adjustment on the demodulator was set to give a reading of 000 on the display for the pressure transducer.

4. Valve A was then closed and water was introduced into one of the beakers until the difference in water levels between the two beakers was 30 mm. This was equivalent to a head difference of 90 mm on the inclined manometer. The gain control was now adjusted to give a display reading of 300 on the demodulator for the transducer.

5. Valve A was then opened and the water level difference in the beakers returned to zero. The zero adjustment was then set to give a reading of 000 on the display.

6. This procedure was repeated 5 or 6 times until the reading on the display would return automatically to 000 when stage 5 was carried out.

The relationship between the display obtained from

the pressure transducer and the readings from the inclined manometer is shown on Fig 3.26. It can be seen that the transducer results agree very favourably with the results obtained from the inclined manometer. From the results it was found that pressure differences of ± 0.1 mm could be measured with good accuracy, and head differences of ± 0.05 mm with reasonable accuracy.

The only difficulty experienced in using the pressure transducer was its sensitivity to the pressure fluctuations caused by the turbulent fluctuation of the velocity component u' with time. One possible method of tackling this problem was to connect the carrier demodulator to a micro computer via an analogue-to-digital converter. A number of pressure tranducer readings could then be recorded over a period of time and the average reading taken. The simplest and least expensive method was a partial clamping of both tubes entering the transducer until only a small amount of water could pass through the clamp. This method was adopted and dampened the pressure fluctuations satisfactorily but had the slight disadvantange of increasing the response time of the pressure transducer by about 30 seconds per reading.

3.4.5 Pitot Tube Selection and Calibration.

It was decided to use a Pitot static tube to measure the local velocities throughout the cross section. This was because a Pitot tube is easy to use, robust and can also be used as a Preston tube in measuring the boundary shear if the depth of flow is sufficient.

A Pitot tube is generally an "L" shaped hollow tube used to measure the dynamic energy of a flow. Perhaps more common in hydraulics is the Pitot static tube which is shown on Fig 3.27. Two tubes run up the stem of the Pitot tube. The inner tube measures the dynamic energy of the flow ($Y + \frac{v^2}{2g}$). while the other tube leads to small holes in the wall of the Pitot tube and so measures only the static energy of the flow (Y). The difference in pressure between the static tube and the dynamic tube is equal to the velocity head, $\frac{v^2}{2g}$. If both tubes are connected to the pressure transducer, then a quick method is available for measuring the local velocities.

The accuracy of the Pitot static tube can be checked by recording a grid of velocity points at one cross section and then integrating these points over the flow cross sectional area to give a mean channel velocity. This will now yield a channel discharge which can now be compared to the discharge obtained from the orifice plate meter. For all tests carried out a series of velocity points were recorded and

integrated over the cross sectional area of the flow by planimetry to give a channel discharge. This discharge is compared with the discharge obtained from the orifice meter on Fig 3.28 and it can be seen that the discharge obtained from the Pitot static tube measurements compares very favourably with the orifice plate readings. Most discharges obtained were within±3% of the orifice meter. On the basis of these results, it was considered appropriate to use the Pitot static tube to measure the local velocities in the channel and flood plain. The size of Pitot static tube chosen was 4 mm outside diameter. This was becuse the Pitot static tube would be used as a Preston tube and it would be necessary to measure the shear velocities very close to the channel wall. The Pitot static tube chosen had a OD of 4 mm and a stem of 800 mm. The nose was a hemispherical shape and the Pitot static tube can be seen on Fig 3.27.

3.4.6 Shear Stress Measurements.

Direct and indirect methods have been developed to measure boundary shear stress and its distribution around a channel perimeter. Direct methods essentially involve the suspension of a "floating element device" just above the channel bed. The forces which act on the element are measured. It was decided too impractical to adopt this approach because of the difficulties which can be experienced in setting up the apparatus and also because of the nonuniform distribution of shear stress around the channel boundary.

Indirect methods of measuring the shear stress on a boundary involve measuring an intermediate parameter such as velocity. Perhaps the simplest indirect method is to measure the vertical velocity profiles above the channel boundary using a Pitot tube and then calculate U_* from the logarithmic velocity equation:

$$\frac{U}{U_*} = 5{\cdot}75 \log \frac{U_* y}{\nu} + 5{\cdot}5 \qquad (3.9)$$

where U is the local point velocity, y is the distance from the boundary, ν is the kinematic viscosity and U_* is the shear velocity given by:

$$U_* = \sqrt{\frac{\tau_o}{\rho}} \qquad (3.10)$$

The local shear stress τ_o can now be calculated from Equation (3.10). The problem experienced with this method is that Equation (3.9) only applies for two dimensional flow conditions. The effects of a side wall are such that Equation (3.9) no longer directly applies. The logarithmic velocity profile method was considered unsuitable because of the low width to depth ratios in many of the tests.

Myers (Ref 36) attempted to use the hot film technique to measure shear stress for his series of experiments. The principle is based on measuring the amount of current required by the hot film to maintain a constant temperature at

the probe. The amount of heat energy lost from the probe is proportional to the ambient velocity. Myers found that the probe became very easily contaminated with impurities in the water.

The method finally adopted by Myers and the present author to measure the shear stress around the perimeter of the channel was a method developed by Preston (Ref 43) in 1954. By placing a small Pitot tube on the wall of a pipe, Preston was able to develop a universal non-dimensional relationship for the difference between the total pressure recorded by the Pitot tube and the static pressure at the wall in terms of skin friction. The relationship is as follows:

$$\frac{P - p_o}{\rho V^2} = F\left[\frac{\tau_o d^2}{\rho V^2}\right] \qquad (3.11)$$

where P is the total pressure, p is the static pressure, d is the Pitot tube diameter, ν is the kinematic viscosity of the fluid and τ_o is the local shear stress at the wall. The function F has been determined from extensive tests to be:

$$\log \frac{\tau d^2}{\rho \nu^2} = \bar{2}\cdot 604 + \frac{7}{8} \log \frac{(P-p_o)\, d^2}{\rho \nu^2} \qquad (3.12)$$

This relationship has been shown to be valid for:

$$\log \frac{(P-p_o)\, d^2}{\rho \nu^2} > 5\cdot 0 \qquad (3.13)$$

Various investigators (Ref 23, Ref40) are in general agreement with Preston's findings and Patel (Ref 40) has suggested a

modification to Equation (3.12):

$$y^* = 0{\cdot}8287 - 0{\cdot}1381x^* + 0{\cdot}1437x^{*2} - 0{\cdot}0062x^{*3} \qquad (3.14)$$

where $$y^* = \log \frac{\tau_o d^2}{4\rho v^2} \qquad (3{\cdot}15)$$

and $$x^* = \log \frac{(P-p_o)d^2}{4\rho v^2} \qquad (3{\cdot}16)$$

valid for the range :

$$1{\cdot}5 < \log \frac{(P-p_o)d^2}{4\rho v^2} < 3{\cdot}5 \qquad (3.17)$$

Cruff (Ref 15) compared the Preston tube technique with the Karman-Prandtl logarithmic velocity law for a series of tests in an open channel. He found that both methods compared favourably. Hwang and Laursen (Ref 25) were able to extend Preston's work to the estimation of local shear for boundaries with rough surfaces. Ghosh and Roy (Ref 21) successfully applied Hwang and Laursen's method and Preston's method to channels with rough and smooth boundaries.

The Preston tube technique was later adopted by most investigators in establishing the shear distribution in a

compound channel. Rajaratnam (Ref 49) reported that a Pitot static tube could be used as a Preston tube without any adverse effects. In private correspondence with Prof. Rajaratnam, the author established the validity of using the existing type of 4 mm OD Pitot static tube for boundary shear stress measurements, with one qualification as mentioned in the following paragraph. It was therefore decided to use the same Pitot static tube used to measure the local velocities in the channel, which in turn can be used to calculate the boundary shear stress.

One disadvantage of the Preston tube technique as reported by Preston is that the tube diameter must not be greater than 1/5 of the boundary layer thickness. The Pitot tube used for shear measurements was 4 mm outside diameter implying that the Pitot tube could not be used to measure the shear stress in depths of flow less than 20 mm. Depths in the flood plain were frequently below this depth and during such tests smaller Preston tubes of diameter 1.6 mm and 3.0 mm borrowed from the Aeronautics Department were used to obtain the shear stress in the flood plain. The shear stress obtained from the small tubes compared well with the results from the Pitot static tube in a series of tests carried out in the main channel as can be seen on Fig 3.29. It was therefore considered valid to use the Preston tubes of different diameters as appropriate.

It was decided to calibrate the Preston tube by measuring the shear stress distribution around the perimeter of

the channel with the flow confined to the main channel. The average shear stress could then be calculated by integrating the shear stress distribution around the perimeter of the channel. The following force equilibrium equation should then be satisfied:

$$\rho g A_c S = \tau_c P_c \qquad (3.18)$$

where A_c is the channel cross sectional area, S is the water surface slope, and τ_c is the average shear stress around the channel perimeter, P_c. A plot of the measured mean boundary shear stress (τ_c) against the calculated value, ρgRS is shown on Fig 3.29 indicating a significant spread of results. The spread of results may be attributed, in part, to the inaccuracy of the Preston tube method, but much more likely, the spread of results reflects a degree of uncertainty of both the bed slope and the water surface slope as already discussed and shown on Fig 3.21.

SEE NOTE OPPOSITE

In Chapter 4, it will be shown that the friction factor- Reynolds number relationship which was most accurate in predicting the value of λ_c for the smooth glass fibre channel was :-

$$\frac{1}{\sqrt{\lambda_c}} = 2{\cdot}0 \log(Re\sqrt{\lambda_c}) - 1{\cdot}3 \qquad (3.19)$$

Independent check on the measurement of shear stress

In view of the degree of uncertainty in the channel bed and water surface slopes and the implications for the measurement of boundary shear stress as illustrated on Fig. 3.29, it was decided to conduct an independent series of shear stress measurements. This work was carried out in the Department of Geology, University of Glasgow, in an hydraulic flume incorporating a much more rigid channel bed relatively free from channel bed undulations. The 4 mm outside diameter Pitot-static tube was tested as well as the 1.6 mm and 3.0 mm diameter Preston tubes for comparative purposes. A Table is given below indicating calculated and measured shear stresses with percentage errors also indicated.

Test Series	Calculated shear stress ρgRS	Measured shear stress	Tube diameter	% Error
Series A	0.582 (N/m^2)	0.557 0.571 0.565	4.0 mm 3.0 mm 1.6 mm	+ 4.3 + 1.8 + 2.9
Series B	0.451 (N/m^2)	0.446 0.436 0.429	4.0 mm 3.0 mm 1.6 mm	+ 1.2 + 3.4 + 4.8
Series C	0.324 (N/m^2)	0.347 0.325 0.330	4.0 mm 3.0 mm 1.6 mm	- 7.2 - 0.4 - 1.8
Series D	0.288 (N/m^2)	0.279 0.289 0.296	4.0 mm 3.0 mm 1.6 mm	+ 3.2 - 0.4 - 2.8
Series E	0.205 (N/m^2)	0.208 0.209 0.213	4.0 mm 3.0 mm 1.6 mm	- 1.3 - 1.8 - 4.1

The data above indicated that the 4 mm diameter Pitot-static tube is adequate for shear stress measurement with the percentage errors, with the exception of one point, being under $\pm$ 5%. Thus it can be argued that the spread of results on Fig. 3.29 is much more due to slope inaccuracies.

This was a similar equation suggested by Tracy and Lester (Ref 65) for smooth rectangular channels and represents the median line through the results. The value of λ_c in Equation (3.19) was computed from the Darcy-Weisbach equation :-

$$\lambda_c = \frac{8g R_c S}{V_c^2} \qquad (3.20)$$

and involves the mean channel velocity measurements and not the boundary shear measurements. If Equation (3.16) is combined with Equation (3.20) eliminating the water surface slope, the following is obtained :-

$$\frac{8\tau_c}{\rho\lambda_c} = V_c^2 \qquad (3.21)$$

thus providing a relationship between boundary shear stress and mean channel velocity. The measured values of shear stress τ_c, can now be compared directly from those calculated from Equation (3.21) using the velocity measurements and friction factors from Equation (3.19). The correlation is shown on Fig 3.30 indicating again a spread of results, but confirming that the shear stress measurements were satisfactory, varying approximately with the velocity squared. For tests involving overbank flow, a more accurate measurement of the water surface slope could now be obtained by assuming that the force equilibrium equation for the total channel cross section was satisfied:

$$\rho g A_t S = \tau_c' P_c' + \tau_f' P_f' \qquad (3.23)$$

where At equals the total cross sectional area of the channel and flood plain, τ_c' and τ_f' are the mean interacting average shear stresses in the channel and flood plain, Pc' and Pf' are the solid boundaries of the channel and flood plain. It was found that very little adjustment was necessary to the measured slope in order to satisfy Equation (3.23) and that the new adjusted slope always lay within the range of likely slopes measured from the surveying level and the pointer gauge.

3.5 Experimental Procedure.

A total of 136 test runs were carried out during the present investigation and the experimental procedure outlined below was adopted for each run.

1. A flood plain section was inserted into the flume to give the required channel and flood plain geometry. As mentoned earlier, a total of 16 different channel geometry arrangements were tested. The configurations of flood plain sections for each geometry tested is shown on Fig 3.15.

2. The bed slope was adjusted to give a slope which would lie between 1/800 and 1/3000. The required slope was obtained by adjusting the screw jacks and reading the bed level every 0.5 metres down the flume using a surveying

level and a pointer gauge attached to the instrument carriage.

3. The pump was switched on and a discharge which would give overbank flow was selected by adjusting the gate valve accordingly. The discharge could then be evaluated from the orifice plate and the manometer.

4. The water surface profile of the channel flow was measured at 1 m intervals along the flume using a surveying level and the pointer gauge. The water surface slope was plotted and compared to the bed slope. If there was a significant difference in the two slopes, the tailgate was raised or lowered accordingly and the water surface profile determined again.

5. Using the Pointer gauge on the instrument carriage, the flow depths in the channel and flood plain were recorded.

6. The Pitot static tube was connected to the pressure transducer by means of clear plastic tubing and any air in the system was bled out, since air bubbles seriously effected the transducer's response.

7. The Pitot static tube was thenplaced in a beaker of water to give a zero pressure difference across the static head and dynamic head of the Pitot static tube. The carrier demodulator was checked for a zero reading and if not, adjusted accordingly.

8. The Pitot static tube was then removed from the beaker into the flow and placed at known positions throughout the cross-sectional area of the channel and flood plain flow to

give a velocity traverse.

9. If the depth of flow in the flood plain was less than 20 mm, a smaller diameter Preston tube was connected to the pressure transducer and used to determine the boundary shear in the flood plain.

10. Point velocity measurements were taken over a grid at intervals of approximately 20 mm both in the horizontal and vertical directions. Boundary shear stress measurements were taken at intervals of around 20-50 mm around the entire wetted perimeter.

11. After completion of the test run, the Pitot tube was placed in the beaker of water and the carrier demodulator was checked for zero reading. Invariably the reading would return to zero.

12. The velocity and shear stress data was then entered on the the ICL2988 mainframe computer and processed by the program in Appendix 1 into a graphical representation of the vertical velocity profiles across the channel and flood plain and boundary shear stress distribution.

13. The boundary shear distribution was integrated by planimetry to give the average shear stress in the channel τ_c', and in the flood plain τ_f'. The vertical velocity profiles were also integrated by planimetry to give depth averaged velocities. The lateral velocity profiles were then plotted and planimetered to give the average velocities in the channel V_c', and in the flood plain V_f'.

14. The average velocities were then multiplied by the

corresponding channel and flood plain areas to give a total discharge,

$$Q = V_c' A_c + V_f' A_f \qquad (3.22)$$

Q was compared to the discharge obtained from the manometer and the differences were usually of the order of 3%.

15. At the end of each test run the recorded data would include the following parameters :-

a) Total discharge Q

b) Bed slope and Water surface slope S_o, S_w

c) Channel depth Y_c

d) Flood plain depth Y_f

e) Point velocities integrated to give Vc' and Vf'

f) Shear stresses integrated to give τ_c' and τ_f'

g) Bankfull depth h, channel and flood plain widths Bc and Bf

The overall testing programme is summarised on Fig 3.31 with a flow chart illustrating all the activities clearly shown.

3.6 Role of experimental error

At the conclusion of this Chapter it has been shown that considerable confidence can be placed on both the point velocity data and the measured shear stress data. However, undulations in the channel bed of the order $\pm$ 0.5 mm have given rise to uncertainties in determining accurate channel bed slopes and water surface slopes. This in turn has resulted in some uncertainty in the criteria of accuracy in establishing completely uniform flow.

It will be seen in later chapters that this uncertainty is reflected in data correlations in the form of a spread of results for each cross-sectional geometry. This is particularly the case for correlations of the friction factor in Chapter 4, the non-dimensional velocity ratio V_c'/V_c in Chapter 4 and non-dimensional shear stress ratios τ_c'/τ_c in Chapter 5.

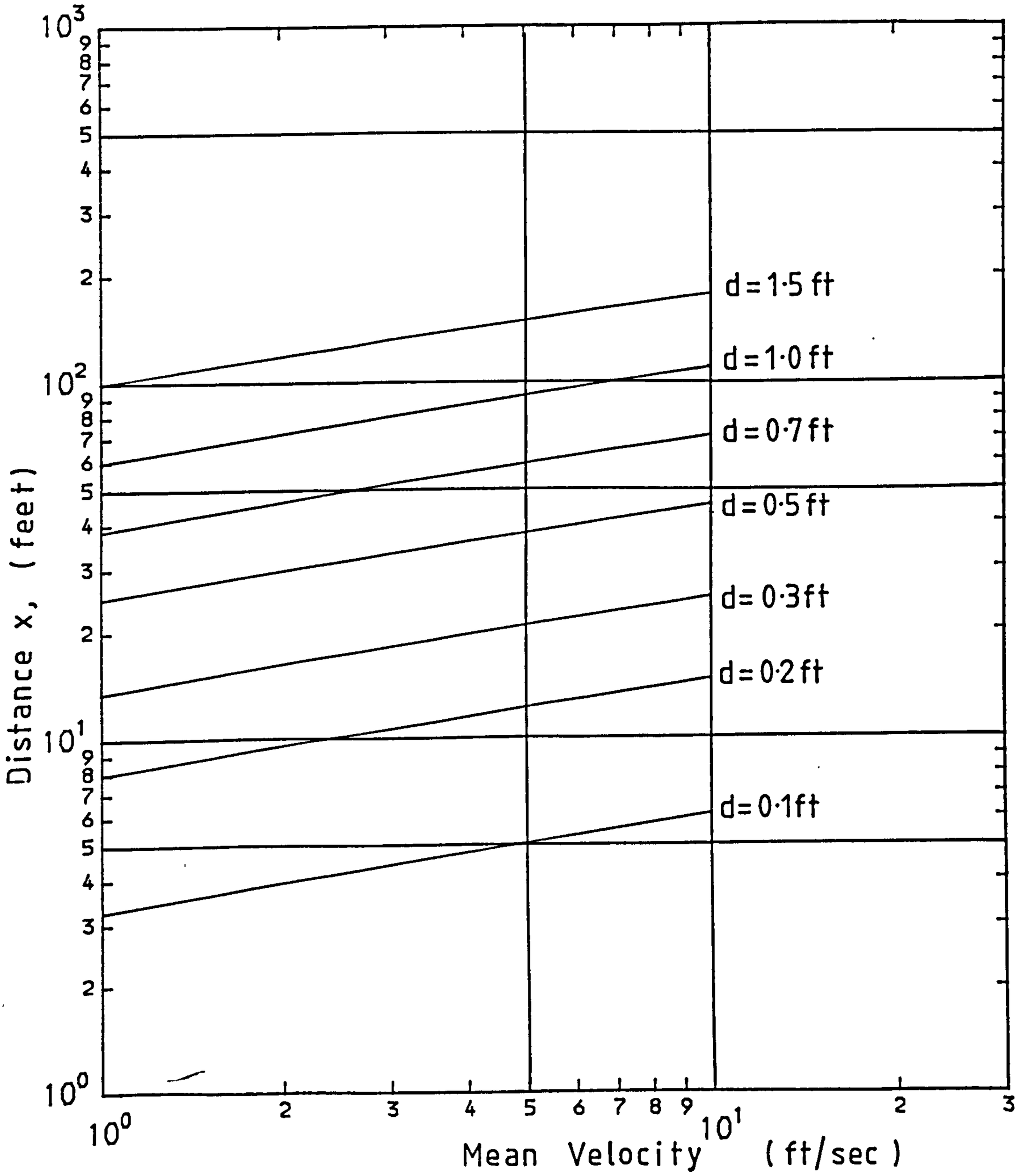

Fig 3·1 Boundary Layer Development with Channel velocity and distance downstream from Channel Entrance.

SYMBOL	GEOMETRY	RUN NO	(mm) h	(mm) B_c	(mm) B_f	No of tests
△	K	1—10	102	400	400	10
▽	A	11—22	52	400	400	12
□	B	23—30	52	200	400	8
◇	C	31—37	52	400	200	7
○	G	38—45	152	200	600	8
⊞	L	46—53	152	200	400	8
⊠	N	54—61	152	200	200	8
⊕	J	62—70	152	400	400	9
⊗	R	71—78	152	400	200	8
✠	MYERS	79—88	102	254	356	10
⌖	RAJARATNAM	89—93	98	711	508	5
⌘	P	94—103	102	200	400	10
⊹	H	104—113	102	200	600	10
⋇	M	114—121	102	200	200	8
ϴ	CRORY	122—126	102	254	356	6
ϰ	CRORY	127—130	102	203	356	4
λ	CRORY	131—133	102	153	356	3
μ	CRORY	134—137	102	102	356	4
*	0	138—145	52	200	200	8
#	I	146—153	52	200	600	8
$	S	154—161	102	400	200	8
@	E	162—167	102	600	200	6

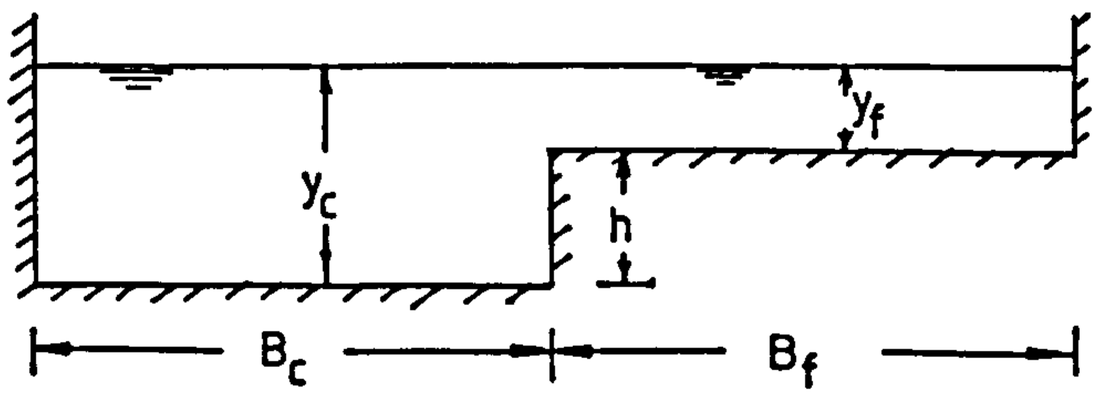

Fig 3·2 Range of Geometries of Asymmetrical Smooth Channels Tested by the Author and Other Investigators.

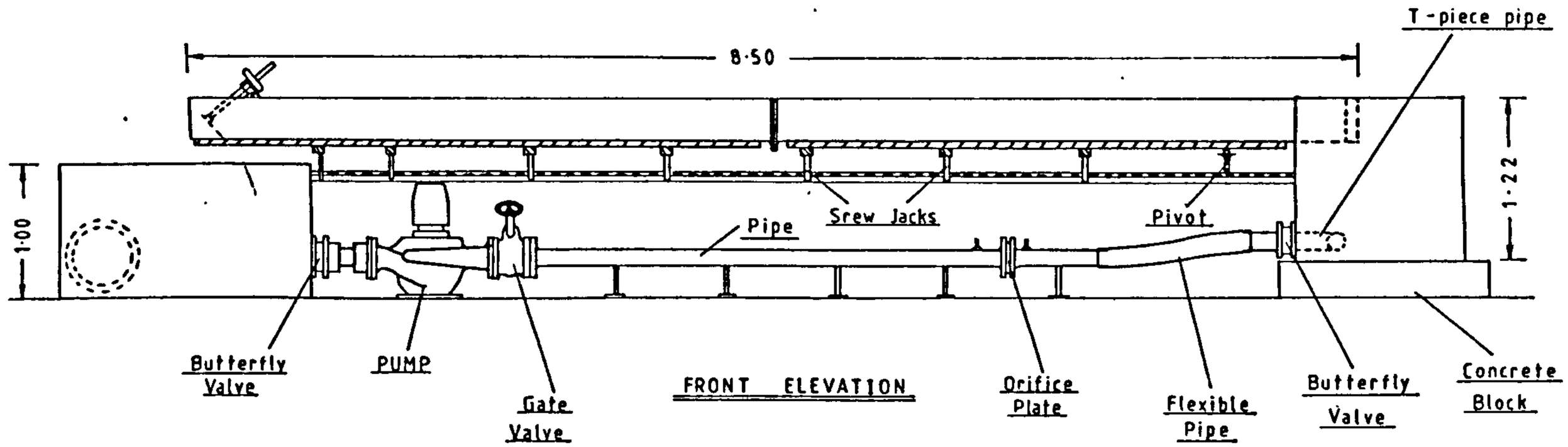

all dimensions in metres

instrument carriage is not shown

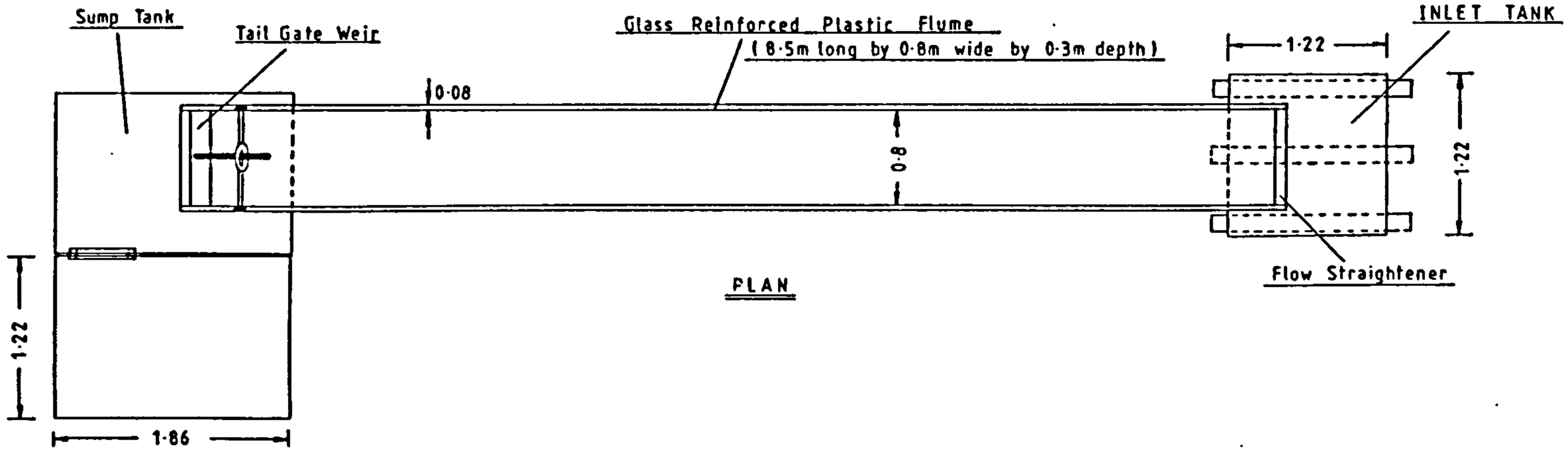

Fig 3·3 Overall Diagram of Model

UNIVERSITY OF GLASGOW DEPARTMENT OF CIVIL ENGINEERING	
HYDRAULIC FLUME	
J. BAIRD 13th June 1983	SCALE 1:80

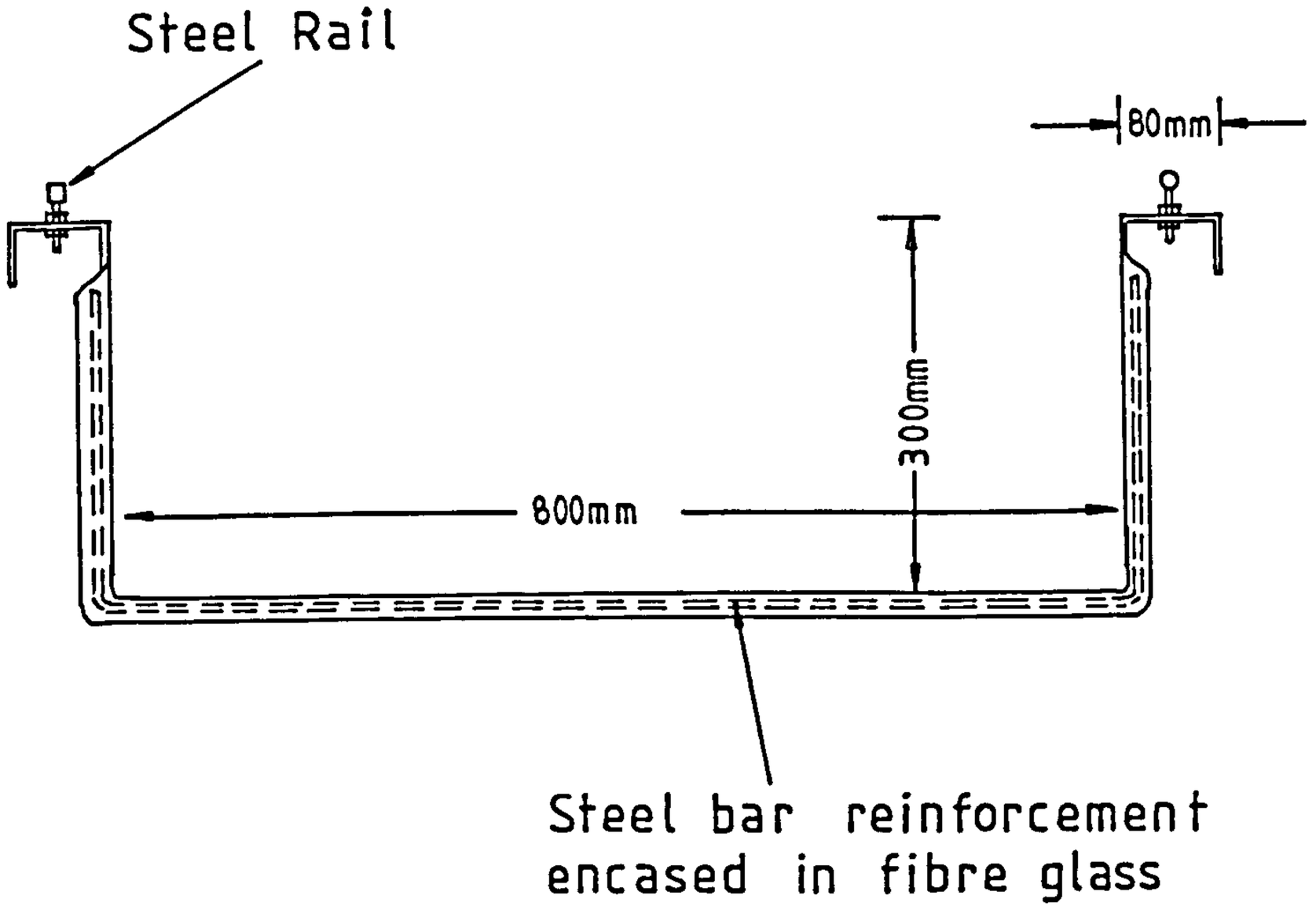

Fig 3·4 Cross Section of Channel.

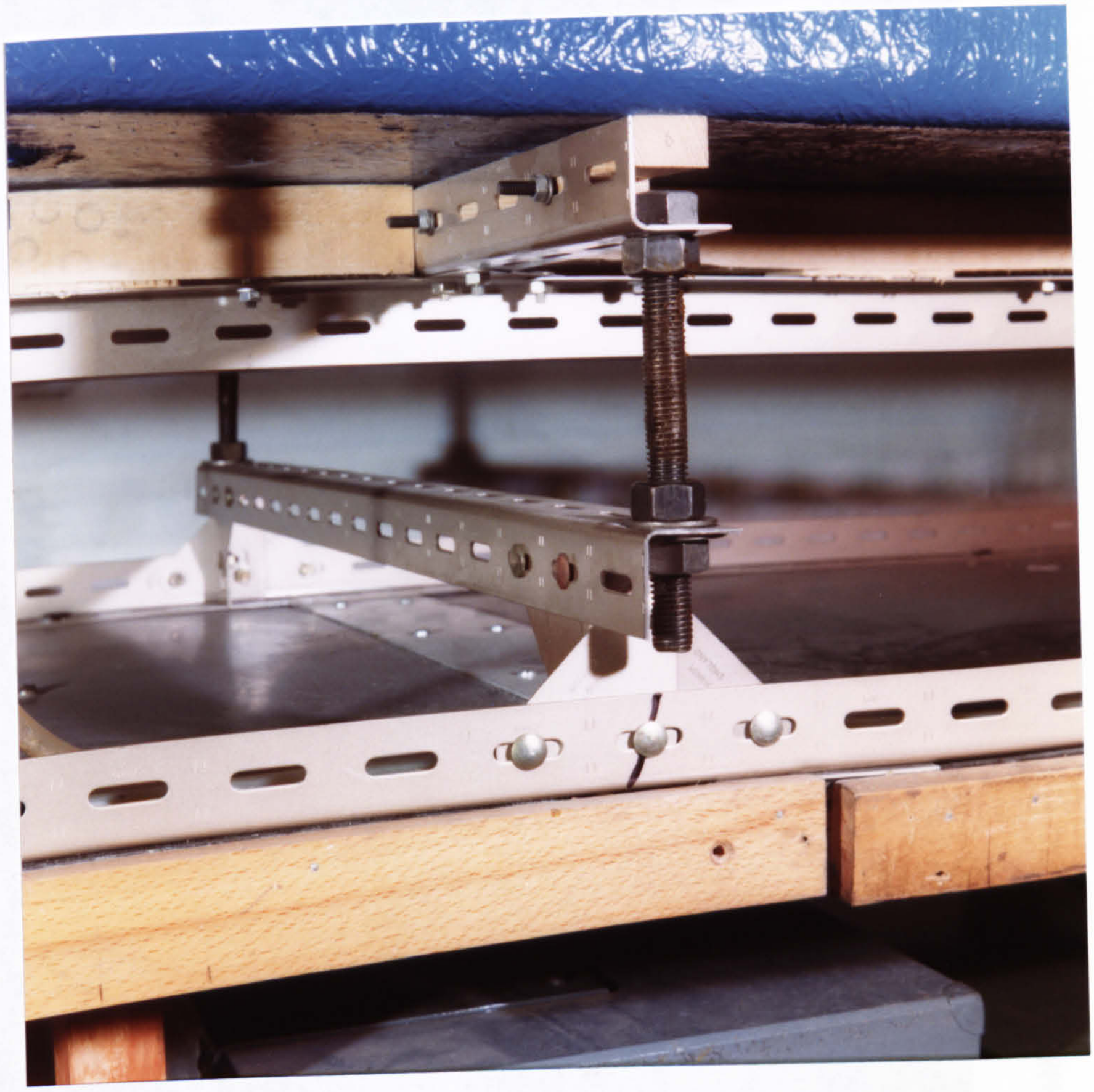

Fig 3·5 Screw jack Arrangement

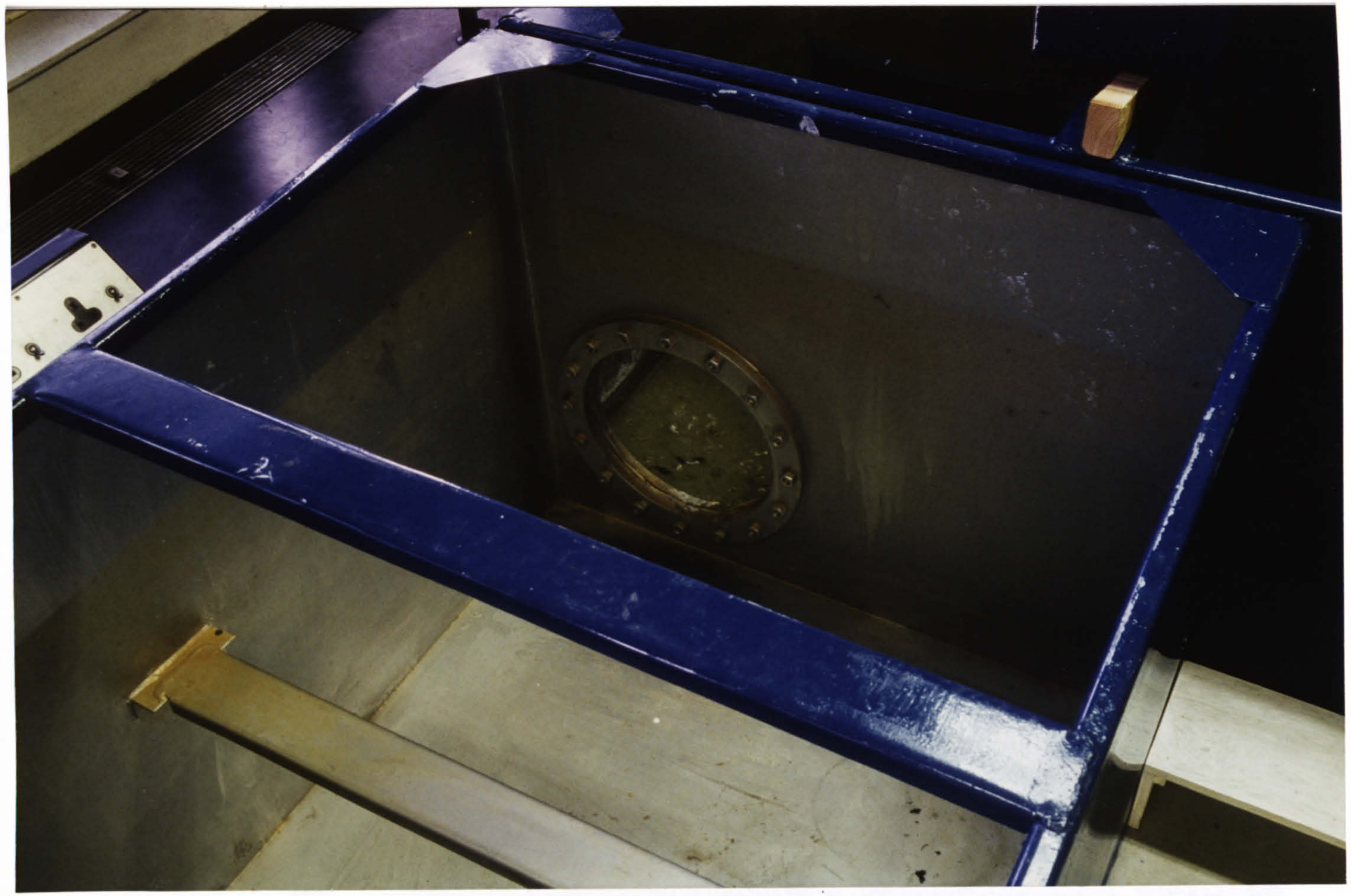

FIG 3.6 FLANGE ARRANGEMENT BETWEEN THE TWO SUMP TANKS.

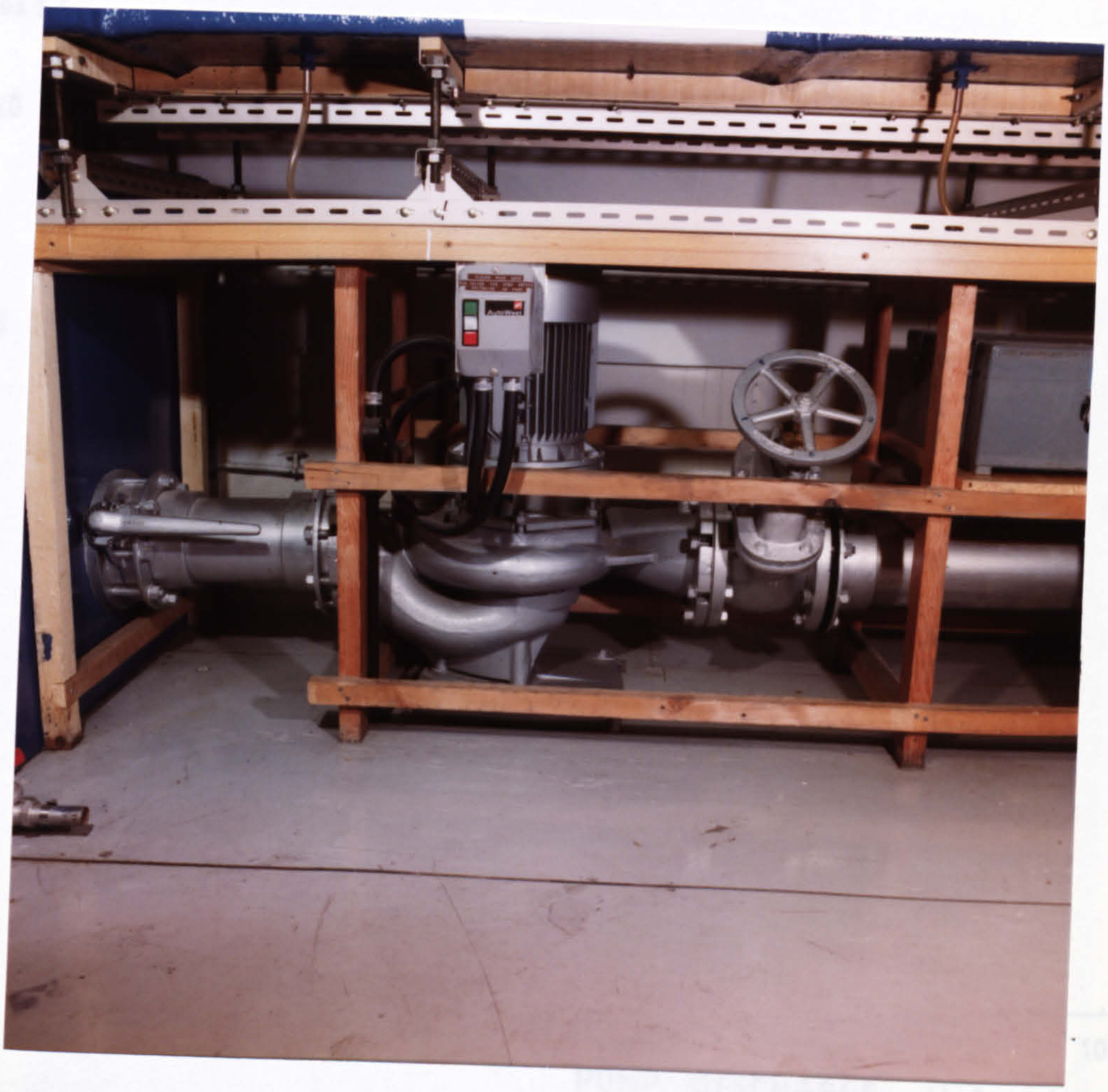

FIG 3.7 SUMP TANK PIPE SECTION, MYSON MSK 150-4210 PUMP AND GATE VALVE.

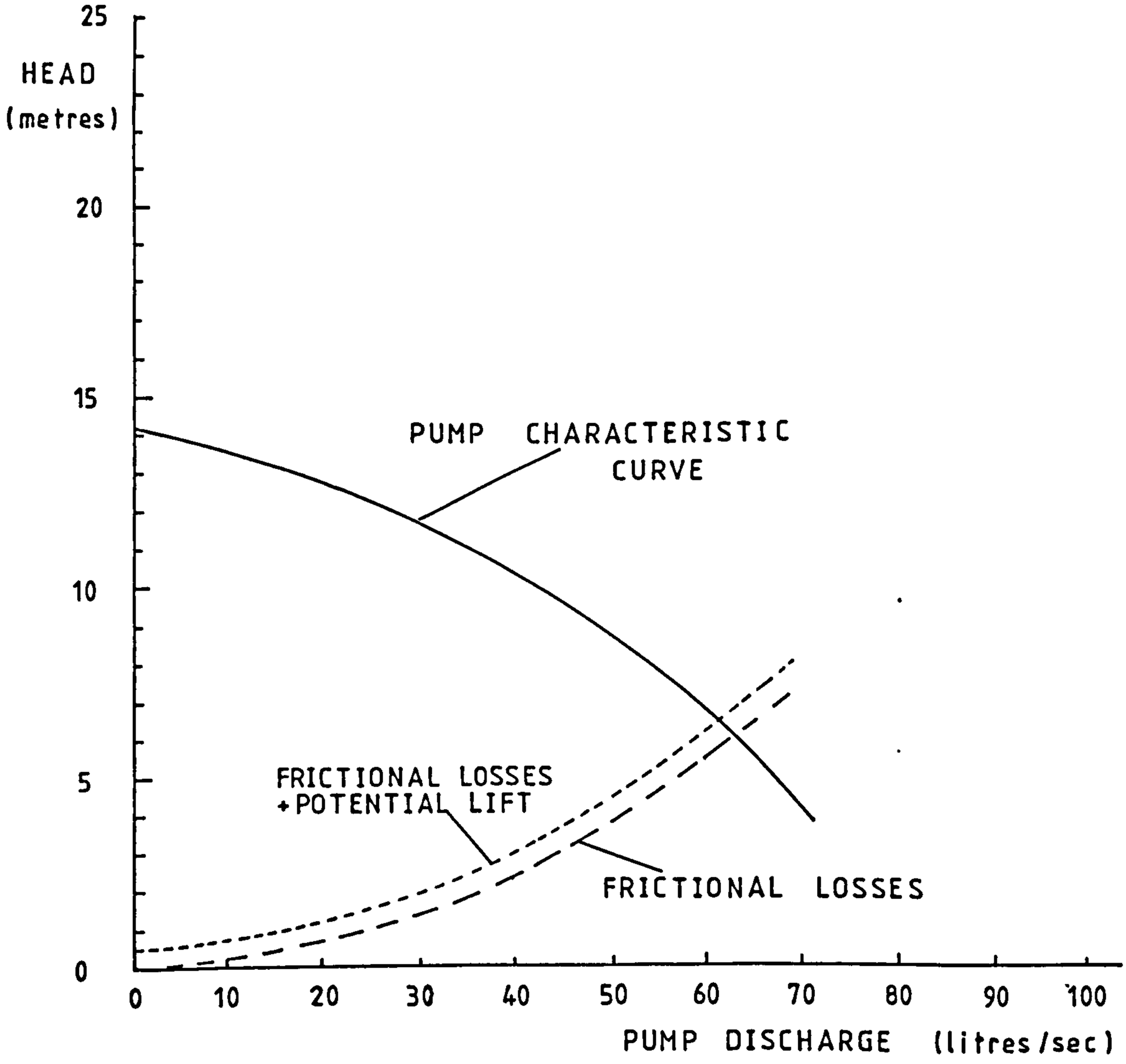

Fig 3·8 Performance Characteristics of the MYSON MSK 150-4210 Pump.

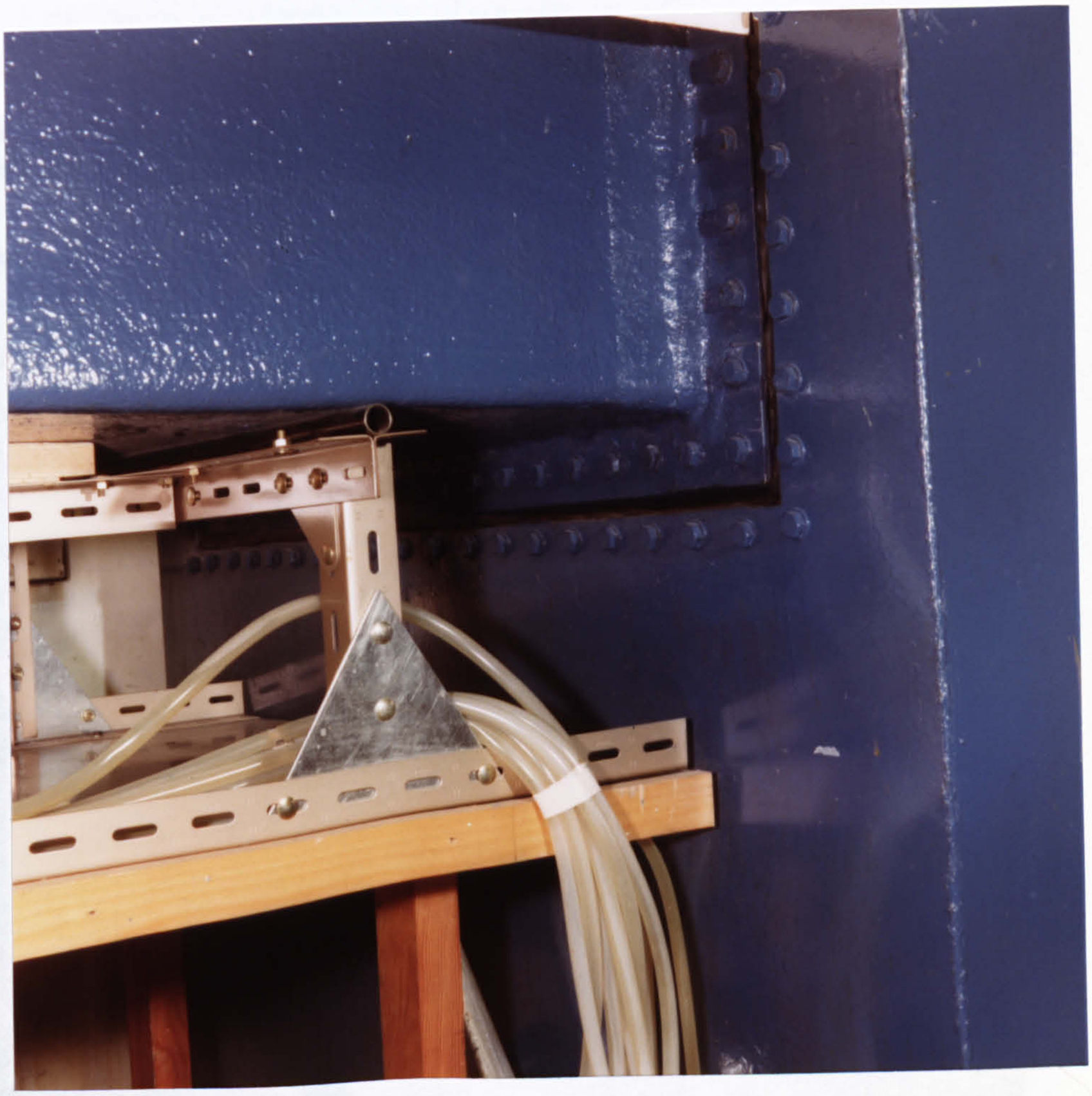

FIG 3.9 INLET TANK JOINT AND CHANNEL PIVOT ARRANGEMENT.

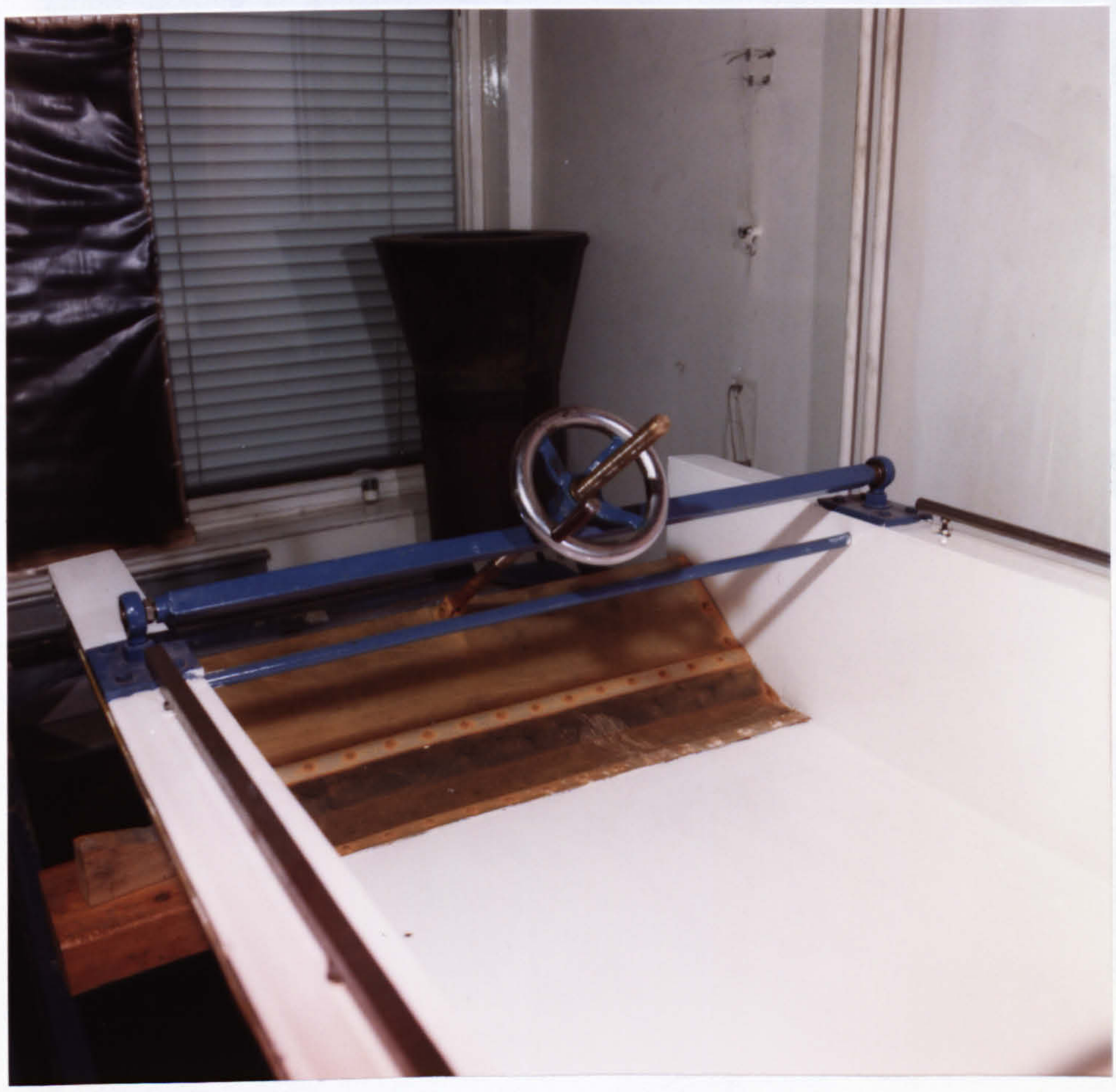

FIG 3 . 10 TAILGATE WEIR ARRANGEMENT.

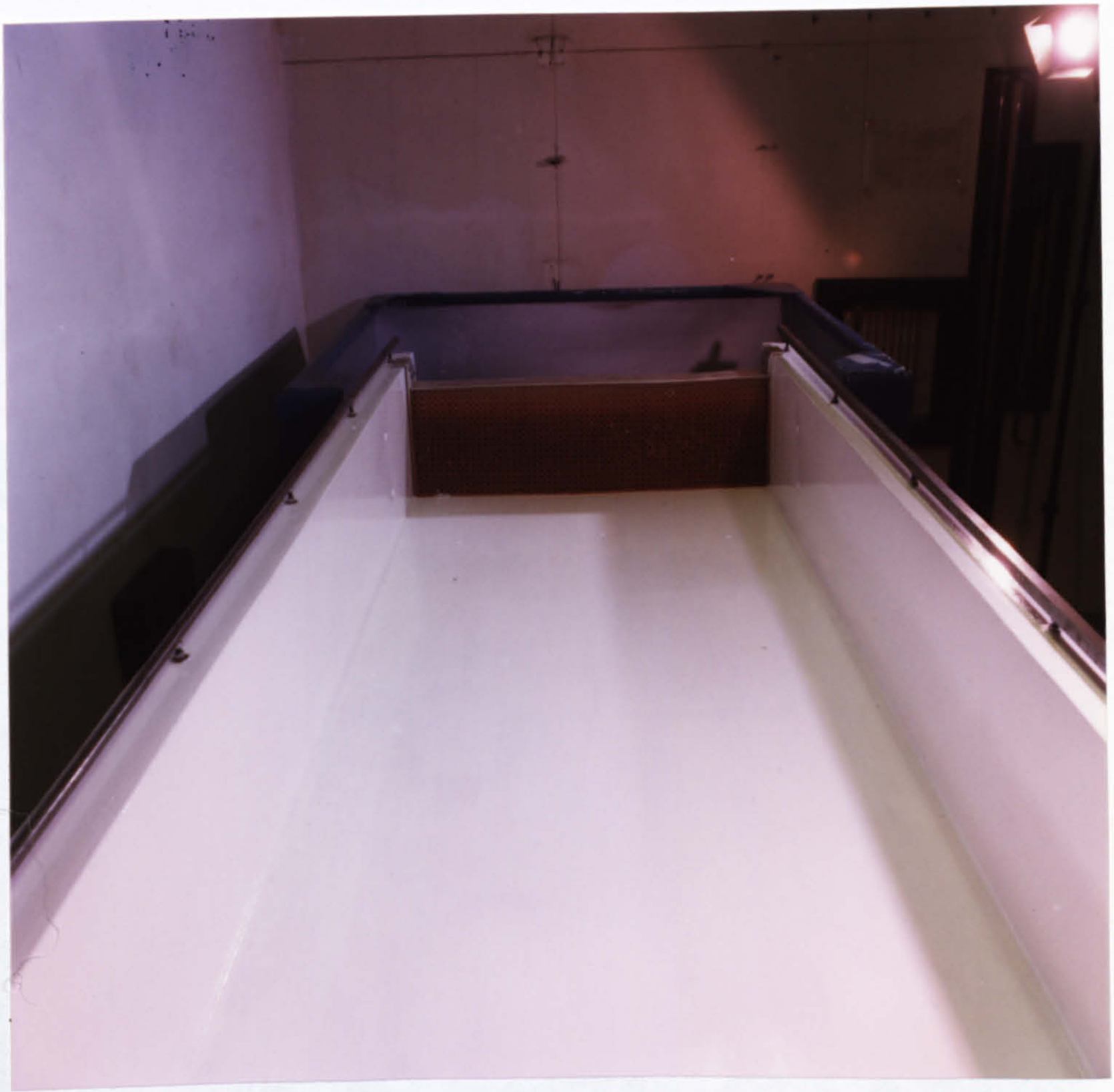

FIG 3.11 HONEYCOMB FLOW STRAIGHTENERS AT CHANNEL ENTRANCE.

FIG 3.12 T- PIECE SECTION IN THE INLET TANK
(HONEYCOMB FLOW STRAIGHTENER ALSO SHOWN).

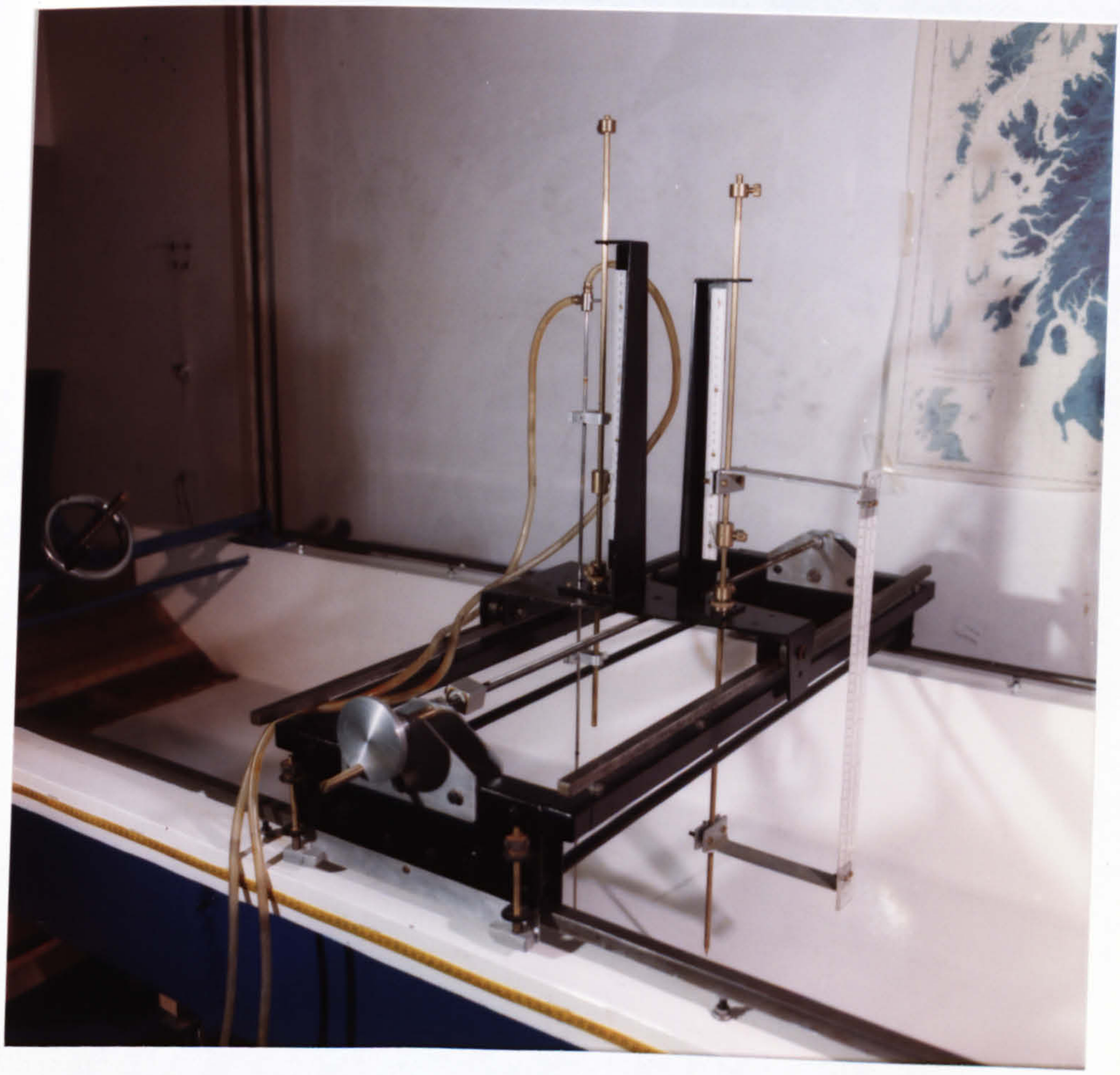

FIG 3. 13 INSTRUMENT CARRIAGE.

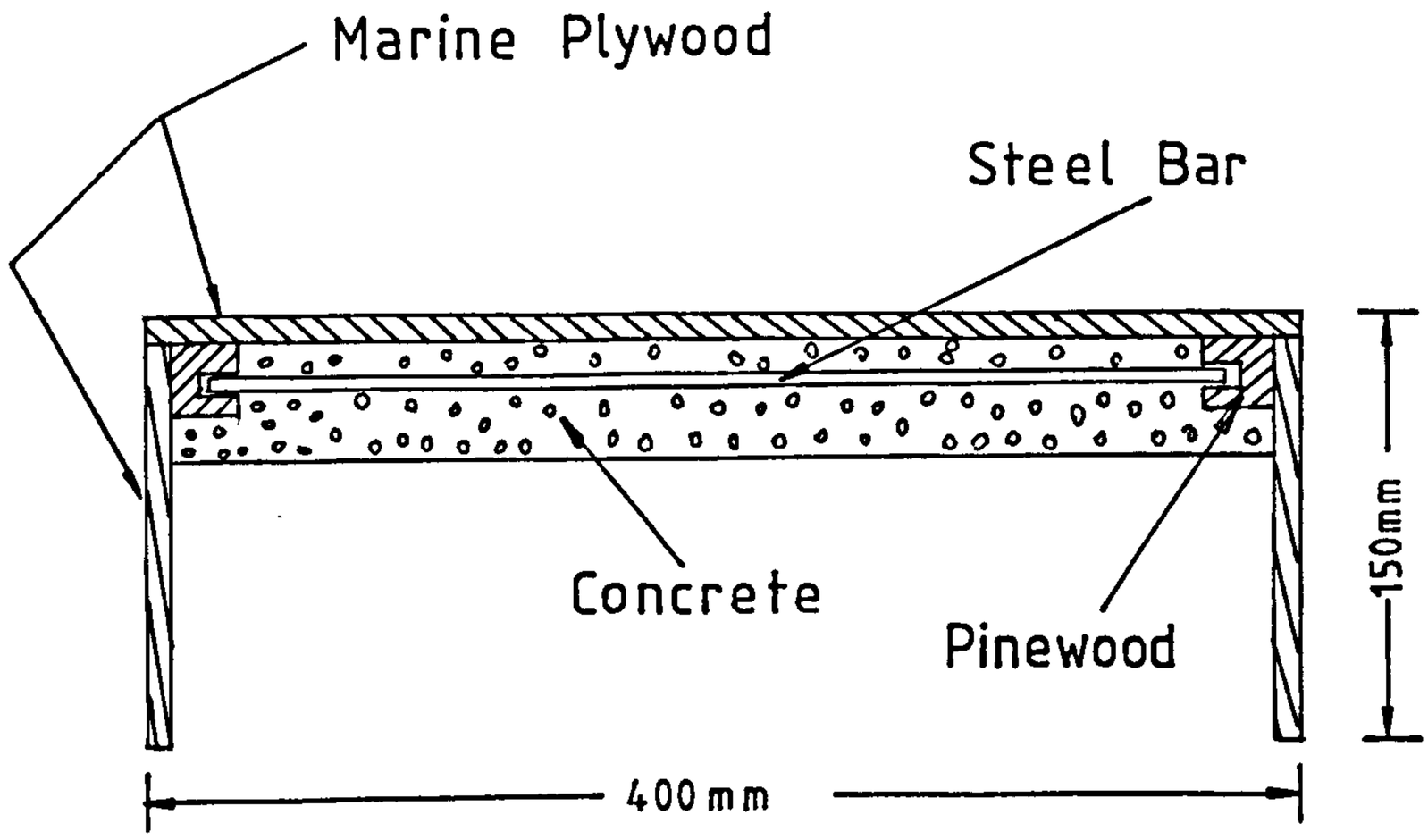

Fig 3·14 Typical Cross Section of Wooden Flood Plain Insert.

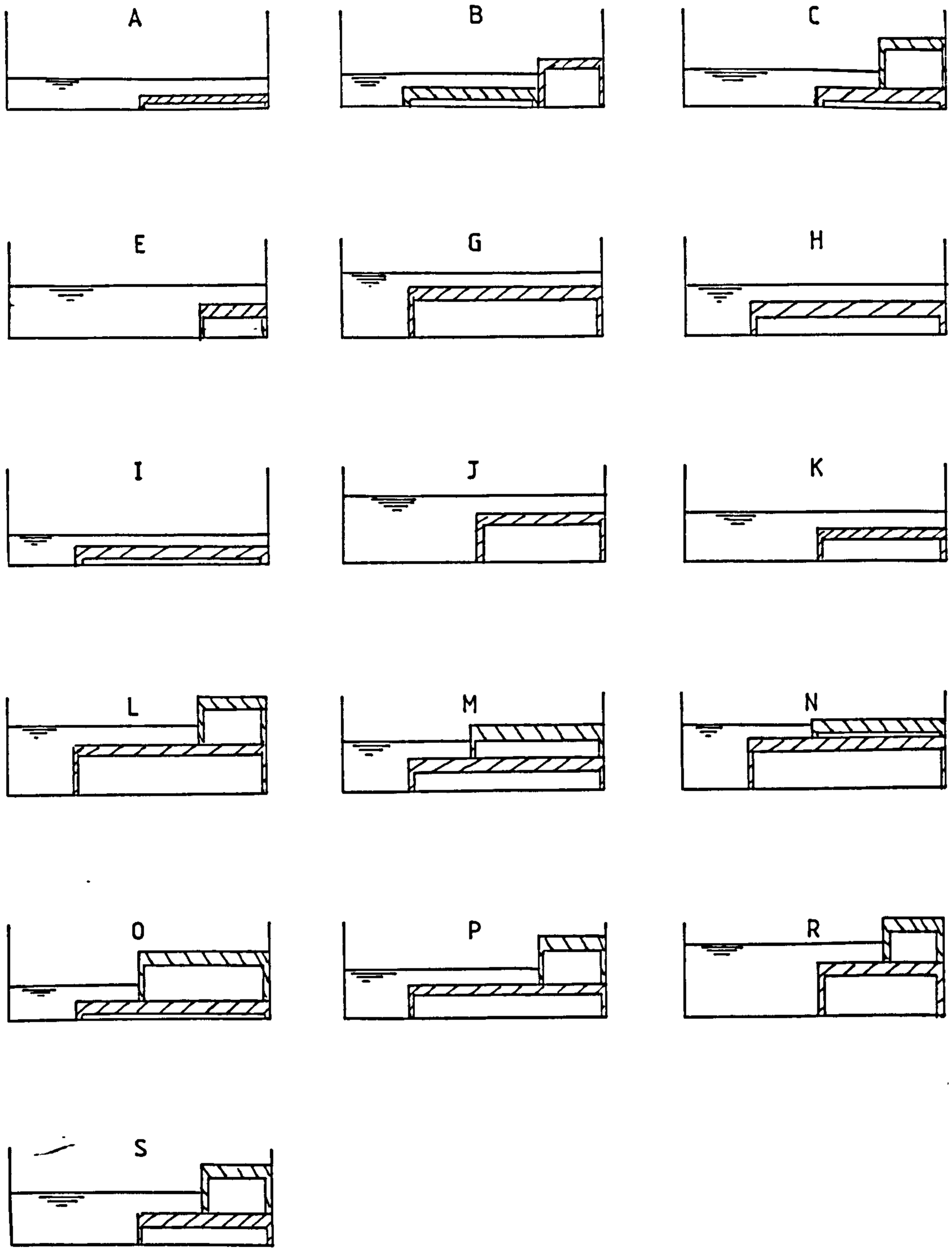

Fig 3·15 Combinations of Flood Plains to give Geometries tested.

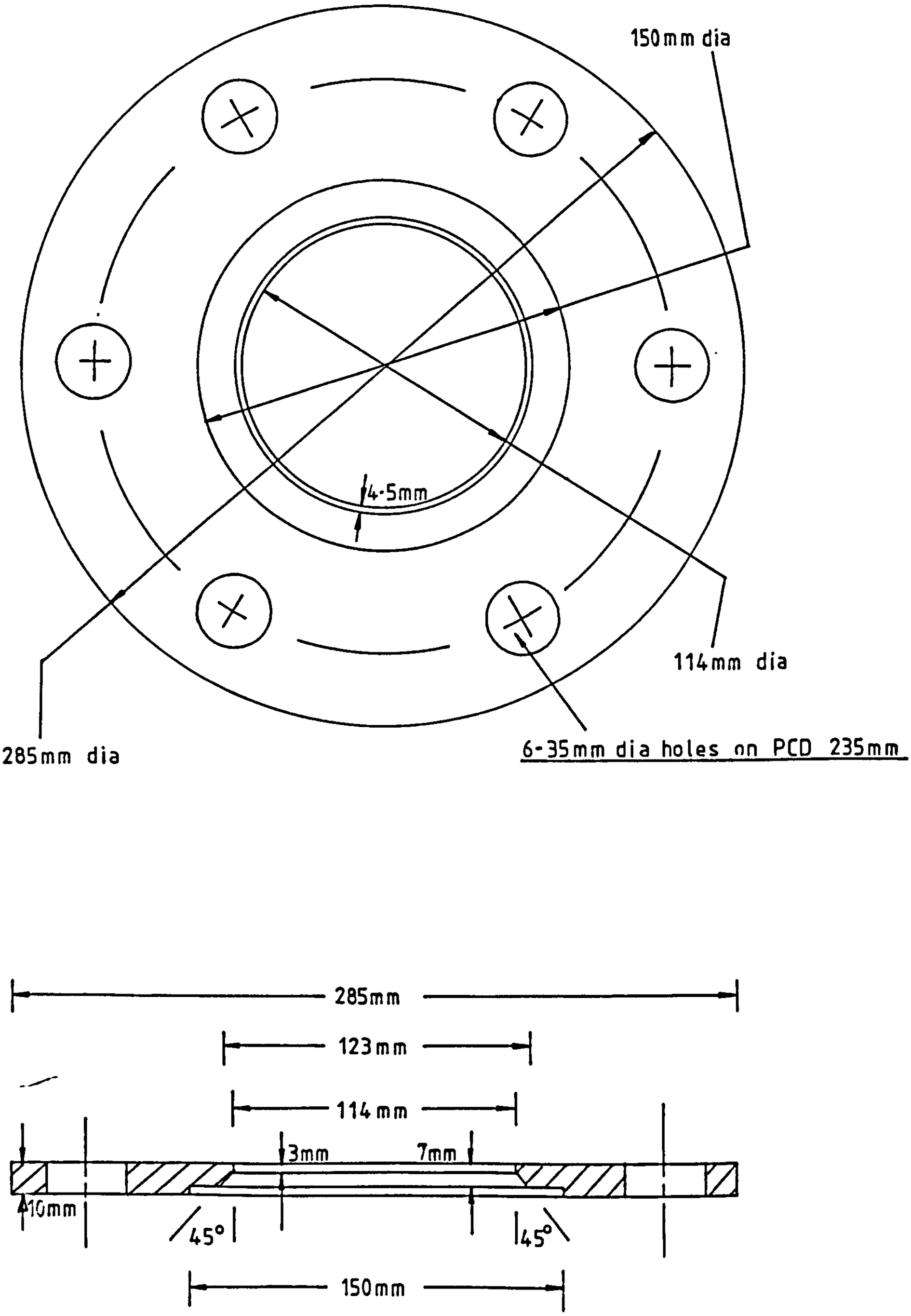

Fig 3·16 Orifice Plate Details

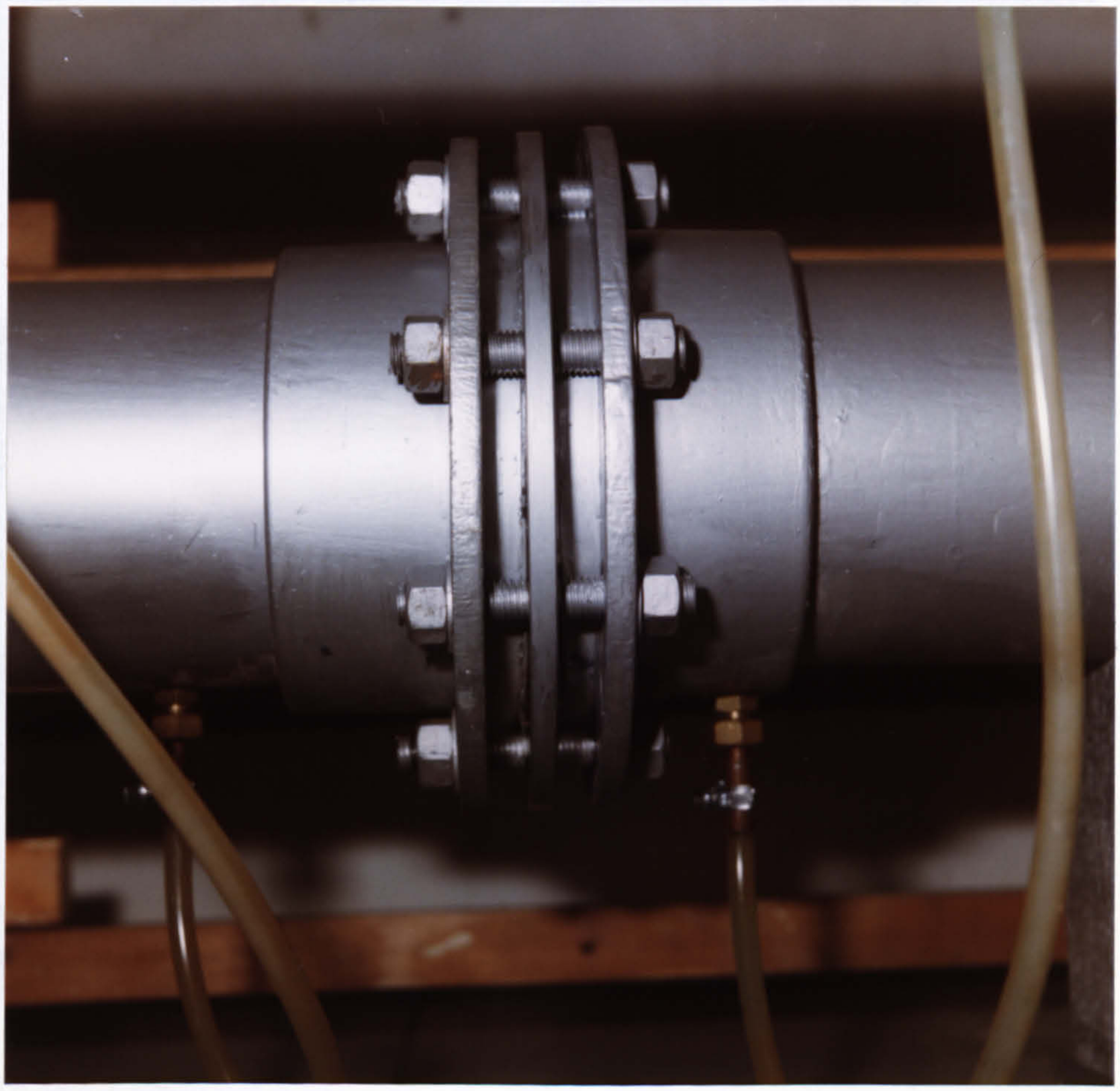

FIG 3.17 PHOTOGRAPH SHOWING POSITION OF ORIFICE PLATE WITH D AND $D/2$ TAPPINGS.

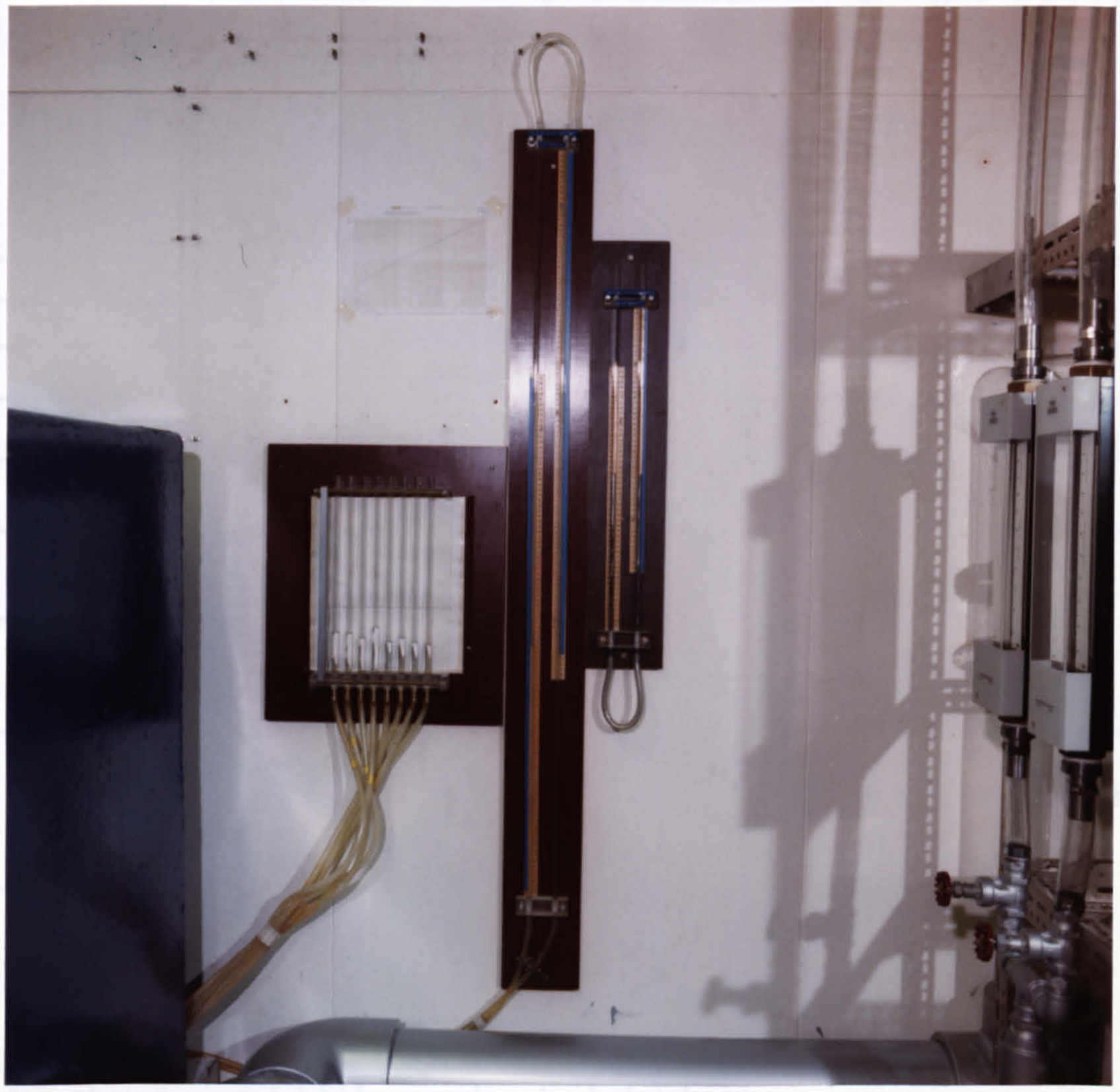

FIG 3.18 MANOMETER BOARD SHOWING WATER AND MERCURY MANOMETERS.

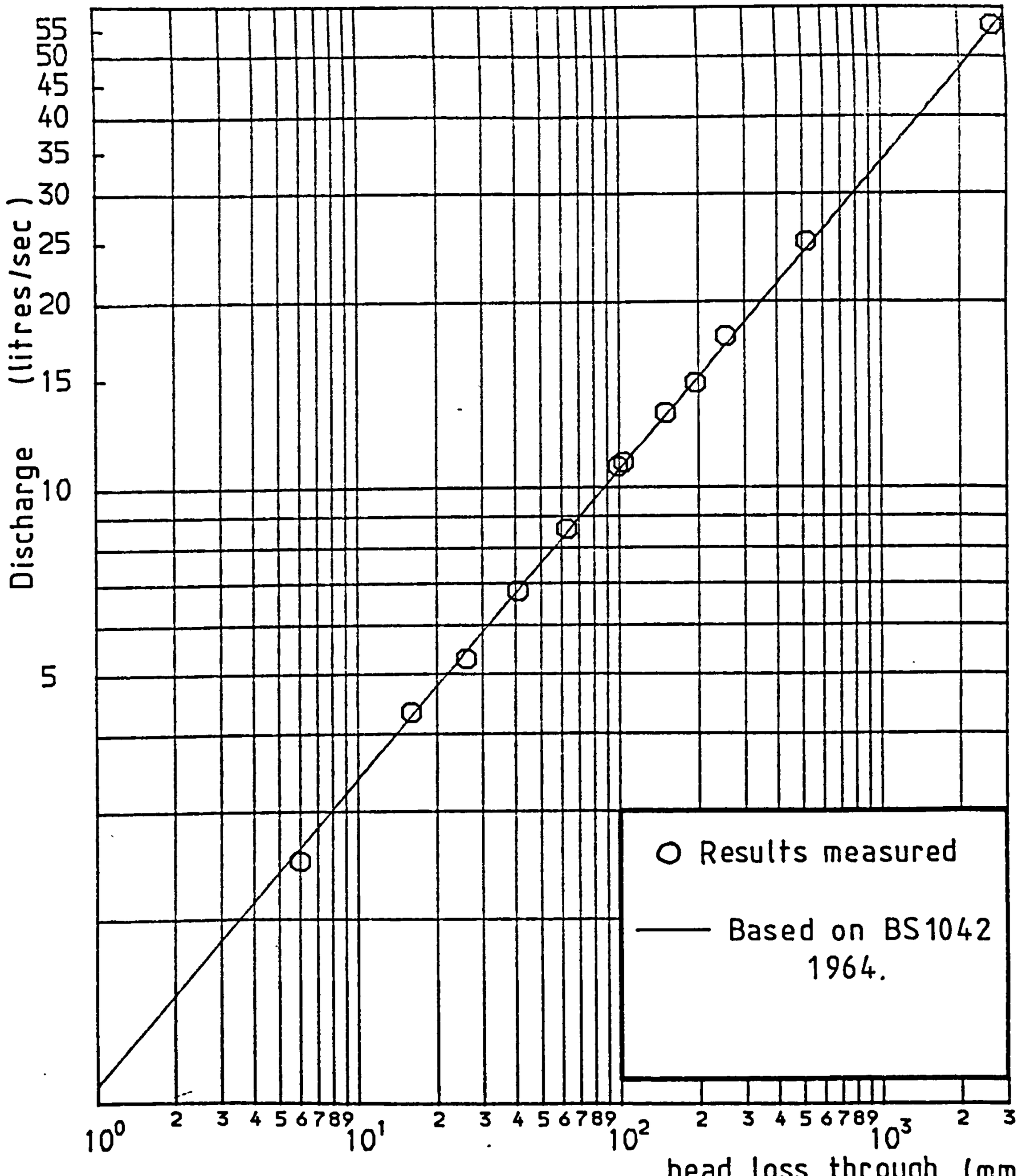

Fig 3.19 Relationship between measured discharge and orifice reading

FIG 3.20 SURVEYING LEVEL USED TO DETERMINE CHANNEL SLOPE.

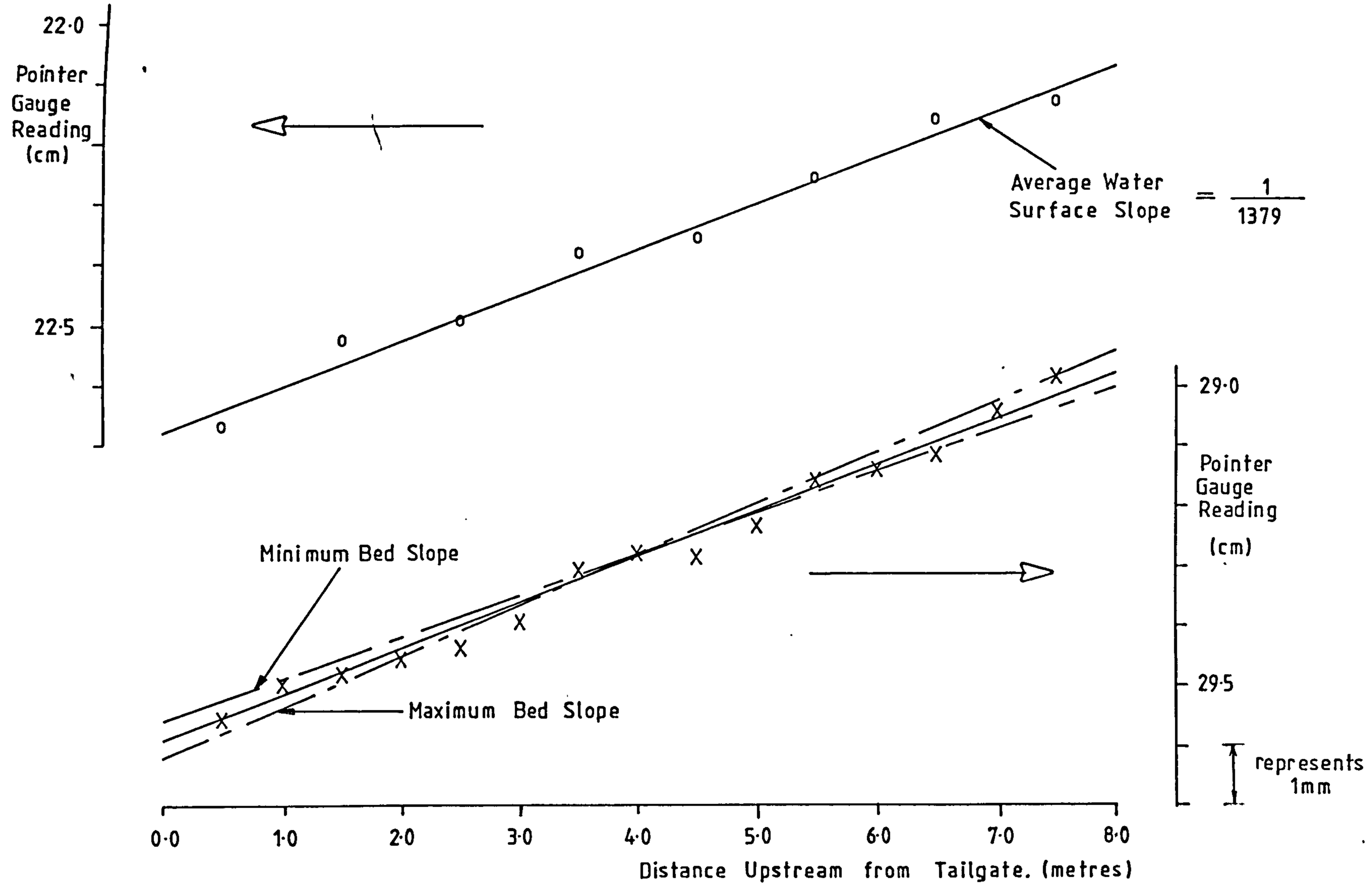

Fig 3·21 Typical Bed and Water Surface Profiles

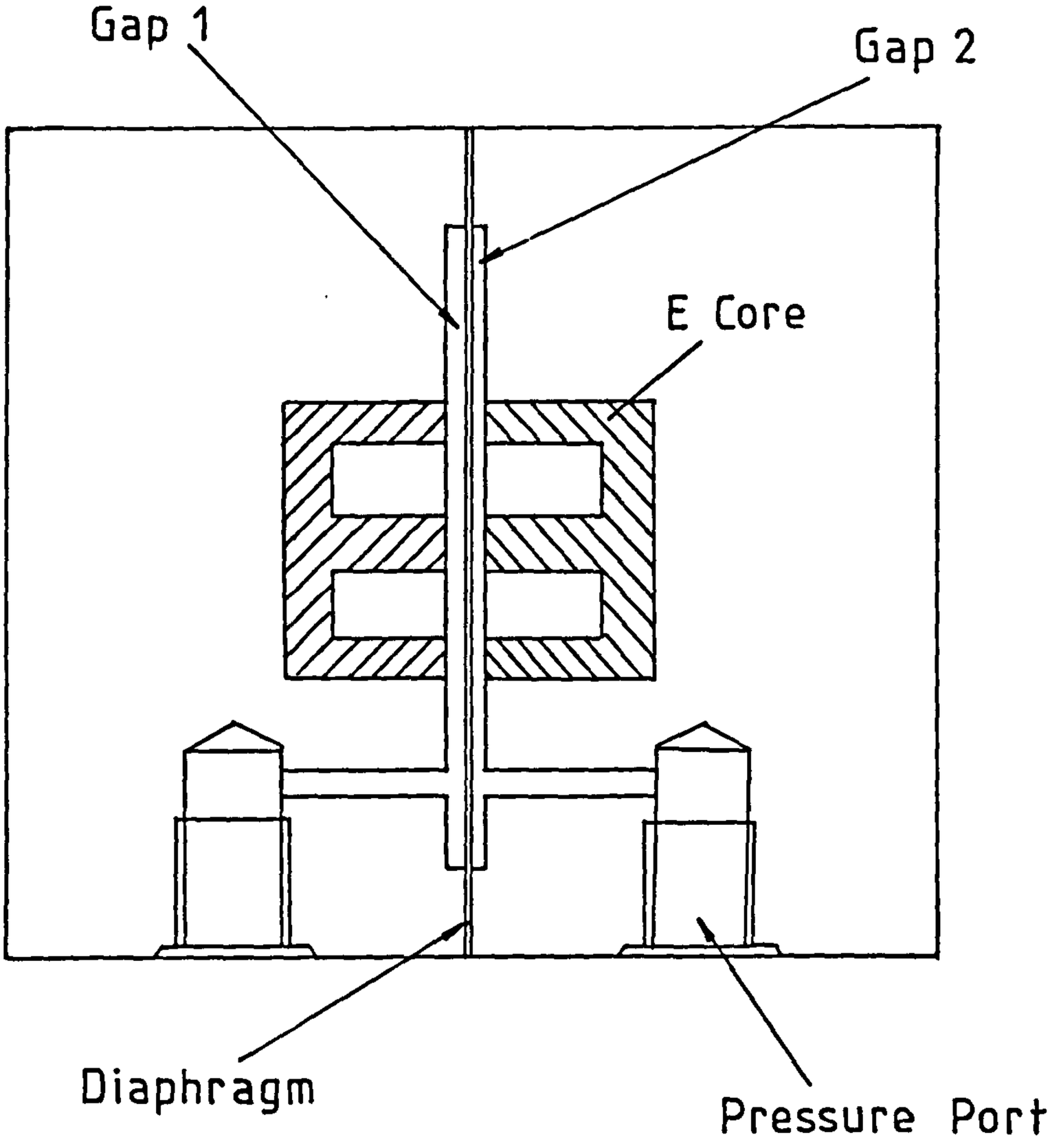

Fig 3·22 Schematic Diagram of the Variable Magnetic Reluctance Transducer.

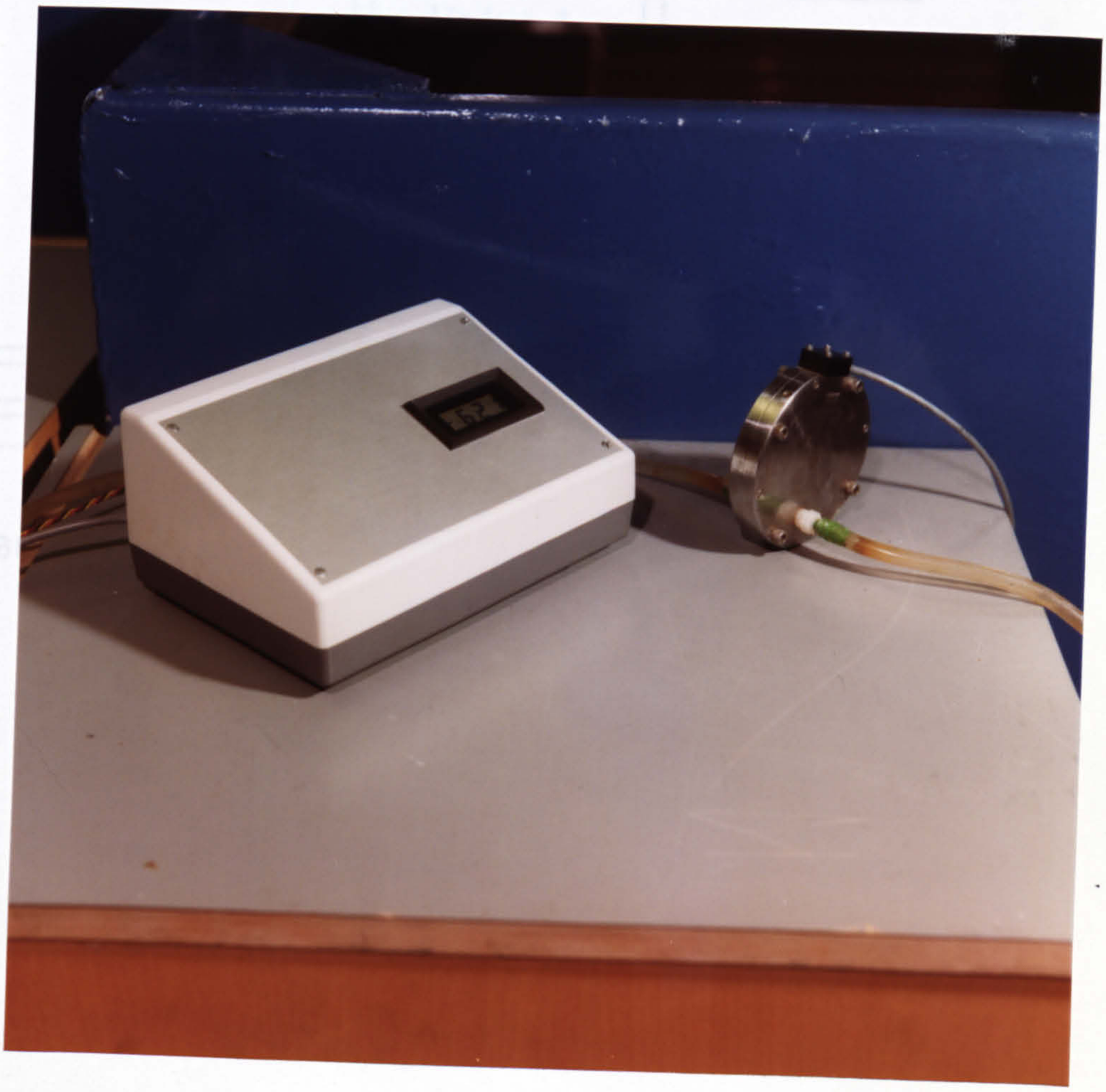

FIG 3.23 PRESSURE TRANSDUCER AND CARRIER DEMODULATOR.

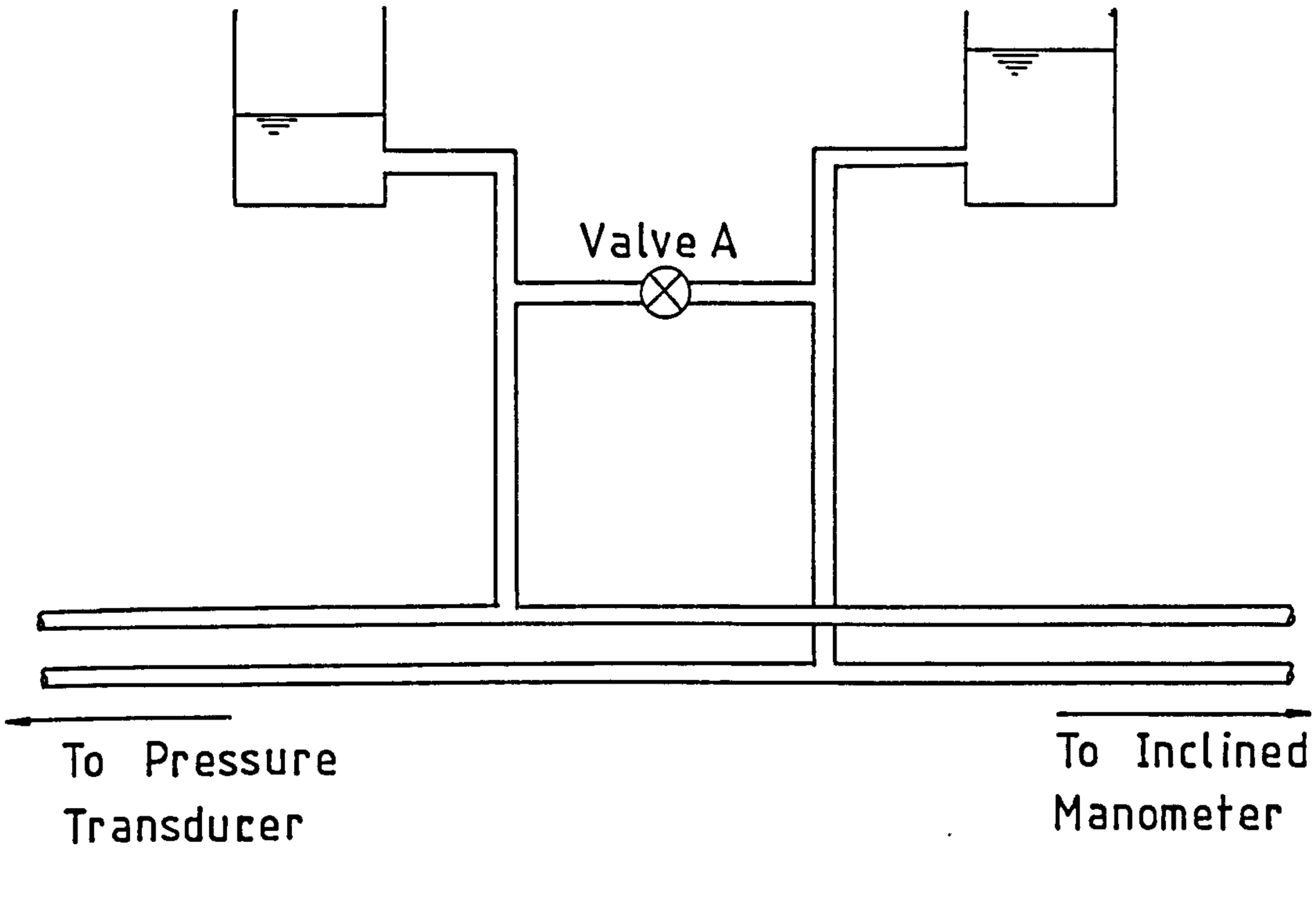

Fig 3·24 Beaker Arrangement used for Pressure Transducer Calibration

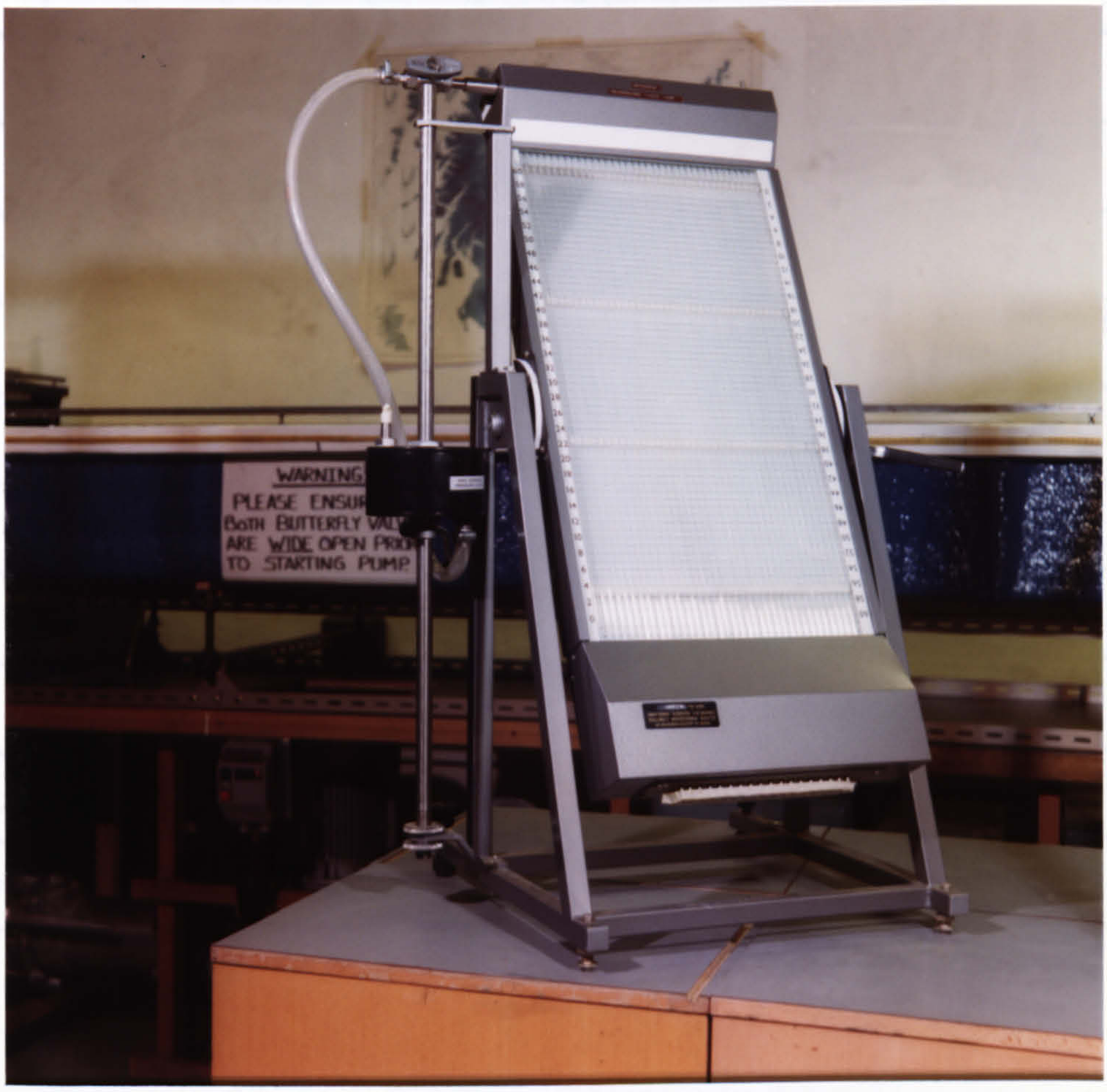

FIG 3 . 25 INCLINED MANOMETER USED TO CALIBRATE THE PRESSURE TRANSDUCER.

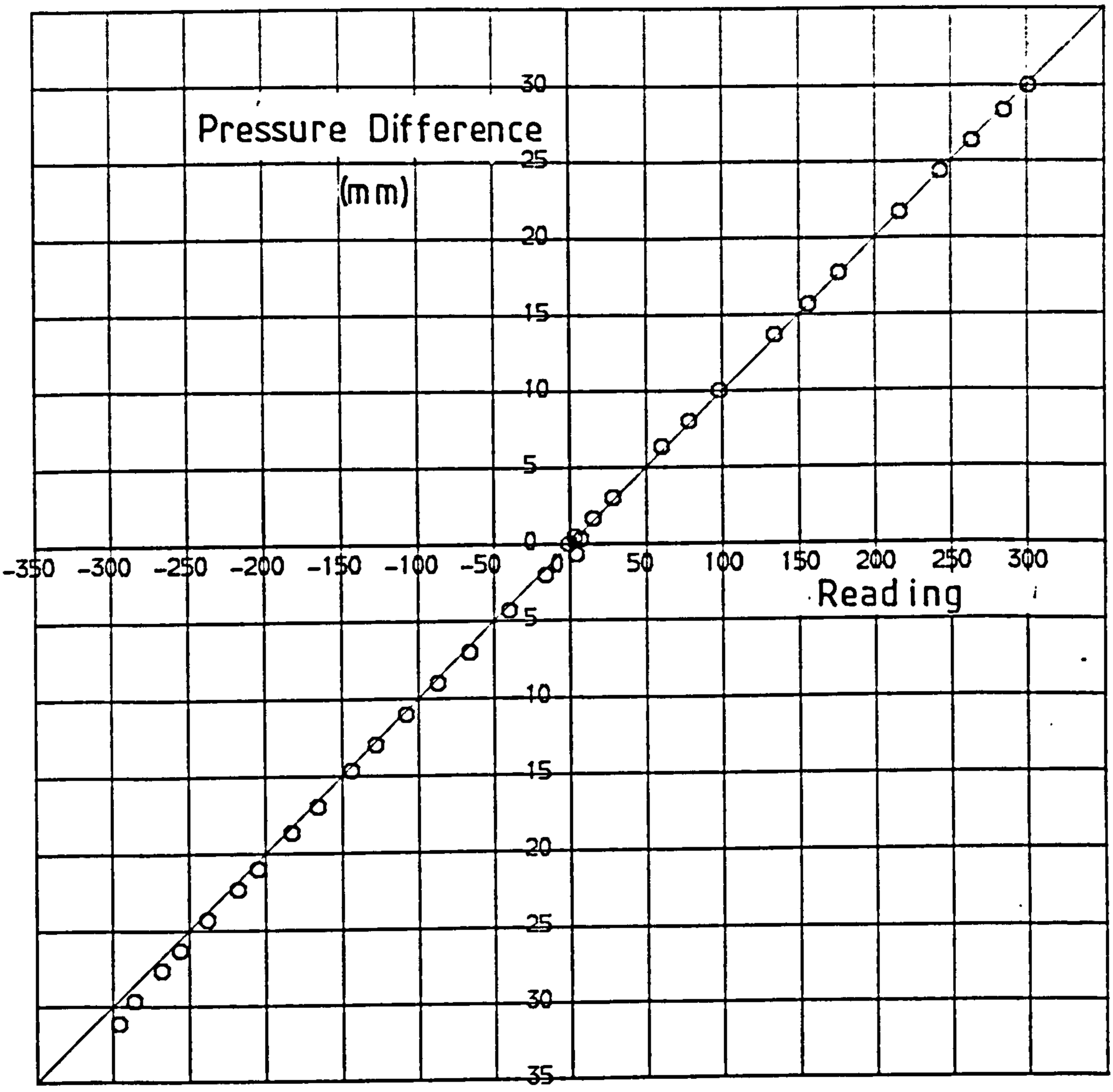

Fig 3·26 Pressure Transducer Calibration showing linear Relationship between Reading and Pressure Difference

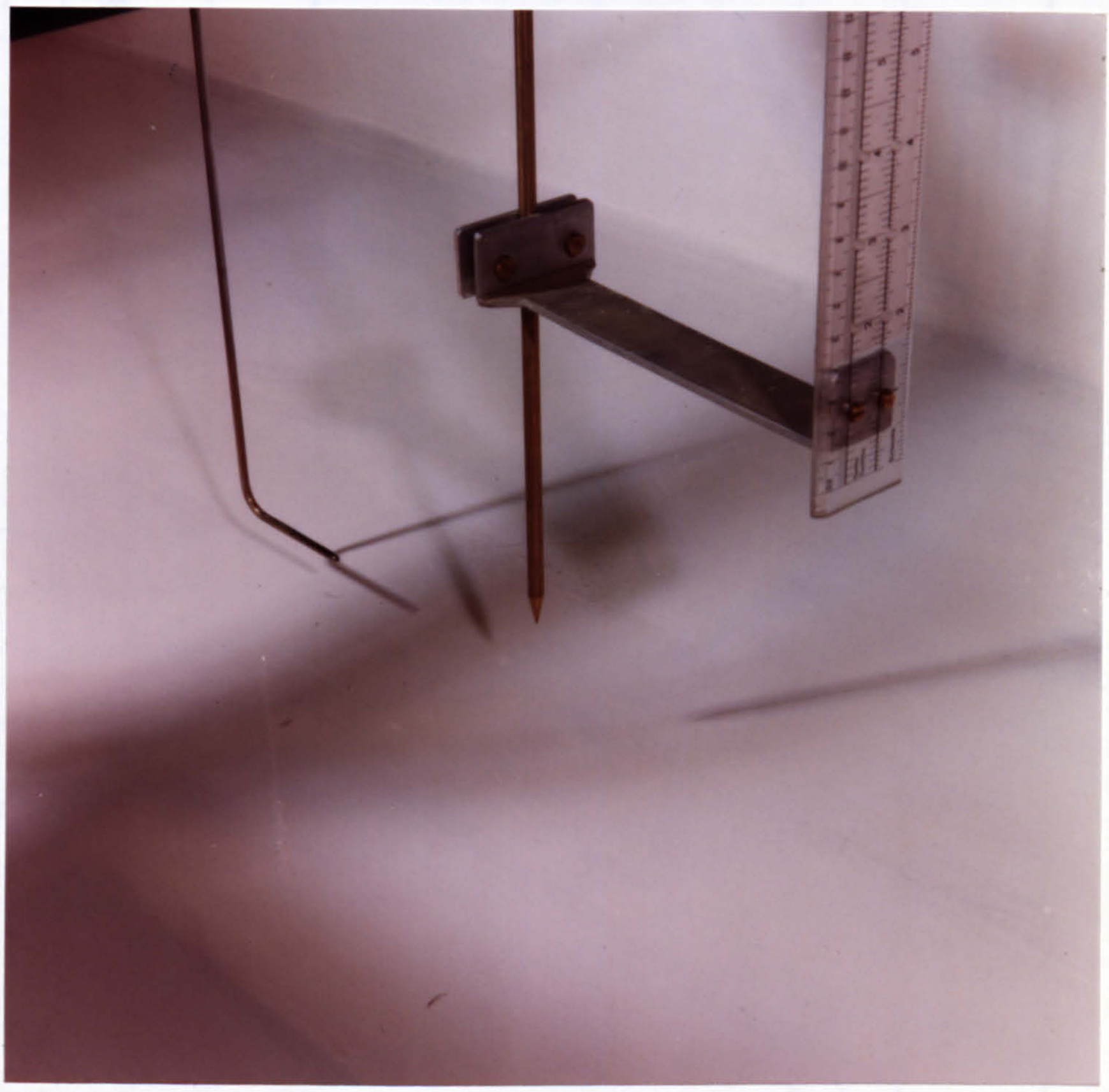

FIG 3.27 WATER LEVEL POINTER AND PITOT STATIC TUBE.

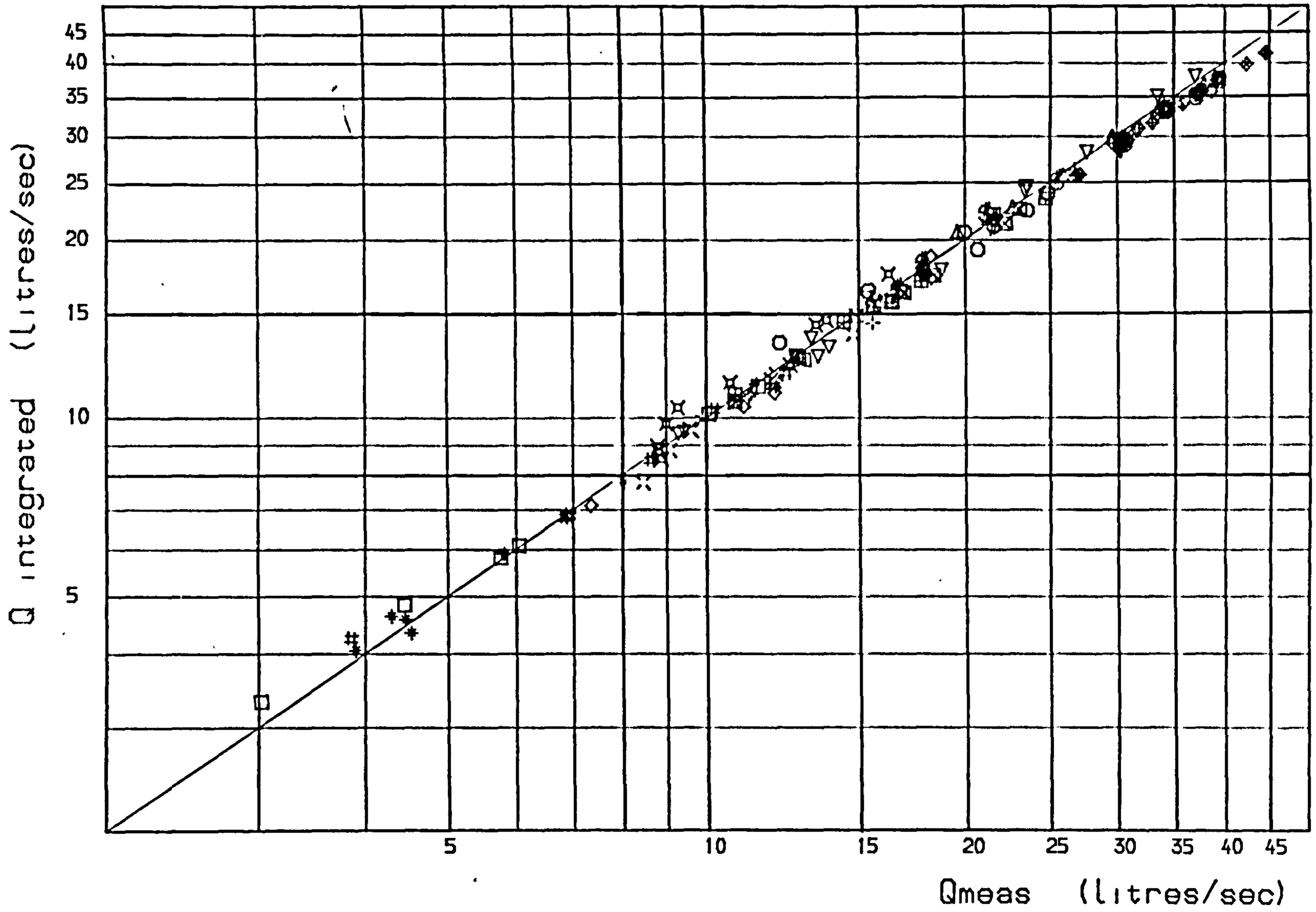

Fig 3·28 Measured discharge against integrated discharge.

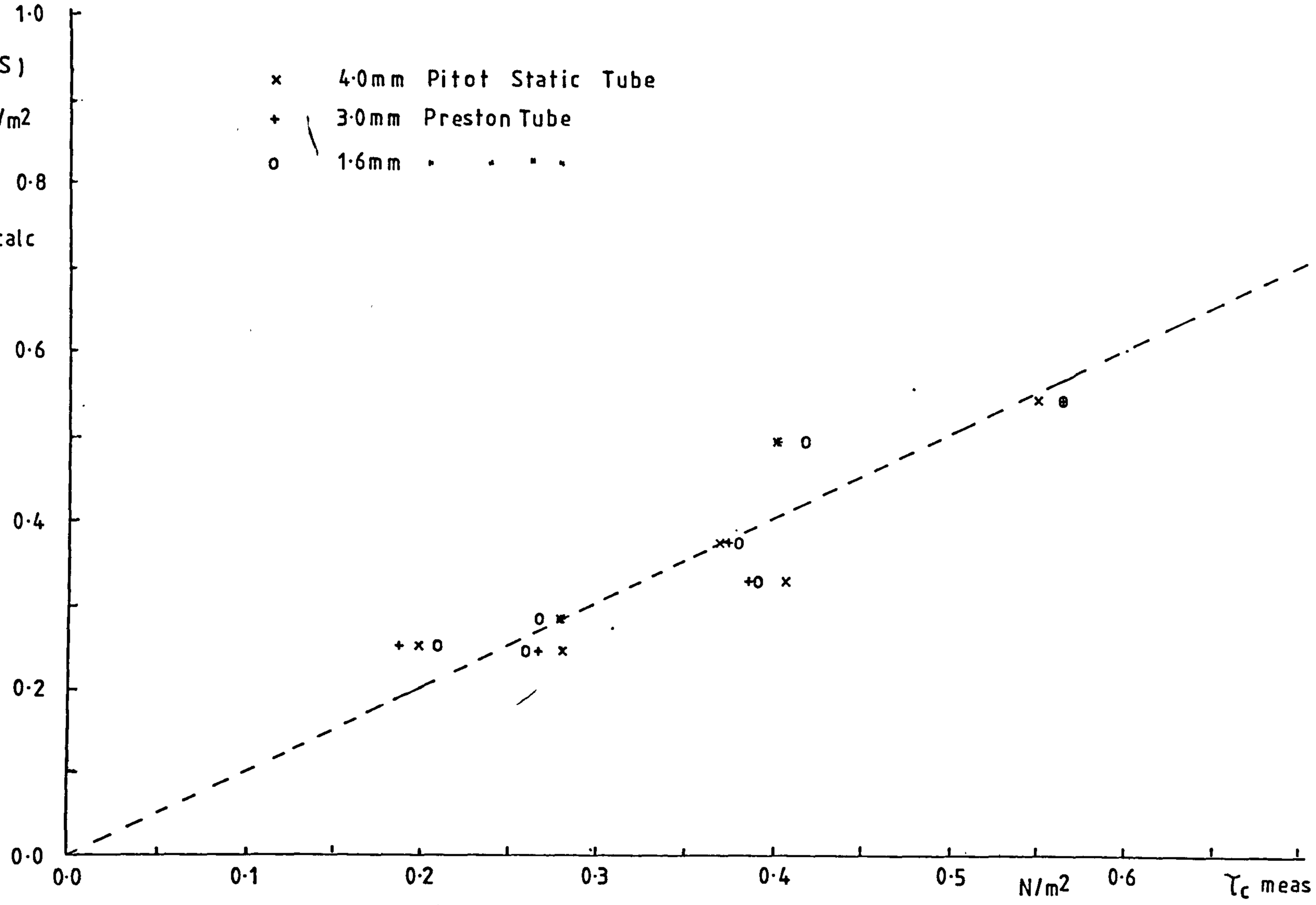

Fig3·29 Comparison of Calculated Shear and Measured Shear.

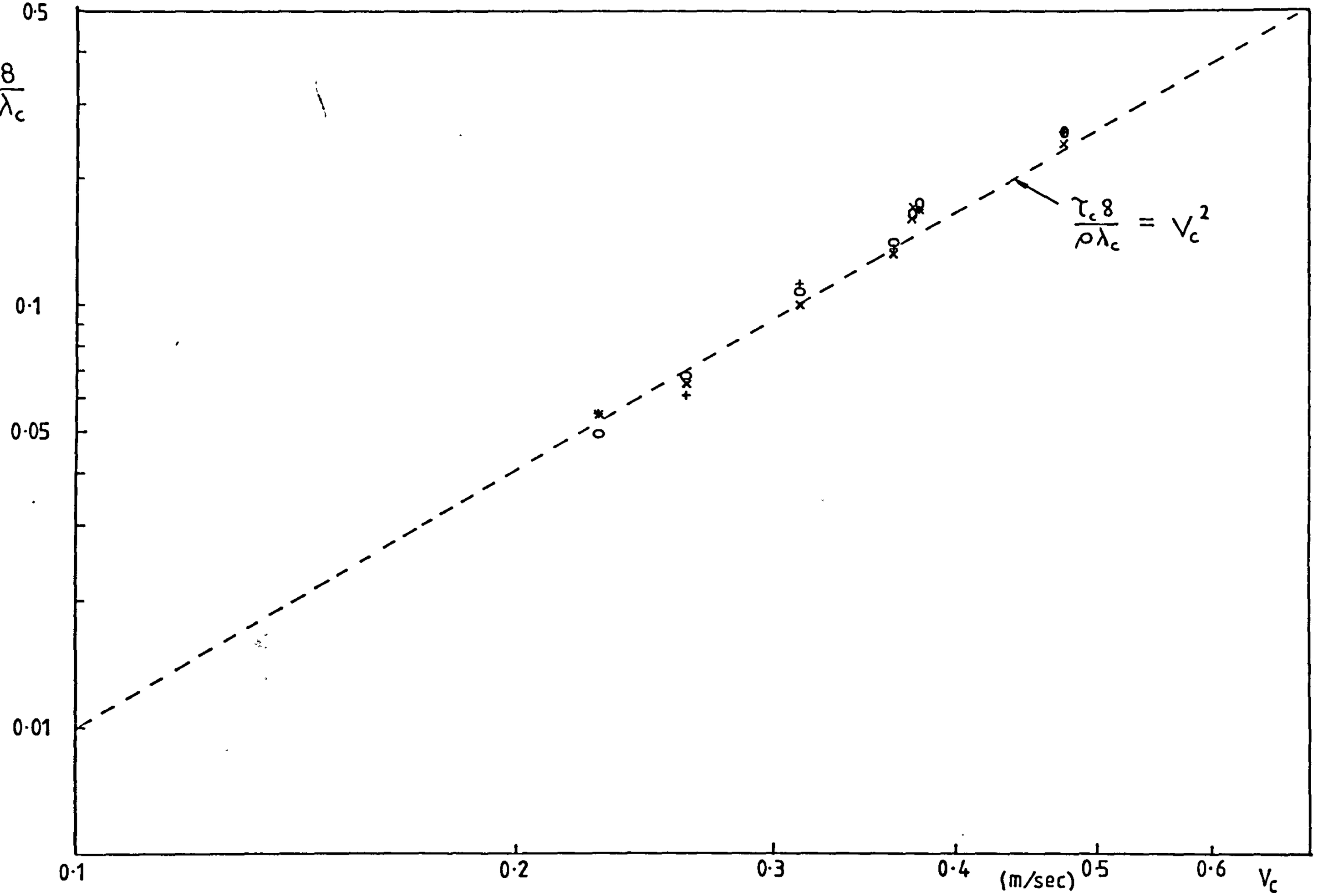

Fig 3·30 Comparison of measured Shear and Velocity in Channel.

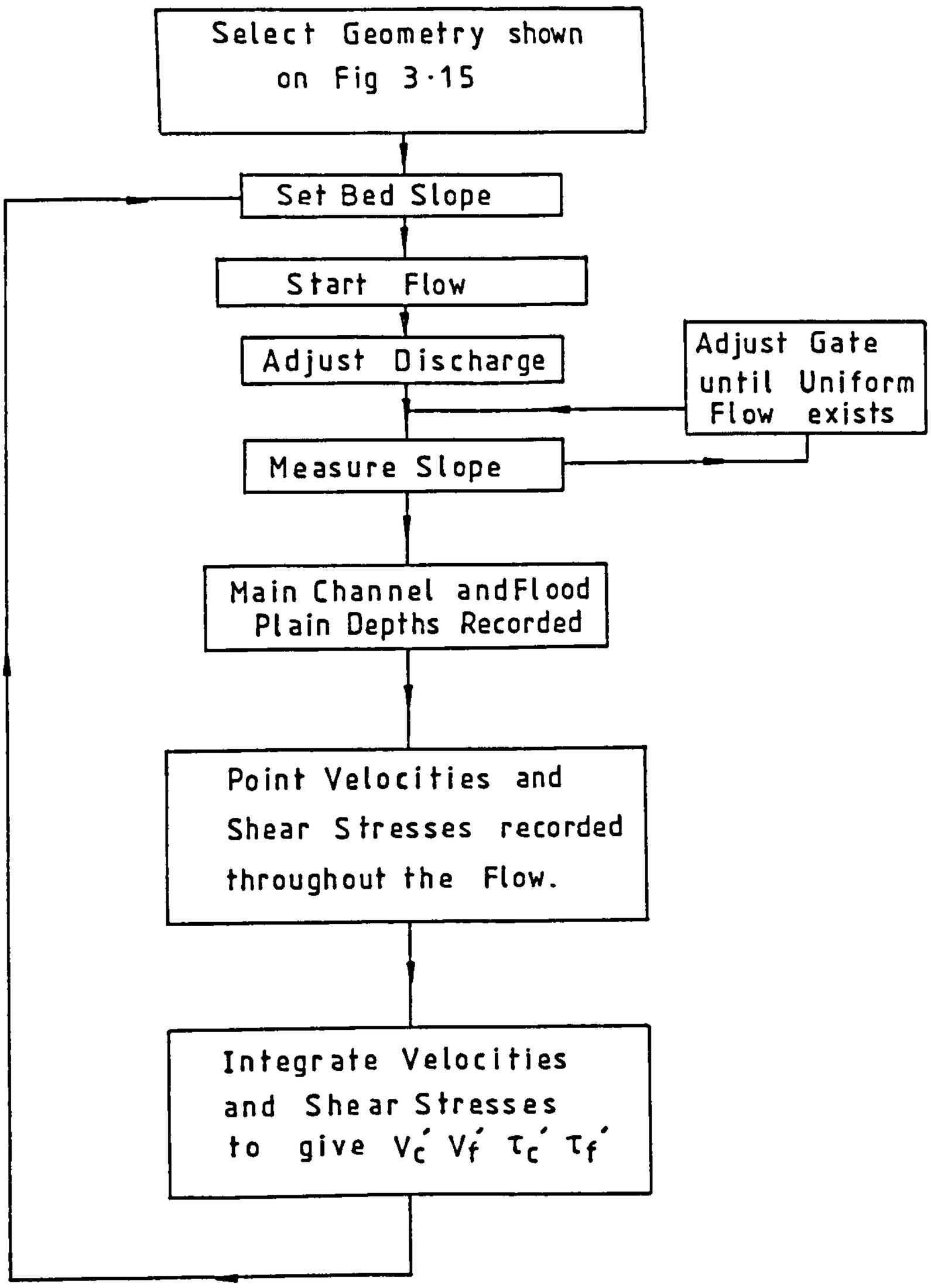

Fig 3·31 Flow Chart showing Experimental Procedure.

BLANK IN ORIGINAL

CHAPTER FOUR

THE EFFECT OF THE INTERACTION MECHANISM ON FLOW VELOCITIES IN THE CHANNEL AND FLOOD PLAIN

Table of Contents

4.4.3 Results of Point Velocity Measurements.

4.4.3.1 General Considerations.

4.4.3.2 The effect of varying the Relative Depth.

4.4.3.3 The effect of varying the Bankfull Depth.

4.4.3.4 The effect of varying the channel width.

4.4.3.5 The effect of varying the floodplain width.

4.4.3.6 The effect of B_f/B_c on the degree of interaction.

4.5 Conclusions.

4.1 Introduction.

In chapter 3 the experimental model was described and an outline given of the experimental procedure carried out for a series of 136 tests. This chapter will present the results of these tests in terms of the local velocity distributions and stage-discharge relationships.

It can be appreciated that before the effects of the channel/flood plain interaction on the channel and flood plain can be quantified, an understanding regarding the hydraulic behaviour of the flow must be obtained when the flow is confined to the channel alone and the flood plain alone. It was therefore considered necessary to establish the friction factors for the flume with the channel and flood plain isolated. A series of such tests were carried out and their description and results are presented in section 4.2.

From the literature review it became apparent that the channel/flood plain interaction transferred momentum from the channel to the flood plain at low flood plain depths resulting in the stage-discharge relationship for the cross section being significantly altered at low flood plain depths. It was therefore decided that initial testing of the compound channel

flow should involve establishing the stage-discharge relationship for channel depths which include overbank flow. These series of tests are presented in section 4.3 and a comparison is made between the results obtained and various methods of discharge prediction as presented in the literature review.

Section 4.4 deals essentially with the 136 full tests carried out for varying cross-sectional geometries, discharges, depths and slopes. Velocity profiles for the channel and flood plain are presented. The mean velocities in the channel and flood plain during interaction are obtained using planimetry, and comparisons are made with the predicted velocities obtained from the established friction factor equations.

4.2 Confined Flow.

4.2.1 General Considerations.

As suggested in the previous section, the importance of establishing the frictional resistance to flow in the channel and flood plain during non-interacting flow conditions cannot be underestimated. Only with this knowledge can the extent of the channel/flood plain interaction be quantified.

Various formulae exist for describing the flow rates in simple channels and such formulae have been presented briefly in section 2.5. It was decided to use two of the discharge equations during this work. These were Manning's equation :

$$Q = \frac{1}{n} A R^{2/3} \sqrt{S} \qquad (4.1)$$

and the Darcy Weisbach equation :

$$Q = A \sqrt{\frac{8gRS}{\lambda}} \qquad (4.2)$$

Mannings Equation was chosen since it gives a quick and reasonably accurate prediction of the stage-discharge relationship especially for uniform flow conditions. Also it is widely used by engineers in practice and therefore readily understood. The main drawback with Mannings Equation is the assumption of a constant n value for all flow depths. The Darcy Weisbach equation was also chosen because it made use of the friction coefficient λ which is non-dimensional and has been shown to be a function of the Reynolds number for smooth channels. The Task Force on friction factors in open channel flows (Ref 58) recommended the emphasis of the use of λ by research workers and engineering teachers. For roughnesses of the type found in the natural river, the friction factor is

independent of the Reynolds number and therefore Mannings Equation can be considered appropriate. However, for smooth channel flow Mannings n may demonstrate limitations since it is not a function of the Reynolds number, and may vary with bed slope or flow depth.

The semi-empirical equation for the friction factor in pipe flow was given in section 2.5 as the Karman-Prandtl smooth pipe equation :

$$\frac{1}{\sqrt{\lambda}} = 2{\cdot}0 \log(Re\sqrt{\lambda}) - 0{\cdot}8 \qquad (4.3)$$

As suggested in section 2.5 much experimental work has been carried out in attempting to establish the significance of Equation (4.3) when applied to open channels rather than pipe flow. Henderson (Ref 24) suggested it could be used quite satisfactorily. Most investigators agree with the general form of equation (4.3) for smooth open channels :

$$\frac{1}{\sqrt{\lambda}} = A \log(Re\sqrt{\lambda}) - B \qquad (4.4)$$

The variations in the constants A and B are presented in Table (2.1) and it can be seen that there is significant disagreement over the value of B. It was therefore decided to look at the relevance of such a relationship and establish the value of B for a series of tests with flow confined to the

channel and to the flood plain. Also the accuracy of Mannings Equation was investigated and the appropriate value of n determined for the channel and flood plain.

4.2.2 Experimental Work.

Flood plain sections were positioned in the flume to give a channel width of 0.4 metres. The flood plain section was of sufficient height to give flow depths in the channel up to 150 mm. From the use of the surveying level it was possible to determine the channel bed slope which was found to lie between the range 1/1350 and 1/1450. As previously explained, due to the slight nonuniformity in the bed of the channel, it was difficult to achieve more accurate bed slopes. The pump was switched on and a discharge selected which would give a flow depth in the channel less than the bankfull depth. Uniform flow was obtained by adjusting the tailgate weir until the water surface slope was equal to the bed slope. The water depth and discharge were recorded and from equations (4.1) and (4.2) an appropriate value of n and λ obtained. A series of similar tests were carried out for the flood plain and the results of such tests are presented in the following section.

4.2.3 Results and Conclusions.

It was found from the above experiments that the values of Mannings n obtained for the channel and flood plain were 0.01 and 0.011 respectively. Figs 4.2(a) to 4.2(d) present non-dimensional stage-discharge relationships for each series of tests. The depth was divided by the bankfull depth h, as shown on Fig 4.1. The non-dimensional discharge was obtained by dividing the measured discharge by the expected discharge at bankfull depth based on the estimated value of Mannings n. Thus the effects of the slope range could be minimised. The curve shown on each graph represents the discharge estimated at that particular depth from the chosen Mannings n, divided by the bankfull depth. Figs 4.2(a),(b) and (c) represent the results obtained for flow confined to the channel with varying channel widths. It can be seen that a Mannings n of 0.01 overlays the curve on to the data for each channel width.

For Fig 4.2(d), which represent tests carried out with the flow confined to the flood plain, a Mannings n of 0.011 was a reasonable estimate of the roughness coefficient. The difference in Mannings n was to be expected since the channel perimeter was made from smooth fibre glass which gave a reasonably polished surface. The flood plain surface was slightly rougher since its surface was constructed from marine plywood which, even though was coated with at least 3 coats of

varnish, still absorbed the varnish to leave a slightly rougher surface than the channel.

As mentioned earlier in this Chapter, the Task Force on Friction Factors in Open Channels (Ref 58) recommended the use of λ in engineering research carried out in open channels, since λ will most accurately describe the frictional resistance of a channel boundary. It has been shown for smooth channels that the friction factor λ , is dependent on the Reynolds Number alone in the generalized form :

$$\frac{1}{\sqrt{\lambda}} = A\log(Re\sqrt{\lambda}) - B \qquad (4.5)$$

where $$Re = \frac{4 R_c V_c}{\nu} \qquad (4.6)$$

and $$\lambda = \frac{8 g R_c S}{V_c^2} \qquad (4.7)$$

where R_c is the hydraulic radius, V_c is the mean velocity in the channel, set at a longitudinal bed slope of S, and ν is the kinematic viscosity. Opinion varies among researchers as to the most appropriate values of the constants A and B, and this particular aspect has been dealt with in the literature review in Chapter 2. However most investigators have found the value of A to approximate to 2.0, therefore it was decided to fix A at 2.0 and to calculate the values of Re and λ and plot these results with curves representing Equation (4.5) with B set at various

values. These graphs are presented on Figs 4.3 (a) to (d). The values of B chosen are B=0.8, 1.3, 1.6, and 1.8. Figs 4.3 (a) to (c) show the results obtained for the three channel widths to be tested more extensively later, namely Bc=0.2 m, 0.4 m, and 0.6 m. During these tests flow was confined to the channel. Although there is considerable spread in the results, the appropriate value of B approximated to 1.3. An interesting point to note is that for varying channel width, the friction factor λ appears only to be a function of the Reynolds number. Kazimipour and Apelt (Ref 29, Ref 30) suggested that the friction factor was also a function of the width to depth ratio of the flow. The apparent contradiction could be explained since the range of width to depth ratios tested in the current investigation was small.

Fig 4.3 (d) shows the results of tests carried out with flow confined to the flood plain. Again there is considerable spread in the results which seem to suggest that the appropriate value of B for the flood plain might be 1.6. This would appear reasonable since Mannings n for the flood plain was greater than the channel. From the comparison of Mannings Equation and the Darcy relationship, it can be reasoned :

$$\frac{R^{1/6}}{n} = \sqrt{\frac{8g}{\lambda}} \qquad (4.8)$$

which suggests that $\lambda \propto n^2$

or $$\frac{\lambda_f}{\lambda_c} = \left(\frac{n_f}{n_c}\right)^2 \qquad (4.9)$$

therefore $$\left(\frac{0{\cdot}011}{0{\cdot}01}\right)^2 = 1{\cdot}1^2 = \frac{\lambda_f}{\lambda_c} \qquad (4.10)$$

Thus Bc=1.3 for the channel and Bf=1.6 for the flood plain would seem reasonable.

4.3 Rating Curves with Overbank Flow.

4.3.1 Introduction.

The previous section presented results of tests carried out with flow confined to either the channel or the flood plain. In this section a series of tests which permit channel/ flood plain interaction will be described. The friction factors determined from the previous section will be used to calculate the expected discharges at an equivalent depth, and hence comparison will demonstrate the effect of the interaction mechanism on the stage-discharge relationships during overbank flow.

All tests have been carried out with the same channel and flood plain widths. 8 series of tests are presented, each series having a different longitudinal bed slope. The value

of the bankfull depth has also been varied.

4.3.2 Tests and Results.

For each series of tests the bed slope remained fixed. A discharge was chosen and the tailgate weir adjusted accordingly to give uniform flow along the channel. The flow depth and the discharge were then recorded. The discharge was then varied and new uniform flow conditions set up. A number of results were recorded for each series until a stage-discharge relationship could be established for overbank flow conditions. The results obtained for these tests are presented on Figs 4.4(a) to (h). It can be seen that the rating curves have been presented non-dimensionally. The non-dimensional graphs were obtained by dividing the flow depth by the bankfull depth,and by dividing the discharge by the bankfull discharge based on a Mannings n of 0.01 which is the friction factor previously established for the main channel.

Also shown on each graph is the predicted discharge using three different methods previously described in the literature review. First, Mannings Equation is presented assuming that the channel and flood plain can be considered as two separate channels with the vertical interface at the channel/flood plain interface being considered as a solid boundary.

A further method of discharge estimation is presented which involves considering the channel and flood plain as a single channel, and estimating the hydraulic radius based on the total cross sectional area and the total wetted perimeter of the compound channel. It can be seen that at very low flood plain depths, this method predicts a sudden reduction in the total discharge of the channels due to the inadequacy of the hydraulic radius in describing the channel geometry. As the flood plain is inundated, there is a sudden increase in the total wetted perimeter with only a slight increase in cross sectional area. Since R=A/P, a sudden reduction in R, and hence Q, occurs.

A third method of discharge estimation is presented on Figs 4.4(a) to (h) which is based on the formula given in BS 1042:Part 3C:1981 :-

$$Q = A\ C\sqrt{RS} \qquad (4.11)$$

$$C = \frac{1}{n} R^{1/y} \qquad (4.12)$$

$$y = \frac{1}{\log R} \log\left[\left(\frac{1}{2} - \frac{n\sqrt{g}}{0{\cdot}26}(1-\log R)\right) + n\sqrt{\frac{1}{4}\left(\frac{1}{n} - \frac{\sqrt{g}}{0{\cdot}13}(1-\log R)\right)^2 + \frac{\sqrt{g}}{0{\cdot}13}\left(\frac{1}{n} + \sqrt{g}\log R\right)}\right] \qquad (4.13)$$

where R is the hydraulic radius for the total cross section and n is the estimated roughness of the channel.

Each of the series of tests demonstrate quite clearly a departure from the three relationships normally adopted in estimating the carrying capacity of a channel during overbank flow. This departure is particularly significant at low flood plain depths. To discuss these results it is considered helpful to present an idealized stage-discharge relationship which is based on the results shown on Figs 4.4(a) to (h). This representative rating curve is shown on Fig 4.5.

It is clear from Fig 4.5 there is a definite reduction in the carrying capacity of the compound channel at small depths on the flood plain. In some cases discharges obtained at bankfull depth were occurring at depths approximately 10 - 15% greater than bankfull depth, suggesting that within such depths, as the water rises, the discharge remains essentially constant. It has been shown that this phenomenon is probably due to a turbulent shear interaction mechanism which is occurring at the channel/ flood plain boundary and is effectively causing an increased resistance to flow. It is difficult to quantify the extent of such a mechanism on the discharge capacity of the channel based on the information shown on Fig 4.4 (a) to (h). However, one or two observations can be made. First, at depths ratios of Yc/h=1.2, the reduction in discharge, compared with the separate channels method of estimating discharge, was around 20%. At low flood plain depths all three methods proved to be inaccurate. For the reasons given above, the single channel

method gave a sudden reduction in the carrying capacity of the channel. At increased depths of flow, i.e. Yc/h>1.2, the single method of discharge estimation became more accurate, suggesting that the compound channel was behaving more like a single channel. The BS3680:Part 3C:1983 method, with its complicated format, did not appear to offer any greater accuracy in the estimation of discharge, raising the question of whether such a formula can justify its use.

An interesting point to note are the results shown on Fig 4.4 (a). Two different rating curve relationships were measured for the same geometry and channel bed slope. One rating curve was obtained by commencing testing below the bankfull depth and increasing the discharge and flow depths in succession. The second rating curve was obtained by operating the system at a high flow depth and discharge and successively lowering the discharge and flow depth. It can be seen that a certain amount of hysteresis was displayed in the results. It is difficult to understand why this should have been since sufficient time was given between the recording of each result, thus establishing steady state conditions. One possible explanation could be non-uniform flow conditions or an error in measuring bed slope or water surface slope. A further possible explanation could be given by considering the work carried out by Blalock and Sturm (Ref 7). As described in the literature review, they were able to show that for compound channel flow, two critical depths of

minimum specific energy could occur. One above bankfull depth and the other below bankfull depth. If this is the case, then perhaps the increasing flow depths were based on the critical depth which occurred below bankfull depth and the falling limb of the rating curve was based on the critical depth over the tailgate weir arising from flow over the bankfull depth. A similar display of hysteresis was also described by Sellin (Ref 54 , Ref 55) where he observed an unstable region of flow just above and below the bankfull depth.

4.3.3 Conclusions of the Stage-Discharge results.

From the series of results obtained, it has become apparent that an interaction mechanism retards the flow carrying capacity of the compound channel at depths just above bankfull depth. At greater depths, however, this interaction mechanism loses its influence with the flow virtually reverting to a single channel.

Three methods of discharge prediction have been presented and it is clear that no method accurately predicts the discharge at low flood plain depths. At subsequent increases in depth, the single channel method of discharge estimation becomes more accurate, with the single channel method increasing in inaccuracy. The third method, proposed by BS3680:Part 3C:1983 offers no improvement in accuracy and it is proposed that such a

method does not justify its use.

4.4 Velocity Profiles.

4.4.1 Introduction.

The experiments presented in section 4.3 revealed quite clearly the existence of the turbulent shear mixing region between the channel and the flood plain over bank flow. The effects of the interaction mechanism on the overall carrying capacity of the compound channel was found to be significant. However, a more comprehensive study was now carried out for 16 different channel geometries. These tests permitted a detailed determination of the flow distribution in both the channel and the flood plain.

4.4.2 Experimental work.

A total of 136 test runs were carried out for 16 different compound channel geometries and the experimental procedure adopted for each test run has been described in Chapter 3. A Pitot tube was placed in the flow and a complete velocity traverse was obtained. A typical velocity traverse grid is shown on Fig 4.6. The channel geometry and flow details for each test run are described in Table 4.1. Also presented in these tables are the mean channel and flood plain velocities during the

turbulent interaction. A brief explanantion of the determination of these mean velocites is now given.

1. As already mentioned each test run of the overbank flow tests involved the discharge measurement, Q, channel depth measurements, Yc and Yf, bed slope and water surface slope measurements, as well as the full range of point velocity measurements as shown on Fig 4.6.

2. After each test was complete all the relevant data was entered and stored on computer. Each test run had an associated datafile stored on computer disk.

3. A computer program was written which would present the vertical velocity profiles at various distances across the channel and flood plain.

4. The profiles were integrated using planimetry to give a mean vertical velocity at the corresponding lateral distance into the flow.

5. The mean vertical velocities were plotted against their lateral positions in the channel or flood plain. By integrating using planimetry the lateral velocity profile now obtained, it was possible to determine the mean channel or flood plain velocity during interaction conditions.

6. Such mean velocities could be checked against the overall discharge obtained from the orifice plate by the relationship :

$$Q_m = V_c' A_c + V_f' A_f \qquad (4.14)$$

where Vc' and Vf' are the channel and flood plain velocities during channel/flood plain interaction, Ac and Af are the corresponding cross-sectional areas and Qm is the discharge obtained from the orifice plate and manometer. Fig 3.28 in Chapter 3 shows that the overall discharge obtained from the channel and flood plain velocities lay within ±3% of the measured discharge. It was therefore considered reasonable to assume that the integrated mean values of the channel and flood plain velocity were accurate.

A computer program was written which would give a visualisation of the flow distribution during channel/flood plain interaction. This program which is presented in Appendix 1 displays the results in two forms: first, isovels or contours of equal velocity for both the channel and flood plain; secondly, lateral velocity profiles in the channel and flood plain for selected heights above the bed. Both graphs are presented on Fig 4.7 for each test run carried out.

4.4.3 Results of Point Velocity Measurements.

4.4.3.1 General Considerations.

Before discussing the results of Fig 4.7 in detail, consider first a typical lateral velocity profile across the compound section as shown on Fig 4.7 (b). From consideration of momentum transfer per unit area from faster layers to slower, Reynolds devised an expression for the turbulent shear stress generated in the form,

$$\tau_r = \rho u'v' \qquad (4.15)$$

where u' and v' are the fluctuating components of velocity. This was modified by Prandtl who made the assumption that u' is of the same order of magnitude as v' and that $u' = l\left(\frac{du}{dy}\right)$. Thus the general equation of turbulence becomes :

$$\tau = \rho l^2\left(\frac{du}{dy}\right)^2 \qquad (4.16)$$

where l is the mixing length, approximated to 0.4y where y is the distance from the solid boundary.

If Equation (4.16) is modified for lateral velocity profiles the following equation is obtained :

$$\tau = \rho l_z\left(\frac{du}{dz}\right)^2 \qquad (4.17)$$

Unfortunately, the equation cannot be solved for a compound channel as the turbulent shear stress τa, and the lateral mixing length l_z are both unknown. In fact, the value of l_z for low flood plain depths is more likely to reflect the scale of the vortices formed by the interaction effect and hence proportional to the flood plain depth Yf, although it is doubtful if this argument can be applied to large flood plain depths when $Yf/Yc \rightarrow 1$.

However Equation (4.17) does indicate that the turbulent shear stress generated is caused by the velocity difference between the main channel and flood plain and its magnitude is a function of the lateral velocity gradient across the channel/ flood plain junction. When the turbulent shear stress is large , so is the degree of momentum transfer per unit area between layers.

The actual momentum transfer between layers is a product of the shearing stress and the area of flow over which the stress acts. In this case the area can be taken as the flood plain depth with a longitudinal channel length of unity. At very low flood plain depths the velocity gradient, and hence shear stress, is a maximum as shown on the sketch below. Multiplied by the flood plain depth to give the momentum transfer, it is clear that the maximum momentum transfer will occur at a particular

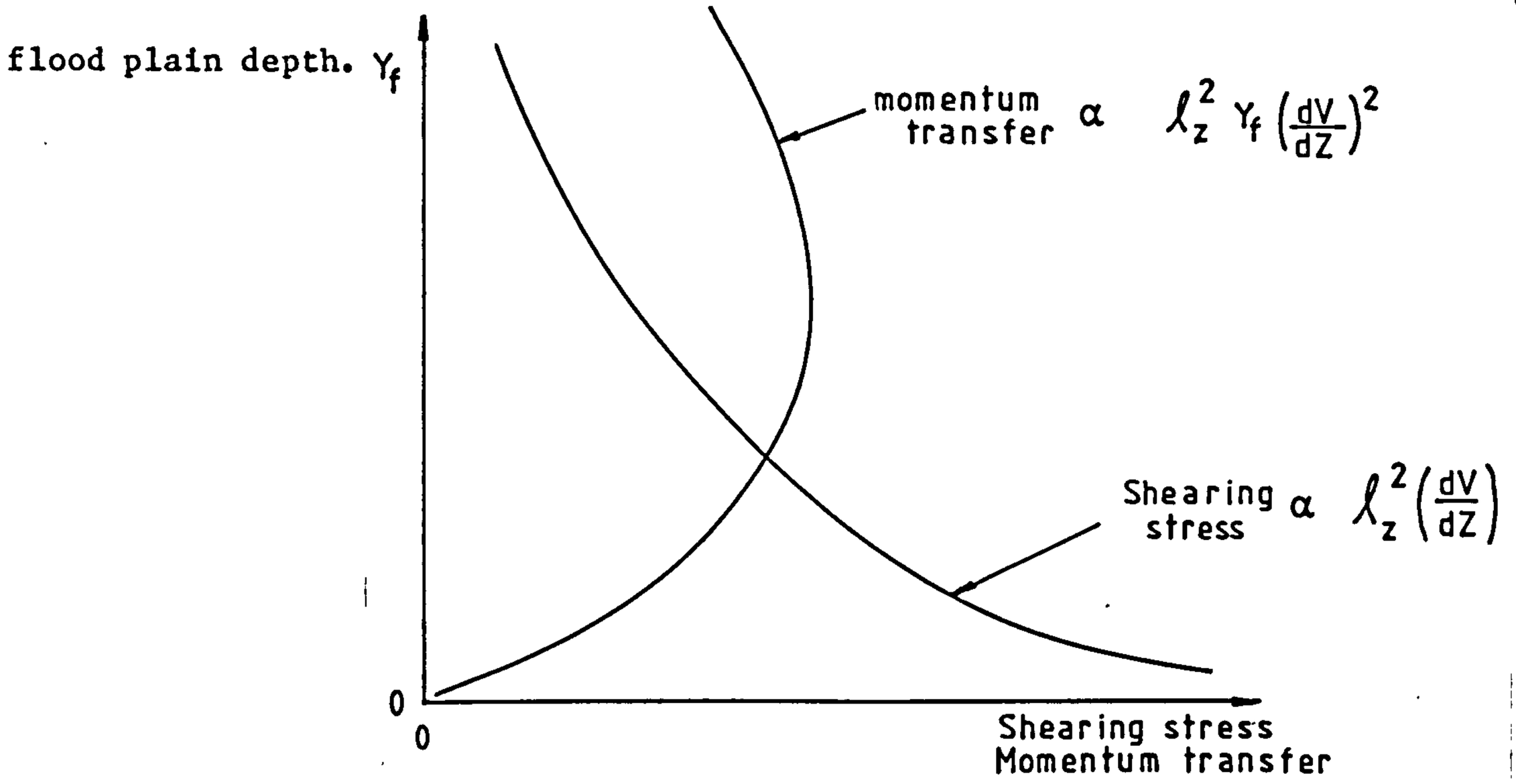

A further point of note concerns the extent of spreading of the shear layer across the channel and flood plain. This has been investigated by Rajaratnam and Ahmadi(Ref 3, Ref 48) who produced an inconclusive result. They found that the total spreading width b_t of the shear layer could be given by :

$$\frac{b_t}{Y_f} - 6\left(\frac{Y_c}{Y_f} - 1\right) \qquad (4.18)$$

which implies $b_t \doteqdot 6\ h$, where h is the bankfull depth. Unfortunately Equation (4.18) cannot be applied with any confidence as Rajaratnam and Ahmadi tested only one value of h. However, it is worthwhile looking out for this point in discussing the author's results with three values of h.

A final point of note before discussing the results proper, concerns the predicted velocity defect in the main channel due to momentum transfer to the flood plain as shown on the sketch shown on Fig 4.7(b). A glance at the results on Fig 4.7 reveals that the velocity defect in the main channel is not always apparent, in fact in some cases the maximum velocity filament occurred in the main channel in the region next to the flood plain junction, where the velocity defect was to be expected. The reasons for this are not immediately obvious, but it became clear that the phenomenon occurred generally at higher discharge rates. A possible explanation could be the influence of secondary currents, but also possible is the influence of a hidden meander along the straight fixed bed channel driven by a non-uniformity in the channel bed.

Having pointed this out, it should be noted however that a measured velocity defect did occur in practically all cases, as can be evidenced by Figs 4.8(a) to (c) showing that the mean channel velocity during interaction was always less than the mean channel velocity when the main channel is isolated (i.e. $V_c'/V_c > 1.0$).

The results investigate the effect of five parameters:-

Y_f/Y_c	the relative depth
h	the bankfull depth

Bc the main channel width

Bf the flood plain width

S the longitudinal bed slope

To investigate these parameters effectively a total of 136 test runs were carried out with each series of test runs related to a specific geometry as shown on Fig 4.9.

For a given geometrical cross-section, the relative flow depth Yf/Yc was varied as well as the longitudinal bed slope.

4.4.3.2 The effect of Varying the Relative Depth.

This effect is clearly indicated for each geometry tested. It can be seen, for instance, for the Geometry K that for a low value of Yf/Yc (Run 4) as shown on Fig 4.7, there is a steeply varying velocity gradient, indicating a high turbulent shear stress at the channel/ flood plain junction and hence a high degree of momentum transfer per unit area. For a larger Yf/Yc (Run 8) the velocity gradient is not as great, suggesting a far less significant shear layer. The effect is even more clearly seen when comparing Run 18 and Run 11 on Fig 4.7 for the case of a bankfull depth of 52mm. At high Yf/Yc values, for the case of Run No 11, the flood plain velocity, if anything, appears as great as the main channel velocity with the maximum velocity

filament occurring on the flood plain.

Large shear interaction for low values of Yf/Yc is especially clear for the results involving bankfull depths of 0.152m, as illustrated in Runs 65 and 68. In these cases the flood plain velocities near the junction are greatly increased and the lateral velocity gradient (dV/dz) very pronounced, so as to give a large shearing stress. It should also be remembered that large shearing stresses in turn, correspond to large values of apparent shear stress τa, which as already described, is a measure of the effect of momentum transfer per unit area on the main channel and the flood plain, resisting on and assisting the other, i.e. it should be remembered that although τa increases with smaller values of Yf/Yc, the actual amount of momentum transfer is given by $\tau a \times Yf \times l$, which from the literature survey, has a peak around relative depths,(Yf/Yc) of 0.2 to 0.3.

Thus a first conclusion from Fig 4.7 is that the relative depth term Yf/Yc is a most important parameter in describing the lateral velocity profile($\frac{dV}{dz}$) and the degree of turbulent shear existing during interaction. This may be true, however, only to the extent that Yf/Yc is the main parameter influencing the velocity difference between the channel and the flood plain.

4.4.3.3 The Effect of Varying the Bankfull Depth.

The effect of varying h can be studied most effectively by keeping all the other parameters constant, namely S, Bc, Bf, and Yf/Yc. It was decided first to keep Bf/Bc, Bc/h, Bf/h constant, and Yf/Yc constant but with h varying. This can be seen by comparing Run 8 (Bf/Bc=1,Yf/Yc=0.33, h=0.102m) and Run 139 (Bf/Bc=1,Yf/Yc=0.33, h=0.052). Run 139 is basically a 1/2 scale model of Run 8, although Run 139 has a greater bed slope. It can be seen from Fig 4.7 that a larger value of h gives a smaller lateral velocity gradient than the smaller scale model. Provided the mixing length l_z is the same in both, then the turbulent shear stress appears greater in the smaller model since the shear stress can be given by :

$$\tau \propto (l_z)^2 \cdot \left(\frac{dV}{dz}\right)^2 \qquad (4.19)$$

However, this may be misleading in the sense that l_z may be determined by the flood plain depth Yf, and hence the l_z term in the smaller model may be approximately 1/4 of the larger. Furthermore, it is not clear from these Figures if the larger model (larger h) has simply transferred more momentum, hence providing a decrease in main channel velocity and increase in flood plain velocity. This will be discussed in greater detail in a later section. It is worth pointing out that the apparent shear stress, τa, for the larger model was 1.29N/m^2 whereas for

the smaller model τ_a was 0.51N/m^2 . For Froude type scaling, by definition, the value of τ_a should increase linearly with model scale, which is not quite the case in this particular example. However, similarity of the lateral velocity profiles might be expected, but this is not evident.

An alternative approach in investigating the effect of h is to take constant values of Bc, Bf, Bf/Bc and Yf/Yc. This can be done by looking at the Geometries B ,P and L described on Fig 4.9. If Run 29 (Yc=0.068, h=0.052, Yf/Yc=0.23), Run 46 (Yc=0.197, h=0.152m, Yf/Yc=0.23) and Run 99 (Yc=0.132m, h=0.102m, Yf/Yc =0.23) are considered, then Bc, Bf, Bc/Bf and Yf/Yc remain constant. From the three test runs, it can be seen that Run 46 has a very shallow lateral velocity gradient (h=0.152m) , whereas Runs 29 and 99 have substantial lateral velocity gradients. It is not clear at this stage if this is an effect of bankfull depth h, or the differing ratios of Bc/h and Bf/h, or even the differing Bed slopes.

The variation in the three lateral velocity profiles can be seen more clearly on Fig 4.10, which is a non-dimensional plot of the mean channel and flood plain velocities during interaction (Vc' and Vf'), divided by the mean velocity for the entire cross section. It can be seen that the smallest h value (or largest Bc/h and Bf/h value) produces the steepest lateral velocity gradient, and presumably the greatest

extent of turbulent shear stress.

As well as this, the effect of the shear interaction is greatest in the channel with the smallest value of h (h= 0.052m) as can be seen from Figs 4.8(a) to (c). If the ratio Vc'/Vc is only considered, when h = 0.052m, Vc'/ Vc is 0.88, whereas when h = 0.102 m, Vc'/ Vc is 0.92 and when h= 0.152 m, Vc'/Vc= 0.93. This indicates the greater effect of the turbulent shear when h is smaller or Bc/h and Bf/h is larger. The ratio Bf/Bc was held constant in each case.

This argument can be carried a stage further by considering the non-dimensional apparent shear stress $\frac{\tau_a}{\rho g Y_f S}$ which is a measure of the effect of the interaction on a particular geometry and will be discussed in Chapter 6. When h = 0.052m, $\frac{\tau_a}{\rho g Y_f S}$ is 12.1, when h = 0.102m, $\frac{\tau_a}{\rho g Y_f S}$ is 5.0 and when h = 0.152m, $\frac{\tau_a}{\rho g Y_f S}$ is 3.68, showing again that the smaller h values, for constant Bf/Bc and Yf/Yc produce greater interaction effects.

This process will be investigated more thoroughly in later chapters, but suffice to say meanwhile, that the ratios Bc/h and Bf/h appear to be significant in the effect of the turbulent shear interaction. In the interests of brevity, other geometries will be considered in a later analysis of the results in Chapter 6.

4.4.3.4 The effect of varying the channel width.

In this analysis it is required to keep the bankfull depth h constant, the flood plain width Bf, constant and Yf/Yc constant. To this end the author has chosen the results for the tests carried out with h=0.1m and Bf=0.2m. Thus, three values of Bc are available, 0.2m, 0.4m, and 0.6m, corresponding to Geometries M, S and E. Particular tests, namely Run 119, Run 158 and Run 164 give a Yf/Yc value of approximately 0.18. These tests shown on Fig 4.7 show a a steep lateral velocity gradient across the channel/flood plain interface, suggesting high turbulent shear stresses. In fact, the approximate non-dimensional plot of the lateral velocity gradients for these tests is shown on Fig 4.11 and indicatesa fairly steep lateral velocity profile for each value of Bc.

The effect of varying Bc appears unclear when investigating its effect on the values of Vc'/Vc (interacting mean channel velocity over the isolated mean channel velocity), where Vc'/Vc is 0.95-0.96 when Bc is 0.2m, Vc'/Vc is approximately 0.94 when Bc is 0.4m, and Vc'/Vc is 0.95 when Bc is 0.6m. From this isolated example it can be seen that the effect of the shear interaction appears to increase slightly with Bc and then decrease at larger values of Bc. Further evidence of this will be seen later when the non-dimensional apparent shear stress $\frac{\tau_a}{\rho g Y_f S}$, which is a further measure of the effect of the

interaction, is discussed. When Bc is 0.2m, $\frac{\tau_a}{\rho g Y_f S}$ is 4.5, while when Bc=0.4m, $\frac{\tau}{\rho g Y_f S}$ is 13.2 and when Bc=0.6m, $\frac{\tau}{\rho g Y_f S}$ is 12.1. Thus there is a dramatic increase in the effect of the shear layer as Bc increases from 0.2m to 0.4m, and a levelling off, or even a slight decrease as Bc increases from 0.4m to 0.6m.

Of course, this effect could also be interpreted as a function of Bc/h which has the three values of 1.91, 3.92 and 5.9, or alternatively a function of Bc/Bf which has the three values of 0.92, 1.93, and 2.82.

4.4.3.5 The effect of varying the floodplain width.

In this case the bankfull depth requires to be held constant as well as Bc and the relative depth, Yf/Yc. When h=0.052m for instance, Bc may be taken as 0.2m and Bf varied from 0.2m, 0.4m to 0.6m. This corresponds to geometries O, B and I. The same process can in fact be carried out for h=0.1m and h=0.15. In the interests of brevity, the results for each bankfull depth are given in the following tables :

B_f	V_c'/V_c	$\tau_a/\rho g Y_f S$	Run
0·2	0·95	5·0	144
0·4	0·91	7·6	26
0·6	0·89	9·2	148

Bc = 0·2
h = 0·052
Y_f/Y_c = 0·27

B_f	V_c'/V_c	$\tau_a/\rho g Y_f S$	Run
0·2	0·97	4·5	119
0·4	0·88	12·8	95
0·6	0·88	11·4	109

Bc = 0·2
h = 0·1
Yf/Yc = 0·18

B_f	V_c'/V_c	$\tau_a/\rho g Y_f S$	Run
0·2	0·93	11·5	60
0·4	0·91	12·5	52
0·6	0·86	19·2	39

Bc = 0·2
h = 0·152
Yf/Yc = 0·13

The data in the Tables above indicate quite clearly the effect of increasing Bf with Bc, h, and Yf/Yc held constant. The effect of the channel/flood plain interaction increases significantly as Bf (or Bf/h) is increased. This is more clearly illustrated on the graphs shown on Fig 4.12 for the full range of relative depths, but including only two values of h.

It can be seen that Vc'/Vc becomes smaller as Bf is increased, indicating an increase in the effect of the shear layer at larger values of Bf/h. It can also be seen that Bc/h is an influential factor in determining the relative depth (Yf/Yc), at which the maximum interaction effect occurs. In Fig 4.12(a) where Bc/h=4, maximum interaction occurs at approximately Yf/Yc=0.3, whereas for Fig 4.12(b) where Bc/h=1.32, the maximum interaction occurs at Yf/Yc values of 0.15.

Bc/h also appears influential in the value of relative depth at which Vc'/Vc=1.0.

4.4.3.6 The effect of B_f/B_c on the degree of interaction.

So far it has been found that the effect of the interaction in terms of Vc'/Vc increases with Bf, but not necessarily with Bc. Previous authors have emphasised the importance of the ratio Bf/Bc on the degree of interaction.

Therefore it was thought important to investigate this effect on the values of Vc'/Vc. Clearly there is a large number of results which can be compared. Therfore, it was considered in the interests of brevity and clarity, to take the minimum value of Vc'/Vc found for each geometry tested and plot this parameter against Bf/Bc. This graph is shown on Fig 4.13. It is clear from this graph that the interaction effect increases with Bf/Bc, probably levelling off at higher values of Bf/Bc, say around 5.0.

Unfortunately, Fig 4.13 obscures completely the effect of the bankfull depth h, of which three values are incorporated. The most obvious solution is, therefore to separate the terms Bc/h and Bf/h as shown on Fig 4.14.

This is an interesting graph revealing a much stronger correlation between Vc'/Vc and the geometrical parameters Bc/h and Bf/h. The interaction effect increases with Bf/h up to a value of approximately 5.0 after which further increases in the flood plain width have little effect on the retardation of flow in the main channel. This is not altogether surprising because, when Bf/h >5, the shear layer due to interaction will be fully developed across the flood plain, and hence further increases in Bf/h will not effect the interaction. This agrees to a certain extent with the postulation of Rajaratnam and Ahmadi who showed that the extent of spreading of the mixing layer is proportional to the bankfull depth.

Another point of interest from this graph is that for a constant value of Bf/h, the effect of interaction decreases with increasing Bc/h. This again is to be expected since for a given value of h, the mixing layer extends a certain distance into the main channel retarding the flow (Vc'/Vc). When the value of Bc is increased, the extent of the mixing layer does not increase and hence the velocity defect will have a smaller relative effect on the main channel. Thus when $Bc/h \rightarrow \infty$, $Vc'/Vc \rightarrow 1.0$. It should be pointed out that the dashed lines shown on Fig. 4.14 represent the author's interpretation based on experimental data combined with reasoning above.

4.5 Conclusions.

In this chapter the effect of the interaction on the velocities in the channel and the flood plain have been investigated. It has been shown, after establishing the friction factors for the channel and flood plain, that the interaction reduces the discharge carrying capacity of a channel at depths slightly greater than bankfull level. Normal discharge equations such as Mannings, Darcy etc, do not recognise this effect and therefore can give misleading results.

It has also been shown that considerable redistribution of the velocities in the channel and flood plain occur as a result of the turbulent shear at the channel/flood plain interface. It is clear that this shear is a function of the velocity gradient across the interface. Furthermore it has

been shown that this velocity gradient varies with the geometrical and flow characteristics of the total cross-section, namely Bc/h, Bf/h and the relative depth Yf/Yc. As the ratio Bf/h increases, the velocity ratio Vc'/Vc decreases indicating an increase in the interaction mechanism. At values of $B_f/h>12$ the velocity defect levels off as shown on Fig 4.14 with subsequent increases in Bf/h having little increased influence on the turbulent shear at the interface. The ratio Bc/h also has an influence on the velocity defect suggesting that as Bc/h increases, the interaction mechanism decreases.

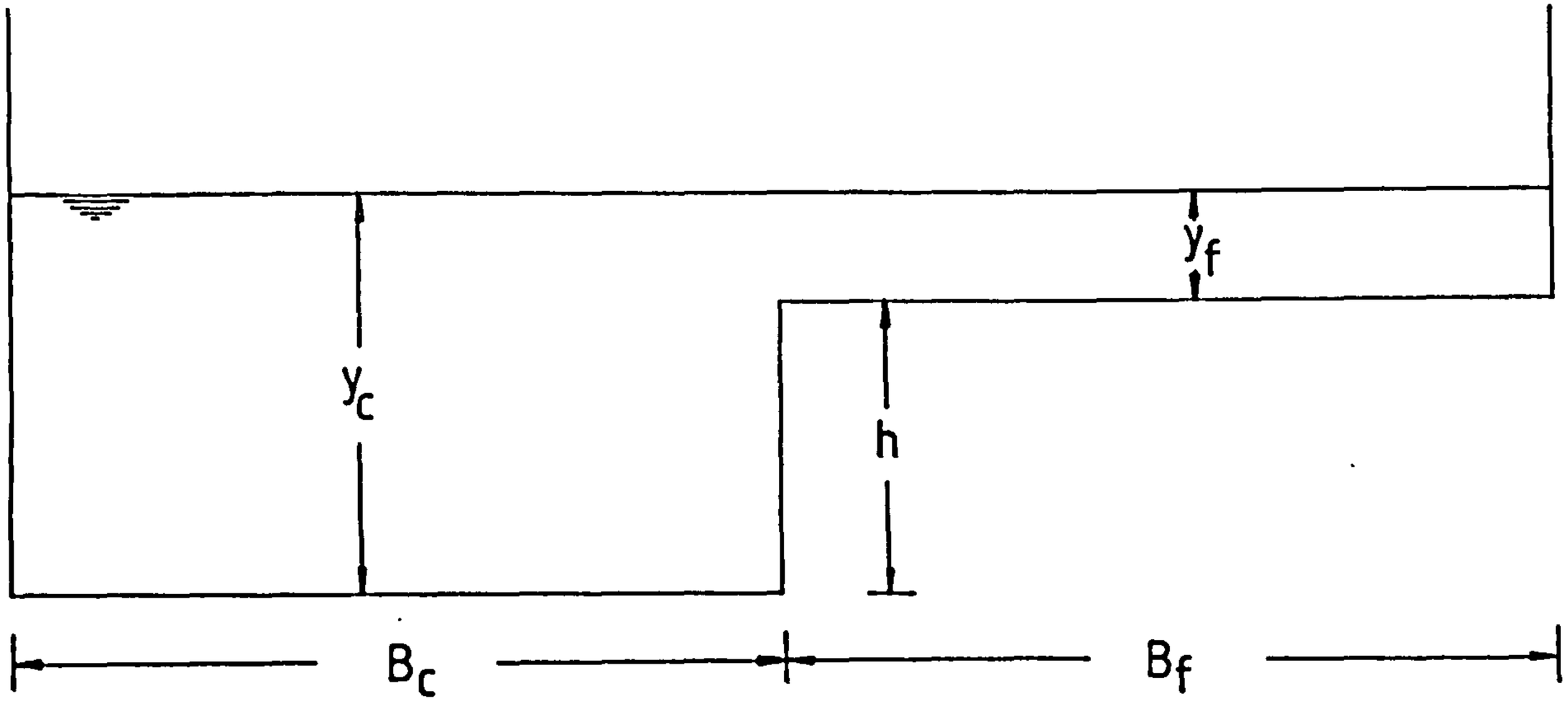

Fig 4·1 General Definition of Terms Used.

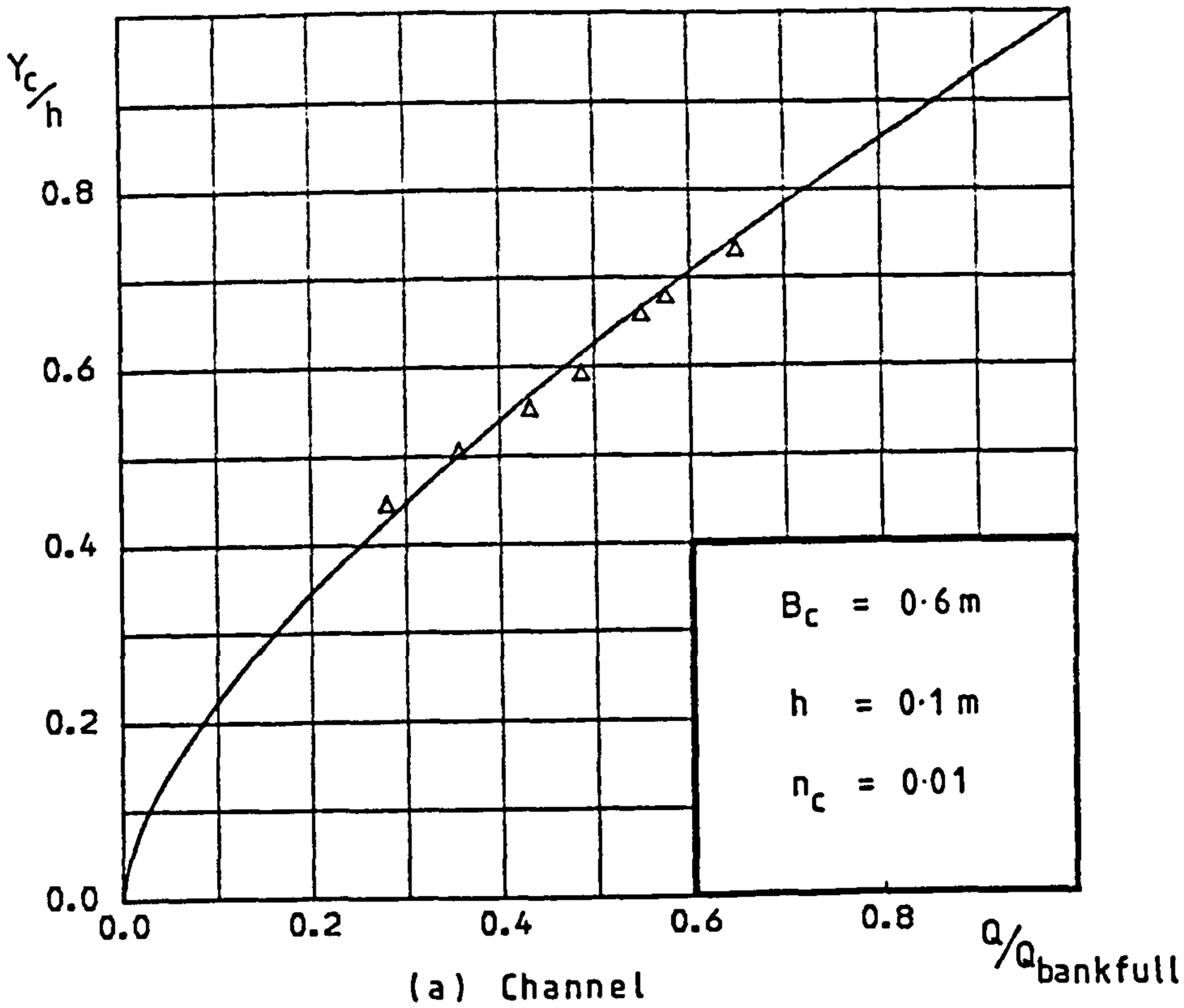

(a) Channel

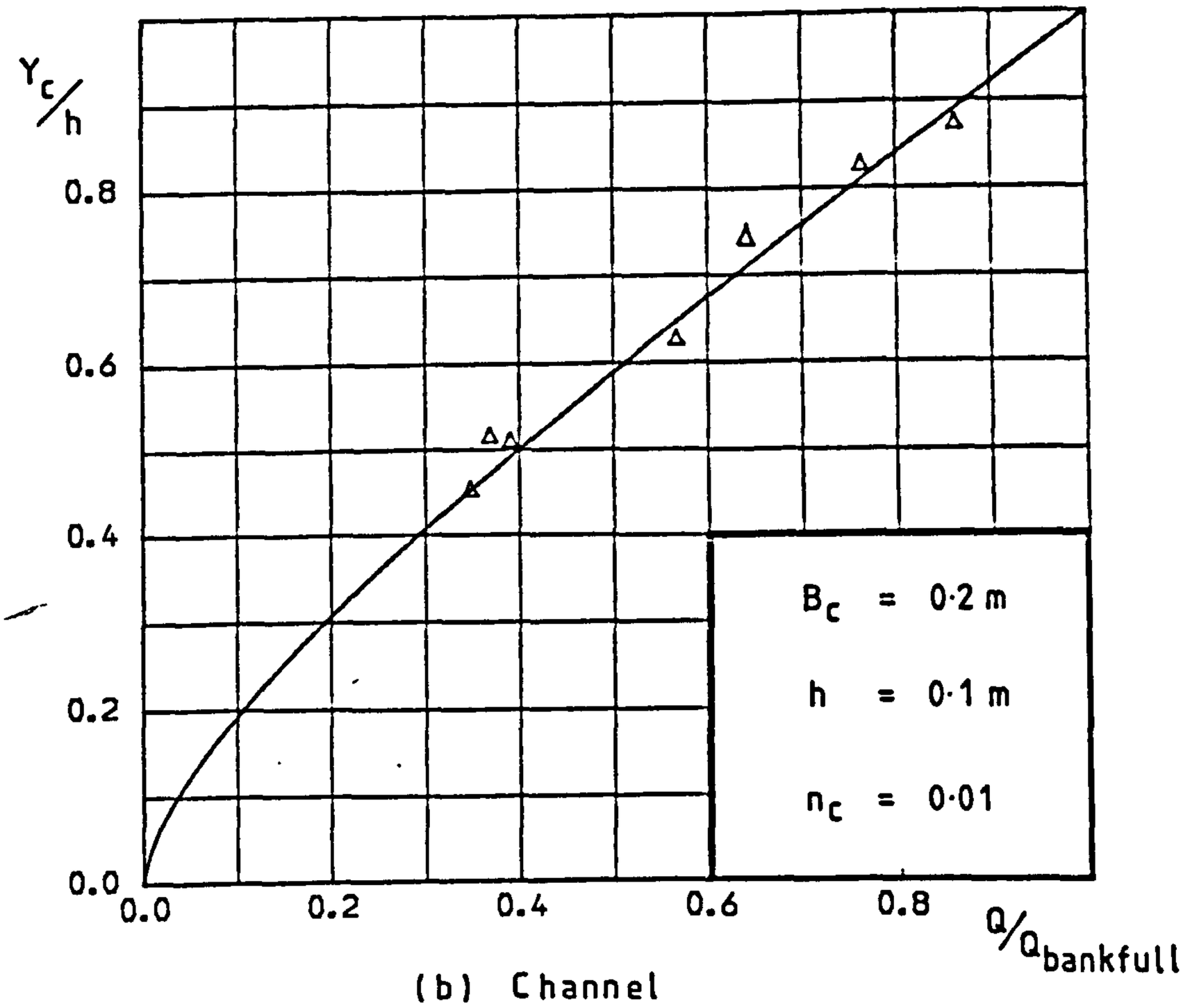

(b) Channel

Fig 4·2 Stage-Discharge Relationship for Rectangular Section

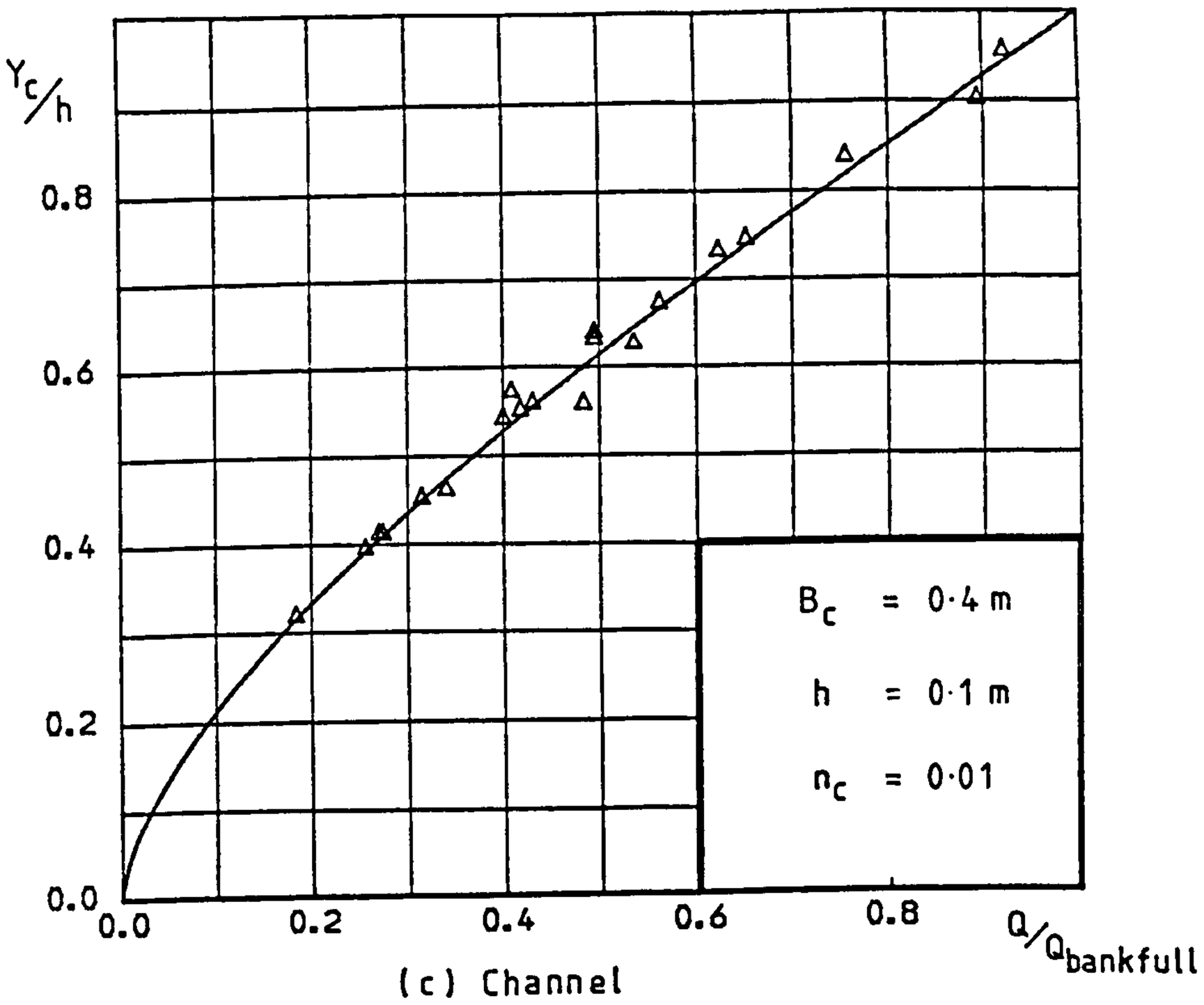

(c) Channel

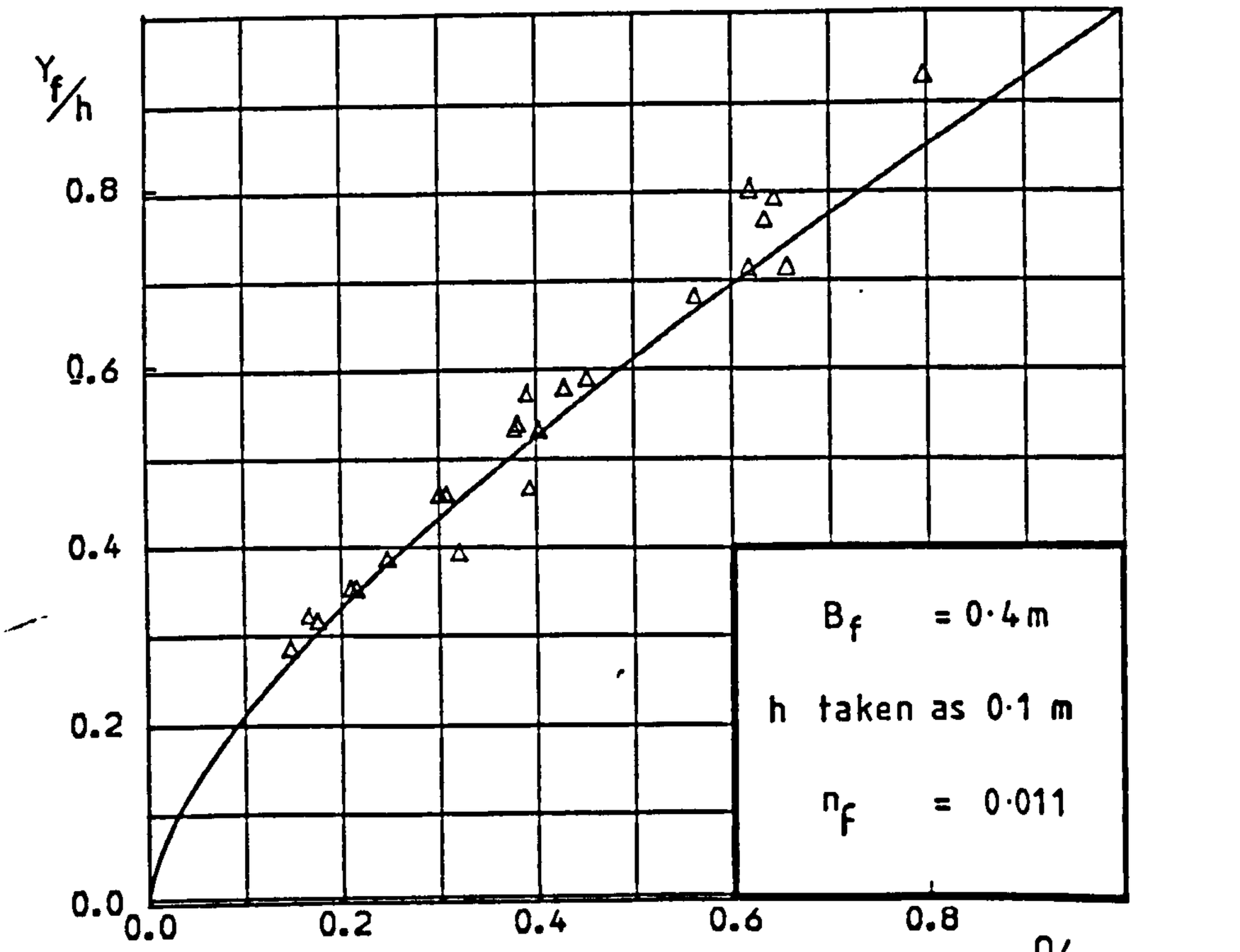

(d) Flood Plain

Fig 4·2 Stage-Discharge Relationship for Rectangular Section

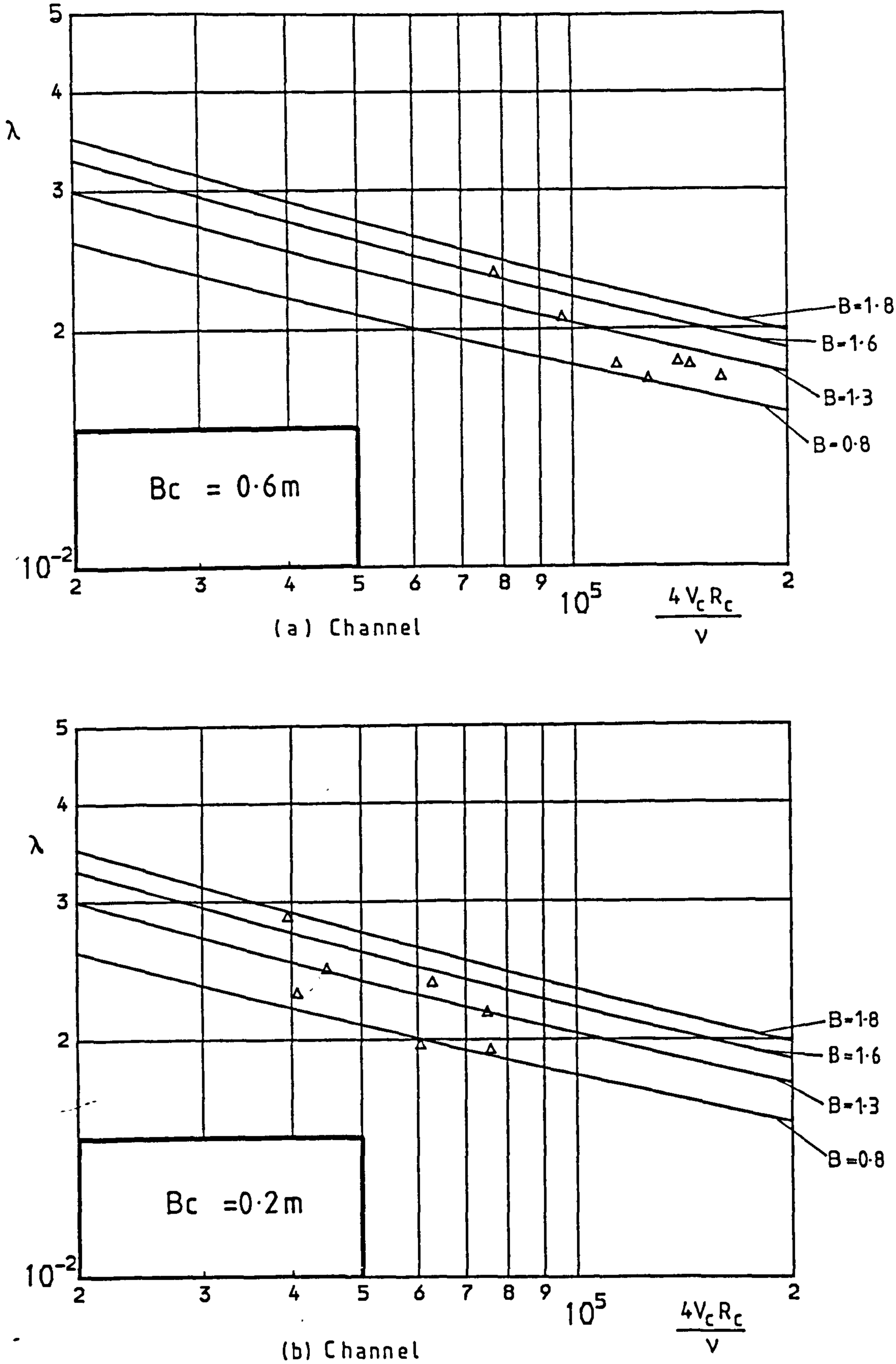

Fig 4·3 λ – Re Relationship for Rectangular Section

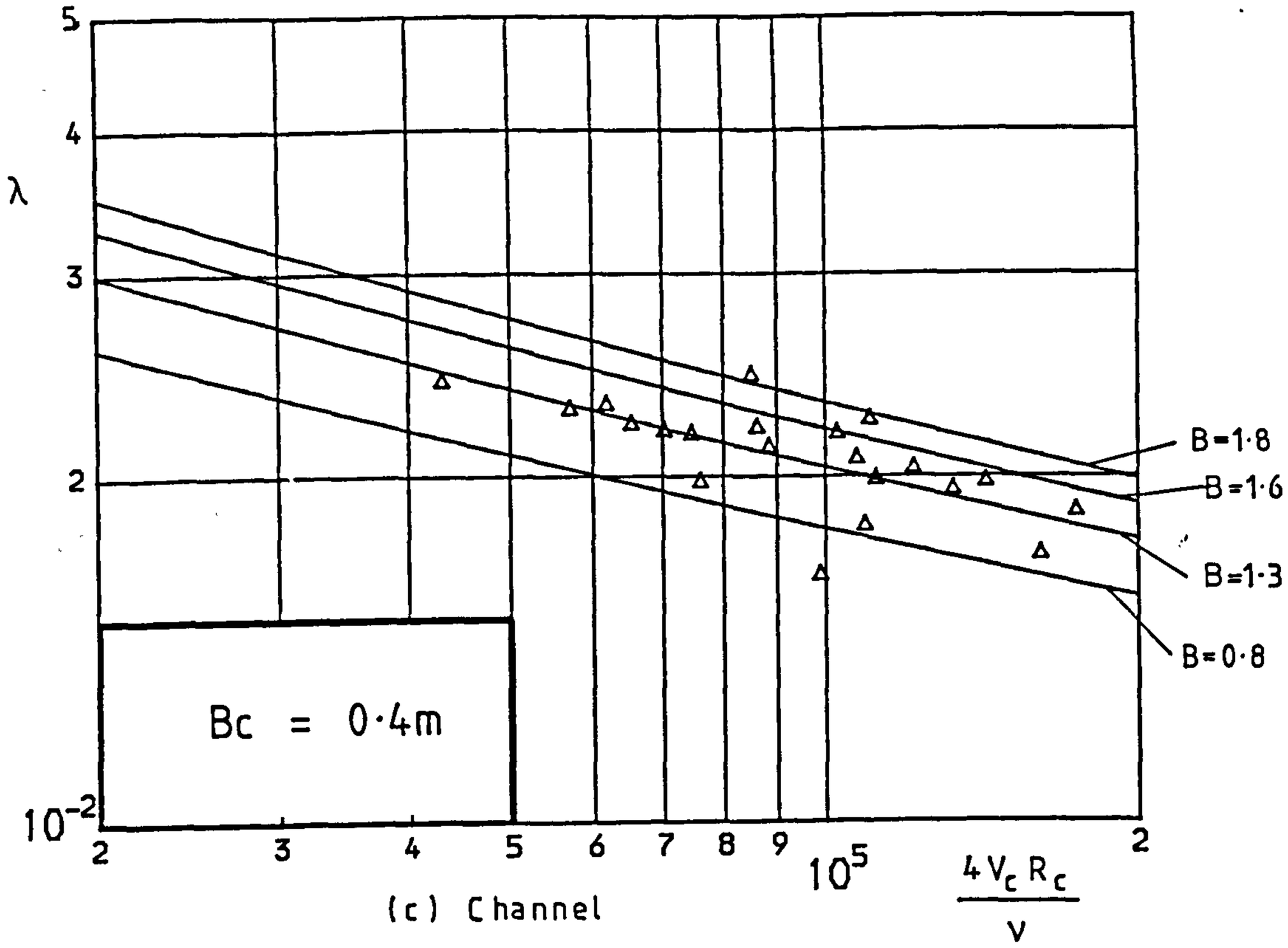

(c) Channel

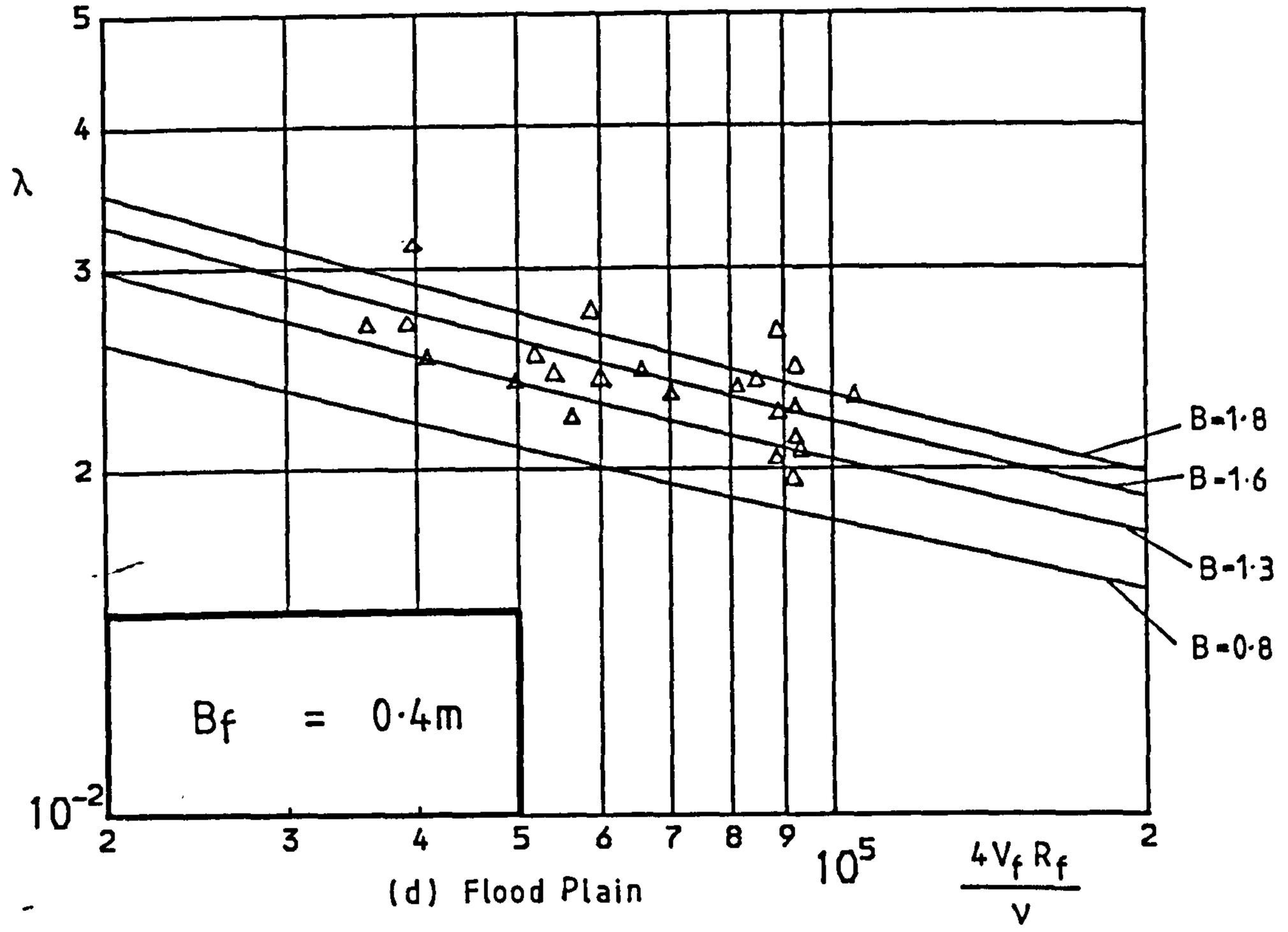

(d) Flood Plain

Fig 4·3 λ–Re Relationship for Rectangular Section

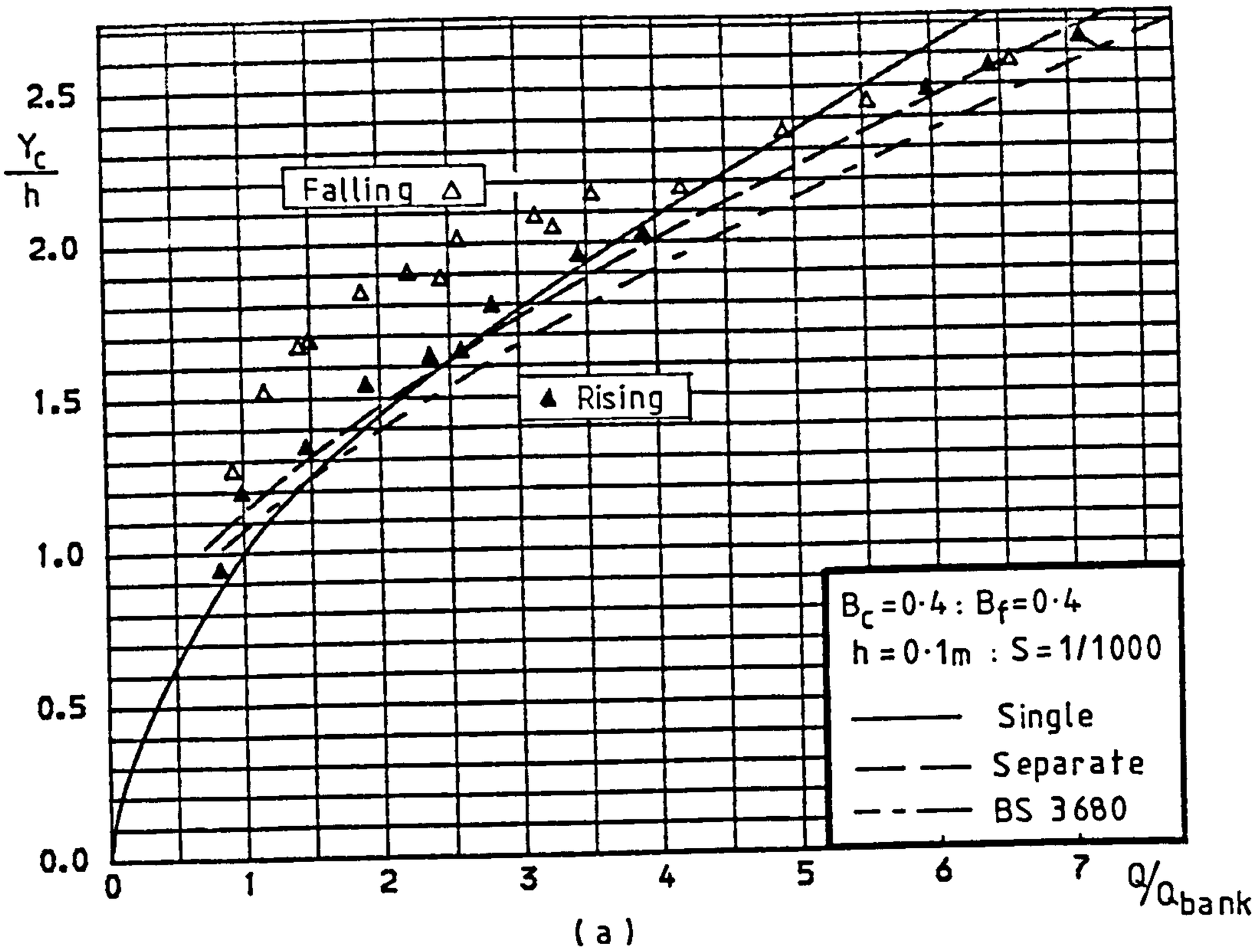
2.5
Yc/h
2.0
1.5
1.0
0.5
0.0
Falling △
▲ Rising
Bc=0·4 : Bf=0·4
h=0·1m : S=1/1000
Single
Separate
BS 3680
0
1
2
3
4
5
6
7
Q/Qbank
(a)

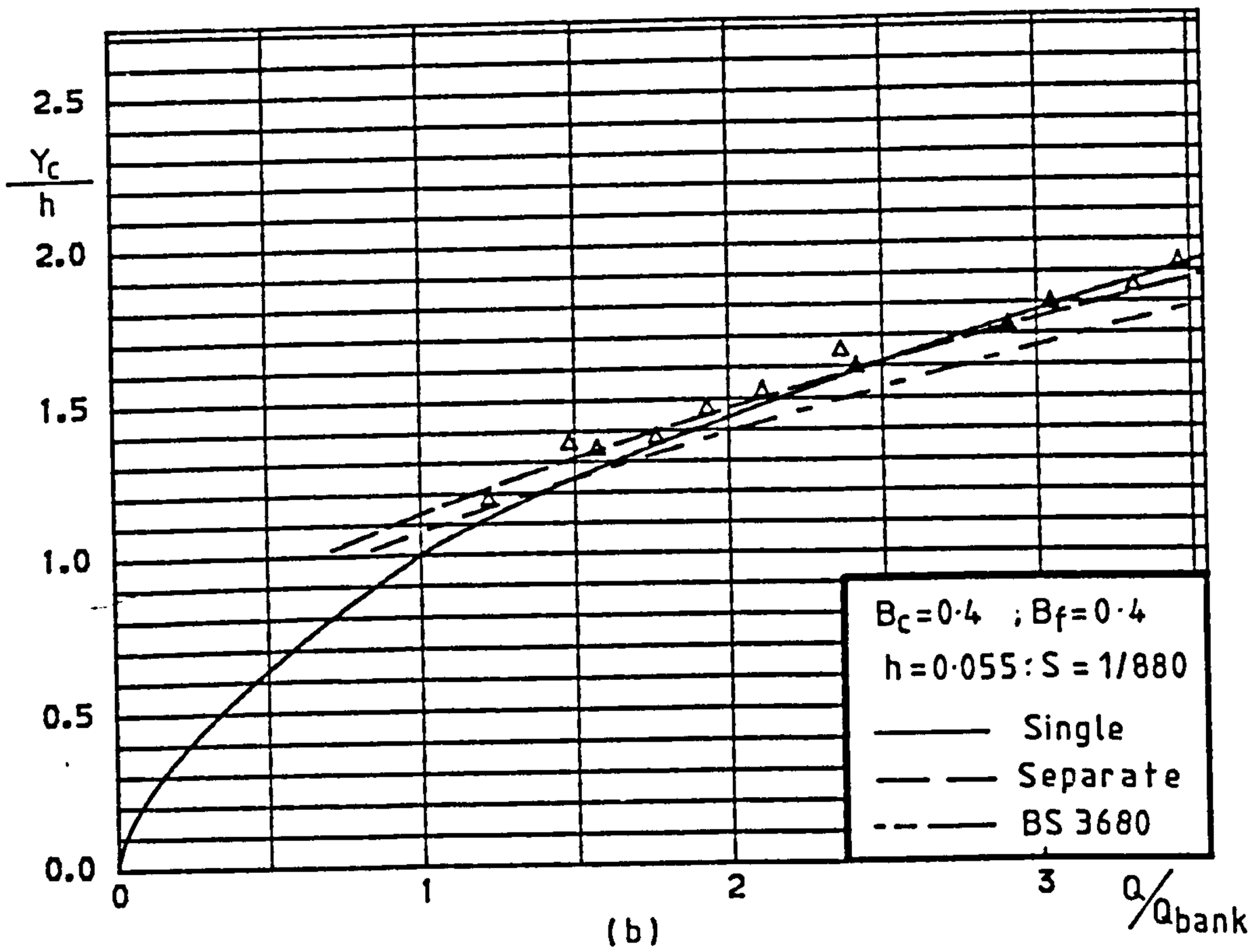
2.5
Yc/h
2.0
1.5
1.0
0.5
0.0
Bc=0·4 ; Bf=0·4
h=0·055 : S=1/880
Single
Separate
BS 3680
0
1
2
3
Q/Qbank
(b)

Fig 4·4

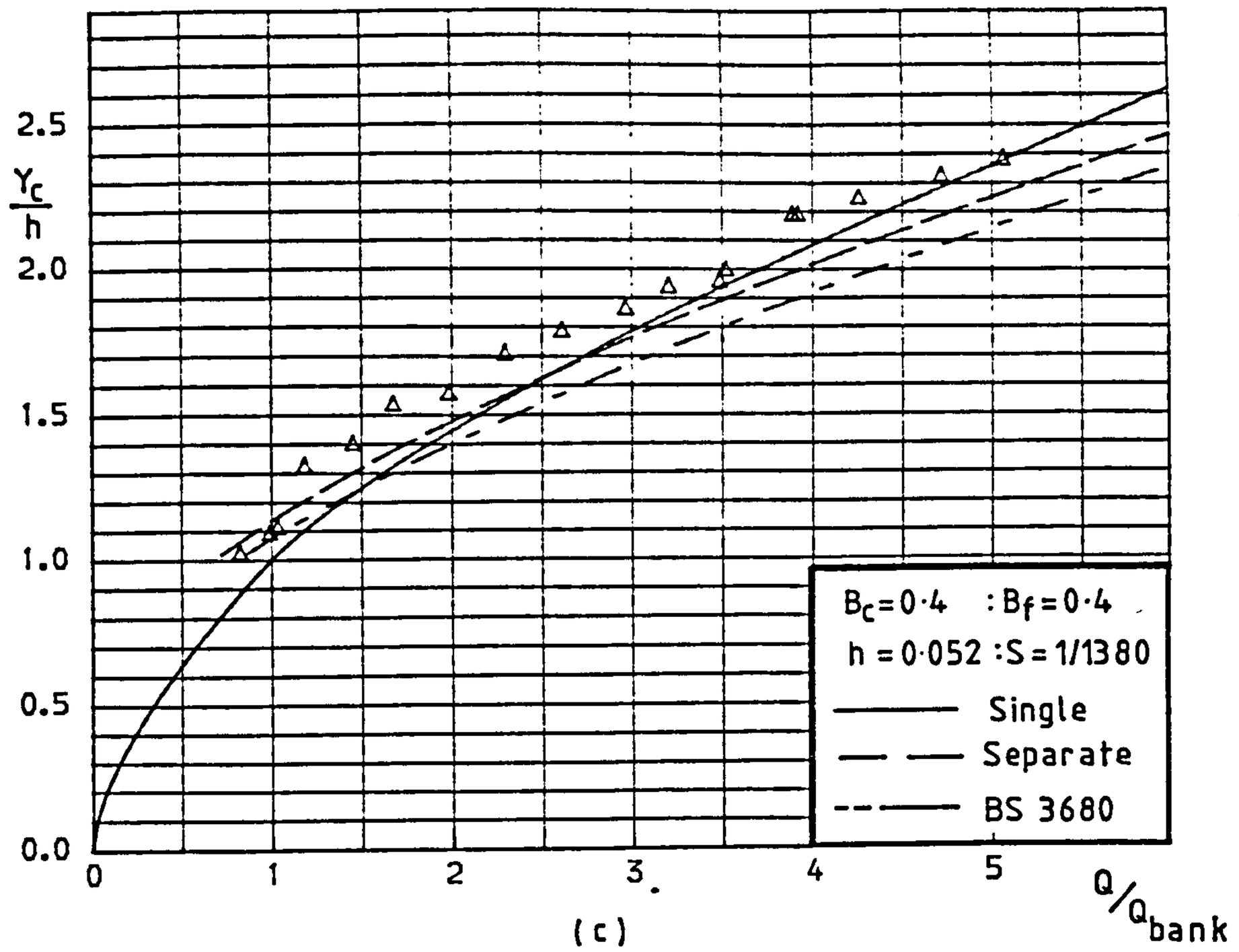
2.5
Yc/h
2.0
1.5
1.0
0.5
0.0
0
1
2
3
4
5
Q/Qbank
Bc=0·4 : Bf=0·4
h=0·052 : S=1/1380
Single
Separate
BS 3680
(c)

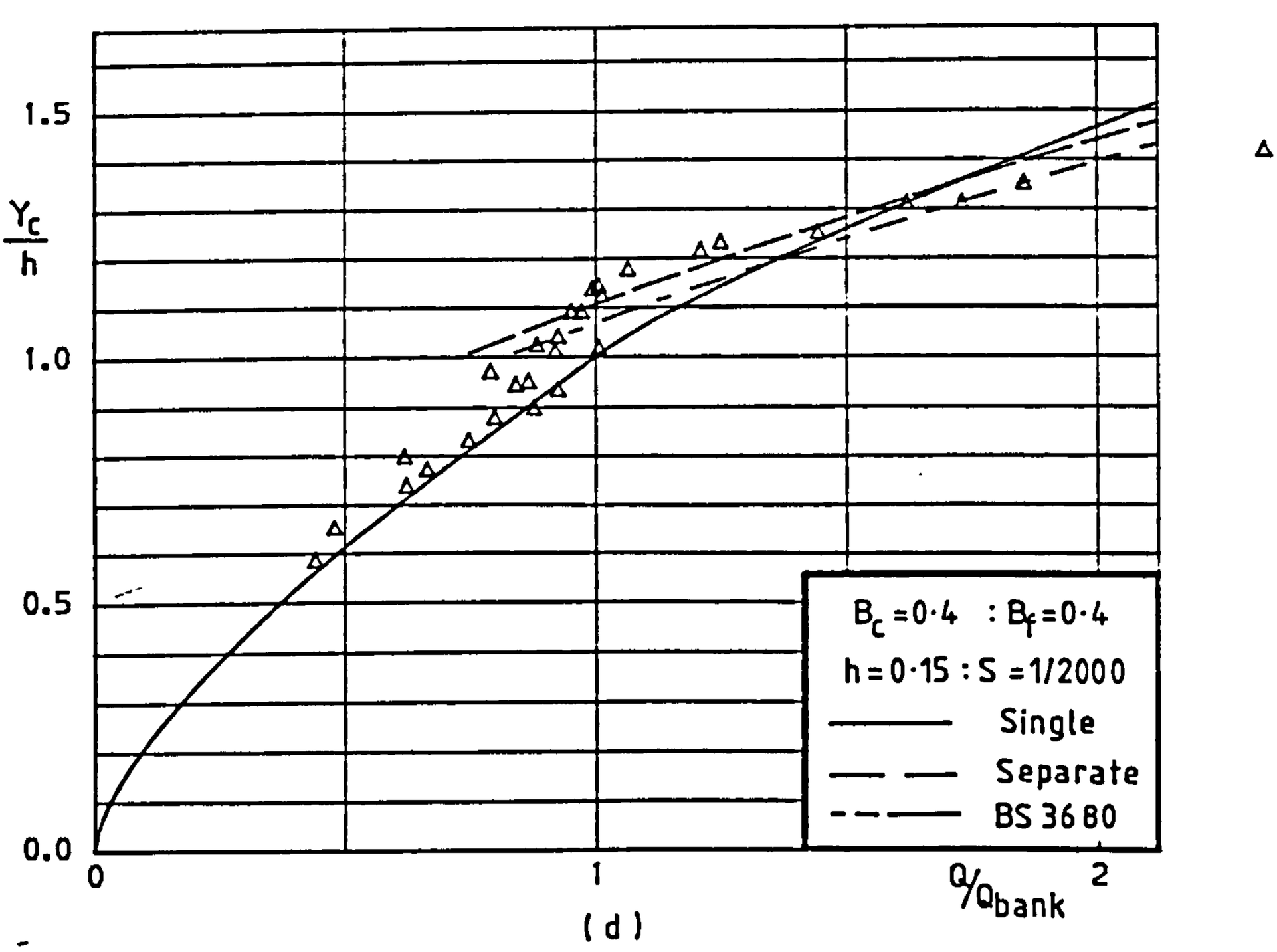
1.5
Yc/h
1.0
0.5
0.0
0
1
2
Q/Qbank
Bc=0·4 : Bf=0·4
h=0·15 : S=1/2000
Single
Separate
BS 3680
(d)

Fig 4·4

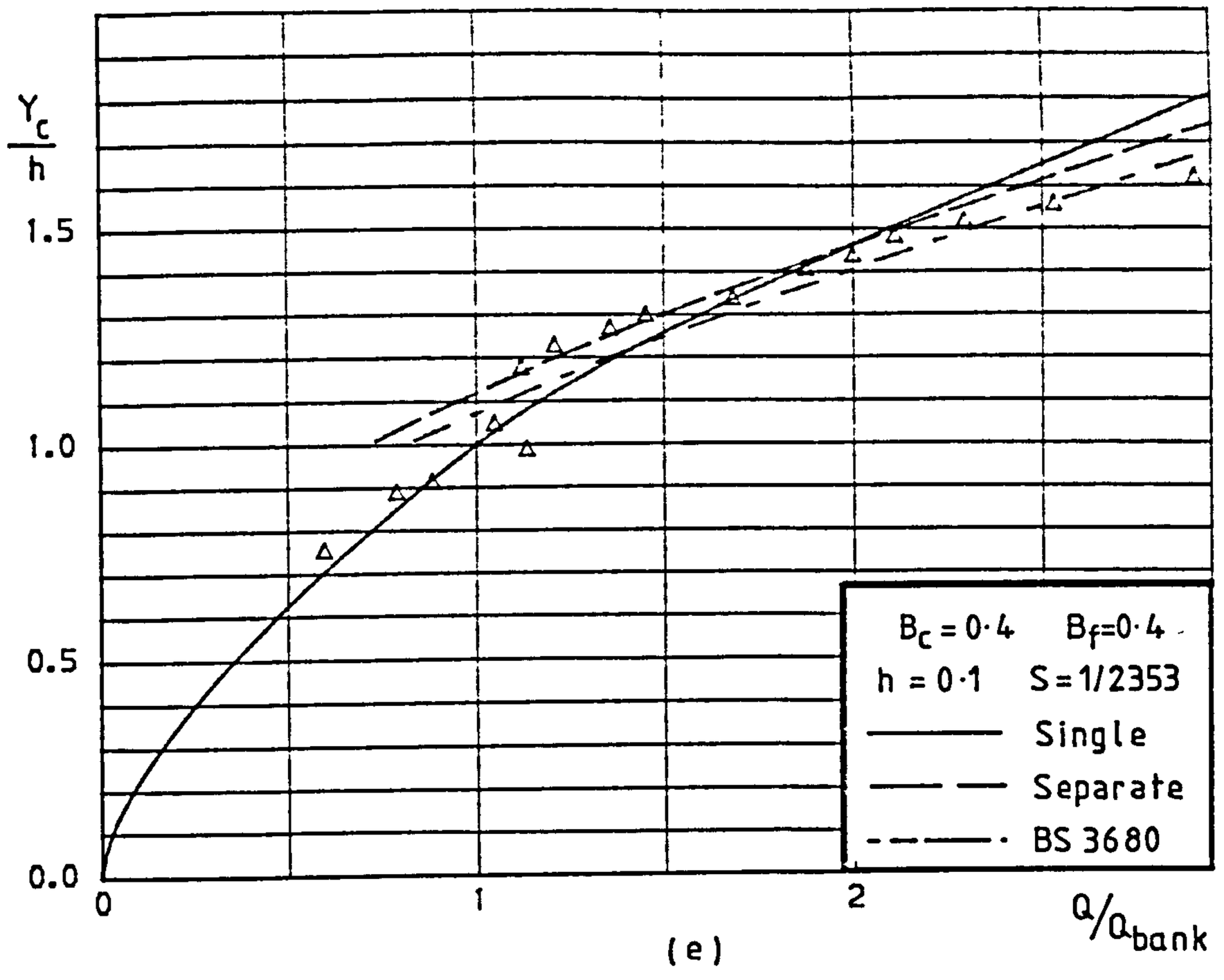
Yc/h
1.5
1.0
0.5
0.0
0
1
2
Q/Qbank
Bc = 0·4 Bf=0·4
h = 0·1 S = 1/2353
Single
Separate
BS 3680

(e)

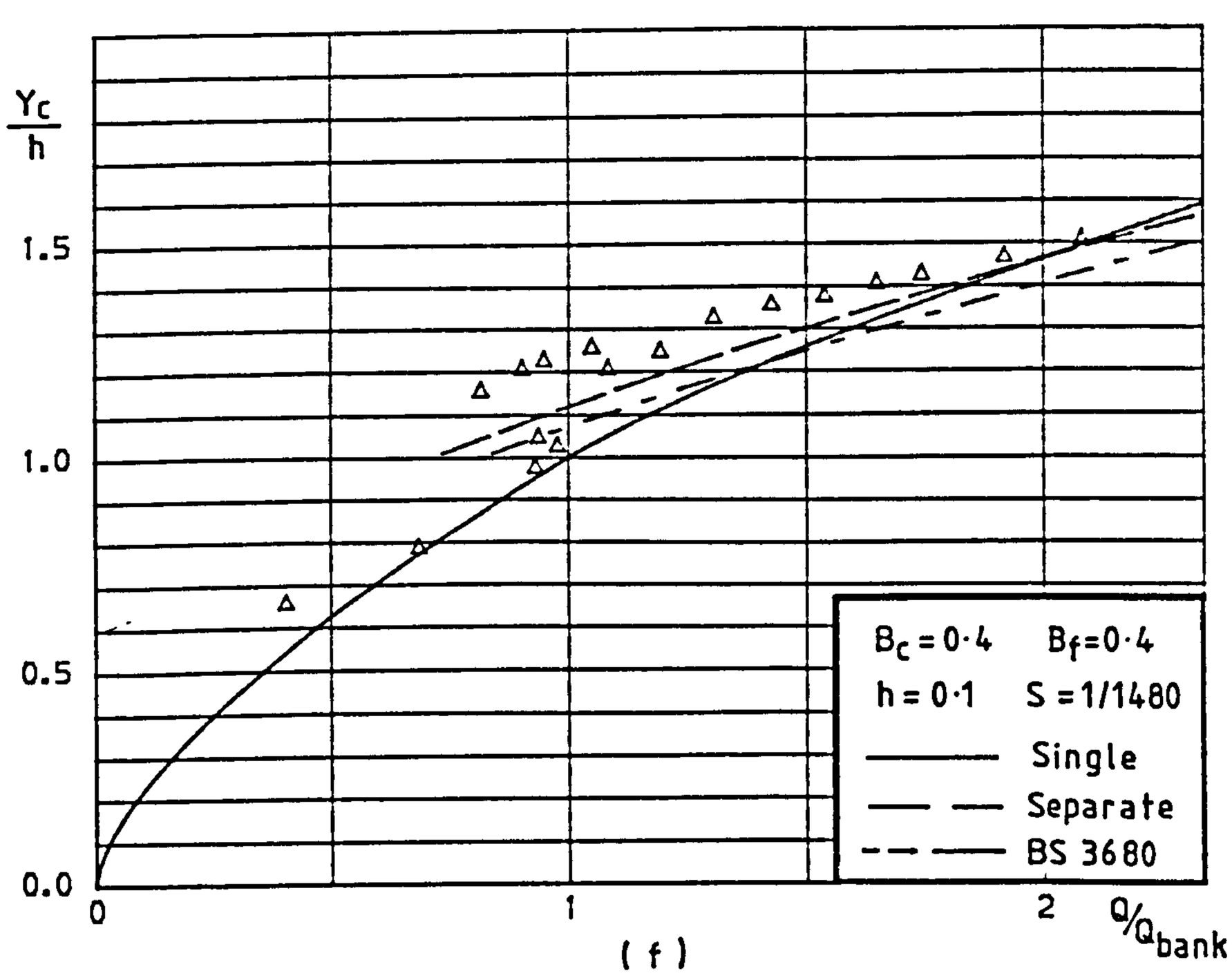
Yc/h
1.5
1.0
0.5
0.0
0
1
2
Q/Qbank
Bc = 0·4 Bf=0·4
h = 0·1 S = 1/1480
Single
Separate
BS 3680

(f)

Fig 4·4

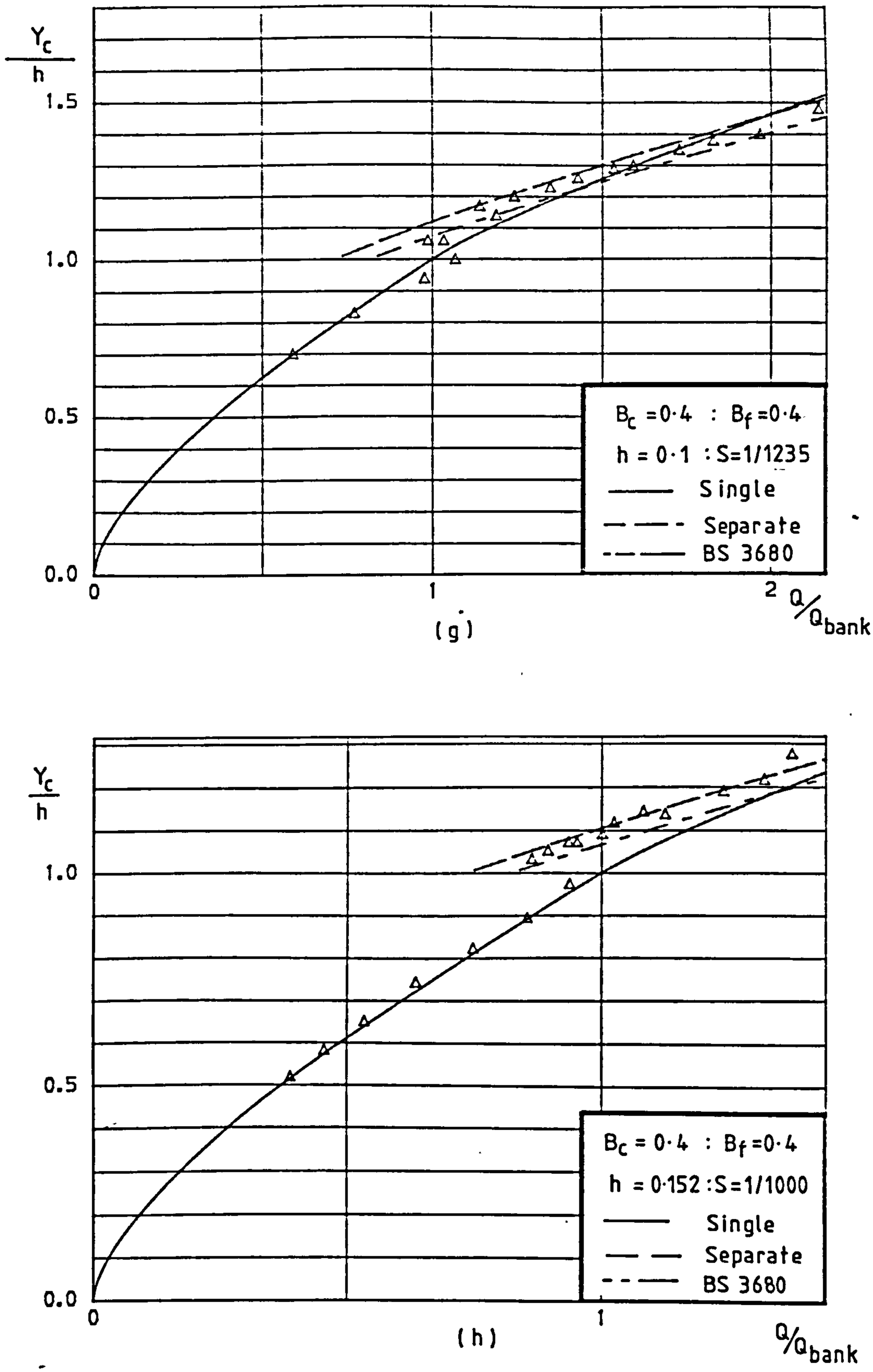
Yc/h
1.5
1.0
0.5
0.0
0
1
2
Q/Qbank
(g)
Bc =0·4 : Bf =0·4
h = 0·1 : S=1/1235
Single
Separate
BS 3680
Yc/h
1.0
0.5
0.0
0
1
(h)
Q/Qbank
Bc = 0·4 : Bf =0·4
h = 0·152 : S=1/1000
Single
Separate
BS 3680

Fig 4·4

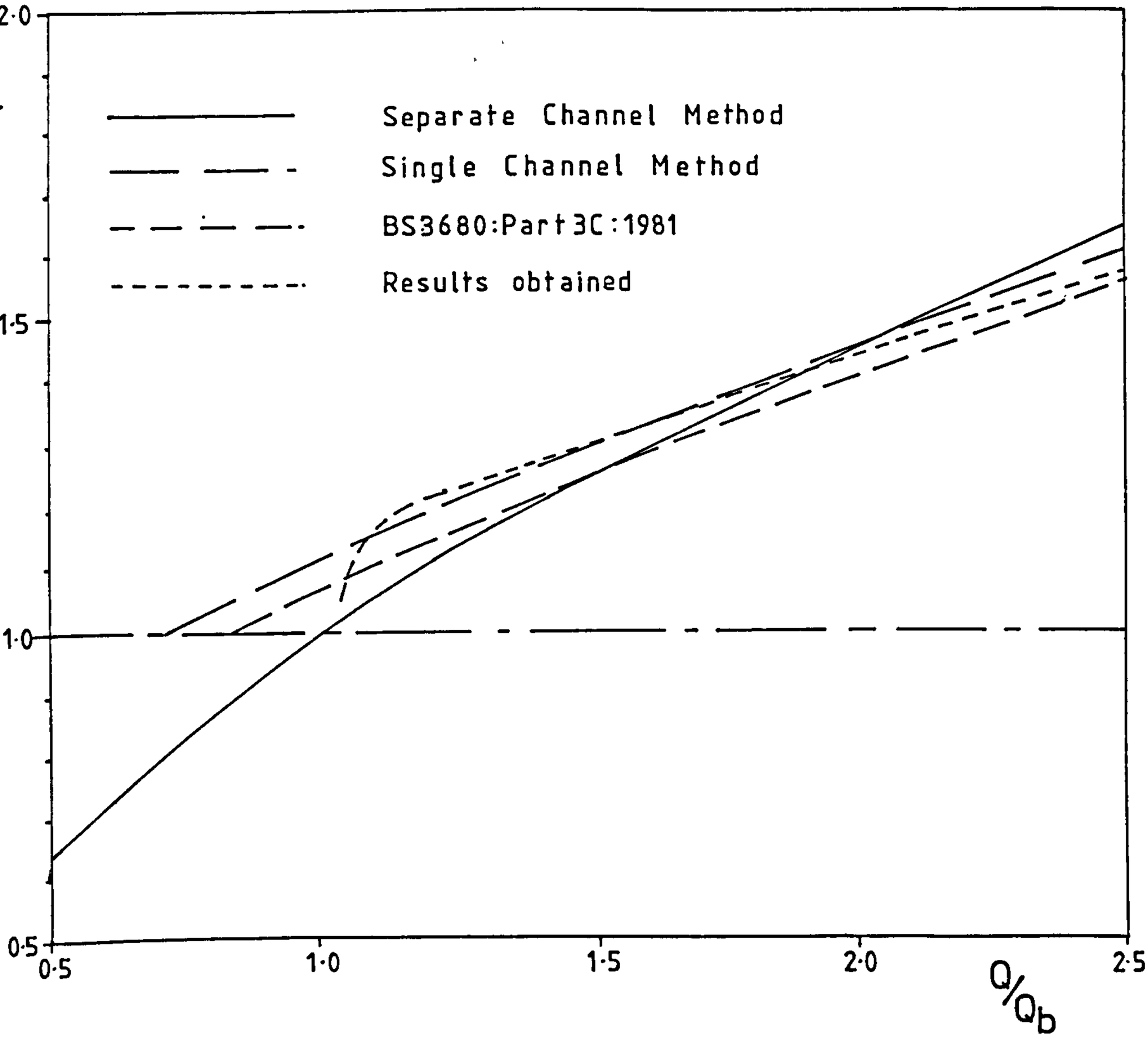

Fig 4·5 An Idealized Stage-Discharge Relationship.

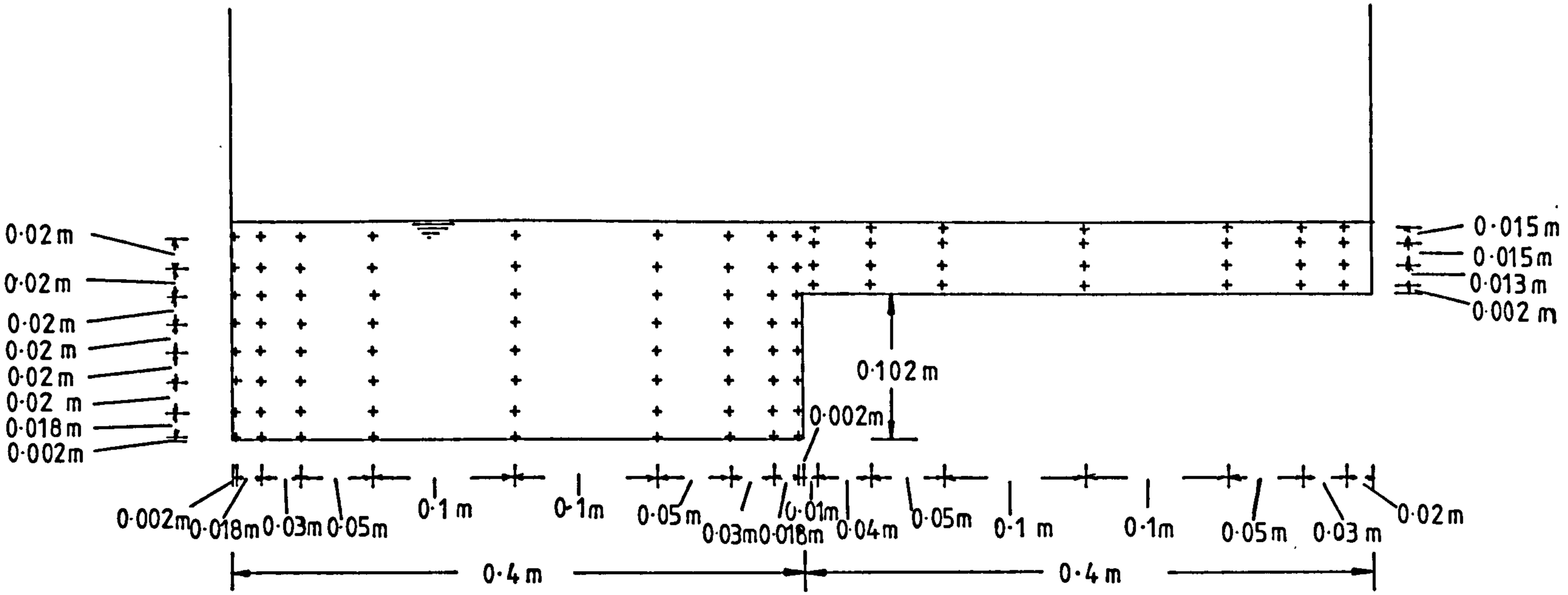

Fig 4·6 A Typical Velocity Traverse for Geometry Configuration "A".

		(m)	(m)	(m)	(m)		(m/sec)	(m/sec)
Geom	Run	Yc	Bc	Bf	h	$Slope^{-1}$	V'c	V'f
K1	1	0.1340	0.400	0.400	0.102	934.0	0.554	0.370
K2	2	0.1260	0.400	0.400	0.102	958.0	0.530	0.340
K3	3	0.1200	0.400	0.400	0.102	1027.0	0.502	0.234
K4	4	0.1150	0.400	0.400	0.102	1192.0	0.471	0.200
K5	5	0.1480	0.400	0.400	0.102	1480.0	0.465	0.380
K6	6	0.1320	0.400	0.400	0.102	2165.0	0.355	0.240
K7	7	0.1200	0.400	0.400	0.102	3103.0	0.299	0.160
K8	8	0.1510	0.400	0.400	0.102	2096.0	0.387	0.330
K9	9	0.1300	0.400	0.400	0.102	2337.0	0.354	0.200
K10	10	0.1210	0.400	0.400	0.102	2977.0	0.305	0.130
A12	11	0.1470	0.400	0.400	0.052	2419.0	0.395	0.390
A5	12	0.1110	0.400	0.400	0.052	7615.0	0.195	0.171
A6	13	0.0920	0.400	0.400	0.052	880.0	0.502	0.390
A7	14	0.1000	0.400	0.400	0.052	960.0	0.500	0.430
A8	15	0.0800	0.400	0.400	0.052	1169.0	0.407	0.263
A9	16	0.0830	0.400	0.400	0.052	1876.0	0.326	0.230
A10	17	0.1250	0.400	0.400	0.052	1522.0	0.446	0.440
A11	18	0.0750	0.400	0.400	0.052	2744.0	0.275	0.125
A1	19	0.1030	0.395	0.400	0.052	1412.0	0.410	0.370

Table 4·1

Geom	Run	Yc (m)	Bc (m)	Bf (m)	h (m)	Slope^{-1}	Vc' (m/s)	Vf' (m/s)
A2	20	0.0810	0.395	0.400	0.052	1719.0	0.325	0.240
A3	21	0.0700	0.395	0.400	0.052	1733.0	0.305	0.145
A4	22	0.0960	0.395	0.400	0.052	2007.0	0.335	0.290
B1	23	0.1050	0.185	0.404	0.052	1800.0	0.310	0.305
B2	24	0.0925	0.185	0.404	0.052	1463.0	0.320	0.285
B3	25	0.0765	0.185	0.404	0.052	1711.0	0.270	0.200
B4	26	0.0710	0.185	0.404	0.052	1678.0	0.260	0.185
B5	27	0.1020	0.185	0.400	0.053	1978.0	0.302	0.284
B6	28	0.0790	0.185	0.400	0.053	1801.0	0.264	0.210
B7	29	0.0685	0.185	0.400	0.053	2738.0	0.195	0.132
B8	30	0.1240	0.185	0.400	0.053	2285.0	0.310	0.325
C1	31	0.0700	0.395	0.200	0.052	1497.0	0.350	0.210
C2	32	0.0960	0.395	0.200	0.052	1727.0	0.375	0.340
C4	33	0.0850	0.395	0.200	0.052	1448.0	0.385	0.275
C5	34	0.0860	0.392	0.193	0.052	2716.0	0.292	0.180
C6	35	0.0640	0.392	0.193	0.052	2192.0	0.275	0.092
C7	36	0.1010	0.392	0.193	0.052	1622.0	0.395	0.330

Table 4·1

Geom	Run	Yc (m)	Bc (m)	Bf (m)	h (m)	Slope^{-1}	V'c (m/s)	V'f (m/s)
C8	37	0.0725	0.392	0.193	0.052	4330.0	0.230	0.185
G1	38	0.1700	0.192	0.607	0.152	797.0	0.495	0.280
G2	39	0.1740	0.192	0.607	0.152	571.0	0.560	0.395
G3	40	0.2090	0.192	0.607	0.152	1477.0	0.402	0.380
G4	41	0.1880	0.192	0.607	0.152	1222.0	0.415	0.340
G5	42	0.1760	0.192	0.603	0.152	2326.0	0.285	0.260
G6	43	0.1860	0.192	0.603	0.152	2024.0	0.310	0.260
G7	44	0.1980	0.192	0.603	0.152	2041.0	0.326	0.295
G8	45	0.1635	0.192	0.603	0.152	3462.0	0.230	0.125
L1	46	0.1970	0.190	0.397	0.152	1168.0	0.435	0.405
L2	47	0.1800	0.190	0.397	0.152	1285.0	0.400	0.300
L3	48	0.1695	0.190	0.397	0.152	1106.0	0.430	0.225
L4	49	0.1890	0.190	0.397	0.152	991.0	0.460	0.380
L5	50	0.1845	0.190	0.397	0.152	1746.0	0.355	0.250
L6	51	0.1790	0.190	0.397	0.152	1643.0	0.350	0.244
L7	52	0.1750	0.190	0.397	0.152	1965.0	0.320	0.220
L8	53	0.1690	0.190	0.397	0.152	2174.0	0.305	0.170

Table 4·1

Geom	Run	Yc (m)	Bc (m)	Bf (m)	h (m)	Slope^{-1}	V'c (m/s)	V'f (m/s)
N1	54	0.1950	0.191	0.213	0.152	1067.0	0.475	0.395
N2	55	0.1830	0.191	0.213	0.152	1205.0	0.435	0.330
N3	56	0.1990	0.191	0.213	0.152	1044.0	0.485	0.410
N4	57	0.1685	0.191	0.213	0.152	1018.0	0.460	0.265
N5	58	0.1685	0.191	0.211	0.152	2138.0	0.310	0.185
N6	59	0.1790	0.191	0.211	0.152	1614.0	0.390	0.275
N7	60	0.1740	0.191	0.211	0.152	1709.0	0.350	0.240
N8	61	0.1930	0.191	0.211	0.152	1757.0	0.370	0.305
J1	62	0.1870	0.390	0.404	0.152	1979.0	0.435	0.295
J2	63	0.1720	0.390	0.404	0.152	1648.0	0.470	0.200
J3	64	0.1720	0.390	0.404	0.152	1397.0	0.505	0.235
J4	65	0.1600	0.390	0.404	0.152	1291.0	0.500	0.130
J5	66	0.1780	0.390	0.404	0.152	1482.0	0.485	0.285
J6	67	0.1840	0.390	0.404	0.152	1344.0	0.515	0.350
J7	68	0.1560	0.390	0.404	0.152	1836.0	0.420	0.105
J8	69	0.1680	0.390	0.404	0.152	1681.0	0.455	0.180
J9	70	0.1660	0.390	0.404	0.152	1963.0	0.425	0.140

Table 4·1

Geom	Run	Yc (m)	Bc (m)	Bf (m)	h (m)	Slope'	Vc' (m/s)	Vf' (m/s)
R1	71	0.1555	0.390	0.200	0.152	1937.0	0.425	0.070
R2	72	0.1660	0.390	0.200	0.152	1761.0	0.455	0.180
R3	73	0.1730	0.390	0.200	0.153	1685.0	0.470	0.240
R4	74	0.1755	0.390	0.200	0.153	1658.0	0.480	0.270
R5	75	0.1795	0.390	0.200	0.153	1647.0	0.485	0.295
R6	76	0.1850	0.390	0.200	0.153	1638.0	0.490	0.320
R7	77	0.1920	0.390	0.200	0.153	1664.0	0.492	0.370
R8	78	0.2010	0.390	0.200	0.153	1803.0	0.485	0.375
P1	94	0.1220	0.193	0.396	0.101	1486.0	0.340	0.210
P2	95	0.1230	0.193	0.396	0.101	1005.0	0.395	0.240
P3	96	0.1280	0.193	0.396	0.101	1720.0	0.325	0.220
P4	97	0.1350	0.193	0.396	0.101	1198.0	0.395	0.305
P5	98	0.1440	0.193	0.396	0.101	1185.0	0.415	0.350
P6	99	0.1320	0.193	0.396	0.101	1044.0	0.420	0.320
P7	100	0.1080	0.193	0.396	0.101	924.0	0.410	0.085
P8	101	0.1190	0.193	0.396	0.101	1552.0	0.340	0.160
P9	102	0.1250	0.193	0.396	0.101	2145.0	0.290	0.160

Table 4-1

Geom	Run	Yc (m)	Bc (m)	Bf (m)	h (m)	Slope^{-1}	Vc (m/s)	Vf (m/s)
P10	103	0.1280	0.193	0.396	0.101	1209.0	0.385	0.260
H1	104	0.1500	0.194	0.601	0.101	1223.0	0.390	0.360
H2	105	0.1290	0.194	0.601	0.101	1097.0	0.390	0.280
H3	106	0.1280	0.194	0.601	0.101	1821.0	0.300	0.210
H4	107	0.1210	0.194	0.601	0.101	1176.0	0.370	0.190
H5	108	0.1320	0.194	0.601	0.101	876.0	0.440	0.345
H6	109	0.1230	0.194	0.601	0.101	1126.0	0.380	0.237
H7	110	0.1200	0.194	0.601	0.101	1231.0	0.365	0.187
H8	111	0.1585	0.194	0.601	0.101	1270.0	0.420	0.390
H9	112	0.1155	0.194	0.601	0.101	1135.0	0.380	0.160
H10	113	0.1250	0.194	0.601	0.101	1839.0	0.305	0.185
M1	114	0.1120	0.193	0.210	0.101	1113.0	0.395	0.120
M2	115	0.1250	0.193	0.210	0.101	1046.0	0.430	0.245
M3	116	0.1410	0.193	0.210	0.101	1249.0	0.415	0.305
M4	117	0.1130	0.193	0.210	0.101	1528.0	0.345	0.090
M5	118	0.1150	0.193	0.210	0.101	1088.0	0.407	0.184
M6	119	0.1230	0.193	0.210	0.101	1453.0	0.365	0.185

Table 4·1

Geom	Run	Yc (m)	Bc (m)	Bf (m)	h (m)	Slope^{-1}	Vc (m/s)	Vf (m/s)
M7	120	0.1270	0.193	0.210	0.101	1135.0	0.415	0.250
M8	121	0.1370	0.193	0.210	0.101	1530.0	0.370	0.275
CRORY	122	0.1562	0.254	0.356	0.102	3800.0	0.257	0.226
CRORY	123	0.1467	0.254	0.356	0.102	3800.0	0.252	0.213
CRORY	124	0.1329	0.254	0.356	0.102	3800.0	0.237	0.174
CRORY	125	0.1280	0.254	0.356	0.102	3800.0	0.219	0.166
CRORY	126	0.1183	0.254	0.356	0.102	3800.0	0.210	0.136
CRORY	127	0.1410	0.203	0.356	0.102	3800.0	0.212	0.173
CRORY	128	0.1321	0.203	0.356	0.102	3800.0	0.193	0.152
CRORY	129	0.1233	0.203	0.356	0.102	3800.0	0.178	0.125
CRORY	130	0.1100	0.203	0.356	0.102	3800.0	0.197	0.062
CRORY	131	0.1550	0.153	0.356	0.102	3800.0	0.200	0.194
CRORY	132	0.1467	0.153	0.356	0.102	3800.0	0.180	0.183
CRORY	133	0.1333	0.153	0.356	0.102	3800.0	0.167	0.146
CRORY	134	0.1634	0.102	0.356	0.102	3800.0	0.206	0.204
CRORY	135	0.1467	0.102	0.356	0.102	3800.0	0.168	0.167
CRORY	136	0.1333	0.102	0.356	0.102	3800.0	0.161	0.146
CRORY	137	0.1187	0.102	0.356	0.102	3800.0	0.126	0.098

Table 4·1

Geom	Run	Yc (m)	Bc (m)	Bf (m)	h (m)	Slope^{-1}	V'c (m/s)	V'f (m/s)
01	138	0.0650	0.196	0.209	0.050	1524.0	0.285	0.135
02	139	0.0755	0.196	0.209	0.050	1376.0	0.320	0.220
03	140	0.0890	0.196	0.209	0.050	1325.0	0.345	0.305
04	141	0.0985	0.196	0.209	0.050	1121.0	0.403	0.360
05	142	0.0830	0.196	0.209	0.050	1161.0	0.355	0.290
06	143	0.0760	0.196	0.209	0.050	2276.0	0.247	0.175
07	144	0.0695	0.196	0.209	0.050	1557.0	0.285	0.170
08	145	0.0610	0.196	0.209	0.050	999.0	0.340	0.120
I1	146	0.0930	0.196	0.604	0.050	1909.0	0.285	0.260
I2	147	0.0750	0.196	0.604	0.050	726.0	0.405	0.290
I3	148	0.0680	0.196	0.604	0.050	913.0	0.348	0.205
I4	149	0.0840	0.196	0.604	0.050	3278.0	0.205	0.168
I5	150	0.0775	0.196	0.604	0.050	1324.0	0.308	0.230
I6	151	0.0870	0.196	0.604	0.050	1570.0	0.308	0.273
I7	152	0.0735	0.196	0.604	0.050	1593.0	0.277	0.197
I8	153	0.0620	0.196	0.604	0.050	1304.0	0.287	0.104

Table 4.1

Geom	Run	Yc (m)	Bc (m)	Bf (m)	h (m)	Slope^{-1}	V'c (m/s)	V'f (m/s)
S1	154	0.1195	0.392	0.203	0.100	1084.0	0.505	0.275
S2	155	0.1110	0.392	0.203	0.100	2019.0	0.365	0.125
S3	156	0.1130	0.392	0.203	0.100	1698.0	0.395	0.158
S4	157	0.1050	0.392	0.203	0.100	1389.0	0.420	0.100
S5	158	0.1220	0.392	0.203	0.100	856.0	0.573	0.350
S6	159	0.1400	0.392	0.203	0.100	1341.0	0.490	0.345
S7	160	0.1055	0.392	0.203	0.100	890.0	0.520	0.200
S8	161	0.1210	0.392	0.203	0.100	1601.0	0.420	0.220
E1	162	0.1145	0.590	0.209	0.100	1818.0	0.425	0.150
E2	163	0.1190	0.590	0.209	0.100	1647.0	0.460	0.180
E3	164	0.1225	0.590	0.209	0.100	1614.0	0.470	0.205
E4	165	0.1255	0.590	0.209	0.100	1555.0	0.485	0.245
E5	166	0.1060	0.590	0.209	0.100	1395.0	0.460	0.190
E6	167	0.1100	0.590	0.209	0.100	1200.0	0.507	0.170

Table 4·1

Contour Values	Velocity (m/s)
1	0·1
2	0·15
3	0·2
4	0·25
5	0·3
6	0·35
7	0·4
8	0·45
9	0·5
10	0·55
11	0·6

Fig 4·7 (a) Key to Contour Values shown on Fig 4·7

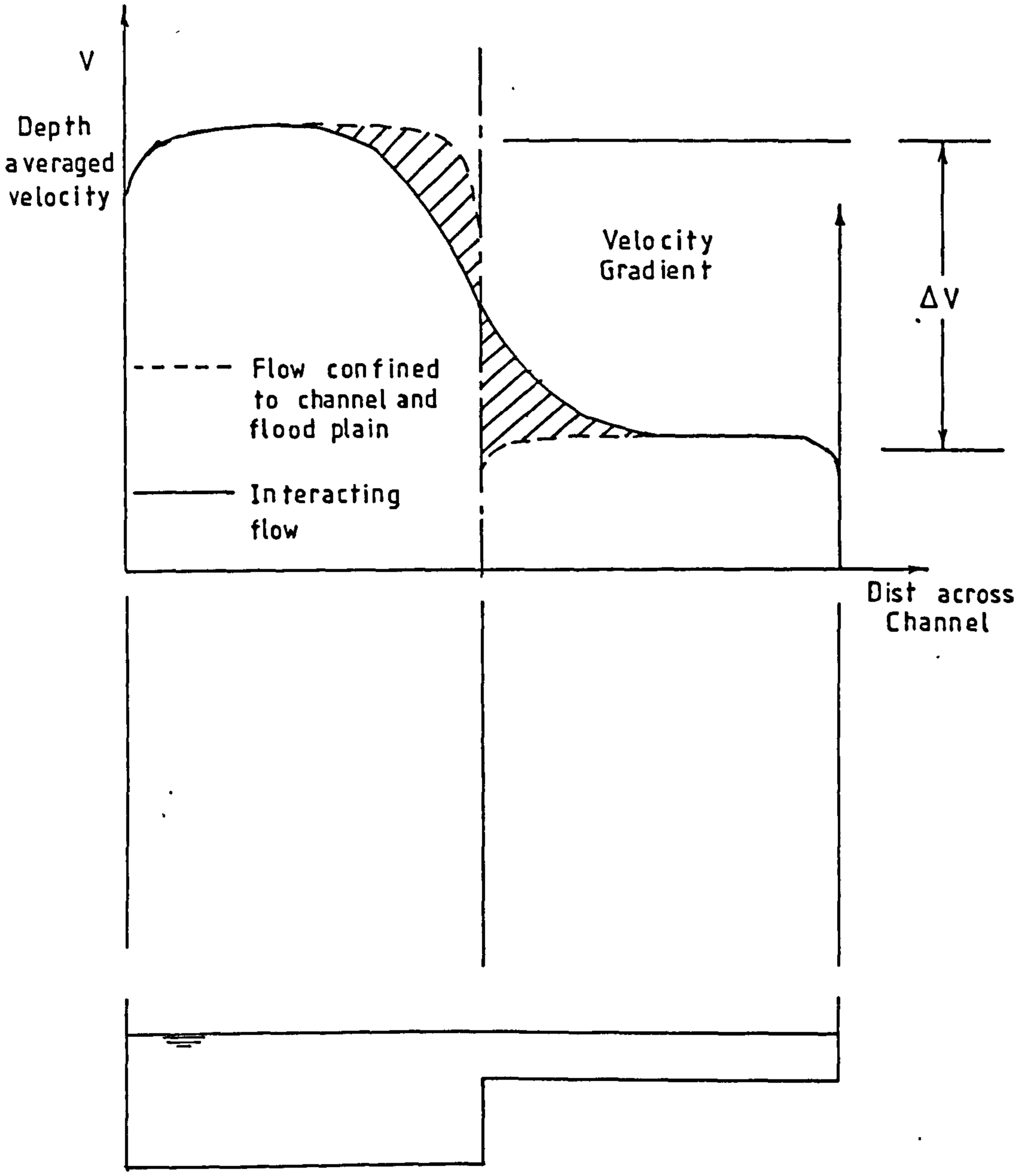

Fig 4·7(b) Velocity Profiles for Flow Confined and Unconfined to the Channel.

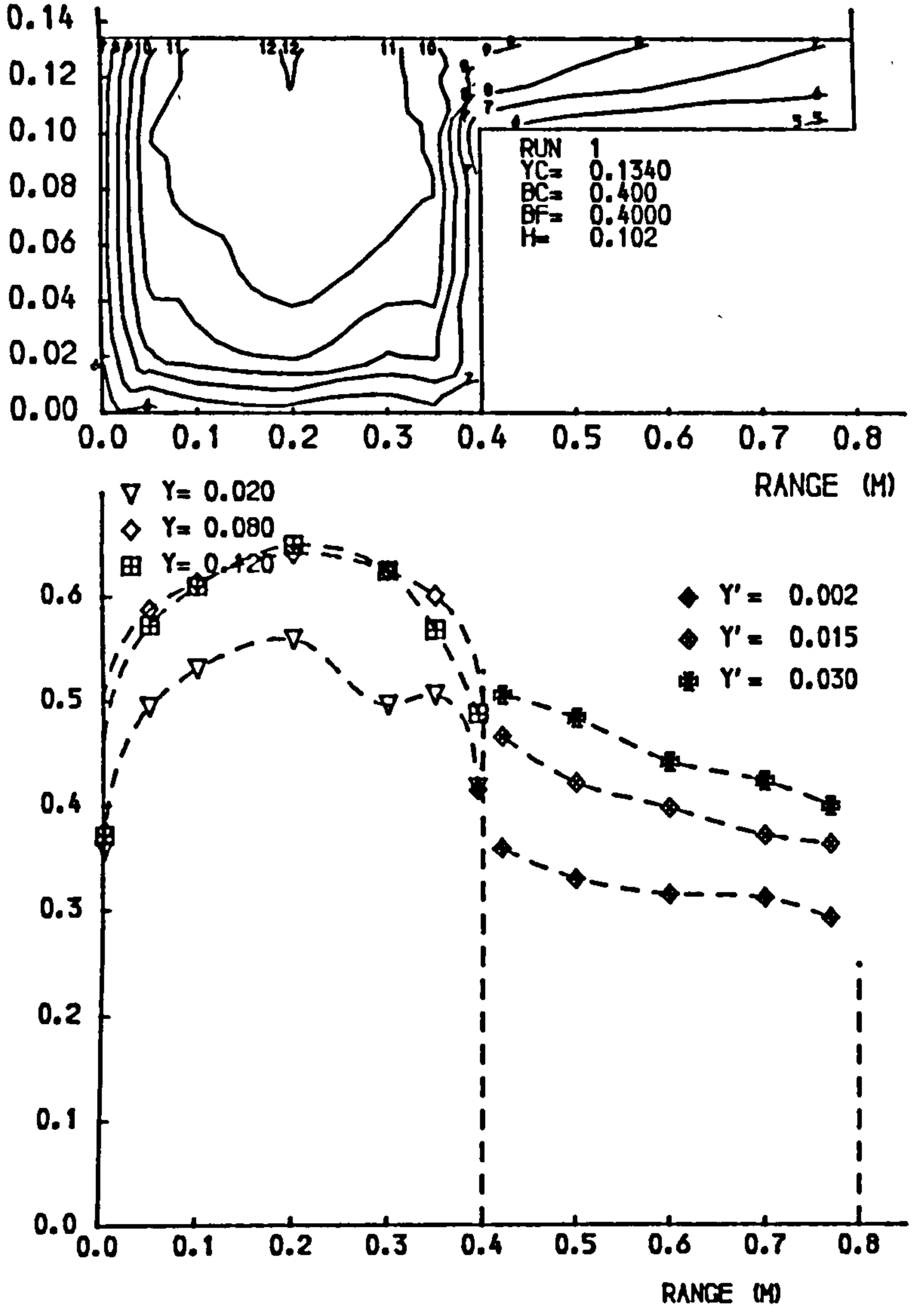

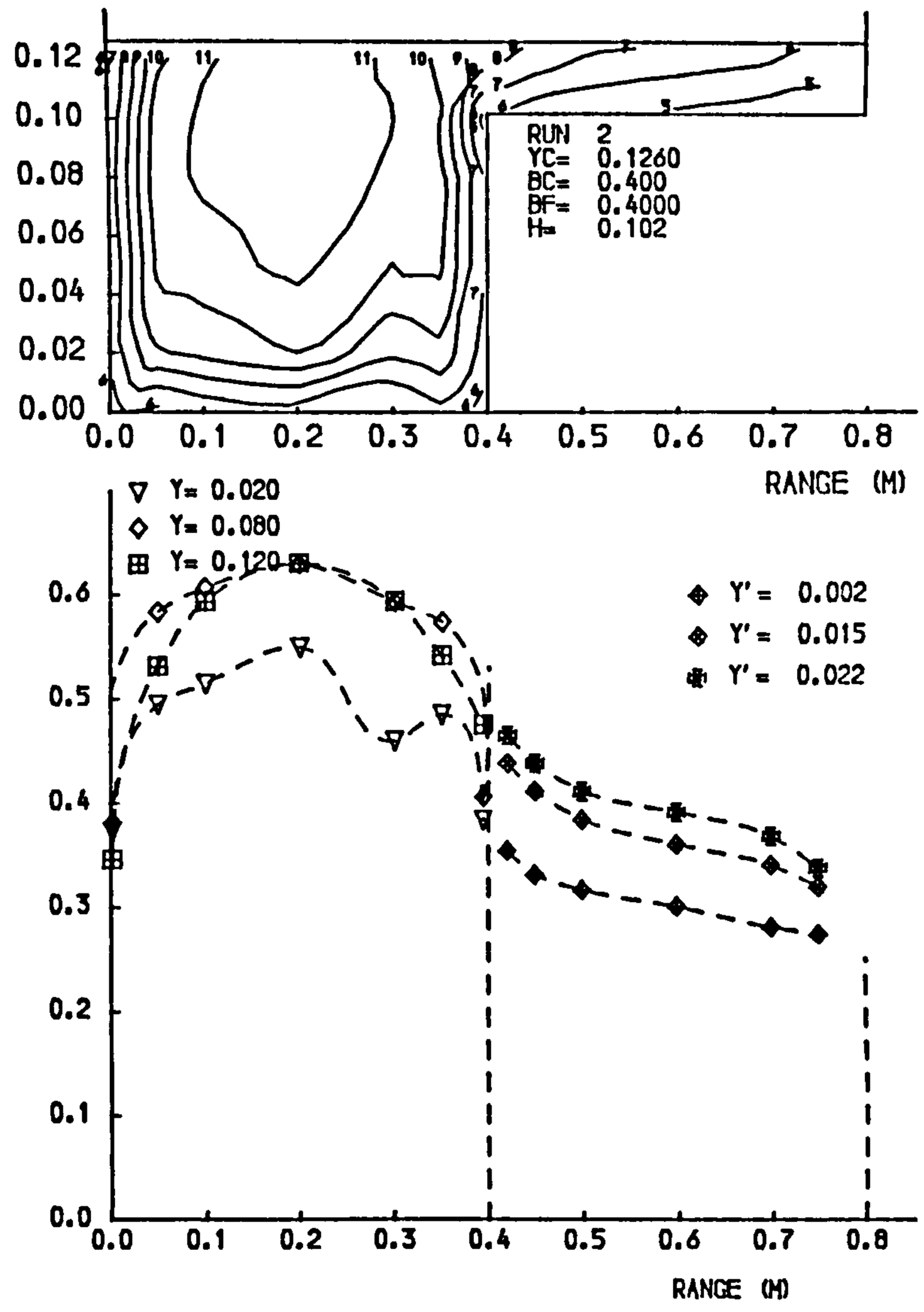

Fig 4·7 Isovels and lateral velocity profiles.

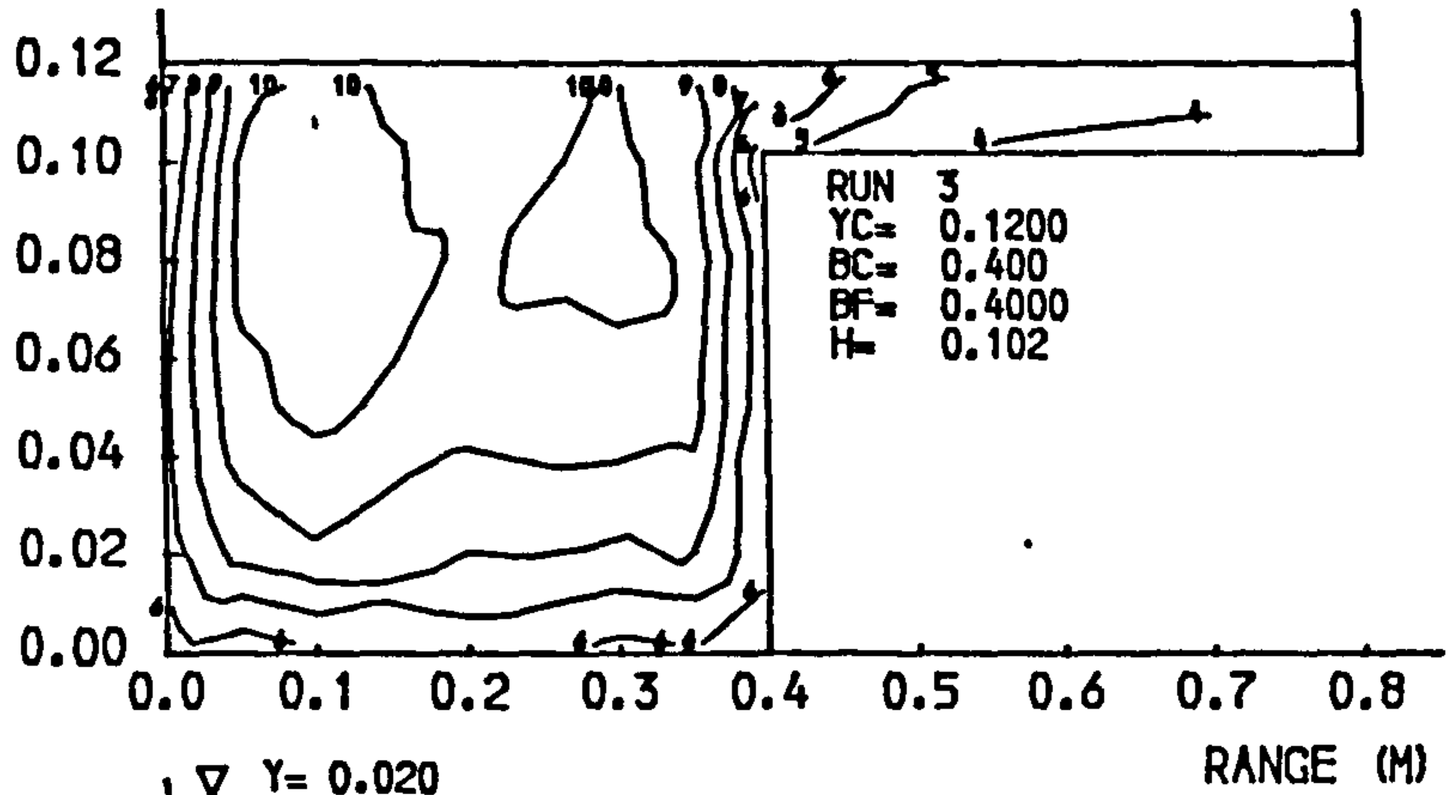

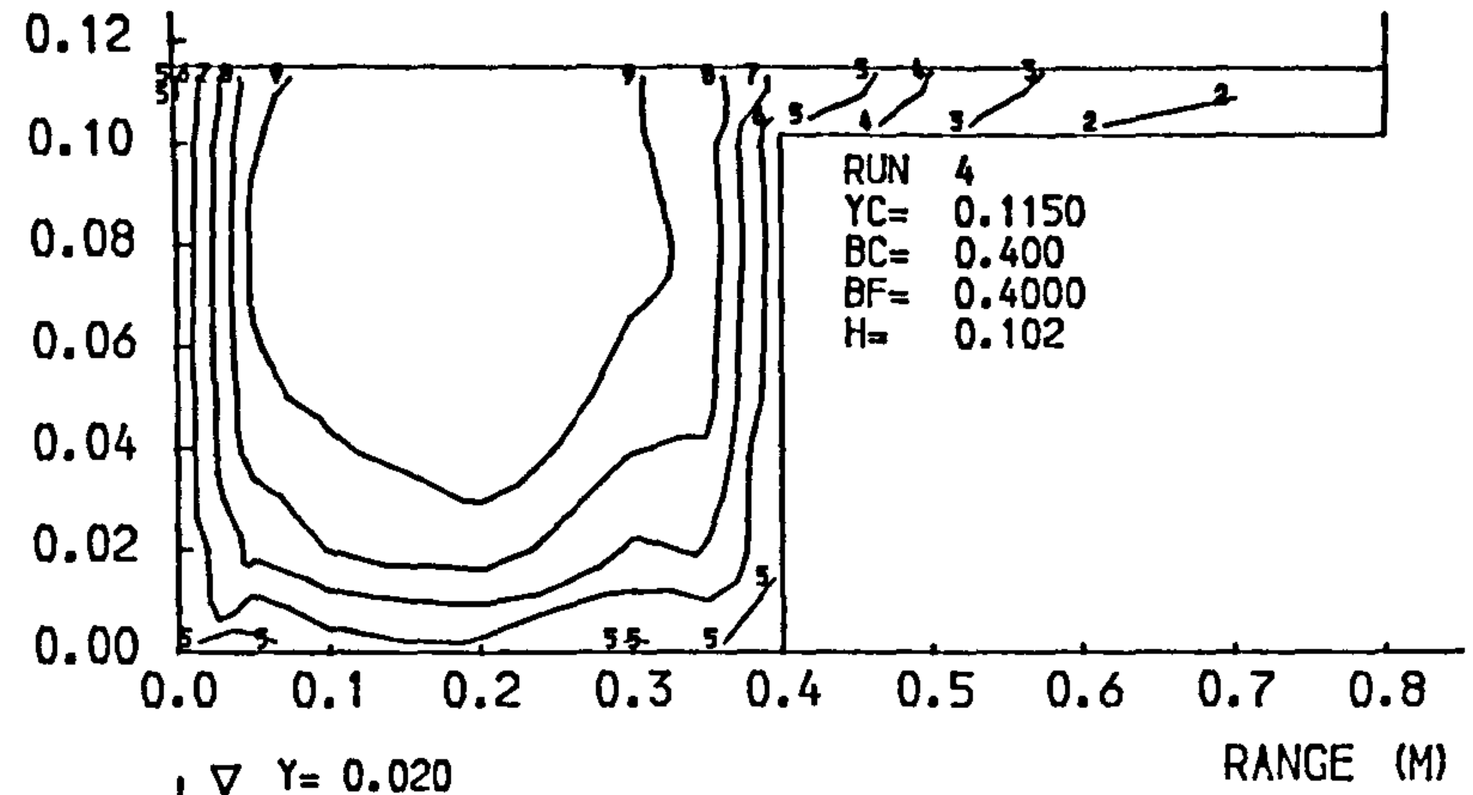

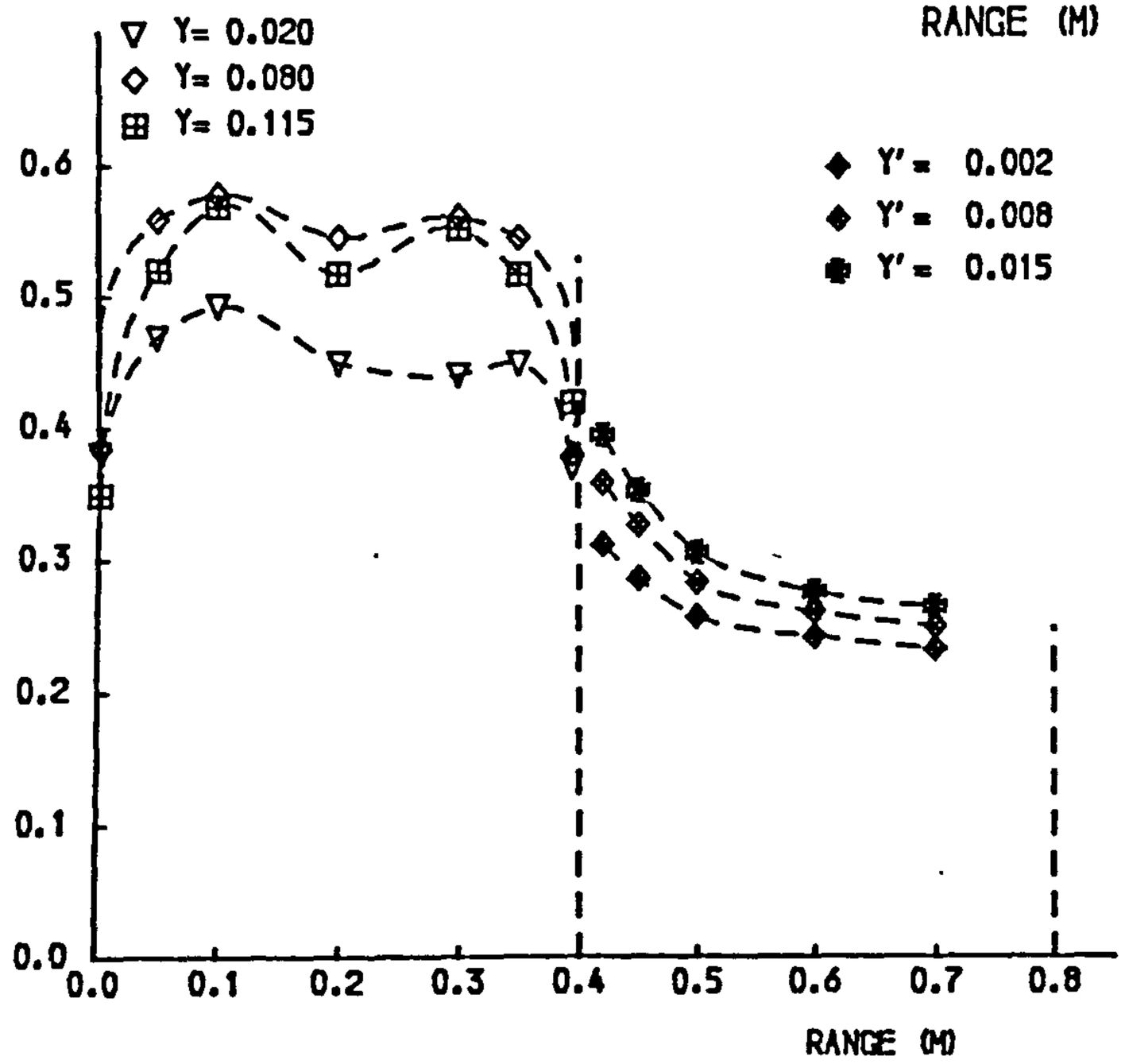

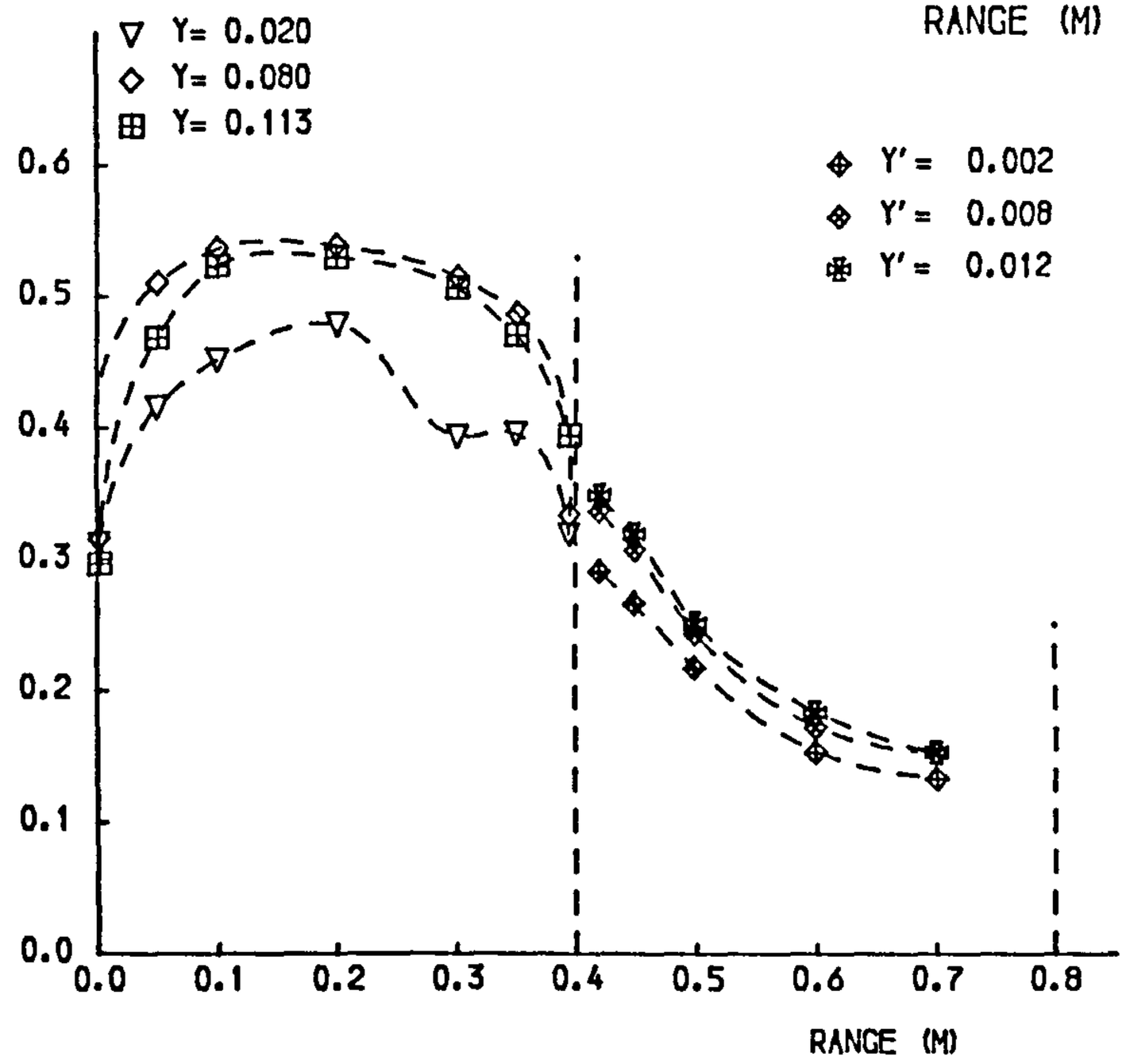

Fig4·7 Isovels and lateral velocity profiles.

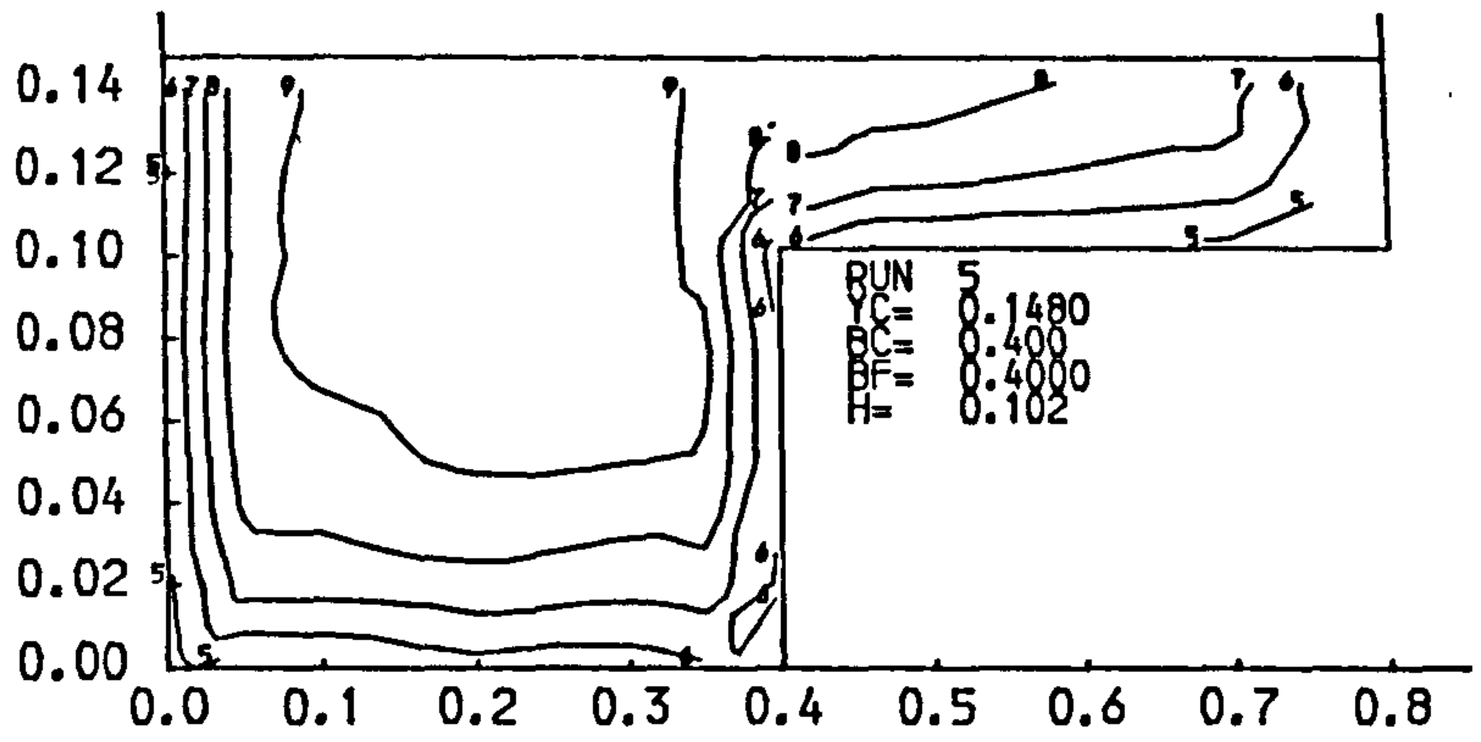

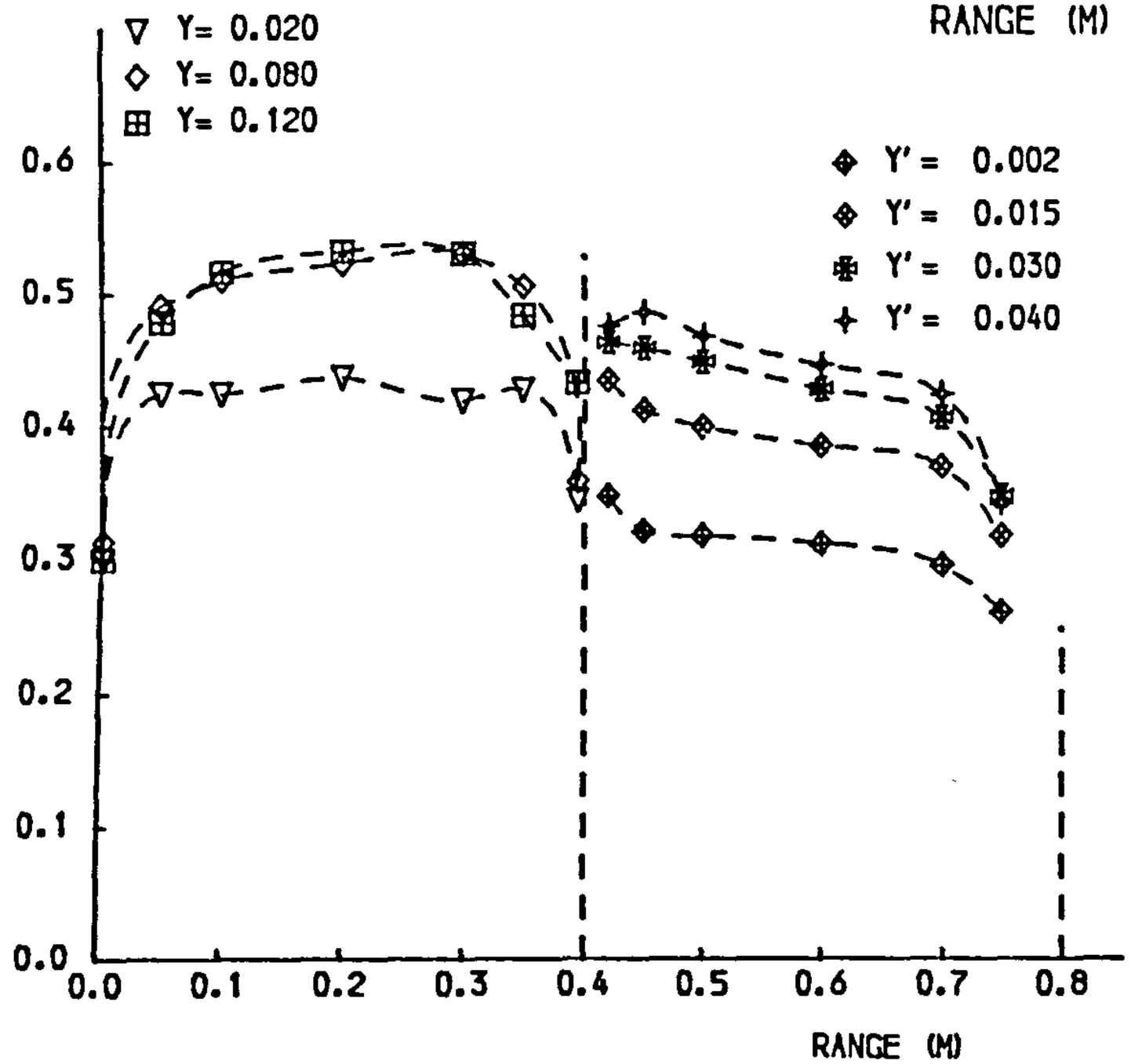

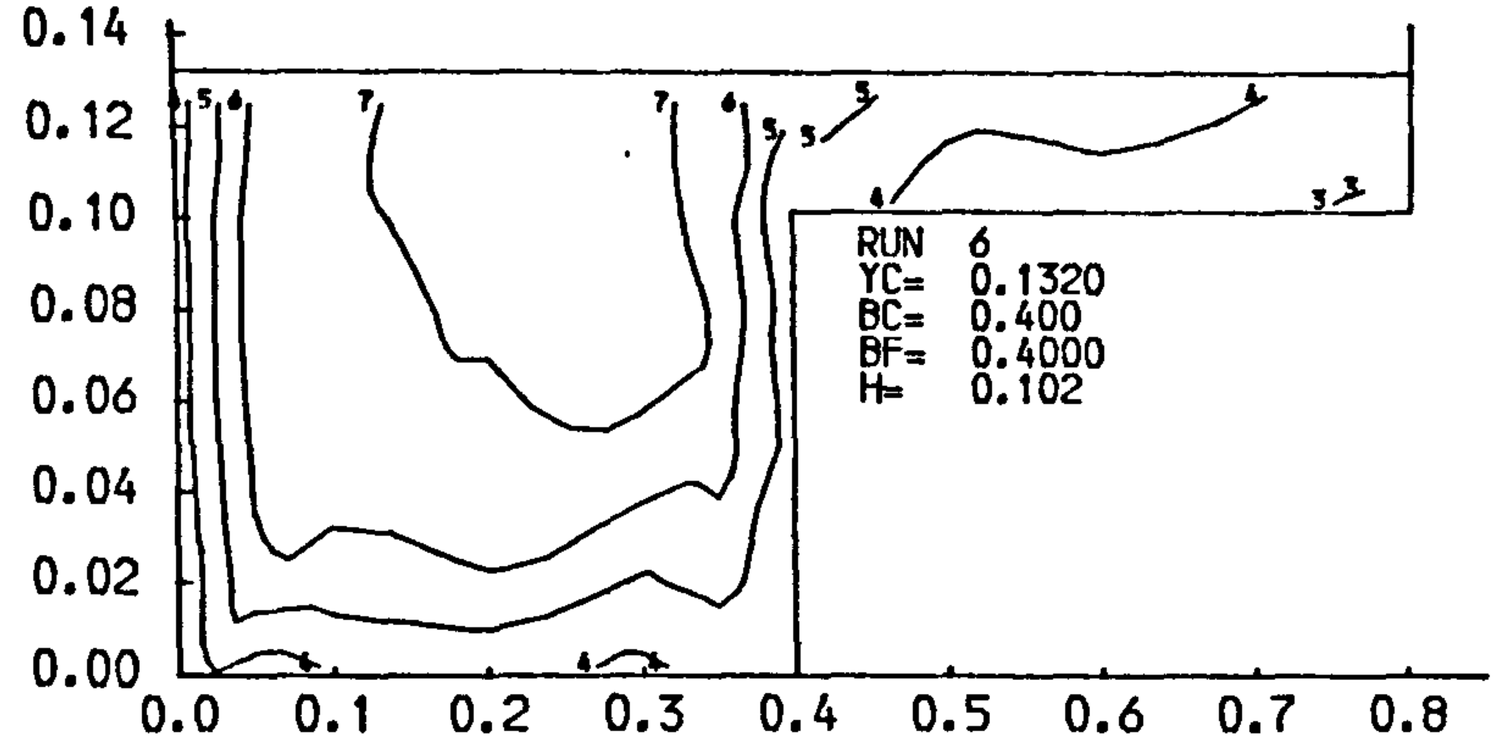

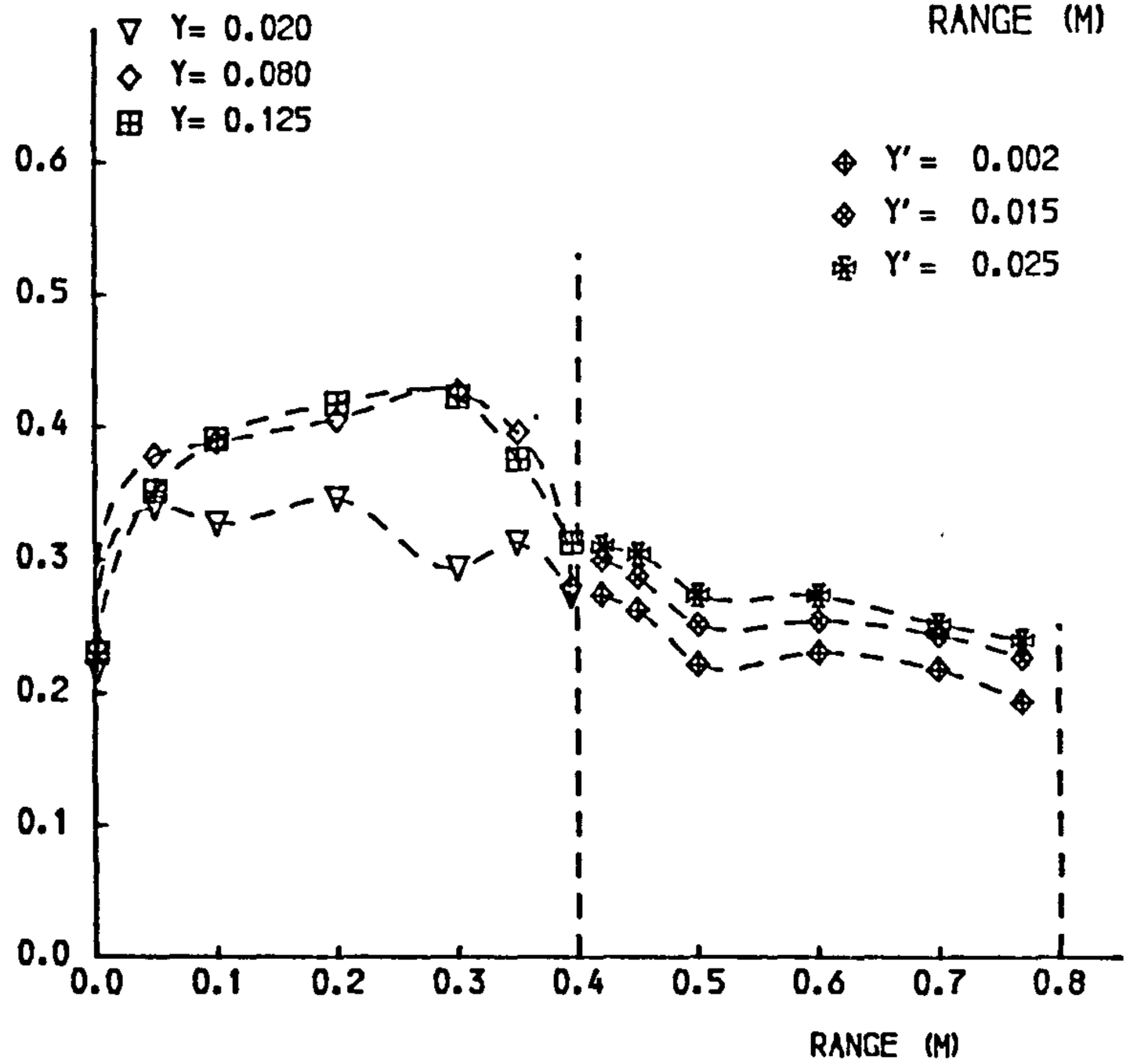

Fig 4·7 Isovels and lateral velocity profiles.

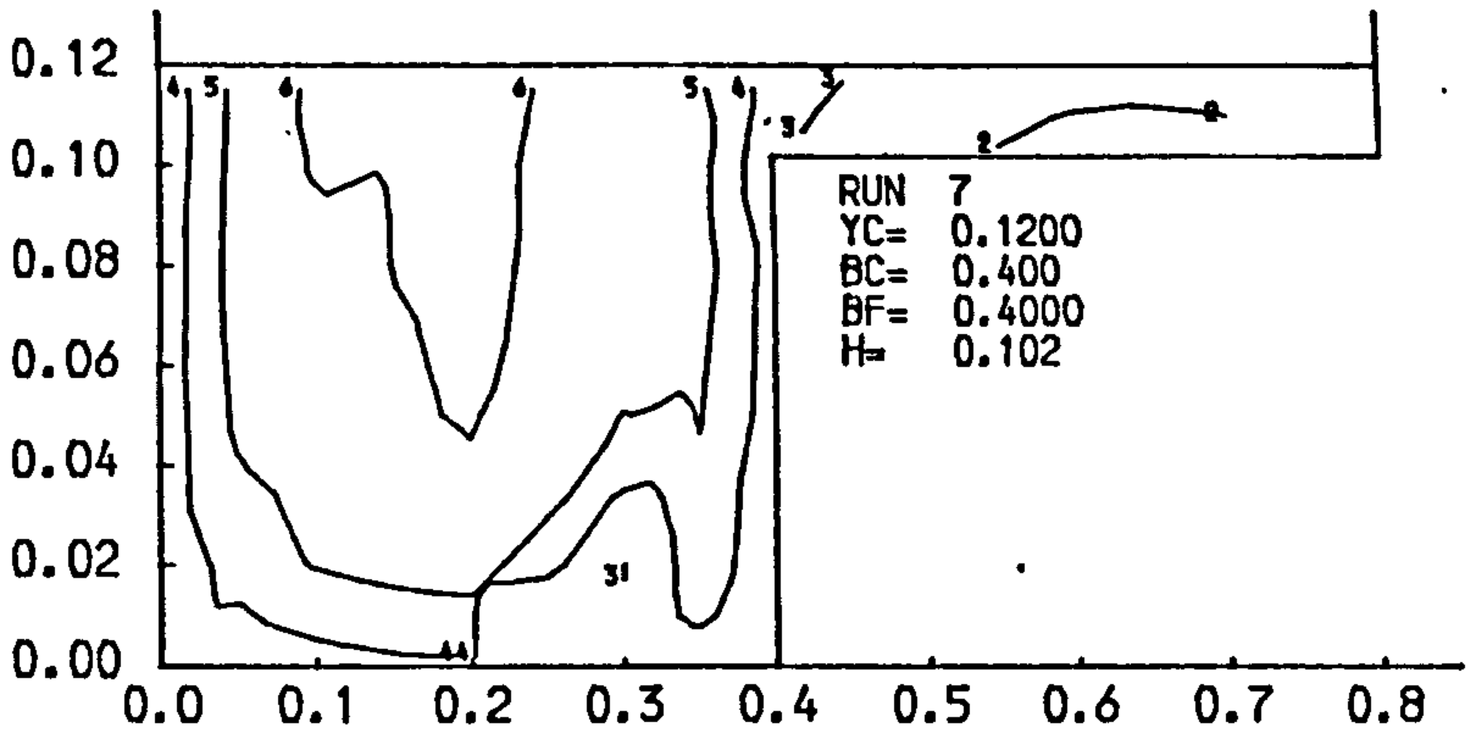

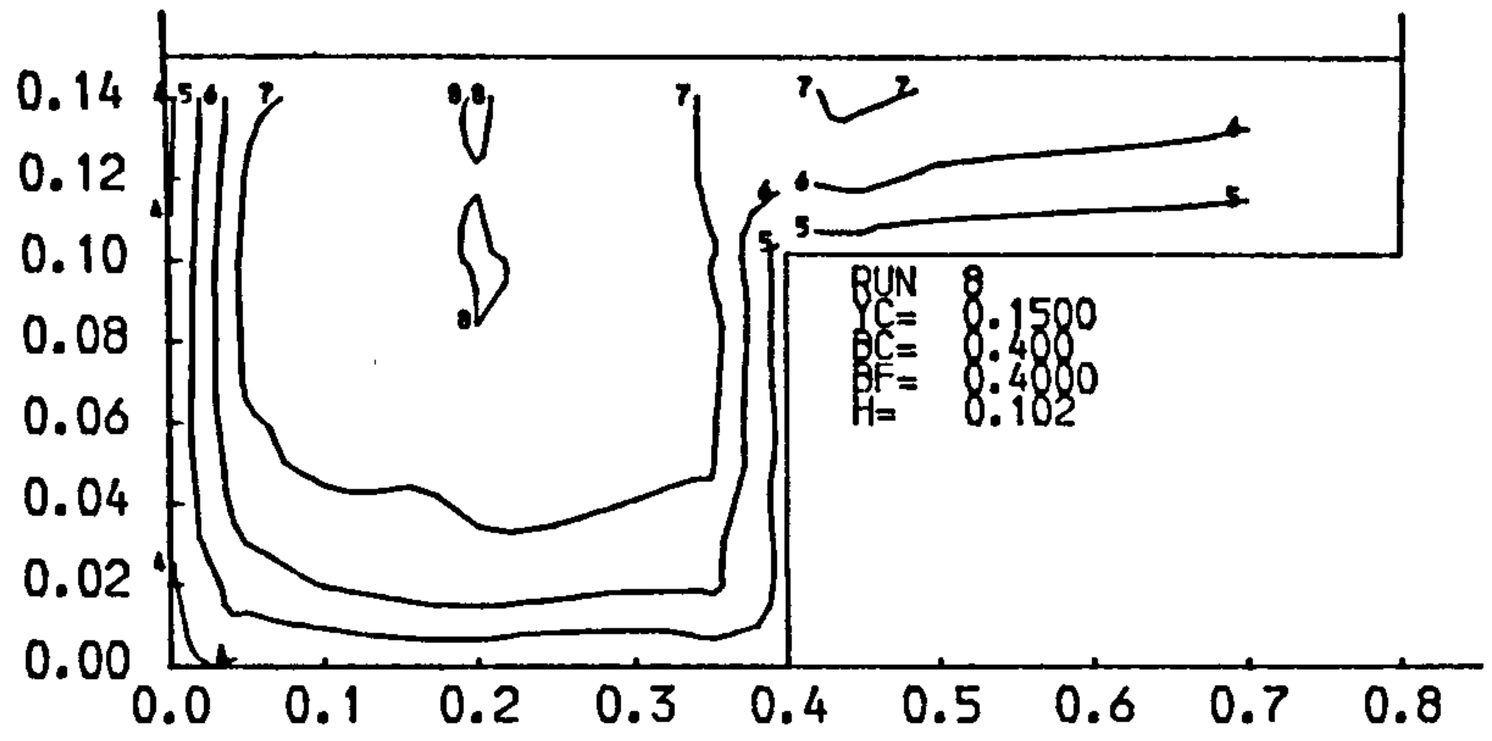

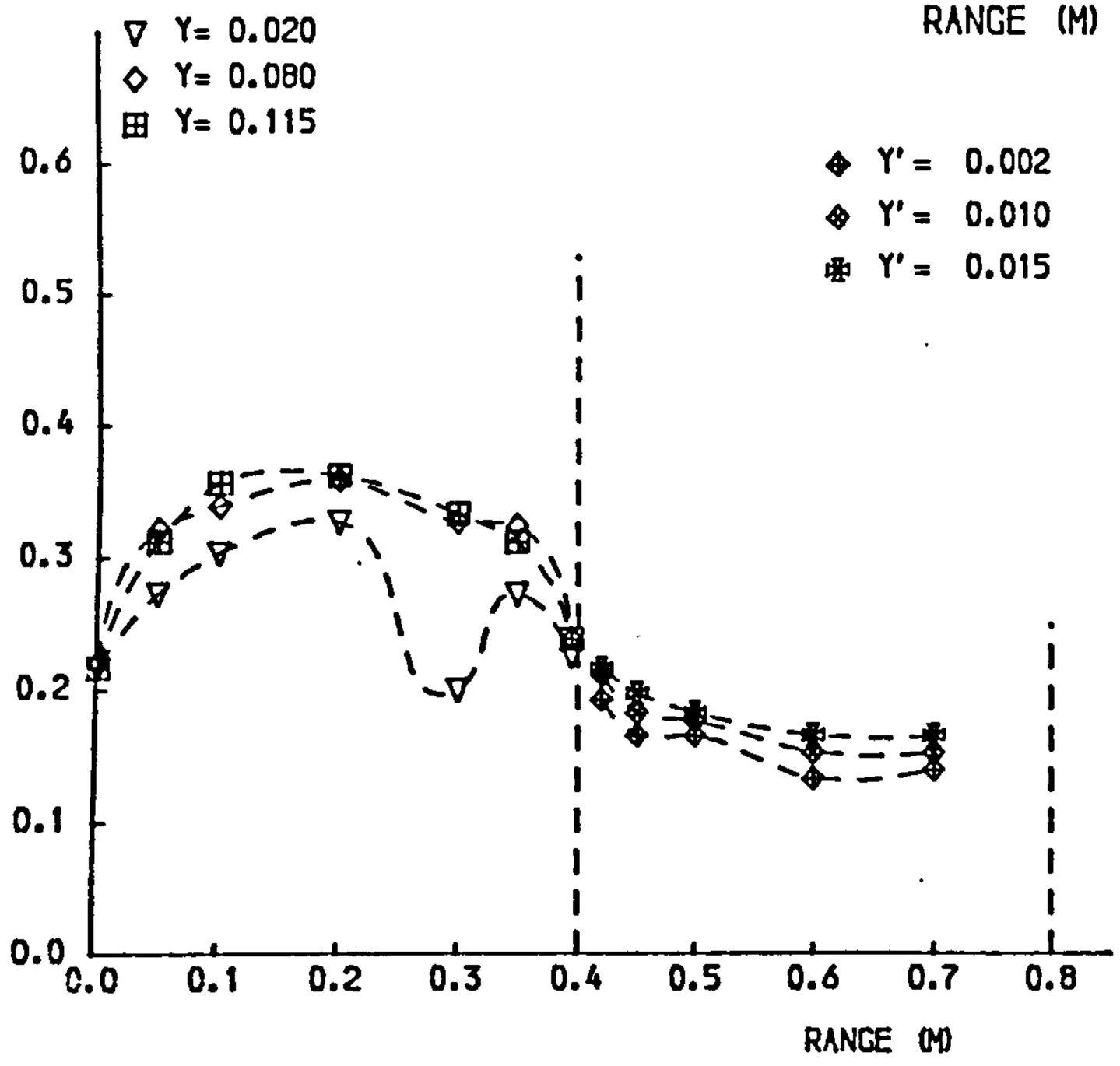

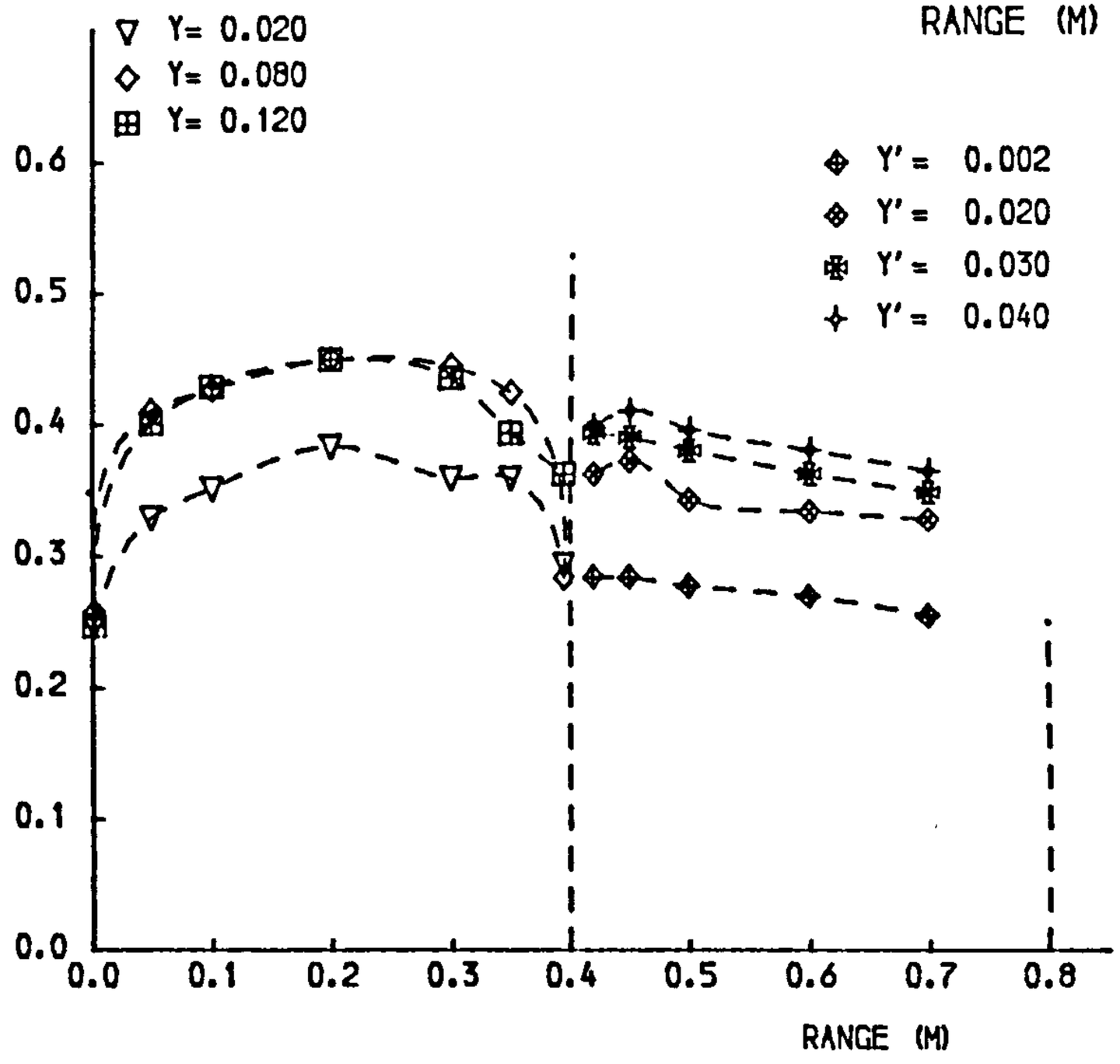

Fig 4·7 Isovels and lateral velocity profiles.

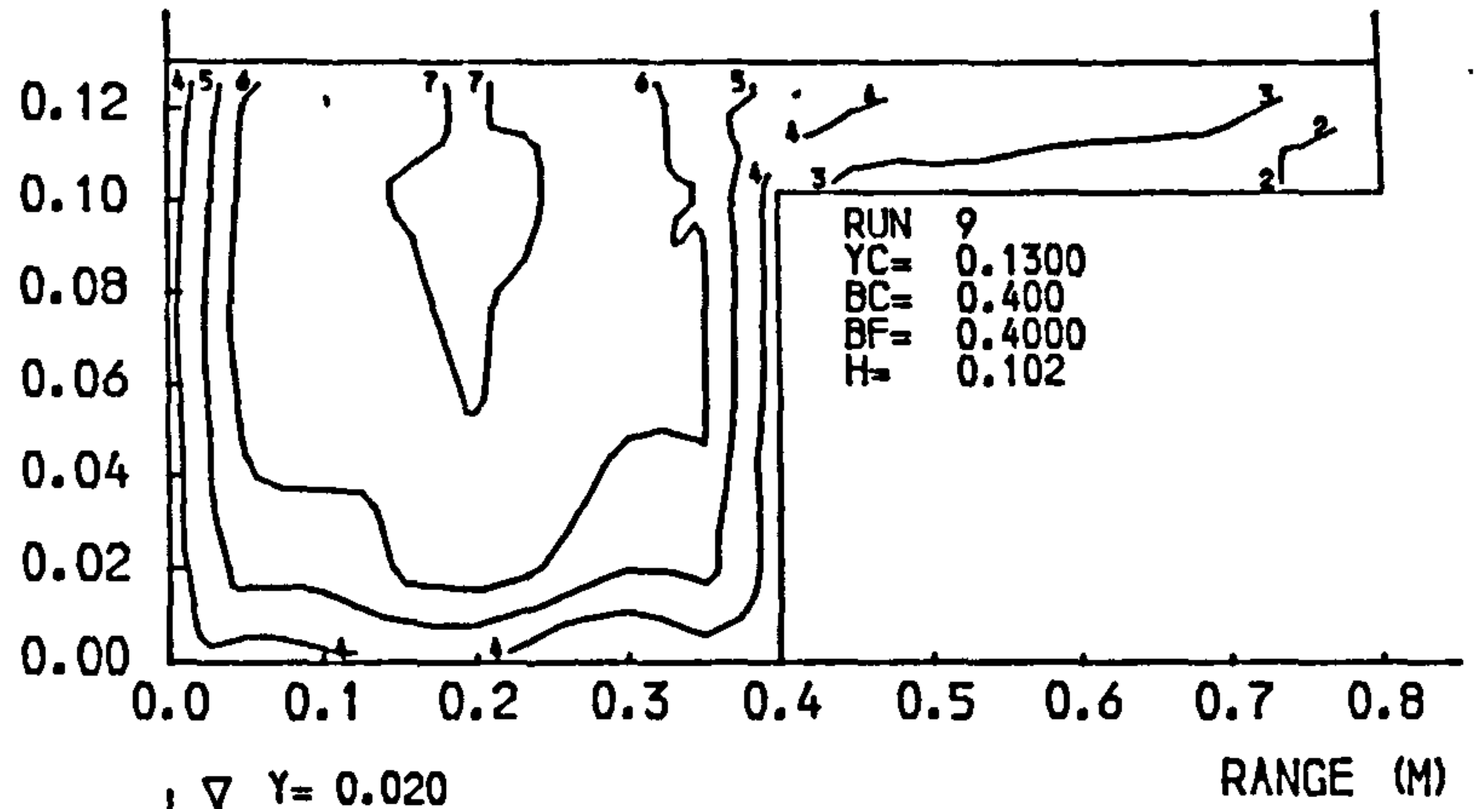

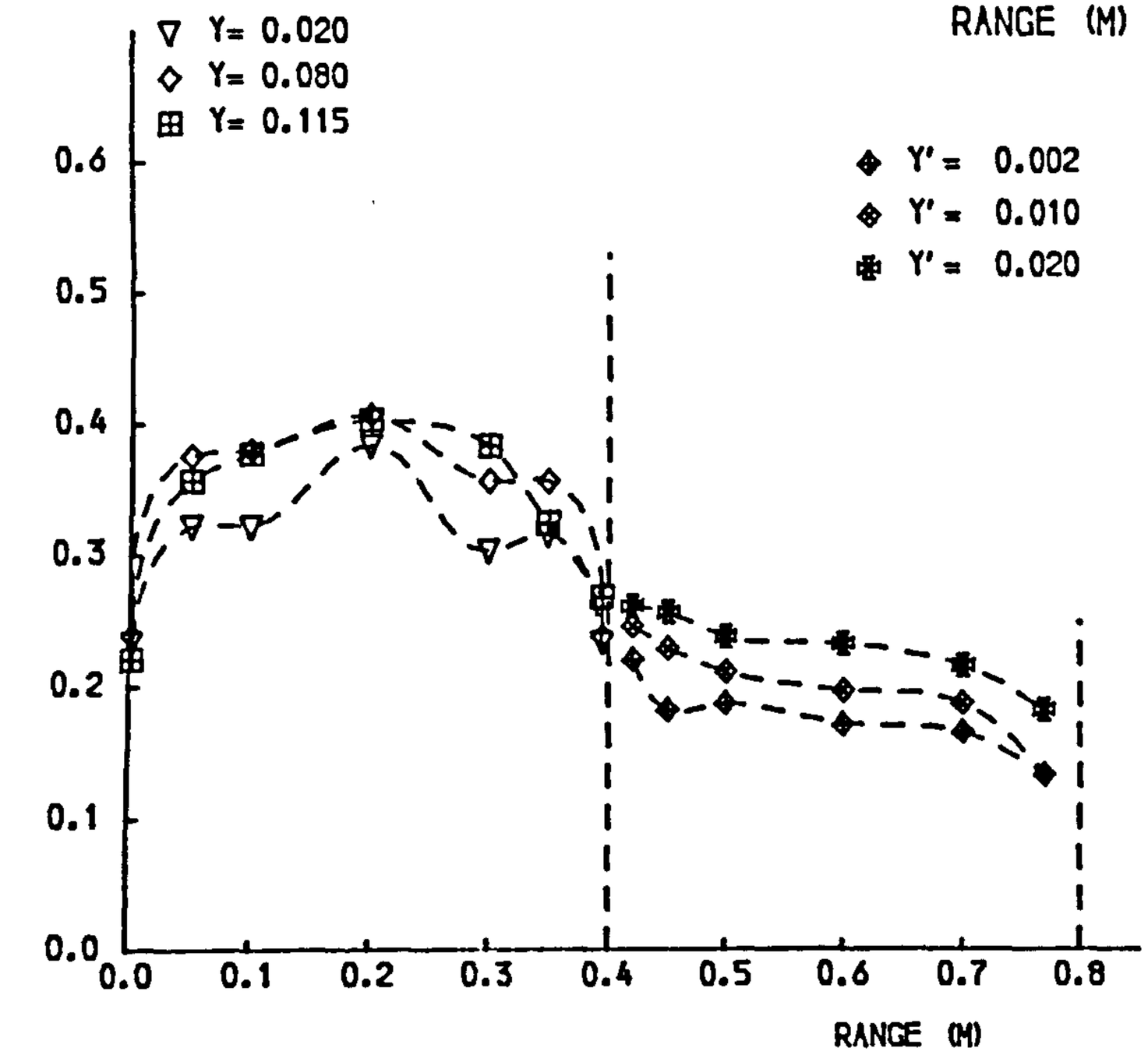

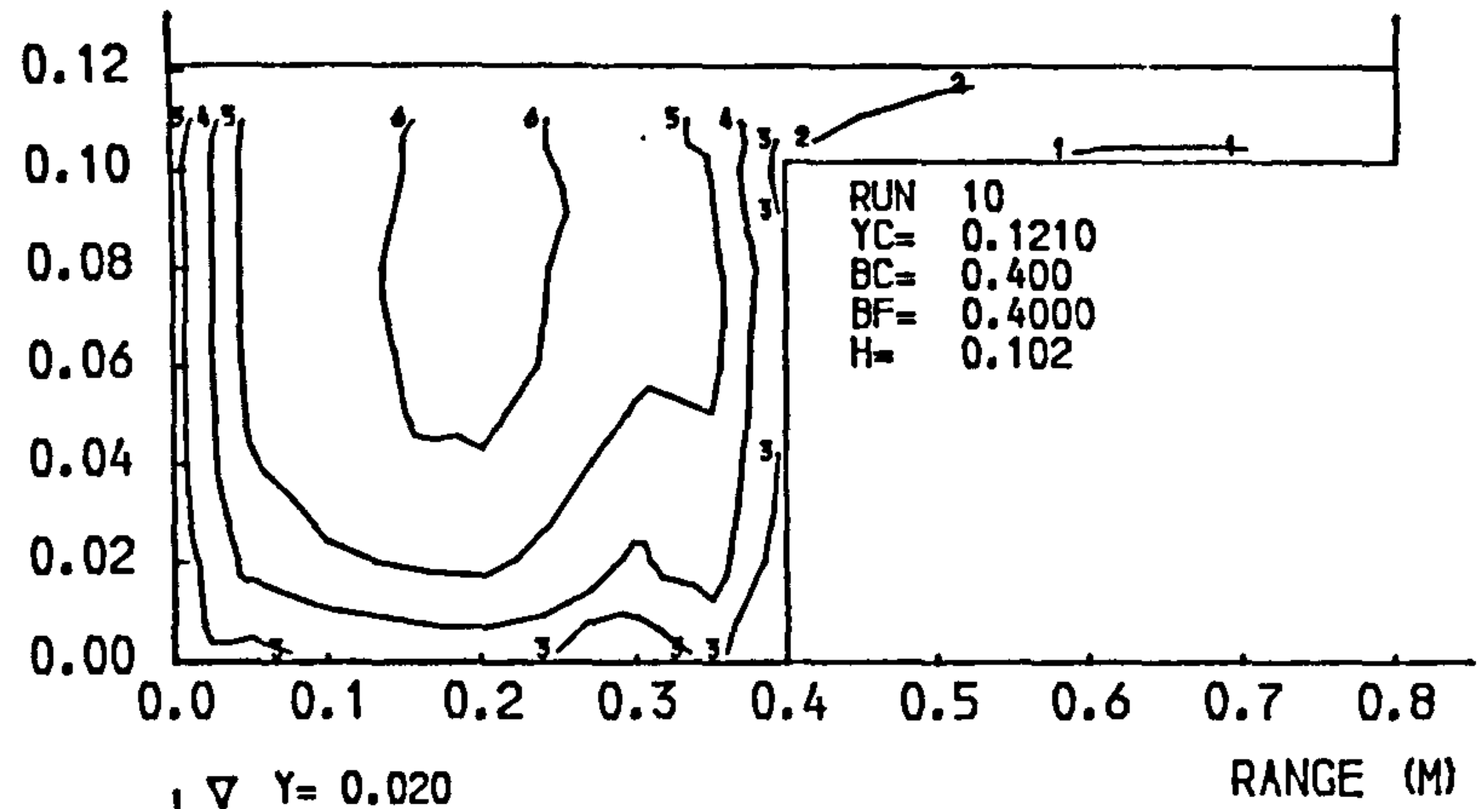

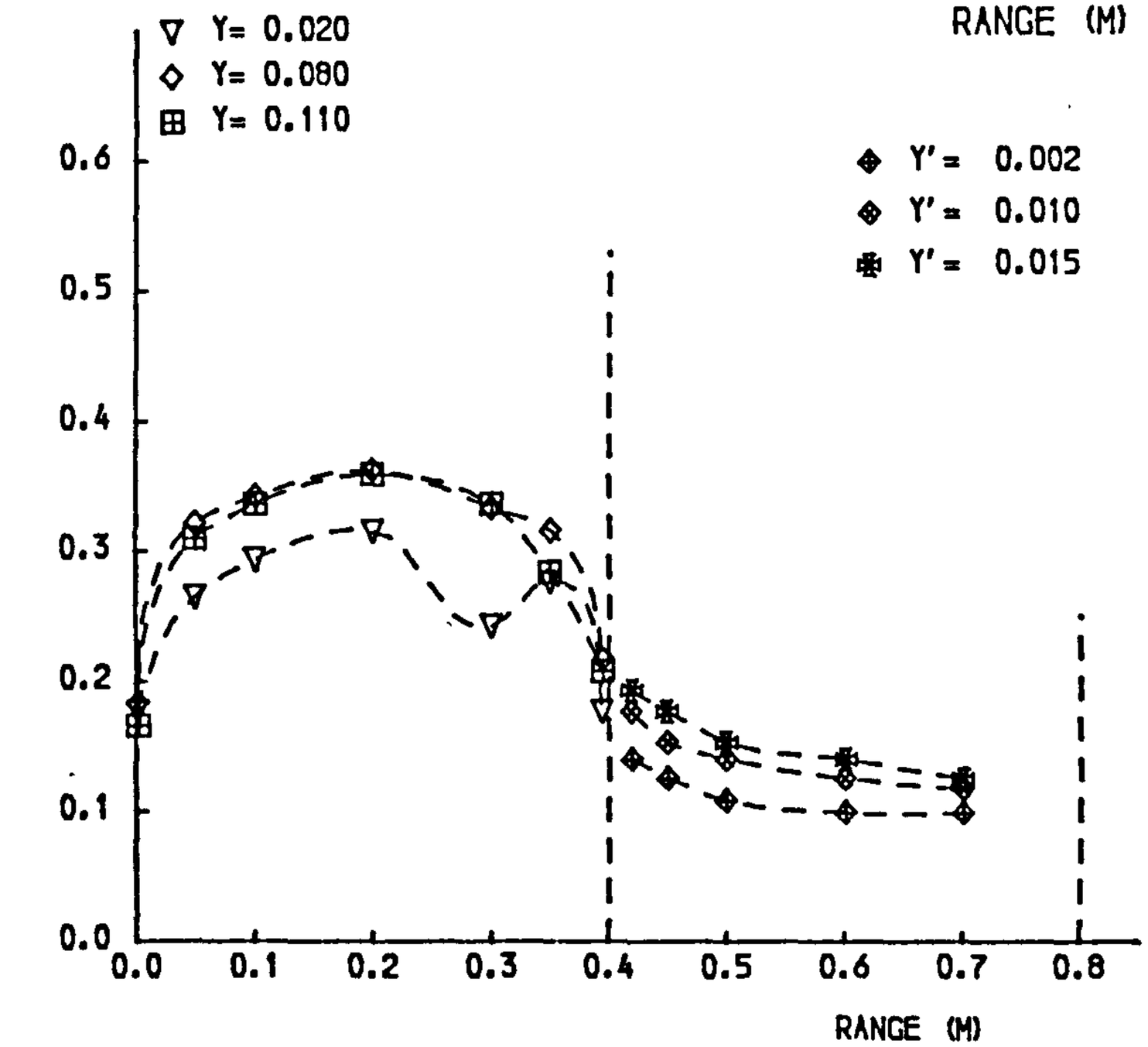

Fig 4·7 Isovels and lateral velocity profiles.

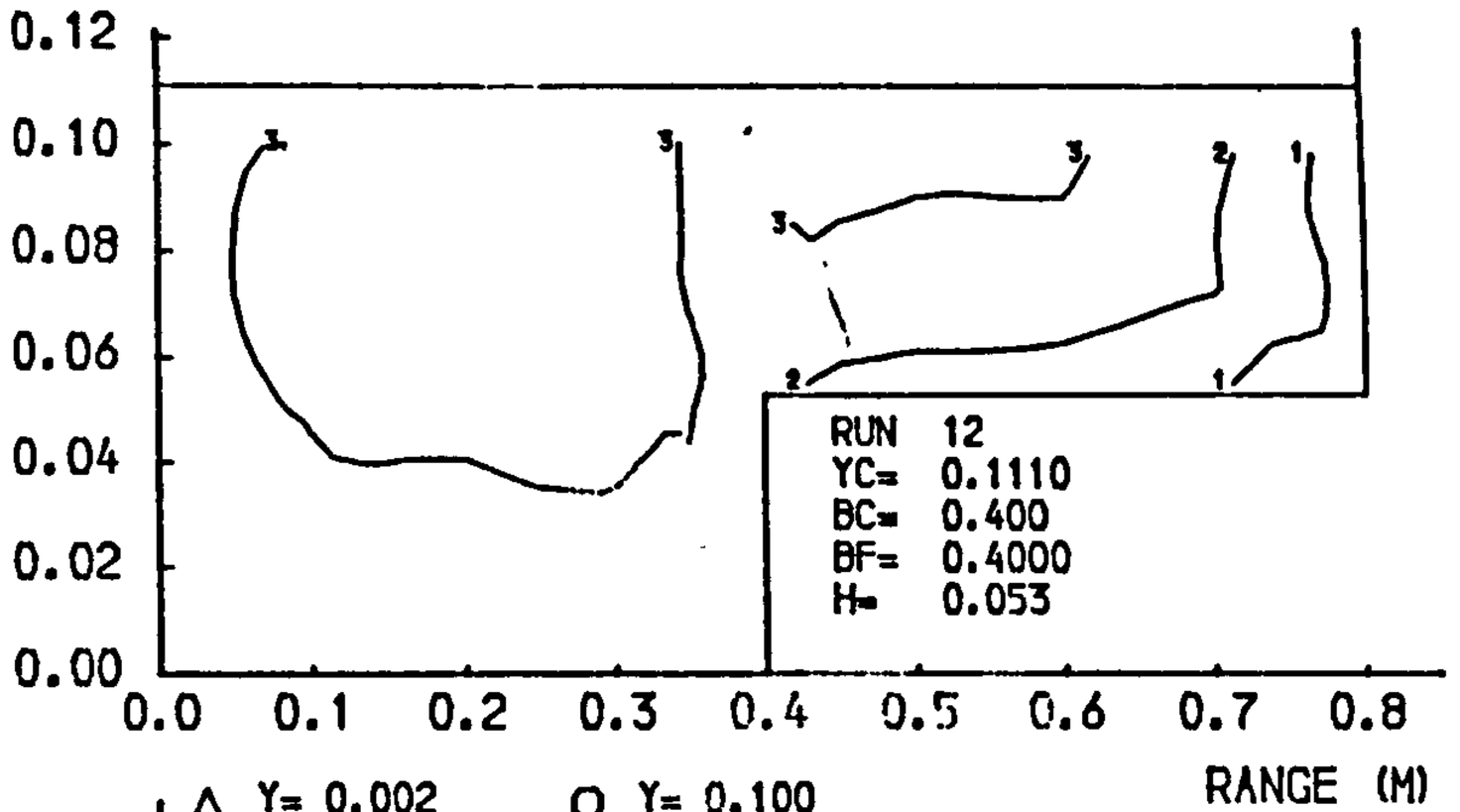

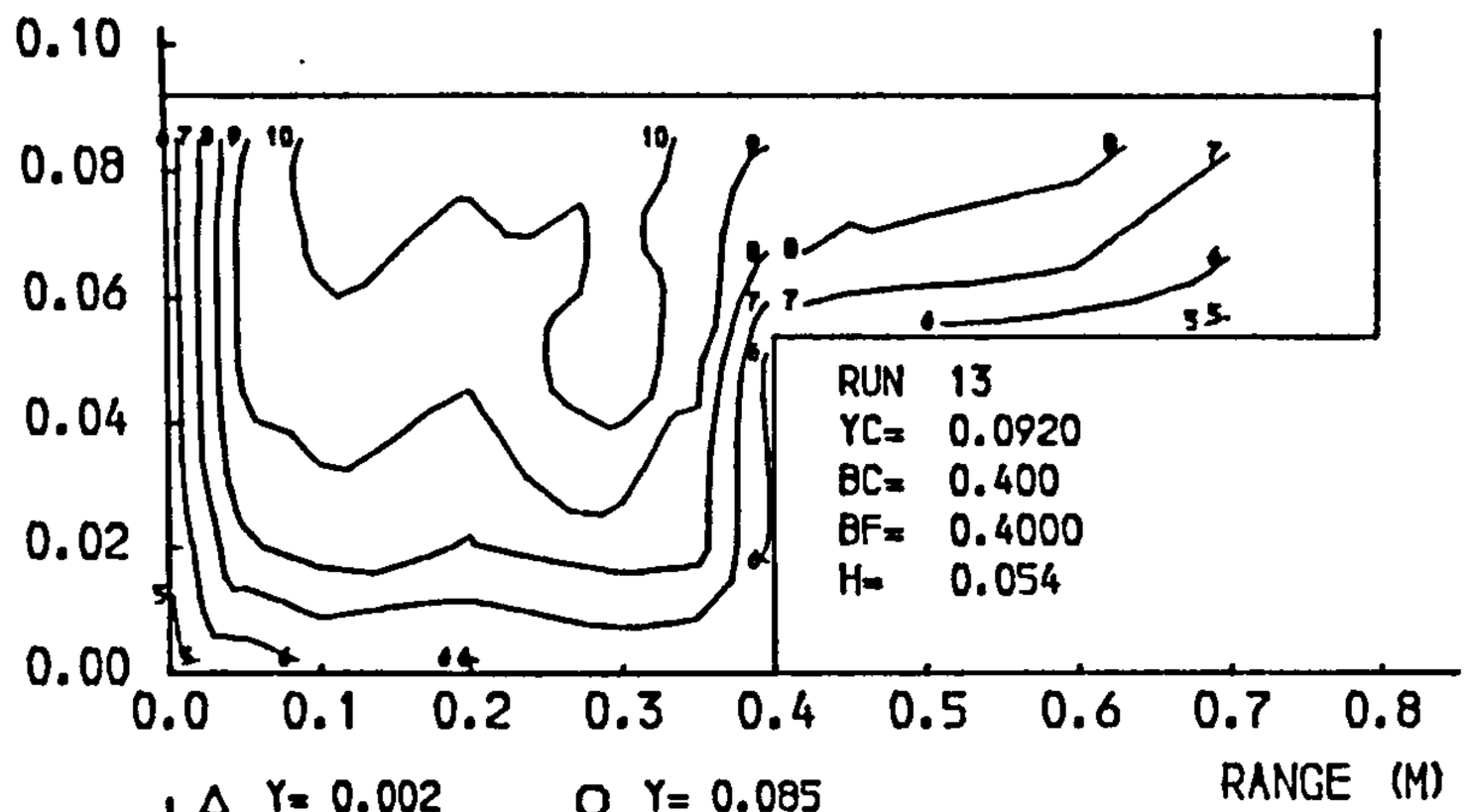

Fig 4·7 Isovels and lateral velocity profiles.

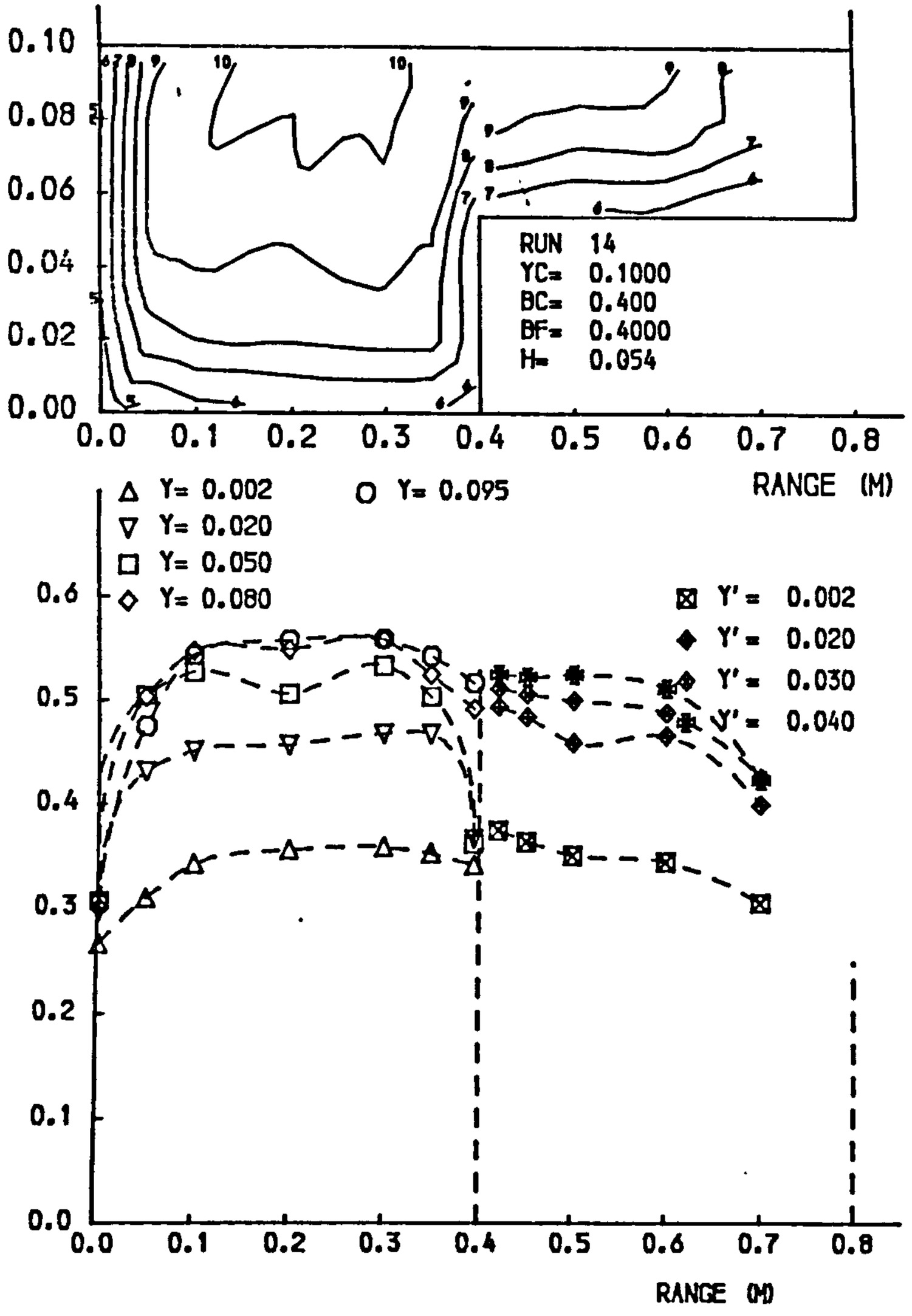

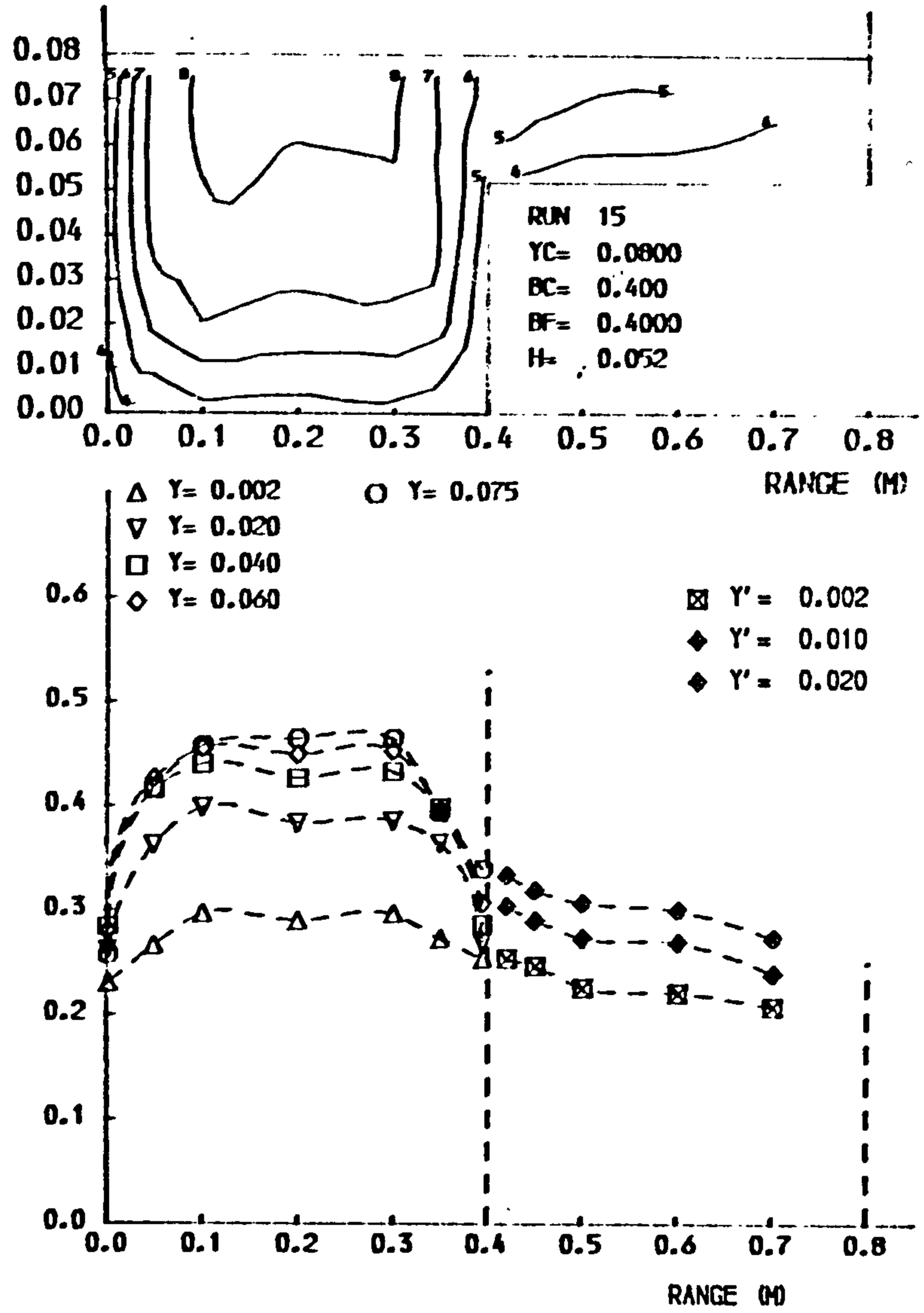

Fig 4·7 Isovels and lateral velocity profiles.

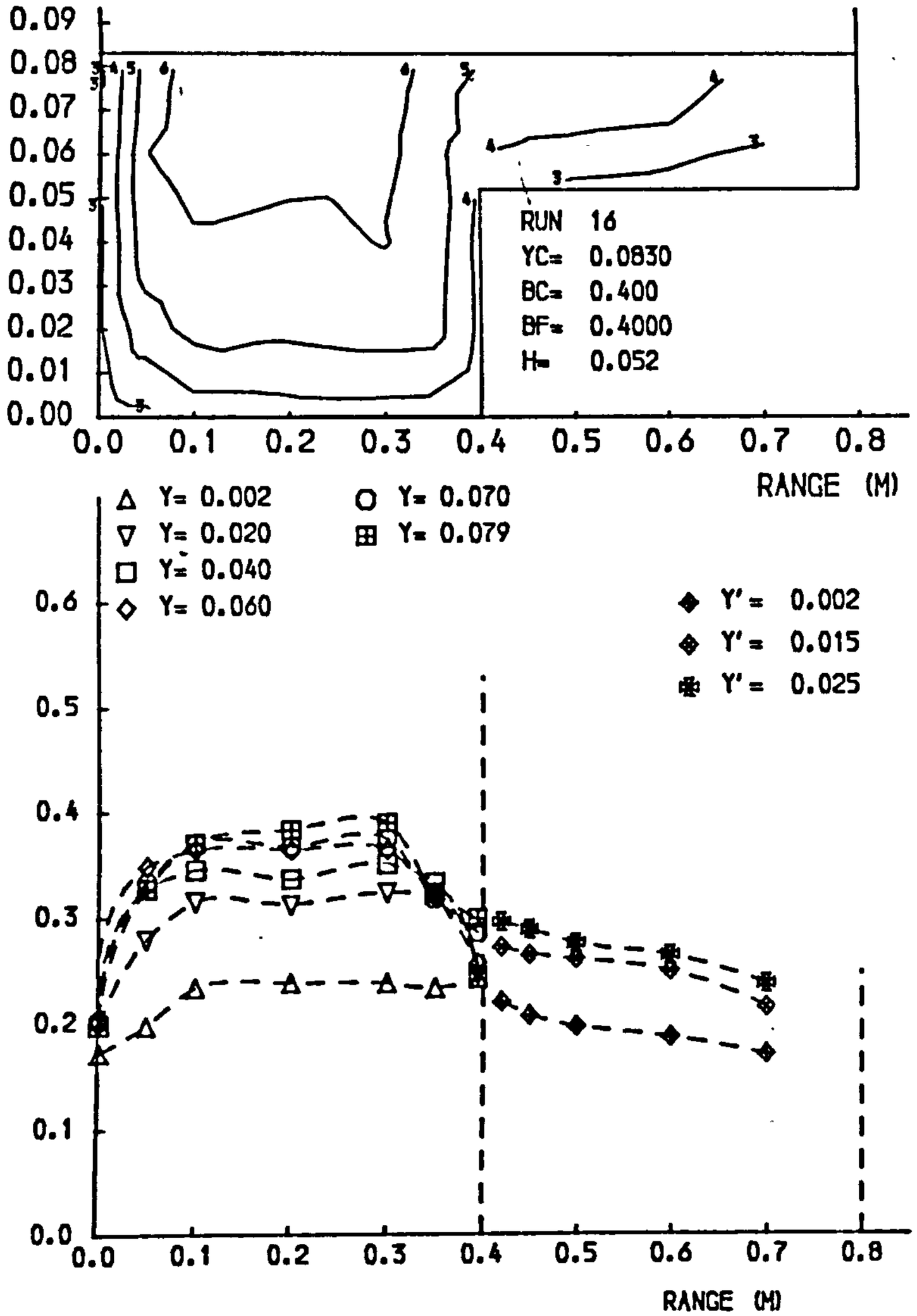

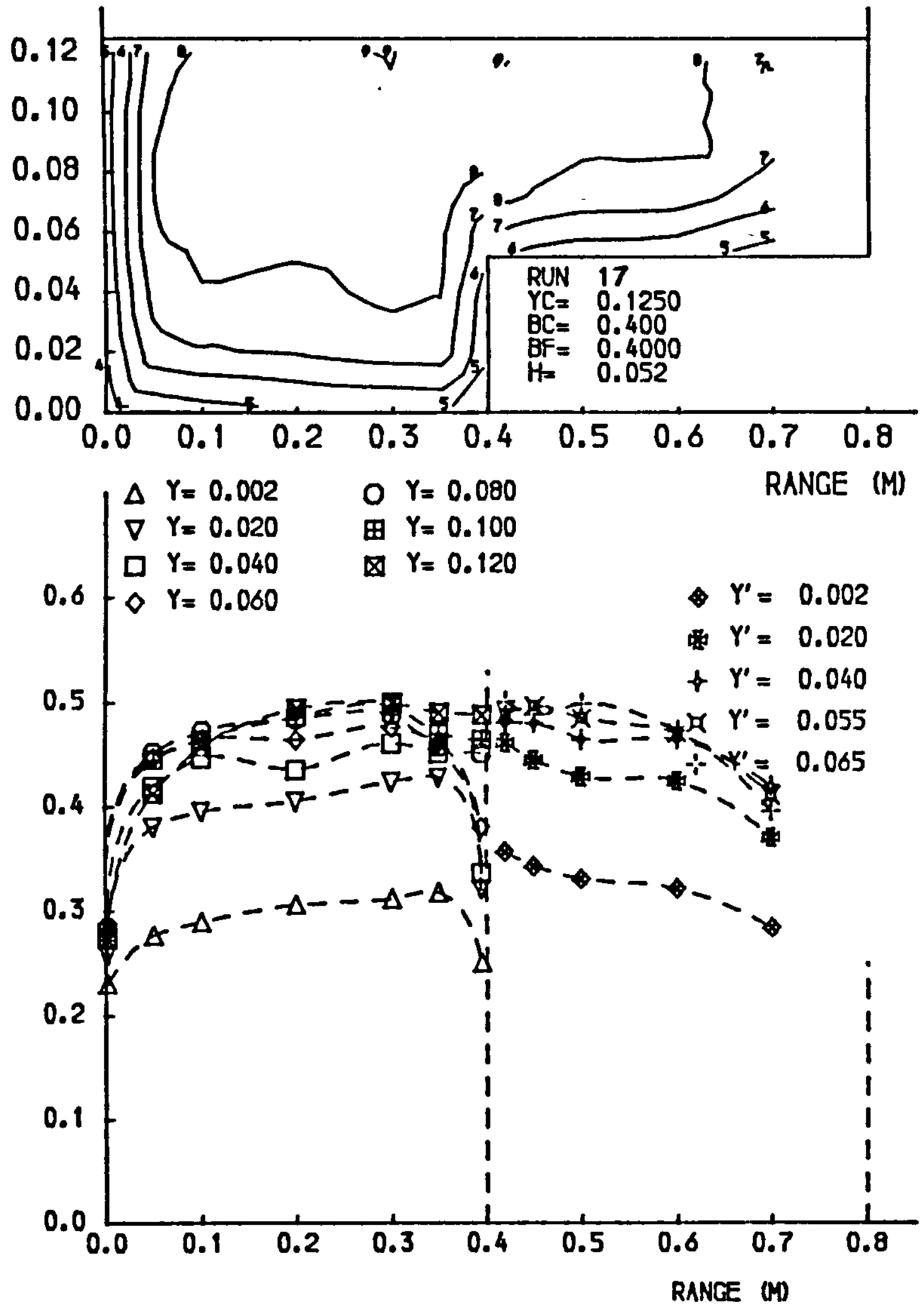

Fig 4·7 Isovels and lateral velocity profiles.

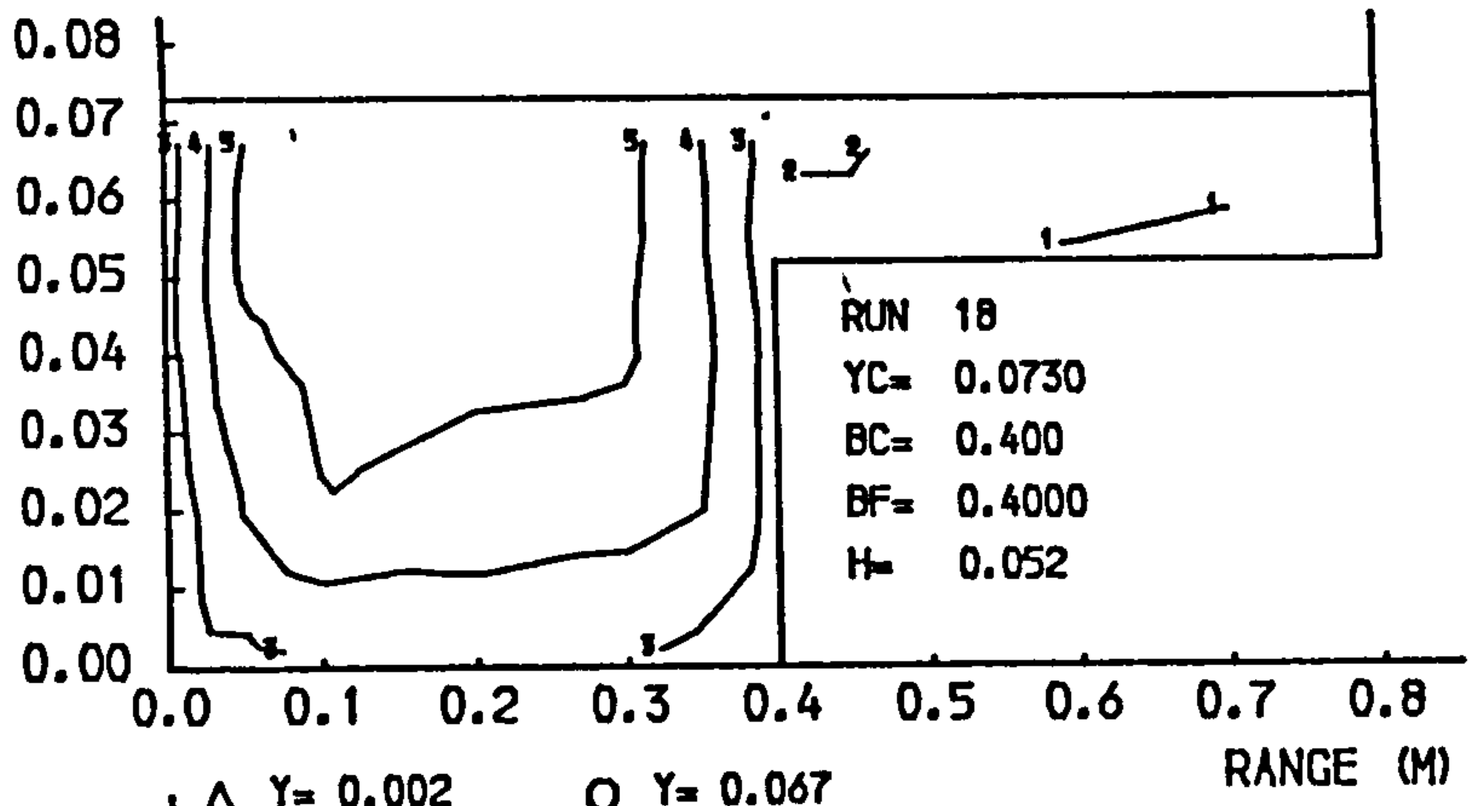

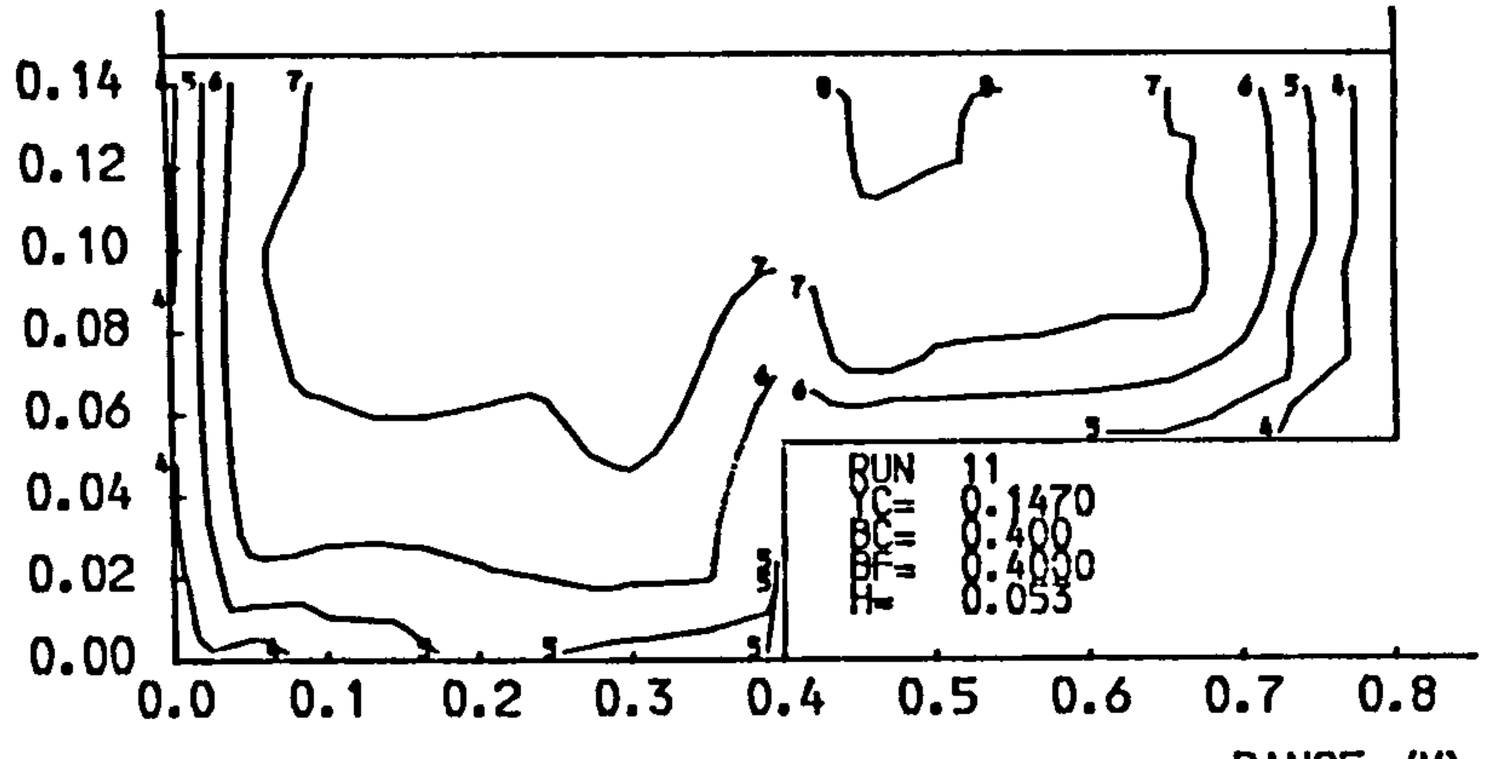

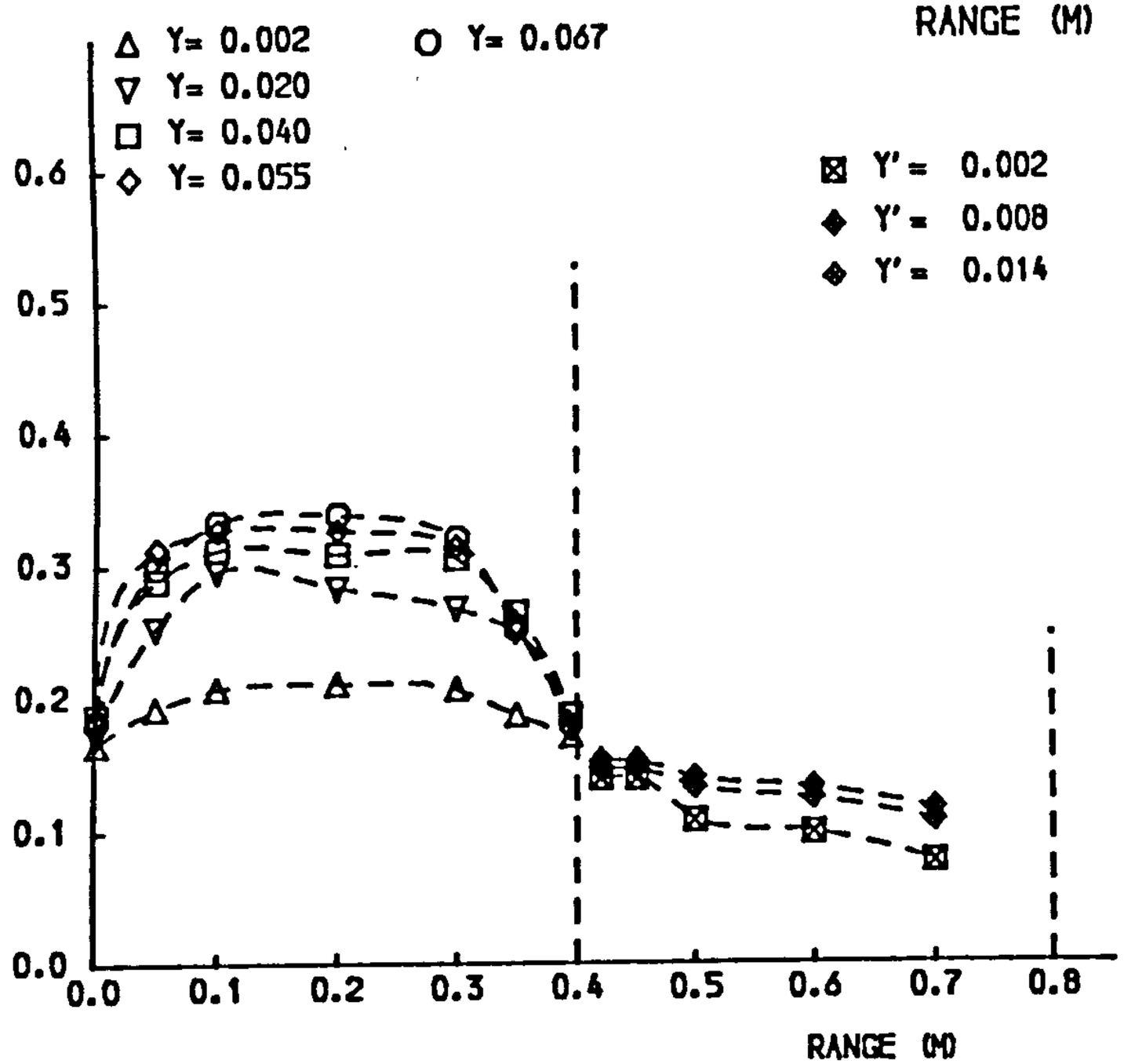

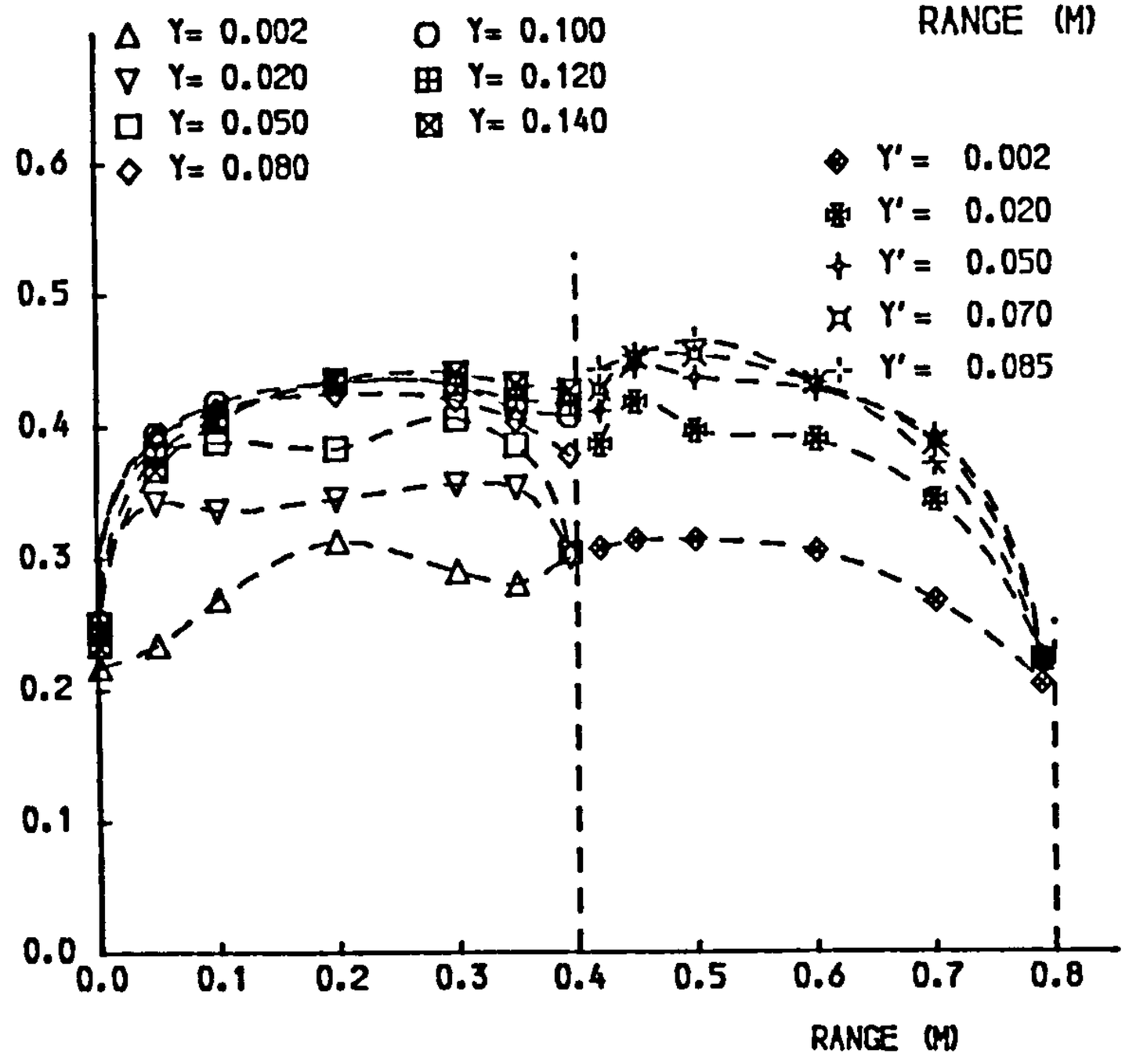

Fig 4·7 Isovels and lateral velocity profiles.

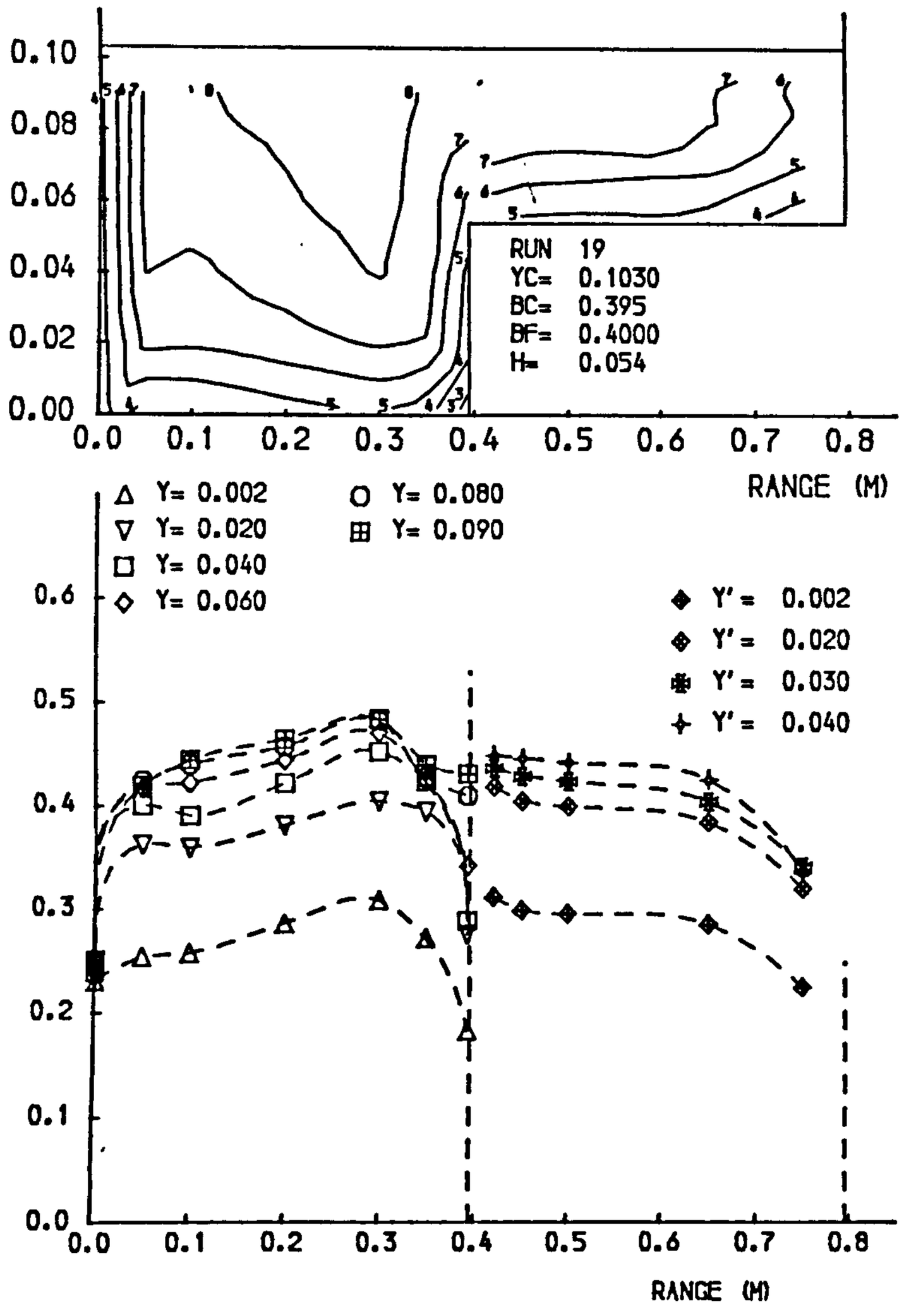

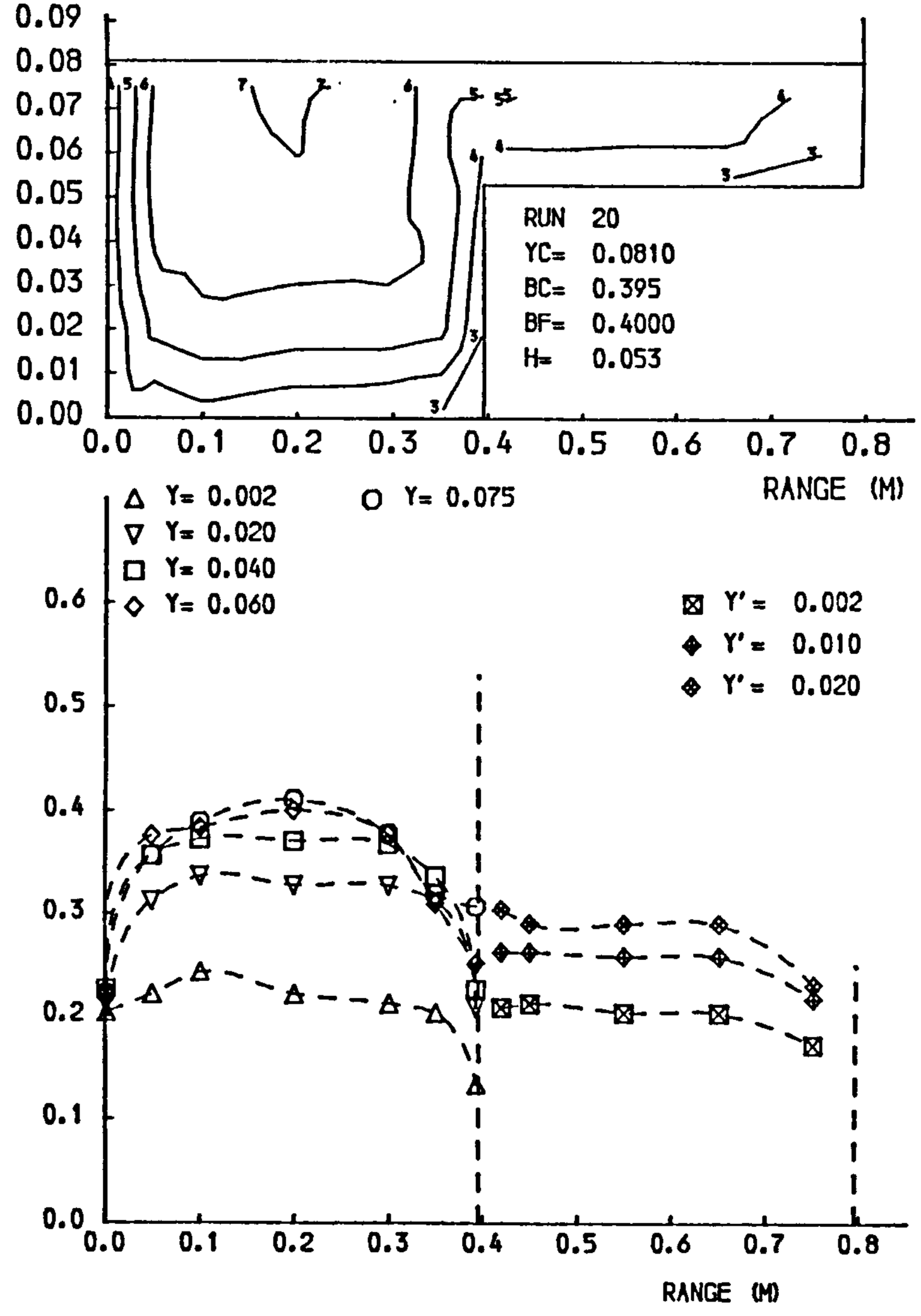

Fig 4·7 Isovels and lateral velocity profiles.

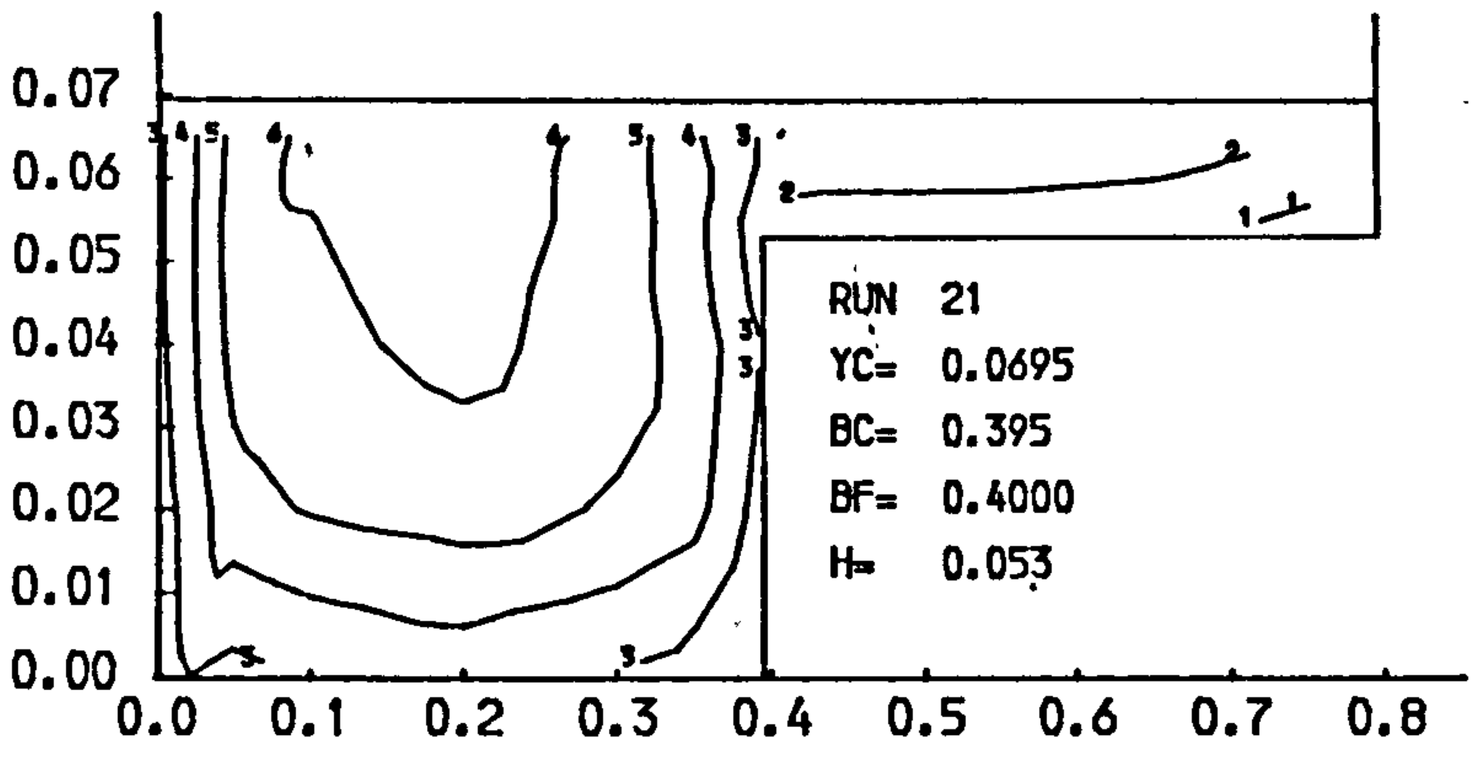

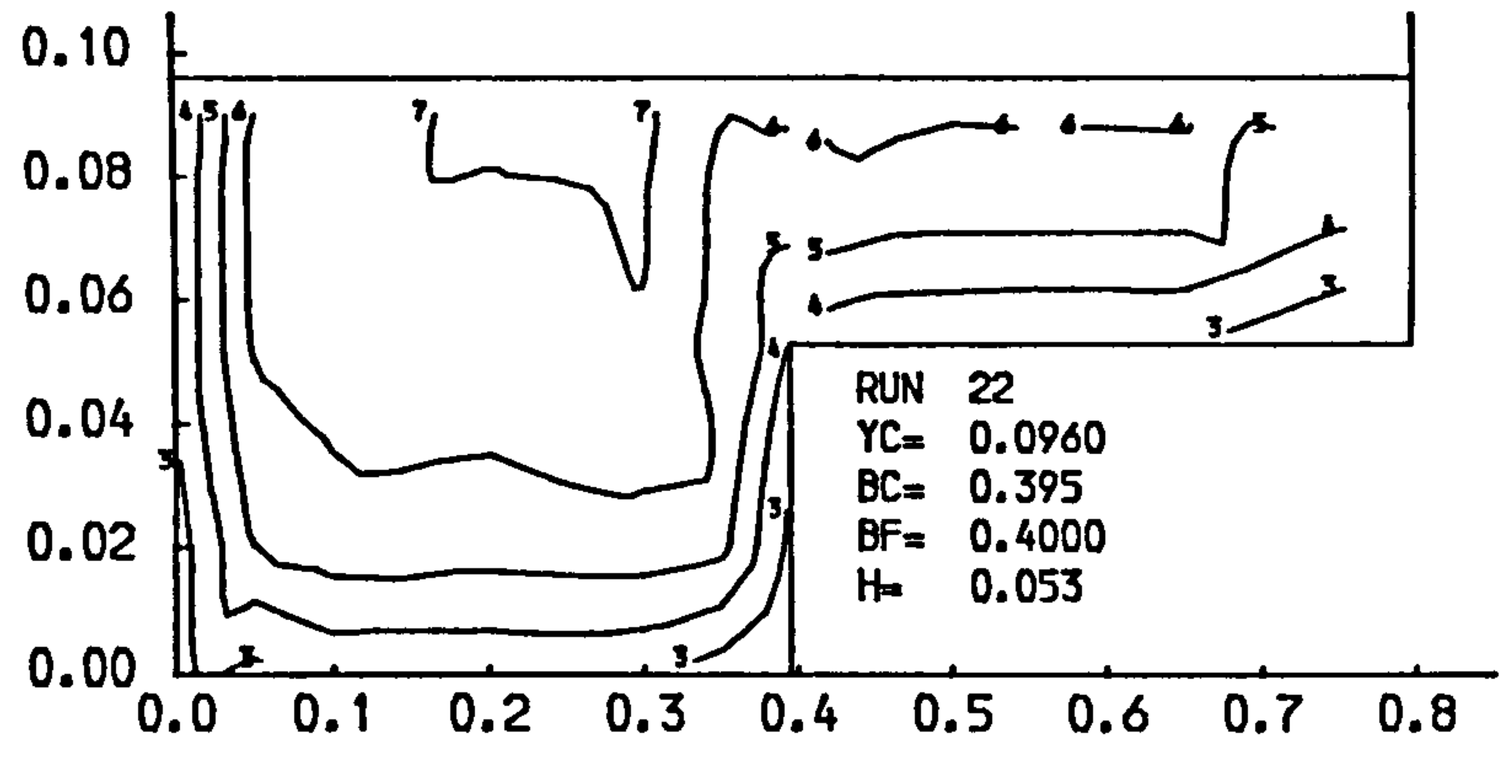

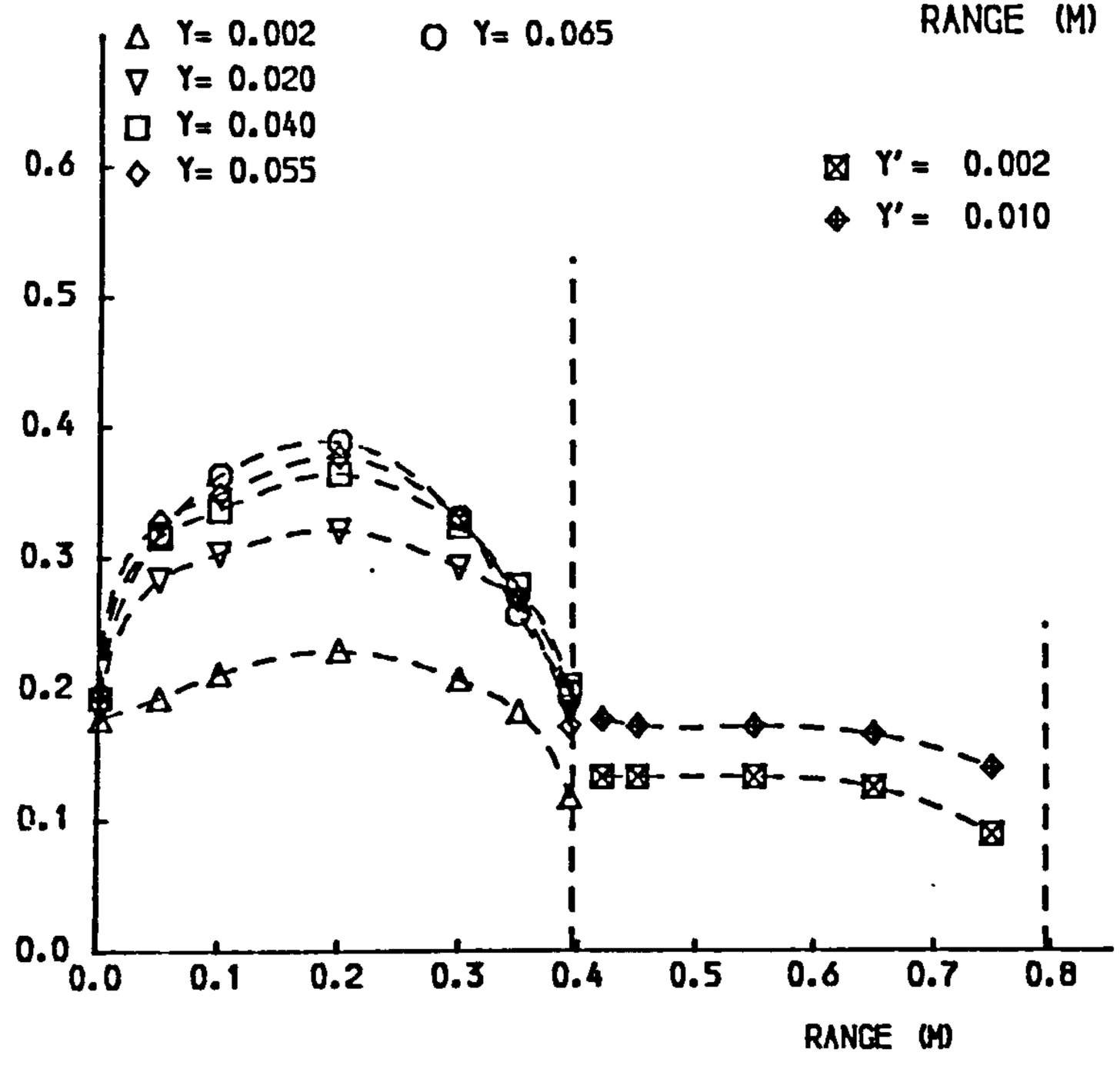

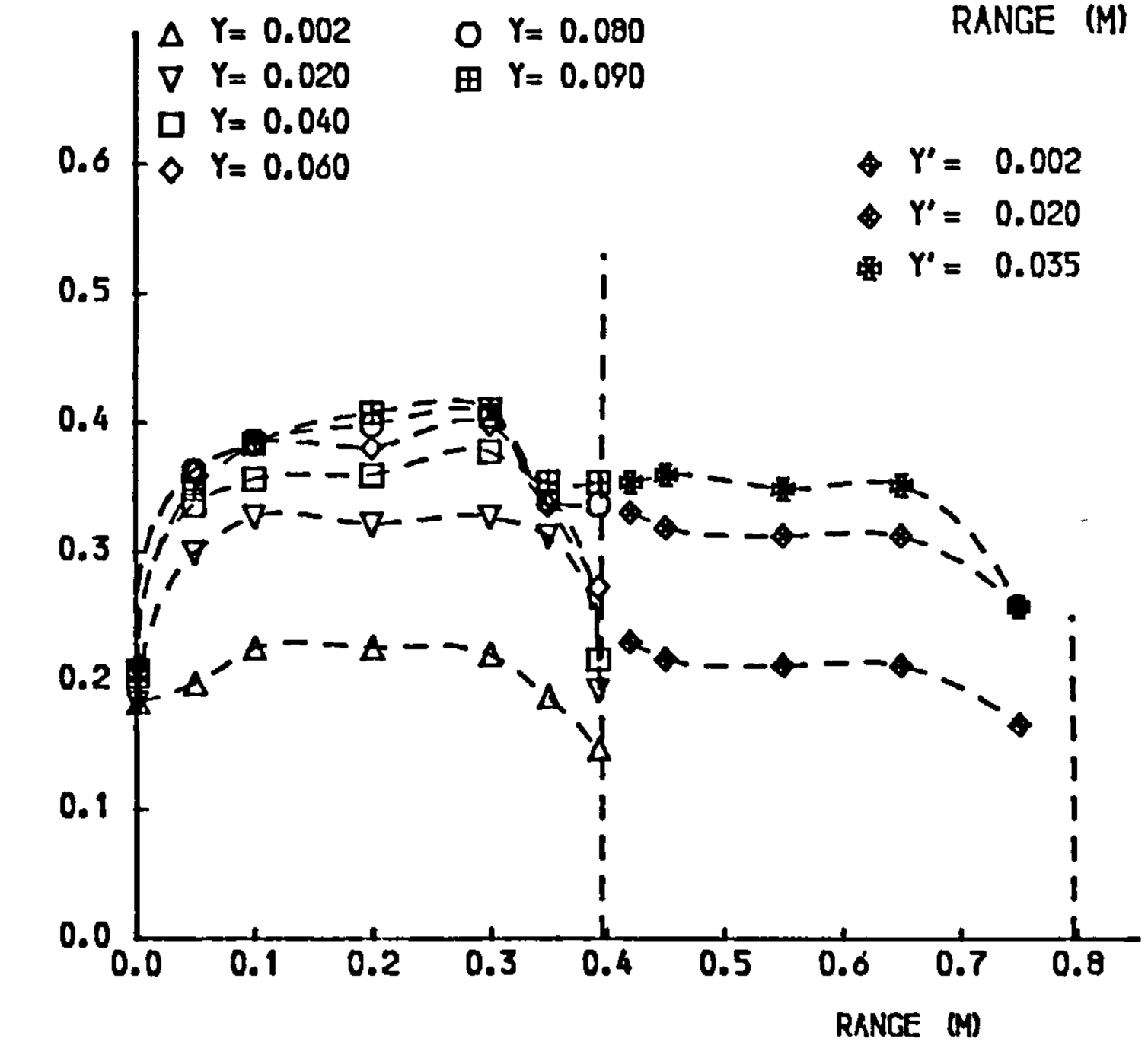

Fig 4·7 Isovels and lateral velocity profiles.

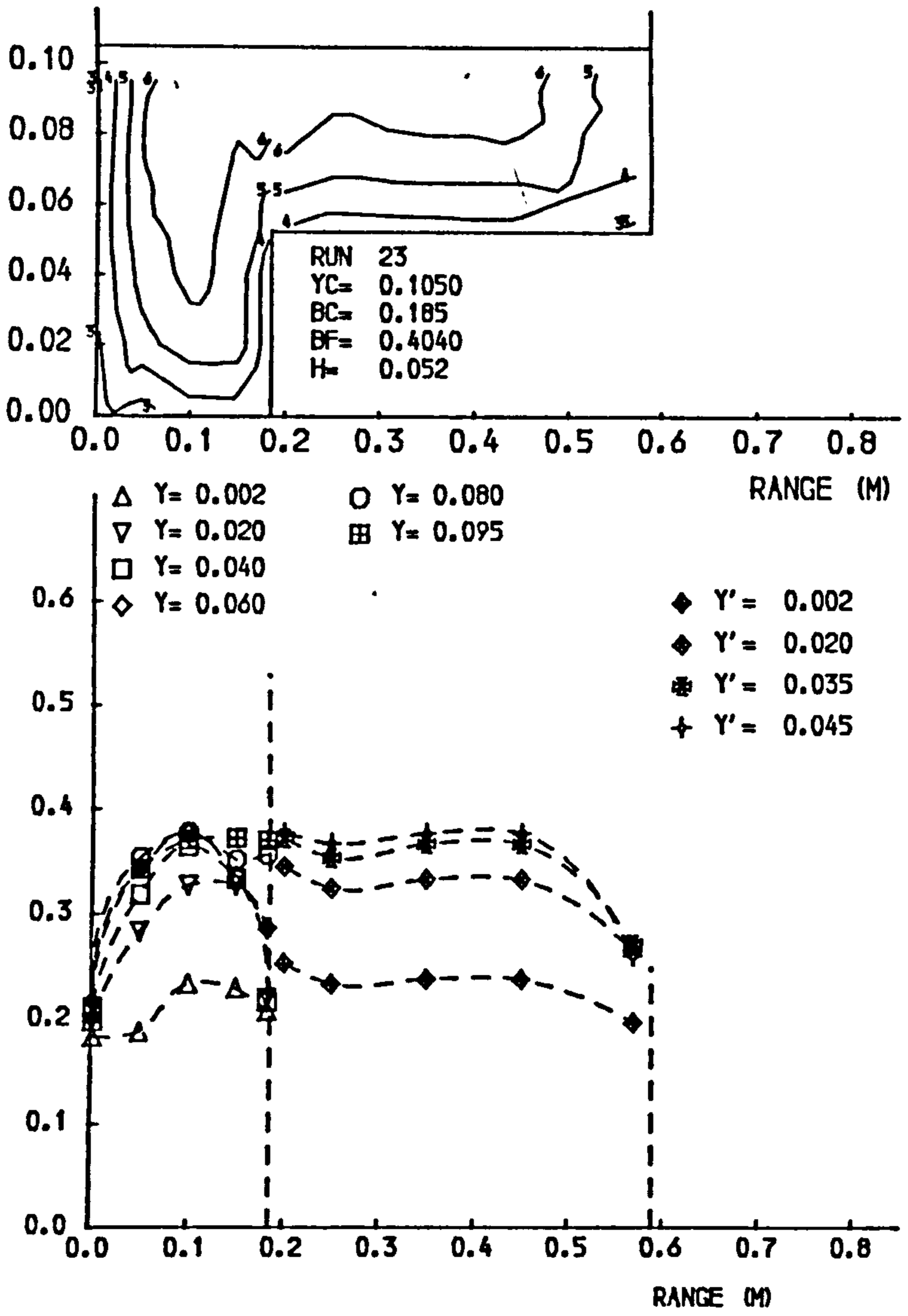

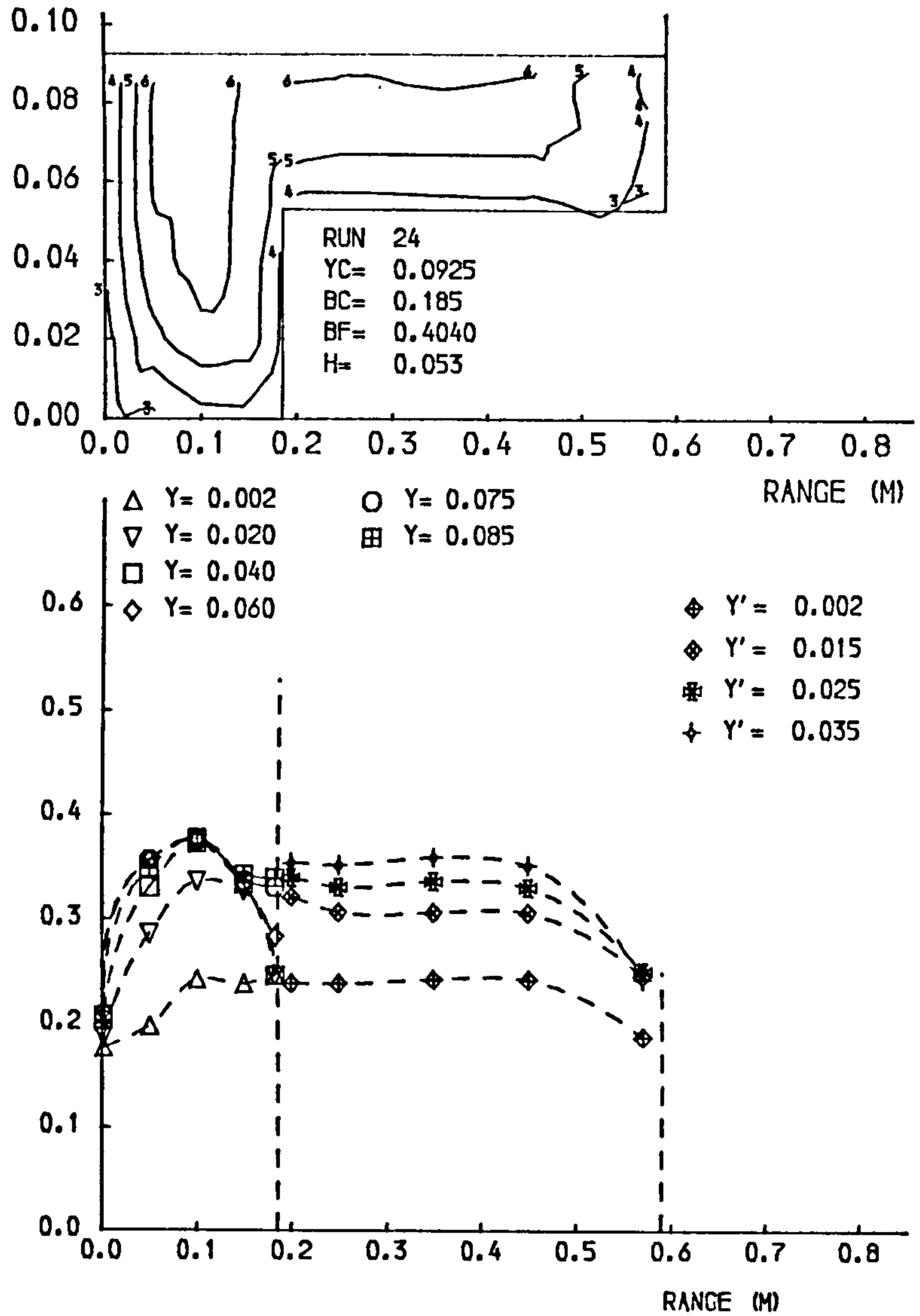

Fig 4·7 Isovels and lateral velocity profiles.

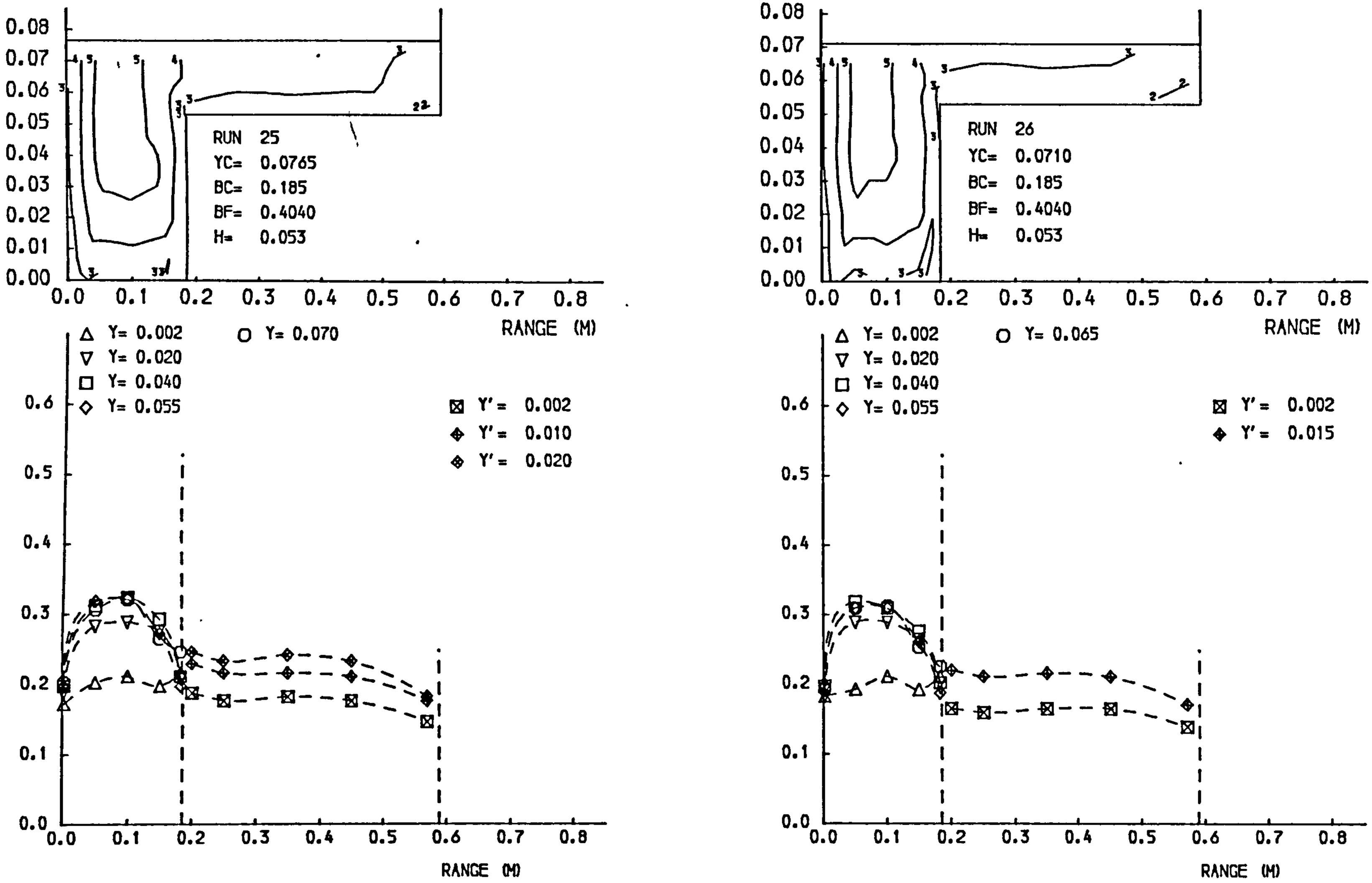

Fig 4·7 Isovels and lateral velocity profiles.

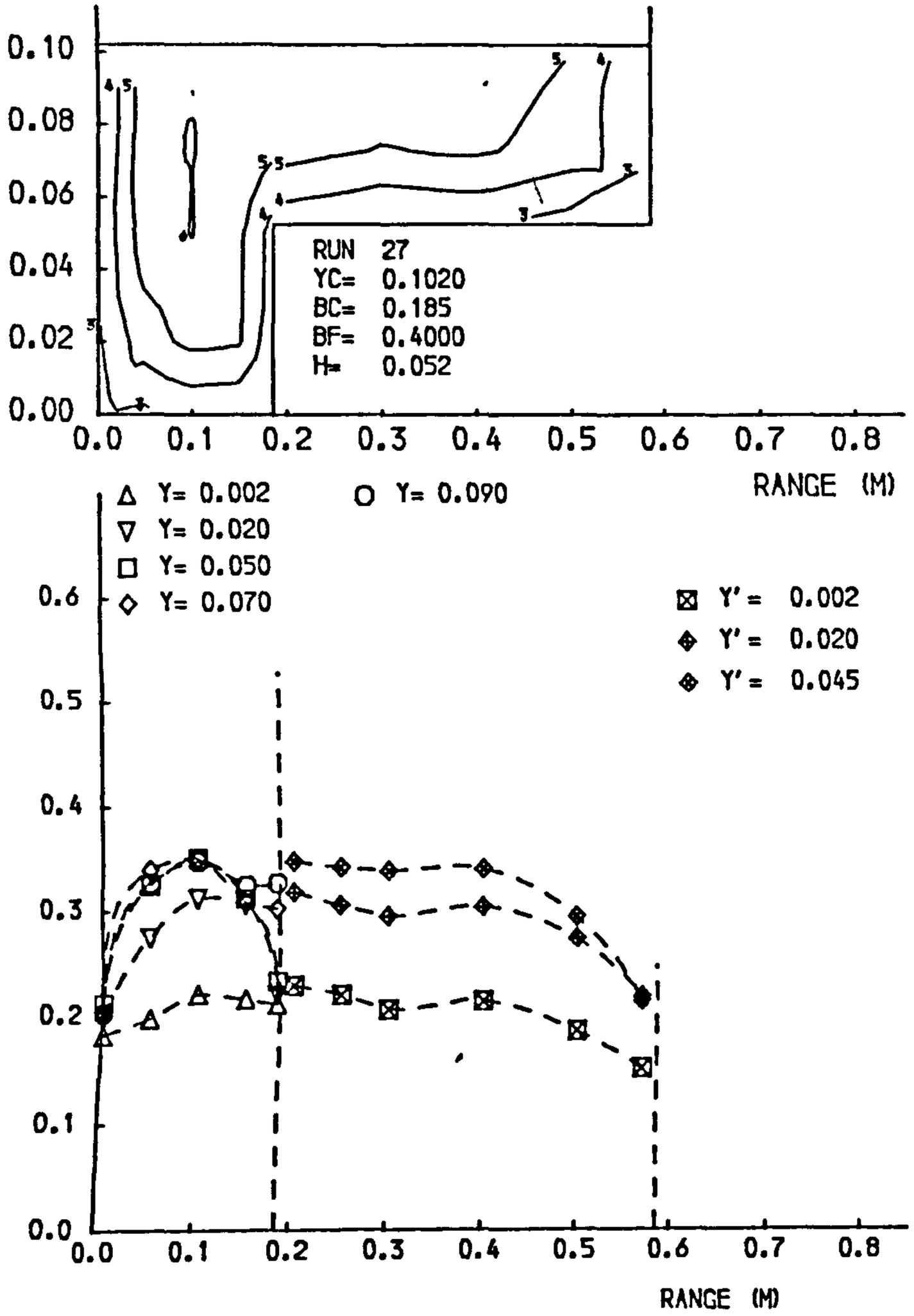

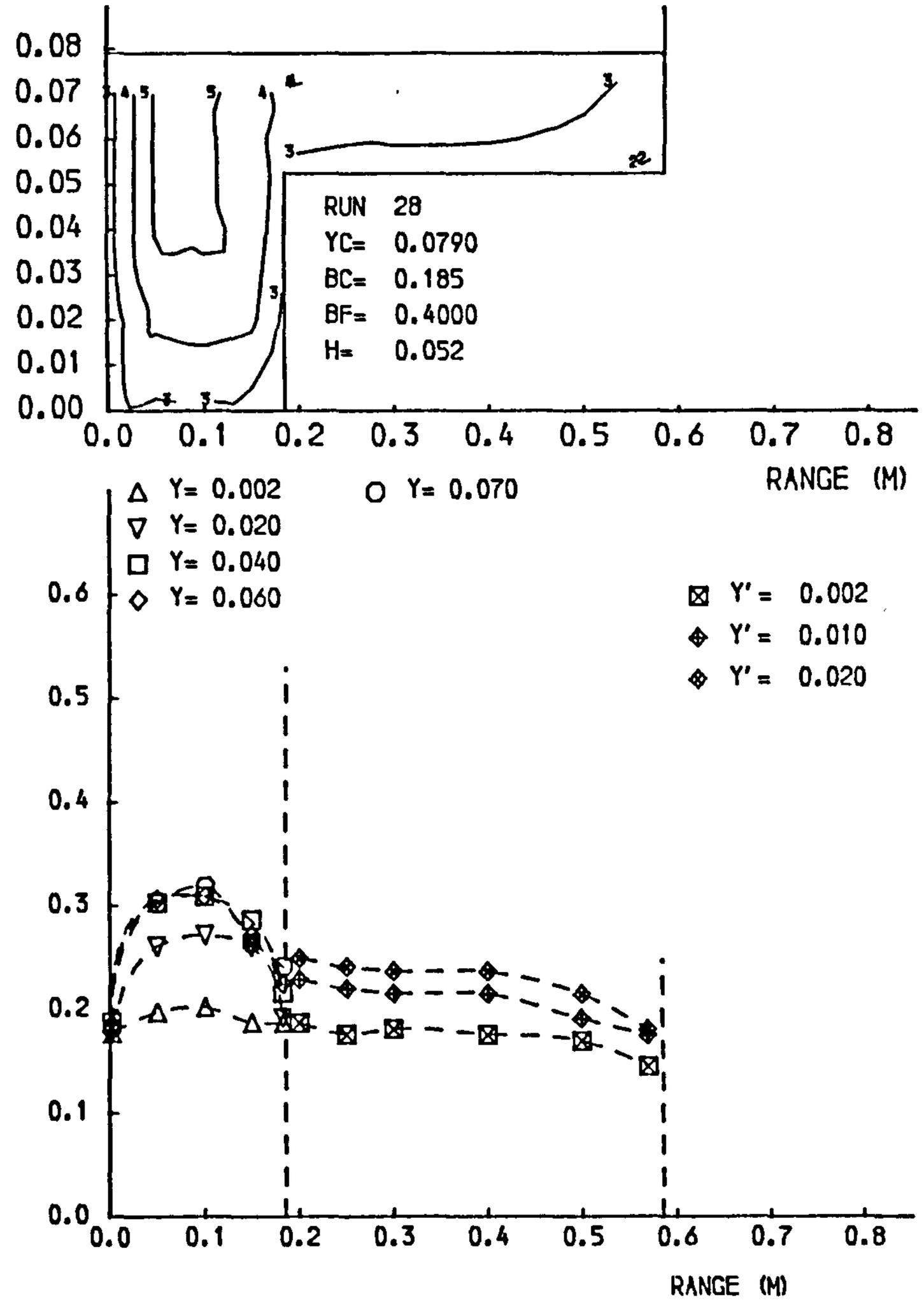

Fig 4·7 Isovels and lateral velocity profiles.

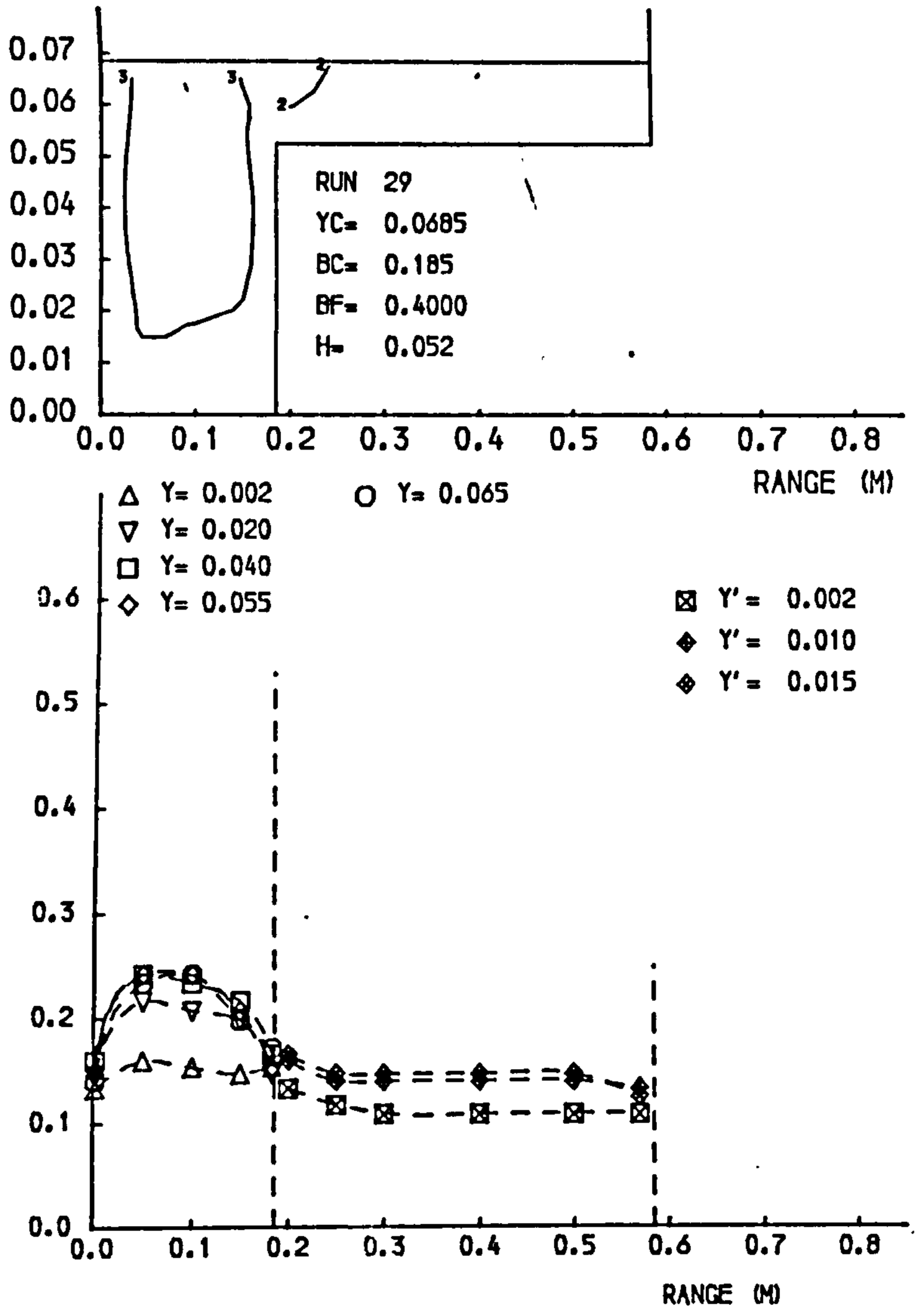

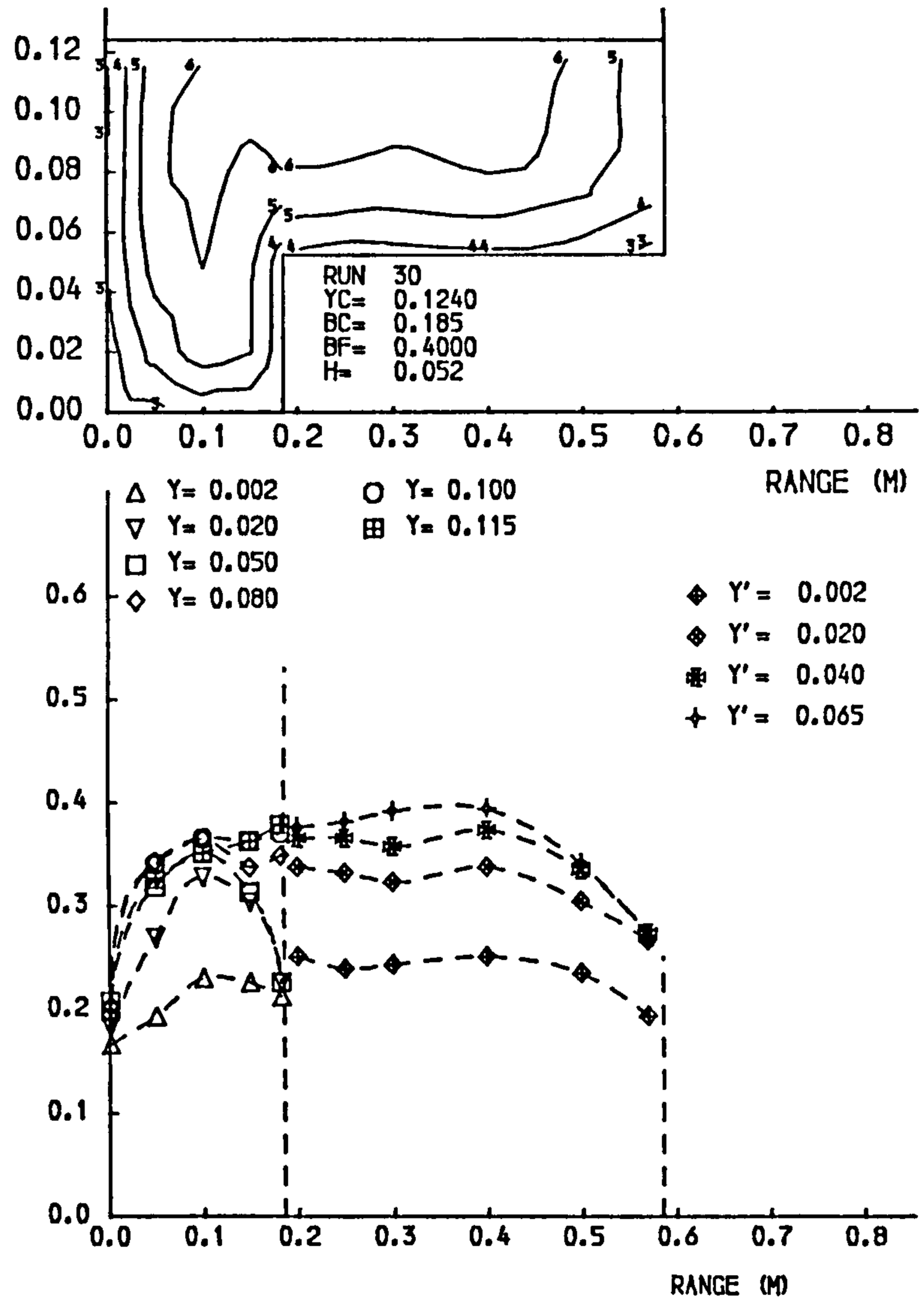

Fig 4·7 Isovels and lateral velocity profiles.

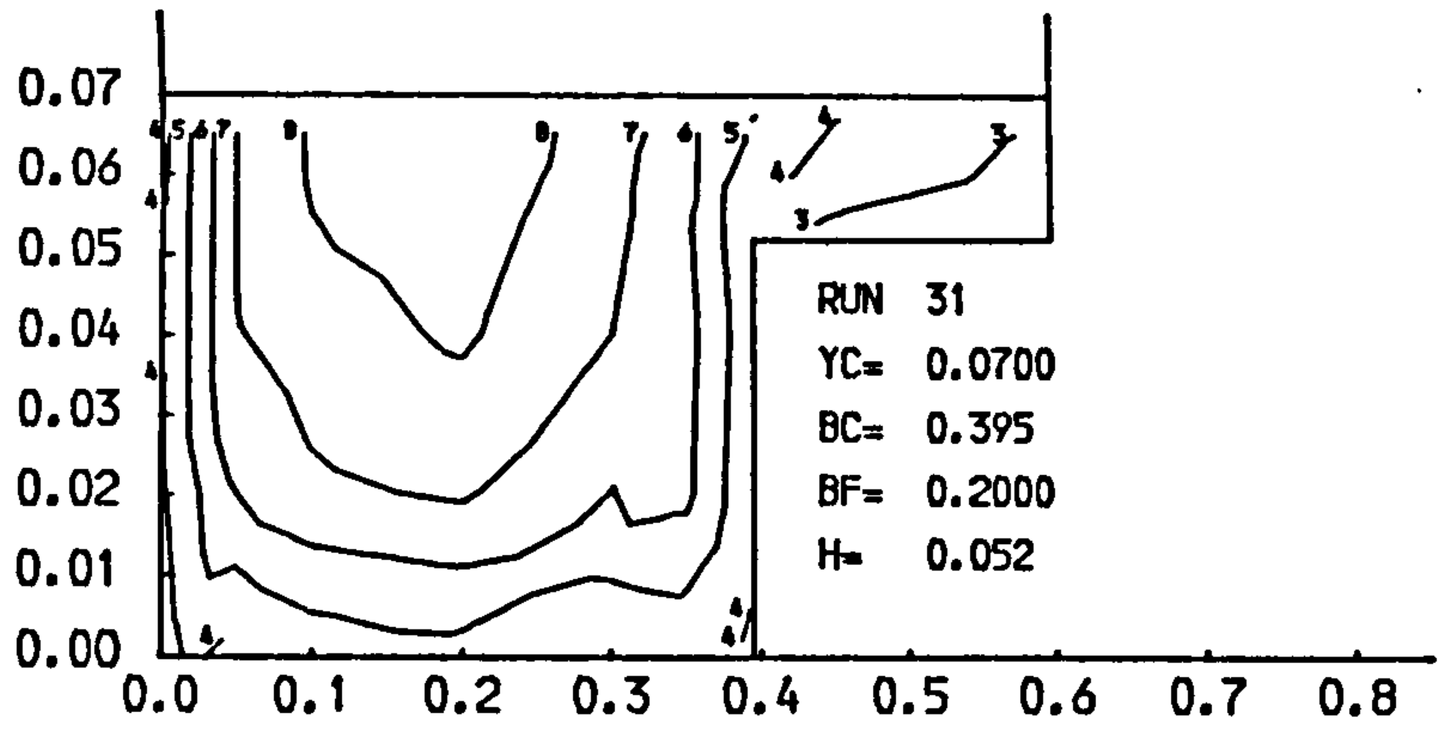

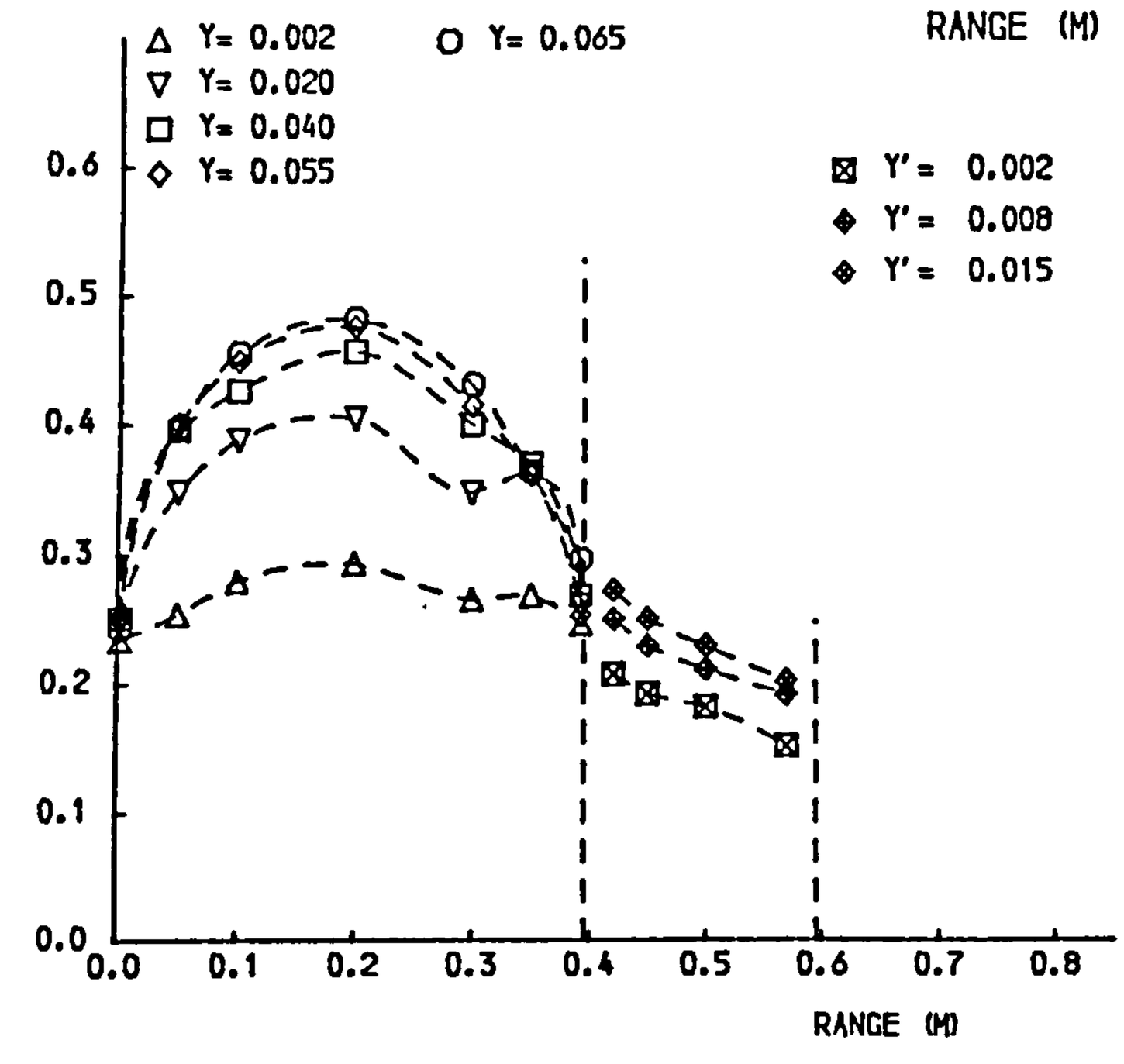

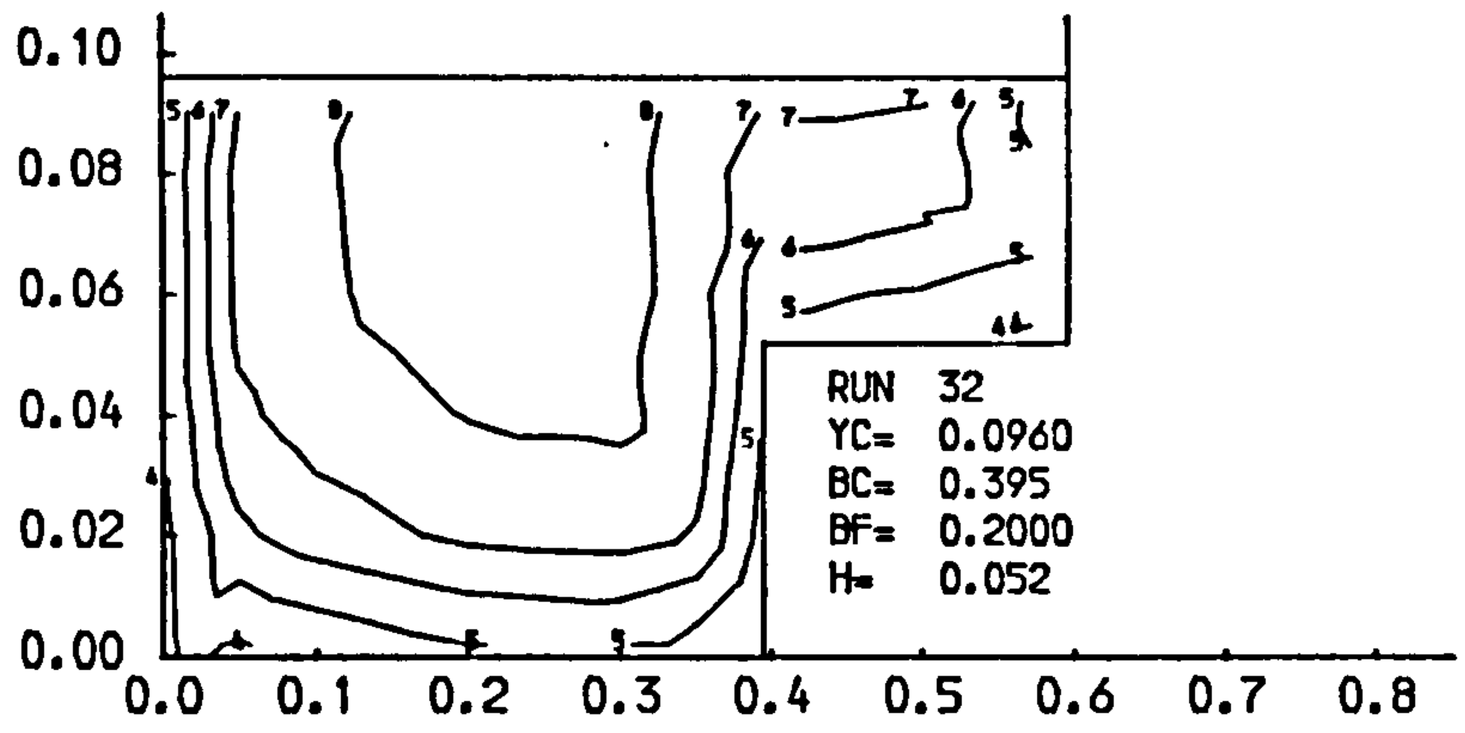

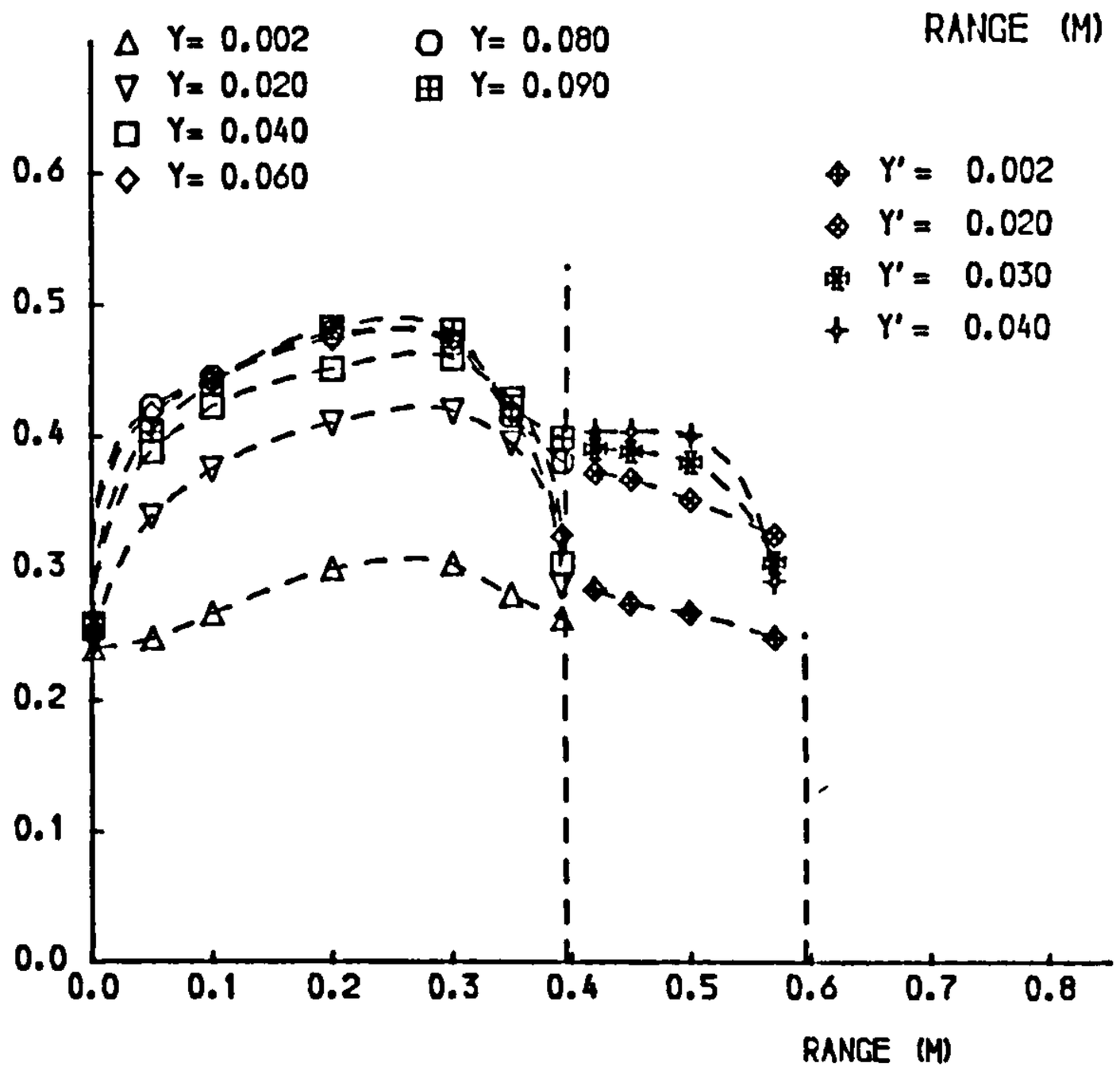

Fig 4·7 Isovels and lateral velocity profiles.

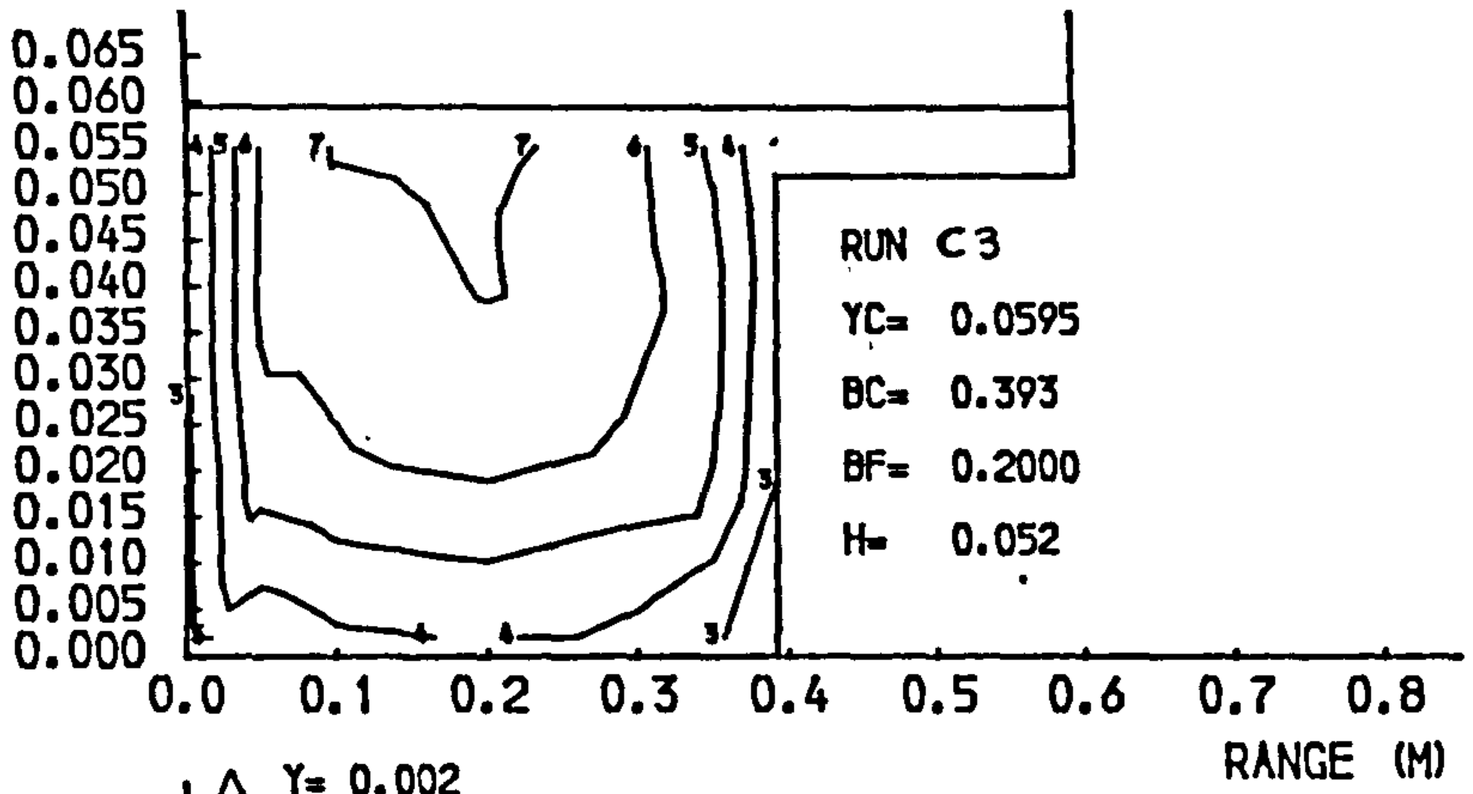

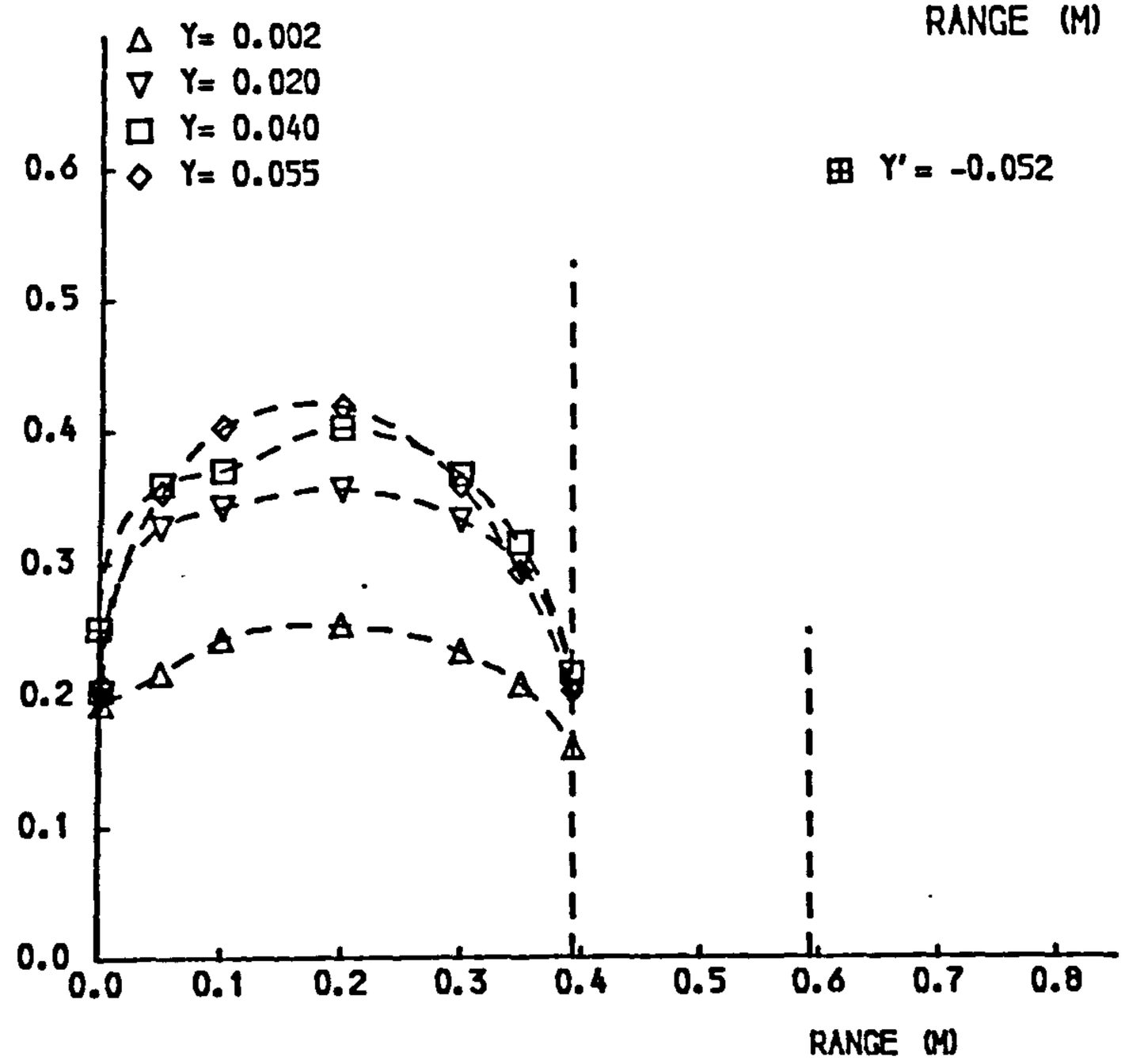

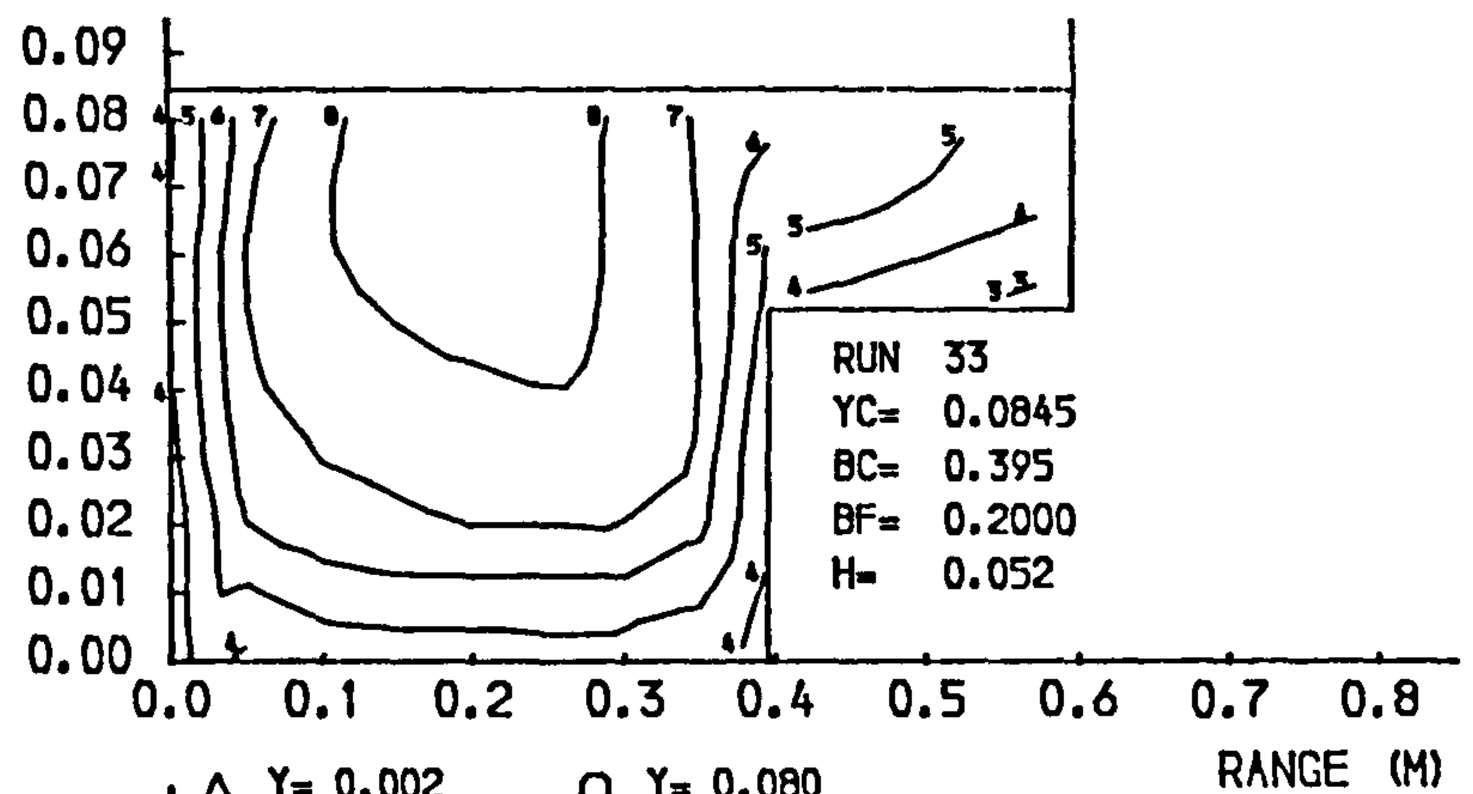

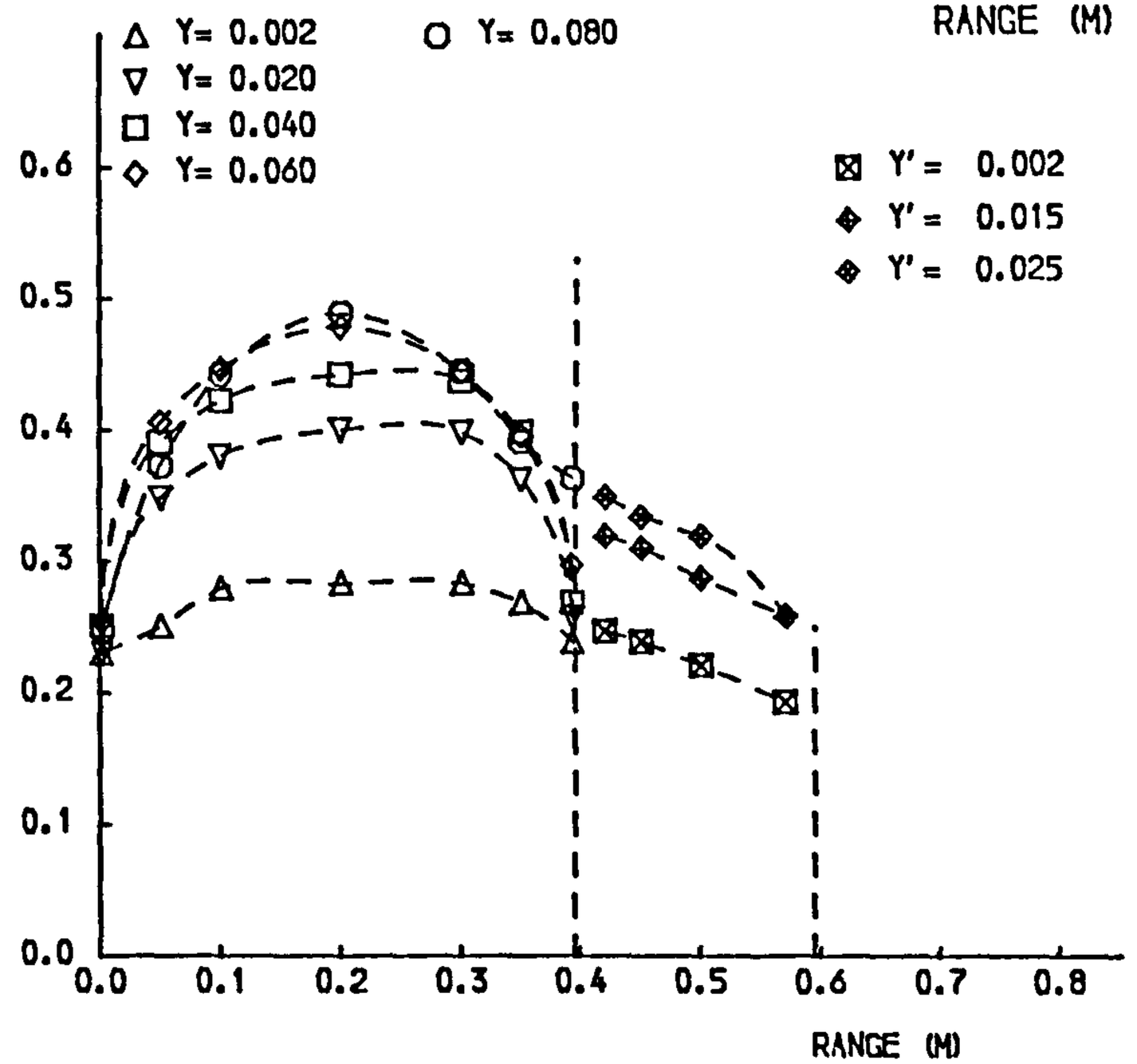

Fig 4·7 Isovels and lateral velocity profiles.

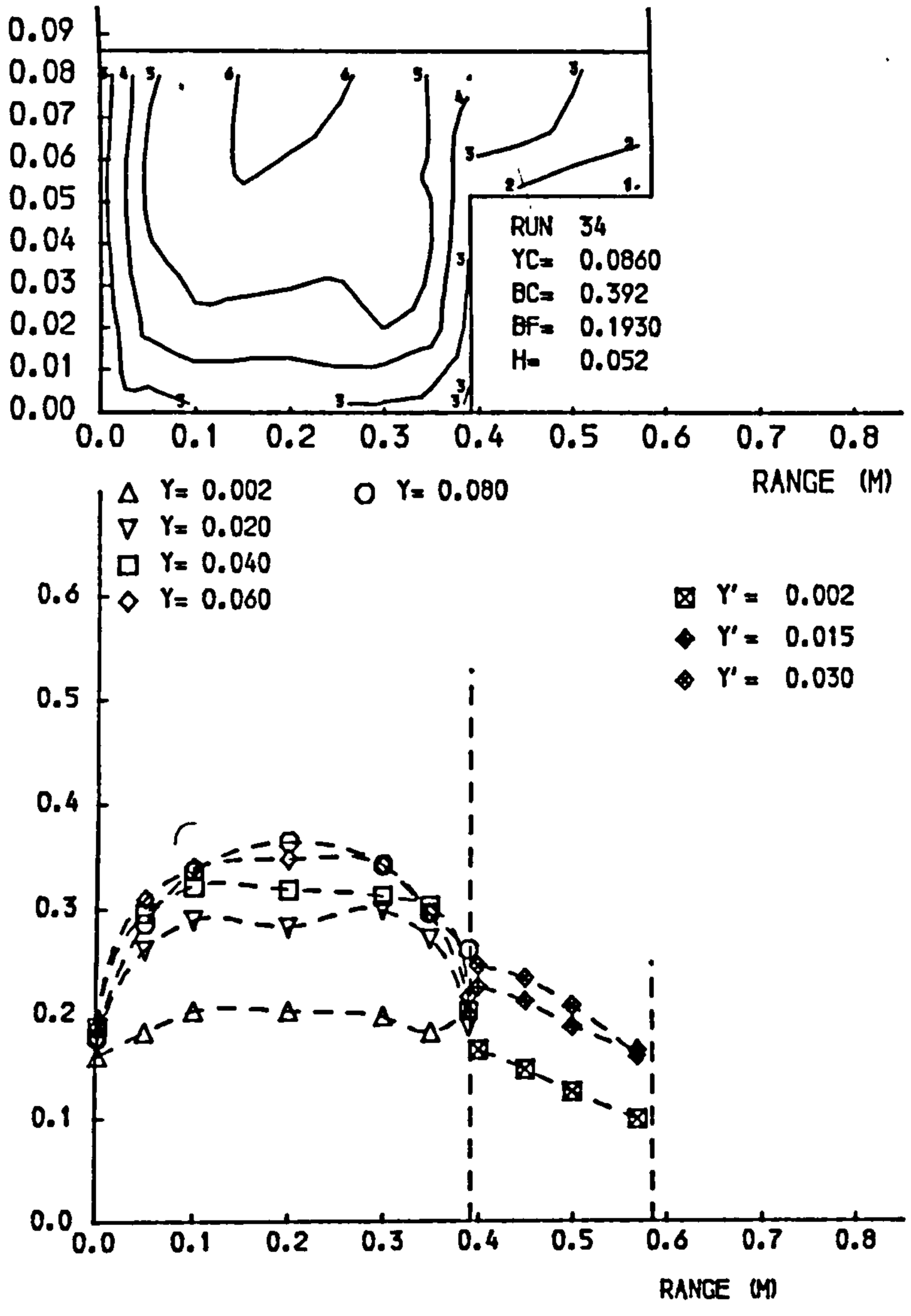

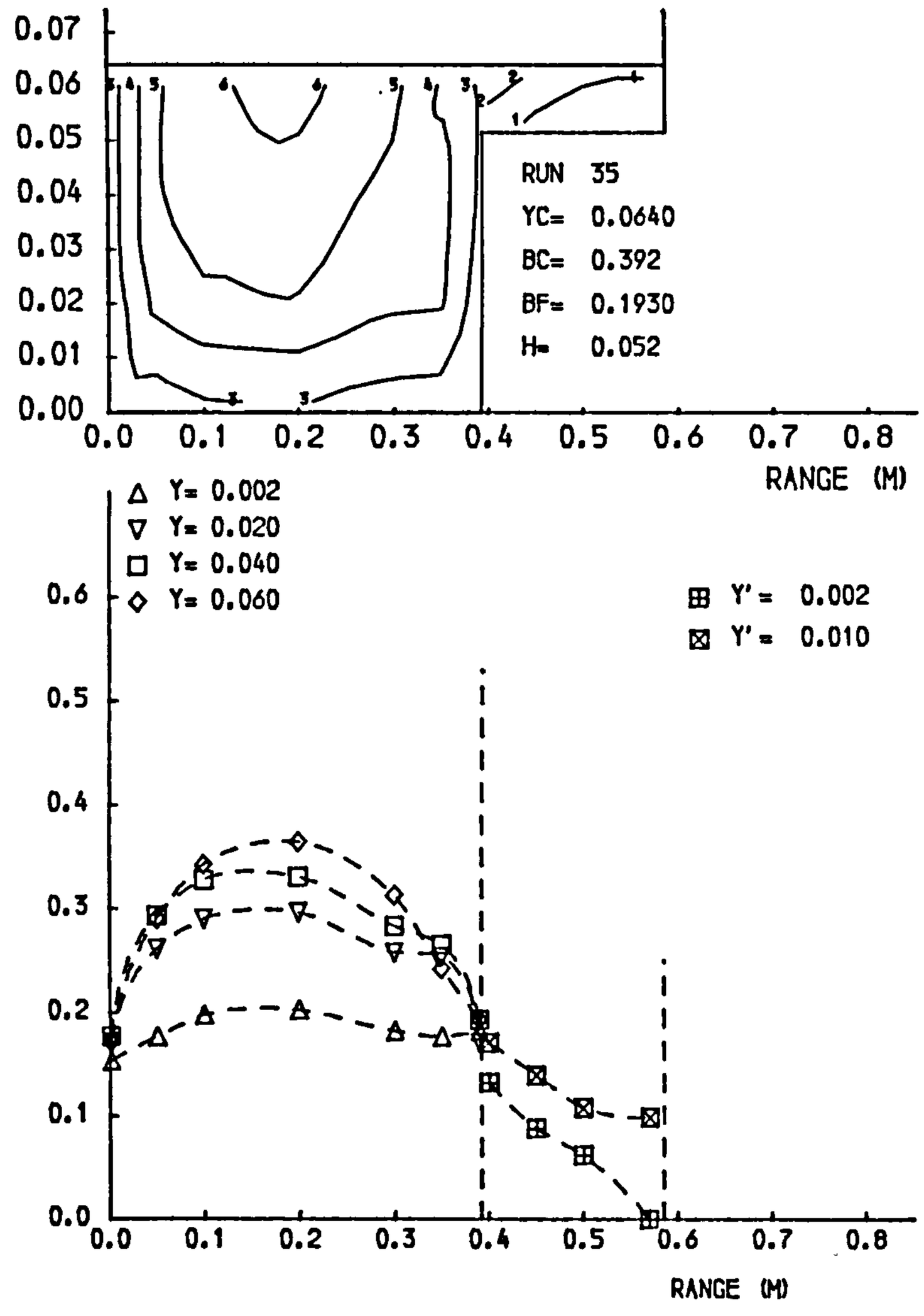

Fig 4·7 Isovels and lateral velocity profiles.

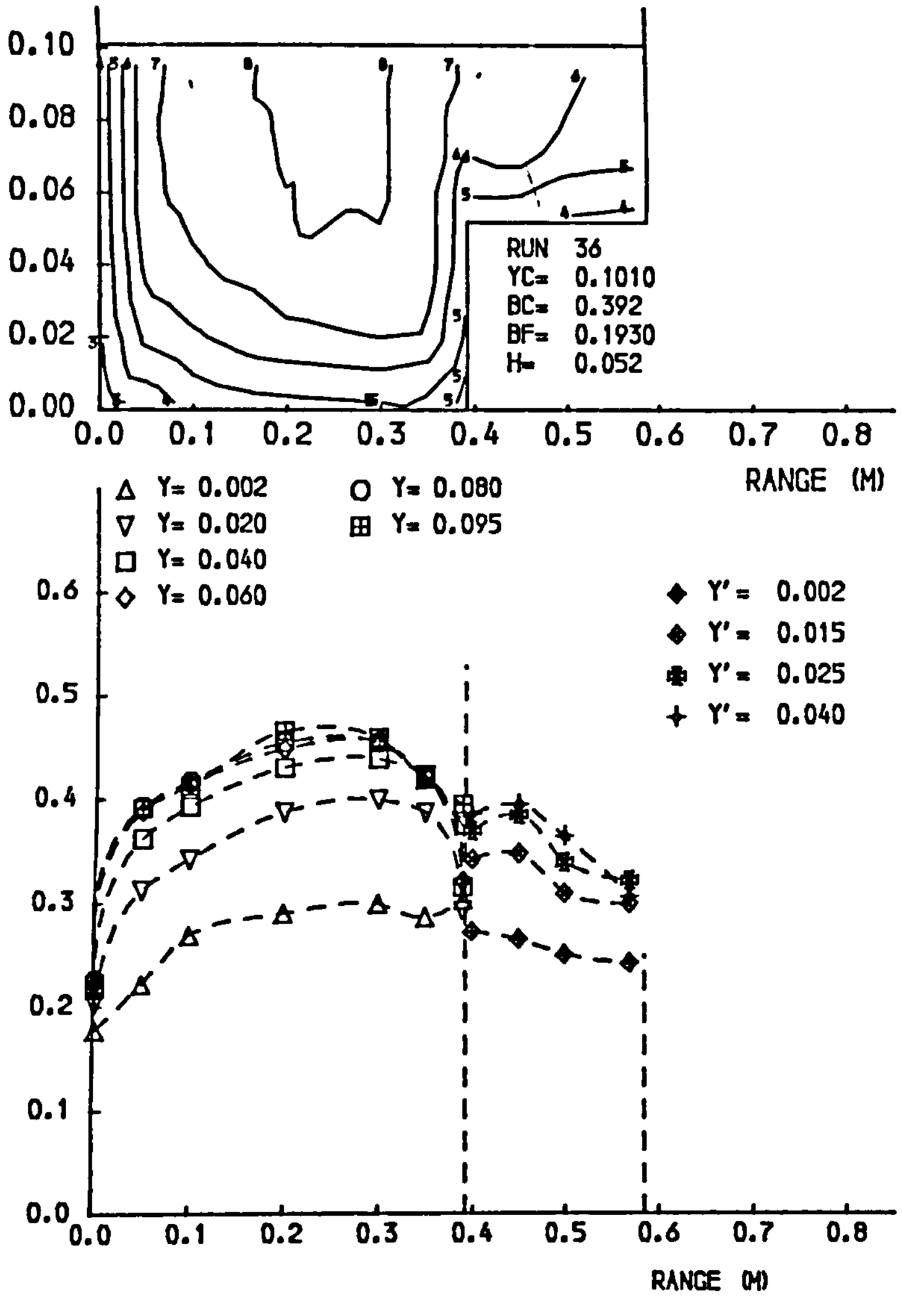

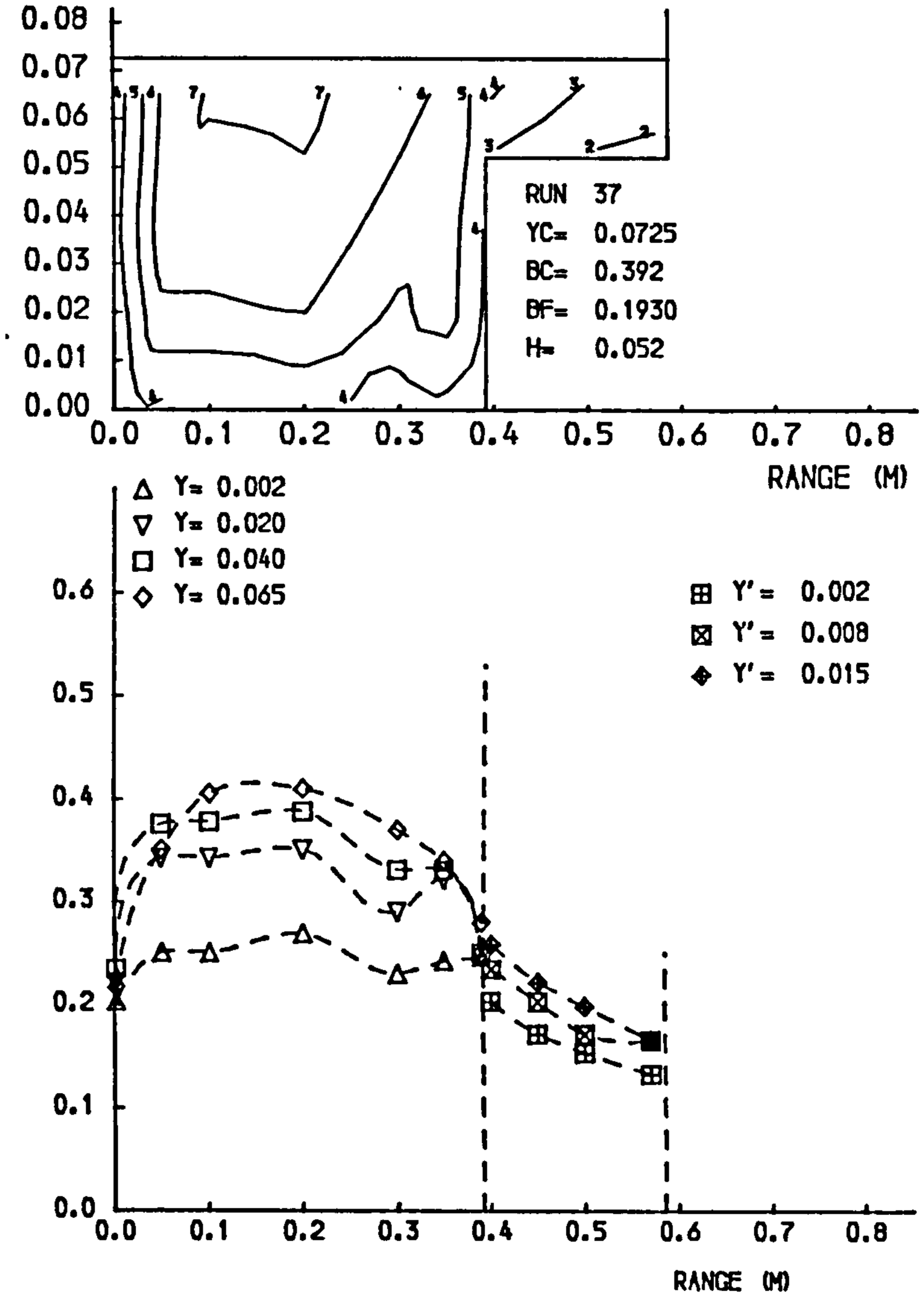

Fig 4·7 Isovels and lateral velocity profiles.

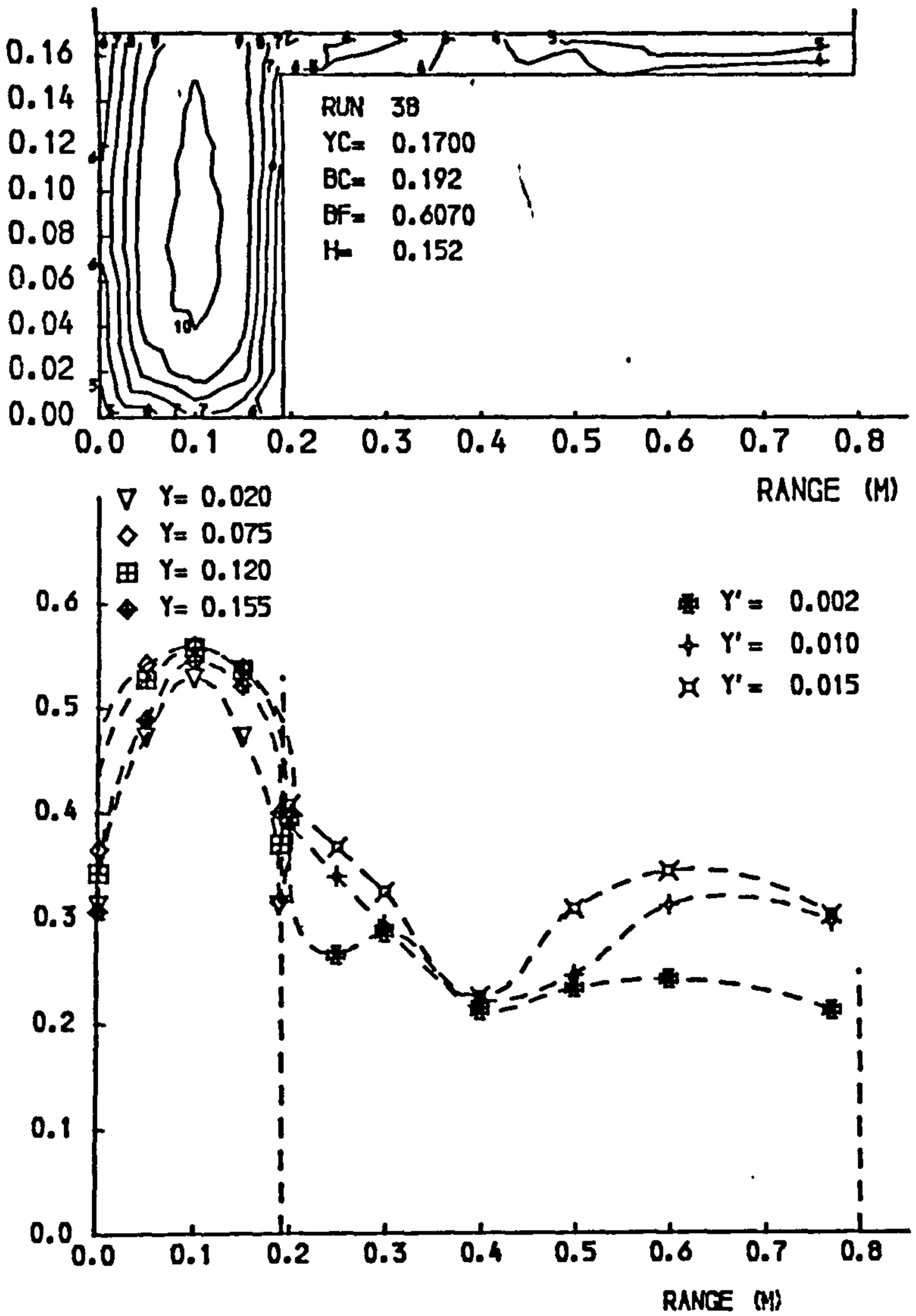

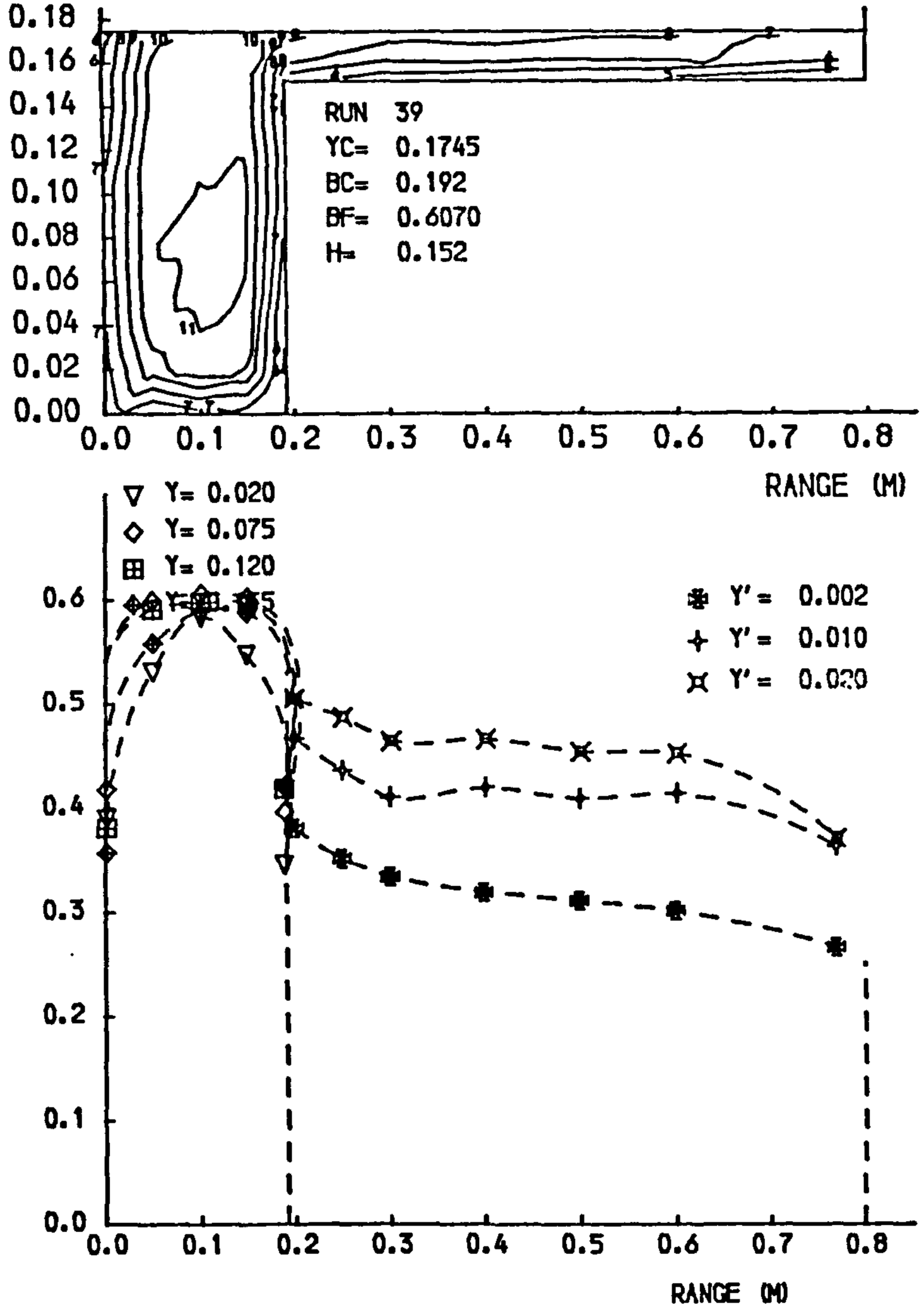

Fig 4·7 Isovels and lateral velocity profiles.

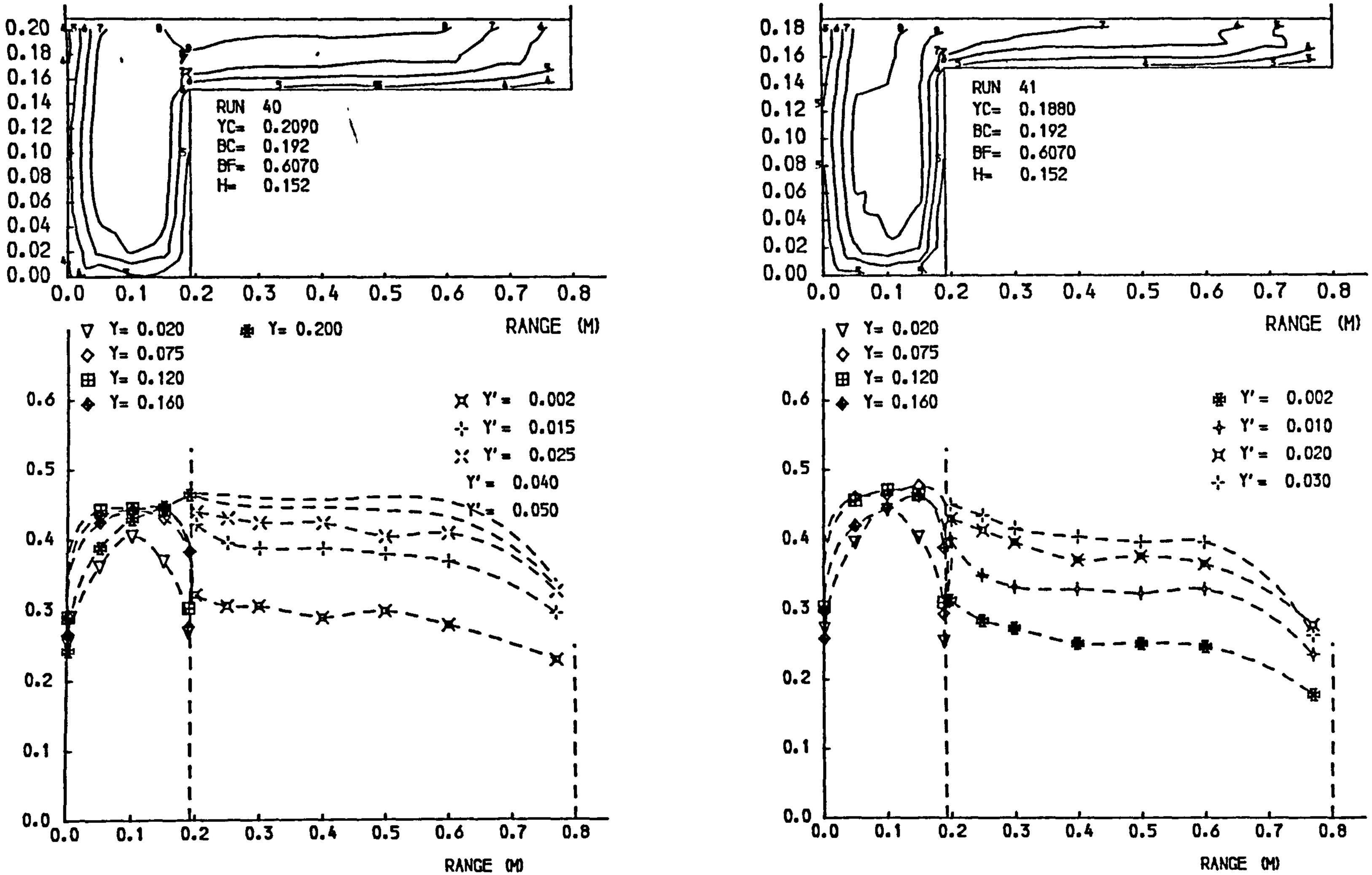

Fig 4·7 Isovels and lateral velocity profiles.

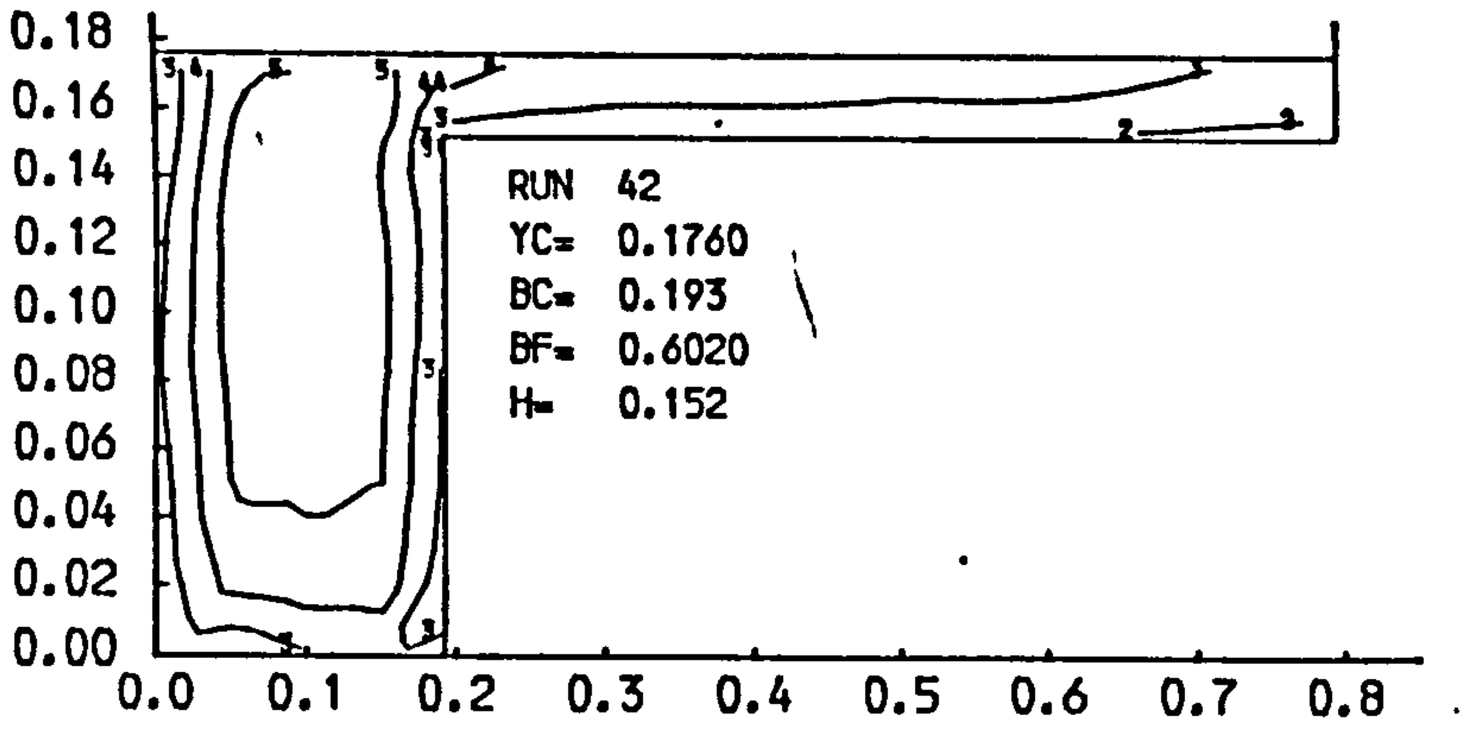

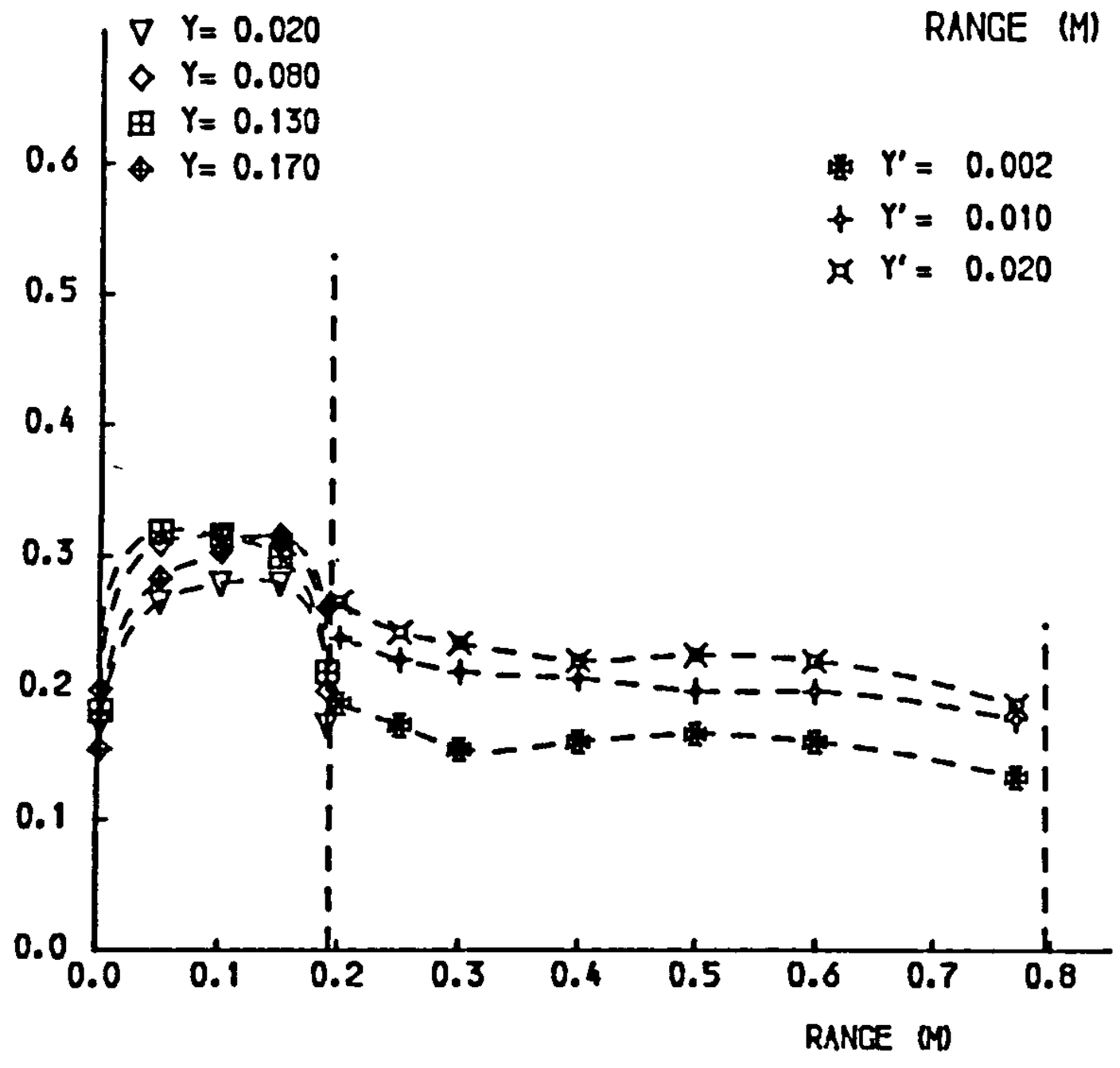

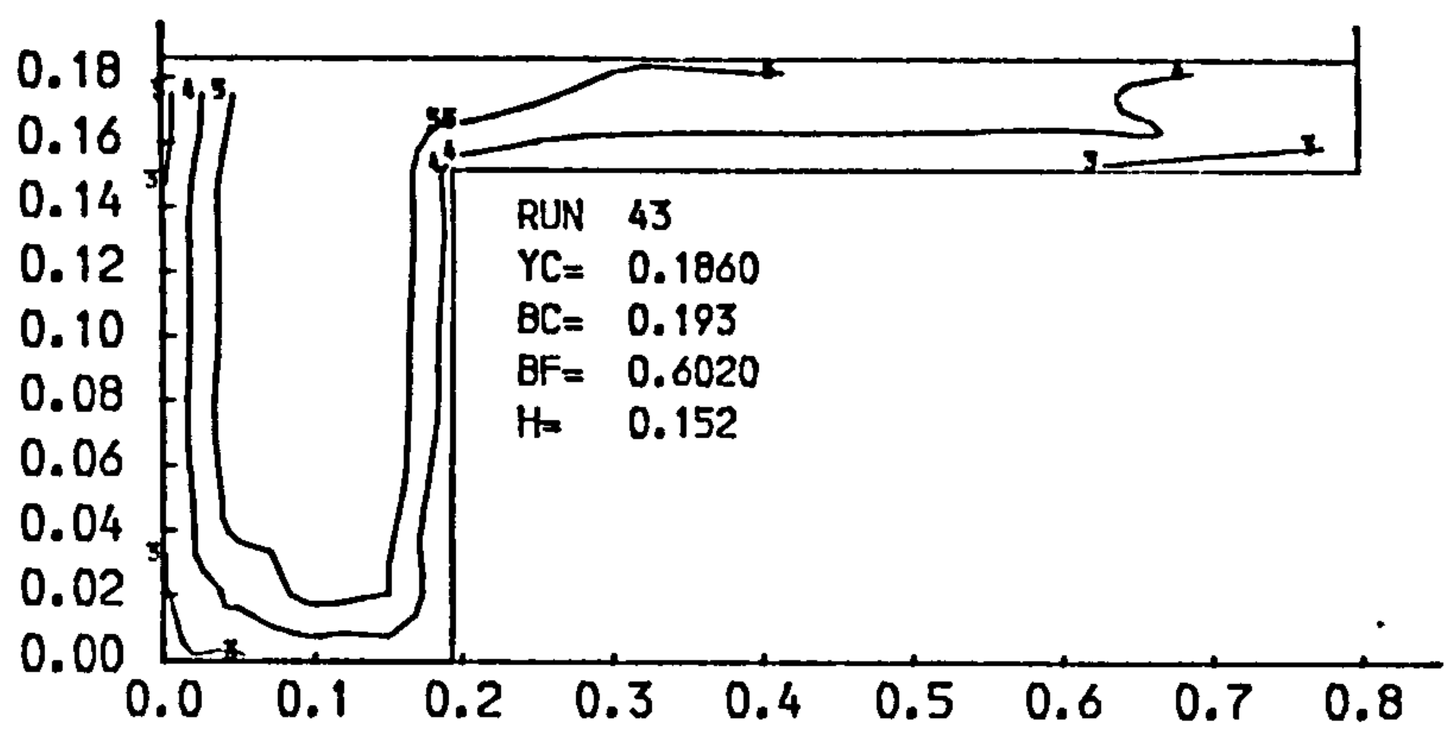

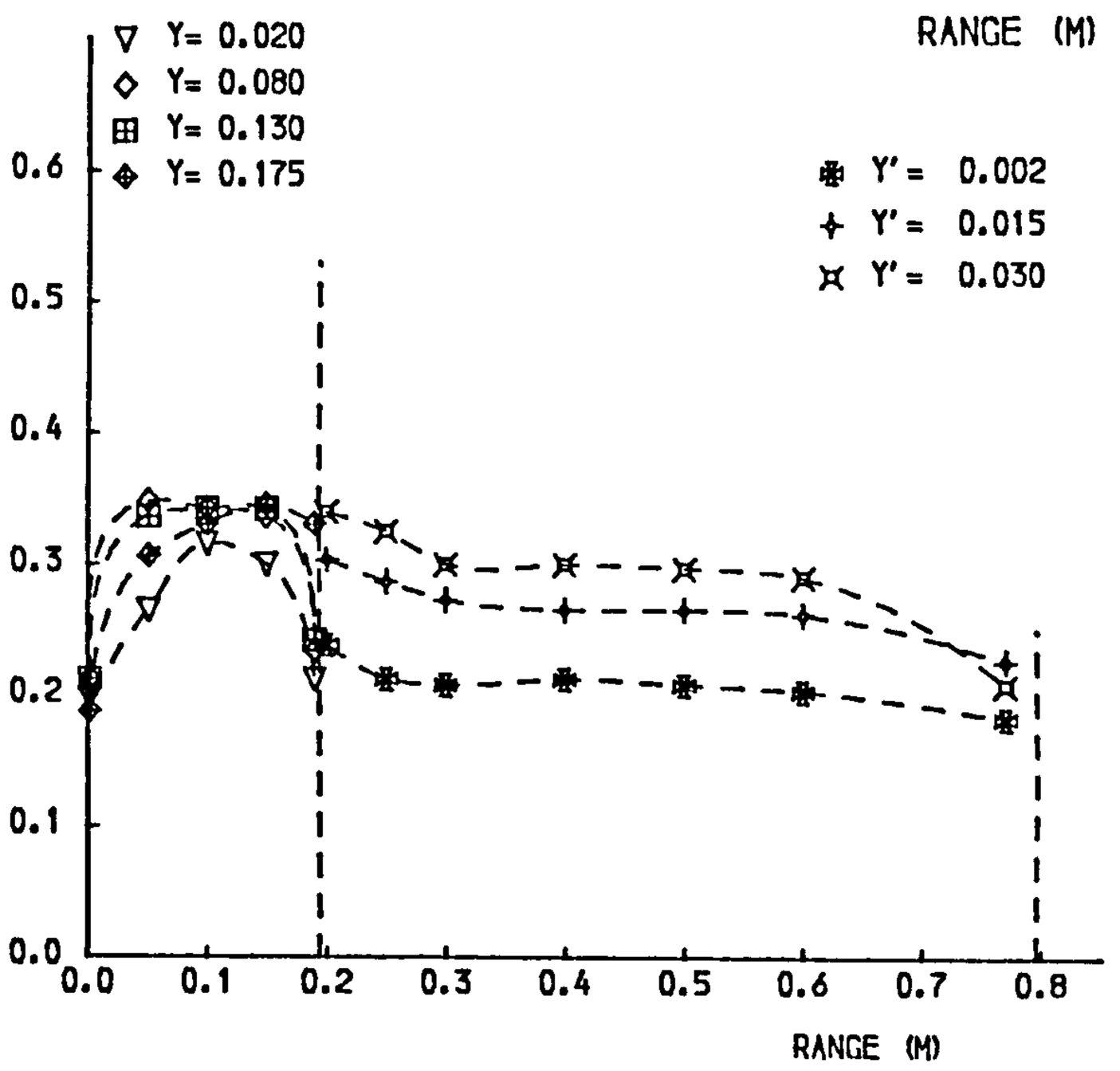

Fig 4·7 Isovels and lateral velocity profiles.

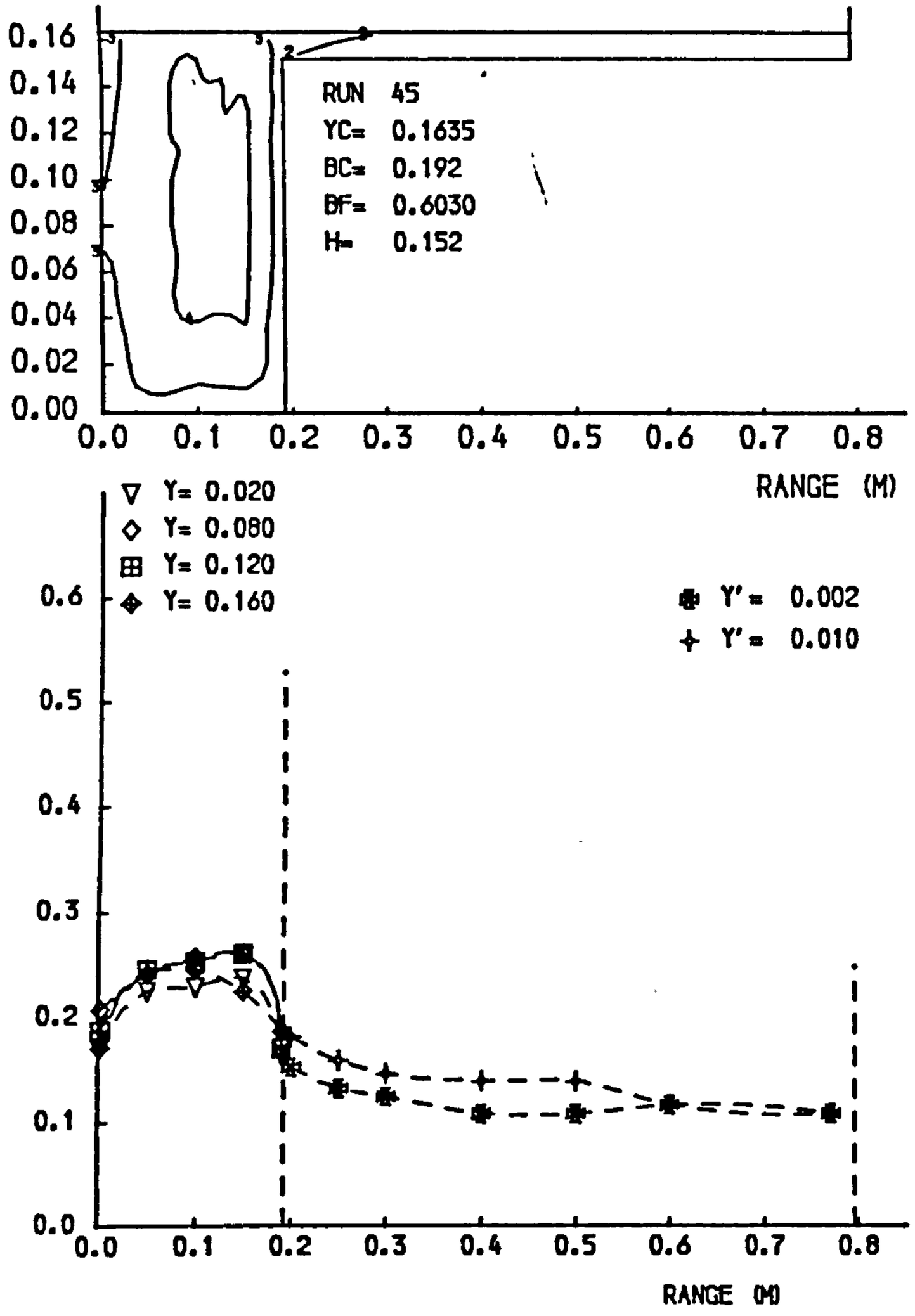

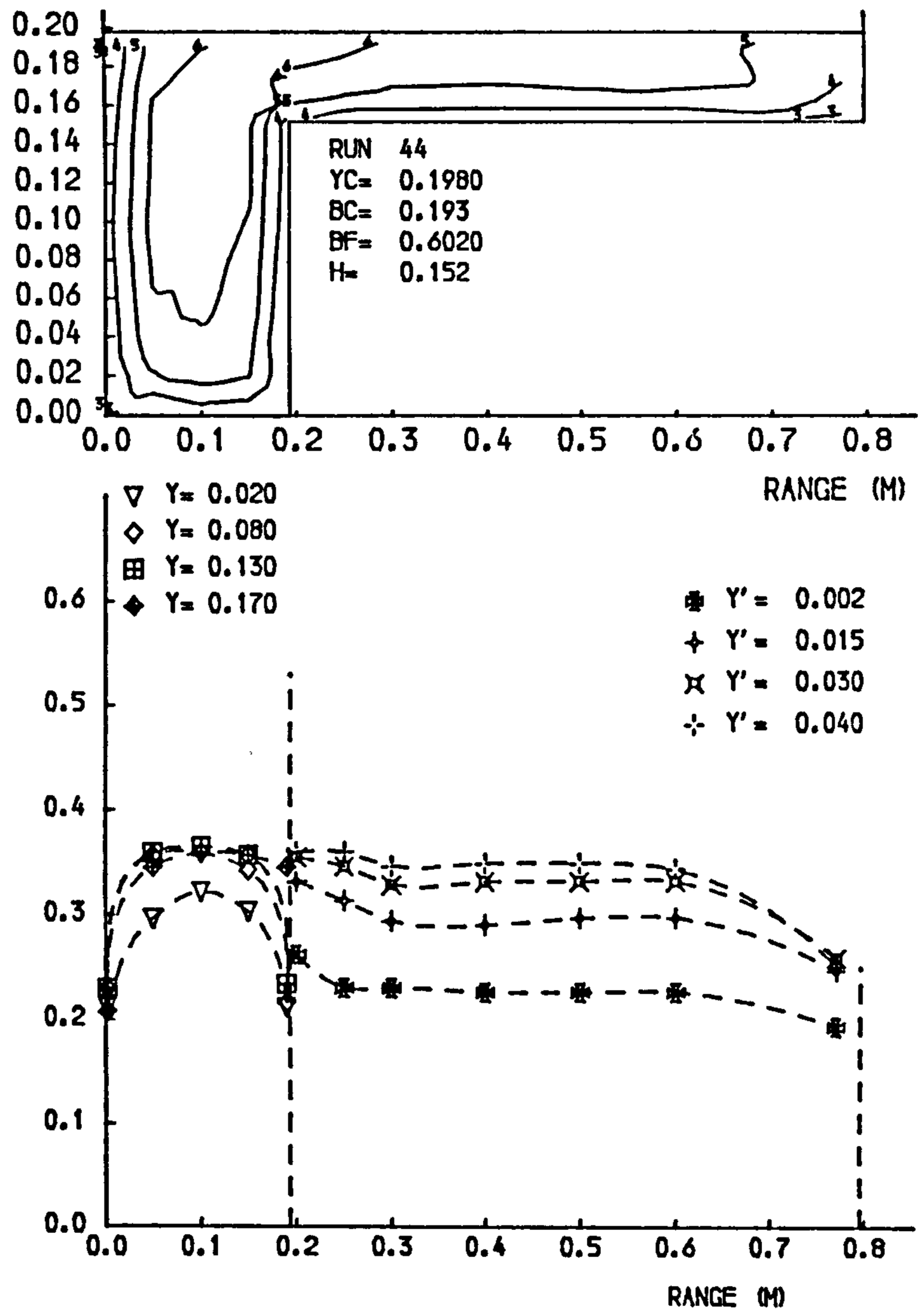

Fig 4·7 Isovels and lateral velocity profiles.

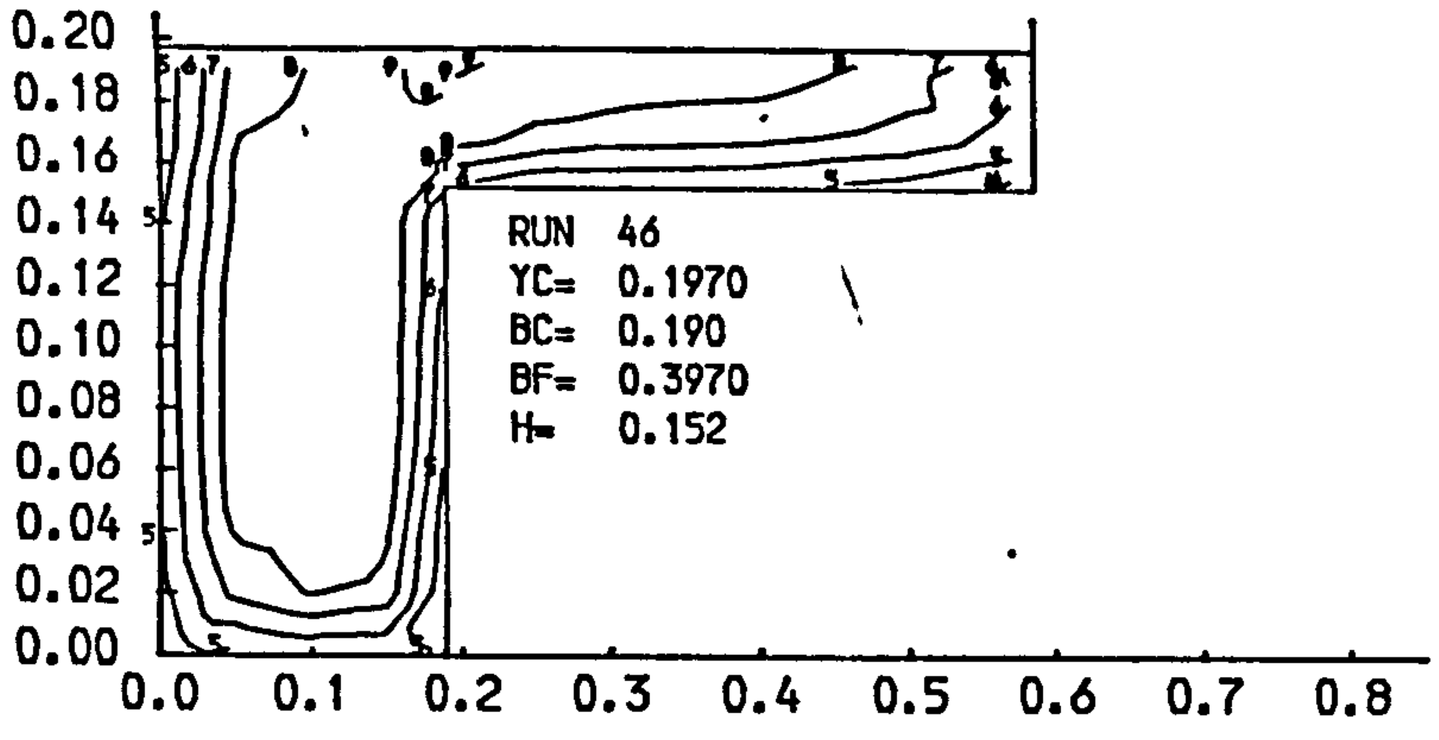

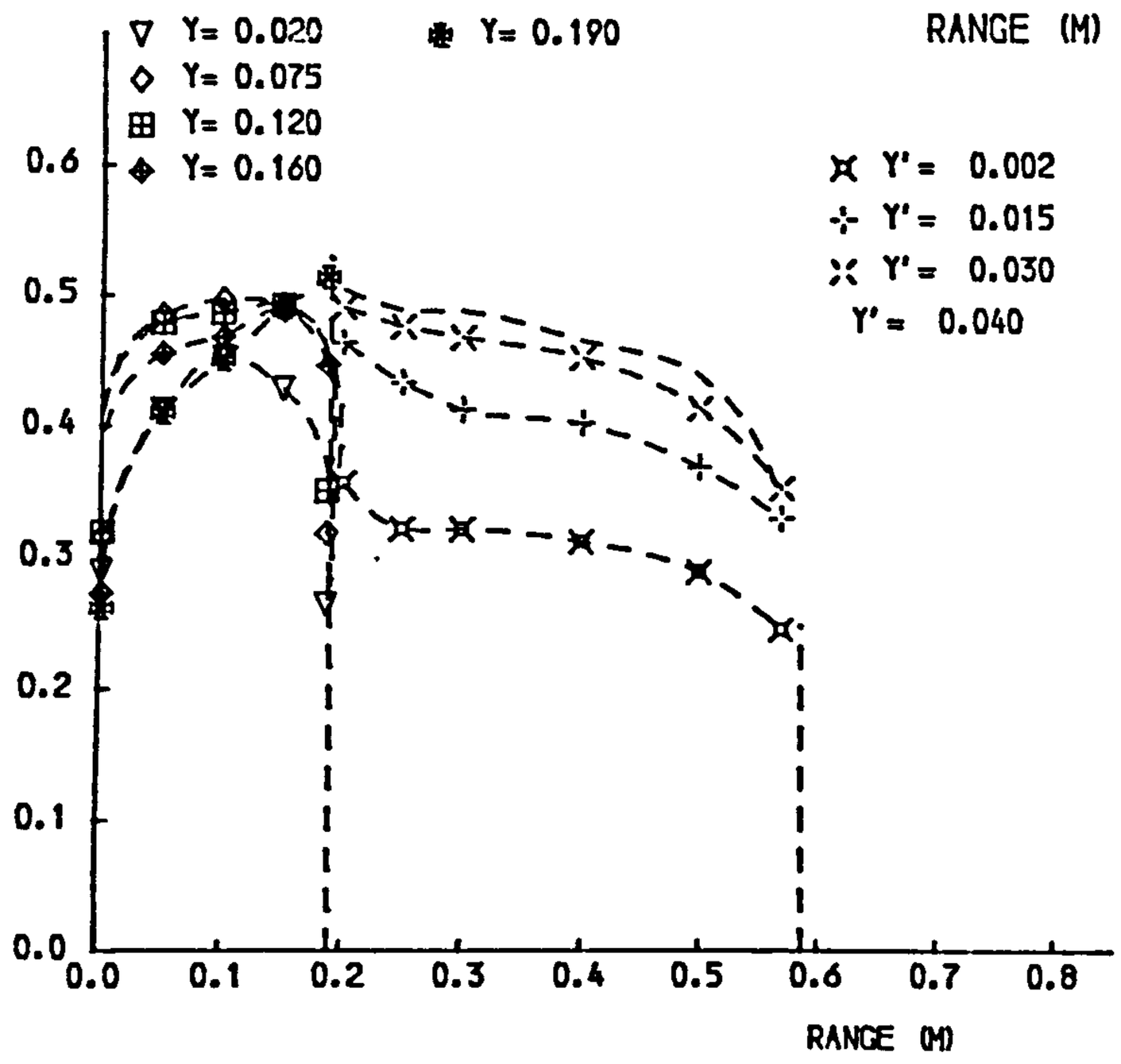

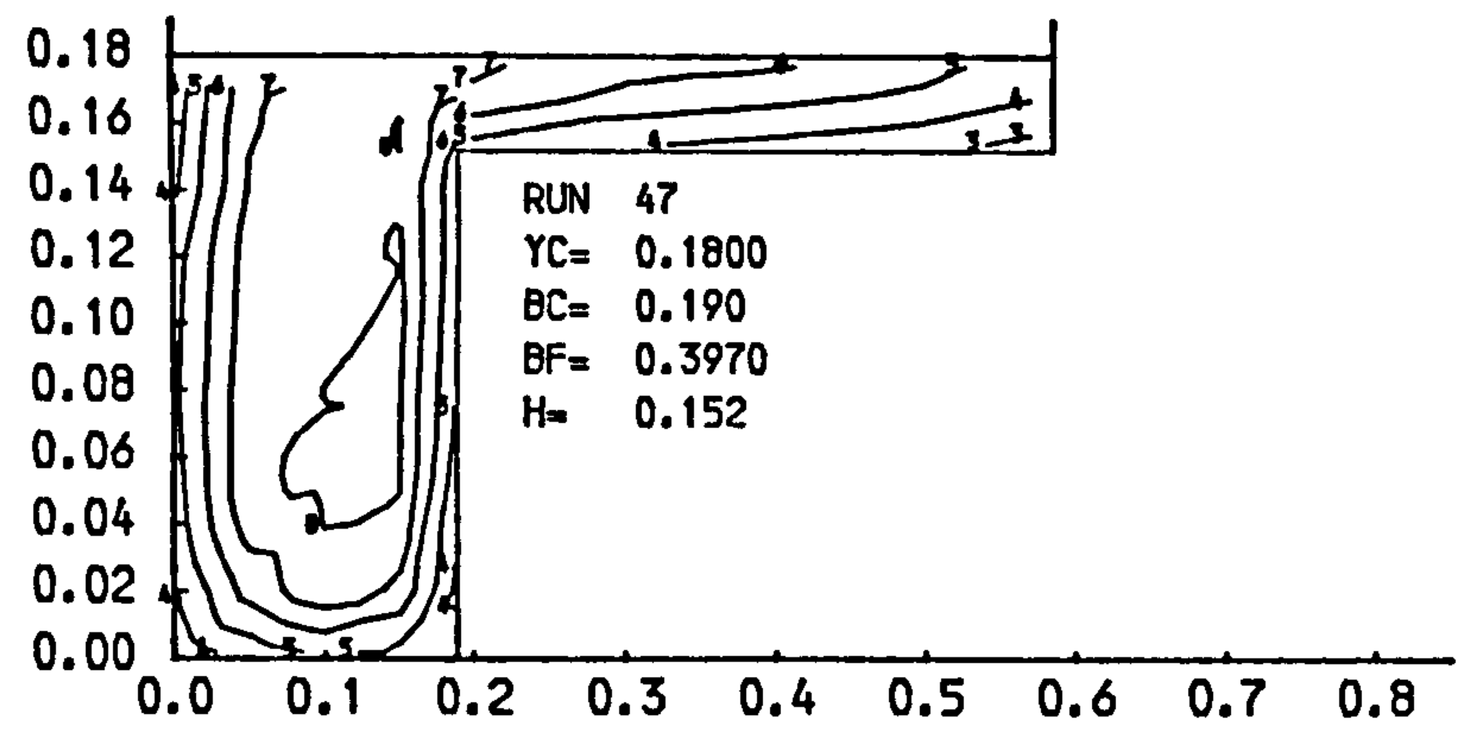

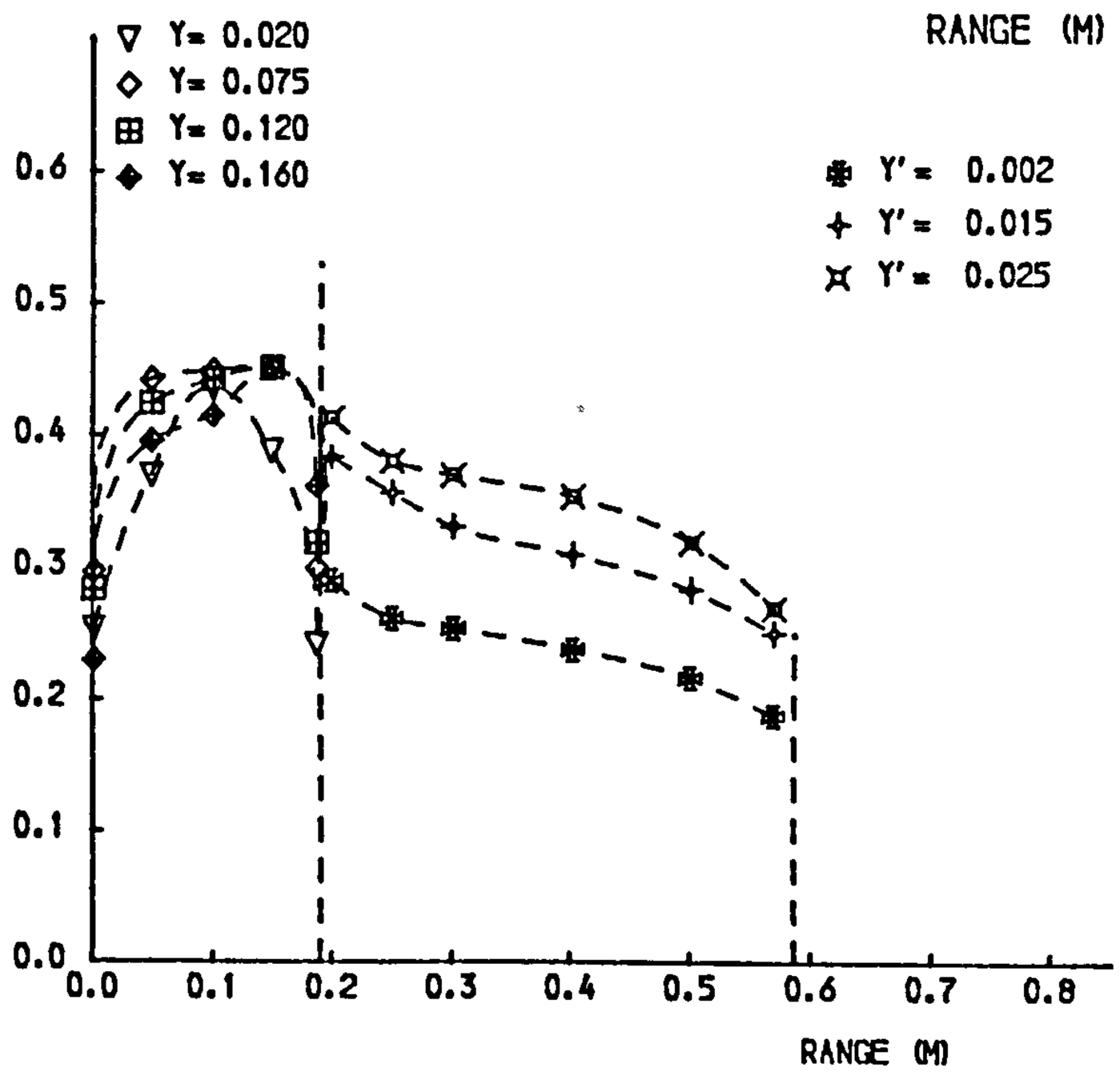

Fig 4·7 Isovels and lateral velocity profiles.

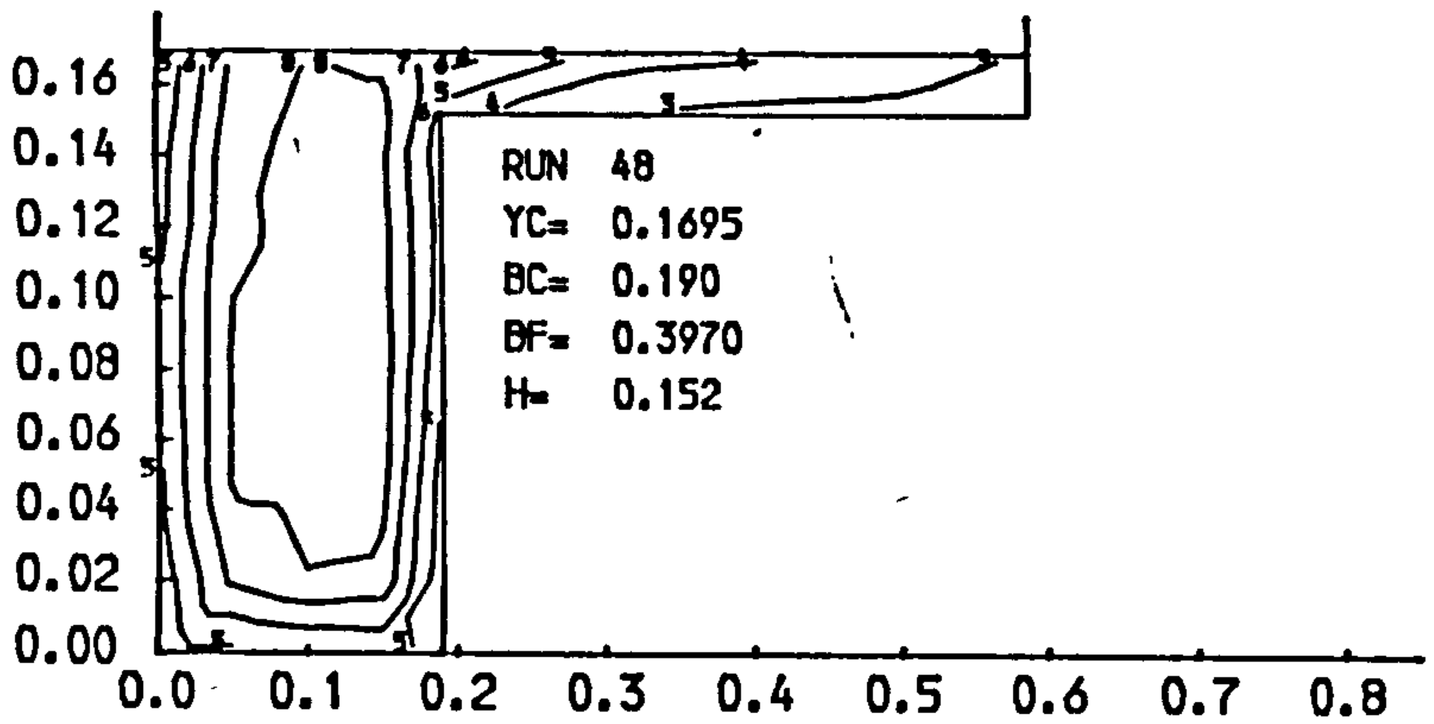

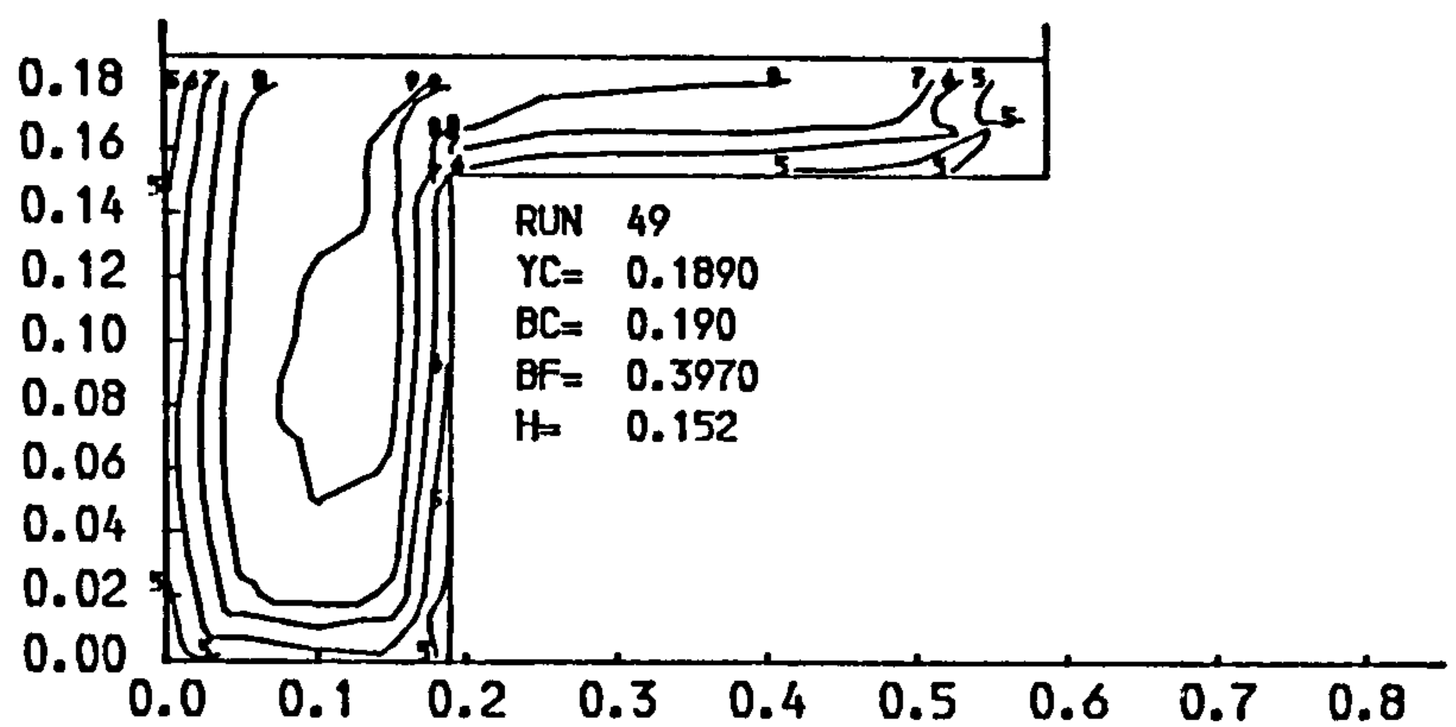

Fig 4·7 Isovels and lateral velocity profiles.

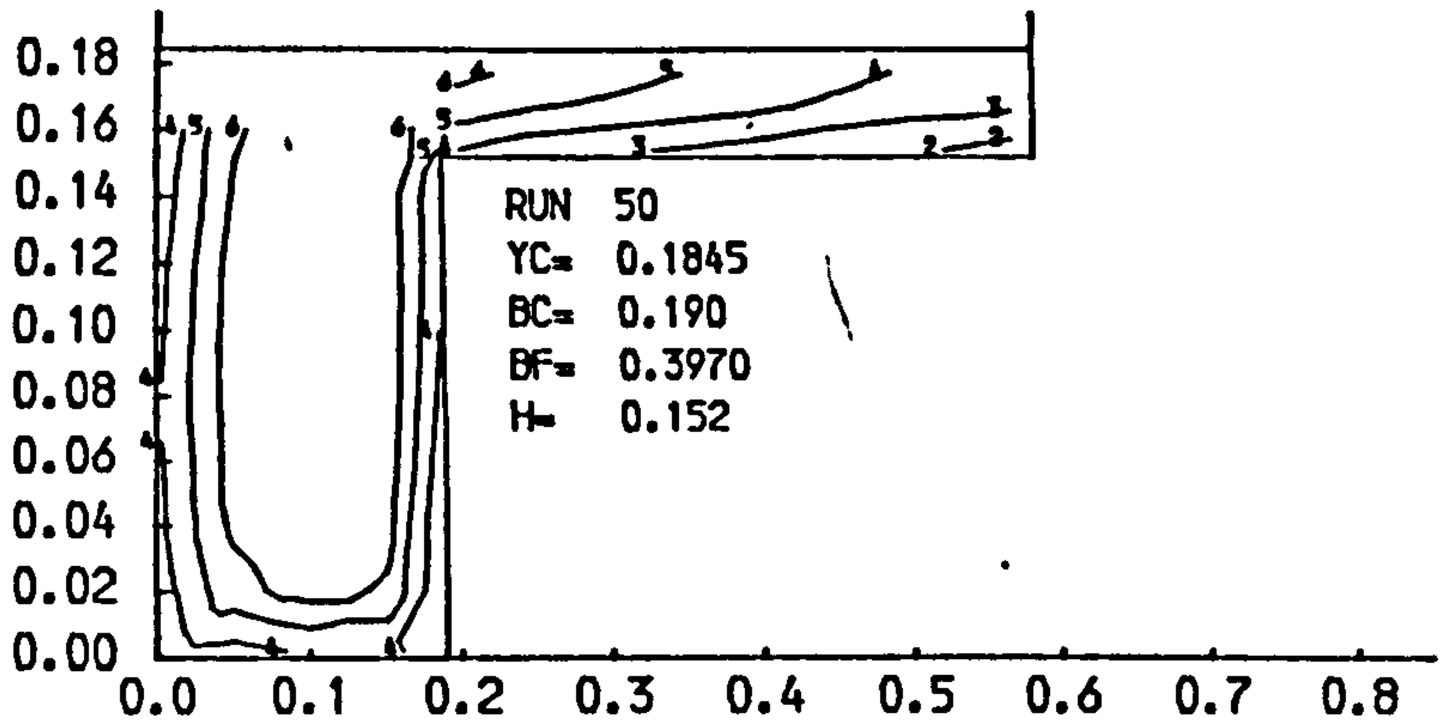

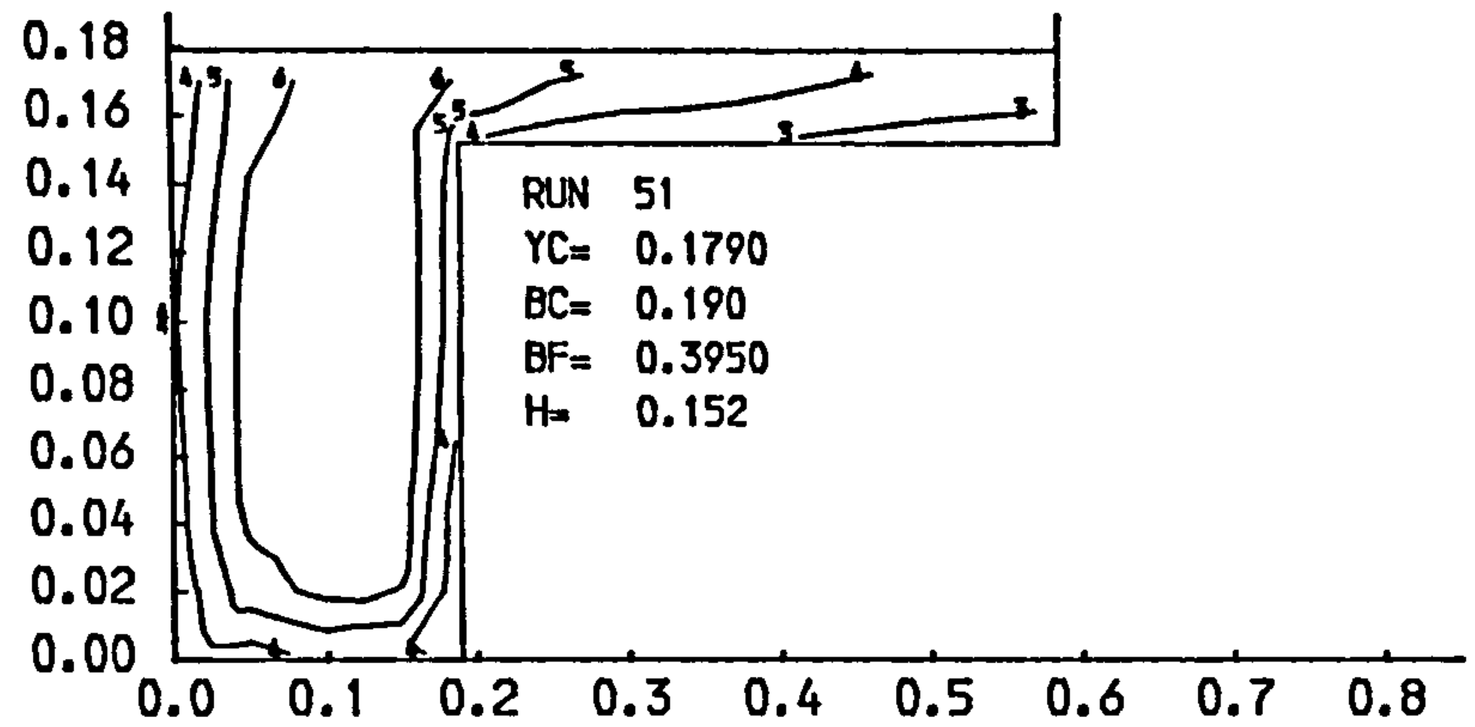

Fig 4·7 Isovels and lateral velocity profiles.

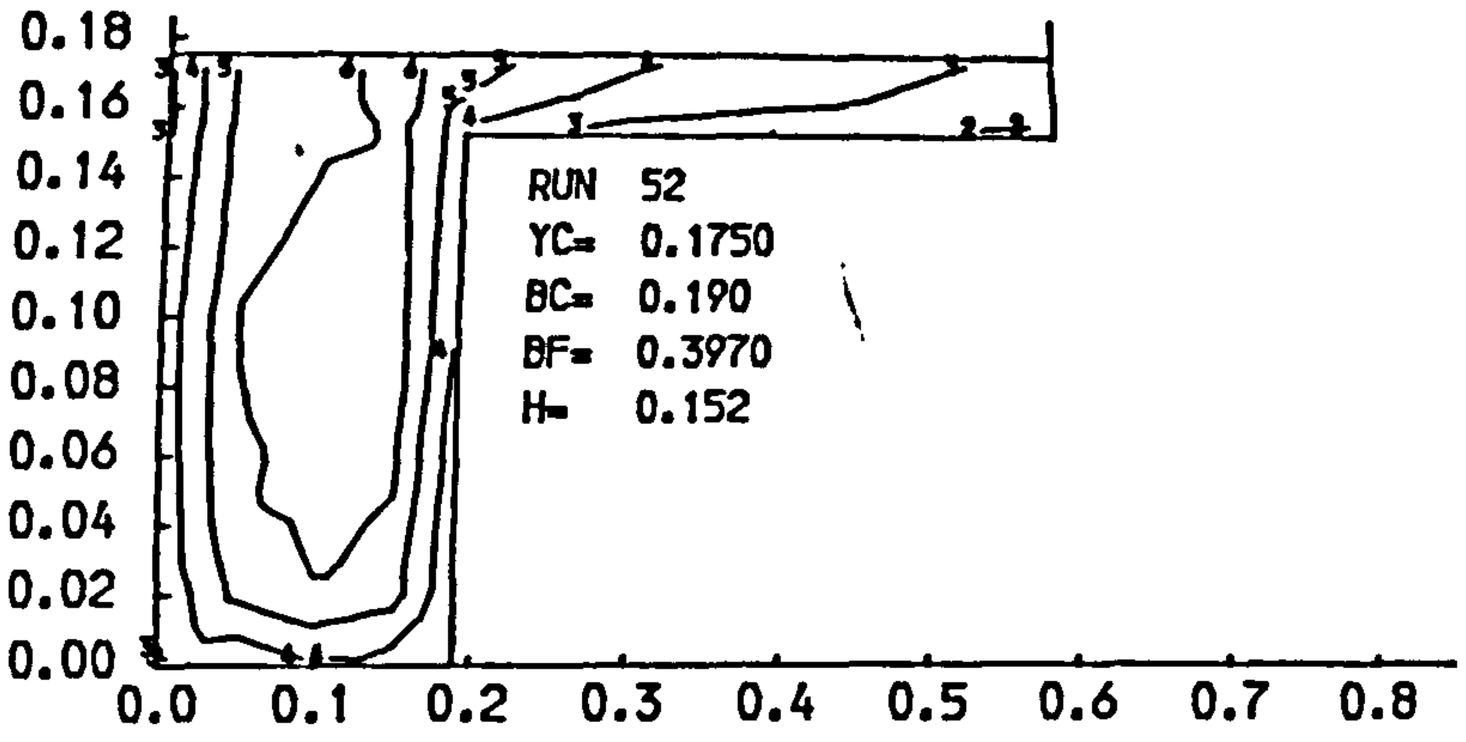

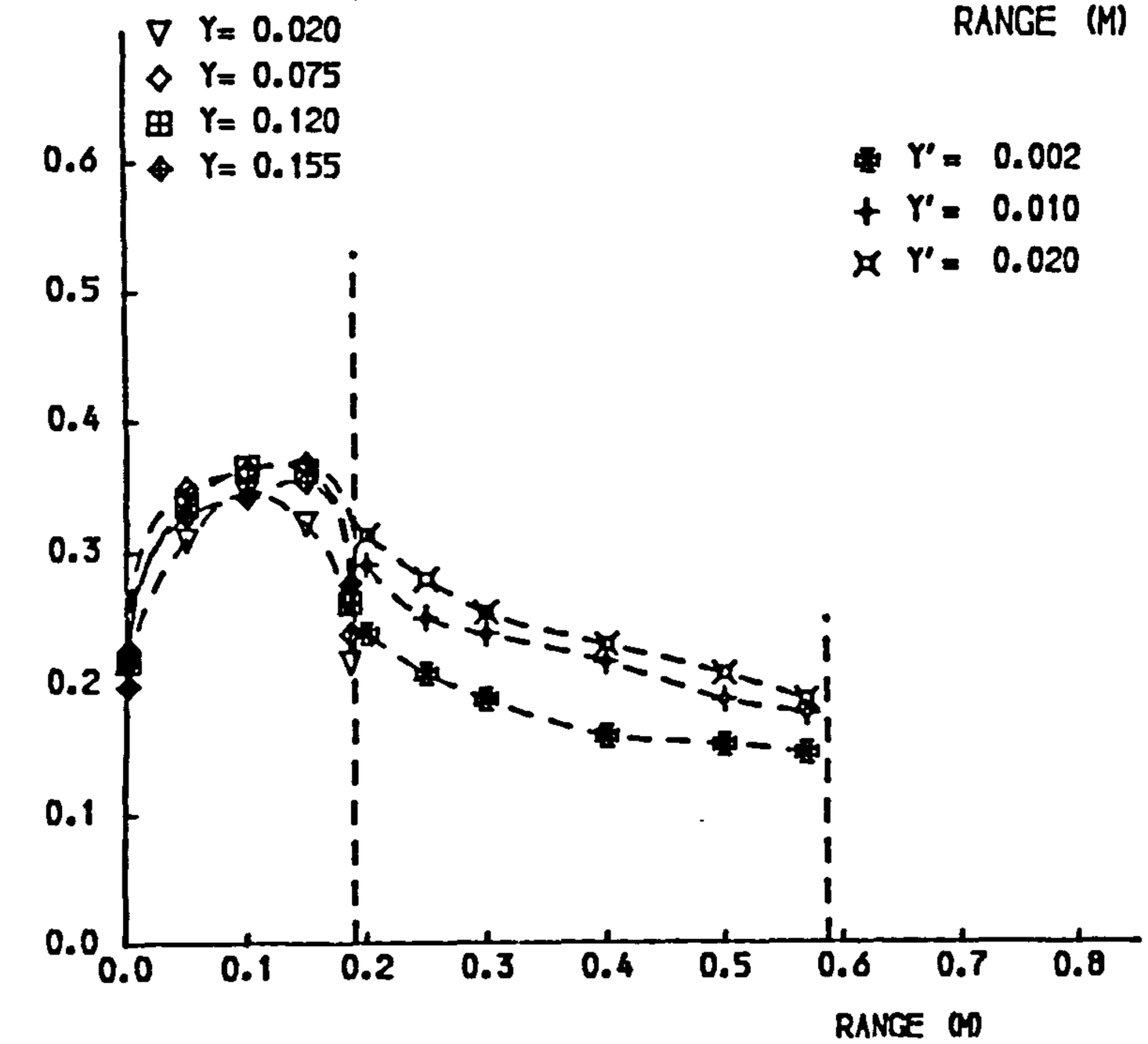

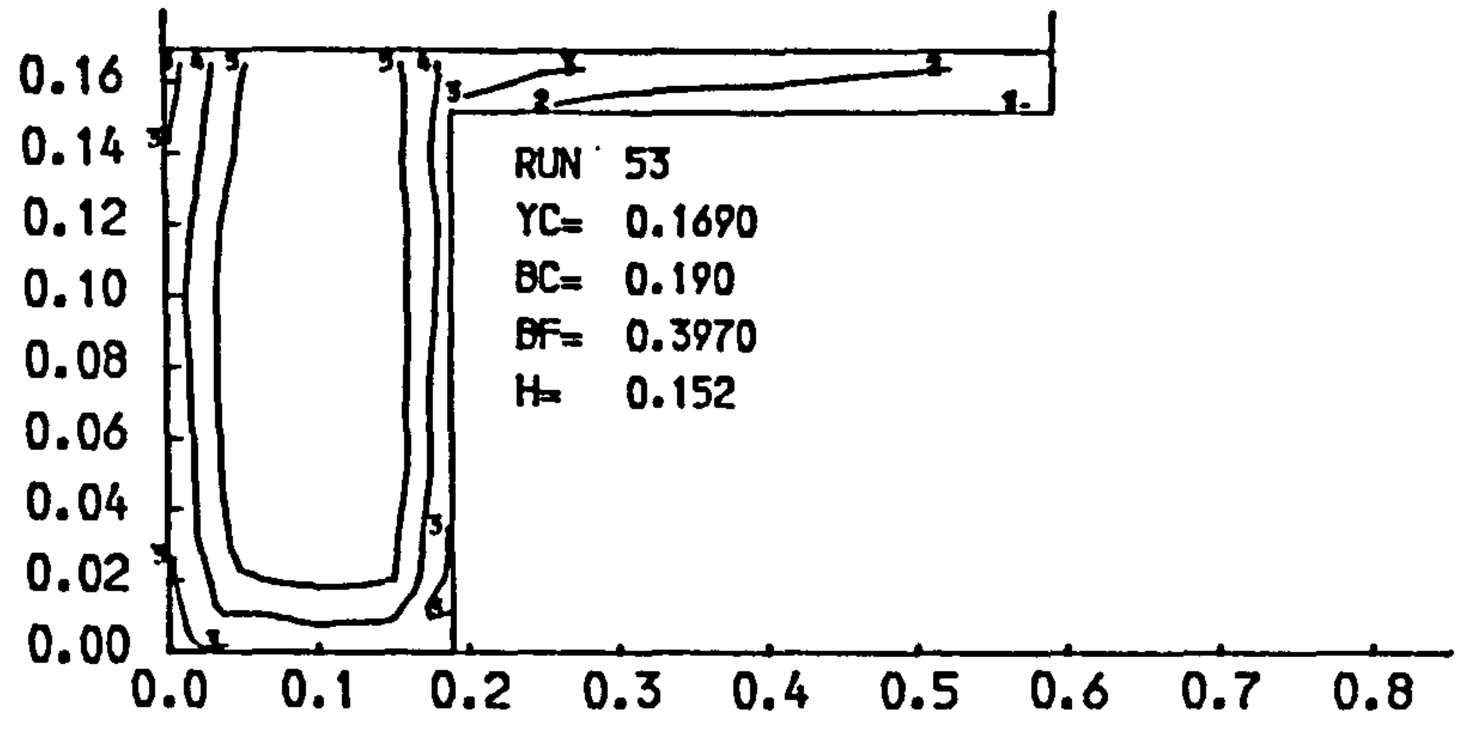

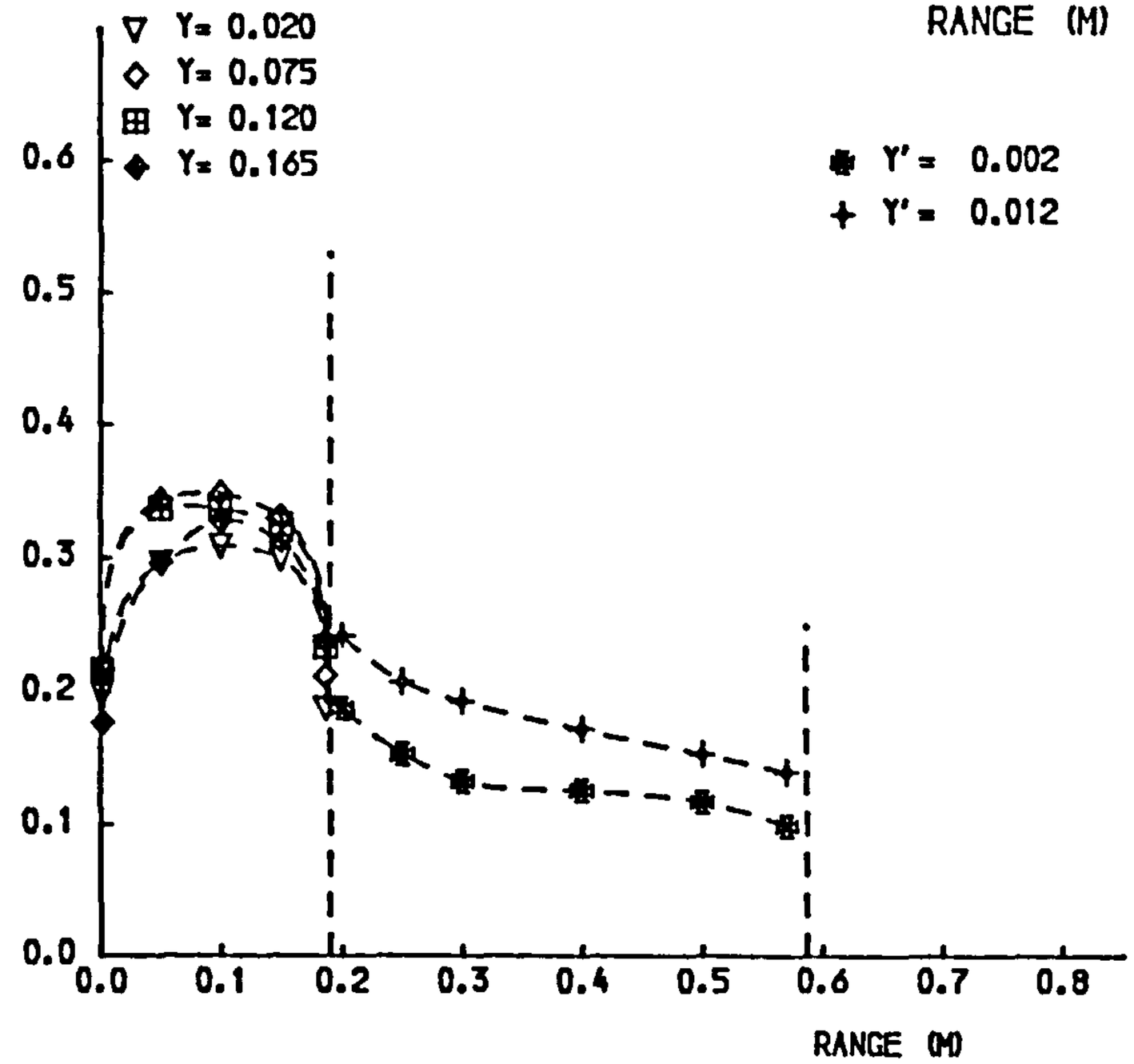

Fig 4·7 Isovels and lateral velocity profiles.

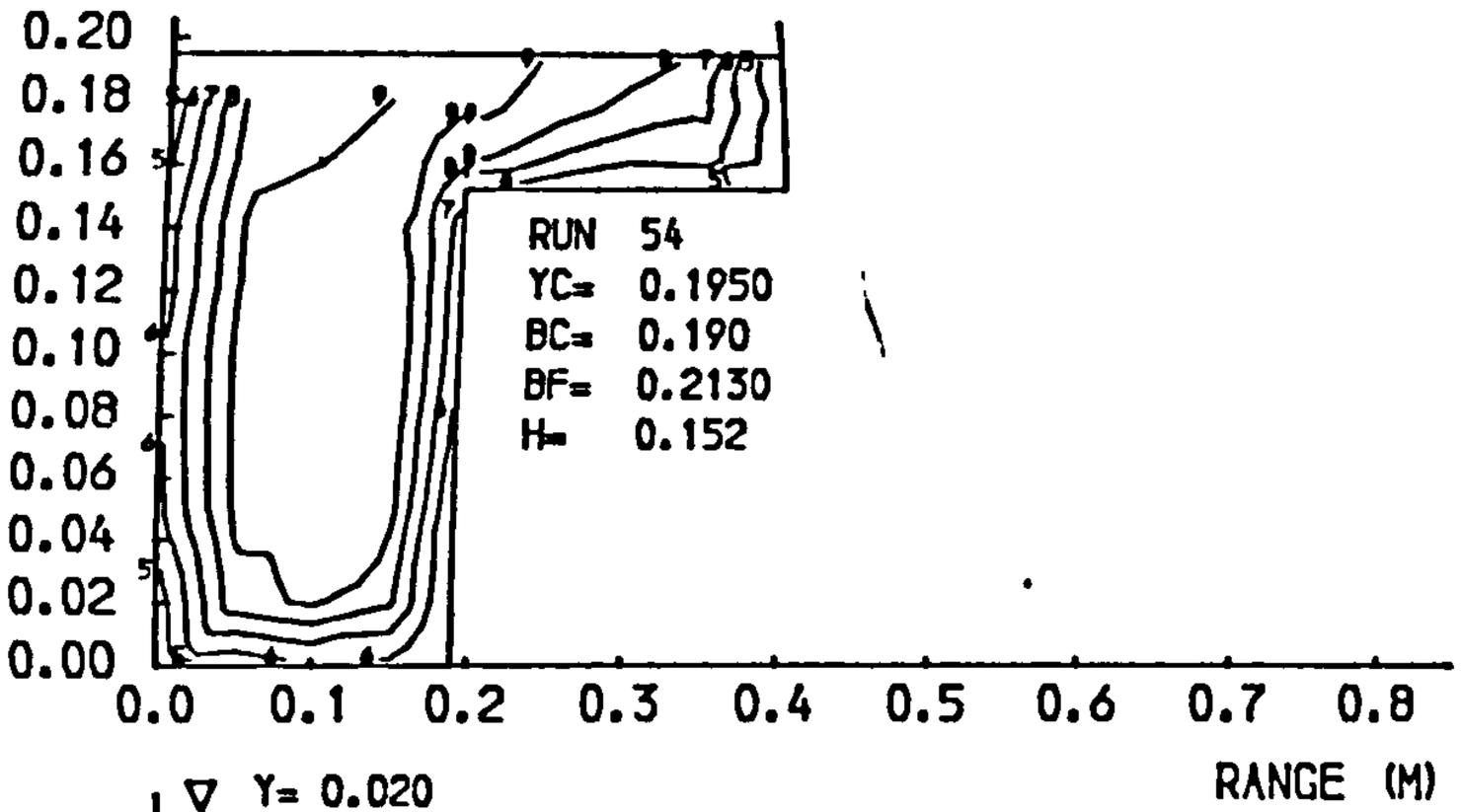

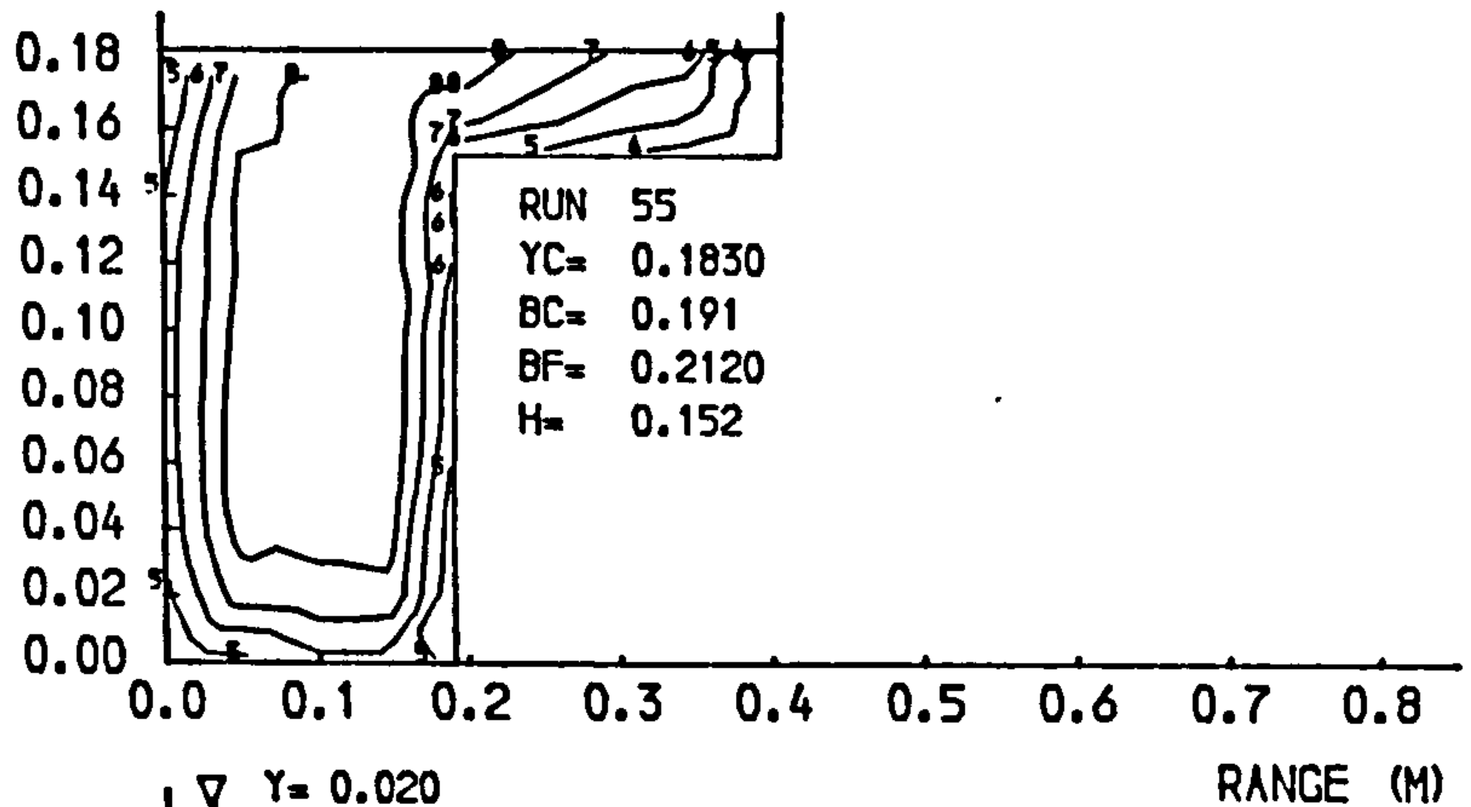

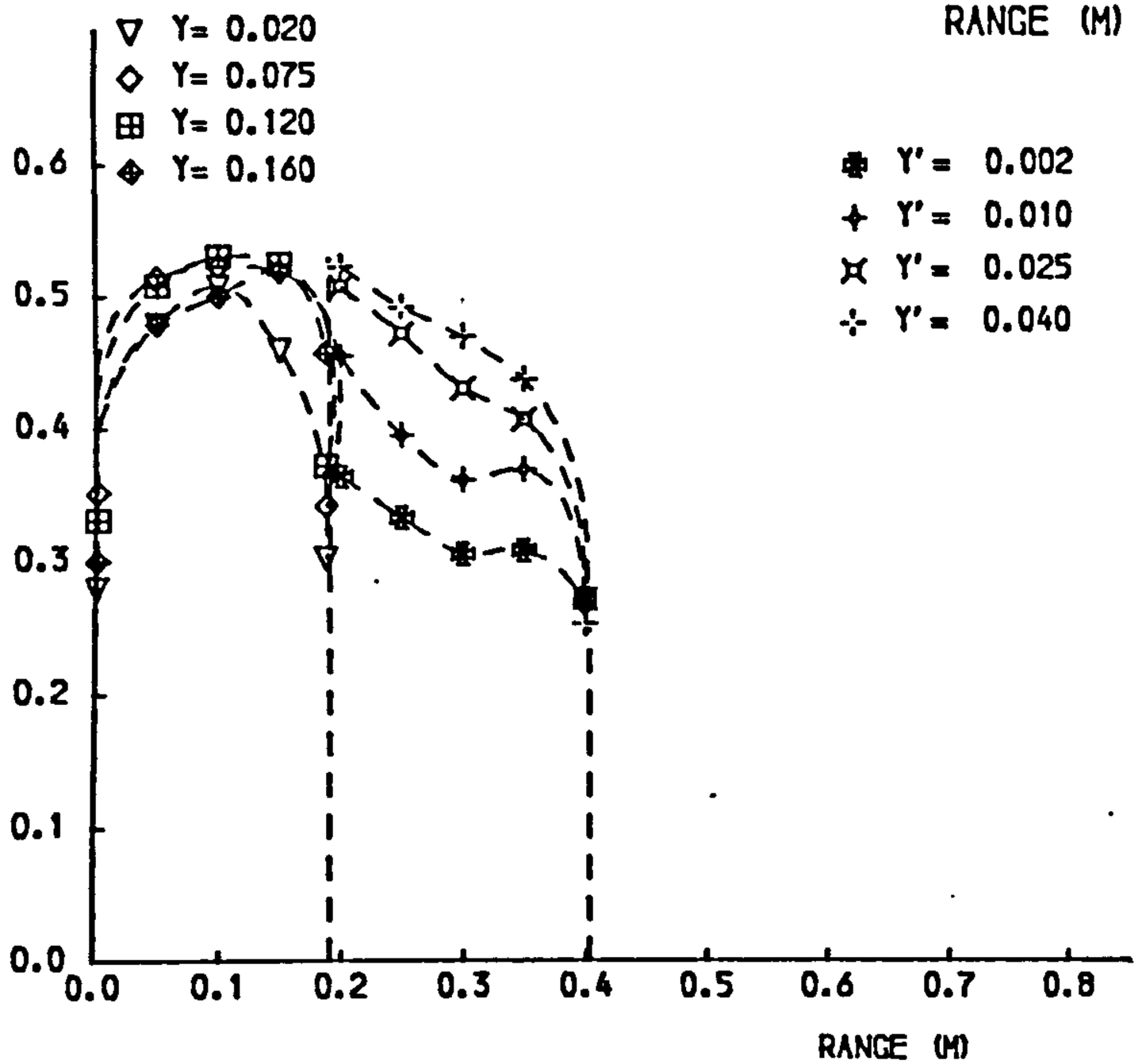

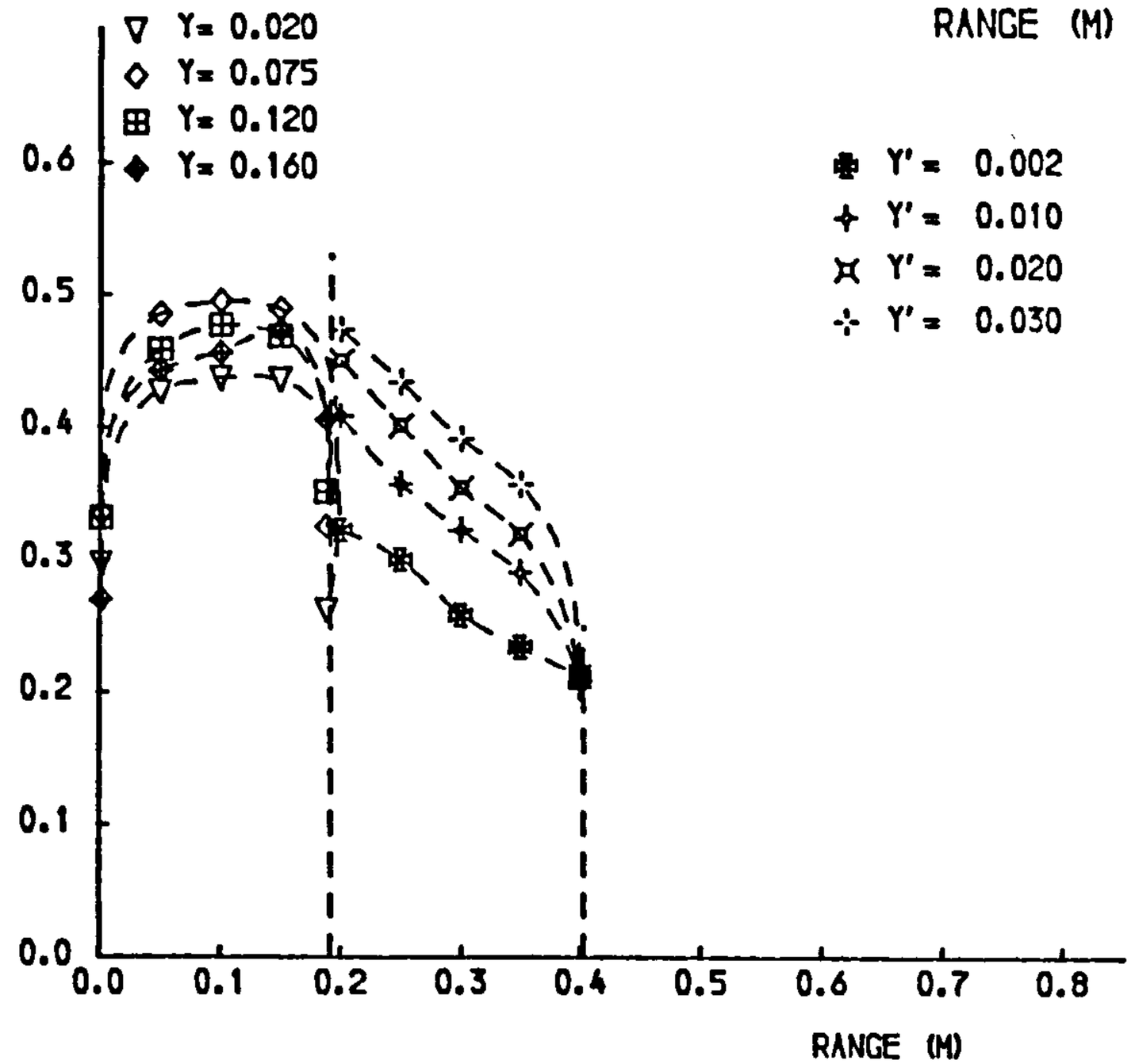

Fig 4·7 Isovels and lateral velocity profiles.

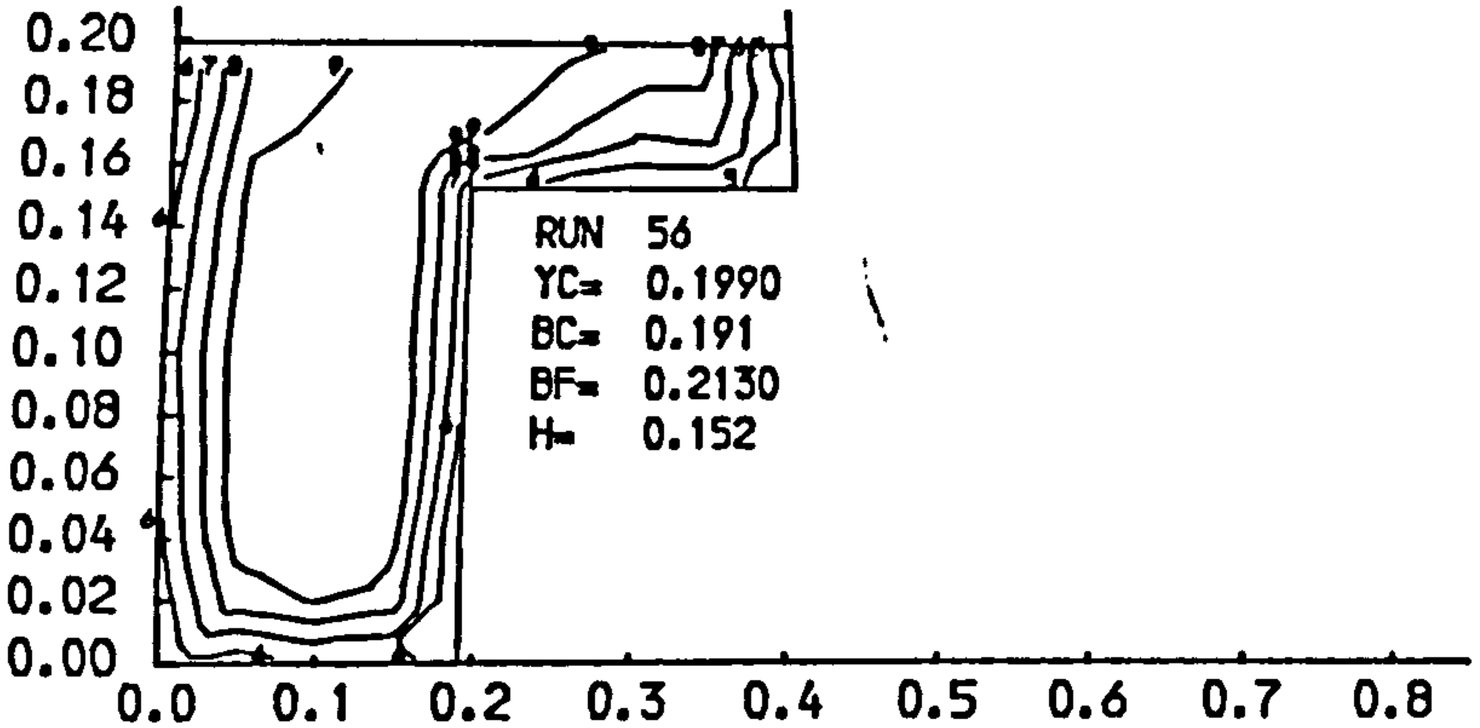

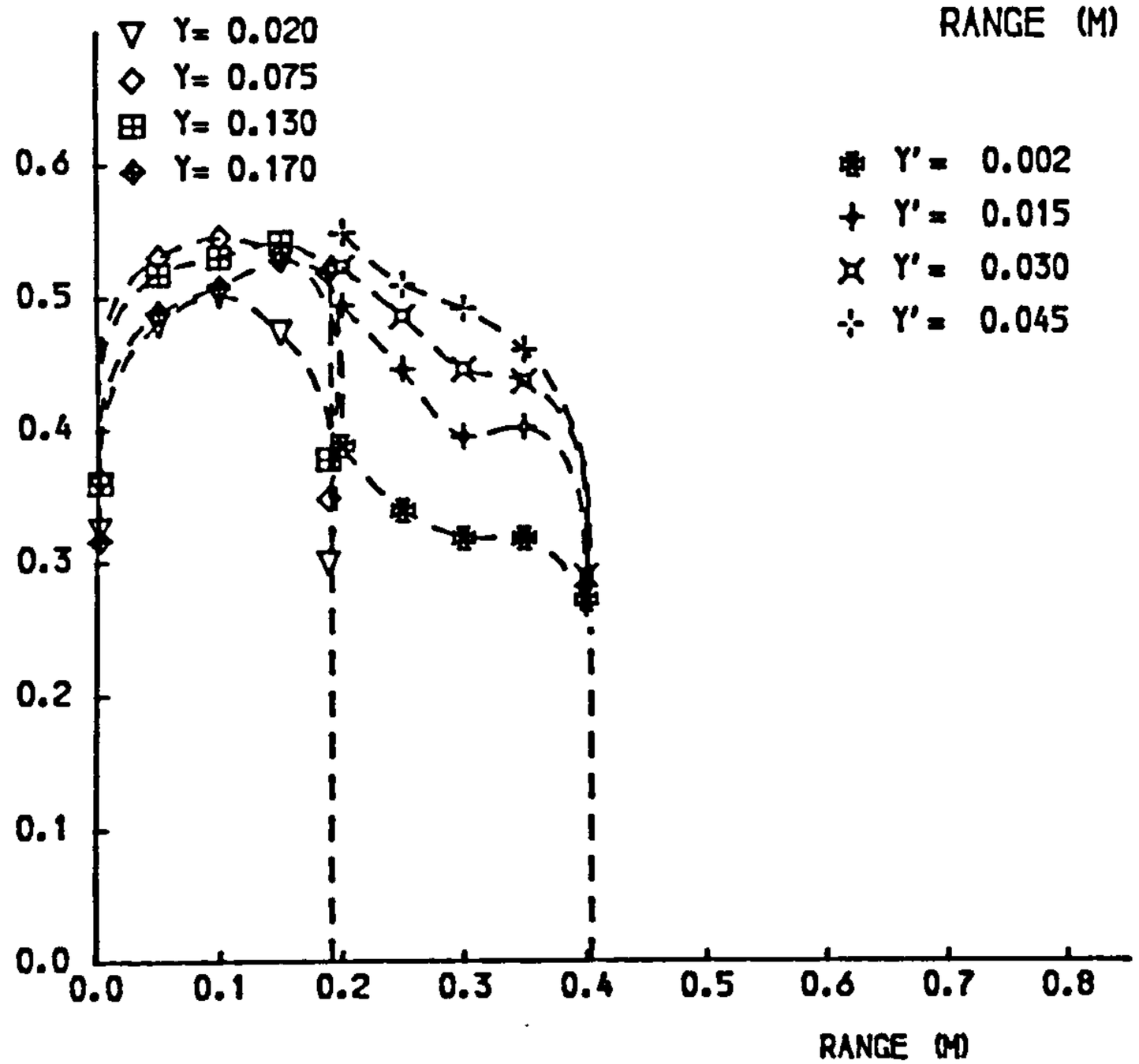

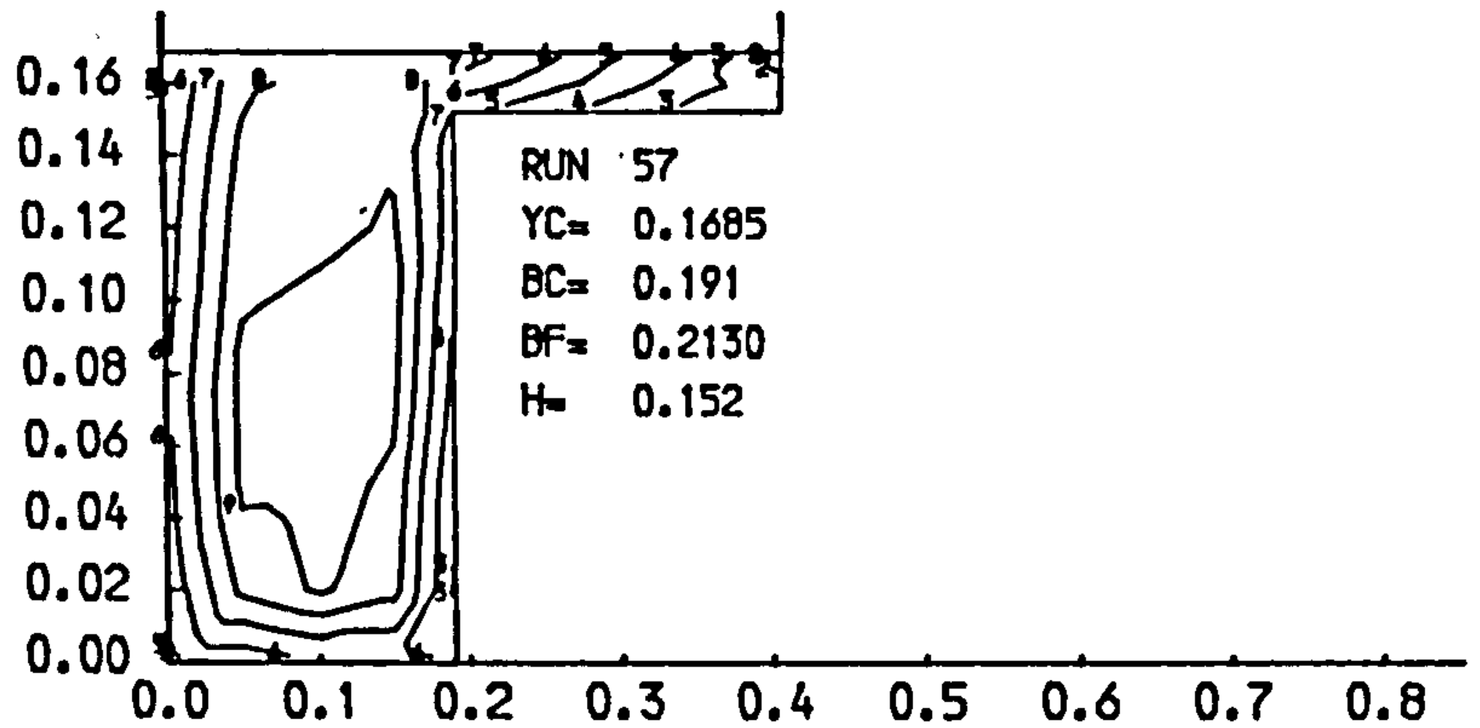

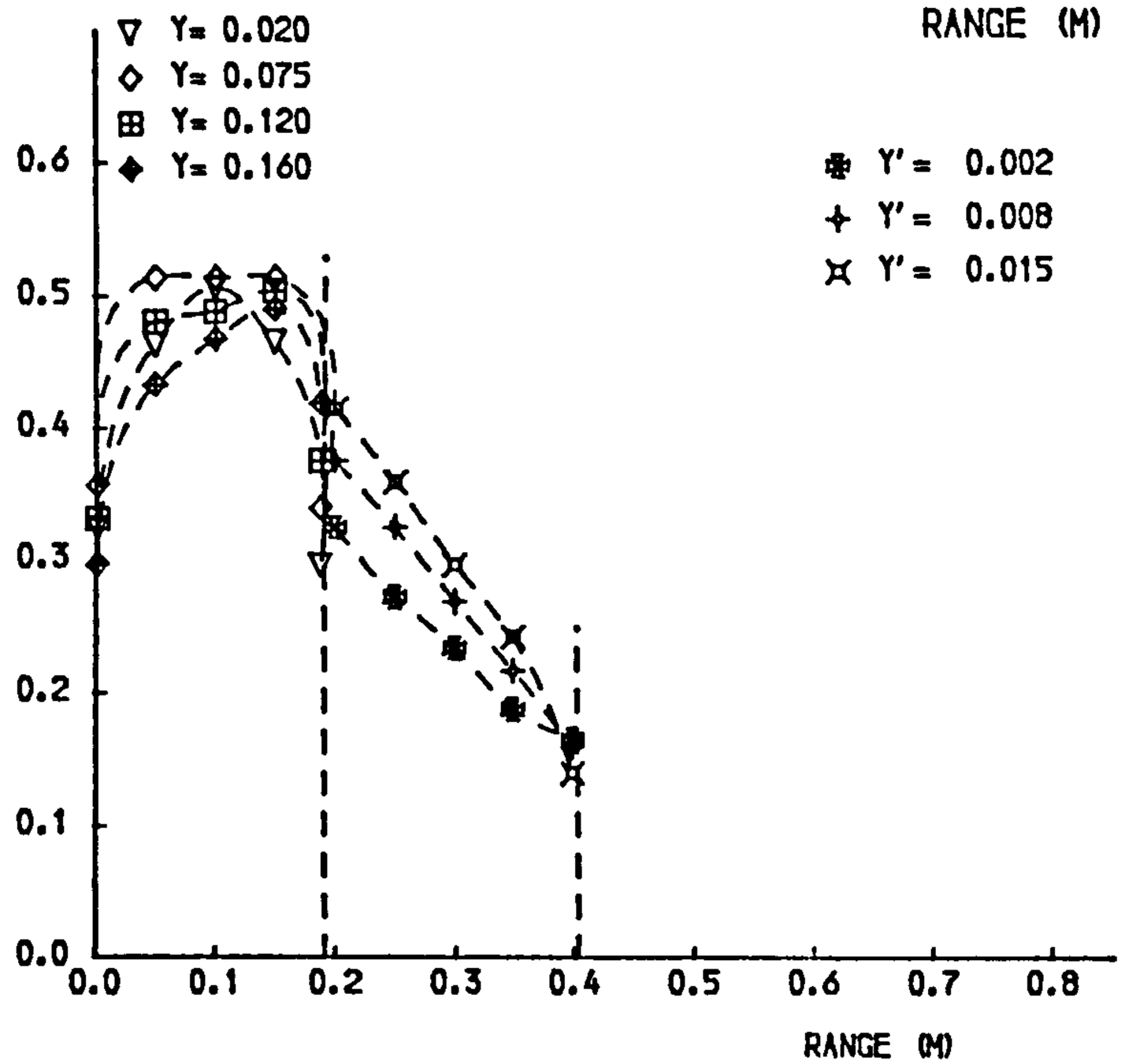

Fig 4·7 Isovels and lateral velocity profiles.

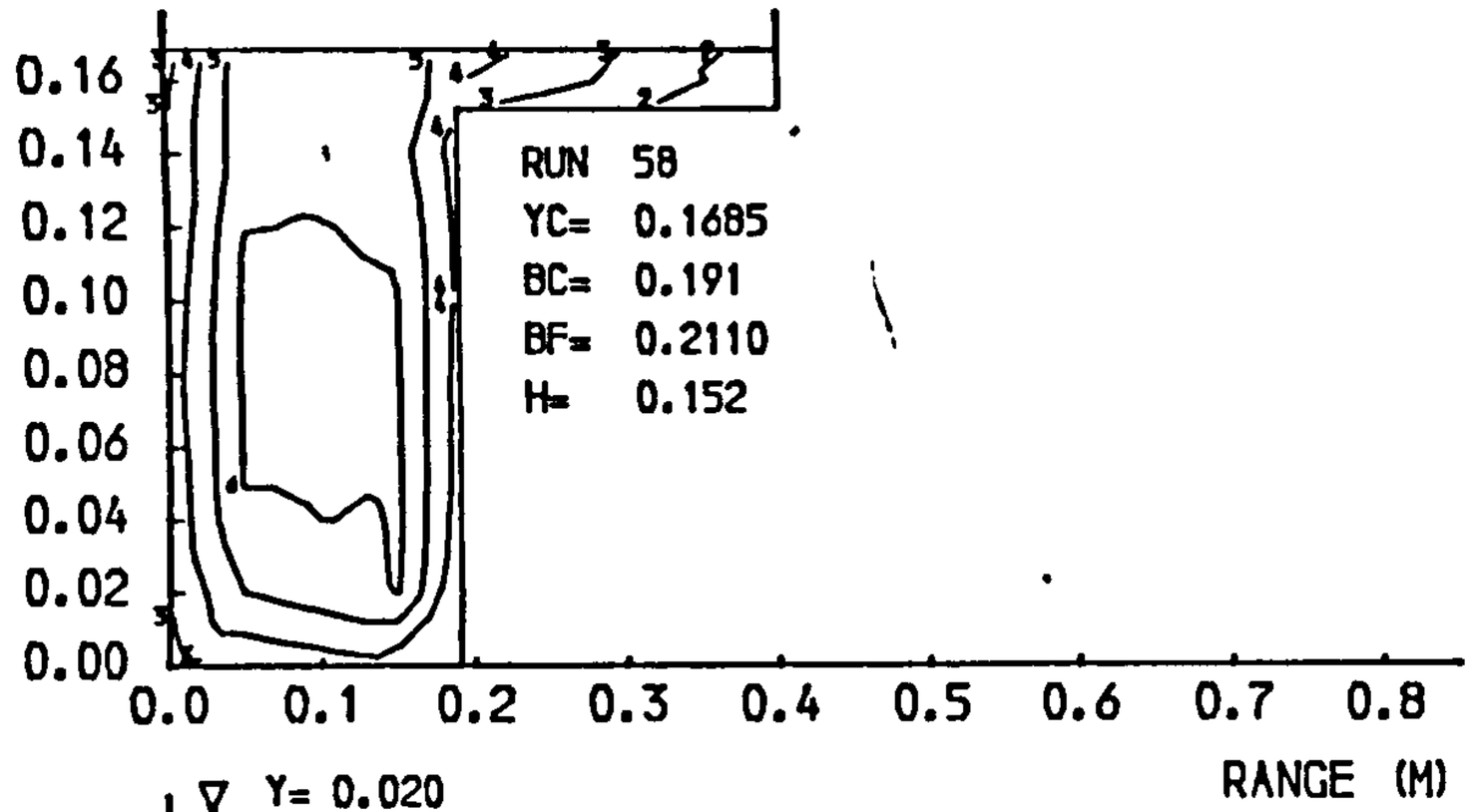

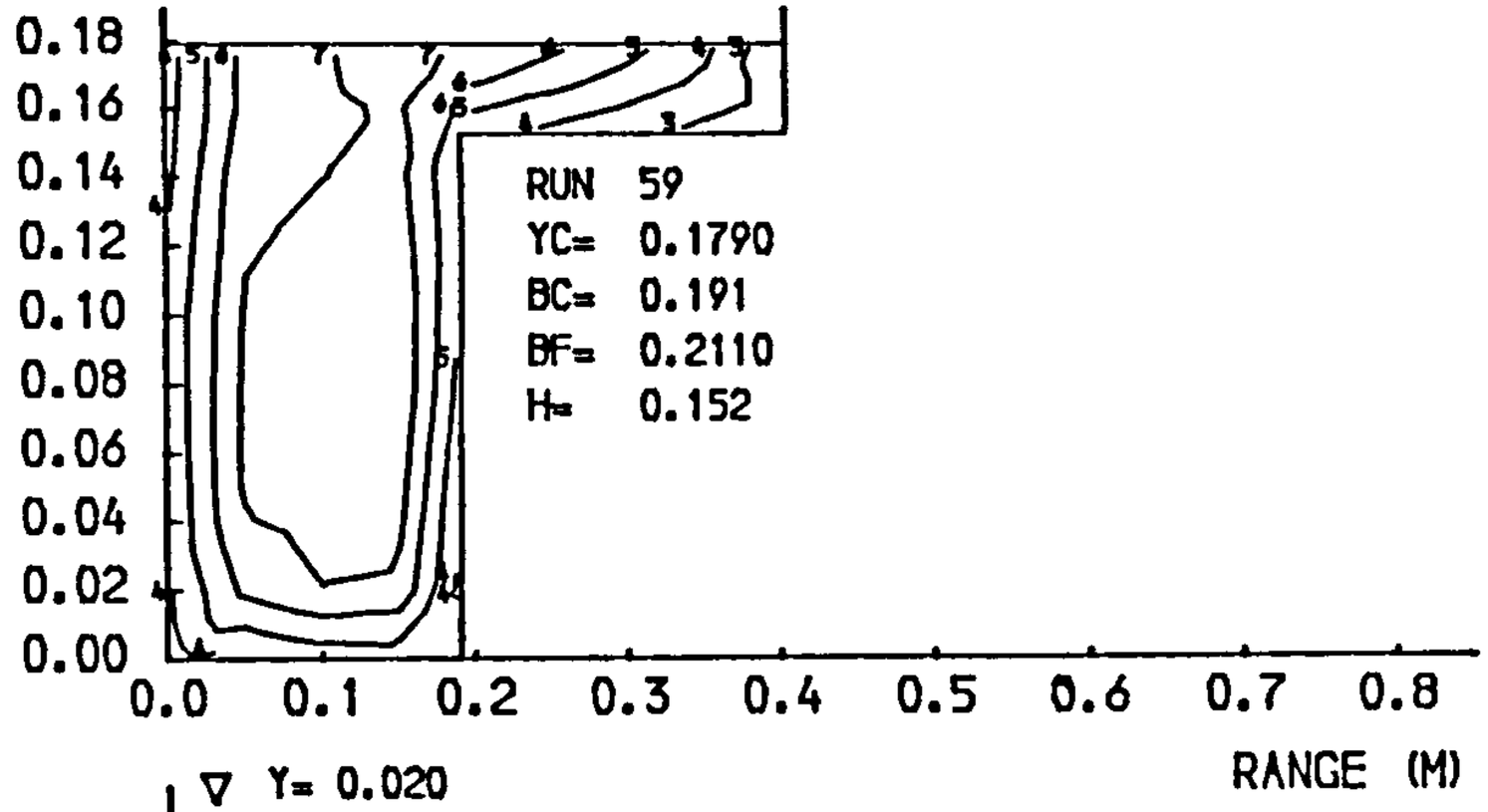

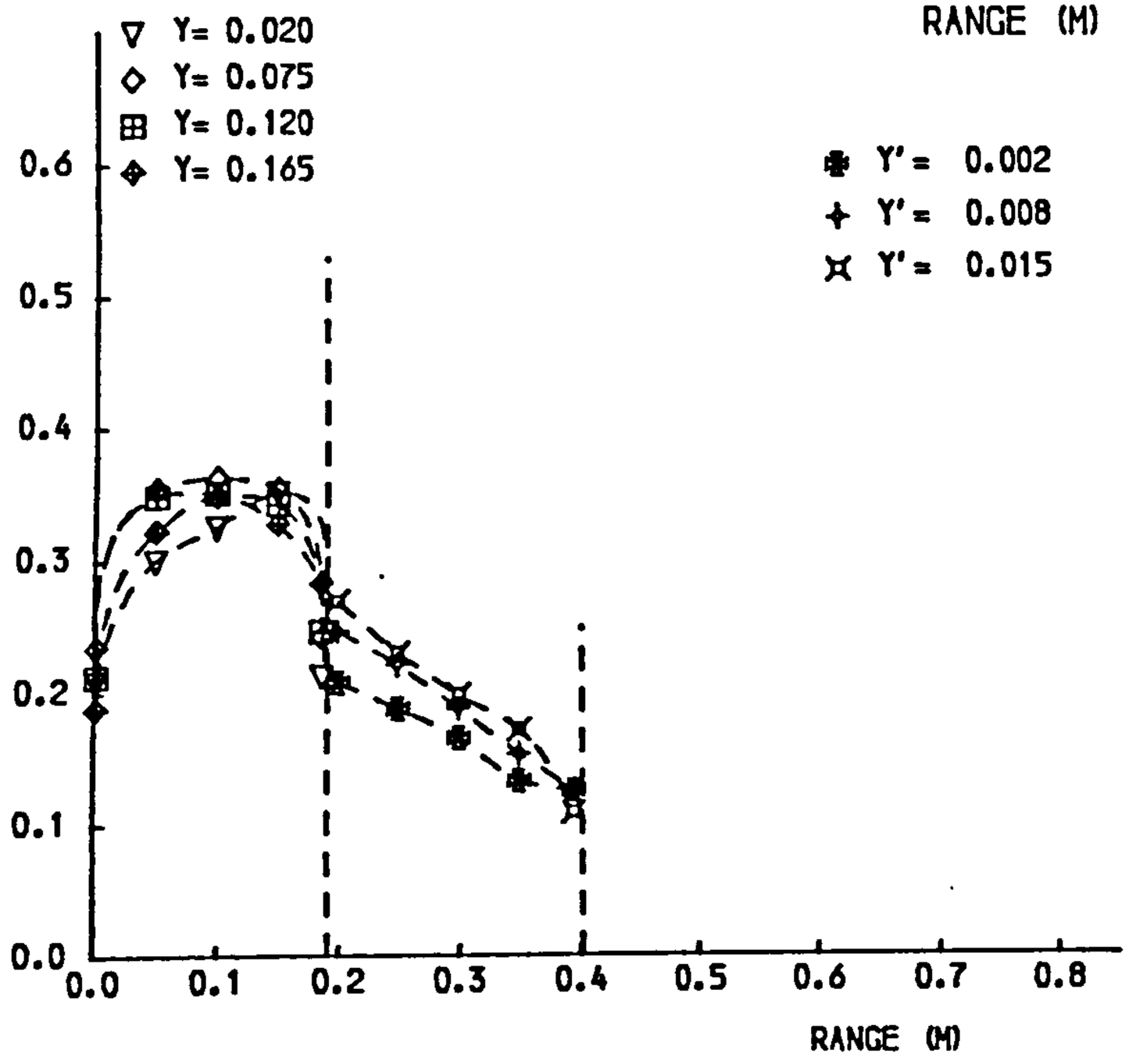

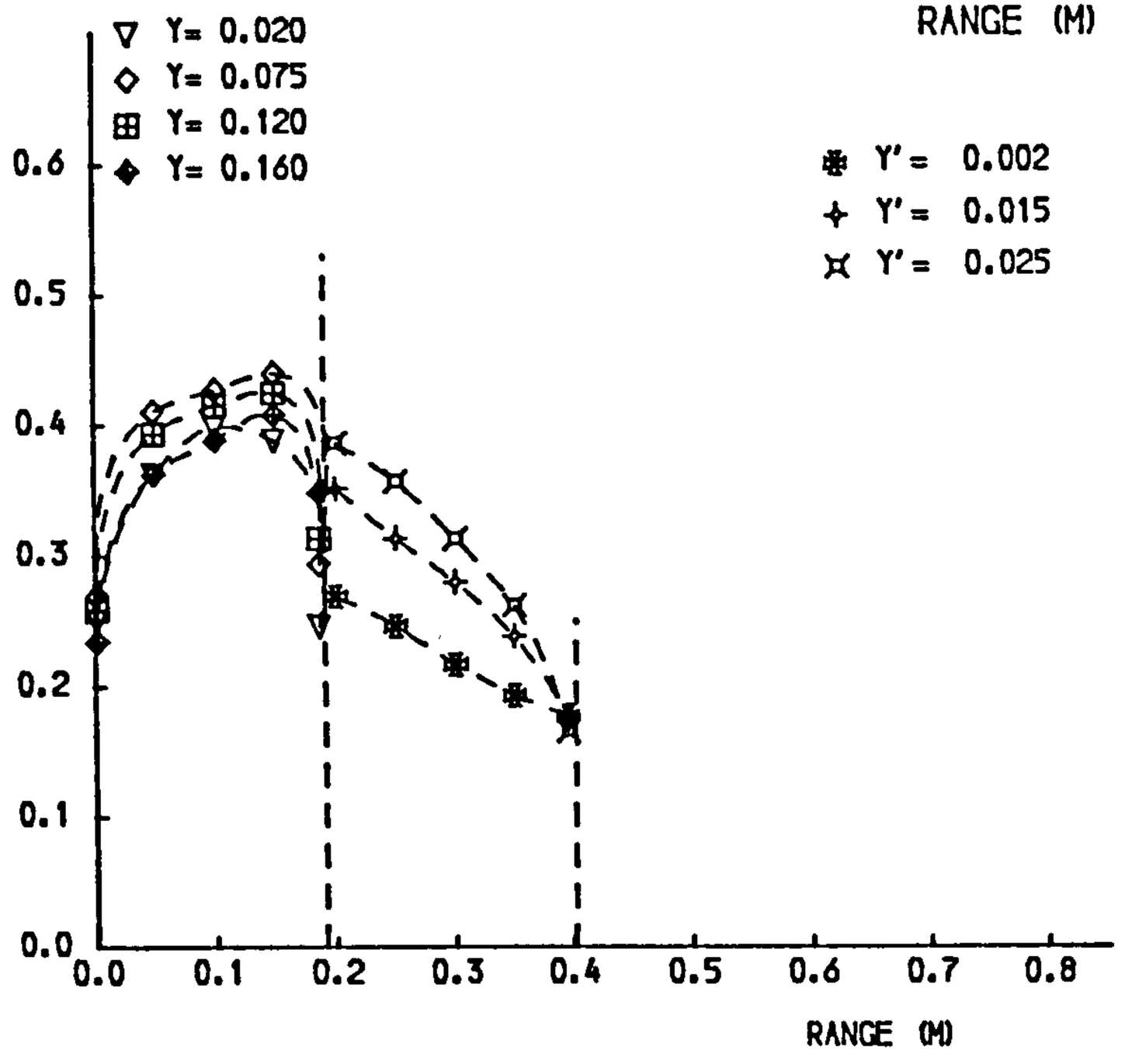

Fig 4·7 Isovels and lateral velocity profiles.

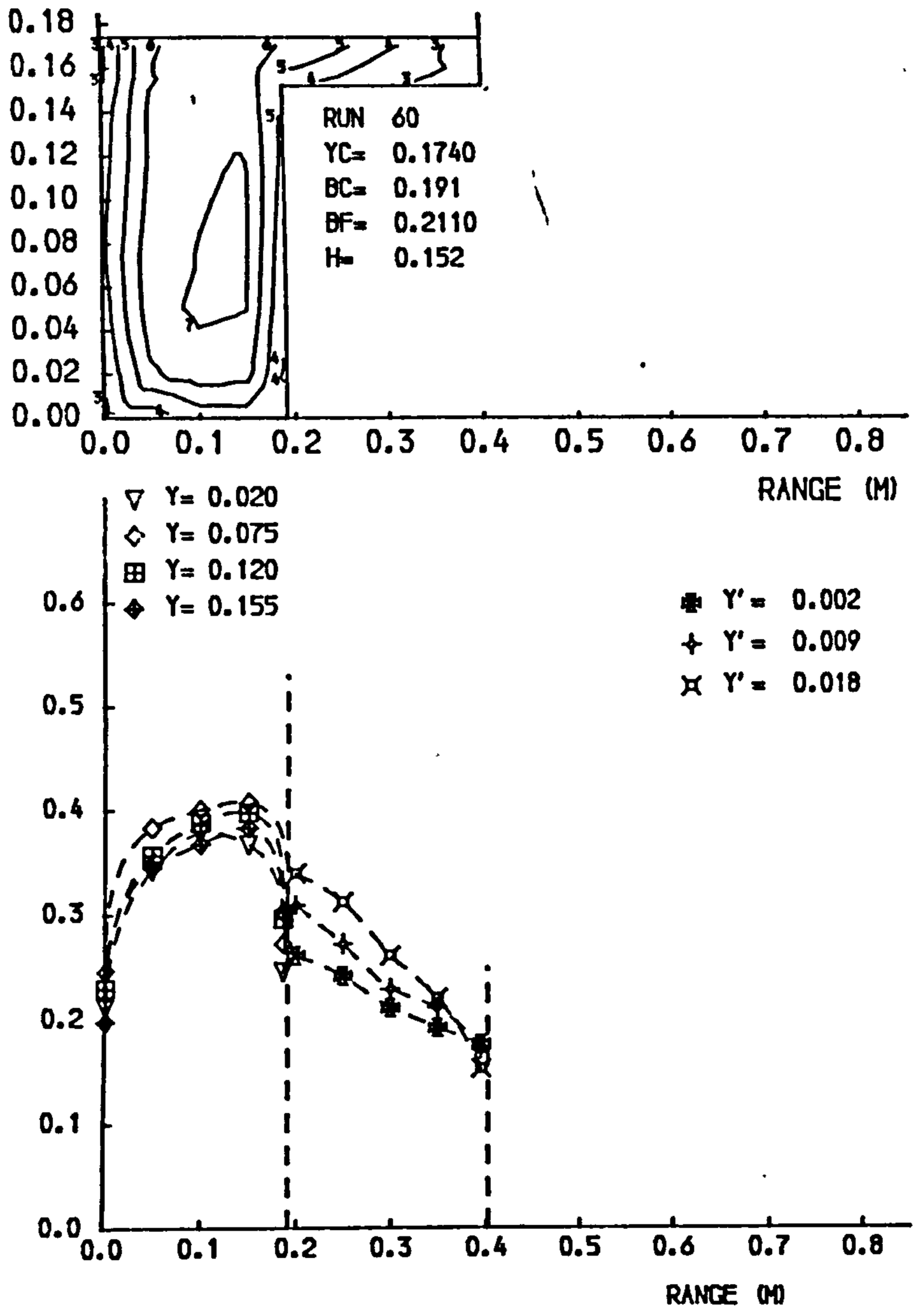

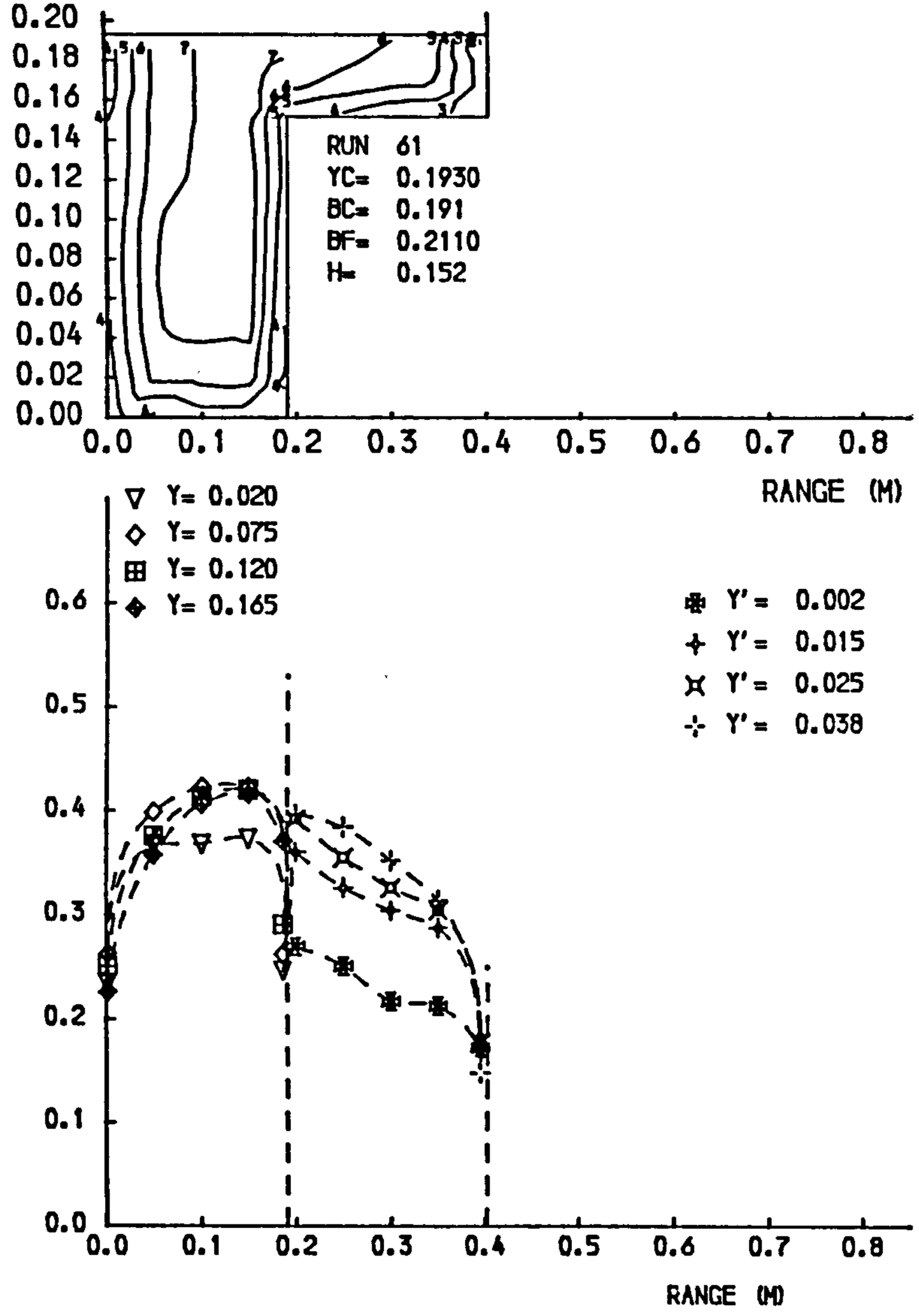

Fig4·7 Isovels and lateral velocity profiles.

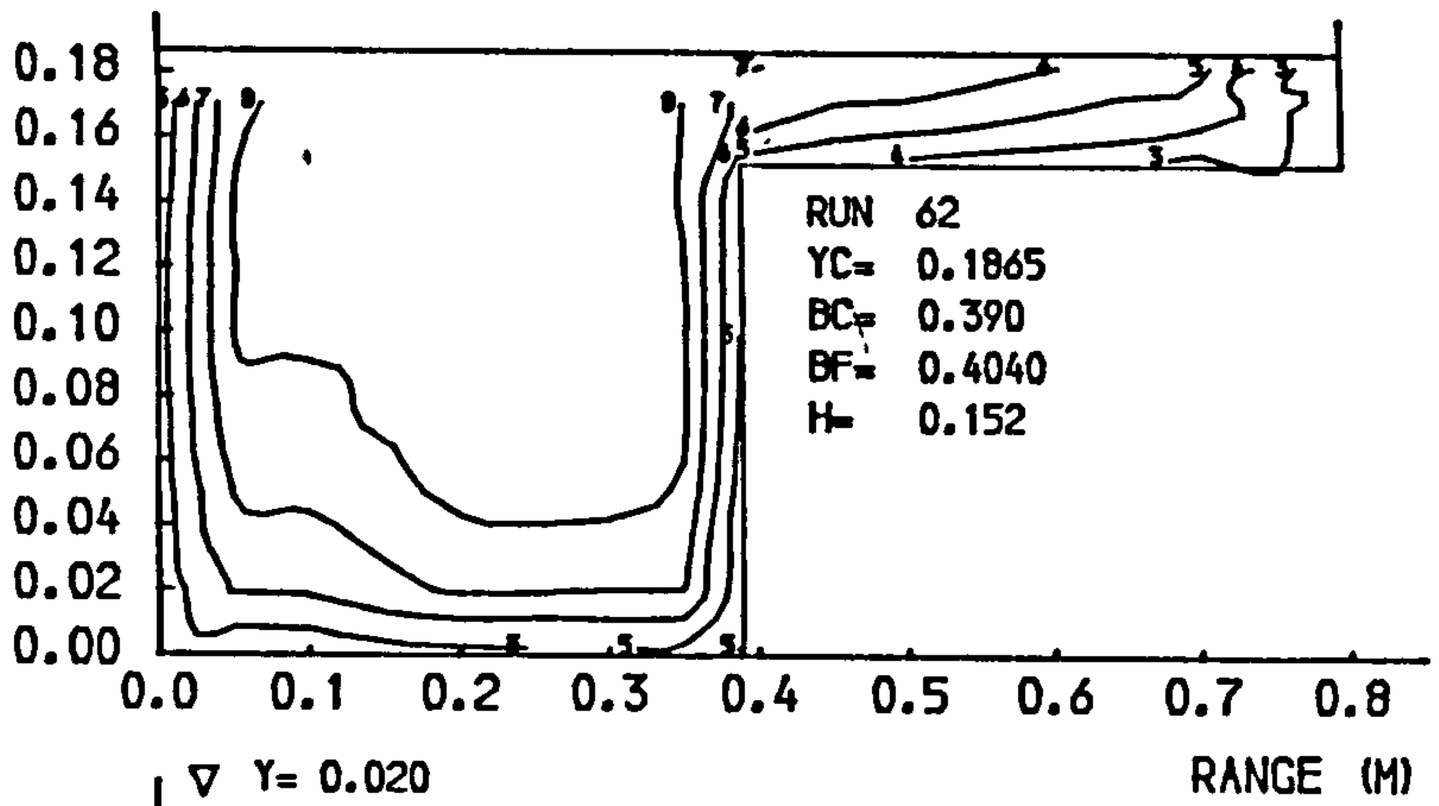

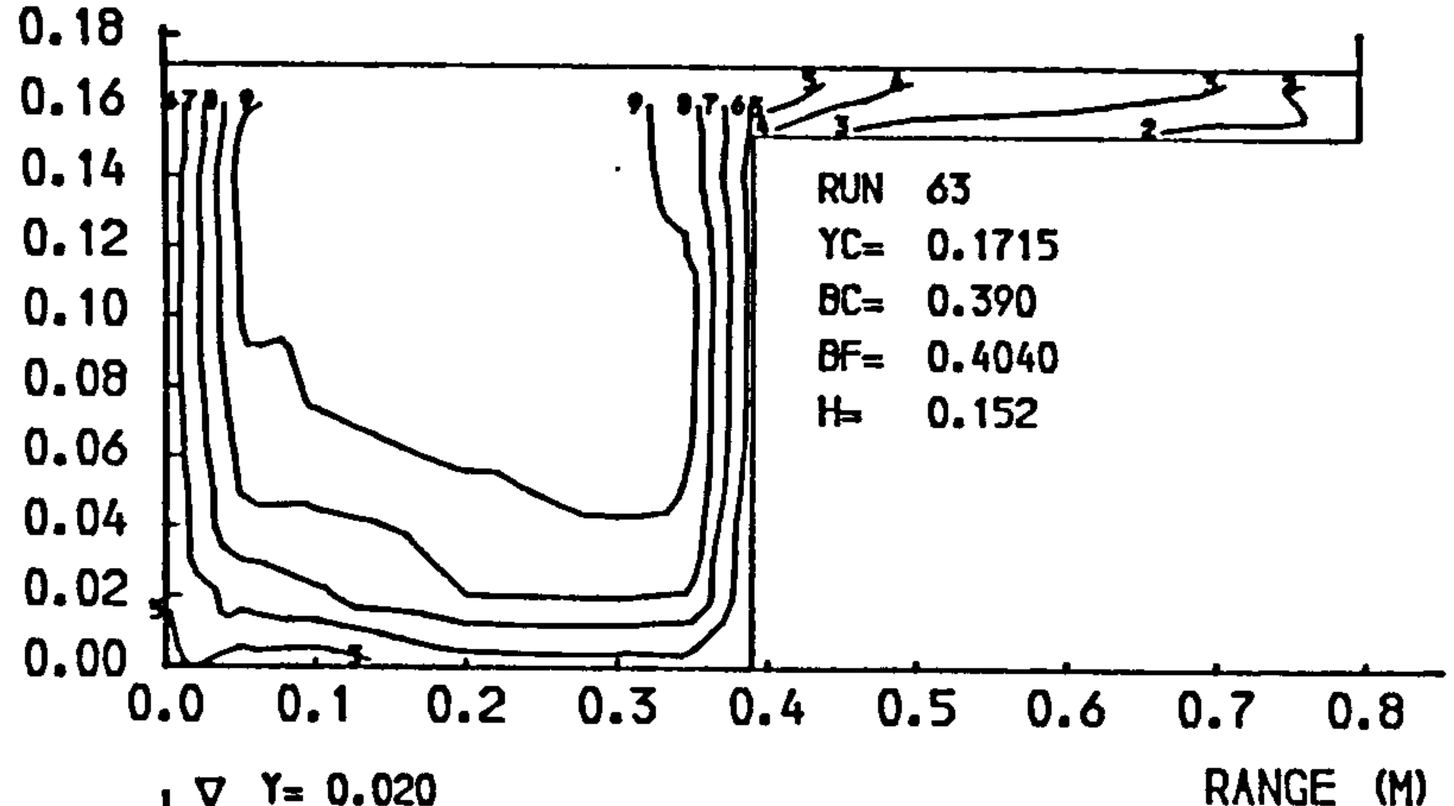

Fig 4·7 Isovels and lateral velocity profiles.

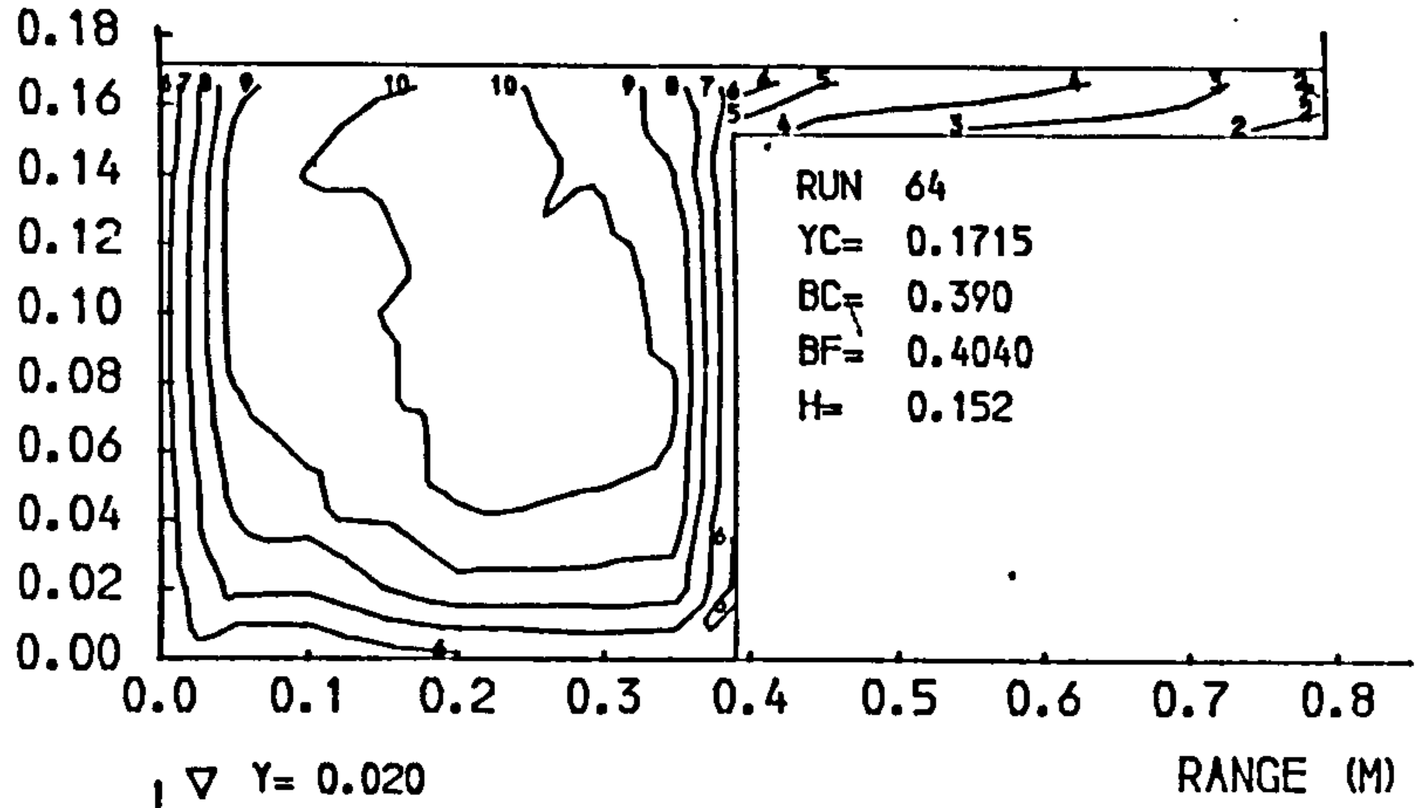

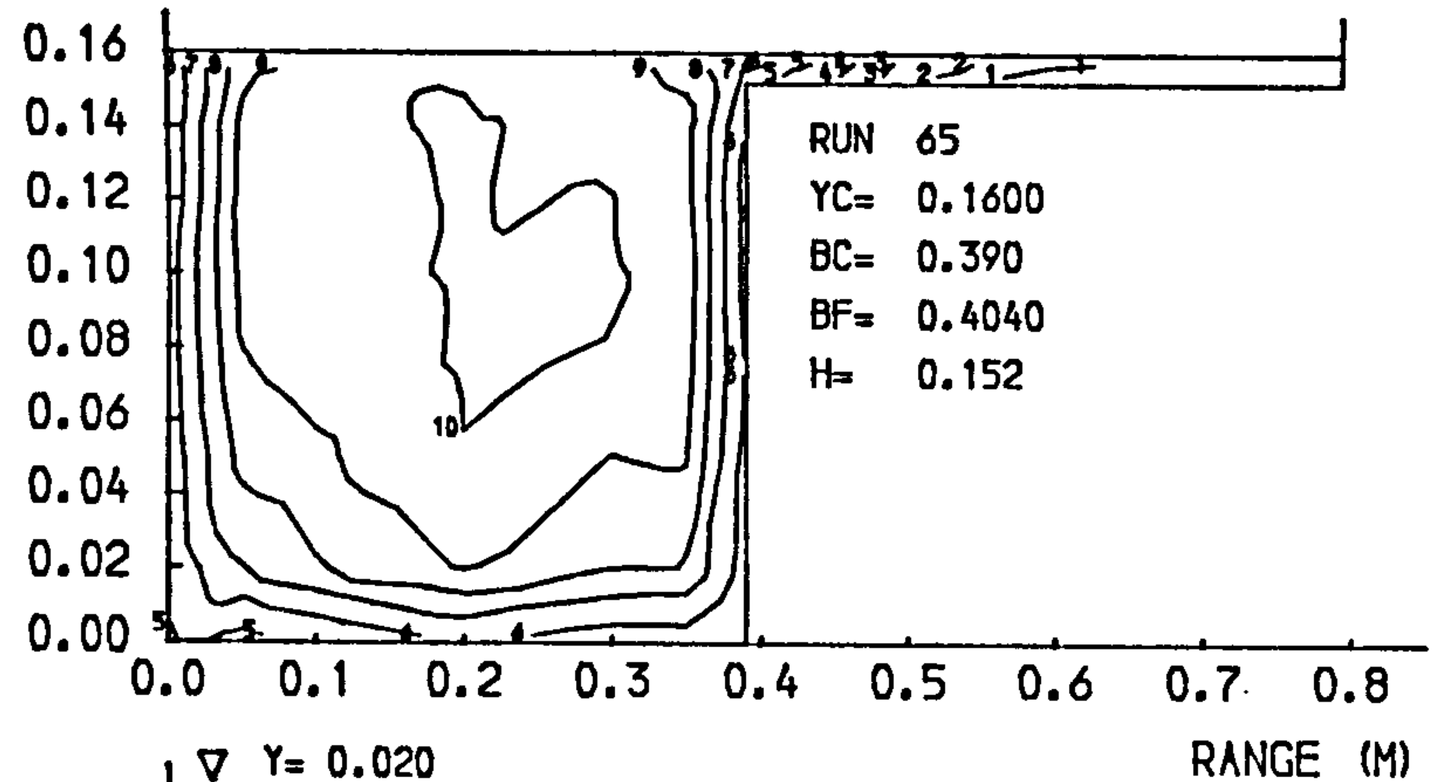

Fig 4·7 Isovels and lateral velocity profiles.

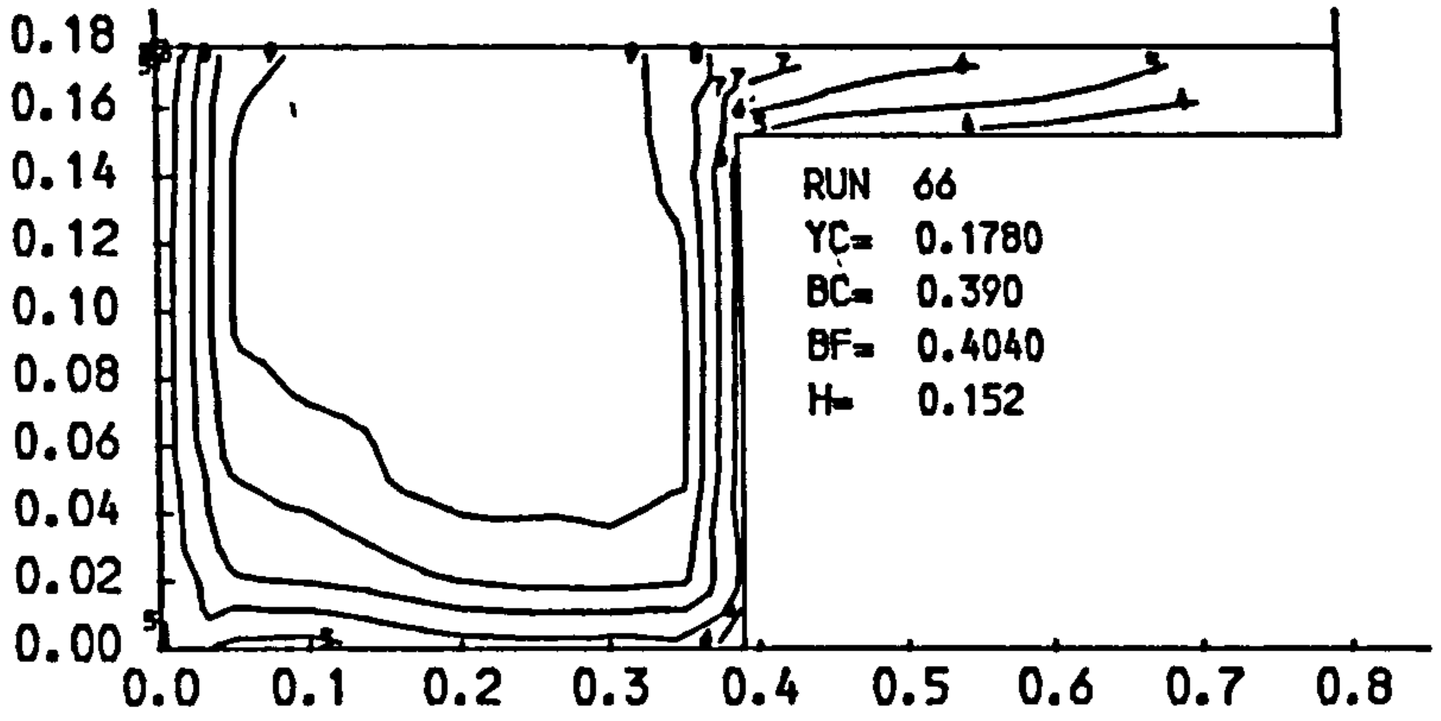

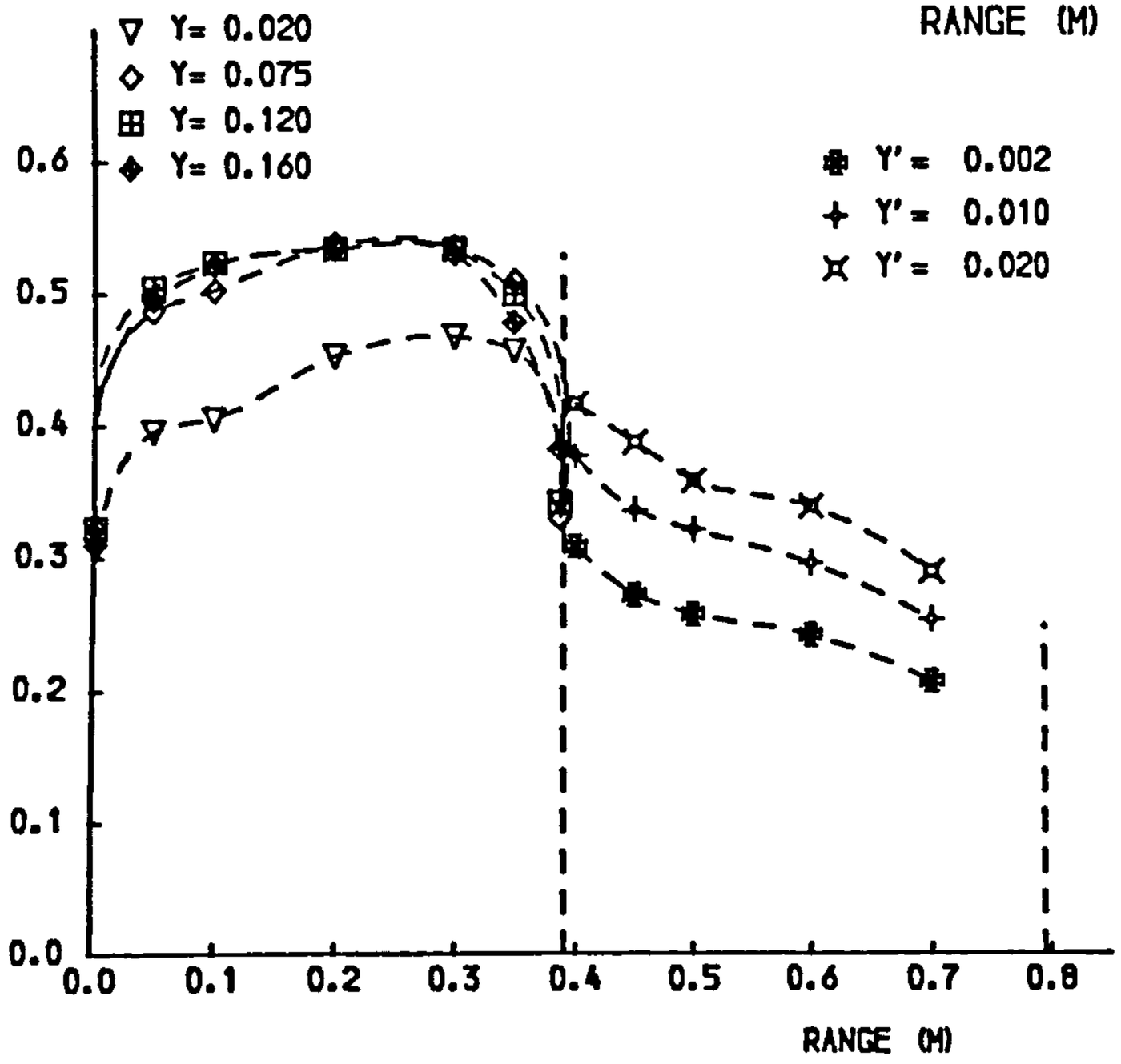

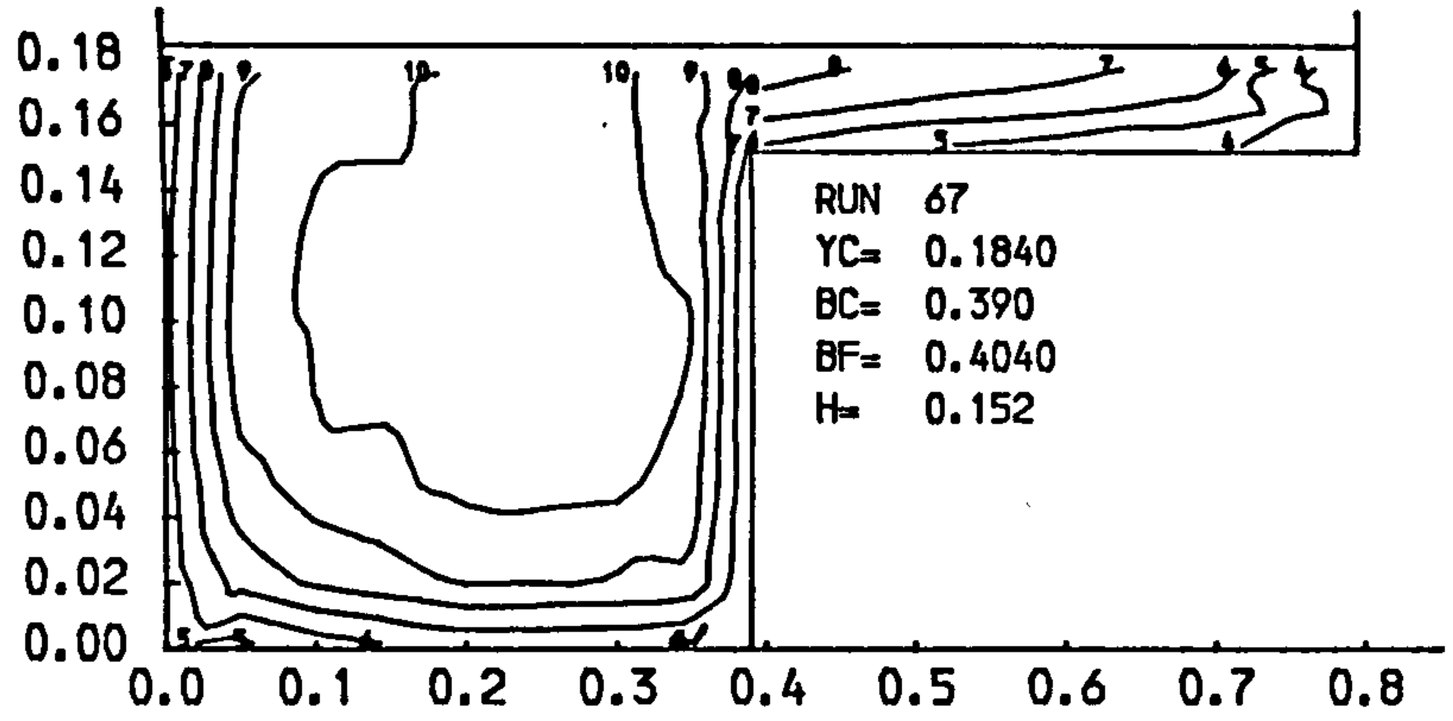

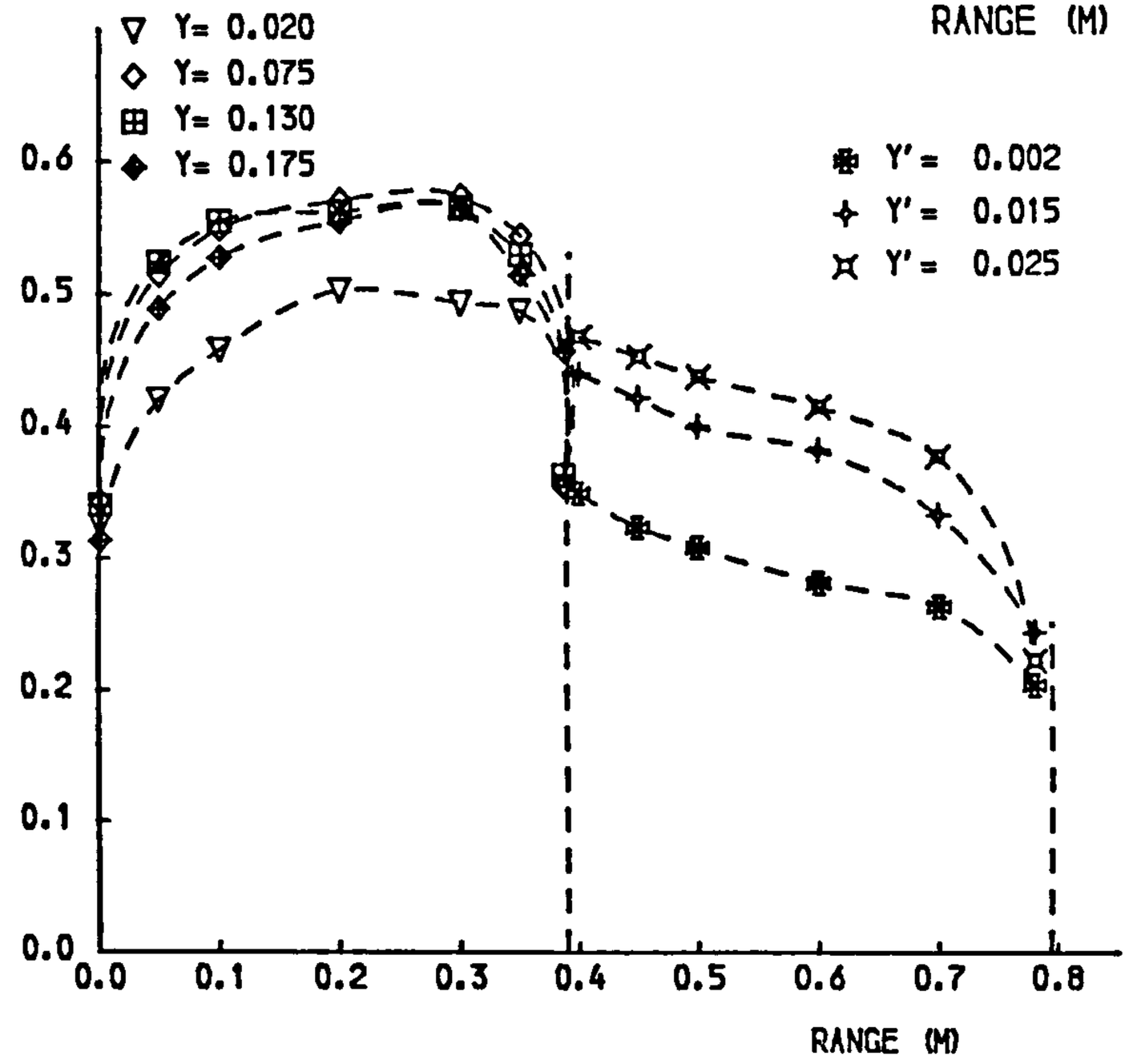

Fig 4-7 Isovels and lateral velocity profiles.

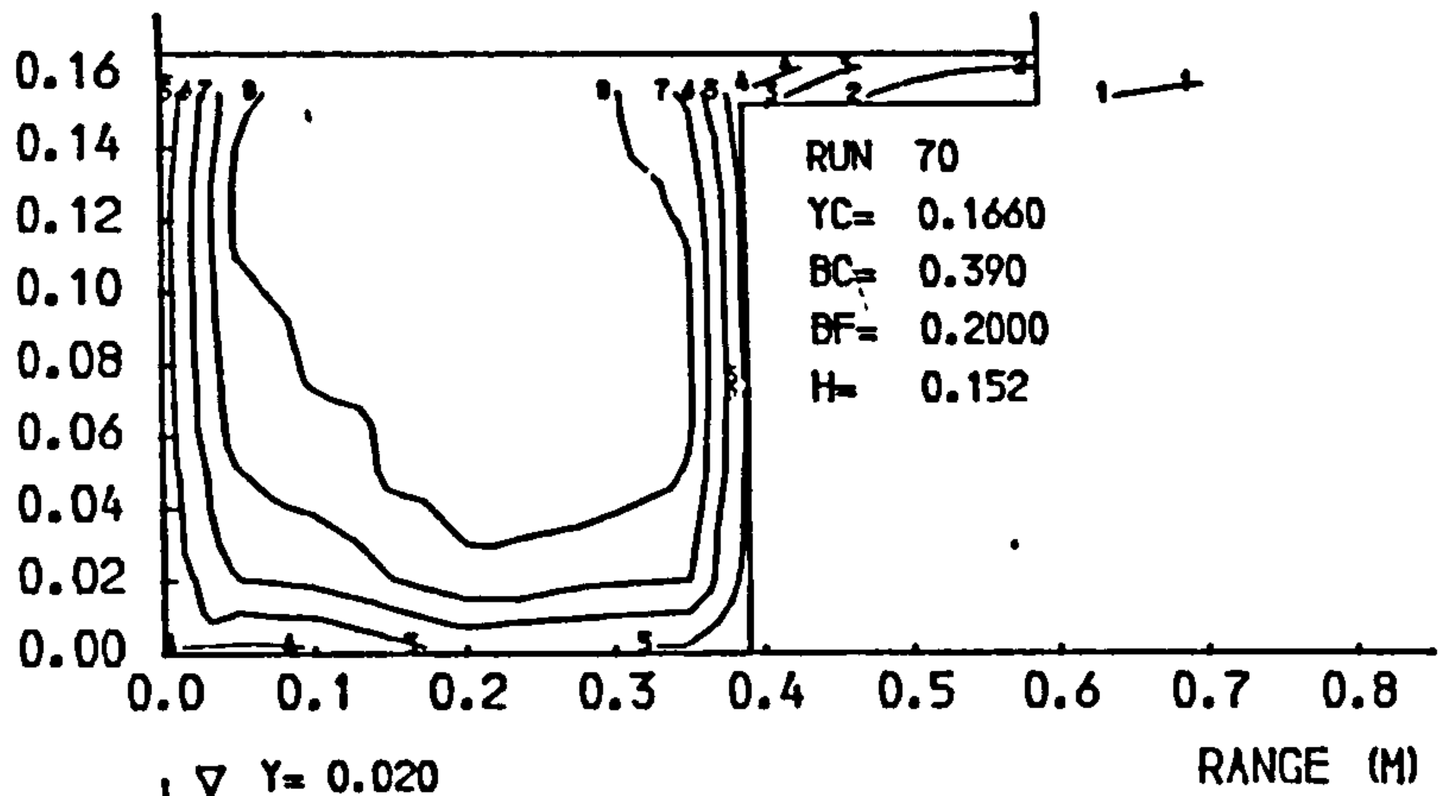

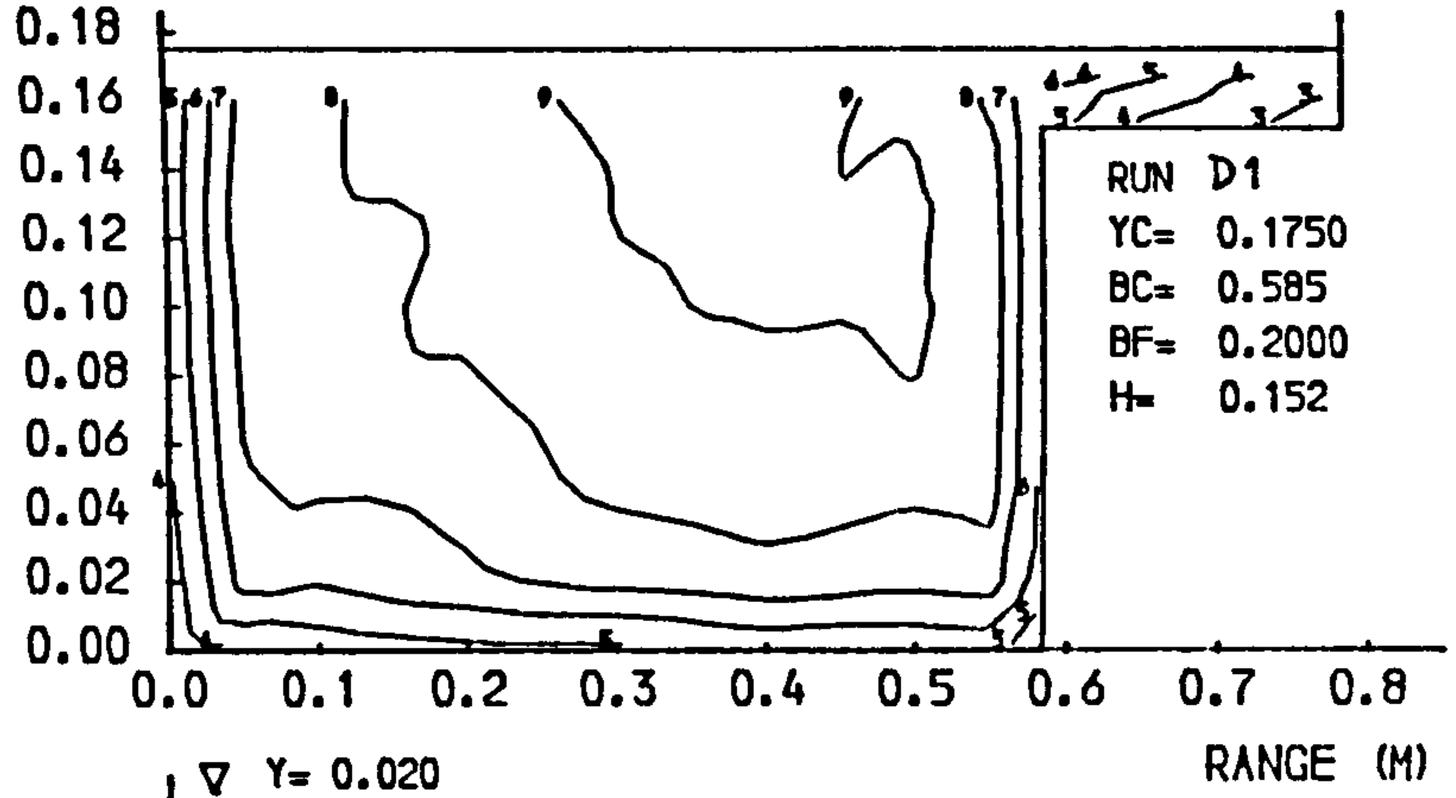

Fig 4·7 Isovels and lateral velocity profiles.

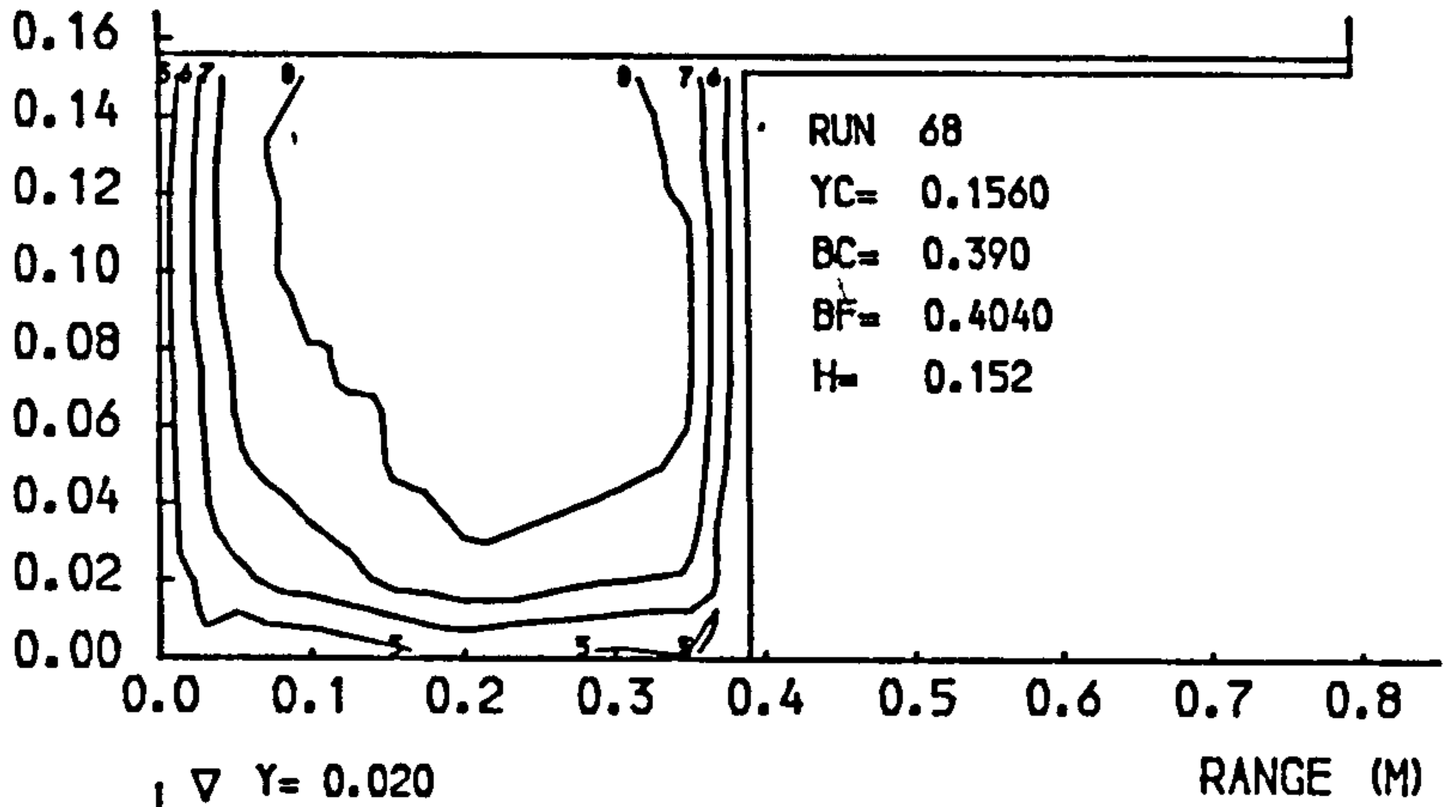

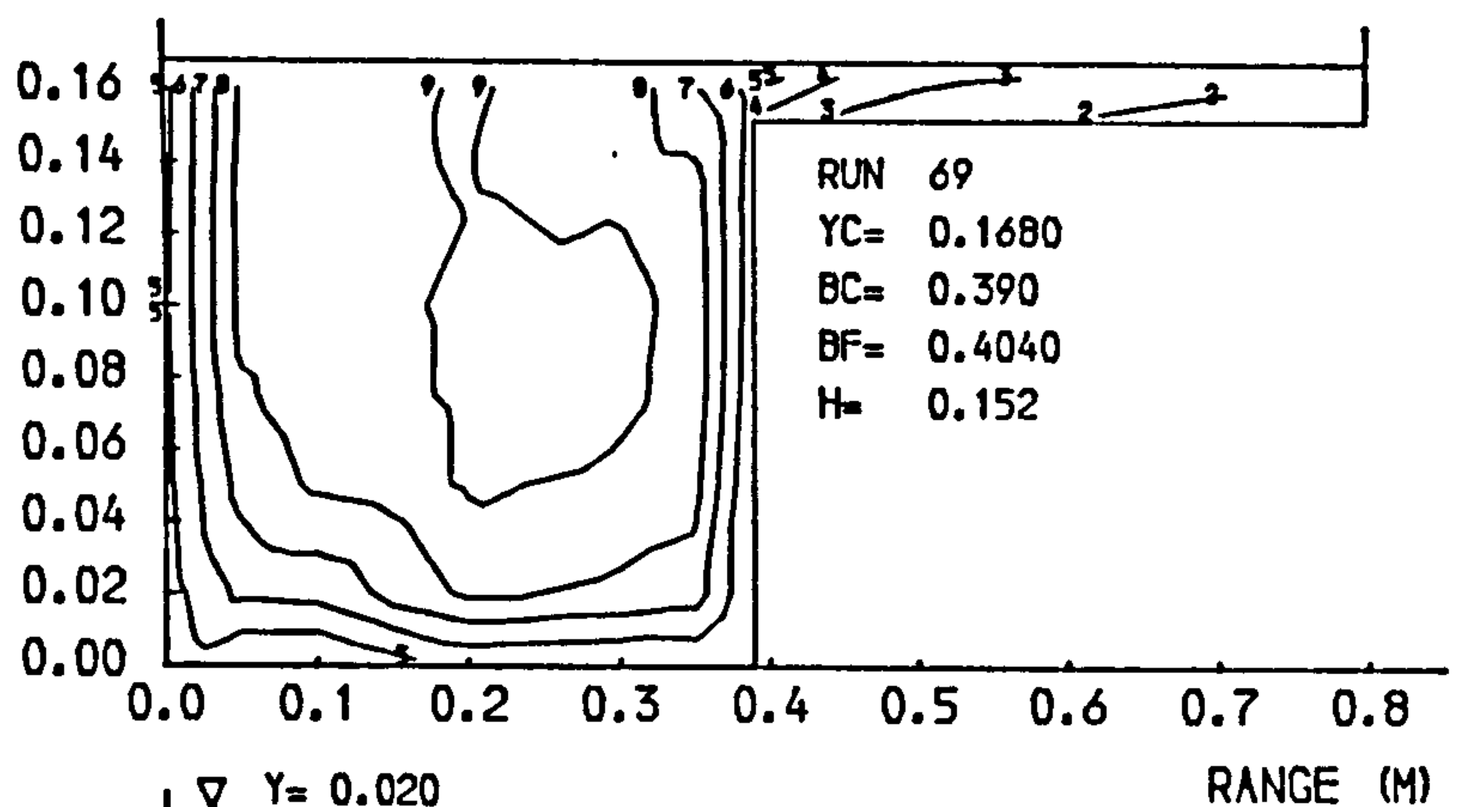

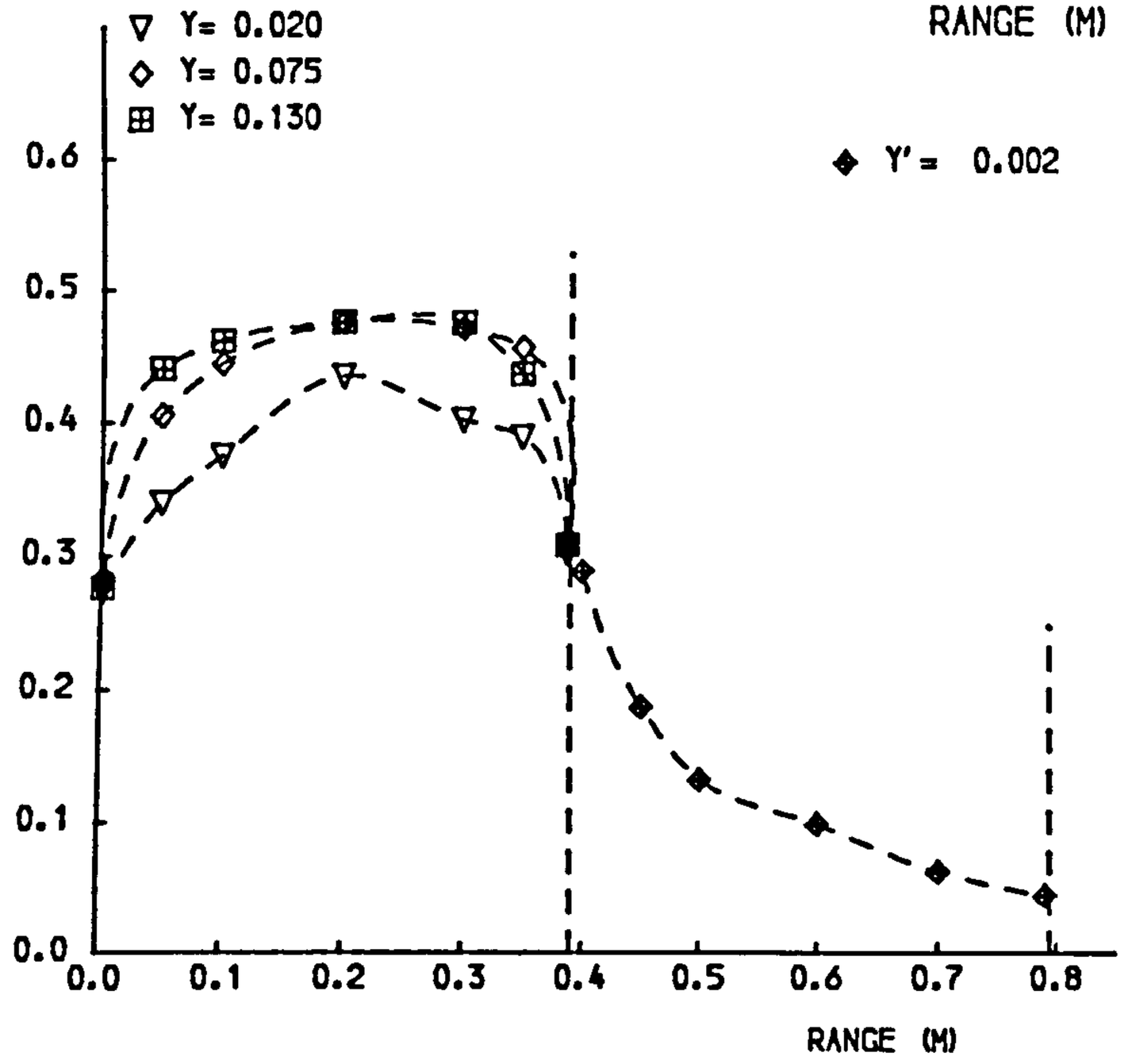

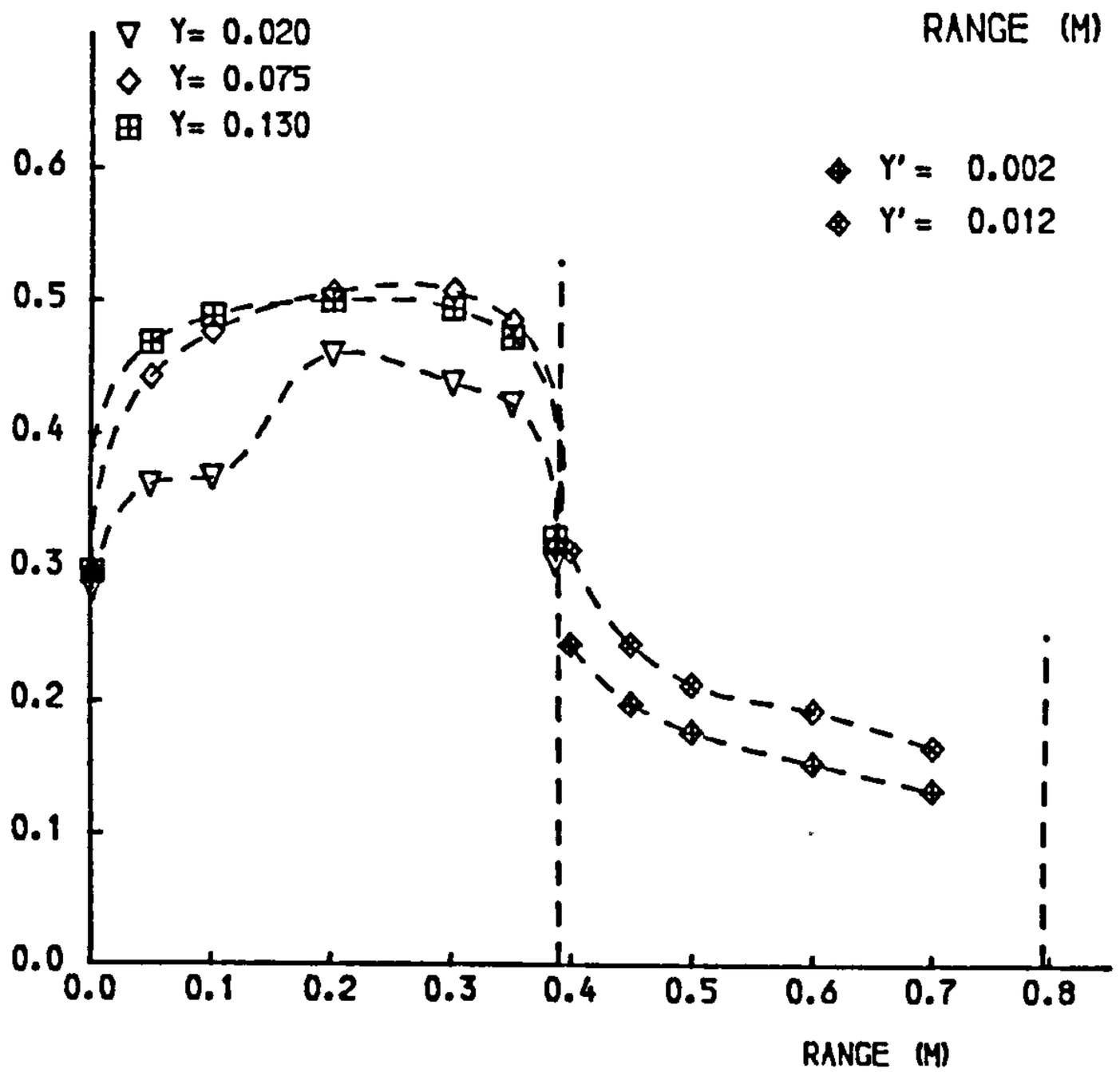

Fig 4·7 Isovels and lateral velocity profiles.

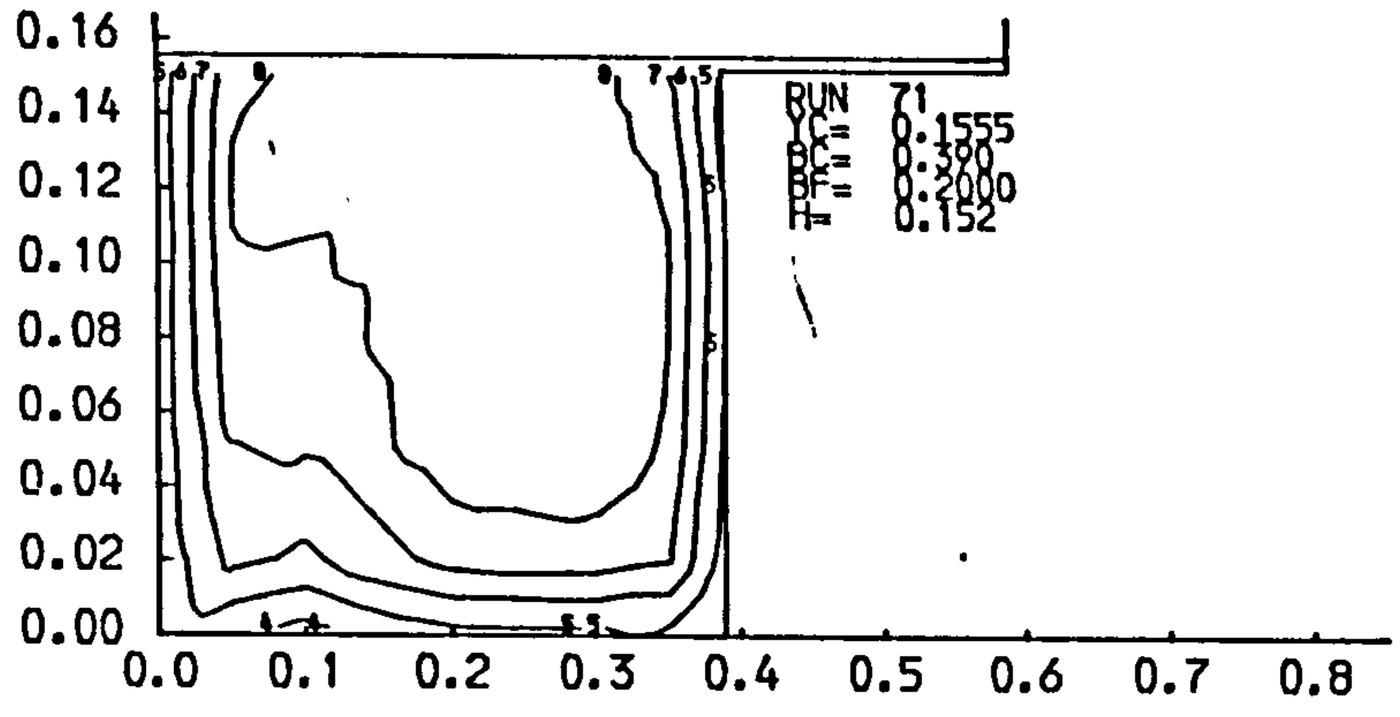

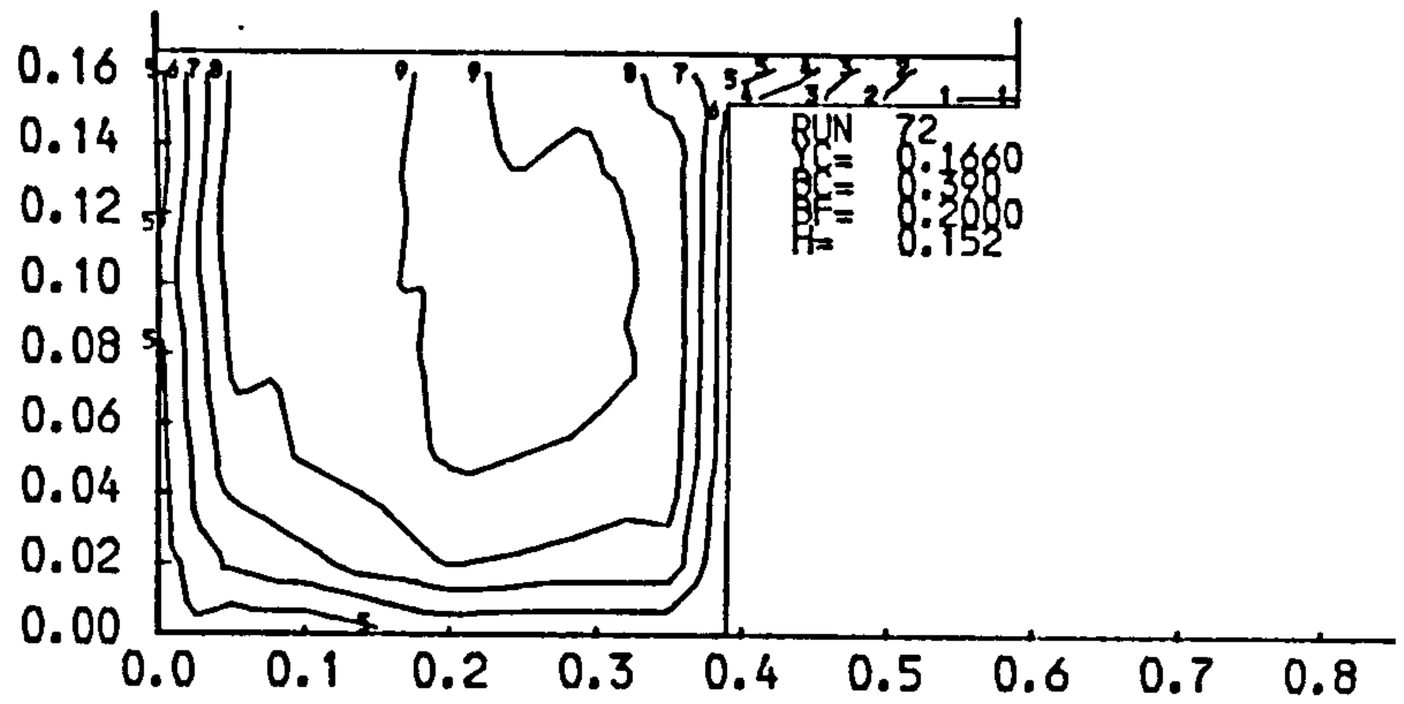

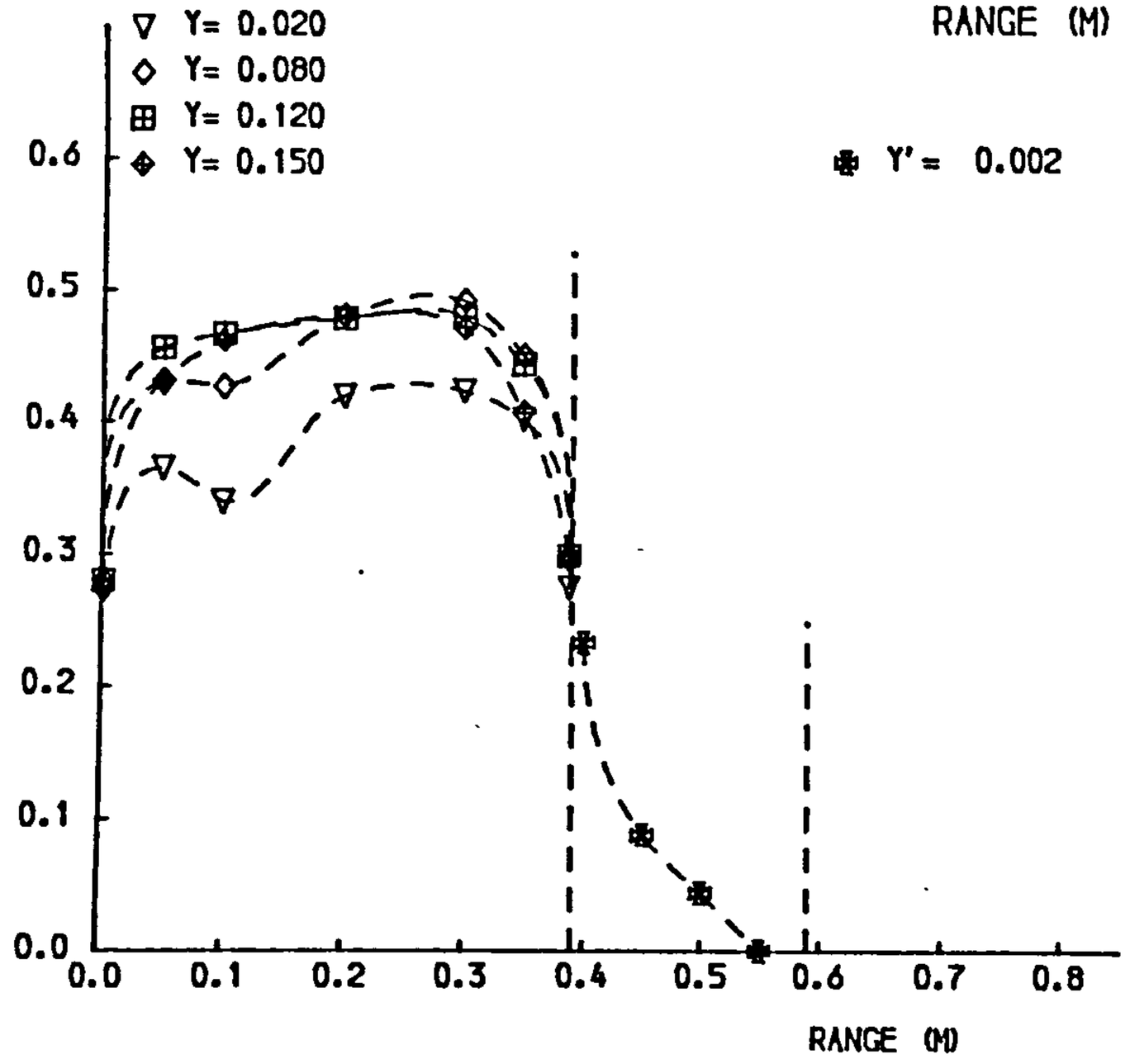

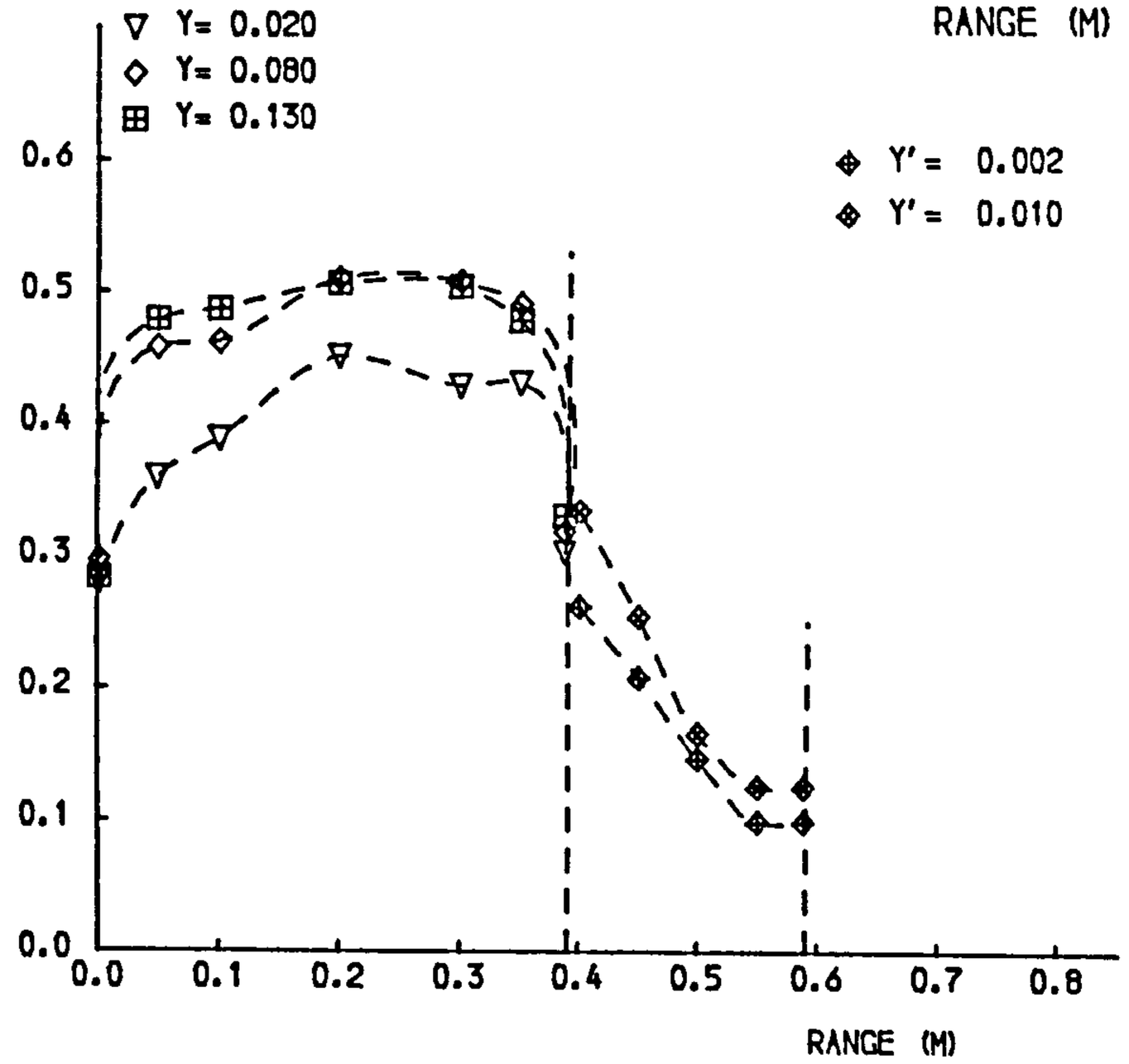

Fig 4·7 Isovels and lateral velocity profiles.

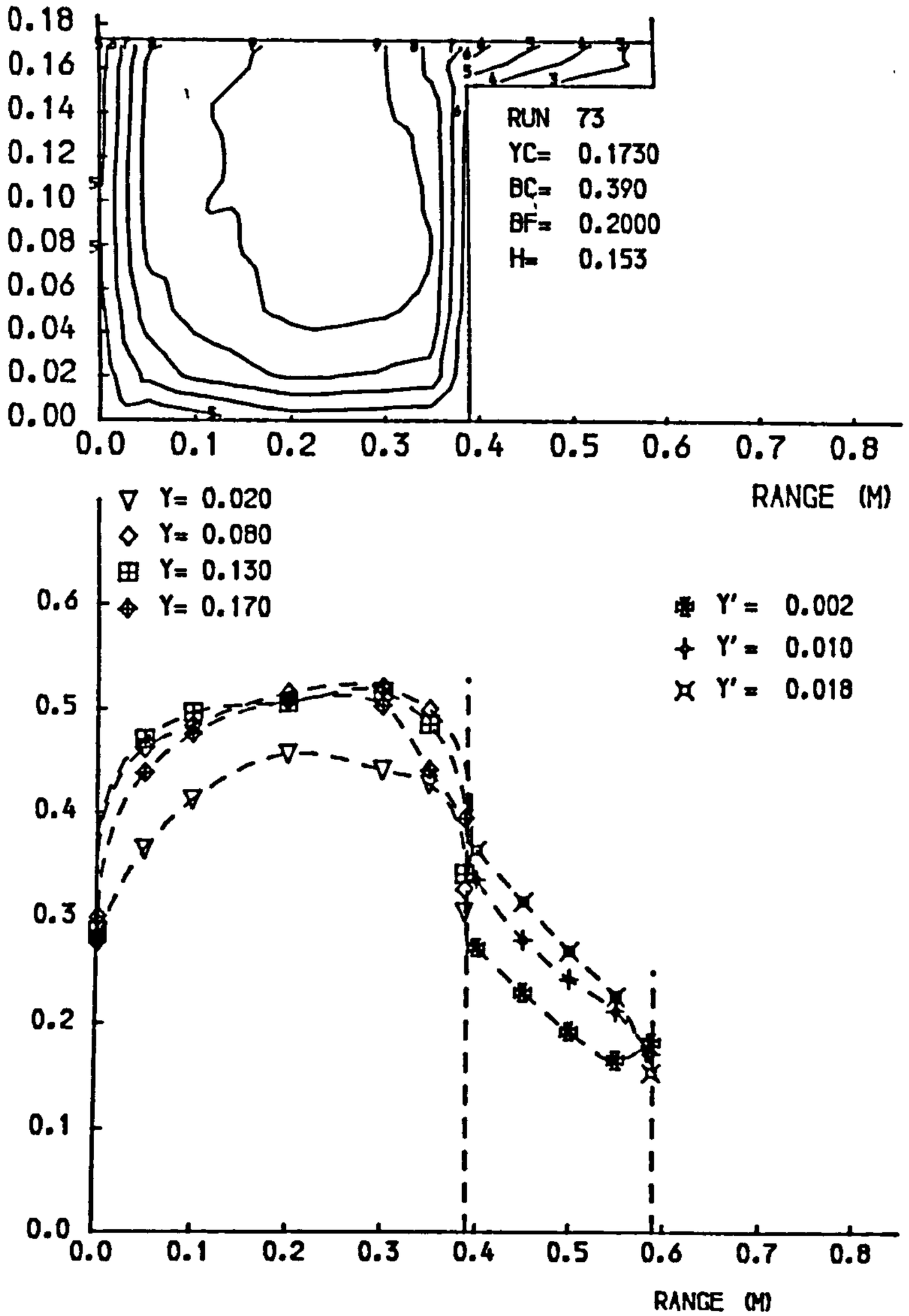

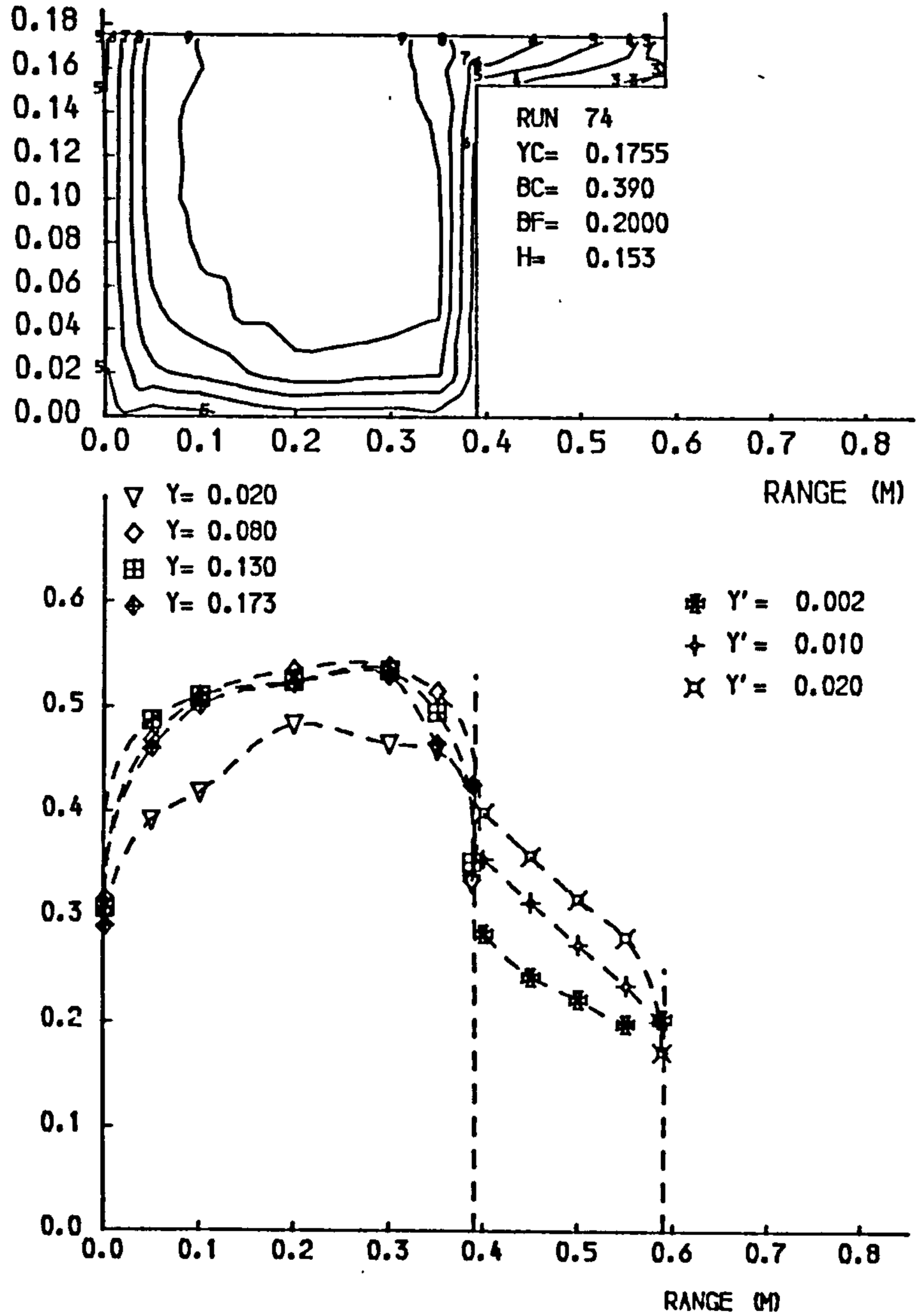

Fig 4·7 Isovels and lateral velocity profiles.

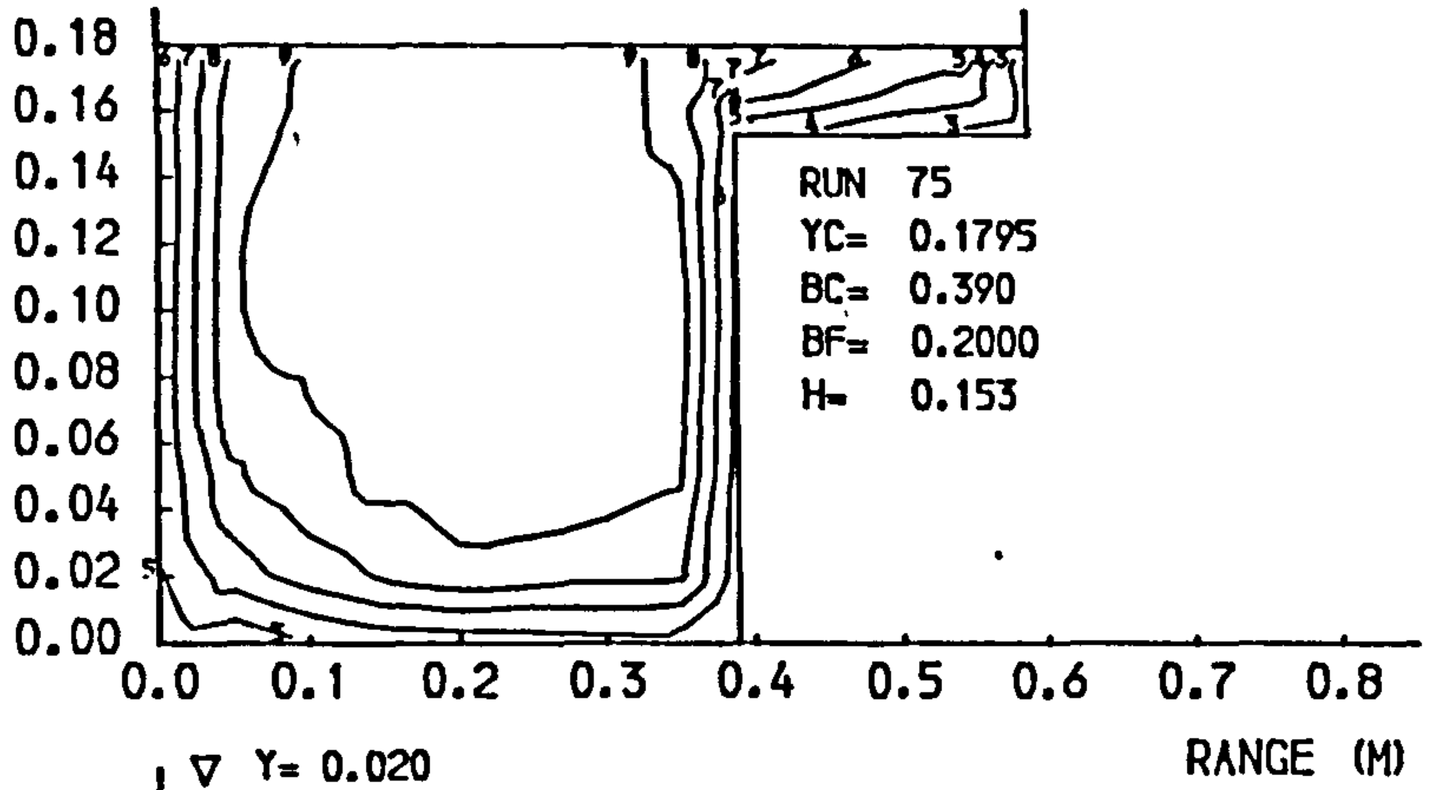

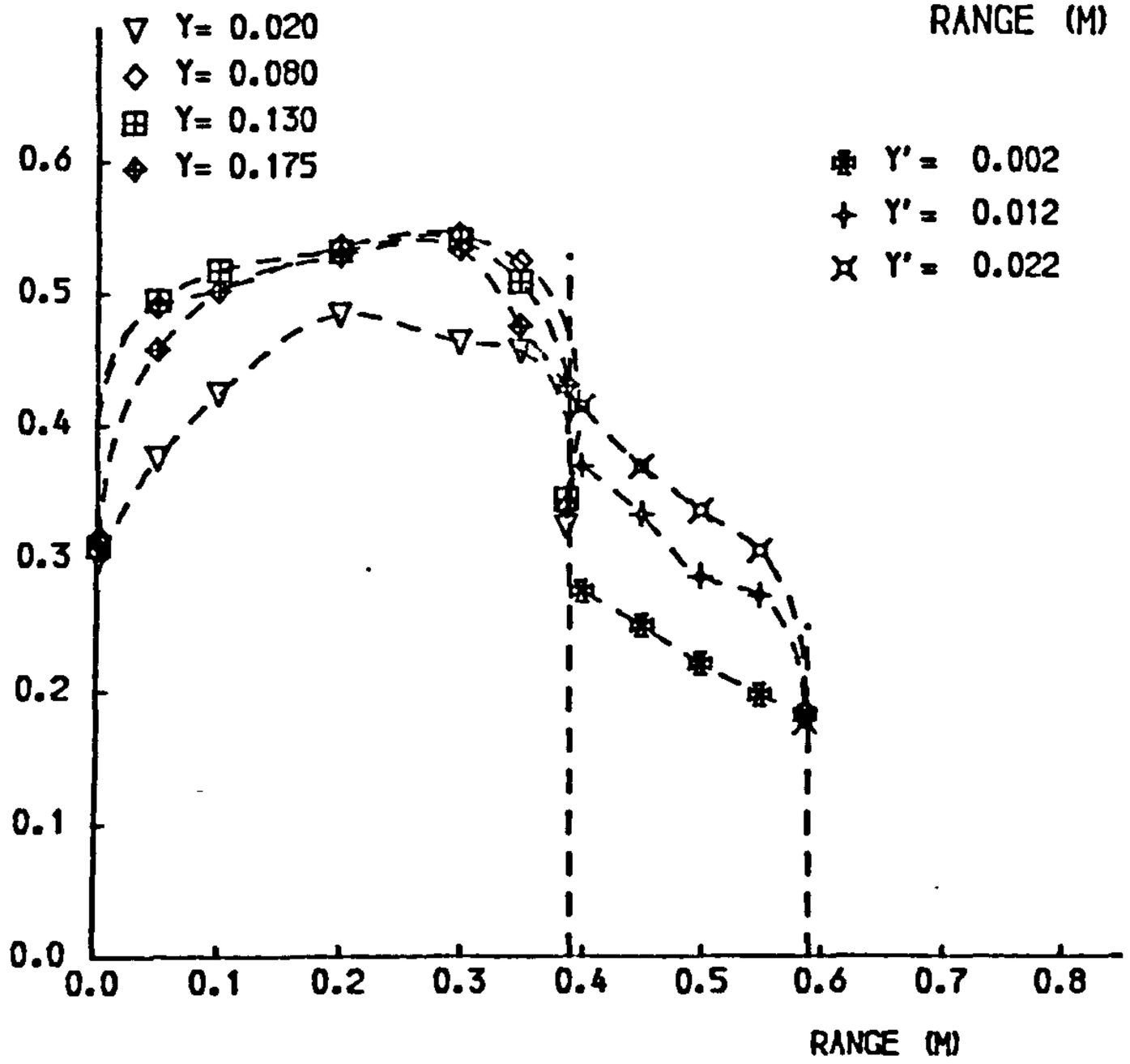

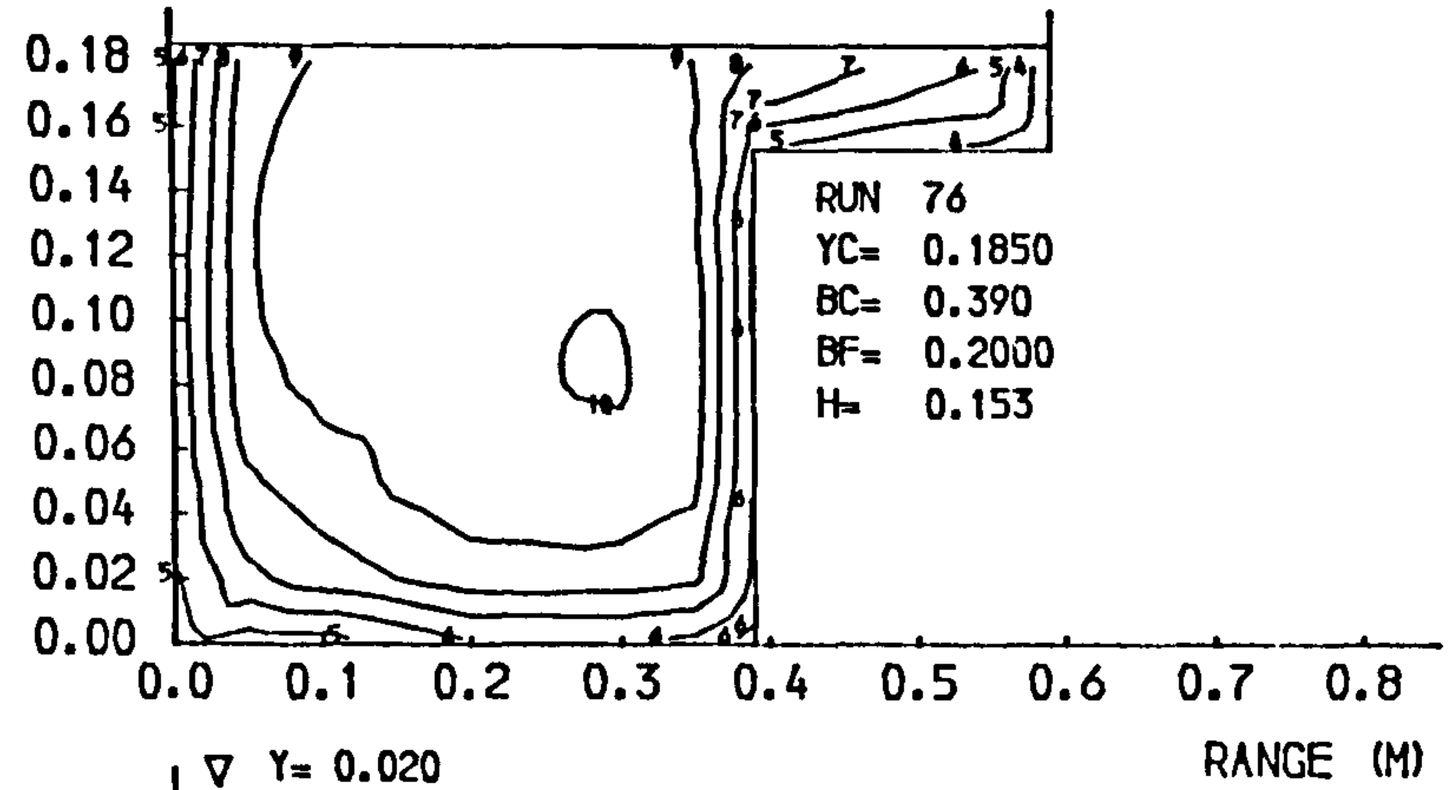

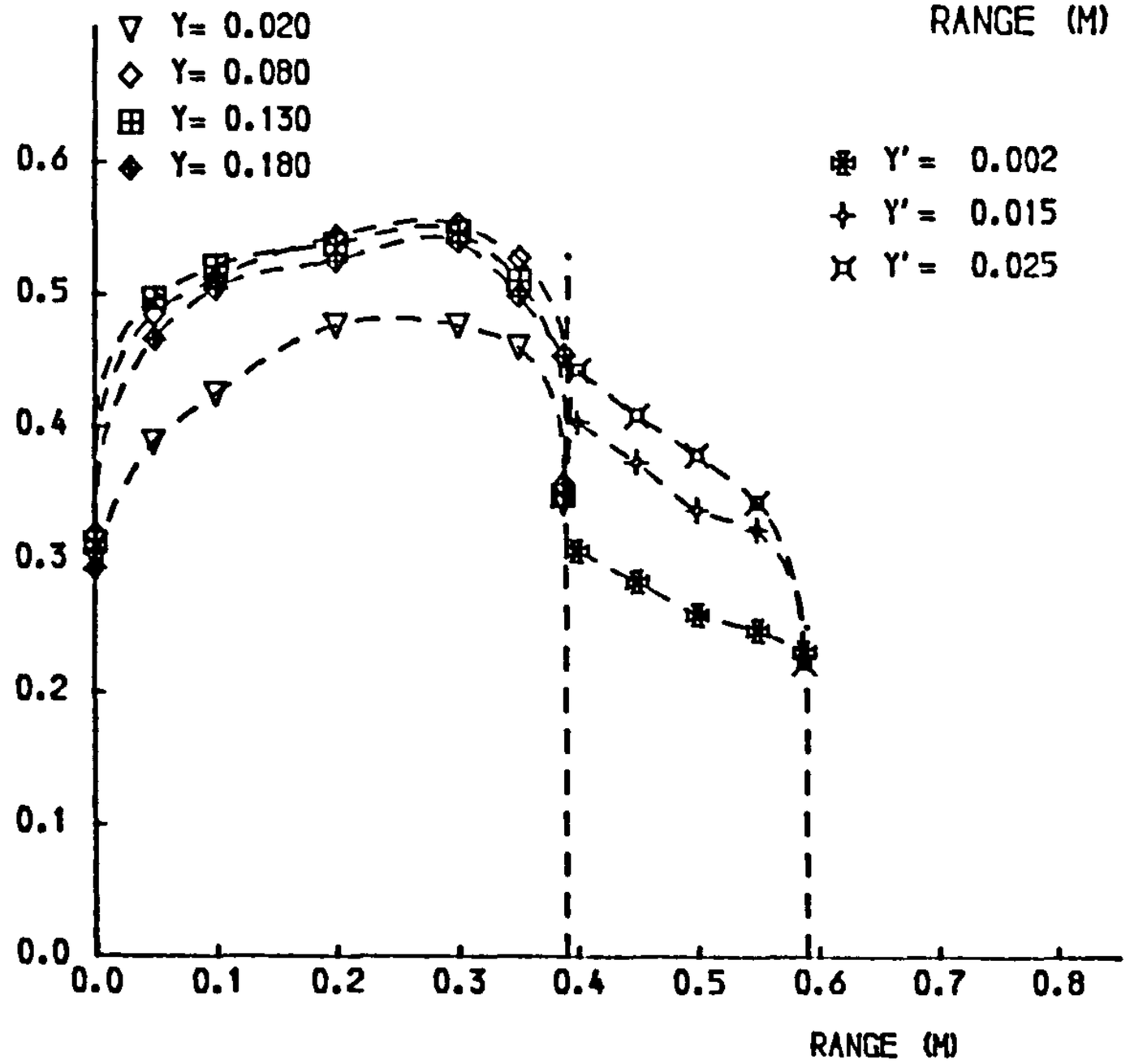

Fig 4·7 Isovels and lateral velocity profiles.

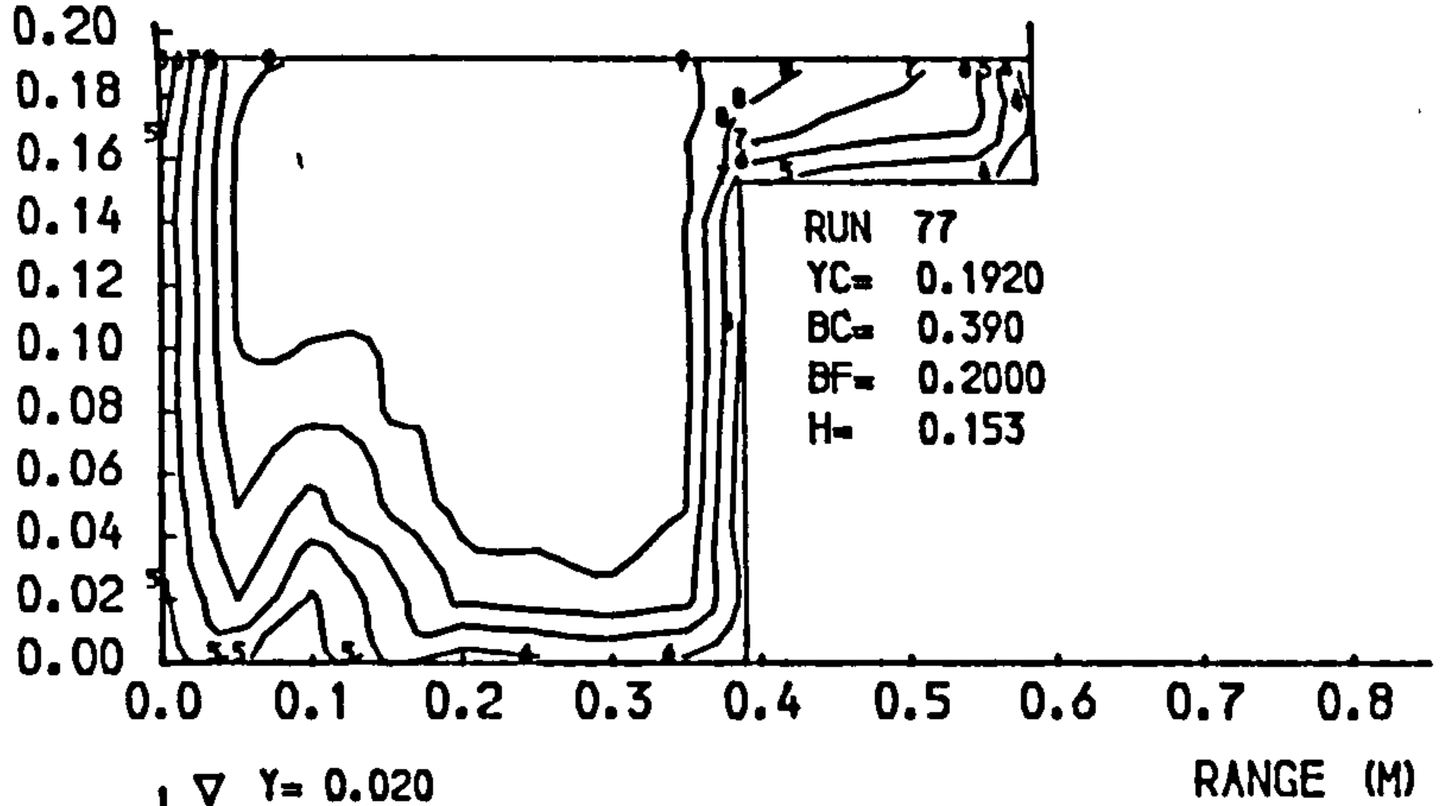

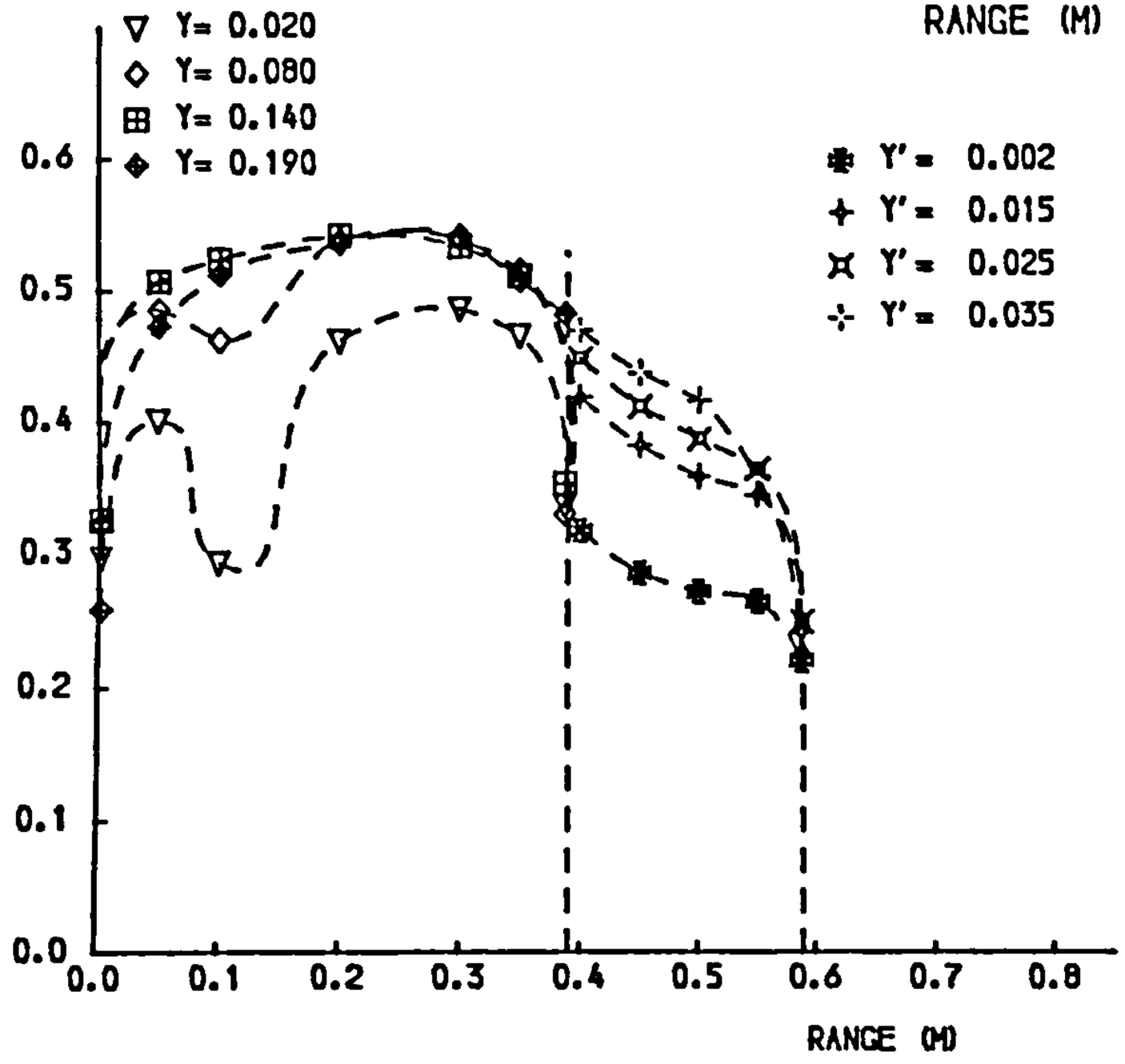

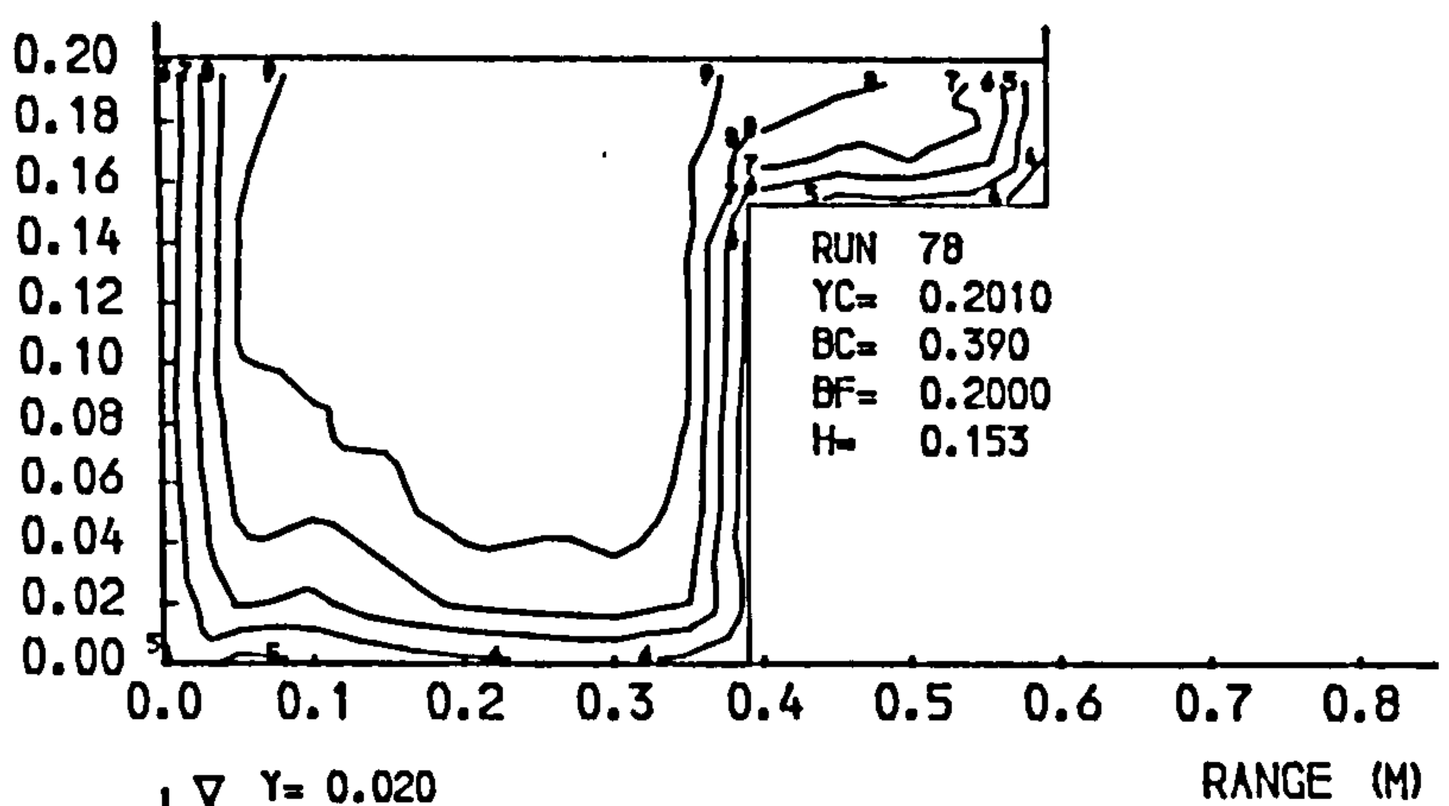

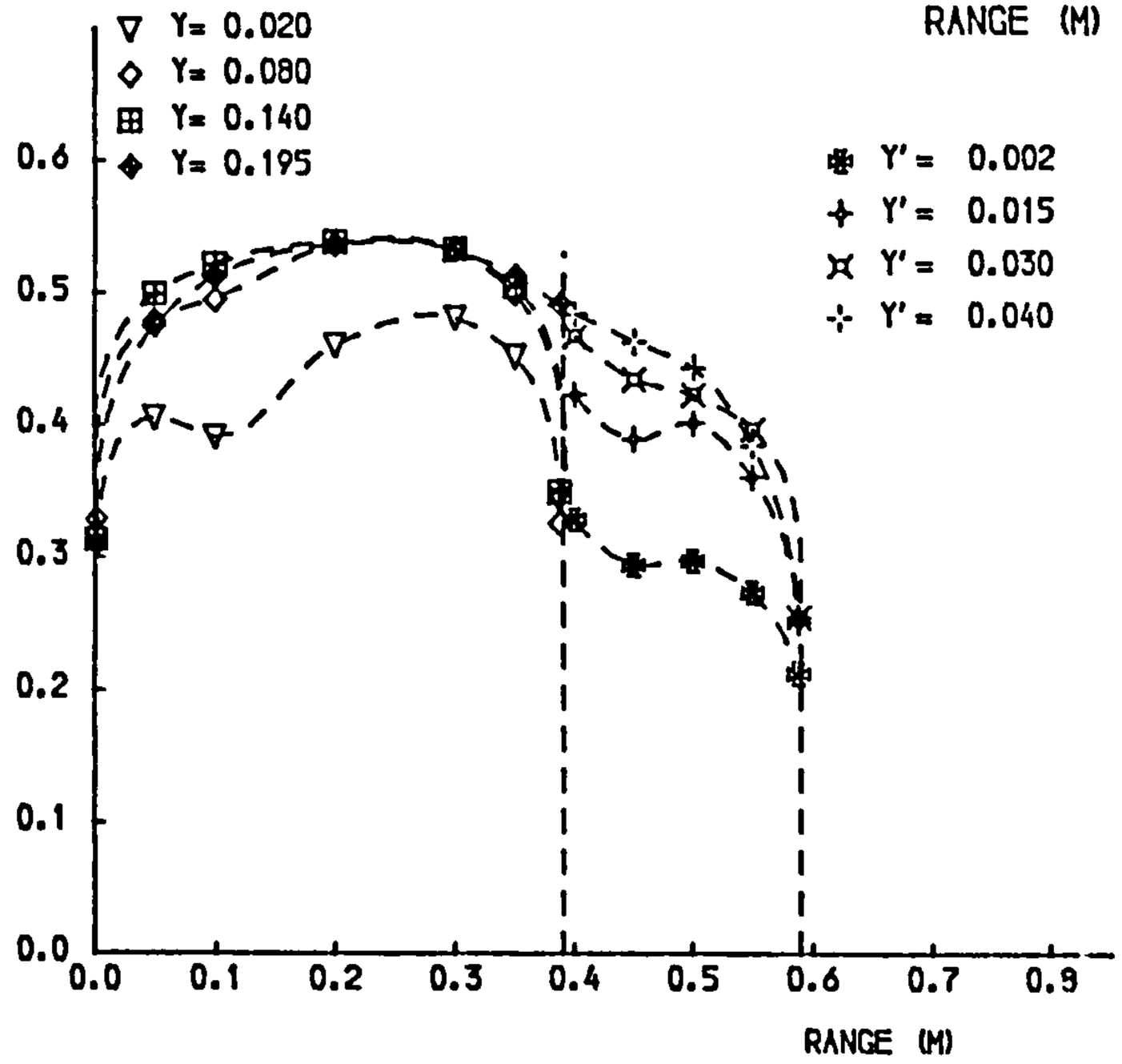

Fig 4·7 Isovels and lateral velocity profiles.

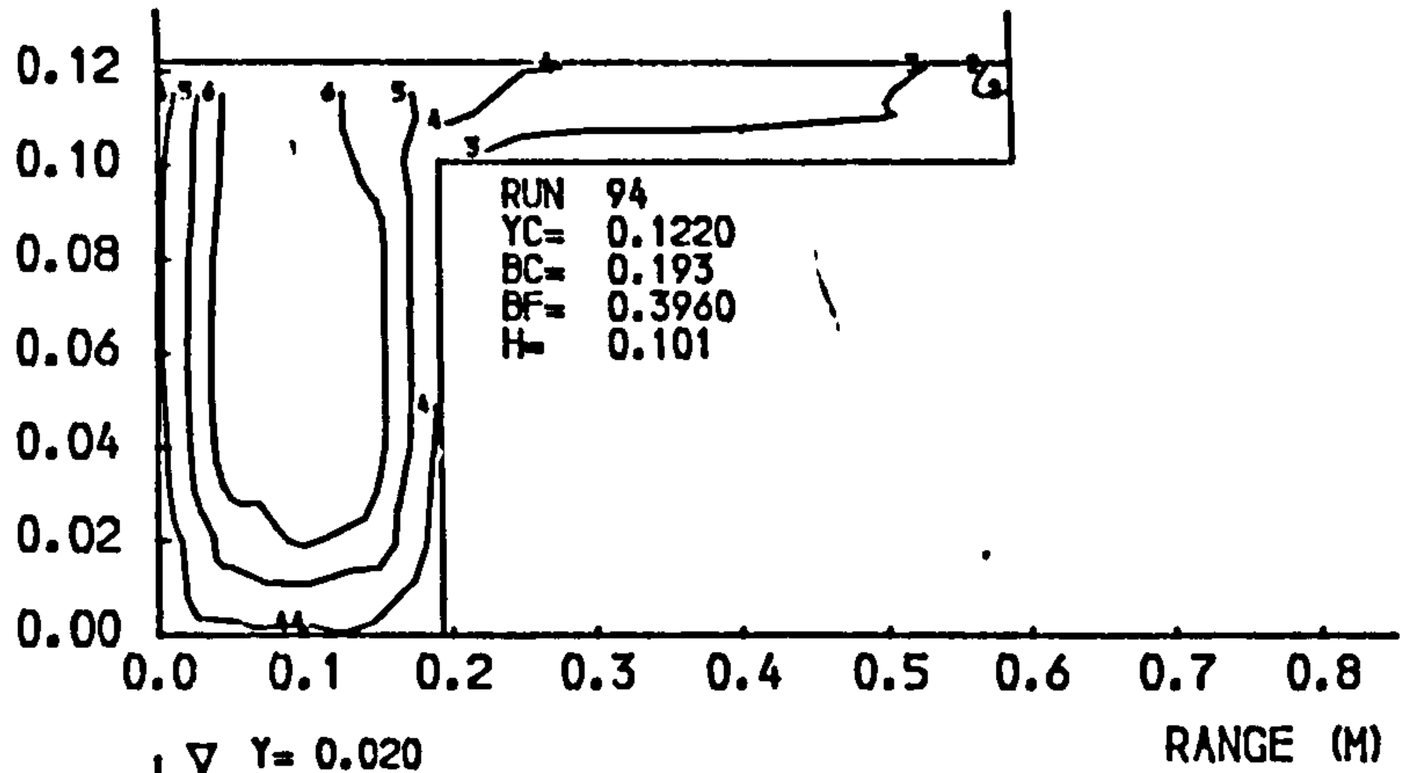

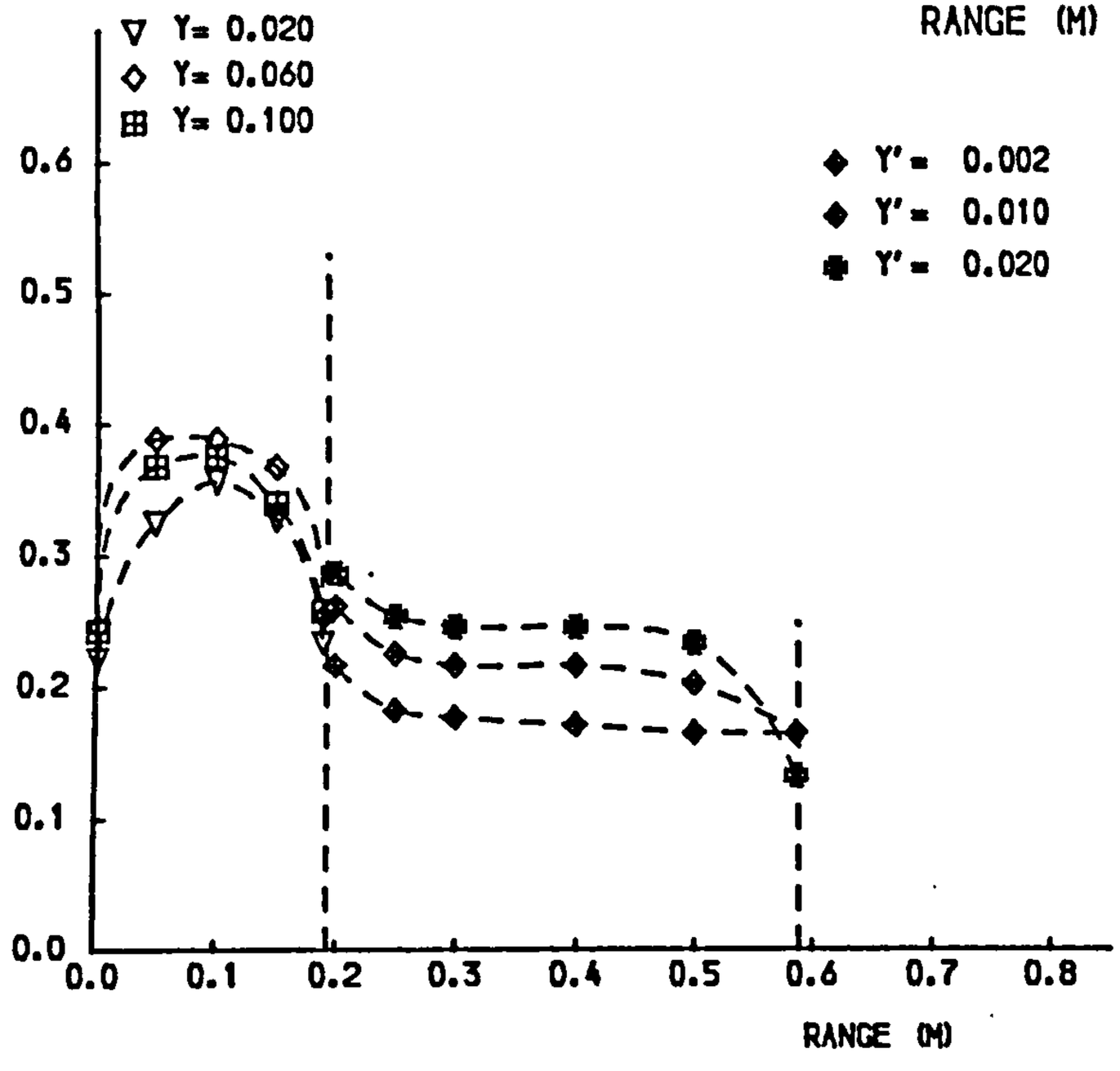

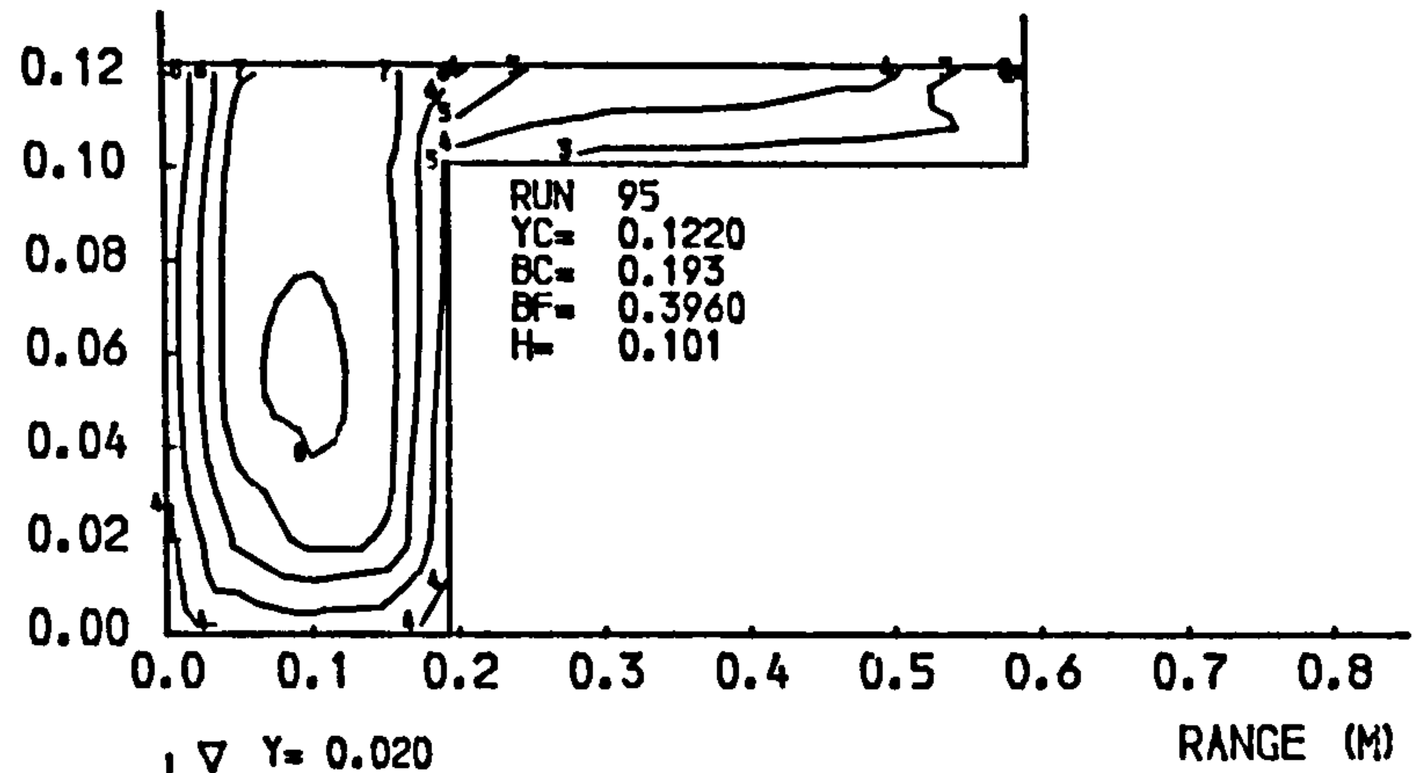

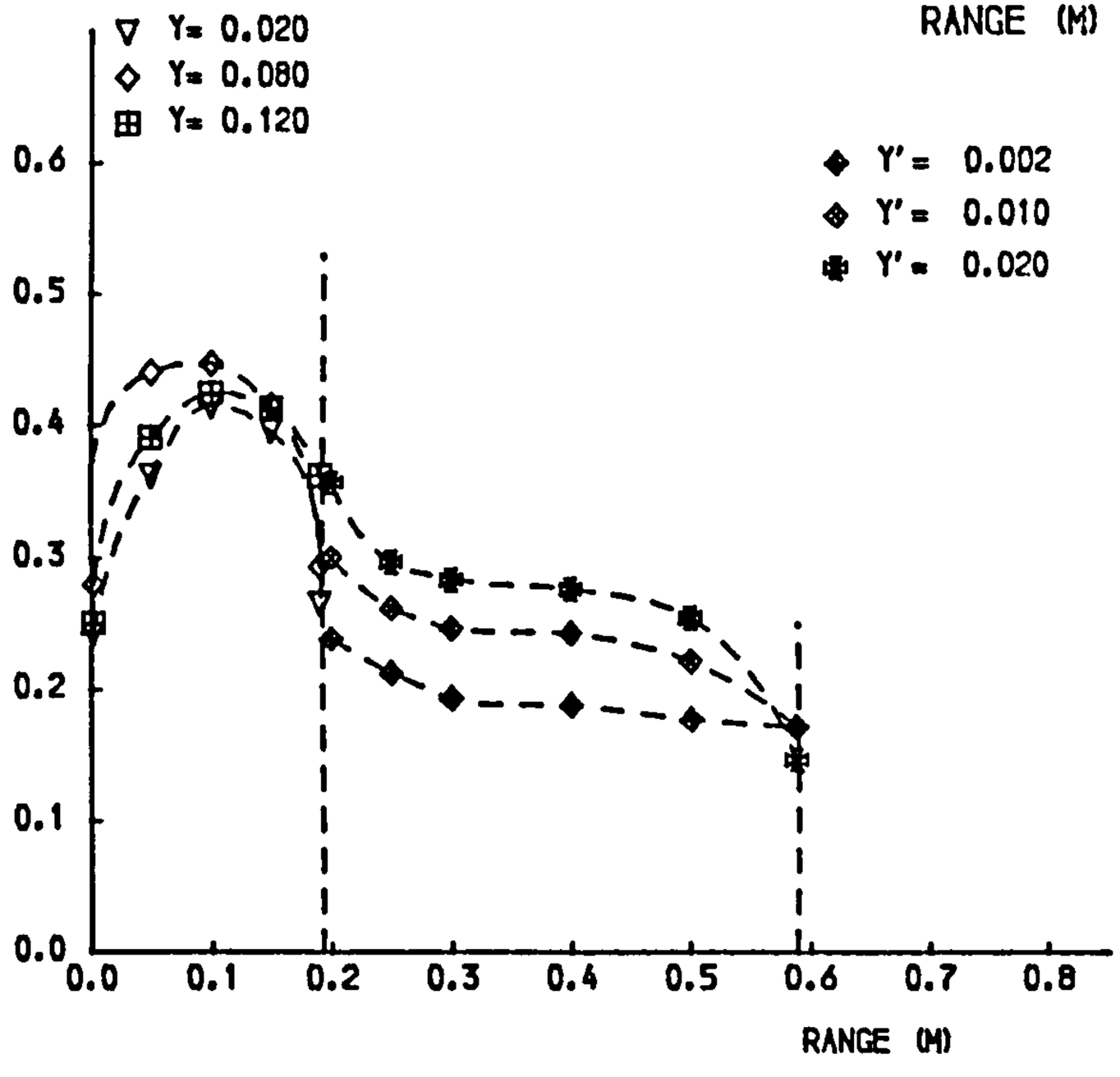

Fig 4·7 Isovels and lateral velocity profiles.

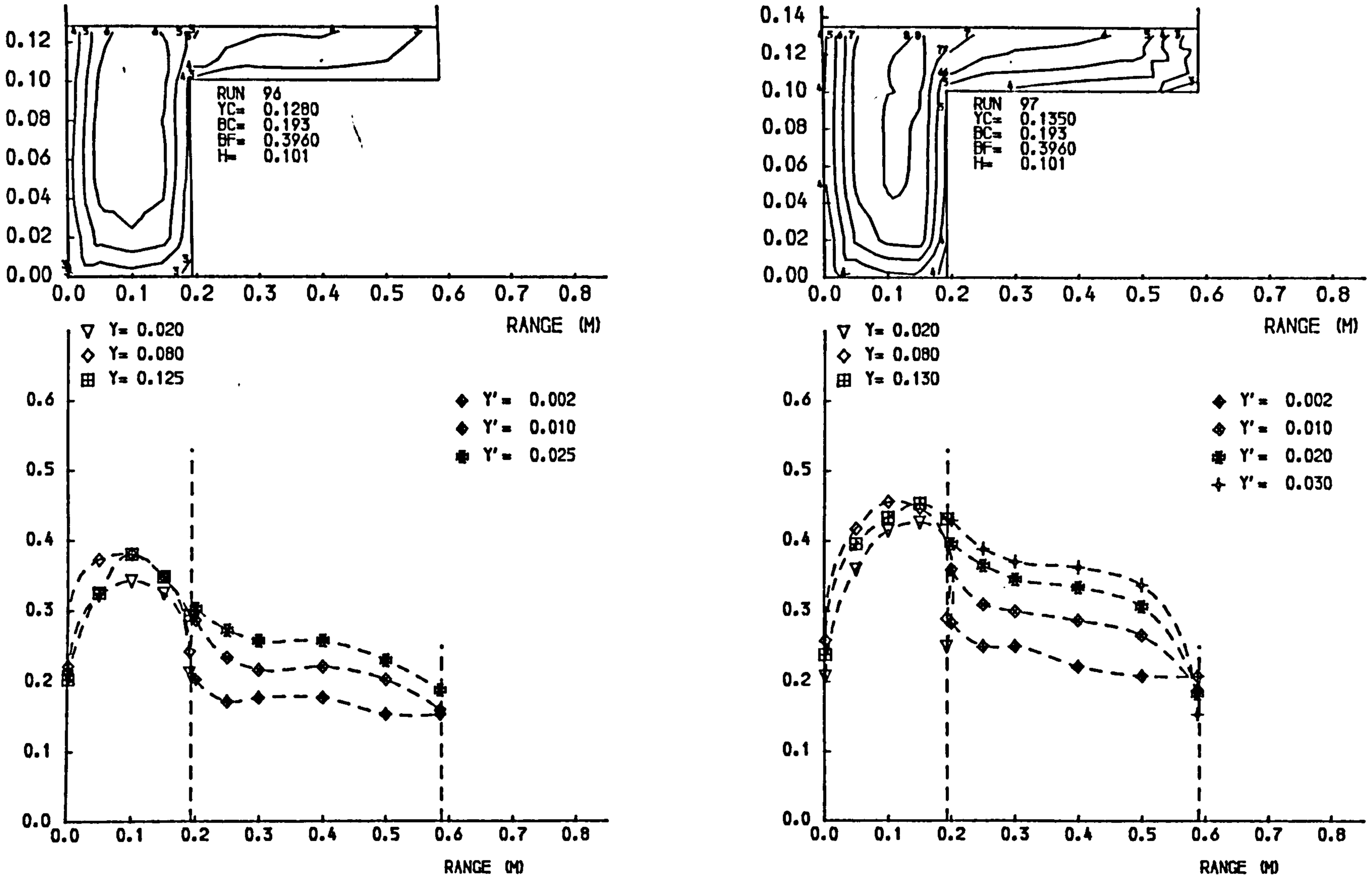

Fig 4·7 Isovels and lateral velocity profiles.

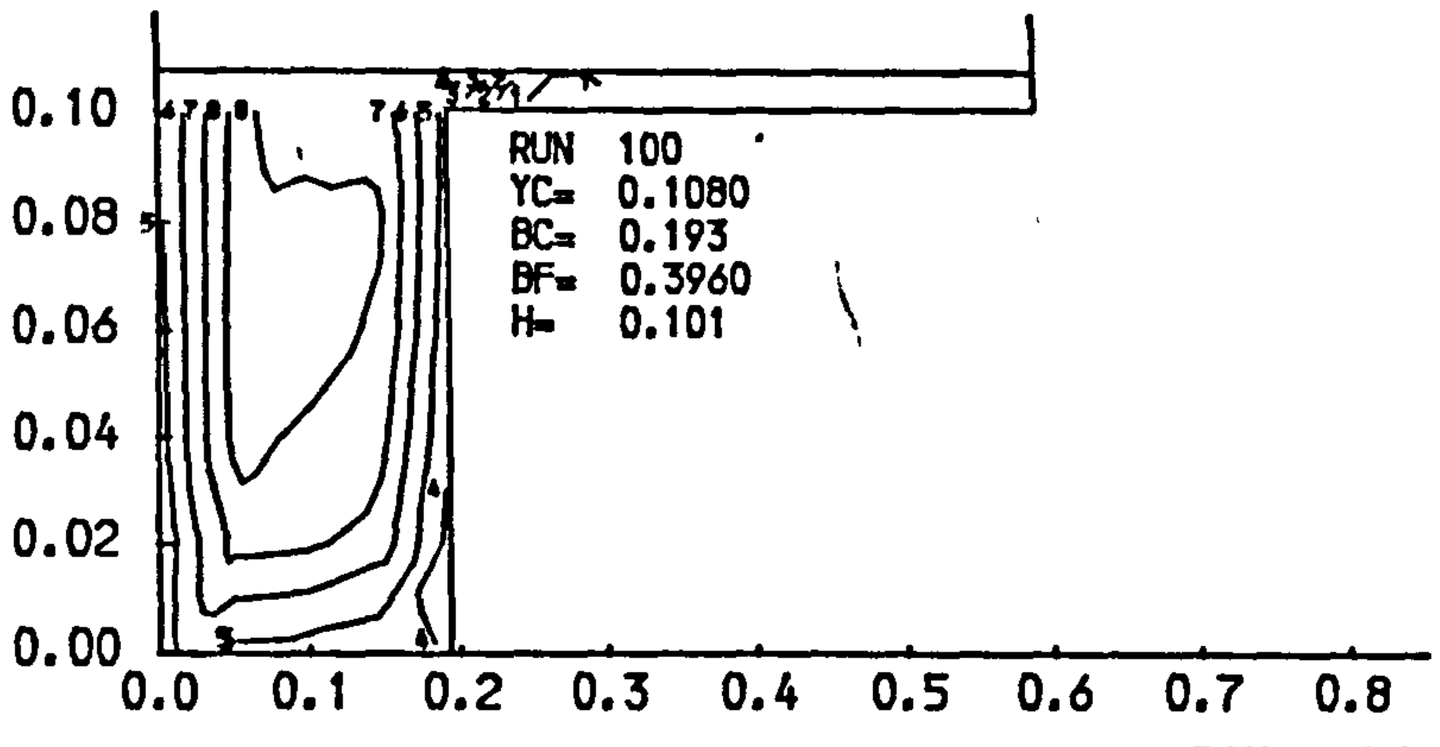

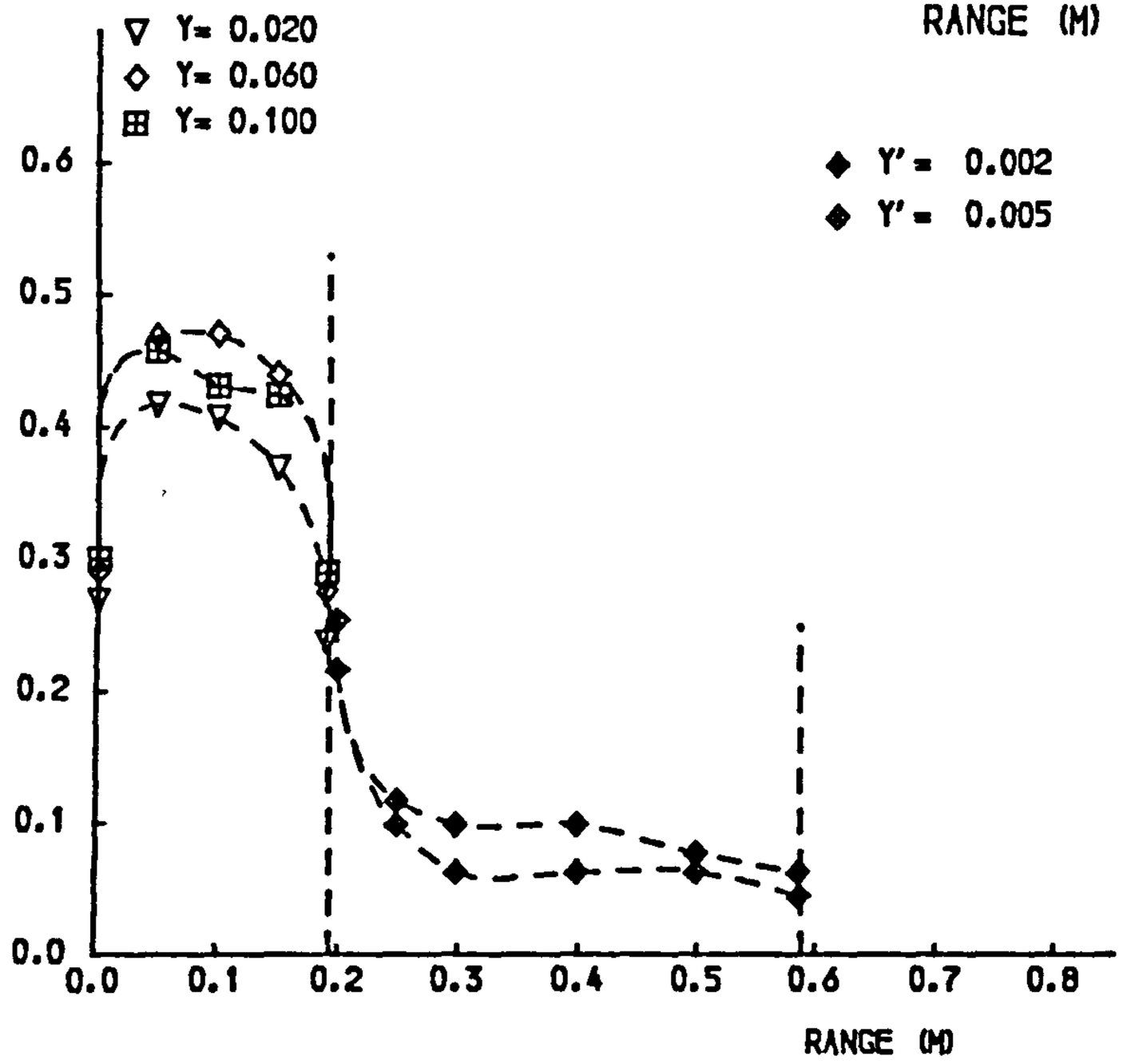

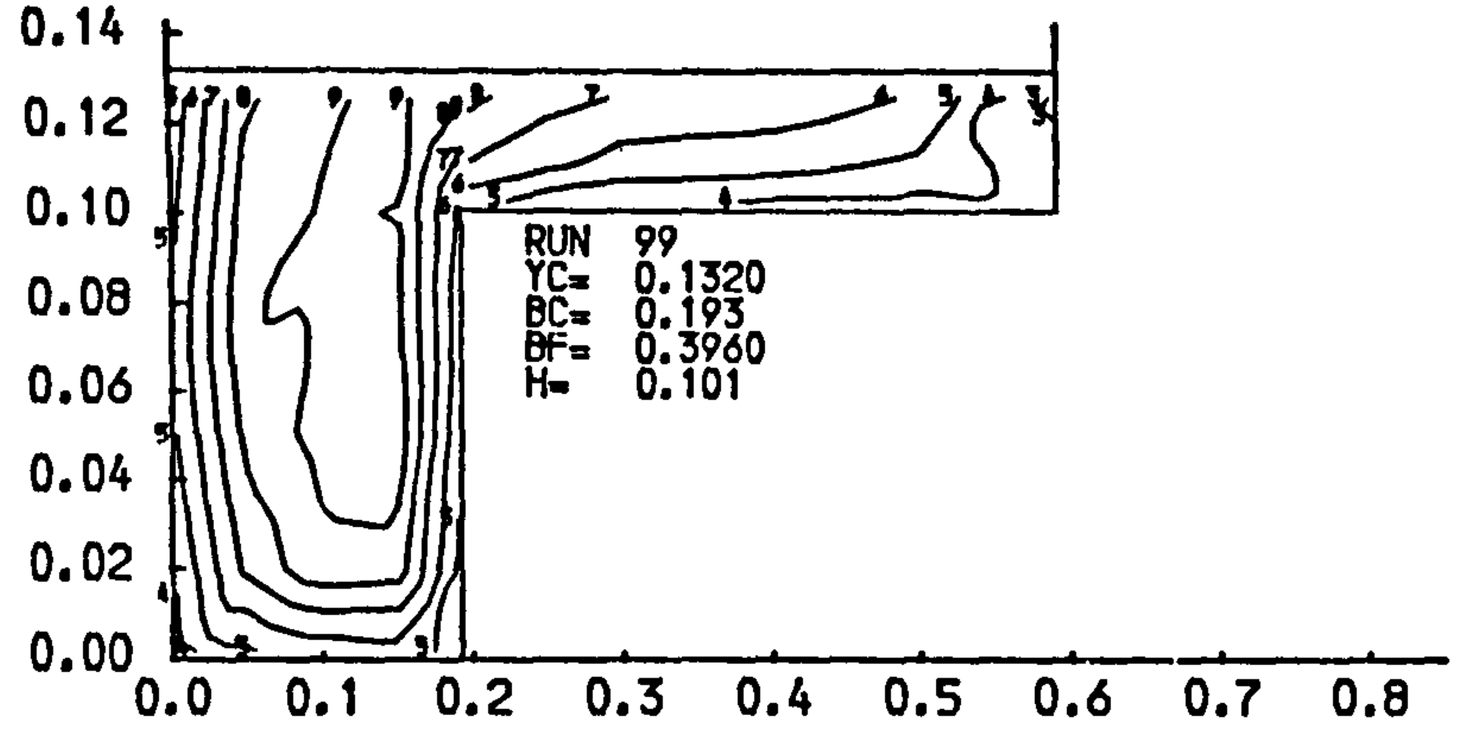

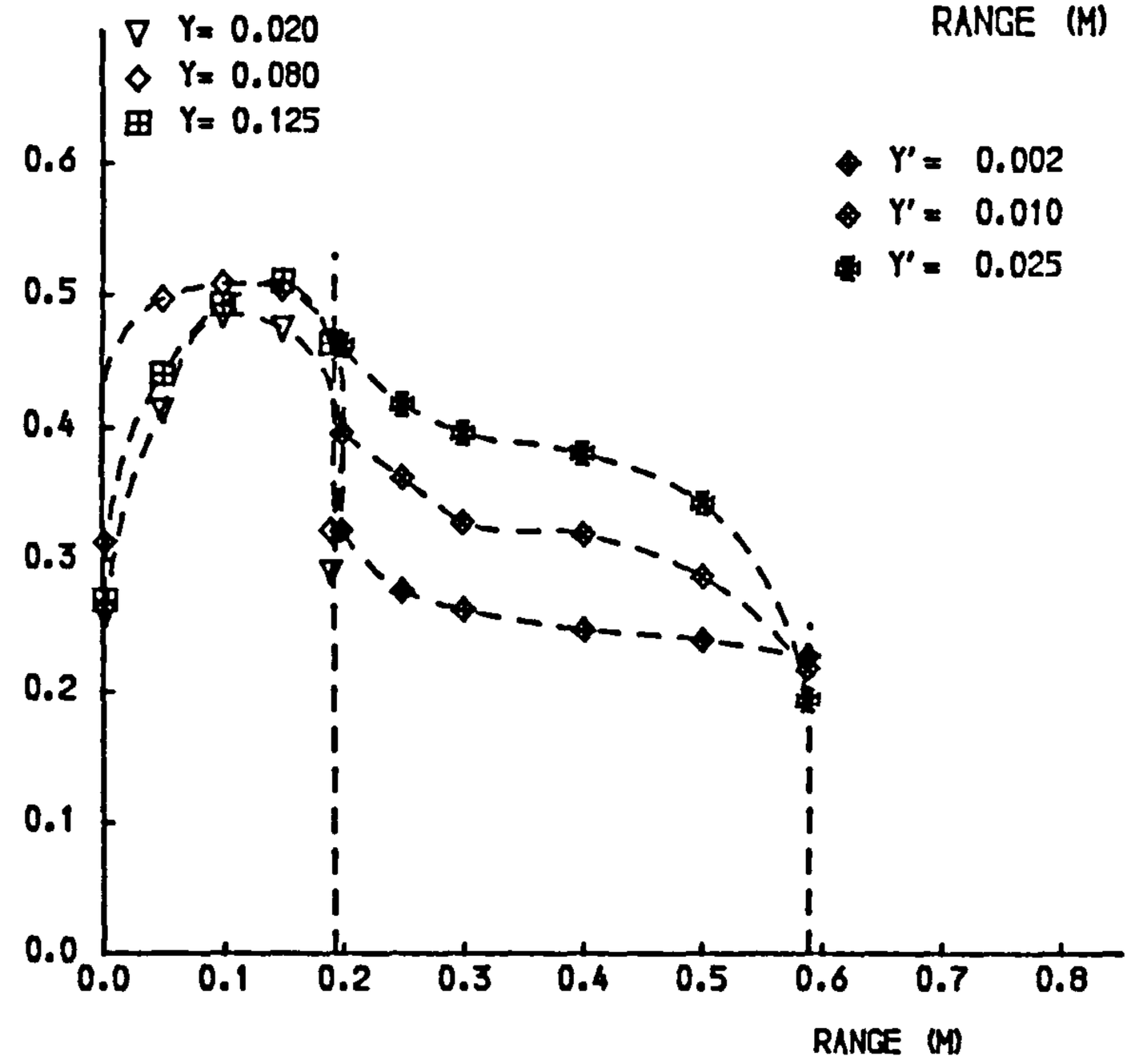

Fig 4·7 Isovels and lateral velocity profiles.

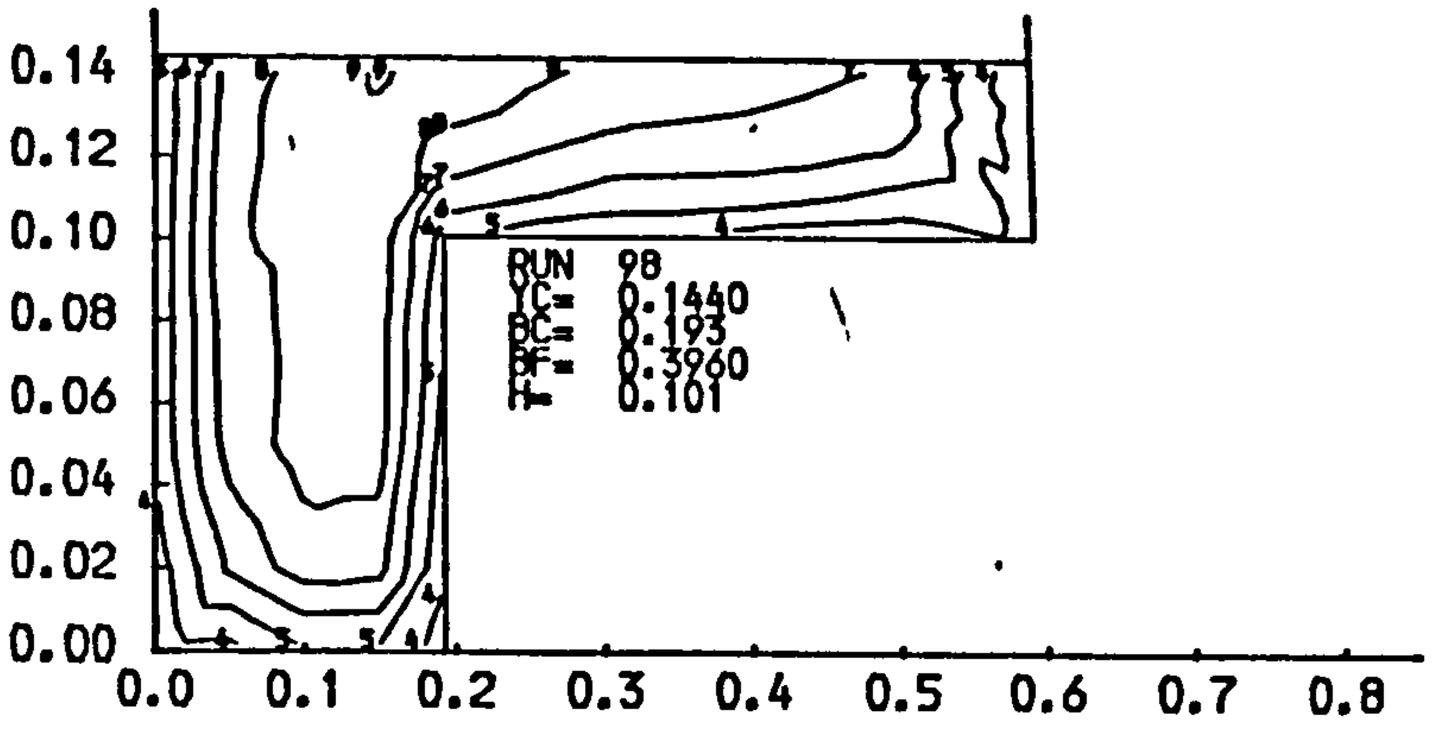

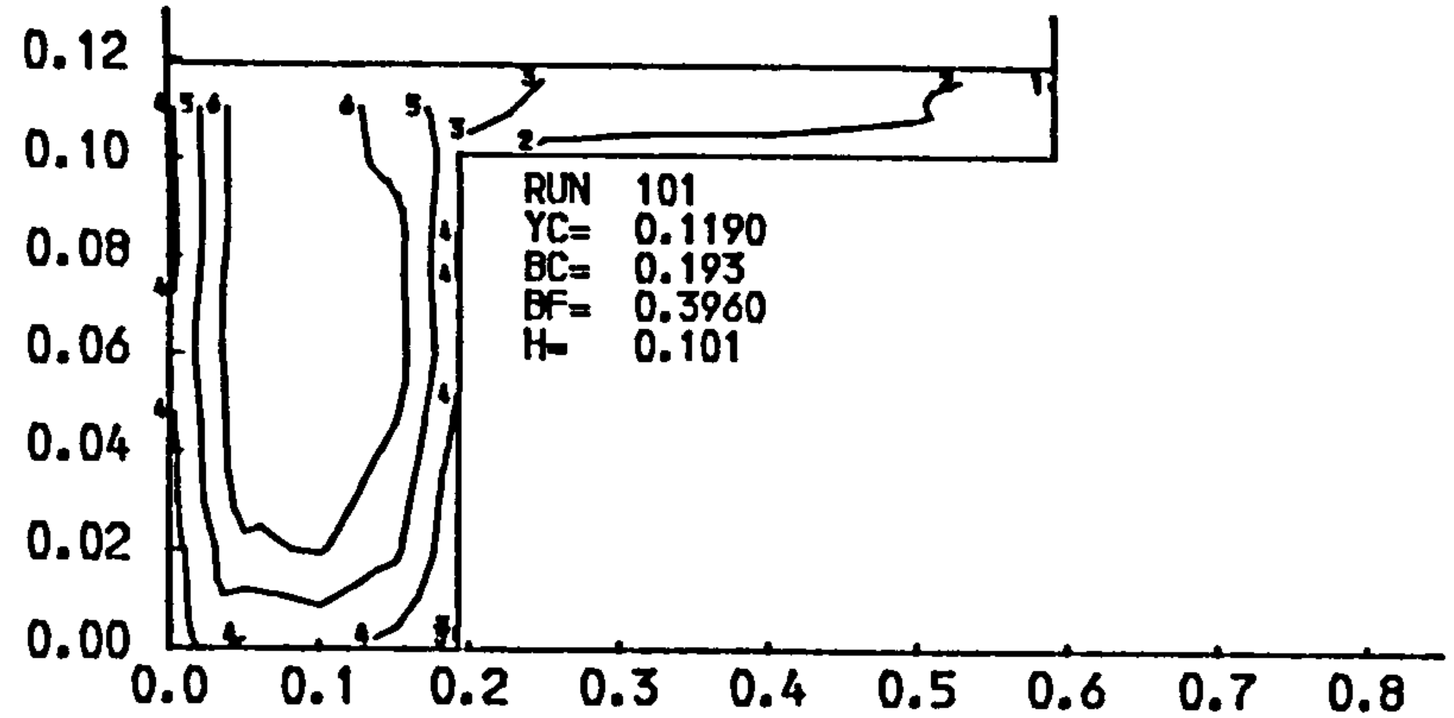

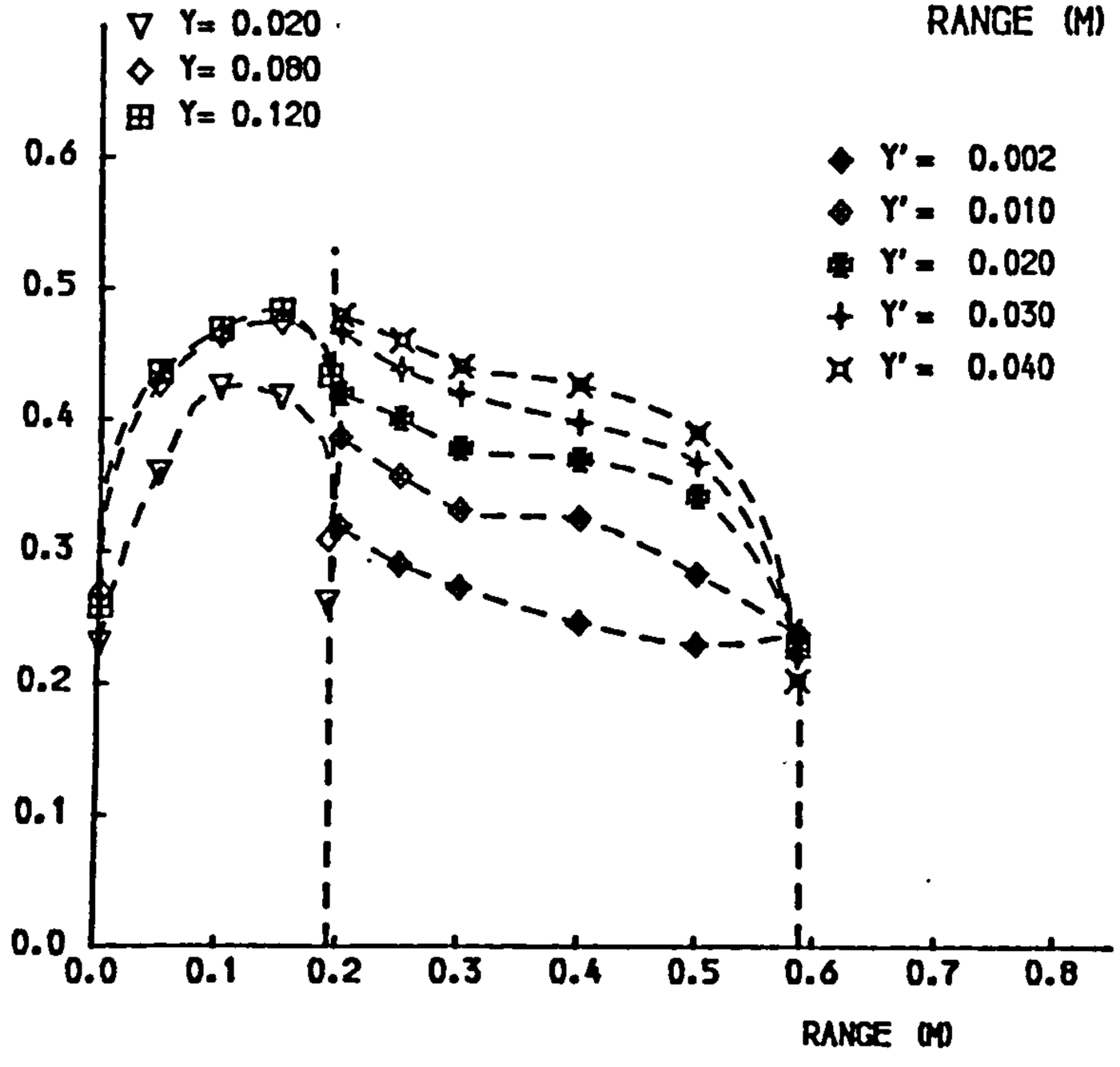

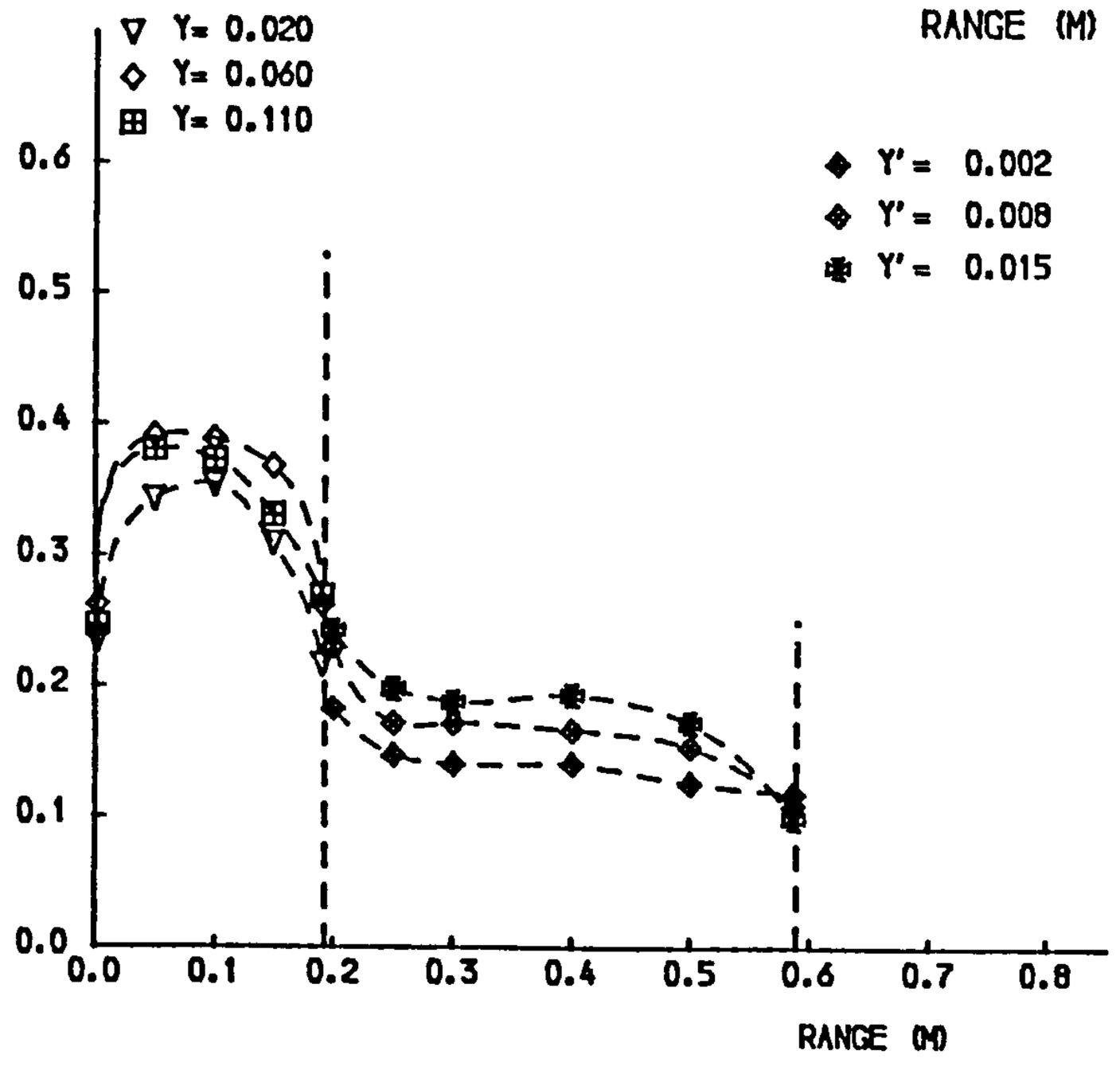

Fig 4·7 Isovels and lateral velocity profiles.

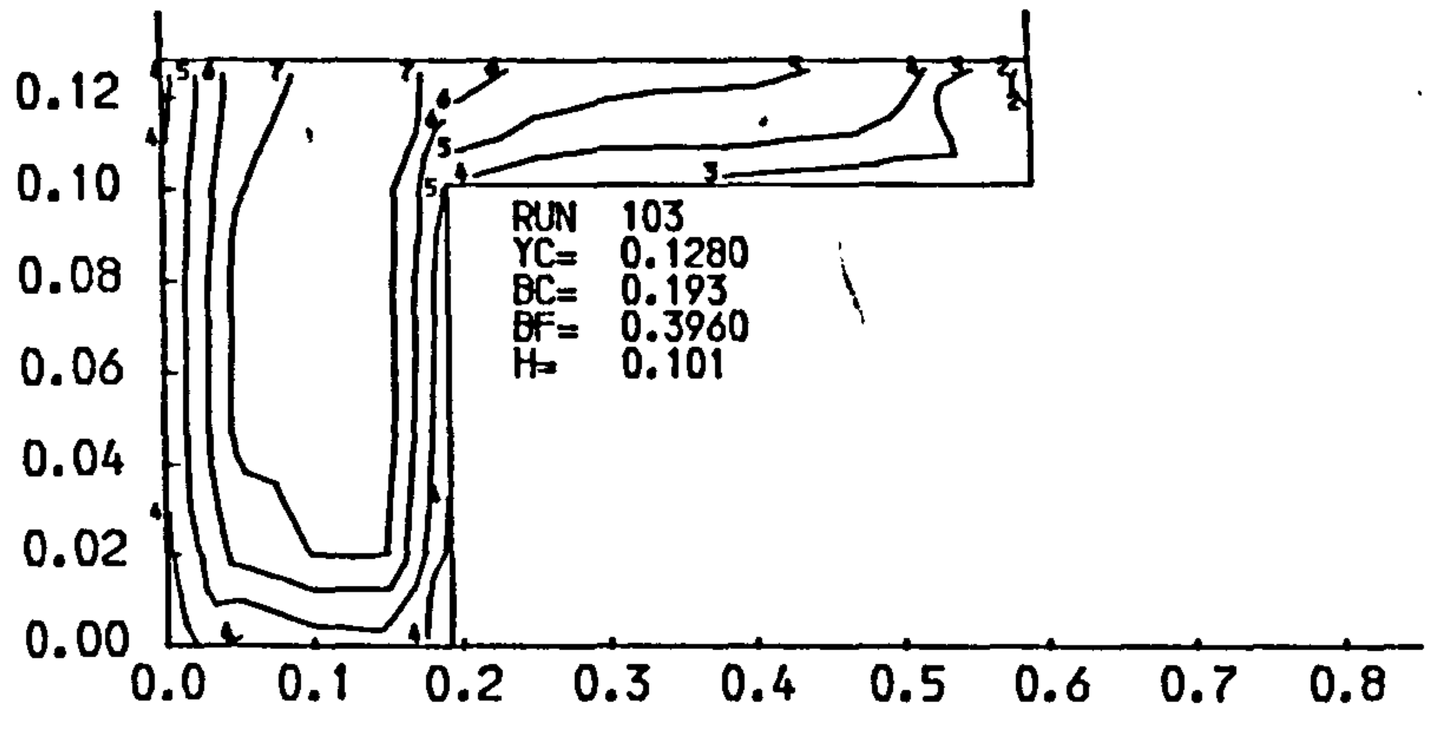

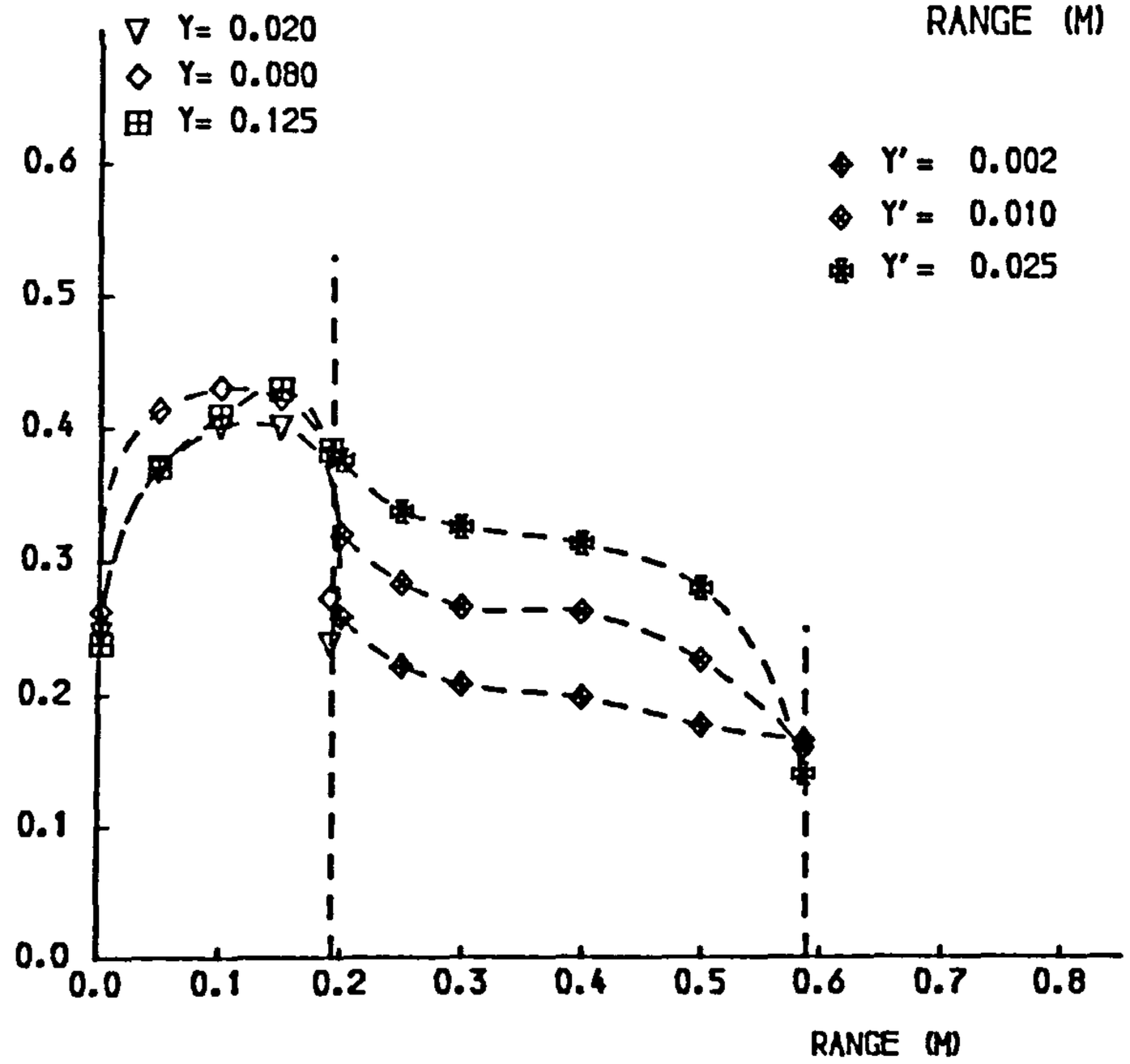

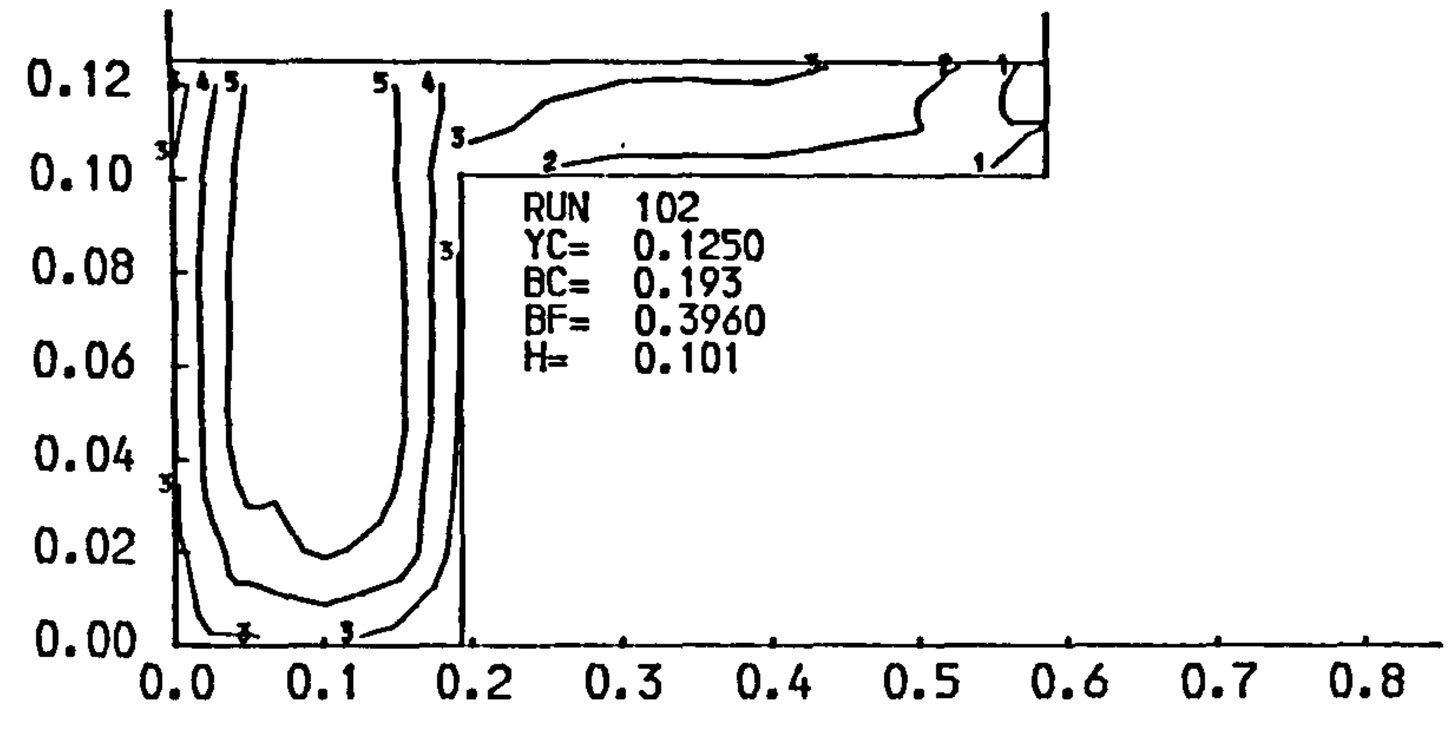

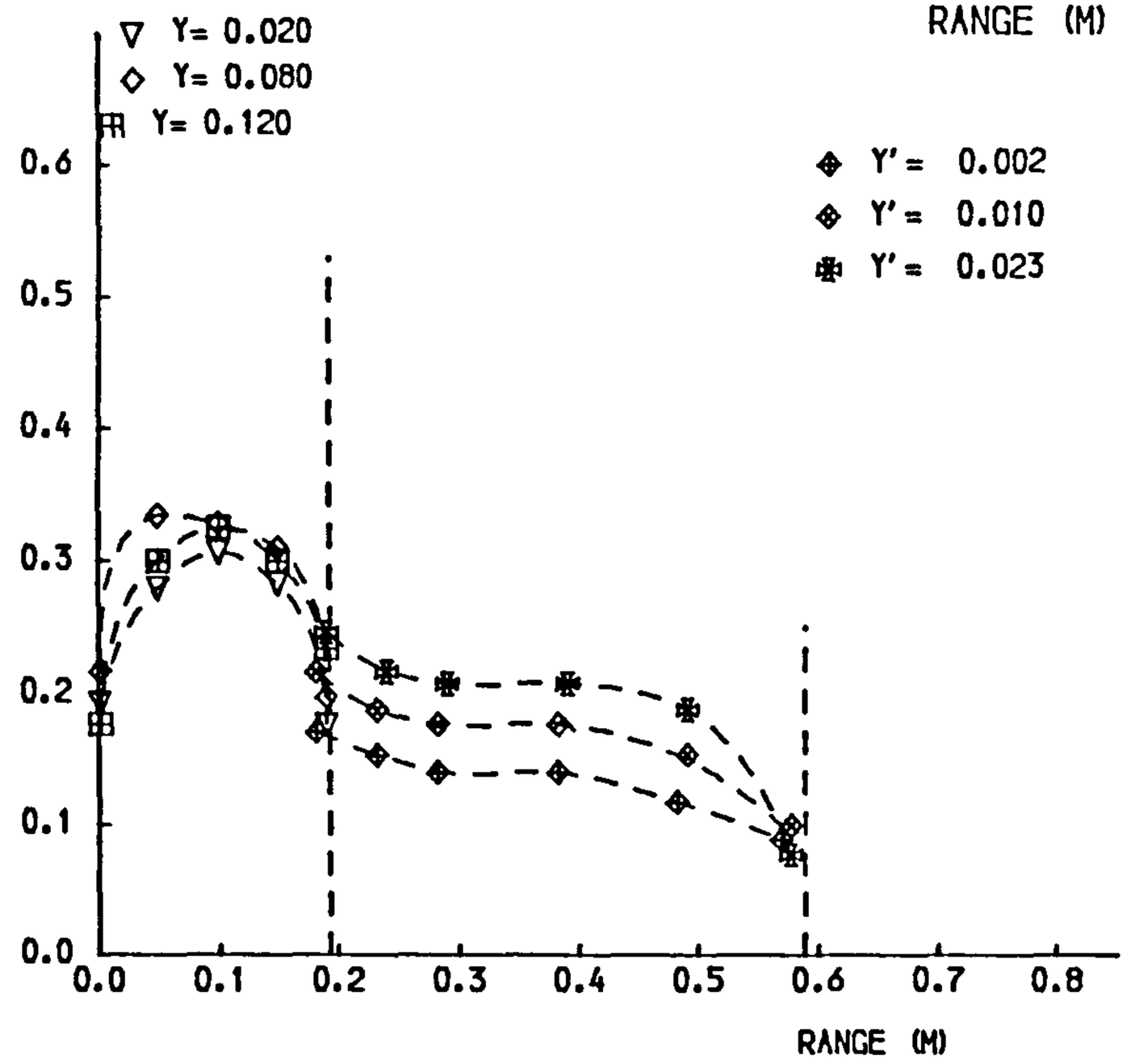

Fig 4·7 Isovels and lateral velocity profiles.

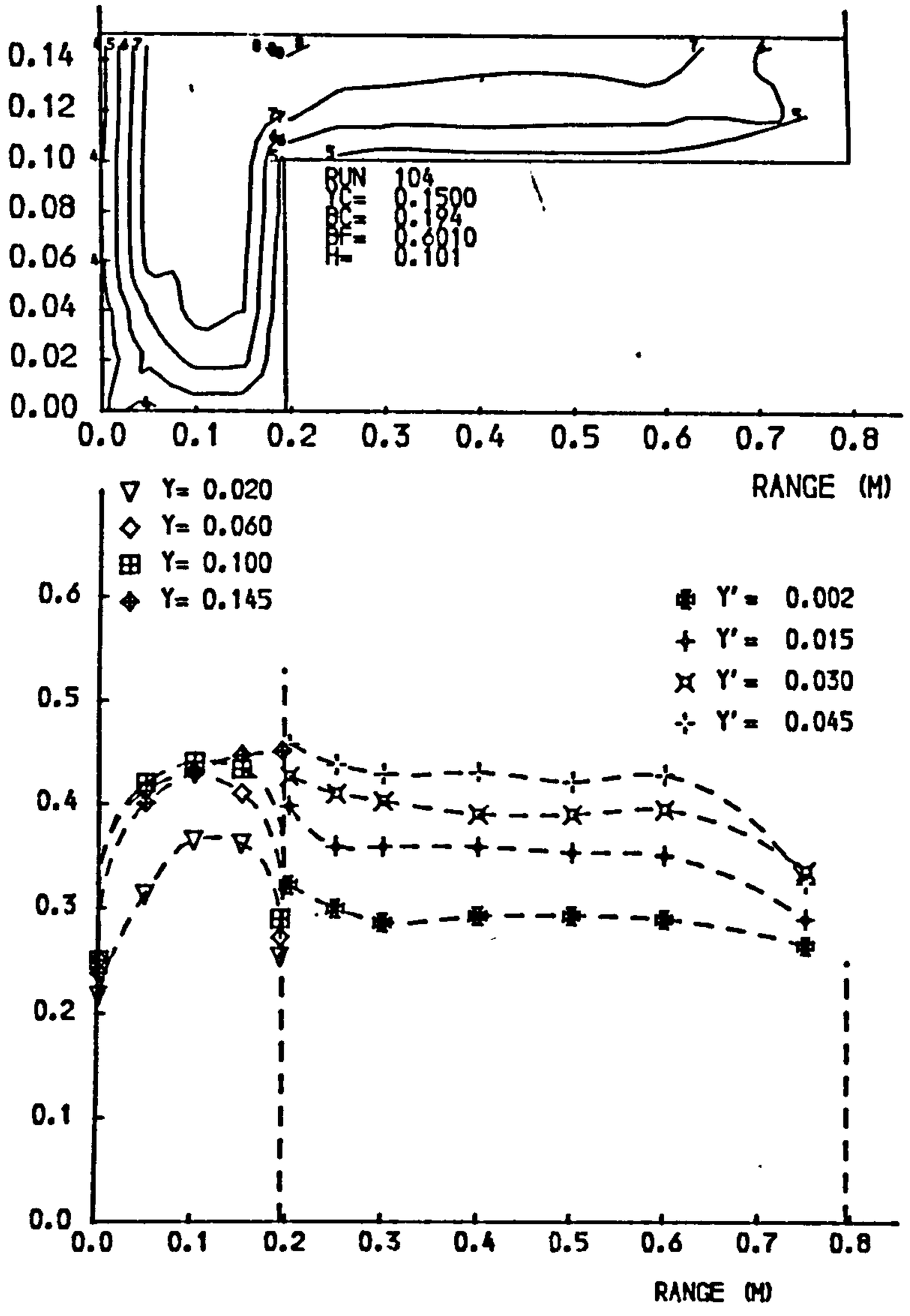

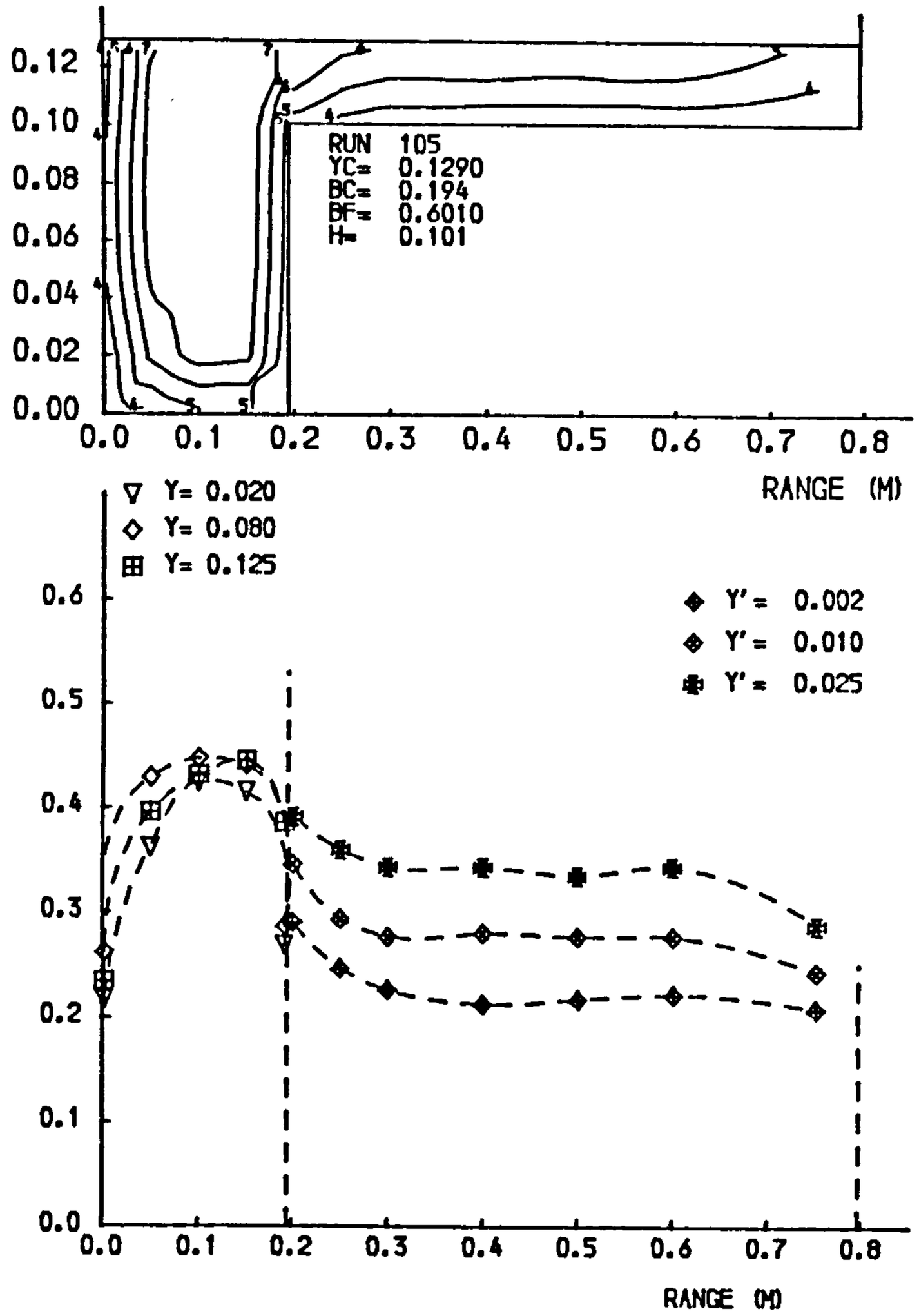

Fig 4·7 Isovels and lateral velocity profiles.

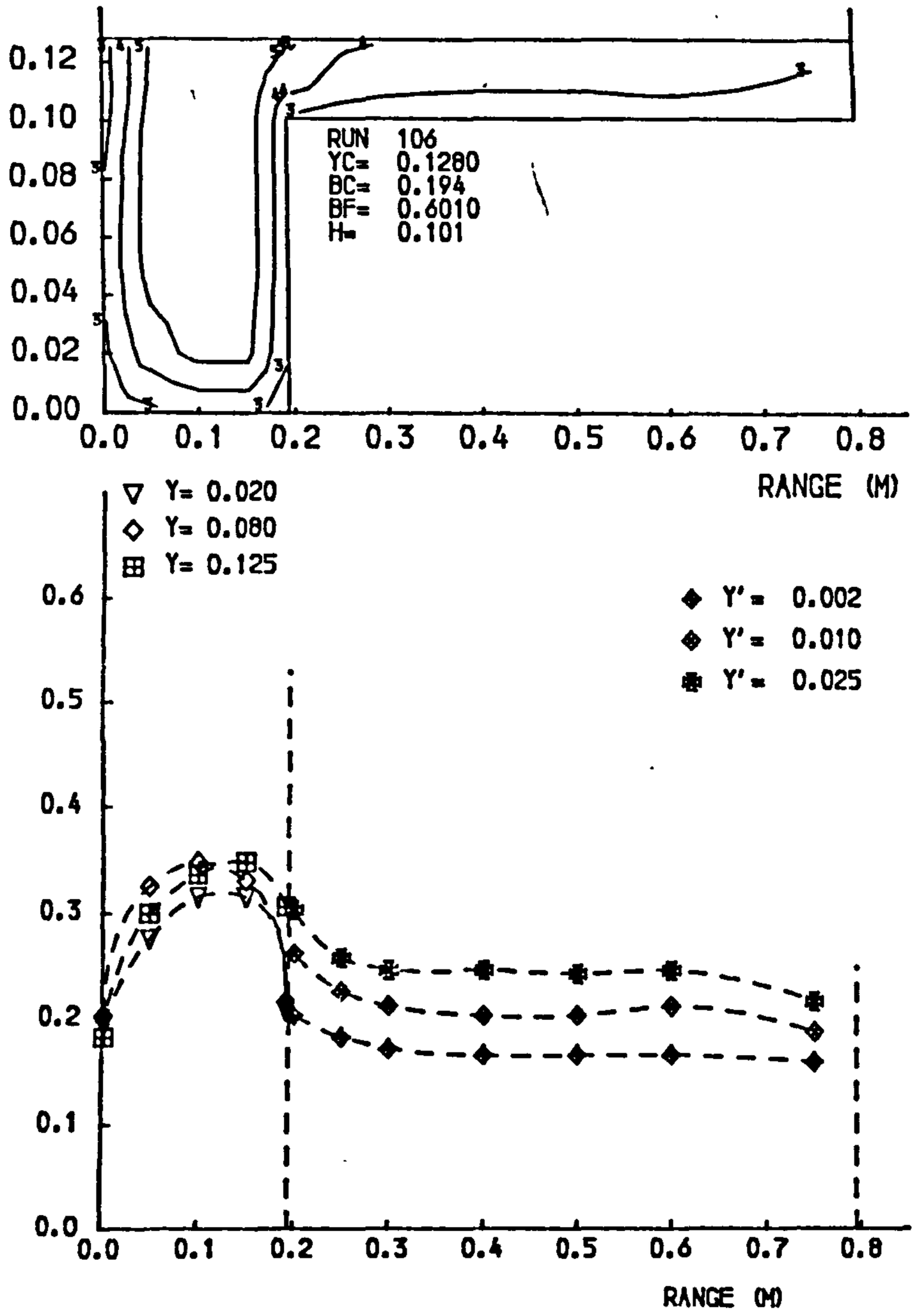

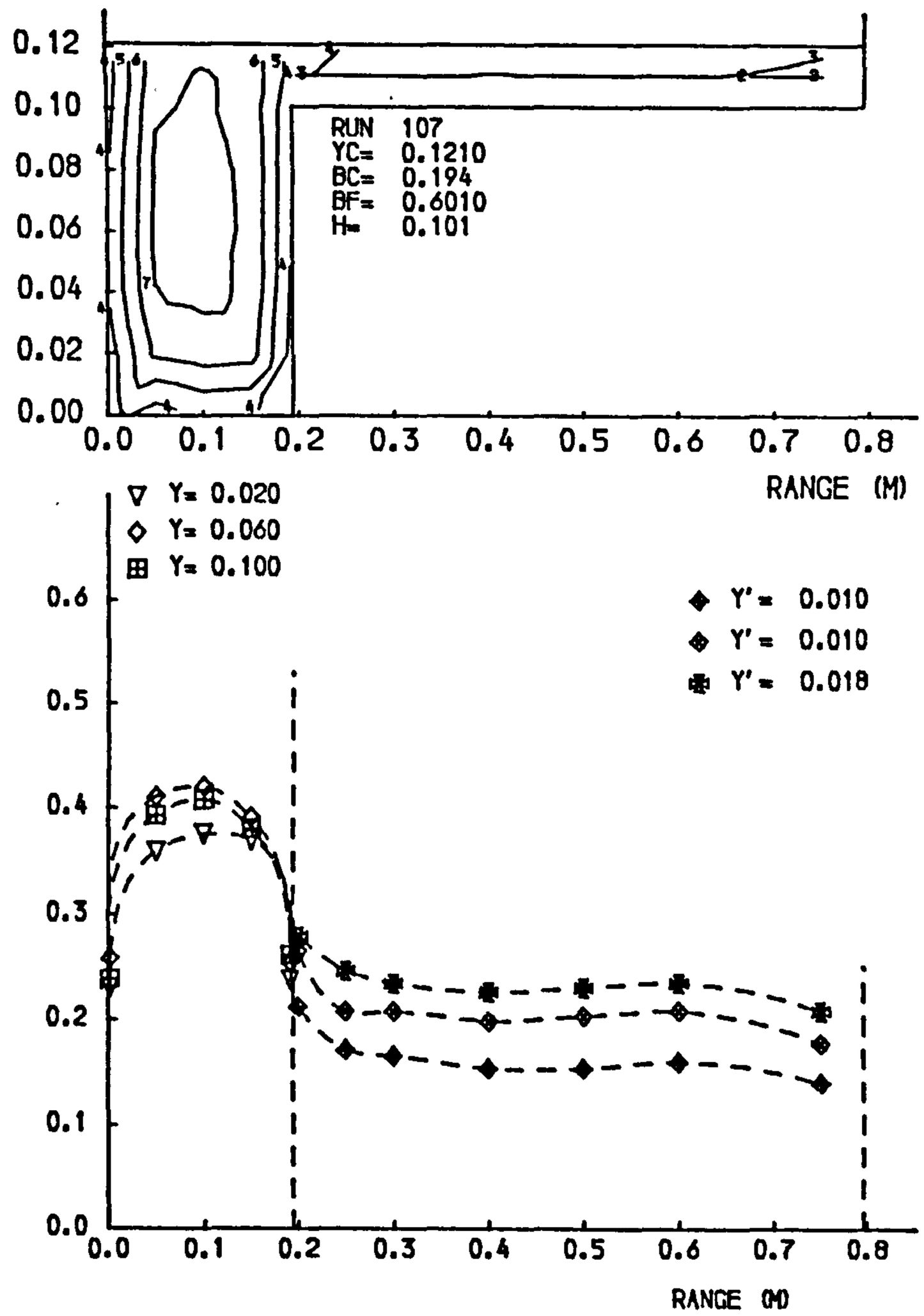

Fig 4·7 Isovels and lateral velocity profiles.

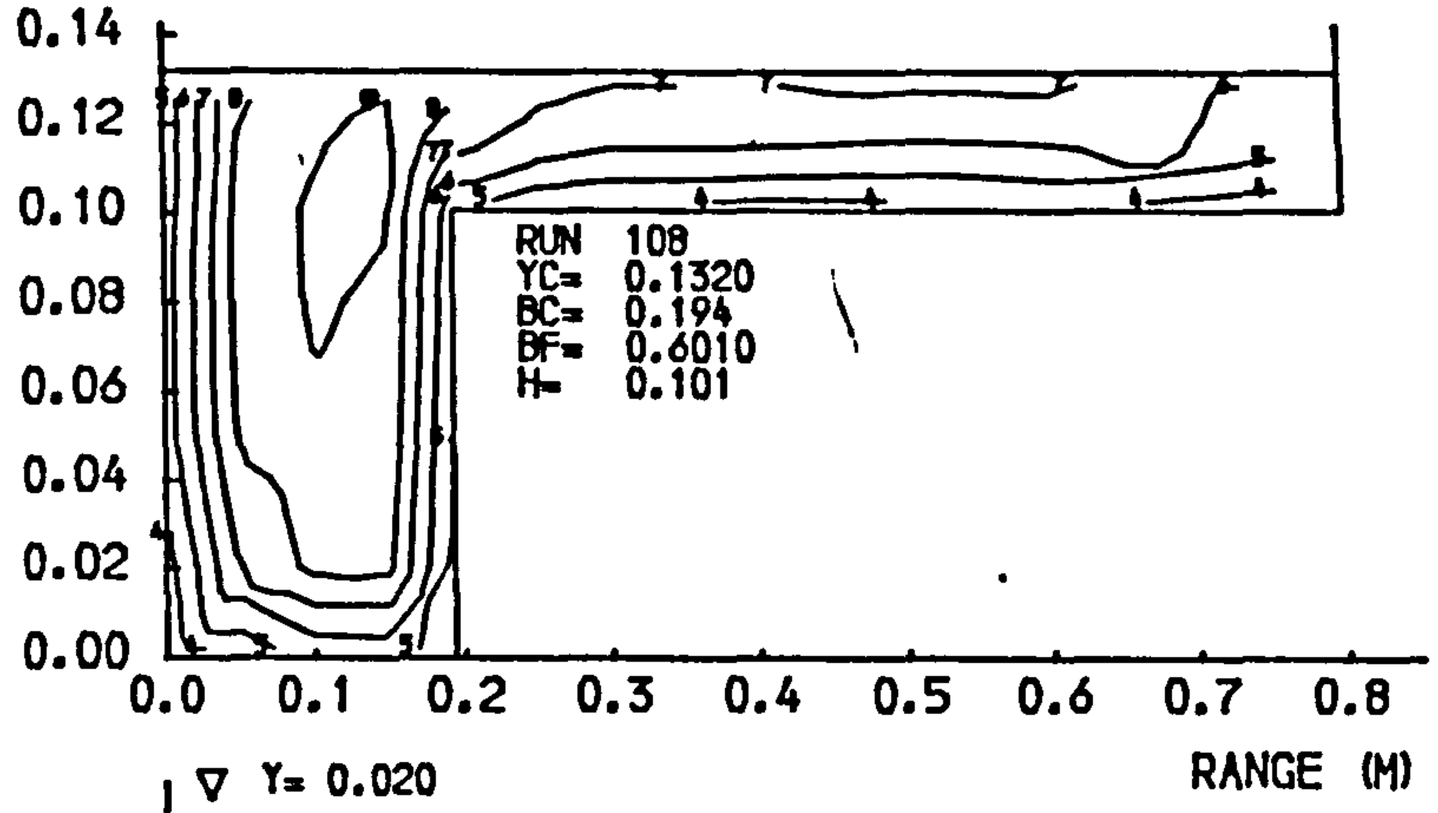

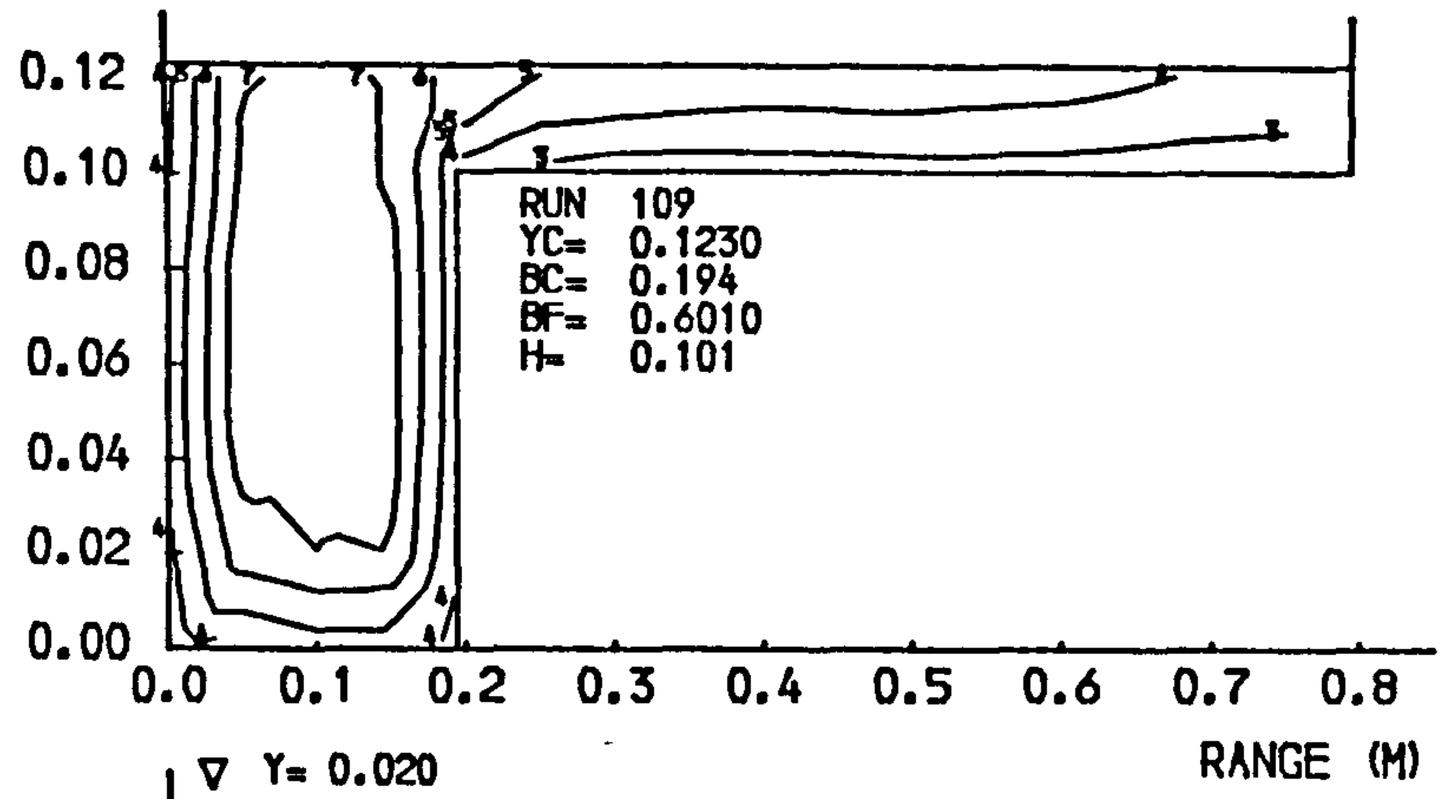

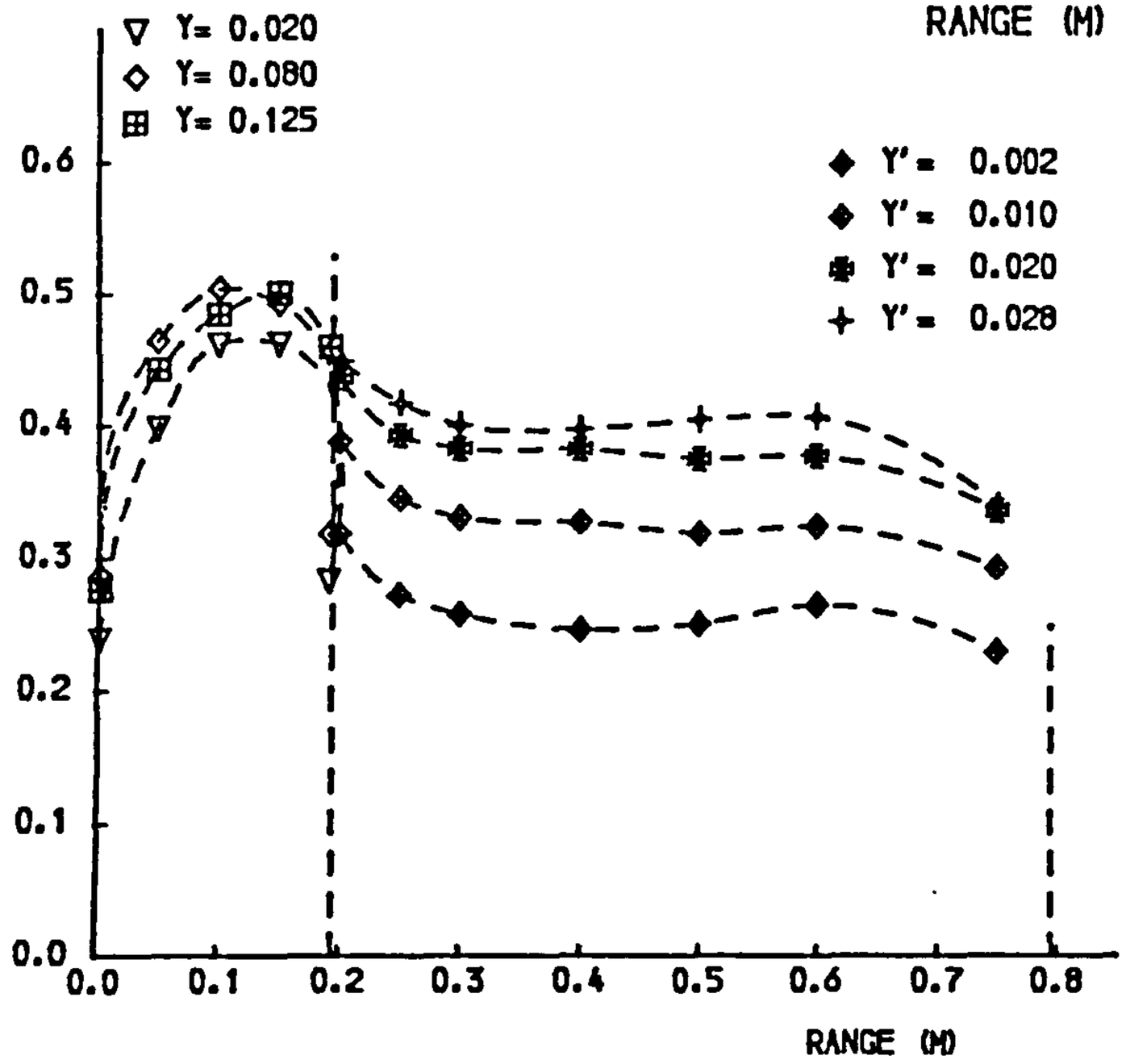

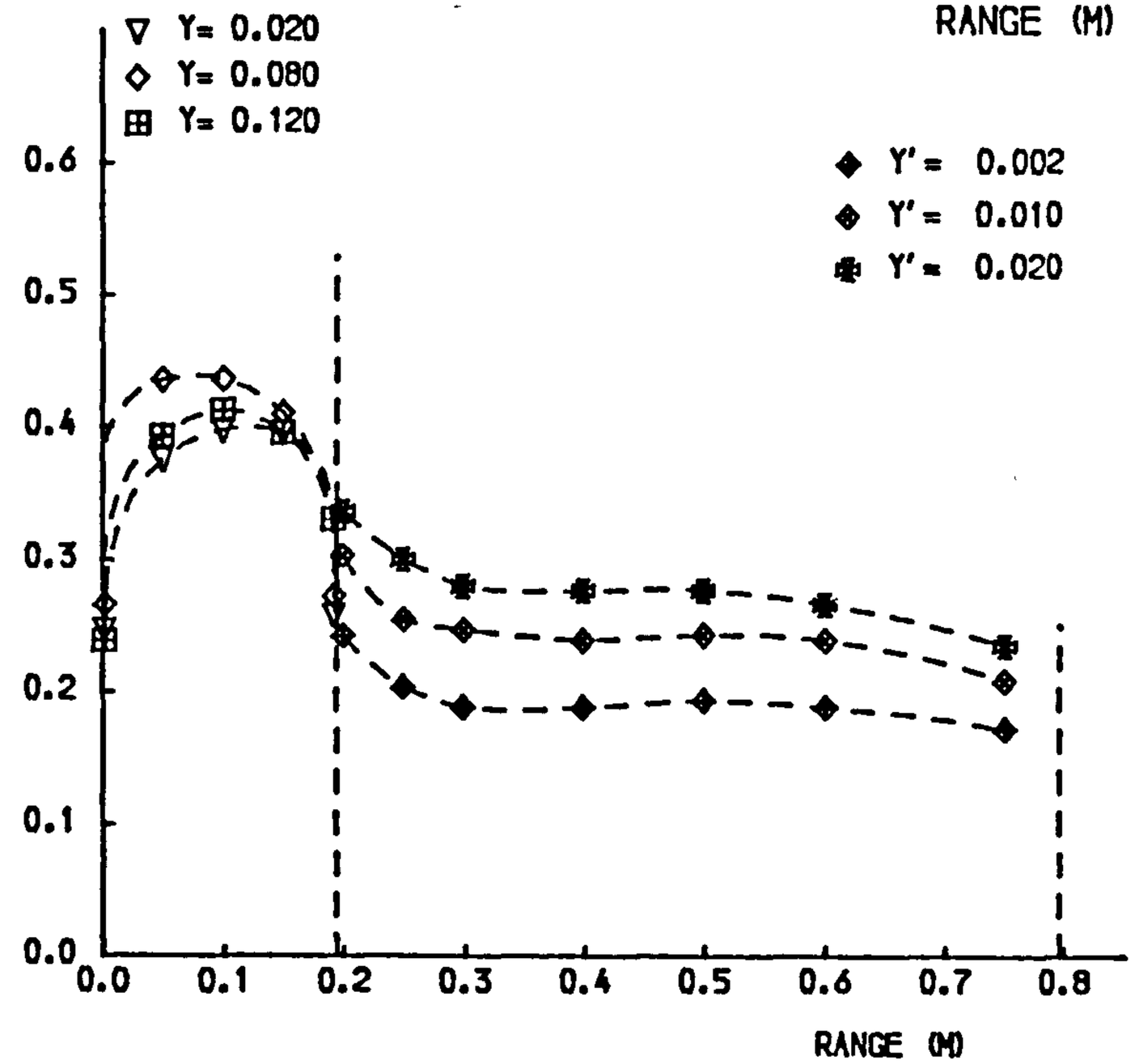

Fig 4·7 Isovels and lateral velocity profiles.

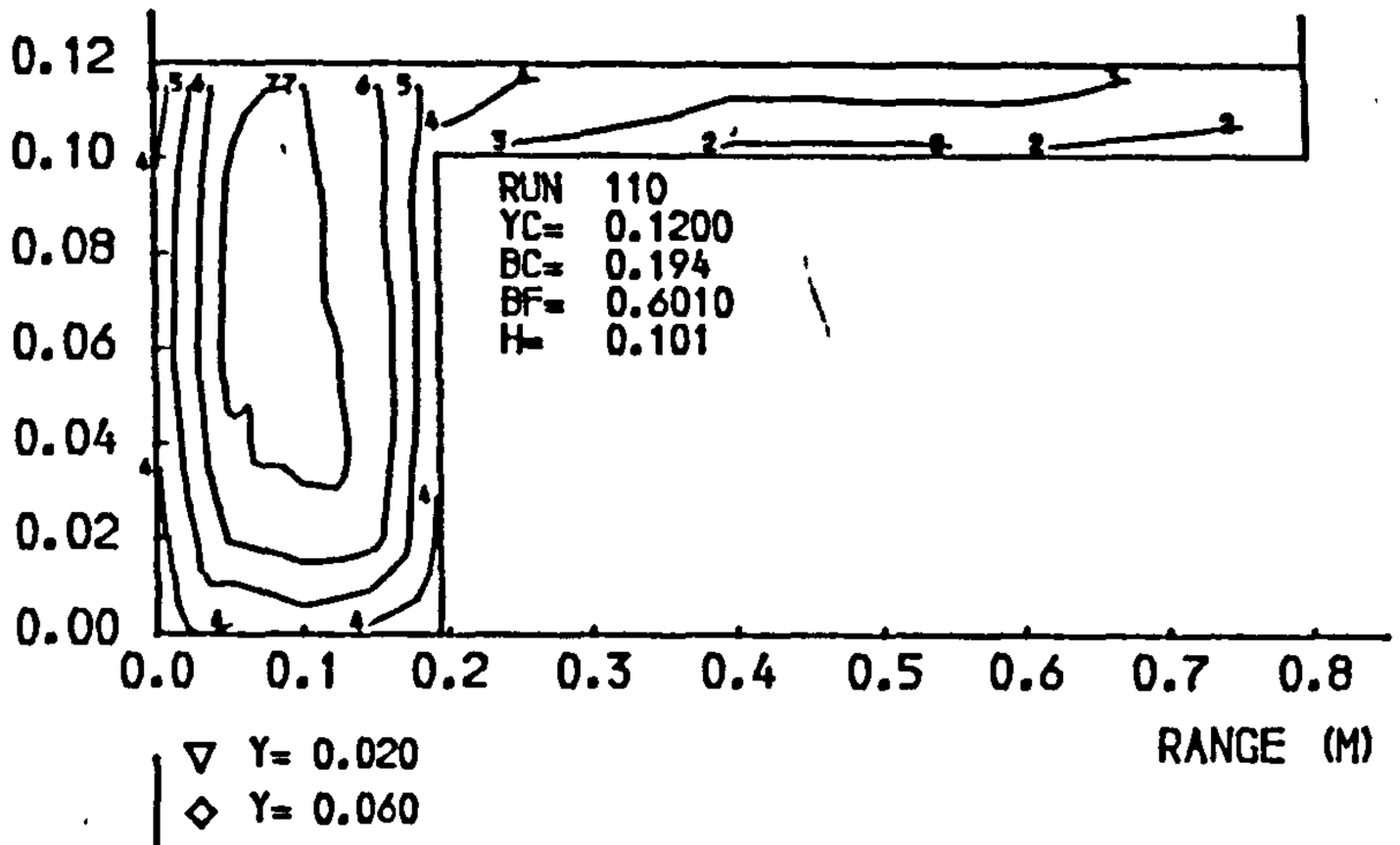

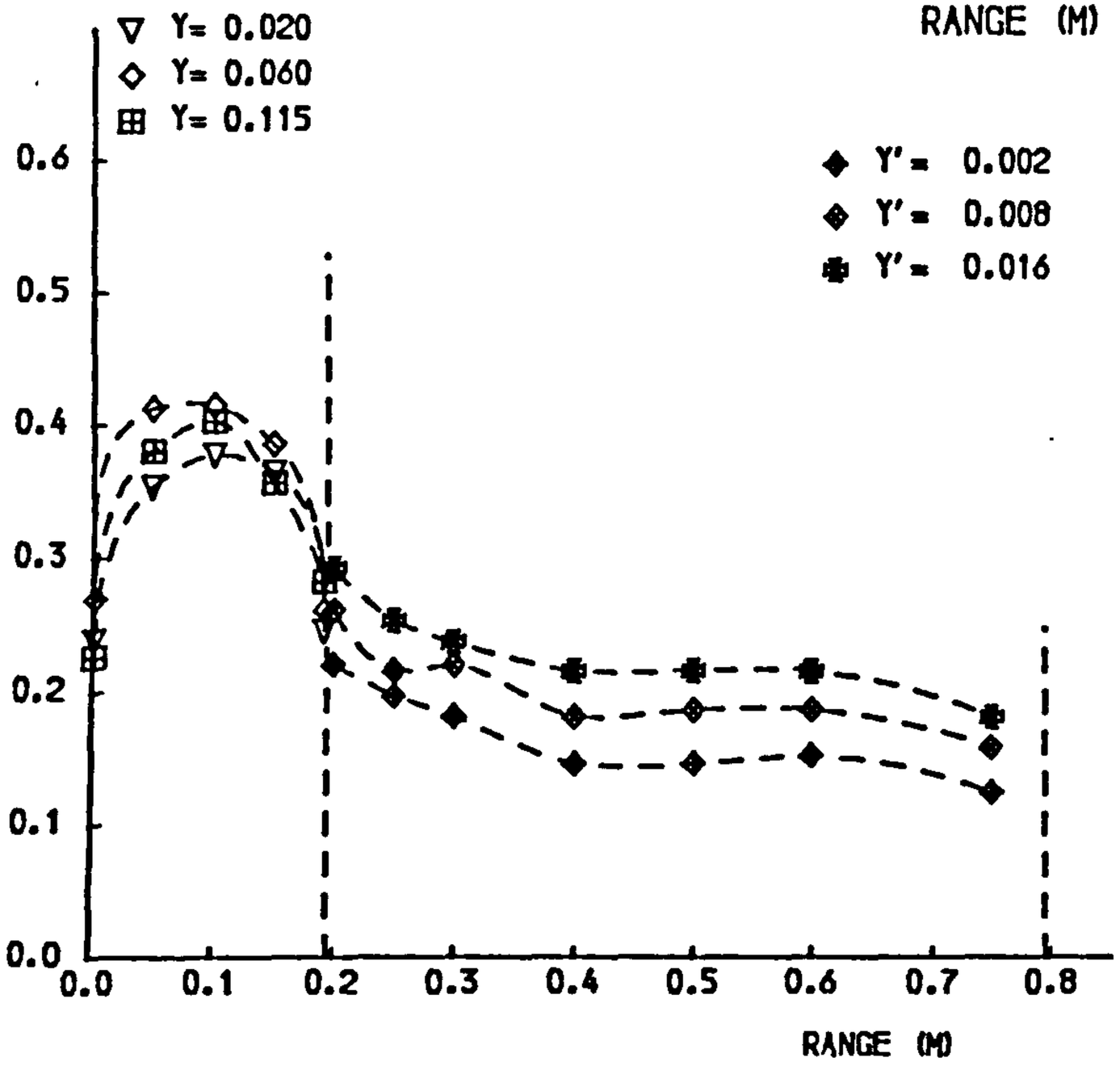

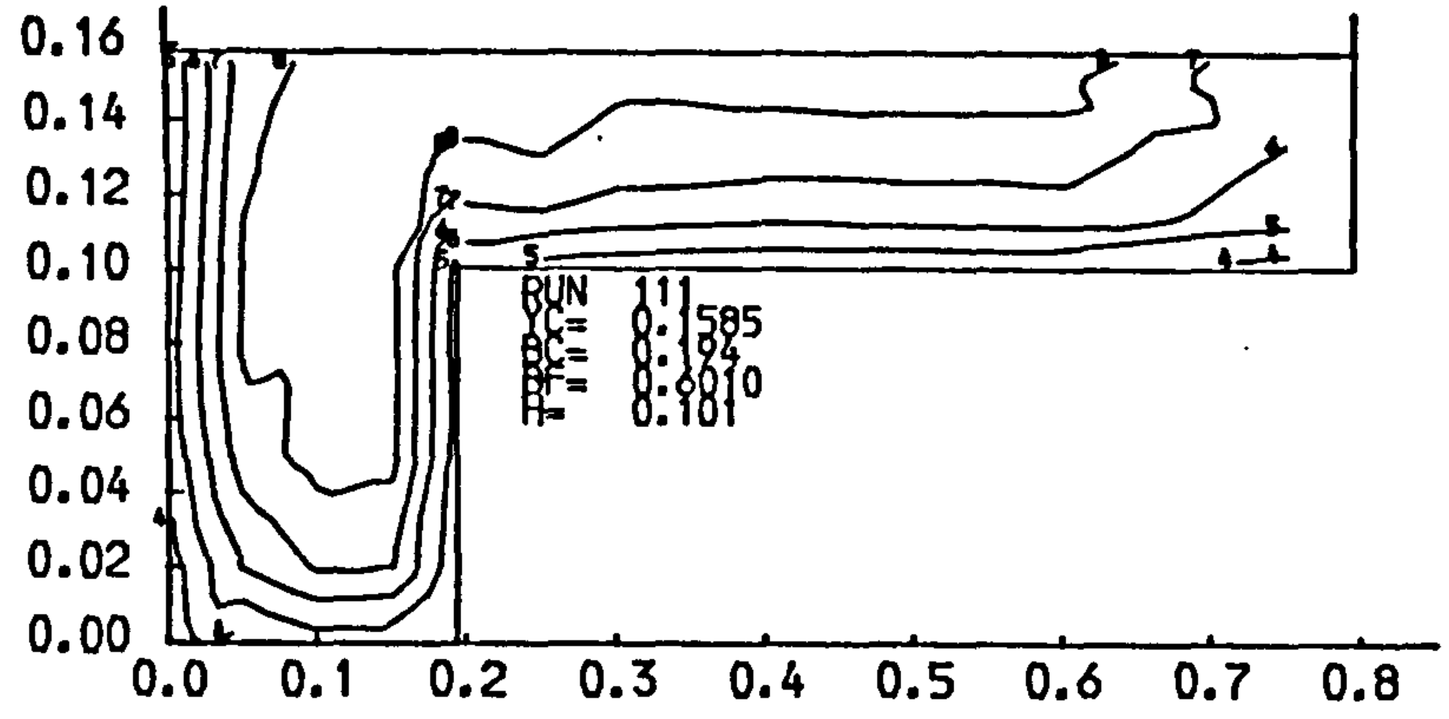

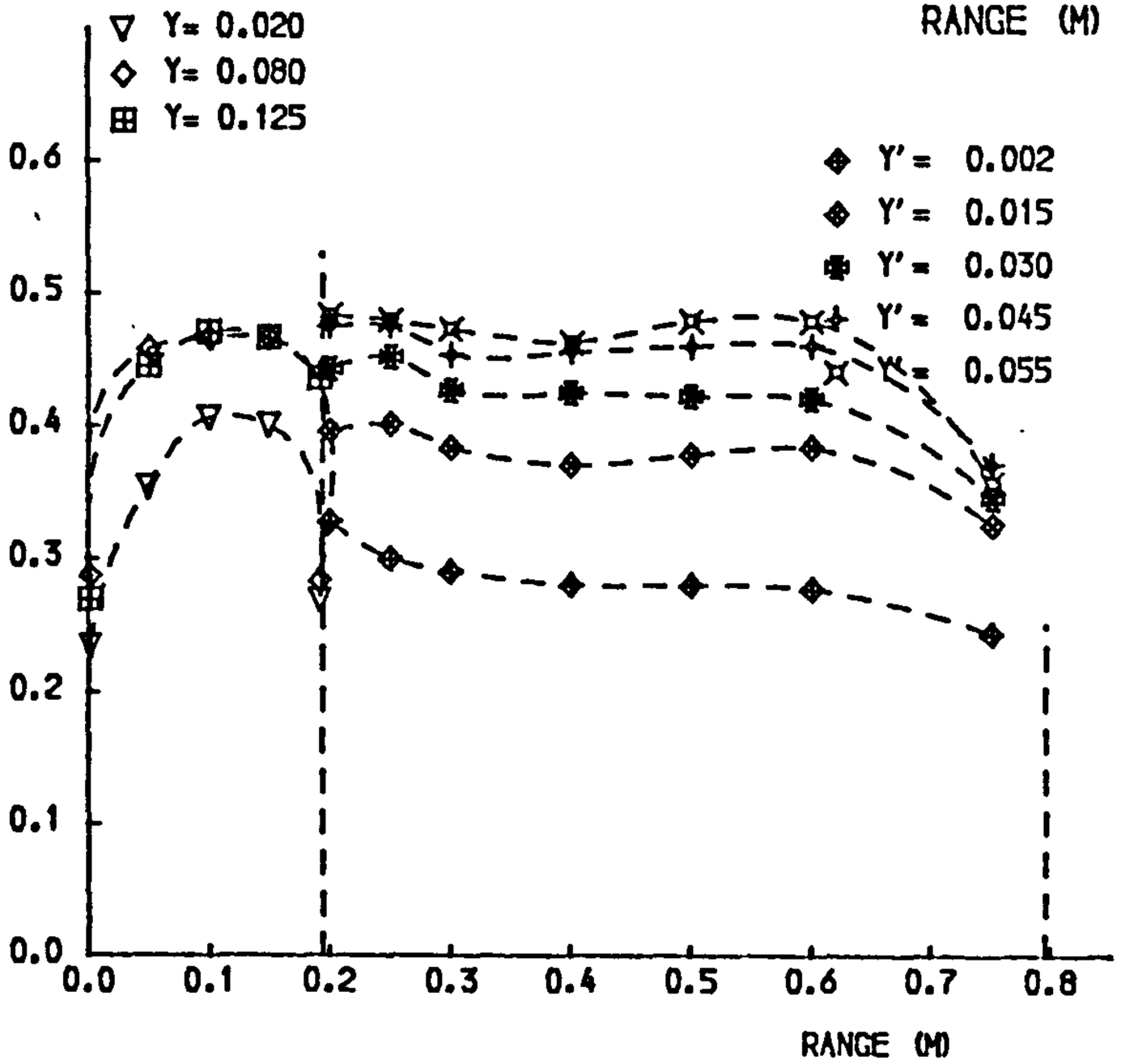

Fig 4·7 Isovels and lateral velocity profiles.

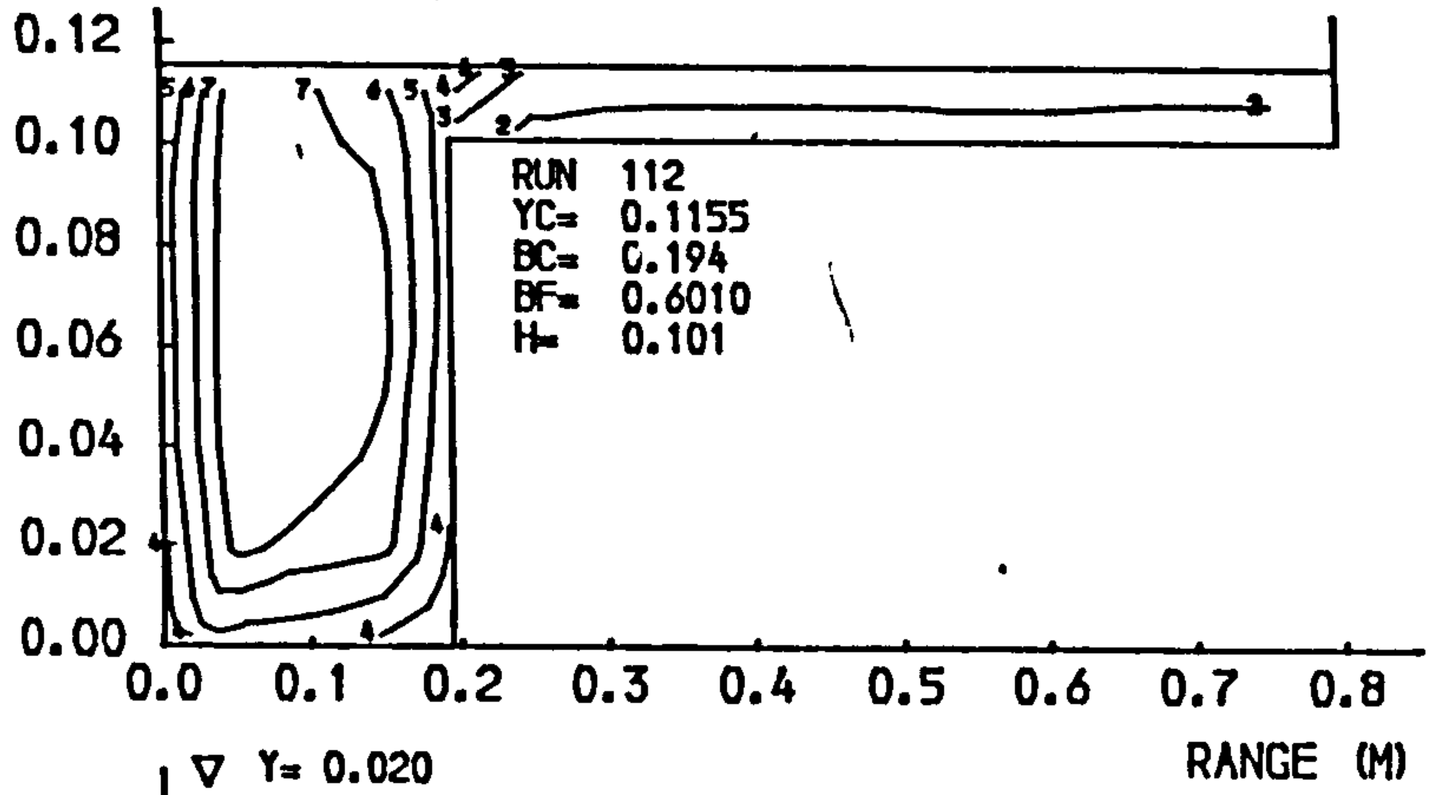

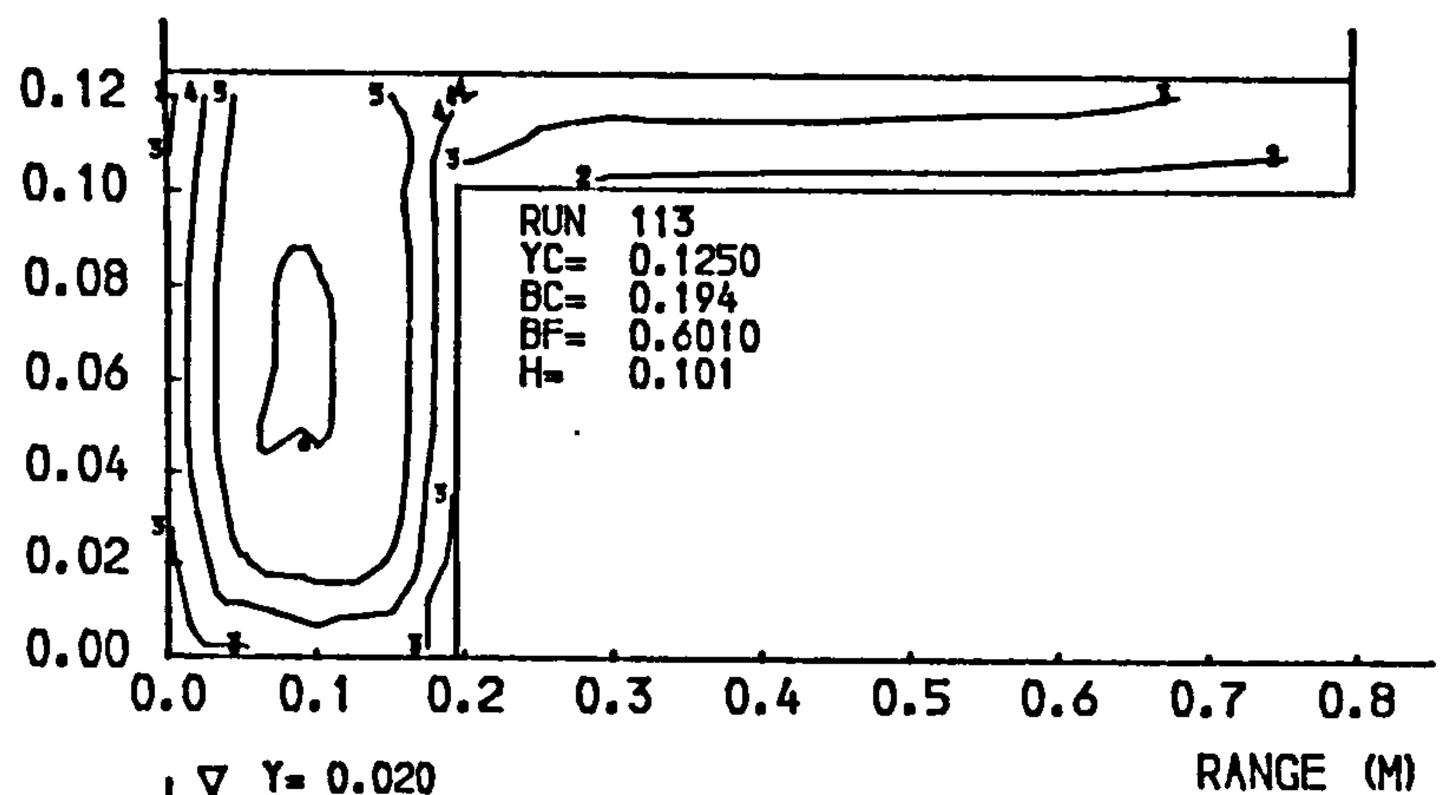

Fig 4·7 Isovels and lateral velocity profiles.

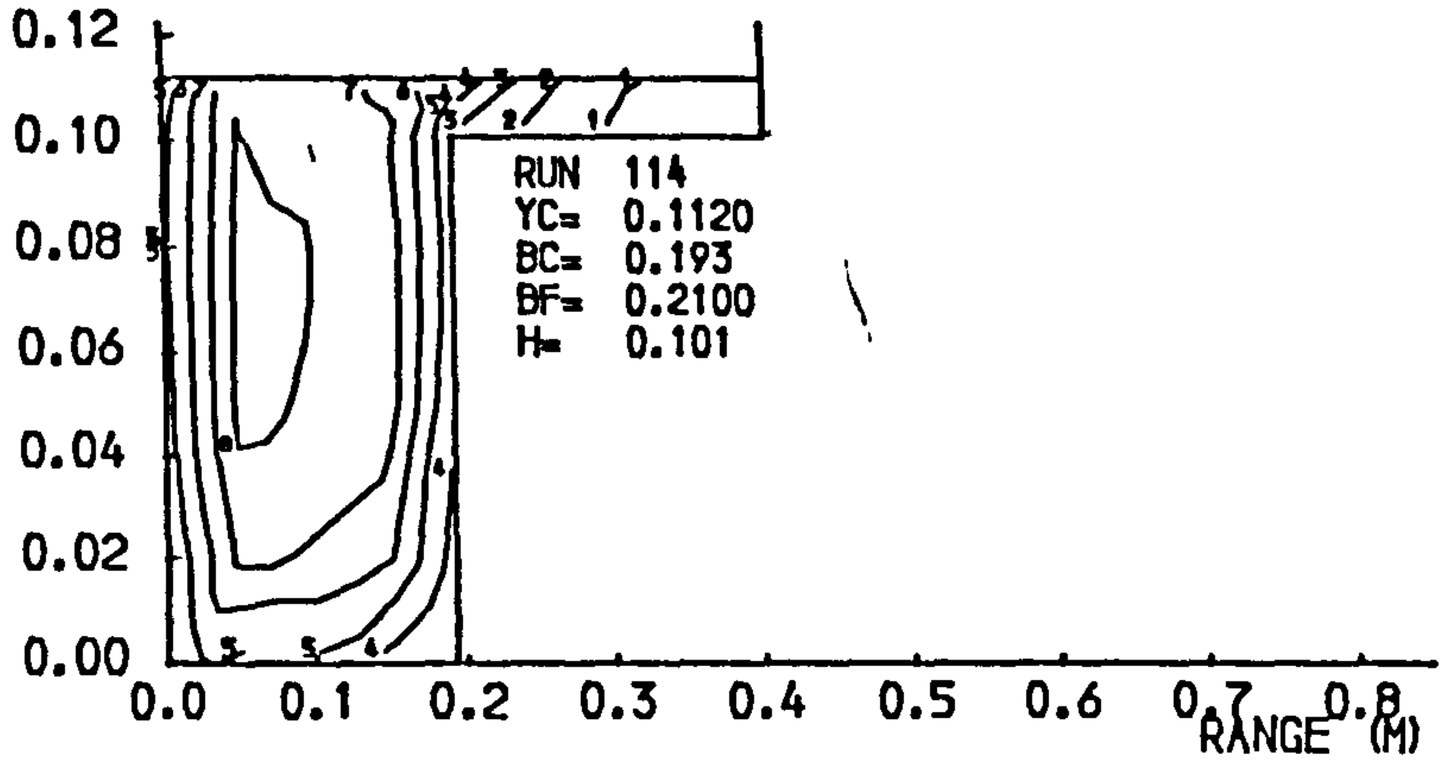

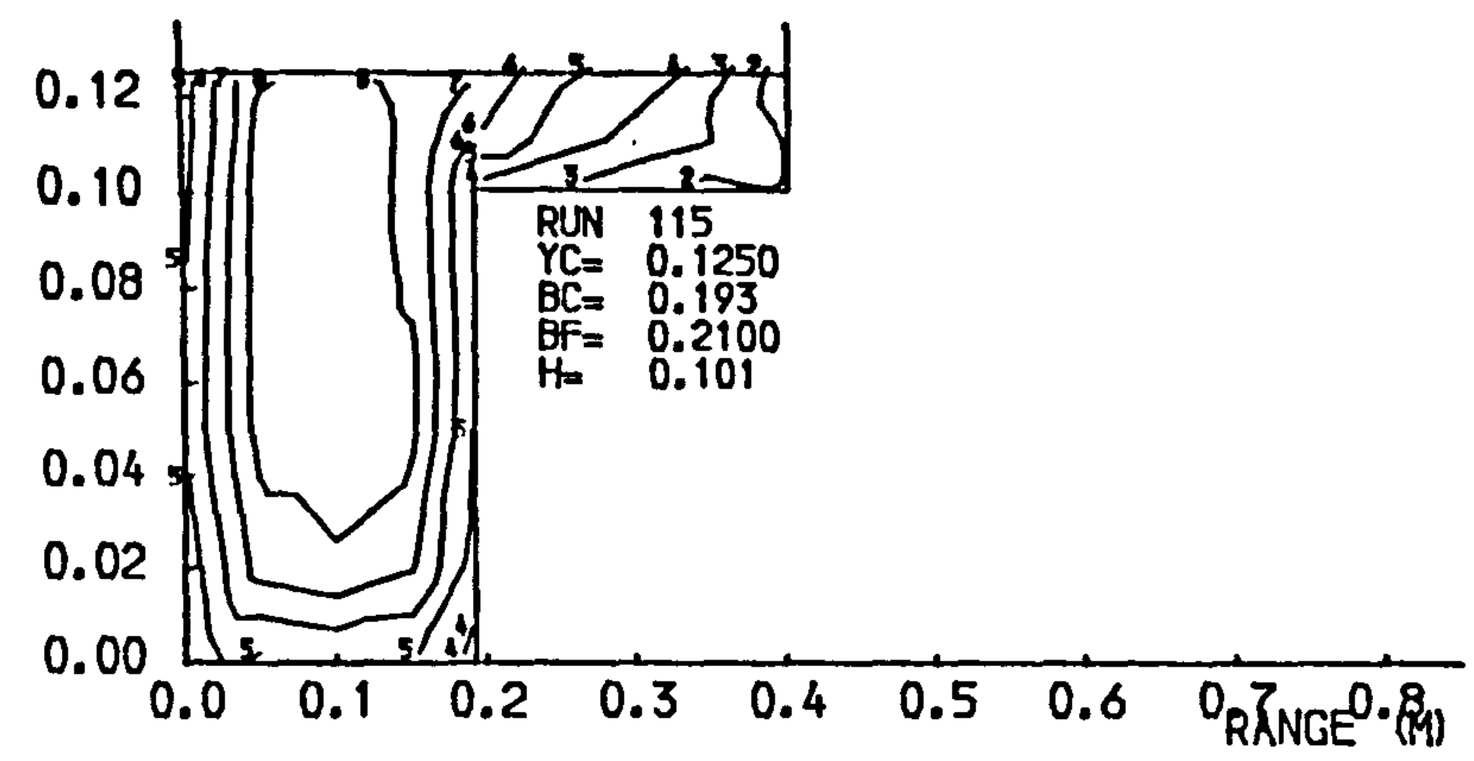

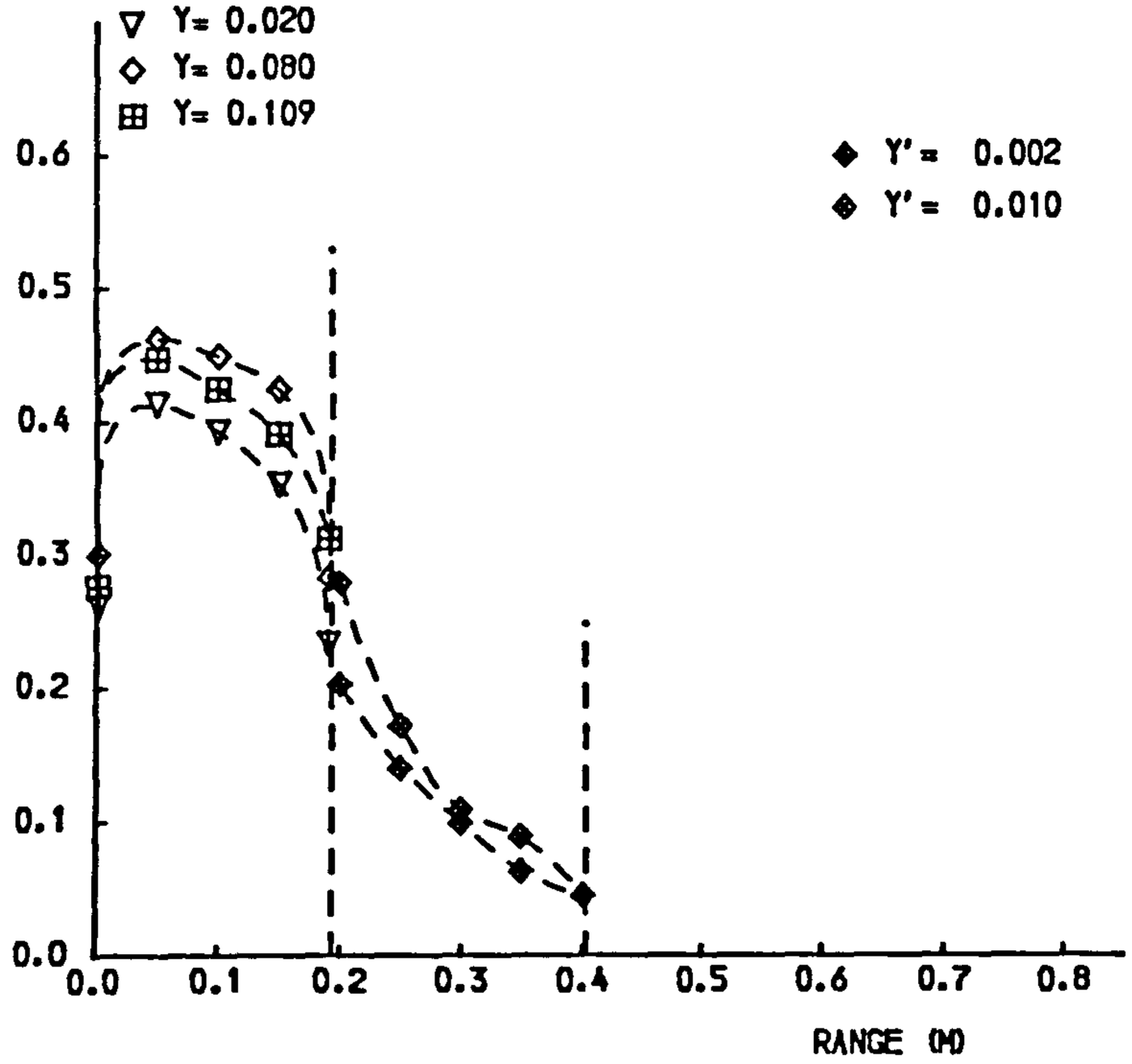

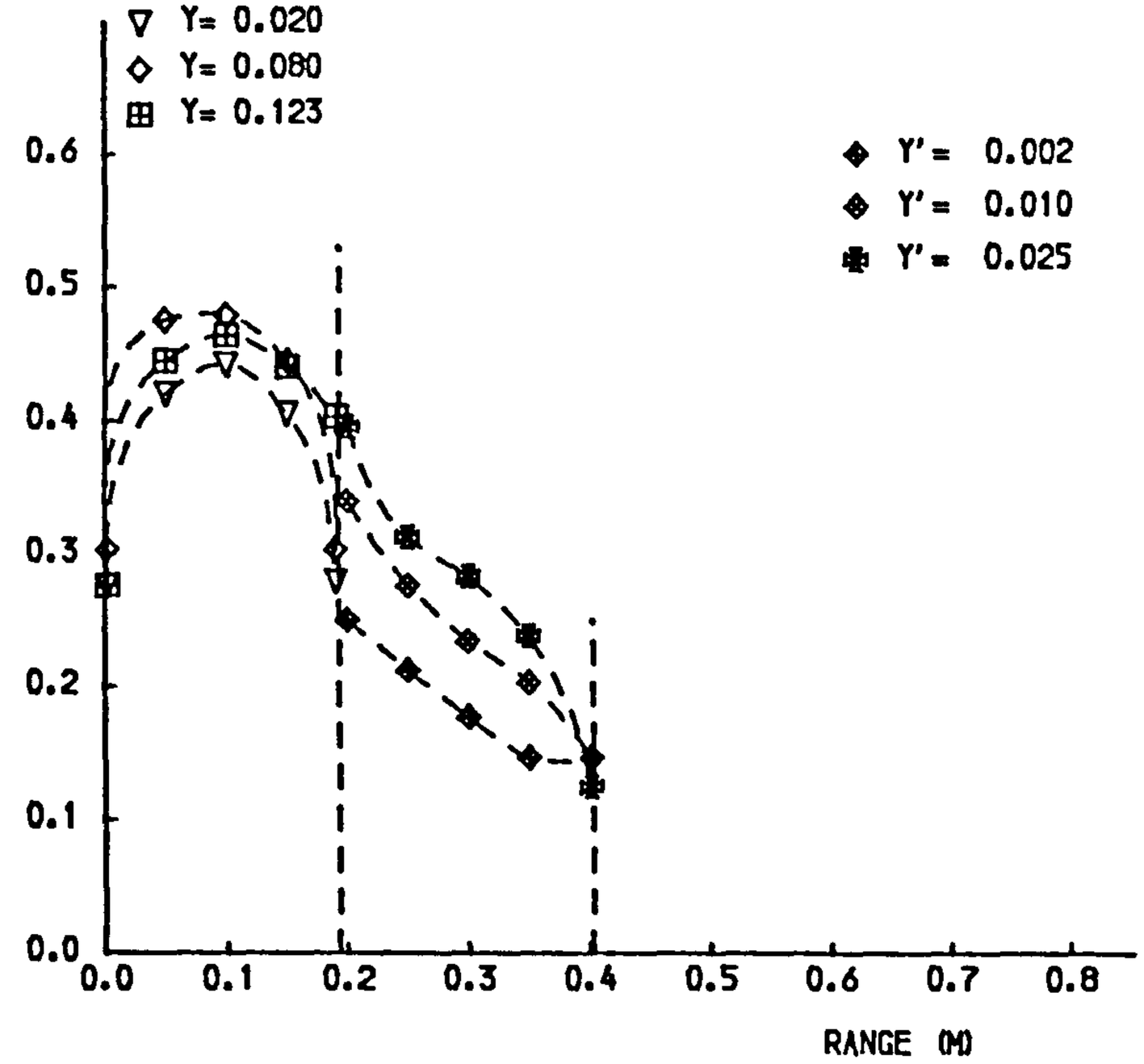

Fig 4·7 Isovels and lateral velocity profiles.

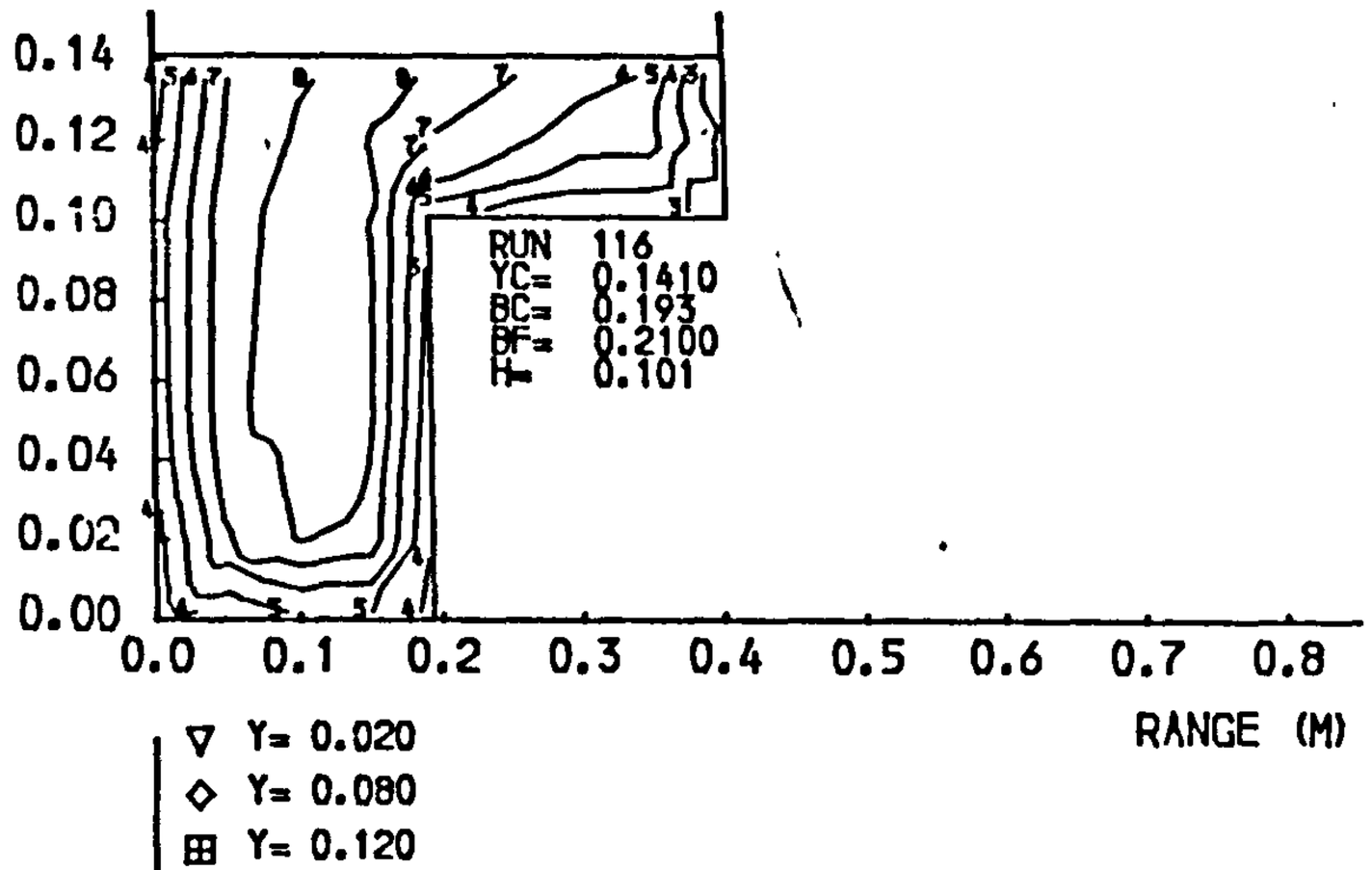

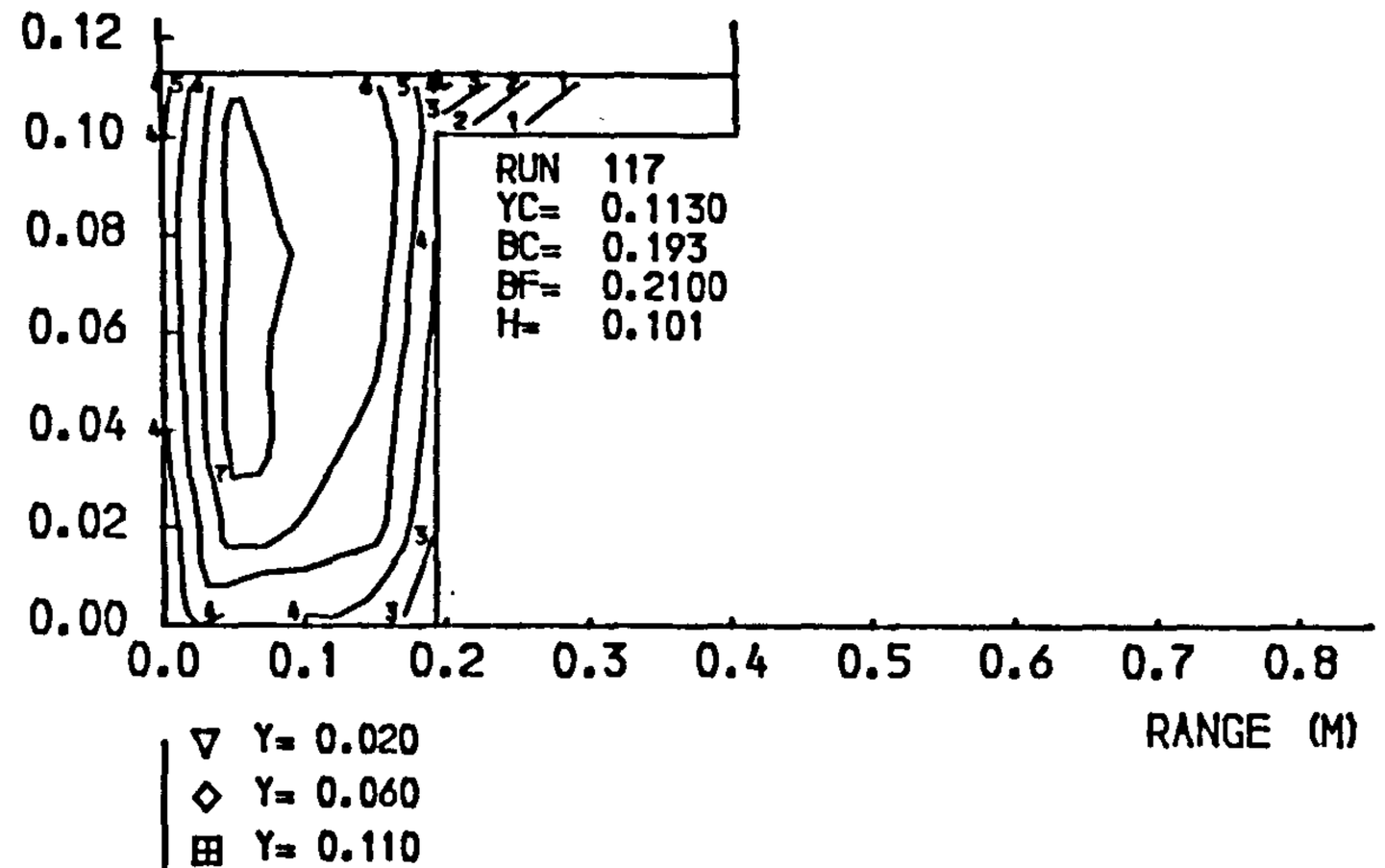

Fig 4·7 Isovels and lateral velocity profiles.

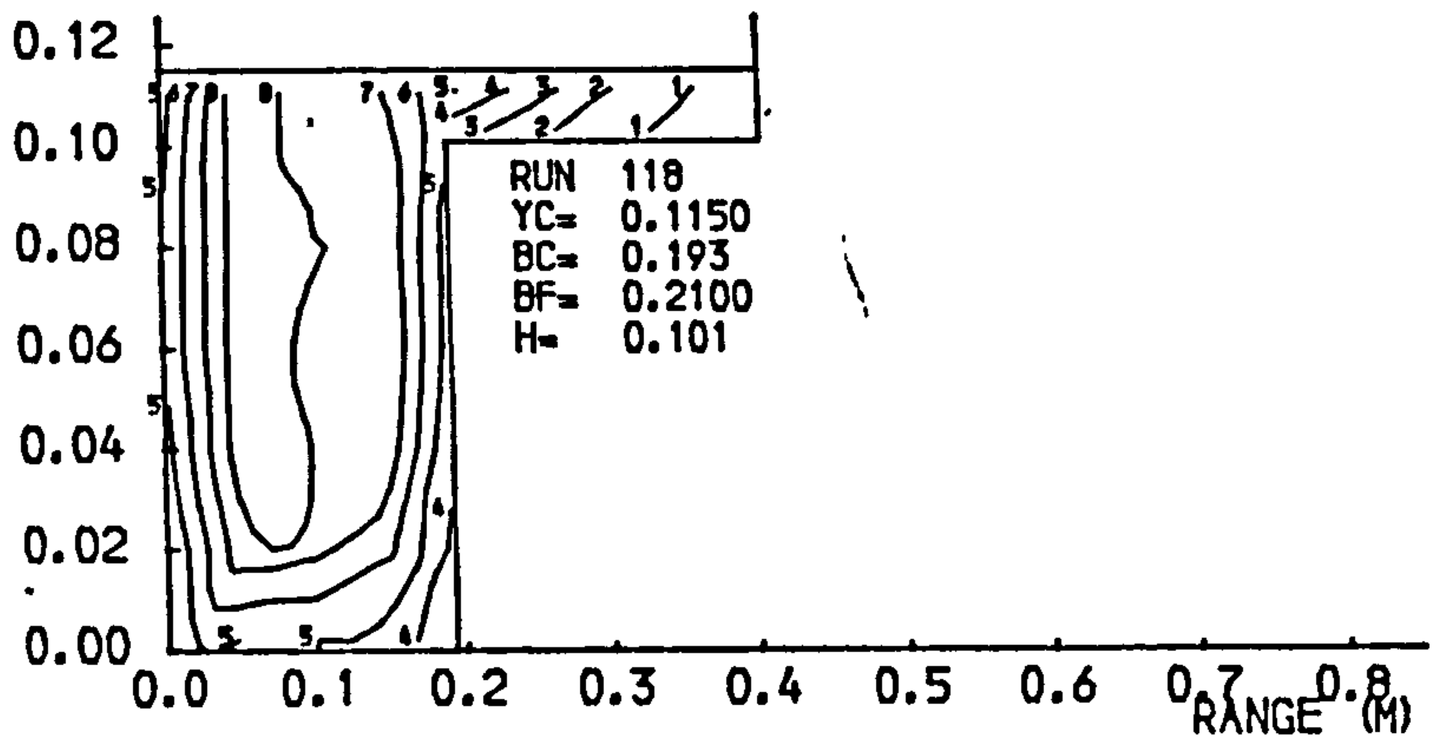

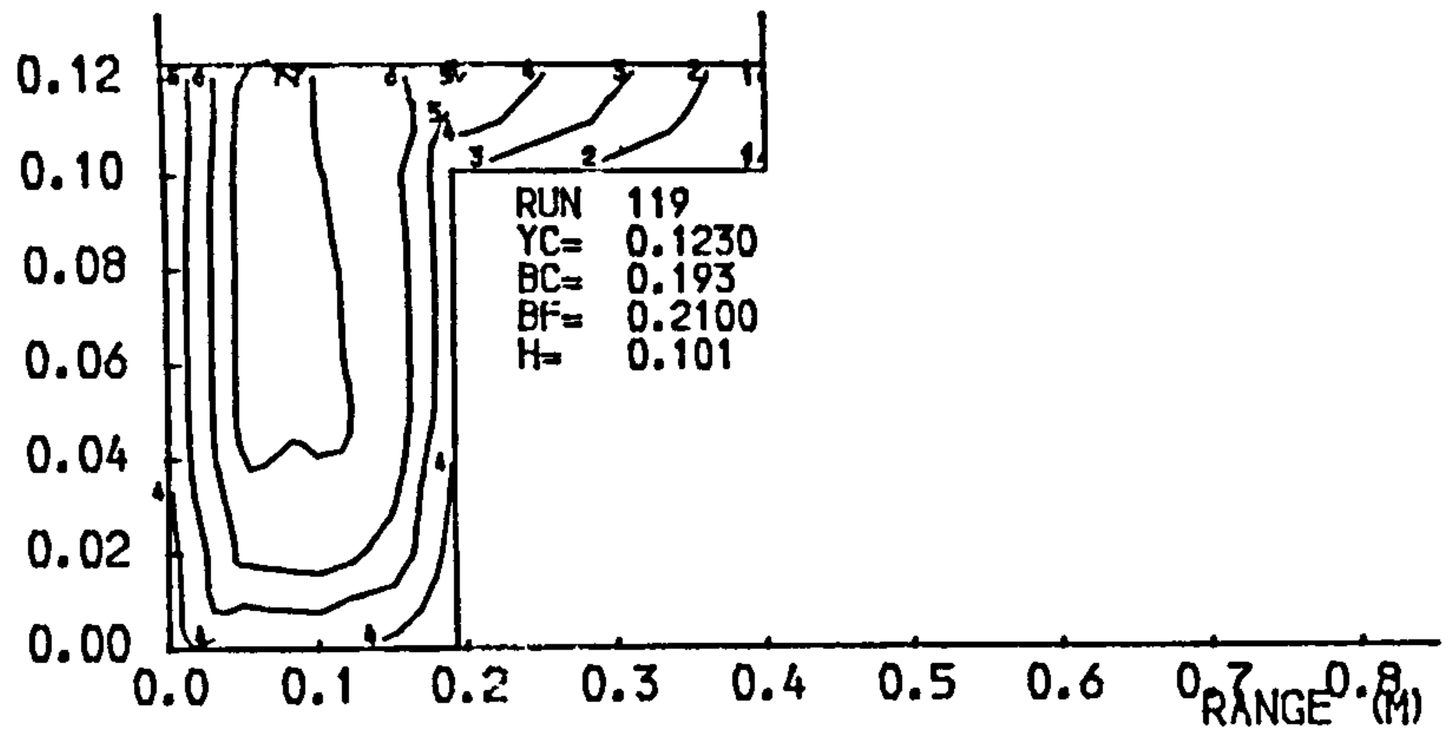

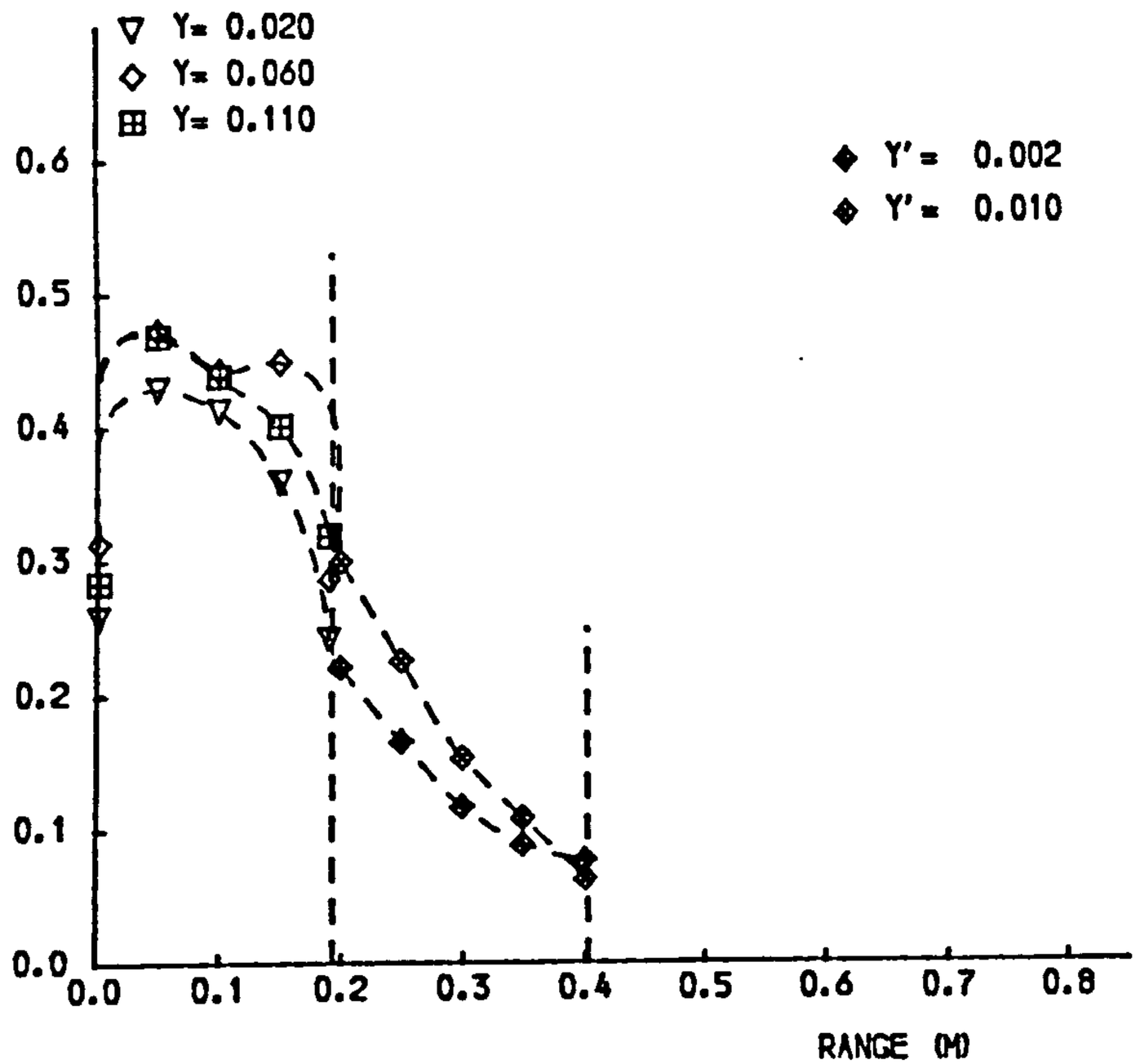

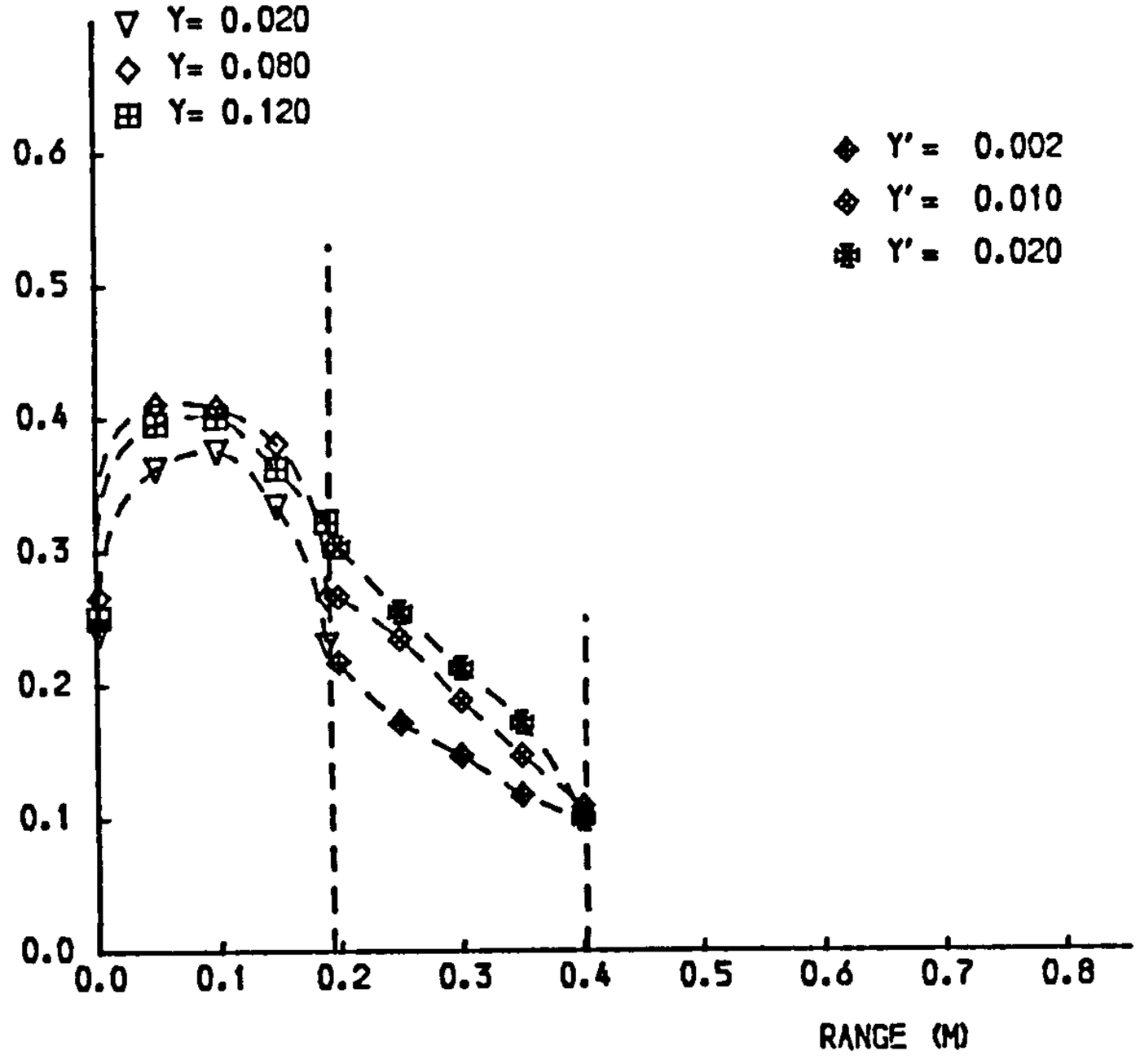

Fig 4·7 Isovels and lateral velocity profiles.

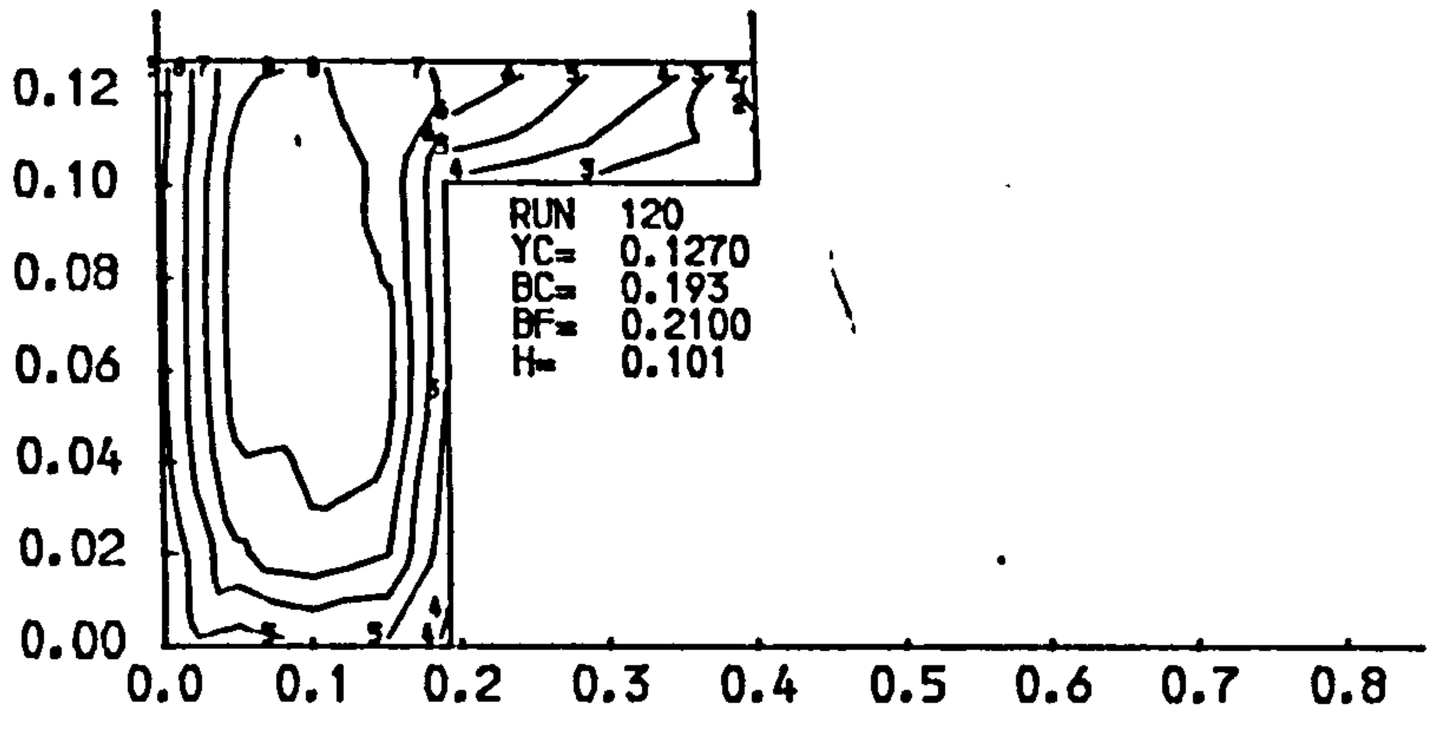

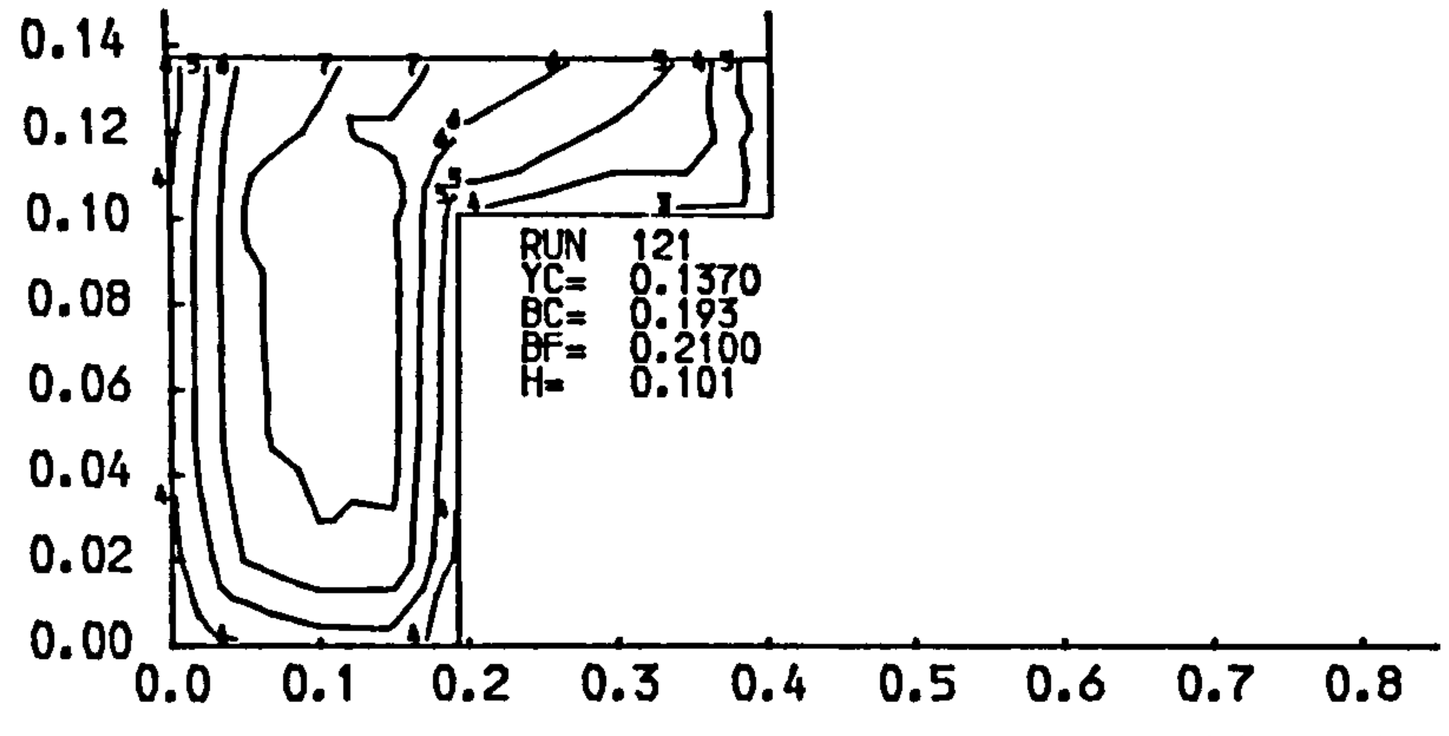

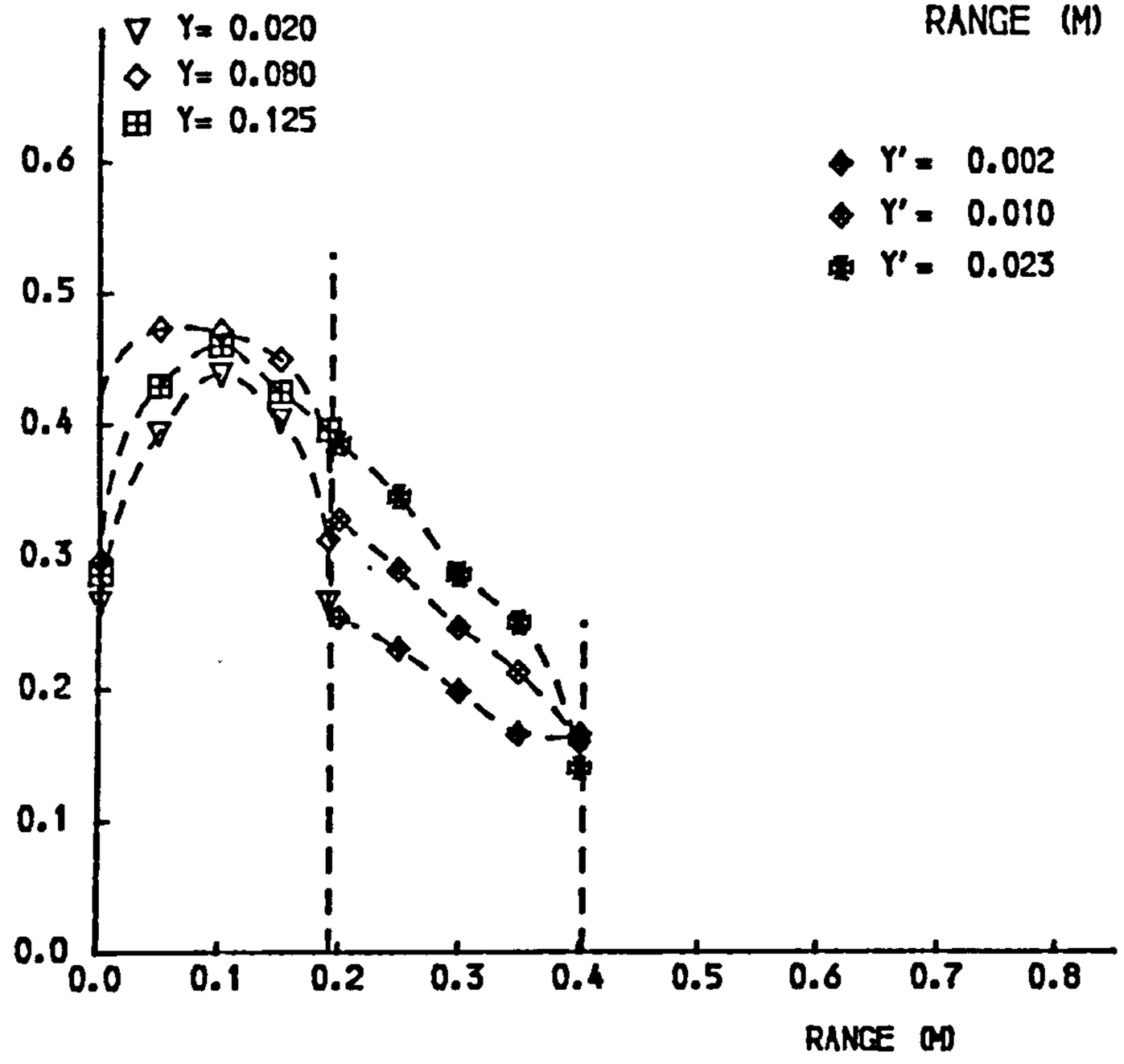

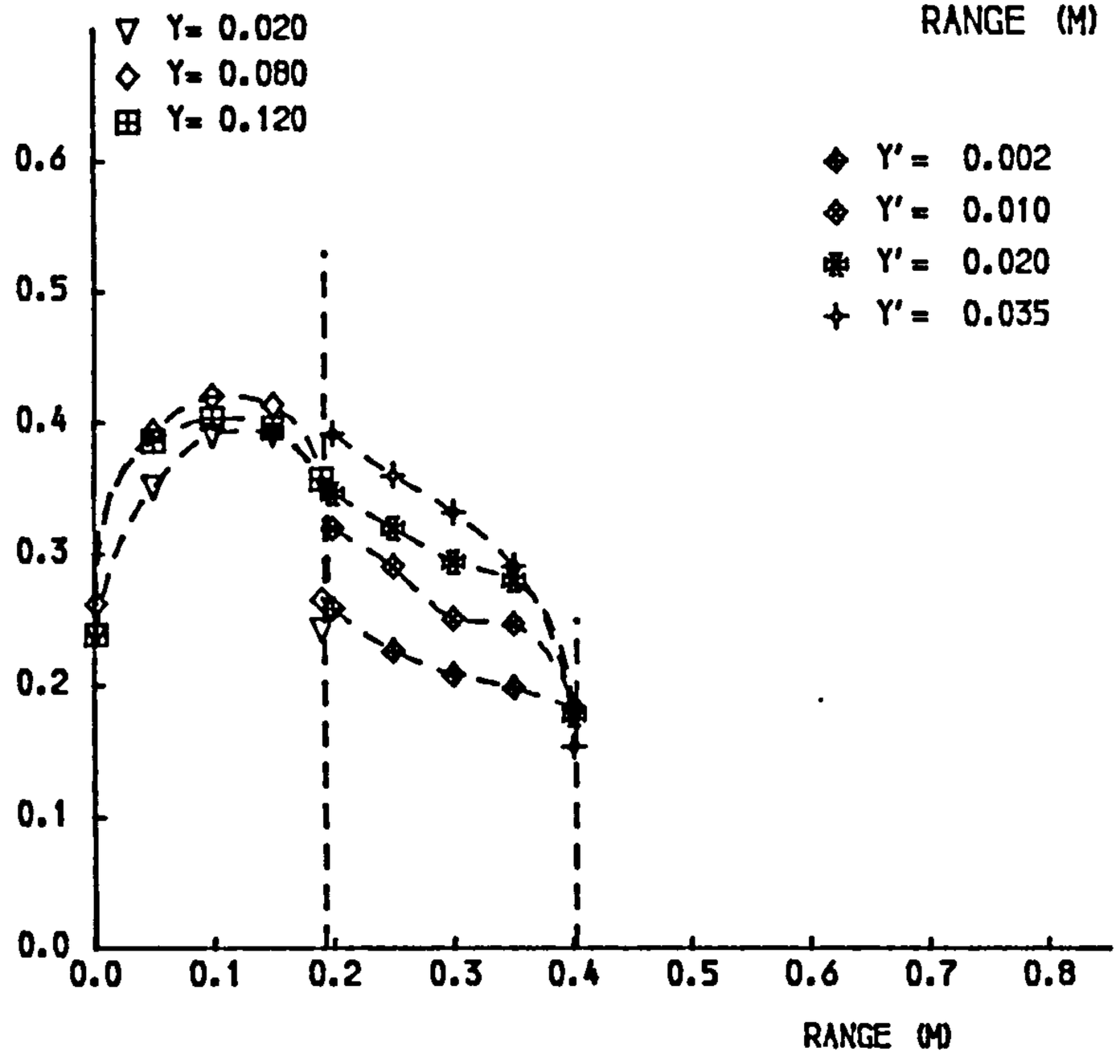

Fig 4·7 Isovels and lateral velocity profiles.

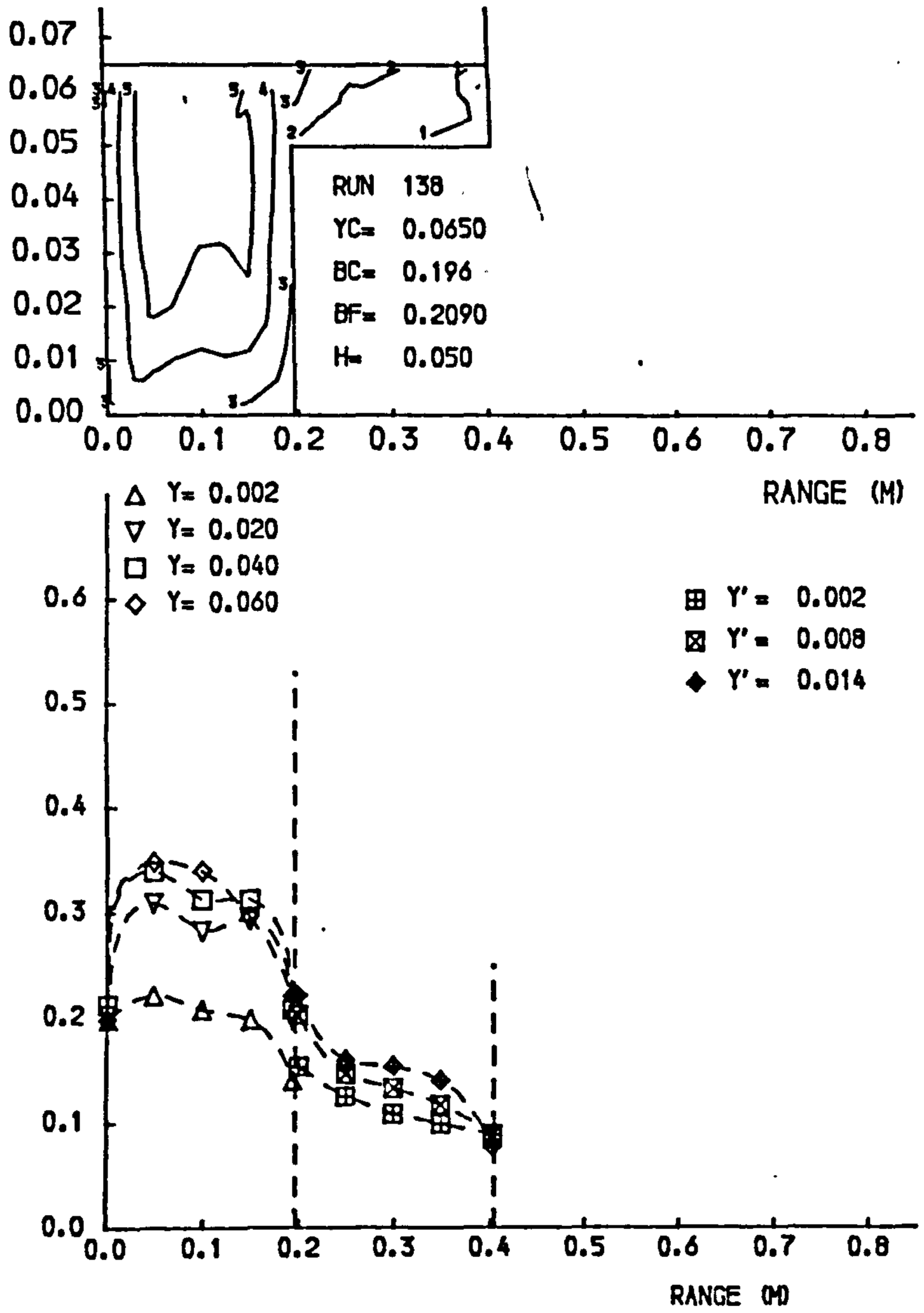

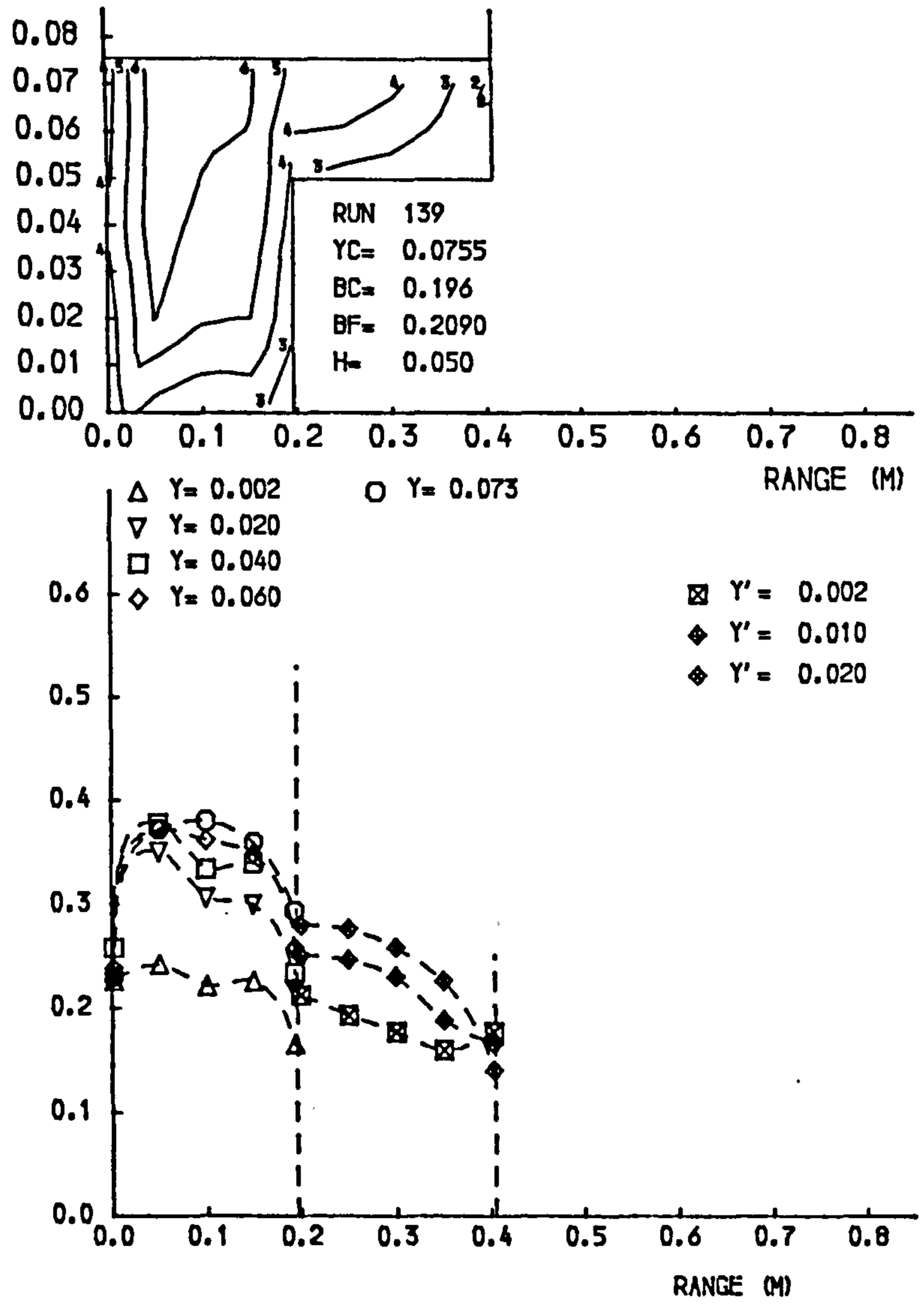

Fig 4·7 Isovels and lateral velocity profiles.

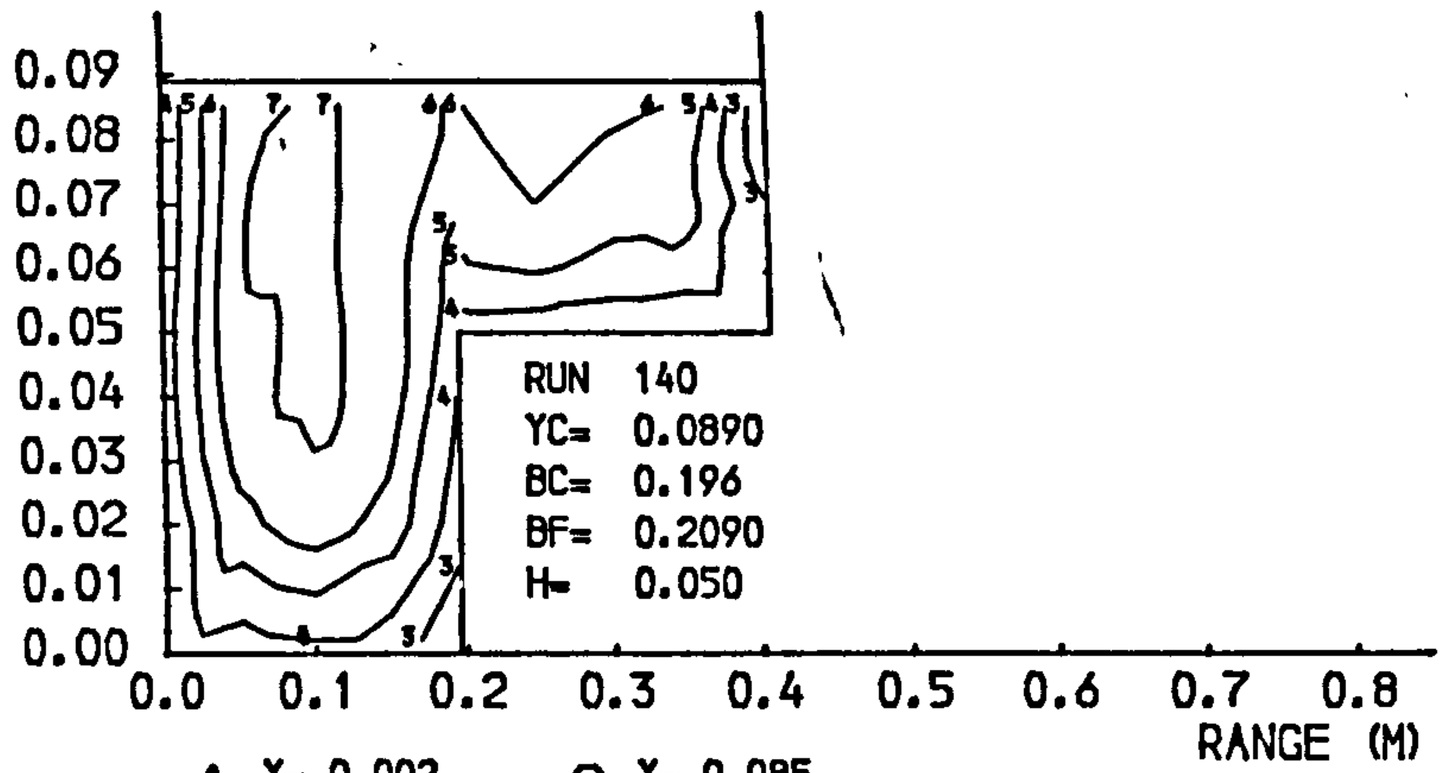

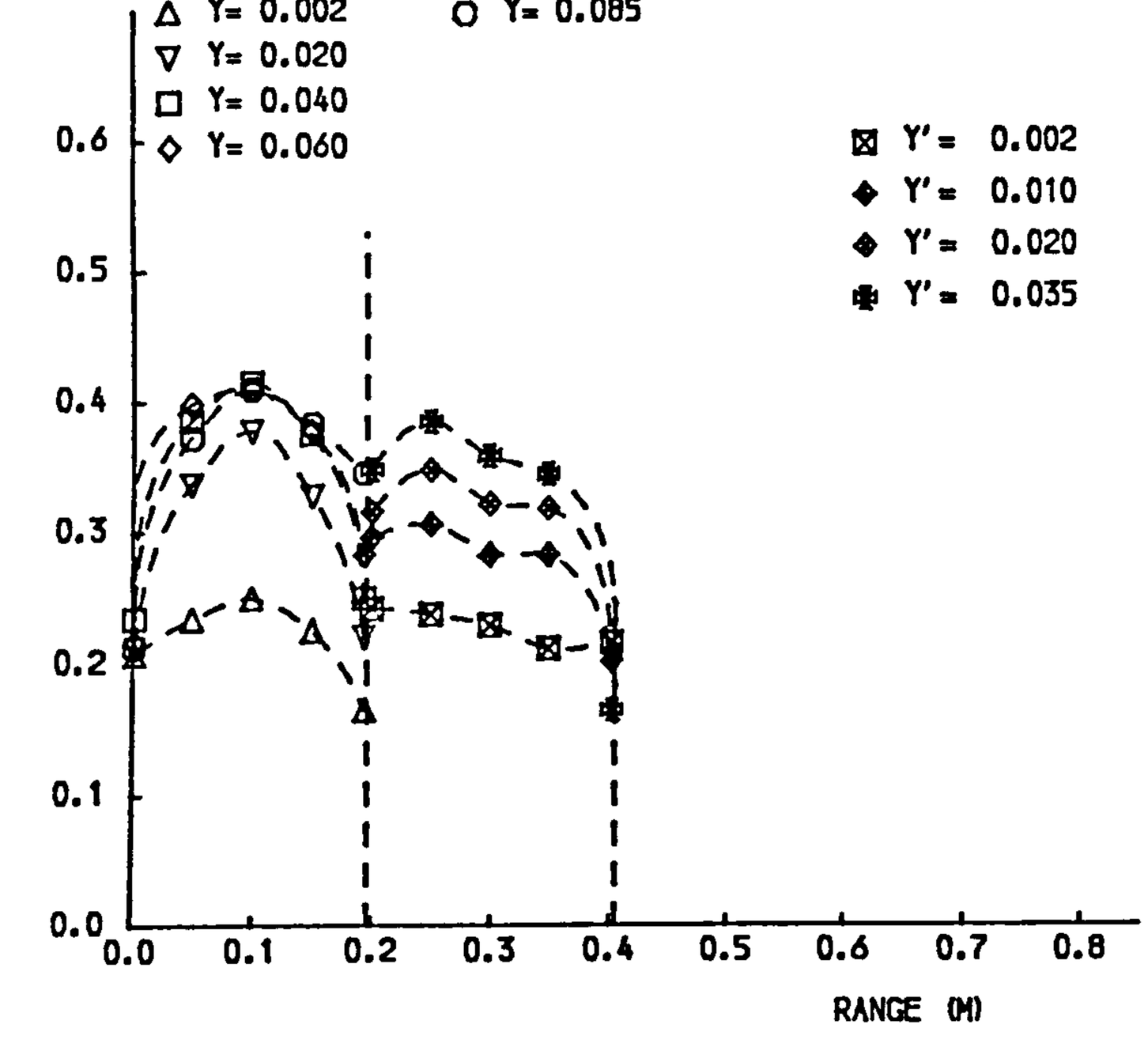

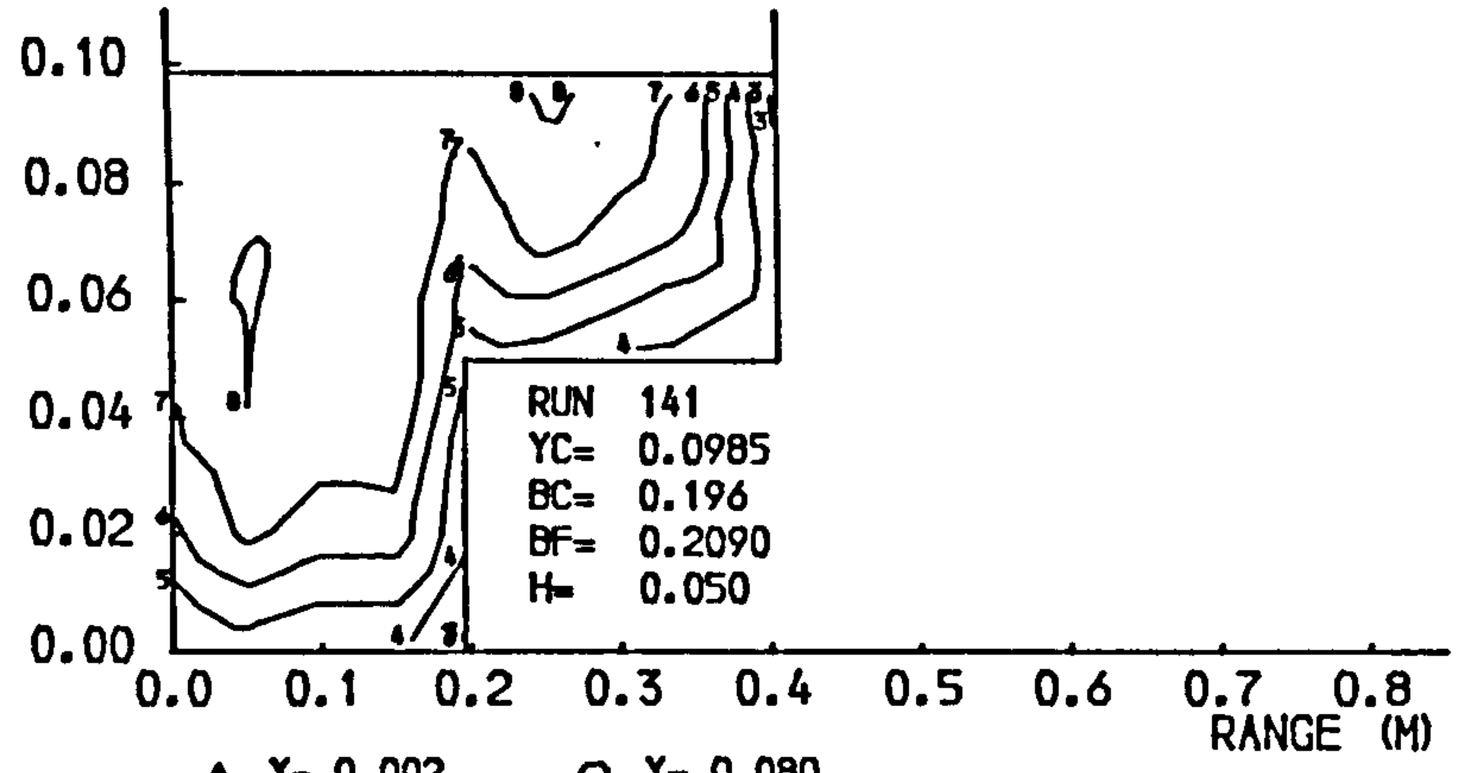

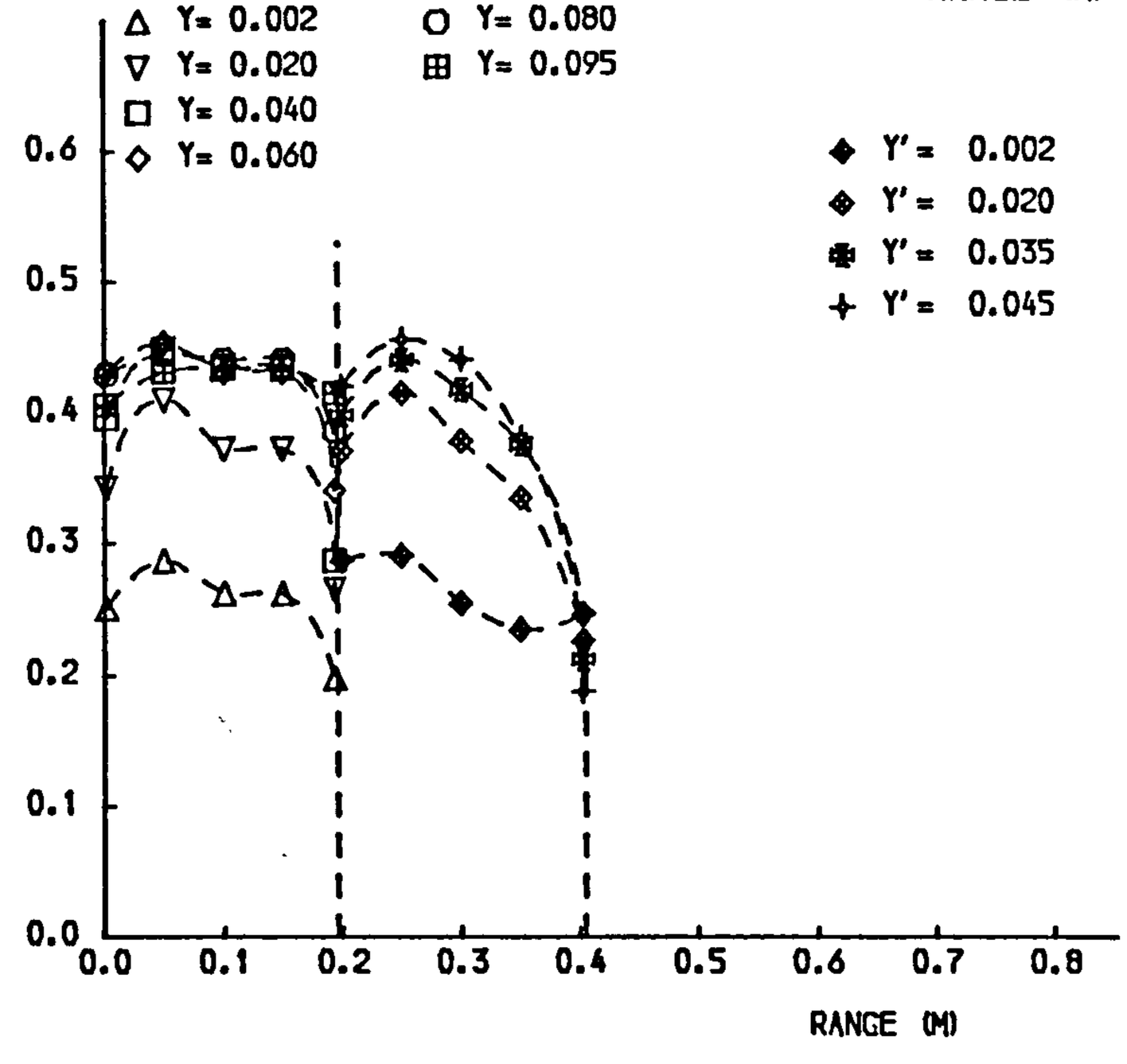

Fig 4·7 Isovels and lateral velocity profiles.

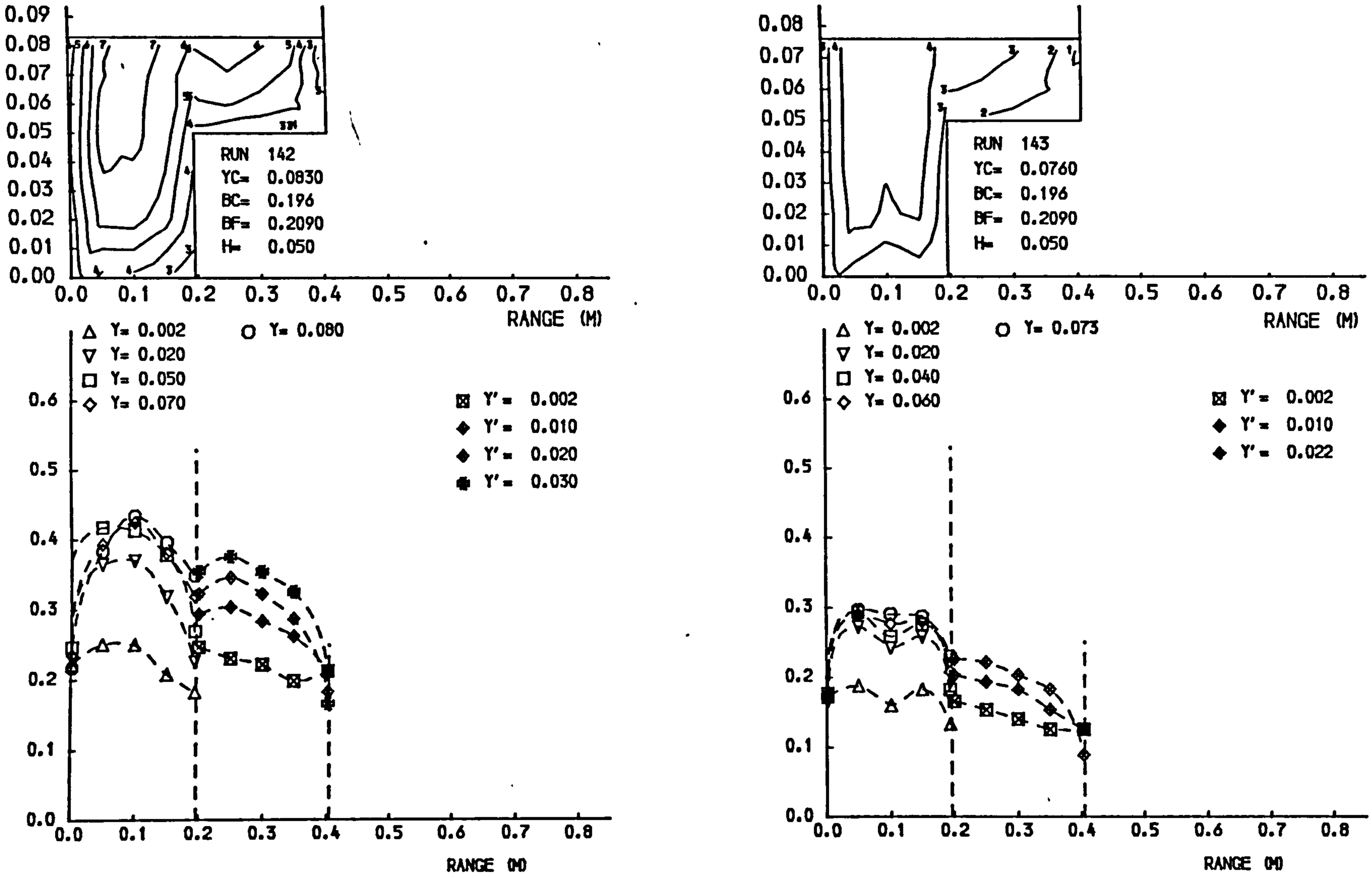

Fig 4·7 Isovels and lateral velocity profiles.

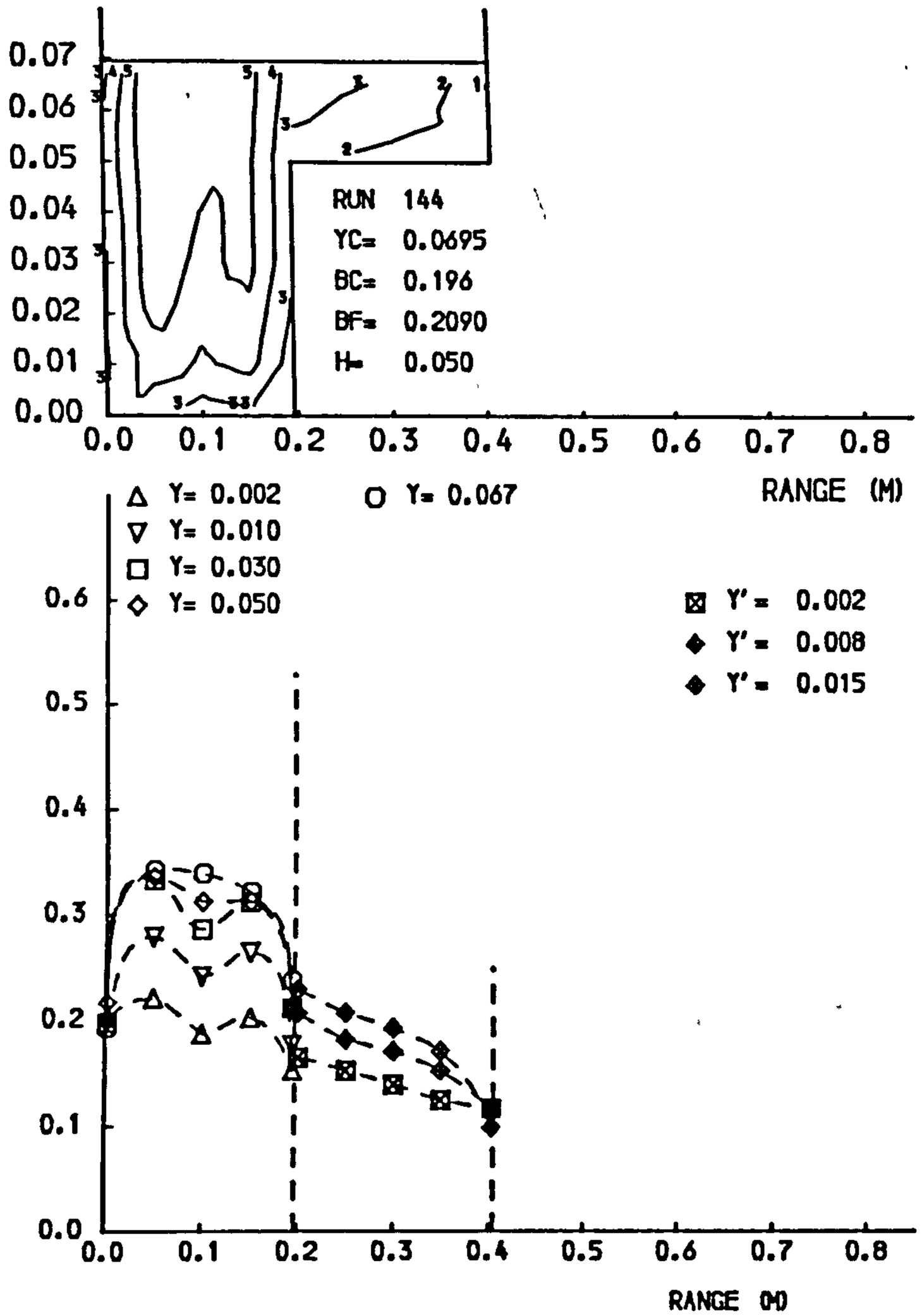

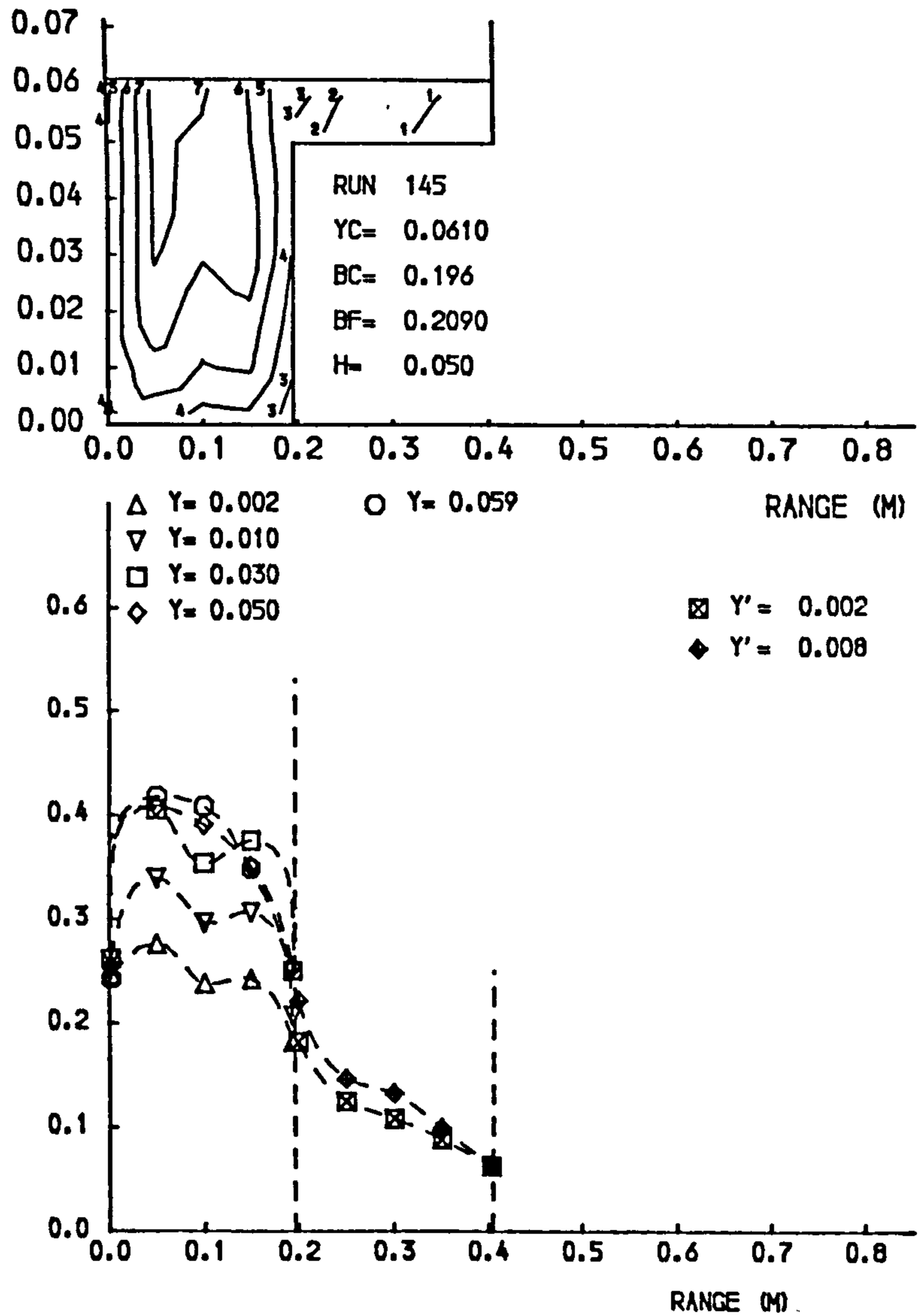

Fig 4·7 Isovels and lateral velocity profiles.

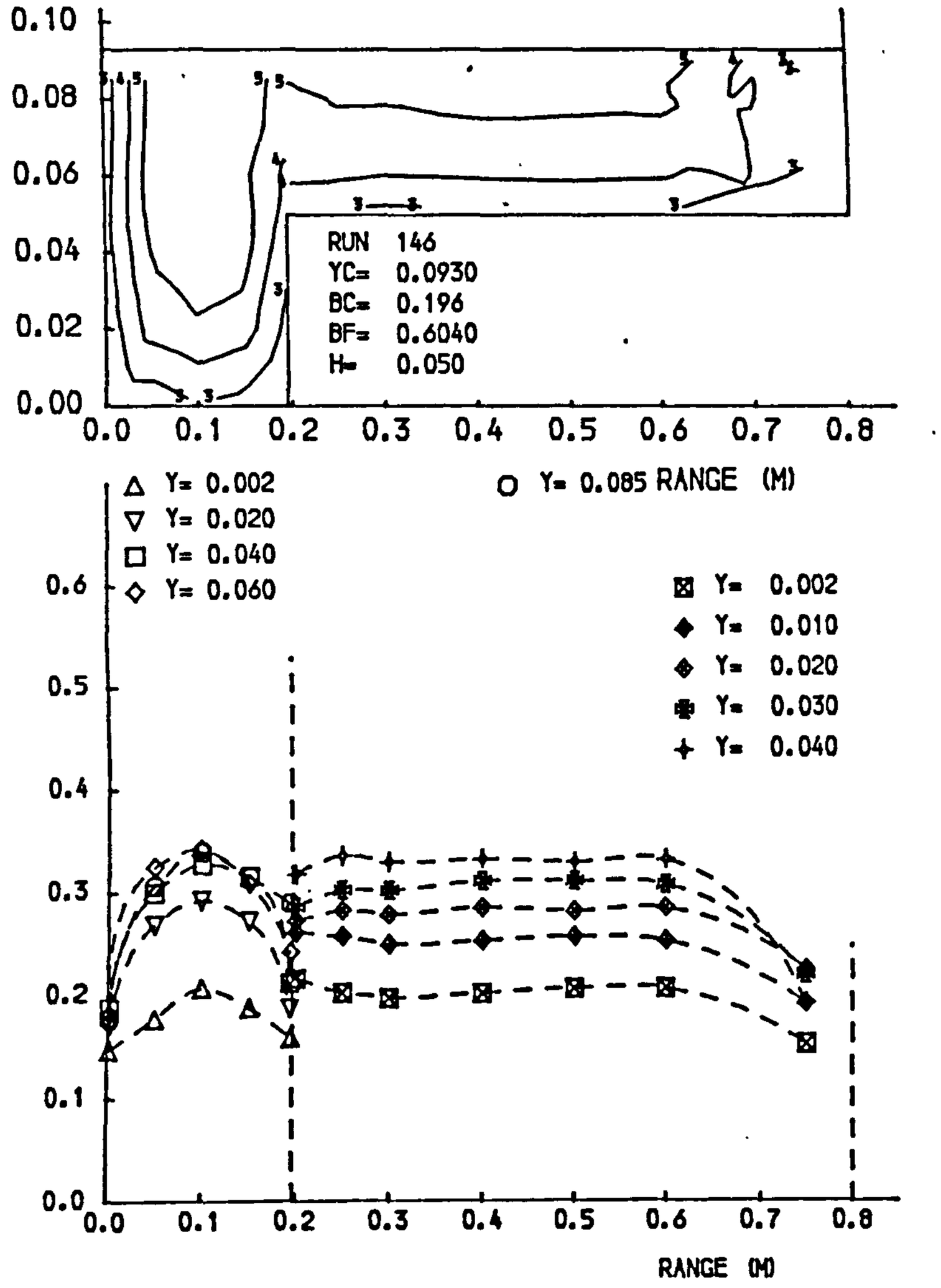

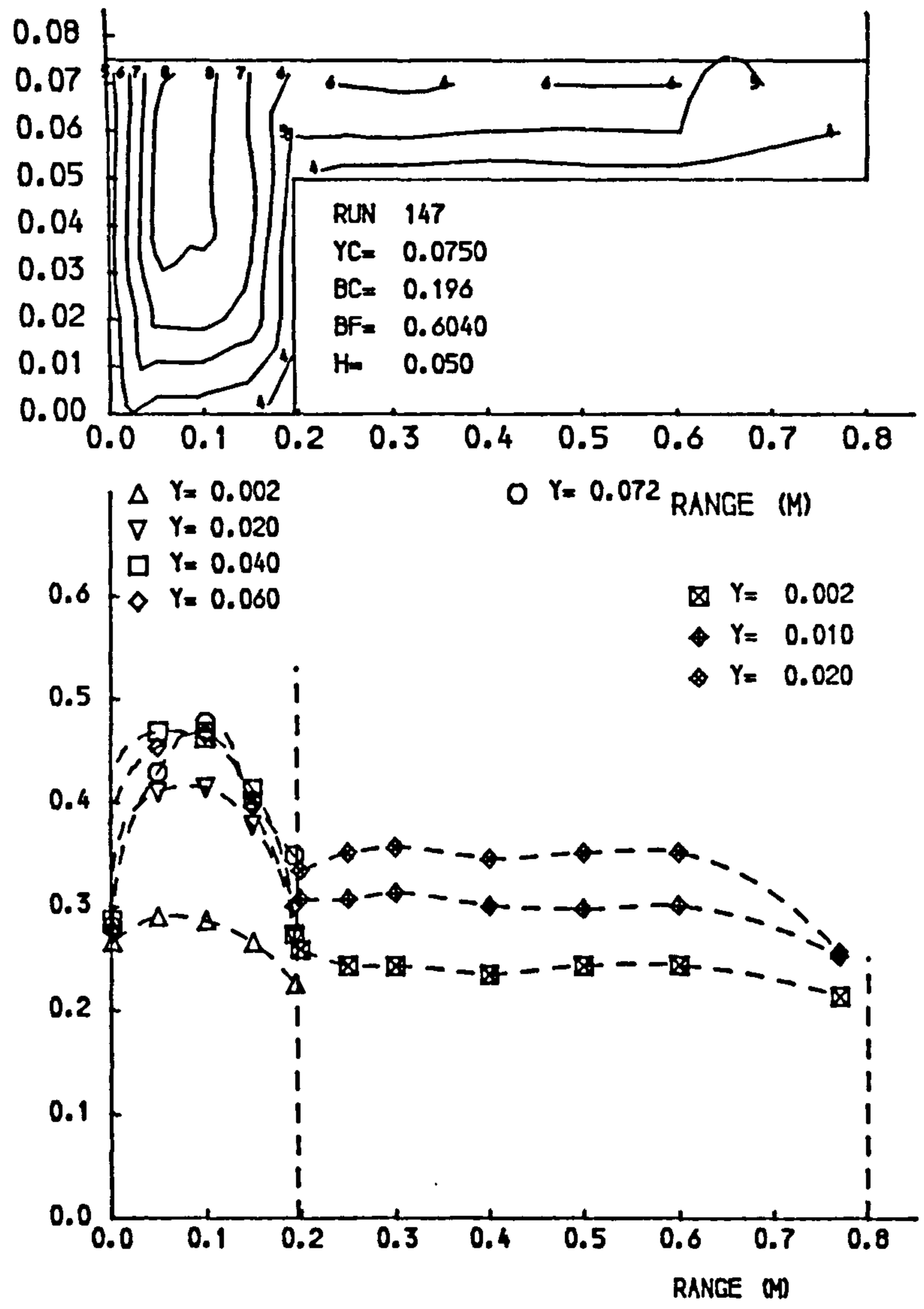

Fig 4·7 Isovels and lateral velocity profiles.

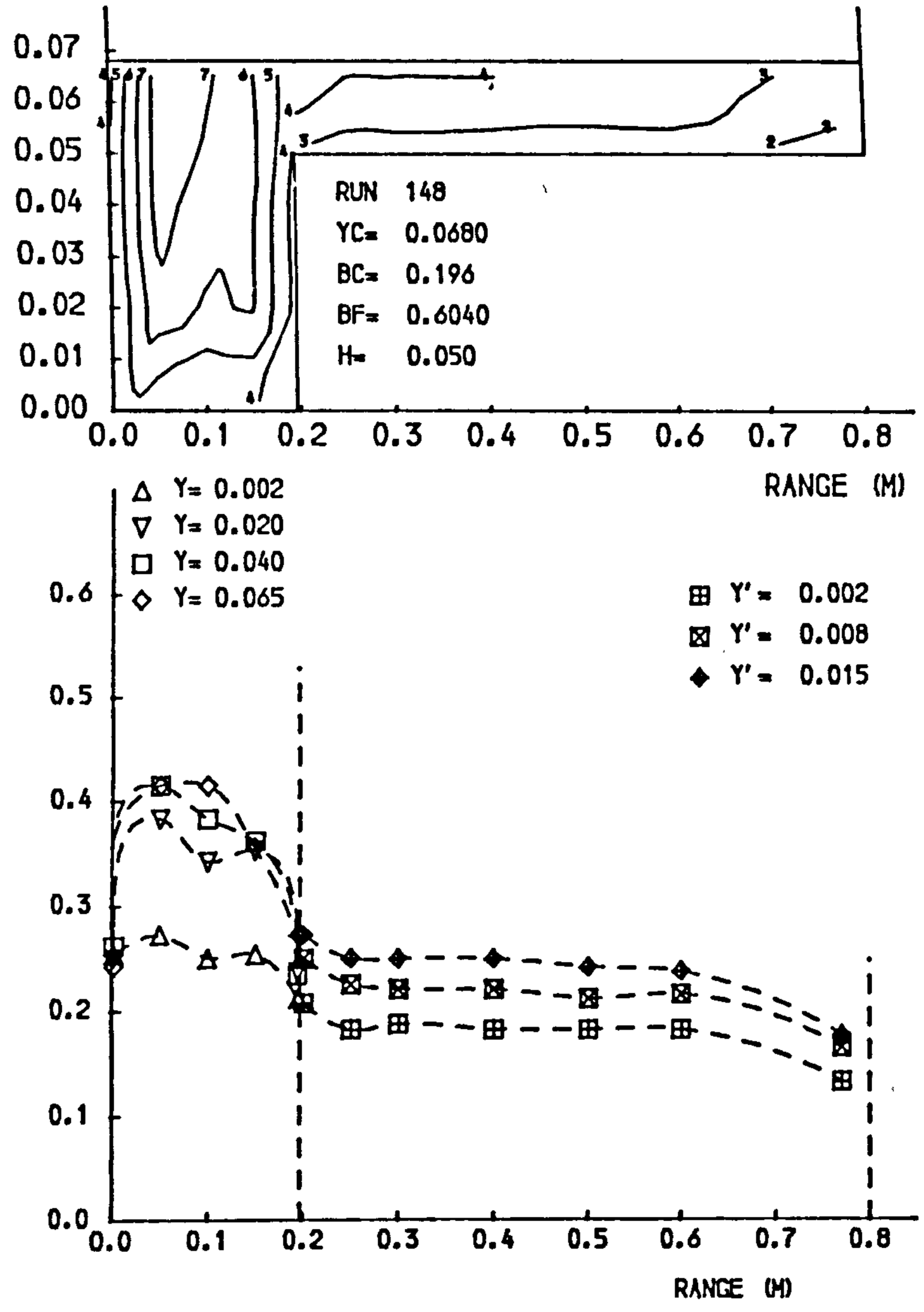

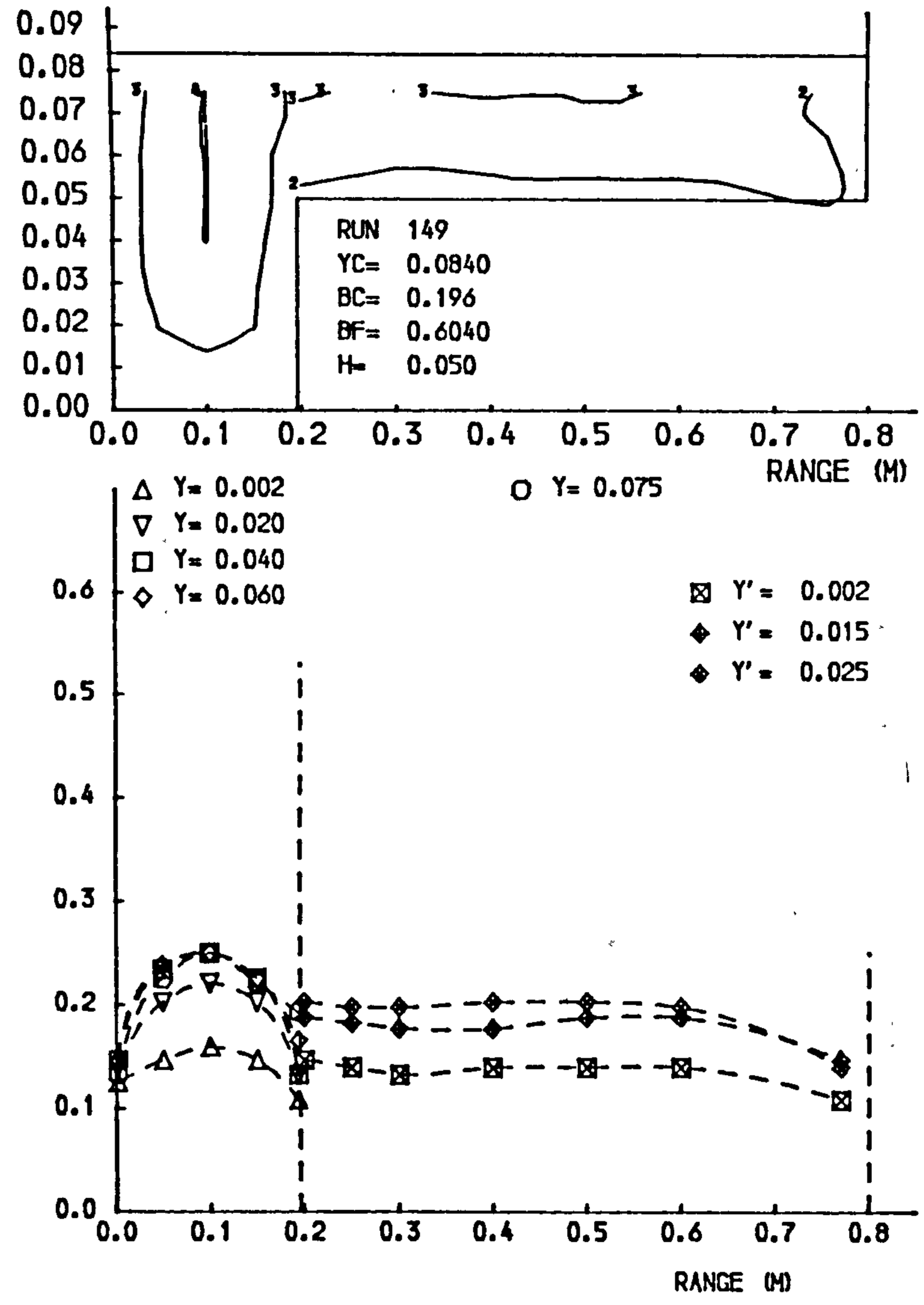

Fig 4·7 Isovels and lateral velocity profiles.

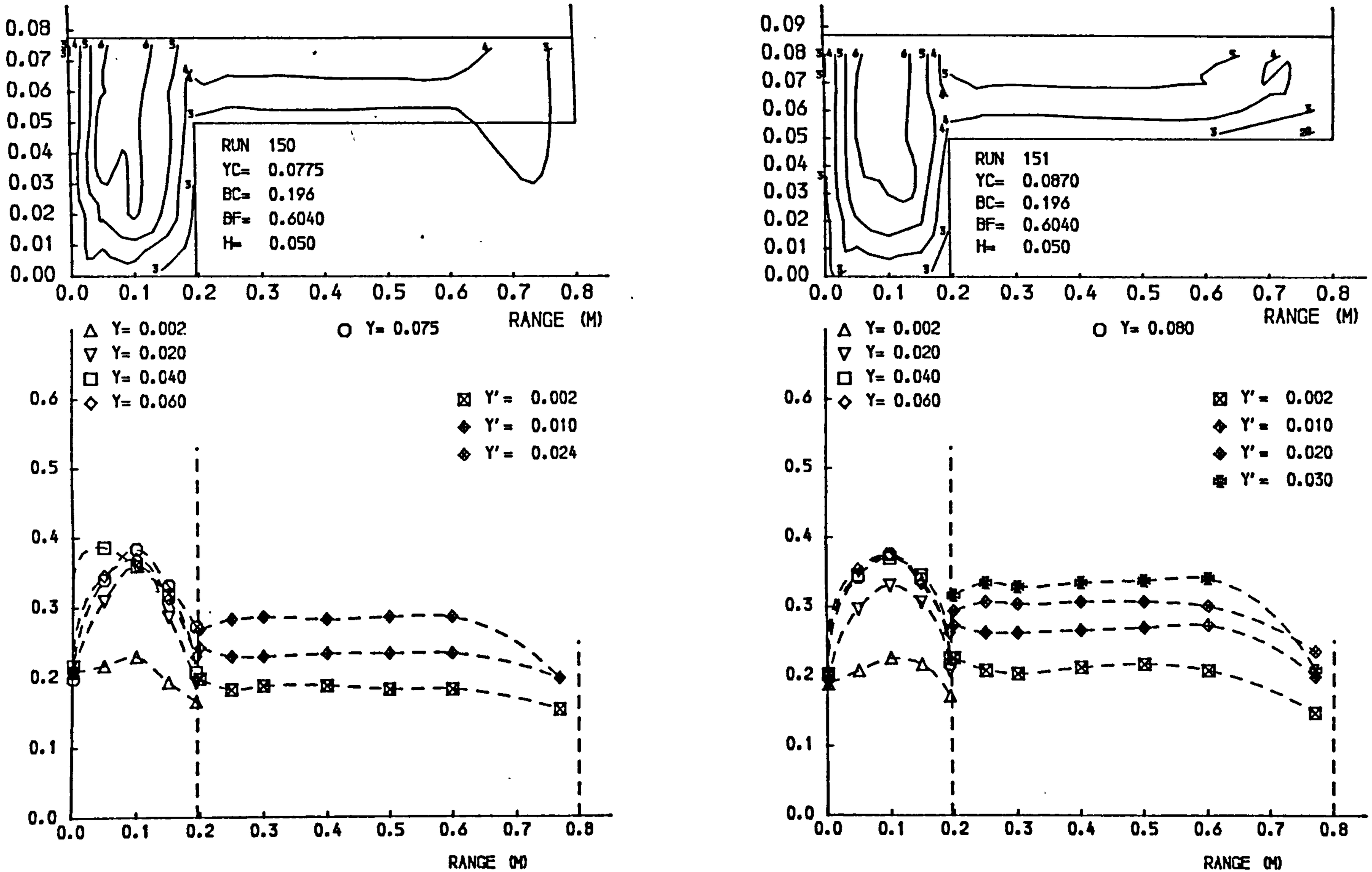

Fig 4·7 Isovels and lateral velocity profiles.

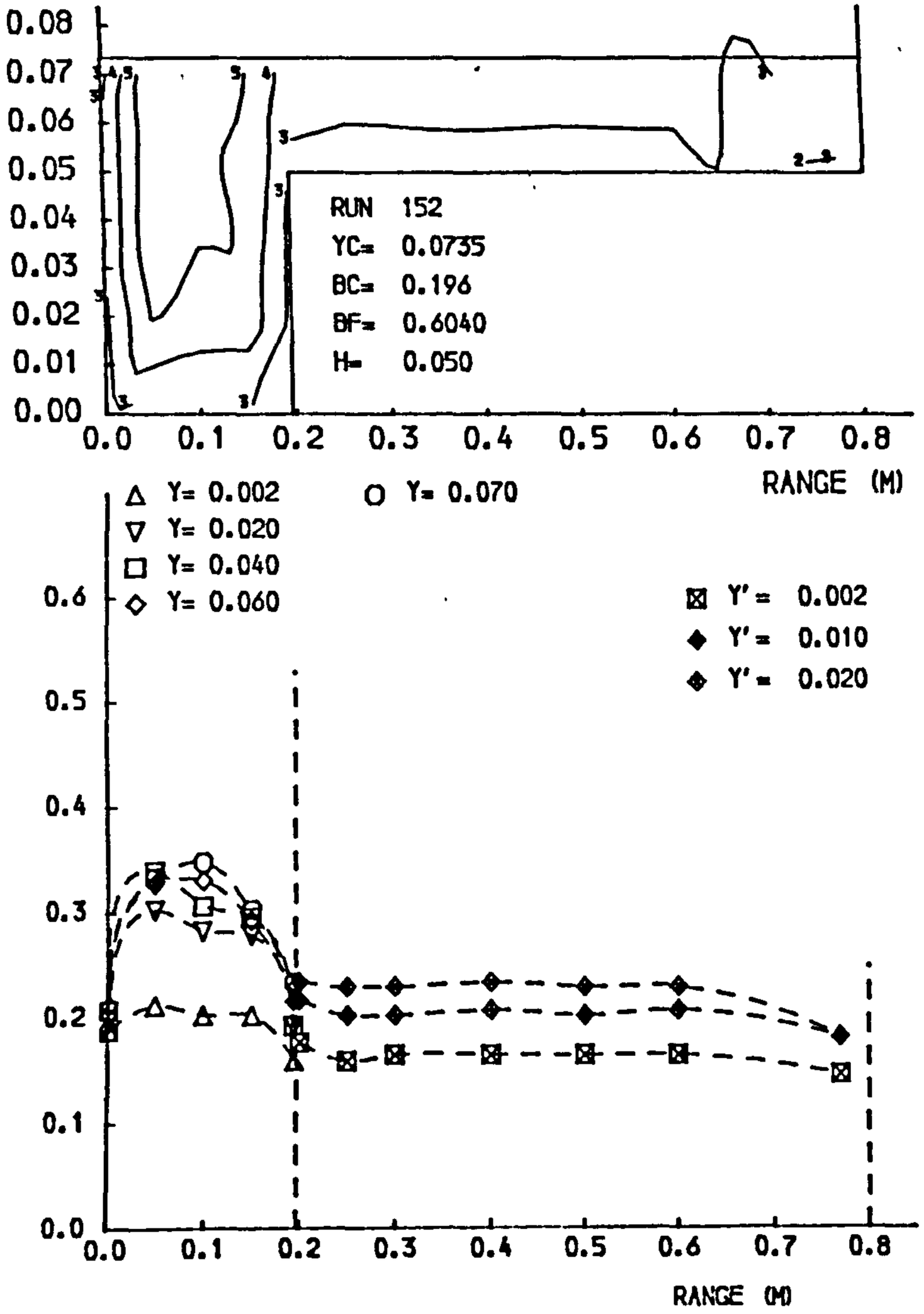

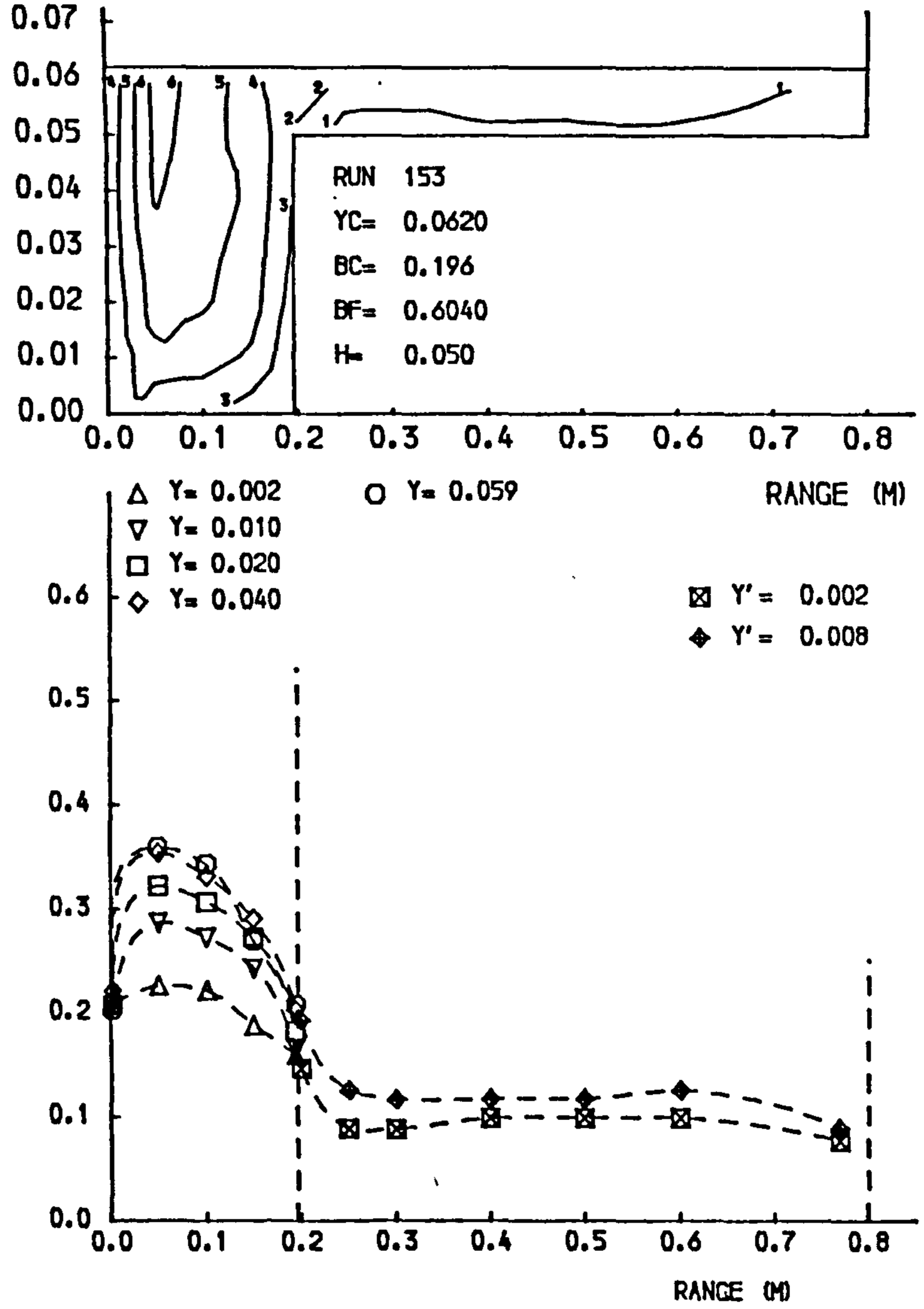

Fig 4·7 Isovels and lateral velocity profiles.

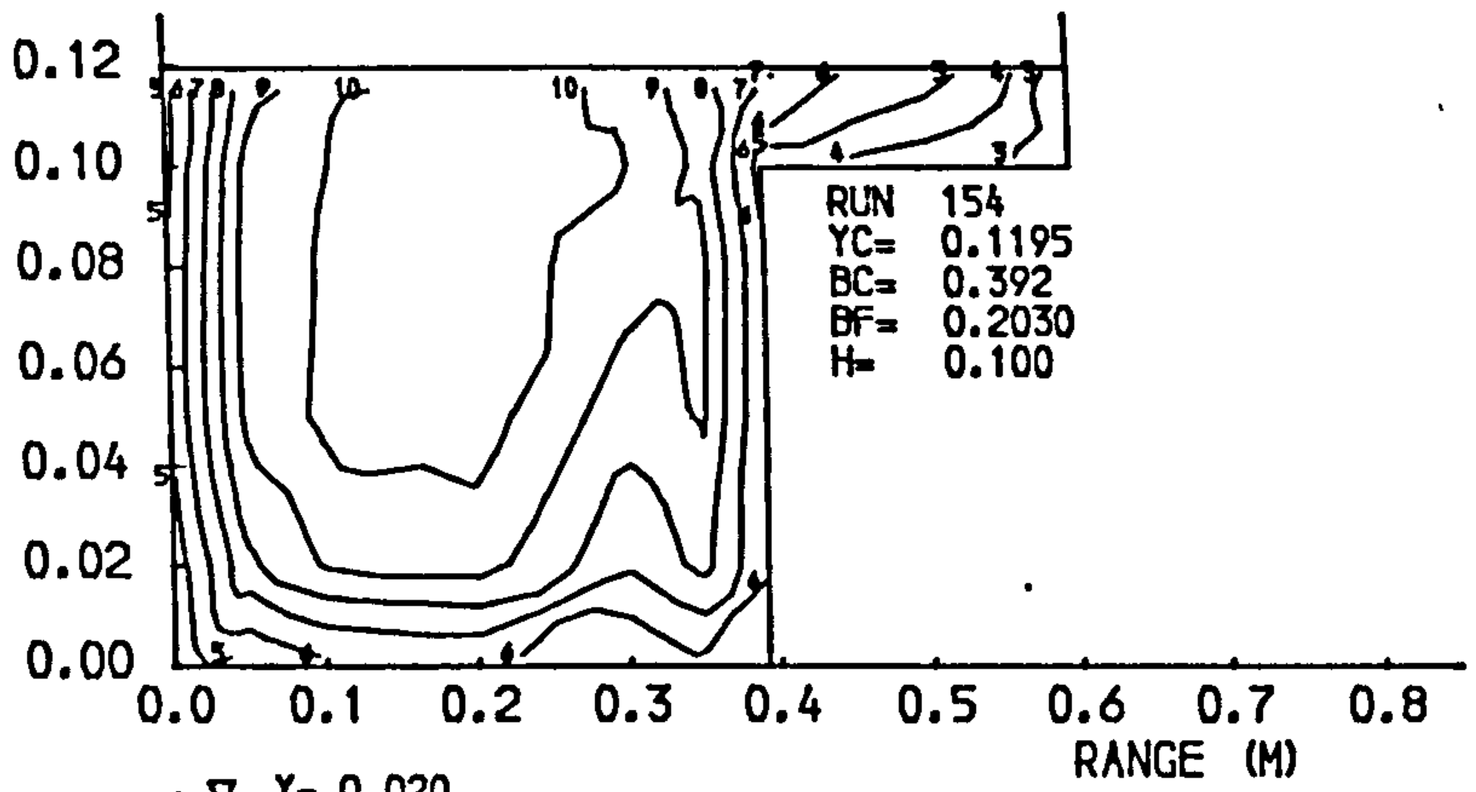

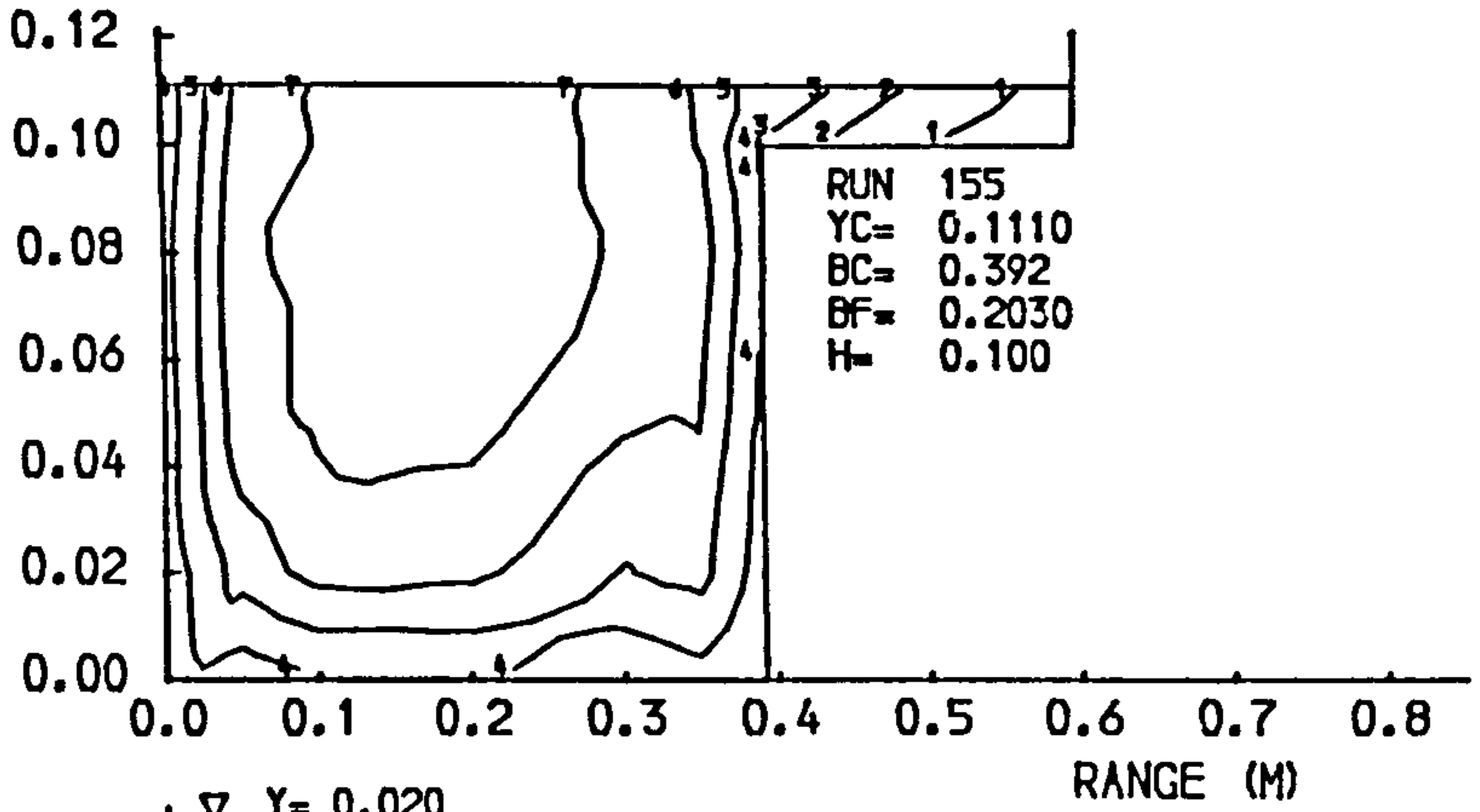

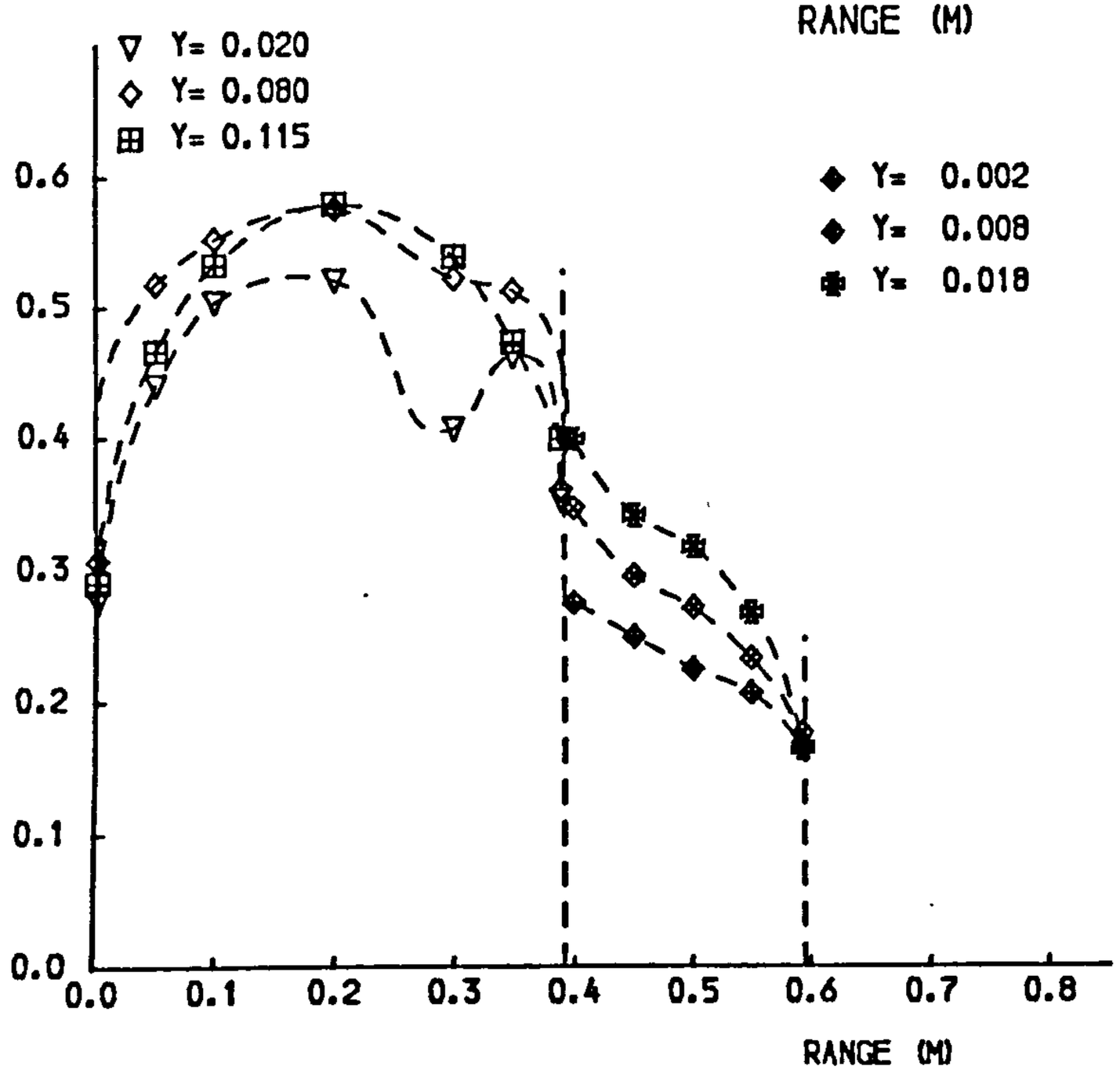

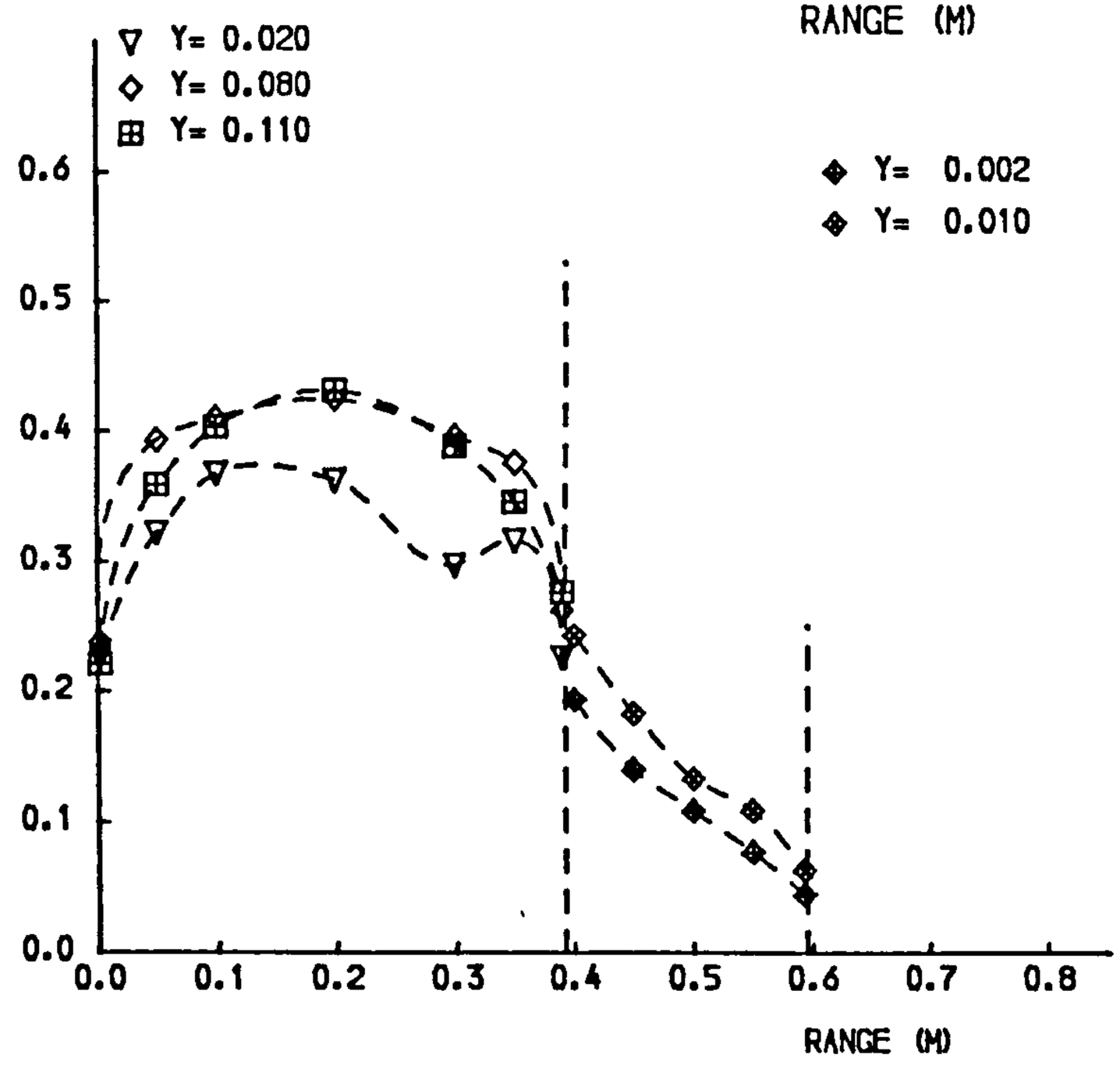

Fig 4·7 Isovels and lateral velocity profiles.

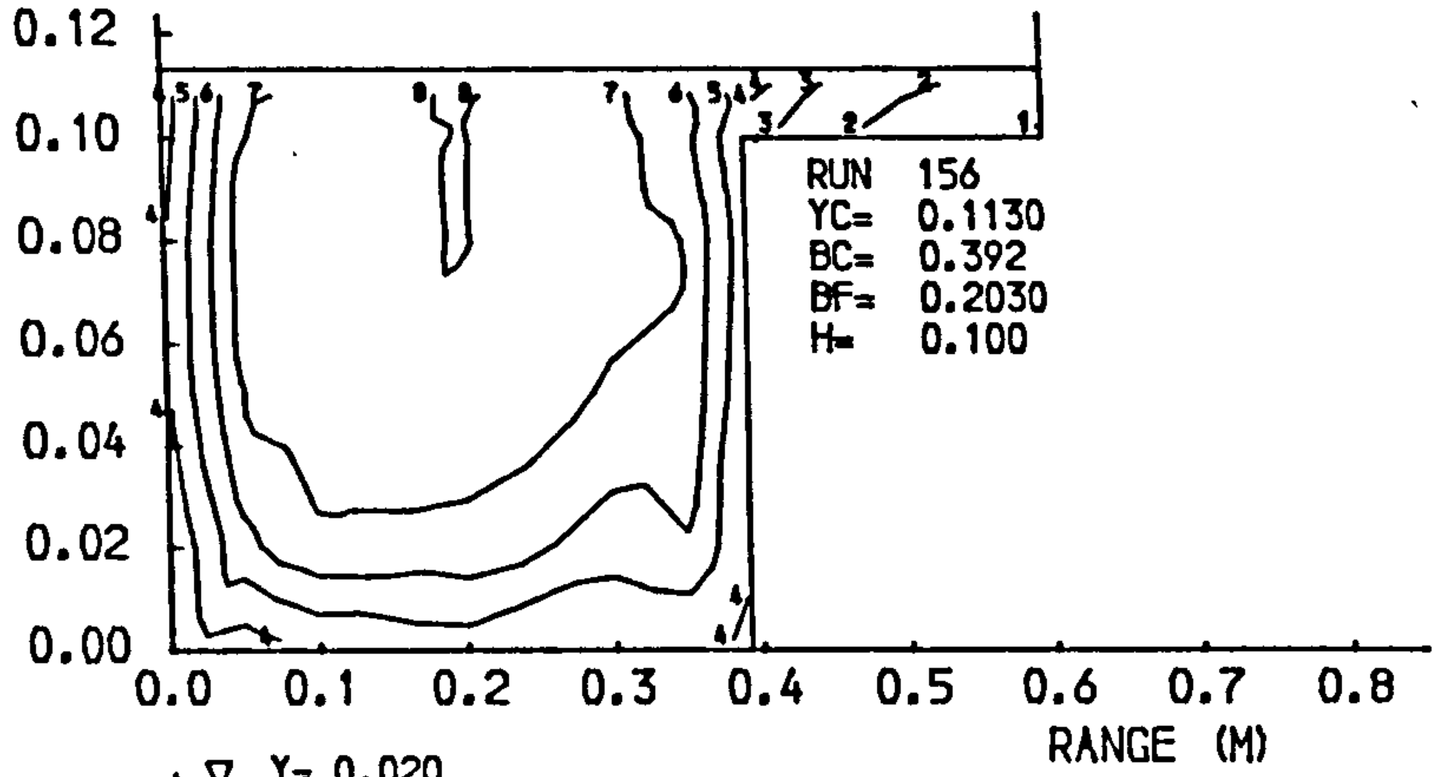

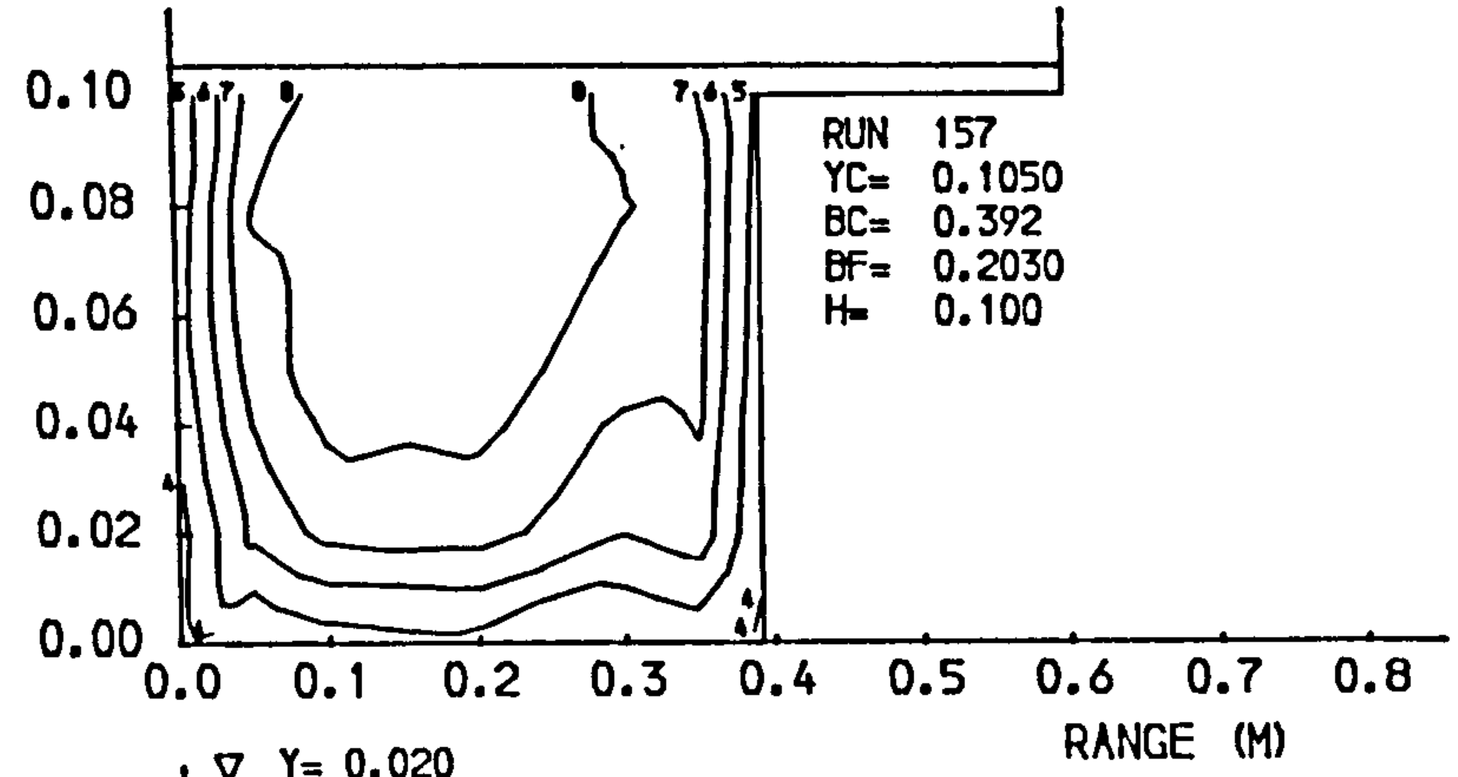

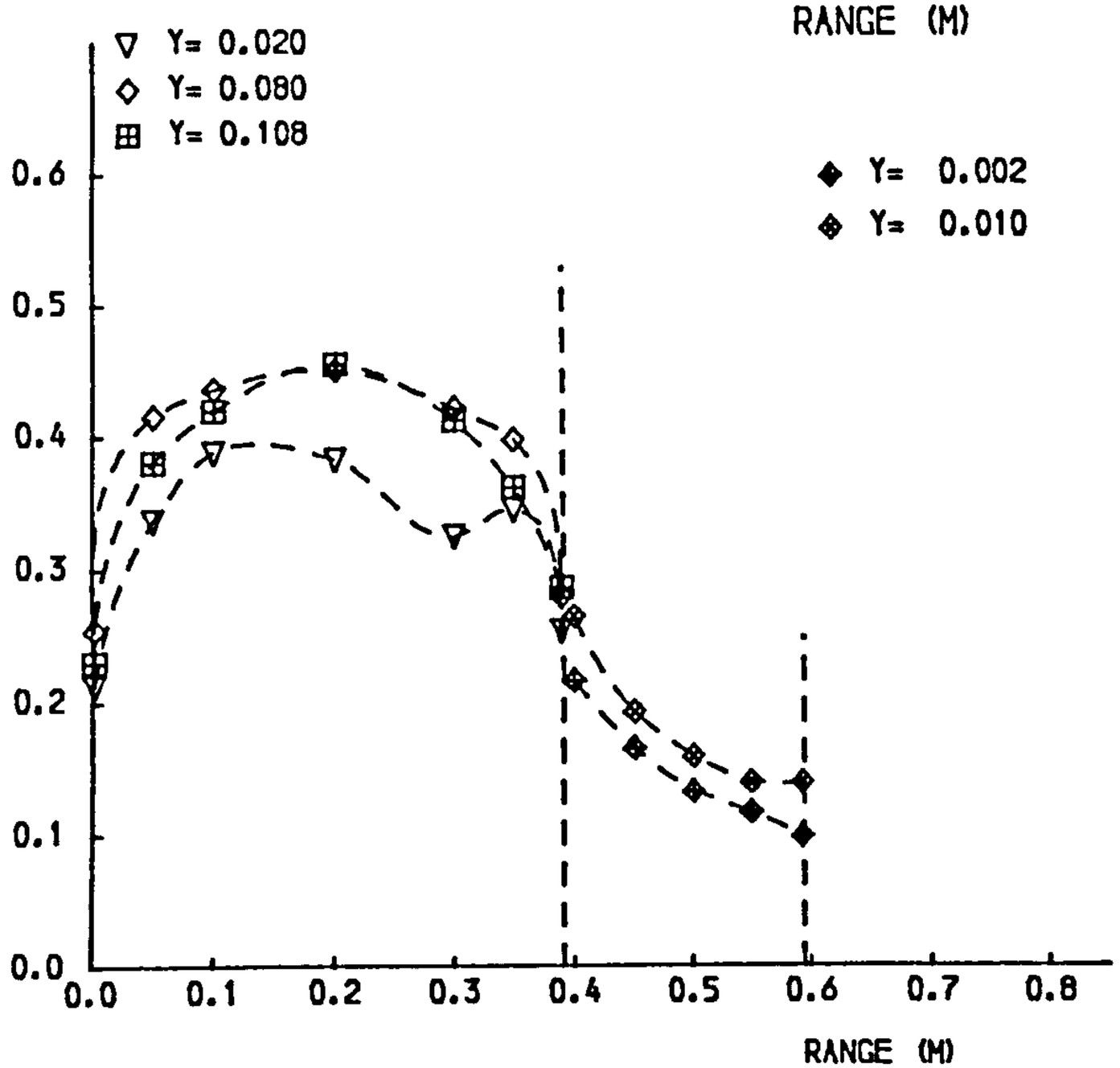

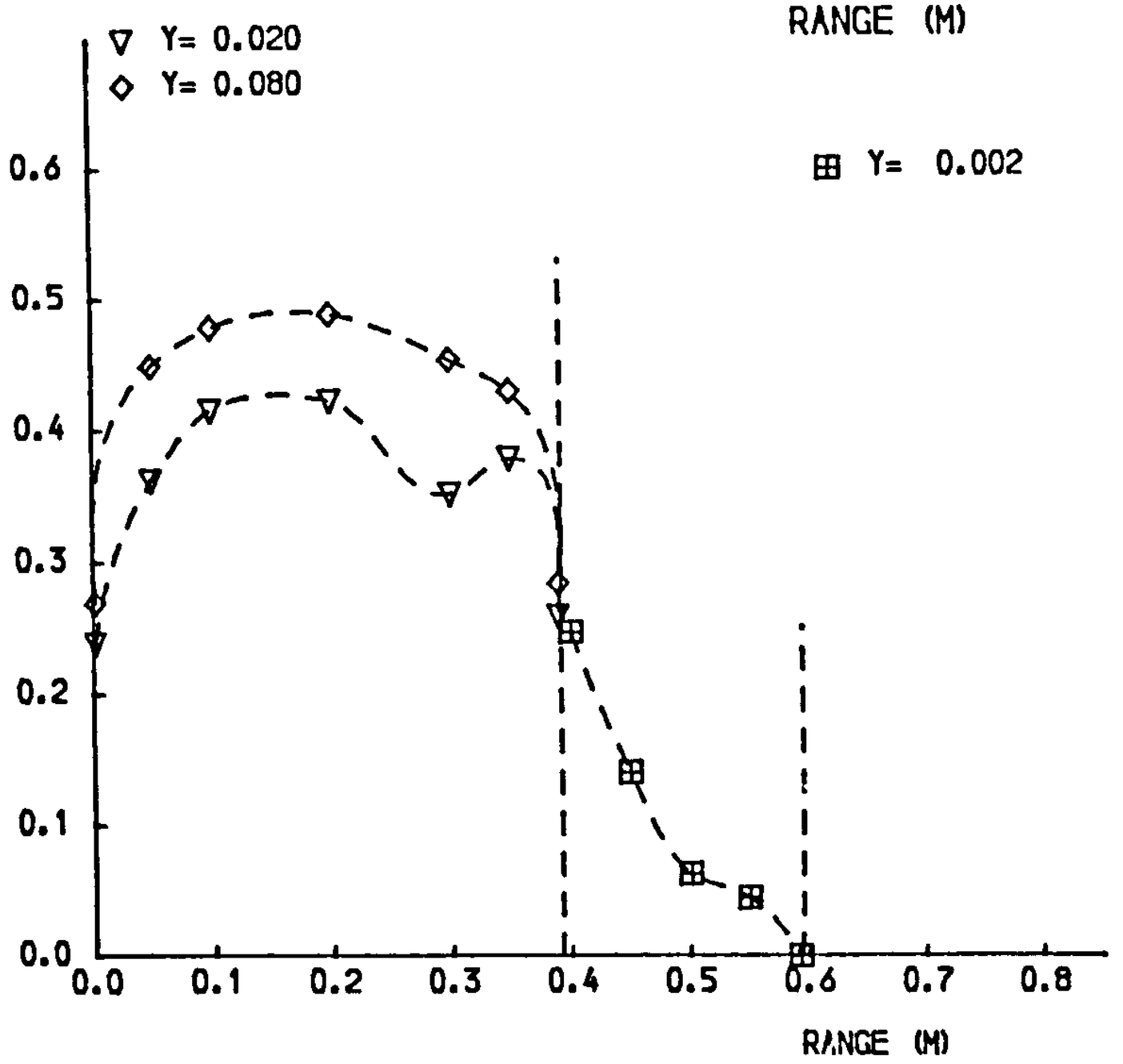

Fig 4·7 Isovels and lateral velocity profiles.

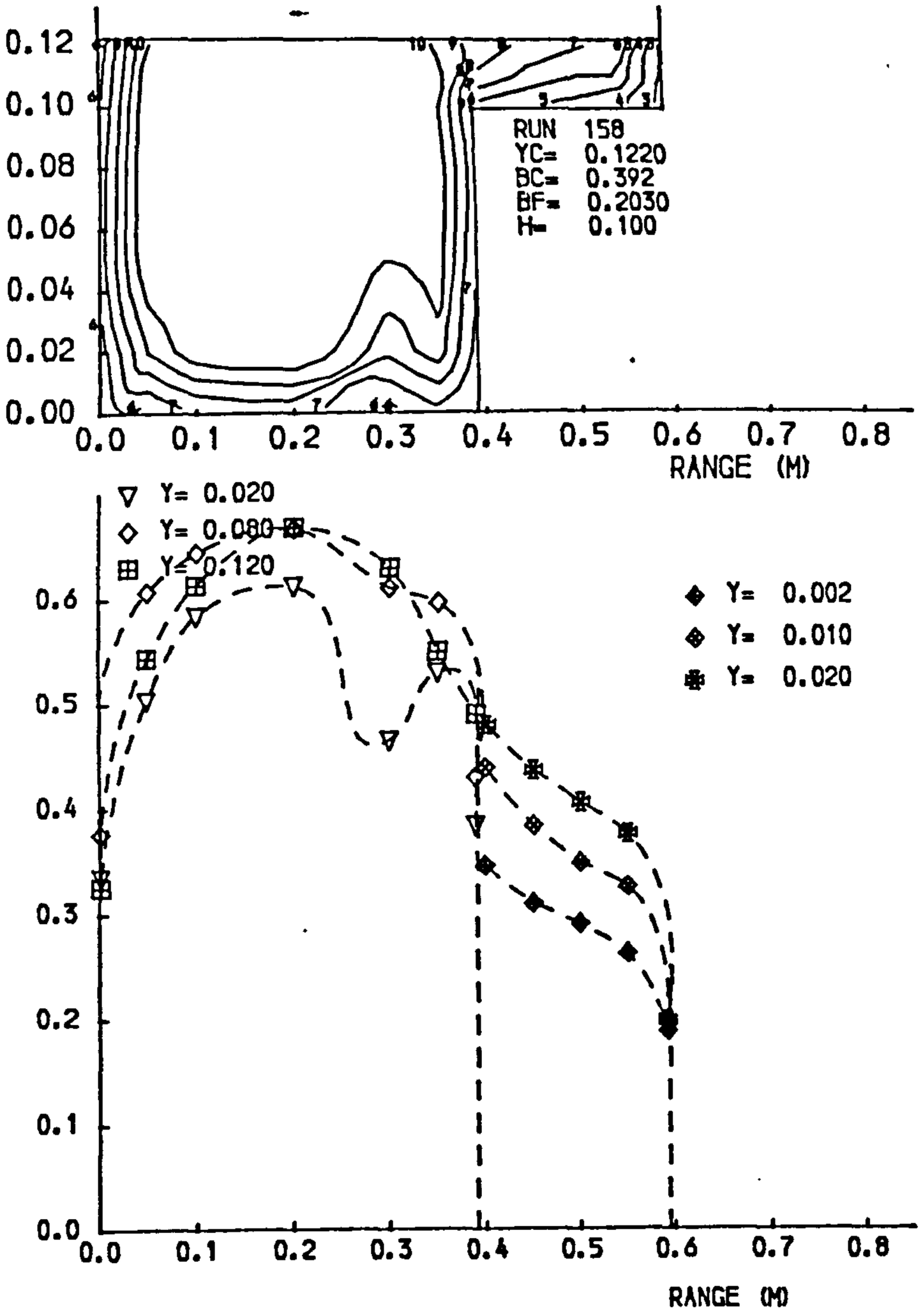

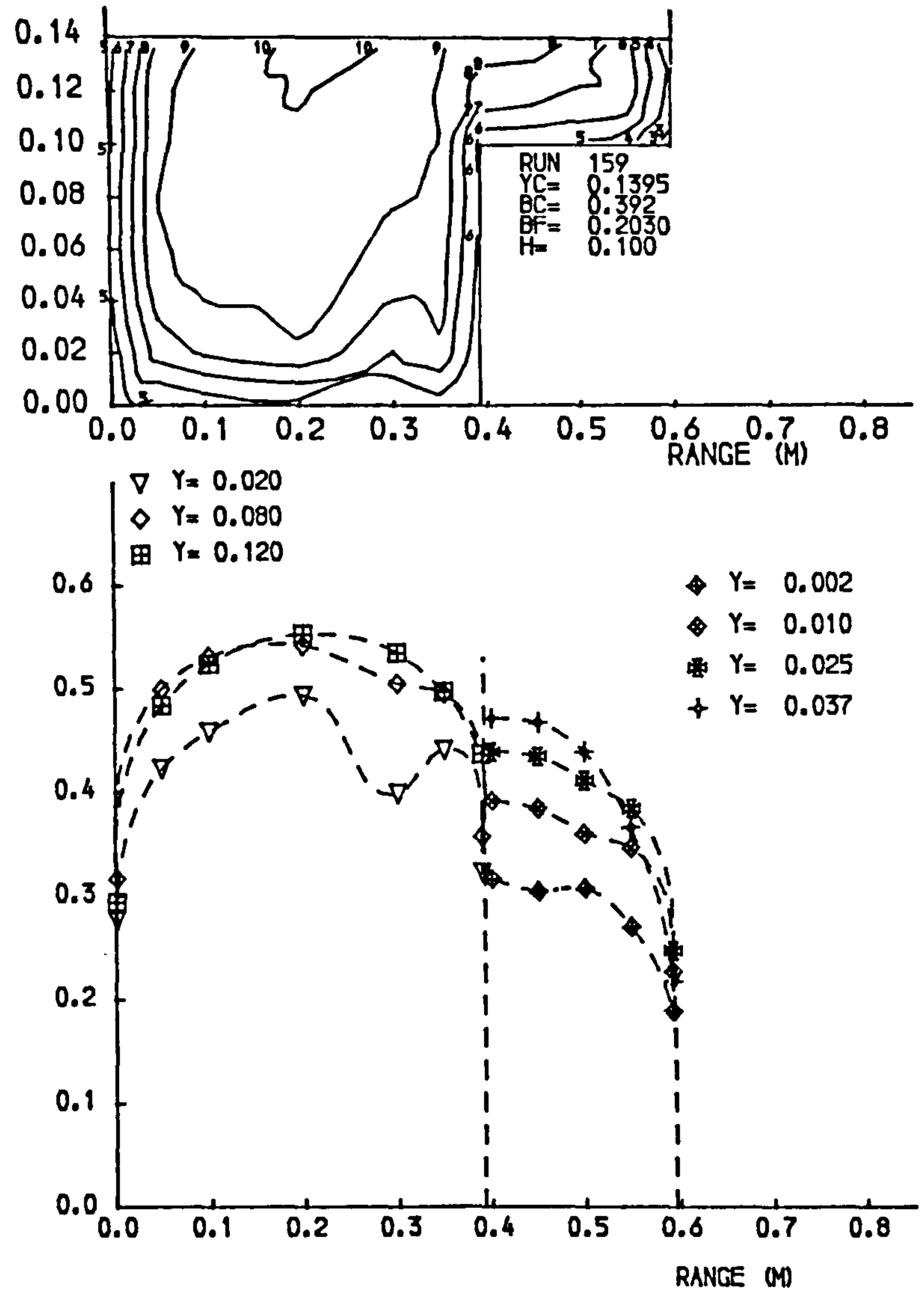

Fig 4·7 Isovels and lateral velocity profiles.

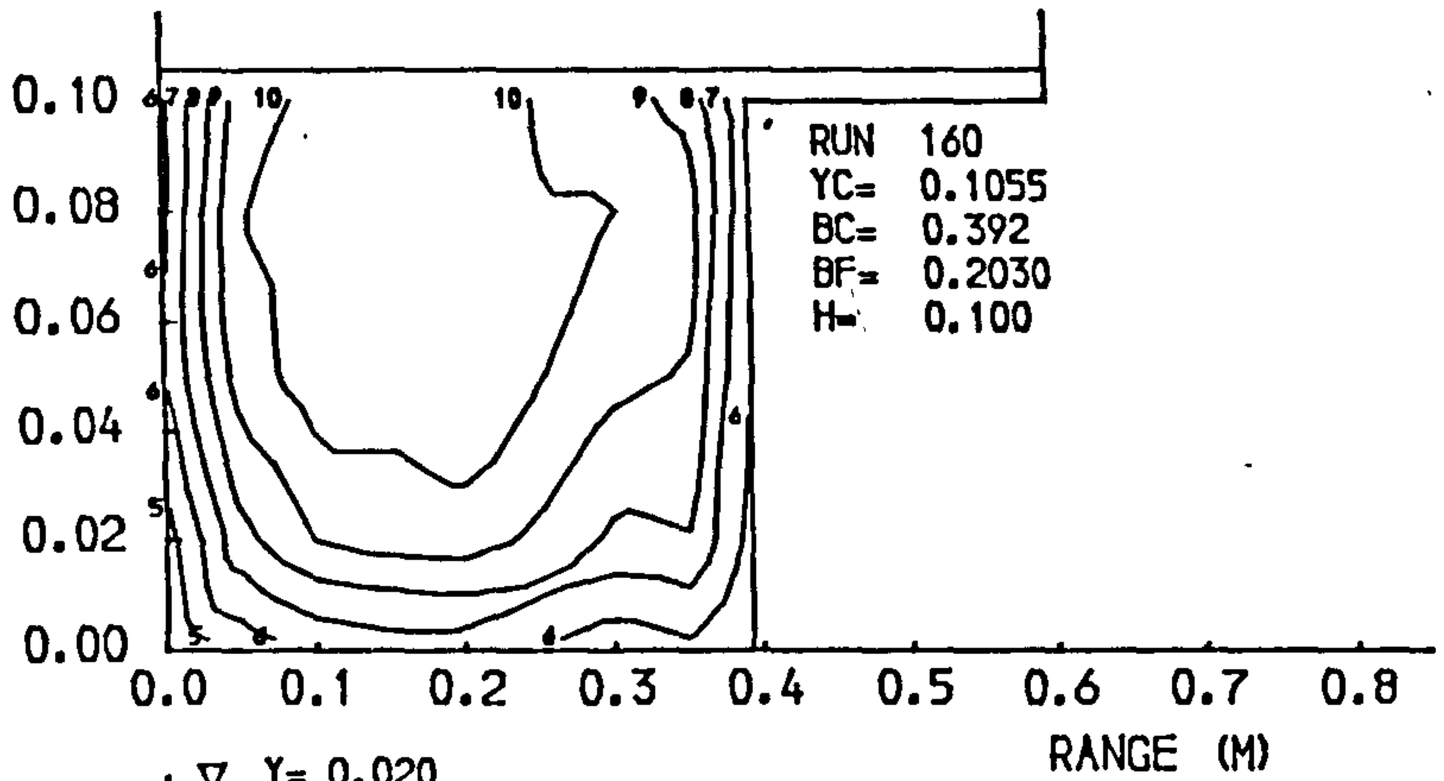

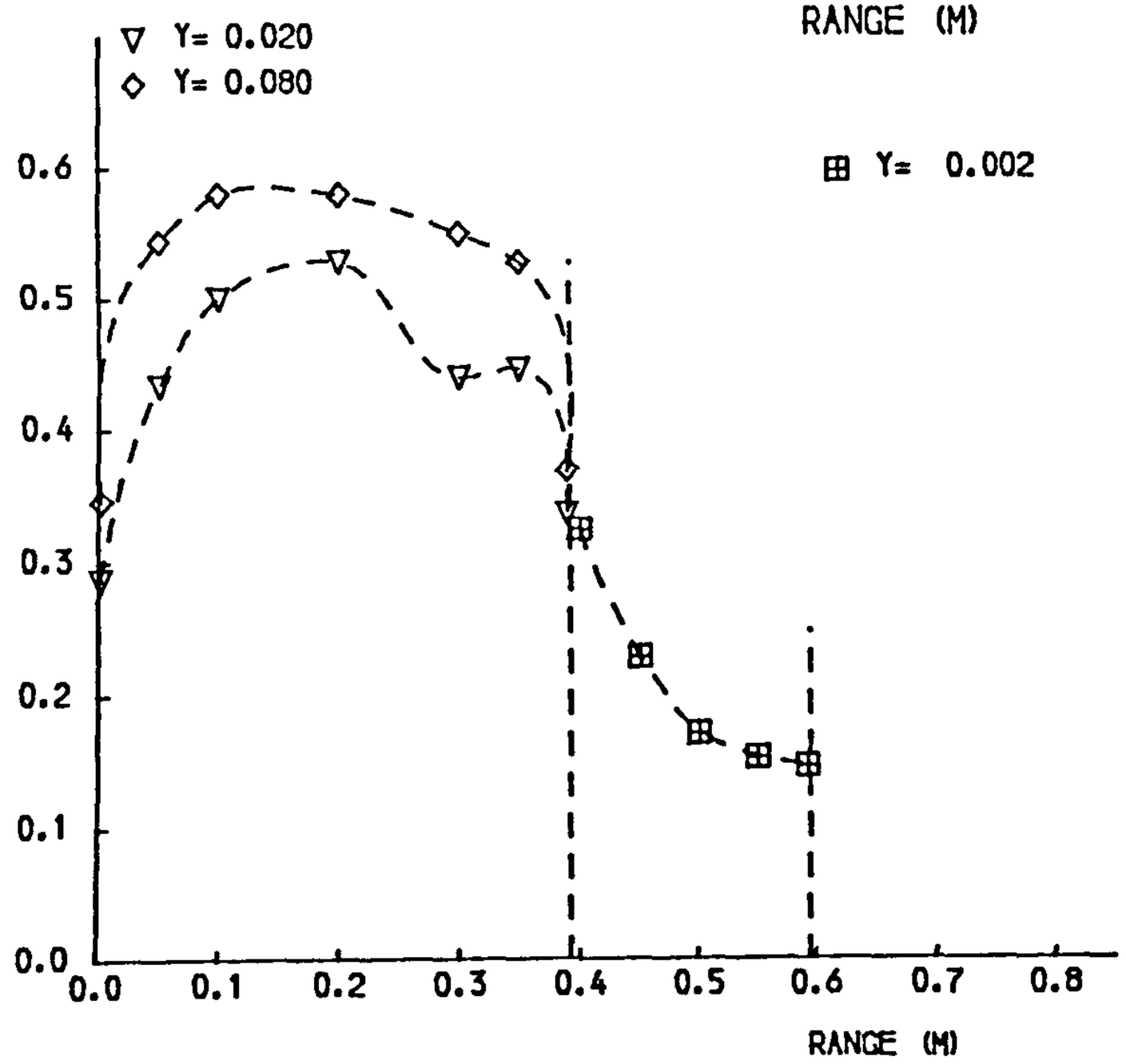

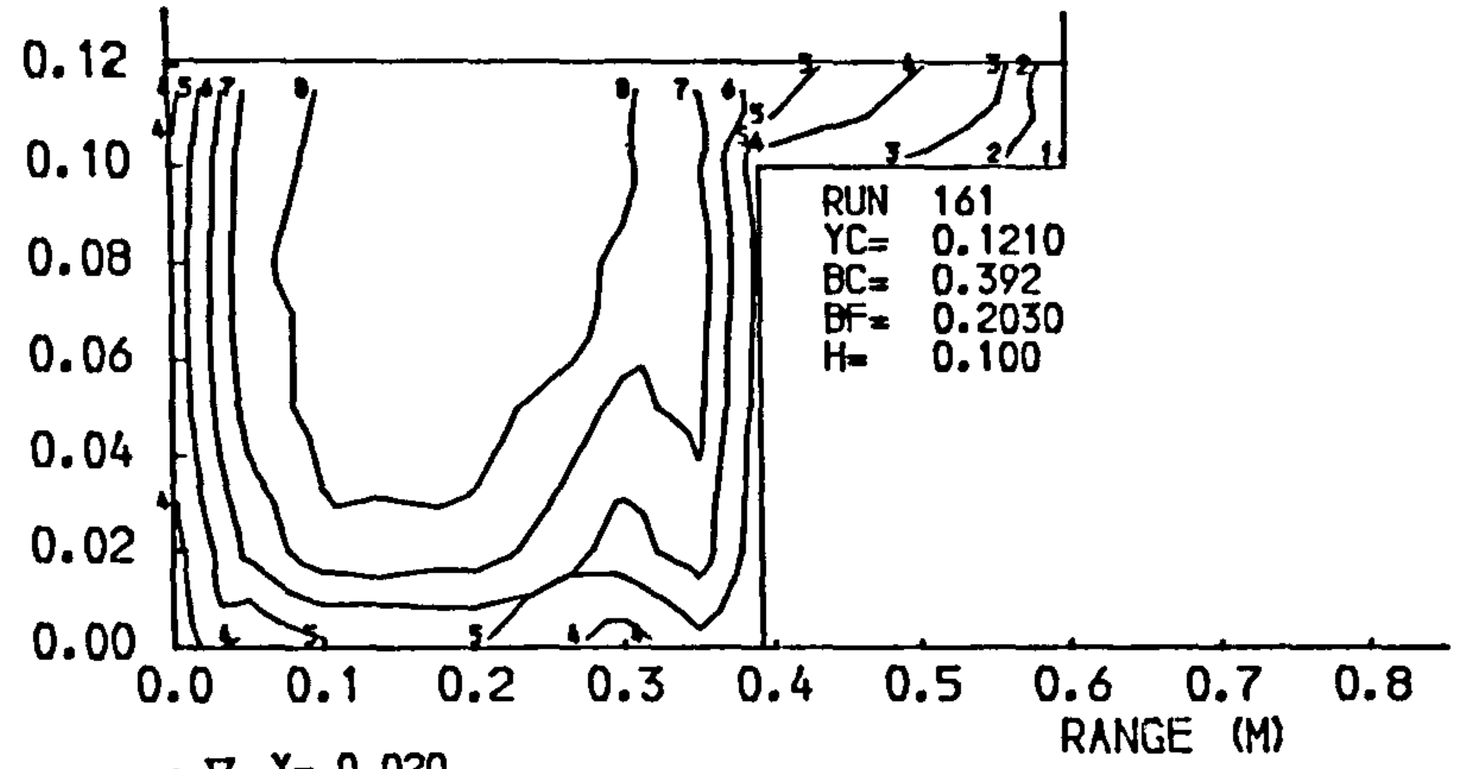

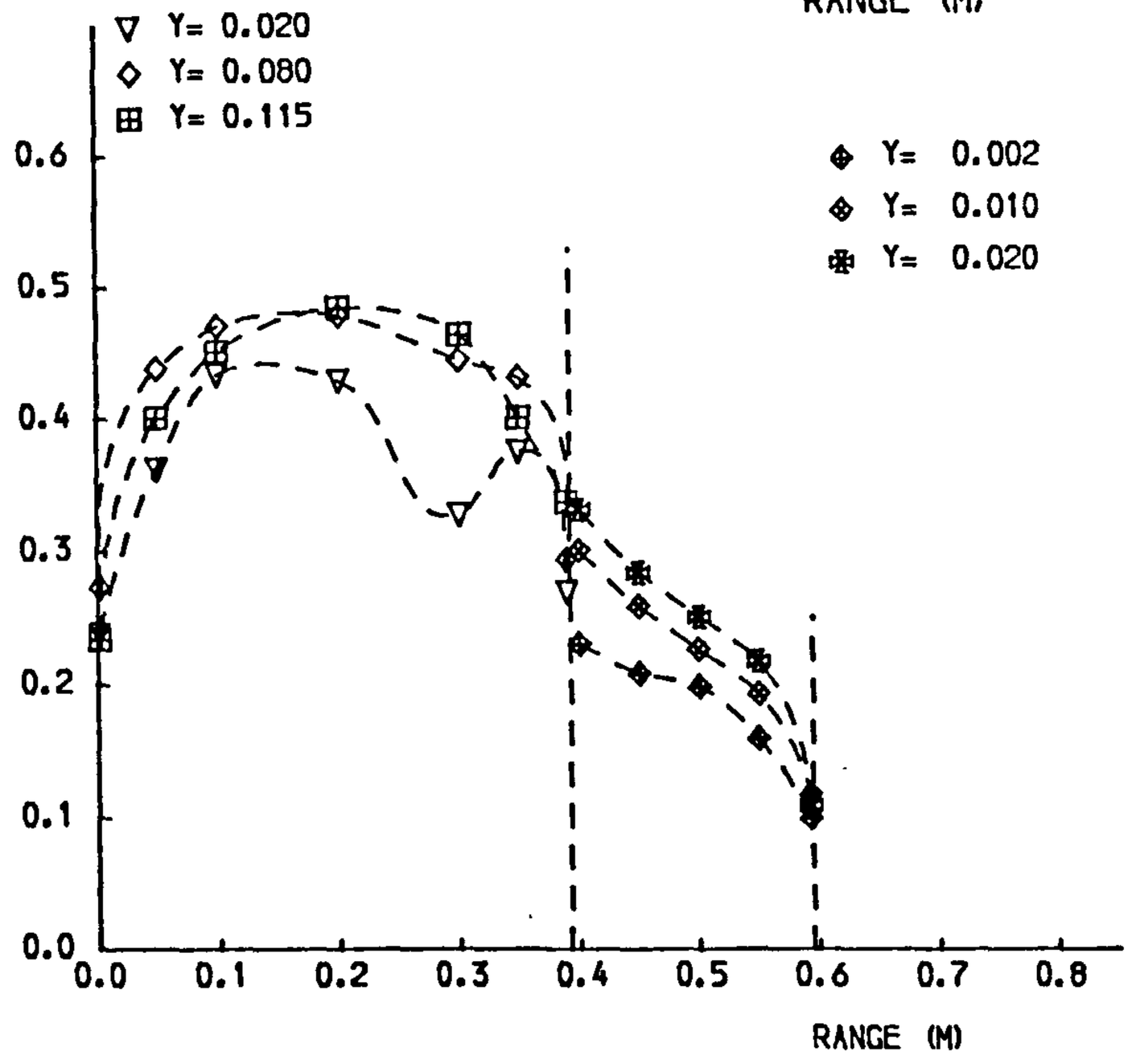

Fig 4·7 Isovels and lateral velocity profiles.

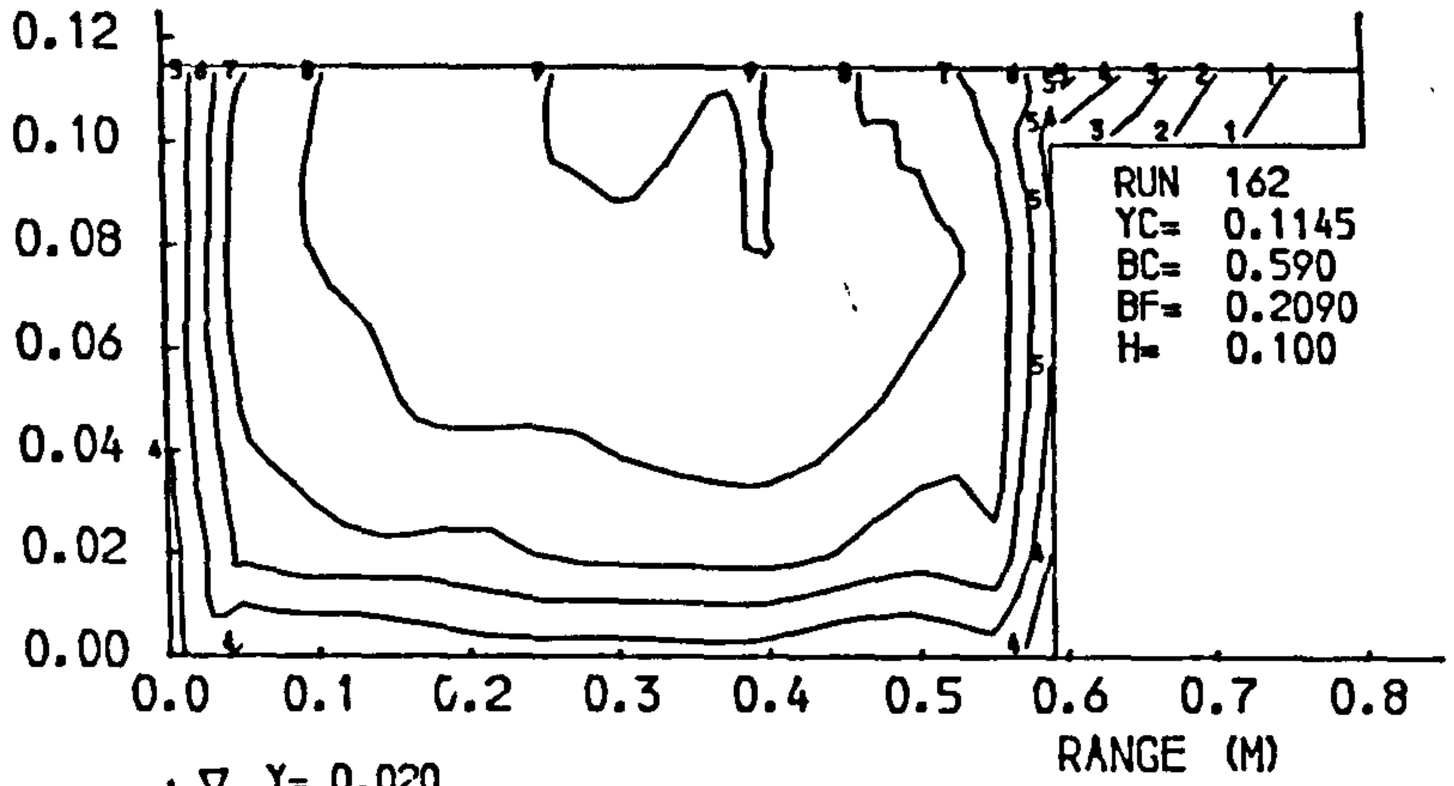

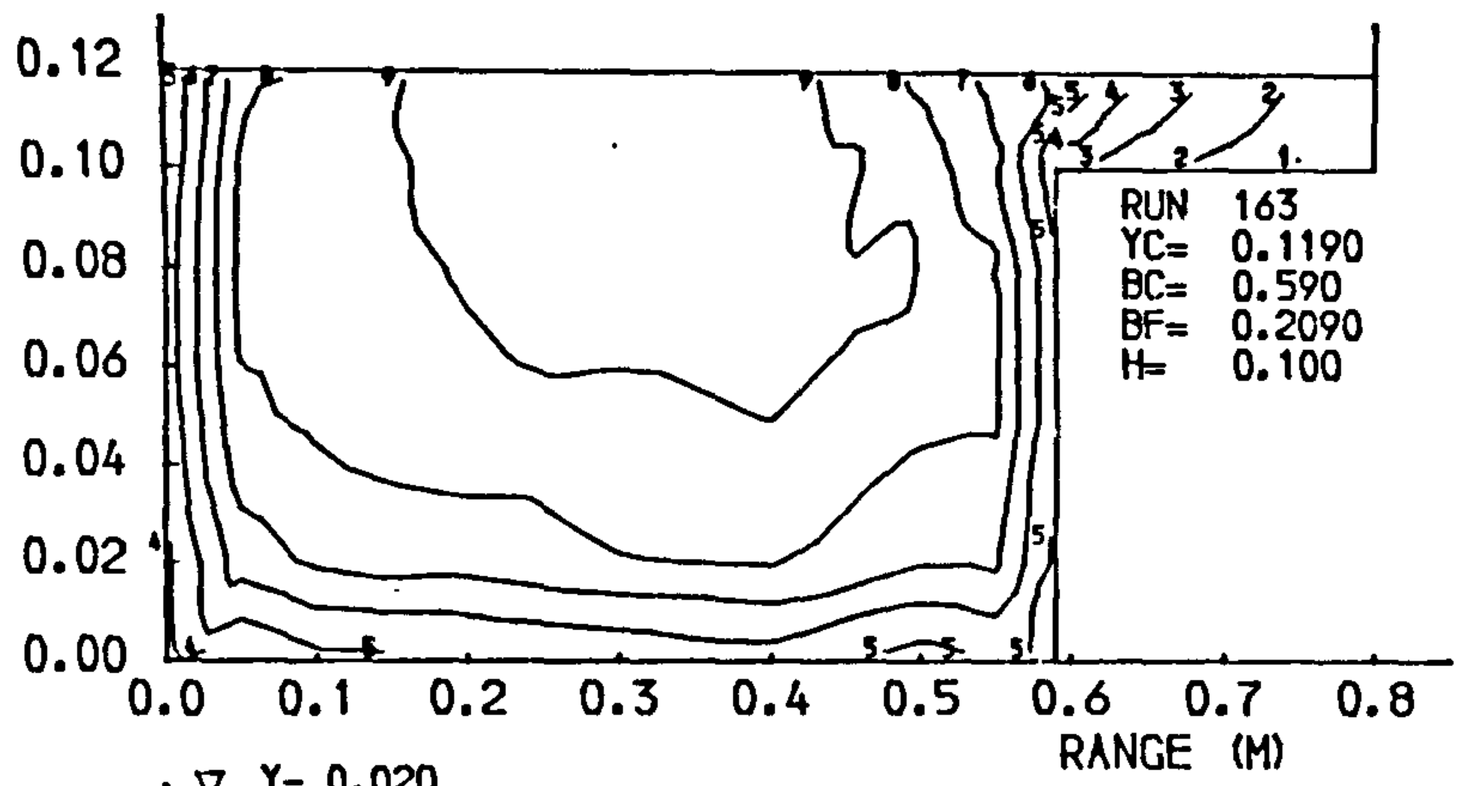

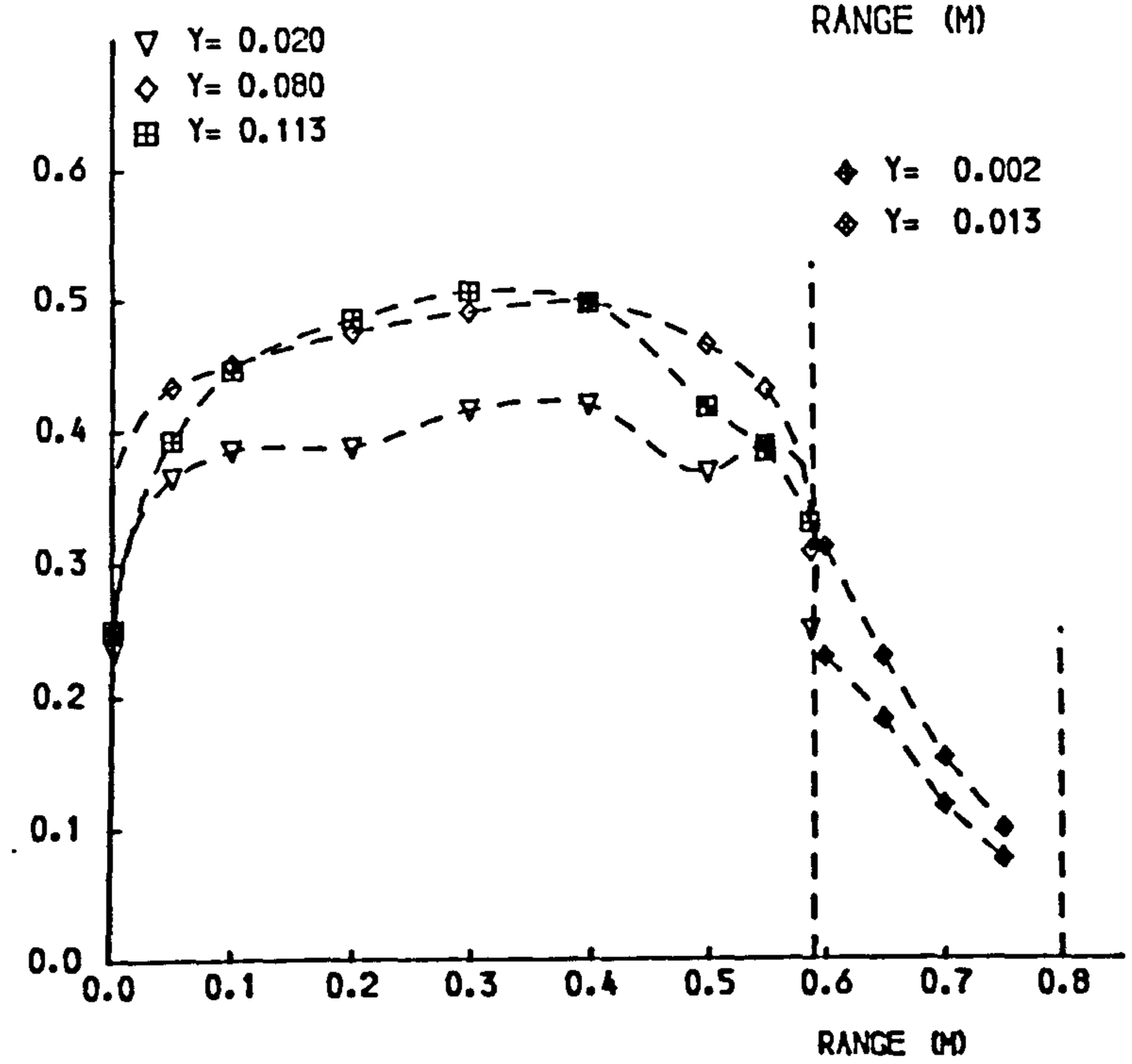

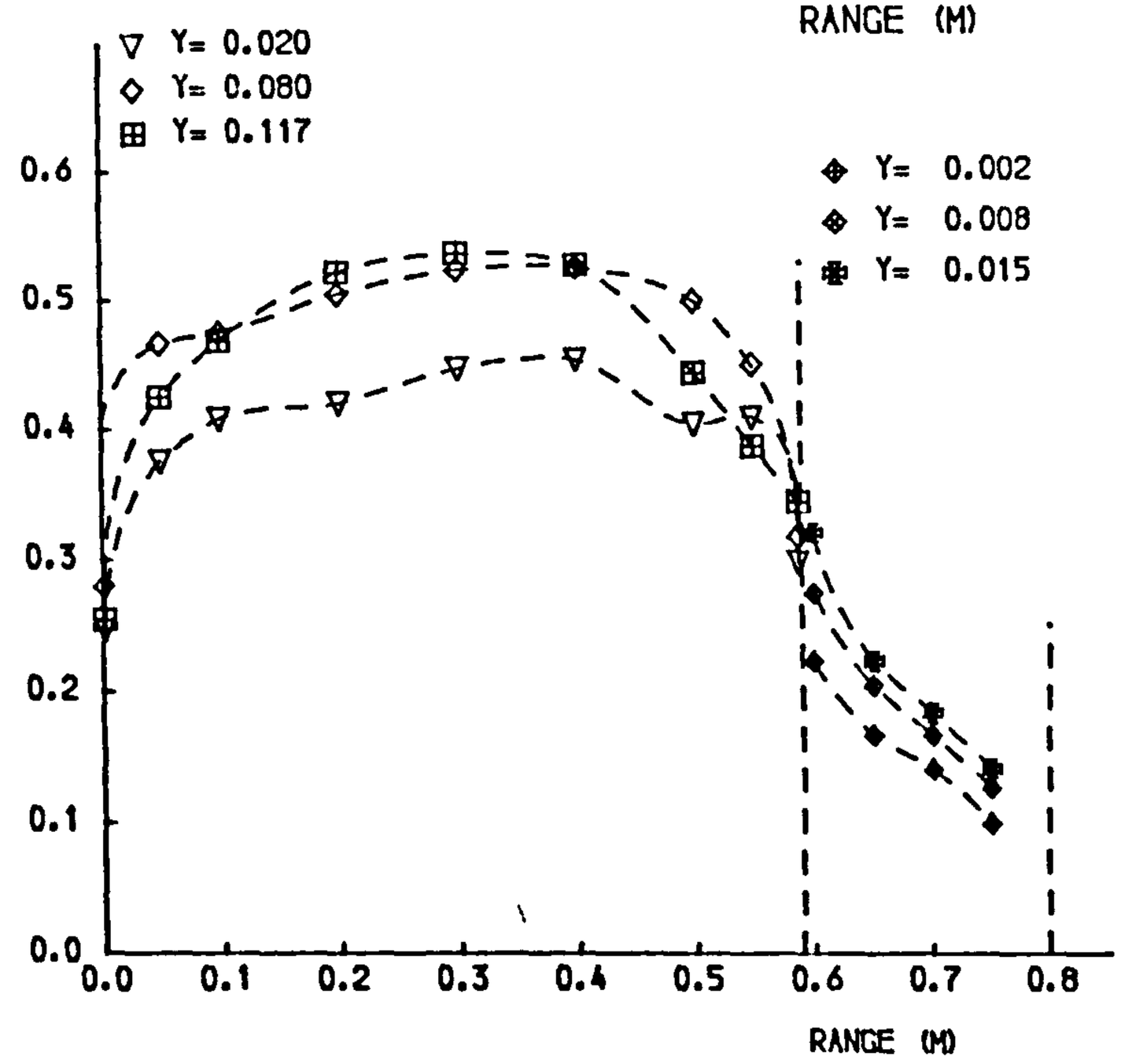

Fig 4·7 Isovels and lateral velocity profiles.

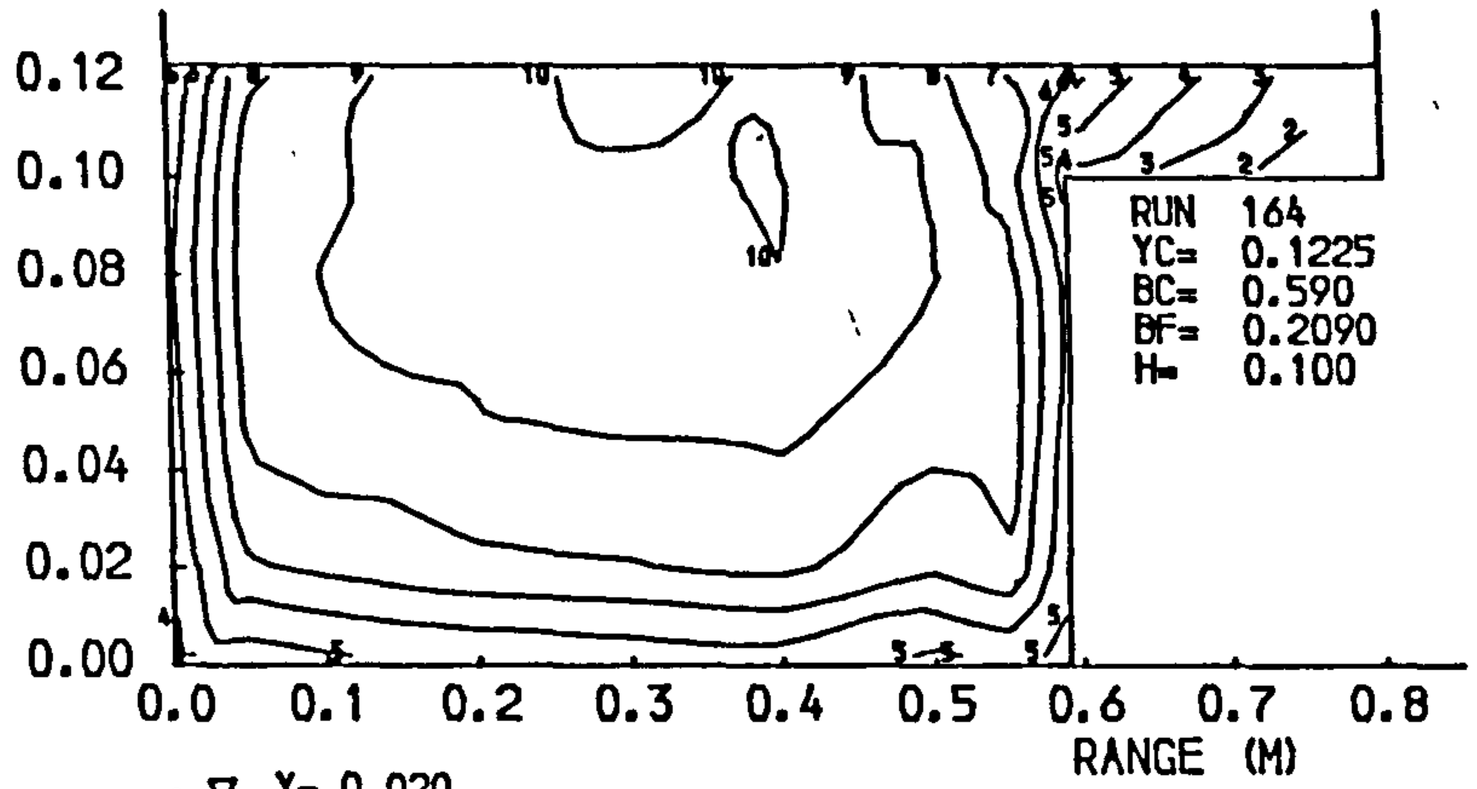

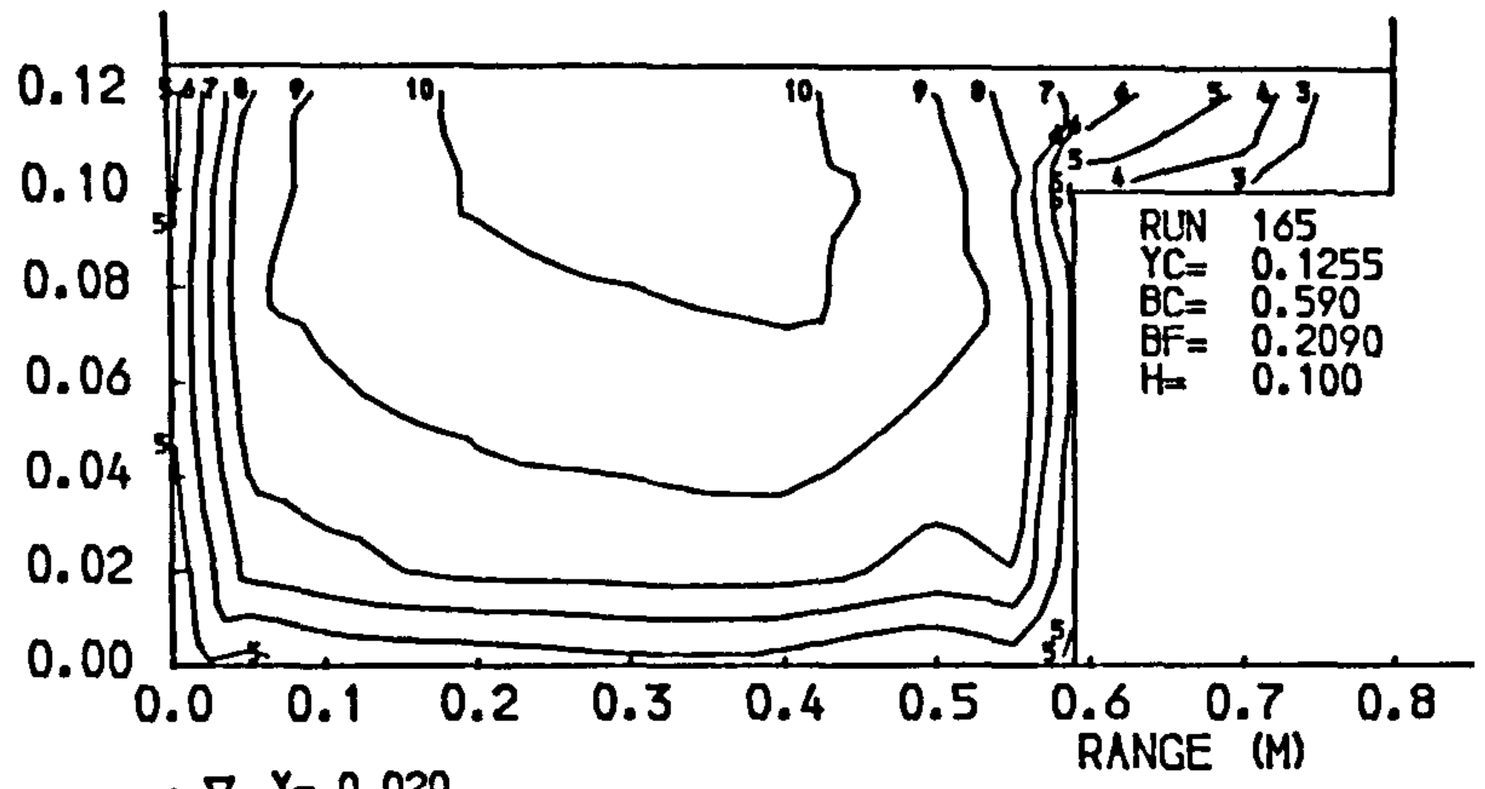

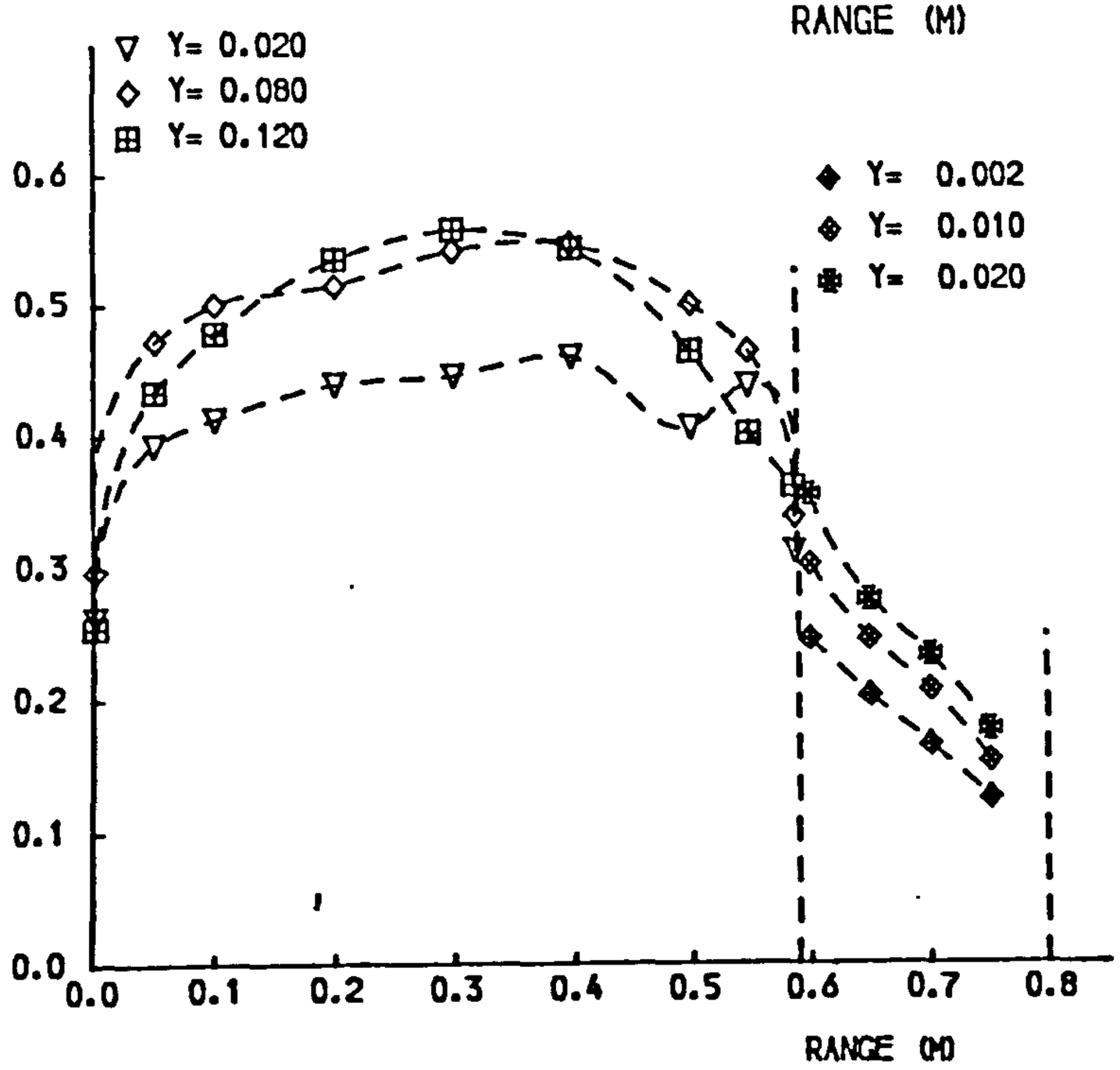

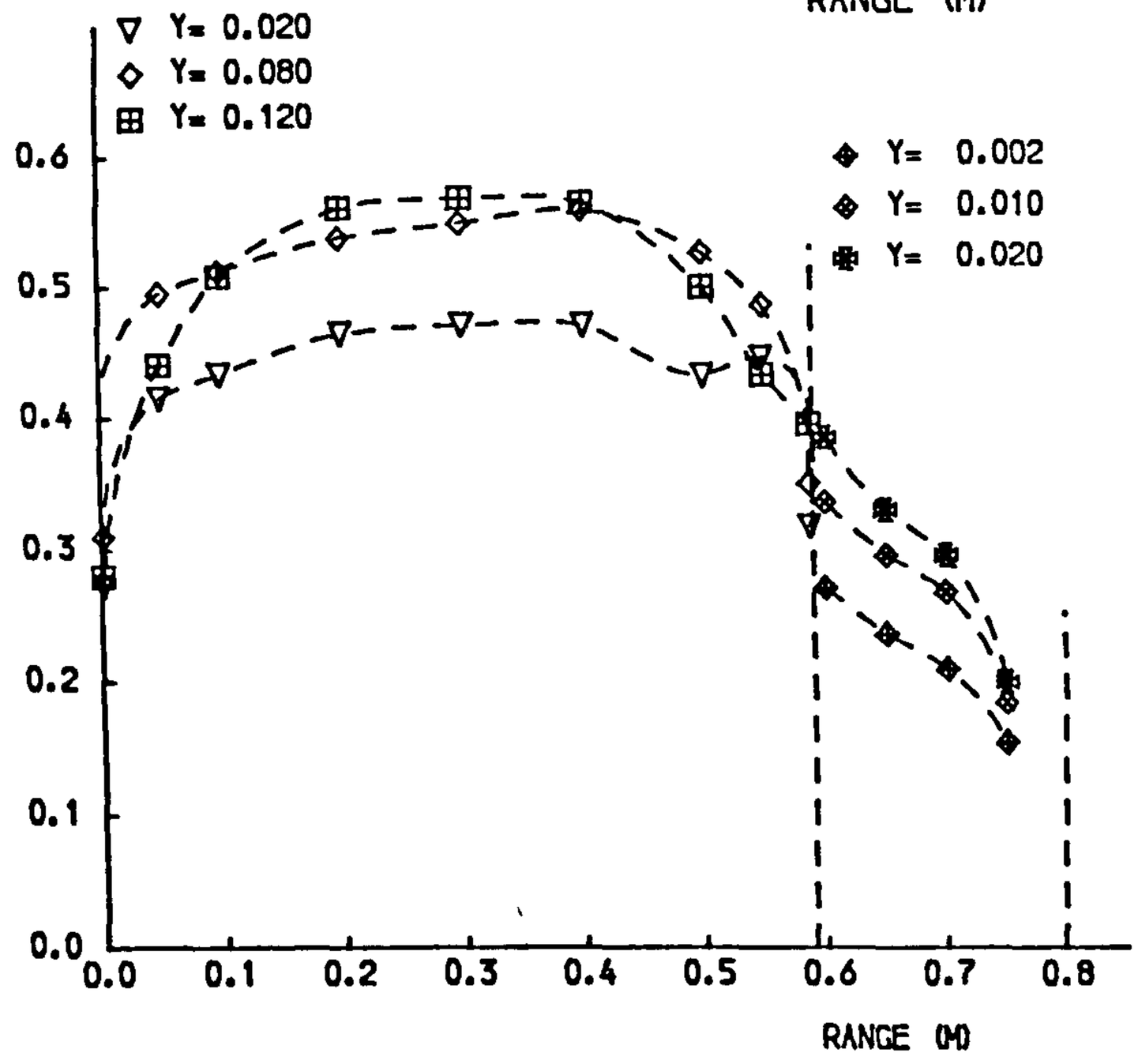

Fig 4·7 Isovels and lateral velocity profiles.

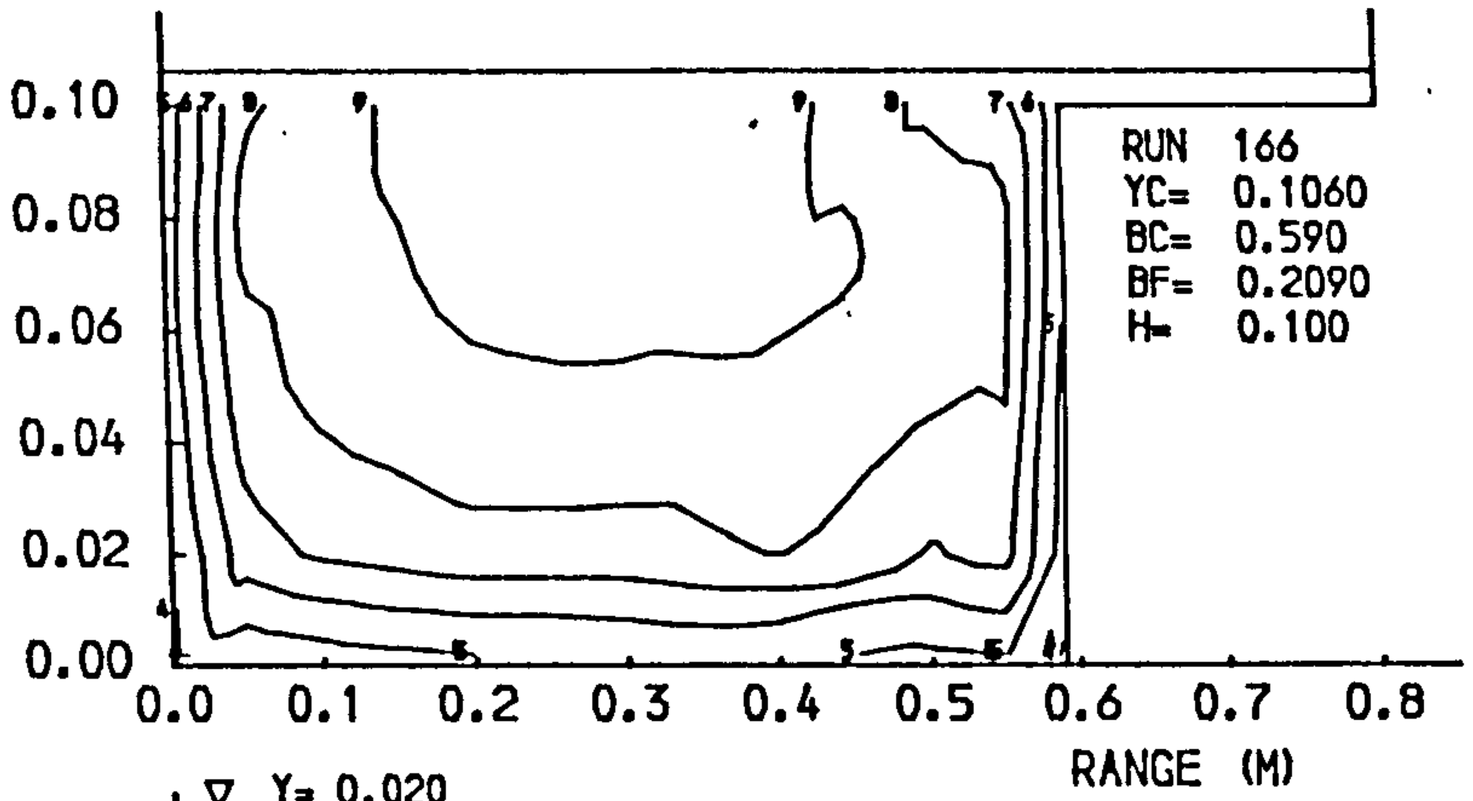

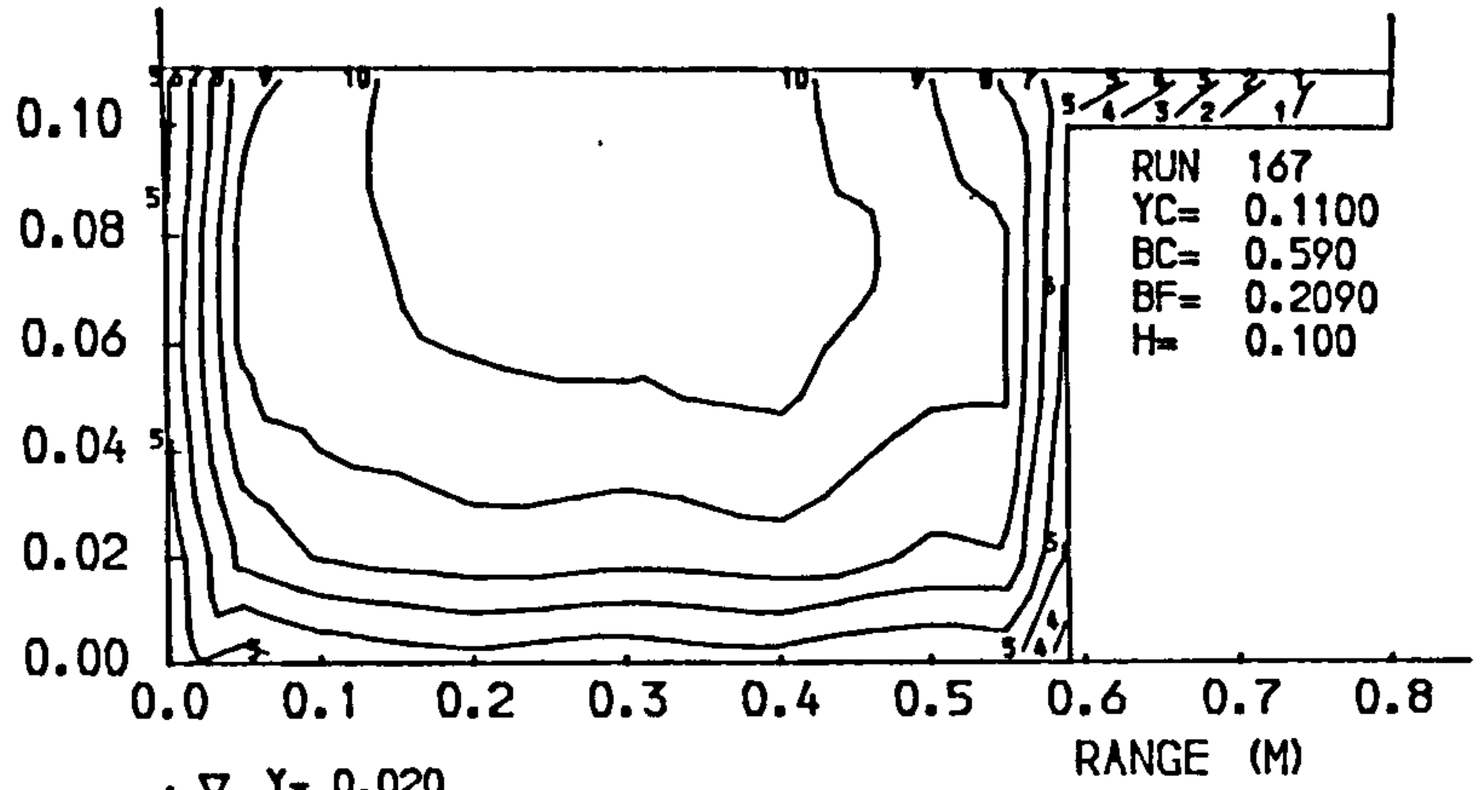

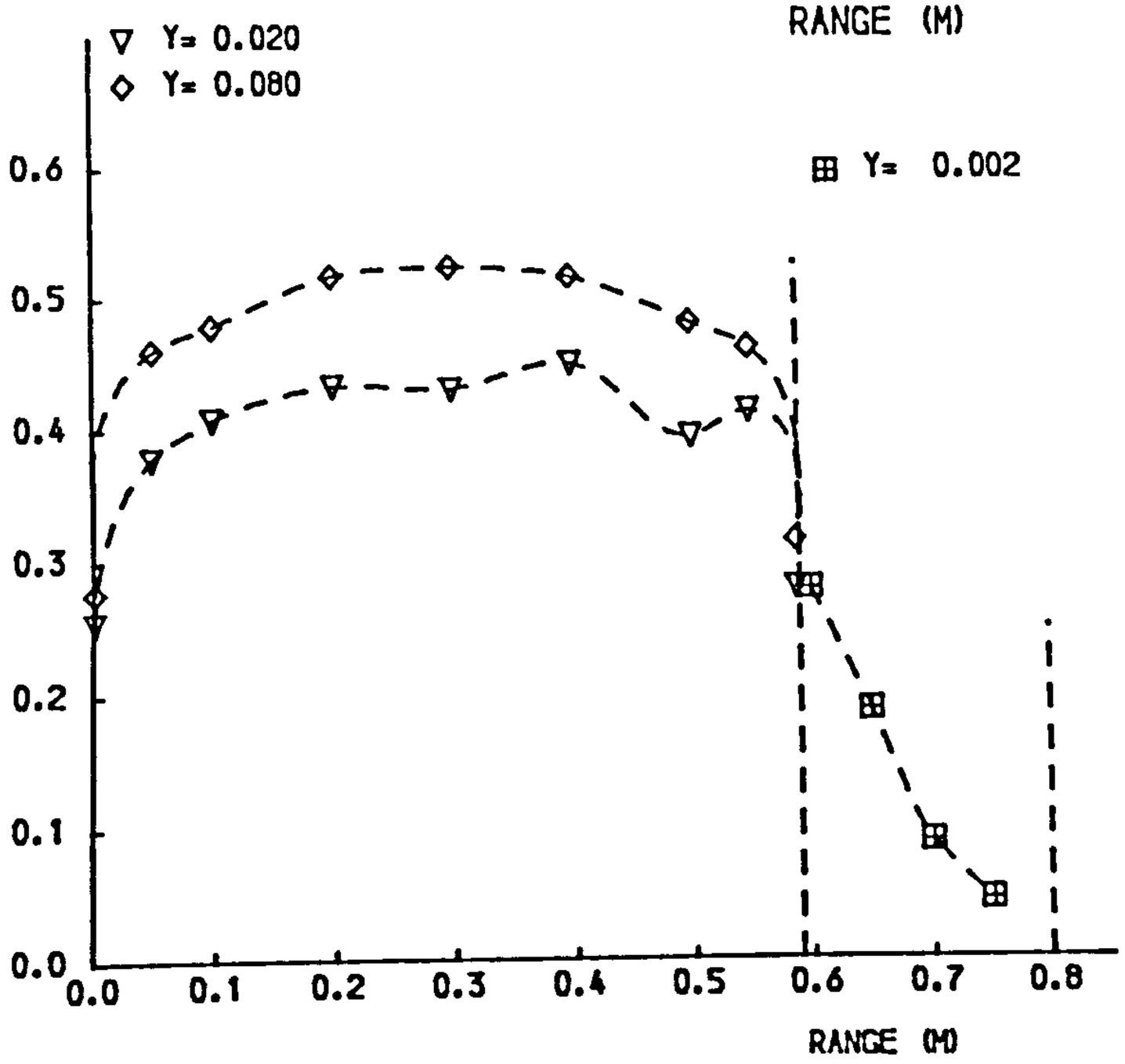

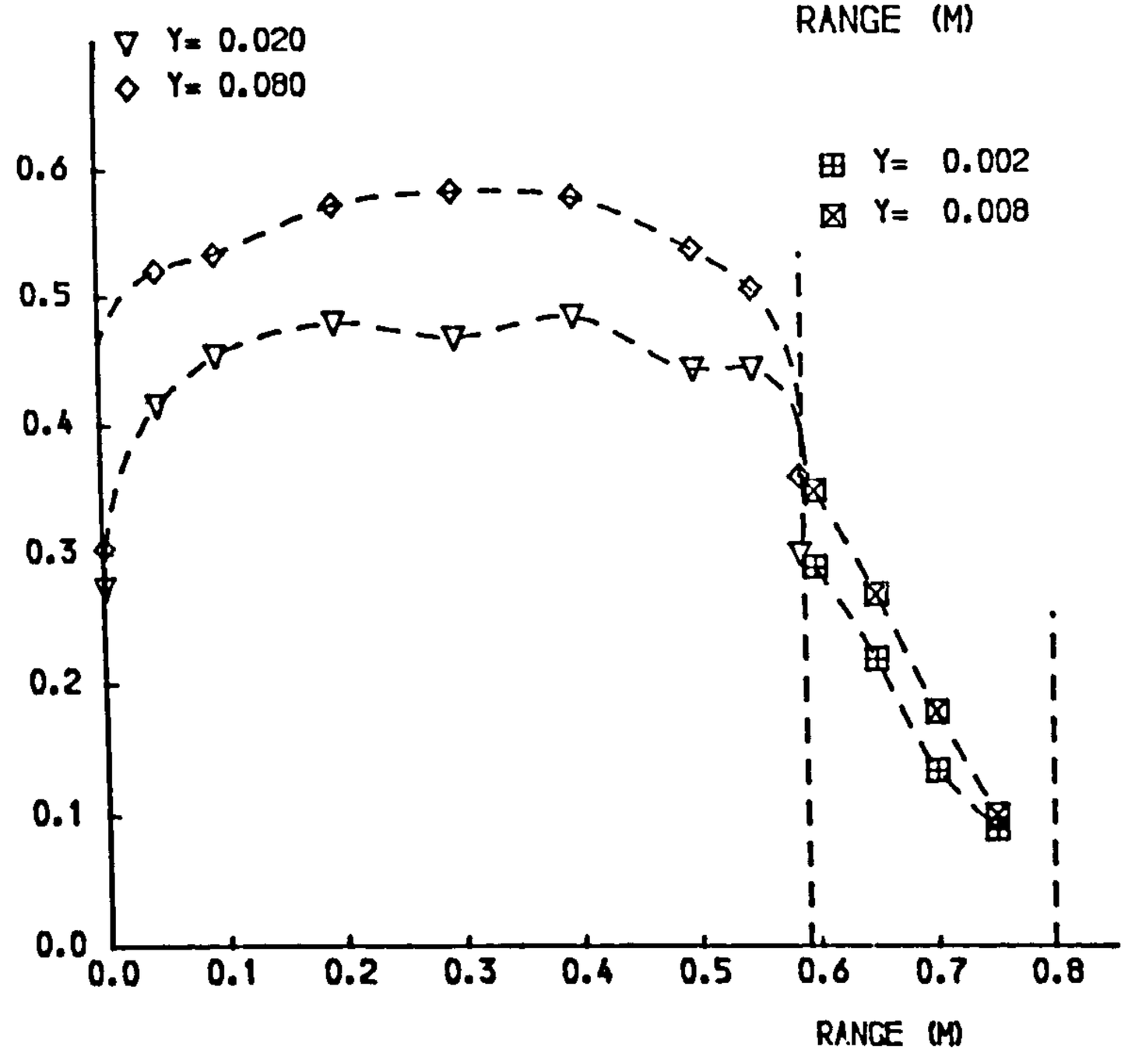

Fig 4·7 Isovels and lateral velocity profiles.

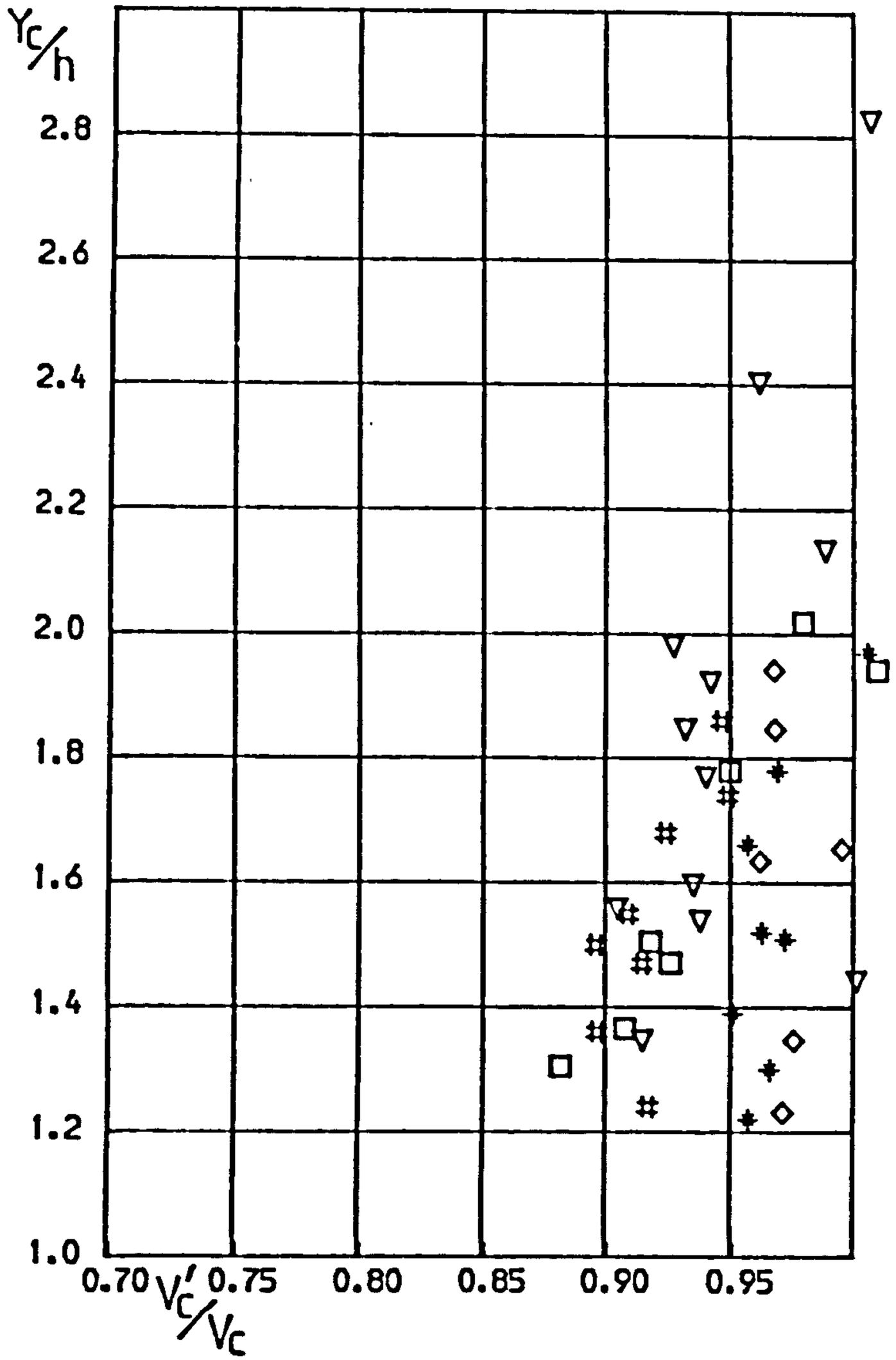

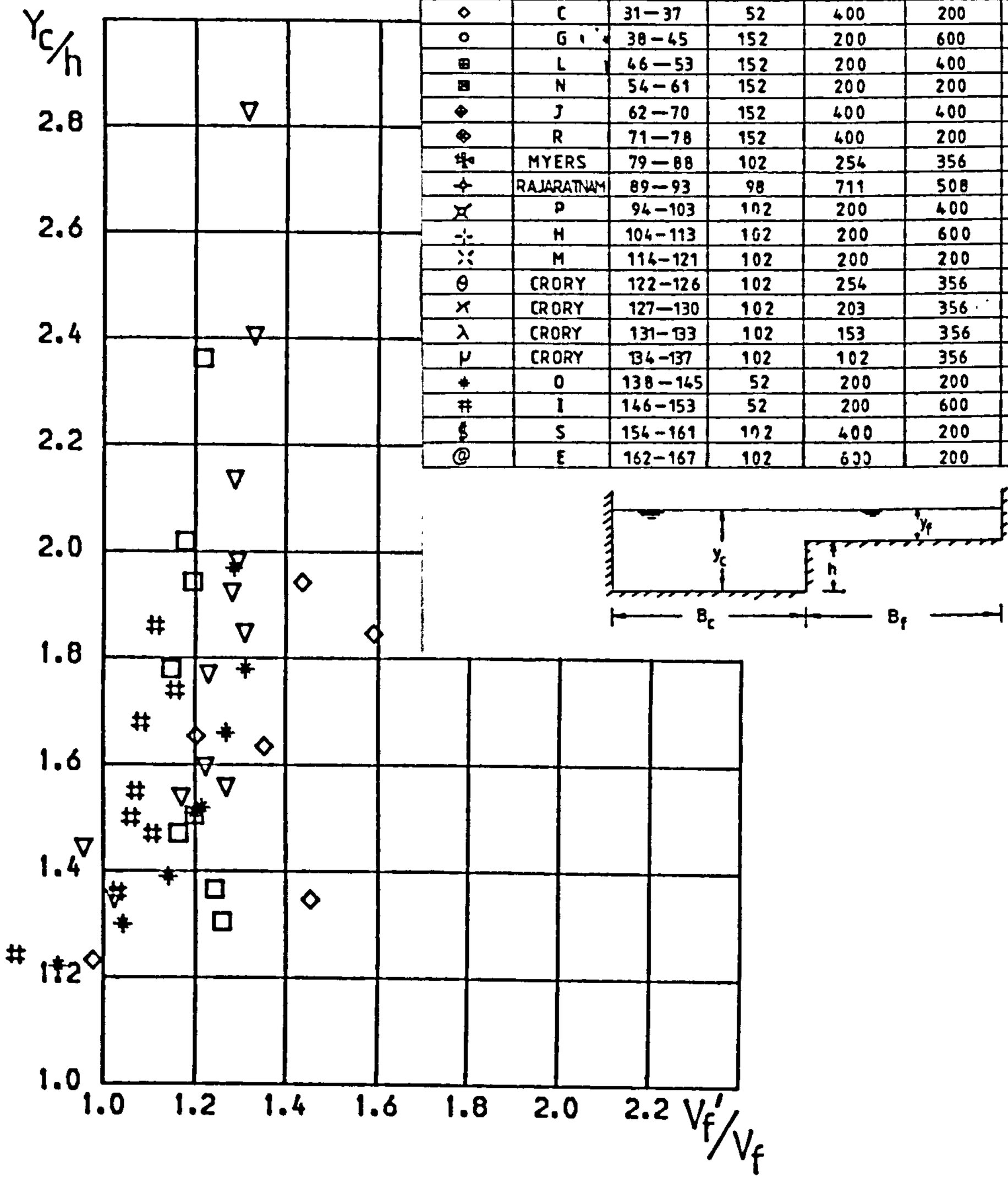

SYMBOL	GEOMETRY	RUN NO	(mm) h	(mm) B_c	(mm) B_f	No of tests
△	K	1 — 10	102	400	400	10
▽	A	11 — 22	52	400	400	12
□	B	23 — 30	52	200	400	8
◇	C	31 — 37	52	400	200	7
○	G	38 — 45	152	200	600	8
⊞	L	46 — 53	152	200	400	8
⊠	N	54 — 61	152	200	200	8
◈	J	62 — 70	152	400	400	9
◈	R	71 — 78	152	400	200	8
⊕	MYERS	79 — 88	102	254	356	10
✧	RAJARATNAM	89 — 93	98	711	508	5
⊠	P	94 — 103	102	200	400	10
⊹	H	104 — 113	102	200	600	10
⊠	M	114 — 121	102	200	200	8
θ	CRORY	122 — 126	102	254	356	6
✕	CRORY	127 — 130	102	203	356	4
λ	CRORY	131 — 133	102	153	356	3
μ	CRORY	134 — 137	102	102	356	4
*	O	138 — 145	52	200	200	8
#	I	146 — 153	52	200	600	8
$	S	154 — 161	102	400	200	8
@	E	162 — 167	102	600	200	6

Fig 4·8(a) (Vc'/Vc) and (Vf'/Vf) against (yc/h) for h= 50 mm.

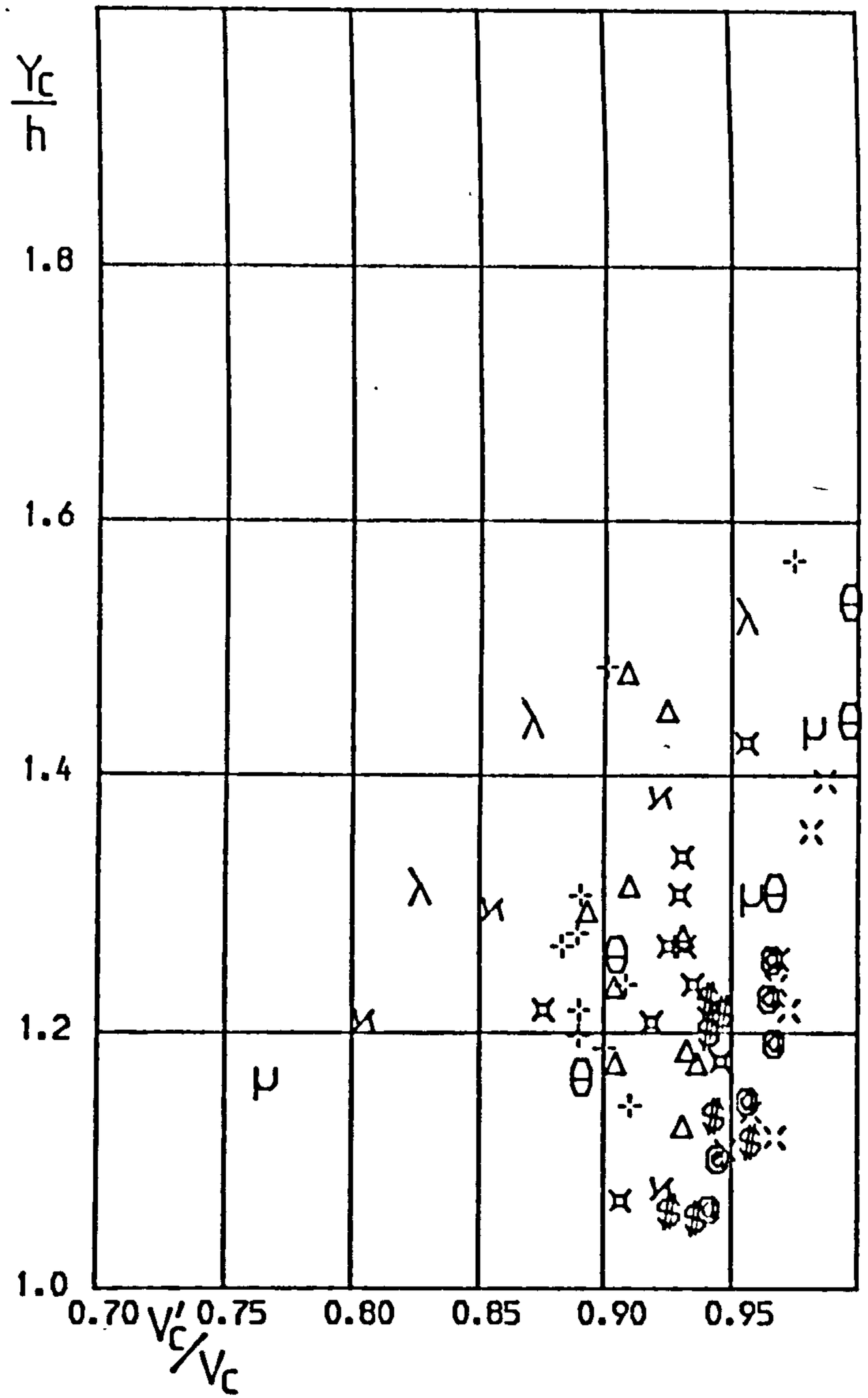

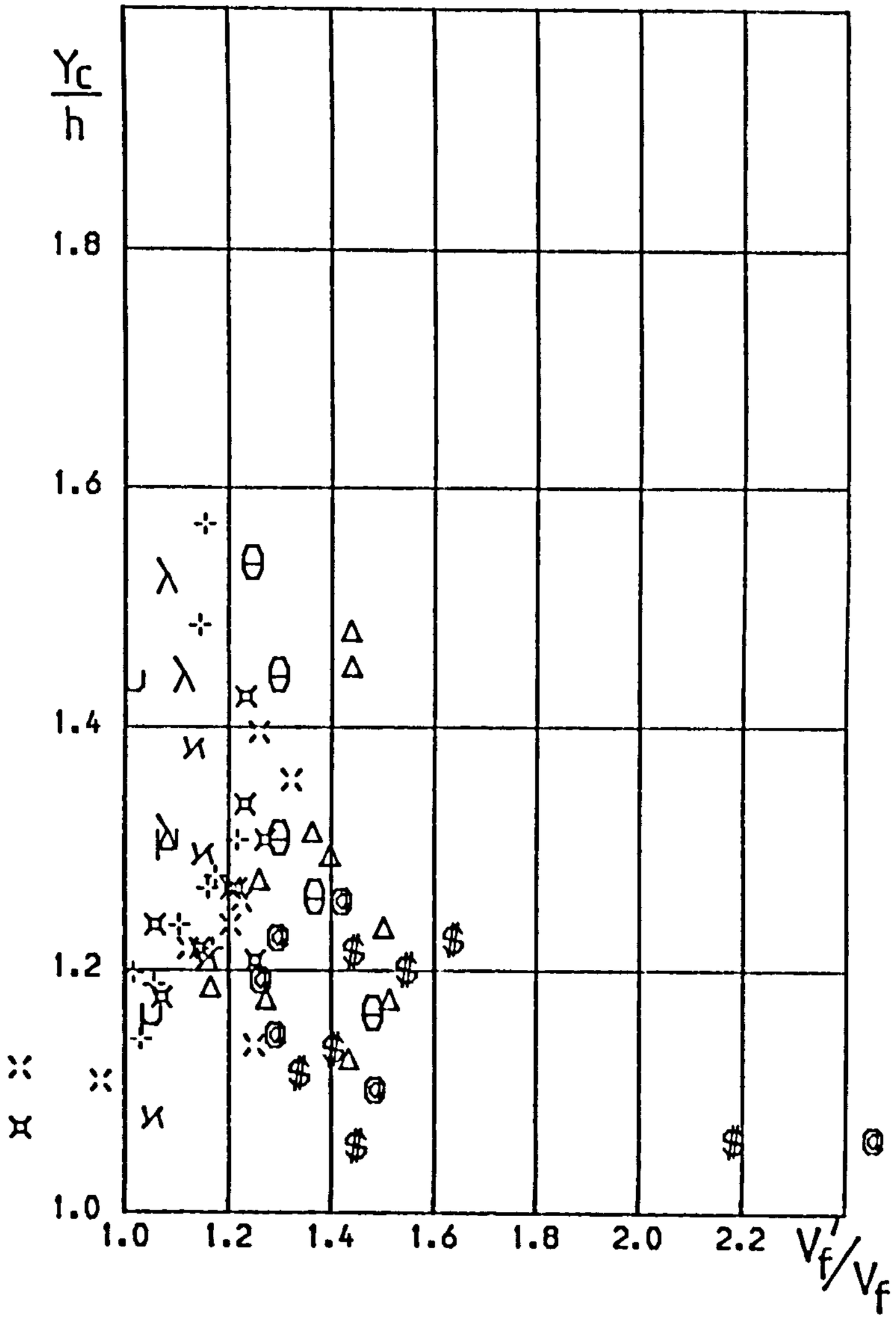

Fig 4·8(b) (V'c/Vc) and (Vf'/Vf) against (yc/h) for h= 100 mm.

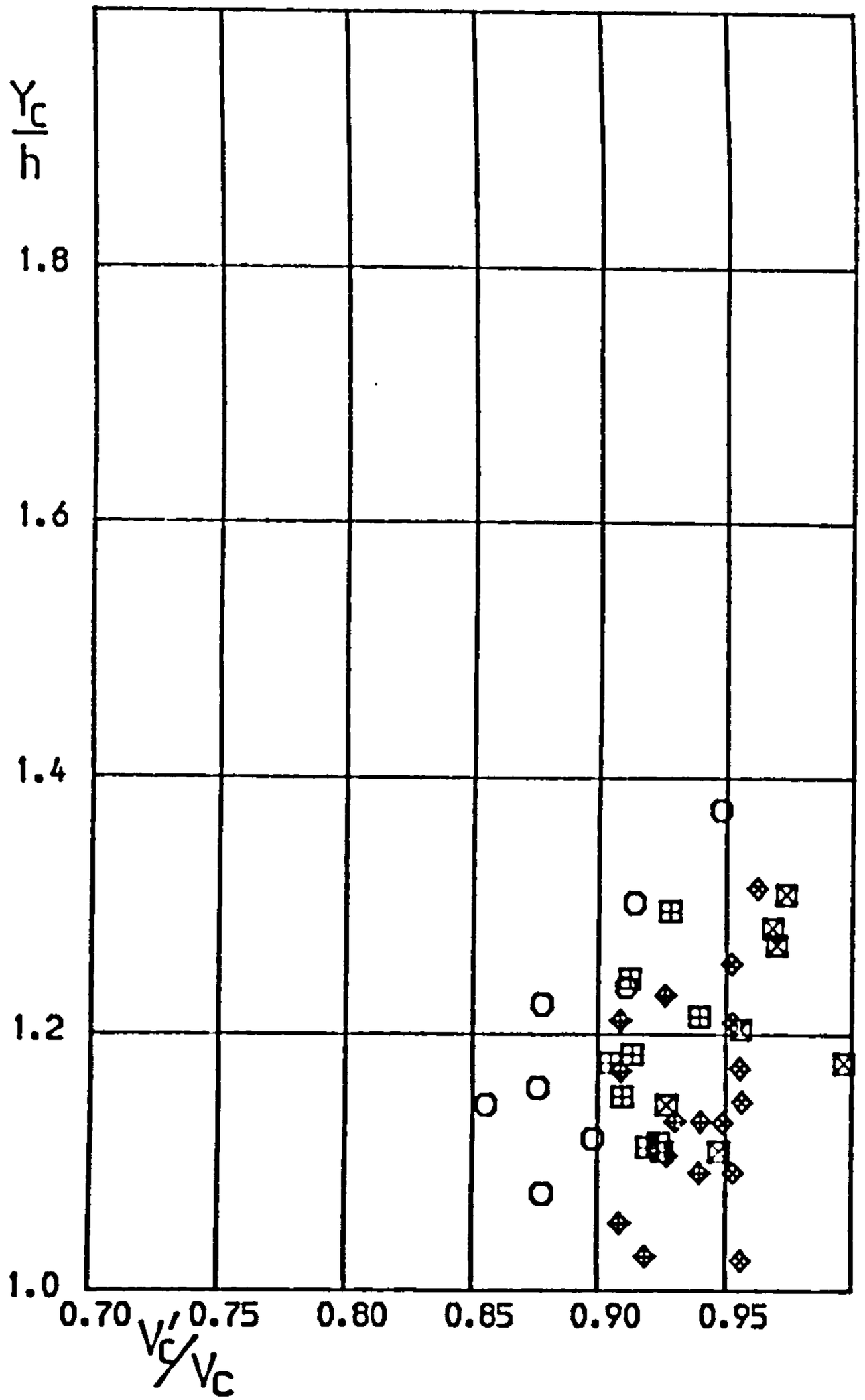

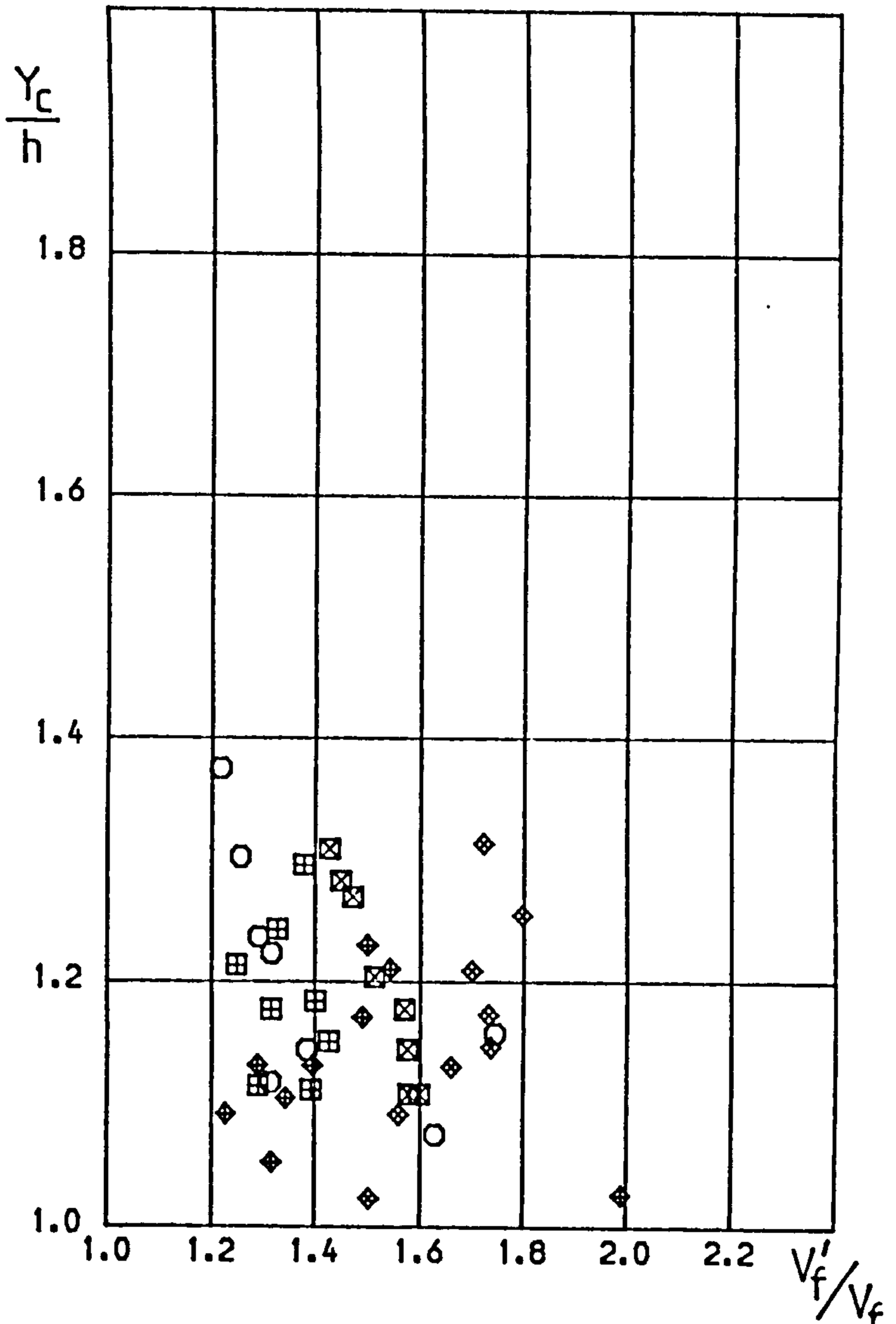

Fig 4·8(c) (Vc'/Vc) and (Vf'/Vf) against (yc/h) for h= 150 mm.

SYMBOL	GEOMETRY	RUN NO	(mm) h	(mm) B_c	(mm) B_f	No of tests
△	K	1—10	102	400	400	10
▽	A	11—22	52	400	400	12
□	B	23—30	52	200	400	8
◇	C	31—37	52	400	200	7
○	G	38—45	152	200	600	8
⊞	L	46—53	152	200	400	8
⊠	N	54—61	152	200	200	8
⊕	J	62—70	152	400	400	9
⊗	R	71—78	152	400	200	8
✠	MYERS	79—88	102	254	356	10
⌖	RAJARATNAM	89—93	98	711	508	5
⌘	P	94—103	102	200	400	10
⌖	H	104—113	102	200	600	10
⌘	M	114—121	102	200	200	8
ϑ	CRORY	122—126	102	254	356	6
ϰ	CRORY	127—130	102	203	356	4
λ	CRORY	131—133	102	153	356	3
μ	CRORY	134—137	102	102	356	4
*	O	138—145	52	200	200	8
#	I	146—153	52	200	600	8
$	S	154—161	102	400	200	8
@	E	162—167	102	600	200	6

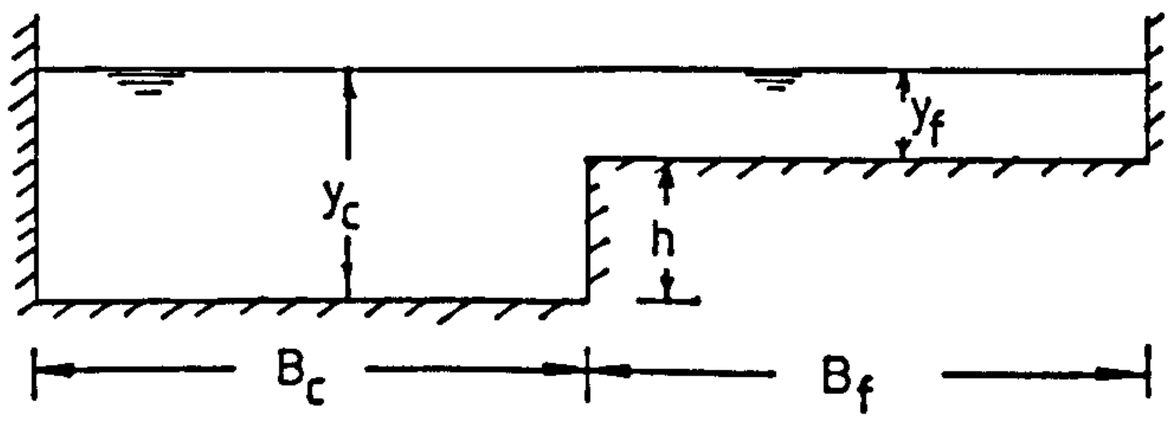

Fig 4·9 Range of Geometries of Asymmetrical Smooth Channels Tested by the Author and Other Investigators.

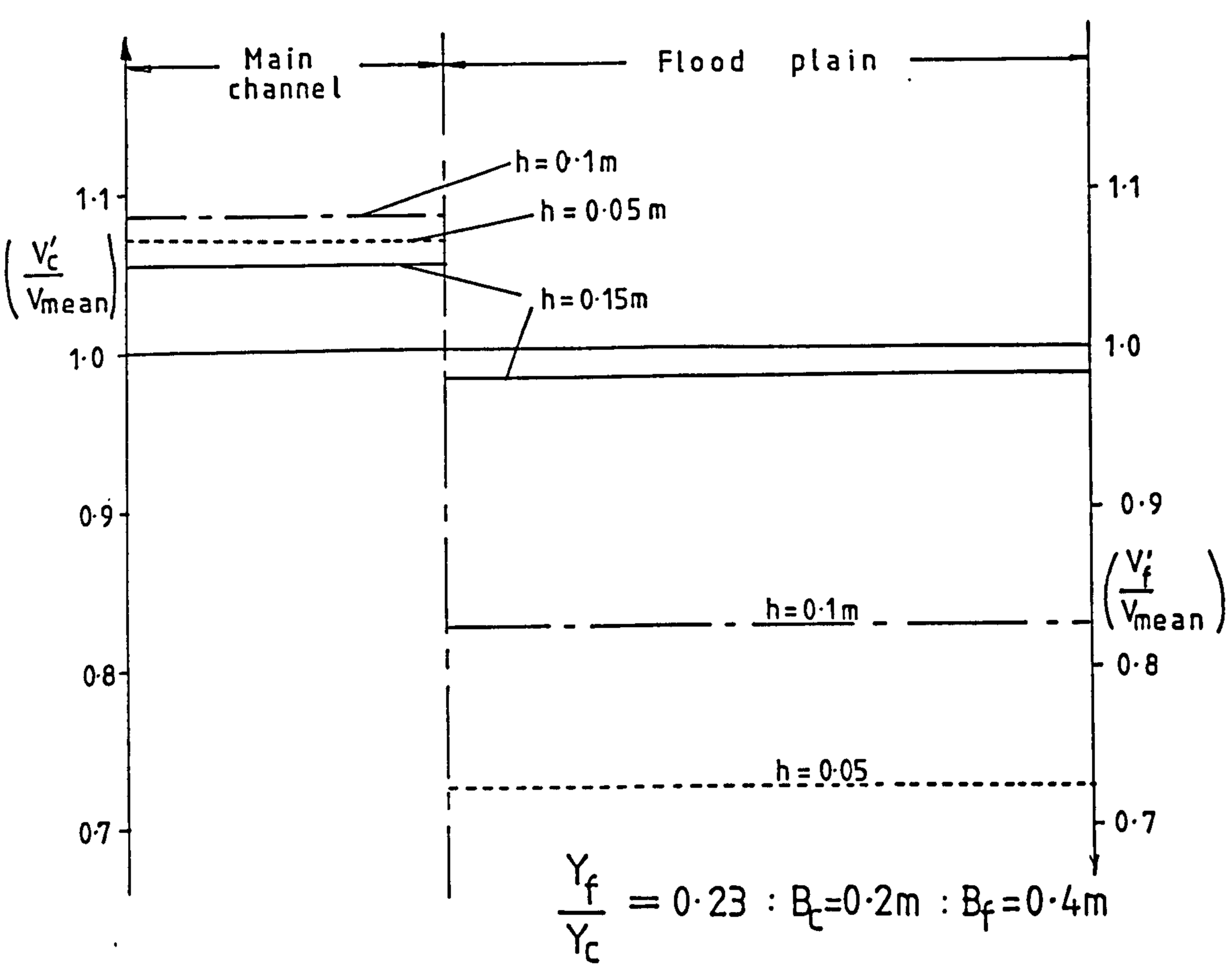

Fig 4·10 Variation of lateral velocity profiles with bankfull depth.

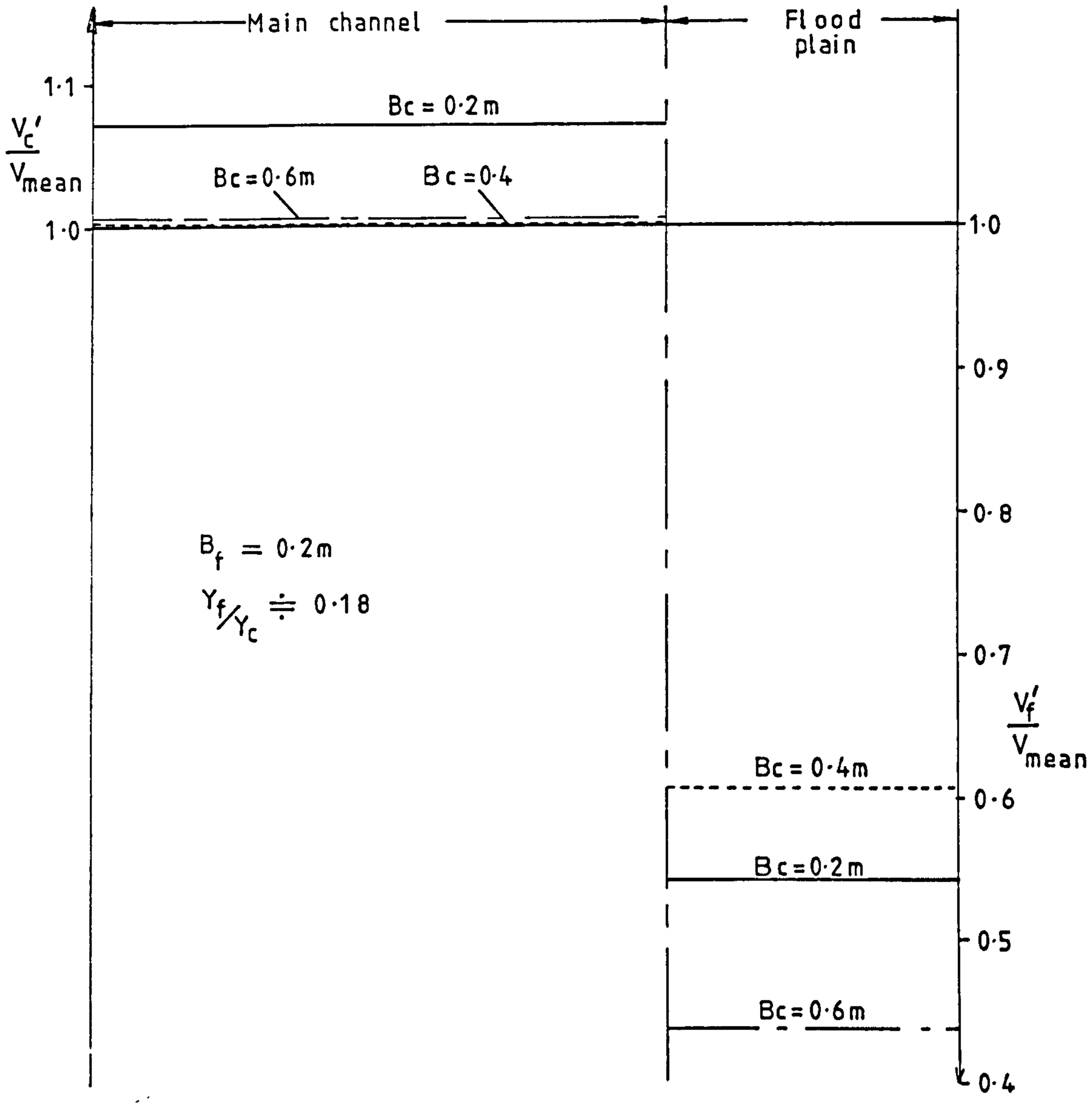

Fig 4·11 Variation of lateral velocity profiles with channel width.

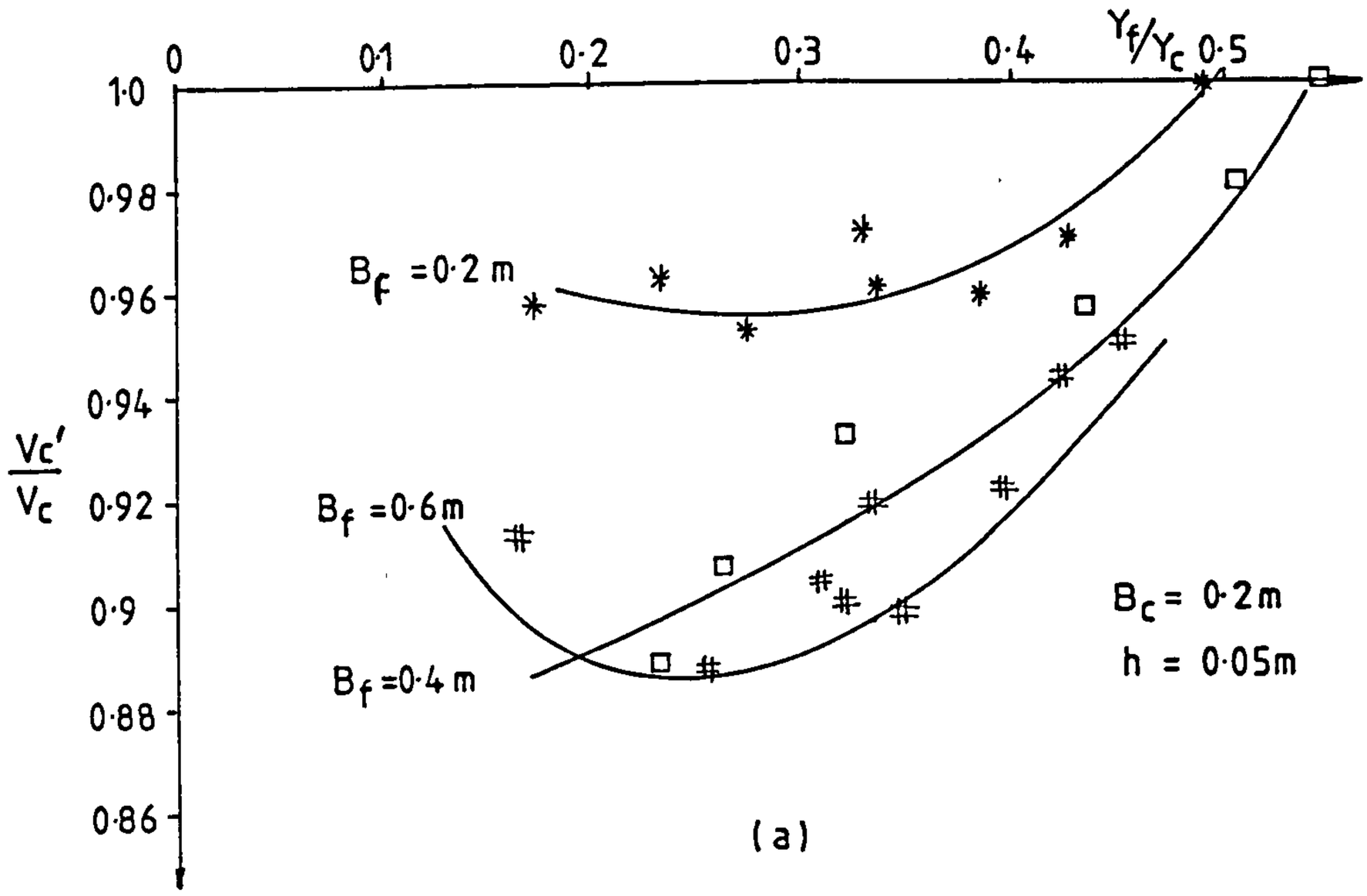

Fig 4·12 Relationship between channel velocity defect and the flood plain width.

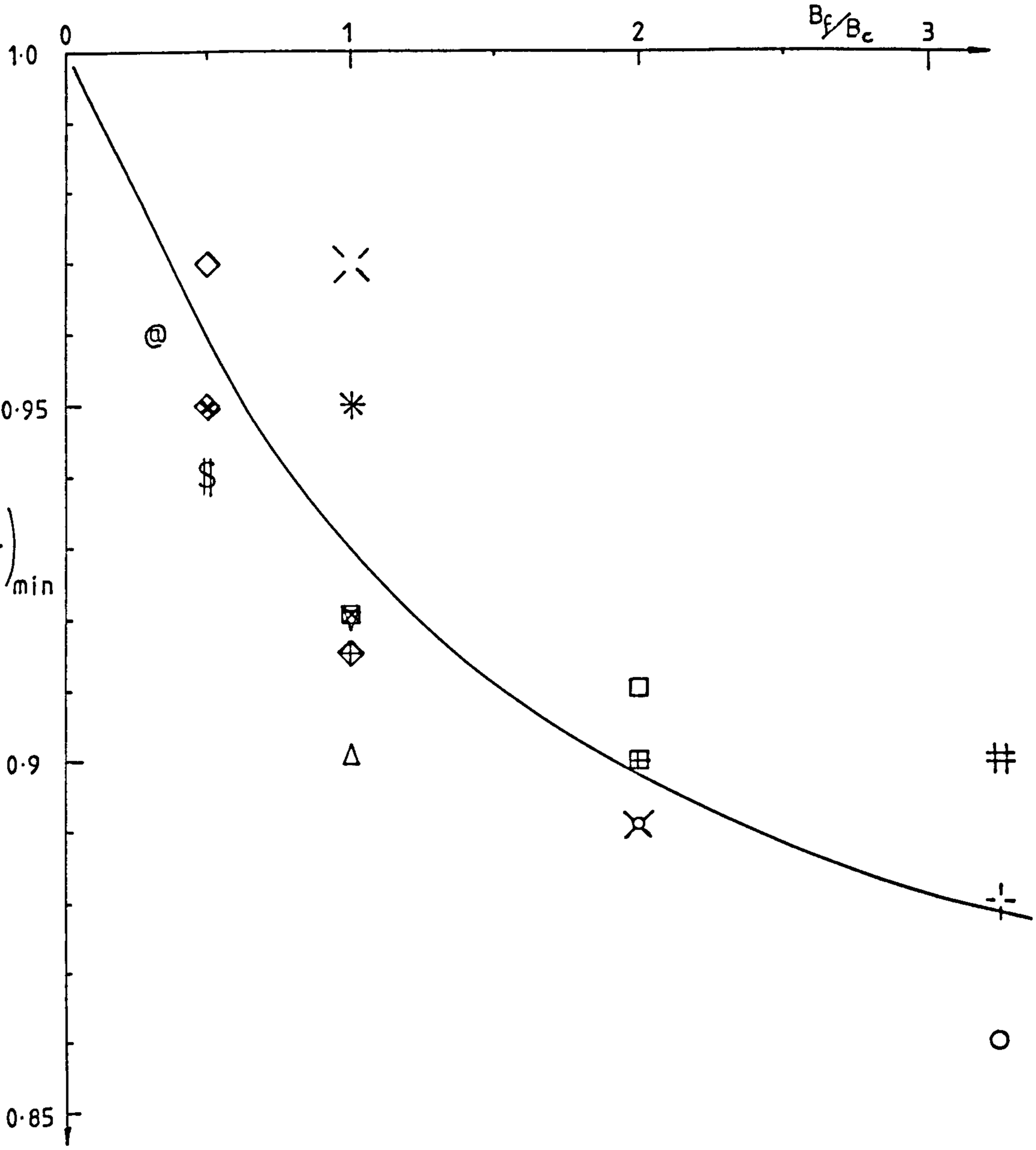

Fig 4·13 Relationship between width ratio and maximum velocity defect.

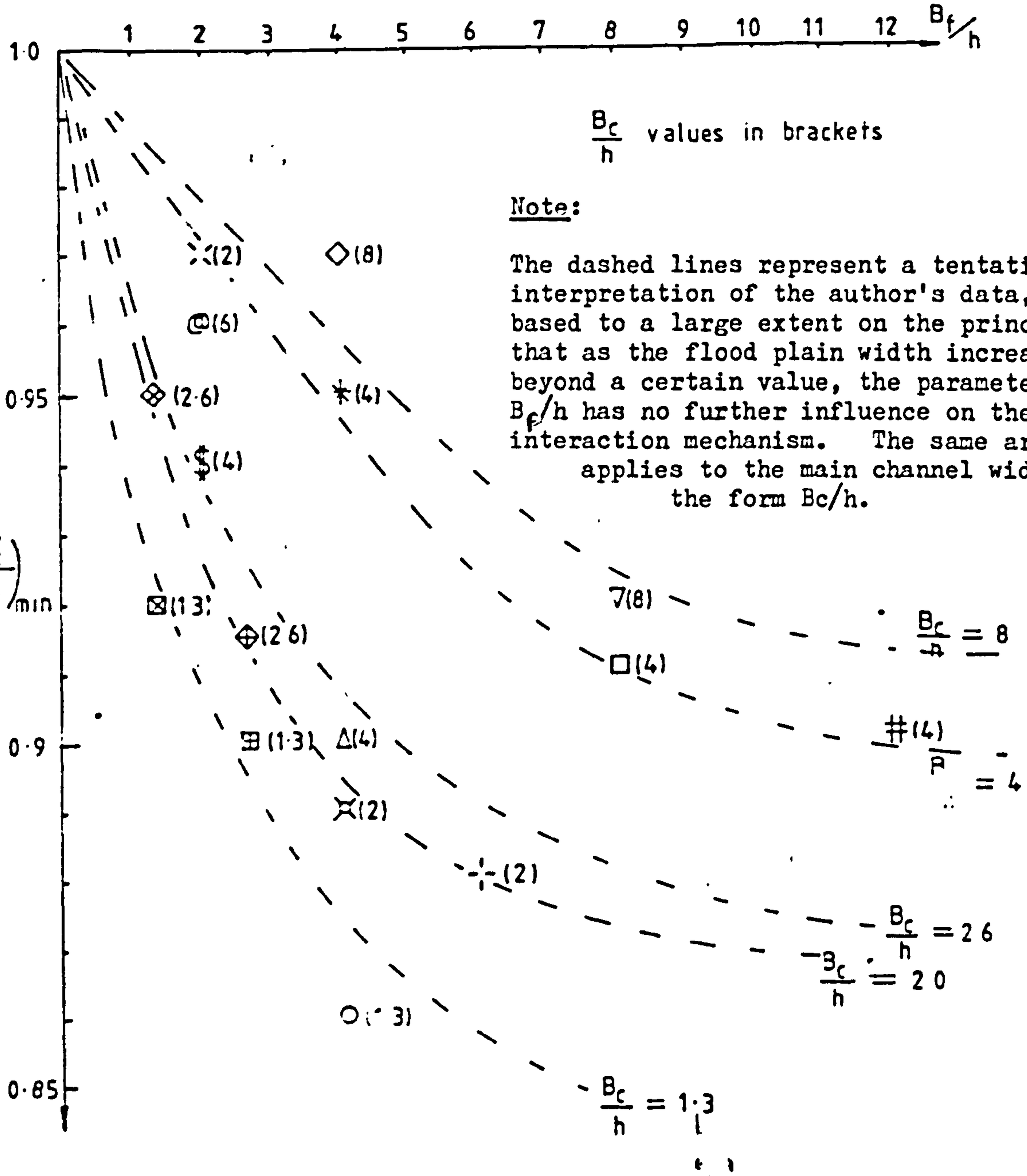

Note:

The dashed lines represent a tentative interpretation of the author's data, based to a large extent on the principle that as the flood plain width increases beyond a certain value, the parameter B_f/h has no further influence on the interaction mechanism. The same argument applies to the main channel width in the form Bc/h.

Fig 4·14 Relationship between channel and flood plain widths and the maximum velocity defect.

CHAPTER FIVE

THE EFFECT OF THE INTERACTION MECHANISM ON BOUNDARY SHEAR STRESSES.. IN THE CHANNEL AND FLOOD PLAIN.

Table of Contents

5.3.4.1 The main channel alone.

5.3.4.2 The flood plain.

5.3.4.3 The whole cross section.

5.3.5 Conclusions.

5.1 Introduction.

Chapter 4 discussed the effects of the channel/flood plain interaction mechanism on the magnitude and distribution of the velocity profiles in both the channel and flood plain. It was shown that, at flow depths greater than the bankfull depth, the mean velocities in the channel could be reduced by up to 15% as a direct result from channel/flood plain interaction. Increases in mean flood plain velocities were also observed for similar flow depths. Such changes in the flow distribution has developed from the existence of a lateral velocity gradient across the channel and flood plain. Velocity gradients in turbulent flow are generally characterised by high turbulent shear regions which attempt to transfer the momentum from fast flow to slower regions of flow. The momentum transfer occurring during overbank flow can be quantified by recording the boundary shear stress distribution around the perimeter of the channel. In this chapter the principle of boundary shear measurement is discussed and applied to compound channel flow. The redistribution of velocities in the channel and flood plain cause a redistribution of boundary shear stresses. This redistribution in shear stresses will be compared to the expected mean shear stresses determined if flow is confined to the channel and the flood plain.

The boundary shear distribution will also be used to highlight regions of high scour since the greater shear exerted on the perimeter of the channel results in an increased likelihood of bed erosion.

Finally, the mean shear stresses in both the channel and flood plain will be discussed in relation to the corresponding mean velocities obtained and presented in Chapter 4.

It must be pointed out at this stage that the most important aspect of the shear stress results will be described in Chapter 6 where the shear stresses will be used to determine the "Apparent shear stress" which can be considered as an imaginary shear stress which occurs at the channel flood plain boundary during channel/flood plain interaction.

5.2 Theoretical Considerations.

As fluid passes an object, i.e. through a pipe or down a channel, it exerts a force on the wetted surface. This force is essentially caused by friction which exists between the boundary and the fluid.

Measurement of this shear force has, until the early fifties been very difficult, except for tests carried out in long pipes or channels where the average shear stress can be related to the average pressure drop along a known length. Two distinct approaches have since been developed to measure the shear stress on a boundary surface.

First, direct methods have been developed which essentially involve suspending a small element of known surface area, just above the boundary and measuring the forces required to maintain the element in the same position. The direct method would require very small elements if the boundary shear distribution is to be obtained since the average shear stress over the element only is recorded. Due to the difficulties in setting up such a method, it was decided to look at indirect methods as a way of recording the boundary shear stress.

Indirect methods involve measuring an intermediate parameter such as heat transfer or local velocities which can be related to shear stresses by an inner boundary law. Perhaps the simplest method involves recording the velocity profile away from the boundary. Such a profile can be related to the Von Karman - Prandtl equation :-

$$\frac{U}{U_*} = 5{\cdot}75 \log \frac{y U_*}{\nu} + 5{\cdot}5 \qquad (5.1)$$

where U_* is the shear velocity given by the equation :-

$$U_* = \sqrt{\frac{\tau_o}{\rho}} \qquad (5.2)$$

and where U is the local velocity a distance of y from the boundary, τ_o is the shear stress and ν is the kinematic viscosity of the fluid. By plotting the velocity profile on semi-logarithmic graph paper, it is possible to determine the shear velocity. Thus it is clear that the shear stress τ_o can be determined from a knowledge of the shear velocity. However, Equation (5.1) only applies to 2 dimensional flow where the side walls have no influence on the vertical velocity profile. The width to depth ratios of tests carried out in this study were such that the velocity profile would be 3-dimensional. Furthermore, it has been shown that the channel/flood plain interaction mechanism restructures the flow distribution resulting in equations like Equation (5.1) no longer being applicable.

Another method of indirect shear stress measurement is the hot wire or hot film anemometry technique. This method essentially measures the amount of heat transfer from the wire or film to the flow which can be related to a shear stress. The main difficulty commonly experienced using this method is the amount of contamination which occurs from impurities and air bubbles. Thus such a method is more suited to

air flow measurements and is not always successful in the present type of study.

A third method which was finally adopted for this investigation was a method developed by Preston (Ref 43) in 1953. This method which became known as the Preston tube technique involves positioning a Pitot tube on the boundary surface, measuring the dynamic pressure and the static pressure and relating them to a shear stress. Preston demonstrated the following relationship :-

$$\frac{(P-p_o)d^2}{\rho\nu^2} = Fn\left[\frac{\tau_o d^2}{\rho\nu^2}\right] \qquad (5.3)$$

where P is the dynamic pressure, p_o is the static pressure, d is the Pitot tube diameter, ρ is the density of the fluid and ν is the kinematic viscosity. Preston proposed the following equation for pipe flow :-

$$\log\frac{\tau_o d^2}{4\rho\nu^2} = 2{\cdot}604 + \frac{7}{8}\log\frac{(P-p_o)d^2}{4\rho\nu^2} \qquad (5.4)$$

where the definitions are as above.

Experimental results obtained in 1958 by Bradshaw and Gregory (Ref 8) at NPL and by Smith and Walker (Ref 78) cast considerable doubt on the validity of the relationship proposed by Preston. However, further work by Head and

Rechtenberg (Ref 23) and Patel (Ref 40) confirmed the validity of Equation (5.3). Furthermore, Patel was able to improve the accuracy of Prestons calibration in Equation (5.4) and suggested the following relationship :-

$$y^* = 0{\cdot}8287 - 0{\cdot}1381x^* + 0{\cdot}1437x^{*2} - 0{\cdot}006x^{*3} \qquad (5.5)$$

where $$y^* = \log \frac{\tau_o d^2}{4\rho\nu^2} \qquad (5.6)$$

and $$x^* = \log \frac{(P-p_o)\, d^2}{4\rho\nu^2} \qquad (5.7)$$

Patel suggested that such a relationship was valid for the range :-

$$1.5 < y^* < 3.5 \qquad (5.8)$$

Many investigators have applied the Preston tube technique to channel flow with considerable success.

5.3 Experimental Work.

5.3.1 Initial Tests.

As indicated in the previous section it was decided to use the Preston tube technique as a means for determining the shear stress distribution in the channel and the flood plain during overbank flow conditions. This method has been used extensively by previous investigators into the shear stress distributions in rectangular channels. Myers(Ref 36),Ghosh and Jena(Ref 20) , Crory and Elsawy (Ref 14), Rajaratnam and Ahmadi (Ref 48) and Hadjipanos et al (Ref 22) have all used the Preston tube technique in compound channel flow with success. Myers (Ref 36) compared the shear stress measurements obtained from 3 different Preston tubes. He calculated the mean shear stress by integrating the shear stress distribution obtained for each test by planimetry and compared this with the mean shear stress calculated from the weight component of the flow down the channel. He found that the 6.35 mm OD Preston tube gave results 21.4% lower than the calculated stresses. A 3.175 mm OD Preston tube was found to give stresses 22.2% less than the calculated stresses. Finally, using the Patel calibration relationship with a Preston tube of outside diameter 1.82 mm, he found that the measured shear stress was 1.32% greater than the calculated shear stress. He proceeded

to use this Preston tube as a means of determining the shear stress distribution in his compound channel during overbank flow.

Considering the difficulties that Myers experienced in selecting a suitable Preston tube, it was decided to look carefully at the shear stress values obtained in the present study with flow confined to the main channel.

Rajaratnam (Ref 49) suggested that a Pitot static tube could be used to measure the shear stresses in a channel. He was able to show that the pressure difference recorded by a Pitot static tube resting on the channel wall was the same as the pressure difference recorded by a Preston tube of the same OD. In his investigations, Rajaratnam used a hemispherical nosed Pitot static tube. Since the only available Pitot static tube for the present study had an elliptical nose, it was hoped that a similar relationship would apply. Private correspondence with Prof. Rajaratnam in fact confirmed that an elliptical nosed Pitot static tube should be adequate for this type of experimental work. It was necessary to verify this and therefore a series of tests was carried out to look at the shear stress measurements recorded from the elliptical nosed Pitot static tube and two Preston tubes of different outside diameters. The shear stresses were also compared with the calculated stresses from a consideration of the weight component of flow acting down the channel. Such tests were carried out with flow confined to the

main channel thus simplifying the shear stress distribution.

First, uniform flow was established in the channel and the flow depth and discharge recorded. The water surface slope was determined using the pointer gauge on the instrument carriage and the surveying level. The elliptical nosed Pitot static tube was connected to the pressure transducer and positioned around the perimeter of the channel at 30mm intervals. For some tests, the Pitot static tube was used, then under the same flow conditions, a Preston tube of 3mm outside diameter was used to determine the shear stress distribution. Finally a third Preston tube of 1.6 mm diameter was connected to the pressure transducer and used to determine the boundary shear stress distribution. Each distribution was integrated by planimetry to give the mean shear stress in the channel. The shear stress measurements were taken a sufficient distance downstream from the channel entrance to give fully developed turbulent flow. The calculated shear stress, τc_{calc} can be found from a consideration of the equilibrium of forces down the channel :-

$$\tau c_{calc} P_c = \rho g A_c \sin\theta \qquad (5.9)$$

where θ is the inclination of the channel relative to the horizontal, ρ is the density of the water, g is the gravitational constant, Ac is the cross-sectional area of the channel and P_c is the wetted perimeter. If θ is small, then $\sin\theta$ can be taken as

the channel slope. Substituting the hydraulic radius for Ac and Pc gives the relationship :-

$$\tau_{c_{calc}} = \rho\, g\, Rc\, S \qquad (5.10)$$

The shear stress obtained from the Preston tubes and the Pitot static tube can be compared to the calculated shear stress from Equation (5.10) and so the accuracy of the Preston tube technique can be measured. Fig 5.1 shows this relationship which gives a good correlation between the results. However there does seem to be considerable spread in results. It was indicated in Chapter 3 that difficulty was experienced in measuring the water surface slope to a sufficient degree of accuracy, therefore the spread of results may not necessarily be due to the inaccuracy of the Preston tube but more likely to be caused by the inaccuracy of the water surface slope measurement.

It was decided as an extra check to relate the shear stress measurements in the main channel to the measured mean velocities in the channel which could be determined with good accuracy from the orifice plate flow meter.

It was shown in Chapter 4 that the friction factor λ_c, for flow confined to the channel could be given by the relationship :-

$$\frac{1}{\sqrt{\lambda_c}} = 2{\cdot}0 \log(Re\sqrt{\lambda_c}) - 1{\cdot}3 \qquad (5.11)$$

where $Re=4V_c R_c/\nu$ and λ_c is given by the Darcy-Weisbach equation :-

$$\lambda_c = \frac{8 g R_c S}{V_c^2} \qquad (5.12)$$

Combining Equations (5.12) and (5.10) and elimating the water surface slope gives the relationship :-

$$\tau_c = \frac{V_c^2 \rho \lambda_c}{8} \qquad (5.12\,a)$$

Equation (5.12a) gives a relationship between τ_c and Vc and the results of such a relationship is shown in Fig 5.2. λ_c was determined from Equation (5.11) with Re based on the measured channel velocity, Vc. It can be seen that there is still some spread in the results although not as significant as the spread on Fig 5.1. Therefore, it seemed reasonable to have a good degree of confidence in the shear stress measurements obtained from the Pitot static tube, as the results obtained were not significantly different from the smaller diameter Preston tubes.

5.3.2 Overbank Flow Conditions.

It has been shown that the 4 mm Pitot static tube which has been used to obtain the local velocity points for the tests presented in chapter 4, can also be used to record the shear stress distribution around the channel. As indicated in the previous section, the measured water surface could vary from the actual water surface slope and so the shear stress measurements enabled a more accurately determined water surface slope. Consider the force equilibrium equation for the compound channel shown on Fig 5.3. For a element of flow of length unity :-

$$\tau_c' P_c' + \tau_f' P_f' = \rho g A_t \mathrm{Sin}\theta \qquad (5.12b)$$

where τ'c and τf' are the measured shear stresses in the channel and flood plain respectively, Pc' is the wetted channel perimeter and is equal to h+Bc+Yc, Pf' is the wetted perimeter of the flood plain and is equal to Yf+Bf, At is the total cross-sectional area of the cross sectional area of the compound channel and θ is the angle of the channel slope relative to the horizontal. Fig 5.5 shows Equation (5.12b) for some of the tests carried out, and it can be seen that there is considerable spread in the results. This spread is mainly due to the inaccuracy of the water surface slope measurement. If θ is small enough (as was the case in the present investigations) then sinθ can be taken as S, the

channel slope. Equation (5.12b) can be used to establish a more accurate water surface slope since the shear stresses can be determined reasonably accurately.

A series of 16 different channel geometries were tested as outlined in chapter 3, with 136 test runs being carried out. The shear stress measurements were recorded at the same time as the local velocity profiles. The velocity points recorded always included points which lay on the channel boundary and so these results could be used to record the shear stresses. Care was taken to ensure that the Pitot tube rested firmly on the channel boundary since it was soon discovered that the pressure difference recorded by the pressure transducer was very sensitive to the position of the Pitot tube relative to the channel wall. One difficulty with the Preston tube technique is that the Preston tube OD must be less than 1/5th the boundary layer thickness for Preston's relationship to be valid. Since flow in the channel and flood plain were always fully developed, this implied that the depth of flow must always be five times greater than the Pitot tube diameter. The Pitot tube tube OD was 4 mm, therefore it could not be used for shear stress measurements at depths of flow less than 20 mm. This condition was always satisfied in the main channel. However to encourage maximum interactive forces between the channel and the flood plain, low flood plain depths were necessary and often this would involve flow depths in the flood plain less than 20 mm. During such

tests, the Pitot tube was used to determine only the velocity distribution in the flood plain. The shear stresses were determined after the velocity traverse was recorded by replacing the Pitot tube with the Preston tube of outside diameter 1.6 mm. The Preston tube would then be positioned around the perimeter of the flood plain.

5.3.3 Results and Discussion.

The flow conditions and shear stresses obtained from the 136 tests are shown on Table 5.1. Also included in this table are the results of the experimental work carried out by Rajaratnam and Ahmadi(Ref 48), Myers (Ref 36) and Crory (Ref 14). Their work has been integrated into the present study to enable the development of a broad understanding of the interaction problem. The actual shear stress distributions recorded in the present study are shown in Fig 5.4 in a similar manner to the point velocity measurements of Chapter 4. These figures were produced by computer and the program used is presented in Appendix 1. All shear stress measurements shown are in Newtons/metre^2 . The tests used to produce the velocity profiles were also used to produce the shear stress measurements. It follows that the parameters varied included the relative depth Yf/Yc, the bankfull depth h, the main channel width and flood plain width, Bc and Bf respectively. As with the velocity distributions it is important to investigate the effect of each

parameter separately with the other parameters held constant.

According to past investigations, the lateral boundary shear stress distribution should appear similar to the sketch below, indicating a shear defect in the main channel and a shear stress increase on the flood plain.

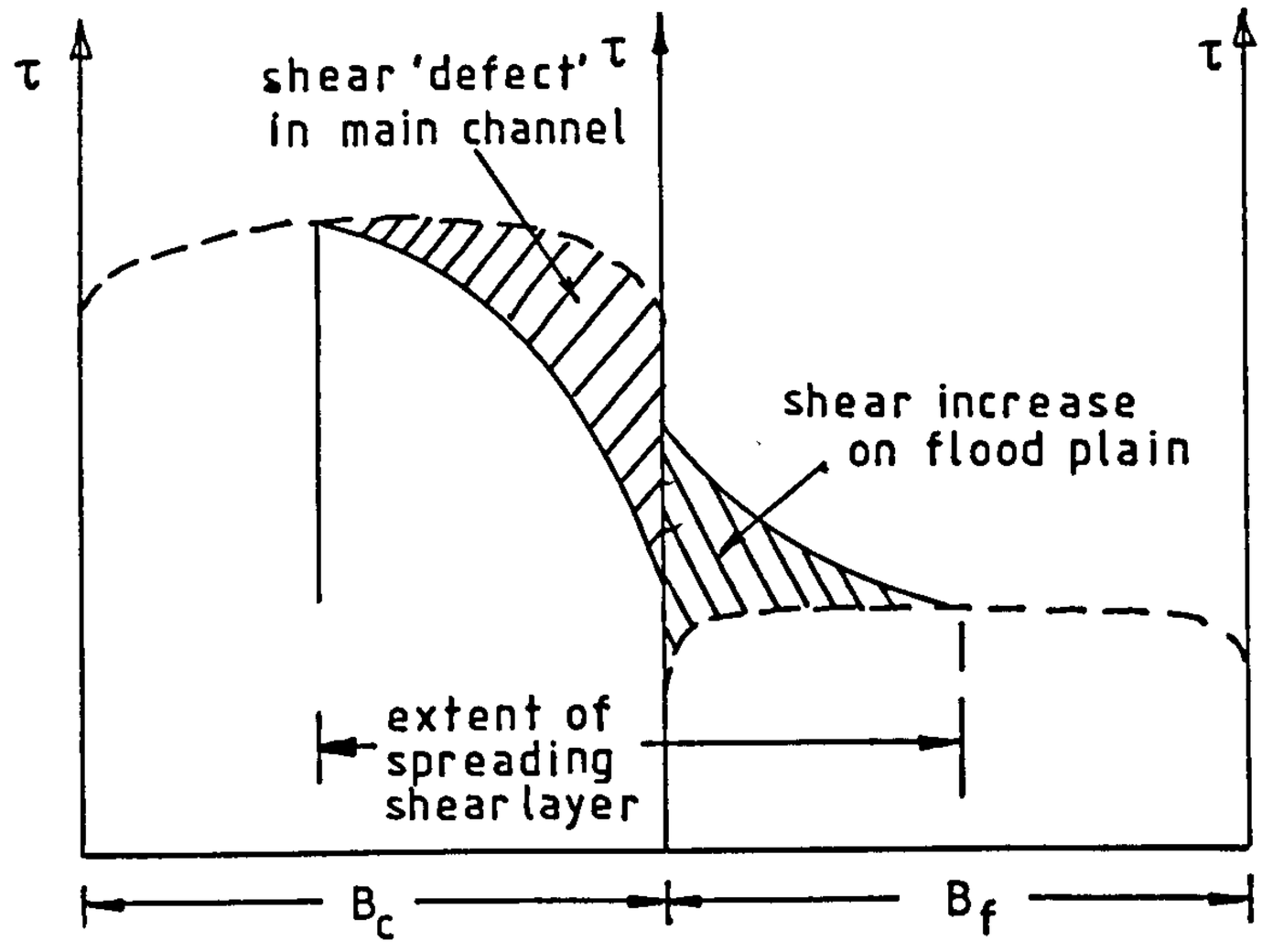

The reason for this shape of lateral shear distribution (as mentioned in Chapter 4) is due to the momentum transfer from the faster layers in the main channel to the slower layers on the flood plain.

The central question in this chapter is concerned with the reasons for a redistribution of shear stress during overbank flow and the factors which influence the magnitude of redistribution. A secondary question might also be how this lateral shear distribution might be related to the lateral velocity profiles described in Chapter 4.

As already described, a region of turbulent shear exists only in the presence of a velocity gradient, as in the case of a channel with flood plain flow. In this case a gradient is being produced by a strong velocity difference between the main channel and flood plain. The velocity gradient in turn produces shearing vortices (or eddies) which transfer energy and momentum away from the main channel and onto the flood plain. The momentum or energy transfer produces a lower mean velocity in the main channel and an increased velocity in the flood plain.

For turbulent flows the boundary shear stress is proportional to the velocity squared ($\tau \propto V^2$) as a first approximation, and thus a reduction or increase of velocity will be reflected in a subsequent reduction or increase in boundary shear stress. Thus for this type of flow, $\tau_{f'}/\tau_f > 1$ and $\tau_{c'}/\tau_c < 1$, where $\tau_{c'}$ and $\tau_{f'}$ are the mean shear stresses in the channel and flood plain during overbank flow. τ_c and τ_f are the expected shear stresses in the channel and flood plain assuming a vertical wall at the channel/flood plain interface. Hence it is clear

that the velocity difference is the root cause of any boundary shear redistribution.

The question remains as to which parameters influence the velocity gradient and hence the redistribution of shear, and which parameters determine the effect of momentum transfer on the flow regimes in the main channel and flood plain.

Certainly the major parameter is the velocity difference between the channel and the flood plain, where this may be characterised by the relative depth Yf/Yc, and the relative roughness term n_f/n_c, although the latter was not a subject of this investigation. As the relative depth decreases towards zero the intensity of the interaction increases, although it should be noted that the degree of momentum transfer is really the product of the intensity of the interaction and the flood plain depth Yf. Thus there is likely to be a relative depth where the degree of momentum transfer is maximised, and hence the term $\tau c'/\tau c$ mimimised.

The parameters describing the effect of the interaction are generally geometric in nature and characterised by the bankfull depth h, main channel width Bc, flood plain width Bf and the longitudinal bed slope S.

The bankfull depth may be influential in determining the extent of spreading of the turbulent shear layer into the channel and flood plain. The main channel may be influential in the sense that once an interaction has been set up, the shear defect will spread a certain distance into the main channel. As Bc is increased, the effect of the interaction becomes relatively less and less.

A similar argument can be applied to the influence of the flood plain width Bf. The shear layer will spread a certain distance into the flood plain, governed mainly by the relative depth. If the flood plain width is extented beyond this distance, the effect on the main channel will be negligible as the velocity distribution near the main channel is not affected.

The other question raised concerns the link between the lateral velocity profiles and the shear stress profiles presented in this chapter. An "Order of magnitude" correlation can be attempted based on Equation (5.13), describing the link between the mean boundary shear stress and the mean velocity :

$$\tau = \frac{\rho \lambda}{8} V^2 \qquad (5.13)$$

Thus the lateral distribution of boundary shear stress from the main channel to the flood plain could be given by :

$$\frac{d\tau}{dz} = \frac{\rho\lambda}{8} \cdot \frac{d(V^2)}{dz} \qquad (5.14)$$

Representative values for the term $\frac{d(V^2)}{dz}$ could be given by the velocities in the channel and flood plain Vc' and Vf'.

Hence

$$\frac{d(V^2)}{dz} \doteq \frac{(V_c^2) - (V_f^2)}{dz} \qquad (5.15)$$

giving

$$\frac{d\tau}{dz} \doteq \frac{\rho\lambda}{8} \frac{(V_c' - V_f')(V_c' + V_f')}{dz} \qquad (5.16)$$

or (5.17)

A typical value of λ is 0.02, and the experimental values in Chapter 4 suggest that (Vc'+Vf') generally lies between 0.3 and 1.0.

Thus

$$\frac{d\tau}{dz} \approx 0{\cdot}75 \rightarrow 2{\cdot}5 \frac{dV}{dz} \qquad (5.18)$$

where dV is a representative velocity difference given by Vc'-Vf'. Equation (5.18) indicates that the lateral gradient for shear stress should be of the same order or greater than the lateral velocity gradients in Chapter 4, and also that similar geometric and relative depth terms should affect the interaction mechanism.

5.3.3.1 The effect of varying the relative depth.

An analysis of the results shows that the influence of the relative depth term Yf/Yc is similar for each of the 16 geometries tested. In the interests of brevity, a representative geometry has been chosen, namely geometry G(0), where Bc=0.2 m, Bf=0.6 m and h=0.152 m. To surmount the problem of varying bed slopes, the results are plotted in a non-dimensional form either as $\tau_{c'}/\tau_{mean}$, or $\tau_{c'}/\tau_{c}$ where τ_{mean} is the average shear stress for the whole cross section. Similar considerations apply to the flood plain shear. Fig 5.6 shows the relationship between the shear stress ratio $\tau_{c'}/\tau_{c}$ and the relative depth Yf/Yc. Several points are worthy of note :

(i) The effect of the interaction decreases rapidly as the relative depth increases.

(ii) The interaction has a maximum effect in the main channel at a given relative depth (in this case 0.15). This depth is also the depth at which maximum momentum transfer occurs.

(iii) The interaction effect on the flood plain does not exhibit any maximum point. This can be explained by the fact that although the degree of momentum transfer decreases with Yf/Yc>0.15, the effect $\tau_{f'}/\tau_{f}$ continues to increase at relative depths less than 0.15 because it is operating on a smaller body of fluid (or area). This is not the case for the main channel where the area of flow

remains much more constant for small variations of relative depth.

An alternative method of looking at the effect of relative depth on the redistribution of boundary shear is the plot of the non-dimensional lateral shear distribution shown on Fig 5.7 for Test runs 45, 39, 43 and 40. This graph illustrates clearly the relationship between the lateral shear stress gradient and the depth of flow. Increasing the relative depth has the effect of decreasing the mean lateral gradient which is not totally surprising since the velocity difference is also decreasing. A point of note concerns the case when Yf/Yc=0.273, where the average flood plain shear is greater than the average main channel shear. This is surprising in view of the fact that the flood plain velocity is still slightly less than the main channel velocity. Overall, it can be seen that the variation in lateral shear stress gradient with relative depth, takes a very similar form to the variation of $\tau_{f'}/\tau_f$ with relative depth as shown on Fig 5.6.

One final comment concerns the comparison of lateral shear stress gradients and the lateral velocity gradients (Chapter 4) for the same geometric cross section and relative depths of flow. The lateral velocity gradients for geometry G are shown on Fig 5.8. Comparison of Fig 5.8 and Fig 5.7 shows that the order of magnitude of the gradients is the

same with a tendency to give a larger gradient for the shear distribution at low relative depths, and a larger velocity gradient for the higher relative depths.

5.3.3.2 The effect of the bankfull depth.

It is necessary to maintain a constant relative depth, channel width and flood plain width before any appraisal can be made concerning the effect of the bankfull depth on the lateral shear stress distribution across the channel and flood plain widths. Obviously a number of runs can be compared. However, in the interests of brevity, only three geometries will be discussed, although similar trends can be observed in other tests.

Consider geometries B, L and P. All three cross sections have a constant Bc and Bf of 0.2 m and 0.4 m repectively. To be more precise, now consider Runs 29, 46 and 99. All three Runs have a relative depth of Yf/Yc=0.23. Thus the only variable for these runs is the bankfull depth which varies from 0.05 m to 0.15 m. Fig 5.9 shows the lateral shear distribution across the channel and flood plain where τ_{mean} is the average shear stress across the full cross section. It is clear that for higher bankfull depths a shallower gradient exists across the channel/flood plain interface. As the bankfull depth decreases, the shear gradient increases, indicating that at lower

bankfull depths, the momentum transfer mechanism is stronger. It is not clear whether this is strictly correct since for a given Yf/Yc, the flood plain depth decreases with decreasing bankfull depth, resulting an increased velocity difference. It is difficult to demonstrate the effects of h since h is inherent in the relative depth term. i.e :

$$\frac{Yf}{Yc} = \frac{Yf}{(Yf+h)} \qquad (5.19)$$

5.3.3.3 The effect of the main channel width.

If the relative depth Yf/Yc, the flood plain width and the bankfull depth can be held constant, then the effect of the channel width on the lateral shear gradient can be assessed. Due to difficulty in operating the experimental flume, only one geometry was investigated with a channel width of Bc=0.6 m. Therefore it is necessary to consider Geometries M(%:Bf=0.2m: Bc=0.2m: h=0.1m), S($:Bf=0.2m: Bc=0.4m: h=0.1m) and E(@:Bf=0.2m: Bc=0.6m: h=0.1m). Fig 5.10 shows the effect of the channel width on the lateral shear stress gradient for these geometries. To be more accurate, the term $\frac{\tau_c' - \tau_f'}{\tau_{mean}}$ used in the graph can be regarded as a measure of the shear gradient across the channel/flood plain interface, and hence gives an indication of the amount of momentum transfer between the two flows. One obvious fact from Fig 5.10 is that the interaction mechanism

clearly reduces as the relative depth increases for all the geometries. This has been observed in an earlier section. Of importance is that as the channel width increases from 0.2 m to 0.4 m for a given relative depth, the lateral shear gradient is reduced. The behaviour of the shear gradient at further increases in channel width is not clear as can be seen from Geometry E where Bc=0.6 m. It is fair to note, however, that the shear gradient does not continue to decrease as larger channel widths are approached. One reasonable argument for this might be due to the interaction mechanism reaching a maximum spreading distance into the main channel with channel widths greater than this distance having little effect on the interaction mechanism.

5.3.3.4 The effect of the flood plain width.

First, to give three different values of Bf, a channel width of Bc=0.2 m must be considered in this particular section. It is possible to compare results for all three bankfull depths, but in the interests of brevity, a bankfull depth of 0.1 m will only be considered. For geometries M, P and H, the channel width is 0.2 m and the bankfull depth is 0.1 m. Bf varies between 0.2 m and 0.6 m. Fig 5.11 presents these three geometries with reference to the amount of shear redistribution occurring in both the channel and flood plain.

Generally, as the flood plain increases, a greater reduction in shear occurs in the channel with a corresponding increase in shear in the flood plain. This is in broad agreement with the findings of Chapter 4 where Fig 4.12 clearly showed a similar trend when the mean channel and flood plain velocities are considered.

Again there is a particular relative depth at which the shear stress ratio $\tau_{c'}/\tau_c$ is a minimum, and hence the interaction mechanism is a maximum. This is because the interaction mechanism is a product of the turbulent intensity and the area over which it acts, namely the flood plain depth. Also apparent is that the depth at which this mechanism is greatest can also vary with the geometrical parameters, although it is not clear how this depth varies at this stage.

5.3.3.5 The effect of Bc/h and Bf/h.

Clearly there is a complex realtionship between the geometrical parameters and the shear redistribution which occurs during overbank flow. An interesting relationship was developed in Chapter 4 when the minimum channel shear stress ratio for each cross section was considered along with the ratios Bf/h and Bc/h. As found in Chapter 4, it was necessary to separate the channel and flood plain width terms since any relationship which solely used the ratio Bf/Bc would obscure the

effects of the bankfull depth term. In this section, the minimum shear stress ratios $\tau c'/\tau c$ for each geometry have been considered and an interesting relationship developed.

Considering Fig 5.12, the most important observation is that when Bf/h increases beyond approximately 10, further increases in the flood plain width have negligble effect on the shear stress redistribution in the main channel. This is in keeping with the work of Rajaratnam and Ahmadi(Ref 48). The correlation with Bf/h is of the form :

$$1 - \left[\frac{\tau_c'}{\tau_c}\right]_{min} = (1 - e^{-0.5\,B_f/h}) \quad f(\frac{h}{B_c}) \qquad (5.20)$$

The other observation is the decreasing interaction effect as Bc/h increases. This is also to be expected, since as the main channel width increases, then the effect of the interaction becomes relatively less and less. The function which will describe the effect of Bc/h can be attained by considering a value of Bf/h where the term$(1 - e^{-0.5\frac{B_f}{h}})$ =1, namely Bf/h=12. The small graph on Fig 5.12 shows the values of Bc/h attained and the final relationship can be given as :

$$1 - \left[\frac{\tau_c}{\tau_c}\right]_{min} = 0.3\,(\frac{h}{Bc})^{0.33}\,(1 - e^{-0.5\frac{B_f}{h}}) \qquad (5.21)$$

Equation (5.21) is a tentative proposal which will give the expected maximum shear defect to occur in the channel for a given

channel and flood plain geometry. It must be remembered that such a equation only applies to channels where smooth channel laws are relevant. It should be noted that the dashed lines shown on Fig. 5.12 are simply the author's interpretation based on the above reasoning and the spread of experimental data.

5.3.4 Friction factor results for overbank flow.

Having measured both the shear stress and point velocities throughout the compound channel, it is possible to produce a series of friction factor - Reynolds number diagrams (λ-Re) for the cases of the main channel alone during the interaction, similarly the flood plain, and finally the entire channel/flood plain cross section.

Thus for each experimental result it is possible to calculate a friction factor and Reynolds number based on measured velocities :

$$\lambda_c = \frac{8 g R_c S}{V_c'^2} \qquad (5.22)$$

$$\lambda_f = \frac{8 g R_f S}{V_f'^2} \qquad (5.23)$$

$$\lambda_t = \frac{8 g R_t S}{V_t} \qquad (5.24)$$

$$Re_c = \frac{4 V_c' R_c}{\nu} \qquad (5.25)$$

$$Re_f = \frac{4\ V_f' R_f}{\nu} \qquad (5.26)$$

and

$$Re_t = \frac{4\ V_t R_t}{\nu} \qquad (5.27)$$

where Vc', Vf' and V_t are the measured values of mean velocity in the channel, flood plain and total cross section respectively.

5.3.4.1 The main channel alone.

This result is shown in Fig 5.13 where the experimental points are compared with the smooth channel equation, namely :

$$\frac{1}{\sqrt{\lambda_c}} = 2{\cdot}0 \log(Re\sqrt{\lambda_c}) - 1{\cdot}3 \qquad (5.28)$$

Fig 5.13 shows that the effective friction factor for the main channel alone during interaction is increased above the non-overbank flow case by a factor varying between 0% -32%. This is in fact in line with the proposition that $\tau_{c'} \propto (Vc')^2$ as substitution in Equation (5.22) shows that $\lambda_c' \propto \frac{1}{\tau_c'}$ or :

$$\frac{\lambda_c'}{\lambda_c} = \frac{\tau_c}{\tau_c'} \qquad (5.29)$$

The minimum value of $\tau_{c'}/\tau_c$ is in the region of 0.75, giving a maximum value of $\lambda_{c'}/\lambda_c = 1{\cdot}32$.

5.3.4.2 The flood plain.

Fig 5.14 shows that the effective friction factor for the flood plain during interaction is greatly reduced from the case of isolated flow. Using a similar argument to the previous section, this probably reflects the value of $\frac{\tau'_f}{\tau_f} \propto \frac{\lambda_f}{\lambda'_f}$, with experimental values of $\tau_f/\tau_{f'}$ being as low as 1/3, which again is of the same order as the reduction in $\frac{\lambda'_f}{\lambda_f}$.

5.3.4.3 The whole cross section.

Fig 5.15 shows the friction factor - Reynolds number relationship for the whole cross section, indicating a considerable spread in the results. Clearly there is no simple relationship between Re_t and λ_t . The amount of momentum transfer occurring for different channel and flood plain geometries is obviously obscuring the relationship, and confirms again the need to establish the geometrical and flow parameters before attempting to determine the appropriate resistance to flow for a channel during overbank flow.

A final point of interest from these particular set of results involves the relationship between the measured values of shear stress and velocity for all geometries. The classical equation for turbulent flows links the two in the form :

$$\tau = \frac{\lambda \rho}{8} V^2 \qquad (5.29)$$

where τ is the mean shear stress and V is the mean velocity. The question remains as to whether this relationship applies to overbank flow conditions. Fig 5.16 shows this relationship between $\tau_{c'}$ and Vc' for the main channel alone, with the assumption that fully developed flow was always occurring. Clearly a squared relationship can be observed, indicating that Equation (5.29) is still perfectly valid for overbank flow conditions in the channel.

5.3.5 Conclusions.

Clearly there is exists a strong relationship between the velocities recorded and presented in Chapter 4 and the shear stress measurements discussed in this Chapter. It follows then that similar conclusions exist for the shear stress results.

Generally, during channel/flood plain interaction, the shear stresses in the channel are reduced with a corresponding increase in boundary shear stresses in the flood plain. The extent of this redistribution is dependent on the geometrical and flow parameters of the compound channel. As the relative depth increases the interaction mechanism is reduced.

However, there is a depth at which maximum redistribution of shear occurs. Also apparent is the increase in interaction with increases of Bf/h and h/Bc. However, there are values of Bf/h and h/Bc beyond which further increases have very little effect on the turbulent shear mechanism.

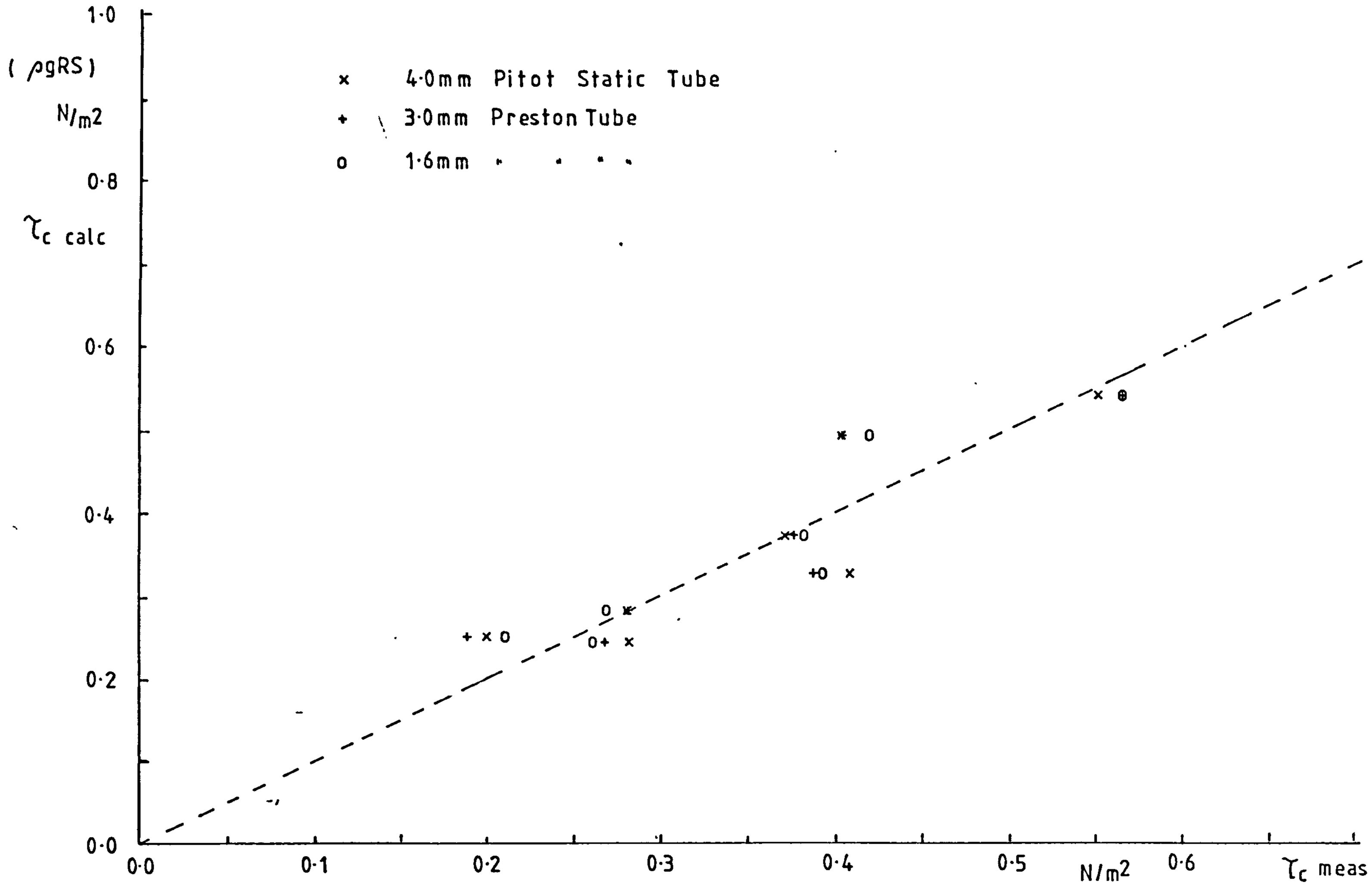

Fig 5·1 Comparison of Calculated Shear and Measured Shear.

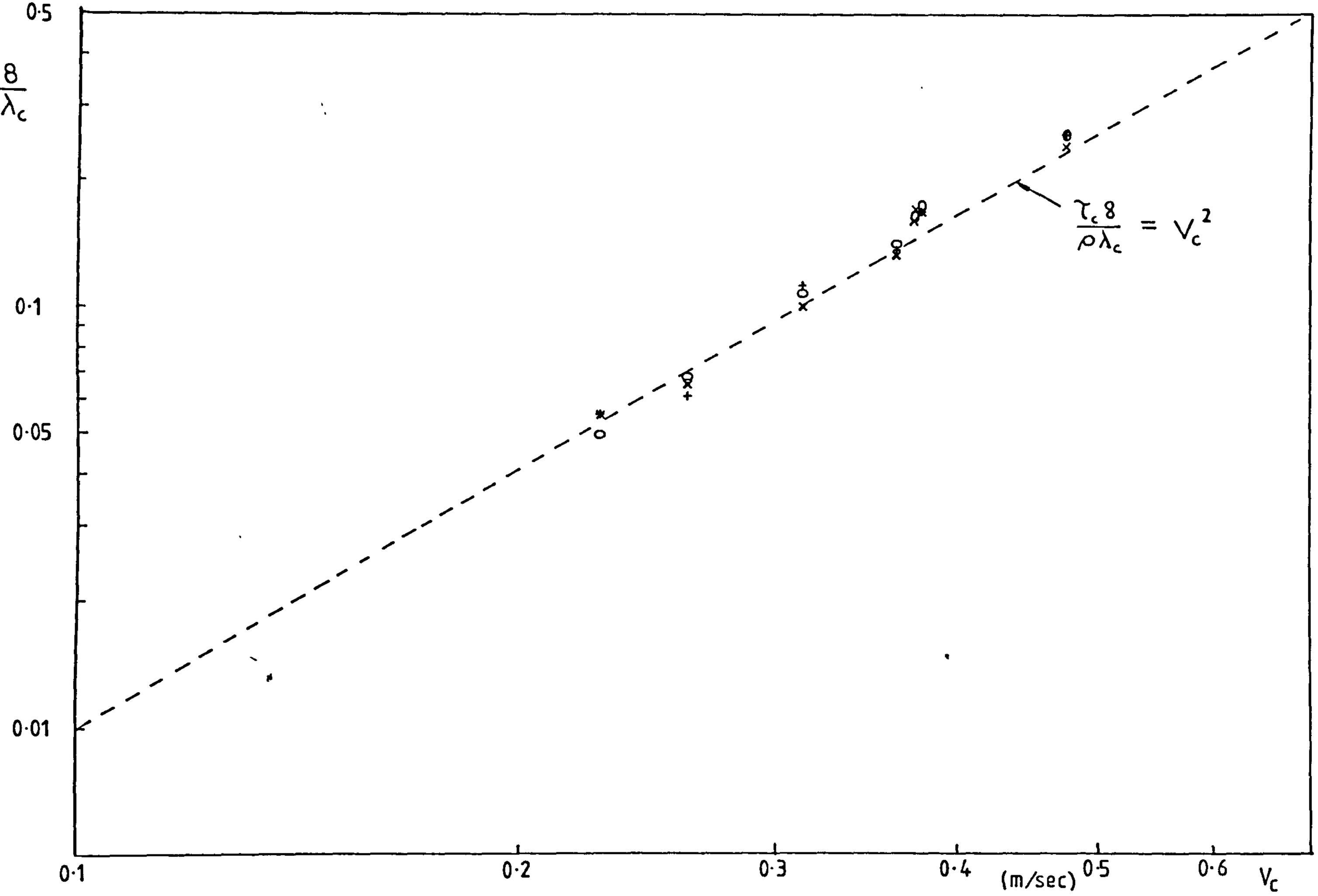

Fig 5·2 Comparison of measured Shear and Velocity in Channel.

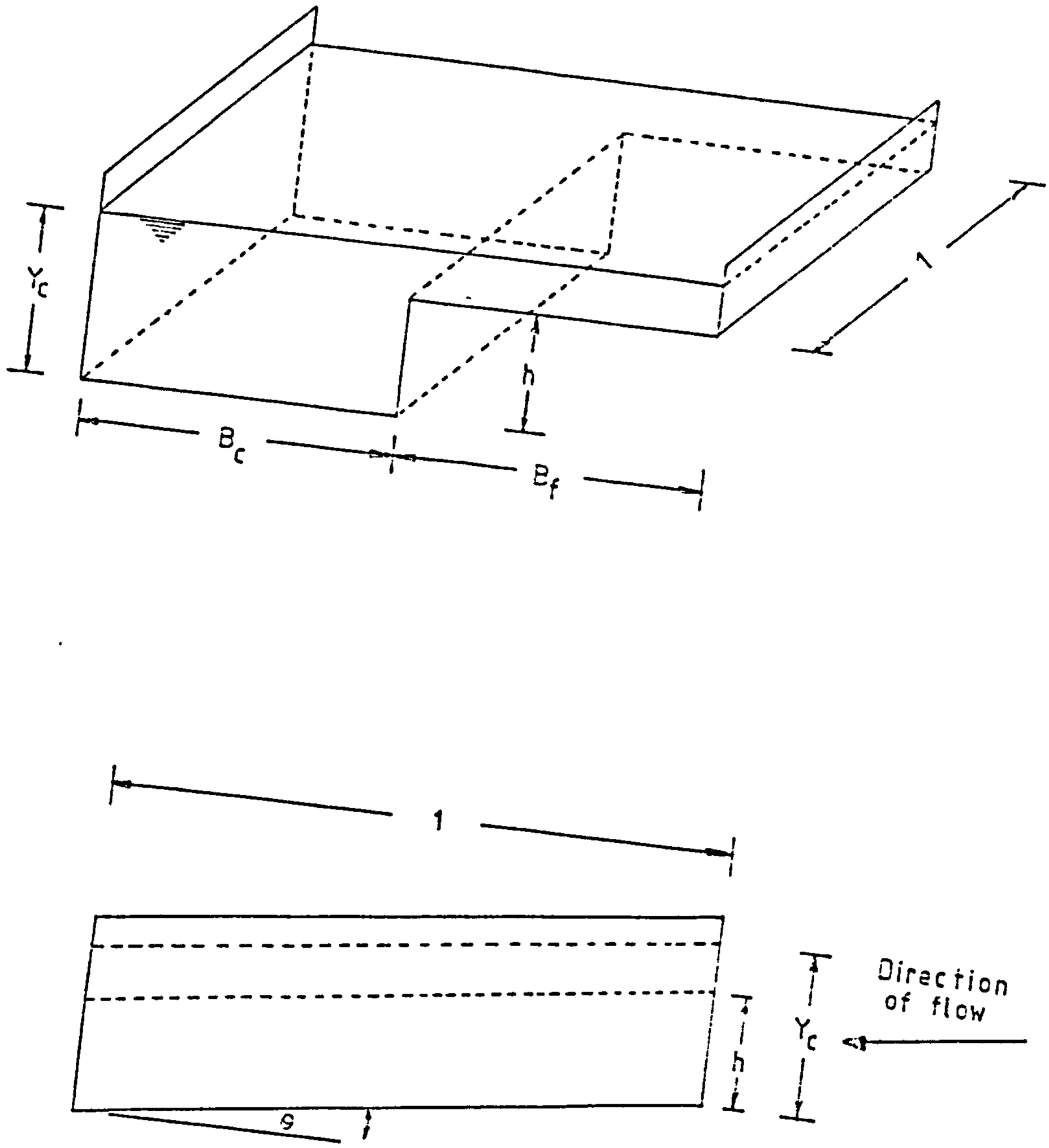

Fig 5·3 Element of flow in Compound Channel.

Test	Run	Yc (m)	Bc (m)	Bf (m)	h (m)	τ_c' (N/m^2)	τ_f' (N/m^2)
K1	1	0.1340	0.400	0.400	0.102	0.708	0.571
K2	2	0.1260	0.400	0.400	0.102	0.651	0.486
K3	3	0.1200	0.400	0.400	0.102	0.598	0.371
K4	4	0.1150	0.400	0.400	0.102	0.501	0.273
K5	5	0.1480	0.400	0.400	0.102	0.490	0.439
K6	6	0.1320	0.400	0.400	0.102	0.294	0.249
K7	7	0.1200	0.400	0.400	0.102	0.211	0.103
K8	8	0.1510	0.400	0.400	0.102	0.336	0.345
K9	9	0.1300	0.400	0.400	0.102	0.288	0.194
K10	10	0.1210	0.400	0.400	0.102	0.219	0.114
A12	11	0.1470	0.400	0.400	0.052	0.346	0.374
A5	12	0.1110	0.400	0.400	0.052	0.090	0.080
A6	13	0.0920	0.400	0.400	0.052	0.627	0.563
A7	14	0.1000	0.400	0.400	0.052	0.613	0.595
A8	15	0.0800	0.400	0.400	0.052	0.424	0.320
A9	16	0.0830	0.400	0.400	0.052	0.272	0.215
A10	17	0.1250	0.400	0.400	0.052	0.463	0.514
A11	18	0.0750	0.400	0.400	0.052	0.196	0.088
A1	19	0.1030	0.395	0.400	0.052	0.408	0.443
A2	20	0.0810	0.395	0.400	0.052	0.273	0.243
A3	21	0.0700	0.395	0.400	0.052	0.249	0.164
A4	22	0.0960	0.395	0.400	0.052	0.277	0.274

Table 5·1

Test	Run	Yc (m)	Bc (m)	Bf (m)	h (m)	τ_c' (N/m^2)	τ_f' (N/m^2)
B1	23	0.1050	0.185	0.404	0.052	0.259	0.294
B2	24	0.0925	0.185	0.404	0.052	0.281	0.296
B3	25	0.0765	0.185	0.404	0.052	0.209	0.169
B4	26	0.0710	0.185	0.404	0.052	0.197	0.144
B5	27	0.1020	0.185	0.400	0.053	0.244	0.244
B6	28	0.0790	0.185	0.400	0.053	0.198	0.178
B7	29	0.0685	0.185	0.400	0.053	0.112	0.082
B8	30	0.1240	0.185	0.400	0.053	0.249	0.279
C1	31	0.0700	0.395	0.200	0.052	0.325	0.170
C2	32	0.0960	0.395	0.200	0.052	0.347	0.317
C4	33	0.0850	0.395	0.200	0.052	0.374	0.314
C5	34	0.0860	0.392	0.193	0.052	0.215	0.140
C6	35	0.0640	0.392	0.193	0.052	0.205	0.090
C7	36	0.1010	0.392	0.193	0.052	0.378	0.373
C8	37	0.0725	0.392	0.193	0.052	0.137	0.012
G1	38	0.1700	0.192	0.607	0.152	0.616	0.350
G2	39	0.1740	0.192	0.607	0.152	0.799	0.619
G3	40	0.2090	0.192	0.607	0.152	0.394	0.419
G4	41	0.1880	0.192	0.607	0.152	0.431	0.366
G5	42	0.1760	0.192	0.603	0.152	0.205	0.155

Table 5·1

Test	Run	Yc (m)	Bc (m)	Bf (m)	h (m)	τ_c' (N/m^2)	τ_f' (N/m^2)
G6	43	0.1860	0.192	0.603	0.152	0.241	0.226
G7	44	0.1980	0.192	0.603	0.152	0.263	0.268
G8	45	0.1635	0.192	0.603	0.152	0.135	0.065
L1	46	0.1970	0.190	0.397	0.152	0.467	0.482
L2	47	0.1800	0.190	0.397	0.152	0.403	0.318
L3	48	0.1695	0.190	0.397	0.152	0.465	0.265
L4	49	0.1890	0.190	0.397	0.152	0.526	0.511
L5	50	0.1845	0.190	0.397	0.152	0.313	0.243
L6	51	0.1790	0.190	0.397	0.152	0.307	0.242
L7	52	0.1750	0.190	0.397	0.152	0.257	0.187
L8	53	0.1690	0.190	0.397	0.152	0.234	0.134
N1	54	0.1950	0.191	0.213	0.152	0.553	0.503
N2	55	0.1830	0.191	0.213	0.152	0.473	0.368
N3	56	0.1990	0.191	0.213	0.152	0.580	0.525
N4	57	0.1685	0.191	0.213	0.152	0.534	0.309
N5	58	0.1685	0.191	0.211	0.152	0.243	0.173
N6	59	0.1790	0.191	0.211	0.152	0.374	0.289
N7	60	0.1740	0.191	0.211	0.152	0.307	0.252
N8	61	0.1930	0.191	0.211	0.152	0.337	0.292

Table 5·1

Test	Run	Yc (m)	Bc (m)	Bf (m)	h (m)	τ_c' (N/m^2)	τ_f' (N/m^2)
J1	62	0.1870	0.390	0.404	0.152	0.409	0.304
J2	63	0.1720	0.390	0.404	0.152	0.488	0.233
J3	64	0.1720	0.390	0.404	0.152	0.564	0.294
J4	65	0.1600	0.390	0.404	0.152	0.562	0.252
J5	66	0.1780	0.390	0.404	0.152	0.514	0.369
J6	67	0.1840	0.390	0.404	0.152	0.581	0.451
J7	68	0.1560	0.390	0.404	0.152	0.394	0.144
J8	69	0.1680	0.390	0.404	0.152	0.455	0.230
J9	70	0.1660	0.390	0.404	0.152	0.402	0.162
R1	71	0.1555	0.390	0.200	0.152	0.406	0.131
R2	72	0.1660	0.390	0.200	0.152	0.459	0.239
R3	73	0.1730	0.390	0.200	0.153	0.487	0.307
R4	74	0.1755	0.390	0.200	0.153	0.501	0.321
R5	75	0.1795	0.390	0.200	0.153	0.514	0.339
R6	76	0.1850	0.390	0.200	0.153	0.523	0.388
R7	77	0.1920	0.390	0.200	0.153	0.524	0.429
R8	78	0.2010	0.390	0.200	0.153	0.504	0.419
MYERS	79	0.1684	0.254	0.356	0.102	0.183	0.181
MYERS	80	0.1638	0.254	0.356	0.102	0.177	0.175
MYERS	81	0.1583	0.254	0.356	0.102	0.170	0.167
MYERS	82	0.1534	0.254	0.356	0.102	0.165	0.158

Table 5·1

Test	Run	Yc (m)	Bc (m)	Bf (m)	h (m)	τ_c' (N/m^2)	τ_f' (N/m^2)
MYERS	83	0.1467	0.254	0.356	0.102	0.153	0.152
MYERS	84	0.1400	0.254	0.356	0.102	0.145	0.140
MYERS	85	0.1333	0.254	0.356	0.102	0.140	0.125
MYERS	86	0.1275	0.254	0.356	0.102	0.133	0.114
MYERS	87	0.1183	0.254	0.356	0.102	0.126	0.089
MYERS	88	0.1116	0.254	0.356	0.102	0.129	0.060
RAJAR	89	0.1128	0.711	0.508	0.098	0.314	0.068
RAJAR	90	0.1228	0.711	0.508	0.098	0.324	0.125
RAJAR	91	0.1445	0.711	0.508	0.098	0.351	0.244
RAJAR	92	0.1814	0.711	0.508	0.098	0.352	0.255
RAJAR	93	0.1085	0.711	0.508	0.098	0.287	0.087
P1	94	0.1220	0.193	0.396	0.101	0.303	0.203
P2	95	0.1230	0.193	0.396	0.101	0.411	0.346
P3	96	0.1280	0.193	0.396	0.101	0.274	0.204
P4	97	0.1350	0.193	0.396	0.101	0.402	0.352
P5	98	0.1440	0.193	0.396	0.101	0.438	0.408
P6	99	0.1320	0.193	0.396	0.101	0.456	0.376
P7	100	0.1080	0.193	0.396	0.101	0.449	0.174
P8	101	0.1190	0.193	0.396	0.101	0.306	0.156
P9	102	0.1250	0.193	0.396	0.101	0.221	0.146
P10	103	0.1280	0.193	0.396	0.101	0.385	0.295

Table 5·1

Test	Run	Yc (m)	Bc (m)	Bf (m)	h (m)	τ_c' (N/m^2)	τ_f' (N/m^2)
H1	104	0.1500	0.194	0.601	0.101	0.388	0.458
H2	105	0.1290	0.194	0.601	0.101	0.400	0.325
H3	106	0.1280	0.194	0.601	0.101	0.237	0.192
H4	107	0.1210	0.194	0.601	0.101	0.363	0.233
H5	108	0.1320	0.194	0.601	0.101	0.504	0.444
H6	109	0.1230	0.194	0.601	0.101	0.382	0.262
H7	110	0.1200	0.194	0.601	0.101	0.354	0.209
H8	111	0.1585	0.194	0.601	0.101	0.441	0.461
H9	112	0.1155	0.194	0.601	0.101	0.385	0.180
H10	113	0.1250	0.194	0.601	0.101	0.245	0.165
M1	114	0.1120	0.193	0.210	0.101	0.416	0.191
M2	115	0.1250	0.193	0.210	0.101	0.483	0.303
M3	116	0.1410	0.193	0.210	0.101	0.441	0.351
M4	117	0.1130	0.193	0.210	0.101	0.316	0.126
M5	118	0.1150	0.193	0.210	0.101	0.436	0.216
M6	119	0.1230	0.193	0.210	0.101	0.349	0.199
M7	120	0.1270	0.193	0.210	0.101	0.449	0.297
M8	121	0.1370	0.193	0.210	0.101	0.349	0.274
CRORY	122	0.1562	0.254	0.356	0.102	0.163	0.166

Table 5.1

Test	Run	Yc (m)	Bc (m)	Bf (m)	h (m)	$\tau_{c'}$ (N/m^2)	$\tau_{f'}$ (N/m^2)
CRORY	123	0.1467	0.254	0.356	0.102	0.149	0.142
CRORY	124	0.1329	0.254	0.356	0.102	0.138	0.124
CRORY	125	0.1280	0.254	0.356	0.102	0.135	0.111
CRORY	126	0.1183	0.254	0.356	0.102	0.128	0.085
CRORY	127	0.1410	0.203	0.356	0.102	0.128	0.132
CRORY	128	0.1321	0.203	0.356	0.102	0.119	0.117
CRORY	129	0.1233	0.203	0.356	0.102	0.114	0.095
CRORY	130	0.1100	0.203	0.356	0.102	0.105	0.059
CRORY	131	0.1550	0.153	0.356	0.102	0.134	0.189
CRORY	132	0.1467	0.153	0.356	0.102	0.125	0.124
CRORY	133	0.1333	0.153	0.356	0.102	0.107	0.104
CRORY	134	0.1634	0.102	0.356	0.102	0.149	0.130
CRORY	135	0.1467	0.102	0.356	0.102	0.109	0.103
CRORY	136	0.1333	0.102	0.356	0.102	0.092	0.083
CRORY	137	0.1187	0.102	0.356	0.102	0.074	0.060
01	138	0.0650	0.196	0.209	0.050	0.237	0.127
02	139	0.0755	0.196	0.209	0.050	0.288	0.218
03	140	0.0890	0.196	0.209	0.050	0.327	0.322
04	141	0.0985	0.196	0.209	0.050	0.437	0.417
05	142	0.0830	0.196	0.209	0.050	0.351	0.331
06	143	0.0760	0.196	0.209	0.050	0.173	0.136
07	144	0.0695	0.196	0.209	0.050	0.234	0.164
08	145	0.0610	0.196	0.209	0.050	0.342	0.159

Table 5.1

Test	Run	Yc (m)	Bc (m)	Bf (m)	h (m)	τ_c' (N/m^2)	τ_f' (N/m^2)
I1	146	0.0930	0.196	0.604	0.050	0.221	0.236
I2	147	0.0750	0.196	0.604	0.050	0.470	0.400
I3	148	0.0680	0.196	0.604	0.050	0.354	0.239
I4	149	0.0840	0.196	0.604	0.050	0.118	0.113
I5	150	0.0775	0.196	0.604	0.050	0.270	0.235
I6	151	0.0870	0.196	0.604	0.050	0.263	0.248
I7	152	0.0735	0.196	0.604	0.050	0.220	0.168
I8	153	0.0620	0.196	0.604	0.050	0.245	0.115
S1	154	0.1195	0.392	0.203	0.100	0.603	0.408
S2	155	0.1110	0.392	0.203	0.100	0.319	0.139
S3	156	0.1130	0.392	0.203	0.100	0.374	0.209
S4	157	0.1050	0.392	0.203	0.100	0.429	0.199
S5	158	0.1220	0.392	0.203	0.100	0.773	0.553
S6	159	0.1400	0.392	0.203	0.100	0.545	0.480
S7	160	0.1055	0.392	0.203	0.100	0.653	0.373
S8	161	0.1210	0.392	0.203	0.100	0.416	0.276
E1	162	0.1145	0.590	0.209	0.100	0.412	0.222
E2	163	0.1190	0.590	0.209	0.100	0.477	0.247
E3	164	0.1225	0.590	0.209	0.100	0.495	0.285

Table 5·1

Test	Run	Yc (m)	Bc (m)	Bf (m)	h (m)	τ_c' (N/m^2)	τ_f' (N/m^2)
E4	165	0.1255	0.590	0.209	0.100	0.524	0.314
E5	166	0.1060	0.590	0.209	0.100	0.493	0.263
E6	167	0.1100	0.590	0.209	0.100	0.592	0.337

Table 5·1

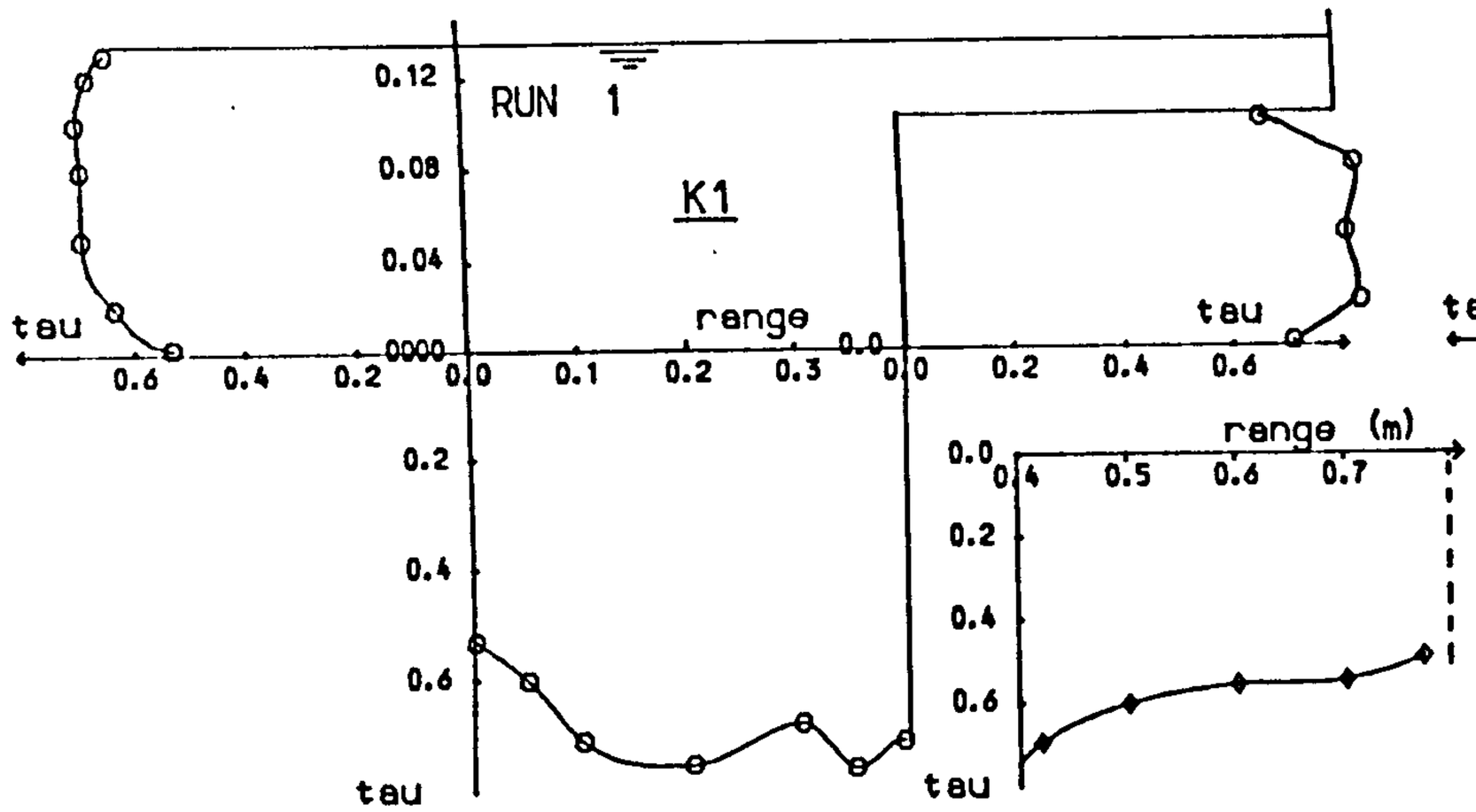

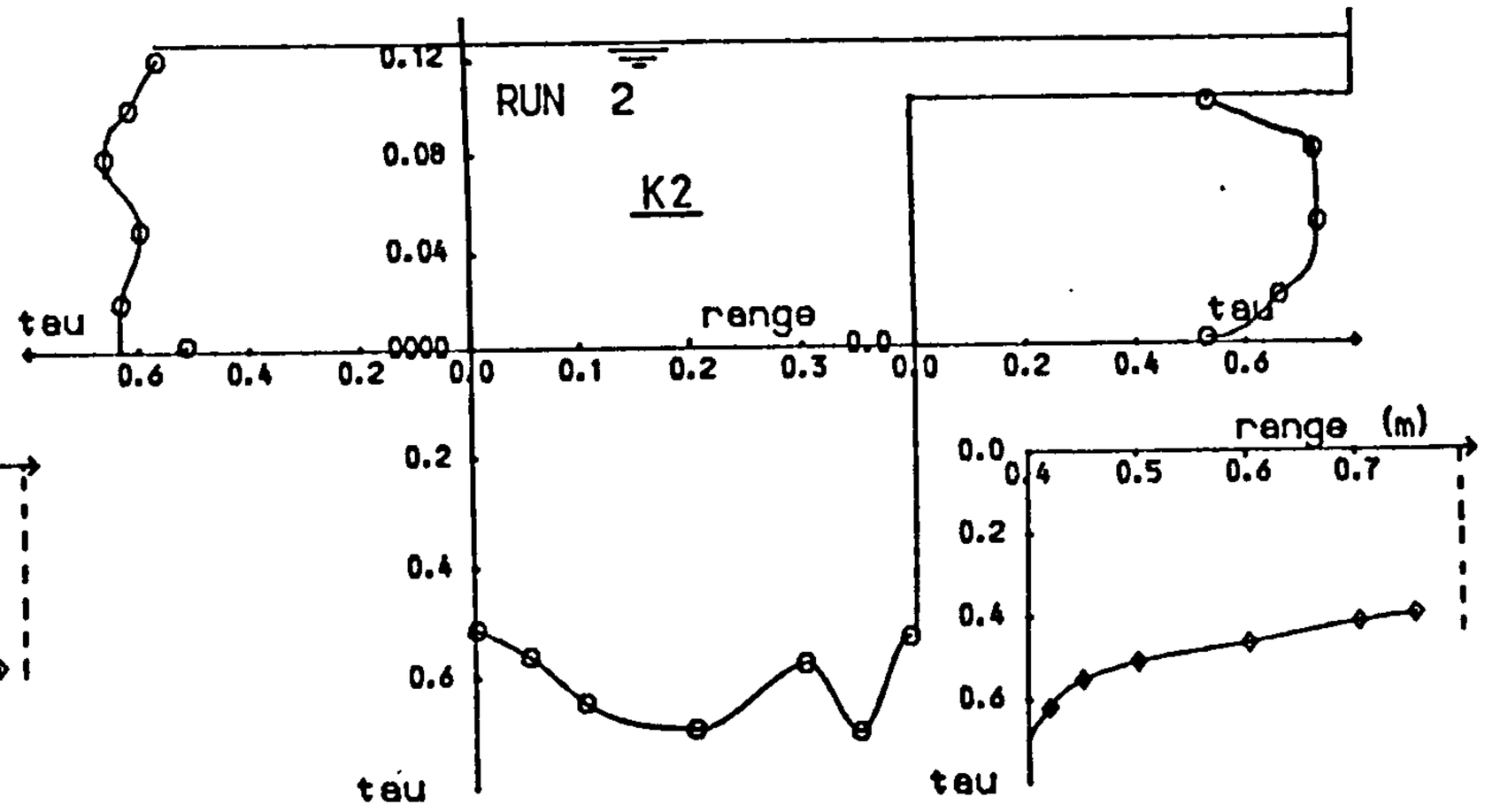

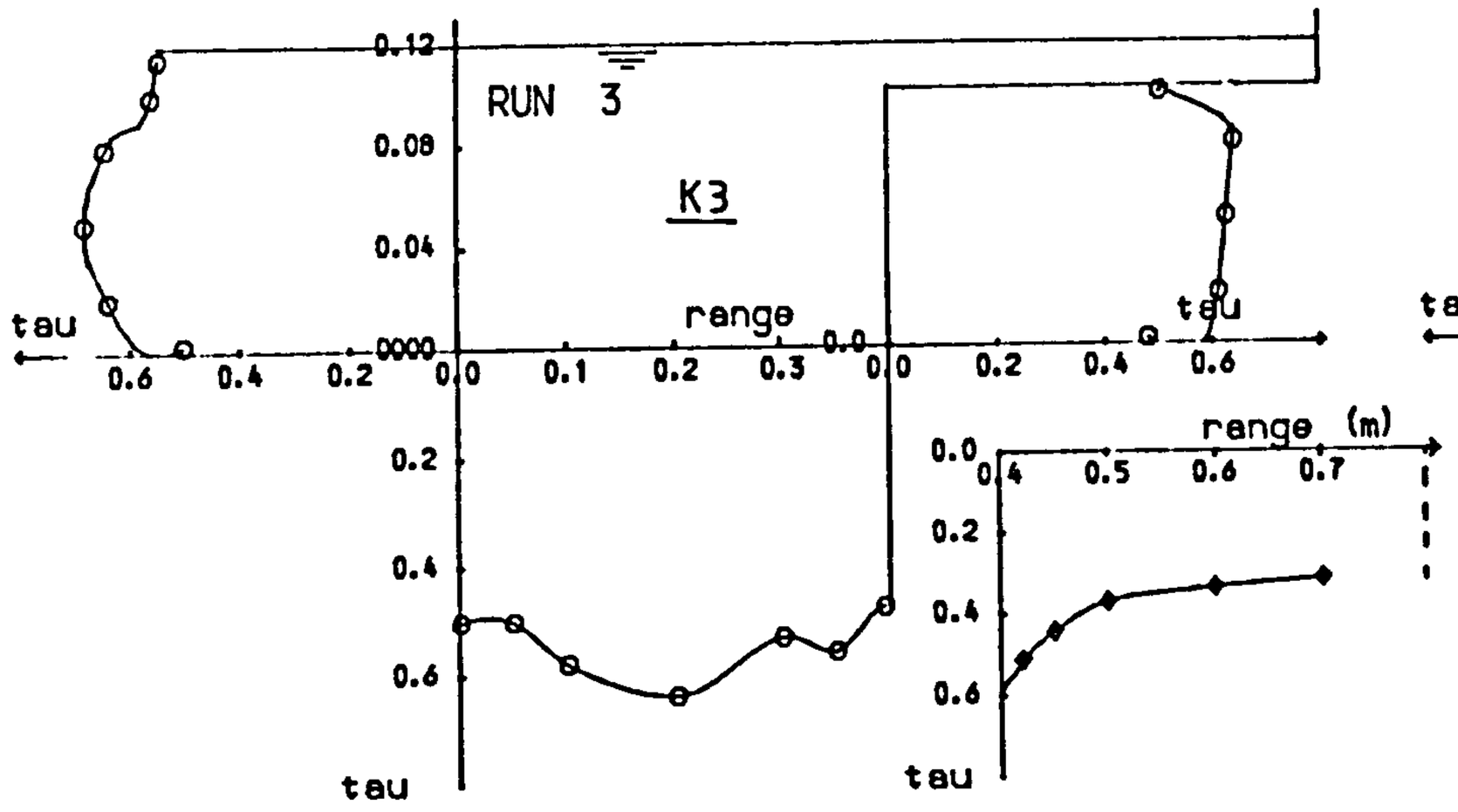

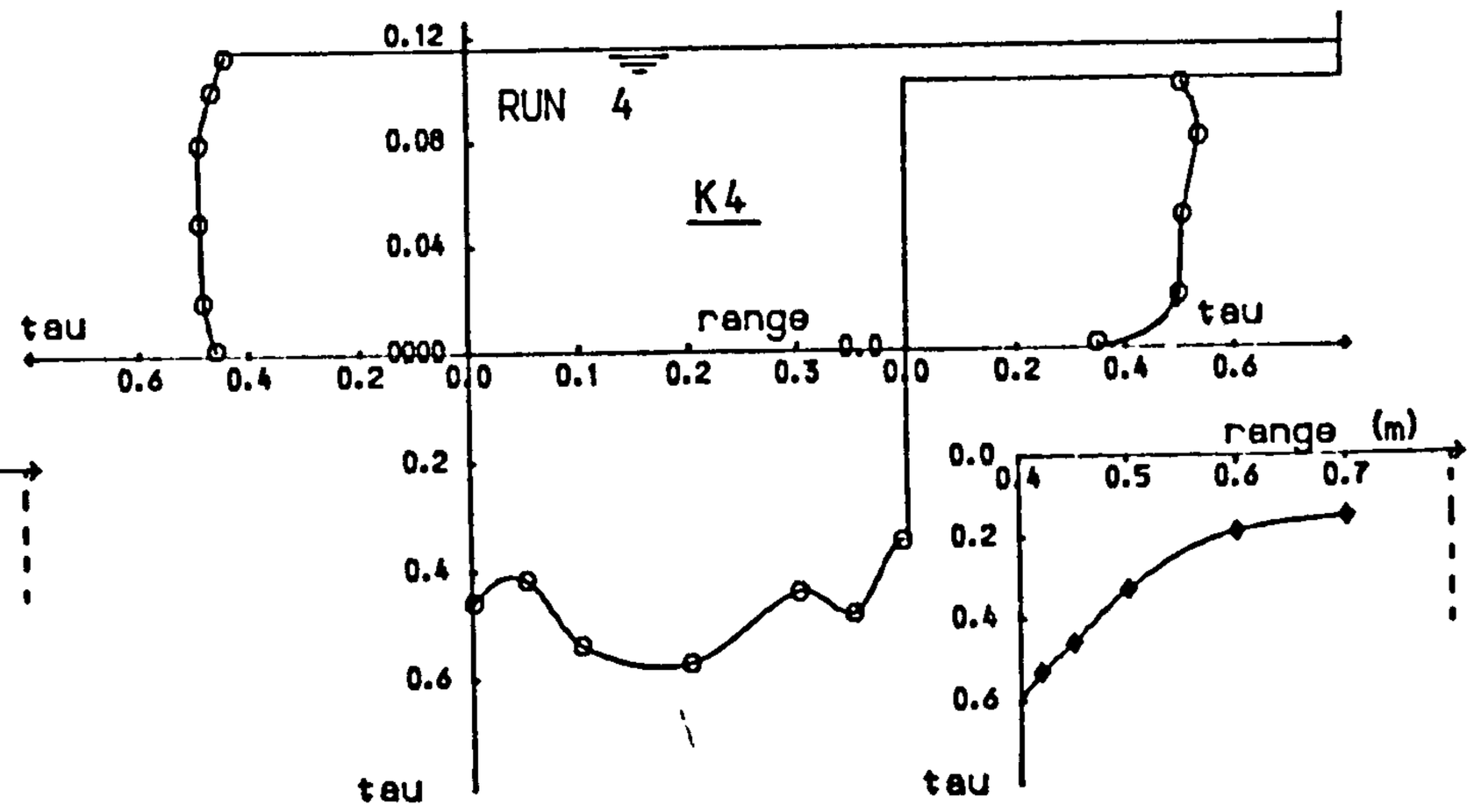

Fig 5·4 Shear stress distribution in channel and flood plain.

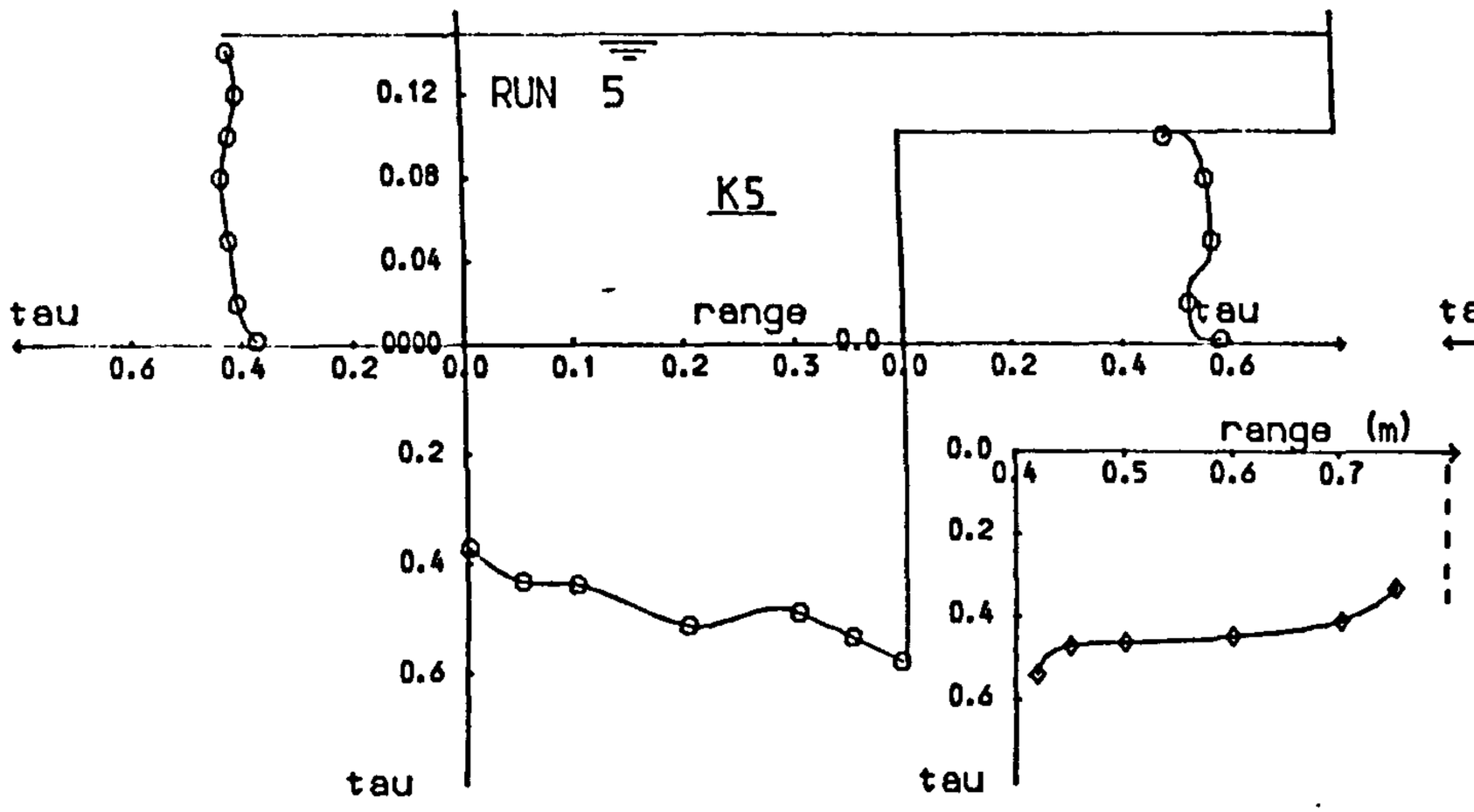

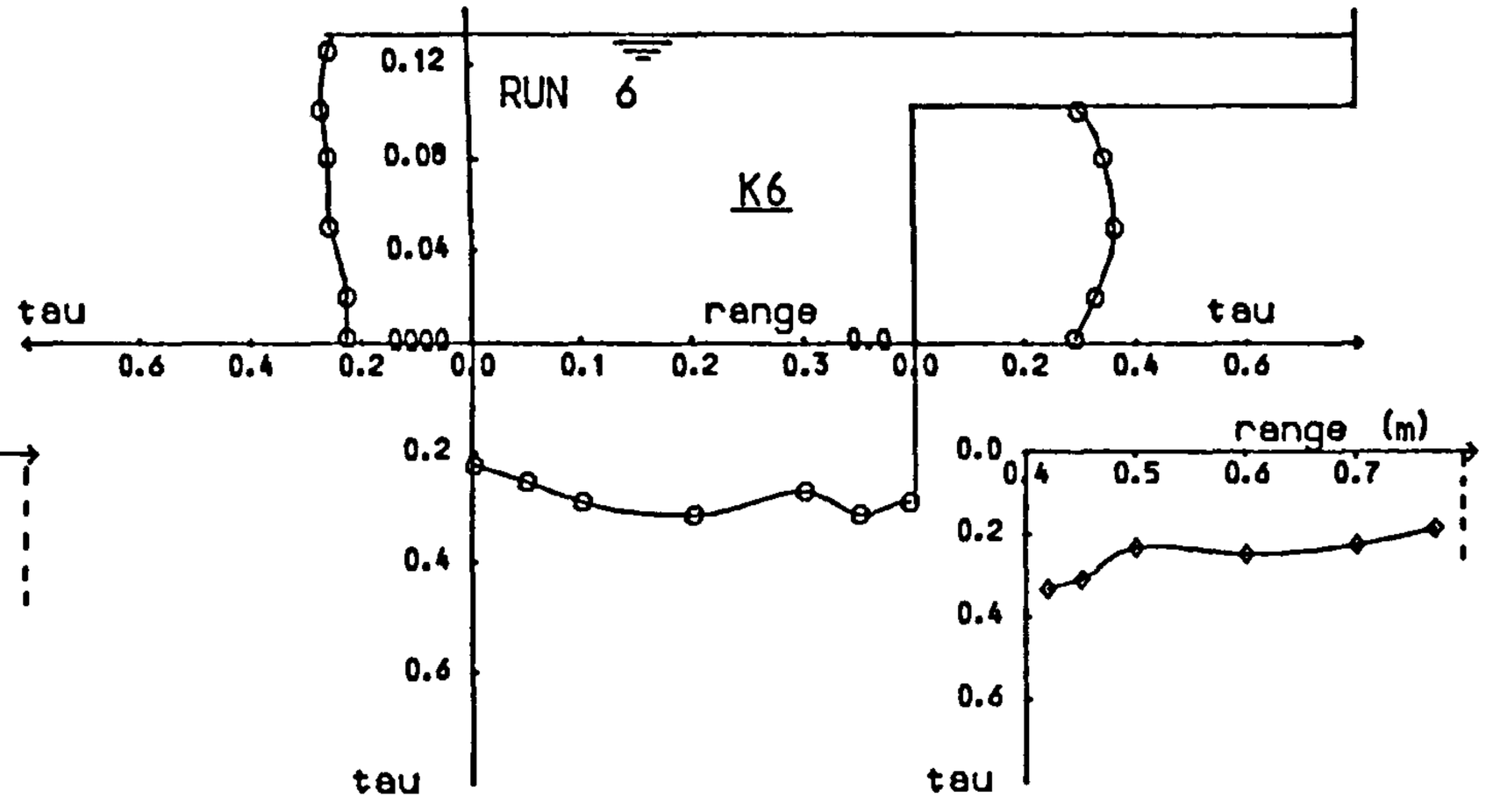

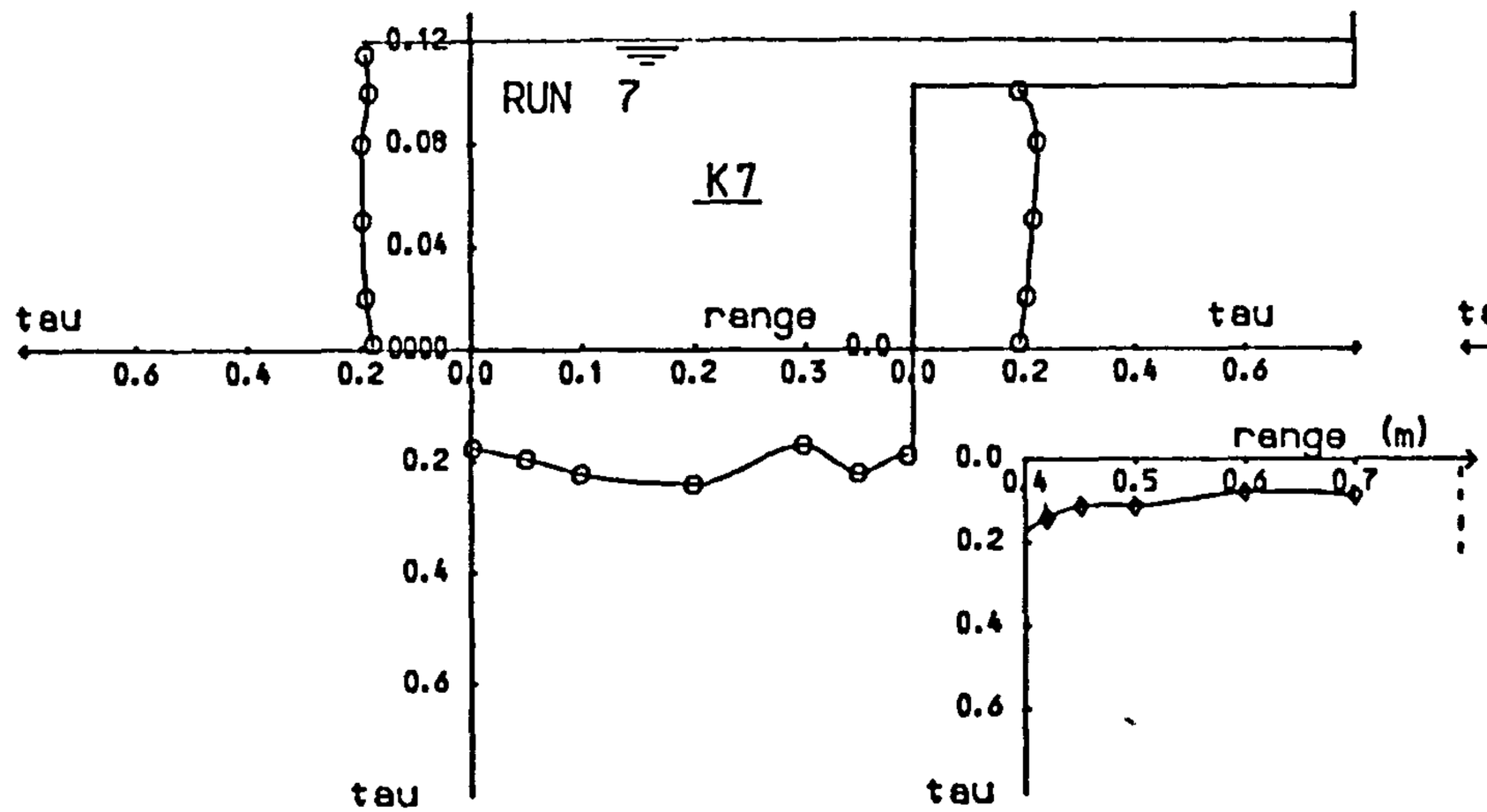

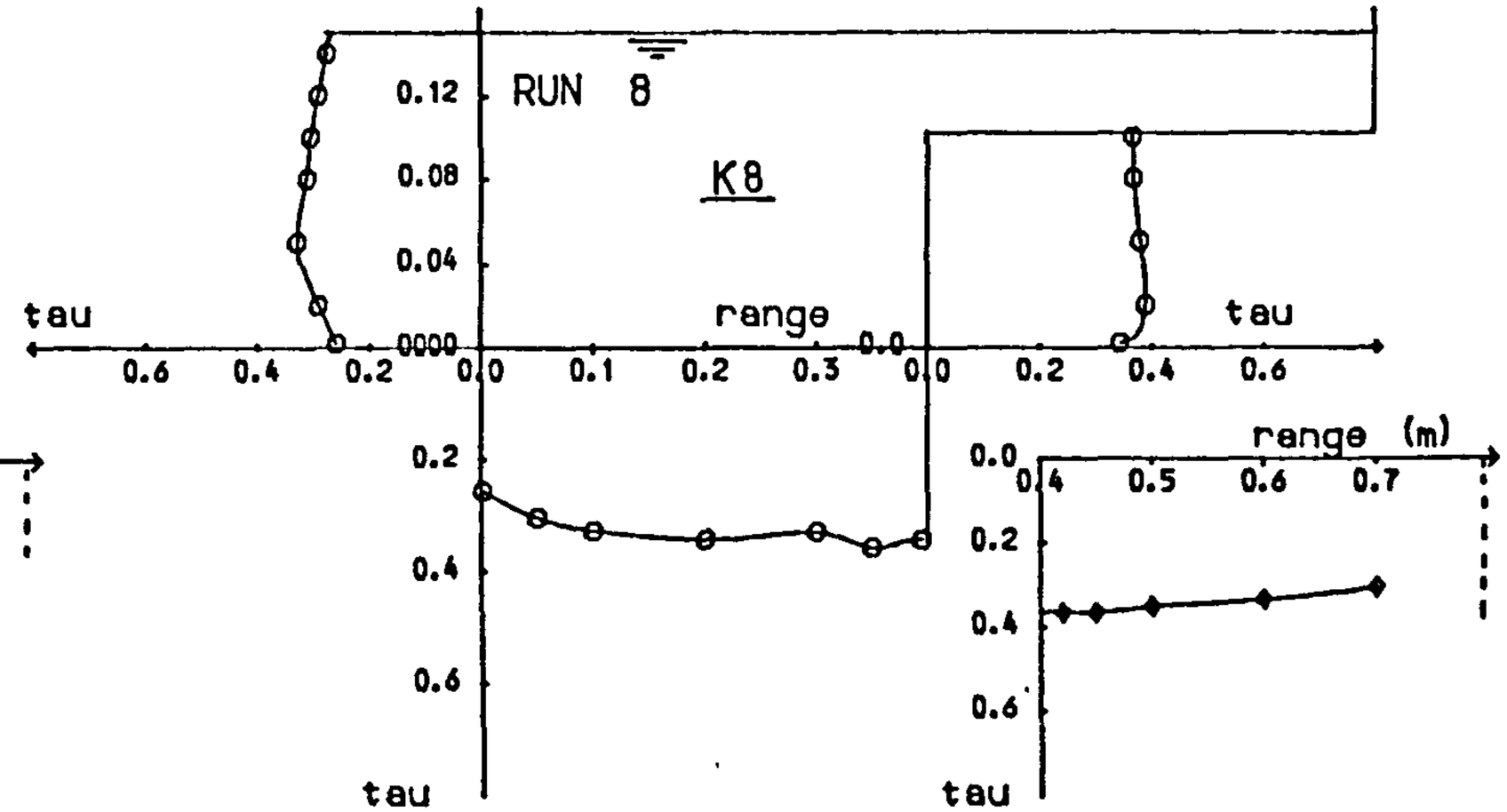

Fig 5·4 Shear stress distribution in channel and flood plain.

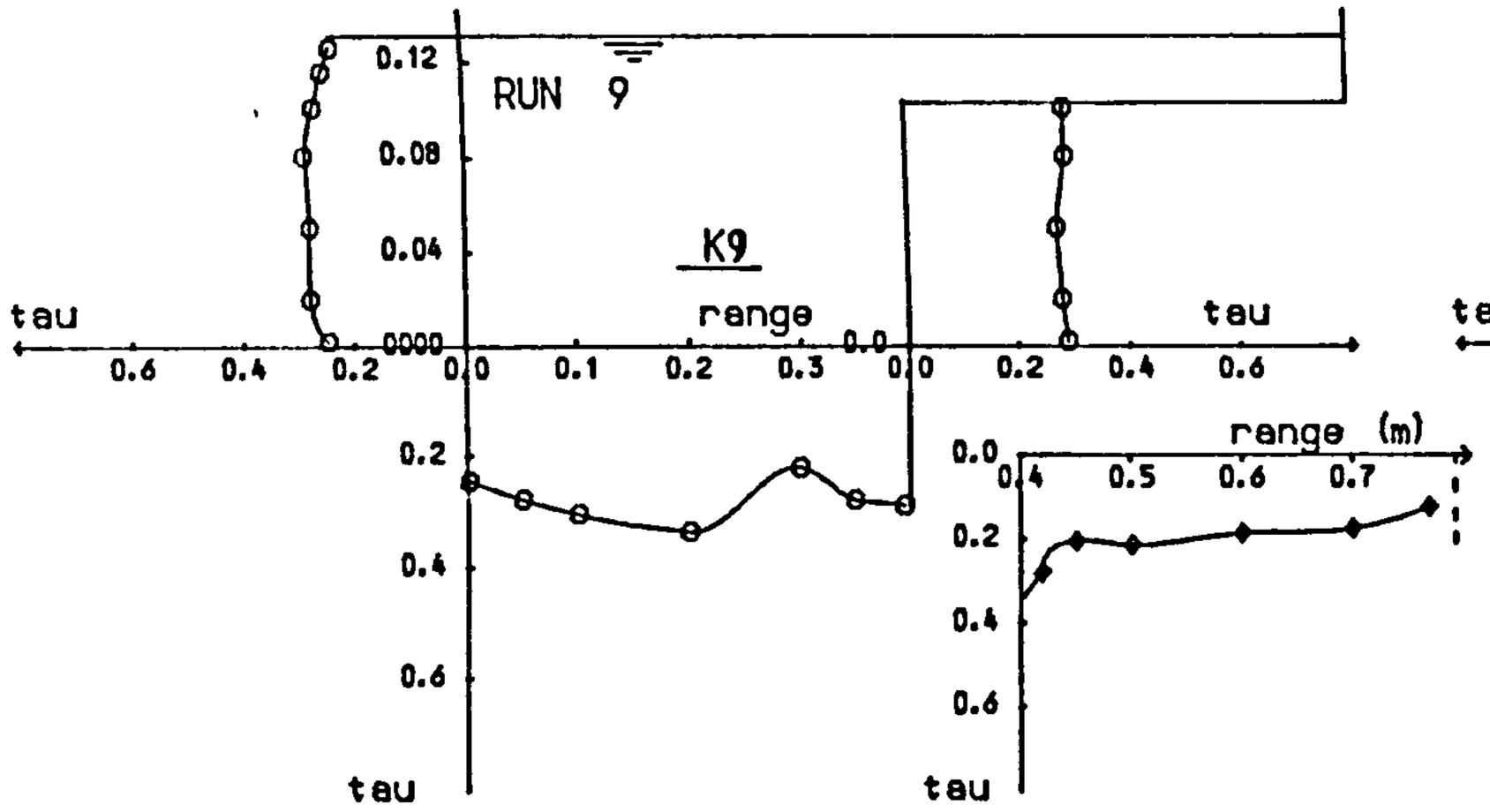

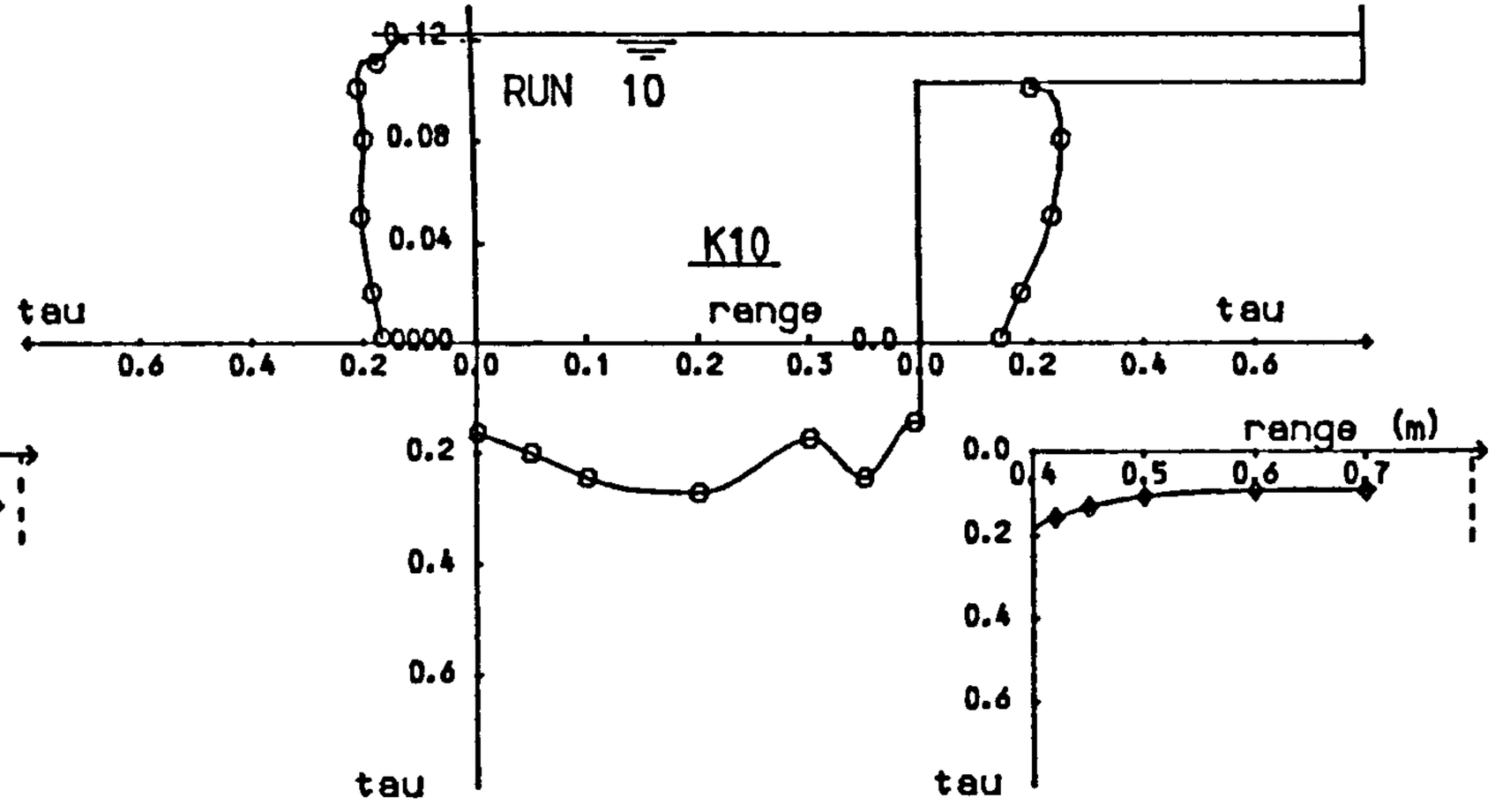

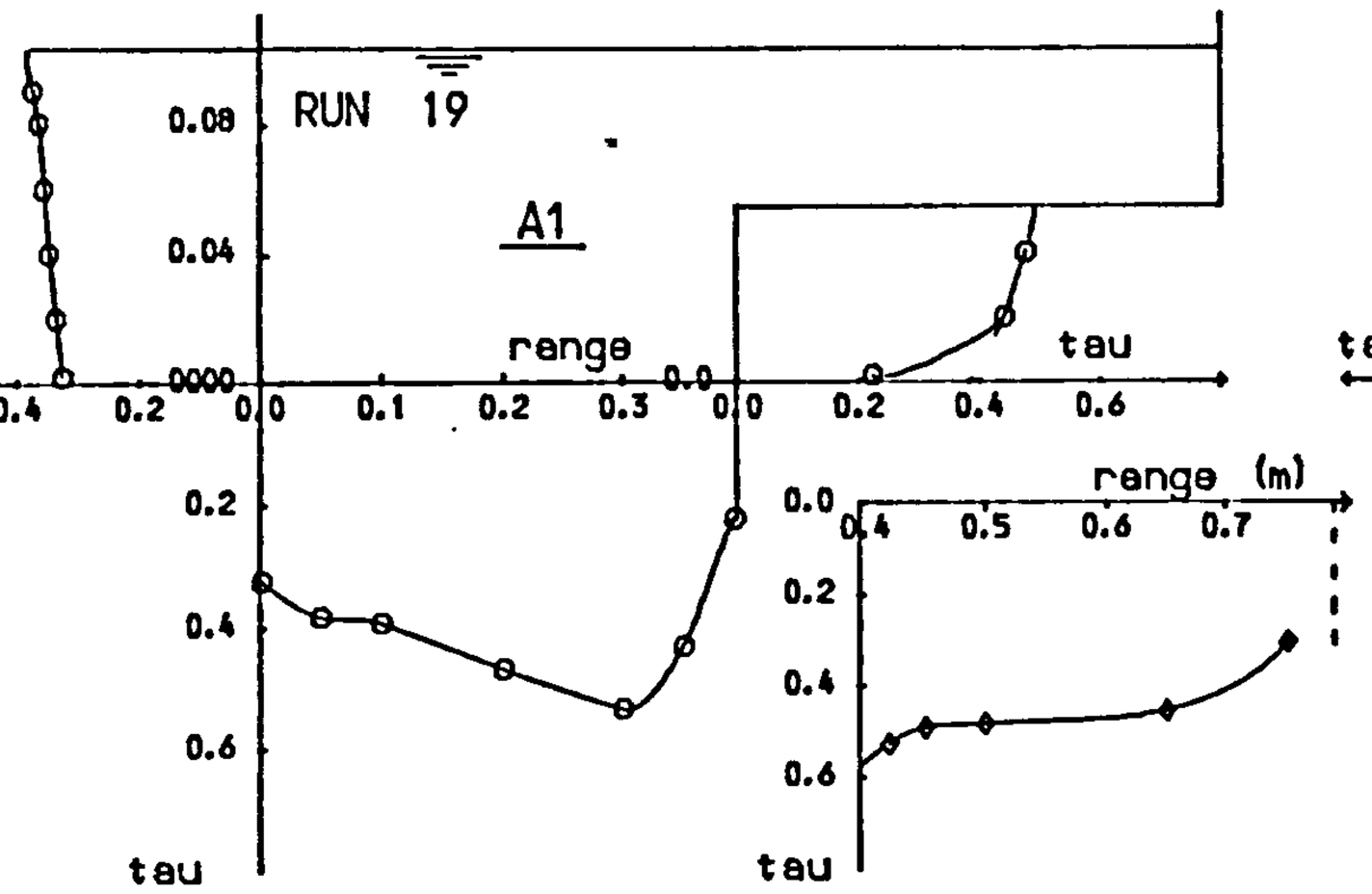

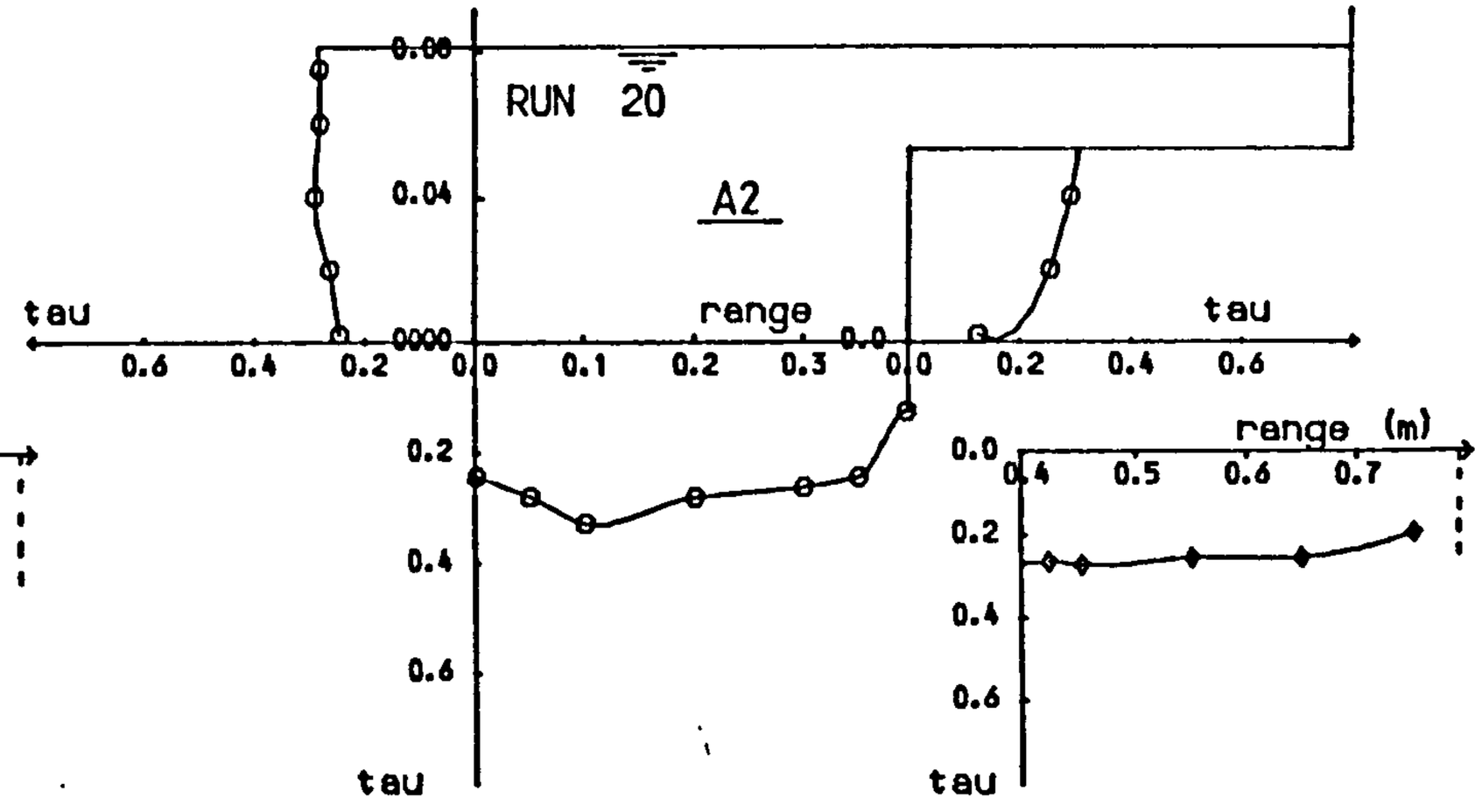

Fig 5·4 Shear stress distribution in channel and flood plain.

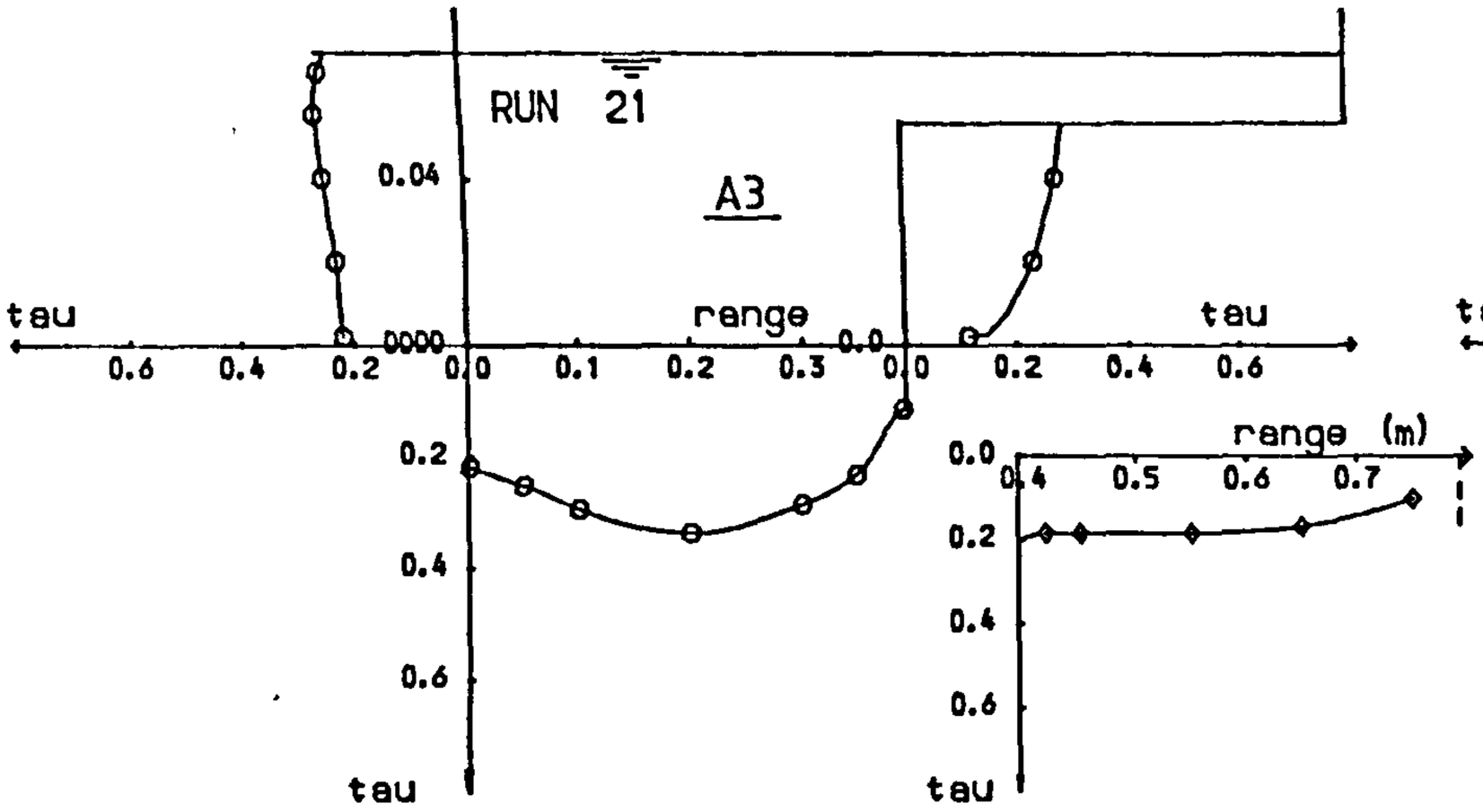

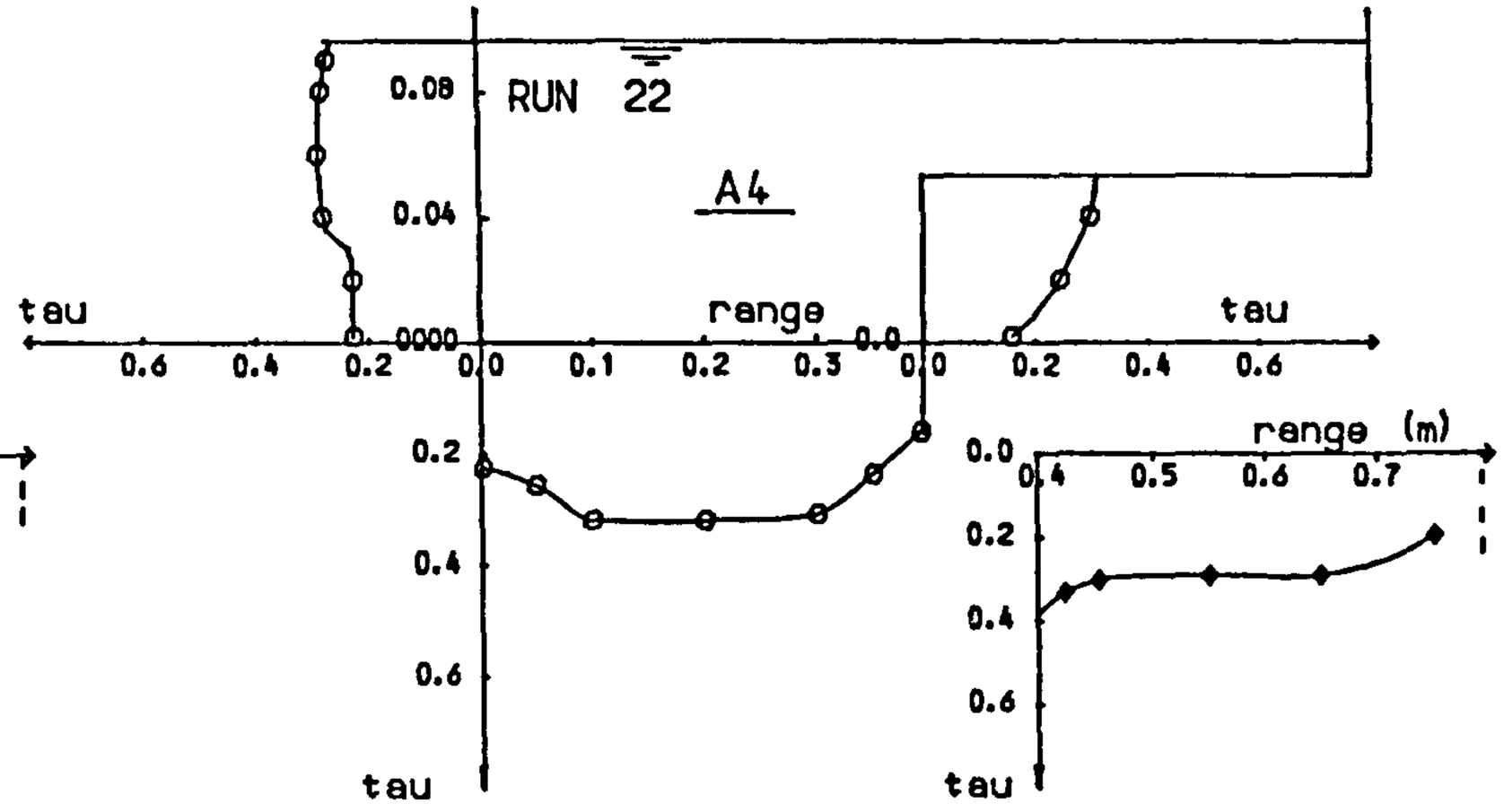

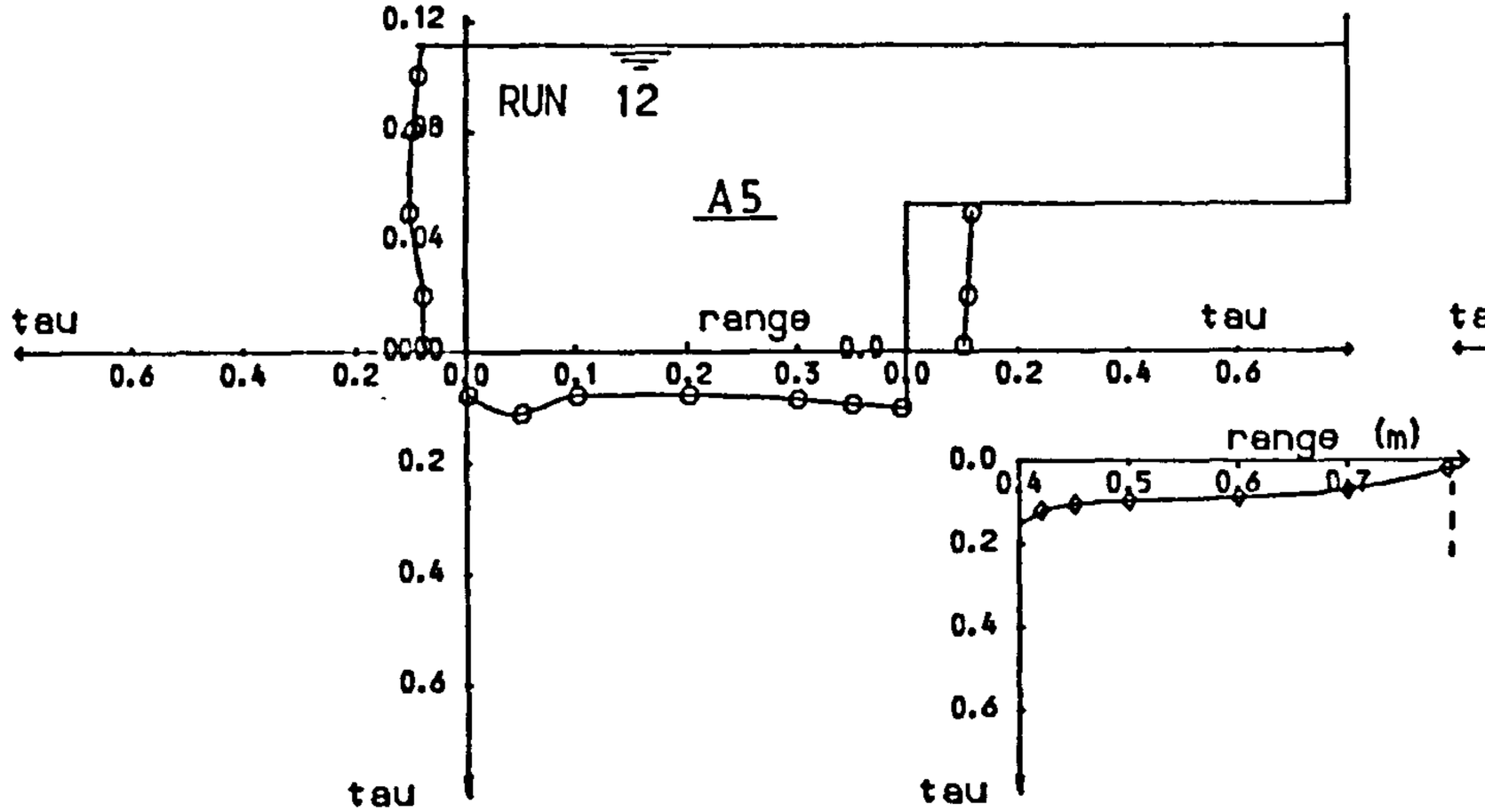

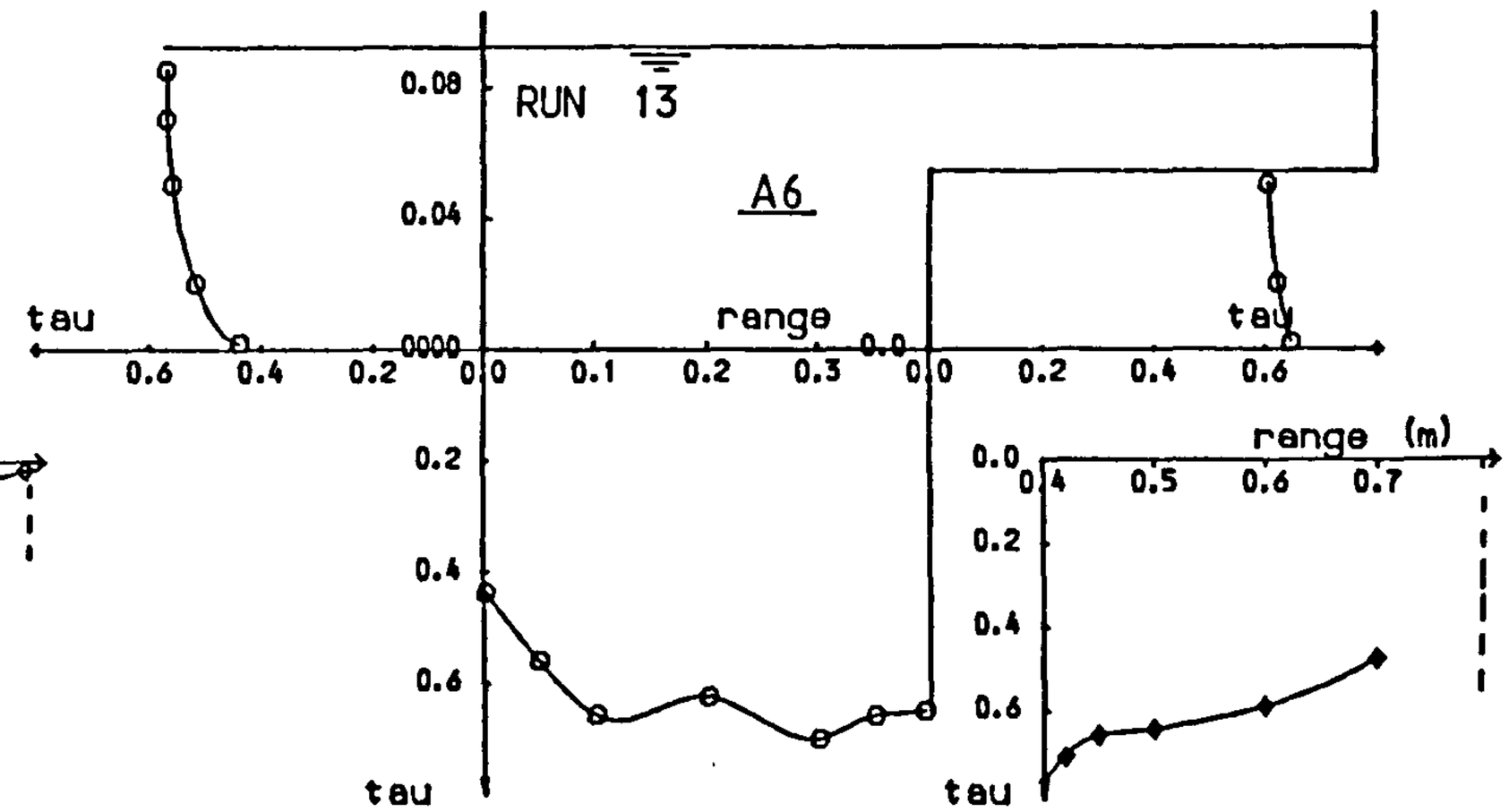

Fig 5·4 Shear stress distribution in channel and flood plain.

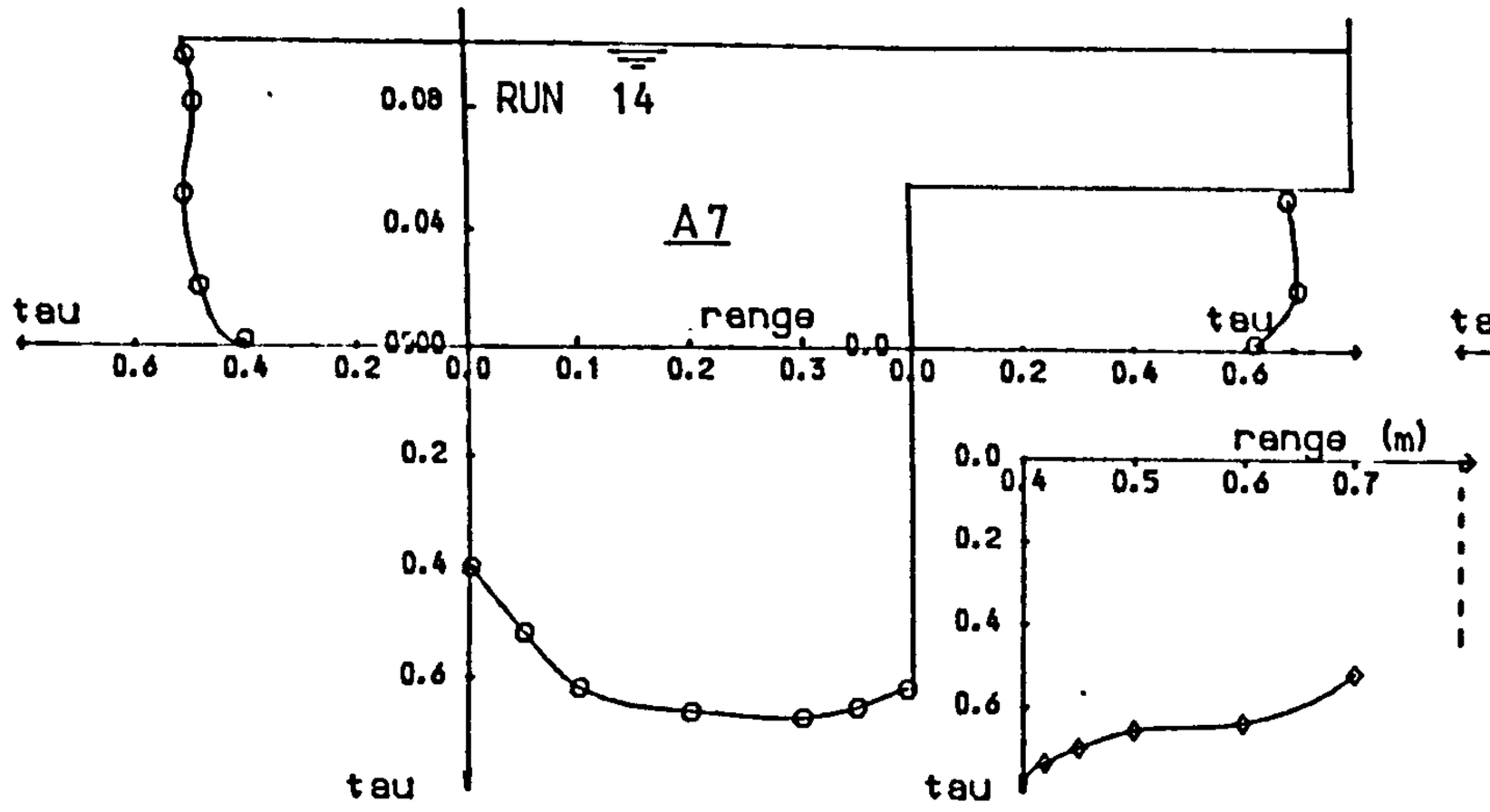

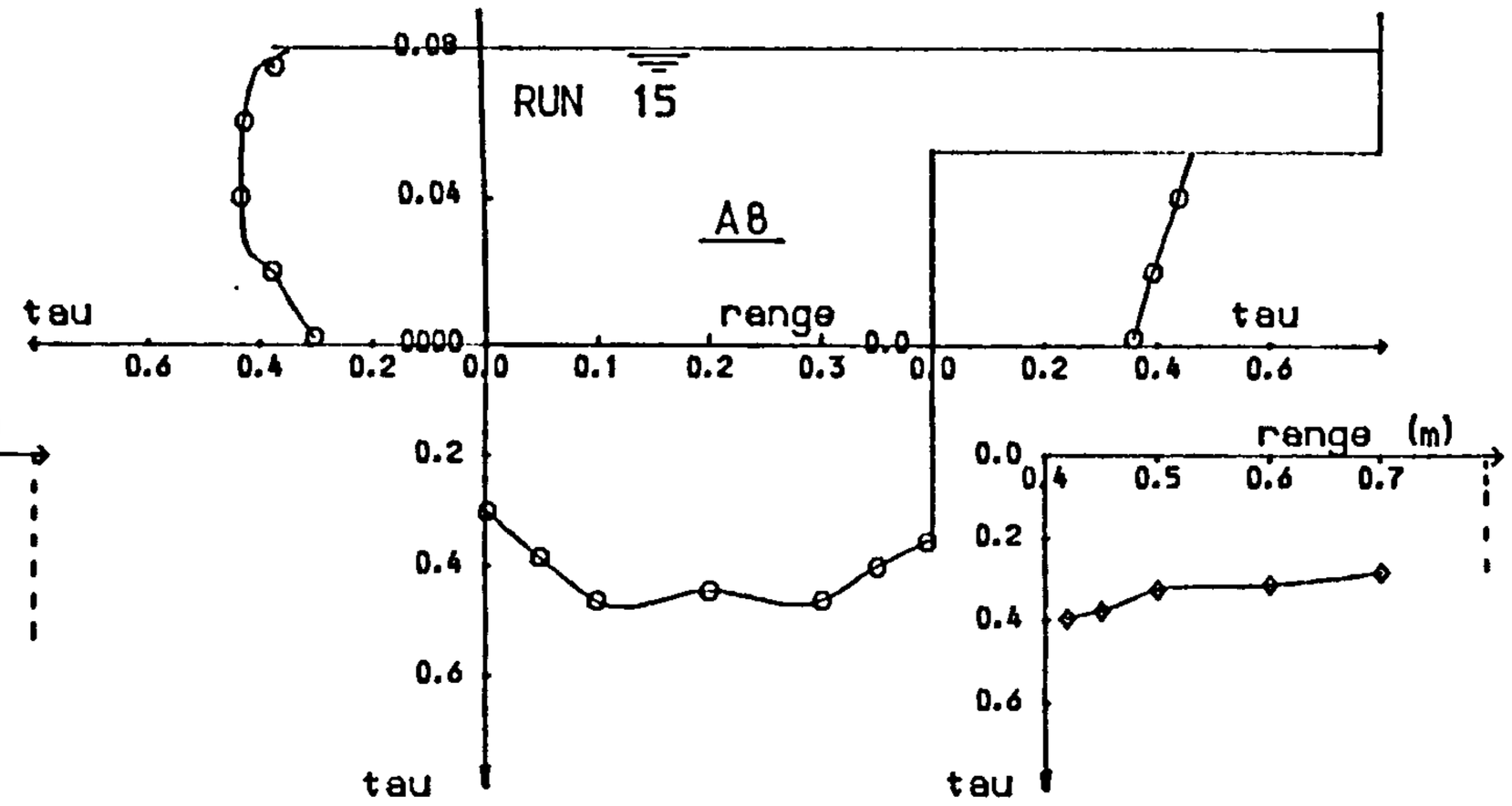

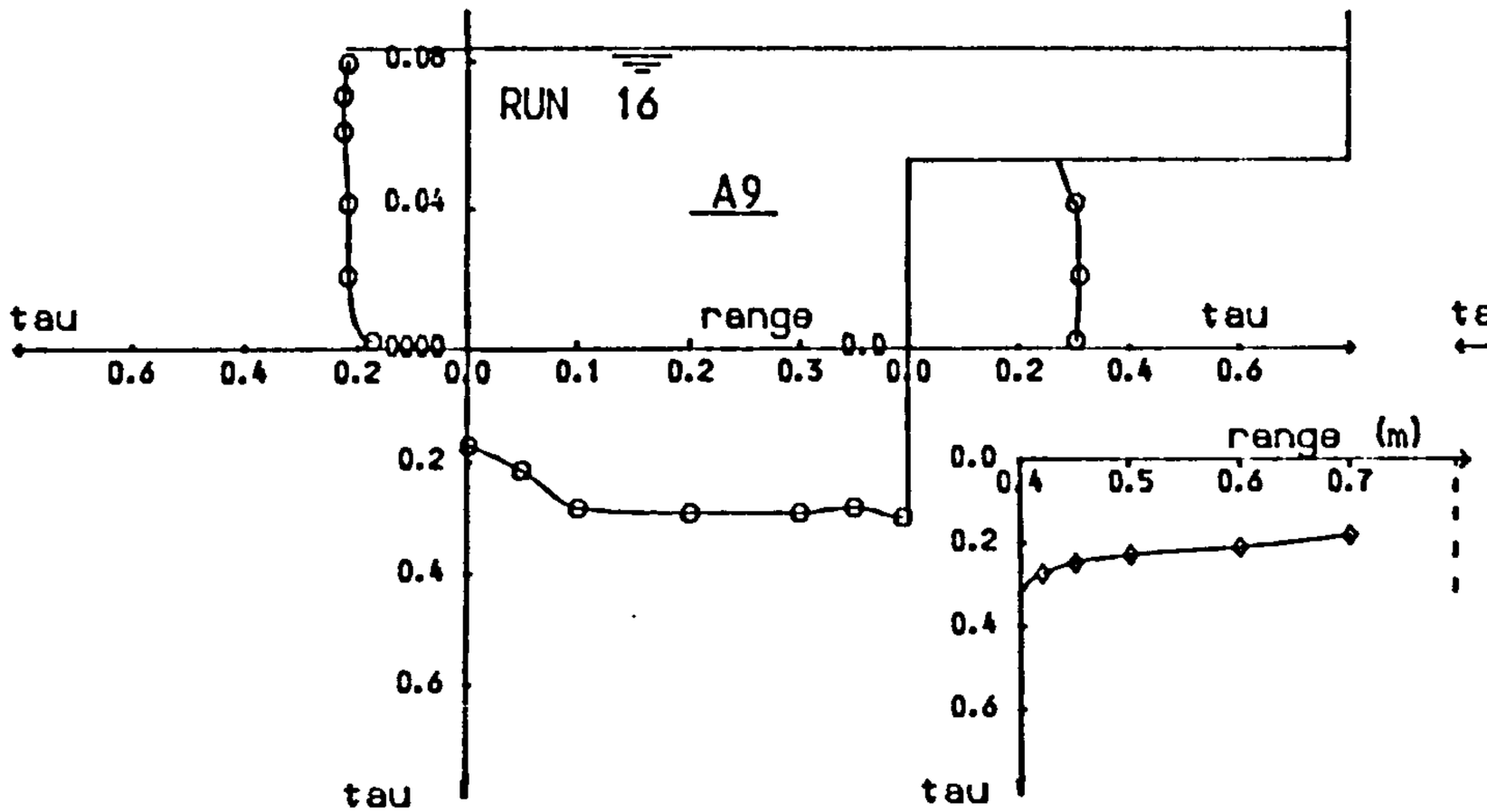

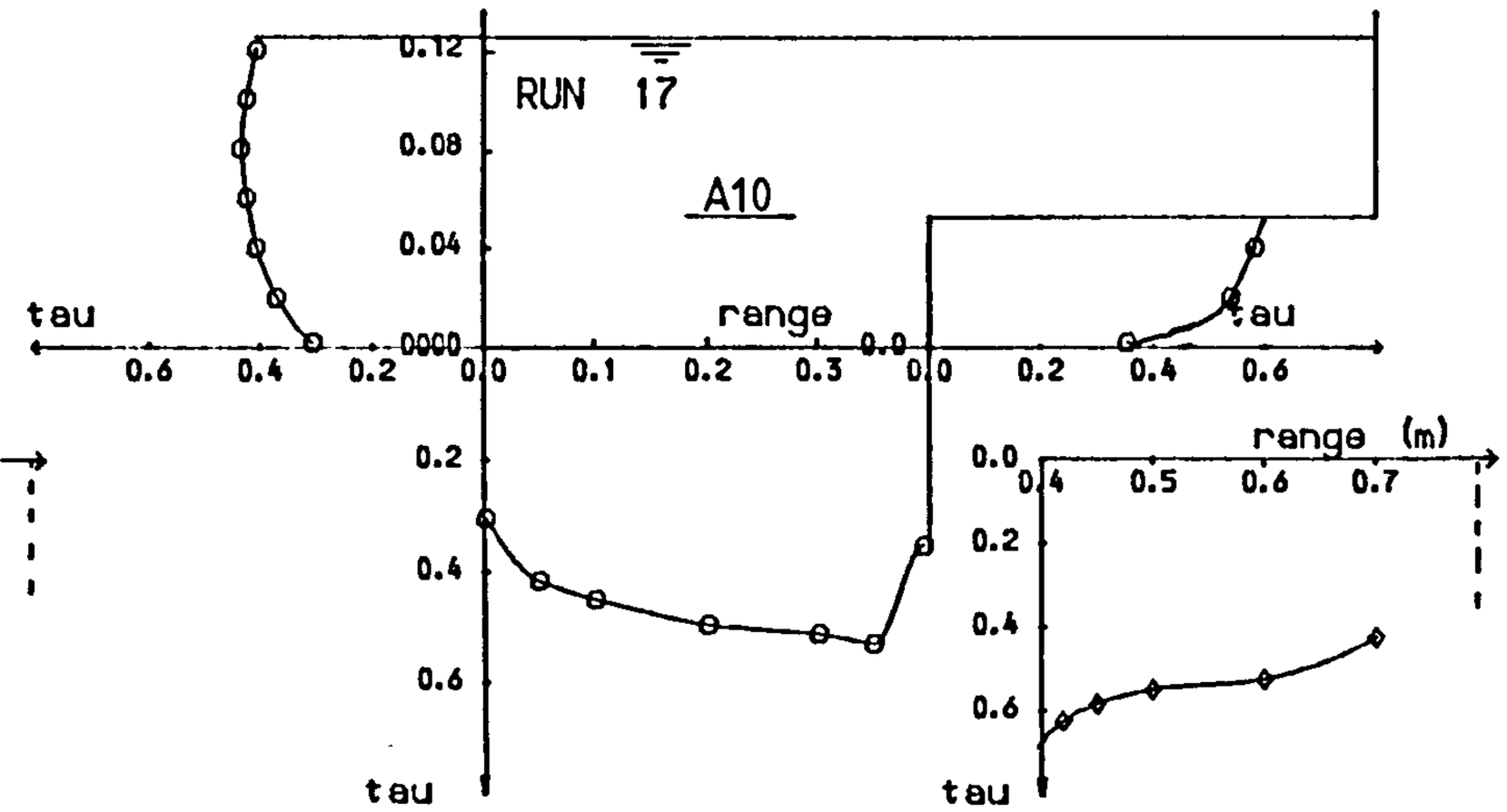

Fig 5·4 Shear stress distribution in channel and flood plain.

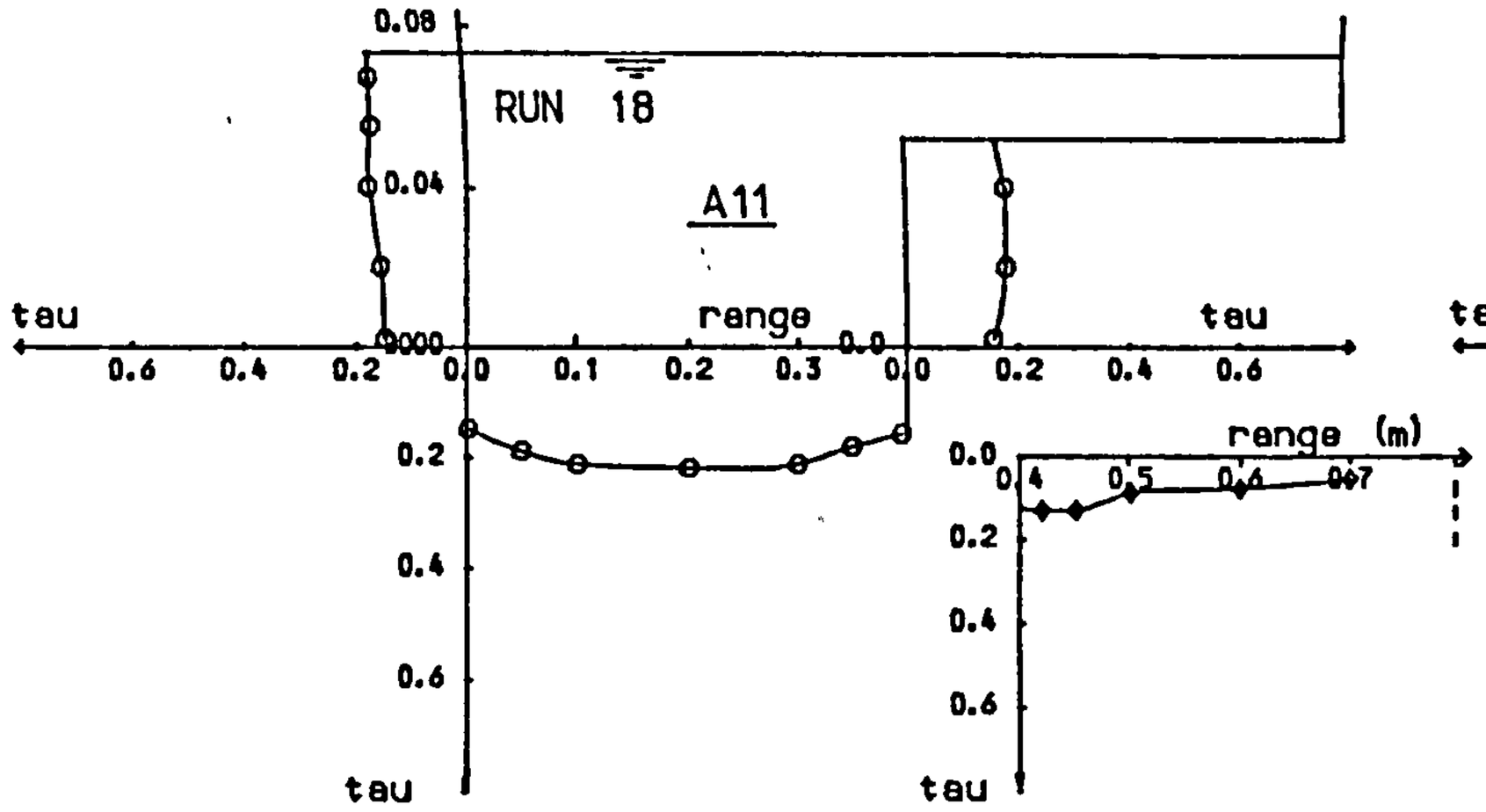

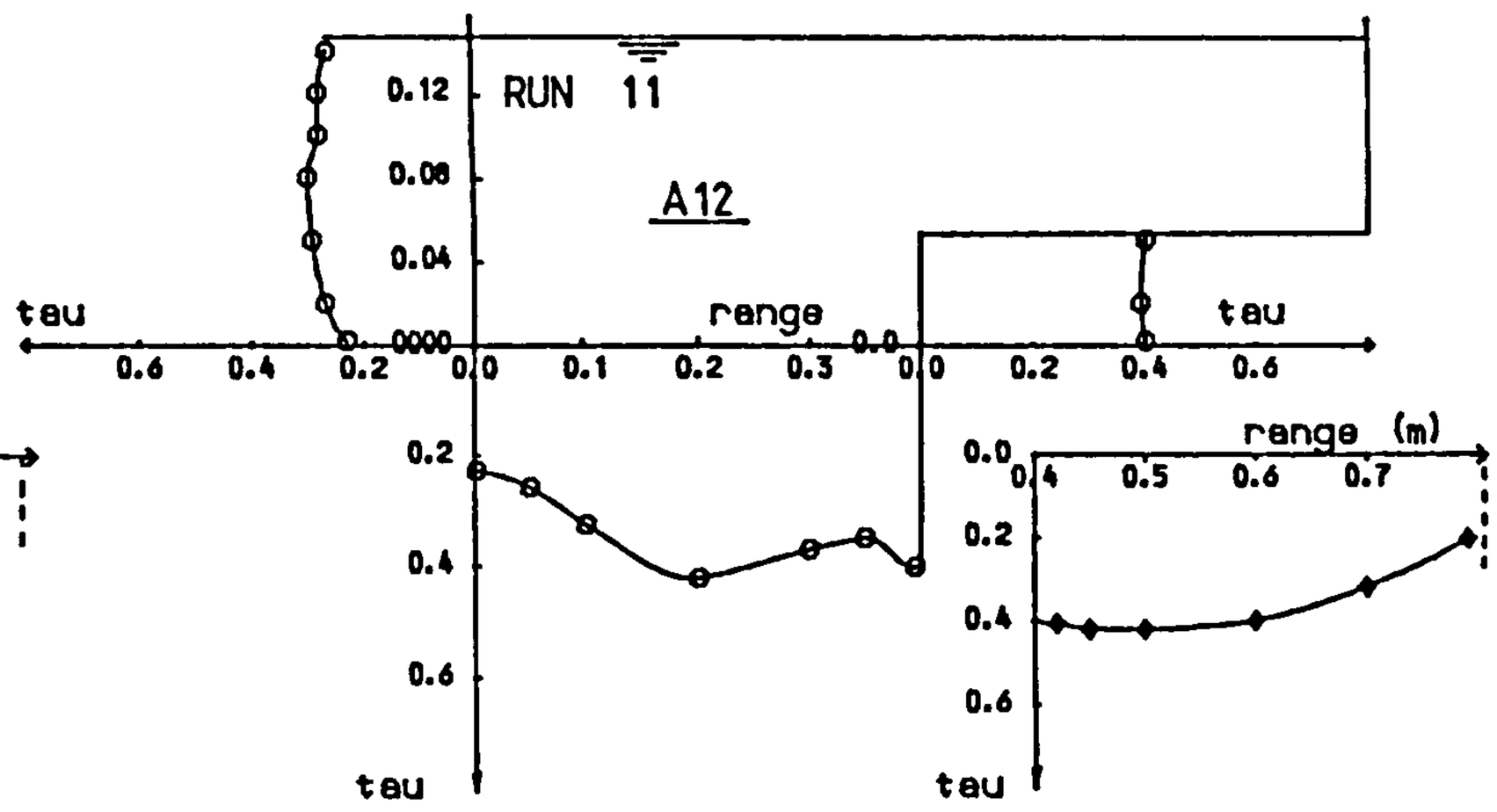

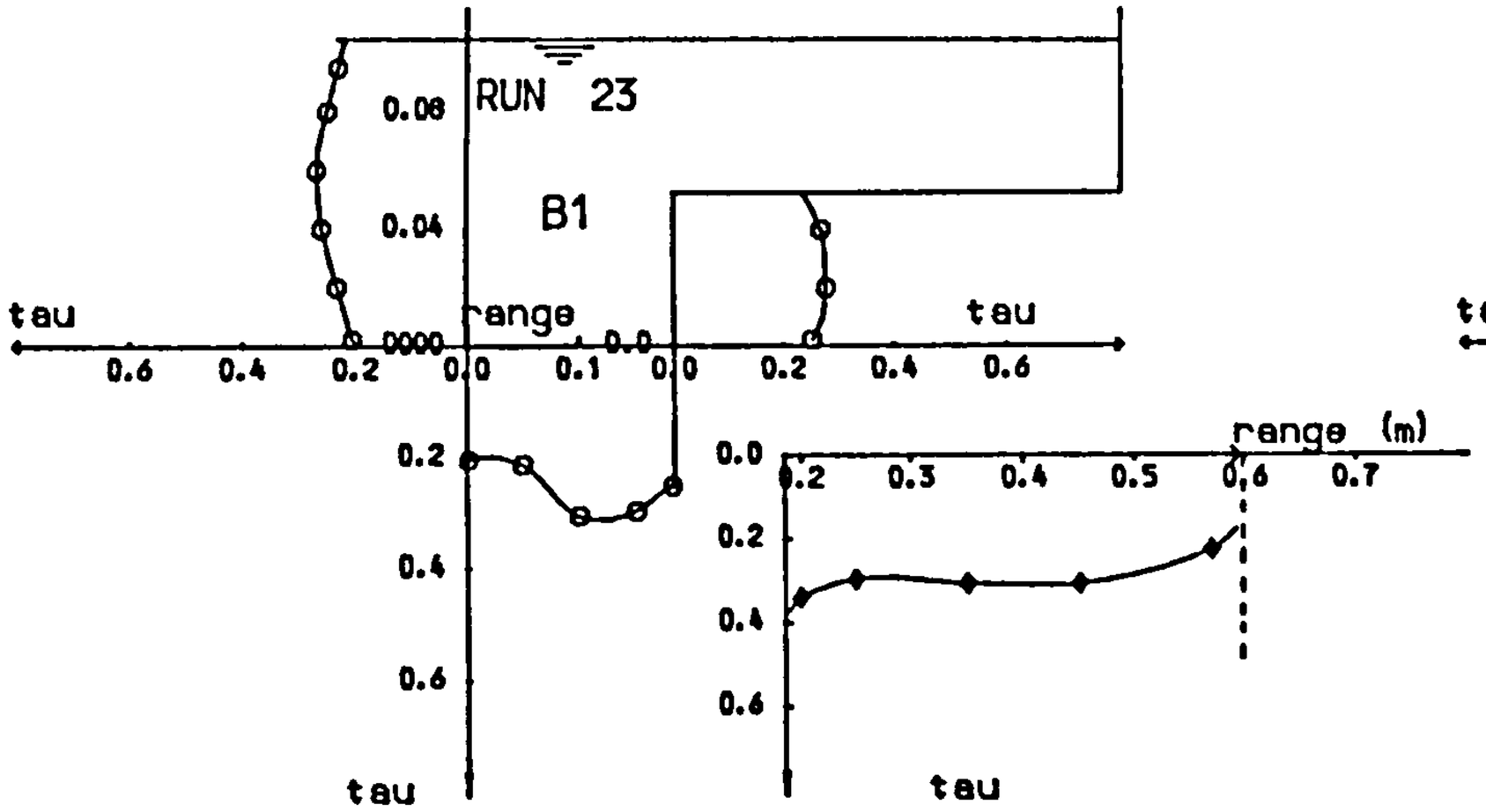

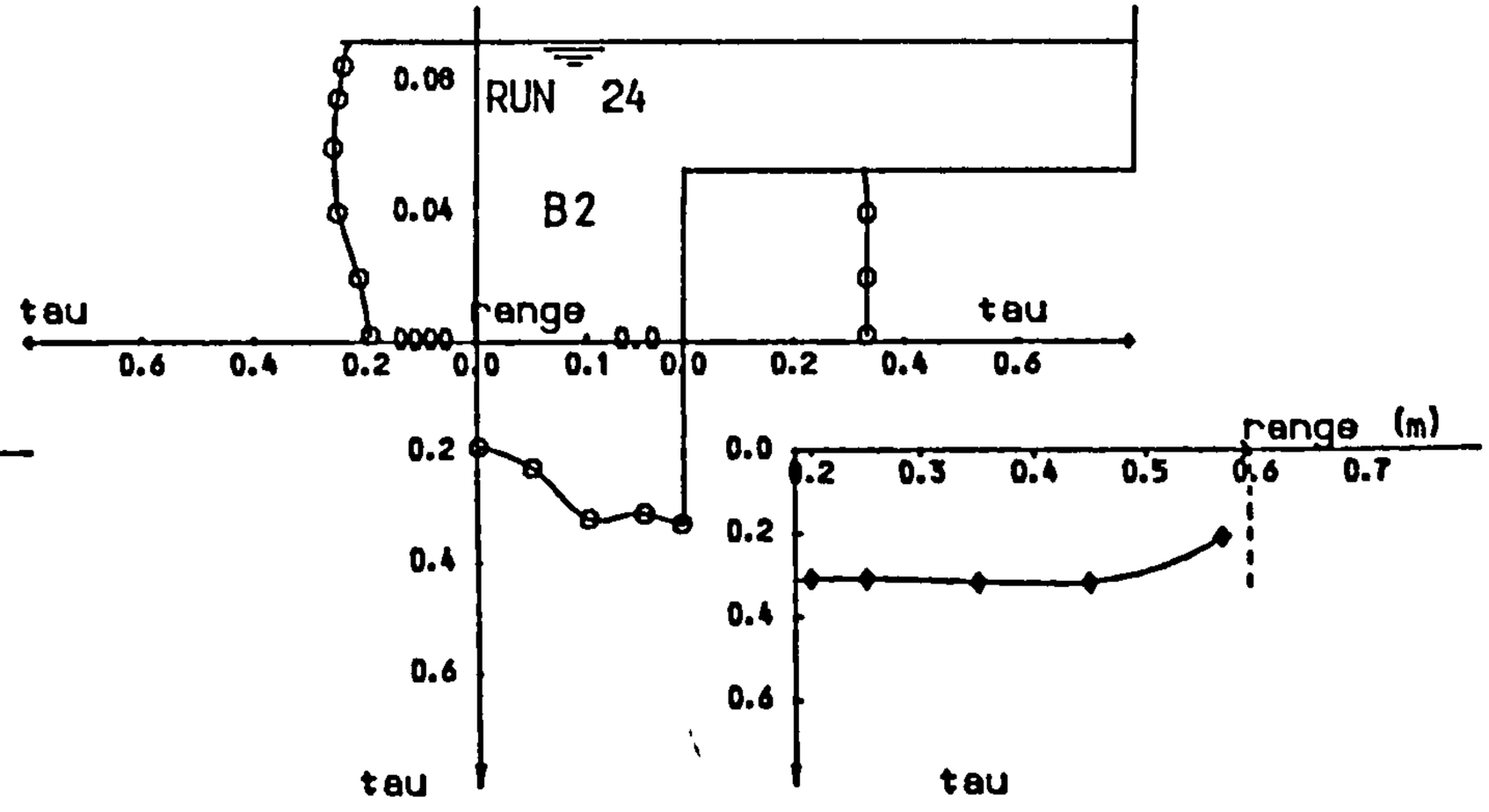

Fig 5·4 Shear stress distribution in channel and flood plain.

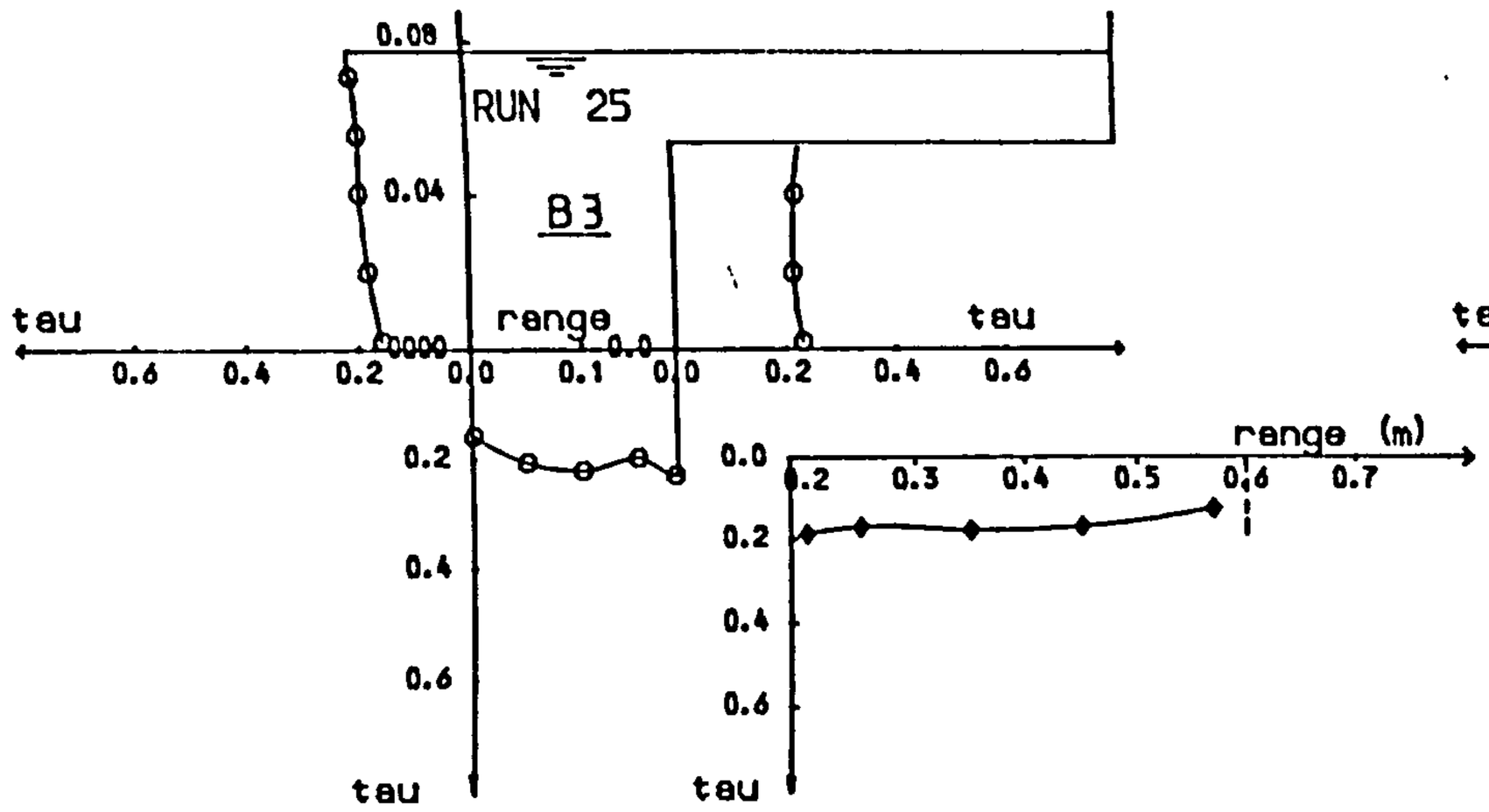

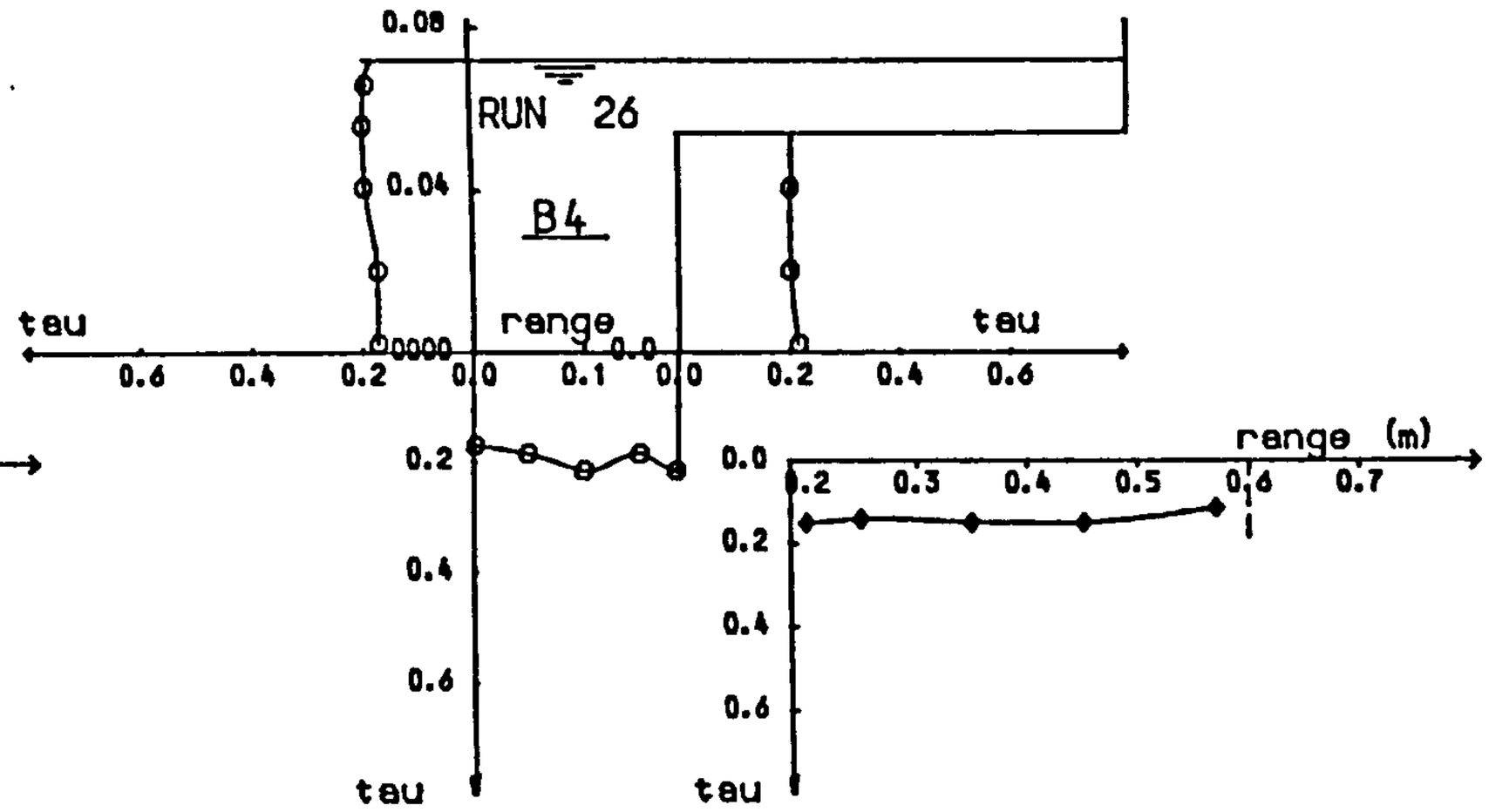

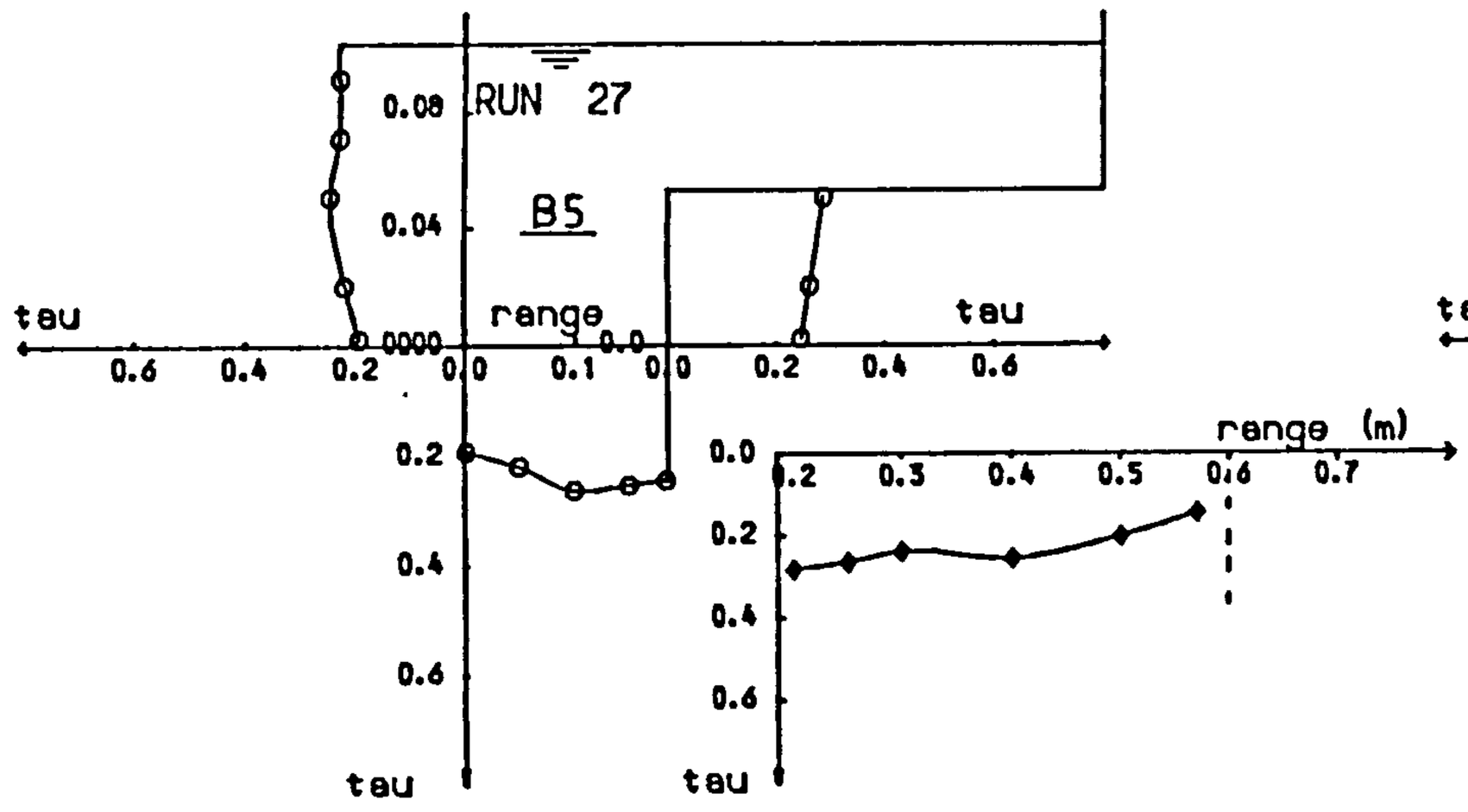

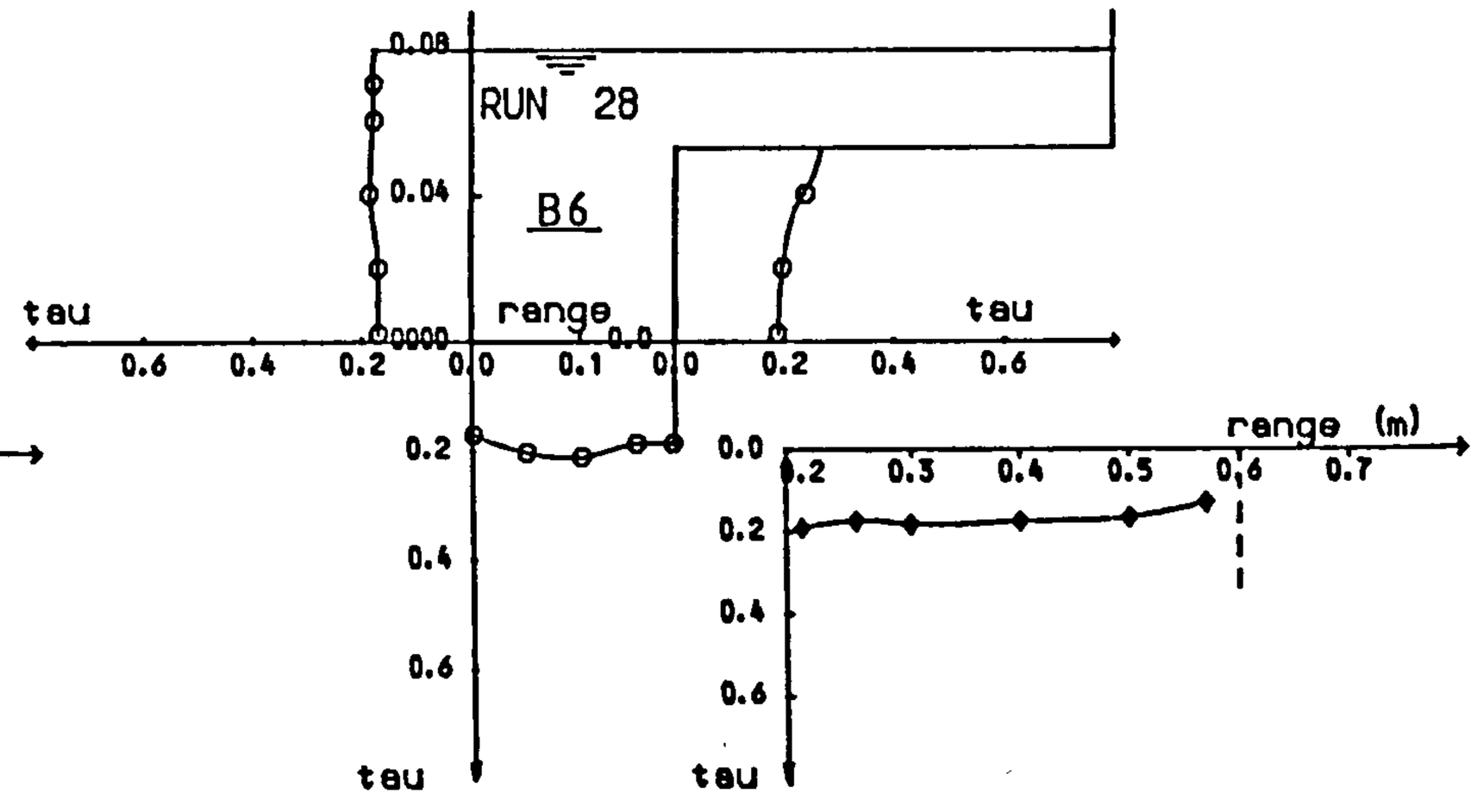

Fig 5·4 Shear stress distribution in channel and flood plain.

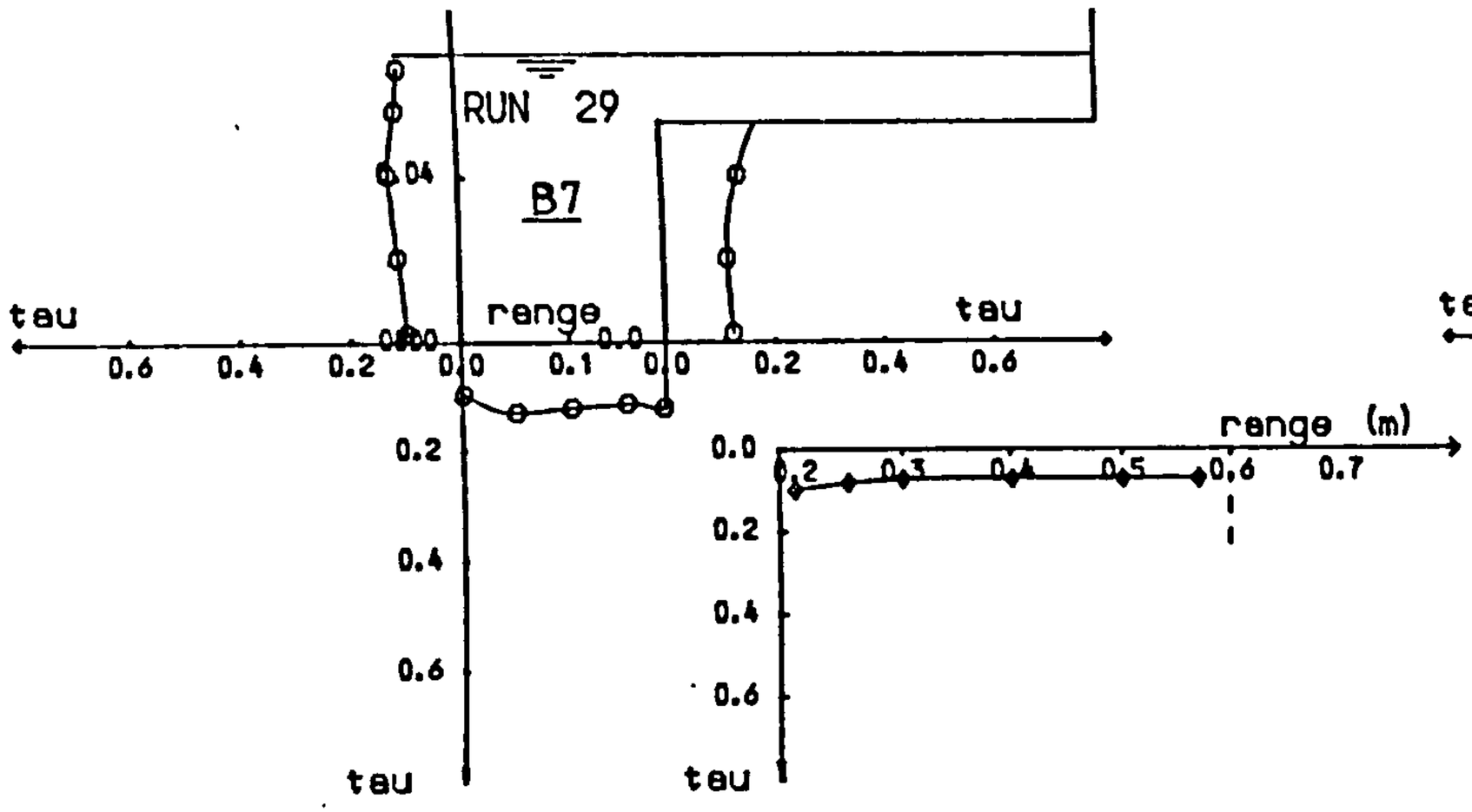

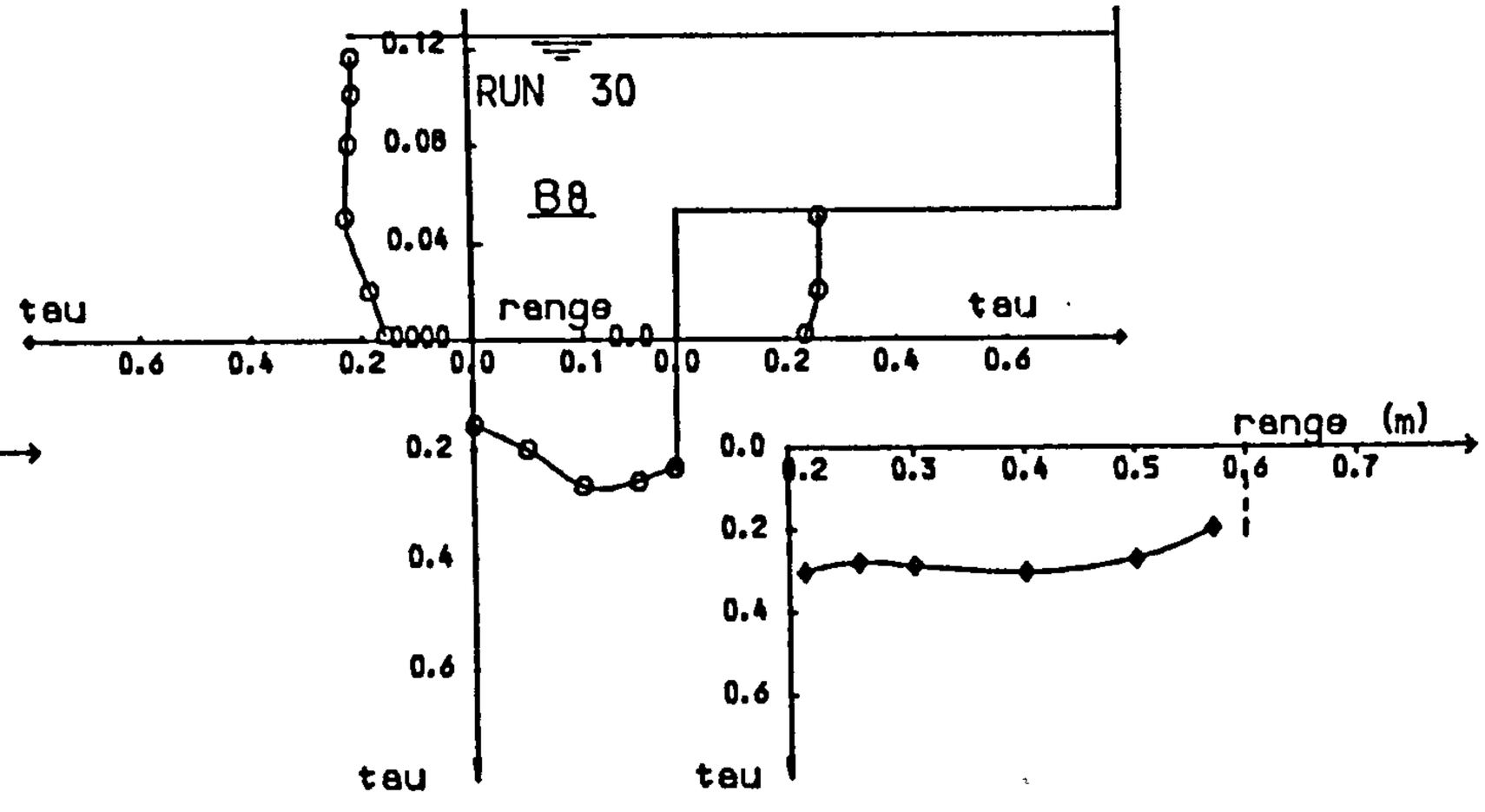

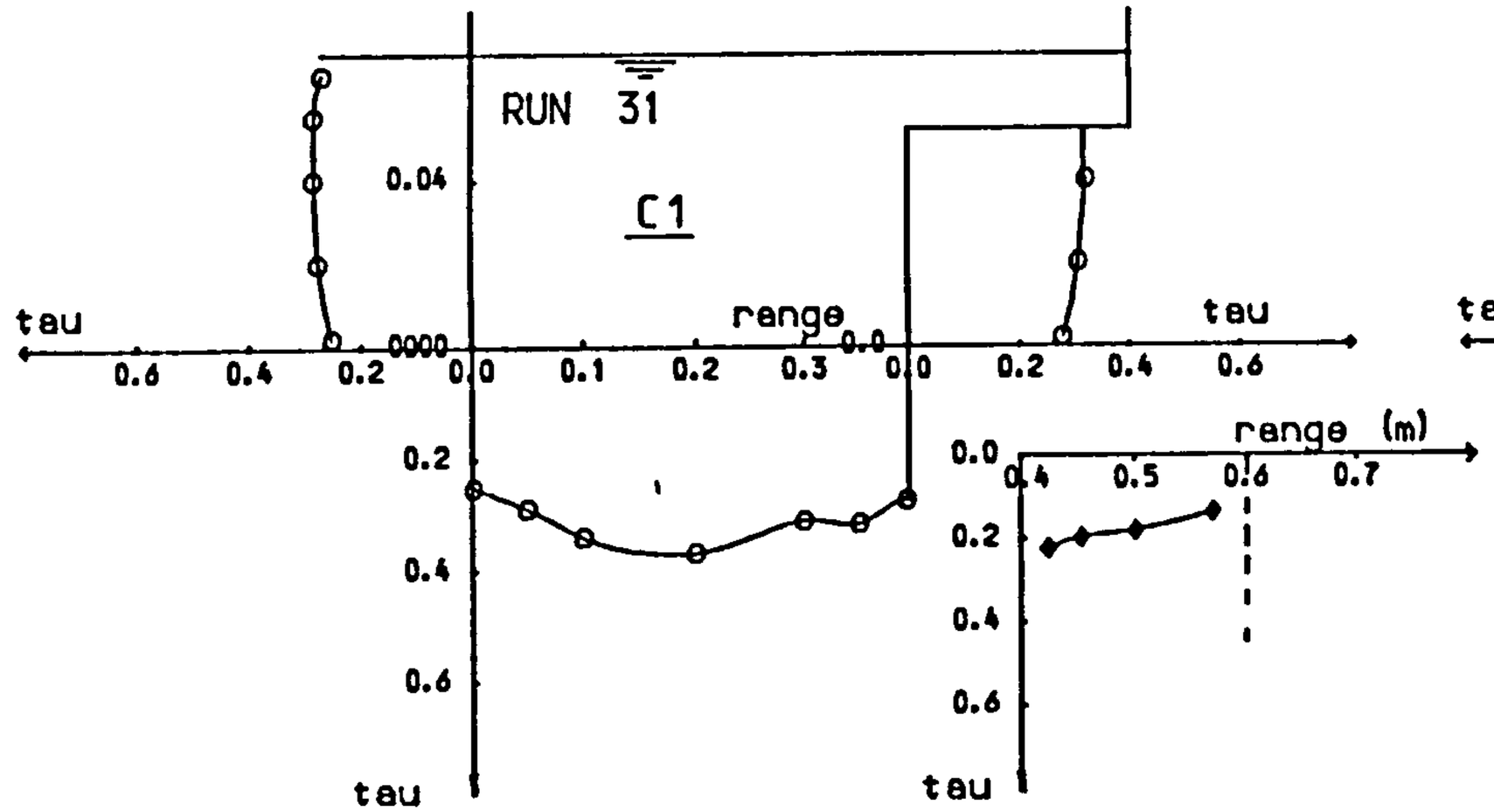

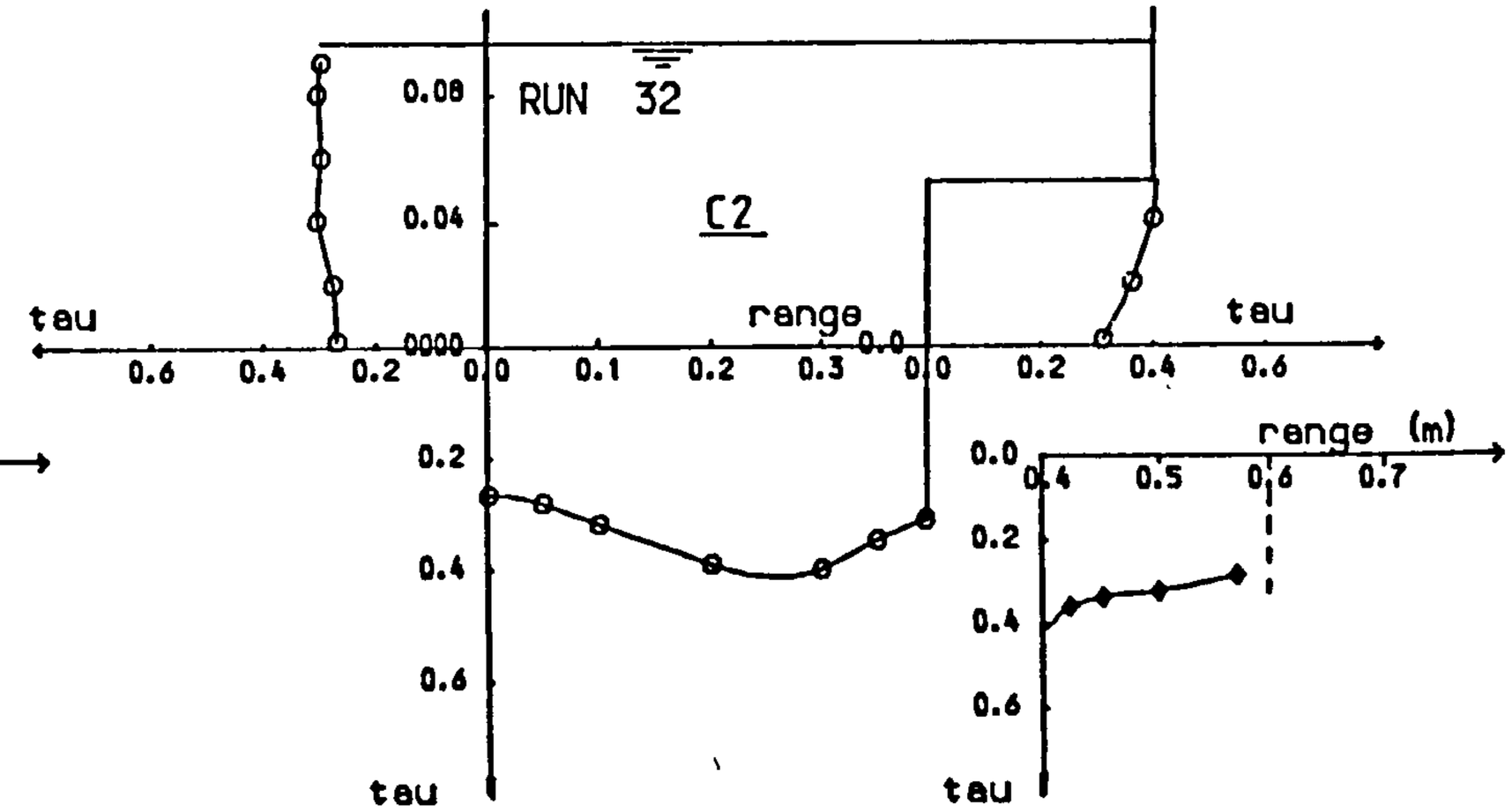

Fig 5·4 Shear stress distribution in channel and flood plain.

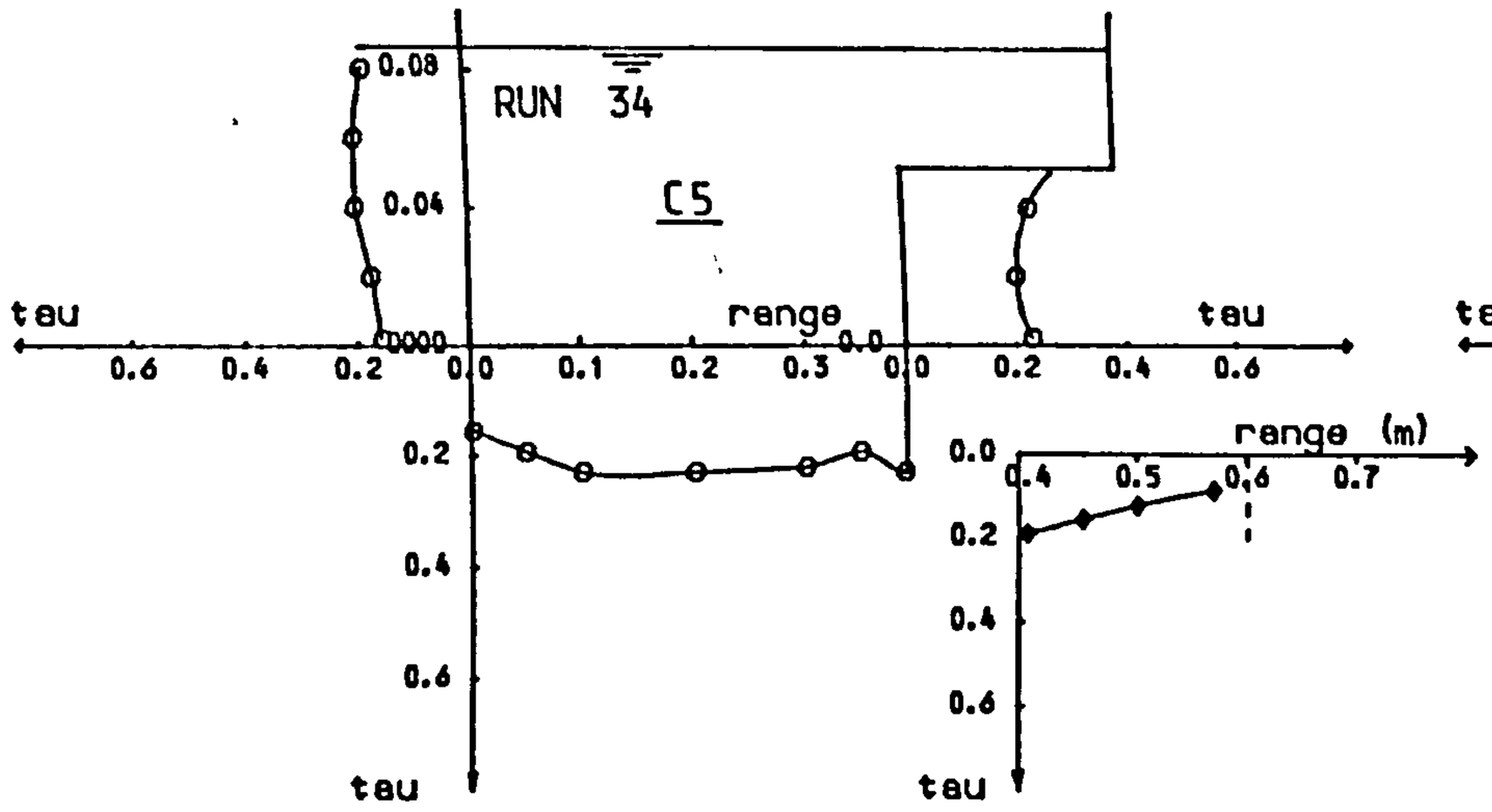

Fig 5·4 Shear stress distribution in channel and flood plain.

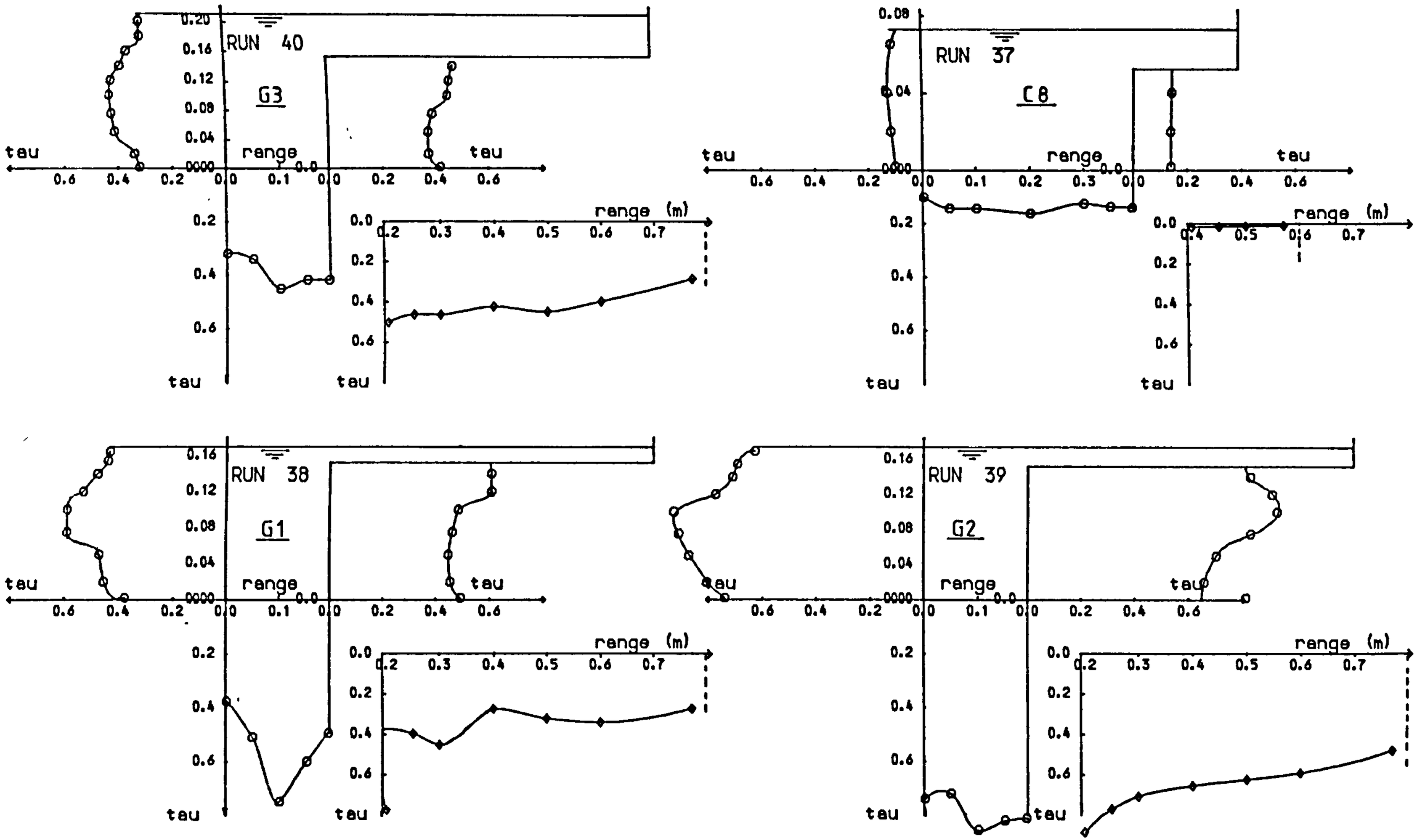

Fig 5·4 Shear stress distribution in channel and flood plain.

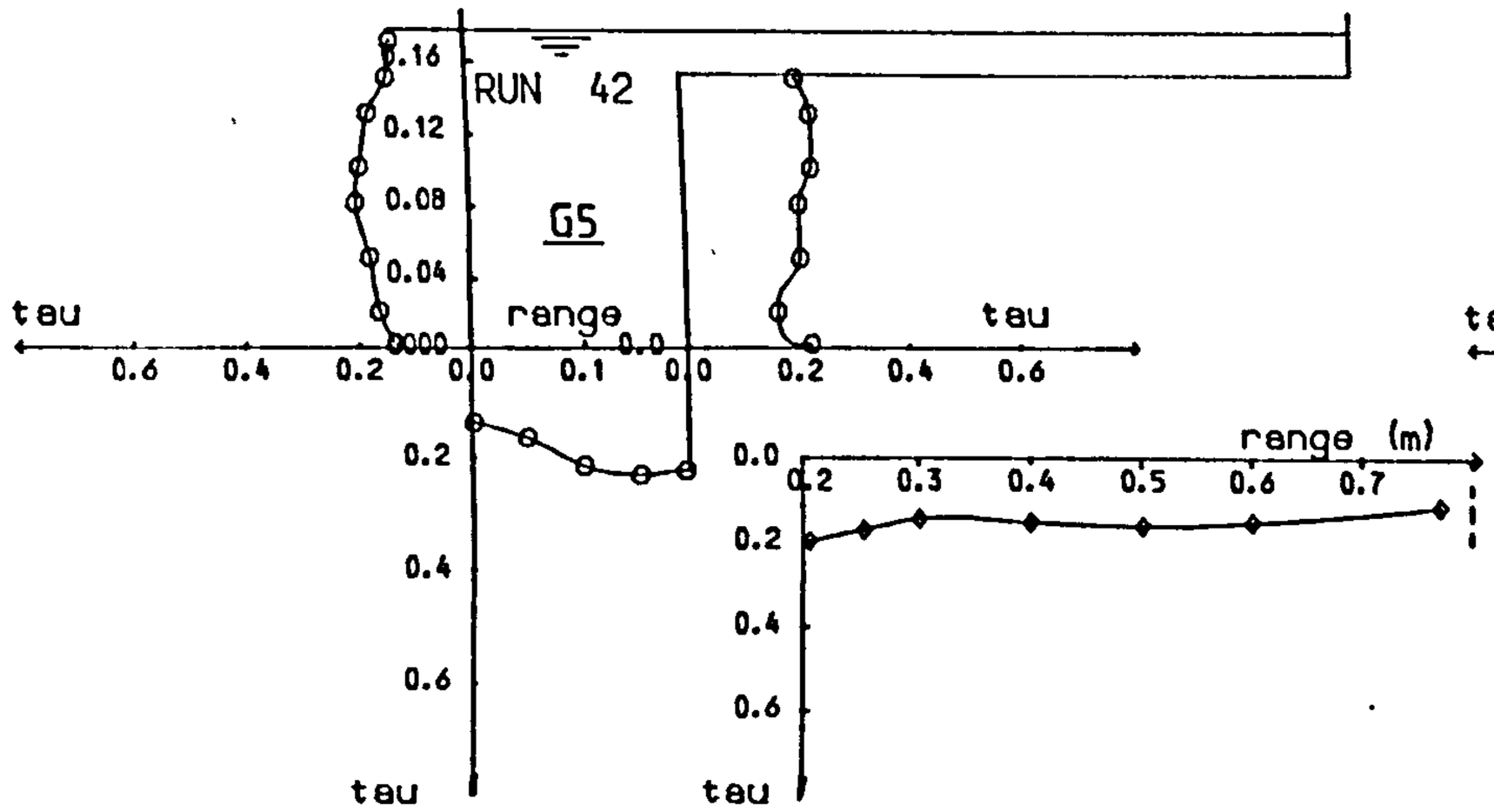

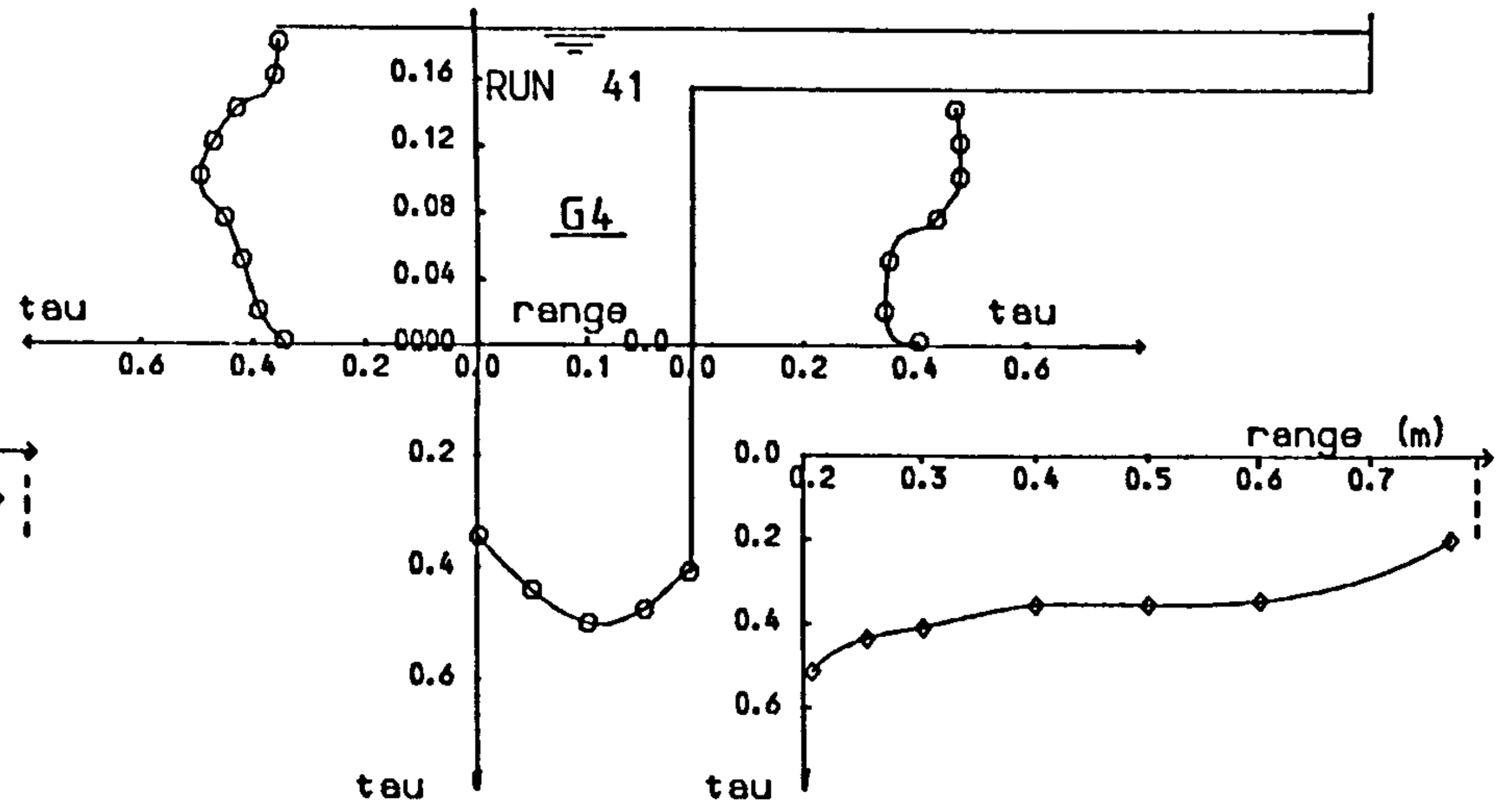

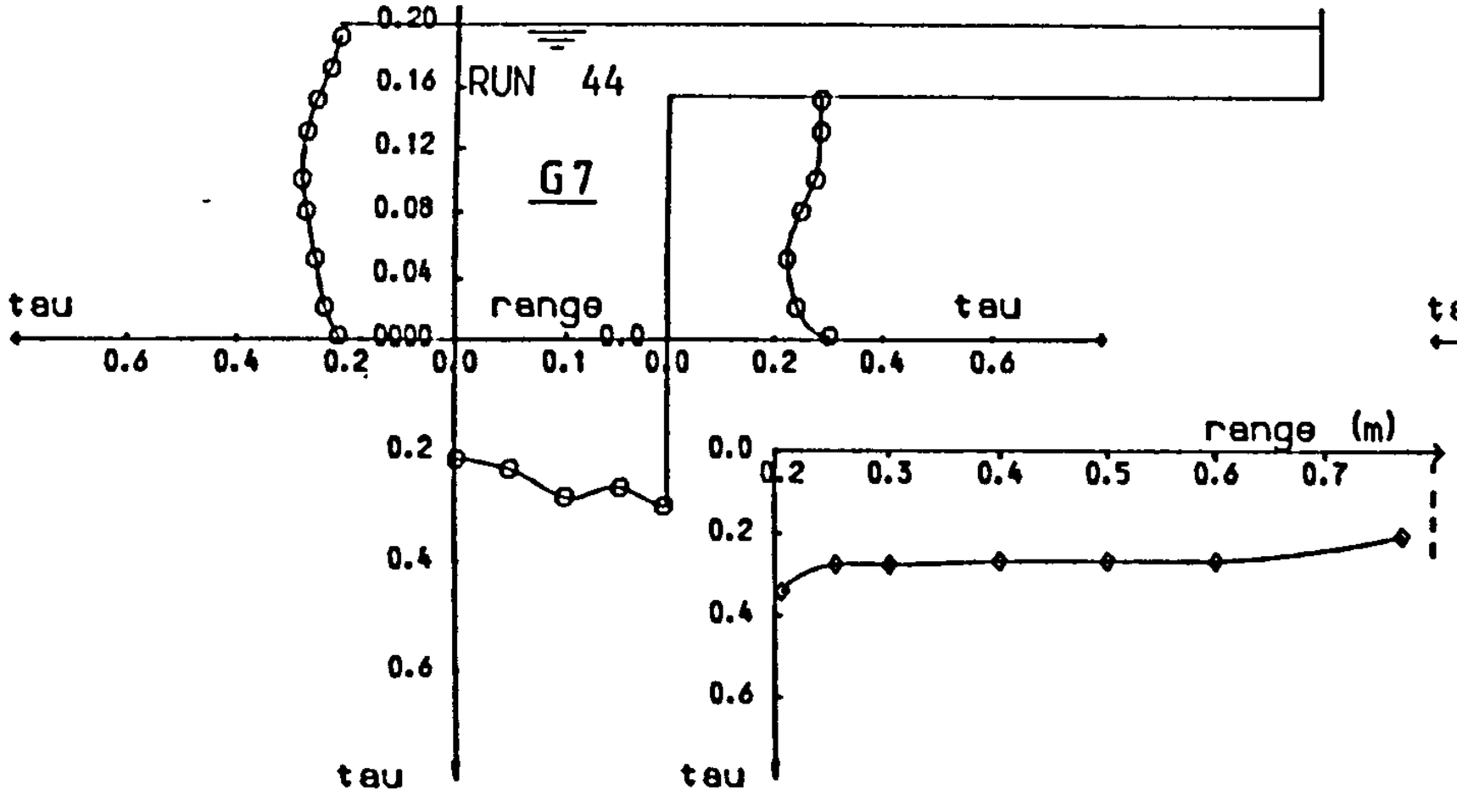

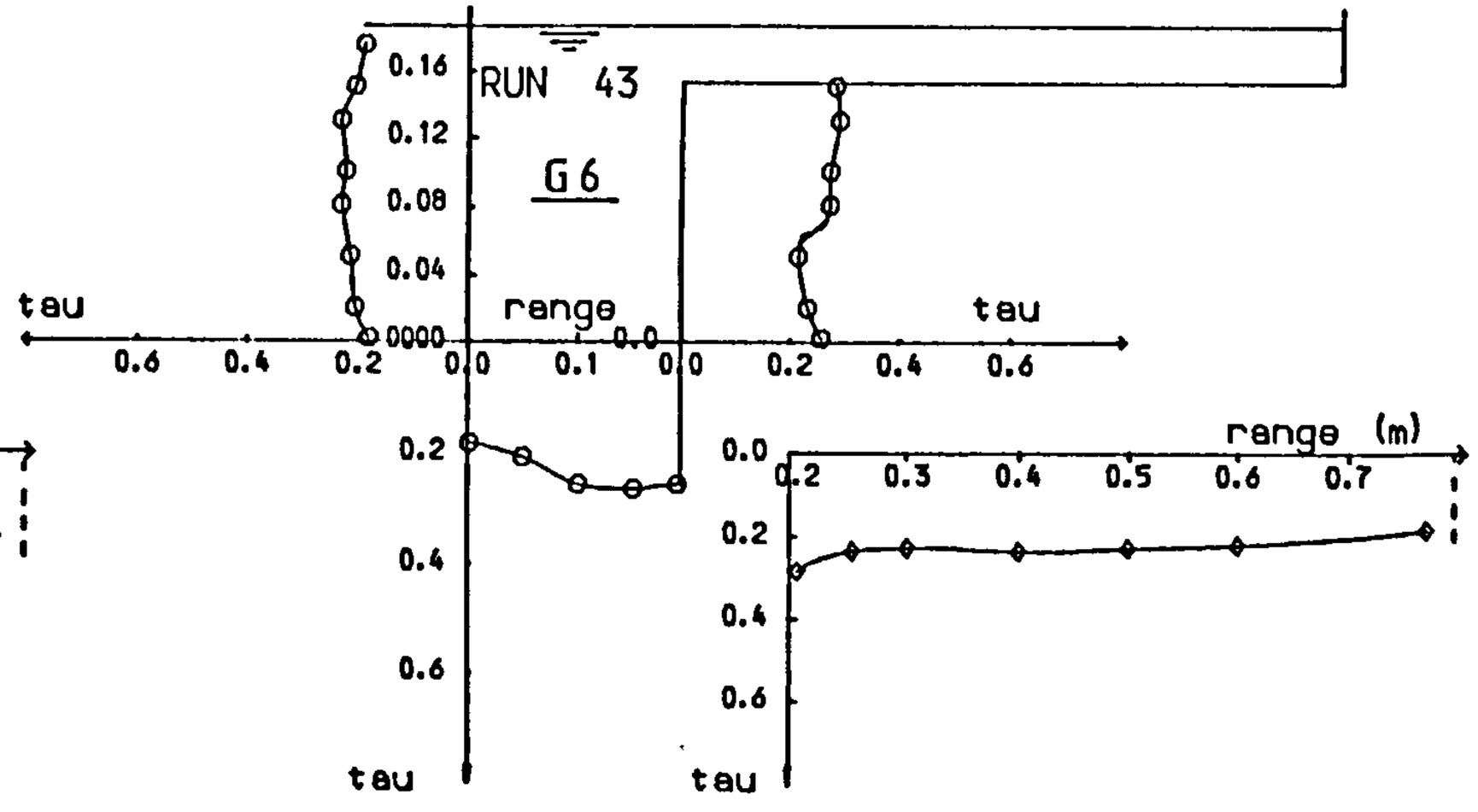

Fig 5·4 Shear stress distribution in channel and flood plain.

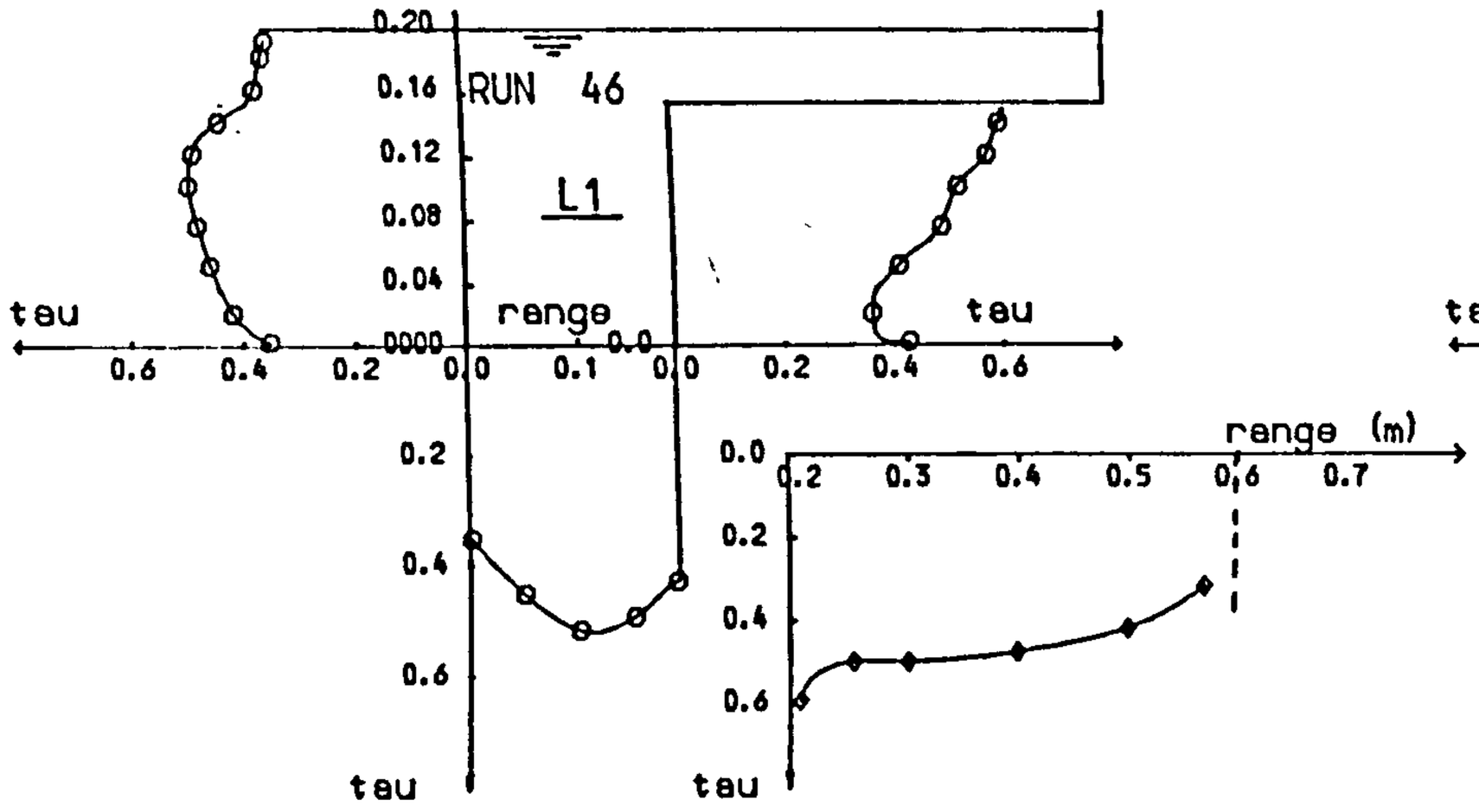

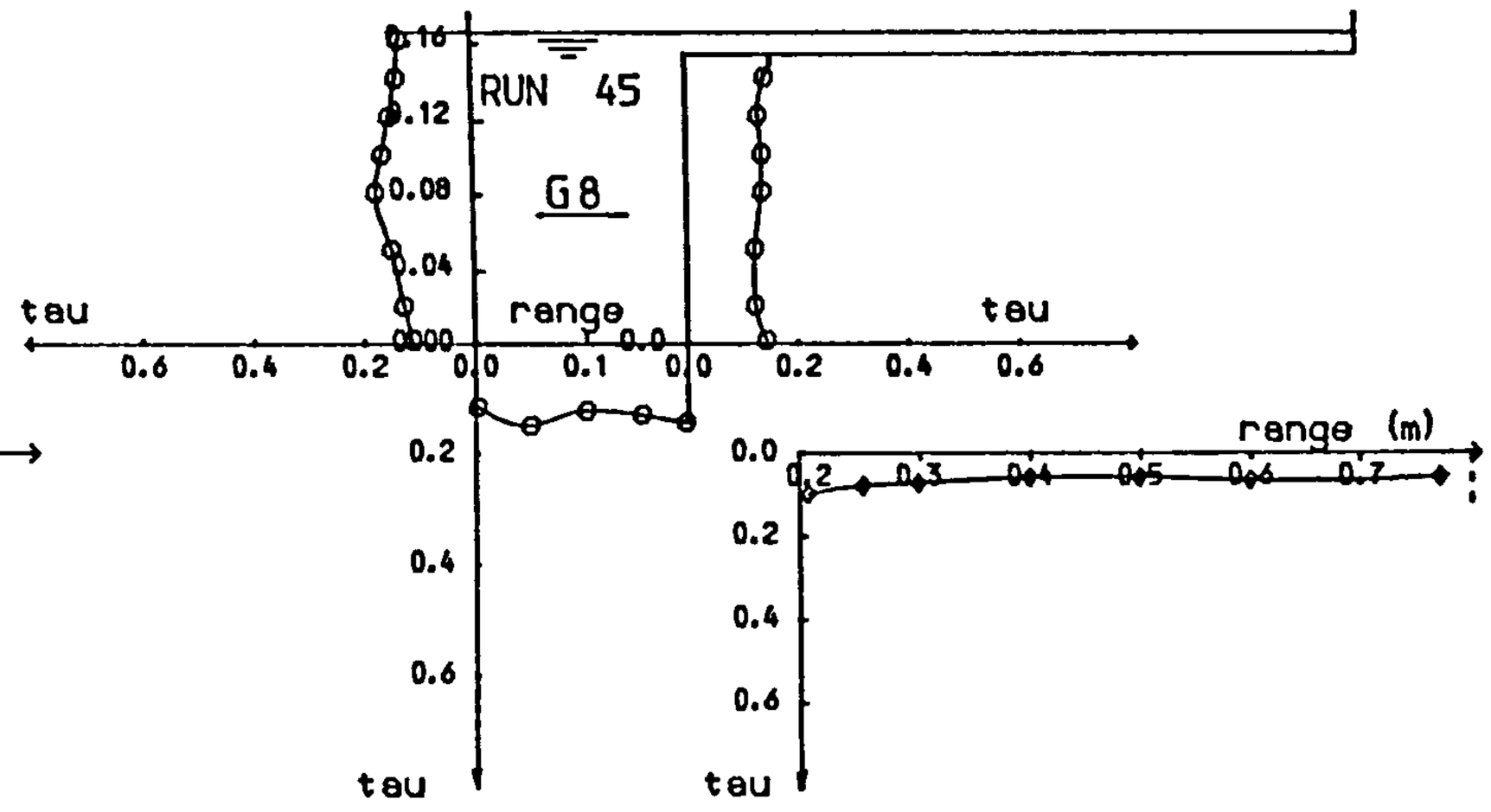

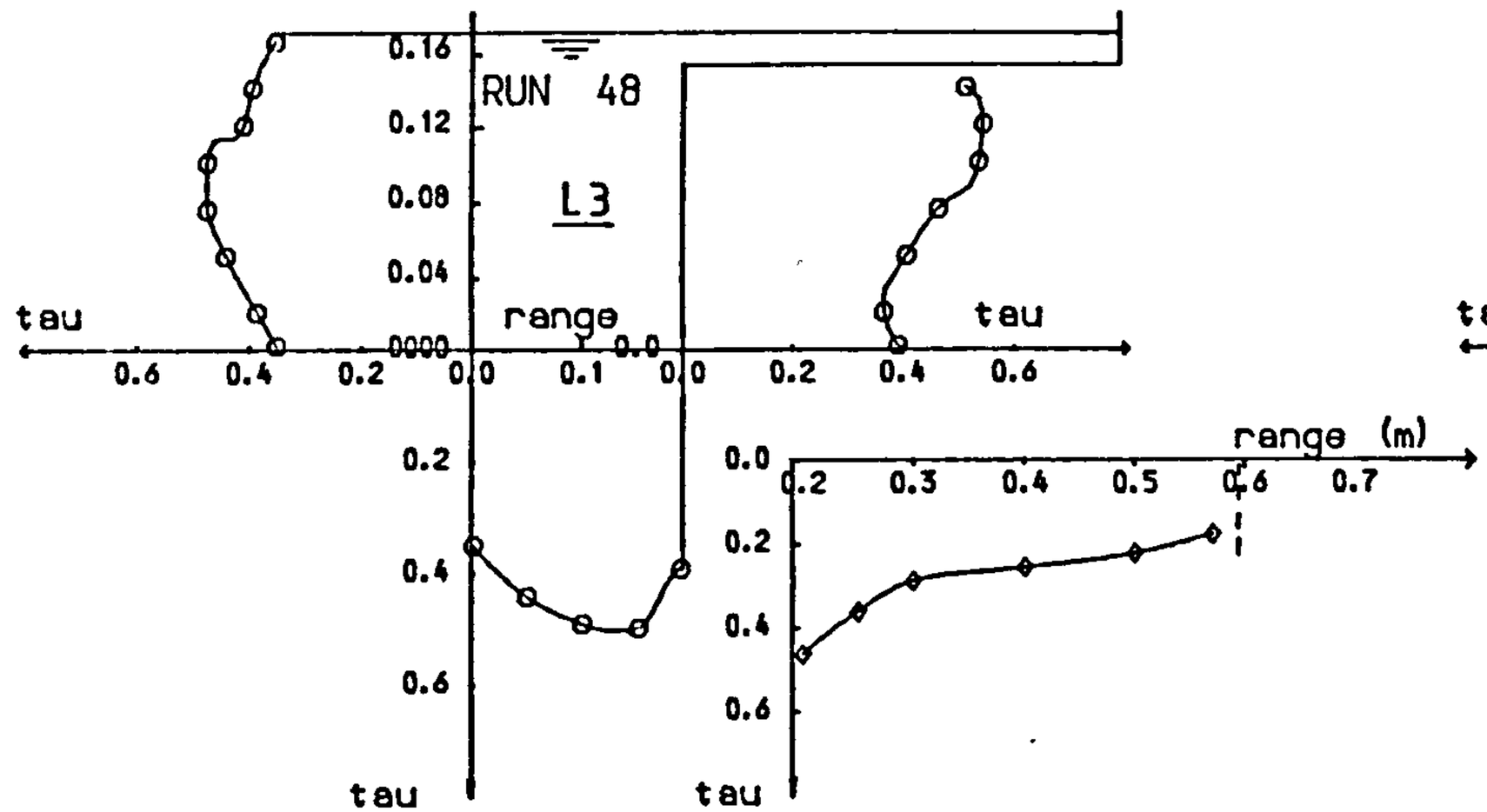

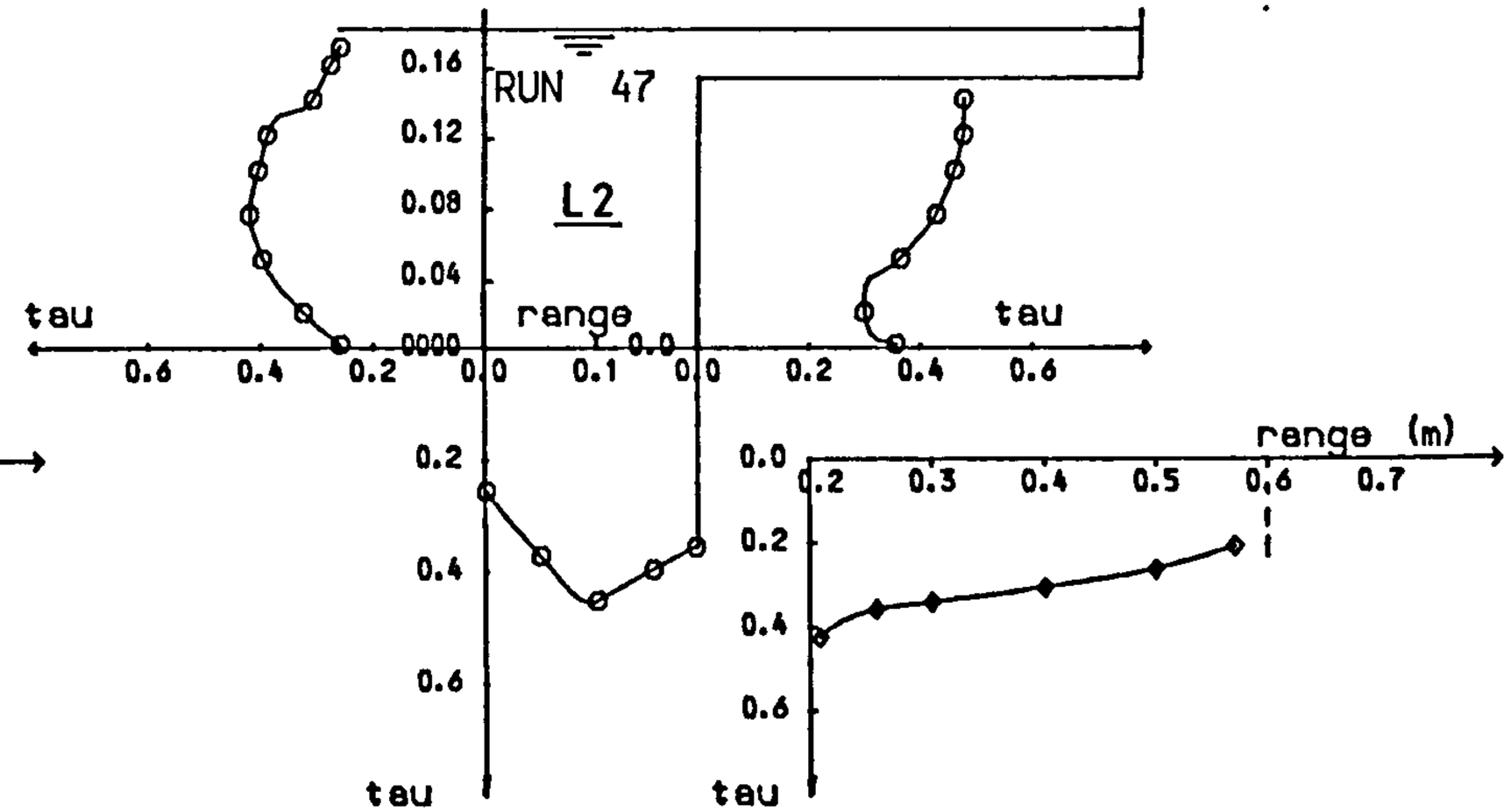

Fig 5·4 Shear stress distribution in channel and flood plain.

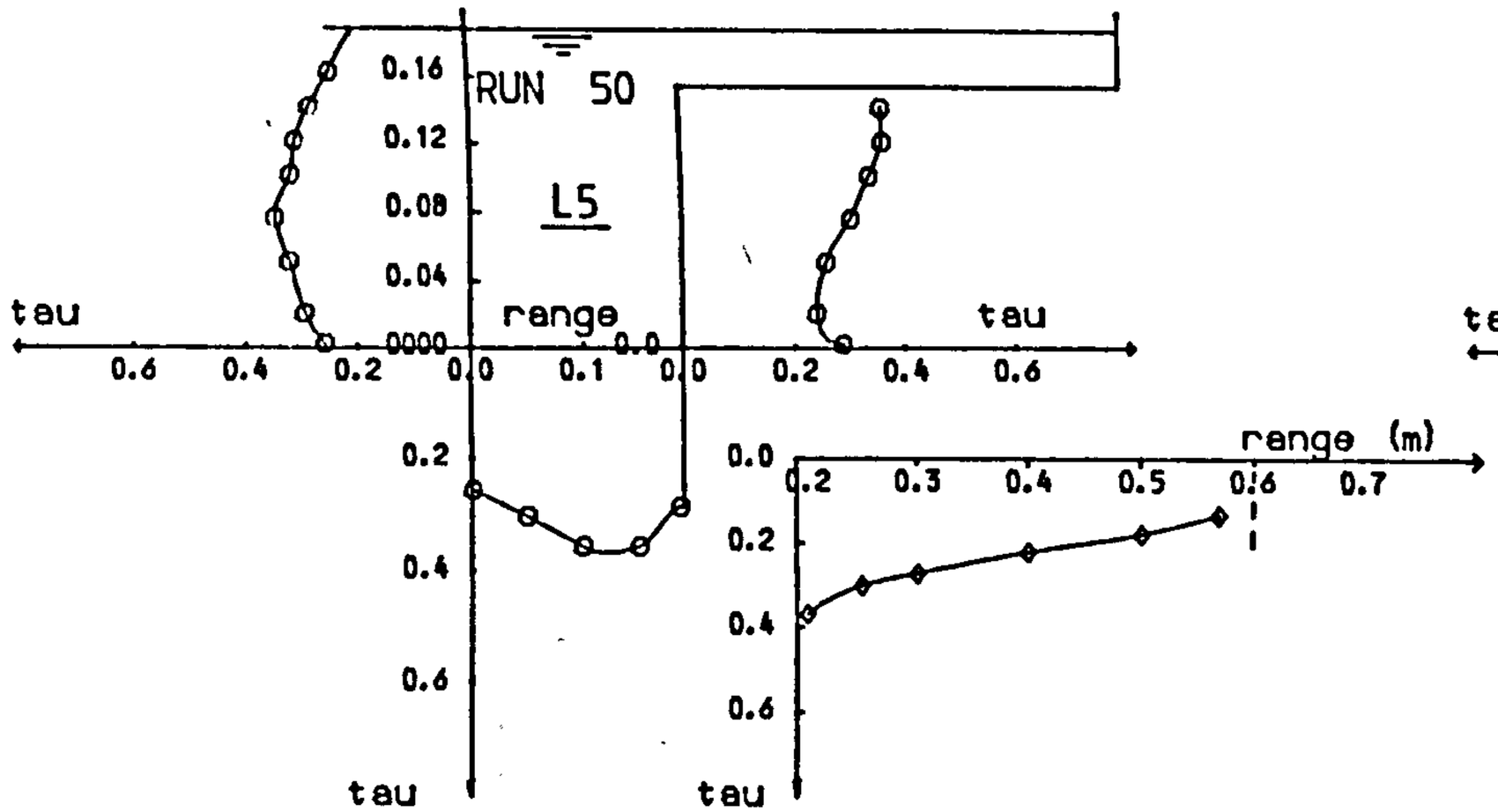

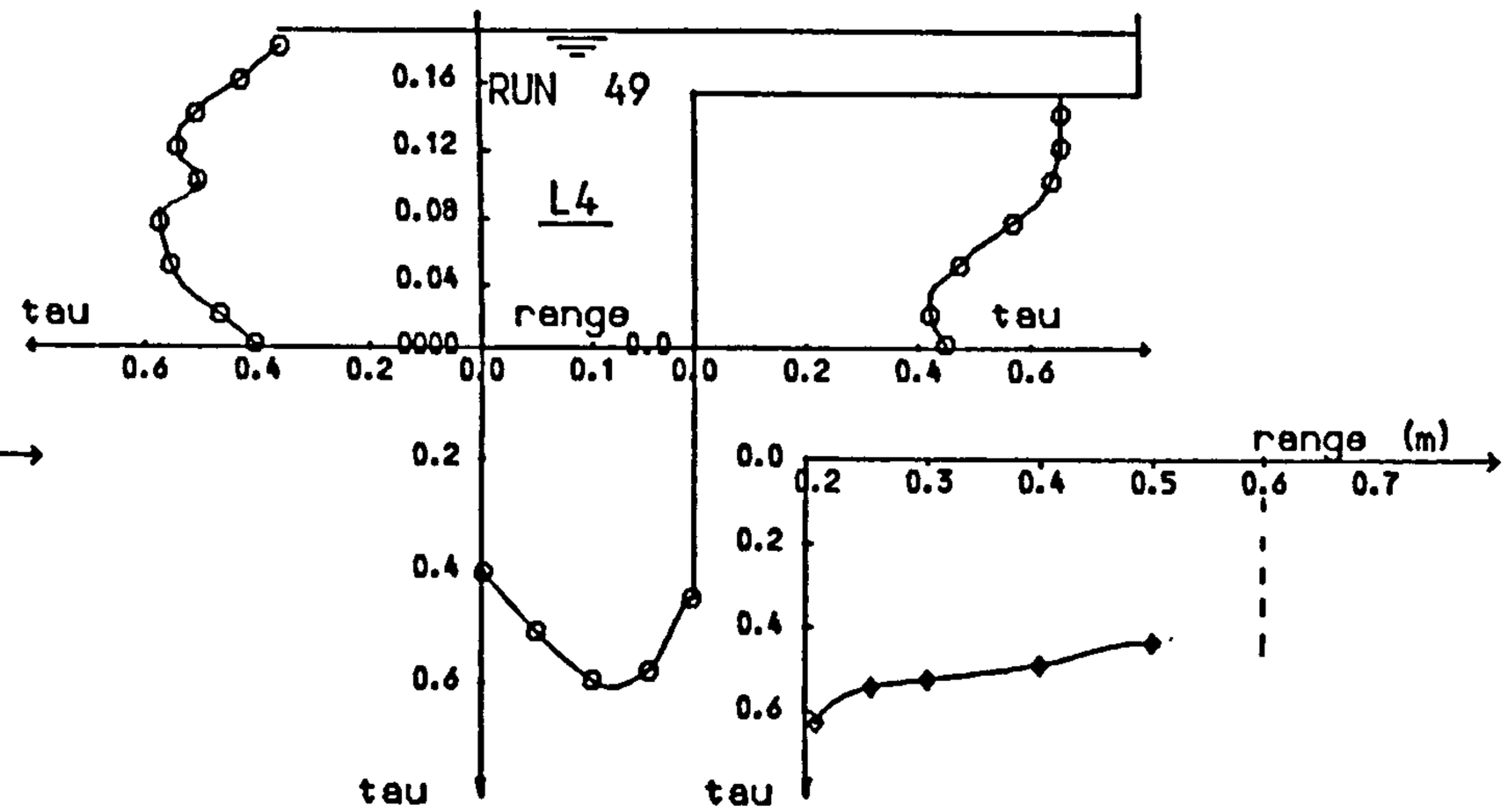

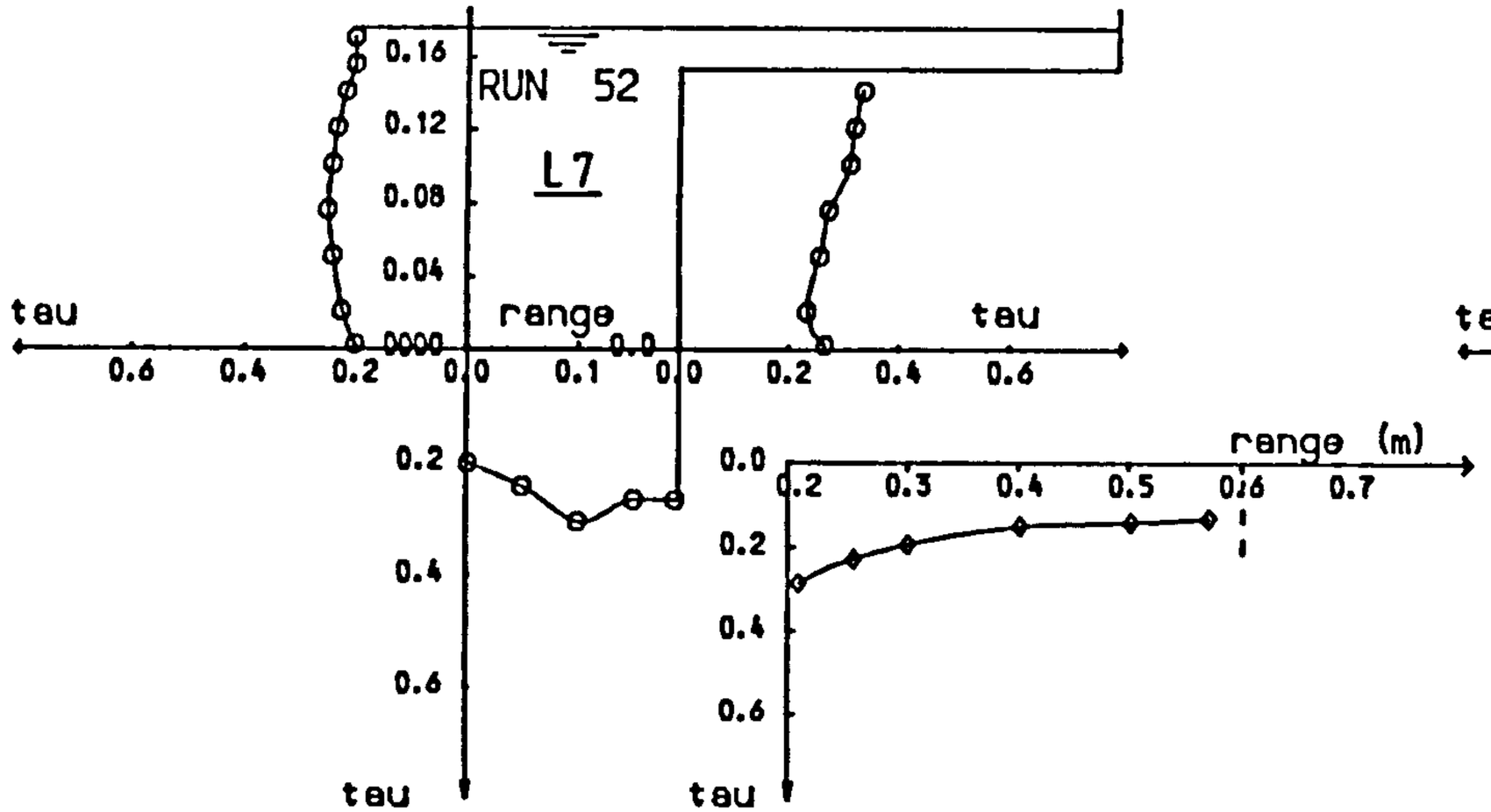

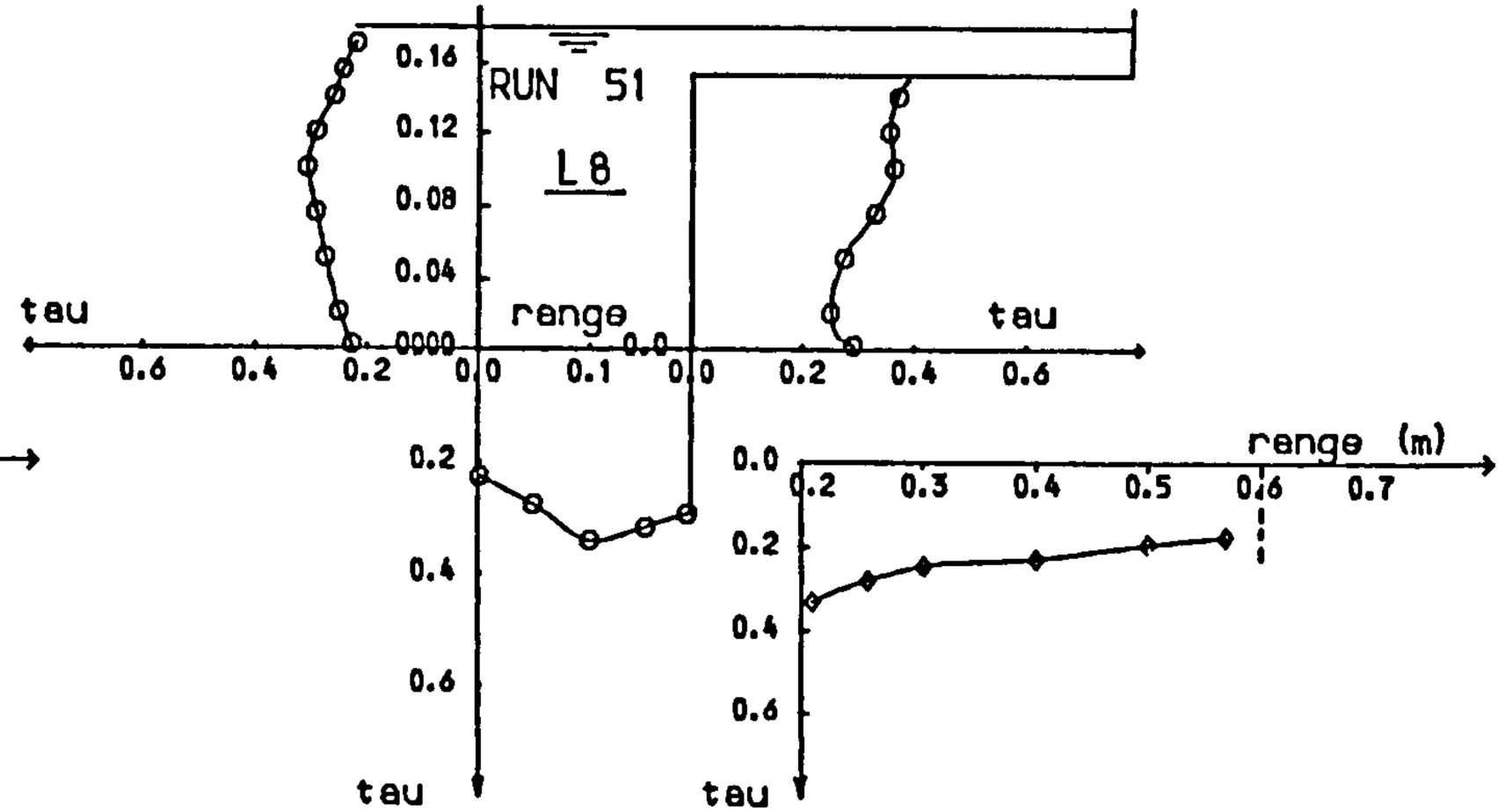

Fig 5·4 Shear stress distribution in channel and flood plain.

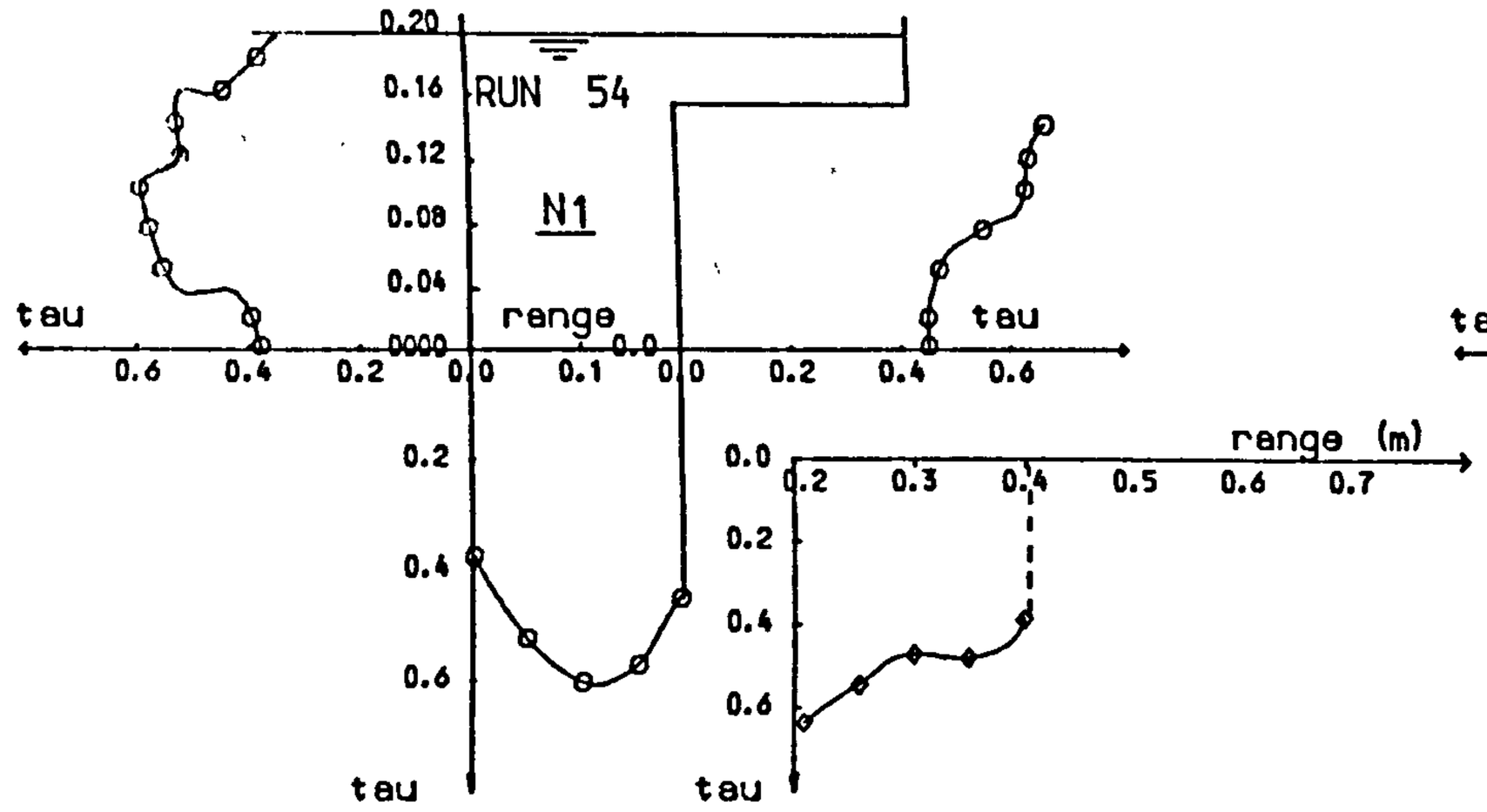

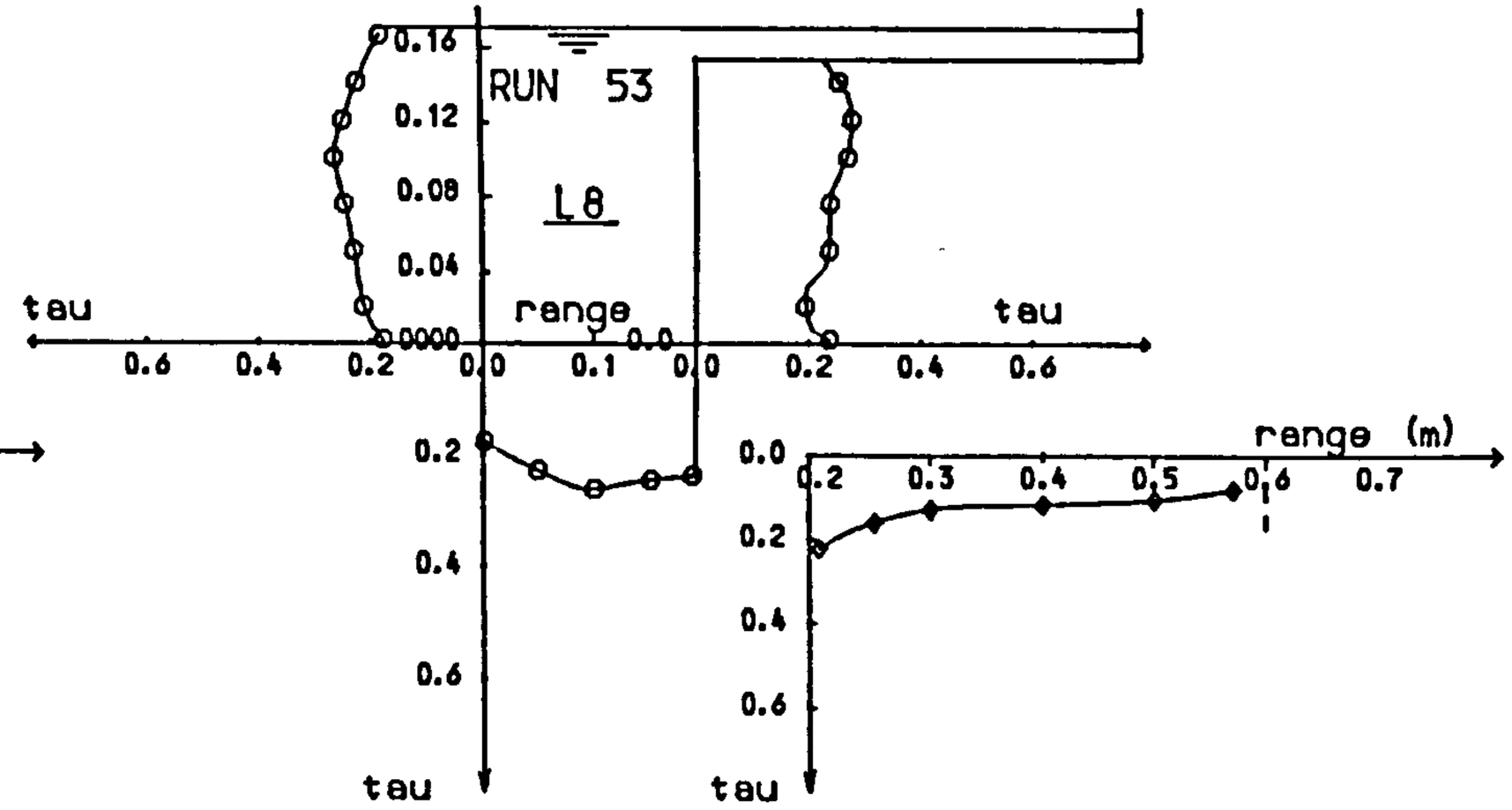

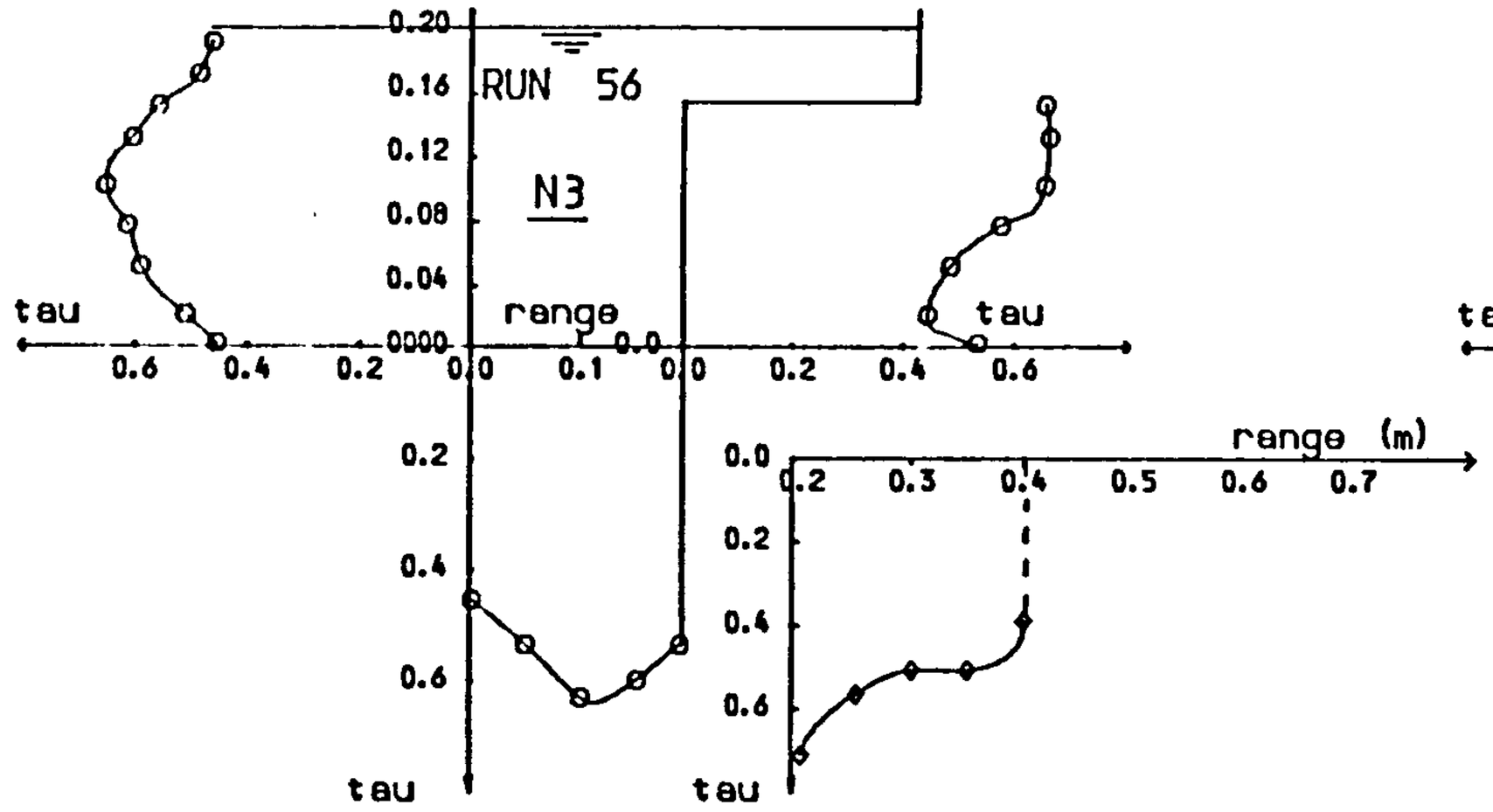

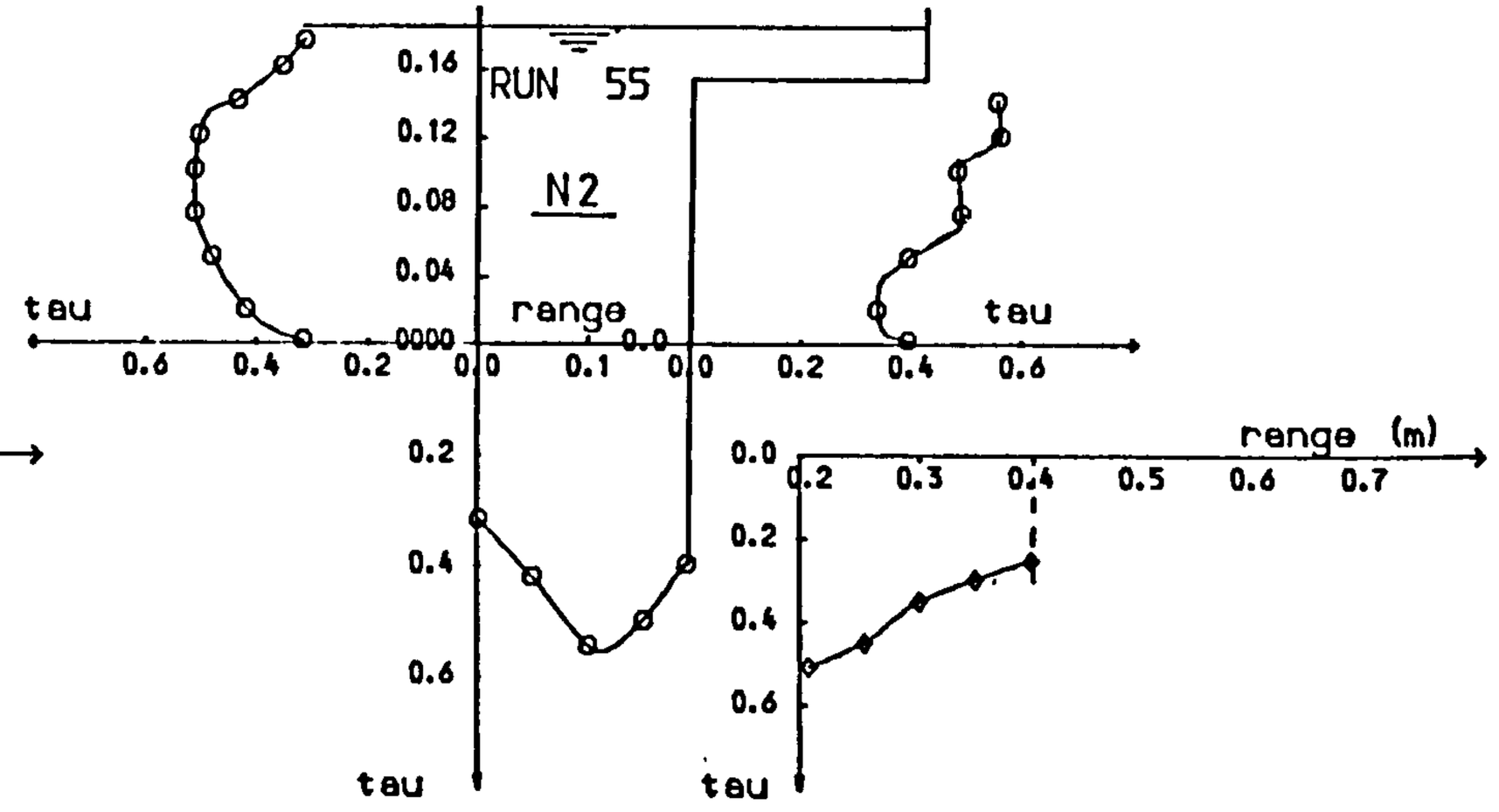

Fig 5·4 Shear stress distribution in channel and flood plain.

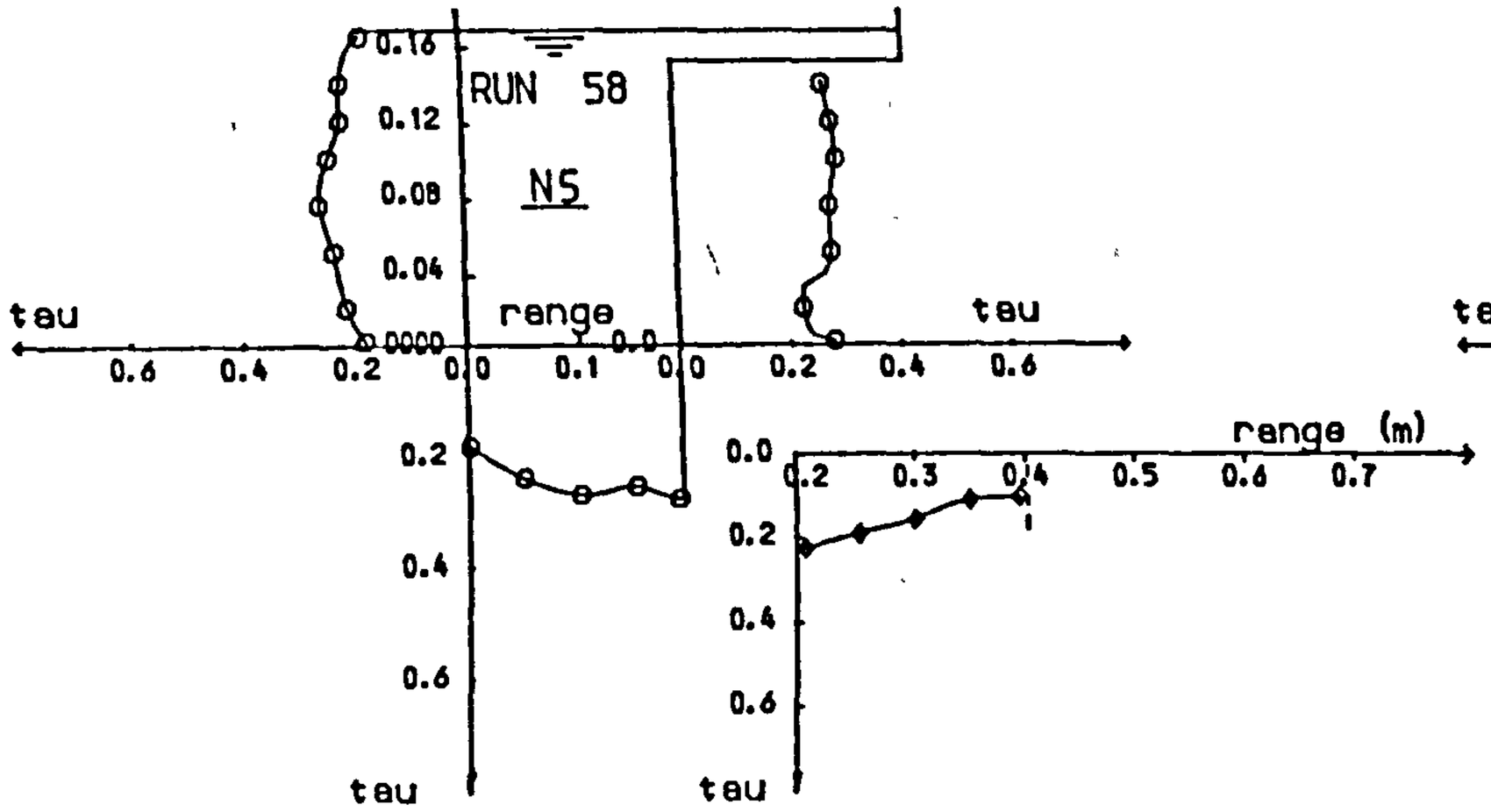

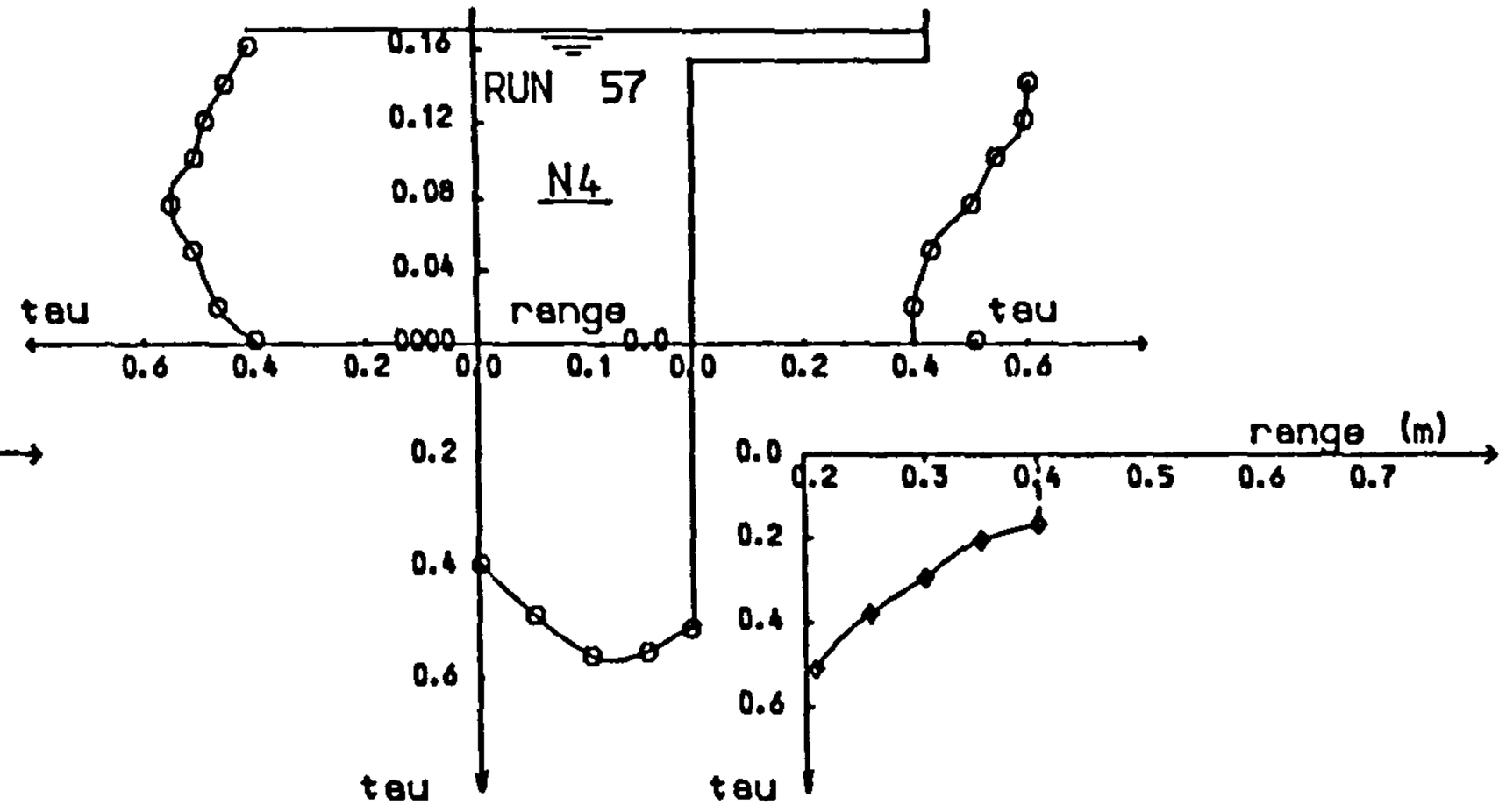

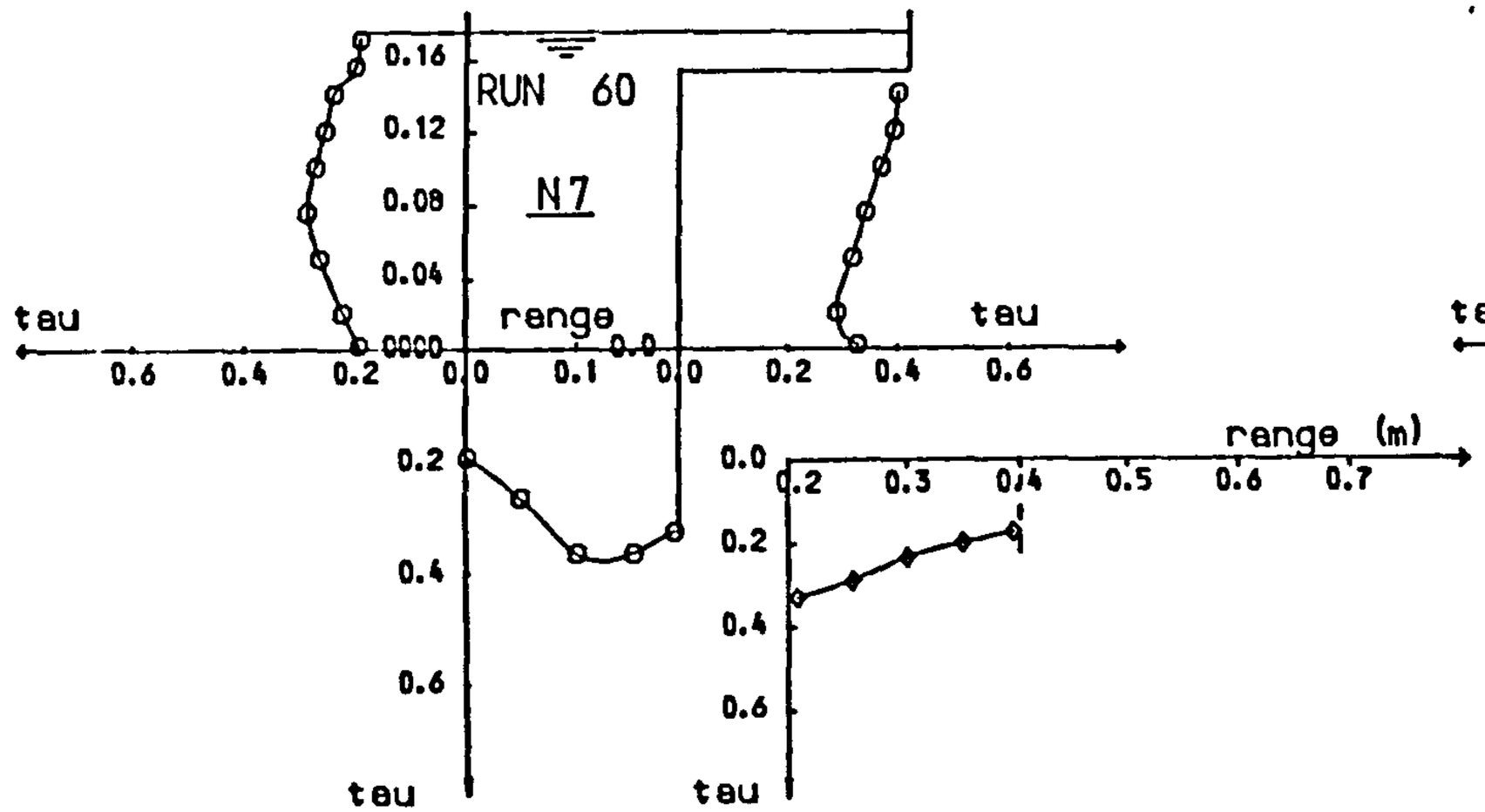

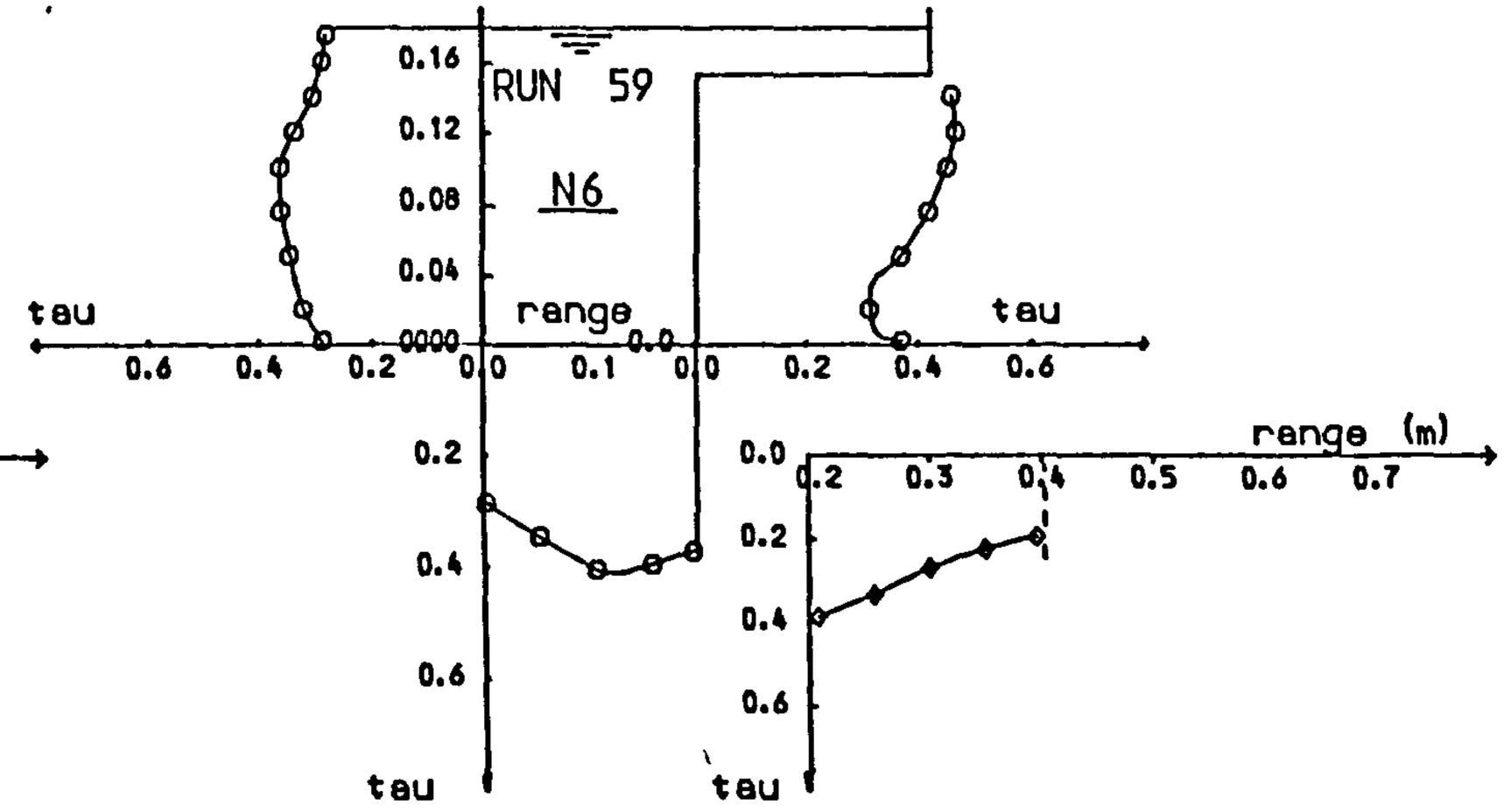

Fig 5·4 Shear stress distribution in channel and flood plain.

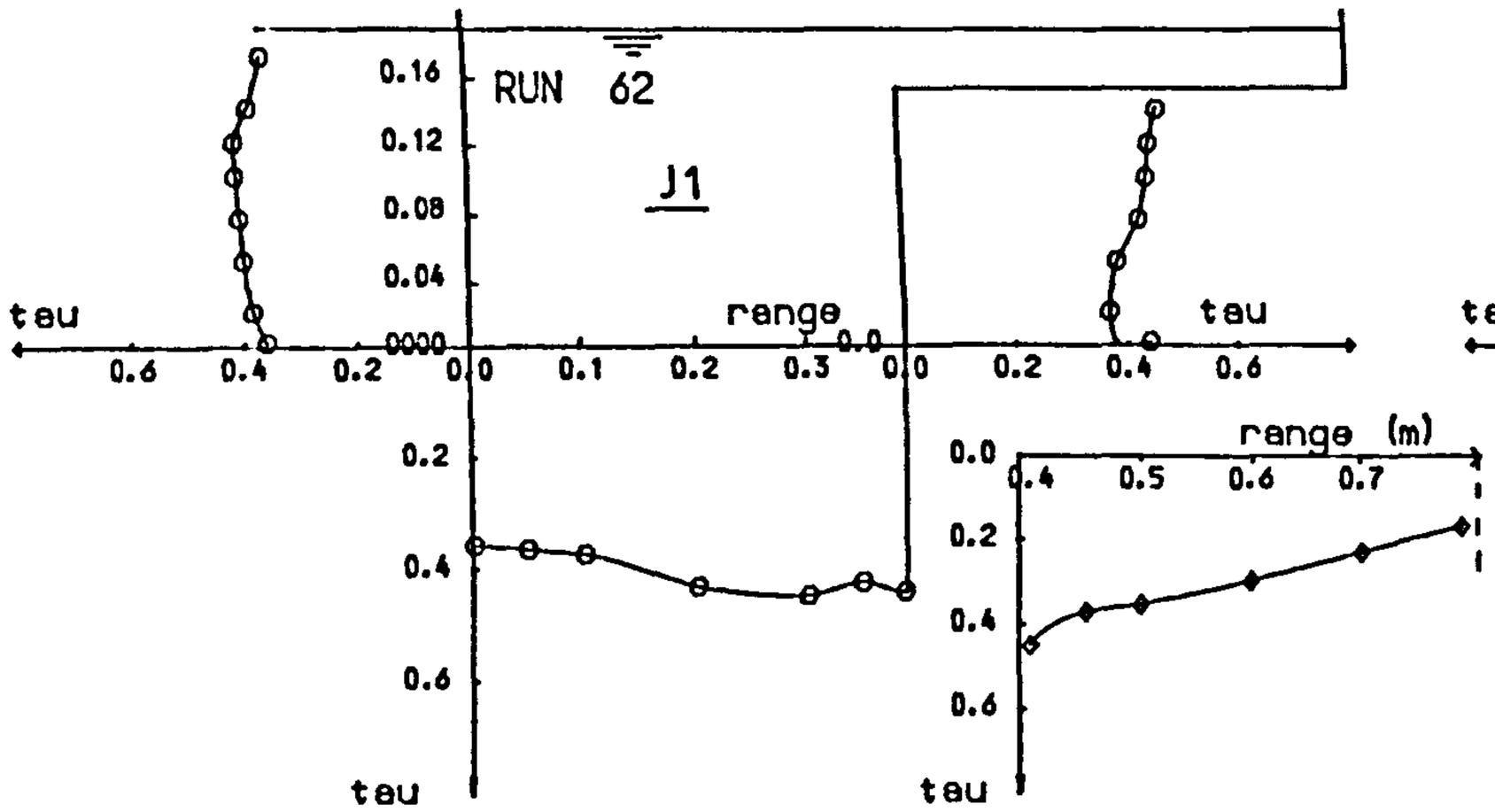

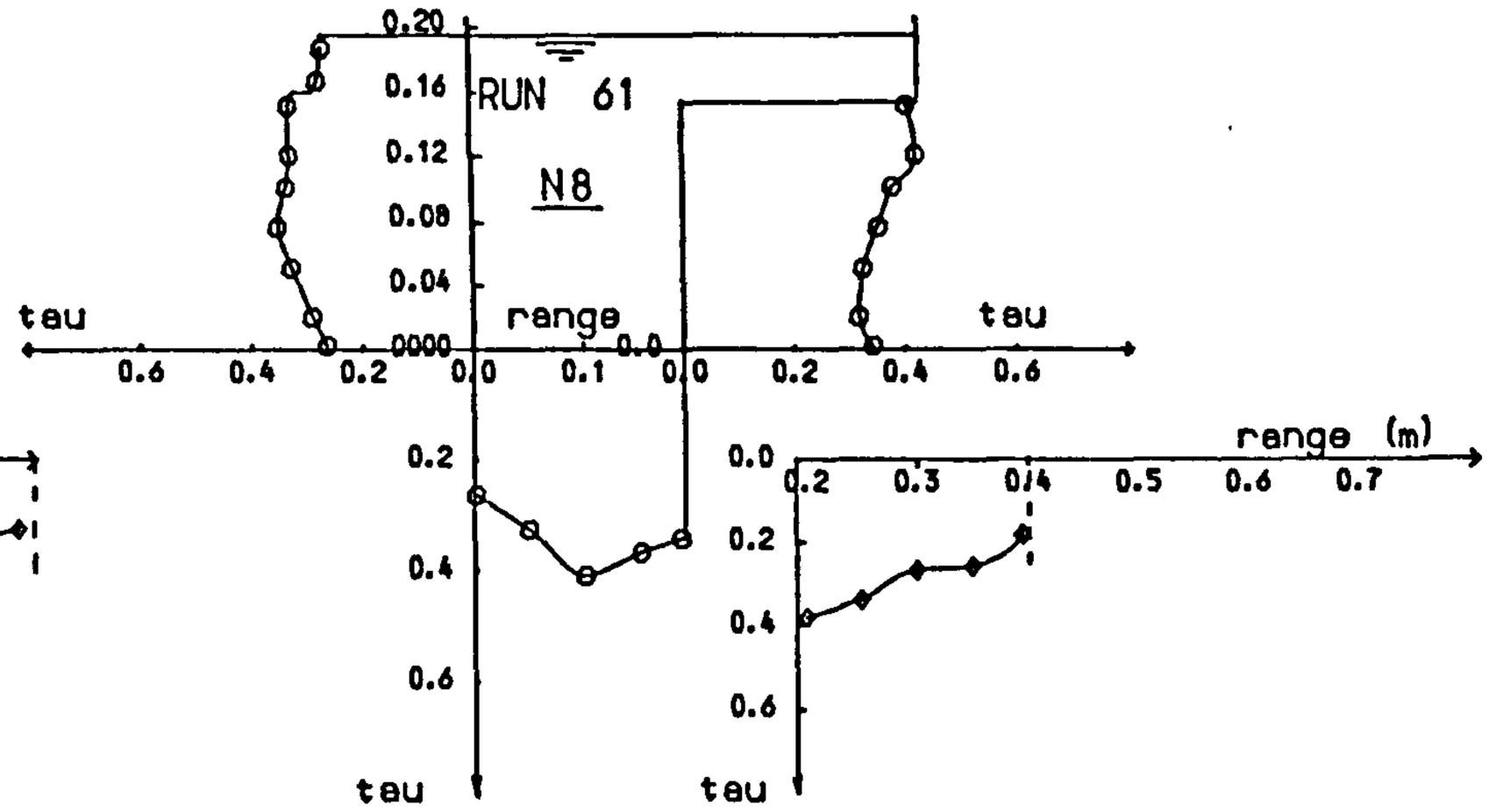

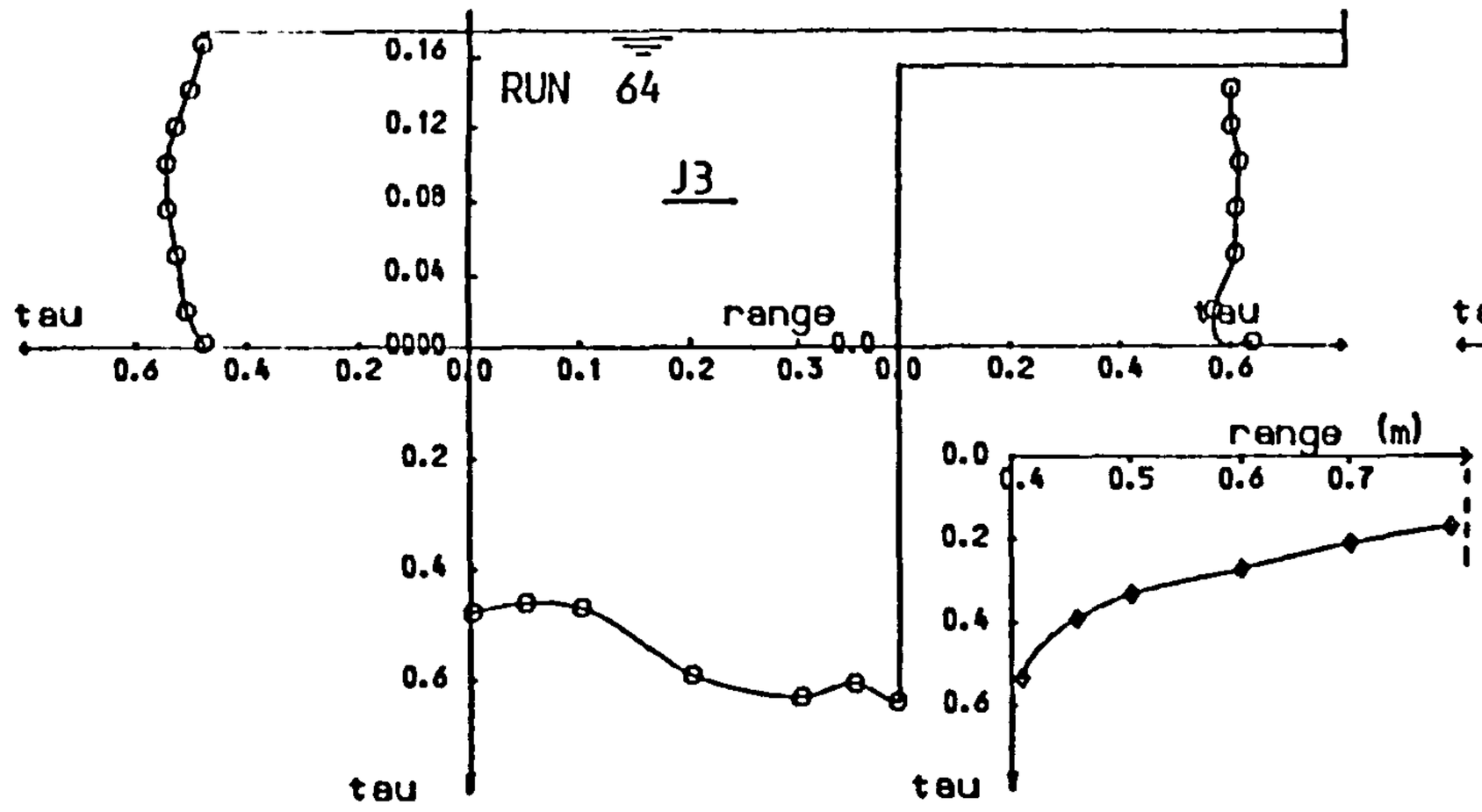

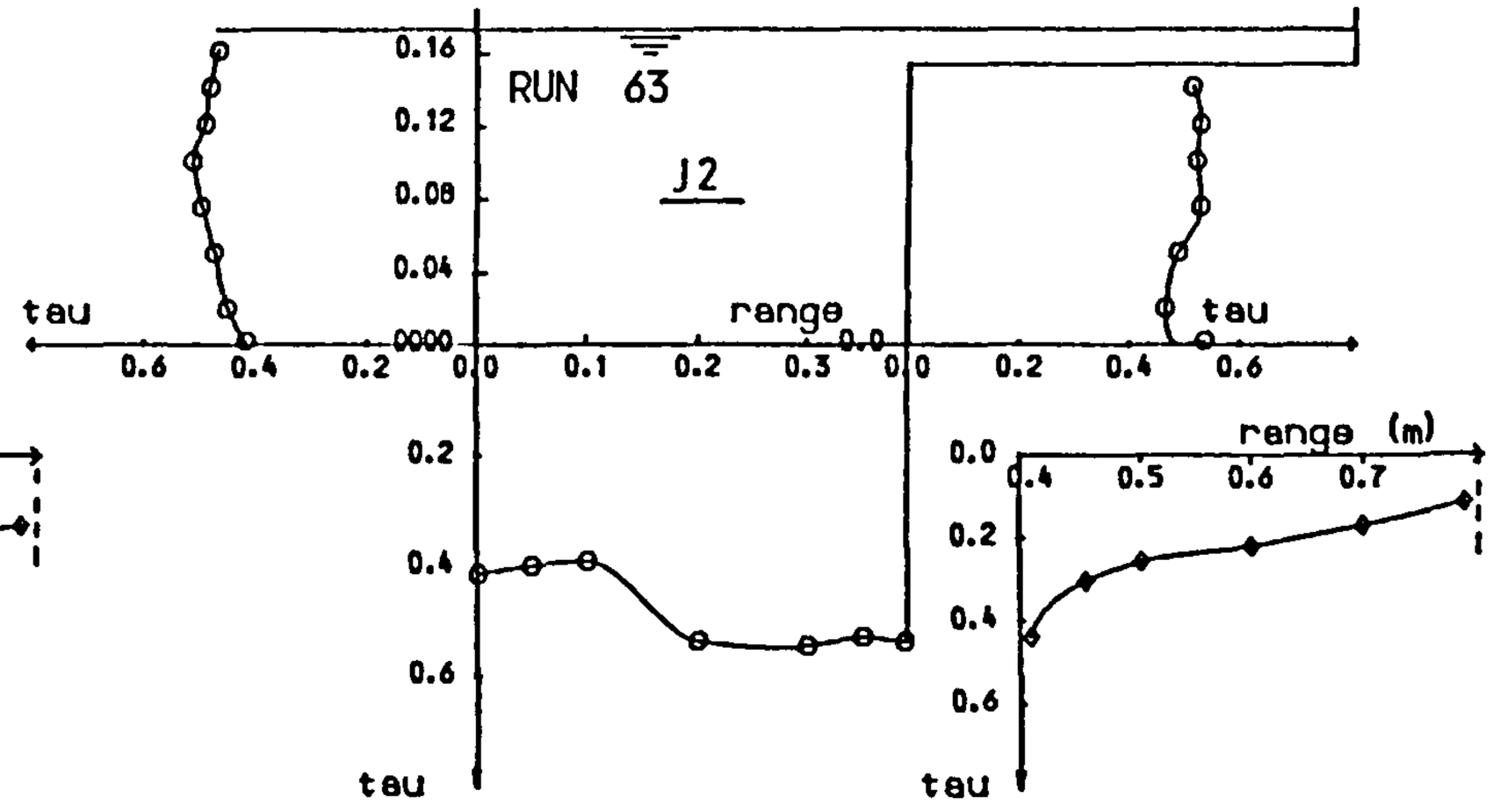

Fig 5·4 Shear stress distribution in channel and flood plain.

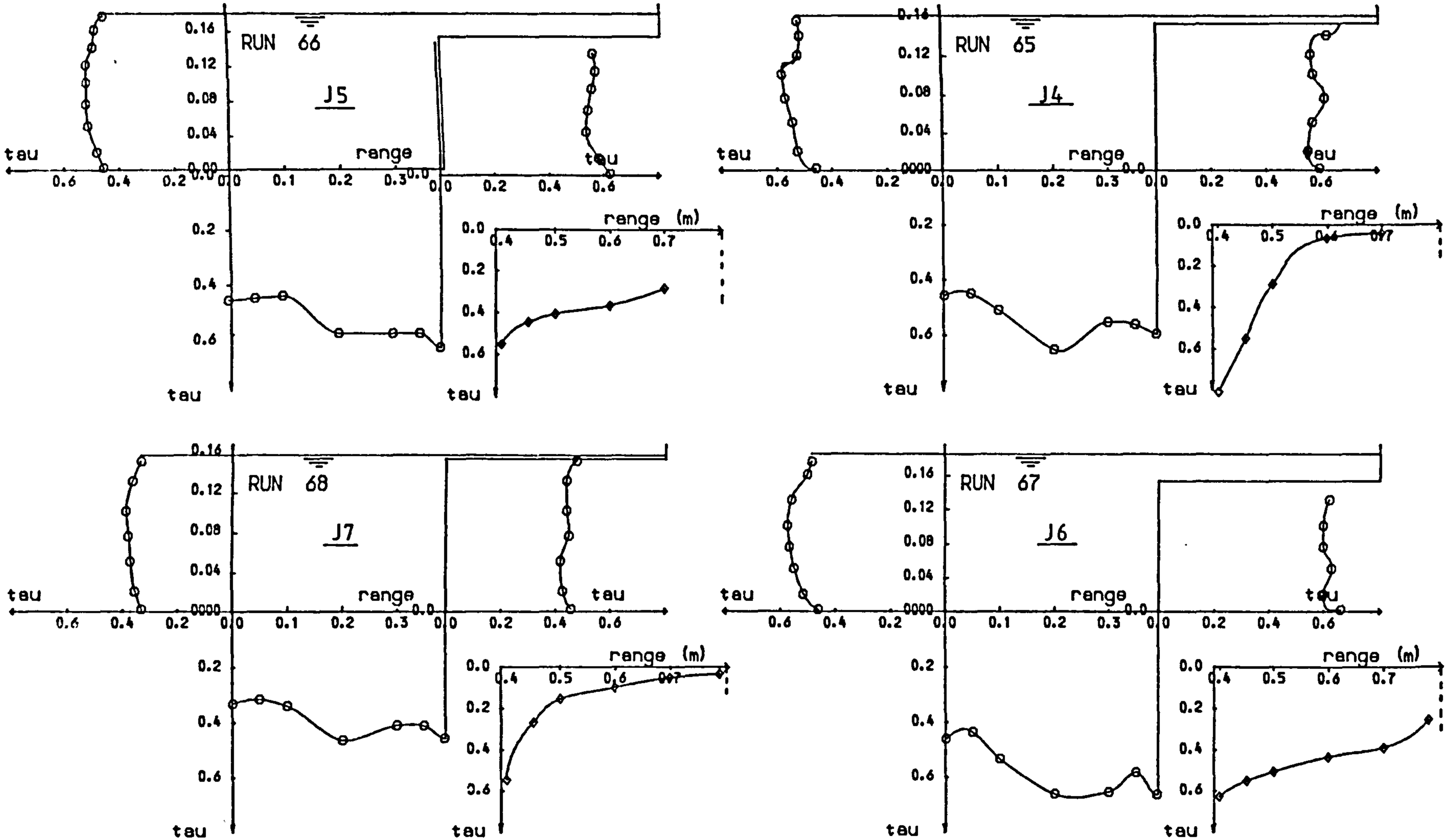

Fig 5·4 Shear stress distribution in channel and flood plain.

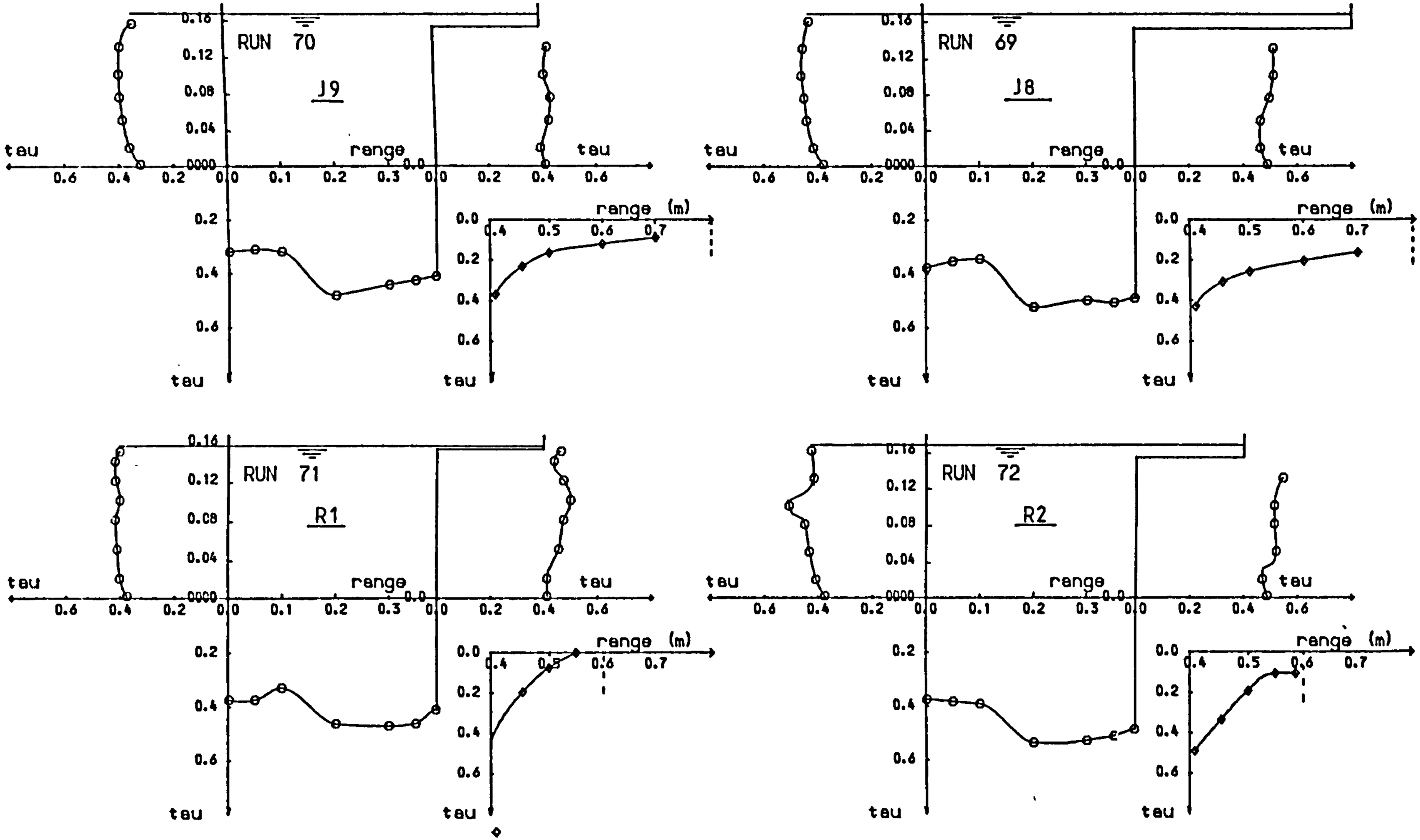

Fig 5·4 Shear stress distribution in channel and flood plain.

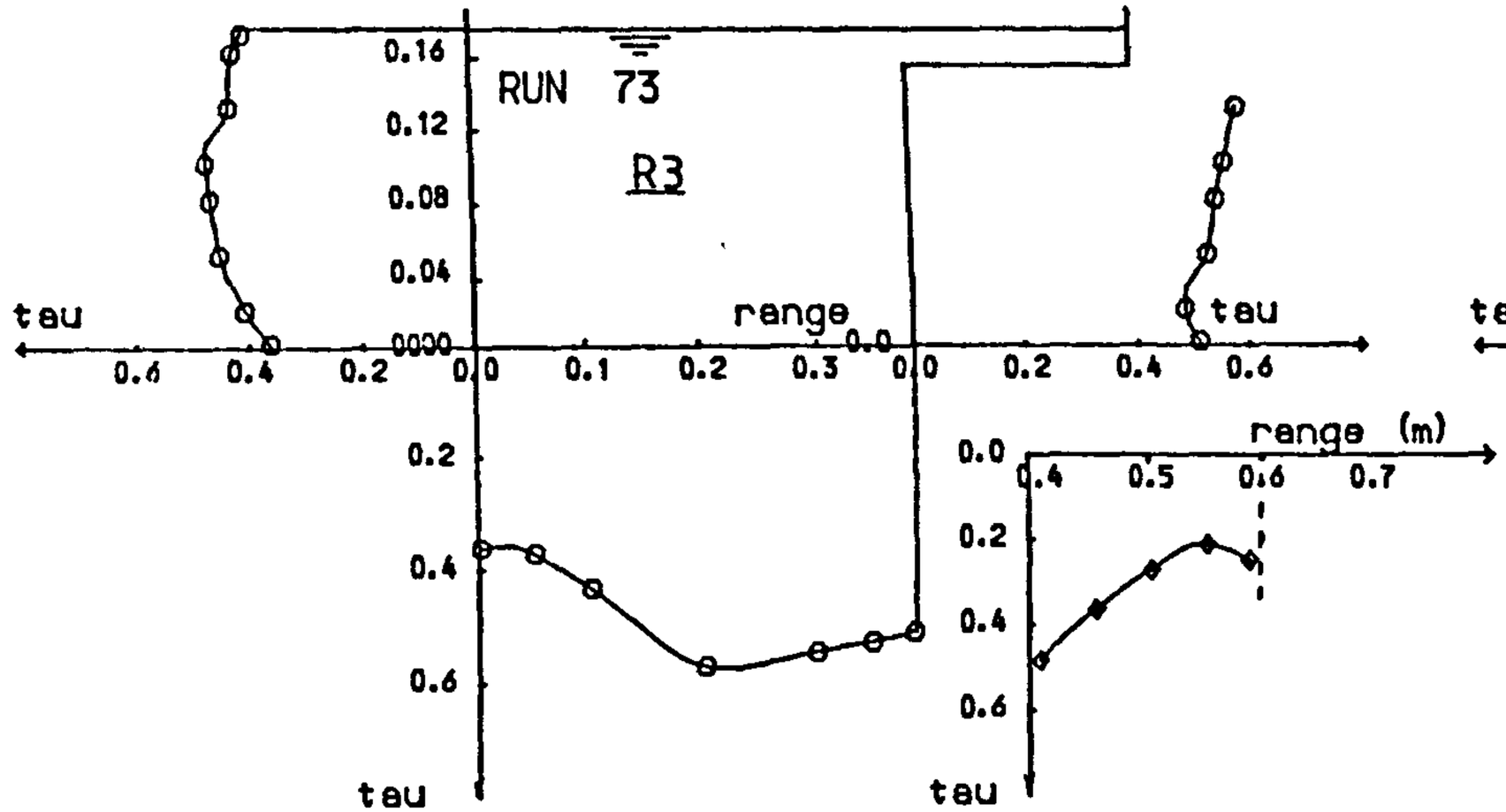

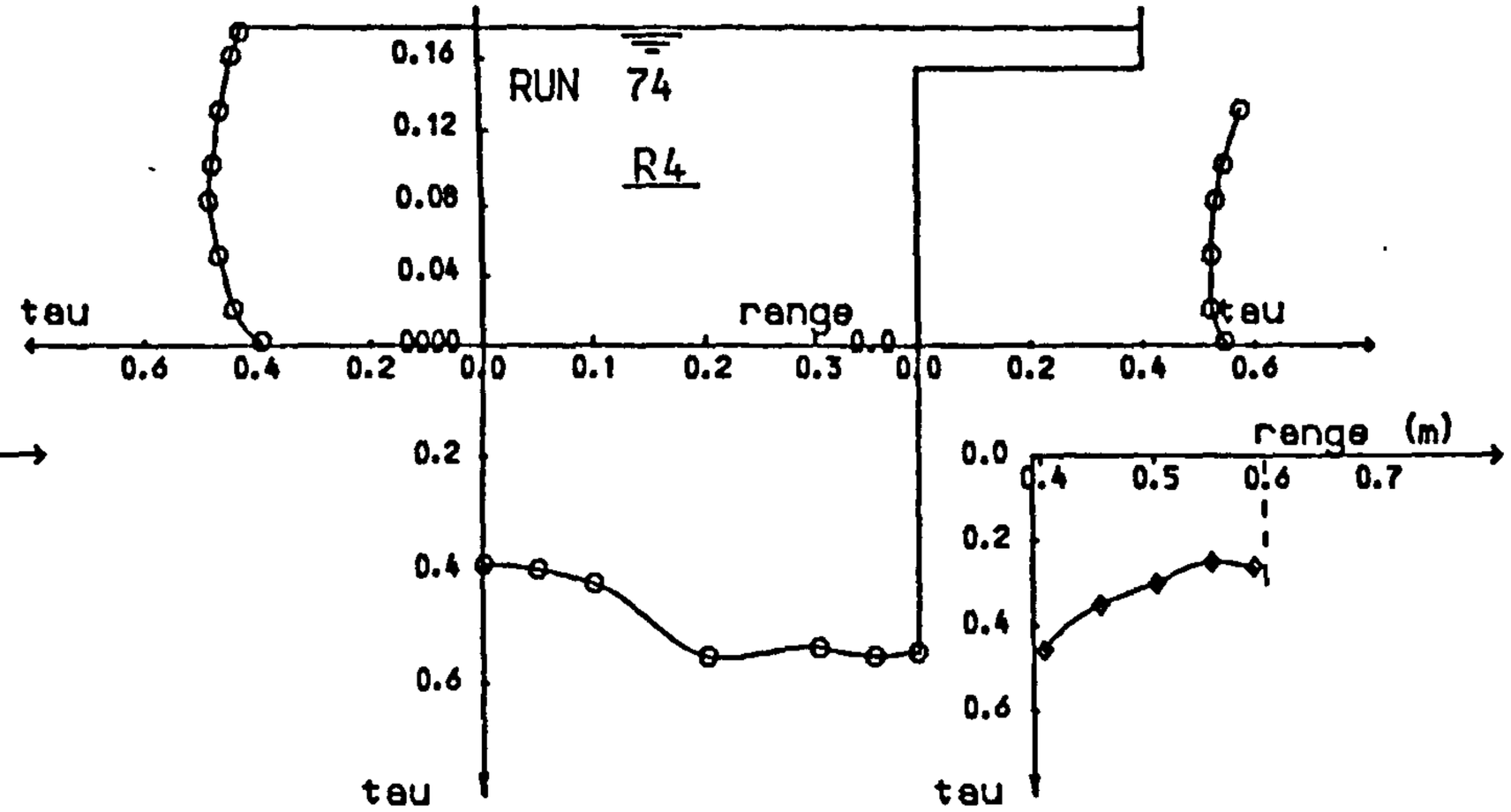

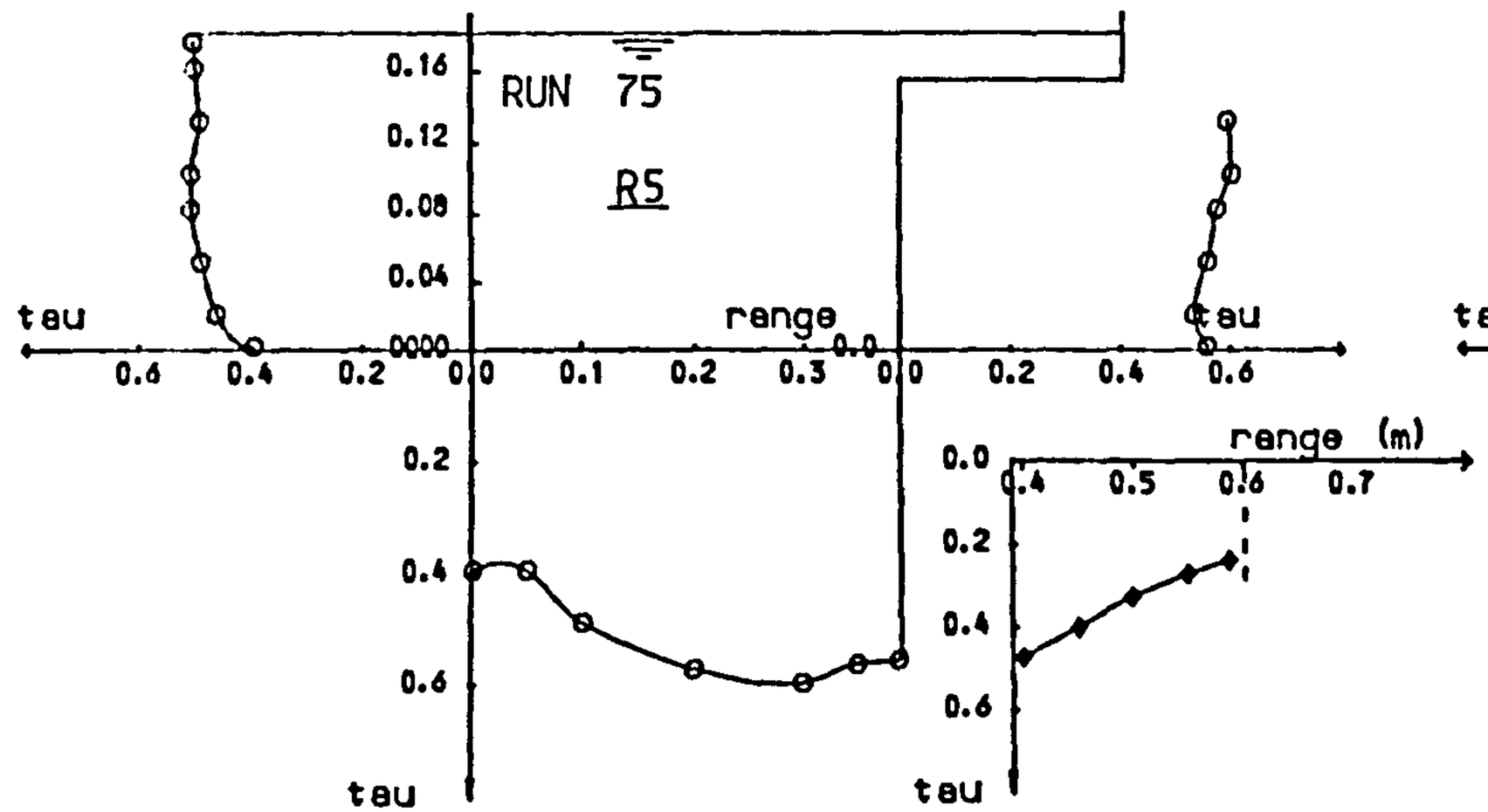

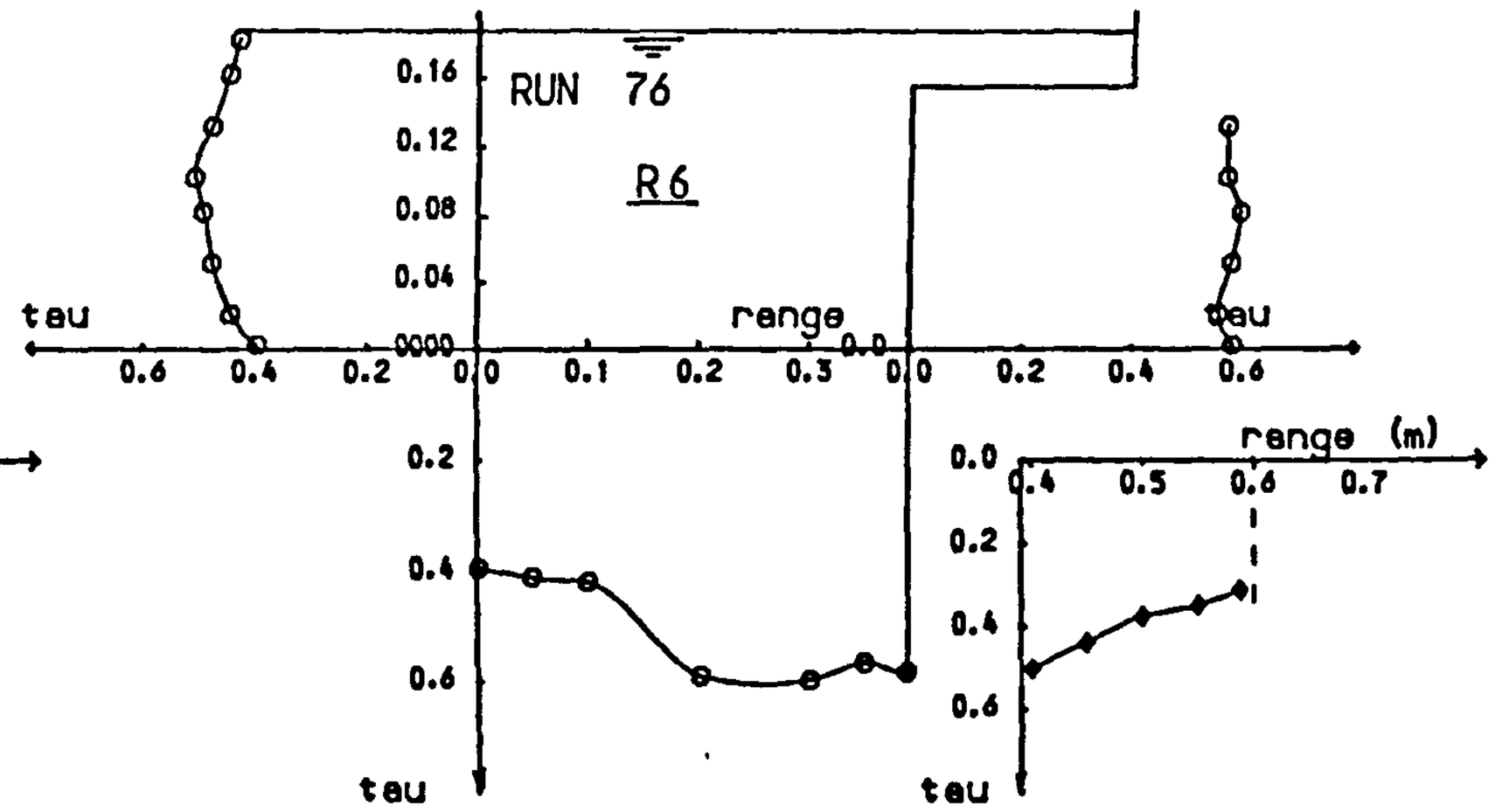

Fig 5·4 Shear stress distribution in channel and flood plain.

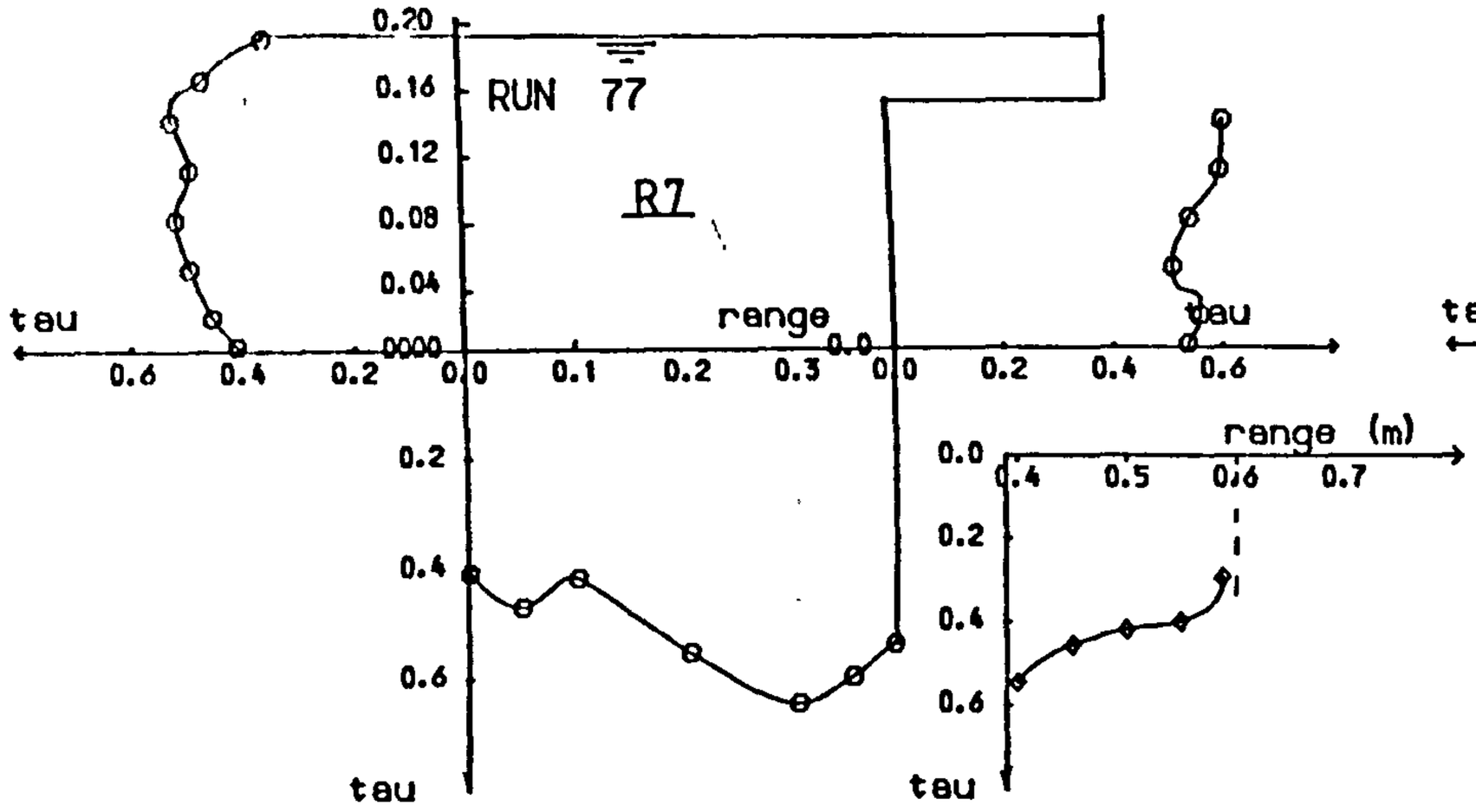

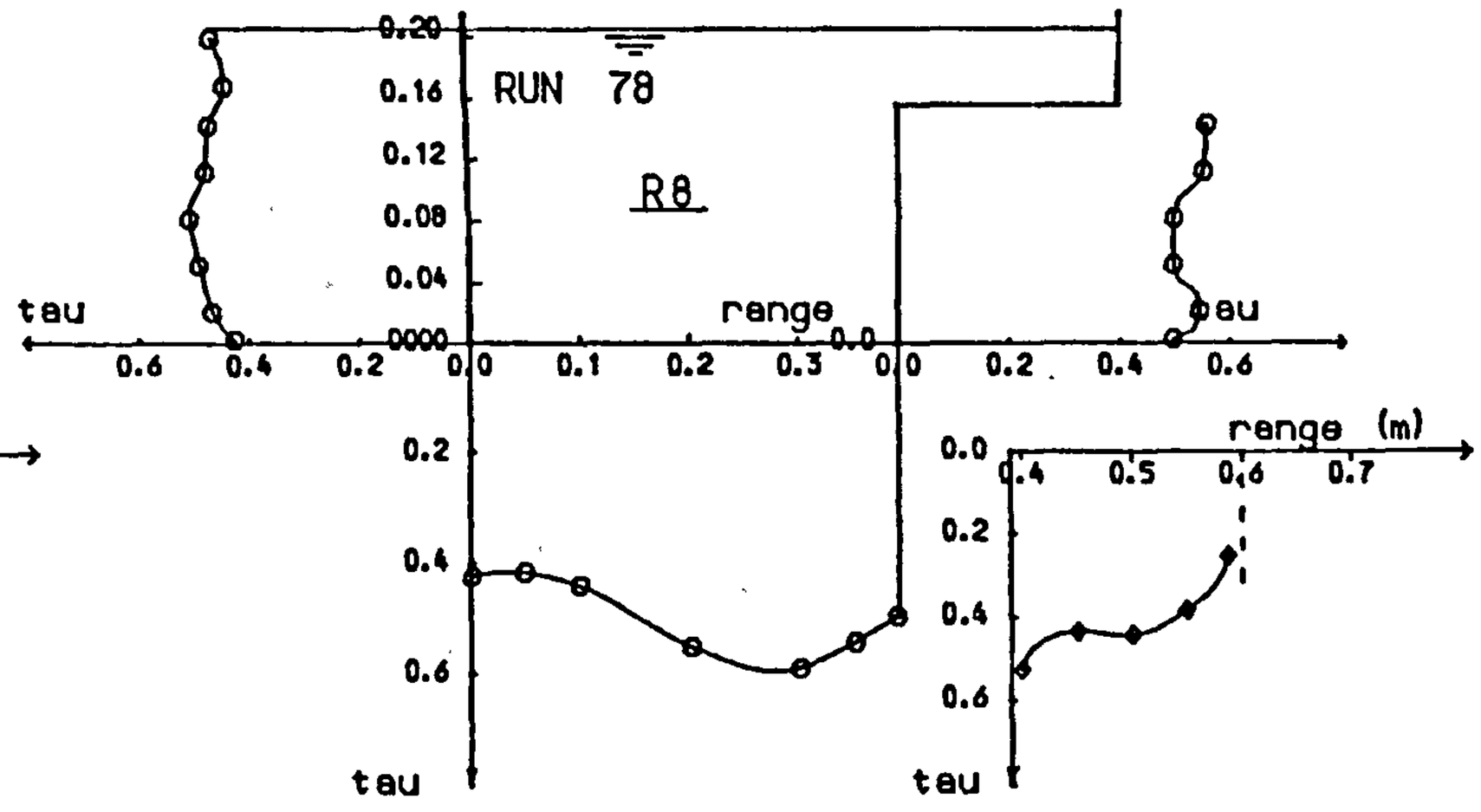

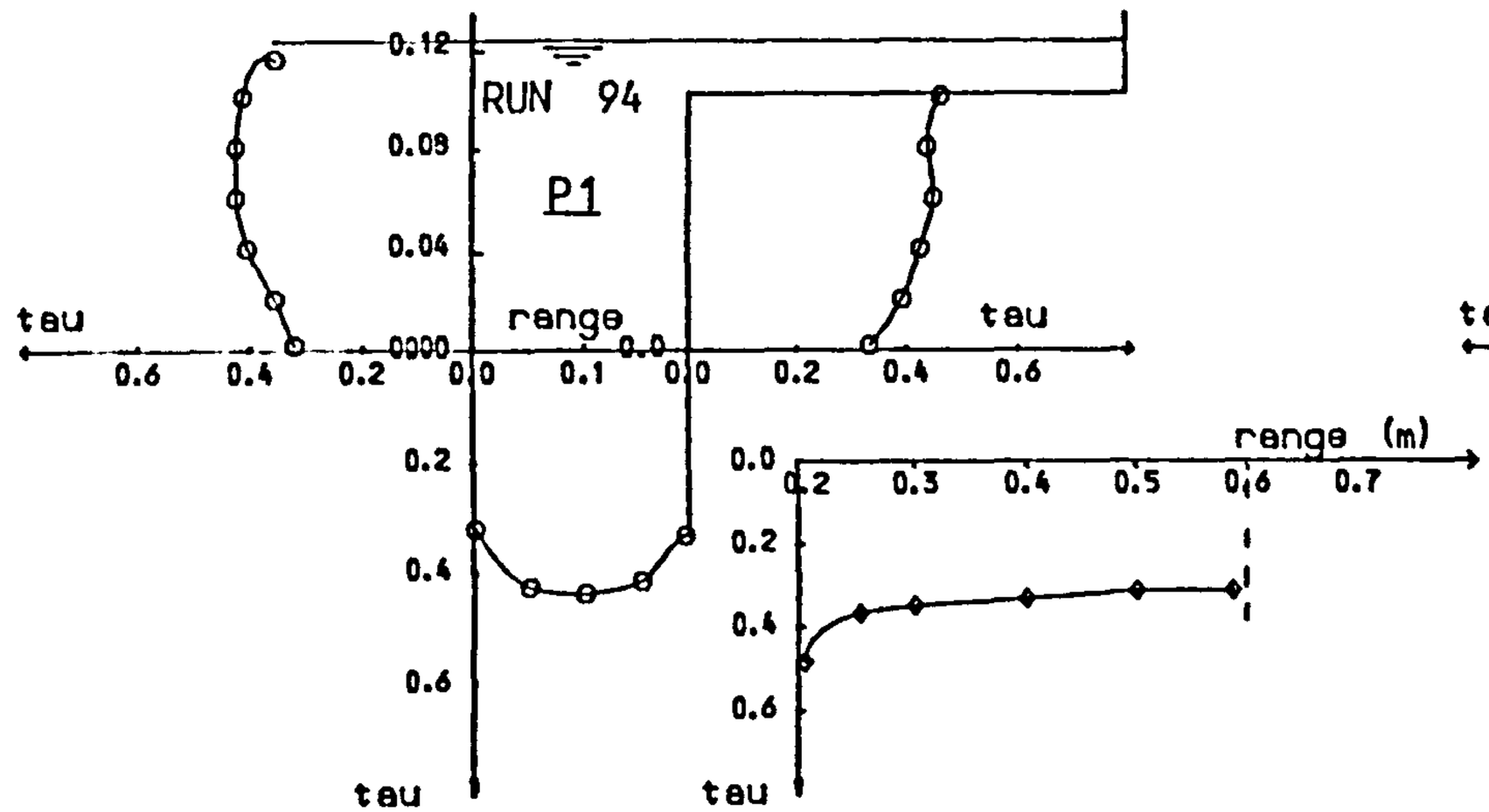

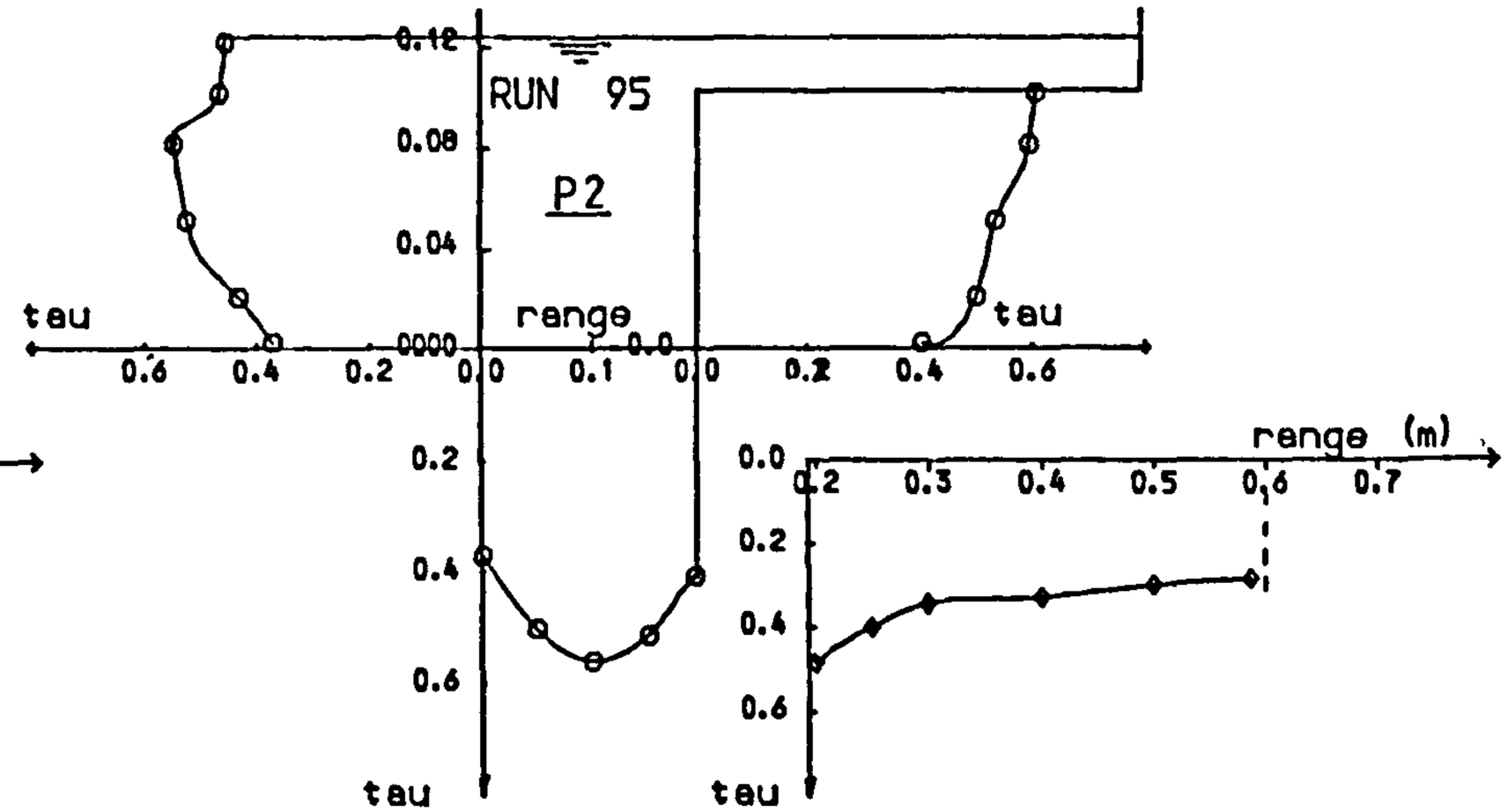

Fig 5·4 Shear stress distribution in channel and flood plain.

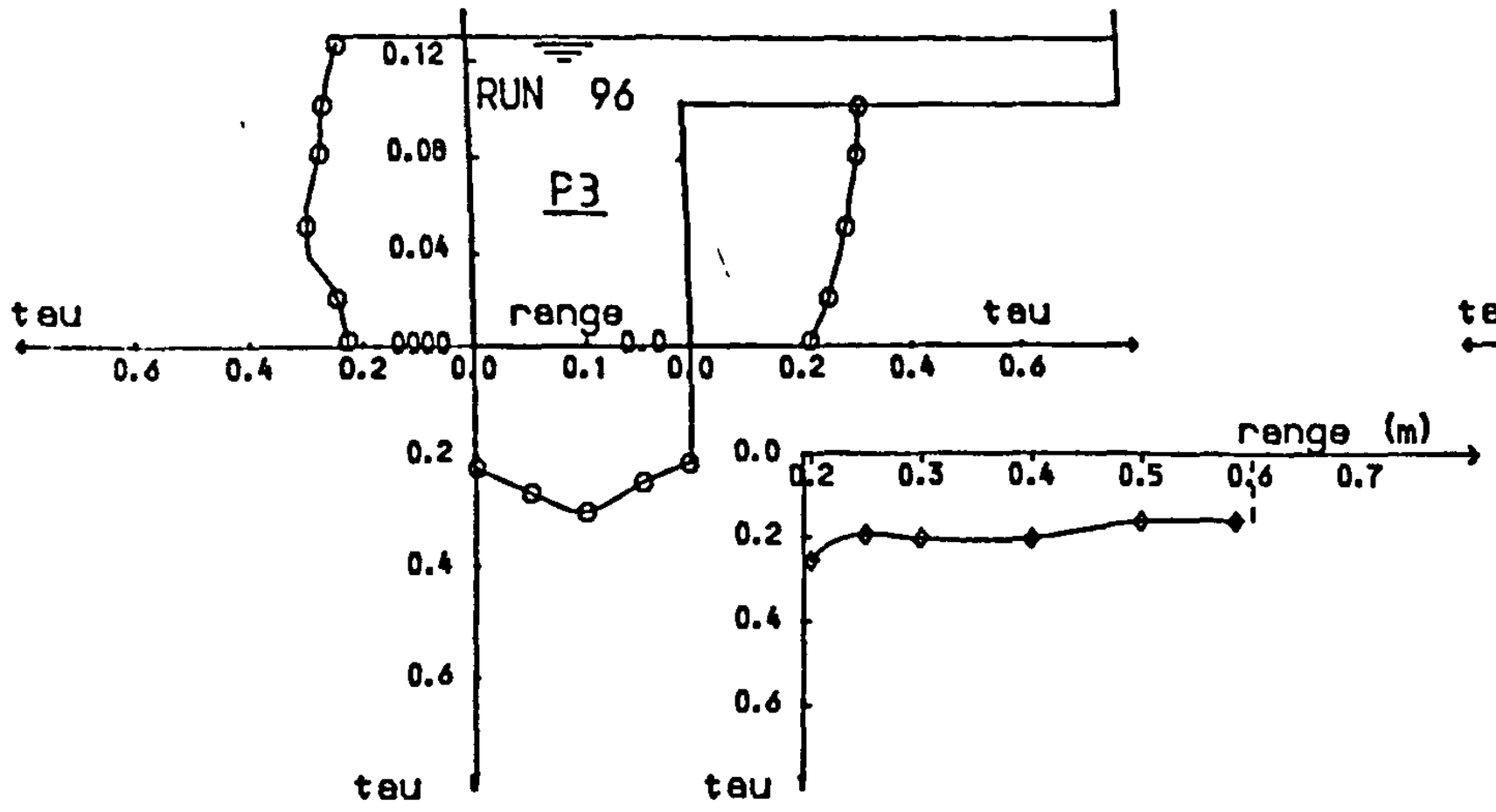

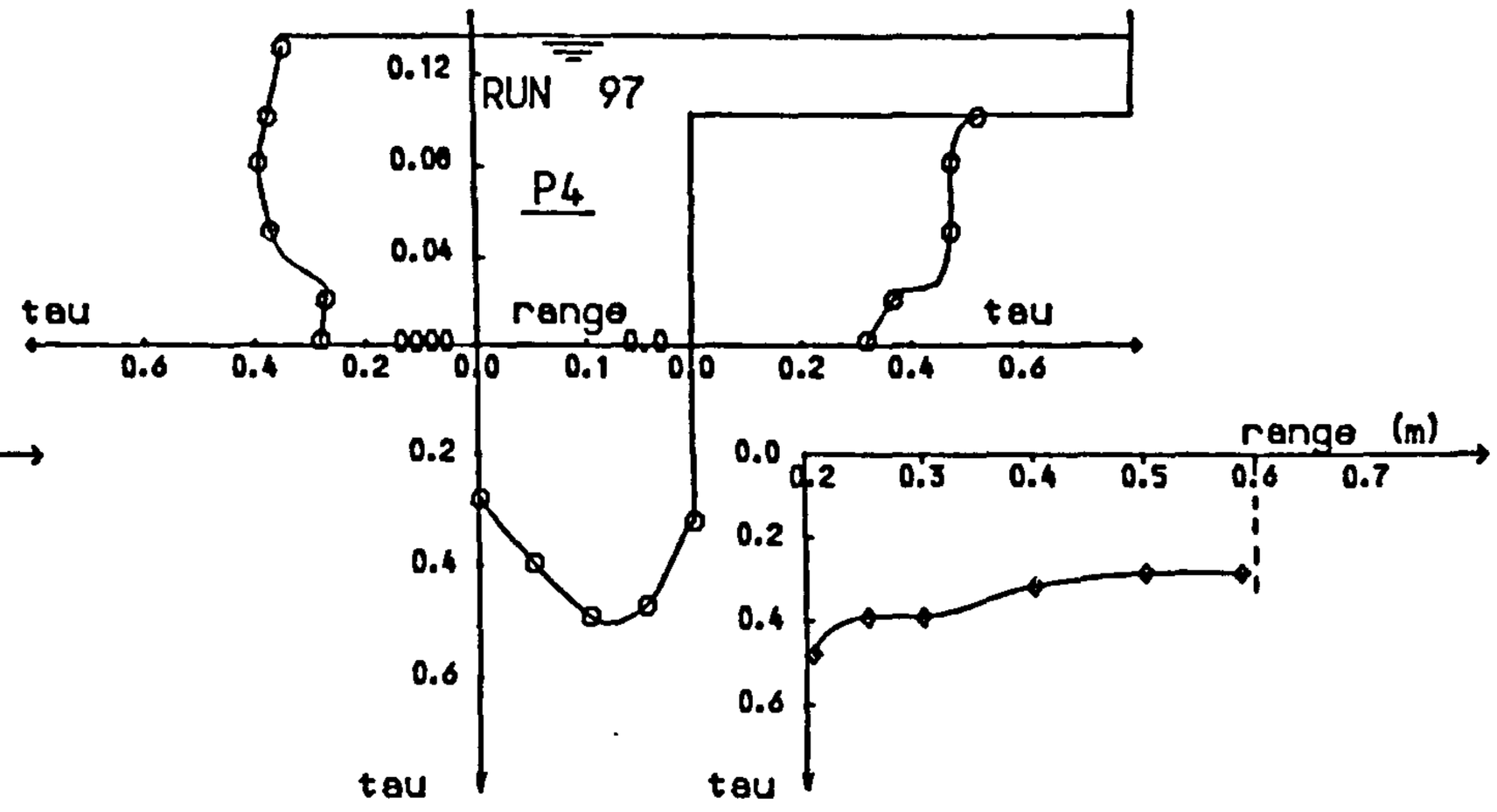

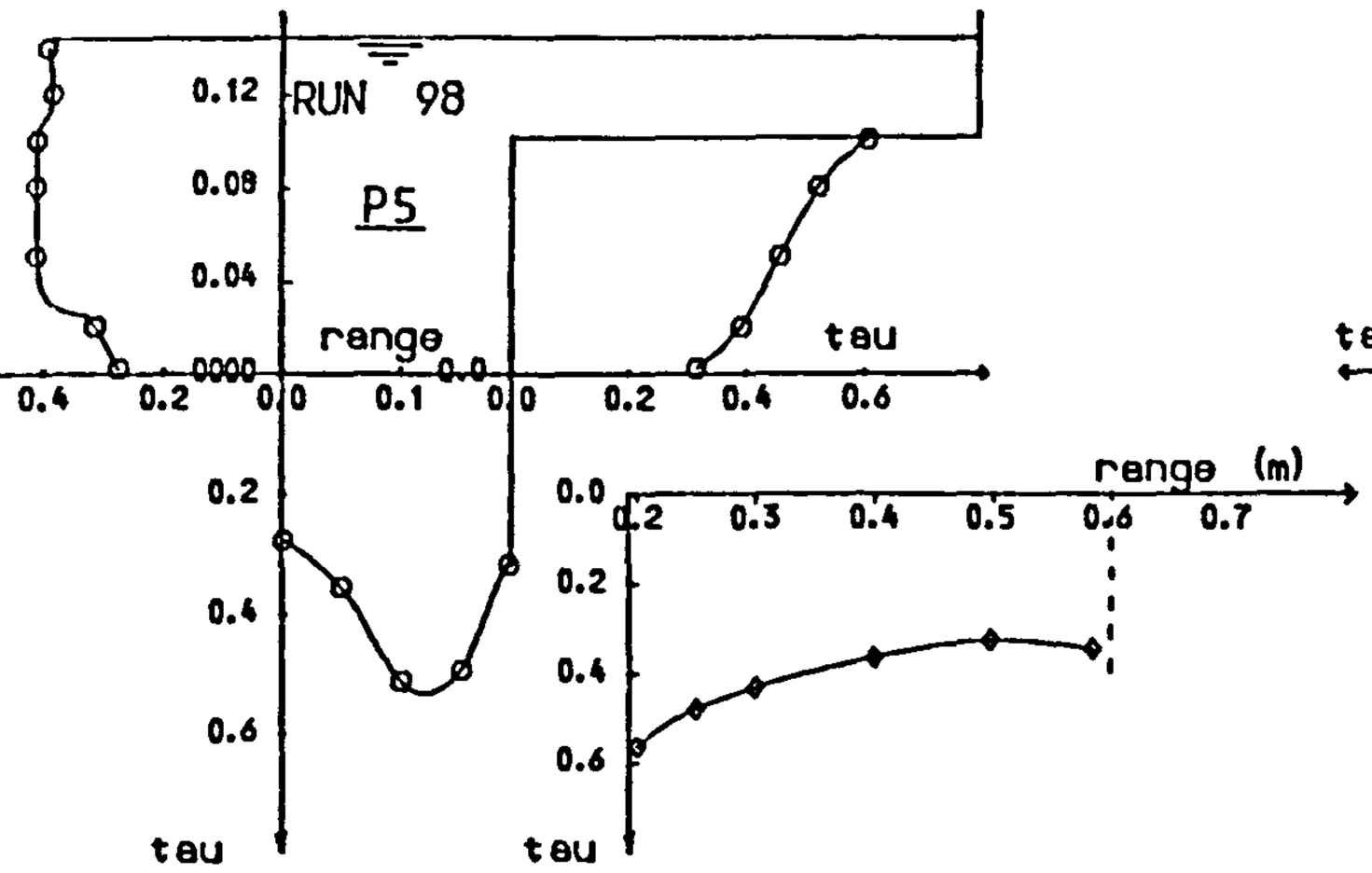

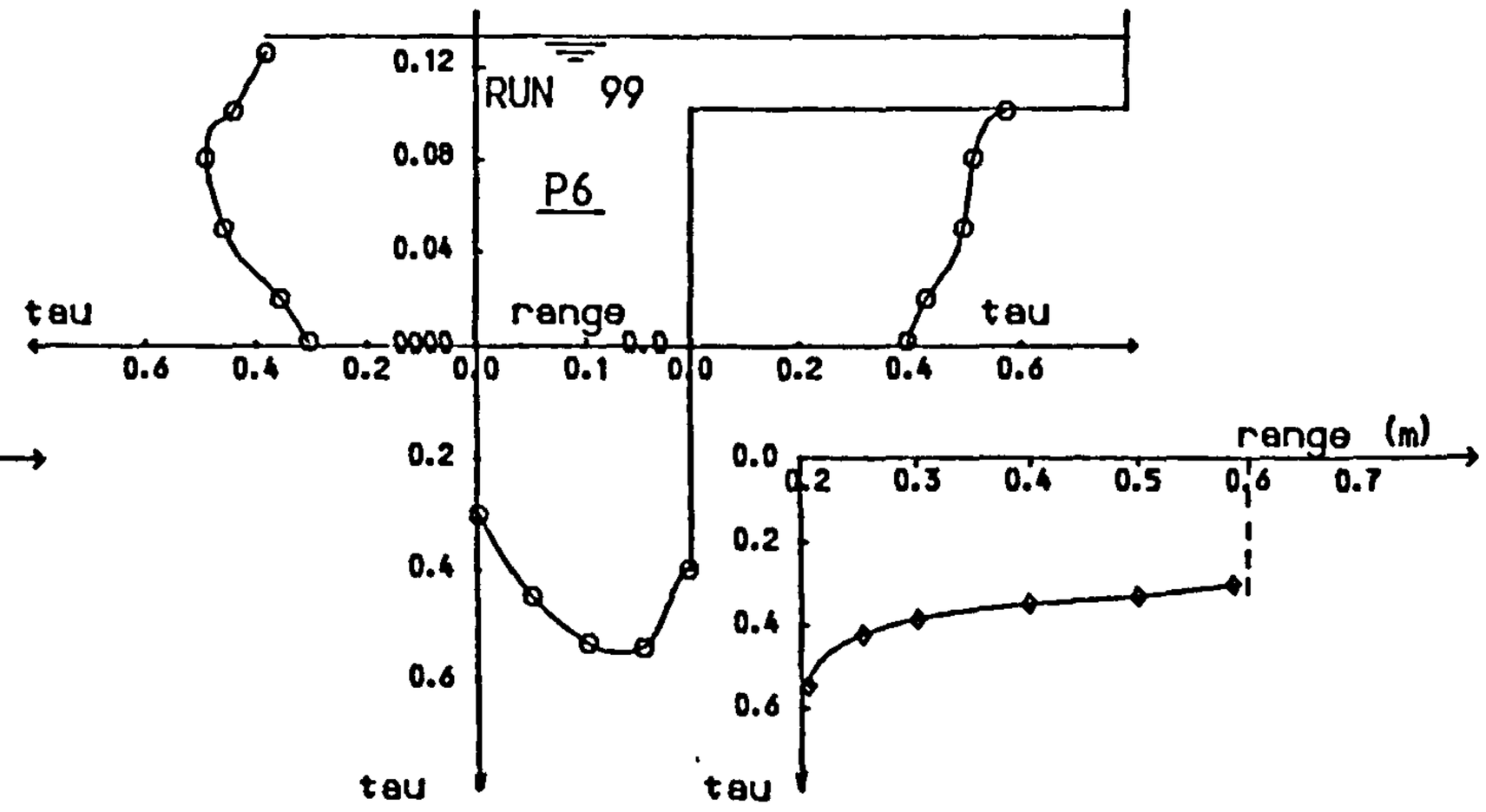

Fig 5·4 Shear stress distribution in channel and flood plain.

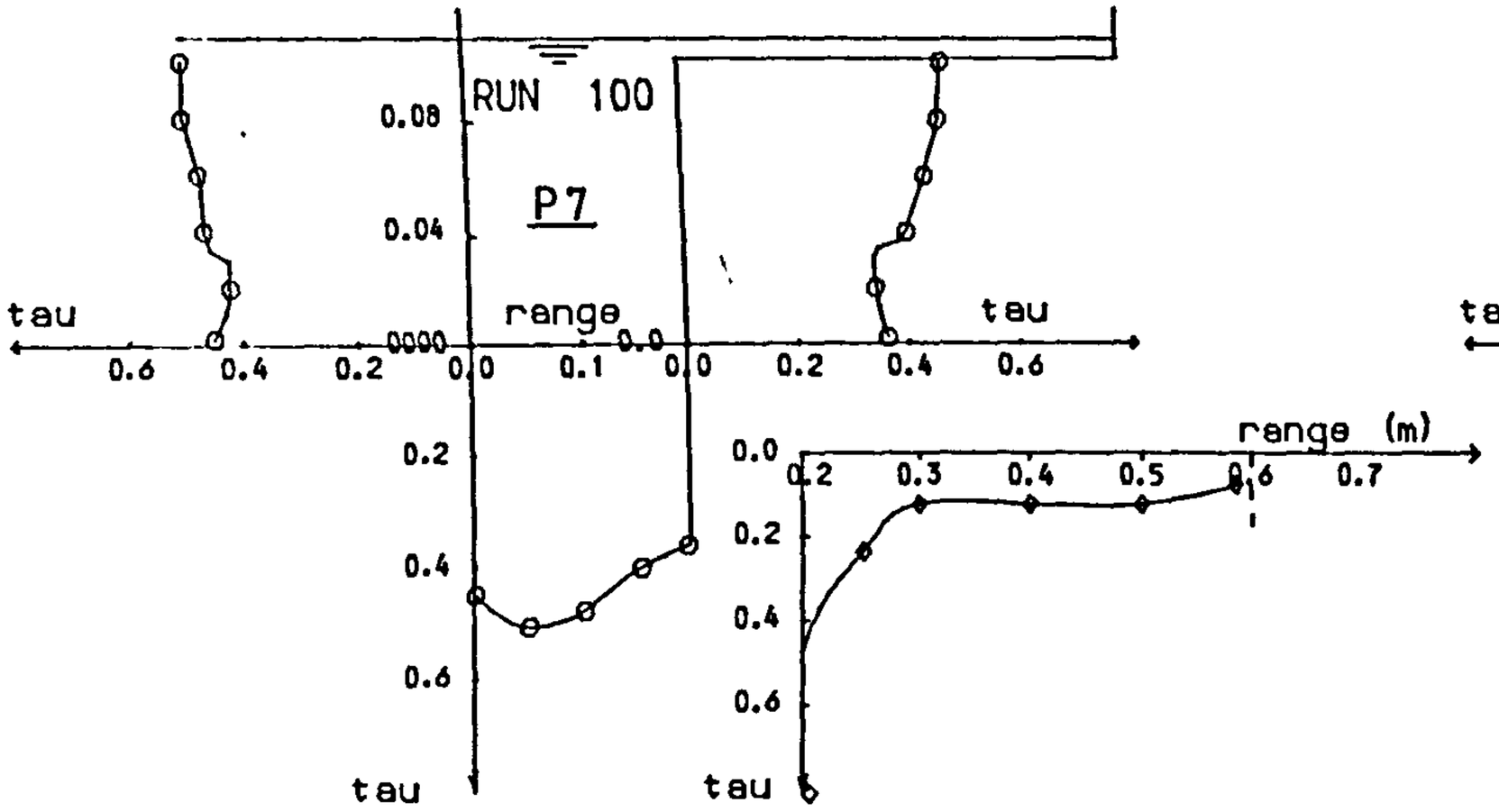

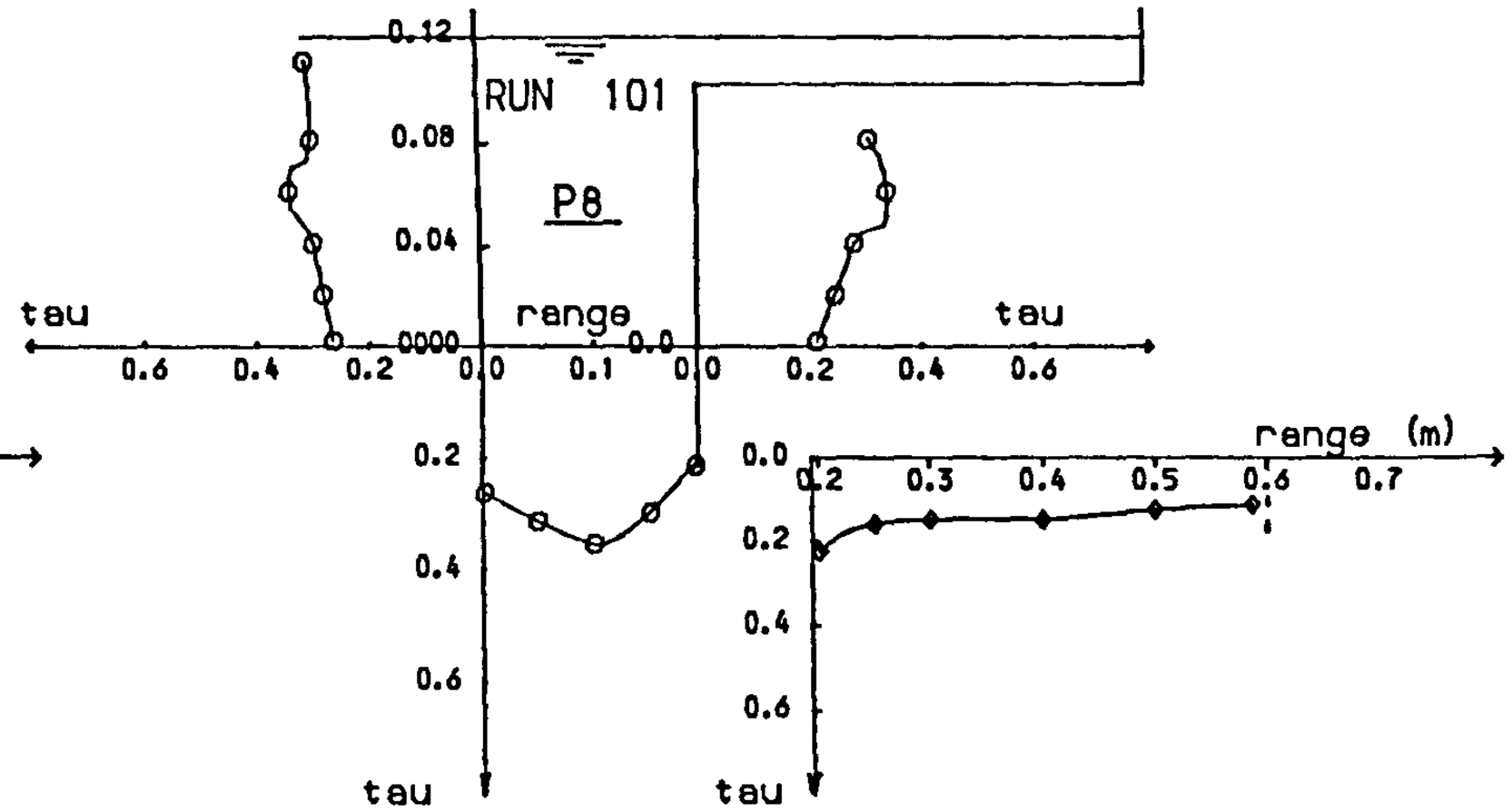

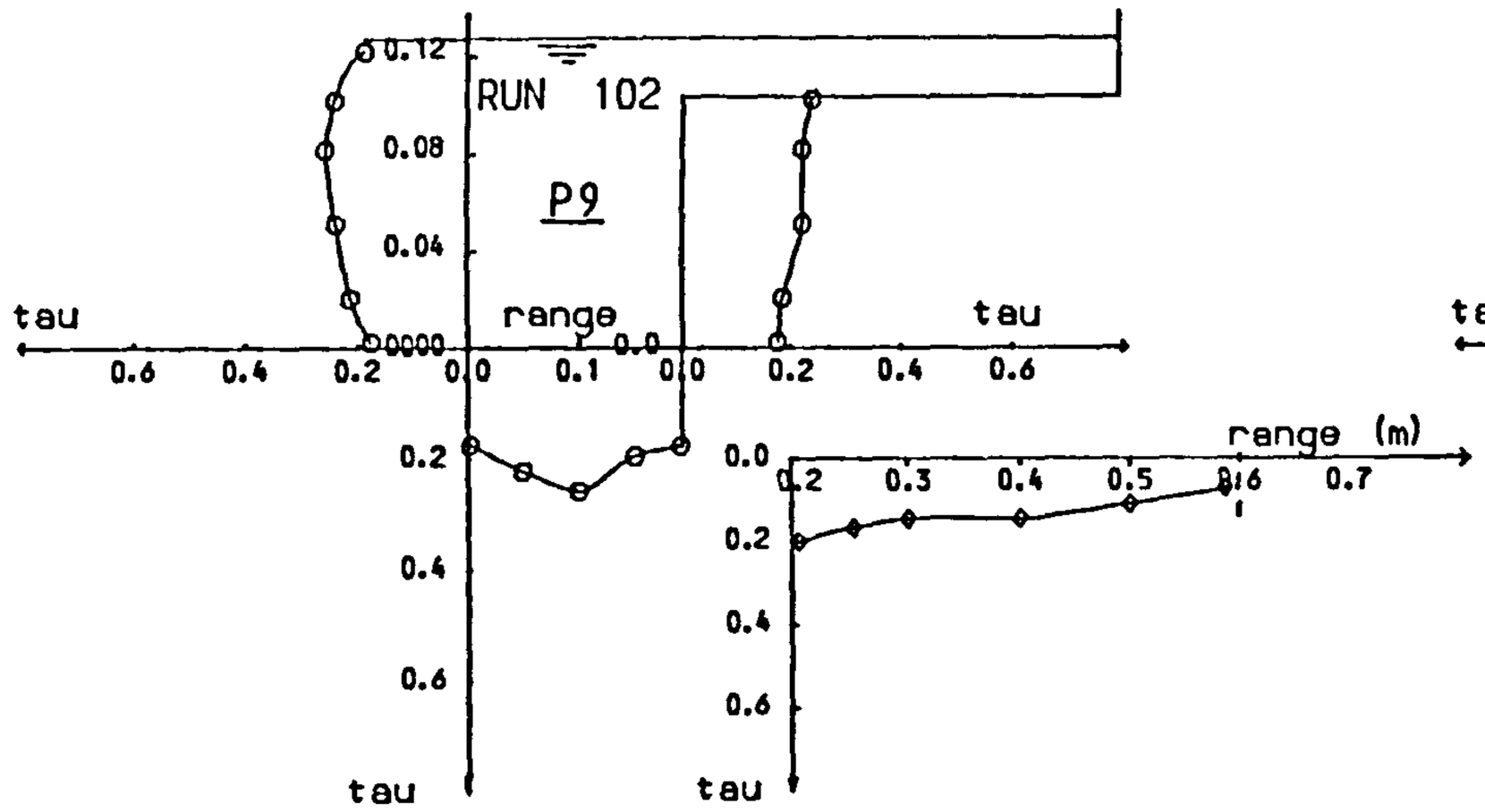

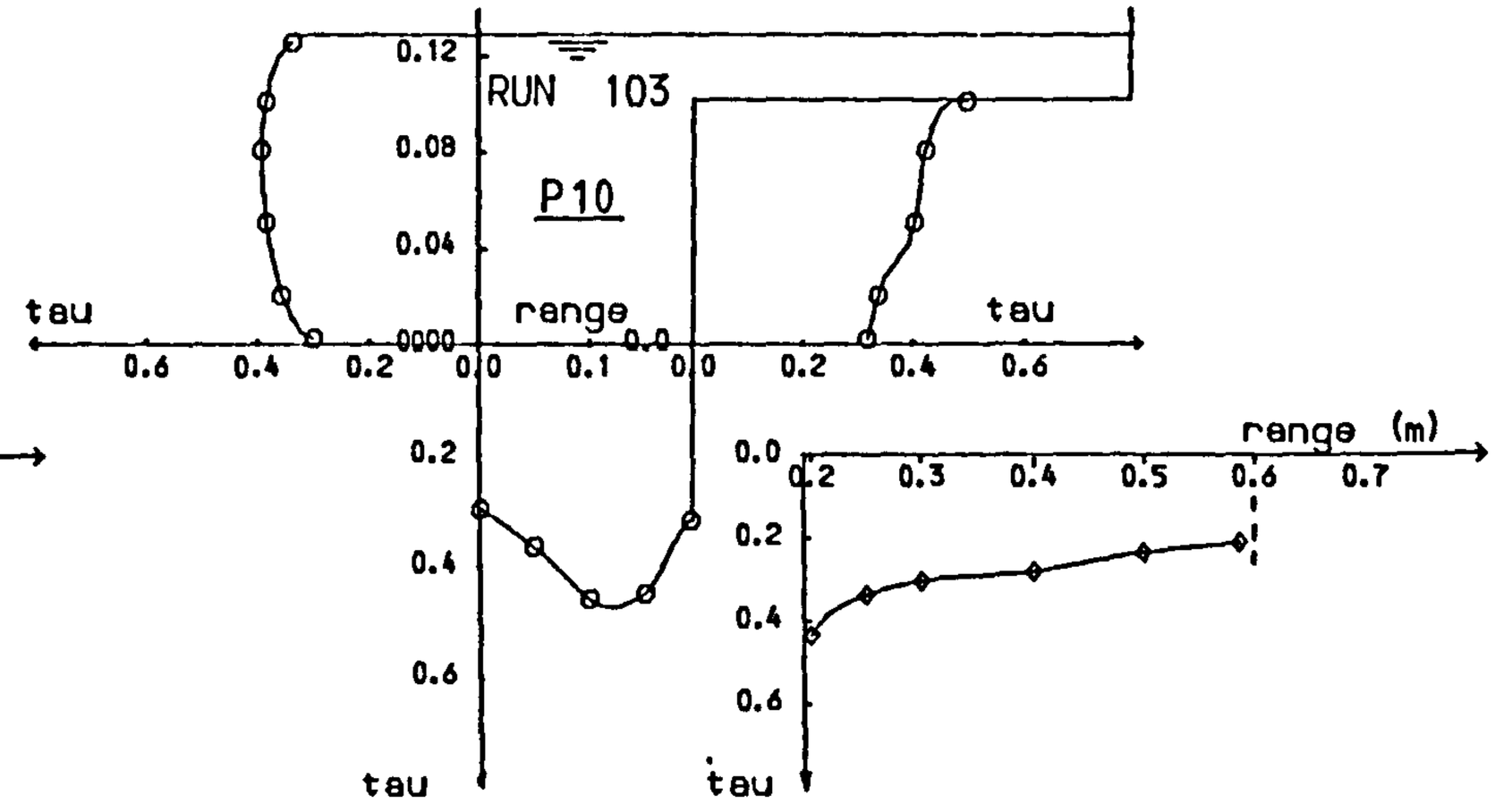

Fig 5·4 Shear stress distribution in channel and flood plain.

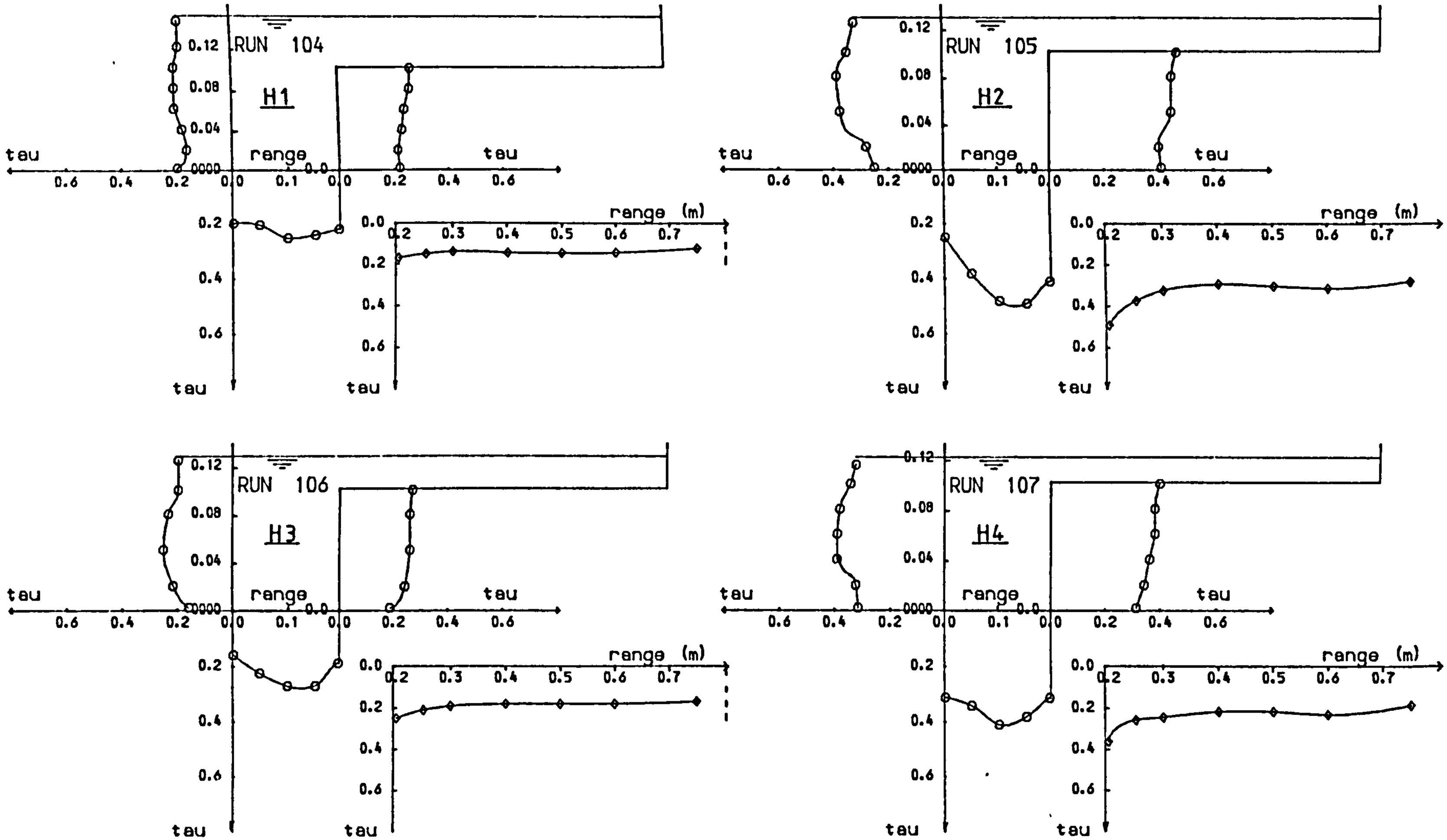

Fig 5·4 Shear stress distribution in channel and flood plain.

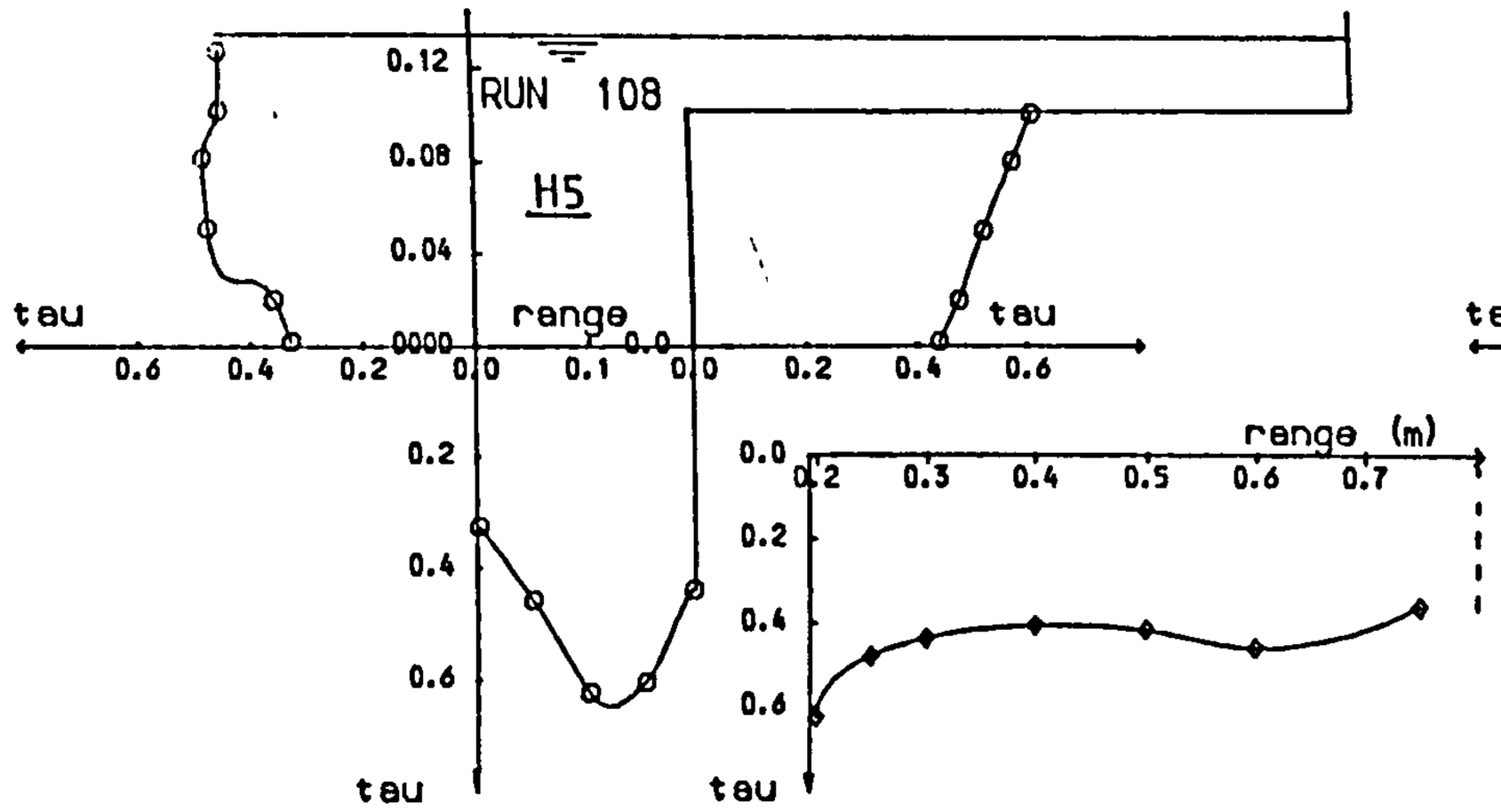

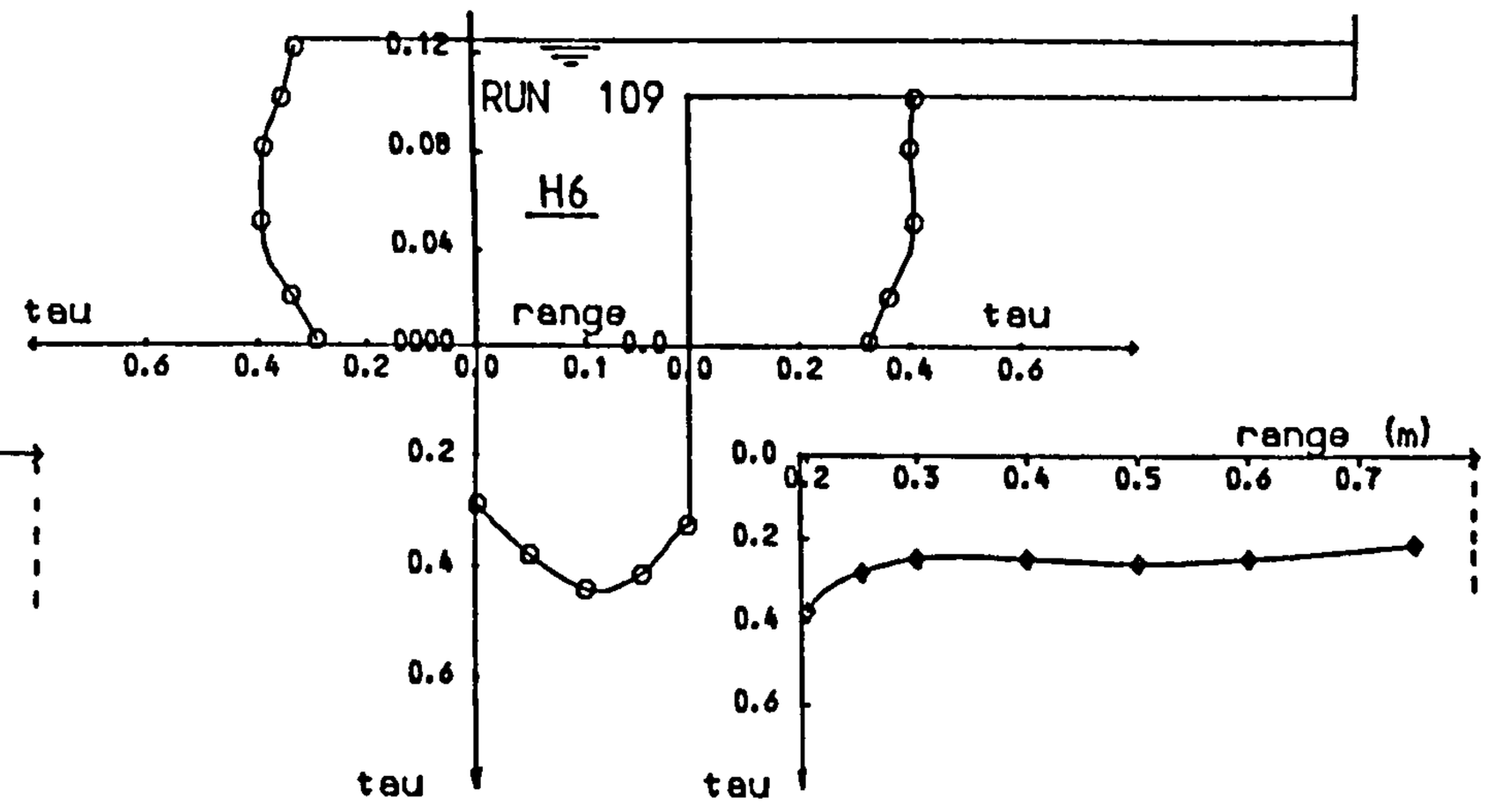

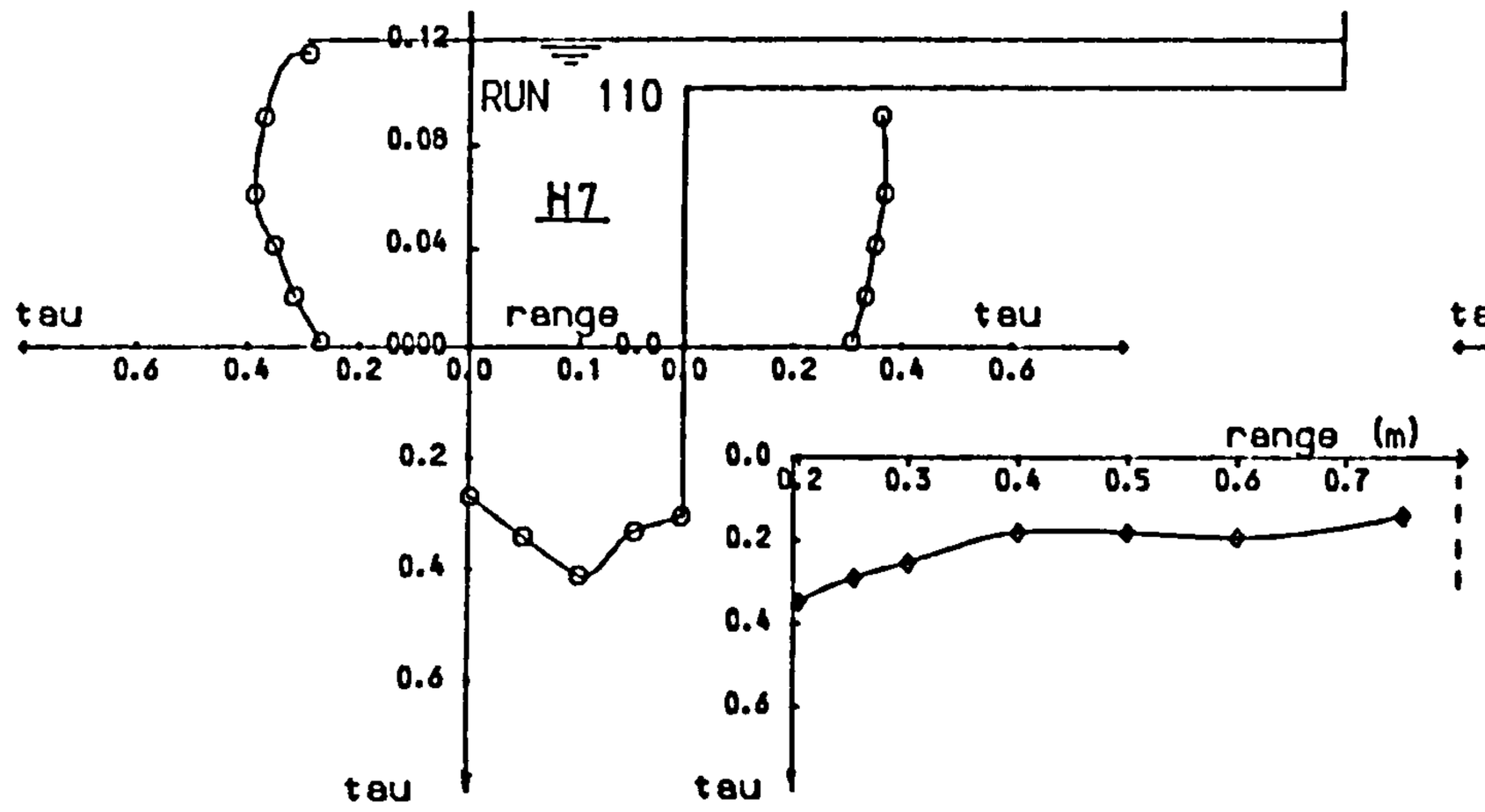

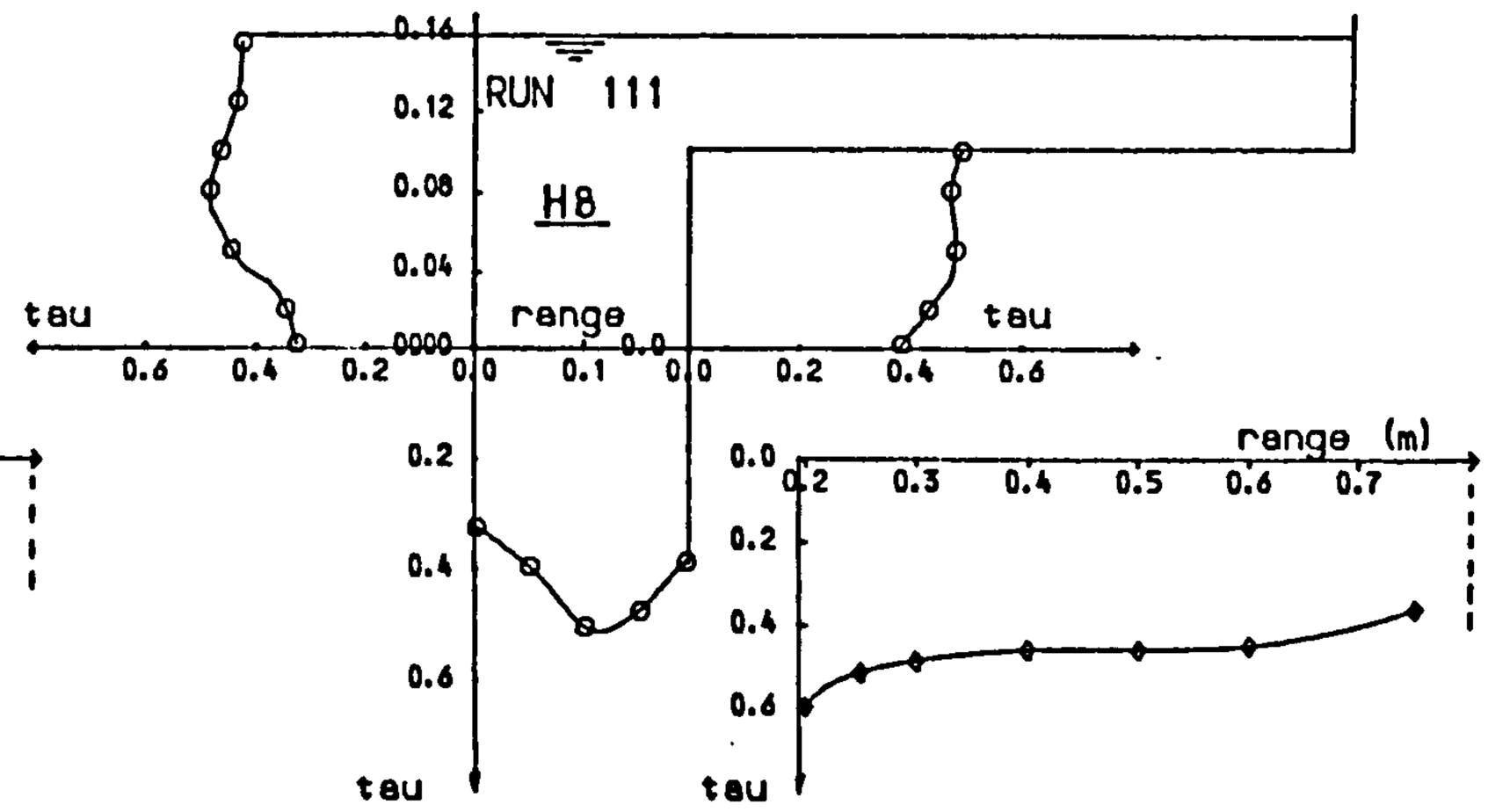

Fig 5·4 Shear stress distribution in channel and flood plain.

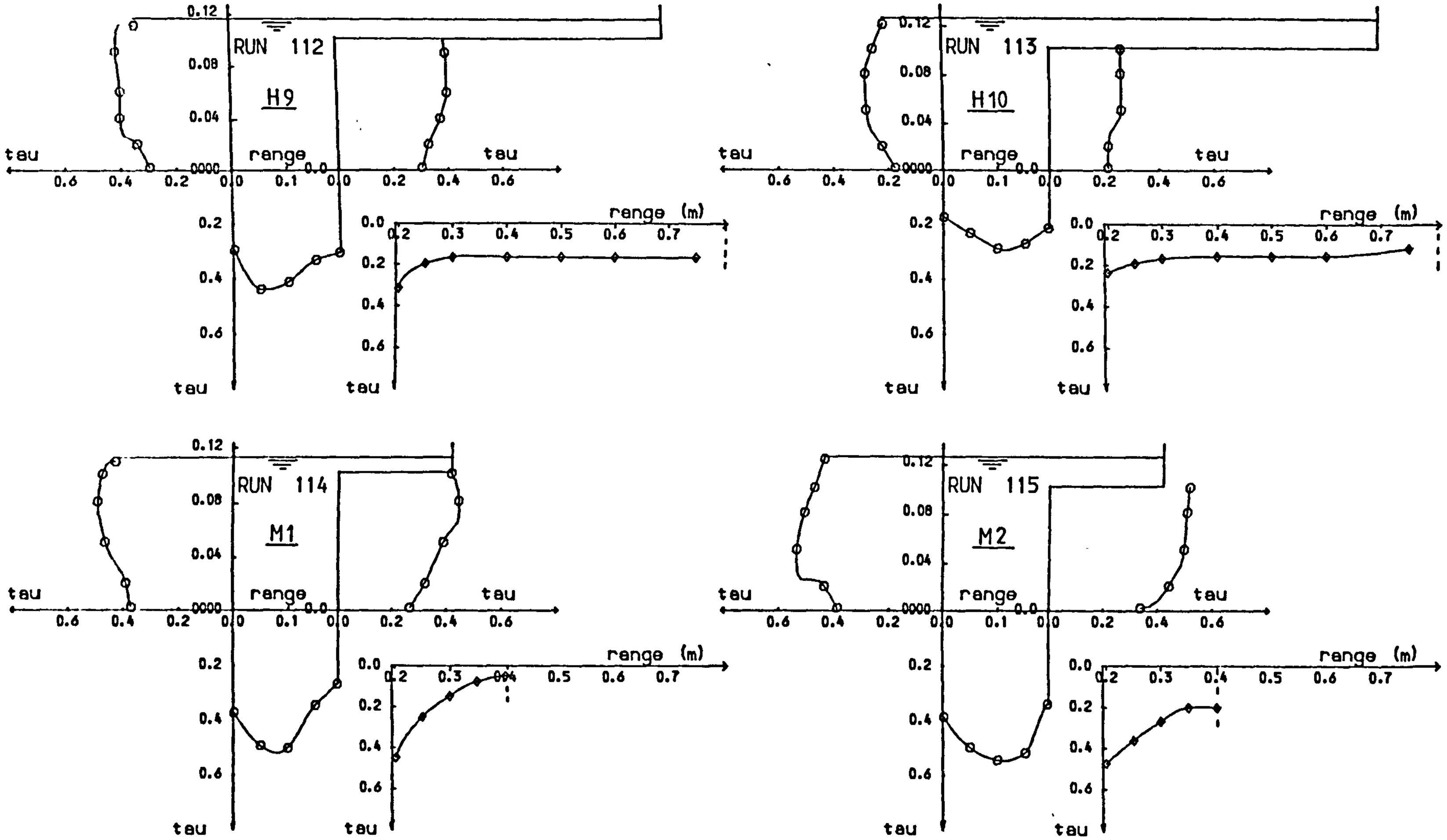

Fig 5·4 Shear stress distribution in channel and flood plain.

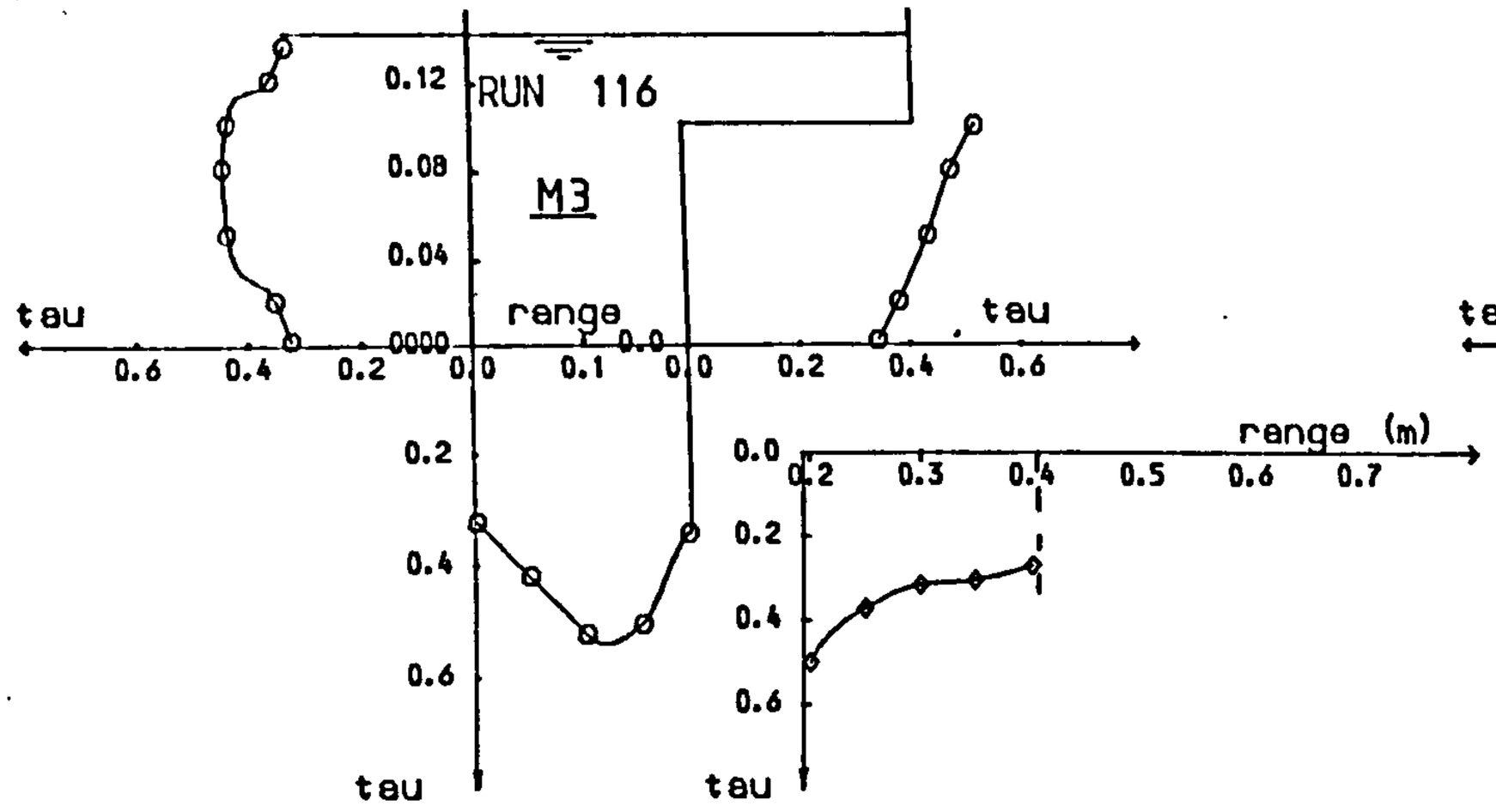

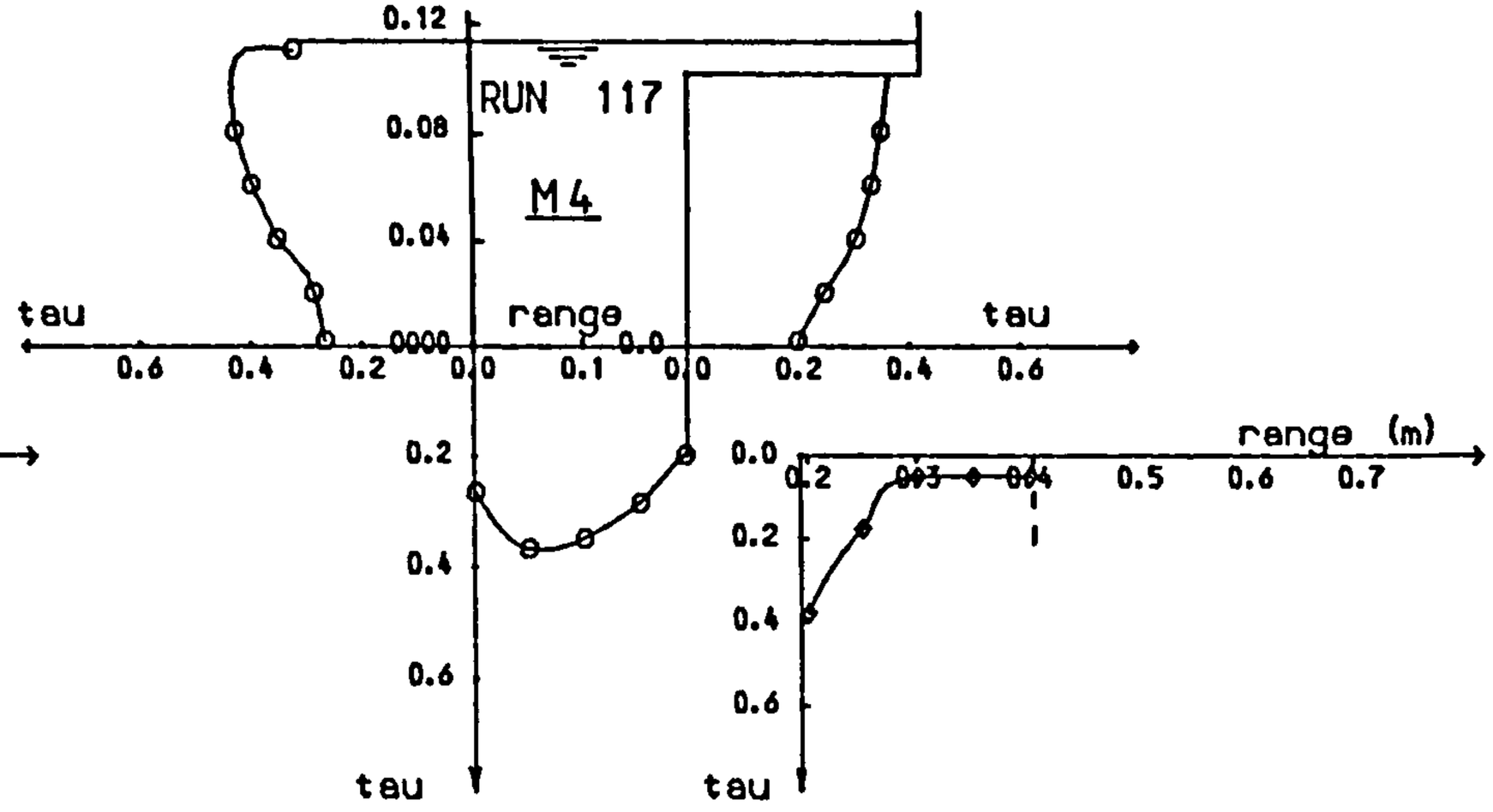

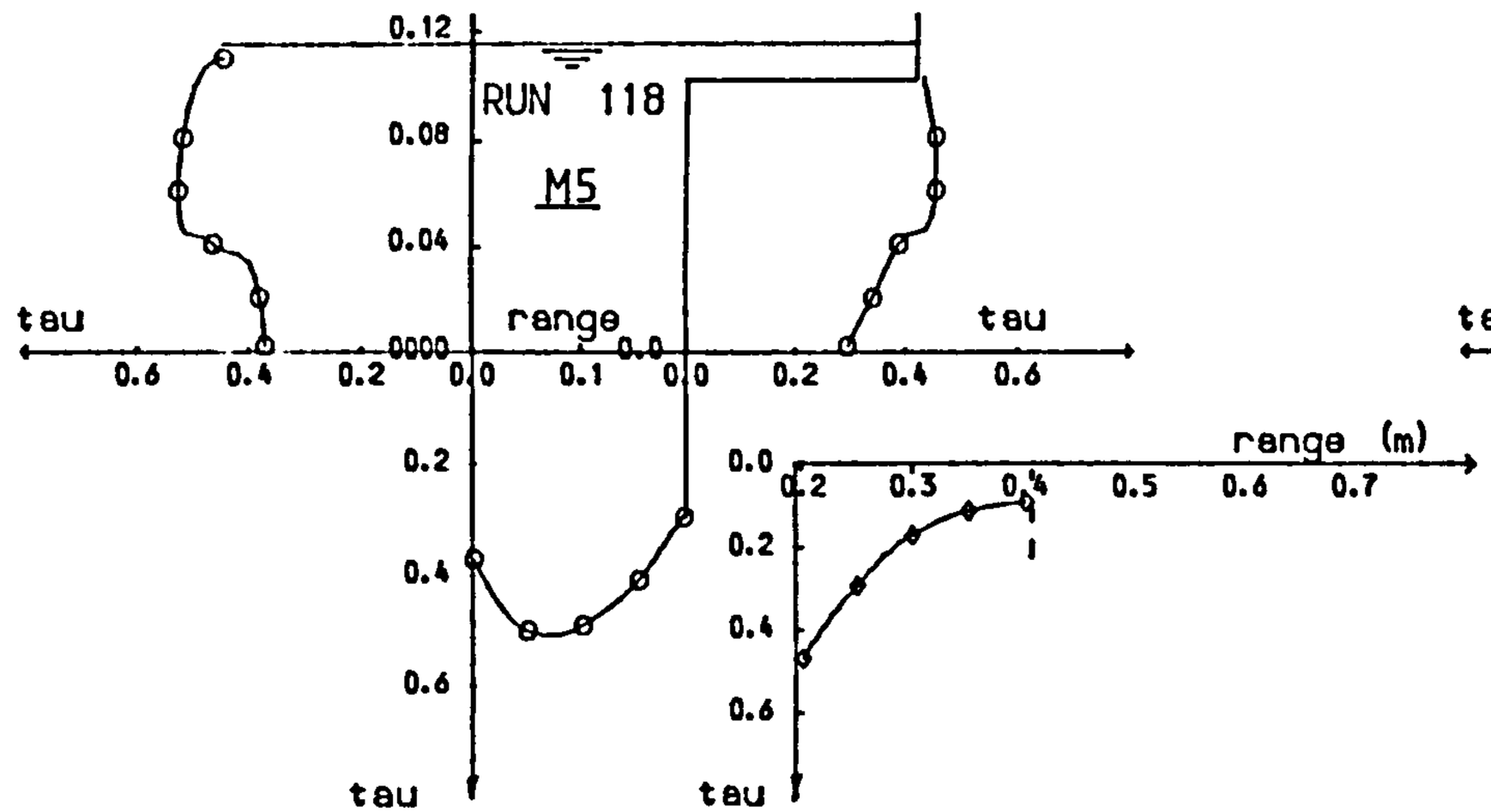

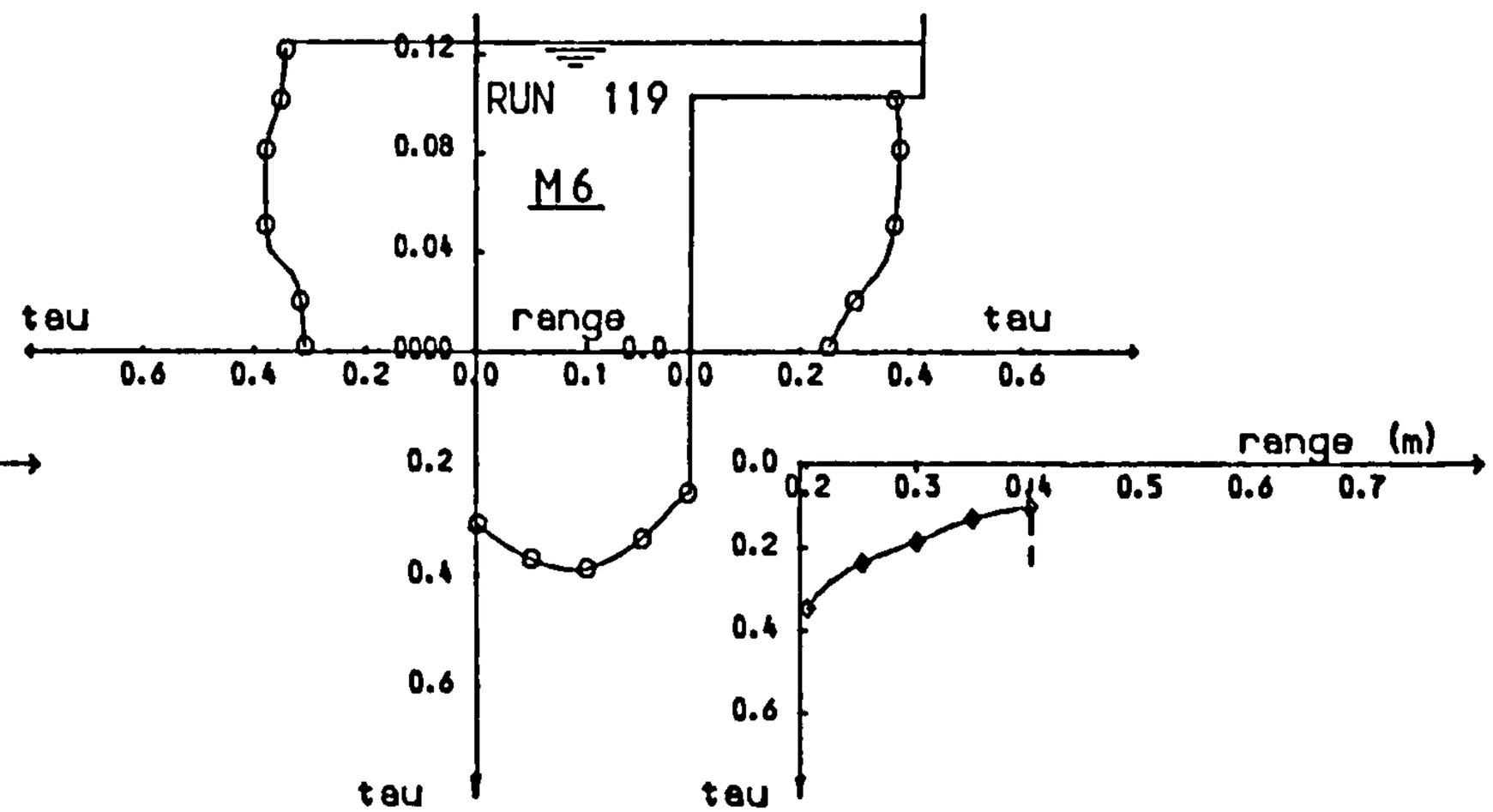

Fig 5·4 Shear stress distribution in channel and flood plain.

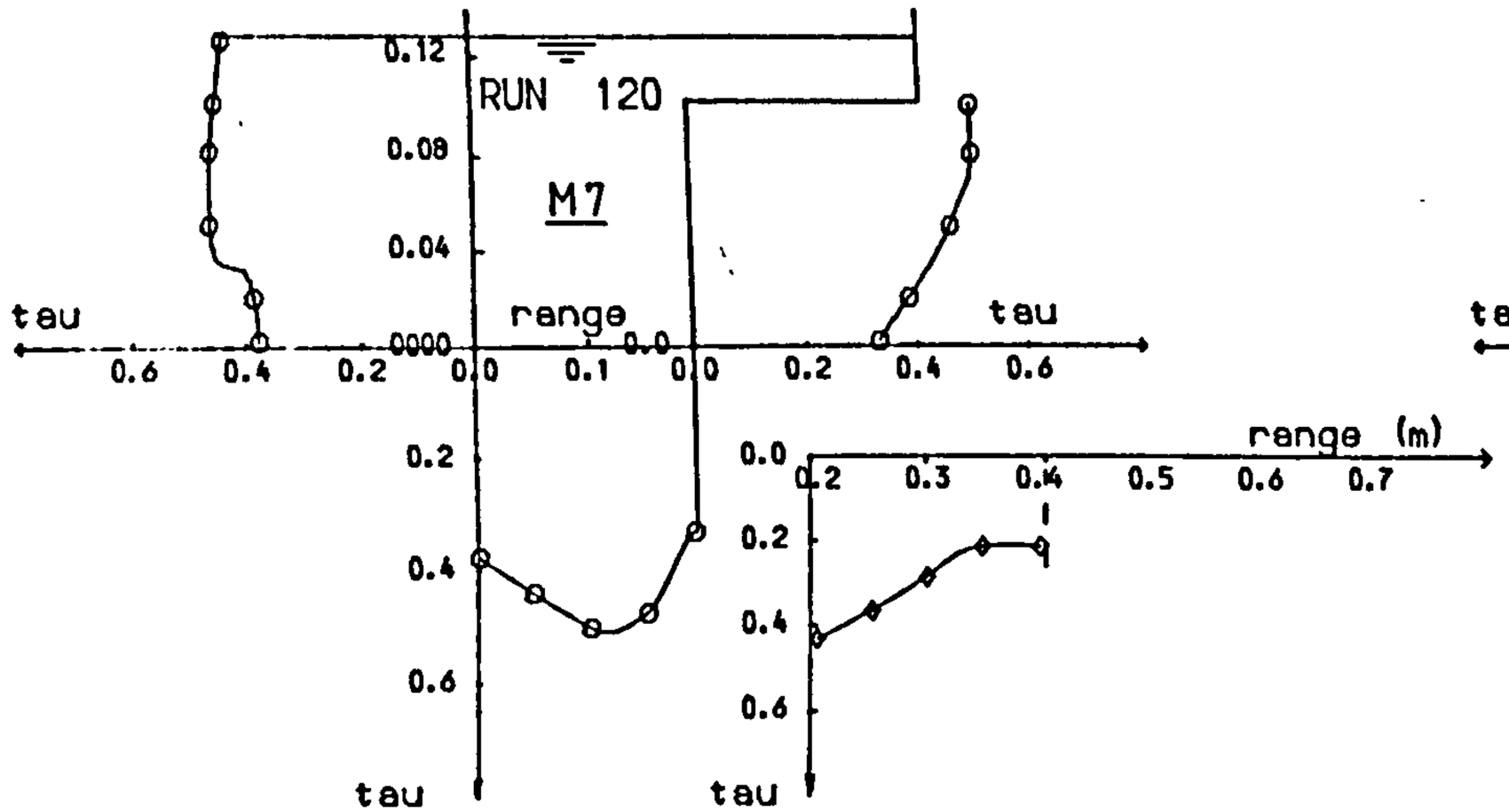

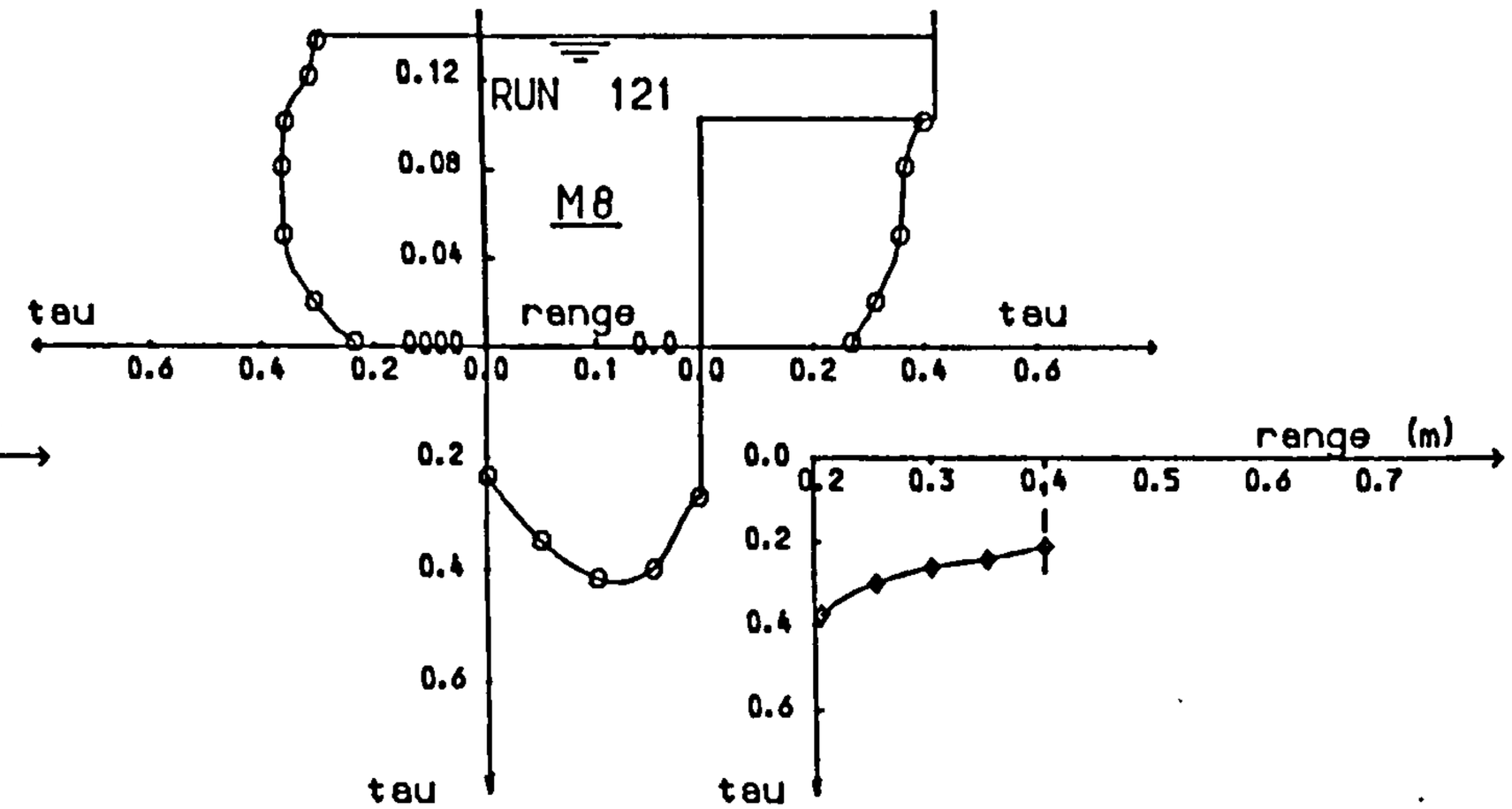

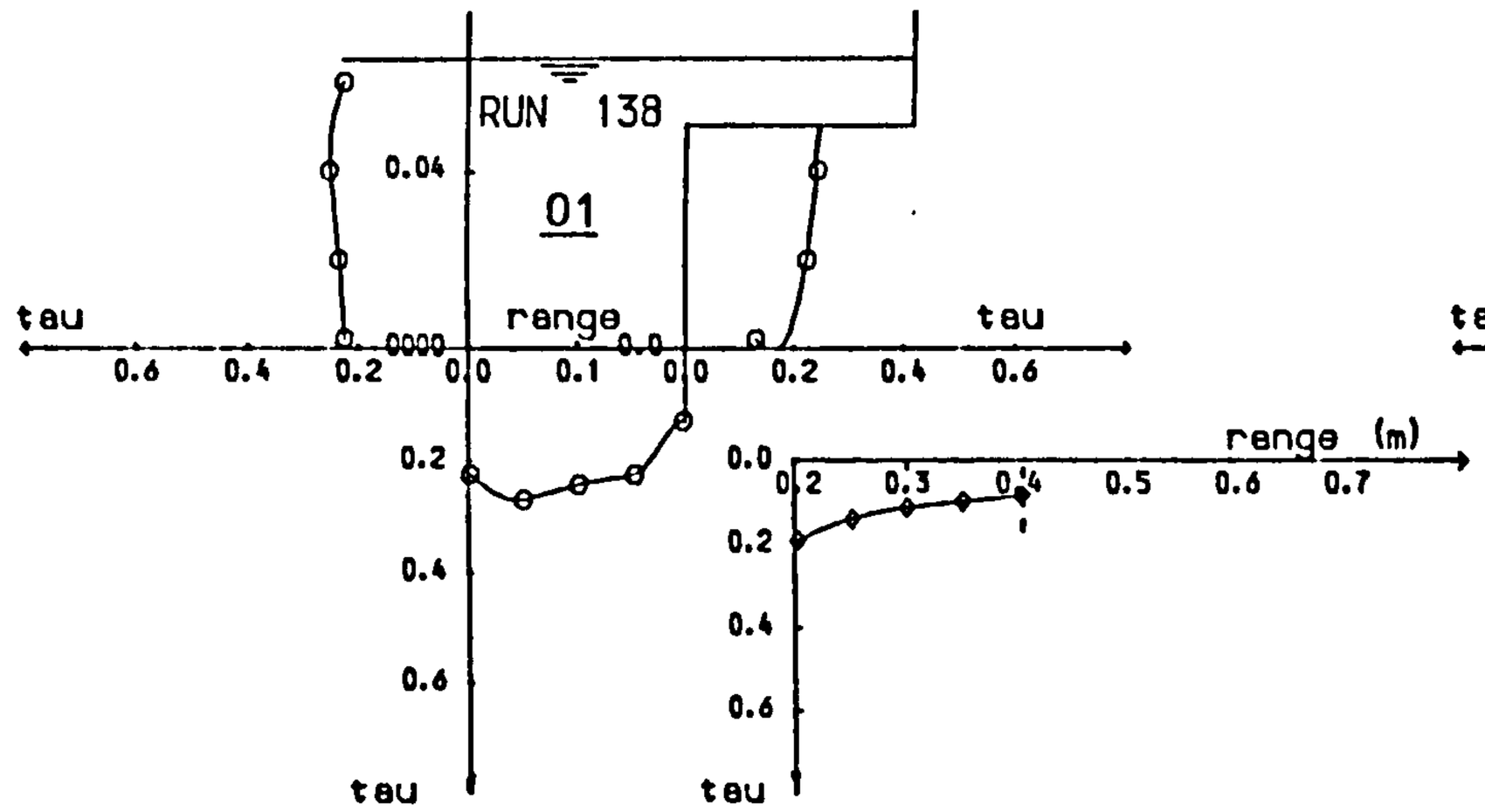

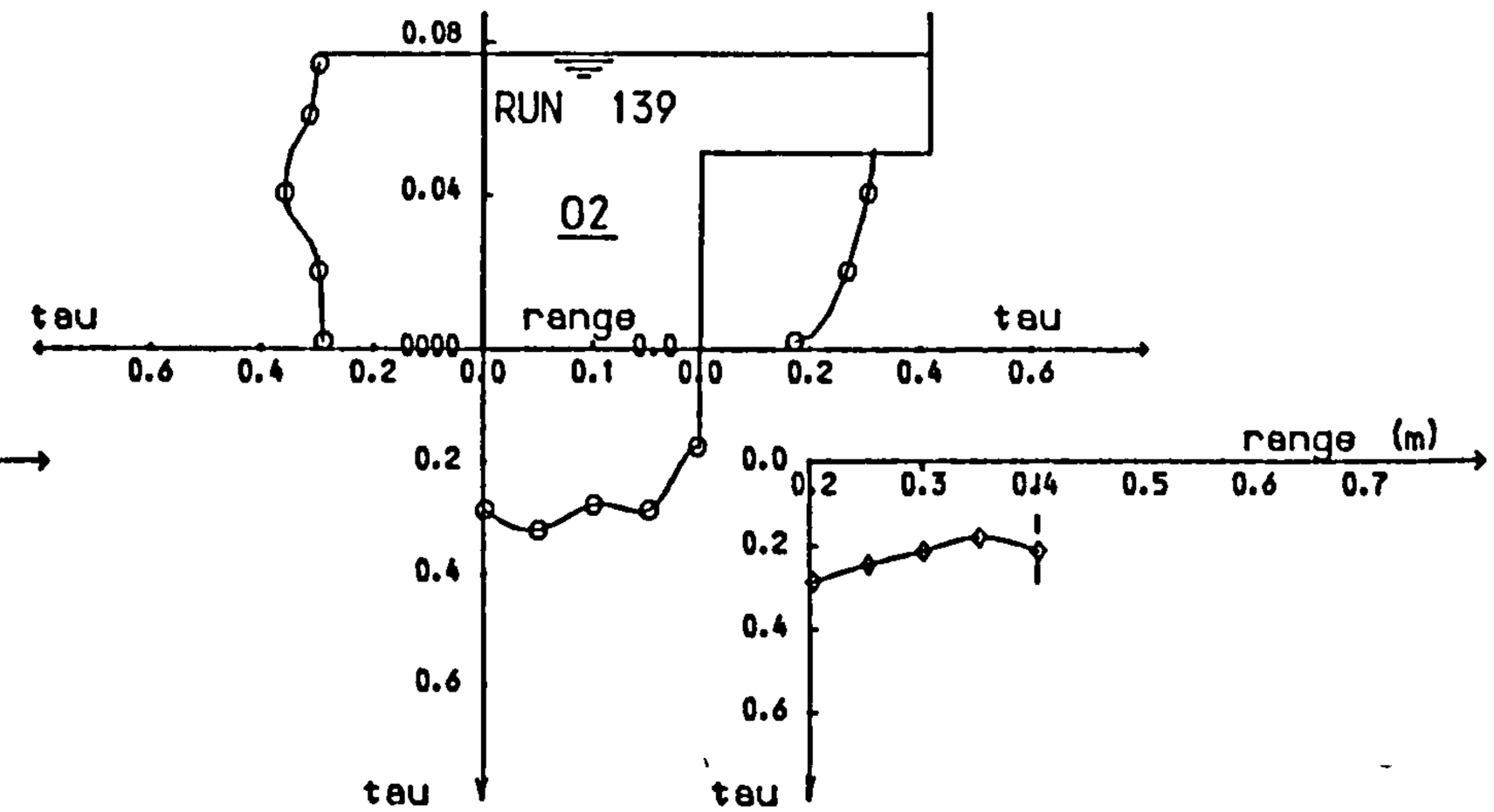

Fig 5·4 Shear stress distribution in channel and flood plain.

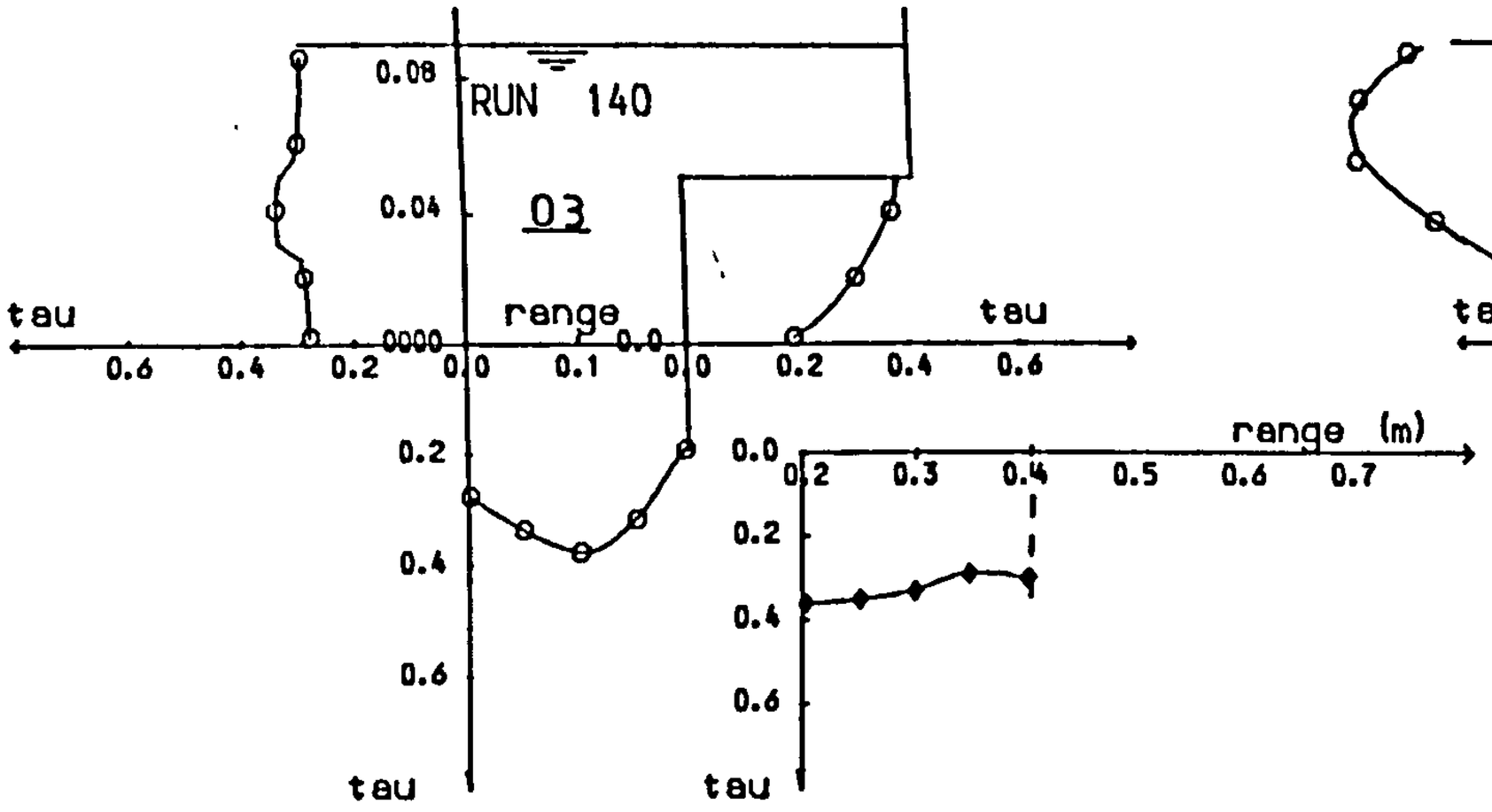

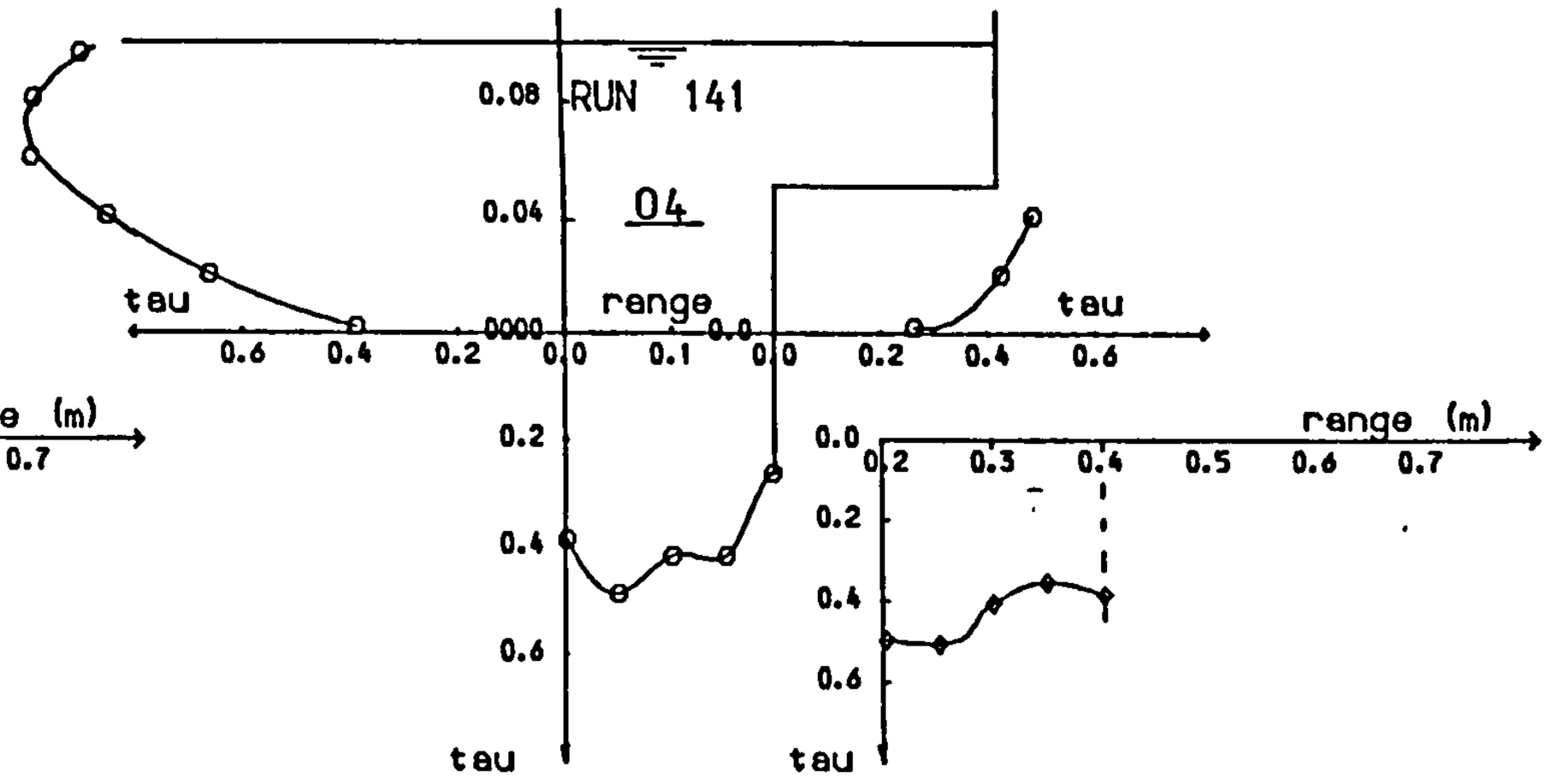

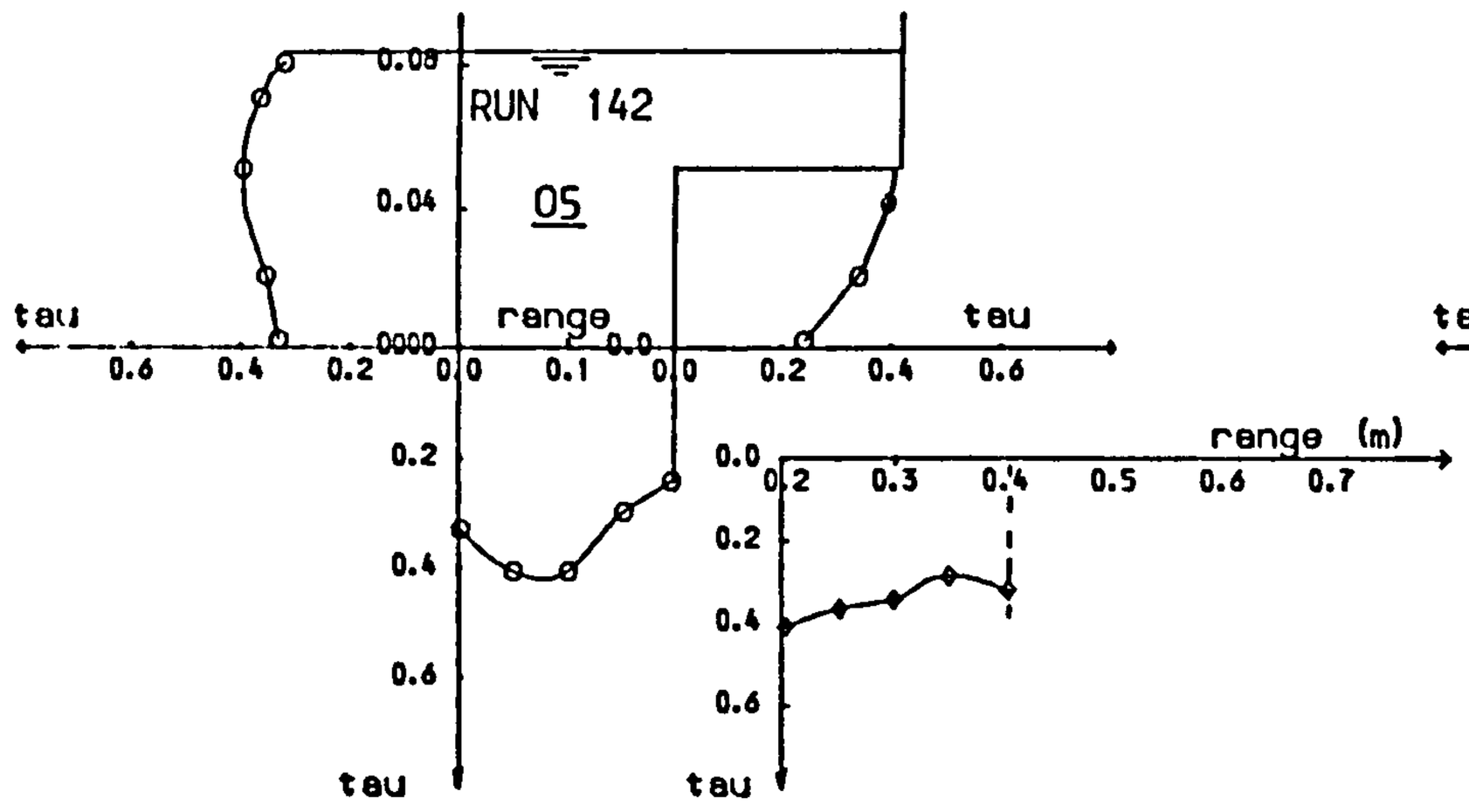

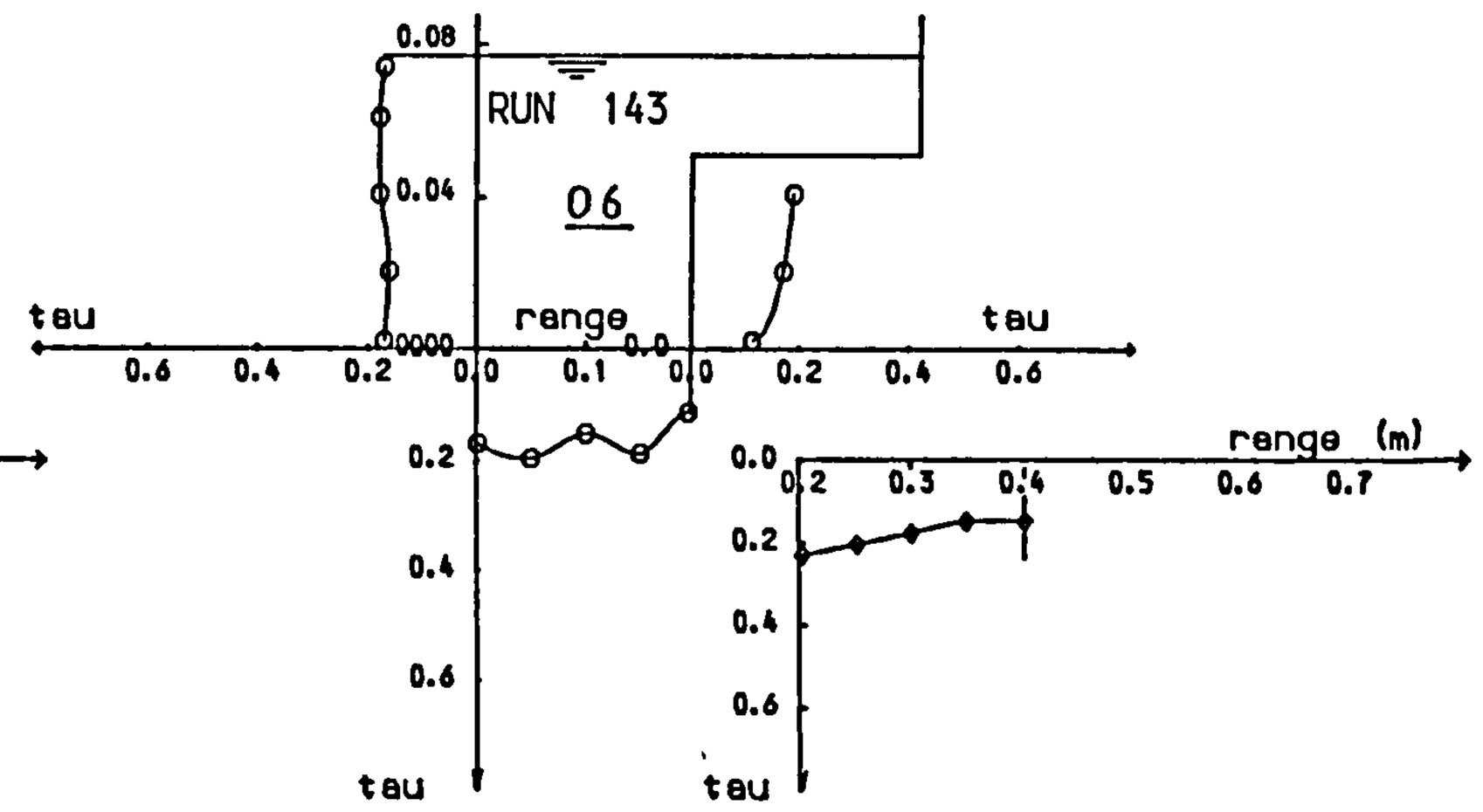

Fig 5·4 Shear stress distribution in channel and flood plain.

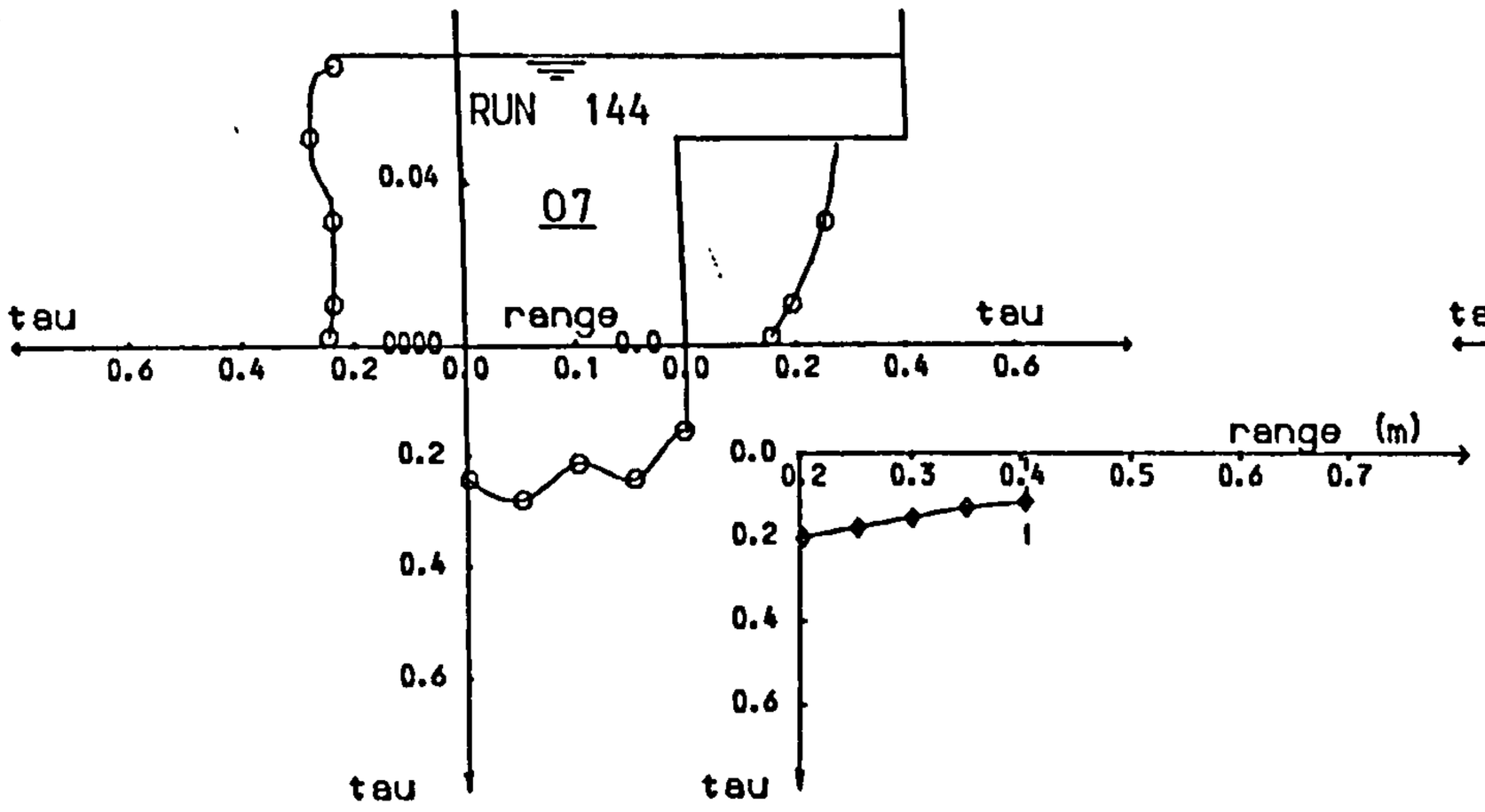

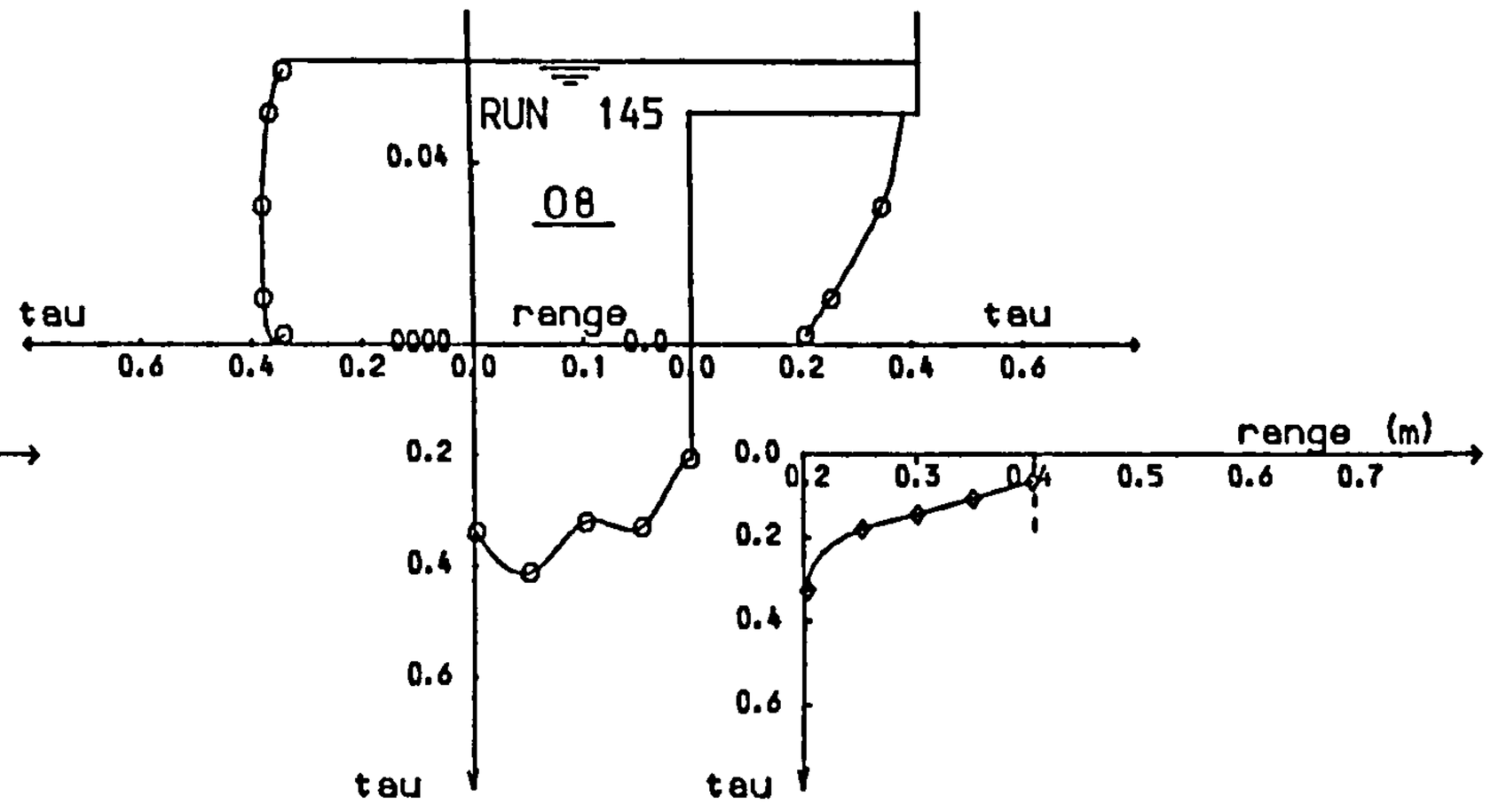

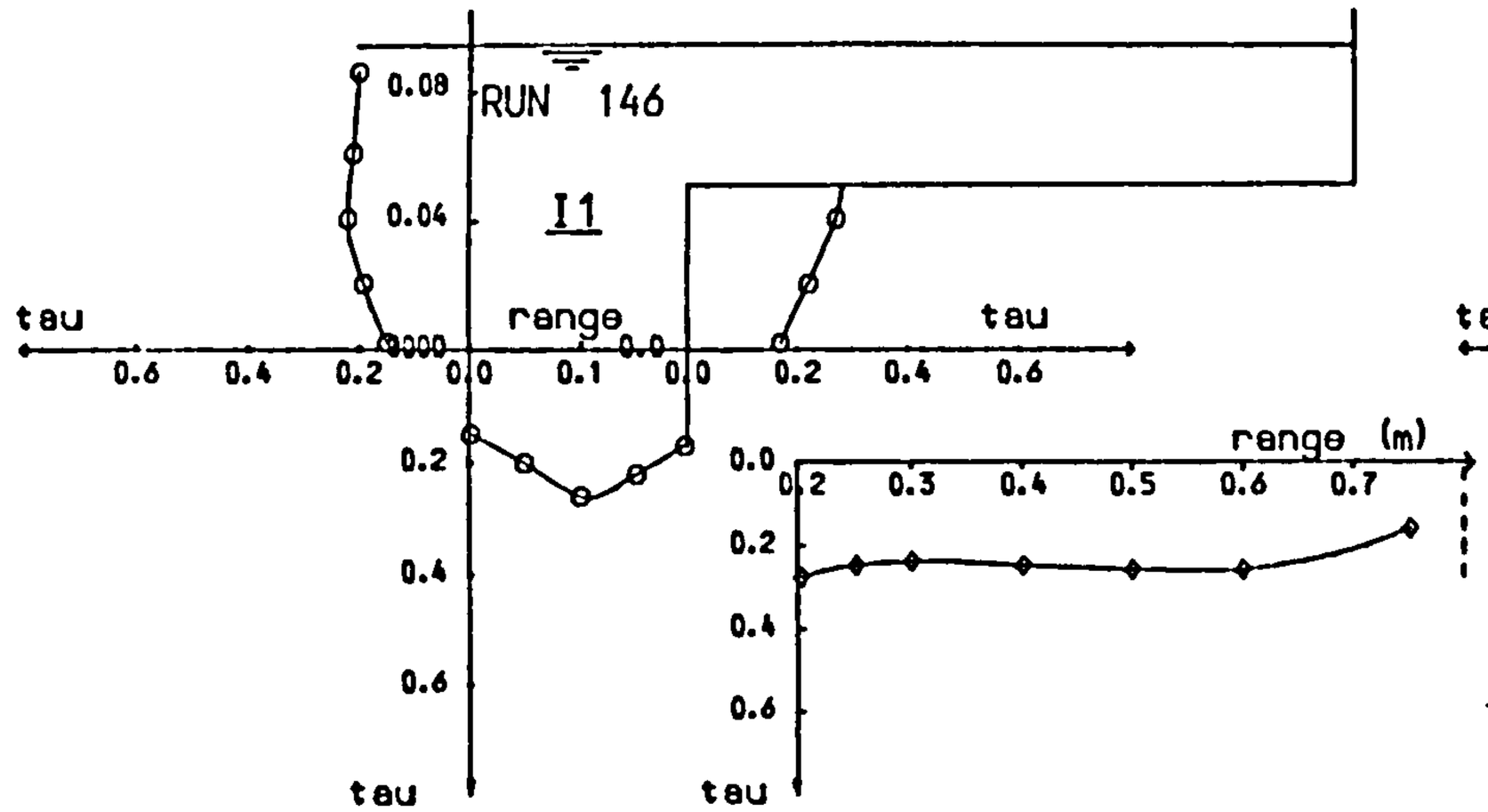

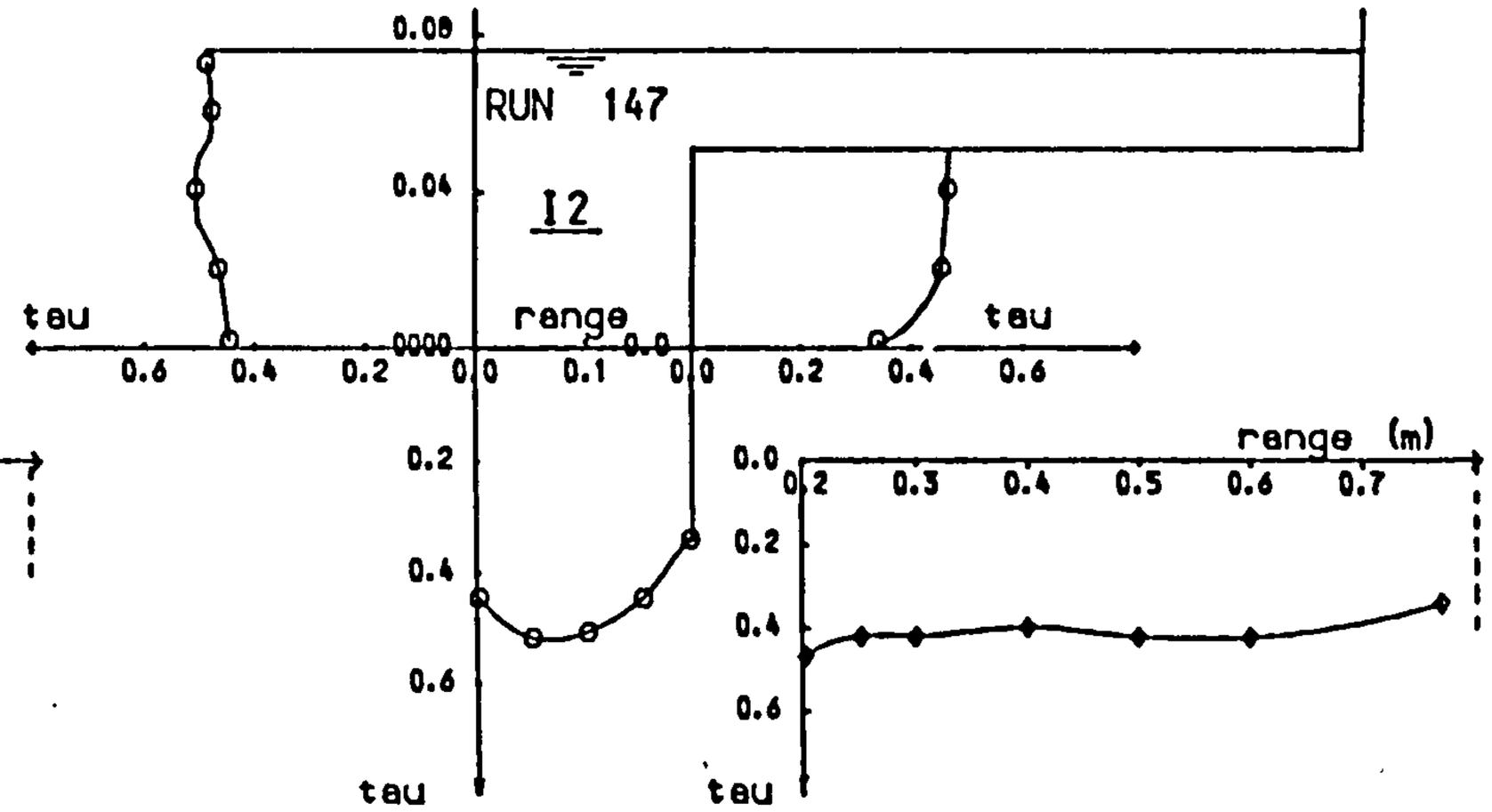

Fig 5·4 Shear stress distribution in channel and flood plain.

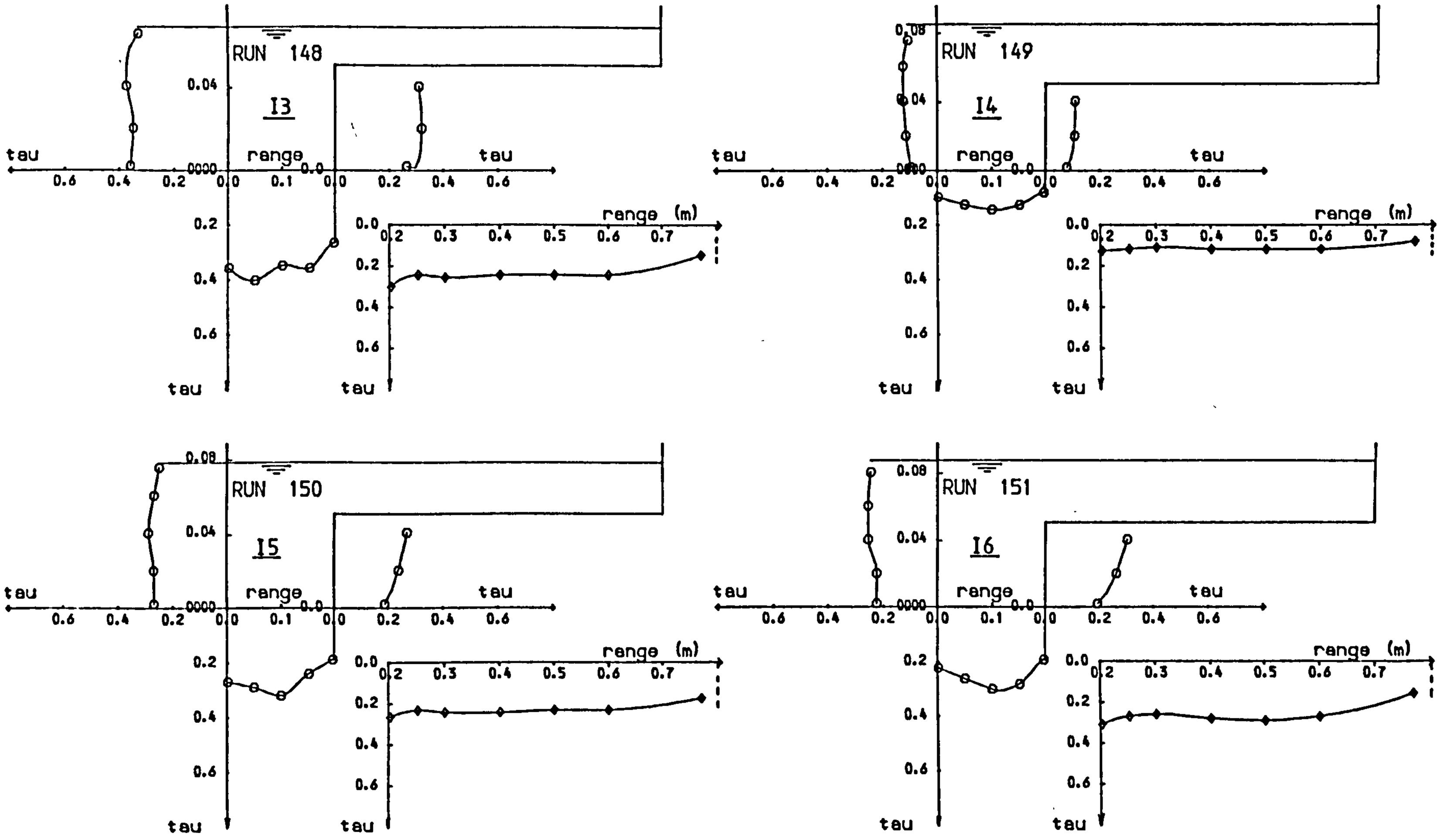

Fig 5·4 Shear stress distribution in channel and flood plain.

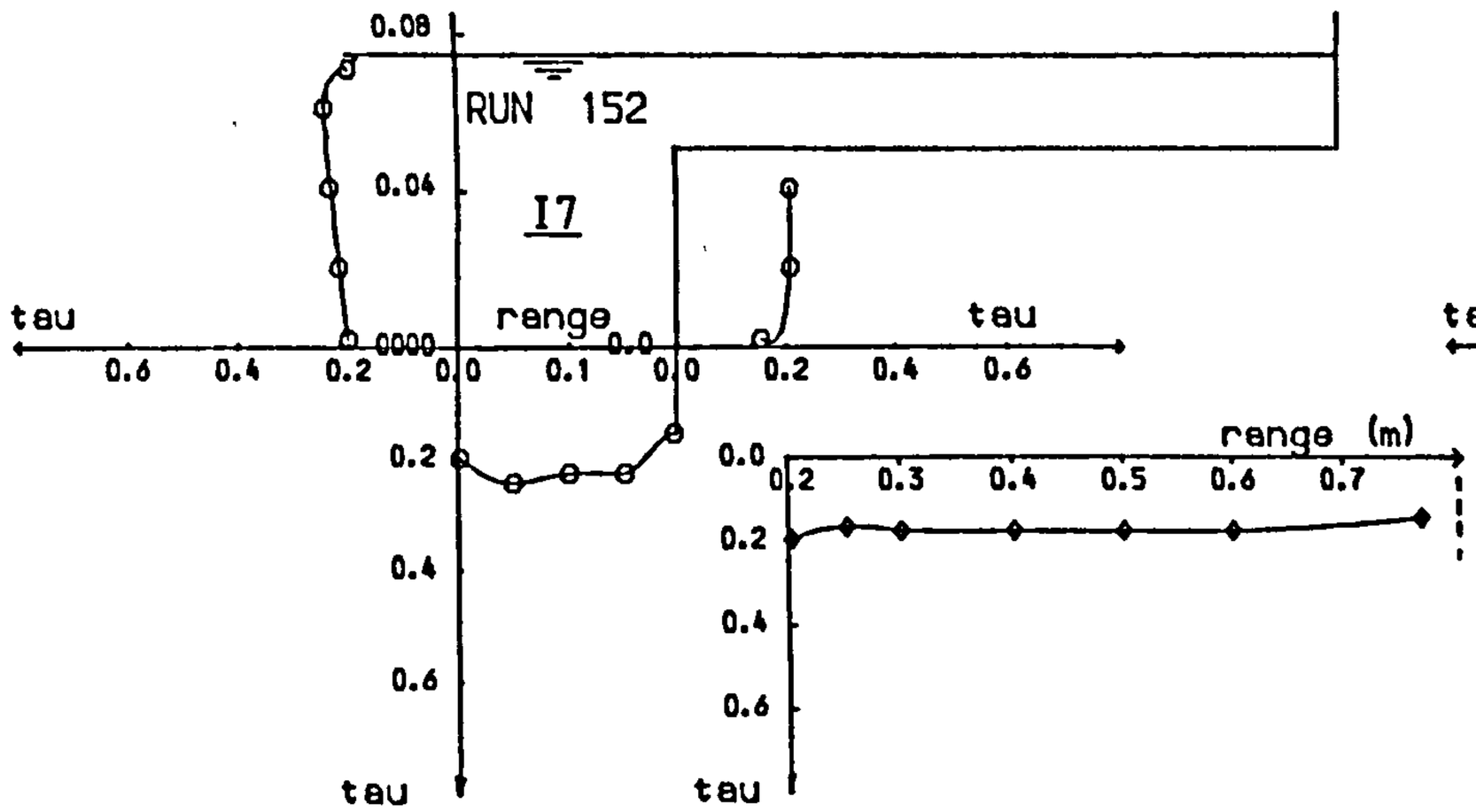

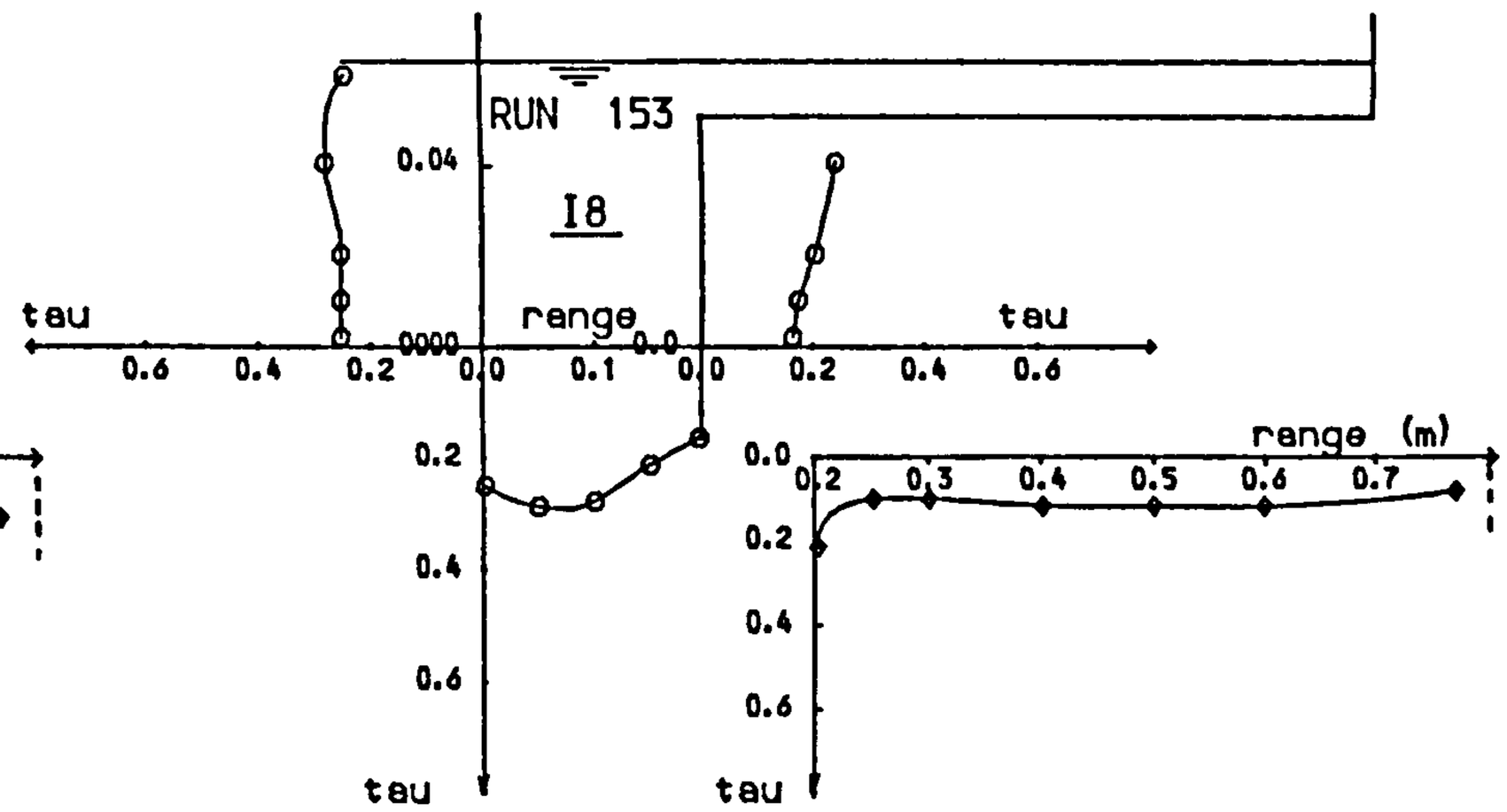

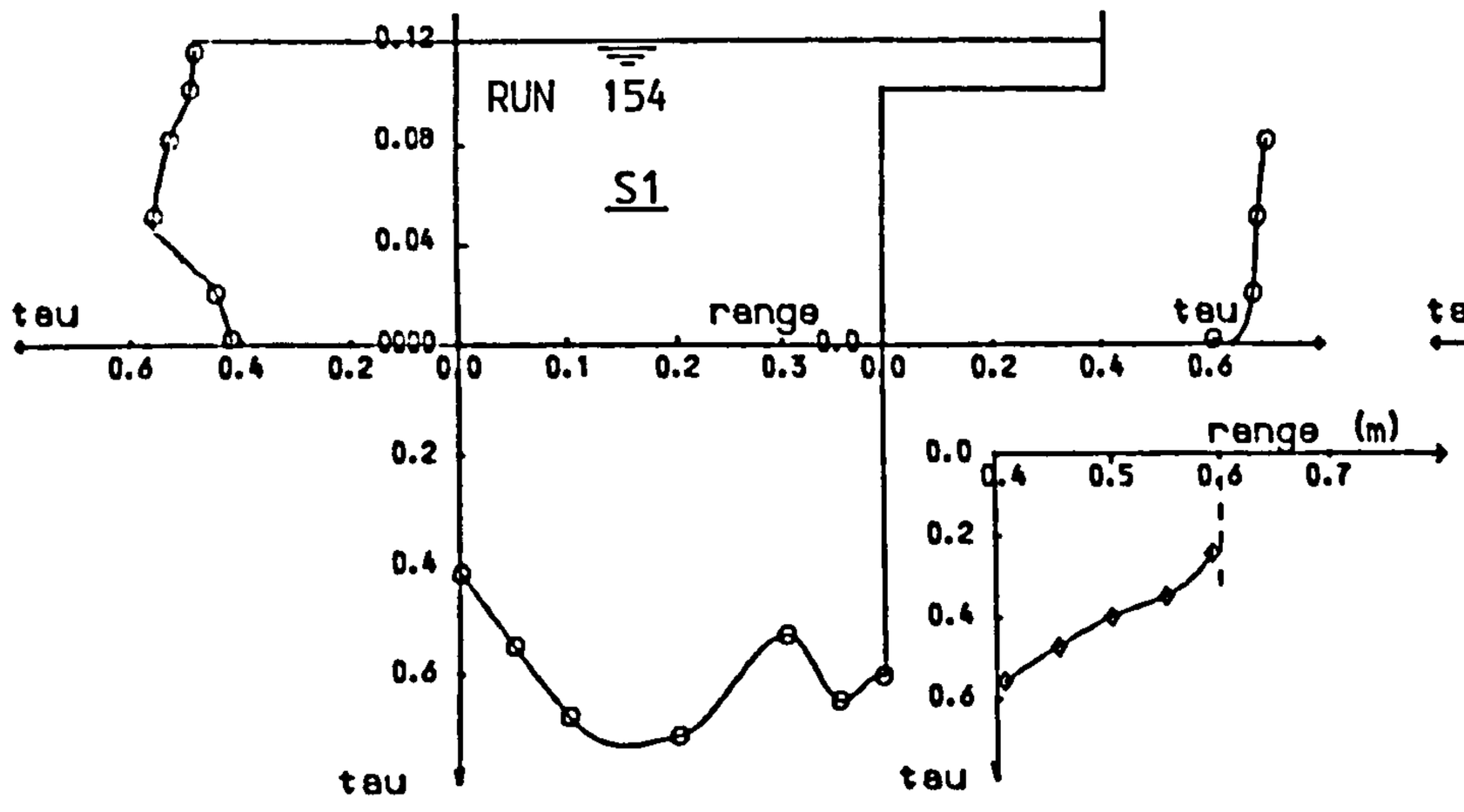

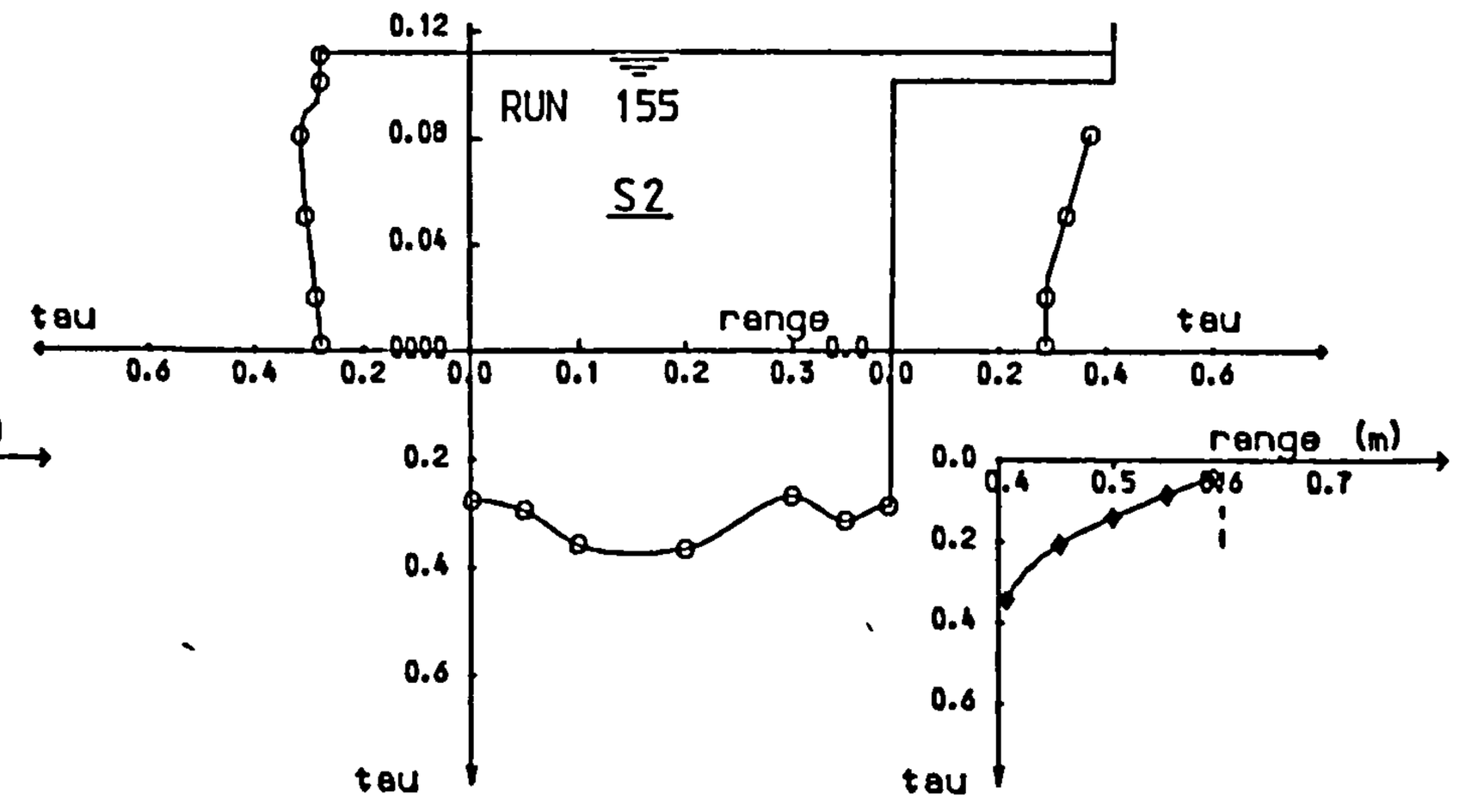

Fig 5·4 Shear stress distribution in channel and flood plain.

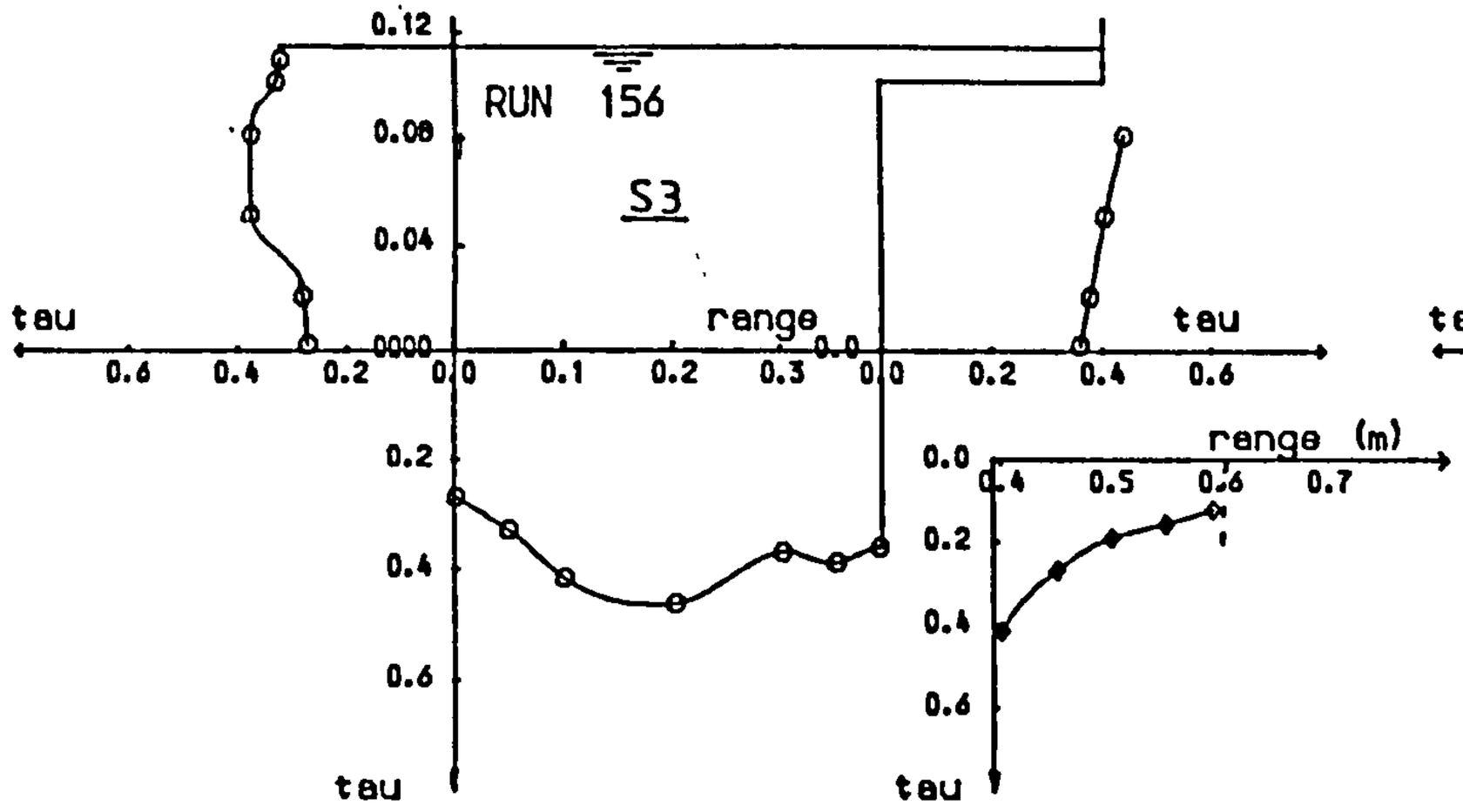

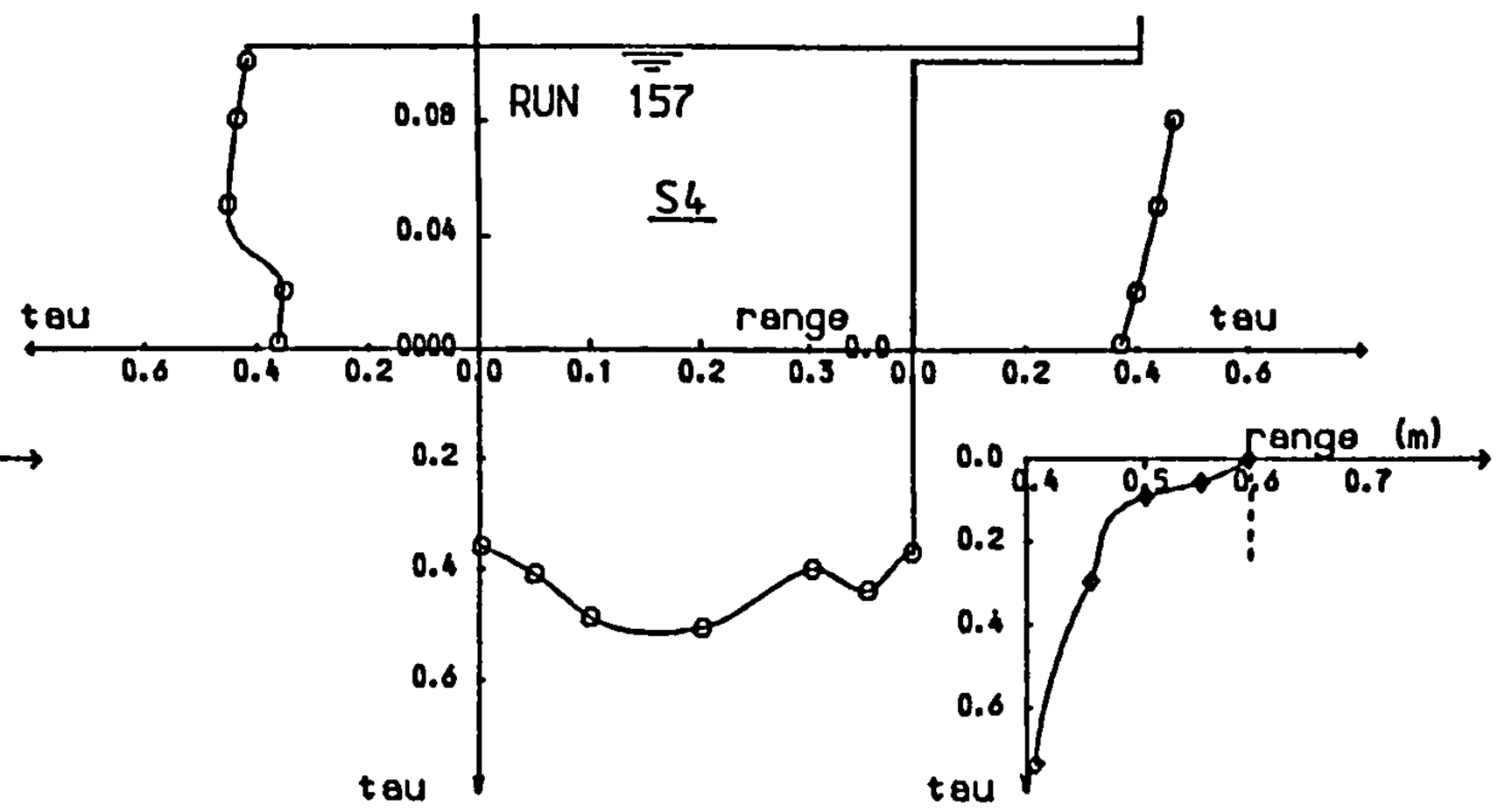

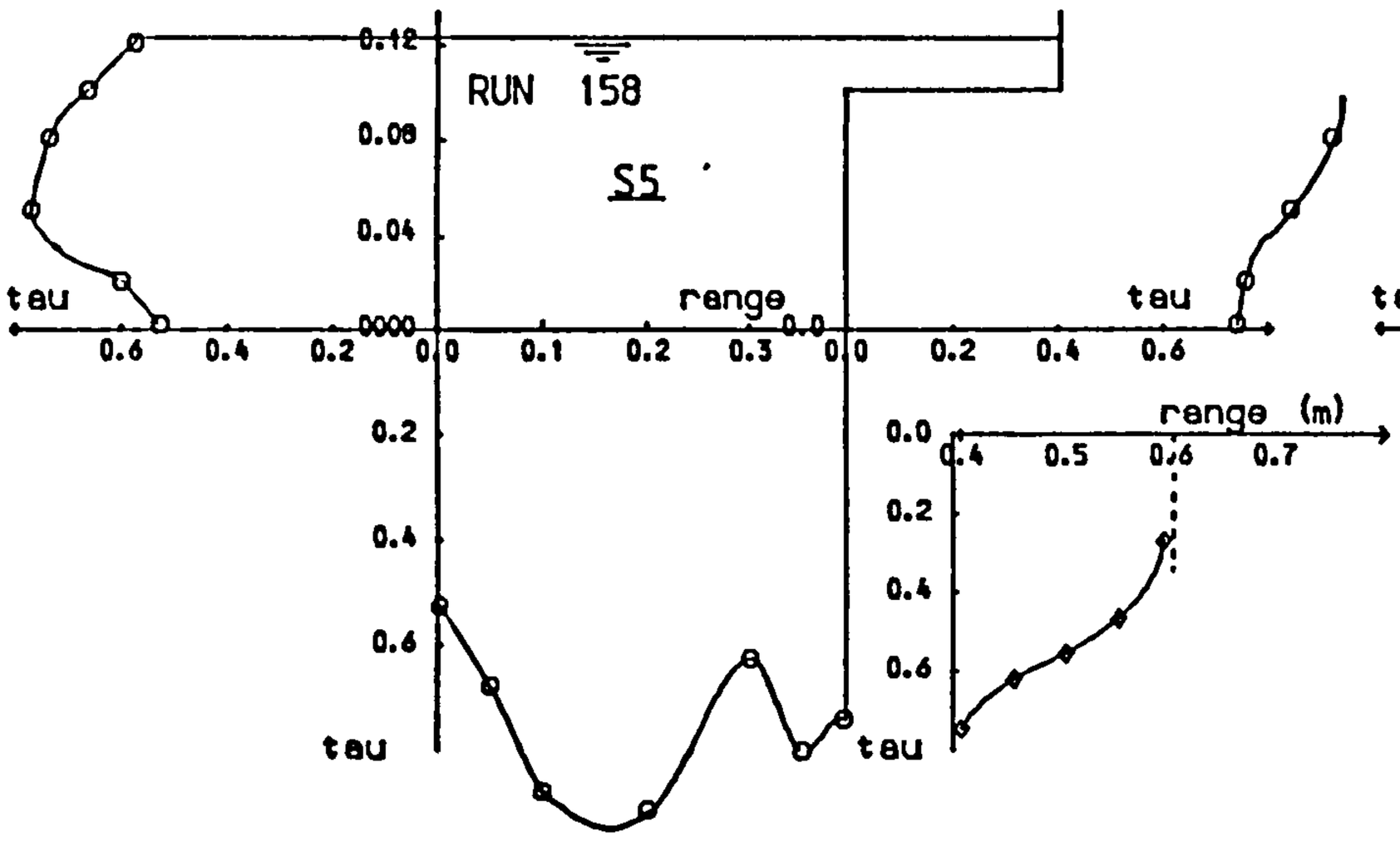

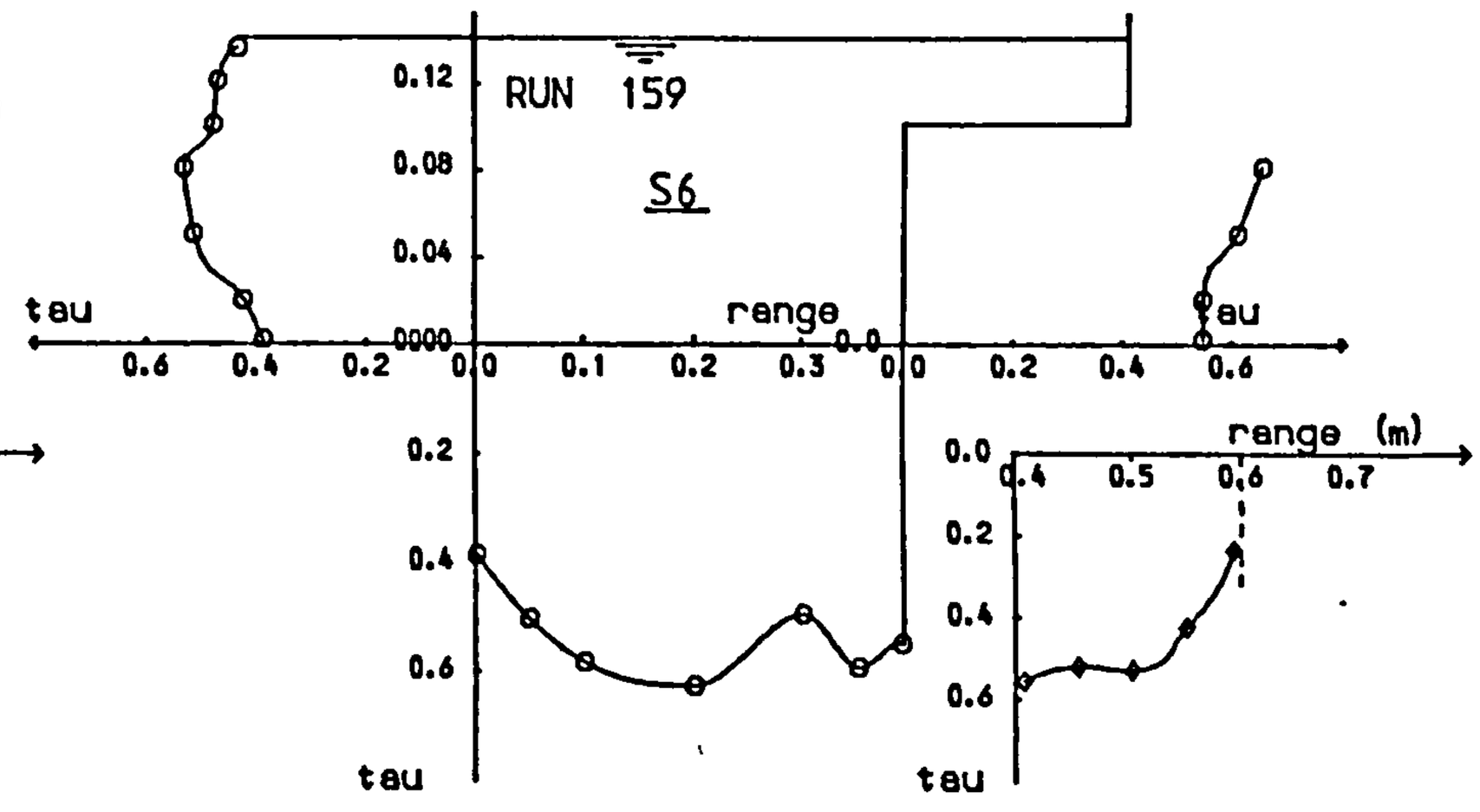

Fig 5·4 Shear stress distribution in channel and flood plain.

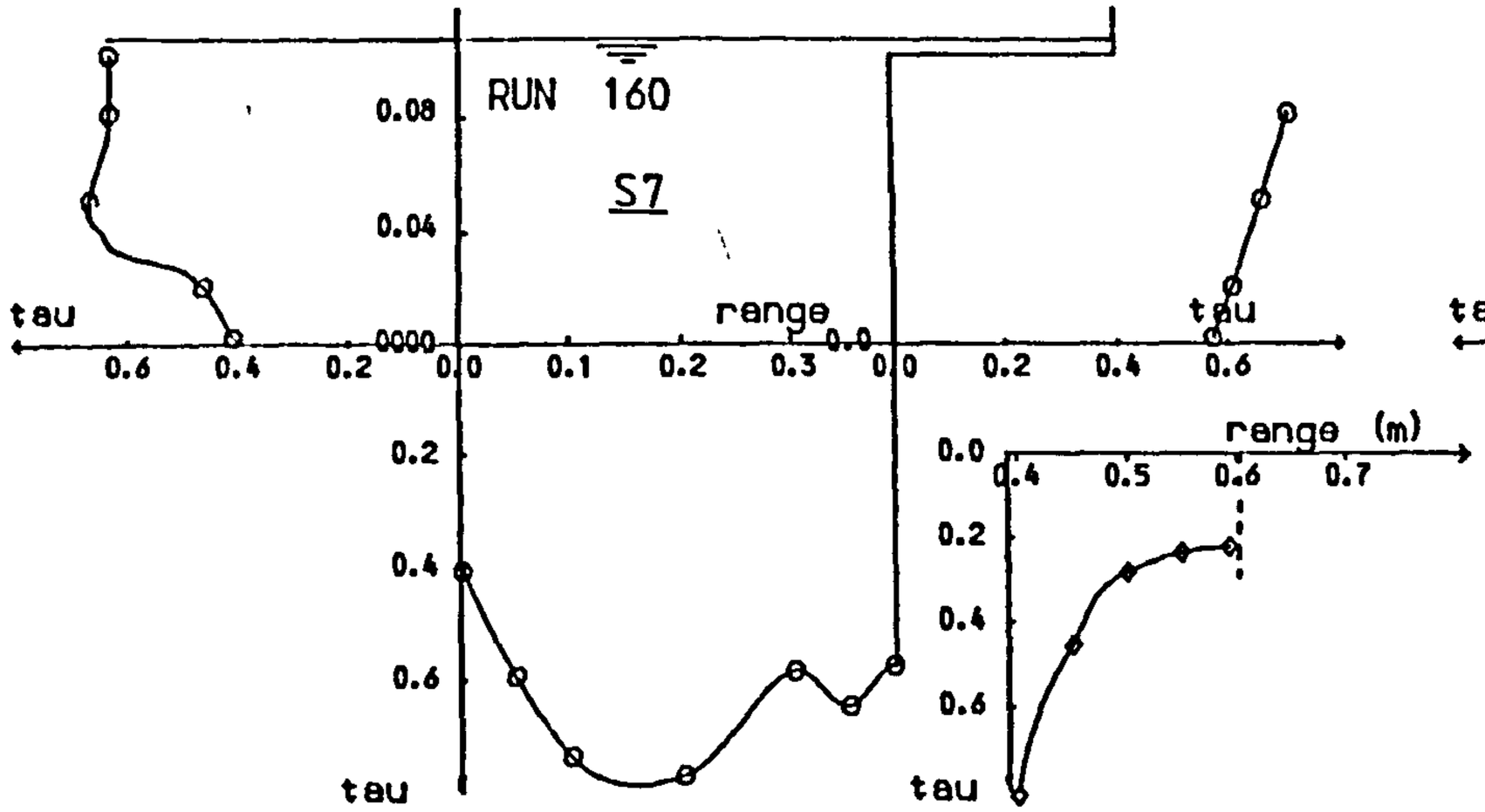

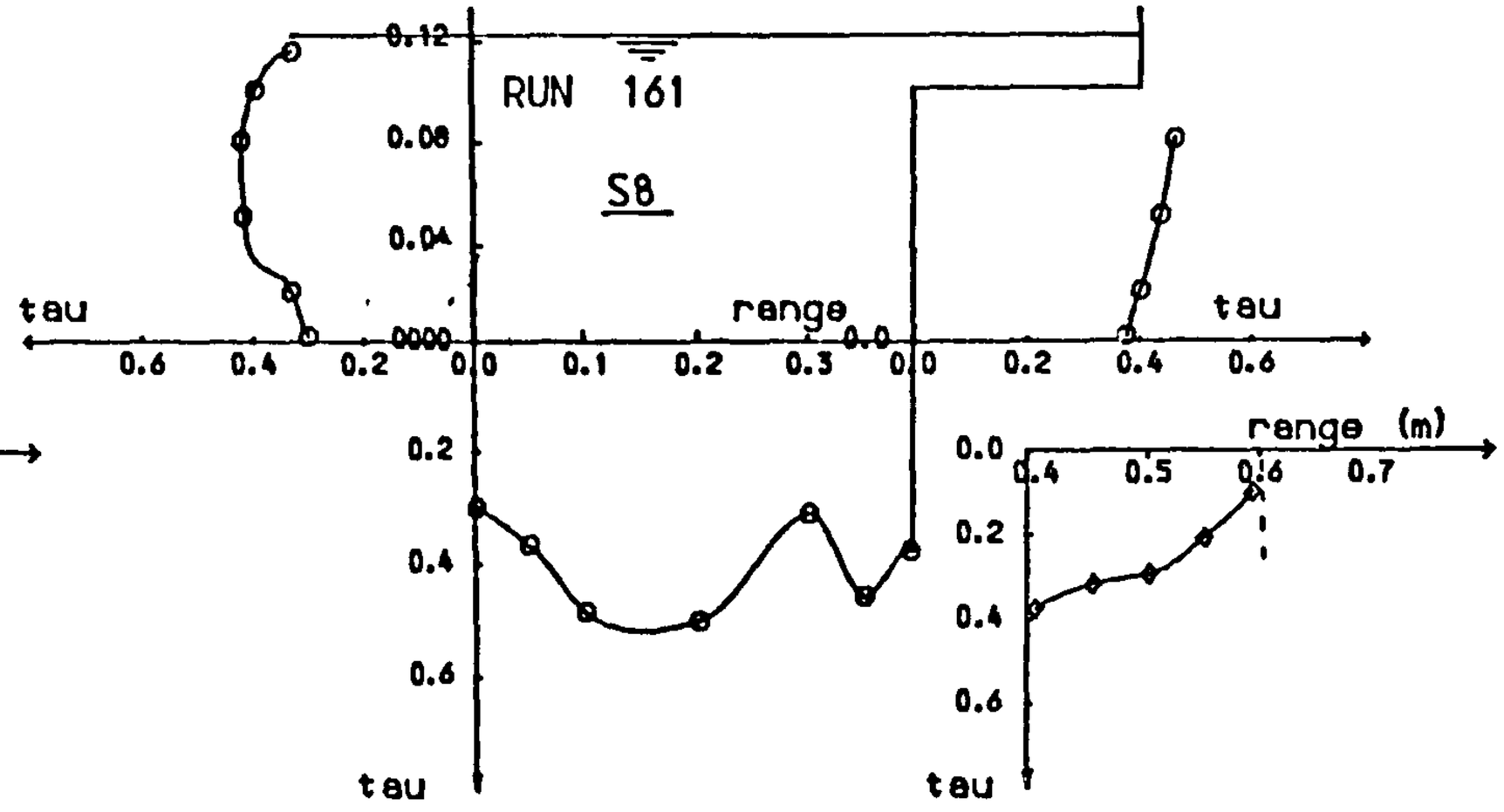

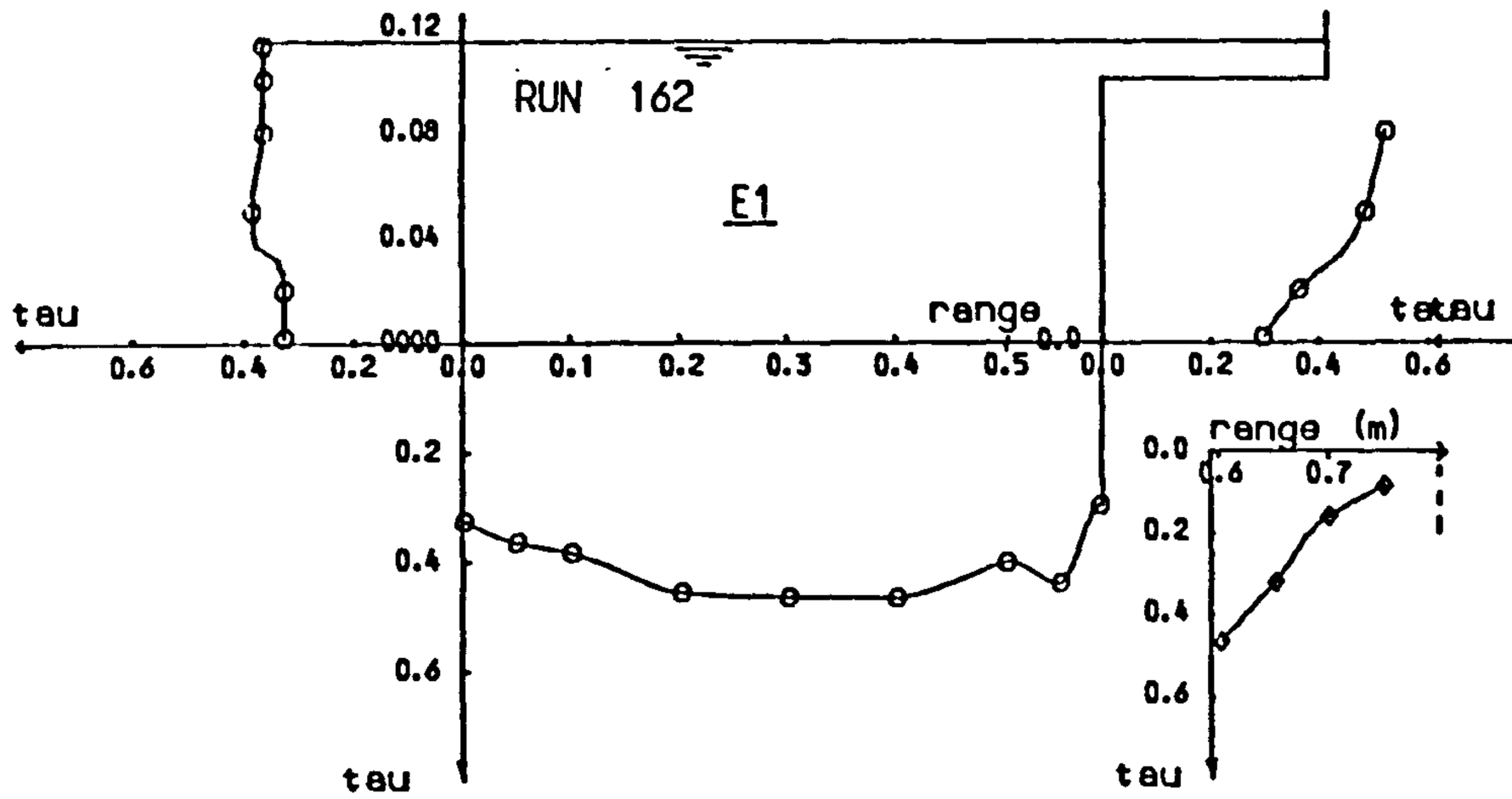

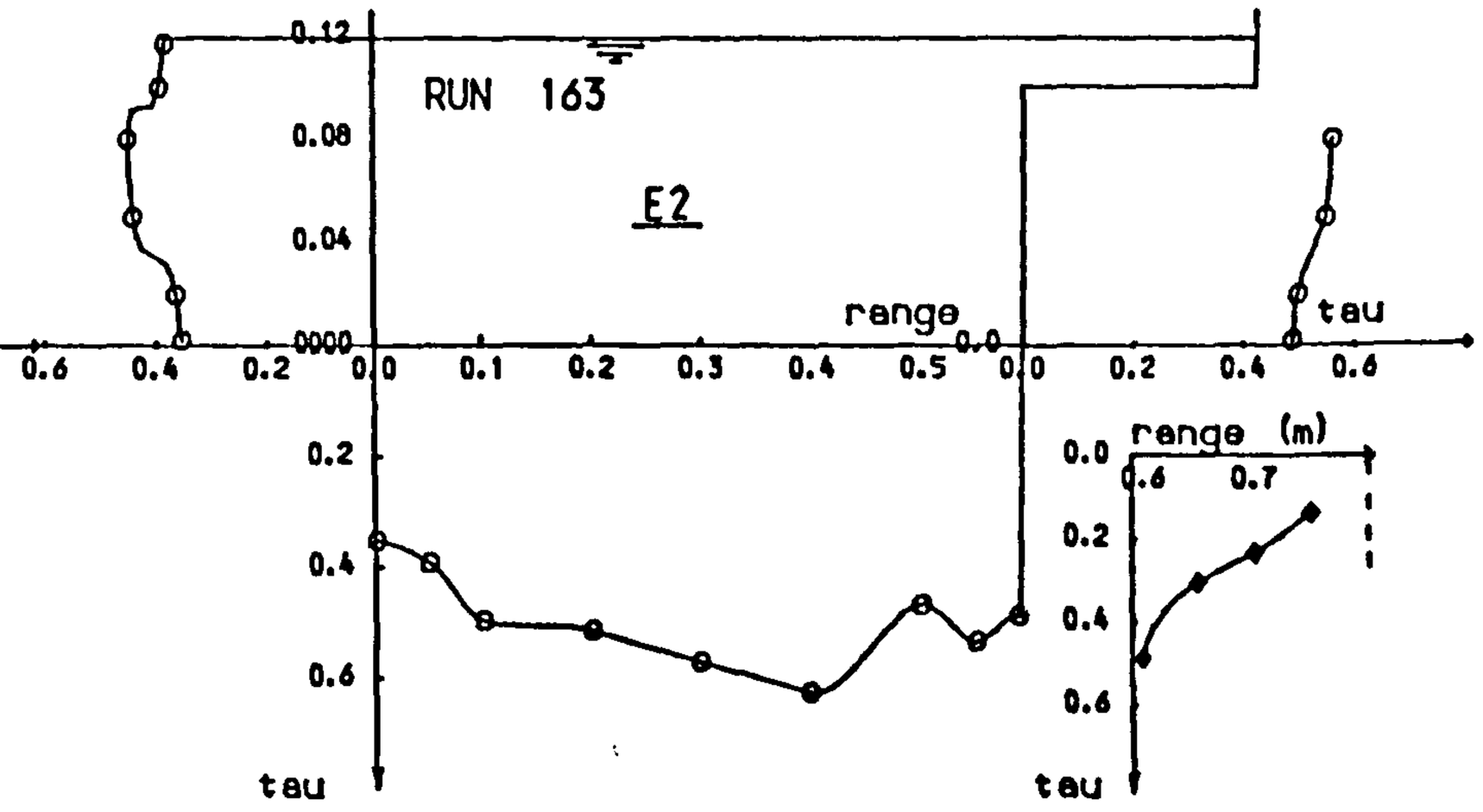

Fig 5·4 Shear stress distribution in channel and flood plain.

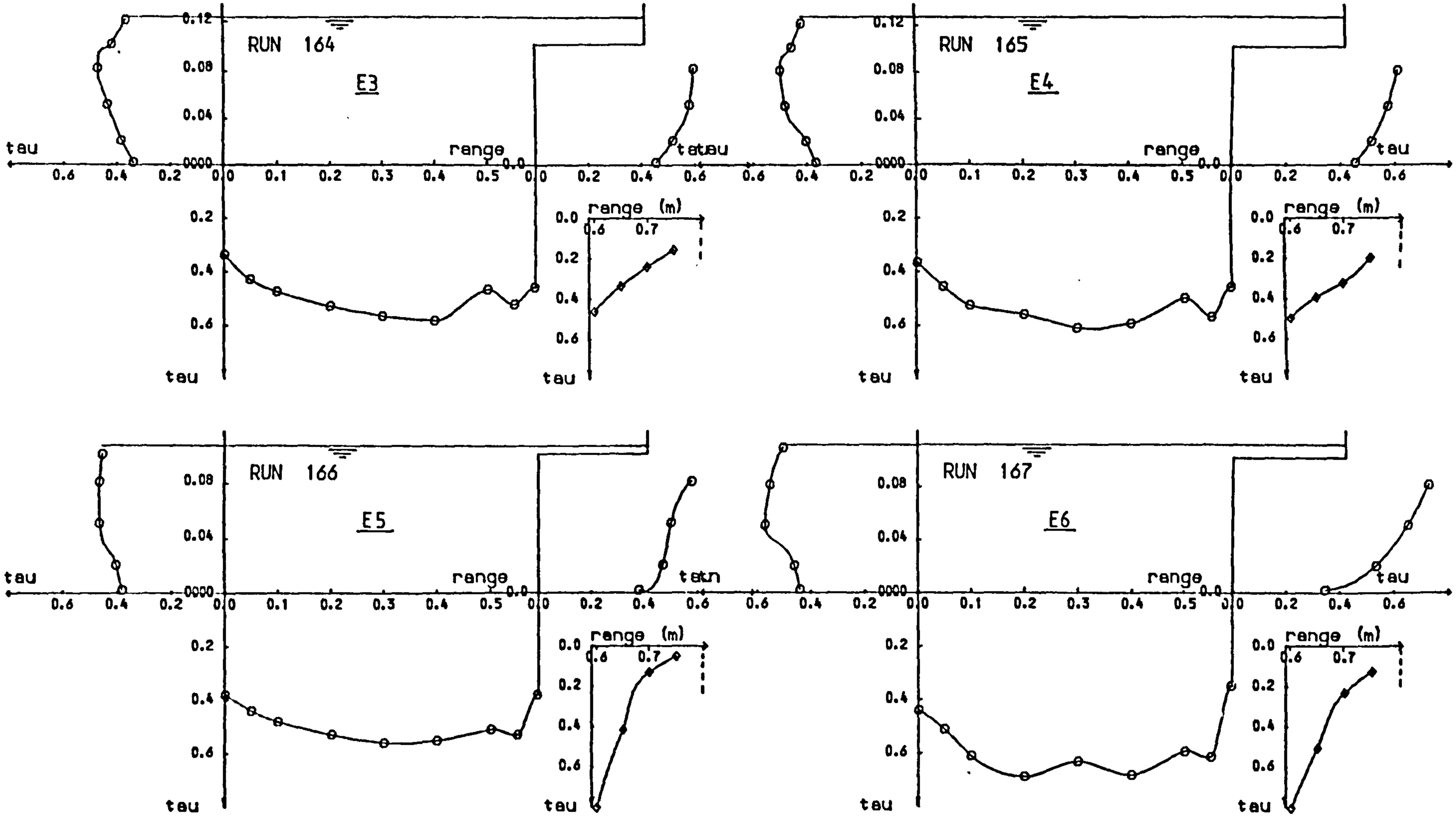

Fig 5·4 Shear stress distribution in channel and flood plain.

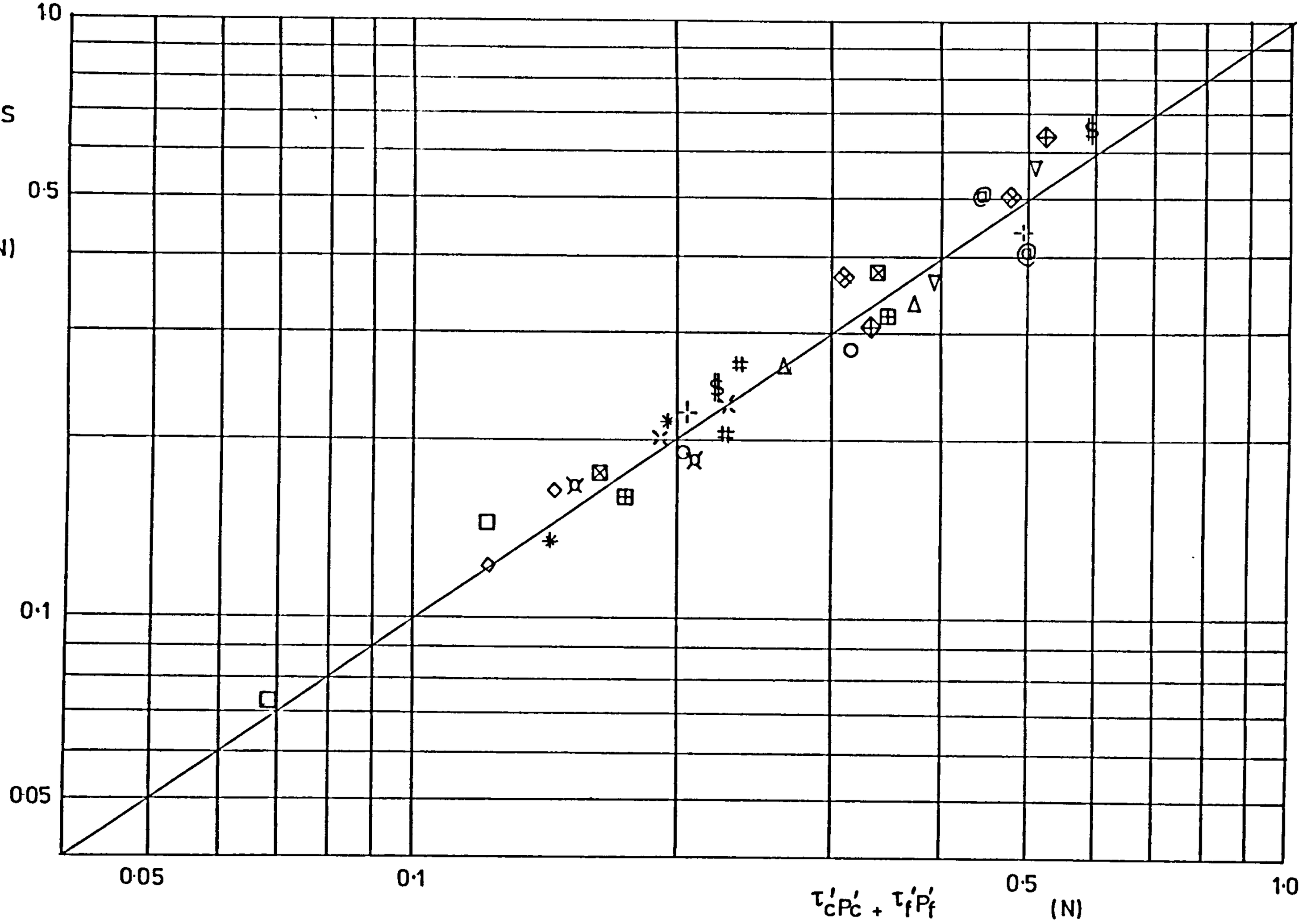

Fig 5·5 Comparison of total measured shear with weight component of flow.

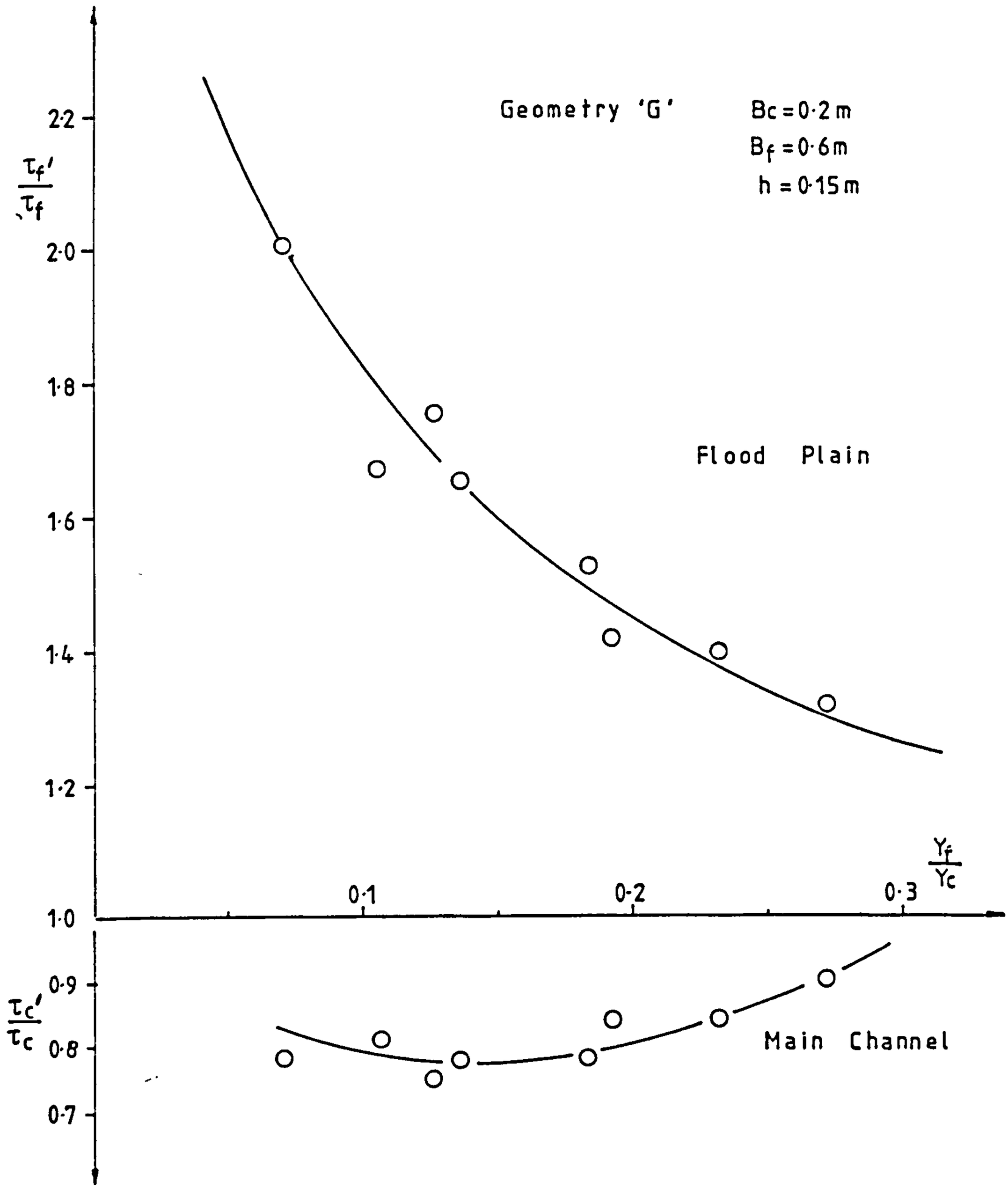

Fig 5·6 Redistribution of boundary shear stress with varying values of relative depth.

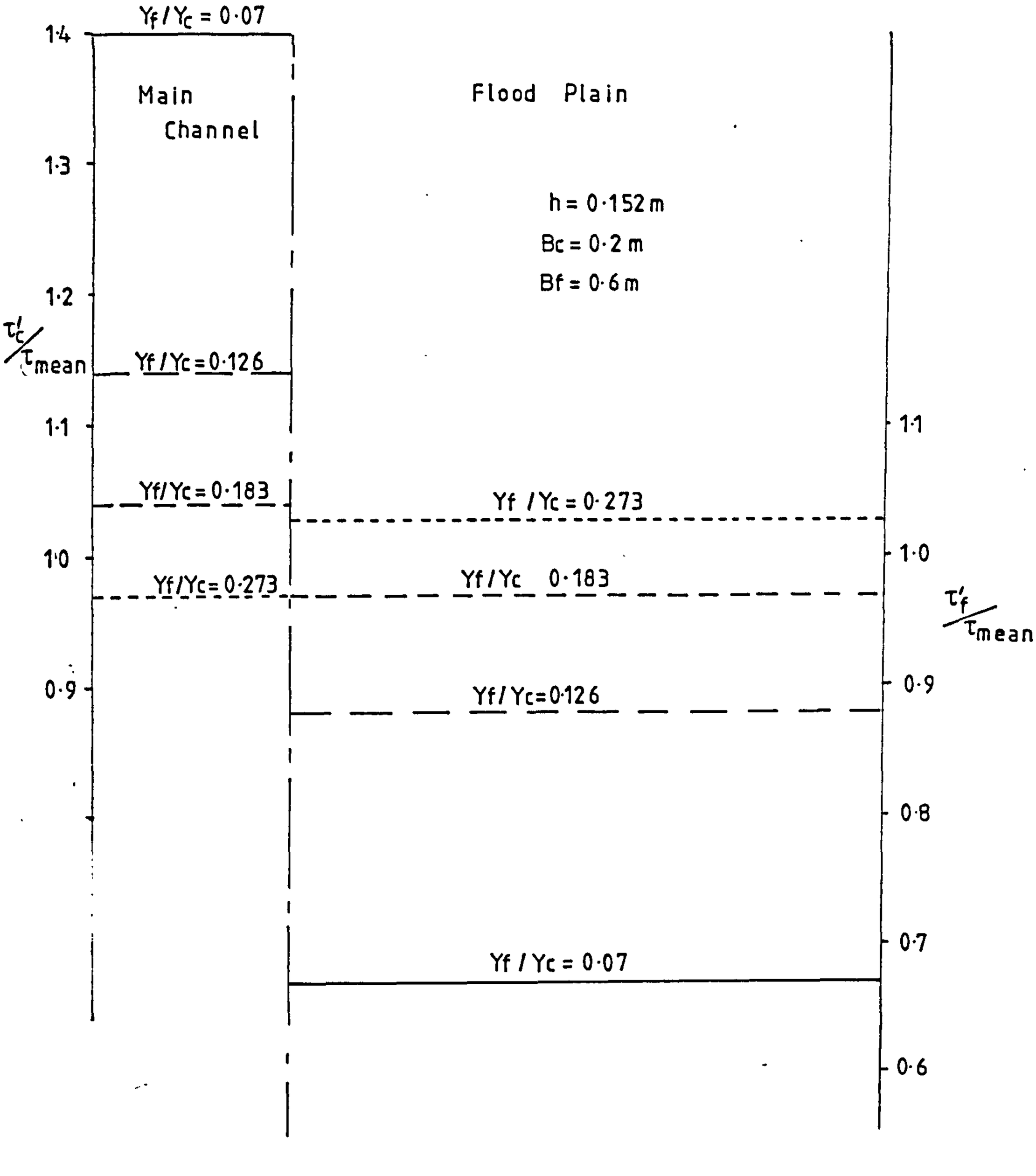

Fig 5·7 Effect of relative depth on lateral shear distribution.

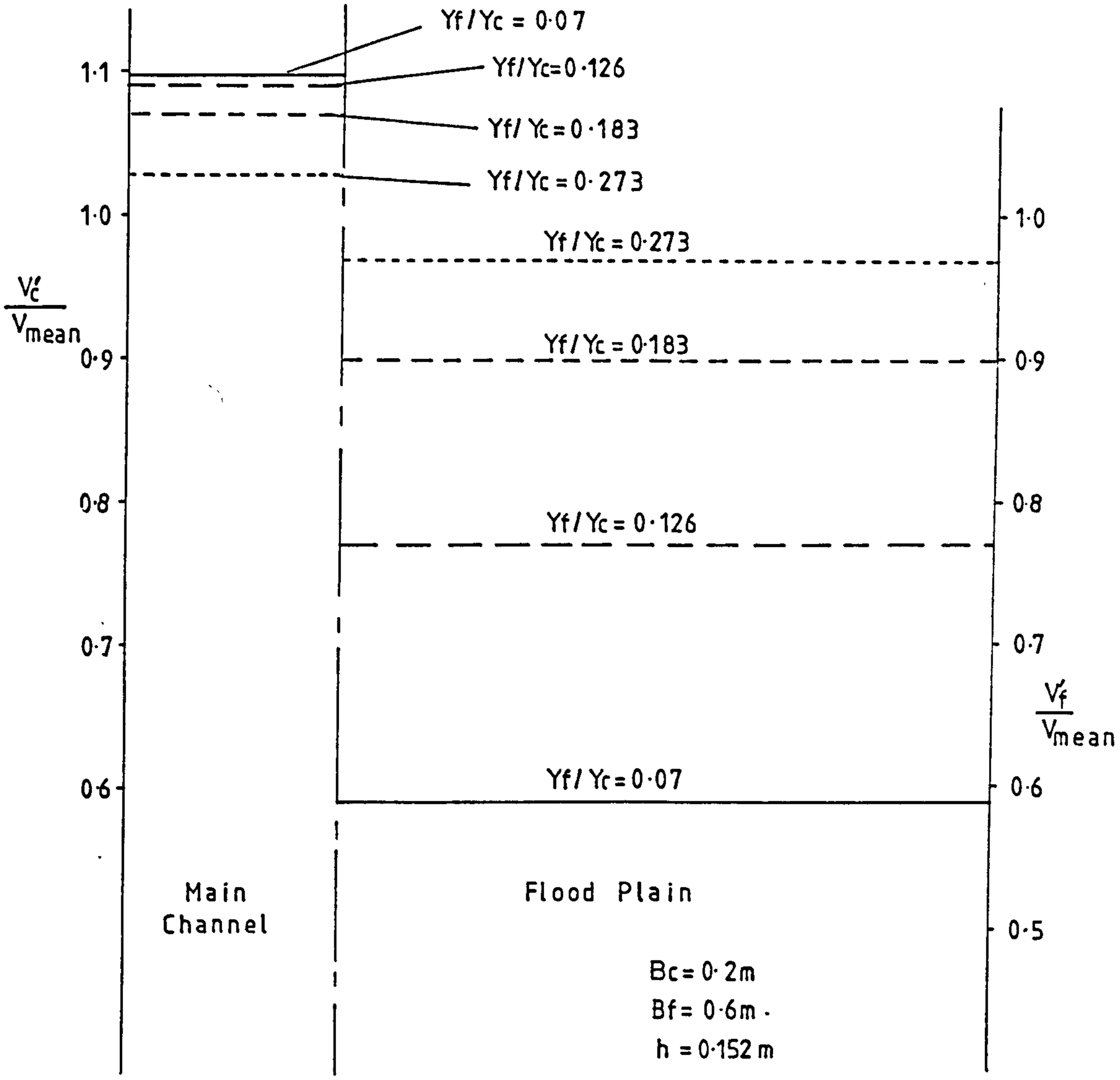

Fig 5·8 Effect of relative depth on lateral velocity distribution.

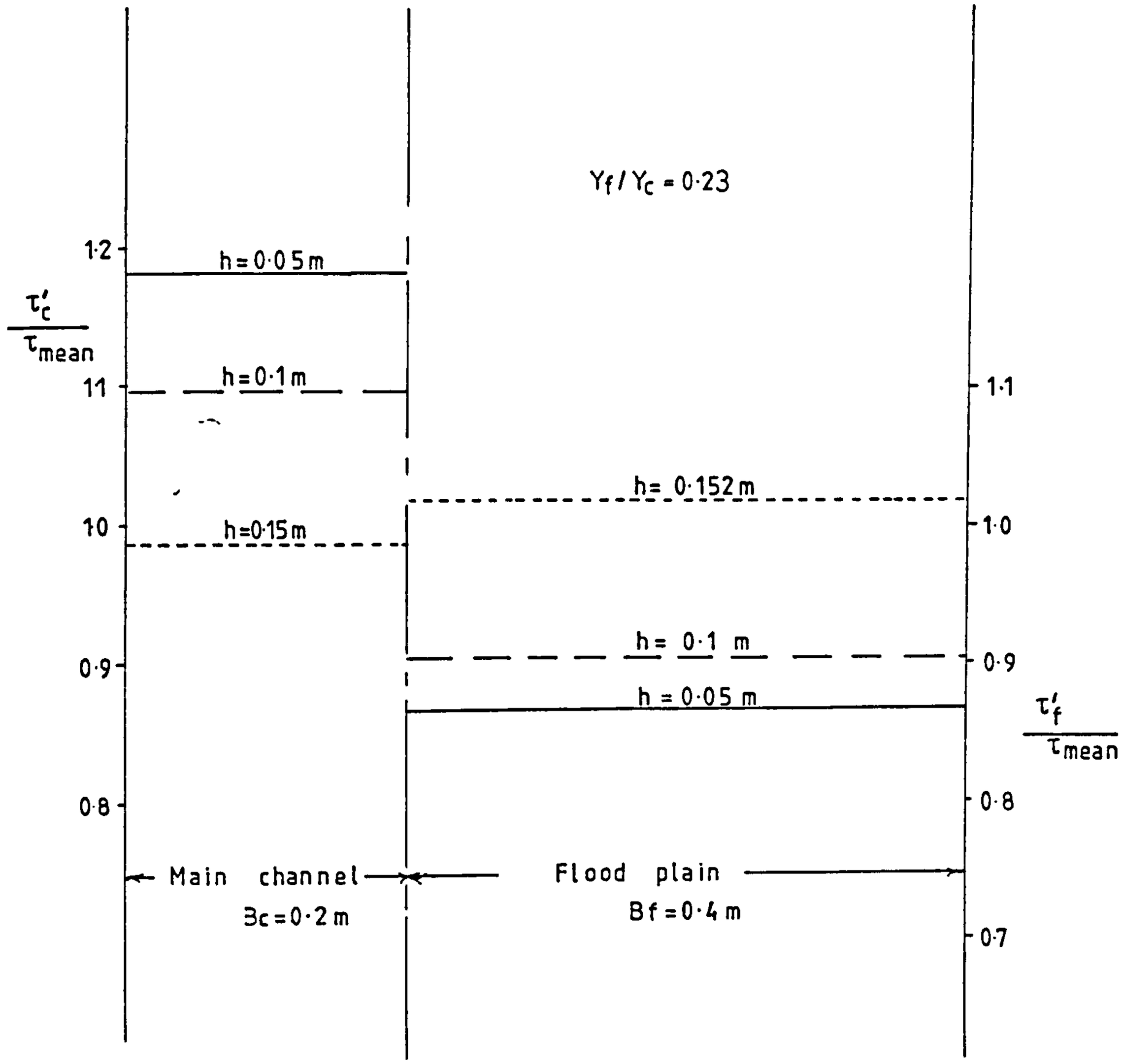

Fig 5·9 Effect of bankfull depth on the lateral shear stress distribution.

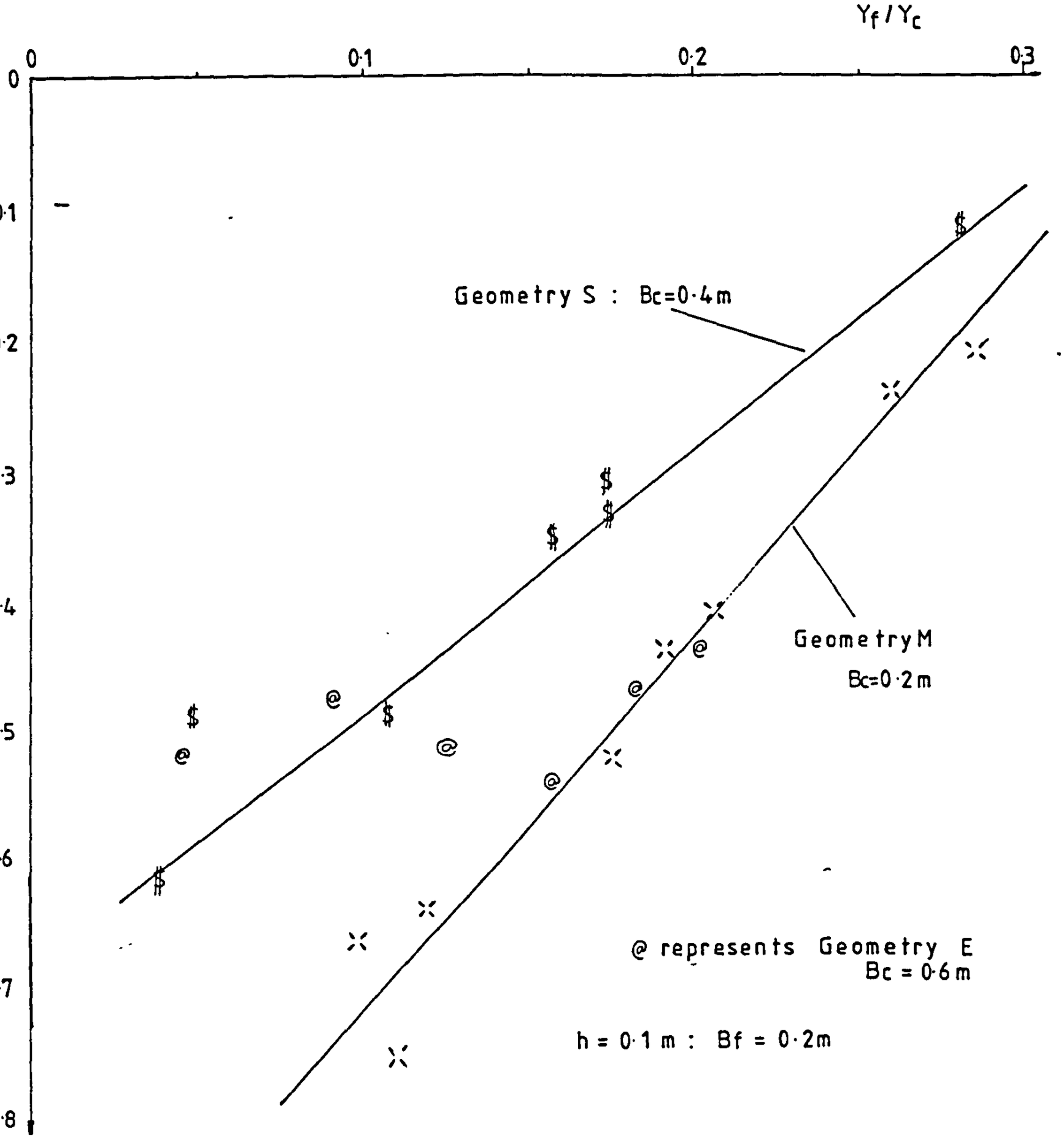

Fig 5·10 Effect of channel width on the lateral shear stress gradient.

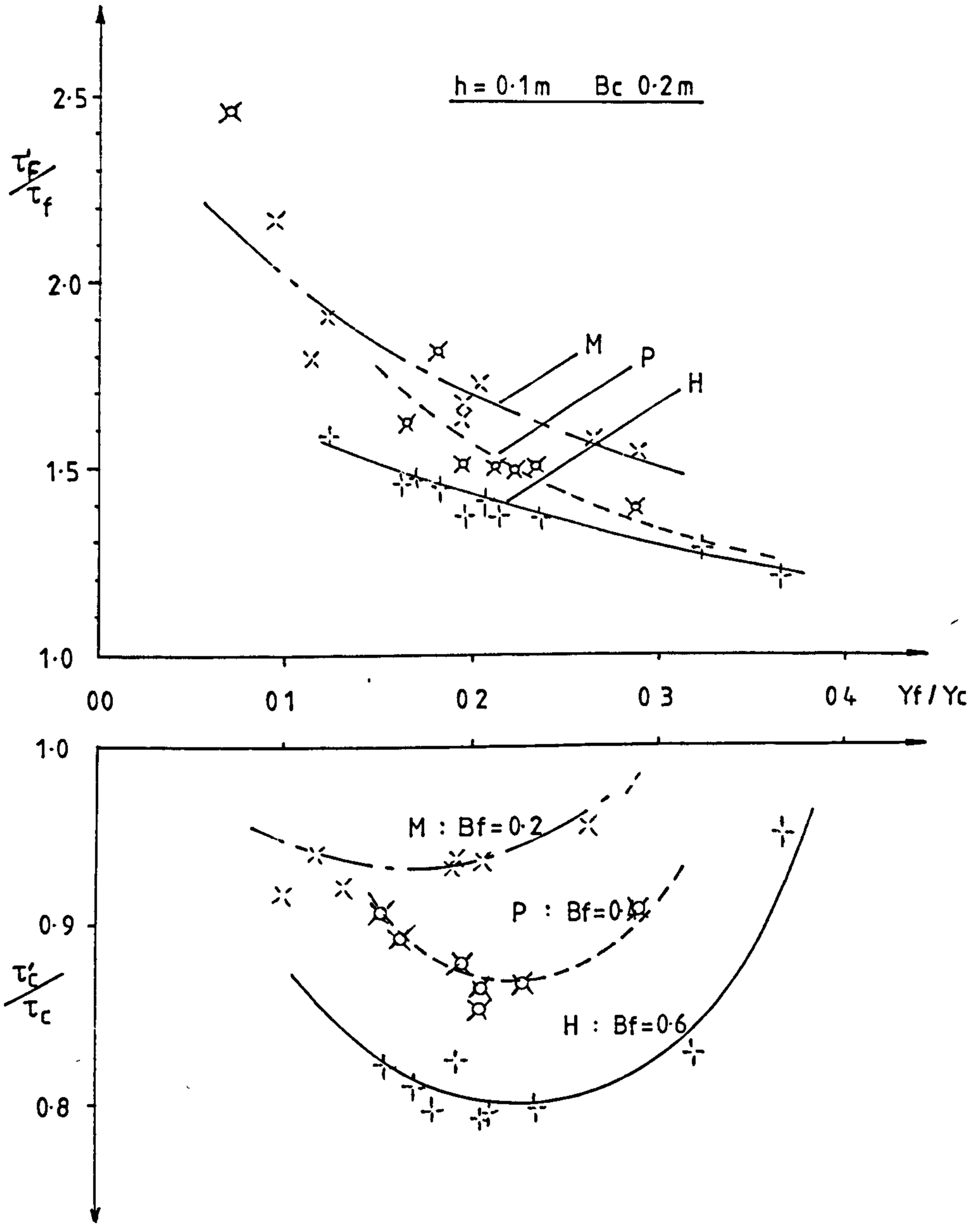

Fig 5·11 Effect of varying flood plain width on redistribution of shear in channel and flood plain.

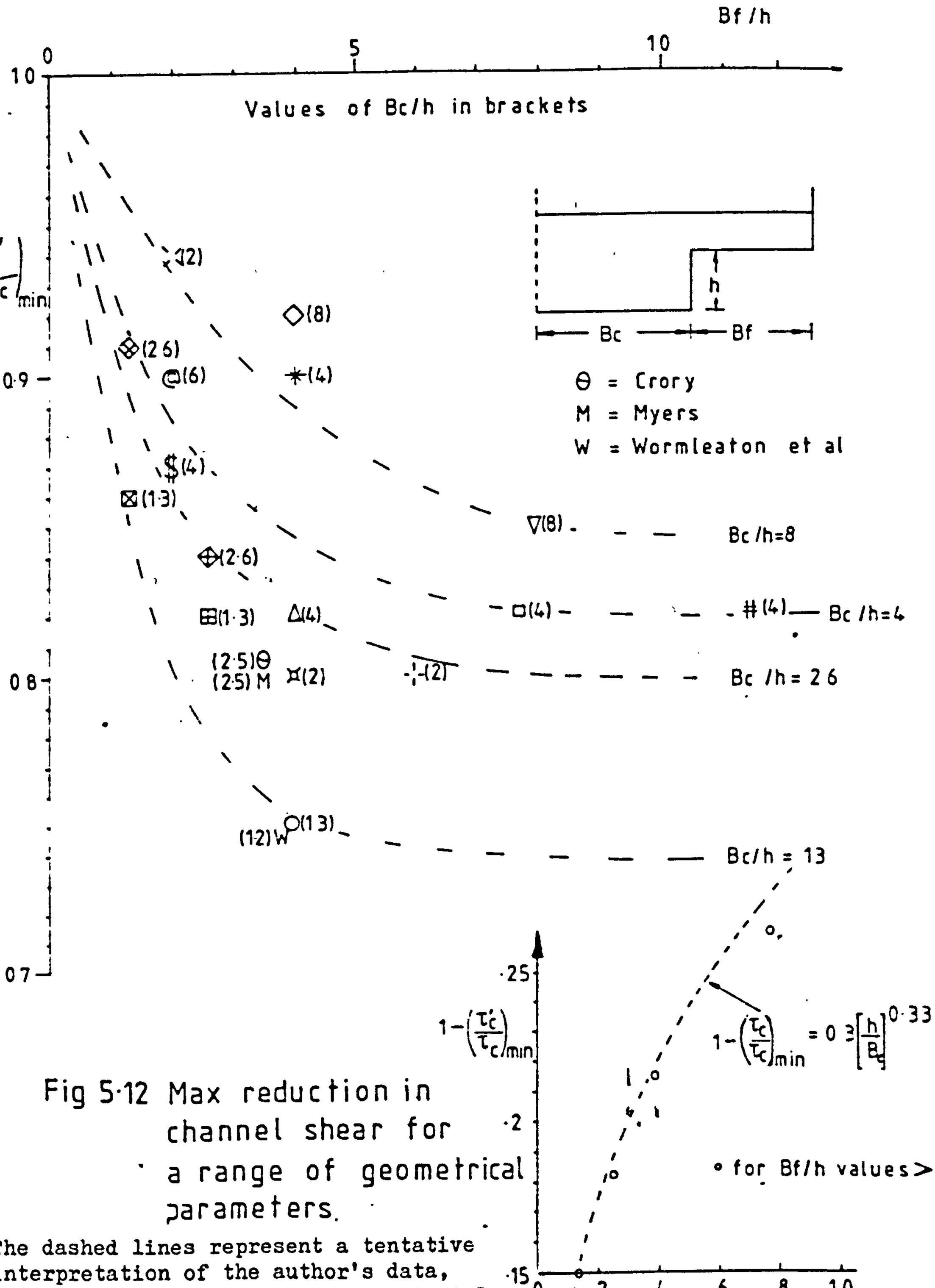

Fig 5·12 Max reduction in channel shear for a range of geometrical parameters.

The dashed lines represent a tentative interpretation of the author's data, based to a large extent on the principle that as the flood plain width increases beyond a certain value, the parameter B_f/h has no further influence on the interaction mechanism. The same argument applies to the main channel width in the form B_c/h.

SYMBOL	GEOMETRY	RUN NO	(mm) h	(mm) B_c	(mm) B_f	No of tests
△	K	1–10	102	400	400	10
▽	A	11–22	52	400	400	12
□	B	23–30	52	200	400	8
◇	C	31–37	52	400	200	7
○	G	38–45	152	200	600	8
⊞	L	46–53	152	200	400	8
⊠	N	54–61	152	200	200	8
◈	J	62–70	152	400	400	9
◈	R	71–78	152	400	200	8
⊕	MYERS	79–88	102	254	356	10
⊹	RAJARATNAM	89–93	98	711	508	5
⋈	P	94–103	102	200	400	10
⊹	H	104–113	102	200	600	10
⋇	M	114–121	102	200	200	8
θ	CRORY	122–126	102	254	356	6
⋌	CRORY	127–130	102	203	356	4
λ	CRORY	131–133	102	153	356	3
μ	CRORY	134–137	102	102	356	4
*	O	138–145	52	200	200	8
#	I	146–153	52	200	600	8
$	S	154–161	102	400	200	8
@	E	162–167	102	600	200	6

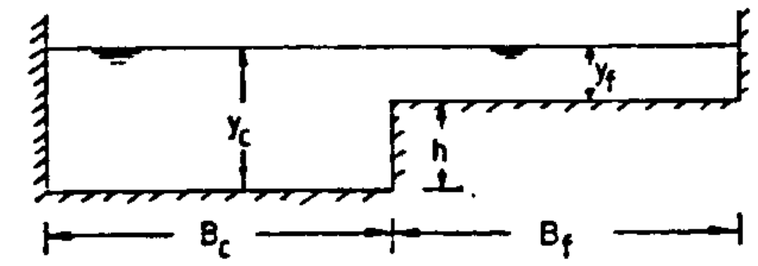

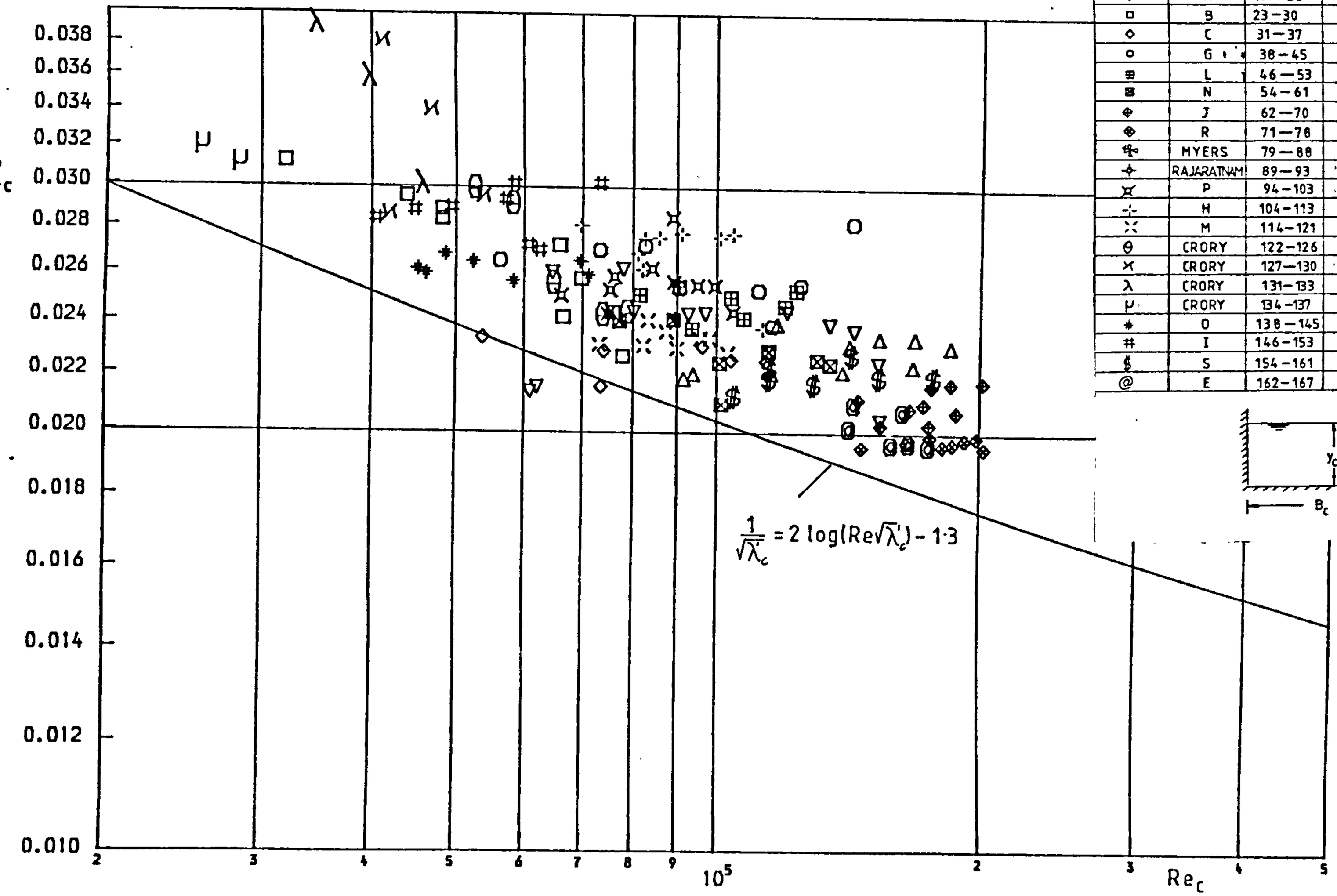

Fig 5.13 Comparison of λ'_c with Re_c

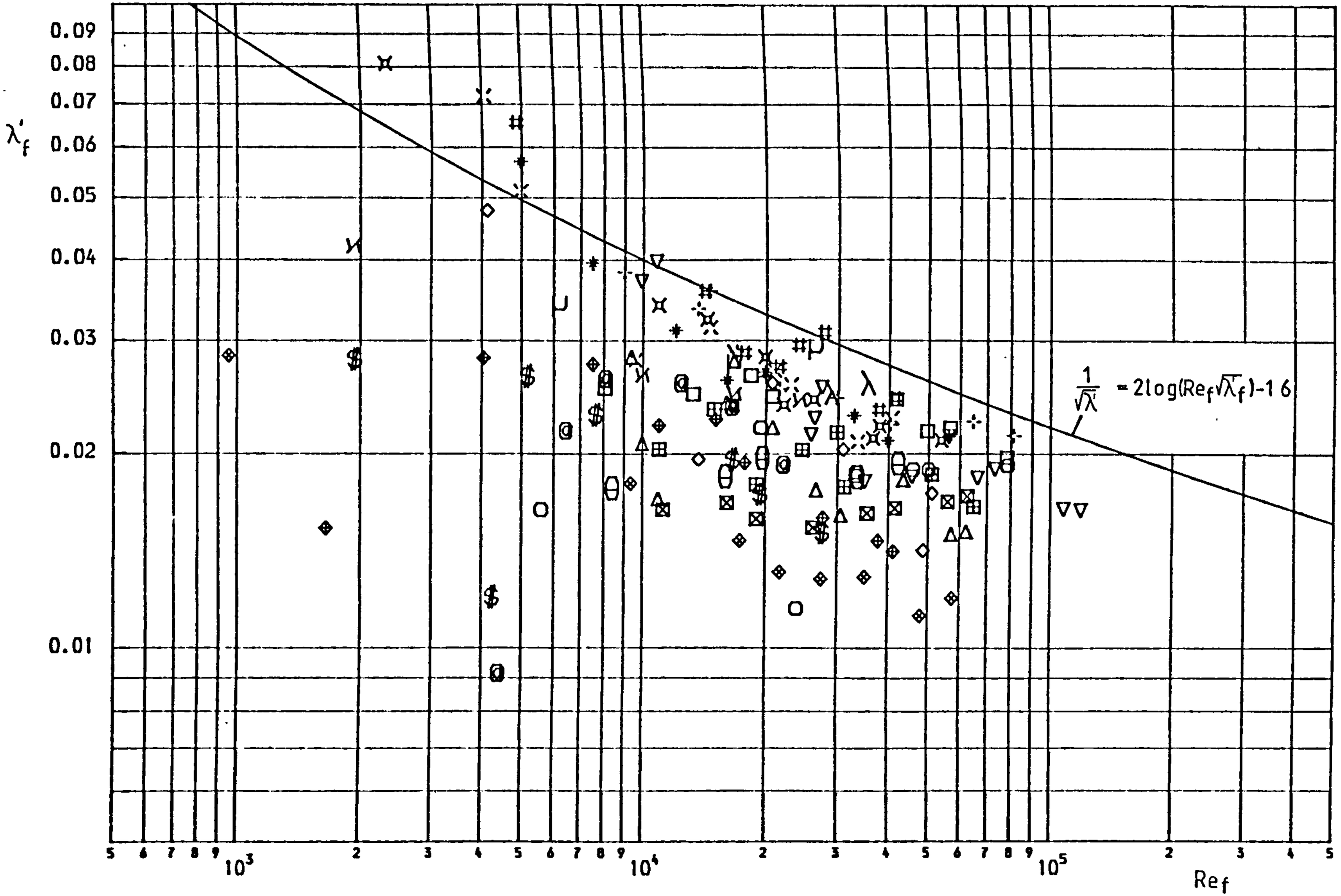

Fig 5.14 Comparison of λ_f' with Re_f

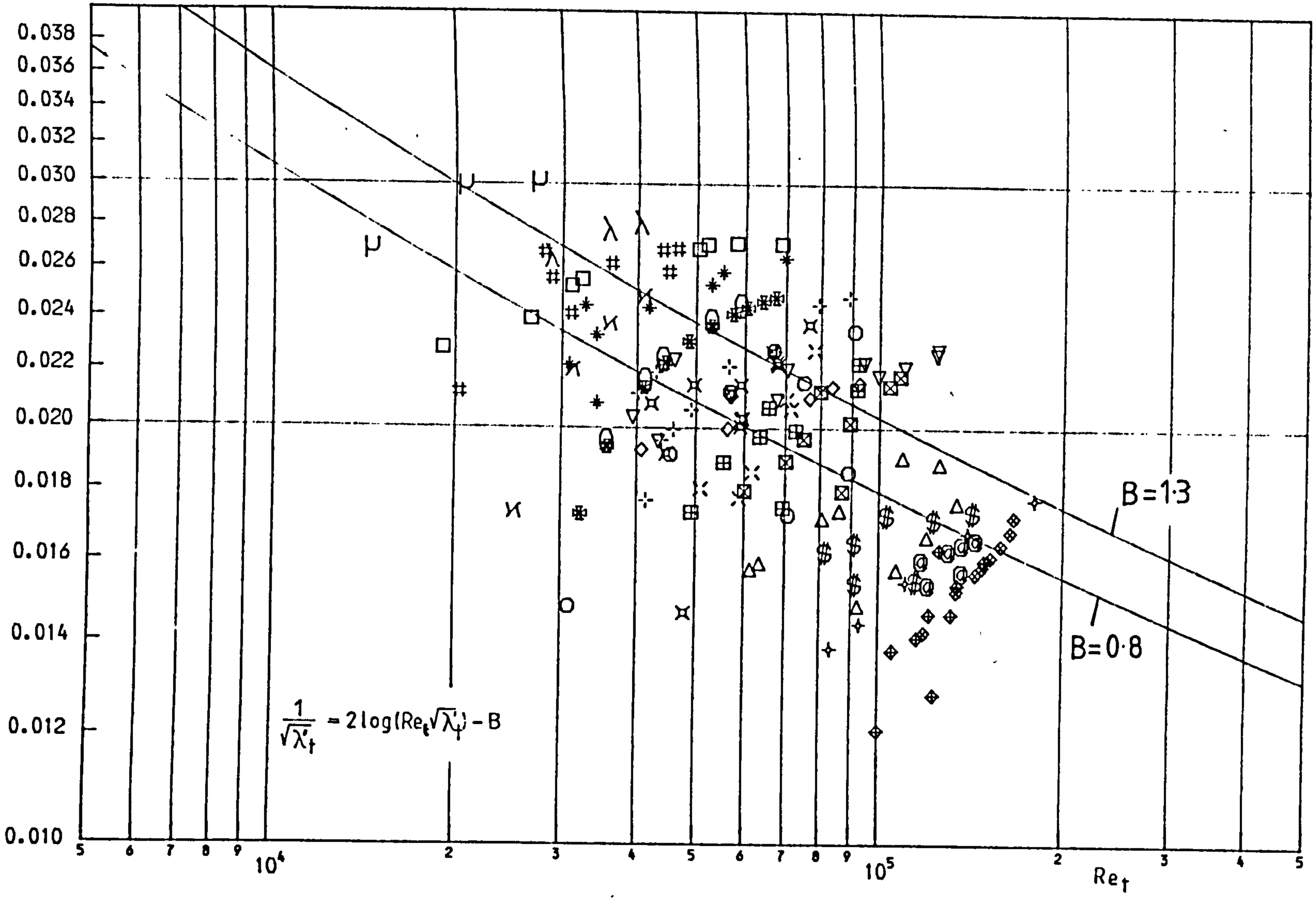

Fig 5·15 Comparison of λ_t with Re_t

SYMBOL	GEOMETRY	RUN NO	(mm) h	(mm) B_c	(mm) B_f	No of tests
△	K	1—10	102	400	400	10
▽	A	11—22	52	400	400	12
□	B	23—30	52	200	400	8
◇	C	31—37	52	400	200	7
○	G	38—45	152	200	600	8
⊞	L	46—53	152	200	400	8
⊠	N	54—61	152	200	200	8
⊕	J	62—70	152	400	400	9
◈	R	71—78	152	400	200	8
⧑	MYERS	79—88	102	254	356	10
✧	RAJARATNAM	89—93	98	711	508	5
⋇	P	94—103	102	200	400	10
⊹	H	104—113	102	200	600	10
✕	M	114—121	102	200	200	8
θ	CRORY	122—126	102	254	356	6
✕	CRORY	127—130	102	203	356	4
λ	CRORY	131—133	102	153	356	3
μ	CRORY	134—137	102	102	356	4
*	O	138—145	52	200	200	8
#	I	146—153	52	200	600	8
$	S	154—161	102	400	200	8
@	E	162—167	102	600	200	6

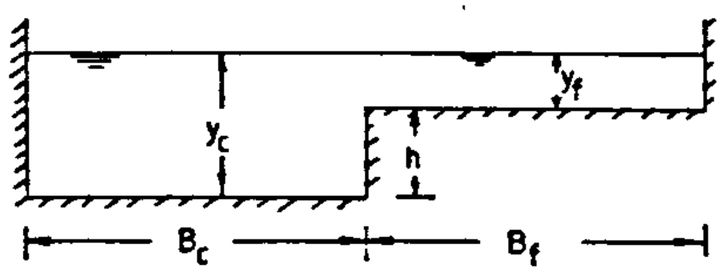

Fig 5·16 Comparison of τ_c' with V_c' showing 'squared' relationship.

CHAPTER SIX

THE APPARENT SHEAR STRESS

Table of Contents

6.1 Introduction.

Up to this point, the effect of the interaction mechanism on the velocities and shear stresses in both the channel and the flood plain have been well demonstrated. It has been shown that the channel velocity and boundary shear are considerably reduced as a result of momentum transfer existing at the channel/flood plain junction. A significant increase in flood plain velocity and boundary shear has also been observed. The redistribution of flow which occurs during overbank flow is a direct result of the turbulent shear mechanism occurring at the channel/flood plain junction. In this chapter, an attempt will be made to relate the intensity of these shear mechanisms to an Apparent shear stress which is considered to act conceptually on the vertical plane which separates the channel from the flood plain.

The reduction in velocity in the channel also implies a transfer of energy from the channel. Some of this energy is transferred to the flood plain with the remainder dissipated in vorticies and eddies formed at the junction. Due to the indeterminant nature of the energy loss, the momentum principle is the most satisfactory method of analysis, applied

in the sense of a force balance for each section of the channel and flood plain, with out of balance forces incorporated in an apparent shear stress term considered to be acting at the channel/flood plain junction.

It has also been shown that the relative changes in shear and velocity which occur are strongly affected by the geometrical parameters of the flow and cross section. An attempt will therefore be made to relate the change in shear (and velocity) to the flow characteristics and geometrical parameters of the compound channel.

6.2 Theoretical Considerations.

Consider the compound channel of unit length shown on Fig 6.1. For uniform flow conditions the equation of force equilibrium in the channel region is given as :-

$$\rho g A_c \sin\theta = \tau_c' P_c' + \text{"OUT OF BALANCE FORCE"} \qquad (6.1)$$

where τ_c' is the interacting channel shear stress distributed around the channel of wetted perimeter Pc' (Pc'=h+Yc+Yf). Ac is the cross sectional area of flow in the channel. $\rho g \sin\theta$ is the weight component of the flow down the channel. If θ is small enough then $\sin\theta = S$ where S is the channel slope. The

"OUT OF BALANCE FORCE" exists due to the momentum transfer mechanism. If this force can be considered as an "Apparent shear force" acting over the channel/flood plain junction depth Yf, then Equation (6.1) can be rewritten :-

$$\tau'_c P'_c + \tau_a Y_f = \rho g A_c S \qquad (6.2)$$

where τ_a is the apparent shear stress and can be considered a measure of the intensity of the interaction mechanism. Since $\rho g A_c S$ can be given by $\tau_c P_c$, where $\tau_c = \rho g R_c S$, then Equation (6.2) becomes :-

$$\tau'_c P'_c + \tau_a Y_f = \tau_c P_c \qquad (6.3)$$

or
$$\tau_a Y_f = \tau_c P_c - \tau'_c P'_c \qquad (6.4)$$

and finally
$$\tau_a = \frac{\tau_c P_c - \tau'_c P'_c}{Y_f} \qquad (6.5)$$

Consider the flow in the flood plain in a similar manner :-

$$\tau'_f P'_f = \text{"OUT OF BALANCE FORCE"} + \rho g A_f S \qquad (6.6)$$

where $\tau_{f'}$ is the measured shear stress in the flood plain acting over the wetted perimeter Pf' (given as Pf'=Bf+Yf), Af is the cross sectional area of the flood plain flow. In this case the "Out of Balance Force", or apparent shear force assists the flow in the flood plain. Equation (6.6) can be rewritten as :-

$$\tau_f' P_f' = \tau_a Y_f + \tau_f P_f \qquad (6.7)$$

which gives $$\tau_a = \frac{\tau_f' P_f' - \tau_f P_f}{Y_f} \qquad (6.8)$$

where τ_f is given as $\rho g A f / P f S$. If the equilibrium of forces across the flood plain and the main channel are considered then Equations (6.3) and (6.7) should simplify to :-

$$\tau_f' P_f' + \tau_c' P_c' = \rho g (A c + A f) S \qquad (6.9)$$

This is the case only if τ_a calculated from Equations (6.5) and (6.8) are the same. In other words, the apparent shear force which resists flow in the main channel must be equal to the apparent shear force which assists flow in the flood plain. This would imply the following relationship :-

$$\frac{\tau_c P_c - \tau_c' P_c'}{Y_f} = \frac{\tau_f' P_f' - \tau_f P_f}{Y_f} \qquad (6.10)$$

or
$$\tau_c P_c + \tau_f P_f = \tau_c' P_c' + \tau_f' P_f' \qquad (6.11)$$

Thus it is clear that the changes in shear which occur in both the flood plain and the channel are caused by the interaction mechanism and interelated by the apparent shear force concept Furthermore, it is possible, from Equations (6.5) or (6.8), to determine the apparent shear stress provided the interacting shear stress and flow parameters are known. The next section will present the apparent shear stress calculated from the results of the 136 tests carried out in the present study.

It would be interesting at this stage to recall past investigations which have considered the apparent shear stress acting at the channel/flood plain junction. In the interest of clarity, some of the work presented in Chapter 2 will be repeated.

Perhaps the first researcher to determine the apparent shear stress for a compound channel was Myers (Ref 36). Fig 6.2 shows the relationship between the apparent shear stress and the relative depth, Yf/Yc for a given channel

geometry. It is obvious from this graph that the apparent shear stress τ_a is a maximum at very low relative depths. If the apparent shear stress is multiplied by the flood plain depth then the apparent shear force per unit length of channel is determined. From Fig 6.3, Myers was able to show that the apparent shear force was a maximum at a relative depth of Yf/Yc=0.3. If the apparent shear force is considered a measure of the increased resistance to flow as a result of channel/flood plain interaction, then it follows that the resistance to flow is a maximum at a relative depth of Yf/Yc=0.3. This would seem reasonable since the present study has confirmed increased resistance to flow in the channel at similar depths, the actual value of Yf/Yc varying with the channel geometry. Furthermore, Myers suggested that the maximum apparent shear force represented 25% of the channel flow weight component.

Rajaratnam and Ahmadi (Ref 3) developed a turbulent shear stress τ^* which could be regarded as a direct measure of the increase in shear which occurred in the flood plain as a result of channel/flood plain interaction. τ^* is a physical shear stress whereas Myers' τa is purely conceptual. However there is obviously similarities. Rajaratnam was able to propose the following relationship :-

$$\frac{\tau *}{\tau_f} = 0{\cdot}15\left[\frac{Y_c}{Y_f} - 1\right]^2 \qquad (6.12)$$

This is an interesting relationship since it confirms Myers findings that the apparent shear stress is strongly dependent on the relative depths of flow in the channel and the flood plain. In fact, a relationship similar to Equation (6.12) will be developed later in this chapter based on results obtained in the present study.

Hadjipanos (Ref 22) presented his apparent shear stress results in different ways, one of which is shown on Fig 6.4. It can be clearly seen that, as the relative depth of flow increases, the apparent shear stress decreases. A further parameter which influences the apparent shear stress is the flood plain roughness. Hadjipanos carried out 4 series of tests, each with varying flood plain roughness. Series "A" tests consisted of smooth flood plains and series "D" tests consisted of the roughest flood plains. It is clear that, as the flood plain roughness increases, the apparent shear stress increases. This is reasonable since the flood plain velocities are lower for rough boundaries and it follows that the greater the difference in velocities between the flood plain and the channel, the greater the turbulent shear mechanism between the flows.

Crory (Ref 14) investigated the influence of the channel/flood plain ratios on the apparent shear stress. She carried out a series of tests with 4 different channel widths and varying depths of flow. Her results are shown on Fig 6.5 and indicate again that, as the flood plain depth decreases, the apparent shear stress increases. Her results further demonstrate the significance of the relative widths of the channel and flood plain on the apparent shear stress. As the flood plain/channel width ratio Bf/Bc increases, the apparent shear stress decreases. However, it must be remembered that Crory only investigated one bankfull depth and therefore was unable to assess its effect on the interaction mechanism. It has been shown in the previous two chapters that the ratio Bf/Bc disguises the effects of the bankfull depth and it is perhaps better to introduce the terms Bf/h and Bc/h as significant geometrical parameters to describe the interaction mechanism.

It is clear that the geometry and roughness coefficients of the compound channel influence the apparent shear stress. As indicated previously, no attempt has been made to vary the relative roughness of the channel and flood plain. Instead, attention has been given to establishing the importance of the geometrical conditions of the flow. In the rest of this chapter, the apparent shear stress will be

presented and discussed in relation to the flow and geometrical parameters of the compound channel.

6.3 Results.

6.3.1 The Apparent shear stress and ΔV.

From Equation (6.5) it was possible to determine the apparent shear stress for the tests carried out in the present study. These results are presented in Table 6.1 together with the appropriate flow parameters. Also included in Table 6.1 are the results obtained by Myers(Ref 36), Rajaratnam (Ref 48) and Crory (Ref 14). As suggested earlier, their work has been used to compare with the results obtained in this study. The apparent shear stresses will now be discussed in more detail.

Wherever turbulent shear stresses exist in fluid flow, there will always be associated velocity gradients. Shear stress is the mechanism whereby fluid is transported from faster regions of flow to slower regions. From a consideration of Prandtl's Momentum transport theory, the shear stress τ at any point in the flow can be represented by :-

$$\tau = (\varepsilon + \mu)\frac{du}{dz} \qquad (6.13)$$

where ε is the eddy viscosity, ν is the viscosity, u is the local velocity of the fluid of distance z from the boundary. The eddy viscosity ε can be given as :-

$$\varepsilon = \rho\, l^2 \frac{du}{dy} \qquad (6.14)$$

where l is regarded as a mixing length of the local flow. In flow regions outside the laminar sub-layer, eddy stresses are very much greater than viscous stresses. Therefore taking μ as being equal to zero and combining Equations (6.13) and (6.14) gives a relationship of the general form :-

$$\tau = \rho \frac{l^2}{(dz)^2}(du)^2 \qquad (6.15)$$

If $\frac{du}{dz}$ is interpreted as the velocity gradient across the flow region, then the shear stress is proportional to the square of the velocity gradient. It may be remembered from Chapter 4 that the higher the velocity gradient existing across the channel/flood plain boundary in a similar manner to that shown on Fig 6.6, the greater the interacting mechanism. It may therefore be possible to relate the apparent shear stress to the velocity gradient which occurs across the channel/flood plain junction during interactive flow. First, however, an

appropriate velocity difference ΔV must be selected which will be characteristic of the velocity gradient occurring. Perhaps the most obvious and easily determined ΔV would be based on the expected mean velocities in the channel and flood plain during isolated flow conditions. This is shown on Fig 6.6. From Equation (6.15) it could be said that the apparent shear stress is a function of ΔV and some length term which defines the $\left(\frac{l}{dz}\right)^2$ term. Vc and Vf were determined for the tests carried out in the present study using Manning's equation with n_c =0.01 and n_f =0.011 for the channel and flood plain respectively.

ΔV was plotted against τ_a for different bankfull depths as shown in Figs 6.7(a) to (d). Also included are the results obtained from other investigators based on the appropriate Manning's n for their experimental flume.

First observations show that as the difference in velocity between the channel and the flood plain increase, the apparent shear stress increases also. This is to be expected if Equation (6.15) is to be considered valid. The results for each geometry tested could be represented by the relationship :-

$$\tau_a = C\ \Delta V^{\alpha} \qquad (6.16)$$

Since Equation (6.16) is presented on Fig 6.7 on logarithmic graph form, the slope of the relationship for each geometry can be taken as α . The range of α would appear to lie between 1.2 and 4.0. It was thought that, from a consideration of Equation (6.15), α would approximate to around 2.0. This was certainly true of some geometries tested. However the variation in α could be explained by remembering that ΔV is only a convenient measure of the difference in velocity at the channel/ flood plain junction. It could be said that the geometrical characteristics of the channel and flood plain would influence the velocity difference at the channel/flood plain junction.

First observations show that the term α is strongly related to the Channel and Flood plain widths. Fig 6.8 shows this to be the case, presenting the relationship between the gradient of the $\tau a - \Delta V$ relationship and Bc/Bf. Clearly as the relative width ratio increased, the term α increased. A relationship for Bc/Bf and α is given on Fig 6.8 as :-

$$\alpha = 2{\cdot}2\left[\frac{B}{B}\right]^{0{\cdot}5} \qquad (6.17)$$

Therefore it could be proposed that Equation (6.16) be written as :-

$$\tau_a = C\ \Delta V^{2{\cdot}2\left(\frac{B_c}{B_f}\right)^{1/2}} \qquad (6.18)$$

An attempt was made to verify the values of the term C. It has been shown in Chapters 4 and 5 that the width terms Bc/h and Bf/h have significance when considering the interaction mechanism. It was therefore decided to determine the value of C by calculating the term $\frac{\tau_a}{\Delta V^{\alpha}}$ and plotting the value of C for each geometry against the Bf/h and Bc/h terms. Thus a generalised relationship for τ_a was proposed :-

$$\tau_a = \Delta V^{2{\cdot}2\left(\frac{B_c}{B_f}\right)^{1/2}} \cdot fn\,[Bc/h\ ,\ Bf/h\,] \qquad (6.19)$$

This relationship is clearly shown on Fig 6.9. It is apparent that for τ_a given Bc/h ratio, there is a definite relationship between the parameter $\frac{\tau_a}{\Delta V^{\alpha}}$ and h/Bf. Given the appropriate roughness coefficients for the channel and flood plain it is now possible to determine the apparent shear stress which is occurring at the flood plain junction during overbank flow with C being determined from Fig 6.9 and α based on the Bc/Bf term. Myers, Crory and Rajaratnam's results are included and compare

well with the present study. However it is not known at this stage how such a relationship as suggested in Equation (6.18) would compare with field data.

Thus a method is available to determine the apparent shear stress a which will occur across the channel/ flood plain boundary during overbank flow provided the velocities in the channel and flood plain can be calculated using the separate channels method. From a knowledge of τ_a, it is possible using Equations (6.5) and (6.8) to determine the change in shear which occurs in the channel and flood plain as a result of channel/flood plain interaction. It was suggested earlier that the shear stress ratios were related to the velocity ratios by the equations :-

$$\frac{\tau_c'}{\tau_c} = \left[\frac{V_c'}{V_c}\right]^2 \qquad (6.20)$$

and

$$\frac{\tau_f'}{\tau_f} = \left[\frac{V_f'}{V_f}\right]^2 \qquad (6.21)$$

Thus it is possible using Equation (6.18) and Fig 6.9 to determine the velocities which will exist in both the channel and flood plain during overbank flow.

6.3.2 The Apparent shear stress and the relative depth.

On analysis of the experimental results it became obvious that a clear relationship existed between the apparent shear stress τa and the relative depths of flow, Yc/Yf in the flood plain and the main channel. In general, as the depth of flow in the flood plain decreases, the apparent shear stress increases. This approach of considering the apparent shear stress from a relative depth point of view does not require any knowledge of the flow distribution in the channel or the flood plain. This section will be concerned with developing this apparent shear stress/ relative depth relationship and discussing its implications with reference to smooth compound channels.

Before any comparison can be made between the non-dimensional term Yc/Yf and τa, the apparent shear stress must also be non-dimensionalized. Because of the scale, turbulent eddies are more likely to be proportional to the flood plain depth, Yf, perhaps it would be appropriate to relate τa to the average shear stress in the flood plain if both channel and flood plain were isolated. It was decided to utilize the average shear stress in the flood plain of infinite width. The term $\frac{\tau_a}{\rho g Y_f S}$ was plotted against Yc/Yf for different bankfull depths as shown on Fig 6.10 (a) to (e). It

is difficult to assess the exact relationship between Yc/Yf and $\frac{\tau_a}{\rho g Y_f S}$ for each of the three bankfull depths tested in the present study. The spread of results obtained would suggest a slope of 2.0 for each geometry. This would imply a relationship of the form :-

$$\frac{\tau_a}{\rho g Y_f S} = \left[\frac{Y_c}{Y_f}\right]^2 \cdot \text{fn[other geometrical parameters]} \quad (6.22)$$

However such a relationship is not suggested in Fig 6.10(d). Again there there is a general trend that as the relative depth Yc/Yf increases, the apparent shear stress increases. The curved relationship shown for each geometry on Fig 6.10(d) would suggest a more complex relationship than that given by Equation (6.22). Linearisation of the relationships shown on Fig 6.10 can be accomplished by considering the idealized $\frac{\tau_a}{\rho g Y_f S}$ vs Yc/Yf relationship shown on Fig 6.11. Here a parameter ψ is substracted from each Yc/Yf value. This value ψ is determined for each investigator's geometry by considering the relative depth at which $\frac{\tau'_c}{\tau_c} = 1$ and hence $\frac{\tau_a}{\rho g Y_f S} = 0$. This gives an equation in the general form :-

$$\log \frac{\tau_a}{\rho g Y_f S} = \alpha_1 \log \left[\frac{Y_c}{Y_f} - \psi\right] + \log F2 \quad (6.23)$$

where α_1 is the slope of the relationship and F2 is a constant.

Equation (6.23) can be rewritten :-

$$\frac{\tau_a}{\rho g Y_f S} = \left[\frac{Y_c}{Y_f} - \psi\right]^{\alpha_1} F2 \qquad (6.24)$$

From Equation (6.24) it is clear that ψ could be interpreted as the value of Yc/Yf where the apparent shear stress is equal to zero.

For most results it was found that once the $\frac{\tau_a}{\rho g Y_f S}$ vs $\frac{Y_c}{Y_f} - \psi$ relationship was linearized, the value of α_1 was generally close to 1.5. As suggested earlier it is difficult to determine an exact value of ψ for each geometry, but a tentative relationship for ψ might be given by the relationship :-

$$\psi \approx 1.0 + 1.5\left(\frac{h}{B_c}\right)^{1.25} \qquad (6.25)$$

indicating that ψ is dependent on the bankfull depth and the channel width. Equation (6.25) implies that ψ will always be greater than 1.0. This is necessary since $\frac{Y_c}{Y_f} - \psi$ can never be less than one.

When Equation (6.26) is applied to the present study and $\frac{\tau_a}{\rho g Y_f S}$ is plotted against $\frac{Y_c}{Y_f} - \psi$ a reasonable linear relationship is obtained as shown on Fig 6.12 (a) to (e). However it must be remembered that such an interpretation might only be possible because of the amount of scatter in the results. Therefore the reliability of Equation (6.25) must be considered with some reservation. Fig 6.12 (e) shows a straight line drawn through each geometry at a slope of 1.5. The general relationship for the apparent shear stress and the relative depth can now be given in the form :-

$$\frac{\tau_a}{\rho g Y_f S} = \left[\frac{Y_c}{Y_f} - \psi\right]^{1.5} F2\,[\text{geometrical parameters}] \qquad (6.26)$$

The value of F2 was determined from Fig 6.12 (e) by the following considerations

$$\log \frac{\tau_a}{\rho g Y_f S} = 1.5 \log\left[\frac{Y_c}{Y_f} - \psi\right] + \log F2 \qquad (6.27)$$

Now when $\frac{Y_c}{Y_f} - \psi = 1.0$, $1.5 \log\left[\frac{Y_c}{Y_f} - \psi\right] = 0.0$ (6.28)

Thus F2= $\frac{\tau_a}{\rho g Y_f S}$ and can be read directly off Fig 6.12 for each geometry tested.

An interesting point to note is the general format of the relationship presented in Equation (6.26). Fig 6.13 shows the general form of this equation. For clarity,

a particular value of ψ and channel geometry has been chosen. Clearly, as the relative depth Yf/Yc increases, the interaction mechanism given by τa, decreases. This is obviously in broad agreement with Myers' findings illustrated on Fig 6.2. Assuming a channel of unit length, the apparent shear force, $\tau_a Yf$ can also be determined from Equation (6.26). Again this relationship shown on Fig 6.13 has close similarities with Myers' apparent shear forces shown on Fig 6.3, with the maximum momentum transfer occurring at a particular relative depth Yf/Yc. Clearly then, the general framework of Equation (6.26) would appear satisfactory in describing the variation in the interaction mechanism with relative depth. The relationship between the values of F2 and the geometrical parameters is a complex one and requires careful analysis.

Up to this point it has been demonstrated that there is a distinct advantage in using the terms Bc/h and Bf/h to describe the geometry of the channel and flood plain in terms of the interaction mechanism. It is therefore reasonable to assume that Bc/h and Bf/h might describe the function F2 since F2 is regarded as a function of the geometrical parameters. Now F2 can be determined from Fig 6.13(e) or from the relationship :-

$$\frac{\tau_a}{\rho g Y_f S\left[\frac{Y}{Y} - \psi\right]^{1.5}} = F2 \qquad (6.29)$$

Fig 6.14 shows the average value of F2 determined from each geometry, plotted against the Bc/h term. First observations might suggest considerable spread in the results with no obvious relationship. However, closer inspection reveals that lines of constant values of Bf/h can be drawn through the data as shown. The slope of each line of constant Bf/h would suggest that Bc/h might be related to F2 in the form :-

$$F2 = \left(\frac{Bc}{h}\right)^{0.5} . F3(Bf/h) \qquad (6.30)$$

where F3 is a function which describes the behaviour of Bf/h. It is a relatively simple procedure for determining the value of F3 for a given Bf/h value. By assuming that Bc/h is equal to 1.0, F3 is equal to F2 and hence the corresponding value of F2 can be read off Fig 6.14 where Bc/h = 1.0. Thus it is possible to plot F3 and Bf/h as shown on Fig 6.15. Clearly, it can be seen that as Bf/h increases, the F3 term increases. However, at subsequent increases in Bf/h, the increase in F3 becomes less significant. A proposed relationship, shown on Fig 6.15 which describes the relationship between F3 and Bf/h is given as :-

$$F3 = 1{\cdot}12\left(1 - e^{-0{\cdot}53\left(Bf/h\right)}\right) \qquad (6.31)$$

This relationship suggests that at very large values of Bf/h, the F3 term tends to reach a maximum of 1·12.

Combining Equations (6.30) and (6.31) gives an overall relationship for F2 as :-

$$F2 = 1{\cdot}12\left(\frac{Bc}{h}\right)^{1/2}\left(1 - e^{-0{\cdot}53\,Bf/h}\right) \qquad (6.32)$$

Thus it is now possible to describe the non-dimensional apparent shear stress term $\frac{\tau_a}{\rho g Y_f S}$ by the relative depths of flow, and the width-to-bankfull terms by combining Equations (6.26) and (6.32) in the form :-

$$\frac{\tau_a}{\rho g Y_f S} = 1{\cdot}12\left(\frac{Y_c}{Y_f} - \psi\right)^{1{\cdot}5}\left(\frac{B_c}{h}\right)^{0{\cdot}5}\left(1 - e^{-0{\cdot}53\,Bf/h}\right) \qquad (6.33)$$

It is now possible to verify this relationship by plotting the L.H.S. of Equation (6.33) with the R.H.S.. This relationship has been presented for all geometries studied on Fig 6.16 (a) to (e). Fig 6.16 (e) shows all the results combined with Myers, Crory and Rajaratnam. The relationship described in Equation (6.33) is drawn through the data suggesting a good correlation for all the results. It is particularly encouraging to observe that other investigations are well

represented as can be seen on Fig 6.16(d). Thus it is possible from a knowledge of the depths of flow in the channel and the flood plain, with the widths of channel and flood plain, to determine the apparent shear stress which is likely to act conceptually at the channel/flood plain interface. With this information, it is also possible to determine the change in boundary shear in the channel and flood plain and hence from Equations (6.20) and (6.21) establish the interacting channel and flood plain velocities.

It is interesting to note the similarity of the Bc/h and Bf/h terms in Equation (6.33) with the corresponding terms presented in Equation (5.21). Clearly the $\tau_{c'}/\tau_c$ term is related to the apparent shear stress. It is therefore encouraging to observe similar relationships determined from two different approaches.

The suitability of Equation (6.33) for channels with two flood plains will be discussed in the following chapter with respect to Hadjipanos and Wormleaton's work and also the work of Ghosh and Jena.

6.4 Conclusions.

Clearly then it has been well demonstrated that the apparent shear stress, which can be considered a measure of the intensity of the interaction mechanism, can be related to the relative depths of flow in the channel and flood plain, the width terms Bc/h and Bf/h and the water surface slope. This relationship can either be presented directly as in Equation (6.33) or by means of velocity differences between the channel and flood plain based on a separate channels method of analysis. Such relationships have only been determined for smooth channels. The suitability of such relationships for full scale rivers is unclear at this stage. From a knowledge of the apparent shear stress it is possible to determine the interacting shear stresses and velocities in the channel, and hence the overall discharge of the channel and flood plain can be assessed.

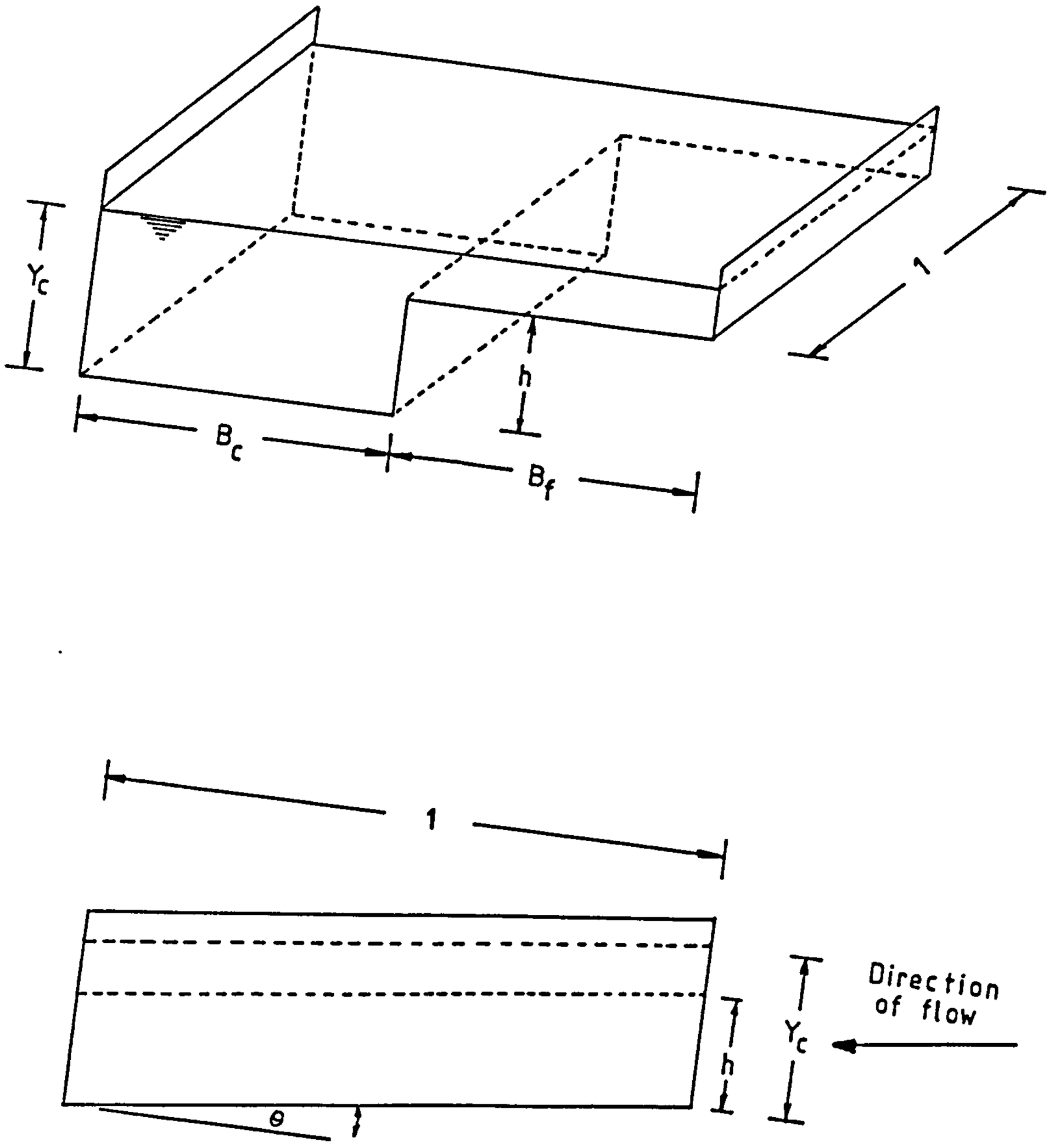

Fig 6.1 Element of flow in Compound Channel.

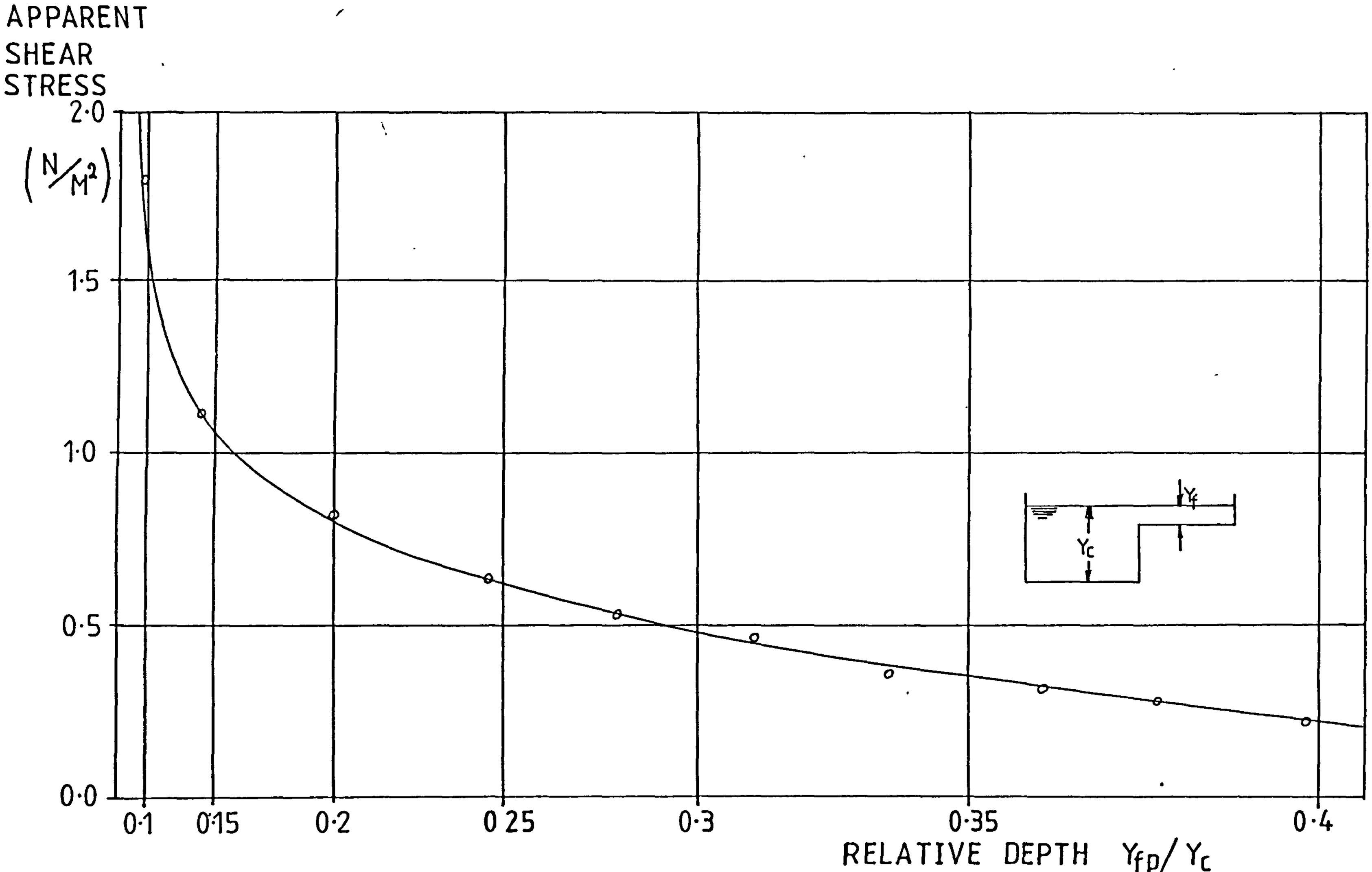

Fig 6·2 APPARENT SHEAR STRESS VERSES RELATIVE DEPTH (MYERS)

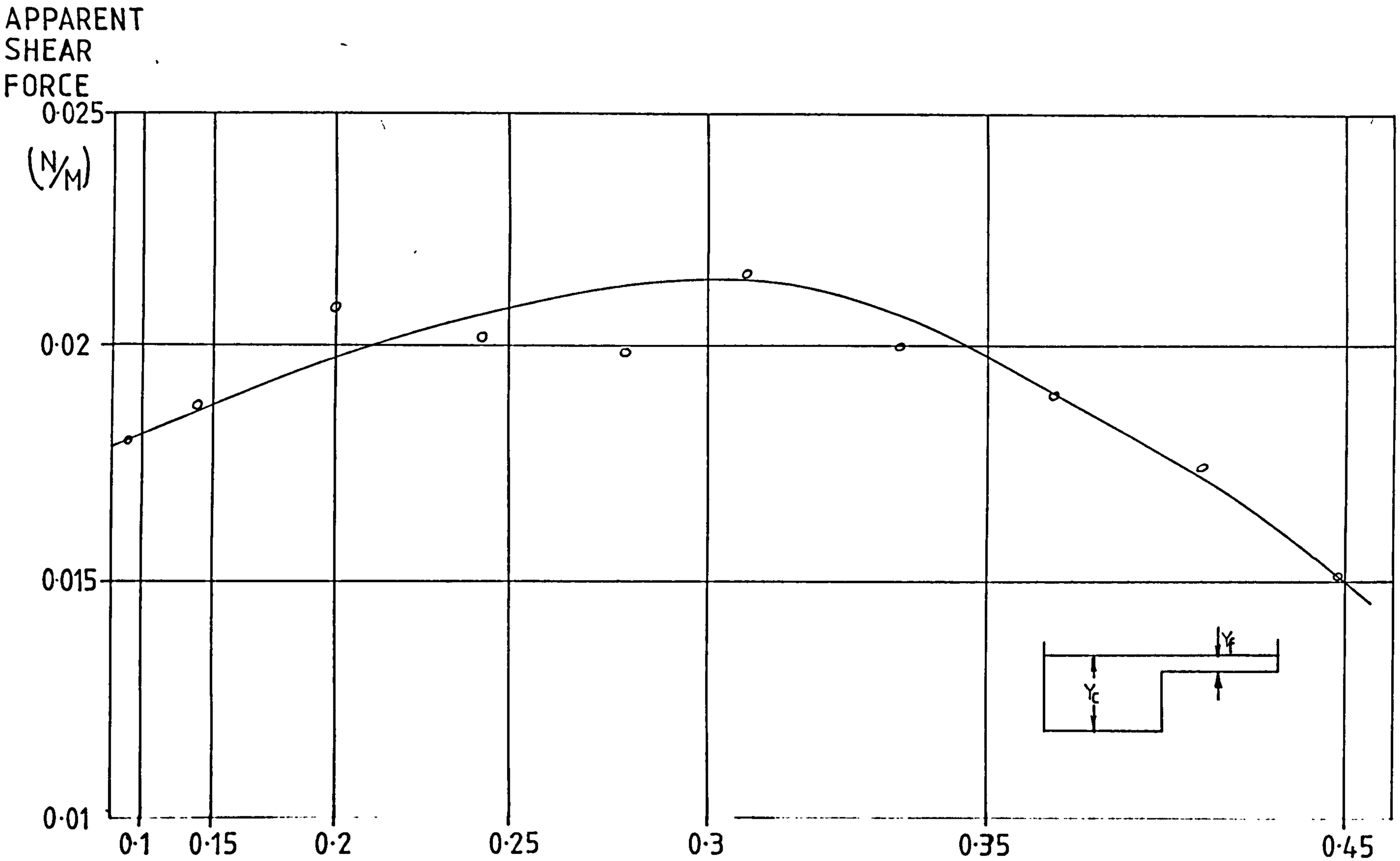

Fig 6·3 APPARENT SHEAR FORCE VERSES RELATIVE DEPTH (MYERS)

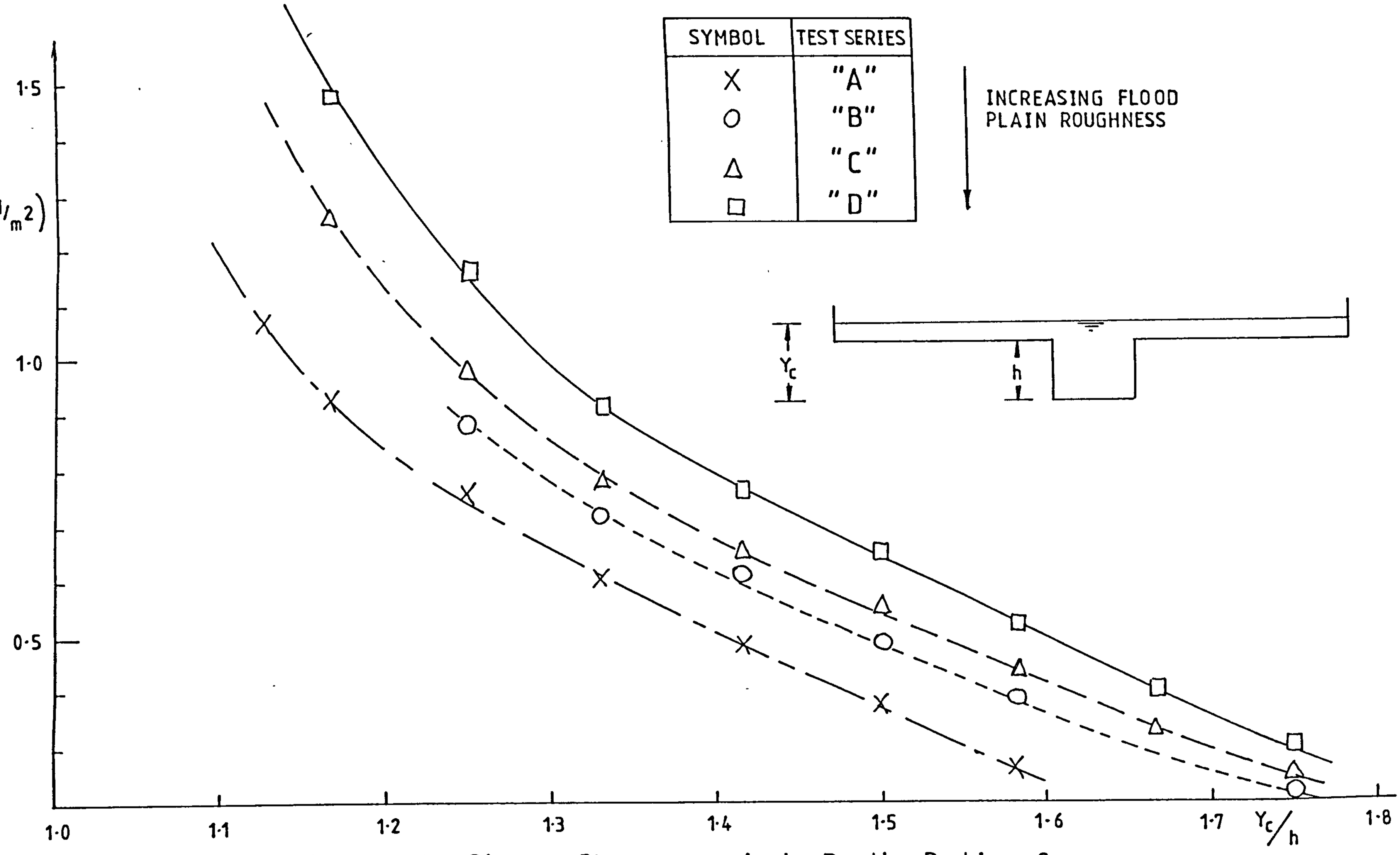

Fig 6·4 Apparent Shear Stress against Depth Ratio & Flood Plain Roughness (Hadjipanos).

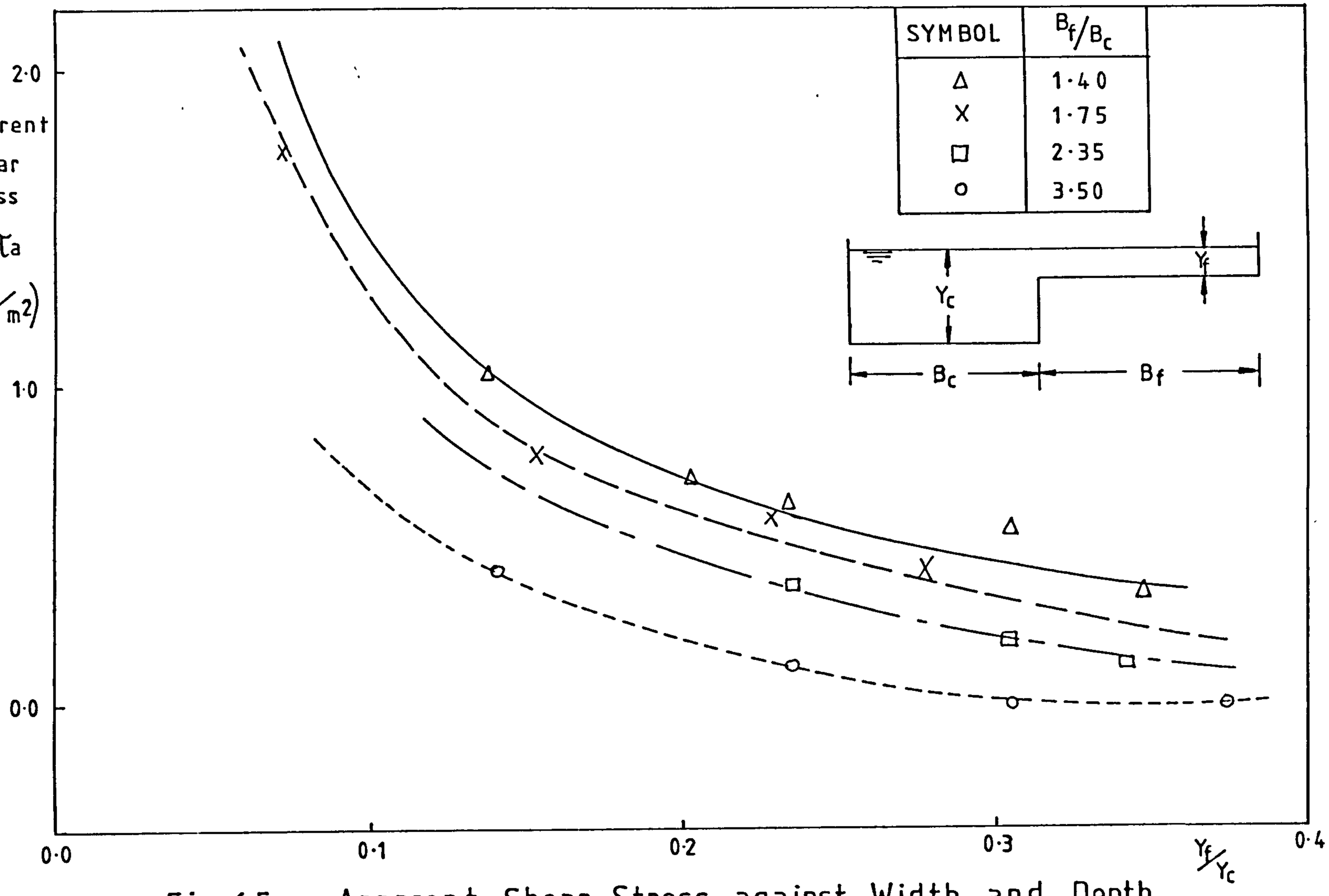

Fig 6·5 Apparent Shear Stress against Width and Depth Ratios (Crory).

Test	Run	Yc (m)	Bc (m)	Bf (m)	h (m)	τ_a (N/m^2)
K1	1	0.1340	0.400	0.400	0.102	3.521
K2	2	0.1260	0.400	0.400	0.102	4.470
K3	3	0.1200	0.400	0.400	0.102	4.808
K4	4	0.1150	0.400	0.400	0.102	5.343
K5	5	0.1480	0.400	0.400	0.102	1.607
K6	6	0.1320	0.400	0.400	0.102	1.762
K7	7	0.1200	0.400	0.400	0.102	1.139
K8	8	0.1510	0.400	0.400	0.102	1.292
K9	9	0.1300	0.400	0.400	0.102	1.295
K10	10	0.1210	0.400	0.400	0.102	1.213
A12	11	0.1470	0.400	0.400	0.052	0.328
A5	12	0.1110	0.400	0.400	0.052	0.111
A6	13	0.0920	0.400	0.400	0.052	1.729
A7	14	0.1000	0.400	0.400	0.052	1.466
A8	15	0.0800	0.400	0.400	0.052	1.535
A9	16	0.0830	0.400	0.400	0.052	0.906
A10	17	0.1250	0.400	0.400	0.052	0.755
A11	18	0.0750	0.400	0.400	0.052	0.172
A1	19	0.1030	0.395	0.400	0.052	1.142

Table 6·1

Test	Run	Yc (m)	Bc (m)	Bf (m)	h (m)	τ_a (N/m^2)
A2	20	0.0810	0.395	0.400	0.052	1.326
A3	21	0.0700	0.395	0.400	0.052	1.544
A4	22	0.0960	0.395	0.400	0.052	0.794
B1	23	0.1050	0.185	0.404	0.052	0.326
B2	24	0.0925	0.185	0.404	0.052	0.547
B3	25	0.0765	0.185	0.404	0.052	0.638
B4	26	0.0710	0.185	0.404	0.052	0.848
B5	27	0.1020	0.185	0.400	0.053	0.217
B6	28	0.0790	0.185	0.400	0.053	0.639
B7	29	0.0685	0.185	0.400	0.053	0.696
B8	30	0.1240	0.185	0.400	0.053	0.119
C1	31	0.0700	0.395	0.200	0.052	0.732
C2	32	0.0960	0.395	0.200	0.052	0.613
C4	33	0.0850	0.395	0.200	0.052	0.864
C5	34	0.0860	0.392	0.193	0.052	0.230
C6	35	0.0640	0.392	0.193	0.052	0.678
C7	36	0.1010	0.392	0.193	0.052	0.683

Table 6.1

Test	Run	Yc (m)	Bc (m)	Bf (m)	h (m)	τ_a (N/m^2)
C8	37	0.0725	0.392	0.193	0.052	-0.311
G1	38	0.1700	0.192	0.607	0.152	4.729
G2	39	0.1740	0.192	0.607	0.152	7.276
G3	40	0.2090	0.192	0.607	0.152	0.853
G4	41	0.1880	0.192	0.607	0.152	1.680
G5	42	0.1760	0.192	0.603	0.152	1.497
G6	43	0.1860	0.192	0.603	0.152	1.334
G7	44	0.1980	0.192	0.603	0.152	0.873
G8	45	0.1635	0.192	0.603	0.152	1.777
L1	46	0.1970	0.190	0.397	0.152	1.392
L2	47	0.1800	0.190	0.397	0.152	1.812
L3	48	0.1695	0.190	0.397	0.152	2.732
L4	49	0.1890	0.190	0.397	0.152	2.059
L5	50	0.1845	0.190	0.397	0.152	0.990
L6	51	0.1790	0.190	0.397	0.152	1.597
L7	52	0.1750	0.190	0.397	0.152	1.440
L8	53	0.1690	0.190	0.397	0.152	1.489

Table 6·1

Test	Run	Yc (m)	Bc (m)	Bf (m)	h (m)	τ_a (N/m^2)
N1	54	0.1950	0.191	0.213	0.152	1.045
N2	55	0.1830	0.191	0.213	0.152	1.153
N3	56	0.1990	0.191	0.213	0.152	0.910
N4	57	0.1685	0.191	0.213	0.152	2.242
N5	58	0.1685	0.191	0.211	0.152	1.417
N6	59	0.1790	0.191	0.211	0.152	0.466
N7	60	0.1740	0.191	0.211	0.152	1.457
N8	61	0.1930	0.191	0.211	0.152	0.614
J1	62	0.1870	0.390	0.404	0.152	1.810
J2	63	0.1720	0.390	0.404	0.152	2.544
J3	64	0.1720	0.390	0.404	0.152	3.418
J4	65	0.1600	0.390	0.404	0.152	9.955
J5	66	0.1780	0.390	0.404	0.152	3.440
J6	67	0.1840	0.390	0.404	0.152	3.187
J7	68	0.1560	0.390	0.404	0.152	12.516
J8	69	0.1680	0.390	0.404	0.152	3.707
J9	70	0.1660	0.390	0.404	0.152	2.780

Table 6·1

Test	Run	Yc (m)	Bc (m)	Bf (m)	h (m)	τ_a (N/m^2)
R1	71	0.1555	0.390	0.200	0.152	6.844
R2	72	0.1660	0.390	0.200	0.152	2.548
R3	73	0.1730	0.390	0.200	0.153	2.206
R4	74	0.1755	0.390	0.200	0.153	2.000
R5	75	0.1795	0.390	0.200	0.153	1.721
R6	76	0.1850	0.390	0.200	0.153	1.605
R7	77	0.1920	0.390	0.200	0.153	1.444
R8	78	0.2010	0.390	0.200	0.153	1.074
Myers	79	0.1684	0.254	0.356	0.102	0.227
Myers	80	0.1638	0.254	0.356	0.102	0.258
Myers	81	0.1583	0.254	0.356	0.102	0.301
Myers	82	0.1534	0.254	0.356	0.102	0.332
Myers	83	0.1467	0.254	0.356	0.102	0.443
Myers	84	0.1400	0.254	0.356	0.102	0.536
Myers	85	0.1333	0.254	0.356	0.102	0.619
Myers	86	0.1275	0.254	0.356	0.102	0.774
Myers	87	0.1183	0.254	0.356	0.102	1.118

Table 6·1

Test	Run	Yc (m)	Bc (m)	Bf (m)	h (m)	τ_a (N/m^2)
Myers	88	0.1116	0.254	0.356	0.102	1.380
Rajar	89	0.1128	0.711	0.508	0.098	4.227
Rajar	90	0.1228	0.711	0.508	0.098	4.312
Rajar	91	0.1445	0.711	0.508	0.098	2.527
Rajar	92	0.1814	0.711	0.508	0.098	1.343
Rajar	93	0.1085	0.711	0.508	0.098	4.144
P1	94	0.1220	0.193	0.396	0.101	1.400
P2	95	0.1230	0.193	0.396	0.101	2.742
P3	96	0.1280	0.193	0.396	0.101	0.936
P4	97	0.1350	0.193	0.396	0.101	1.203
P5	98	0.1440	0.193	0.396	0.101	0.889
P6	99	0.1320	0.193	0.396	0.101	1.456
P7	100	0.1080	0.193	0.396	0.101	5.829
P8	101	0.1190	0.193	0.396	0.101	1.044
P9	102	0.1250	0.193	0.396	0.101	0.739
P10	103	0.1280	0.193	0.396	0.101	1.407

Table 6·1

Test	Run	Yc (m)	Bc (m)	Bf (m)	h (m)	τ_a (N/m^2)
H1	104	0.1500	0.194	0.601	0.101	1.240
H2	105	0.1290	0.194	0.601	0.101	1.936
H3	106	0.1280	0.194	0.601	0.101	1.242
H4	107	0.1210	0.194	0.601	0.101	2.240
H5	108	0.1320	0.194	0.601	0.101	2.309
H6	109	0.1230	0.194	0.601	0.101	2.192
H7	110	0.1200	0.194	0.601	0.101	2.032
H8	111	0.1585	0.194	0.601	0.101	0.653
H9	112	0.1155	0.194	0.601	0.101	2.457
H10	113	0.1250	0.194	0.601	0.101	1.102
M1	114	0.1120	0.193	0.210	0.101	1.966
M2	115	0.1250	0.193	0.210	0.101	0.995
M3	116	0.1410	0.193	0.210	0.101	0.548
M4	117	0.1130	0.193	0.210	0.101	0.950
M5	118	0.1150	0.193	0.210	0.101	1.557
M6	119	0.1230	0.193	0.210	0.101	0.670
M7	120	0.1270	0.193	0.210	0.101	0.878
M8	121	0.1370	0.193	0.210	0.101	0.531

Table 6·1

Test	Run	Yc (m)	Bc (m)	Bf (m)	h (m)	τ_a (N/m^2)
Crory	122	0.1562	0.254	0.356	0.102	0.352
Crory	123	0.1467	0.254	0.356	0.102	0.472
Crory	124	0.1329	0.254	0.356	0.102	0.645
Crory	125	0.1280	0.254	0.356	0.102	0.717
Crory	126	0.1183	0.254	0.356	0.102	1.032
Crory	127	0.1410	0.203	0.356	0.102	0.431
Crory	128	0.1321	0.203	0.356	0.102	0.579
Crory	129	0.1233	0.203	0.356	0.102	0.751
Crory	130	0.1100	0.203	0.356	0.102	1.764
Crory	131	0.1550	0.153	0.356	0.102	0.122
Crory	132	0.1467	0.153	0.356	0.102	0.177
Crory	133	0.1333	0.153	0.356	0.102	0.358
Crory	134	0.1634	0.102	0.356	0.102	-0.188
Crory	135	0.1467	0.102	0.356	0.102	0.006
Crory	136	0.1333	0.102	0.356	0.102	0.126
Crory	137	0.1187	0.102	0.356	0.102	0.447
01	138	0.0650	0.196	0.209	0.050	0.553

Table 6·1

Test	Run	Yc (m)	Bc (m)	Bf (m)	h (m)	τ_a (N/m^2)
02	139	0.0755	0.196	0.209	0.050	0.506
03	140	0.0890	0.196	0.209	0.050	0.503
04	141	0.0985	0.196	0.209	0.050	0.379
05	142	0.0830	0.196	0.209	0.050	0.666
06	143	0.0760	0.196	0.209	0.050	0.327
07	144	0.0695	0.196	0.209	0.050	0.615
08	145	0.0610	0.196	0.209	0.050	1.128
I1	146	0.0930	0.196	0.604	0.050	0.436
I2	147	0.0750	0.196	0.604	0.050	1.910
I3	148	0.0680	0.196	0.604	0.050	1.781
I4	149	0.0840	0.196	0.604	0.050	0.304
I5	150	0.0775	0.196	0.604	0.050	0.916
I6	151	0.0870	0.196	0.604	0.050	0.513
I7	152	0.0735	0.196	0.604	0.050	0.784
I8	153	0.0620	0.196	0.604	0.050	1.330
S1	154	0.1195	0.392	0.203	0.100	2.831
S2	155	0.1110	0.392	0.203	0.100	1.733

Table 6·1

Test	Run	Yc (m)	Bc (m)	Bf (m)	h (m)	τ_a (N/m^2)
S3	156	0.1130	0.392	0.203	0.100	2.280
S4	157	0.1050	0.392	0.203	0.100	6.917
S5	158	0.1220	0.392	0.203	0.100	3.339
S6	159	0.1400	0.392	0.203	0.100	1.426
S7	160	0.1055	0.392	0.203	0.100	11.941
S8	161	0.1210	0.392	0.203	0.100	1.697
E1	162	0.1145	0.590	0.209	0.100	2.281
E2	163	0.1190	0.590	0.209	0.100	1.700
E3	164	0.1225	0.590	0.209	0.100	1.649
E4	165	0.1255	0.590	0.209	0.100	1.561
E5	166	0.1060	0.590	0.209	0.100	7.895
E6	167	0.1100	0.590	0.209	0.100	5.696

Table 6·1

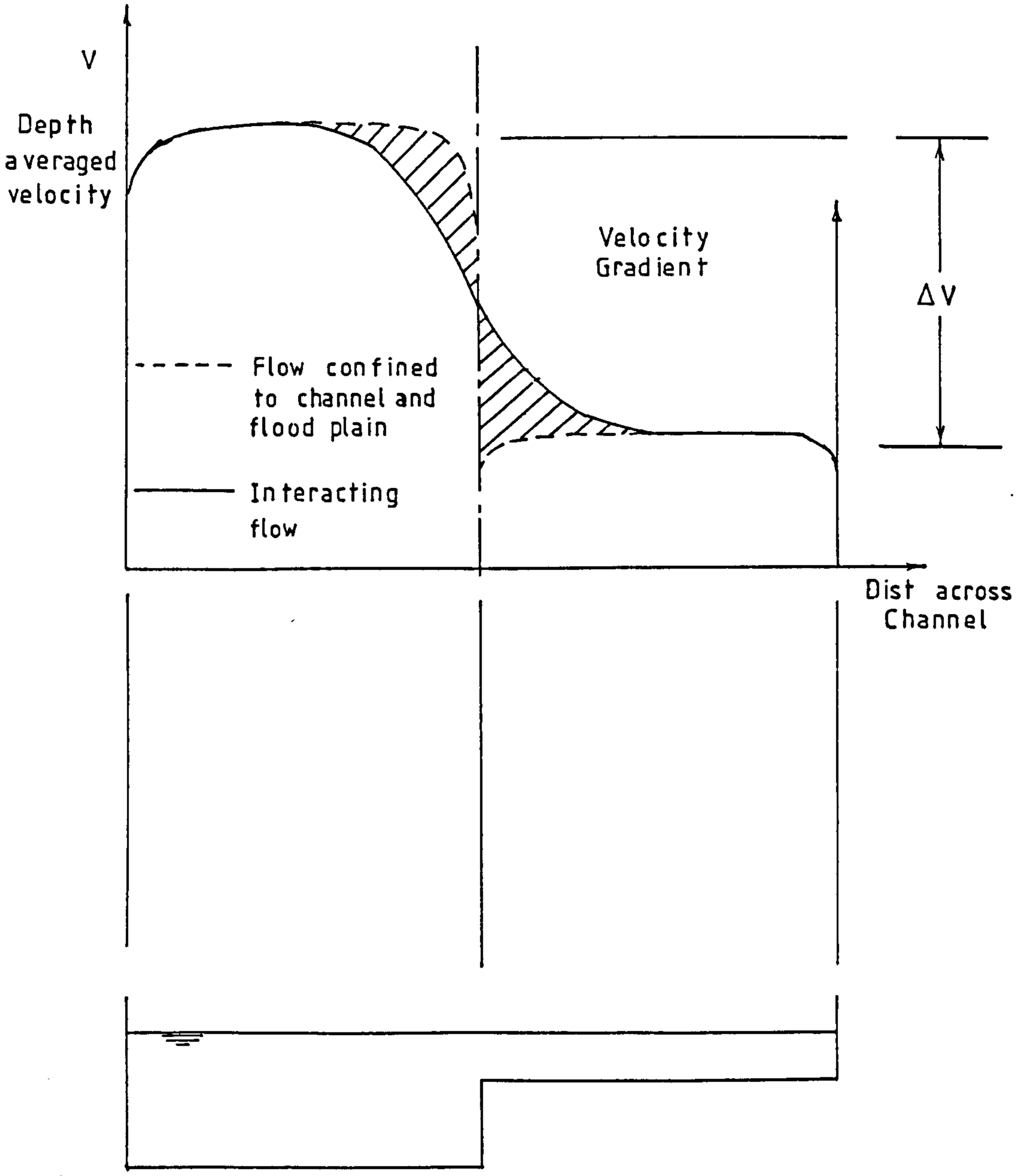

Fig 6·6 Velocity Profiles for Flow Confined and Unconfined to the Channel.

SYMBOL	GEOMETRY	RUN NO	(mm) h	(mm) B_c	(mm) B_f	No of tests
△	K	1–10	102	400	400	10
▽	A	11–22	52	400	400	12
□	B	23–30	52	200	400	8
◇	C	31–37	52	400	200	7
○	G	38–45	152	200	600	8
⊞	L	46–53	152	200	400	8
⊠	N	54–61	152	200	200	8
⊕	J	62–70	152	400	400	9
⊗	R	71–78	152	400	200	8
⊛	MYERS	79–88	102	254	356	10
⊹	RAJARATNAM	89–93	98	711	508	5
⊠	P	94–103	102	200	400	10
⊹	H	104–113	102	200	600	10
⊠	M	114–121	102	200	200	8
θ	CRORY	122–126	102	254	356	6
✕	CRORY	127–130	102	203	356	4
λ	CRORY	131–133	102	153	356	3
μ	CRORY	134–137	102	102	356	4
✱	O	138–145	52	200	200	8
#	I	146–153	52	200	600	8
$	S	154–161	102	400	200	8
@	E	162–167	102	600	200	6

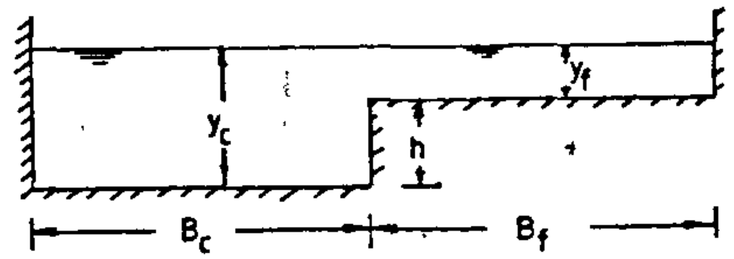

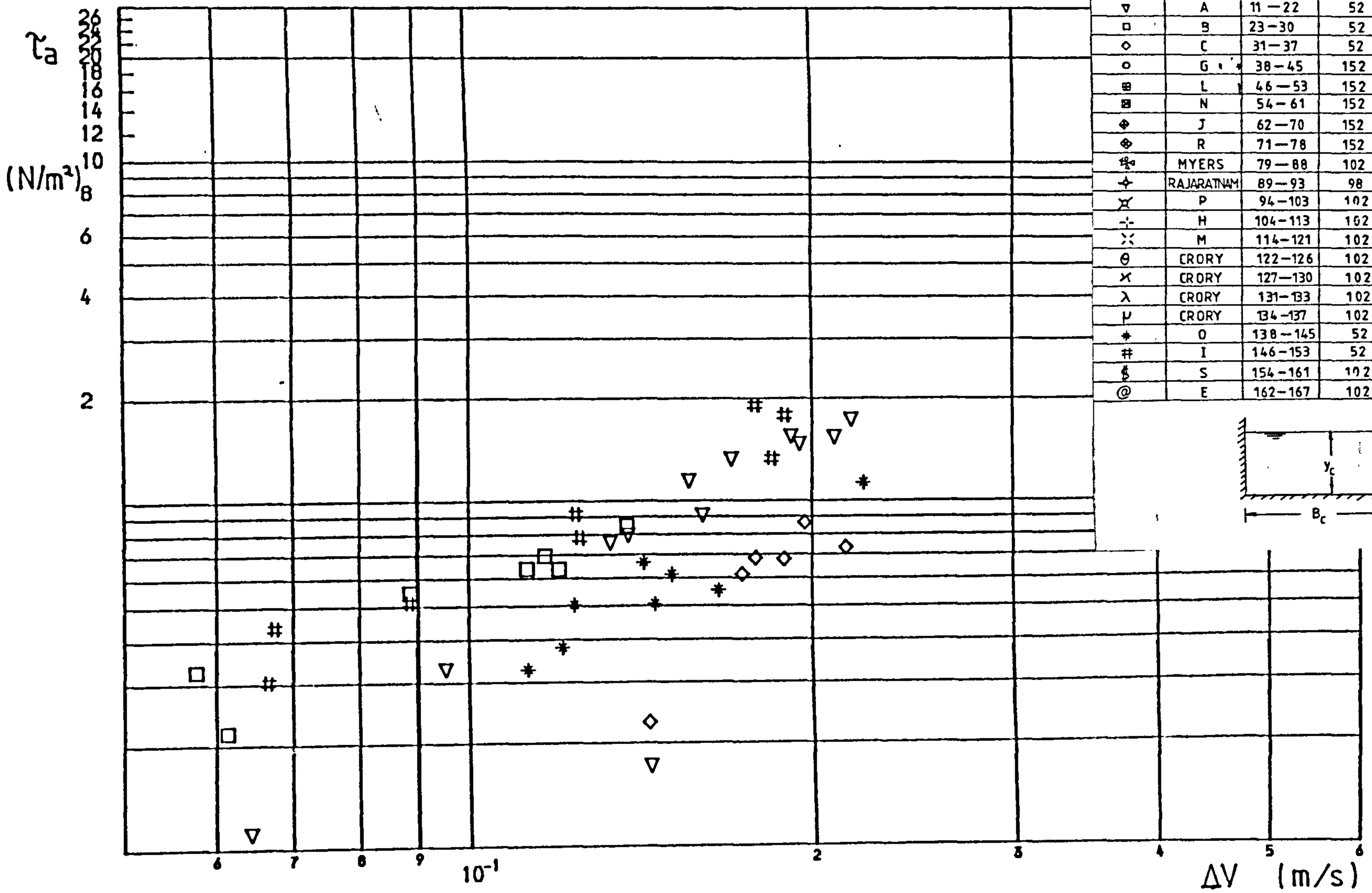

Fig 6·7(a) Apparent shear stress τ_a against ΔV for h= 50 mm

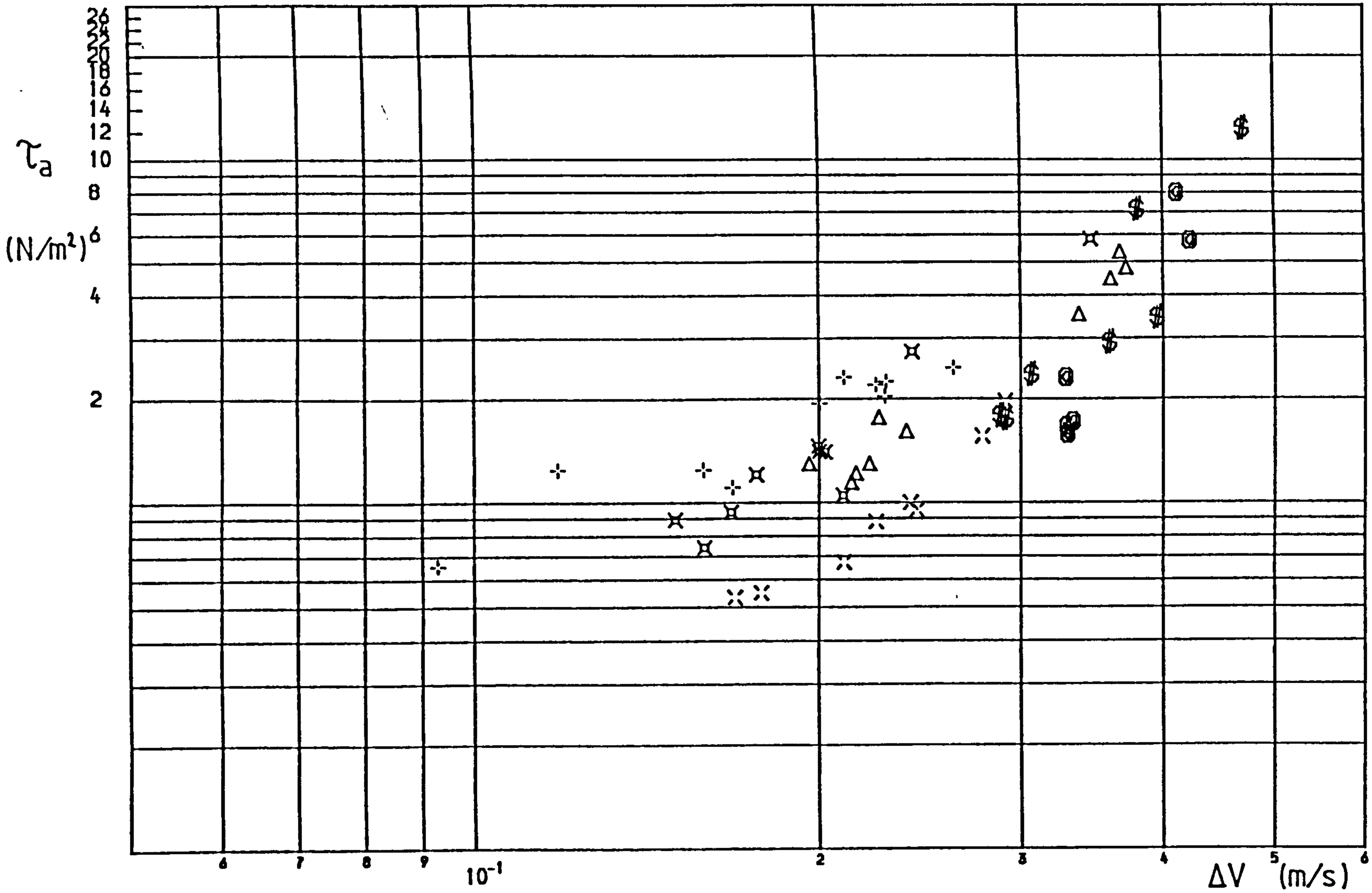

Fig 6·7 (b) Apparent shear stress τ_a against ΔV for h= 100 mm

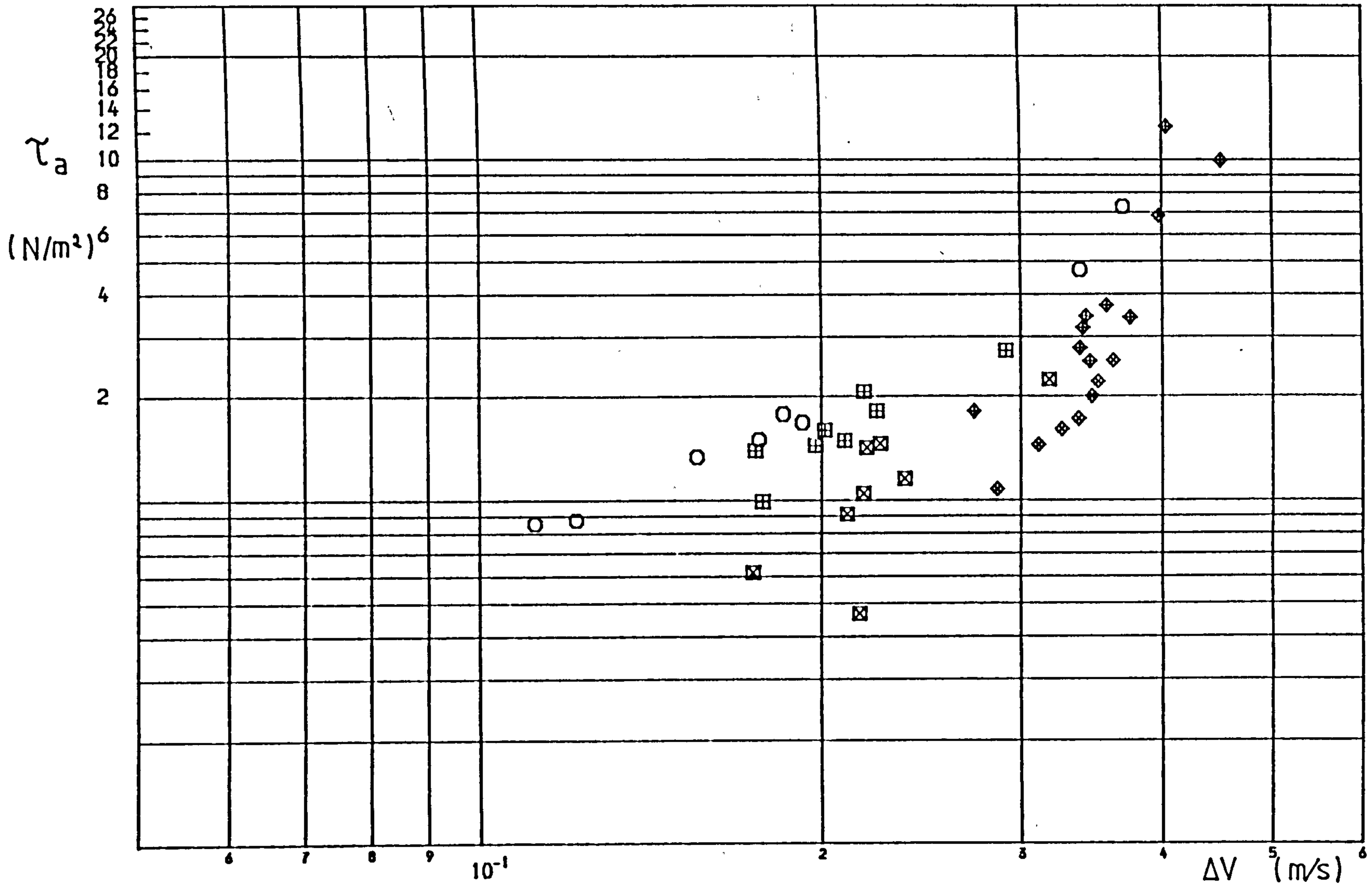

Fig 6·7(c) Apparent shear stress τ_a against ΔV for h= 150 mm

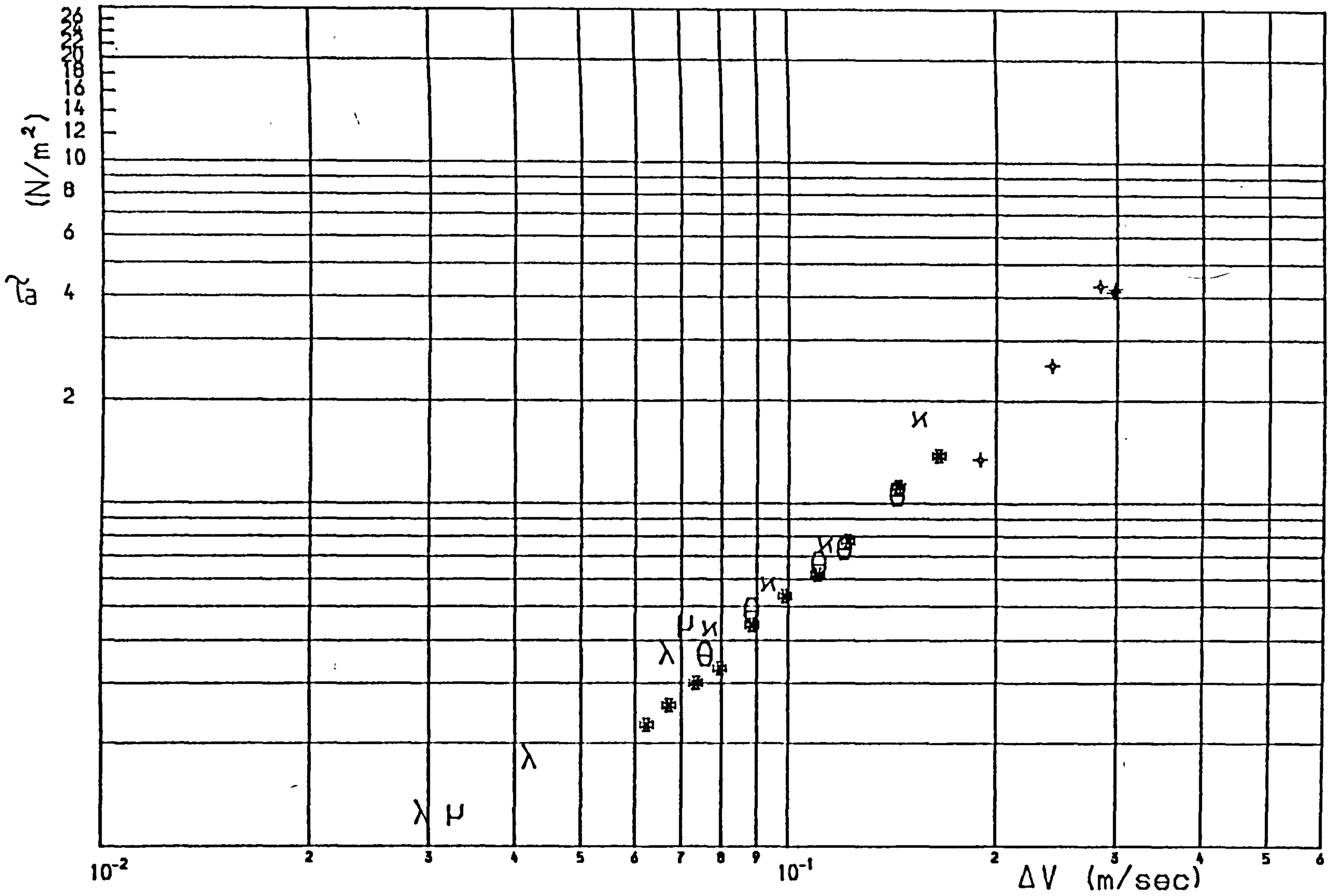

Fig 6·7(d) Apparent shear stress τ_a against ΔV for Myers Rajaratnam and Crory.

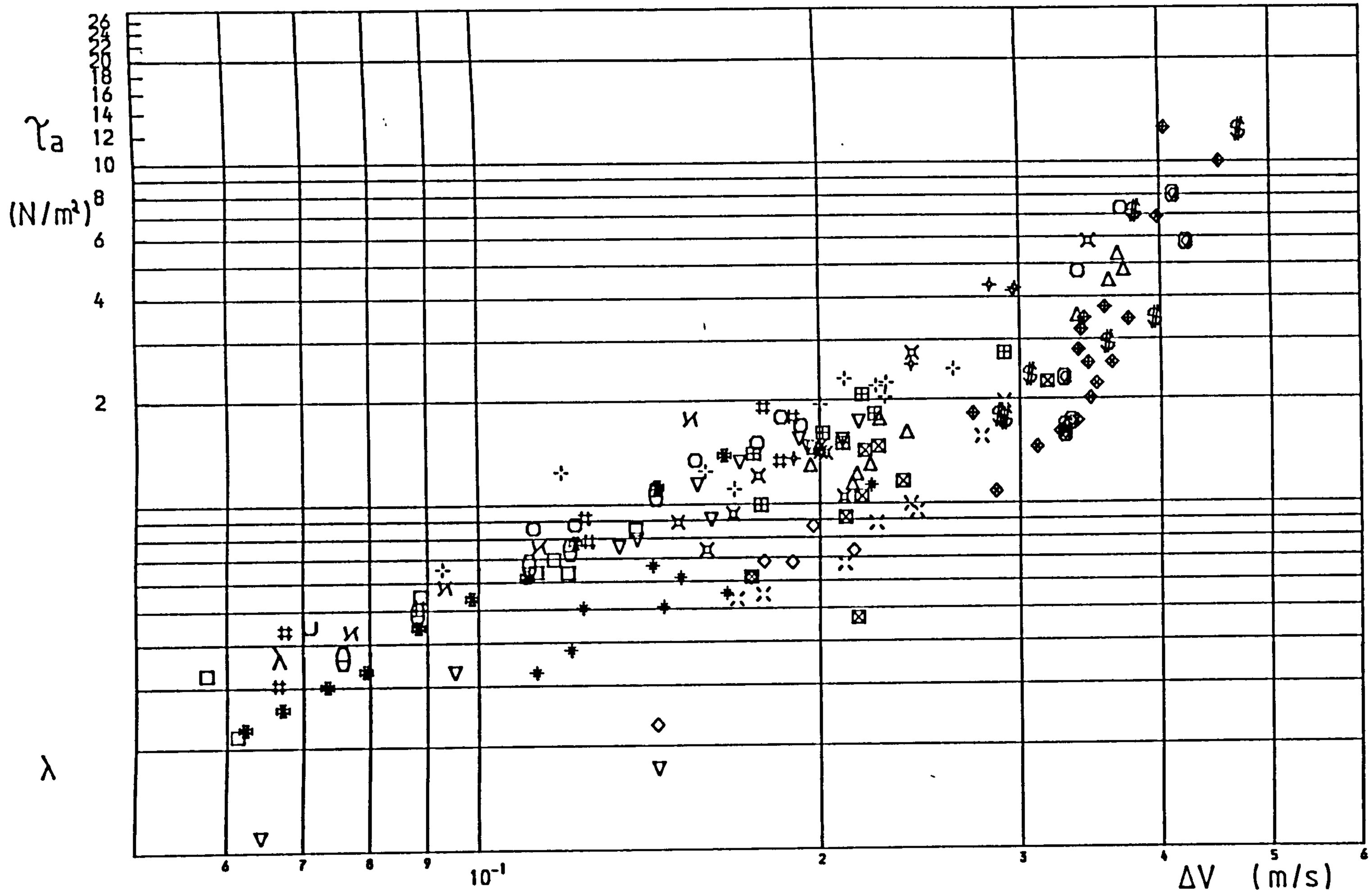

Fig6·7(e) Apparent shear stress τ_a against ΔV for all tests.

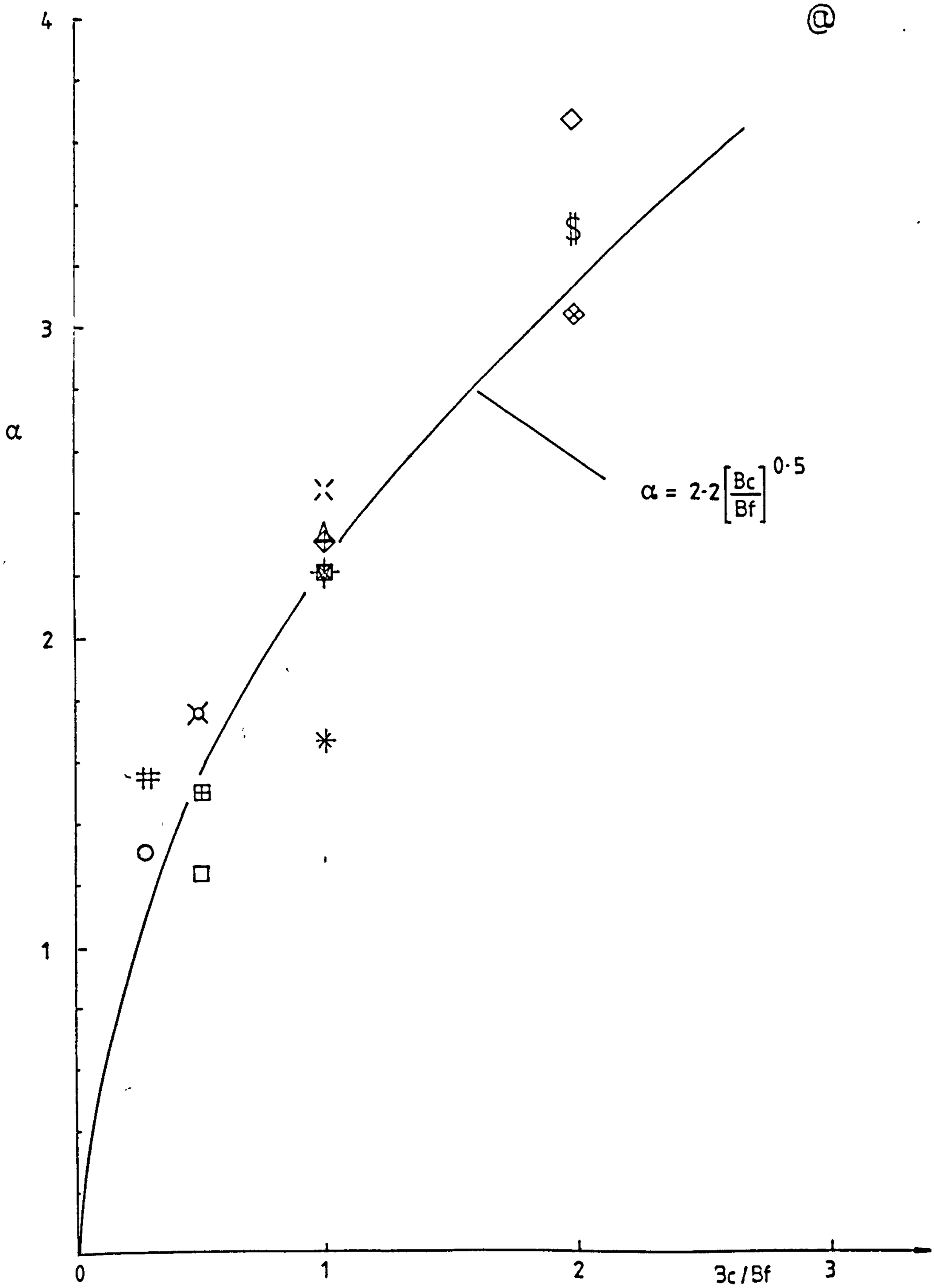

Fig 6·8 Relationship between $\tau a - \Delta V$ slope α for each geometry and the relative widths.

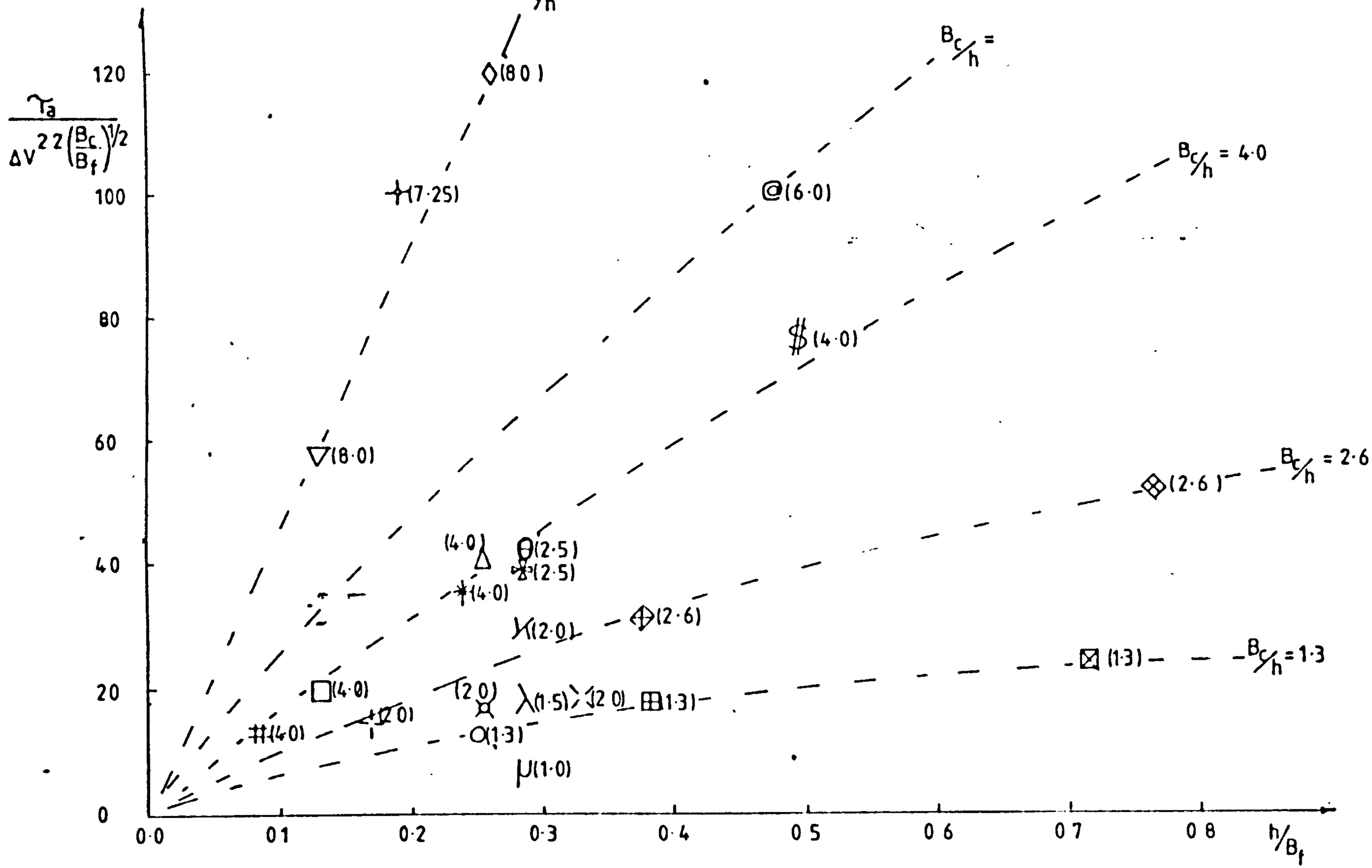

Fig 6·9 Variation of Apparent Shear Stress Parameter with Channel/Flood Plain Geometry.

SYMBOL	GEOMETRY	RUN NO	(mm) h	(mm) B_c	(mm) B_f	No of tests
△	K	1–10	102	400	400	10
▽	A	11–22	52	400	400	12
□	B	23–30	52	200	400	8
◇	C	31–37	52	400	200	7
○	G	38–45	152	200	600	8
⊞	L	46–53	152	200	400	8
⊠	N	54–61	152	200	200	8
⊕	J	62–70	152	400	400	9
⊗	R	71–78	152	400	200	8
⊛	MYERS	79–88	102	254	356	10
✧	RAJARATNAM	89–93	98	711	508	5
⊠	P	94–103	102	200	400	10
⊹	H	104–113	102	200	600	10
⊠	M	114–121	102	200	200	8
θ	CRORY	122–126	102	254	356	6
✕	CRORY	127–130	102	203	356	4
λ	CRORY	131–133	102	153	356	3
μ	CRORY	134–137	102	102	356	4
*	O	138–145	52	200	200	8
#	I	146–153	52	200	600	8
₵	S	154–161	102	400	200	8
@	E	162–167	102	600	200	6

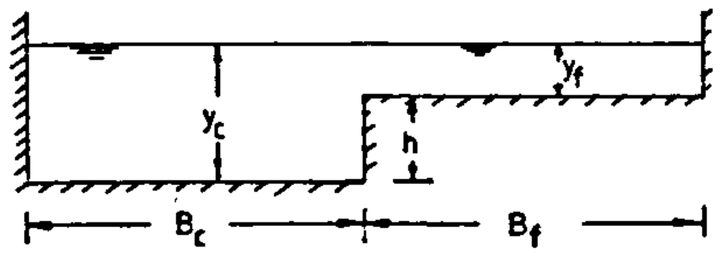

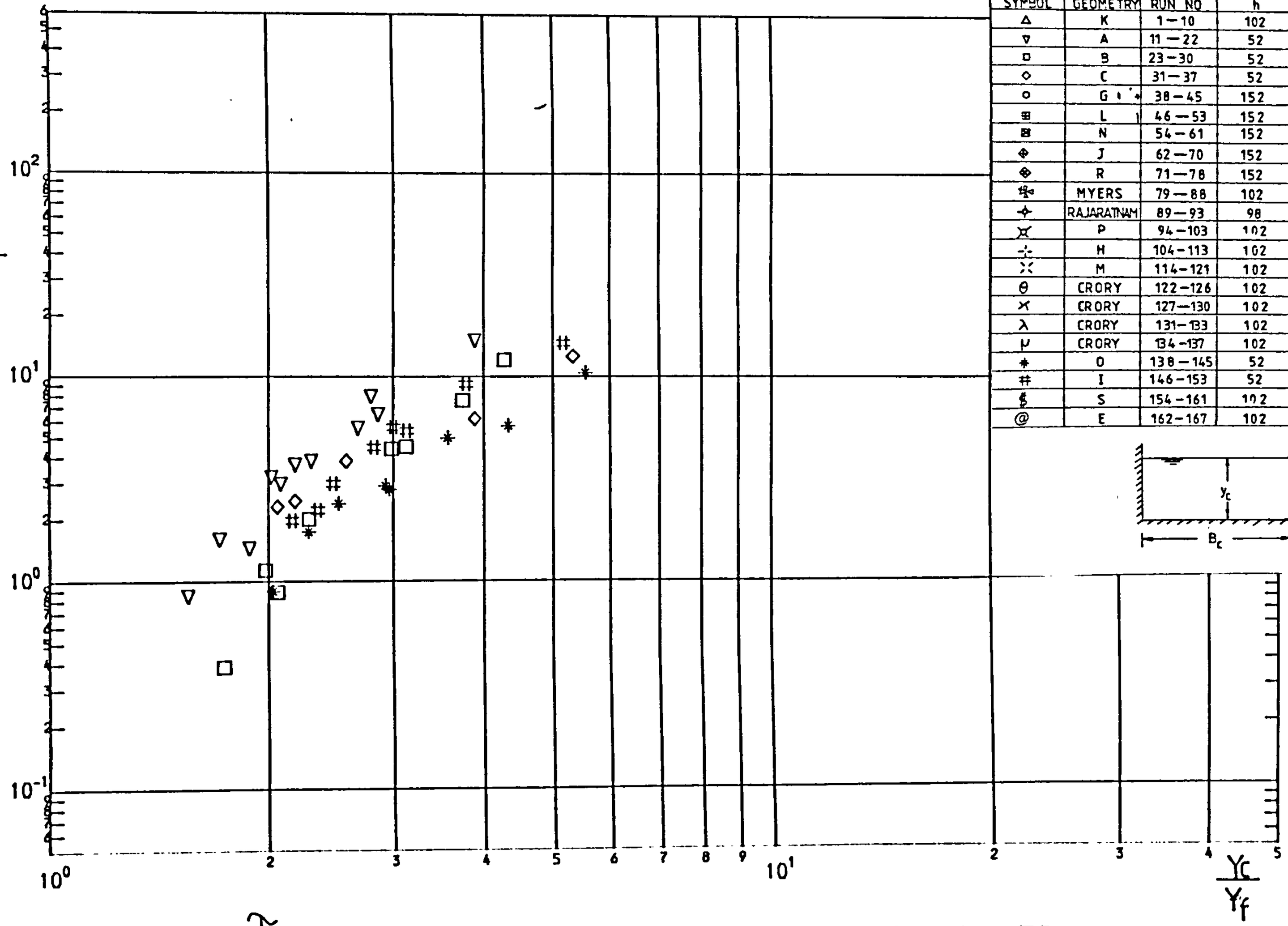

Fig 6·10(a) $\frac{\tau_a}{\rho g Y_f S}$ against Y_c/Y_f for h= 50 mm

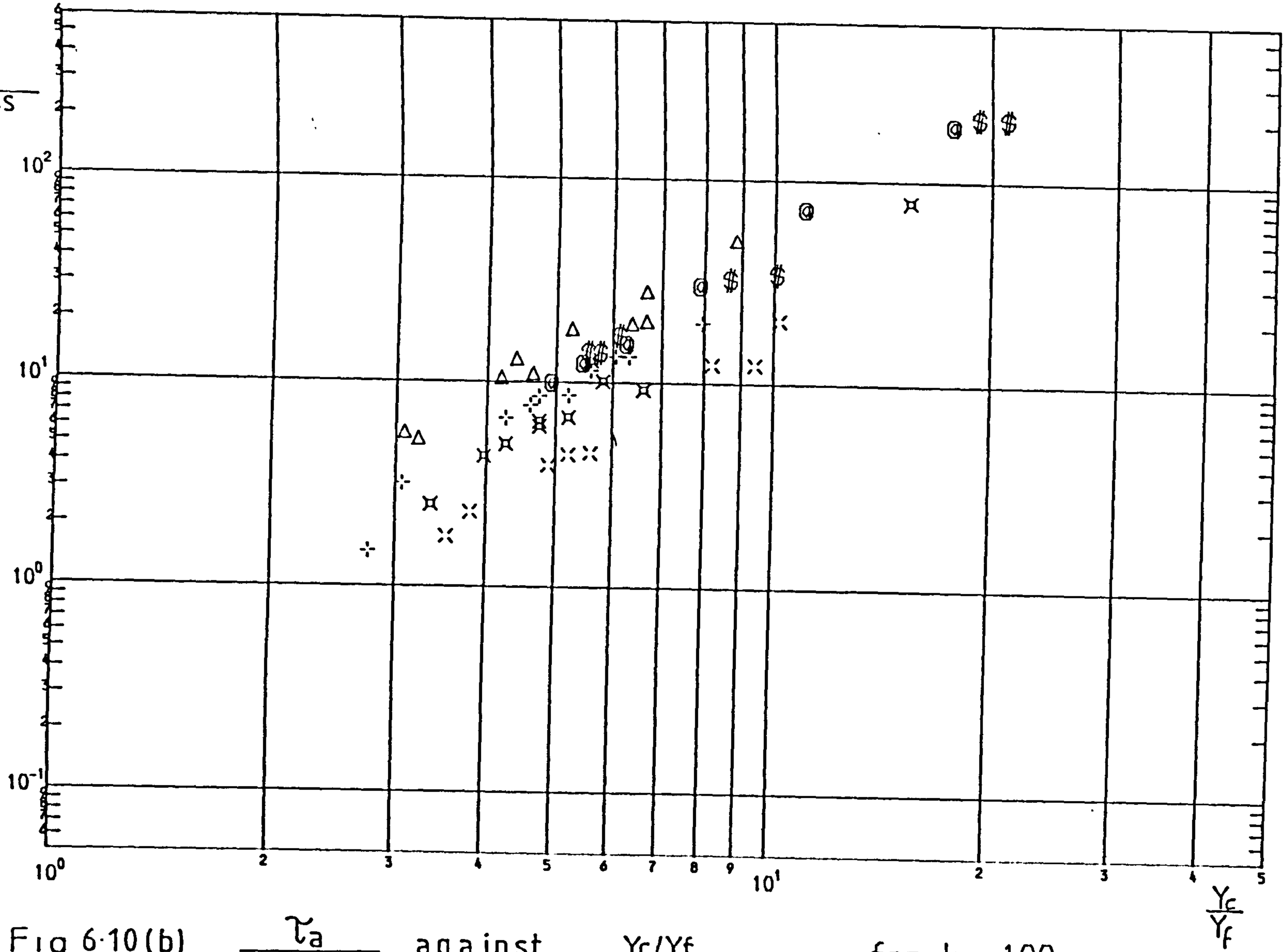

Fig 6·10(b) $\frac{\tau_a}{\rho g Y_f S}$ against Yc/Yf for h= 100 mm

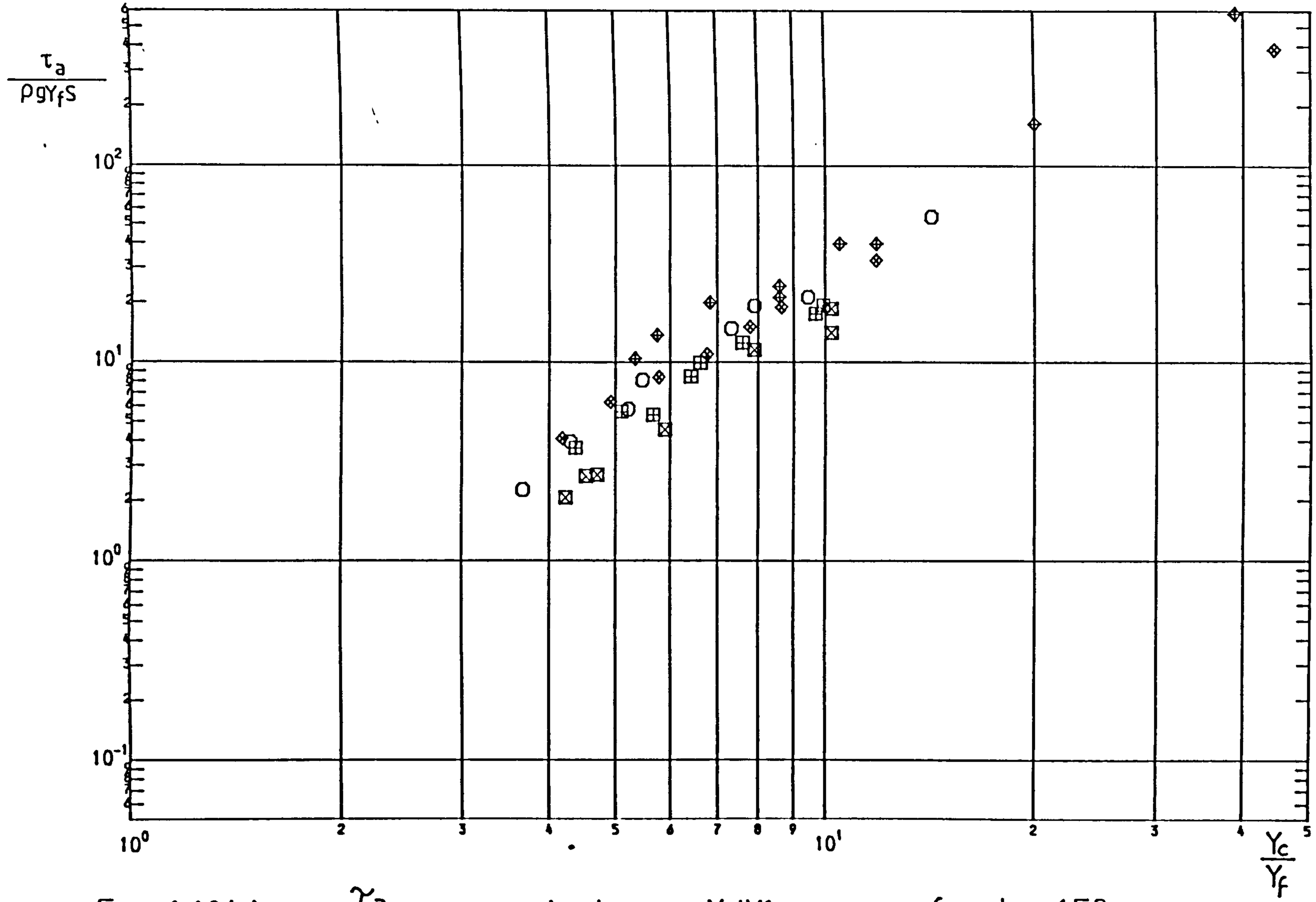

Fig 6·10(c) $\frac{\tau_a}{\rho g Y_f S}$ against Y_c/Y_f for h= 150 mm

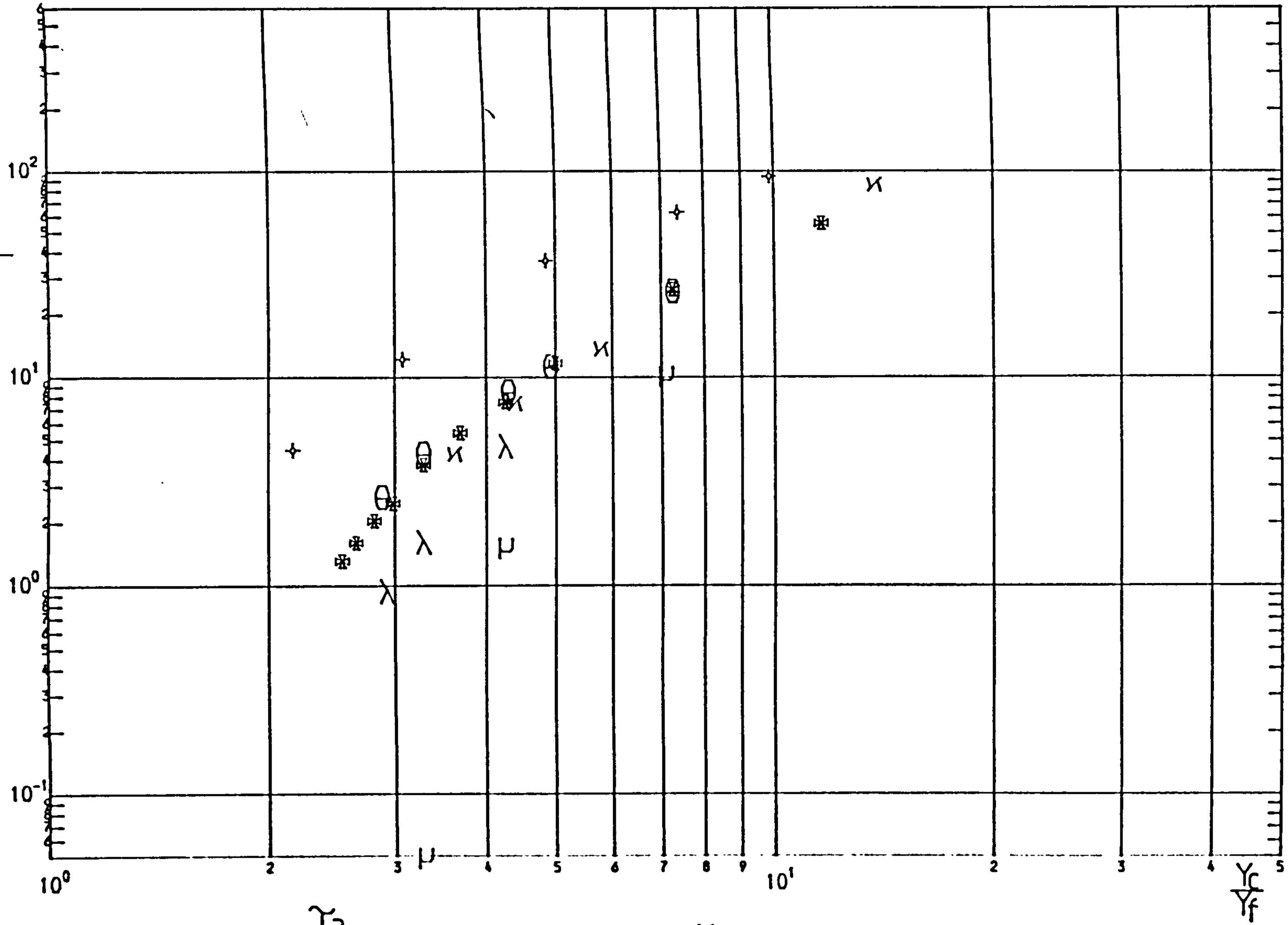

Fig 6·10(d) $\frac{\tau_a}{\rho g Y_f S}$ against $\frac{Y_c}{Y_f}$ for Myers Rajaratnam and Crory.

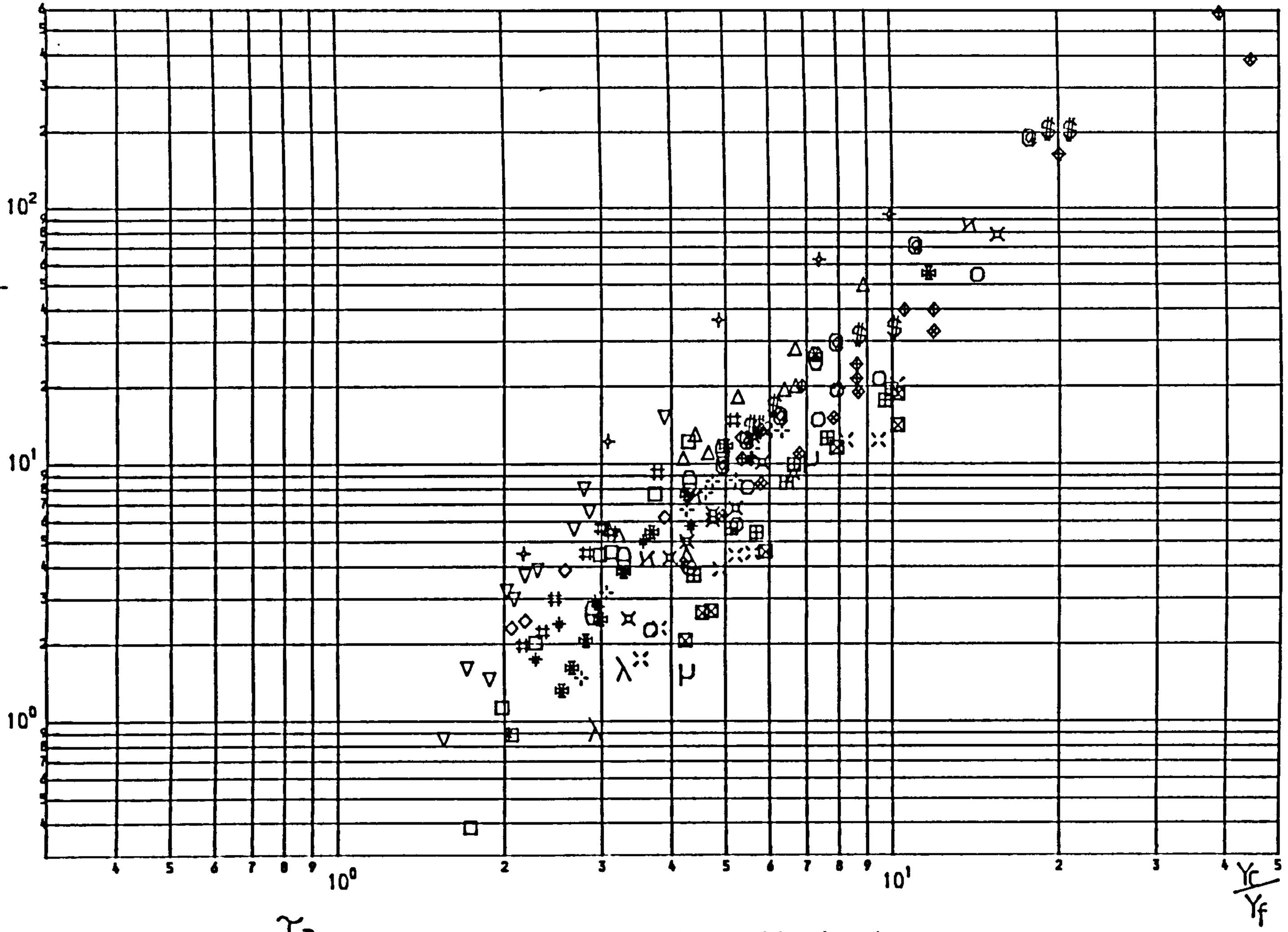

Fig 6·10 (e) $\frac{\tau_a}{\rho g Y_f S}$ against Y_c/Y_f for all tests

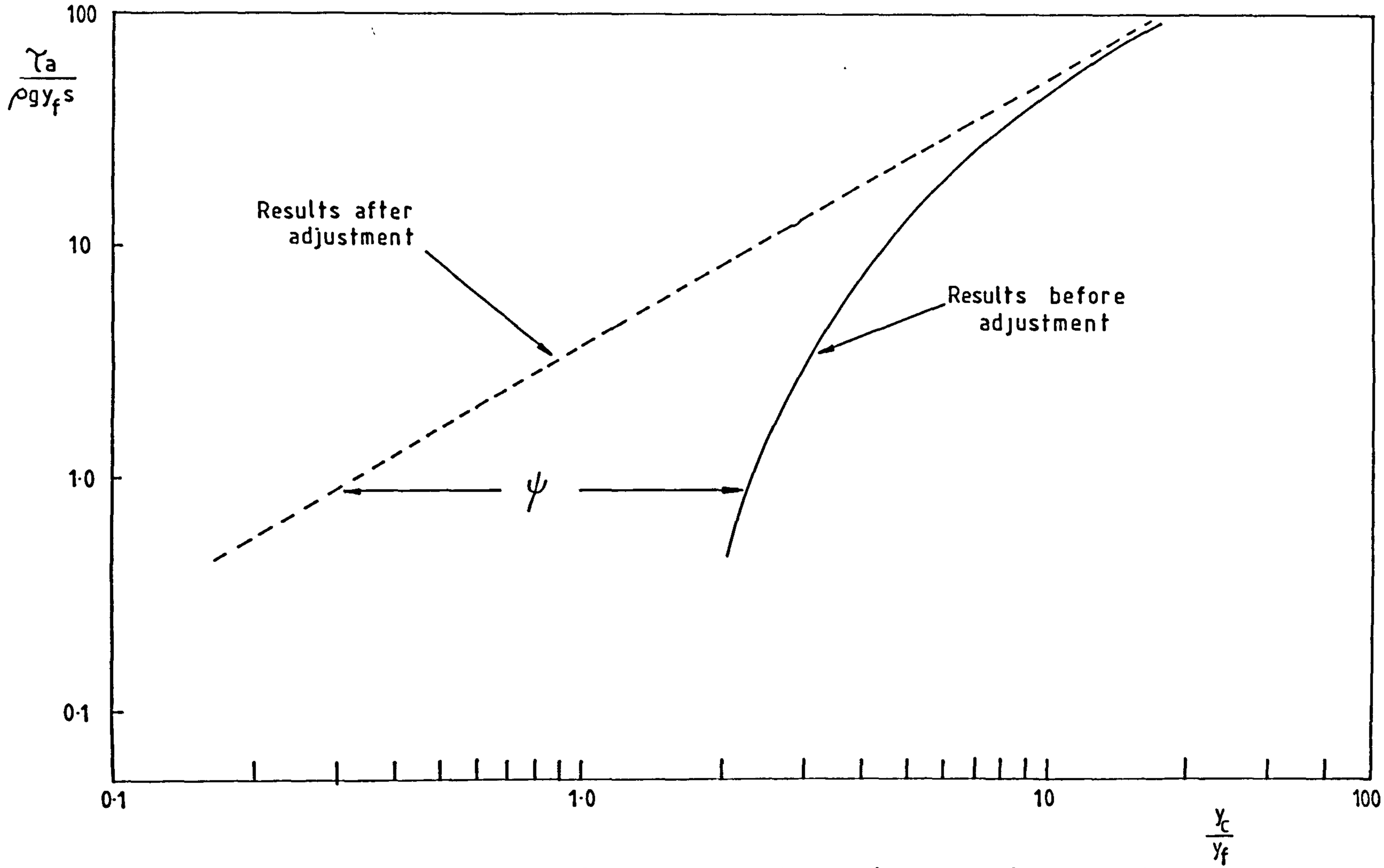

Fig 6·11 A Typical result for a channel geometry before and after the introduction of the parameter ψ.

SYMBOL	GEOMETRY	RUN NO	(mm) h	(mm) B_c	(mm) B_f	No of tests
△	K	1 — 10	102	400	400	10
▽	A	11 — 22	52	400	400	12
□	B	23 — 30	52	200	400	8
◇	C	31 — 37	52	400	200	7
○	G	38 — 45	152	200	600	8
⊞	L	46 — 53	152	200	400	8
⊠	N	54 — 61	152	200	200	8
◈	J	62 — 70	152	400	400	9
⊕	R	71 — 78	152	400	200	8
⋕	MYERS	79 — 88	102	254	356	10
✧	RAJARATNAM	89 — 93	98	711	508	5
⋇	P	94 — 103	102	200	400	10
⊹	H	104 — 113	102	200	600	10
⁙	M	114 — 121	102	200	200	8
θ	CRORY	122 — 126	102	254	356	6
⋌	CRORY	127 — 130	102	203	356	4
λ	CRORY	131 — 133	102	153	356	3
μ	CRORY	134 — 137	102	102	356	4
✱	O	138 — 145	52	200	200	8
#	I	146 — 153	52	200	600	8
⋕	S	154 — 161	102	400	200	8
@	E	162 — 167	102	600	200	6

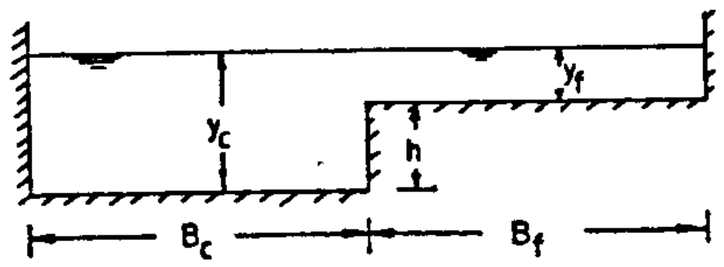

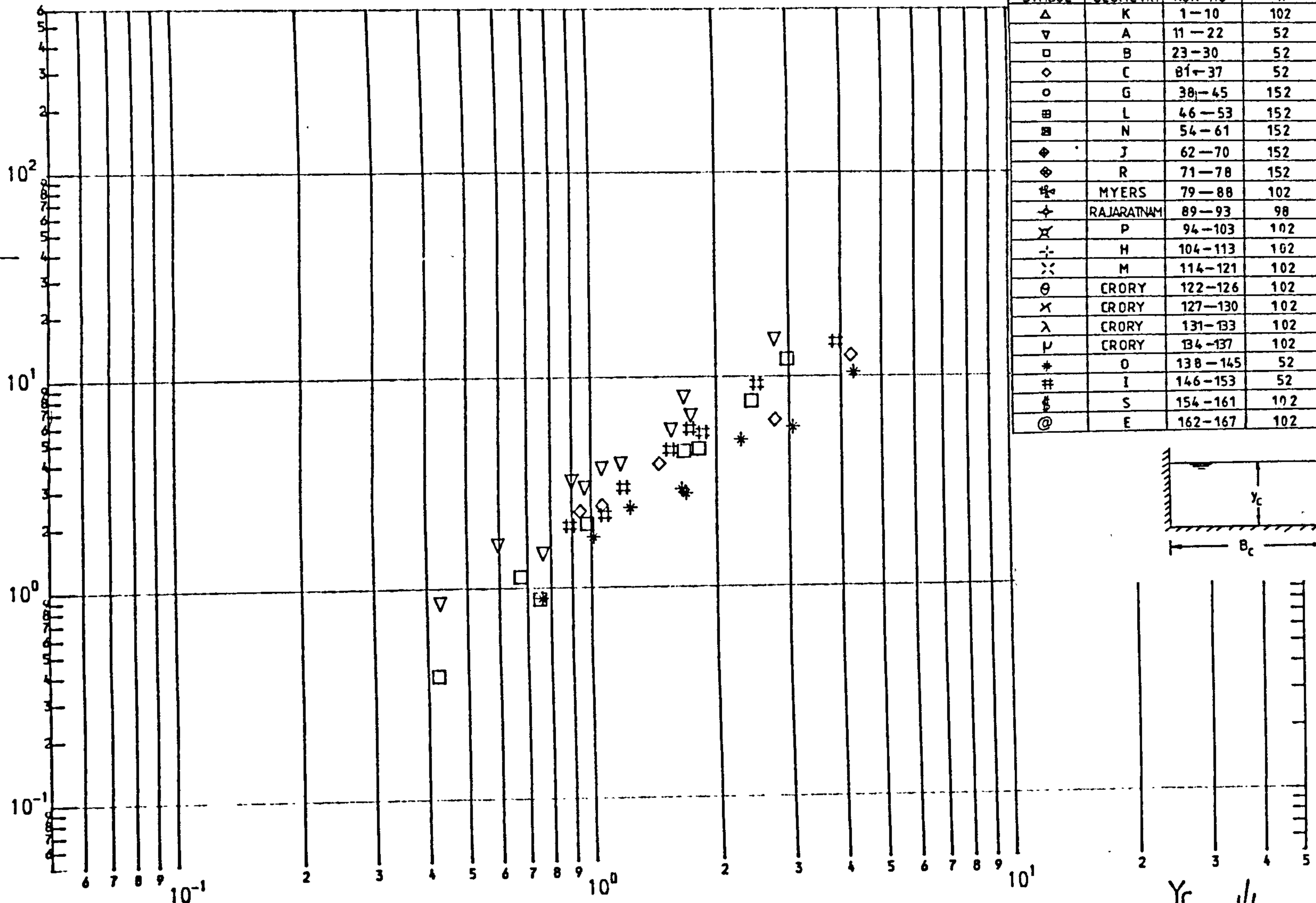

Fig 6·12(a) $\frac{\tau_a}{\rho g Y_f S}$ against $(Y_c/Y_f - \psi)$ h = 50 mm.

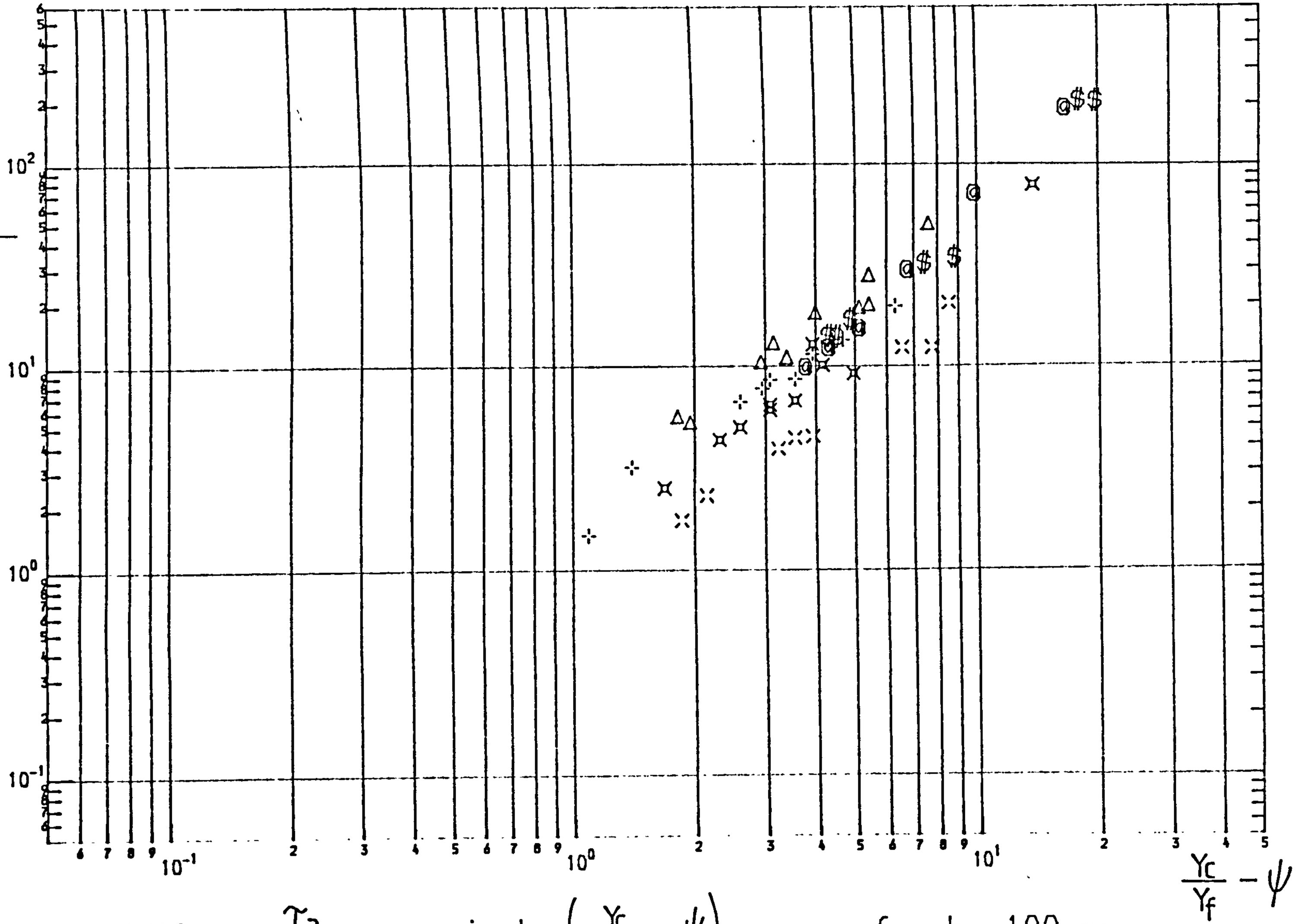

Fig 6·12 (b) $\frac{\tau_a}{\rho g Y_f S}$ against $\left(\frac{Y_c}{Y_f} - \psi\right)$ for h= 100 mm

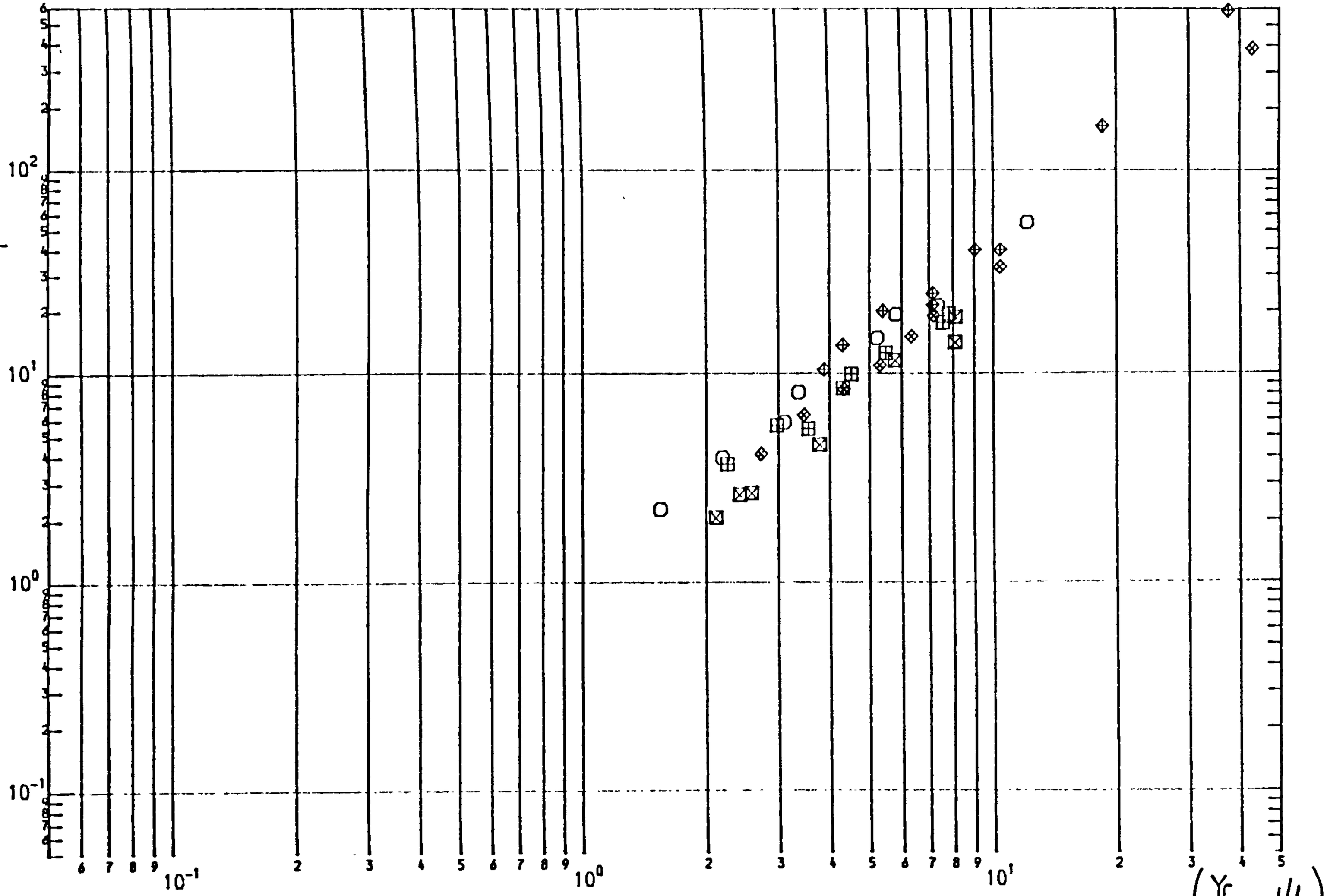

Fig 6·12 (c) $\frac{\tau_a}{\rho g Y_f S}$ against $\left(\frac{Y_c}{Y_f} - \psi\right)$ for h= 150 mm

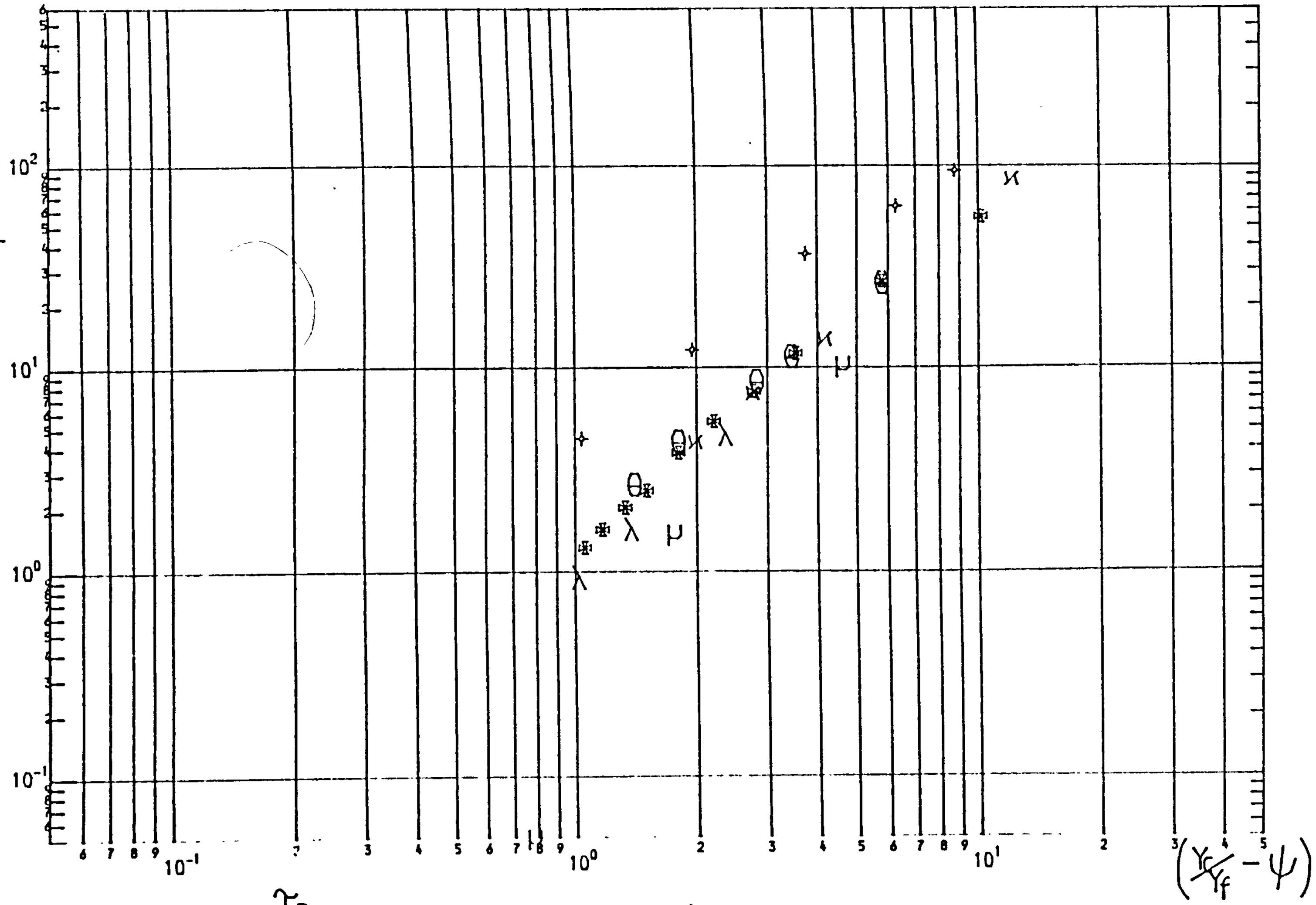

Fig 6·12 (d) $\frac{\tau_a}{\rho g Y_f S}$ against $\left(\frac{Y_c}{Y_f} - \psi\right)$ for Myers Rajaratnam and Crory.

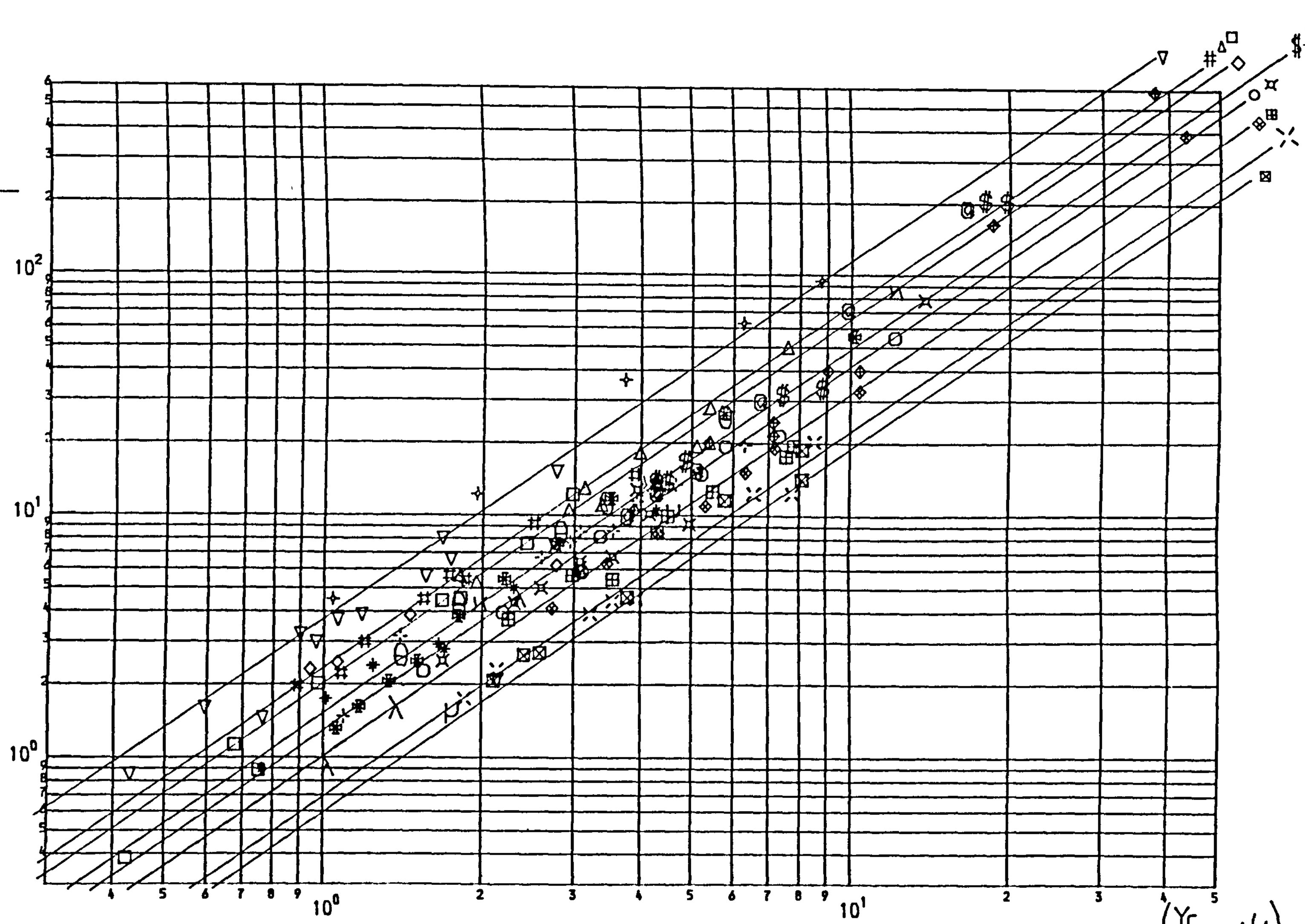

Fig 6·12(e) $\frac{\tau_a}{\rho g Y_f S}$ against $\left(\frac{Y_c}{Y_f} - \psi\right)$ for all tests.

$$\frac{\tau_a}{\rho g Y_f S} = \left(\frac{Y_c}{Y_f} - \psi\right)^{1.5} F_2\,(\text{Geometry})$$

for a given geometry and slope

$$\frac{\tau_a}{Y_f} \;\alpha\; \left(\frac{Y_c}{Y_f} - \psi\right)^{1.5}$$

Assume $\psi = 2$ for instance

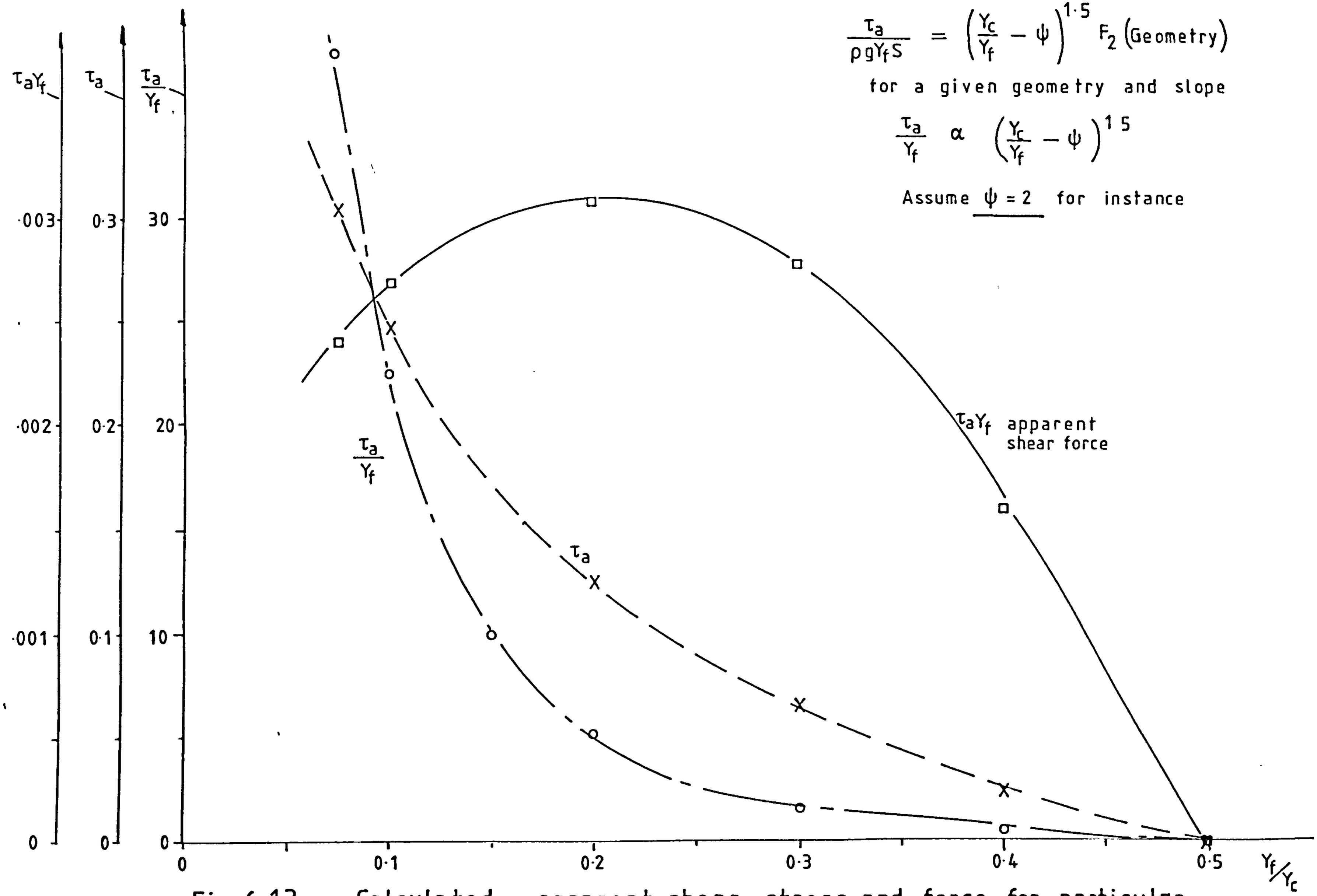

Fig 6·13 Calculated apparent shear stress and force for particular relative depths.

$$\frac{\tau_a}{\rho g Y_f S \left[\frac{Y_c}{Y_f} - \psi\right]^{1.5}} = F2$$

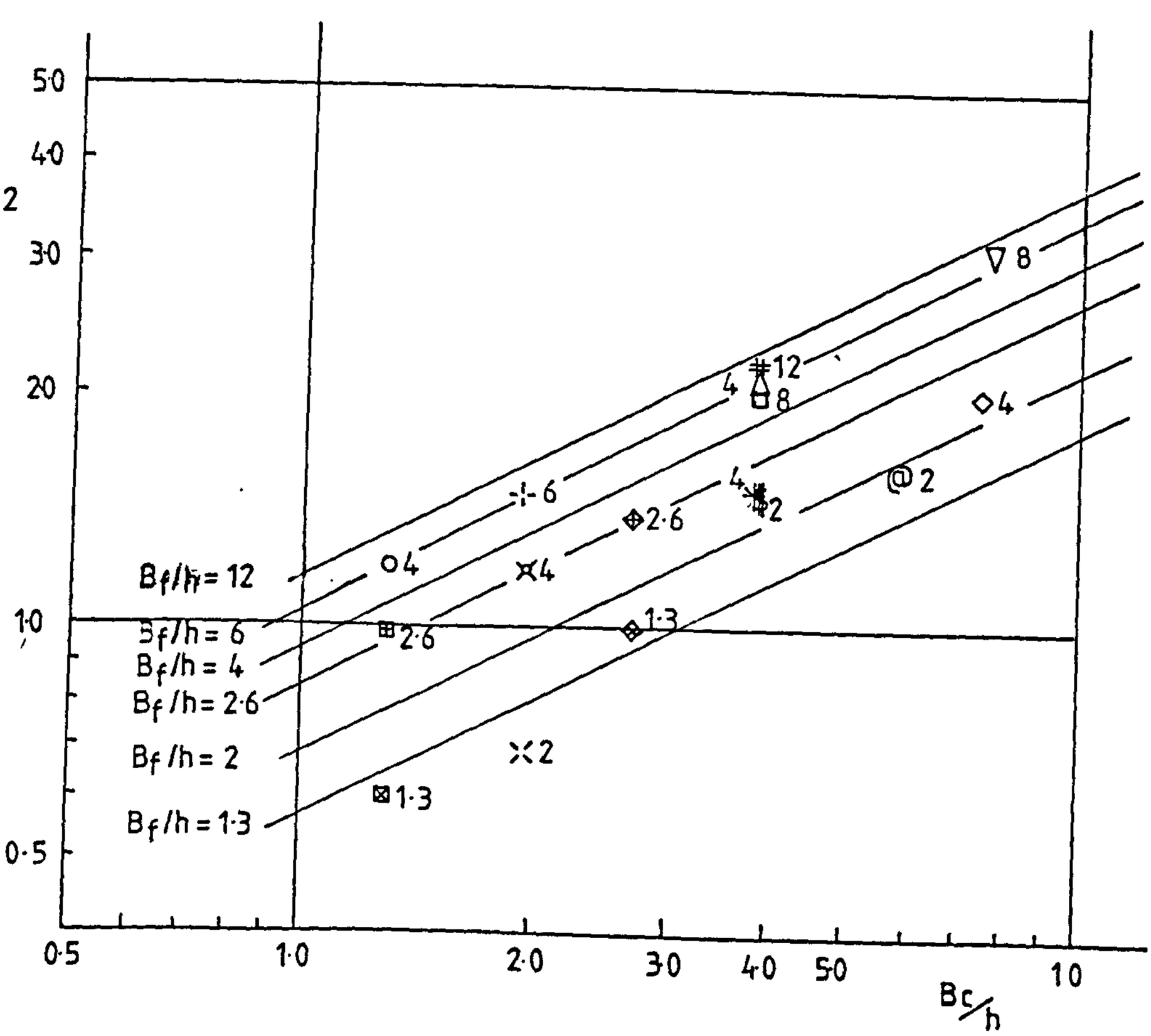

Fig 6·14 Relationship between F2 and B_c/h.

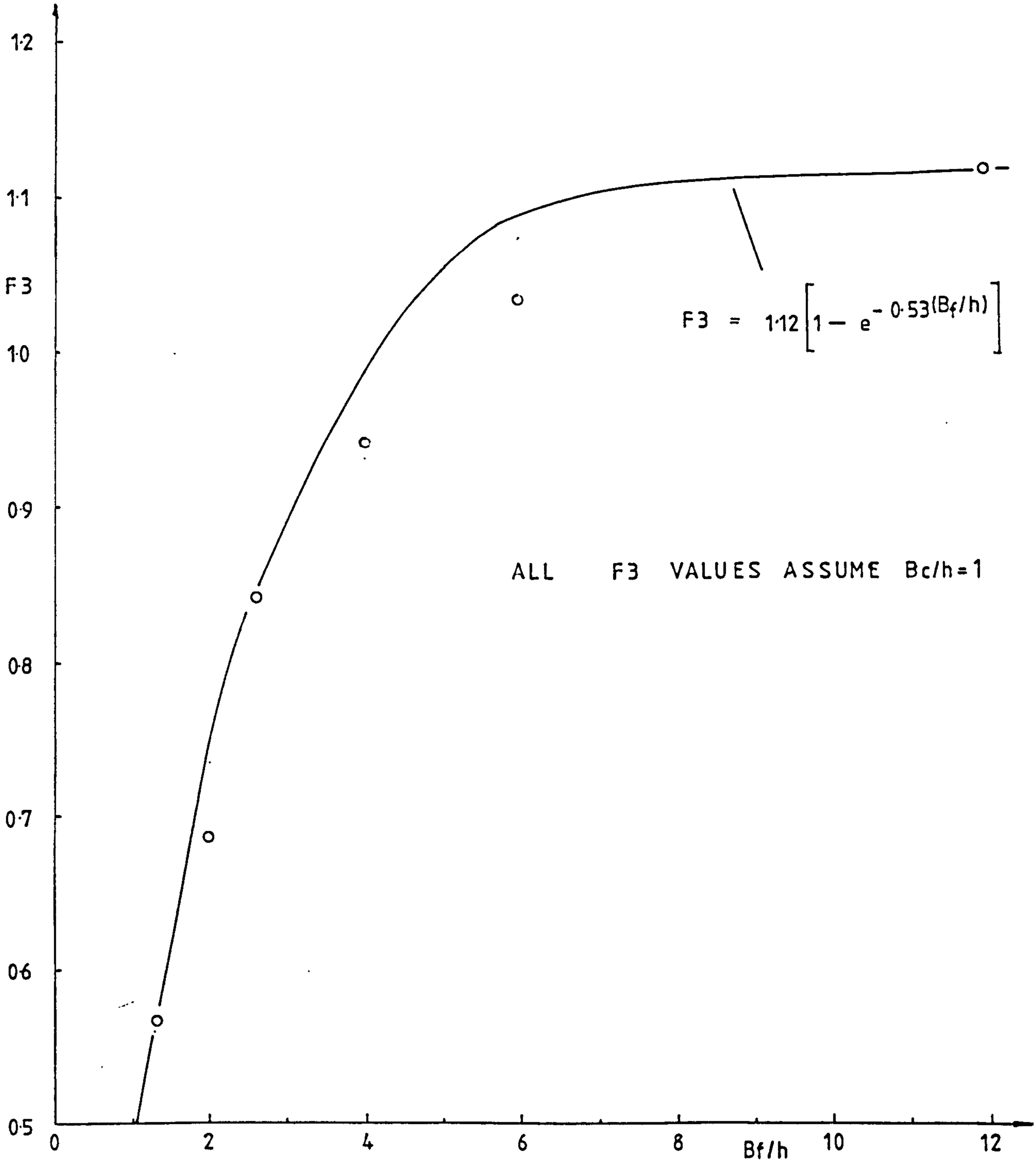

Fig 6·15 Relationship between F3 and B_f/h.

$\frac{\tau_a}{\rho g Y_f S}$

SYMBOL	GEOMETRY	RUN NO	(mm) h	(mm) B_c	(mm) B_f	No of tests
△	K	1—10	102	400	400	10
▽	A	11—22	52	400	400	12
□	B	23—30	52	200	400	8
◇	C	31—37	52	400	200	7
○	G	38—45	152	200	600	8
⊞	L	46—53	152	200	400	8
⊠	N	54—61	152	200	200	8
⊕	J	62—70	152	400	400	9
⊗	R	71—78	152	400	200	8
⊞	MYERS	79—88	102	254	356	10
⊹	RAJARATNAM	89—93	98	711	508	5
⋇	P	94—103	102	200	400	10
⊹	H	104—113	102	200	600	10
⁜	M	114—121	102	200	200	8
θ	CRORY	122—126	102	254	356	6
×	CRORY	127—130	102	203	356	4
λ	CRORY	131—133	102	153	356	3
μ	CRORY	134—137	102	102	356	4
*	O	138—145	52	200	200	8
#	I	146—153	52	200	600	8
$	S	154—161	102	400	200	8
@	E	162—167	102	600	200	6

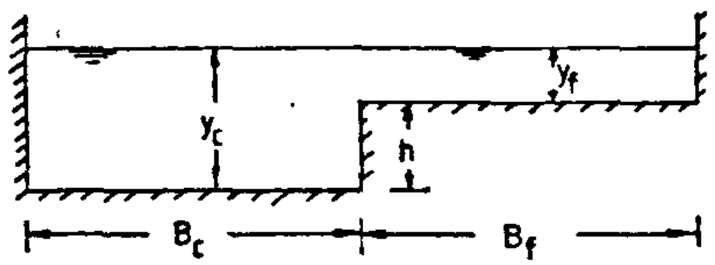

Fig 6·16 (a) $\frac{\tau_a}{\rho g Y_f S}$ against $1{\cdot}12\left(\frac{Y_c}{Y_f}-\psi\right)^{1{\cdot}5}\left(\frac{B_c}{h}\right)^{1/2}\left(1-e^{-0{\cdot}53\frac{B_c}{h}}\right)$ for h= 50 mm $1{\cdot}12\left(\frac{Y_c}{Y_f}-\psi\right)^{1{\cdot}5}\left(\frac{B_c}{h}\right)^{1/2}\left(1-e^{-0{\cdot}53\frac{B_c}{h}}\right)$

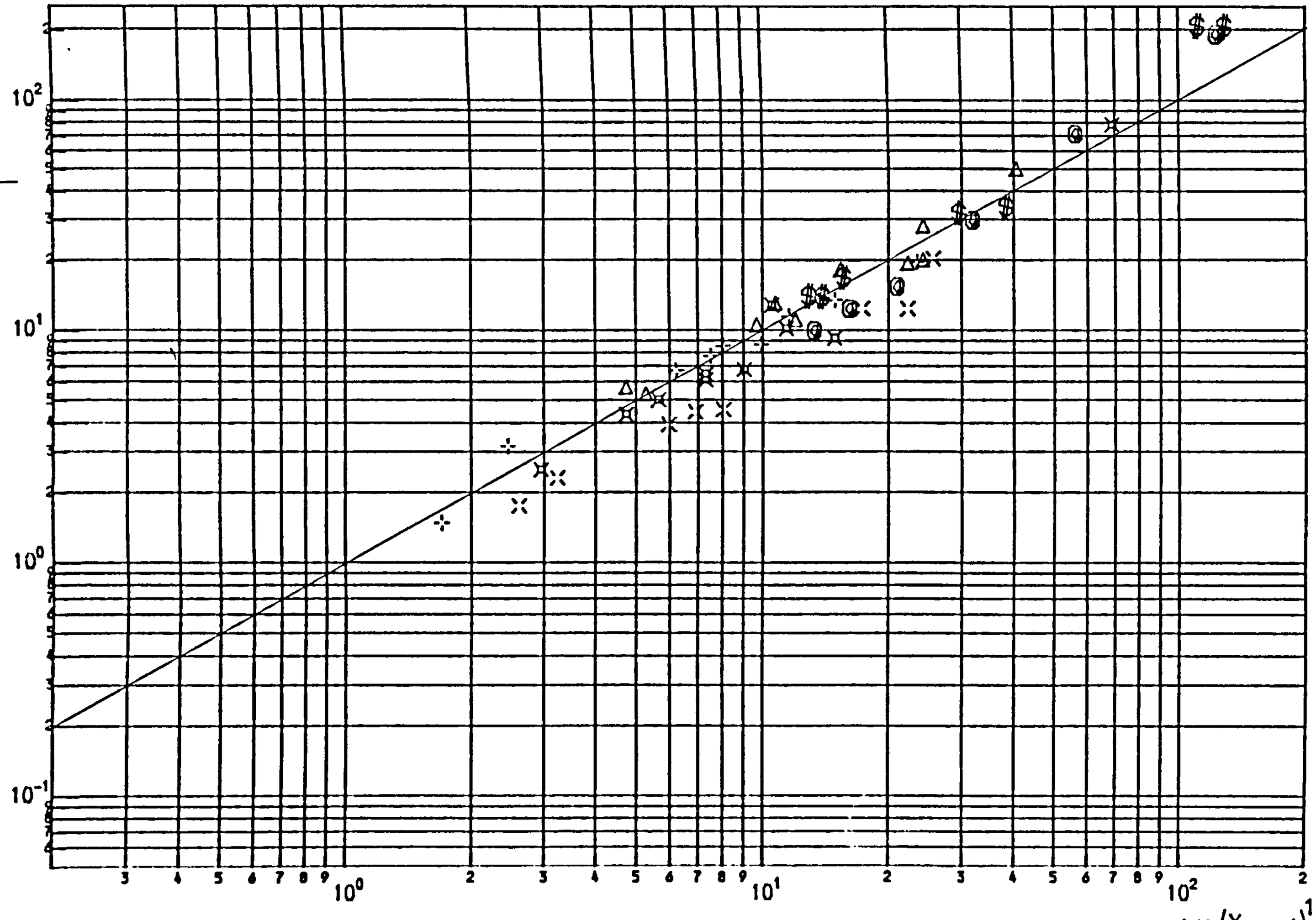

Fig 6·16 (b) $\frac{\tau_a}{\rho g Y_f S}$ against $1{\cdot}12\left(\frac{Y_c}{Y_f}-\psi\right)^{1{\cdot}5}\left(\frac{B_c}{h}\right)^{1/2}\left(1-e^{-0{\cdot}53\frac{B_c}{h}}\right)$ for h = 100 mm

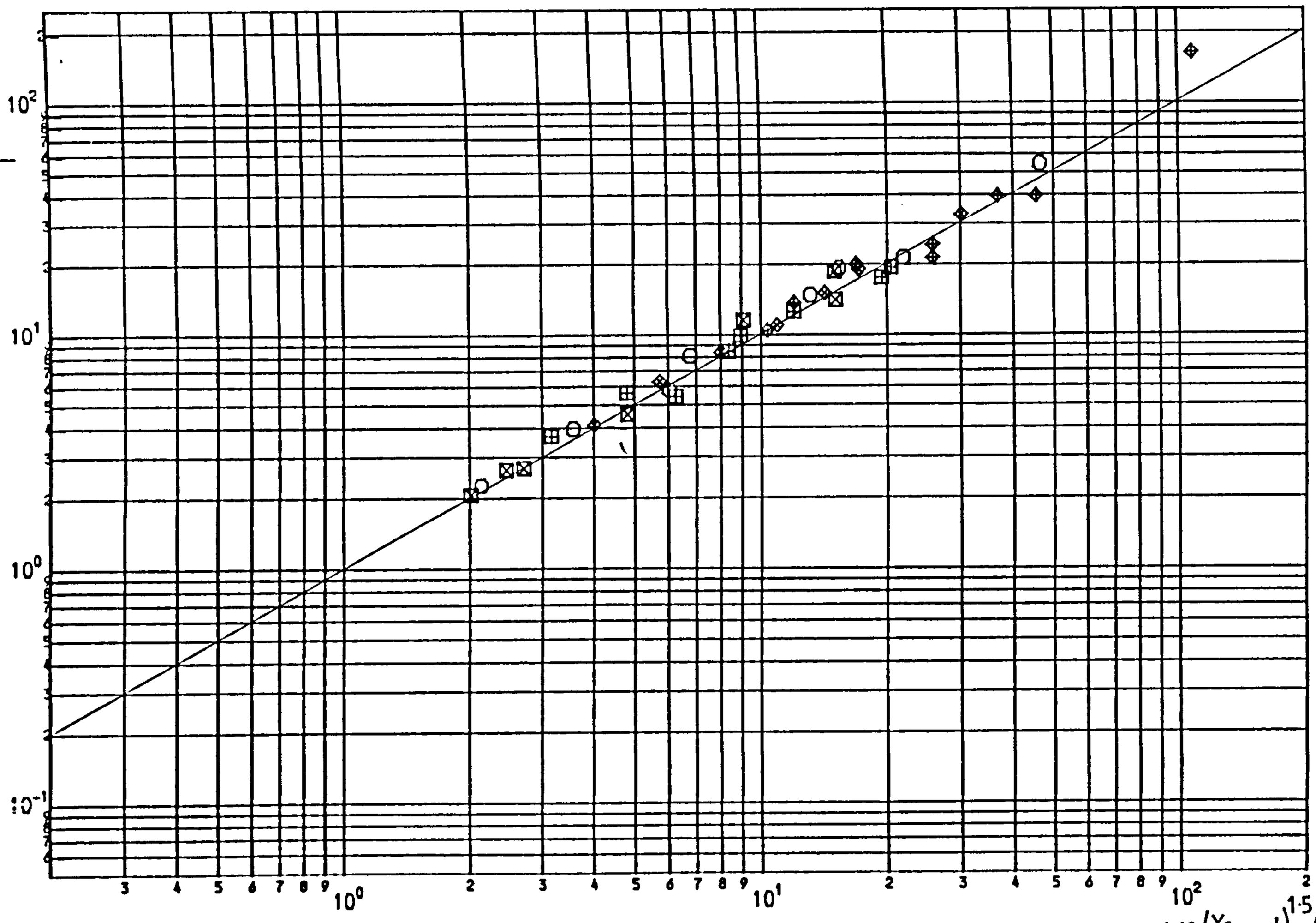

Fig 6·16 (c) $\frac{\tau_a}{\rho g Y_f S}$ against $1{\cdot}12\left(\frac{Y_c}{Y_f}-\psi\right)^{1{\cdot}5}\left(\frac{B_c}{h}\right)^{1/2}\left(1-e^{-0{\cdot}53\frac{B_c}{h}}\right)$ for h= 150 mm

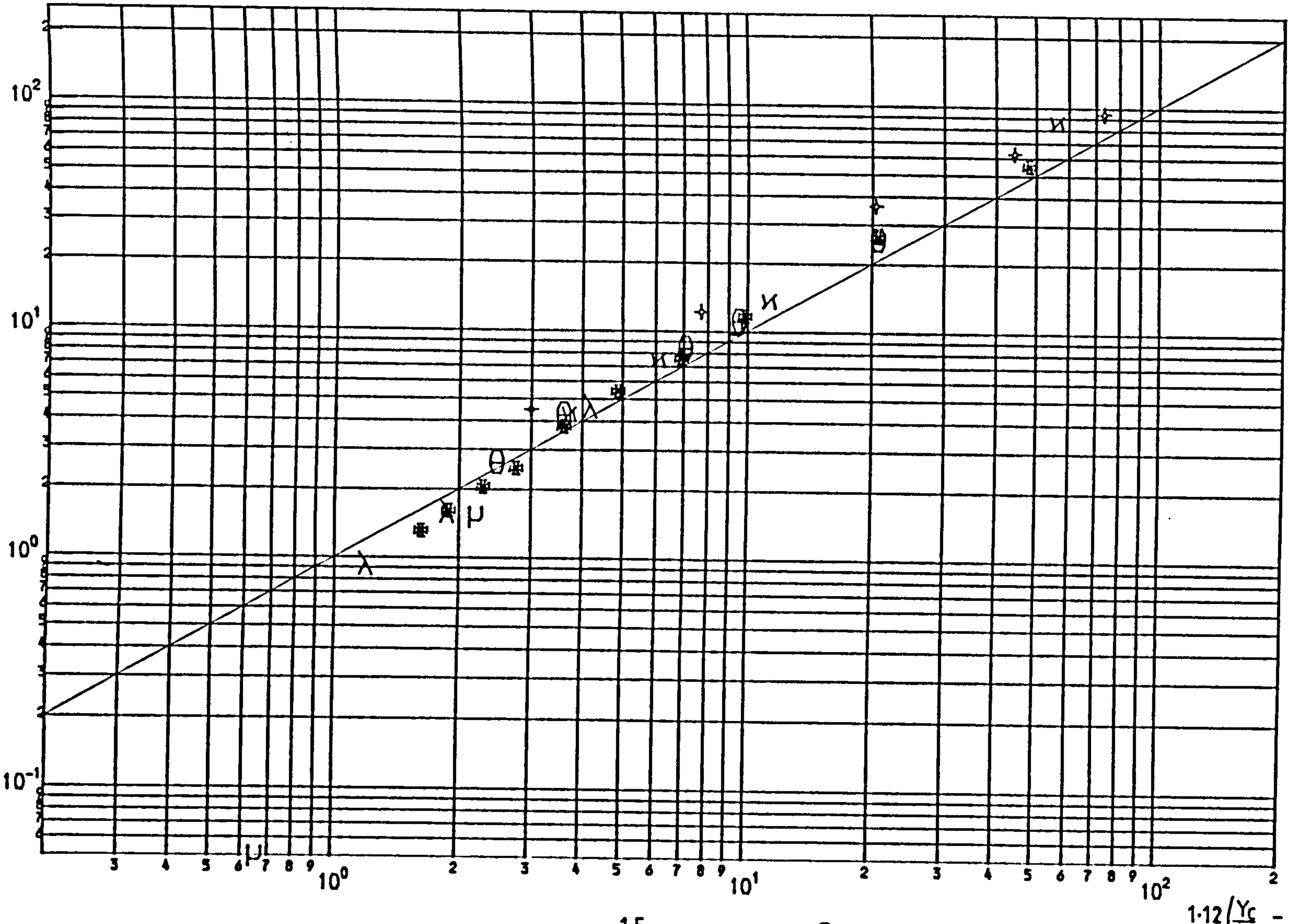

Fig 6·16 (d) $\frac{\tau_a}{\rho g Y_f S}$ against $1{\cdot}12\left(\frac{Y_c}{Y_f}-\psi\right)^{1{\cdot}5}\left(\frac{B_c}{h}\right)^{1/2}\left(1-e^{-0{\cdot}53\frac{B_c}{h}}\right)$ for Myers Rajaratnam and Crory.

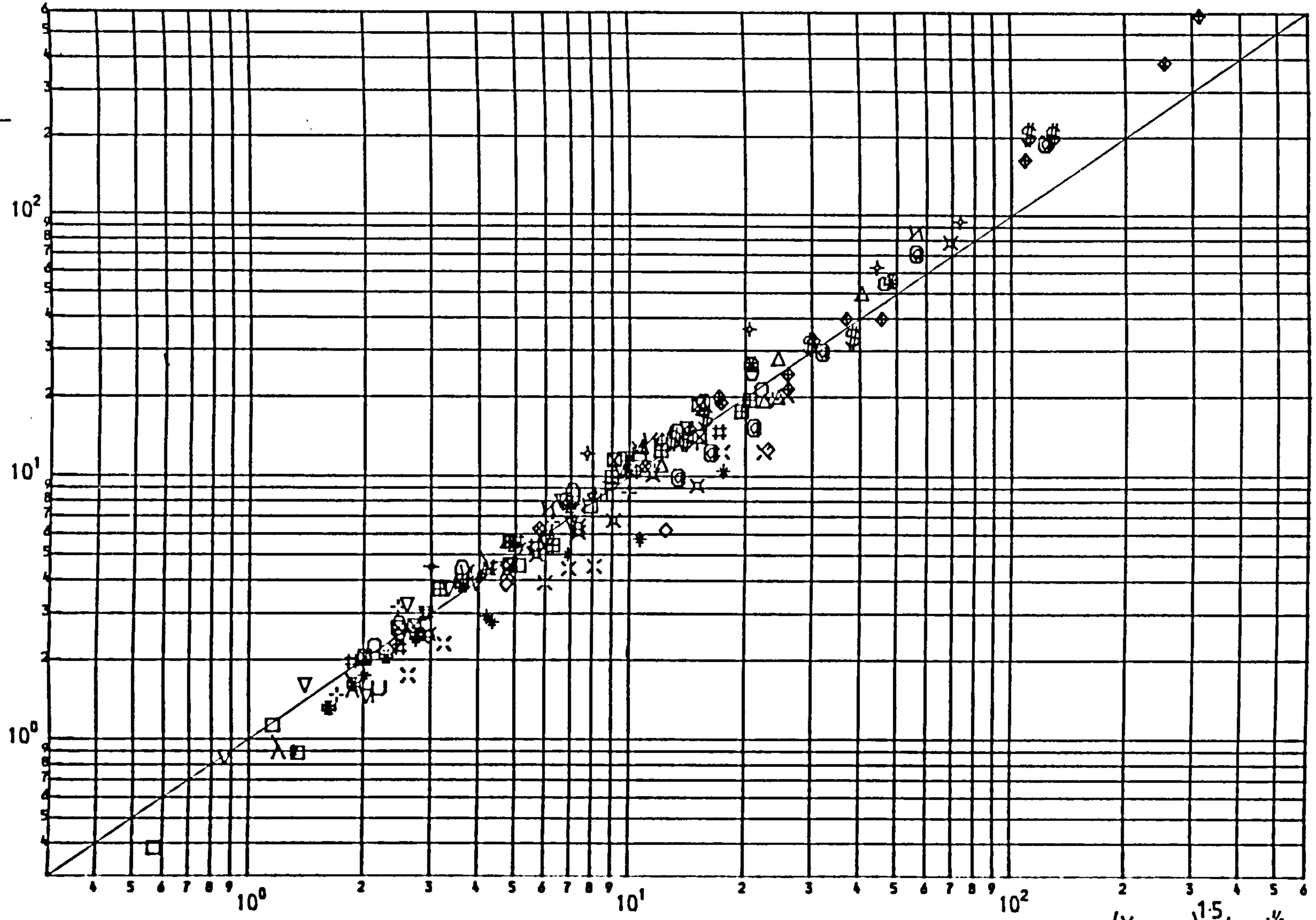

Fig 6·16 (e) $\frac{\tau_a}{\rho g Y_f S}$ against $1{\cdot}12\left(\frac{Y_c}{Y_f}-\psi\right)^{1{\cdot}5}\left(\frac{B_c}{h}\right)^{1/2}\left(1-e^{-0{\cdot}53\frac{B_c}{h}}\right)$

μ

CHAPTER SEVEN

COMPARISON WITH OTHER STUDIES, CONCLUSIONS AND SUGGESTIONS FOR FUTURE RESEARCH.

Table of Contents

7.1 Introduction.

The purpose of the present investigation has been to study the relationship between the geometrical parameters of the compound channel with respect to the interaction mechanism which exists at the channel/flood plain boundary. It has been shown that the amount of turbulent shear at this interface is strongly related to the channel and flood plain widths, the relative depths in the channel and flood plain and the bankfull depth. A relationship has been proposed which attempts to predict the amount of resistance which will occur in smooth boundary channels. Other investigators have produced similar relationships based on their own experimental work. Such work will be discussed in this chapter in the light of the current investigation. Work carried out by Myers, Crory and Rajaratnam has been presented extensively in this study since their work is similar to the author's, involving the use of a main channel flanked by one flood plain.

Some experimental work has been carried out with symmetrical compound channels. Relationships have also been developed in the past in an attempt to express the intensity of the channel/flood plain interaction in such channels. These channels essentially have two zones of interaction, each at the

channel/flood plain junction. If one half of a symmetrical channel is considered, then similarities with asymmetrical channels might be expected. These results/relationships will therefore also be discussed with respect to the current set of results.

The discussion of past investigations can be divided into two main areas. First the relationships developed by other investigators can be compared with the results obtained from the present study. Secondly, the results produced from other investigations can be compared to the relationships developed in this study.

7.2 Past Relationships which have been developed.

Up to this point the results of Crory, Myers, and Rajaratnam and Ahmadi have been presented extensively with the results obtained by the author. No mention, apart from in the literature review, has been made of the relationships which these investigators developed based on their own results. Their work will therefore be presented along with Hadjipanos' relationships developed for Symmetrical compound channels.

7.2.1 Crory's Relationships.

Crory's results have been presented extensively in the current investigation. She carried out 16 experiments on a compound channel whose main channel width was varied for different tests. She also varied the depth of flow in the channel. Using the Preston tube technique, she was able to determine the shear stress distribution and hence average shear in both the channel and the flood plain. She was therefore able to determine the effect of the channel/ flood plain width ratio on the shear stress distribution and proposed the following relationships :-

$$1 - \phi'_c = \frac{B_c}{B_f}\,\frac{h^2}{A_c} \qquad (7.1)$$

and

$$\phi'_f - 1 = \frac{B_c}{B_f}\,\frac{h^2}{A_f} \qquad (7.2)$$

where

$$\Phi_c = \frac{\tau'_c\, P'_c}{\rho g\, A_c S} \qquad (7.3)$$

and

$$\Phi_f = \frac{\tau'_f\, P'_f}{\rho g A_f S} \qquad (7.4)$$

$\tau_{c'}$ and $\tau_{f'}$ are the interacting shear stresses in the channel and flood plain of cross sectional areas Ac and Af respectively. Pc'= Bc + Yc + h and Pf'= Bf + Yf. S is the channel and flood plain slope. Where these equations are

developed from can be seen in Chapter 2. Shear tests were recorded for each test in the present study and therefore it is possible to validate Equations (7.1) and (7.2) in the light of the current investigation. Fig 7.1 and Fig 7.2 shows the relationships proposed by Crory, for all the geometries tested in the current investigation.

Some interesting observations can be made with Fig 7.1. It can be seen that Crory's results do follow Equation (7.1) as does Myers' results. Crory's work involved a bankfull depth of around 0.1 m and flood plain width to channel width ratios Bf/Bc of 1.4 to 3.5. The test carried out by the author with a similar geometry, namely geometry P(✕ :h=0.102 m:Bf/Bc=2.0) lies close to Crory's and Myers' results suggesting that Equation (7.1) is only valid for geometries with the same bankfull depth and channel and flood plain width as Crory tested. This can be explained by remembering that Equation (3.1) can be rewritten :-

$$\Phi'_c = 1 - \left(\frac{h}{Bc}\right)\left(\frac{h}{Yc}\right)\left(\frac{Bc}{Bf}\right) \qquad (7.5)$$

Thus if (h/Yc) tends towards 1.0 , (ie for very low flood plain depths) and (h/Bf) also tends towards 1.0, then obviously $\Phi'c$ will equal zero which can never be so. This is clearly demonstrated on Fig 7.1 where geometries R(◈), N(⊠), S($), E(@), and M(:) all have low flood plain widths for their corresponding bankfull

depths. This gives (h/Bc) values closer to 1.0 resulting in Equation (7.1) no longer being valid. Thus it is clear that Equation (7.1) is valid for the particular geometry that Crory tested but cannot be satisfactorily applied to other cross sections. Crory did not investigate the significance of the bankfull depth h, fully. Comparing geometry P(⋈ :h=0.102m:Bf/Bc=2.0) with geometries B(□ :h=0.05m:Bf/Bc=2.0) and L(⊞ :h=0.150m:Bf/Bc=2.0) show that for a given Bf/Bc ratio, equation (7.1) is not satisfied. Furthermore, it is clear that when Bf/Bc ratios exceed the range tested by Crory, eg, geometry E(@ :h=0.150m:Bf/Bc=0.33), Equation (7.1) becomes increasingly inaccurate.

Similar observations can be made with Equation (7.2) shown on Fig 7.2. Similarly, Equation (7.2) can be rewritten as :-

$$\phi'_f - 1 = \left(\frac{B_c}{B_f}\right)\left(\frac{h}{B_f}\right)\left(\frac{h}{Y_f}\right) \qquad (7.6)$$

It is assumed that Φ'_f' can never be less than 1.0 which suggests that the terms (h/Bf) and (h/Yf) when small will give ϕ'_f values close to 1.0. Consider the geometry I(#:h/Bf=0.0866) where the results on Fig 7.2 are clearly different from Equation (7.2). Equation (7.2) underestimates the value of $\Phi f'$ for this particular geometry. Now consider geometry

R(⊗:h/Bf=0.76). Here the ratio (h/Bf) is much greater, however Equation (7.2) underestimates the value of $\Phi f'$. Clearly the relationship between $\Phi f'$ and the geometrical parameters is more complicated than Crory's relationships might suggest. Although to be fair, the limited range of geometries tested by her made it difficult to assess fully the effects of the channel dimensions on the interaction mechanism.

Crory's results only confirm the findings of Chapters 4, 5 and 6 which suggest that the Bc/Bf term obscures the effect of the bankfull depth term on the interaction mechanism. By introducing the parameters Bc/h and Bf/h, as the author has done, relationships can be developed which will give a good representation of Crory's results.

7.2.2 Rajaratanam and Ahamadi.

Rajaratnam and Ahamdi (Ref 48) proposed a relationship which introduced a longitudinal shear stress $\tau*$, which essentially represents the increase in shear which occurs in the flood plain as a result of channel/flood plain interaction. The interaction, according to Rajaratnam, would never extend into the flood plain beyond a distance of $2.5b_\tau$ where b_τ is given by the relationship :-

$$\frac{b_\tau}{Y_f} = 0.64\left(\frac{Y_c}{Y_f} - 1\right) \qquad (7.7)$$

Rajaratnam therefore calculated τ_* as the increase in shear which is occurring on the flood plain, a distance of $2.5b_\tau$ into the flood plain. Thus there lies the difference between τ_* and τ_a, the apparent shear stress discussed in this study, with τ_a being based on the total width of the flood plain. When considering the relationships developed by Rajaratnam based on τ_*, there must be limited similarities with results which use the apparent shear stress. A relationship proposed by Rajaratnam is given as :-

$$\frac{\tau_*}{\rho g Y_f S} = 0.15\left(\frac{Y_c}{Y_f} - 1\right)^2 \qquad (7.8)$$

Clearly this relationship, shown on Fig 7.3 is not representative of the authors results based on τ_a, with Equation (7.8) underestimating the value of τ_a. Howvever, it is interesting to note that Rajaratnam's own results are clearly greater than Equation (7.8), suggesting that the general increase in results is possibly due to the inherent difference between τ_* and τ_a.

It must be observed that the general framework of Equation (7.8) is reasonable, with $\frac{\tau_a}{\rho g Y_f S}$ generally increasing with $0.15(Yc/Yf-1)^2$ for a given geometry. In fact, this relationship has similarities with the relationship developed in

Equation (7.8) would suggest that the channel and flood plain widths have no effect on the interaction mechanism. Clearly, the results presented in this study have suggested quite the reverse. Rajaratnam made no attempt to vary the channel and flood plain widths, and it is therefore concluded that Equation (7.8) describes well the variation in τ_* for varying relative depths, for Rajaratnam and Ahmadi's particular Experimental flume.

7.2.3 Hadjipanos, Wormleaton and Allen.

In chapter 2, work carried out by Hadjipanos, Wormleaton and Allen was described. Hadjipanos carried out a full regression analysis into the relationship between the apparent shear stress τ_a and various geometrical and roughness parameters. To recall, Hadjipanos carried out a series of experiments with a main channel of width 0.29m and bankfull depth 0.12 m, flanked by two flood plains, each of width 0.46 m. The channel and flood plain widths remained fixed, with only the depth of flow in the channel and flood plain being varied. Four series of tests were carried out with flood plains of varying roughness - Series A, the smooth flood plain, and Series D, the roughest flood plain. Of main concern is the relationships developed by Hadjipanos based on his smooth flood plain

experiments, since direct comparisons with the current investigation are possible.

It was pointed out in Chapter 4 that the intensity of the interaction is strongly related to the lateral velocity gradient at the channel/flood plain boundary. Hadjipanos recognised this point and introduced a velocity gradient parameter $\dot{\gamma}$ which could represent the actual velocity gradient at the interface. $\dot{\gamma}$ is given by the relationship :-

$$\dot{\gamma} = \frac{V_c - V_f}{\frac{1}{2}(B_c + B_f)} \qquad (7.9)$$

where Vc and Vf are the velocities in the channel and flood plain based on non-interacting conditions using Manning's Equation. $\frac{1}{2}$(Bc+Bf) actually represents the distance between the centroids of flow on the channel and flood plain. A further term which Hadjipanos considered significant was $\bar{V}$ given by :-

$$\bar{V} = \frac{Q_t}{A_t} \qquad (7.10)$$

where Qt is the total discharge down the channel and flood plain of total cross sectional area At.

Arranging the significant parameters which influence the interaction mechanism into a non-dimensional relationship, Hadjipanos proposed the following relationship :-

$$\frac{\tau_a}{\rho \overline{V}^2} = 2{\cdot}48 \times 10^4 \left(\frac{\dot{\gamma} Y_f}{V}\right)^{1{\cdot}01} \left(\frac{\overline{V} Y_f}{\nu}\right)^{-1{\cdot}30} \qquad (7.11)$$

where τ_a is the apparent shear stress, ν is the kinematic viscosity and Yf is the depth of flow in the flood plain. Fig 7.4 presents this relationship for the current investigation and also other studies. It would seem that Myers' results satisfy Equation (7.11) reasonably well. Also Crory's results for a similar channel width are well represented. However, it is clear that as the channel width decreases for Crory's results i.e. (Bc=0.153 m: λ) and (Bc=0.102 m: μ), Equation (7.11) no longer gives a good representation of the data.

Similar observations can be made with the current investigations. Reasonable straight line fits can be drawn through each geometry data which will be parallel with Hadjipanos' relationship. The position of each line seems to be dependent on the value of Bc, or rather Bc/h. The arrow shows clearly the displacement required to fit the data. It is also clear that a similar trend exists for varying Bf. Consider geometries H(+: Bc=0.2m: Bf=0.6m), P(¤: Bc=0.2m: Bf=0.4) and M(□: Bc=0.2m: Bf=0.2m). All three geometries have an equal Bc=0.2 m and h=0.102 m. As the flood plain width is reduced, the straight line relationship through each set of data moves downward as shown on Fig 7.4. Such findings can be confirmed by studying other geometries.

The main conclusions that can be drawn from Equation (7.11) and Fig 7.4 is that the data from each geometry show a straight line relationship similar to Equation (7.11) but that the widths of the channel and flood plain have an influence on the apparent shear stress. This influence is not introduced adequately in Equation (7.11). This is understandable since Hadjipanos did not vary the channel or flood plain widths and therefore was in no position to assess the significance of these widths.

However, one advantage of Equation (7.11) is that it is non-dimensional thus giving a dimensionally consistent equation.

A further relationship developed by Hadjipanos, Wormleaton and Allen (Ref 70) is shown on Fig 7.5 and is given by the equation :-

$$\tau_a = 13{\cdot}84\,\Delta V^{0{\cdot}882}\left(\frac{Y_c}{h}\right)^{-3{\cdot}123}\left(\frac{B_f}{B_c}\right)^{-0{\cdot}727} \qquad (7.12)$$

This equation considers the important parameters in determining the apparent shear stress as being ΔV, the difference in mean velocity between the main channel and the flood plain based on Manning's equation, the relative depths of flow, and the relative widths of the channel and flood plain. This equation therefore has some similarities with the relationship developed in

$$\tau_a = \Delta V^{2.2\left[\frac{Bc}{Bf}\right]^{1/2}} \cdot fn\left\{\frac{h}{B_f}, \frac{Bc}{h}\right\} \qquad (7.13)$$

Again it is clear from Fig 7.6 that there is some considerable spread in the results. On closer inspection, it is apparent that the spread is due to the variation in channel and flood plain width. This is certainly because Hadjipanos carried out his experiments in a flume with constant channel/flood plain widths. Consider the three geometries I(#:Bf/h=12), A(▽:Bf/h=8) and B(□:Bf/h=8) which all have a high Bf/h value. Clearly, as Fig 7.6 shows, all τ_a values for these geometries are greater than Equation (7.13) would suggest. Other geometries such as E(@:Bf/h=1.3) and M(><:Bf/h=2) have low Bf/h values and hence are less than the values suggested by Equation (7.13). Generally then, Hadjipanos has not introduced the geometrical parameters fully into Equation (7.13) probably because his experimental results did not contain varying cross sections.

7.2.4 Myers.

A recent investigation was carried out by Myers (Ref 38) with a symmetrical compound channel. The investigation involved tests with a main channel of width 160 mm. Two flood plain widths of 300 mm and 180 mm and two bankfull depths of 80 mm and 120 mm were tested. The average velocities

in the main channel and flood plain were measured and the appropriate Reynolds numbers calculated :-

$$Re_c = \frac{4 V_c' R_c}{\nu} \qquad (7.14)$$

and

$$Re_f = \frac{4 V_f' R_f}{\nu} \qquad (7.15)$$

where ν is the kinematic viscosity, Vc' and Vf' are the mean velocities in the channel and flood plain respectively, and Rc and Rf are the hydraulic radii. Myers studied the relationship between the Reynolds number ratio, Re_c / Re_f, and the relative depth of flow. Fig 7.6 presents his findings. It is clear that for a given relative depth, the Reynolds number ratio decreases as the bankfull depth increases. Similarly, for a constant bankfull depth and relative depth of flow, the Reynolds number ratio reduces with increasing flood plain width.

It is interesting to confirm Myers findings with the present investigation. First, consider 3 geometries with equal channel and flood plain widths. i.e. geometry N(⊠:h=0.15:Bc=0.2:Bf=0.2), geometry N(::h=0.15:Bc=0.2:Bf=0.2) and geometry O(*:h=0.15:Bc=0.2:Bf=0.2). Fig 7.7 shows the Reynolds number ratios against relative depths for the current study. By considering these 3 geometries with varying bankfull depth h, it is clear that similar trends as those found by Myers are evident. For a given relative depth it is obvious that the Reynolds number

ratio is reduced for a reduction in bankfull depth. Similar observations can be made for other geometries.

Another observation made by Myers was the variation in Reynolds number ratio with an increase in flood plain width. Consider the following geometries with a constant h=0.15 m and Bc=0.2 m. Geometry N(⊠:Bf=0.2), L(▣:Bf=0.4) and G(o:Bf=0.6). It is difficult to note any difference in the relationships shown on Fig 7.7 This would suggest that for the present study, there is not a significant variation in Reynolds number ratio for a variation in flood plain width.

7.2.5 Conclusions.

Clearly then, there have been attempts to predict the apparent shear stress Which exists at the channel/flood plain junction. These attempts have been generally based on geometries with fixed channel or flood plain widths. Such relationships have in fact introduced the channel or flood plain width terms without sufficient experimental information to confirm their validity. The results from the current study, with the extensive variation in Bf and Bc, have highlighted this difficulty and the author must therefore conclude that such relationships are only suitable for the particular geometries they were determined from.

7.3 Symmetrical Channel Results.

In the current investigation, Myers, Crory and Rajaratnam's results have been presented extensively with the authors own results. These investigators used channels flanked by only one flood plain and so it was believed that their results could be compared directly with the authors. However work has been carried out in smooth compound channels with two flood plains, namely Hadjipanos, Ghosh and Jena. Their results will be discussed in this section with relationships developed in this thesis.

It is expected that if two flood plain/main channel interfaces exist, as in a symmetrical compound channel, then it is expected that two interaction mechanisms will occur. The two apparent shear stresses when added together will give the out of balance force calculated by measuring the shear stress distribution in the main channel, and considering the non-interacting shear stress.

It might be reasoned that the total apparent shear force for two interacting zones might be twice the apparent shear force for an asymmetrical compound channel. However it is probably the case only for channels of widths greater than twice the distance the interaction mechanism extends into the main channel. Any channel widths less than this might give rise to

compensating effects between the two interaction zones. With this in mind, the results of Hadjipanos, Ghosh and Jena will be compared to the relationships developed in chapter 6.

It was shown that the apparent shear stress τ_a could be determined from the relationship :-

$$\tau_a = \Delta V^{2\,2\left[\frac{Bc}{Bf}\right]^{1/2}} \cdot C\left\{\frac{h}{B_f}, \frac{Bc}{h}\right\} \qquad (7.16)$$

where ΔV is calculated from the use of Manning's Equation. The value of C for a particular geometry can be determined from Fig 7.8. The value of $\frac{\tau_a}{\Delta V^{2.2(Bc/Bf)^{1/2}}}$ has been calculated for both Hadjipanos, Ghosh and Jena's work and plotted against h/Bf where Bf is the width of one flood plain. Taking Bc as half the main channel width it can be seen that the results of these investigators fit closely the function C. This would suggest that Equation (7.16) could well be extended to describe symmetrical channel interaction mechanisms, although it would be necessary to carry out tests on channels with greater Bc/h values since Hadjipanos tested Bc/h=1.2 and Ghosh and Jena tested Bc/h=1.0.

However, until more results are available for symmetrical compound channels with smooth surfaces, caution must be given to the suitability of Equation (7.16) for symmetrical channels.

A further relationship was developed in Chapter 6 involving the relative depth and the non-dimensional form of τa given by the equation :-

$$\frac{\tau_a}{\rho g Y_f S} = 1{\cdot}12\left(\frac{Y_c}{Y_f} - \psi\right)^{1{\cdot}5} \cdot \left(\frac{Bc}{h}\right)^{1/2} \cdot \left(1 - e^{-0{\cdot}53\left(\frac{Bf}{h}\right)}\right) \qquad (7.17)$$

where ψ was tentatively given by the relationship :-

$$\psi = 1{\cdot}0 + 1{\cdot}5\left(\frac{h}{Bc}\right)^{1{\cdot}25} \qquad (7.18)$$

All the geometries tested for the current investigation provided a reasonable fit to Equation (7.17). However, it would be interesting to assess the significance of the Equation to geometries with two flood plains on either side of the main channel. Fig 7.9 shows this relationship for both Hadjipanos, Ghosh and Jena's results. It is clear that, although there is some spread in the results for both investigations, there is a general trend which follows that of the asymmetrical channel. Again it is difficult to ascertain this spread of results but two reasons are likely. First there is likely to be experimental errors due to uncertainty in water surface slopes, shear stress measurements etc. Secondly there is a strong possibility of both interaction zones overlapping. It is not clear what effect the overlapping mechanisms would have on the apparent shear stress.

7.4 Conclusions.

This thesis has presented details of an extensive experimental study into the behaviour of the interaction mechanism which exists at the channel/flood plain junction during overbank flow. In particular, the effect of this interaction has been studied with reference to varying channel geometries in a smooth compound channel with only one flood plain.

It is important to emphasise the nature of the interaction in its proper context of overbank flow in natural rivers. As will be indicated in the following section, there are a number of processes ocurring in a natural river during periods of flooding. Channel meandering, bed roughness laterally sloping flood plains and the interaction mechanism all contribute to the overall resistance of the channel to flow. However this study must be regarded as a first step in assessing the interacting mechanism and its significance in relation to other hydraulic processes.

Chapter 2 presented details of past work carried out in this area of hydraulic research and also touched on basic relationships developed on open channel flow. It was clearly indicated that a turbulent shear mechanism was introduced at the channel/flood plain junction which would have an influence on the hydraulic characteristics of the channel. It is clear from the

past studies, that the mechanism can be given as a function of various geometrical and hydraulic parameters of the channel and flood plain :-

$$\text{Degree of interaction} = \left\{ \frac{Bc}{Bf}, \frac{Bc}{h}, \frac{Bf}{h}, \frac{Yf}{Y}, \Delta V, \frac{n_c}{n_f} \right\}$$

It was considered appropriate to carry out an investigation which would clearly define the relationship between the turbulent shear mechanism and the geometrical parameters of the compound channel.

Chapter 3 described the details of an experimental flume which was designed and built in the Civil Engineering Department at Glasgow University which could be used for a model study. The design details and the constructional procedure was described and the instrumentation used to carry out the study was presented. Before any study could commence, considerable effort was necessary to ensure that all instrumentation was fully calibrated. It was found that by integrating point velocities, recorded by a Pitot tube, using a planimeter, it was possible to determine the mean velocities in the channel and flood plain with reasonable accuracy. Combined with the Preston tube technique, it was also possible to use planimetry to determine the shear stress distribution in the channel and flood plain.

It was decided to investigate a total of 16 different channel geometries in detail and the experimental

procedure carried out for the 136 test runs is also indicated in Chapter 3

Chapters 4, 5 and 6 presented studies of the interaction mechanism described by different parameters. Chapter 4 presented velocity distributions. Chapter 5 discussed how the boundary shear stresses were redistributed as a result of channel/flood plain interaction. Chapter 6 developed the conceptual τa values and related τa to the geometrical parameters of the compound channel. The conclusions of these chapters are best summarised by a number of points :-

i) As the term Bf/h increases, the interaction mechanism correspondingly increases. However, with subsequent increases of Bf/h greater than 12, no further increase in the interaction mechanism occurs. This is clearly demonstrated on Fig 4.14, Fig 5.12 and Fig 6.15.

ii) Another term which describes the interaction mechanism is Bc/h. As Bc/h increases, the interaction mechanism decreases accordingly. Again this is demonstrated on Fig 4.14, Fig 5.12 and Fig 6.14.

iii) The effect of h, the bankfull depth, on the interaction mechanism will depend on the associated values of Bc/h and Bf/h.

iv) The frictional resistance of the channel and flood plain is significantly affected as a result of channel/flood plain interaction. The channel friction factor, λ_c, increases as illustrated on Fig 5.13 and the flood plain friction factor, λ_f,

decreases as shown on Fig 5.14.

v) Two relationships were presented which would enable the apparent shear stress to be determined for smooth channels. One relationship considered the velocity difference which exists between the channel and flood plain based on the use of Manning's equation. Coefficients are introduced which account for the different geometrical parameters Bc/Bf, Bf/h and Bc/h with the overall relationship being given as :-

$$\tau_a = \Delta V^{2.2\left[\frac{Bc}{Bf}\right]^{1/2}} \cdot C\left\{\frac{h}{B_f}, \frac{Bc}{h}\right\} \qquad (7.19)$$

A further relationship which was based on the relative depths of flow in the channel and flood plain was also developed. This eqution could be given as :-

$$\frac{\tau_a}{\rho g Y_f S} = 1{\cdot}12\left(\frac{Y_c}{Y_f} - \psi\right)^{1.5} \cdot \left(\frac{B_c}{h}\right)^{1/2} \cdot \left(1 - e^{-0{\cdot}53\left(\frac{Bf}{h}\right)}\right) \qquad (7.20)$$

where ψ can be regarded as the relative depth at which τ_a will equal zero and is tentatively given as :-

$$\psi \doteq 1{\cdot}0 + 1{\cdot}5\left(\frac{h}{B_c}\right)^{1{\cdot}25} \qquad (7.20(a))$$

Given just a knowledge of the channel geometry, the water surface slope and the depth of flow, Equation (7.20) can be used again to determine the apparent shear stress. Armed with the knowledge of

the apparent shear stress, it is possible to determine, from force equilibrium equations the extent of shear redistribution. Finally, it is possible to determine the velocities in the channel and the flood plain during interaction, since the changes in shear can be related to the square to the changes of velocity.

7.5 Suggestions for Future Research.

The work presented in this thesis has been concerned with the amount of interaction which exists between a channel and its flood plain, and the geometrical parameters which affect it. It is hoped that the effect of the parameters have been well established. To further the knowledge of the interacting behaviour of channels and flood plains, the main aim must be to determine its behaviour in actual rivers. Until field tests results are available in sufficient detail, suitable modelling techniques must be adopted to give good representation at a smaller scale.

Consider what processes are involved in dissipating energy in rivers during overbank flow. These processes can be divided into 5 broad areas :-

1. Bed friction in both the channel and flood plain, with perhaps greater frictional resistance in the flood plain due to vegetation.
2. Form roughness caused by large scale obstructions such as pools, ripples, bars and boulders.
3. Meanders which give rise to run onto and off the flood

plains, resulting in strong turbulent mechanisms.

4. Secondary currents which redistribute channel and flood plain velocities.

5. The turbulent shear interaction which exists between the channel and flood plain, as discussed in this study.

It is not clear how important each area is in determining the carrying capacity of a river during flooding. However, it is important to represent these processes in the hydraulic model. Areas 2 and 3 are unique to a particular river reach and hence difficult to represent on a general hydraulic flume. However it should be possible to model the meandering effects and frictional losses in a hydraulic model. This discussion will be limited to discussing frictional losses.

First, consider the actual channel flow parameters to be found in British rivers. Nixon (Ref 39) has given regime equations based on the bankfull discharge of rivers :-

$$Bc = Q_b^{1/2} \tag{7.21}$$

and

$$h = 0{\cdot}54\, Q_b^{1/3} \tag{7.22}$$

where Bc is the channel width, h is the bankfull depth and Qb is the bankfull discharge. A typical range for Qb is 10 to 500 m^3/sec, hence it is possible to determine the flow

characteristics based on Equations (7.21) and (7.22).

$$10m < Bc < 67m$$

$$1.2m < h < 4.3m$$

$$8m < Bc/h < 16m$$

$$0.9m/s < Vb < 1.8m/s$$

$$4\times10^{6} < Re_b < 3\times10^{7}$$

where Vb and Re_b are the bankfull velocities and Reynolds numbers respectively. If a Mannings n of 0.03 for the river is assumed, it is possible to determine the range of λ_b from the relationship :-

$$\lambda_b = \frac{8 g n^2}{R_b^{1/3}} \qquad (7.23)$$

where Equation (7.23) has been developed from the Darcy and Manning's equations. Based on the typical values given above, expected λ_b values are :-

$$0.045 < \lambda_b < 0.07$$

This range of λ_b and Re_b values for the prototype river is shown on Fig 7.10. Also shown are typical ranges investigated in the current model study. Clearly both the Reynolds numbers and λ_b values are not the same as the values found typically in rivers. This is because of problems associated with scaling up from models, mainly due to conflicting requirements.

First, the open channel flow is dominated by gravitational forces and inertial reactions and is thus based on Froude scaling criteria. Secondly, it is extremely difficult to have correct Reynolds scaling in Froude scale free surface flows, with Reynolds numbers in the prototype being of 2 orders of magnitude greater than the model.

To give good simulation of bed friction, it is necessary to have the same λ values in the model as in the actual river. Obviously this is not the case as can be seen in Fig 7.10 for the present study. Clearly the only way to satisfy this criterion is to use channel and flood plain sections which will give the same $\frac{k}{4R}$ values as in the prototype river. Thus the effective roughness of the model must be carefully chosen.

A second point worth noting from Fig 7.10 concerns the two different regions where the model and prototype values lie. For full scale rivers, the flow is rough and turbulent and thus frictional resistance is independent of the Reynolds number. The model results fall into the region of smooth turbulent flow where viscous forces are influencing the resistance to flow. The significance of these viscous forces on the interaction mechanism is not clear. It may be the case that the turbulence scale of the mechanism, which is of the order of Yf, may not be seriously affected by viscous forces and therefore it may be possible to give adequate representation of the shear mechanism on models

which operate in the smooth turbulent region. The Reynolds number gives an indication of the turbulence which exists in any flow condition. Since turbulence is the process by which the energy loss at the channel/flood plain junction is dissipated, it is considered important to to have large Reynolds numbers in the model. Clearly then, the requirements for any model study which attempts to represent the interaction mechanism in full scale rivers are twofold :-

1. To model the actual λ values which occur in both the prototype channel and flood plain. This will involve careful selection of the appropriate effective roughness values.

2. To attempt to reduce the effects of viscosity and to give adequate turbulence levels in the model to give good representation of the energy cascade principle which will occur as a result of channel/flood plain interaction. This can best be achieved by maximising the model Reynolds numbers for both the channel and flood plain.

SYMBOL	GEOMETRY	RUN NO	(mm) h	(mm) B_c	(mm) B_f	No of tests
△	K	1—10	102	400	400	10
▽	A	11—22	52	400	400	12
□	B	23—30	52	200	400	8
◇	C	31—37	52	400	200	7
○	G	38—45	152	200	600	8
⊞	L	46—53	152	200	400	8
⊠	N	54—61	152	200	200	8
◈	J	62—70	152	400	400	9
◈	R	71—78	152	400	200	8
⋕	MYERS	79—88	102	254	356	10
✣	RAJARATNAM	89—93	98	711	508	5
⋇	P	94—103	102	200	400	10
⊹	H	104—113	102	200	600	10
⋇	M	114—121	102	200	200	8
θ	CRORY	122—126	102	254	356	6
✕	CRORY	127—130	102	203	356	4
λ	CRORY	131—133	102	153	356	3
μ	CRORY	134—137	102	102	356	4
✱	O	138—145	52	200	200	8
#	I	146—153	52	200	600	8
$	S	154—161	102	400	200	8
@	E	162—167	102	600	200	6

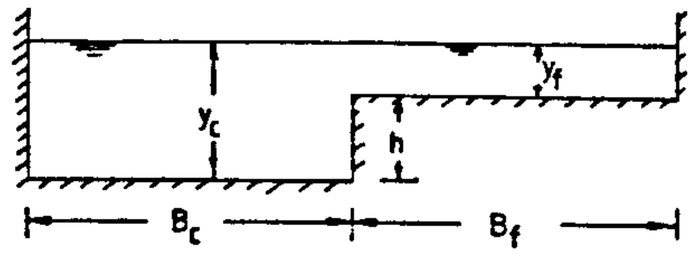

Fig 7·1 Comparison of relationship developed by Crory with the authors' results.

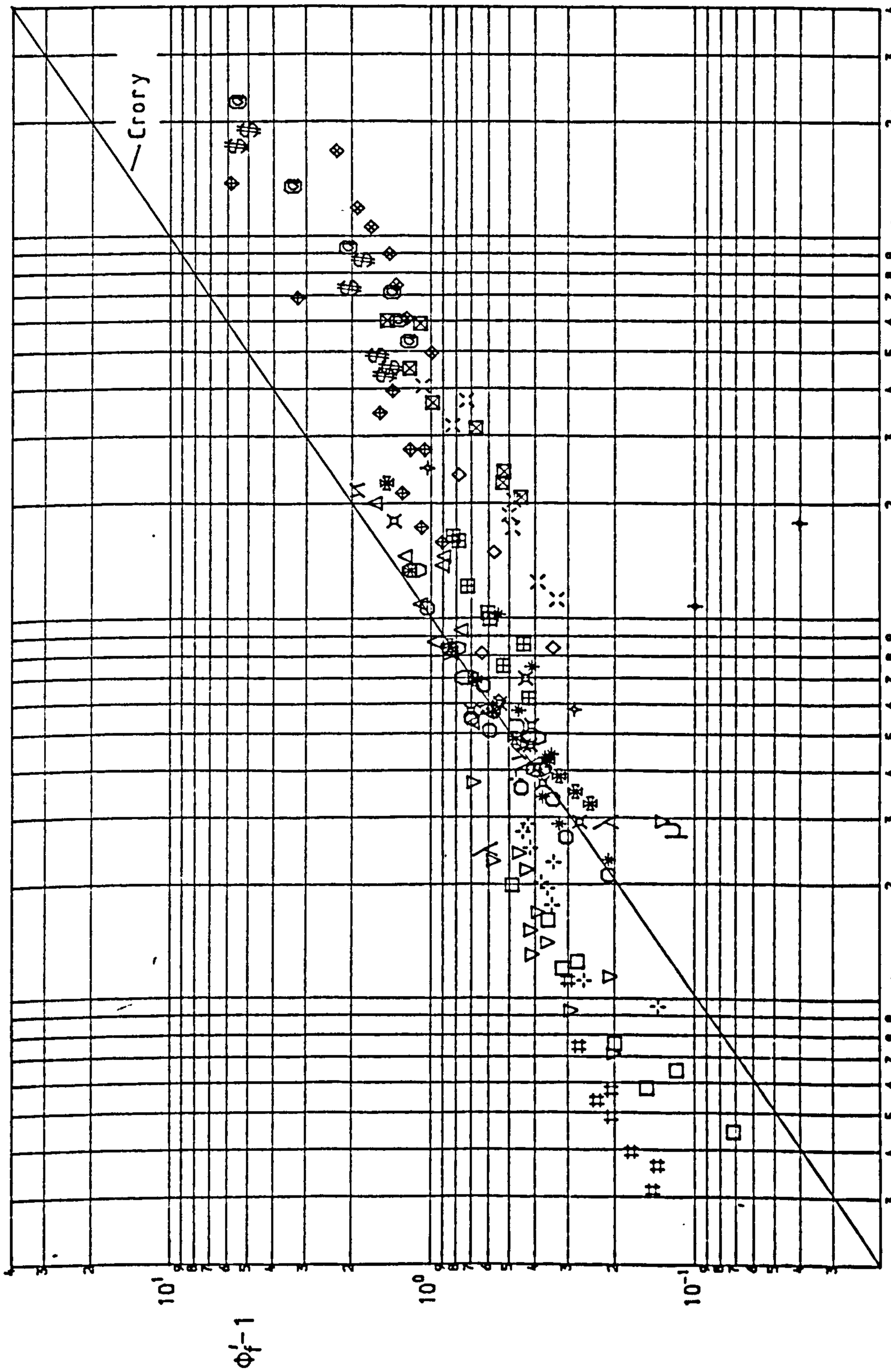

Comparison of relationship developed by Crory with the authors' results.

Fig 7.2

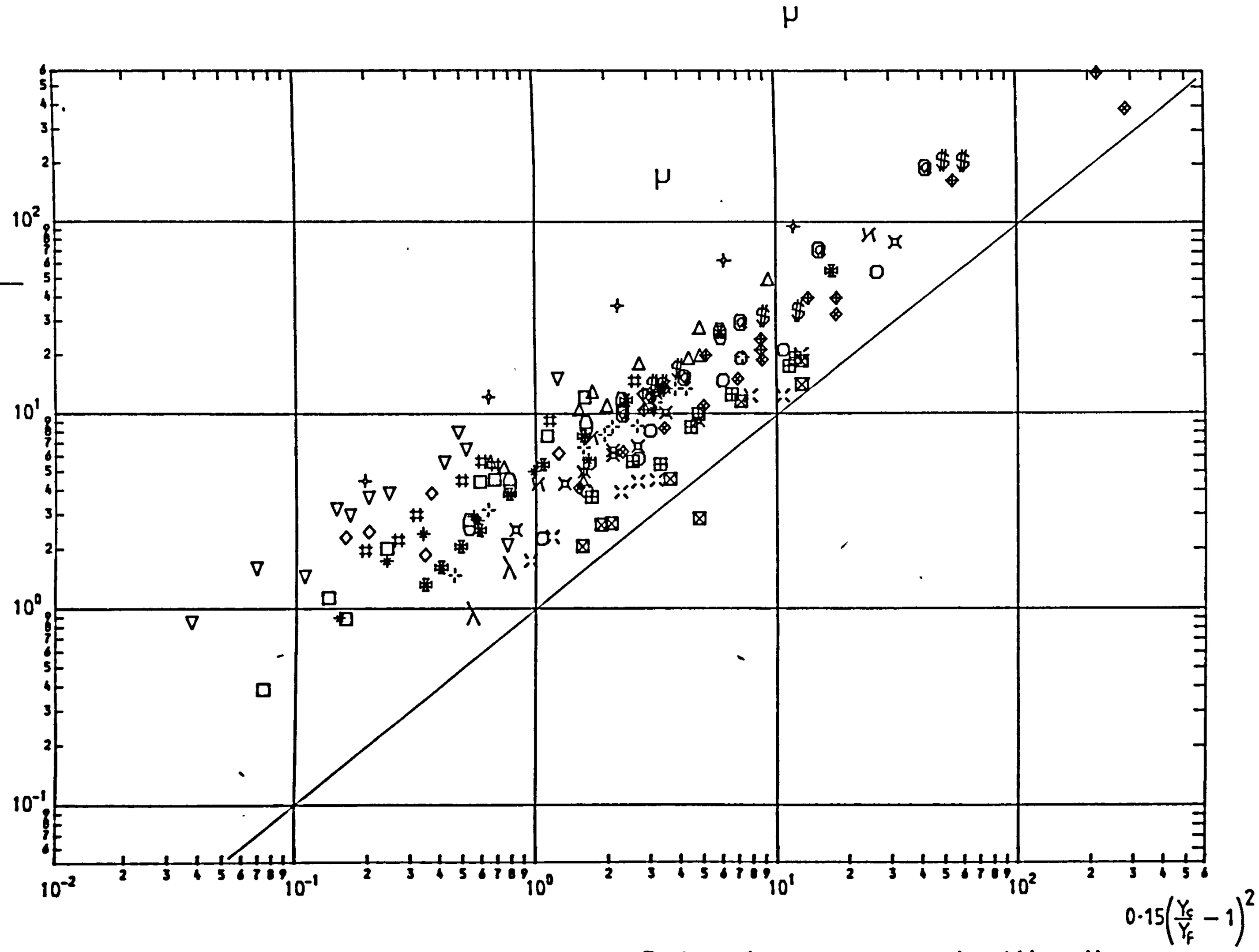

Fig 7·3 Relationship developed by Rajaratam compared with the authors' results.

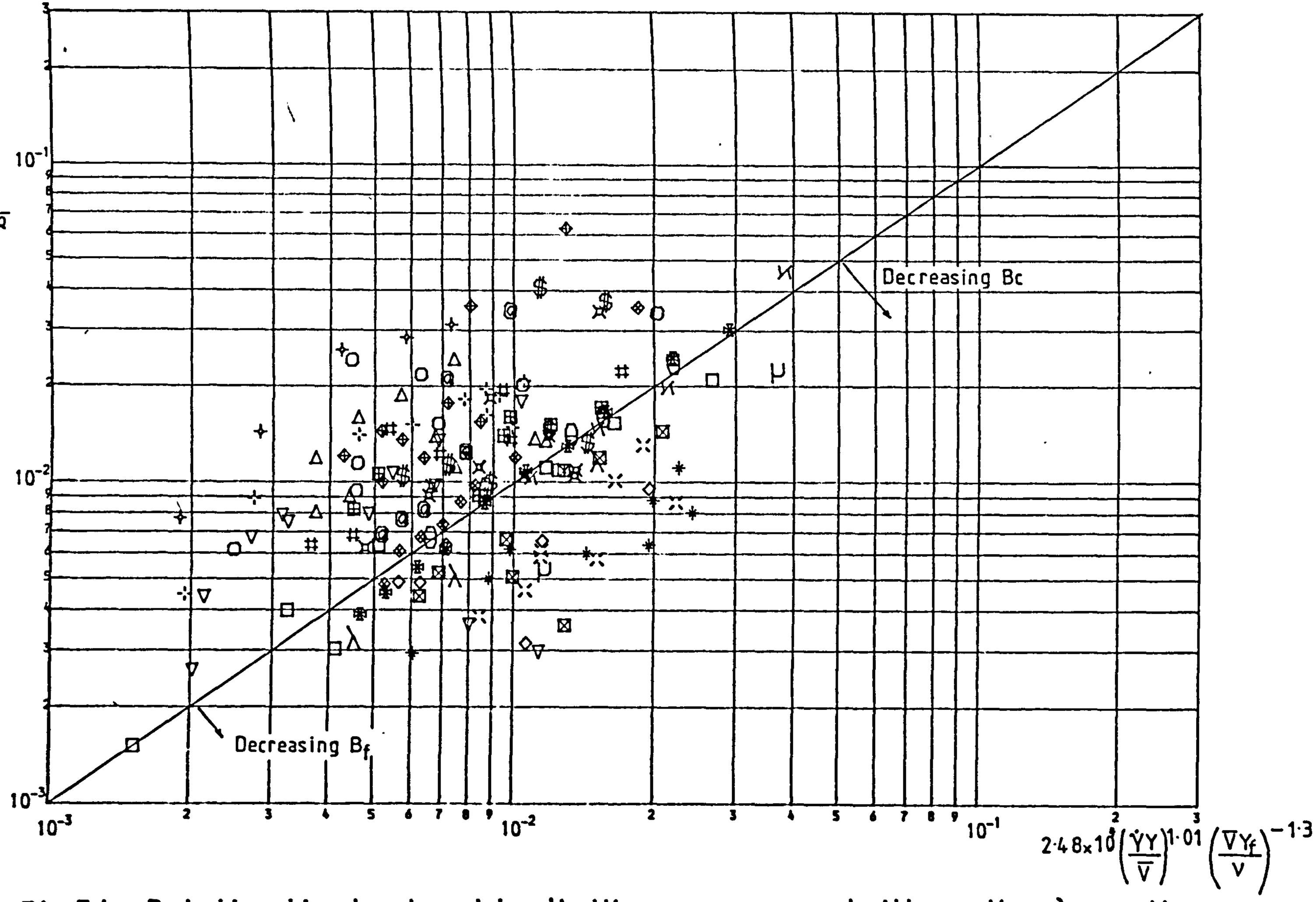

Fig 7·4 Relationship developed by Hadjipanos compared with authors' results.

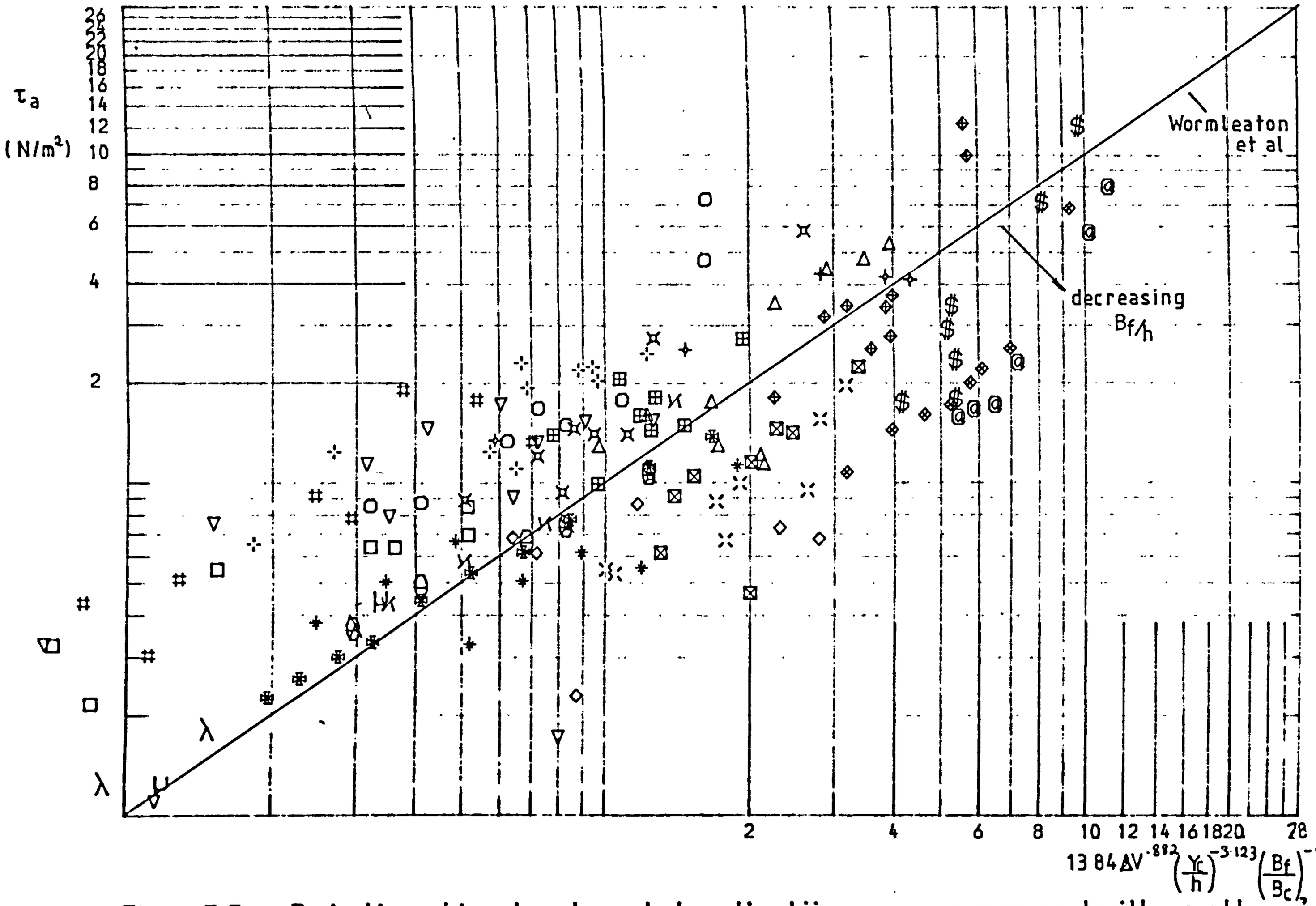

Fig 7·5 Relationship developed by Hadjipanos compared with authors' results.

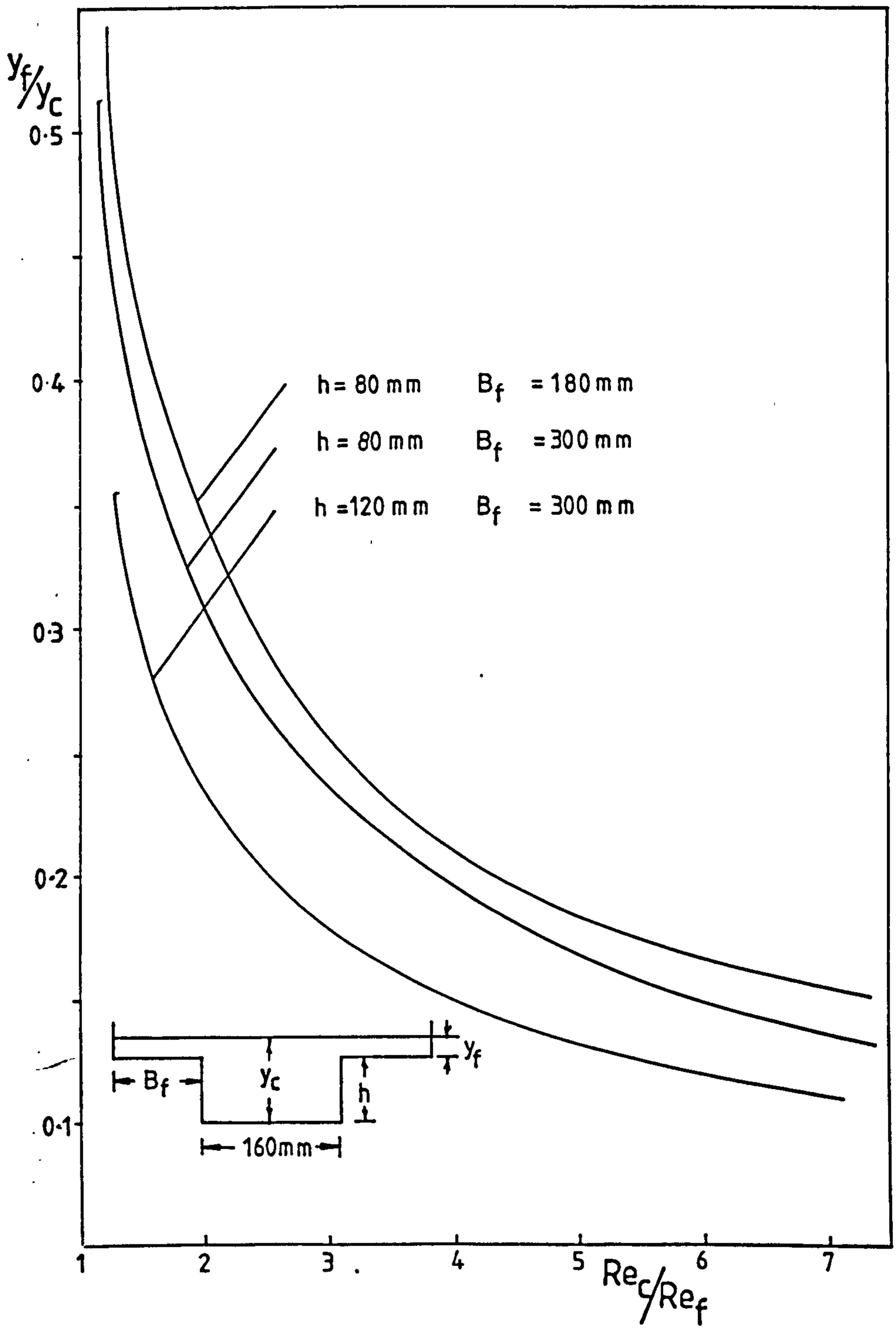

Fig 7·6 Variation of Reynolds number ratio with Relative depth (Myers).

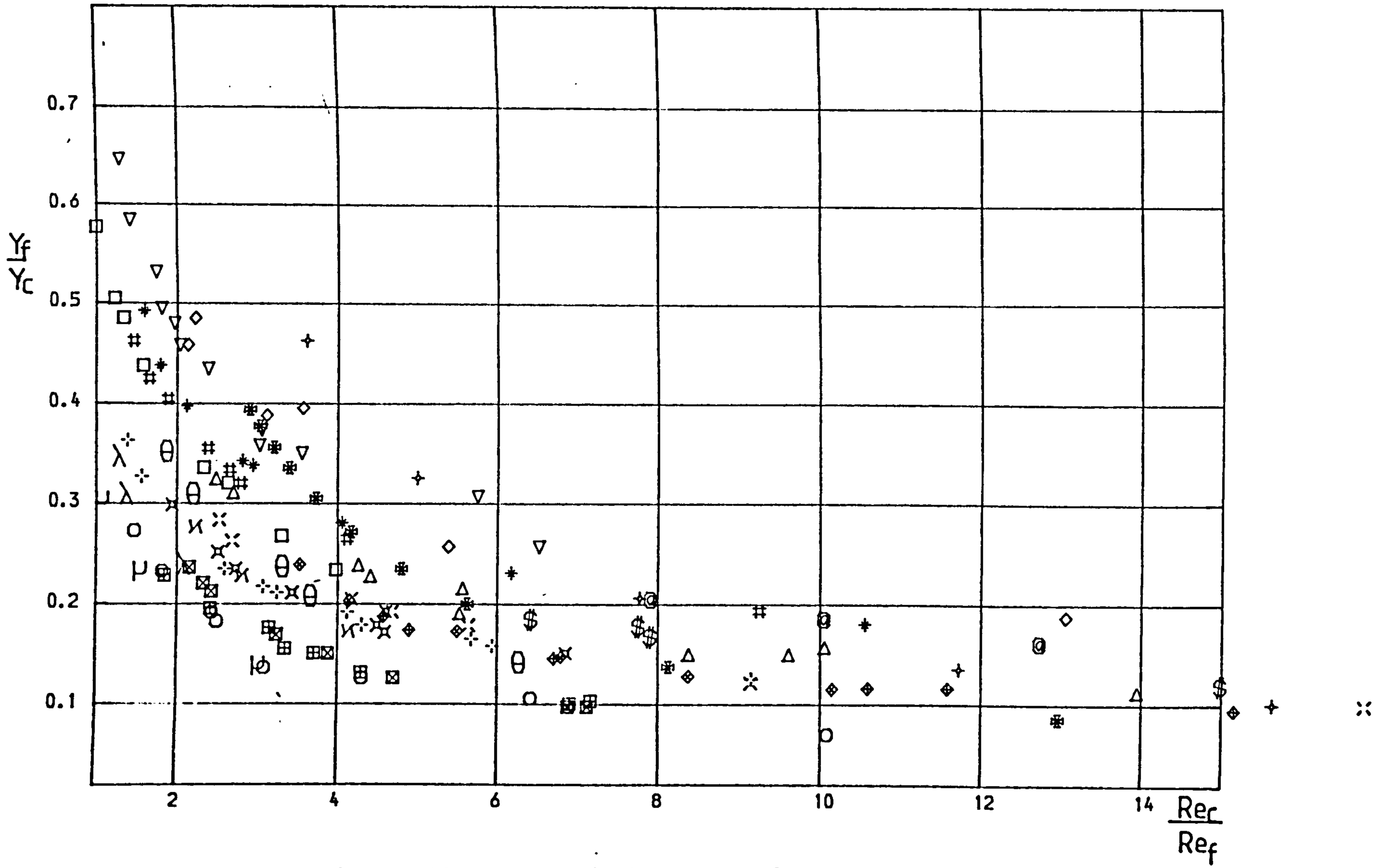

Fig 7·7 Authors' results presented in a form suggested by Myers.

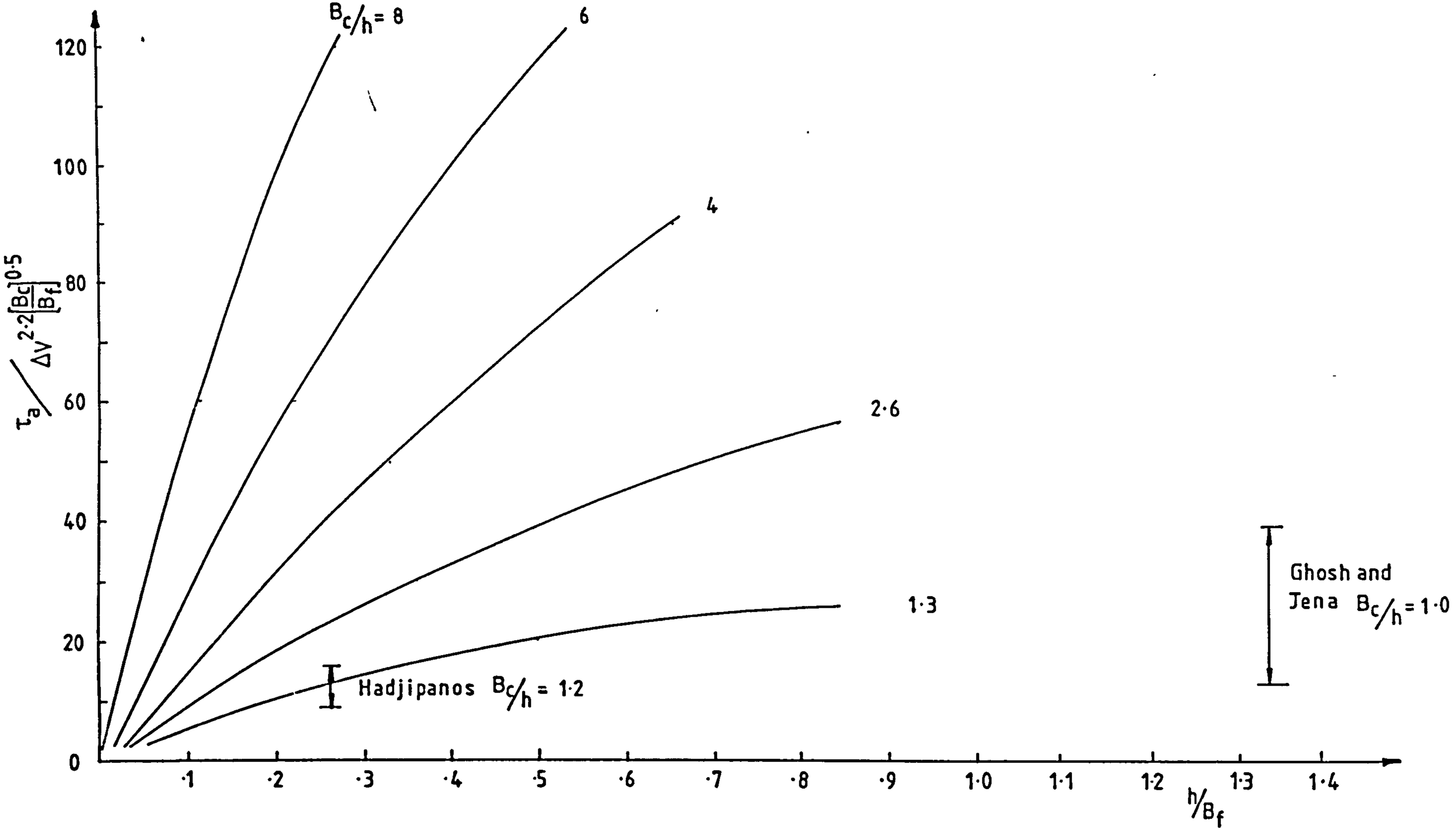

Fig 7·8 Comparison of other Investigations with the Current Study.

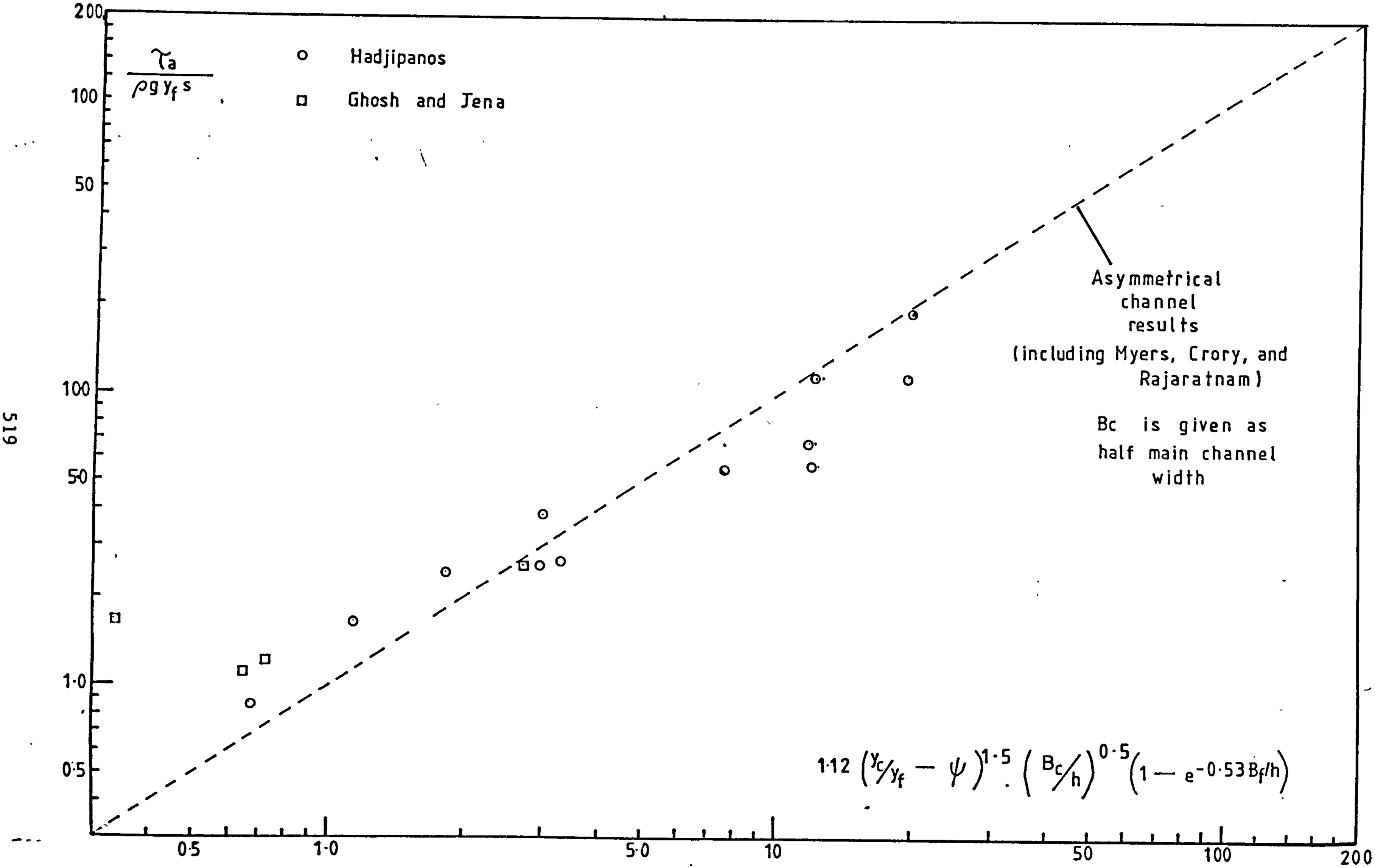

Fig 7·9 Comparison of relationship developed in the present study and other results.

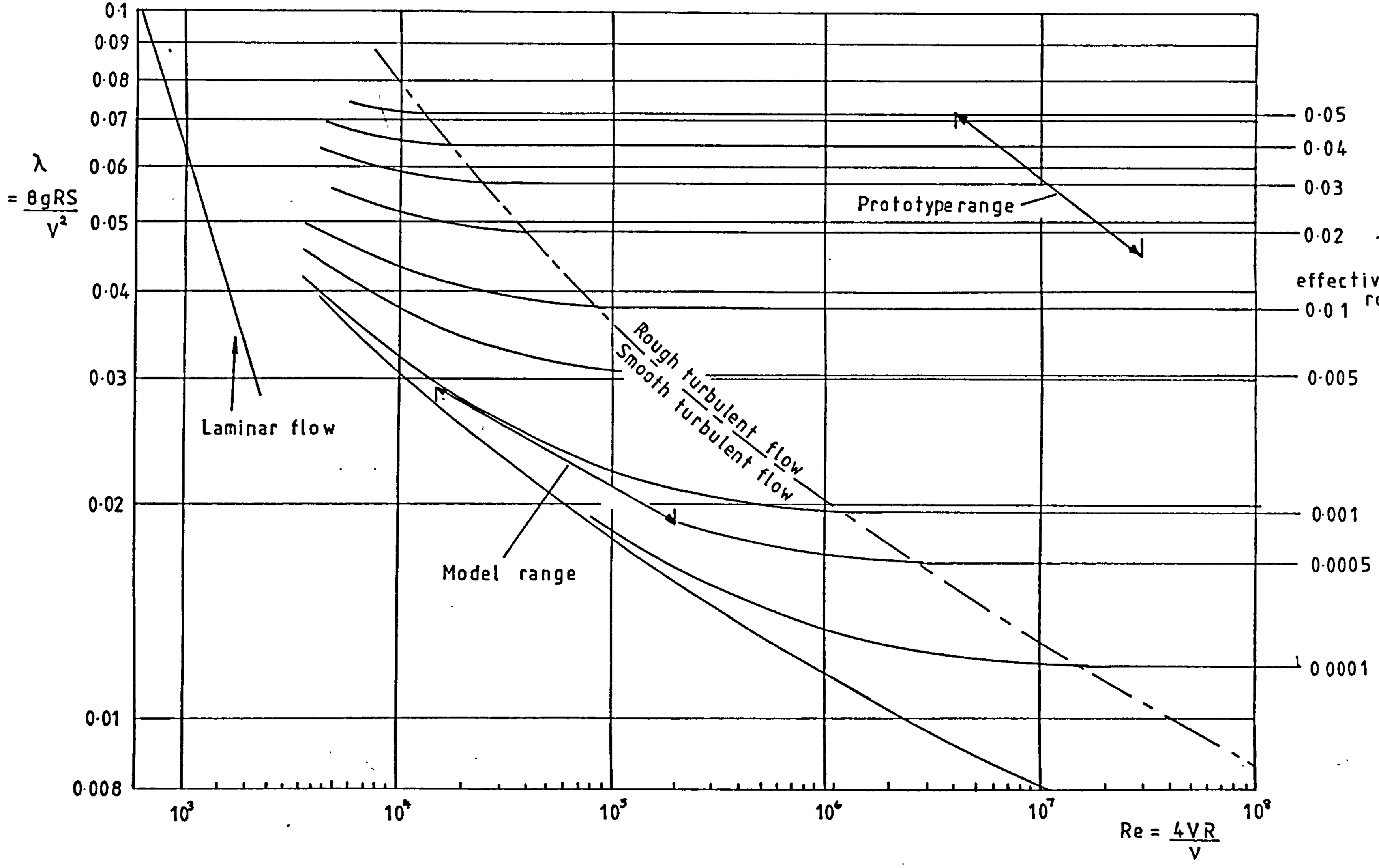

Fig 7·10 Moody's chart showing model and full scale ranges.

BIBLIOGRAPHY

1. Ackers, P., "Resistance to Fluids Flowing in Channels and Pipes", Hydraulic Research Paper No.1, H.M.S.O., London, England, 1958.

2. Agasieva, S.I., Barekyan, A.S., "Change in the Mean Velocities in Main Bed and Chezy's Coefficient during Flood Water", Meteorogia i Geologia, No.9, 1961 (In Russian).

3. Ahamdi, R., "An experimental study of Interaction between main channel and flood plain flows", Doctoral dissertation, University of Alberta, Edmonton, Canada.

4. Barishnikov, N.B, Ivanov, G.N, Sokolov, Yu.N., "Role of Flood Plain in a Flood Discharge of a River Channel", Proc of 14th International Congress of the I.A.H.R, Paris, 1971.

5. Belt, C.B., "The 1973 Flood and man's constriction of the Mississippi river", Science, Vol. 189, No. 4204, page 681.

6. Bhowmik, N.G., Demissie, M., "Carrying Capacity of Floodplains", Jour. Hyd. Div., A.S.C.E., Vol.108, No HY3, March 1982.

7. Blalock, M.E., Sturm, T.W., "Minimum Specific Energy in Compound Open Channel", Journ. Hyd. Div., A.S.C.E., Vol.107, HY6, June 1981.

8. Bradshaw, P., and Gregory, N., "The determination of local turbulent skin friction from observations in the viscous sublayer", Aero. Res. Counc R. and M., No 3202, 1959.

9. BS3680 : Part 3C : 1983, "Methods for determination of the stage-discharge relation".

10. Chow, V.T., "Open Channel Hydraulics", McGraw-Hill Book Co, New York, 1959.

11. Chow, V.T., "Handbook of Applied Hydrology", McGraw-Hill Book Co., Inc., New York, 1964.

12. Crory, P.M., Elsawy, E.M., "An Experimental Investigation into the Interaction Between a River's Deep Section and it's Floodplain", I.A.H.R. Symposium on River Engineering and its Interaction with Hydrological and Hydraulic Research, Section D, Belgrade, Yugoslavia, May 1980.

13. Elsawy, E.M. and Crory, P.M., " Effects of interaction on a channel with one flood plain", International Conference on Water resources engineering, Bangkok, Thailand, January 1978.

14. McKee, P.M., "A study of the hydraulic characteristics of open channels with flood plains", A thesis submitted to Queens University, Belfast in partial fufillment of the Doctor of Philosophy, 1980.

15. Cruff, R.W., "Cross Channel Transfer of Linear Momentum in Smooth Rectangular Channels", U.S.G.S Water Supply Paper 1592-B, 1965.

16. FLUCOMP - A mathematical model available from The Hydraulic Research Station, Wallingford.

17. Fread, D.L., "Flood Routing in Meandering Rivers with Floodplains", 3rd Annual Symposium of the Waterways, Harbours and Coastal Engineering Division, A.S.C.E., Vol.1, Rivers 1976.

19. Ghosh, S.N., Metha, P.J., "Boundary Shear Distribution in a Channel with Varying Roughness Distribution",Proc. I.C.E., Vol.57, March 1974.

18. Ghosh, S.N., "Boundary Shear Distribution in Channels with Varying Wall Roughness", Proc. I.C.E., Vol.59, December,1975.

20. Ghosh, S.N., Jena, S.B., "Boundary Shear Distribution in Open Channel Compound", Proc. I.C.E, Vol. 49, August 1971.

21. Ghosh, S.N., and Roy, N., "Boundary Shear Distribution in open channel flow", Journ. Hyd. Div., A.S.C.E., Vol 96, HY4, April, 1970.

22. Hadjipanos, P., "Flow in compound channels with varying roughness", Thesis presented to London University in 1980 in partial fulfillment of the requirements for the degree of Doctor of Philosophy.

23. Head, M.R., and Rechenberg, I., " The Preston tube as a means of measuring skin friction", Journ. of Fluid Mechanics, Vol 14, Part 1, 1962.

24. Henderson, F.M., "Open Channel Flow", MacMillan Pub. Co., New York, 1966.

25. Hwang, L.S., and Laursen, E.M., "Shear Measurement Technique for rough surfaces", Journal of Hyd. Div., A.S.C.E., Vol 80, HY2, March, 1963.

26. Ippen, A.T., and Drinker, P.A., "Boundary Shear Stress in Curved Trapezoidal Channels", Jour. Hyd. Div., A.S.C.E. Vol.88, HY5, September 1962.

27. James, M., and Brown, R.J., "Geometric parameters that influence flood plain flow", U.S. Army Engineer Waterways Experimental Station, Vicksburg, Miss., June, 1977, Research report H-77-1.

28. Jansen, P.P., "Principles of River Engineering - The non-tidal alluvial river", Pitman, London, 1979.

29. Kazemipour, A.K., Apelt, C.J., "Shape Effects on Resistance to Uniform flow in Open Channels", Jour. Hyd. Res., I.A.H.R., Vol.17, No.2, 1979.

30. Kazemipour, A.K., Apelt, C.J., "New Data on Shape Effects in Smooth Rectangular Channels", Jour. Hyd. Res., I.A.H.R., Vol.20, No.3, 1982.

31. Keulegan, G.H., "Laws of Turbulent Flow in Open Channels", Jour. of Research of the National Bureau of Standards, U.S. Dept. of Commerce, Vol.21, Dec 1938.

32. Manning, R., "Flow in Open Channels and Pipes", Trans., Institution of Civil Engineers (Ireland), Vol.20, 1980.

33. Mosonyi, E.F., "Studies for intake structures of flood detention basins to be established along the upper Rhine", International Conference on the Hydraulic Aspects of Floods and Flood Control, B.H.R.A. Fluid Engineering, London, England, September 1983.

34. Myers, W.R.C., Elsawy, E.M., "Boundary Shear in Channel with Floodplain", Jour. Hyd. Div., A.S.C.E., July 1975.

35. Myers, W.R.C., "Momentum Transfer in a Compound Channel", Jour. Hyd. Res., I.A.H.R., Vol.16, No.2, 1978

36. Myers, W.R.C., "Boundary Shear Stress and Momentum Transfer in Open Channels of Complex Cross-Section", Ph.D Thesis, Queen's University, Belfast, Northern Ireland, 1973.

37. Myers, W.R.C., "Flow Resistance in Wide Rectangular Channels", Journ. Hyd. Div., A.S.C.E., Vol.108, No HY4, April 1982.

38. Myers, W.R.C., "Frictional resistance in Channels with flood plains", Proceedings of the First International Conference on Channels and Channel Controls Structures, Southampton, England, April 1984.

39. Nixon, M., "A study of the bankfull discharges of rivers in England and Wales", Proc., I.C.E., Vol. 12, p 157, No 6322, 1959.

40. Patel, V.C., "Calibration of the Preston Tube and Limitations on its Use in Pressure Gradients", Jour. Fluid Mechanics, Vol.23, 1965.

41. Pillai, N.N., "On Uniform Flow through Small Rectangular Open Channels", Journ. Hydraulic Research, Vol.8, No.4, 1970.

42. Posey, C.J.F., "Shape Effects on Resistance in Flood Plain Channels", Civil Engineering, A.S.C.E., No.CE4, Vol.37, April 1967.

43. Preston, J.H., "The Determination of Turbulent Skin Friction by Means of Pitot Tubes", Jour. Royal Aeronautical Society, Vol.58, 1954.

44. Price, R.K., "A mathematical model for river developments - Theoretical development", Report No. INT 127, December 1975.

45. Radojkovic, M., "Mathematical Modelling of Rivers with Floodplains", 3rd Annual Symposium of the Waterways, Harbours and Coastal Engineering Division, A.S.C.E., Vol.1, Rivers 1976.

46. Radyuk, A.L., "On the Interaction of Streams in a Channel having Irregular Roughness within Width", Idzyetiya vyschih uchebnyh savedemii, Lesnoi Zhurnal, Vol.1, 1967 (In Russian).

47. Rajaratnam, N., Ahmadi, R.M., "Interaction between Main Channel and Floodplain Flows", Jour. Hyd. Div., A.S.C.E., May 1970.

48. Rajaratnam, N., Ahmadi, R.M., "Hydraulics of Channels with Floodplains", Jour. Hyd. Research, I.A.H.R., Vol.19, No.1, pp43-60, 1981.

49. Rajaratnam, N., "On the Preston Tube with a Hemispherical Nose", Civil Engineering and Public Works Review, November 1965.

50. Rao, K.K., "Effect of Shape on the Mean Flow Characteristics of Turbulent Flow through Smooth Rectangular Open Channel", Thesis, University of Iowa, Iwoa City.

51. Reinus, E,. "Steady Uniform Flow in Open Channels", Transactions, Royal Institute of Technology, Stockholm, Sweden, No.179, 1961.

52. Rodi, W., "Turbulence Models and their application in Hydraulics - a state of the art review, I.A.H.R., Delft The Netherlands, 1980.

53. Rodi, W., Celik, I., Demuren, A.O. and Keller, R.J., "New developments in the area of computer applications in Hydraulics and water resources", Special presentation of recent developments, Twentieth I.A.H.R. Congress, Moscow, 1983.

54. Sellin, R.H.J., "A Study of the Interaction between Flow in the Channel of a River and that over its Floodplain", Ph.D Thesis, University of Bristol, Bristol, England, 1961.

55. Sellin, R.H.J., " A Laboratory Investigation into the Interaction between the Flow in the Channel of a River and that over its Floodplain", La Houille Blanche, 7, 1964.

56. Shih, C.C., Grig, N.S., "A Reconsideration of the Hydraulic Radius as a Geometric Quality in Open Channel Hydraulics", Proc. 12th Congress I.A.H.R., Vol.1 (Paper A36), Sept 1967.

57. Spitsin, J.P., "On the Interaction of the Streams of the Main River Bed and the Floodplain", Meterologia i Gidrologia, No.10, 1962 (In Russian).

58. Progress Report of the Task Force on Friction Factors in Open Channels, "Friction Factors in Open Channels", Jour. Hyd. Div., A.S.C.E., Vol.89, No. HY2, March 1963.

59. Taylor, G.I., "The statistical theory of turbulence", Proc. Royal Society of Aero., Vol 151, September 1935 pages 421-464.

60. Tingsanchali, T., Achermann, N.L., "Effects of Overbank Flow in Flood Computations", Jour. Hyd. Div. A.S.C.E., HY7, July 1976.

61. Toebes, G.H., Sooky, A.A., "Hydraulics of Meandering Rivers with Floodplains", Journ. Waterways and Harbours Div., A.S.C.E., Vol.93, WW2, 1967.

62. Toebes, G.H., and Sooky, A.A., "The hydraulics of Meandering rivers with flood plains", Hydromechanics laboratory, Technical Report No. 10, School of Civil Engineering, Purdue University, U.S.A., April, 1965.

63. Townsend, D.R., "Investigation of Turbulence Level in a Region of High Shear Flow", Ph.D Thesis, Queen's University, Belfast, Northern Ireland, 1967.

64. Townsend, D.R., "An Investigation of Turbulence Characteristics in a River Model of Complex Cross-section", Proc., I.C.E., Vol.40, June 1968.

65. Tracy, H.J., Lester, C.M., "Resistance Coefficients and Velocity Distribution in Smooth Rectangular Channel", U.S. Geological Survey, Water Supply Paper, Vol.1592-A, 1961.

66. Udeozo, B.N.C., "Uniform Flow in Idealized Channel-Floodplain Geometries", M.Sc Thesis, Purdue University, Lafayette, Indiana, U.S.A., 1967.

67. Williams, G.P., "Aids in designing Laboratory flumes", U.S. Geological Survey, Washington, January 1971.

68. Ward, R.C., "Floods-A geographical Perspective", McMillan, 1978.

69. Wormleaton, P.R., Allen, J., Hadjipanos, P., "Effects of Shear Stress in Compound Channels", I.A.H.R., 2nd Congress of the Asian and Pacific Regional Division, Taiwan, May 1980.

70. Wormleaton, P.R., Allen, J., and Hadjipanos, P., "Discharge Assessment in Compound channel flow", Journal Hydraulics Division, A.S.C.E., Vol 108, HY9, September, 1982.

71. Wright, R.R., Carstens, M.R., "Linear-Momentum Flux to Overbank Sections", Jour. Hyd. Div., A.S.C.E., Vol.96, HY12, September 1970.

72. Yen, C.L., Overton, D.E., "Shape Effects on Resistance in Floodplain Channels", Jour. Hyd. Div., A.S.C.E., HY1, January 1973.

73. Yen, C.L., and Overton, D.E., "A method for flow computation in floodplain channels", Proc. International Symp. on Stochastic Hydraulics, University of Pittsburgh, 1971.

74. Zheleznyakov, G.V., "Hydraulic Basis of River Hydrometry Methods", Izdateslstro Academii Nauk, U.S.S.R., 1950 (In Russian).

75. Zheleznyakov, G.V., "Relative Deficit of Mean Velocity of Instable River Flow - Kinematic Effect in River beds with Floodplains", Proc 11th International Congress I.A.H.R., Leningrad, 1965.

76. Zheleznyakov, G.V., "Interaction of Channel and Floodplain Streams", Proc 14th International Congress I.A.H.R., Paris, 1971.

77. Zheleznyakov, G.V. and Novikova, N.M., "Kinematic Effect of the flow in Erodible Channels", International Conference of the I.A.H.R., Istanbul, Turkey, 1973.

78. Smith, D.W., and Walker, J.H., "Skin friction Measurements in incompressible flow", N.A.C.A., Technical note 4231, 1958.

APPENDIX ONE

COMPUTER PROGRAMS DEVELOPED FOR STUDY

PROGRAM FOR PLOTTING ISOVELS AND LATERAL VELOCITY PROFILES
PRESENTED IN CHAPTER 4

```
      PROGRAM CONLAT
      DIMENSION VELC(20,20),VELF(20,20),HEIHTC(20),HEIHTF(20)
      DIMENSION RANGEC(20),RANGEF(20),CONT(10),VELC1(20)
      DIMENSION VELF1(20)
      DATA CONT /0.1,0.15,0.2,0.25,0.3,0.35,0.4,0.45,0.5,0.55/
      READ(5,9993) ISET
      WRITE(6,9993) ISET
      READ(5,9995)NT
      WRITE(6,9995)NT
      READ(5,9998)YC,S,BW,BC,H
      READ(5,9999)LL
      READ(5,9997)(RANGEC(I),I=1,LL)
      READ(5,9999)KK
      READ(5,9997)(HEIHTC(J),J=1,KK)
      DO 12 I=1,LL
      READ(5,9997)(VELC(I,J),J=1,KK)
12    WRITE(6,9997)(VELC(I,J),J=1,KK)
      READ(5,9999)LLL
      READ(5,9997)(RANGEF(I),I=1,LLL)
      READ(5,9999)KKK
      READ(5,9997)(HEIHTF(J),J=1,KKK)
      DO 13 I=1,LLL
13    READ(5,9997)(VELF(I,J),J=1,KKK)
      DO 14 J=1,KKK
14    HEIHTF(J)=HEIHTF(J)+H
9999  FORMAT( I2)
9998  FORMAT( 5F10.4)
9997  FORMAT( 12F10.4)
9995  FORMAT( I3)
9993  FORMAT( I1)
C
C
      CALL PAPER(1)
      CALL CTRMAG(12)
      IF(ISET.EQ.1) CALL PSPACE(0.15,0.65,0.7,0.95)
      IF(ISET.EQ.1) CALL CSPACE(0.05,0.7,0.65,1.0)
      IF(ISET.EQ.2) CALL PSPACE(0.85,1.35,0.7,0.95)
      IF(ISET.EQ.2) CALL CSPACE(0.75,1.45,0.65,1.0)
      CALL MAP(0.0,0.8+0.05,0.0,YC+0.01)
      CALL POSITN(0.0,0.0)
      CALL JOIN(BC,0.0)
      CALL JOIN(BC,H)
      CALL JOIN(BW,H)
      CALL JOIN(BW,YC+0.01)
      CALL POSITN(BW,YC)
      CALL JOIN(0.0,YC)
```

```
      SPACE2=0.0
      DO 84 J=2,KK
      JCOUNT=JCOUNT+1
      CALL POSITN(0.0+0.03,0.7-SPACE)
      IF(JCOUNT.GT.4) CALL POSITN(0.4+0.03,0.7-SPACE2)
      SPACE=SPACE+0.035
      IF(JCOUNT.GT.4) SPACE2=SPACE2+0.035
      CALL CTRMAG(18)
      CALL CTRSET(4)
      CALL TYPENC(J+48)
      CALL CTRMAG(10)
      CALL CTRSET(1)
      CALL TYPECS(' Y=',3)
      CALL  TYPENF(HEIHTC(J),3)
84    CONTINUE
      CALL CTRSET(4)
      CALL CTRMAG(15)
      DO 87 J=2,KKK
      DO 86 I=1,LLL-1
      VELF1(I)=VELF(I,J)
86    CONTINUE
      CALL CURVEO(RANGEF,VELF1,1,LLL-1)
      CALL PTPLOT(RANGEF,VELF1,1,LLL-1,JJ+J)
87    CONTINUE
      SPACE=0.0
      DO 85 J=2,KKK
      CALL POSITN(0.6+0.02,0.6-SPACE)
      SPACE=SPACE+0.04
      CALL CTRSET(4)
      CALL CTRMAG(18)
      CALL TYPENC(JJ+J)
      CALL CTRMAG(10)
      CALL CTRSET(1)
      CALL TYPECS(' Y= ',4)
      CALL TYPENF(HEIHTF(J)-H,3)
85    CONTINUE
      CALL PSPACE(0.1,1.4,0.1,0.95)
      IF(ISET.EQ.2) GO TO 83
      CALL CSPACE(0.0,1.5,0.05,1.1)
      CALL CTRMAG(20)
      CALL PLACE(20,35)
      CALL CTRSET(1)
      CALL TYPECS('F',1)
      CALL CTRSET(2)
      CALL TYPECS('IG       ',8)
      CALL CTRSET(1)
      CALL TYPECS('I',1)
      CALL CTRSET(2)
      CALL TYPECS('SOVELS AND LATERAL VELOCITY PROFILES.',37)
83    CALL GREND
      STOP
      END
```

```
      CALL POSITN(0.0,YC+0.01)
      CALL JOIN(0.0,0.0)
      CALL AXES
      CALL CONTIA(VELC,2,LL-1,20,2,KK,20,CONT,3,10,RANGEC,HEIHTC)
      CALL CONTIA(VELF,1,LLL-1,20,2,KKK,20,CONT,1,10,RANGEF,HEIHTF)
      CALL CTRMAG(10)
      CALL PLOTCS(BC+0.05,H-0.008,'RUN ',4)
      CALL TYPENI(NT)
      CALL PLOTCS(BC+0.05,H-0.016,'YC= ',4)
      CALL TYPENF(YC,4)
      CALL PLOTCS(BC+0.05,H-0.024,'BC= ',4)
      CALL TYPENF(BC,3)
      CALL PLOTCS(BC+0.05,H-0.032,'BF= ',4)
      CALL TYPENF(BF,4)
      CALL PLOTCS(BC+0.05,H-0.040,'H=  ',4)
      CALL TYPENF(H,3)
      CALL PLACE(55,75)
      CALL TYPECS('RANGE (M)',9)
      CALL CTRORI(1.0)
      CALL PLACE(30,3)
      CALL TYPECS('DEPTH (M)',9)
      CALL CTRORI(0.0)
C
C
C                START LATERAL VELOCITY PLOTS
C
      CALL PSPACE(0.15,0.65,0.2,0.65)
      CALL CSPACE(0.05,0.7,0.1,0.7)
      IF(ISET.EQ.2) CALL PSPACE(0.85,1.35,0.2,0.65)
      IF(ISET.EQ.2) CALL CSPACE(0.75,1.45,0.1,0.7)
      CALL MAP(0.0,0.8+0.05,0.0,0.7)
      CALL AXESSI(0.1,0.1)
      CALL CTRMAG(15)
      CALL BROKEN(10,10,10,10)
      CALL POSITN(BC,0.0)
      CALL JOIN(BC,0.53)
      CALL POSITN(BW,0.0)
      CALL JOIN(BW,0.25)
      CALL CTRSET(4)
      DO 88 J=2,KK
      IF(H.GT.0.06) J=J+1
      IF(J.GT.KK) GOTO 88
      DO 89 I=2,LL-1
      VELC1(I)=VELC(I,J)
89    CONTINUE
      JJ=48+J
      CALL CURVEO(RANGEC,VELC1,2,LL-1)
      CALL PTPLOT(RANGEC,VELC1,2,LL-1,JJ)
88    CONTINUE
C
      JCOUNT=0
      SPACE=0.0
```

PROGRAM USED TO PLOT GRAPH OF SHEAR STRESS
DISTRIBUTION IN CHANNEL AND FLOOD PLAIN AS
SHOWN IN CHAPTER 5

```
      PROGRAM SHEAR2
      DIMENSION TCL(50),TCB(50),TCR(50)
      DIMENSION VELL(50),VELR(50),VELB(50)
      DIMENSION VELFF(50)
      DIMENSION TCF(50)
      DIMENSION VELC(50,50),VELF(50,50),HEIHTC(20),HEIHTF(20)
      DIMENSION NTES(200),VCDASH(200),VFDASH(200),TCDASH(200)
      DIMENSION TFDASH(200),QMEAS(200)
      DIMENSION DEPTH(200),BCHANN(200),BFLOOD(200),BANKH(200)
      DIMENSION SOLD(200),SNEW(200)
      DIMENSION RANGEC(20),RANGEF(20)
      READ(5,9993)ISET
      READ(5,9994)NT
      READ(5,9996)YC,S,BW,BC,H
      BF=BW-BC
      WRITE(6,9998)YC,S,BW,BC,H
      READ(5,9999)LL
      READ(5,9997)(RANGEC(I),I=1,LL)
      READ(5,9999)KK
      READ(5,9997)(HEIHTC(J),J=1,KK)
      DO 12 I=1,LL
12    READ(5,9997)(VELC(I,J),J=1,KK)
      READ(5,9999)LLL
      READ(5,9997)(RANGEF(I),I=1,LLL)
      WRITE(6,9997)(RANGEF(I),I=1,LLL)
      READ(5,9999)KKK
      READ(5,9997)(HEIHTF(J),J=1,KKK)
      DO 13 I=1,LLL
13    READ(5,9997)(VELF(I,J),J=1,KKK)
9999  FORMAT( I2)
9996  FORMAT(5F10.4)
9997  FORMAT( 12F10.4)
      READ(7,9994)NTESTS
      WRITE(6,9994)NTESTS
      READ(7,9993)IGEO
      DO 10 I=1,NTESTS
      READ(7,9991)NTES(I),DEPTH(I),BCHANN(I),BFLOOD(I),SNEW(I)
     1,BANKH(I),SOLD(I)
      SOLD(I)=1.0/SOLD(I)
10    SNEW(I)=1.0/SNEW(I)
      DO 11 I=1,NTESTS
      READ(7,9998)VCDASH(I),VFDASH(I),TCDASH(I),TFDASH(I)
     1,QMEAS(I)
C
11    CONTINUE
```

```
9993   FORMAT( I1)
9994   FORMAT( I3)
9991   FORMAT( I3,6F10.4)
9998   FORMAT( 7F10.4)
C
C
C
       CALL SHEARCALC(VELL,VELB,VELR,LL,KK,LLL,
      1TCL,TCB,TCR,TCF,NTES,VELC,VELF,VELFF)
C
C
C                DRAW GEOMETRY PF CHANNEL
       IF(ISET.EQ.1) SPACE=0.0
       IF(ISET.EQ.2) SPACE=0.65
       TSP=0.4
       CALL PAPER(1)
       CALL CSPACE(0.0,1.5,0.0,1.1)
       CALL CTRMAG(12)
       CALL PSPACE(0.3+SPACE,0.7+SPACE,0.8-TSP,0.95-TSP)
       CALL MAP(0.0,0.8,0.0,YC+0.01)
       CALL POSITN(0.0,0.0)
       CALL JOIN(BC,0.0)
       CALL JOIN(BC,H)
       CALL JOIN(BW,H)
       CALL JOIN(BW,YC+0.01)
       CALL POSITN(BW,YC)
       CALL JOIN(0.0,YC)
       CALL JOIN(0.0,YC+0.01)
       CALL JOIN(0.0,0.0)
       CALL POSITN(BC/3.0,YC-YC/40.0)
       CALL JOIN(BC/3.0+0.05,YC-YC/40.0)
       CALL POSITN(BC/3.0+0.04,YC-YC/20.0)
       CALL JOIN(BC/3.0+0.01,YC-YC/20.0)
       CALL POSITN(BC/3.0+0.02,YC-YC/40.0*3.0)
       CALL JOIN(BC/3.0+0.03,YC-YC/40.0*3.0)
       CALL PLOTCS(BC/10.0,YC-YC/5.0,'RUN ',4)
       CALL CTRSET(2)
       CALL TYPENI(NT)
       CALL PLOTCS(BC-0.15,YC/10.0,'RANGE',5)
C
C
C                    DRAW LHS WALL
       CALL PSPACE(0.1+SPACE,0.3+SPACE,0.8-TSP,0.95-TSP)
       CALL MAP(0.8,0.0,0.0,YC+0.01)
       CALL CTRSET(4)
       CALL CTRMAG(12)
       CALL PTPLOT(TCL,HEIHTC,2,KK,54)
       CALL CURVEO(TCL,HEIHTC,2,KK)
       CALL CTRMAG(8)
       CALL AXESSI(0.2,0.04)
       CALL POSITN(0.0,YC)
       CALL JOIN(TCL(KK),YC)
       CALL CTRSET(1)
       CALL PLOTNC(0.8,0.0,62)
```

```
      CALL CTRSET(2)
      CALL CTRMAG(12)
      CALL PLOTCS(0.8,YC/10.0,'TAU',3)
C
C           DRAW BASE SHEAR
C
      CALL PSPACE(0.3+SPACE,0.4*BC/0.8+0.3+SPACE,0.6-TSP,0.8-TSP)
      CALL MAP(0.0,BC,0.8,0.0)
      CALL CTRMAG(8)
      CALL AXESSI(0.1,0.2)
      CALL CTRSET(4)
      CALL CTRMAG(12)
      CALL PTPLOT(RANGEC,TCB,2,LL-1,54)
      CALL NSCURV(RANGEC,TCB,2,LL-1)
      CALL CTRMAG(8)
      CALL POSITN(BC,0.0)
      CALL JOIN(BC,TCB(LL-1))
      CALL CTRSET(2)
      CALL CTRMAG(12)
      CALL PLOTCS(-0.1,0.8,'TAU',3)
C
C
C           DRAW RHS WALL SHEAR
C
C
      CALL PSPACE(0.4*BC/0.8+0.3+SPACE,0.5+SPACE+0.4*BC/0.8
     1,0.8-TSP,0.8+0.15*H/(YC+0.01)-TSP)
      CALL MAP(0.0,0.8,0.0,H)
      CALL CTRMAG(8)
      CALL AXESSI(0.2,0.5)
      CALL CTRMAG(12)
      DO 59 J=2,KK
      IF(HEIHTC(J).LT.H) KN=J
59    CONTINUE
      CALL CTRMAG(12)
      CALL CTRSET(4)
      CALL PTPLOT(TCR,HEIHTC,2,KN,54)
      CALL CURVEO(TCR,HEIHTC,2,KN)
      CALL CTRMAG(8)
      CALL CTRSET(5)
      CALL PLOTNC(0.8,0.0,60)
      CALL CTRSET(2)
      CALL CTRMAG(12)
      CALL PLOTCS(0.55,YC/10.0,'TAU',3)
C
C
C           DRAW FLOOD SHEAR
      WRITE(6,998) (RANGEF(I),I=1,LLL-1)
      WRITE(6,998) (TCF(I),I=1,LLL-1)
998   FORMAT( 'VALUES ARE',12F10.4)
      CALL PSPACE(0.4*BC/0.8+0.35+SPACE,0.75+SPACE,0.6-TSP,0.75-TSP)
      CALL CTRMAG(8)
```

```
      CALL MAP(BC,0.8,0.8,0.0)
      CALL AXESSI(0.1,0.2)
      CALL CTRSET(4)
      CALL CTRMAG(12)
      CALL PTPLOT(RANGEF,TCF,1,LLL-1,53)
      CALL CURVEO(RANGEF,TCF,1,LLL-1)
      CALL CTRSET(5)
      CALL PLOTNC(0.8,0.0,60)
      CALL POSITN(0.0,0.8)
      CALL JOIN(0.0-0.03,0.8-0.03)
      CALL POSITN(0.0,0.8)
      CALL JOIN(0.0+0.03,0.8-0.03)
      CALL CTRSET(1)
      CALL CTRSET(2)
      CALL PLOTCS(0.6,-0.05,'RANGE (M)',9)
      CALL PLOTCS(BC-0.08,0.8,'TAU',3)
C
C
      IF(TSP.EQ.0.4) GO TO 76
      IF(ISET.EQ.2) GO TO 76
      CALL PSPACE(0.1,1.35,0.1,1.0)
      CALL CTRMAG(20)
      CALL PLACE(10,35)
      CALL CTRSET(1)
      CALL TYPECS('F',1)
      CALL CTRSET(2)
      CALL TYPECS('IG          ',10)
      CALL CTRSET(1)
      CALL TYPECS('S',1)
      CALL CTRSET(2)
      CALL TYPECS('HEAR STRESS DISTRIBUTION IN CHANNEL AND',39)
      CALL TYPECS(' FLOOD PLAIN.',13)
76    CALL GREND
      STOP
      END
      SUBROUTINE SHEARCALC(VELL,VELB,VELR,LL,KK,LLL,
     1TCL,TCB,TCR,TCF,NTES,VELC,VELF,VELFF)
      DIMENSION VELL(50),VELB(50),VELR(50),TCL(50),VELFF(50)
     1,TCB(50),TCR(50),NTES(200)
      DIMENSION VELC(50,50),VELF(50,50),TCF(50)
      DO 99 I=2,LL-1
99    VELB(I)=VELC(I,2)
      DO 98 J=2,KK
98    VELL(J)=VELC(2,J)
      DO 97 J=2,KK
97    VELR(J)=VELC(LL-1,J)
C
      DO 94 I=1,LLL-1
94    VELFF(I)=VELF(I,2)
      WRITE(6,9989)(VELFF(I),I=2,LLL-1)
9989  FORMAT( 12F10.4)
      CALL READSHEAR(VELR,TCR,2,KK)
```

```
      CALL READSHEAR(VELB,TCB,2,LL-1)
      CALL READSHEAR(VELL,TCL,2,KK)
      CALL READSHEAR(VELFF,TCF,1,LLL-1)
      WRITE(6,8887) (TCR(I),I=2,KK)
      WRITE(6,8887) (TCB(I),I=2,LL-1)
      WRITE(6,8887) (TCL(I),I=2,KK)
      WRITE(6,8887) (TCF(I),I=1,LLL-1)
8887  FORMAT( ' SHEAR ',12F10.4)
      RETURN
      END
C
C
      SUBROUTINE READSHEAR(VEL,TC,NN,NNN)
      DIMENSION VEL(50),TC(50)
      DIA=0.004
      DO 35 I=NN,NNN
      RED=VEL(I)**2.0/19.62
      TC(I)=0.0
      IF(RED.EQ.0.0) GO TO 35
      XSTAR=ALOG10(RED*9810.0*DIA**2.0/4000.0/(0.00000101**2.0))
      YSTAR=0.8287-0.1381*XSTAR+0.1437*XSTAR**2.0-0.0063*XSTAR**3.0
      TC(I)=10.0**YSTAR*4000.0*0.00000101**2.0/DIA**2.0
35    CONTINUE
      RETURN
      END
```